Non-linear Finite Element Analysis of Solids and Structures

Volume 2
Advanced Topics

M. A. Crisfield

WILEY

Non-linear Finite Element Analysis of Solids and Structures

Volume 2: Advanced Topics

To

Kiki, Lou, Max, Arabella
Gideon, Gavin, Rosie and Lucy

Non-linear Finite Element Analysis of Solids and Structures

Volume 2: ADVANCED TOPICS

M. A. Crisfield
Imperial College of Science, Technology and Medicine, London, UK

JOHN WILEY & SONS
Chichester · New York · Weinheim · Brisbane · Singapore · Toronto

Baffins Lane, Chichester,
West Sussex PO19 1UD, England

National 01234 779777
International (+44) 1243 779777
e-mail (for orders and customer service enquiries); cs-book@wiley.co.uk

Visit our Home Page on http://www.wiley.co.uk
or http://www.wiley.com

Reprinted with corrections December 1988, April 2000

Other Wiley Editorial Offices

John Wiley & Sons, Inc., 605 Third Avenue,
New York, NY 10158-0012, USA

VCH Verlagsgesellschaft mbH, Pappelallee 3,
D-69469 Weinheim, Germany

Jacaranda Wiley Ltd, 33 Part Road, Milton,
Queensland 4046, Australia

John Wiley & Sons (Canada) Ltd, 22 Worcester Road,
Rexdale, Ontario M9W 1L1, Canada Loop

John Wiley & Sons (Asia) Pte Ltd, 2 Clementi Loop 02-01,
Jin Xing Distripark, Singapore 129809

British Library Cataloging in Publication Data

A catalogue record for this book is available from the British Library

ISBN 0 471 95649 X

Typeset in 10/12pt Times by Thomson Press (India) Ltd, New Delhi, India
Printed and bound in Great Britain by Bookcraft (Bath) Ltd.
This book is printed on acid-free paper responsibly manufactured from sustainable forestation, for which at least two trees are planted for each one used for paper production.

Contents

Preface

In the preface to Volume 1, I expressed my trepidation at starting to write a book on non-linear finite elements and the associated mechanics. These doubts grew as I worked on Volume 2, which attempts to cover 'advanced topics'. These topics include many areas which are still the subject of considerable controversy. None the less, I have finally completed this second volume, although in so doing, I have almost certainly made mistakes. In persevering, I have received much encouragement from a number of readers of Volume 1 who have urged me not to abandon the second volume and who have made me believe that there is some need for a book of this kind.

As with the subject-matter of the first book, there are many specialist texts which cover the background mechanics. My aim has not been to replace such books and, indeed, I have attempted to reference these books with a view to encouraging wider reading. Instead, my aim has been to emphasise the numerical implementation. As with the earlier volume, an engineering approach is adopted in contrast to a strict mathematical development.

At the end of the Preface of Volume 1, I indicated the subjects that I intended to cover in this second volume. These topics have all been included, but so have a number of other topics that I did not originally envisage including. In particular Chapter 23 covers 'Contact and friction' and Chapter 24 covers 'Nonlinear dynamics' (both 'implicit' and 'explicit'). These important subjects are included because I have now conducted some research in these areas. This is true of most of the topics in the book. However, while I have often given the background to some of my own research, I have also attempted to cover important developments by others. Often, in so doing, I have reinterpreted these works in relation to my own 'viewpoint'. Often, this will not coincide with that of the originator. The reader should, of course, read the originals as well!

The previous paragraph gives the impression that the book is related to research. This is only partially true in that any book, attempting to cover advanced topics, must be concerned with the recent research in the field. However, in addition to these research-related topics, there are many other topics in which the ground work is fairly well established. In these areas, the book is closer to a traditional 'textbook'.

I referred earlier to 'my own research'. Of course, I should have referred to 'the work of my research group'. In particular, I must thank the following (in alphabetical order) for their important contributions: Mohammed Asghar, Michael Dracopoulos, Zhiliang Fan, Ugo Galvanetto, Hans-Bernd Hellweg, Gordan Jelenic, Ahad Kolahi, Yaoming Mi, Gray Moita, Xiaohong Peng, Jun Shi and Hai-Guang Zhong.

Indeed, I wrote Chapter 22 on 'Examples from an up-dated non-linear finite element computer program using truss elements' in conjunction with Dr Shi. This chapter describes a finite element computer program that can be considered as the extension of the simple computer programs described in Volume 1. As with the latter programs, the new program is available via anonymous FTP (ftp://ftp.cc.ic.ac.uk/pub/depts/aero/nonlin2). The aim of the new program is purely didactic and it is intended to illustrate some of the 'path-following' and 'branch-switching techniques' described in Chapter 21.

10 More continuum mechanics

This chapter can be considered as an extension of Chapter 4 in Volume 1. As in the latter chapter, the aim is not to provide a fundamental text on continuum mechanics (for that the reader should consult the references quoted in the Introduction to Chapter 4 and the additional references [H1, M1, O1, T1–T3]). Instead the aim is to pave the way for subsequent work on finite element analysis. For much of this work, Sections 10.1–10.5 will suffice. Section 10.6, which closely follows the work of Hill [H1] (see also Atluri [A1], Ogden [O1] and Nemat-Nasser [N1], gives a more detailed examination of a range of strees and strain measures. This section is not easy and could be skipped (along with Sections 10.7–10.8) at a first reading.

10.1 RELATIONSHIPS BETWEEN SOME STRAIN MEASURES AND THE STRUCTURES

In Section 4.9, we related the Green and Almansi strain measures to the principal stretches, which were introduced in Section 4.8 via the polar decomposition theorem. We will now extend these relationships to some other strain measures.

Our starting-point is the right stretch $\mathbf{U}$ or $\mathbf{U}_R$ and the left stretch $\mathbf{U}_L$ or $\mathbf{V}$ (see 4.126) which can be expressed in terms of the principal stretches, $\lambda_1 - \lambda_3$ via (see 4.139) and (4.145))

$$\mathbf{U} = \mathbf{Q}(\mathbf{N})\text{Diag}(\lambda)\mathbf{Q}(\mathbf{N})^{\mathrm{T}} = \lambda_1\mathbf{N}_1\mathbf{N}_1^{\mathrm{T}} + \lambda_2\mathbf{N}_2\mathbf{N}_2^{\mathrm{T}} + \lambda_3\mathbf{N}_3\mathbf{N}_3^{\mathrm{T}} \tag{10.1a}$$

$$\mathbf{V} = \mathbf{Q}(\mathbf{n})\text{Diag}(\lambda)\mathbf{Q}(\mathbf{n})^{\mathrm{T}} = \lambda_1\mathbf{n}_1\mathbf{n}_1^{\mathrm{T}} + \lambda_2\mathbf{n}_2\mathbf{n}_2^{\mathrm{T}} + \lambda_3\mathbf{n}_3\mathbf{n}_3^{\mathrm{T}} \tag{10.1b}$$

with $\mathbf{Q}(\mathbf{N}) = [\mathbf{N}_1, \mathbf{N}_2, \mathbf{N}_3]$ and $\mathbf{Q}(\mathbf{n}) = [\mathbf{n}_1, \mathbf{n}_2, \mathbf{n}_3]$. In Section 4.2, we showed how the principal direction $\mathbf{N}_1$ and $\mathbf{n}_1$ could be found from an eigenvalue analysis of $\mathbf{C} = \mathbf{F}^{\mathrm{T}}\mathbf{F}$ or of $\mathbf{b} = \mathbf{F}\mathbf{F}^{\mathrm{T}}$. It was assumed that the principal directions were distinct. If two of the principal stretches coincide (say λ_1 and λ_2), the directions $\mathbf{N}_1$ and $\mathbf{N}_2$ (or $\mathbf{n}_1$ and $\mathbf{n}_2$) are not unique and can only be determined to within an arbitrary rotation about $\mathbf{N}_3$ (or $\mathbf{n}_3$). In the following, it will generally be assumed that the stretches and principal directions are distinct. Detail in relation to the case of coinciding stretches will be given in Section 13.8. In the meantime, we note that if all of the stretches coincide, in place of (10.1a) and

(10.1b), we have

$$\mathbf{U} = \mathbf{V} \times \lambda \mathbf{I} \tag{10.1c}$$

Following the forms of (10.1a) and (10.1b), some general strain measures, $\boldsymbol{\varepsilon}$, may be expressed, in the Lagrangian frame, as

$$\boldsymbol{\varepsilon} = \mathbf{Q}(\mathbf{N})\mathbf{Diag}(\boldsymbol{\varepsilon})\mathbf{Q}(\mathbf{N})^{\mathrm{T}} \tag{10.2a}$$

while others may be expressed in the Eulerian frame as

$$\boldsymbol{\varepsilon} = \mathbf{Q}(\mathbf{n})\mathbf{Diag}(\boldsymbol{\varepsilon})\mathbf{Q}(\mathbf{n})^{\mathrm{T}} \tag{10.2b}$$

where the principal strains, $\boldsymbol{\varepsilon}_{1-3}$ (from $\mathbf{Diag}(\boldsymbol{\varepsilon})$) can be related to the principal stretches λ_{1-3} (from $\mathbf{Diag}(\lambda)$). For any one of the principal directions, we can write

$$\varepsilon = f(\lambda) \tag{10.3}$$

where we require that:

1. $f(1) = 0$ so that there is no strain when $\| \mathbf{dx} \| = \| \mathbf{dX} \|$ (see (4.131) and the stretch, λ, is unity.
2. Having expressed ε via a Taylor series,

$$\varepsilon = f(1) + (\lambda - 1)\left.\frac{\partial f}{\partial \lambda}\right|_{\lambda=1} + \frac{(\lambda-1)^2}{2}\left.\frac{\partial^2 f}{\partial \lambda^2}\right|_{\lambda=1} + \cdots \tag{10.4a}$$

in order to coincide with the usual engineering theory strains, $\varepsilon = \lambda - 1$, for small stretches, it follows from (10.4a) that

$$\left.\frac{\partial f}{\partial \lambda}\right|_{\lambda=1} = 1 \tag{10.4b}$$

3. ε should increase strictly monotonically with λ.

The strain measures may either be related to (10.2a) or to (10.2b). We will address this issue later, but will firstly consider some common strain measures in terms of (10.3).

Biot strain (or co-rotated engineering strain):

$$\varepsilon = \lambda - 1 \tag{10.5}$$

Green strain:

$$\varepsilon = \tfrac{1}{2}(\lambda^2 - 1) \tag{10.6}$$

Almansi strain:

$$\varepsilon = \frac{1}{2}\left(1 - \frac{1}{\lambda^2}\right) \tag{10.7}$$

Log strain:

$$\varepsilon = \log_{\mathrm{e}} \lambda \tag{10.8}$$

These measures have already been introduced for truss elements in Chapter 3.

Combining the polar decomposition, $\mathbf{F} = \mathbf{RU}$ (see (4.127)) with (10.1a) and noting that $\mathbf{U}$ is symmetric:

$$\mathbf{C} = \mathbf{F}^{\mathrm{T}}\mathbf{F} = \mathbf{U}^{\mathrm{T}}\mathbf{U} = \mathbf{Q(N)Diag}(\lambda^2)\mathbf{Q(N)}^{\mathrm{T}} = \mathbf{U}^{2*} \tag{10.9}$$

and hence, from (4.73) and (10.9),

$$\begin{aligned}\mathbf{E} &= \tfrac{1}{2}(\mathbf{F}^{\mathrm{T}}\mathbf{F} - \mathbf{I}) = \mathbf{Q(N)Diag}\left(\frac{\lambda^2}{2}\right)\mathbf{Q(N)}^{\mathrm{T}} - \tfrac{1}{2}\mathbf{Q(N)Q(N)}^{\mathrm{T}} \\ &= \mathbf{Q(N)Diag}\left(\frac{\lambda^2 - 1}{2}\right)\mathbf{Q(N)}^{\mathrm{T}} \\ &= \tfrac{1}{2}[\mathbf{C} - \mathbf{I}] = \tfrac{1}{2}[\mathbf{U}^2 - \mathbf{I}]\end{aligned} \tag{10.10}$$

where we have used the relationship

$$\mathbf{Q(N)Q(N)}^{\mathrm{T}} = \mathbf{I} = \sum_{i=1}^{3} \mathbf{N}_i\mathbf{N}_i^{\mathrm{T}}.$$

Equation (10.10) has been derived previously in Section 4.9 (see (4.153)). From the derivation of (10.10), we can identify the Green strain, $\mathbf{E}$, as stemming from the combination of (10.6) and (10.2a).

Using the polar decomposition, $\mathbf{F} = \mathbf{VR}$ of (4.126) and the relationship in (10.1b) for $\mathbf{V}$, the Almansi strain of (4.91) can, in a similar fashion be re-expressed as

$$\mathbf{A(n)} = \tfrac{1}{2}(\mathbf{I} - \mathbf{F}^{-\mathrm{T}}\mathbf{F}^{-1}) = \tfrac{1}{2}(\mathbf{I} - \mathbf{V}^{-\mathrm{T}}\mathbf{V}^{-1}) = \mathbf{Q(n)Diag}\left(\frac{\lambda^2 - 1}{2\lambda^2}\right)\mathbf{Q(n)}^{\mathrm{T}} \tag{10.11}$$

The latter can also be derived by combining (10.2b) with (10.7). Combining (10.2a) with (10.8), the log strain can be written as:

$$\log_{\mathrm{e}}\mathbf{U} = \mathbf{Q(N)Diag}(\log_{\mathrm{e}}(\lambda))\mathbf{Q(N)}^{\mathrm{T}} = \log_{\mathrm{e}}(\mathbf{C}^{1/2}) = \tfrac{1}{2}\log_{\mathrm{e}}\mathbf{C} \tag{10.12}$$

In contrast to the strain measures of (10.10) and (10.11), the log strain can only be computed after a polar decomposition has obtained the principal directions, $\mathbf{N}_i$ and principal stretches, λ_i.

Alternatively (to give a *different* strain measure), using (10.2b) and (10.8), we can write

$$\log_{\mathrm{e}}\mathbf{V} = \mathbf{Q(n)Diag}(\log_{\mathrm{e}}(\lambda))\mathbf{Q(n)}^{\mathrm{T}} \tag{10.13}$$

It was shown in Section 4.9 that the Green strain of (10.10) is invariant to a rigid rotation while the Almansi strain of (10.11) is not. In a similar fashion, $\log_{\mathrm{e}}\mathbf{U}$ is invariant to a rigid rotation while $\log_{\mathrm{e}}\mathbf{V}$ is not.

The Biot strain can be found by combining (10.5) and (10.2a) to give

$$\boldsymbol{E}_{\mathrm{b}} = \mathbf{Q(N)Diag}(\lambda - 1)\mathbf{Q(N)}^{\mathrm{T}} = \mathbf{U} - \mathbf{I} \tag{10.14}$$

A comparison of (10.10) and (10.12) with (10.14) shows that, if the stretches λ are small, $\mathbf{E} \simeq \log_{\mathrm{e}}\mathbf{U} \simeq \boldsymbol{E}_{\mathrm{b}}$.

Alternative strain measures can be derived. For example, (10.5) could be combined with (10.2b) and Hill [H1] combines (10.7) with (10.2a) to produce an Almansi strain

*In this chapter and in Chapter 13, we will use $\mathbf{C}$ for the (right) Cauchy Green tensor (as in (10.9)) and, as a consequence, will now use $\mathbf{D}$ (previously $\mathbf{C}$) for the constitutive matrix (or tensor).

(**A**(**N**)) that differs from the more usual definition of (4.91) and (10.11) in that, in the former, one would have **Q**(**N**)'s rather than **Q**(**n**)'s.

The Almansi strain, **A**(**N**), the Green strain **E** of (10.11), the Biot strain, $\boldsymbol{E}_b$ of (10.14) and the $\log_e \mathbf{U}$ strain of (10.12) can be considered as belonging to a family of strain measures given by Hill [H1] (see also [A1, N1, P1]) which all relate to (10.2a) and for which

$$\boldsymbol{E} = \frac{1}{m}[\mathbf{C}^{m/2} - \mathbf{I}] \qquad \text{if } m \neq 0 \tag{10.15a}$$

$$\boldsymbol{E} = \tfrac{1}{2}\log_e \mathbf{C} \qquad \text{if } m = 0 \tag{10.15b}$$

With $m = -2$, one obtains **A**(**N**), with $m = 1$, $\boldsymbol{E}_b$ in (10.14) and with $m = 2$, the Green strain of (10.10).

We have already considered the second Piola–Kirchhoff stress which is work conjugate to the Green strain of (10.10). In Sections 10.5 and 10.6, we will consider stresses that are work conjugate to some of the other strain measures that have been discussed here.

10.2 LARGE STRAINS AND THE JAUMANN RATE

For some large-strain analysis, it is useful to work in the current configuration using the Cauchy stress. Many formulations have then used the Jaumann rate of Cauchy stress. In particular, it has other been used in large-strain elasto-plastic analyses (see Chapters 12 and 19). In addition it is relevant to hyper-elastic relationships including rubber analyses (Chapter 13). We now give a basic introduction in order to allow the 'Eulerian finite element formulation' to be described in Chapter 12. However, finer points including the integration of the rate equations, plasticity and hyperelasticity follow in later chapters.

Much finite element work on large-strain elaso-plastic analysis has adopted a hypo-elastic approach (see Section 4.12) in relation to the Cauchy stress. A naïve solution might then involve simply updating the Cauchy stress via

$$\boldsymbol{\sigma}_n = \boldsymbol{\sigma}_o + \mathbf{D}_t : \delta\boldsymbol{\varepsilon} \tag{10.16}$$

where subscript o means 'old' and subscript n means 'new' and $\mathbf{D}_t$ is some tangential modular matrix (see the footnote to page 3 for an explanation of the change of notation for the constitutive tensor) which may allow for plasticity (Chapters 6, 14 and 15). The update in (10.16) would imply that, for a rigid-body motion for which $\delta\boldsymbol{\varepsilon} = \mathbf{0}$, the stresses update via $\boldsymbol{\sigma}_n = \boldsymbol{\sigma}_o$. However, we know (Figure 4.10), that the Cauchy stress components (related to a fixed unrotated coordinate system) do change under a rigid-body rotation. Hence a more sensible updating scheme would directly incorporate the rotation of (4.63) so that

$$\boldsymbol{\sigma}_n = \mathbf{R}\boldsymbol{\sigma}_o\mathbf{R}^T + \mathbf{D}_t : \delta\boldsymbol{\varepsilon} = \mathbf{R}\boldsymbol{\sigma}_o\mathbf{R}^T + \Delta t\, \mathbf{D}_t : \dot{\boldsymbol{\varepsilon}} \tag{10.17}$$

where the first term rotates the stresses (Section 4.3.2) and the second is caused by the material constitutive law. In this second term, we have introduced a small time change, Δt, and the strain rate, $\dot{\boldsymbol{\varepsilon}}$ (see also (4.108)). Under a rigid-body rotation, equation (10.17)

(with $\delta\boldsymbol{\varepsilon} = \dot{\boldsymbol{\varepsilon}} = \mathbf{0}$) would have resulted from a small displacement change, $\delta\mathbf{u}$, whereby

$$\delta\mathbf{x}_n = \mathbf{R}\delta\mathbf{x}_o = \delta\mathbf{x}_o + \delta\mathbf{u} = \mathbf{x}_o + \mathbf{v}\,\Delta t \tag{10.18}$$

where the subscript n means 'new' while the subscript o means 'old' and $\mathbf{v}$ is the velocity. From (10.18),

$$\mathbf{R} = \left[\mathbf{I} + \frac{\partial \delta\mathbf{u}}{\partial \mathbf{x}}\right] = \left[\mathbf{I} + \Delta t\,\frac{\partial \mathbf{v}}{\partial \mathbf{x}}\right] \tag{10.19}$$

Now (see also (4.93) for $\delta\boldsymbol{\varepsilon}$), we can write

$$\frac{\partial \delta\mathbf{u}}{\partial \mathbf{x}} = \frac{1}{2}\left[\frac{\partial \delta\mathbf{u}}{\partial \mathbf{x}} + \frac{\partial \delta\mathbf{u}^{\mathrm{T}}}{\partial \mathbf{x}}\right] + \frac{1}{2}\left[\frac{\partial \delta\mathbf{u}}{\partial \mathbf{x}} - \frac{\partial \delta\mathbf{u}^{\mathrm{T}}}{\partial \mathbf{x}}\right] = \delta\boldsymbol{\varepsilon} + \delta\boldsymbol{\Omega} \tag{10.20}$$

or

$$\frac{\partial \mathbf{v}}{\partial \mathbf{x}} = \mathbf{L}(4.109) = \frac{1}{2}\left[\frac{\partial \mathbf{v}}{\partial \mathbf{x}} + \frac{\partial \mathbf{v}^{\mathrm{T}}}{\partial \mathbf{x}}\right] + \frac{1}{2}\left[\frac{\partial \mathbf{v}}{\partial \mathbf{x}} - \frac{\partial \mathbf{v}^{\mathrm{T}}}{\partial \mathbf{x}}\right] \tag{10.21}$$

so that

$$\frac{\partial \mathbf{v}}{\partial \mathbf{x}} = \tfrac{1}{2}[\mathbf{L} + \mathbf{L}^{\mathrm{T}}] + \tfrac{1}{2}[\mathbf{L} - \mathbf{L}^{\mathrm{T}}] = \dot{\boldsymbol{\varepsilon}} + \dot{\boldsymbol{\Omega}} \tag{10.22}$$

The matrices $\delta\boldsymbol{\Omega}$ and $\dot{\boldsymbol{\Omega}}$ in (10.21) and (10.22) are skew-symmetric (or antisymmetric) with zeros on the leading diagonal. Such matrices (say $\mathbf{S}$) satisfy the relationship:

$$\mathbf{S}^{\mathrm{T}} = -\mathbf{S} \tag{10.23}$$

At this stage it is worth emphasising some issues related to the adopted notation. Following the procedure introduced in Chapter 4, we are using $\dot{\boldsymbol{\varepsilon}}$ as the velocity strain tensor (or rate of deformation tensor) although $\dot{\boldsymbol{\varepsilon}}$ is not the rate of a strain measure $\boldsymbol{\varepsilon}$. In a similar fashion, the spin $\dot{\boldsymbol{\Omega}}$ is not the rate of some tensor $\boldsymbol{\Omega}$. We should also note that some authors use $\mathbf{W}$ instead of the current $\dot{\boldsymbol{\Omega}}$ (Bathe [B1] uses $\boldsymbol{\Omega}$) and reserve $\boldsymbol{\Omega}$ for $\dot{\mathbf{R}}\mathbf{R}^{\mathrm{T}}$ which will be introduced later (as $\mathbf{W}$ in (10.70)). In addition, Dienes [D1] refers to the current $\dot{\boldsymbol{\Omega}}$ as the vorticity and not as the spin.

We require (10.17) to give the correct solution of $\mathbf{R}\boldsymbol{\sigma}_o\mathbf{R}^{\mathrm{T}}$ (see Section 4.3.2) for a rigid-body motion in which $\dot{\boldsymbol{\varepsilon}} = \mathbf{0}$ and so, from (10.21) and (10.22), in these circumstances:

$$\frac{\partial \mathbf{v}}{\partial \mathbf{x}} = \mathbf{L} = \dot{\boldsymbol{\Omega}} \tag{10.24}$$

Hence, from (10.19):

$$\mathbf{R} = [\mathbf{I} + \Delta t\,\dot{\boldsymbol{\Omega}}] \tag{10.25}$$

and, from (10.17):

$$\boldsymbol{\sigma}_n = [\mathbf{I} + \Delta t\dot{\boldsymbol{\Omega}}]\boldsymbol{\sigma}_o[\mathbf{I} + \Delta t\dot{\boldsymbol{\Omega}}]^{\mathrm{T}} + \Delta t\,\mathbf{D}_t{:}\dot{\boldsymbol{\varepsilon}} \tag{10.26a}$$

or

$$\boldsymbol{\sigma}_n = \boldsymbol{\sigma}_o + \Delta t\dot{\boldsymbol{\sigma}} = \boldsymbol{\sigma}_o + \Delta t[\dot{\boldsymbol{\Omega}}\boldsymbol{\sigma}_o + \boldsymbol{\sigma}_o\dot{\boldsymbol{\Omega}}^{\mathrm{T}}] + \Delta t\,\mathbf{D}_t{:}\dot{\boldsymbol{\varepsilon}} \tag{10.26b}$$

where, in moving from (10.26a) to (10.26b), we have ignored terms of order Δt^2.

A stricter version of (10.26b) involves

$$\boldsymbol{\sigma}_n = \boldsymbol{\sigma}_o + \int \dot{\boldsymbol{\sigma}}\, dt \tag{10.27}$$

where

$$\dot{\boldsymbol{\sigma}} = \dot{\boldsymbol{\Omega}}\boldsymbol{\sigma} + \boldsymbol{\sigma}\dot{\boldsymbol{\Omega}}^T + \mathbf{D}_{tJC}:\dot{\boldsymbol{\varepsilon}} = \dot{\boldsymbol{\Omega}}\boldsymbol{\sigma} + \boldsymbol{\sigma}\dot{\boldsymbol{\Omega}}^T + \dot{\boldsymbol{\sigma}}_J = \dot{\boldsymbol{\Omega}}\boldsymbol{\sigma} - \boldsymbol{\sigma}\dot{\boldsymbol{\Omega}} + \dot{\boldsymbol{\sigma}}_J \tag{10.28a}$$

and $\dot{\boldsymbol{\sigma}}_J$ is the Jaumann rate of Cauchy stress. (It is also sometimes known as the 'co-rotational rate'.) In (10.28a), the subscripts JC means 'Jaumann rate of Cauchy stress' and they have been added because, as indicated earlier in Chapter 3, we should indicate the type of stress and strain (and now strain rate) measure when specifying a tangential relationship. If a tangential modular matrix is appropriate for one measure, it may need modifying or transforming if it is used with another measure. In relation to hyperelasticity, the issue of transforming constitutive tensors will be discussed further in Section 12.4 and in Chapter 13.

In two dimensions, (10.28a) can be rewritten, using vector notation for $\dot{\boldsymbol{\sigma}}$ and $\dot{\boldsymbol{\varepsilon}}$ with a matrix for $\mathbf{D}_{tJC}$, so that

$$\dot{\boldsymbol{\sigma}} = \dot{\boldsymbol{\sigma}}_J + \omega \begin{bmatrix} 2\tau_{xy} \\ -2\tau_{xy} \\ \sigma_y - \sigma_x \end{bmatrix} = \mathbf{D}_{tJC}\dot{\boldsymbol{\varepsilon}} + \omega \begin{bmatrix} 2\tau_{xy} \\ -2\tau_{xy} \\ \sigma_y - \sigma_x \end{bmatrix} \tag{10.28b}$$

where ω is the spin given by

$$\omega = \frac{1}{2}\left(\frac{\partial \dot{u}}{\partial y} - \frac{\partial \dot{v}}{\partial x}\right)$$

In both (10.28a) and (10.28b) we have related the Jaumann rate of Cauchy stress, $\dot{\boldsymbol{\sigma}}_J$, to the strain rate, $\dot{\boldsymbol{\varepsilon}}$, using a rate type (or incremental) constitutive law (see Section 4.12 and Chapter 6) so that

$$\dot{\boldsymbol{\sigma}}_J = \mathbf{D}_{tJC}(\boldsymbol{\sigma}, \mathbf{F}):\dot{\boldsymbol{\varepsilon}} \tag{10.29}$$

In equation (10.29) the $(\boldsymbol{\sigma})$ following $\mathbf{D}_{tJC}$ indicates that for an elasto-plastic or hypoelastic stress–strain relationship, the tangential modular matrix may be a function of the current stresses, $\boldsymbol{\sigma}$. Also, the $(\mathbf{F})$ term indicates that (for a hyperelastic material) $\mathbf{D}_{tJC}$ may also be a function of the deformation gradient. For a hypoelastic relationship, we need to consider the issue of integrating the rate relationships in (10.28a). This will be discussed, in relation to elasto-plasticity, in Section 19.5.

The Jaumann rate, $\dot{\boldsymbol{\sigma}}_J$ of (10.28a), is one of a number of 'objective rates' which correctly transforms as a result of a rotation, $\mathbf{R}$ (see Section 4.3.2) for which

$$d\mathbf{x}' = \mathbf{R}\, d\mathbf{x} \tag{10.30}$$

so that not only do we have

$$\boldsymbol{\sigma}' = \mathbf{R}\boldsymbol{\sigma}\mathbf{R}^T \tag{10.31}$$

but also

$$\dot{\boldsymbol{\sigma}}'_{obj} = \mathbf{R}\dot{\boldsymbol{\sigma}}_{obj}\mathbf{R}^T \tag{10.32}$$

In the case of the Jaumann rate, using (10.28a), we require (see Section 10.8):

$$\dot{\boldsymbol{\sigma}}'_{\mathrm{J}} = \dot{\boldsymbol{\sigma}}' - \dot{\boldsymbol{\Omega}}'\boldsymbol{\sigma}' + \boldsymbol{\sigma}'\dot{\boldsymbol{\Omega}}' = \mathbf{R}[\dot{\boldsymbol{\sigma}}' - \dot{\boldsymbol{\Omega}}'\boldsymbol{\sigma}' + \boldsymbol{\sigma}'\dot{\boldsymbol{\Omega}}']\mathbf{R}^{\mathrm{T}} \tag{10.33}$$

An alternative way of looking at the objectivity of $\dot{\boldsymbol{\sigma}}_{\mathrm{J}}$ is that, with no real strain-induced stress change, $\dot{\boldsymbol{\sigma}}_{\mathrm{J}}$ is zero from (10.29) and from (10.28a):

$$\dot{\boldsymbol{\sigma}} = \dot{\boldsymbol{\Omega}}\boldsymbol{\sigma} - \boldsymbol{\sigma}\dot{\boldsymbol{\Omega}} \tag{10.34}$$

and hence with $\dot{\boldsymbol{\varepsilon}} = \mathbf{0}$:

$$\boldsymbol{\sigma}_{\mathrm{n}} = \boldsymbol{\sigma}_{\mathrm{o}} + \Delta t\dot{\boldsymbol{\sigma}} = \boldsymbol{\sigma}_{\mathrm{o}} + \Delta t(\dot{\boldsymbol{\Omega}}\boldsymbol{\sigma}_0 - \boldsymbol{\sigma}_0\dot{\boldsymbol{\Omega}}) \simeq (\mathbf{I} + \Delta t\dot{\boldsymbol{\Omega}})\boldsymbol{\sigma}_{\mathrm{o}}(\mathbf{I} + \Delta t\dot{\boldsymbol{\Omega}})^{\mathrm{T}} \simeq \mathbf{R}\boldsymbol{\sigma}_{\mathrm{o}}\mathbf{R}^{\mathrm{T}} \tag{10.35}$$

as it should as a result of a rigid rotation. In the last step in (10.35), we have used (10.25).

In some circumstances (see Section 12.4), it is useful to work with the Jaumann rate of Kirchhoff stress ($\boldsymbol{\tau} = \det(\mathbf{F})\boldsymbol{\sigma}$—see (4.122))—rather than the Jaumann rate of Cauchy stress. In these circumstances, in place of (10.28a), we have

$$\dot{\boldsymbol{\tau}} = \dot{\boldsymbol{\tau}}_{\mathrm{J}} + \dot{\boldsymbol{\Omega}}\boldsymbol{\tau} + \boldsymbol{\tau}\dot{\boldsymbol{\Omega}}^{\mathrm{T}} = \mathbf{D}_{\mathrm{tJK}}:\dot{\boldsymbol{\varepsilon}} + \dot{\boldsymbol{\Omega}}\boldsymbol{\tau} + \boldsymbol{\tau}\dot{\boldsymbol{\Omega}}^{\mathrm{T}} \tag{10.36}$$

where $\mathbf{D}_{\mathrm{tJK}}$ is the tangential modular tensor appropriate to the Jaumann rate of Kirchoff stress and, generally, differs from the $\mathbf{D}_{\mathrm{tJC}}$ in (10.28a) (see Section 12.4).

10.3 HYPERELASTICITY

Hyperelasticity will be considered in detail in Chapter 13. However, with a view to the following Section (10.4) on the 'Truesdell rate', we will here amplify the very basic introduction of Section 4.12. In the first instance, we will consider small strains which are linearly related to the displacements.

Following on from the introduction of Section 4.12, the simplest strain energy function, ϕ, can be expressed as

$$\phi = \phi(\varepsilon) = 2\mu\bar{I}_2 + \frac{\bar{\lambda}}{2}I_1^2 \tag{10.37}$$

where I_1 and $\bar{I}_2$ are strain invariants given by

$$I_1 = \mathrm{tr}(\boldsymbol{\varepsilon}) = \varepsilon_{ii} = \varepsilon_{11} + \varepsilon_{22} + \varepsilon_{33} \tag{10.38}$$

and

$$\bar{I}_2 = \tfrac{1}{2}\mathrm{tr}(\boldsymbol{\varepsilon}^2) = \tfrac{1}{2}\varepsilon_{ij}\varepsilon_{ij} \tag{10.39}$$

and μ and $\bar{\lambda}$ are the Lamé constants (see Section 4.2.3). In two dimensions (plane strain), equation (10.39) degenerates to

$$\bar{I}_2 = \tfrac{1}{2}\varepsilon_{11}^2 + 2\varepsilon_{12}\varepsilon_{21} + \varepsilon_{22}^2 \tag{10.40}$$

From (4.165), it follows that

$$\boldsymbol{\sigma} = \frac{\partial\phi}{\partial\boldsymbol{\varepsilon}} = 2\mu\frac{\partial\bar{I}_2}{\partial\boldsymbol{\varepsilon}} + \bar{\lambda}I_1\frac{\partial I_1}{\partial\boldsymbol{\varepsilon}} = 2\mu\boldsymbol{\varepsilon} + \bar{\lambda}\mathrm{tr}(\boldsymbol{\varepsilon})\mathbf{I} \tag{10.41a}$$

or:

$$\sigma_{ij} = \frac{\partial \phi}{\partial \varepsilon_{ij}} = 2\mu\varepsilon_{ij} + \bar{\lambda}\varepsilon_{kk}\delta_{ij} \tag{10.41b}$$

These are the simple linear Hookean stress–strain relationships of (4.27) and (4.28) which can be rewritten (see (4.29)–(4.31)) as

$$\sigma_{ij} = D_{ijkl}\varepsilon_{kl}; \qquad \boldsymbol{\sigma} = \mathbf{D}:\boldsymbol{\varepsilon} \tag{10.42}$$

with

$$D_{ijkl} = \mu(\delta_{ik}\delta_{jl} + \delta_{il}\delta_{jk}) + \bar{\lambda}\delta_{ij}\delta_{kl}; \qquad \mathbf{D} = 2\mu\,\mathbf{I}_4 + \bar{\lambda}(\mathbf{1}\otimes\mathbf{1}) \tag{10.43}$$

where, in (10.44) $\mathbf{I}_4$ is the fourth-order unit tensor and $\mathbf{1}$ the second-order unit tensor. The relationships in (10.43) satisfy the symmetry conditions, $C_{ijkl} = C_{jikl} = C_{ijlk}$.

From (10.41a), we also have

$$\dot{\boldsymbol{\sigma}} = 2\mu\dot{\boldsymbol{\varepsilon}} + \bar{\lambda}\,\mathrm{tr}(\dot{\boldsymbol{\varepsilon}})\mathbf{I} = \mathbf{D}_t:\dot{\boldsymbol{\varepsilon}} = \mathbf{D}_t:\dot{\boldsymbol{\varepsilon}} = \frac{\partial^2\phi}{\partial\boldsymbol{\varepsilon}\partial\boldsymbol{\varepsilon}}:\dot{\boldsymbol{\varepsilon}} \tag{10.44}$$

In this case, the tangential tensor $\mathbf{D}_t$ equals the secant tensor $\mathbf{D}$ in (10.42).

When the strains are non-linearly related to the displacements, we might adopt a strain measure such as the Green strain ($\mathbf{E}$) so that, in place of (10.37), we would have

$$\phi = \phi(\mathbf{E}) \tag{10.45}$$

and in place of (10.41),

$$\mathbf{S} = \frac{\partial \phi}{\partial \mathbf{E}}; \qquad S_{ij} = \frac{\partial \phi}{\partial E_{ij}} \tag{10.46}$$

Also, in place of (10.44), we would have

$$\dot{\mathbf{S}} = \frac{\partial^2\phi}{\partial\mathbf{E}\partial\mathbf{E}}:\dot{\mathbf{E}} = \mathbf{D}_{t\mathrm{K}2}:\dot{\mathbf{E}}; \qquad \dot{S}_{ij} = \frac{\partial^2\phi}{\partial E_{ij}\partial E_{kl}}\dot{E}_{kl} \tag{10.47}$$

where the fourth-order constitutive tensor $\mathbf{D}_{t\mathrm{K}2}$ (with K2 for the second Piola–Kirchhoff) is now generally not constant but depends on the current strains. A detailed discussion on hyperelasticitly is given in Chapter 13.

10.4 THE TRUESDELL RATE

We will rewrite (10.47) as

$$\dot{\mathbf{S}} = \mathbf{D}_{t\mathrm{K}2}:\dot{\mathbf{E}} \quad \text{or} \quad S_{ab} = D^{t\mathrm{K}2}_{abcd}\dot{E}_{cd} \tag{10.48}$$

(where the movement from a subscript to a superscript is introduced purely according to space). From (10.47), the tangent tensor, $\mathbf{D}_{t\mathrm{K}2}$ can be written as

$$D^{t\mathrm{K}2}_{abcd} = \frac{\partial^2\phi}{\partial E_{ab}\partial E_{cd}} \tag{10.49}$$

We now require the equivalent relationship between the Cauchy strees derivatives, $\dot{\boldsymbol{\sigma}}$, and the velocity strain tensor, $\dot{\boldsymbol{\varepsilon}}$ (see (4.108)). However, it is more convenient to start with the Kirchhoff or nominal stress, $\tau = J\boldsymbol{\sigma}$ (with $J = \det(\mathbf{F})$) which is related to the second Piola-Kirchhoff stresses, $\mathbf{S}$, via (4.122) which is reproduced here as

$$\dot{\tau} = J\dot{\boldsymbol{\sigma}} = \mathbf{F}\dot{\mathbf{S}}\mathbf{F}^{\mathrm{T}} \tag{10.50}$$

Differentiation of (10.50) leads to

$$\dot{\tau} = \mathbf{F}\dot{\mathbf{S}}\mathbf{F}^{\mathrm{T}} + \dot{\mathbf{F}}\mathbf{S}\mathbf{F}^{\mathrm{T}} + \mathbf{F}\mathbf{S}\dot{\mathbf{F}}^{\mathrm{T}} \tag{10.51}$$

Substituting in (10.51) for $\mathbf{S}$ in terms of τ from (10.50) leads to

$$\dot{\tau} = \dot{\mathbf{F}}\mathbf{S}\mathbf{F}^{\mathrm{T}} + \dot{\mathbf{F}}\mathbf{F}^{-1}\tau + \tau\mathbf{F}^{-\mathrm{T}}\dot{\mathbf{F}}^{\mathrm{T}} \tag{10.52}$$

From the non-virtual form of the relationship in (4.112), (10.52) can be re-expressed as

$$\dot{\tau} = \mathbf{F}\dot{\mathbf{S}}\mathbf{F}^{\mathrm{T}} + \mathbf{L}\tau + \tau\mathbf{L}^{\mathrm{T}} = \dot{\tau}_{\mathrm{T}} + \mathbf{L}\tau + \tau\mathbf{L}^{\mathrm{T}} \tag{10.53}$$

where $\mathbf{L}$ is the velocity gradient $\partial\mathbf{v}/\partial\mathbf{x}$ and $\dot{\tau}_{\mathrm{T}}$ is the Truesdell rate of Kirchhoff stress. Like $\dot{\tau}_{\mathrm{J}}$, $\dot{\tau}_{\mathrm{T}}$ is an objective stress rate (see also Section 10.8).[†]

In order to explore further the relationship between (10.48) and (10.53), it is necessary to adopt indicial notation coupled with the relationship (4.113) between $\dot{\boldsymbol{E}}$ and $\dot{\varepsilon}$ whereby:

$$\dot{\mathbf{E}} = \mathbf{F}^{\mathrm{T}}\dot{\boldsymbol{\varepsilon}}\mathbf{F}; \quad \dot{E}_{\mathrm{cd}} = F_{\mathrm{kc}}\dot{\varepsilon}_{\mathrm{kl}}F_{\mathrm{id}} \tag{10.54}$$

Substituting from (10.48) and (10.54) into (10.53) leads to

$$\dot{\tau} = \dot{\tau}_{\mathrm{T}} + \mathbf{L}\tau + \tau\mathbf{L}^{\mathrm{T}} = \mathbf{D}_{\mathrm{tDK}}\dot{\varepsilon} + \mathbf{L}\tau + \tau\mathbf{L}^{\mathrm{T}} \tag{10.55}$$

where

$$D^{\mathrm{tTK}}_{tjkl} = F_{ia}F_{Jb}F_{kc}F_{ld}D^{\mathrm{tK2}}_{abcd} \tag{10.56}$$

Equation (10.56) gives the relationship between the terms in the tangent tensor ($\mathbf{D}_{t\mathrm{TK}}$) relating the Truesdell rate of Kirchhoff stress, $\dot{\tau}_{\mathrm{T}}$ to the velocity strain tensor ($\dot{\varepsilon}$) with the terms in the tangent tensor ($\mathbf{D}_{\mathrm{tK2}}$) relating the rates of the second Piola-Kirchhoff stress and Green strain (see (10.48)). By using the relationship $\mathbf{L} = \dot{\varepsilon} + \dot{\Omega}$ (see (10.22)), we can easily transfer (10.55) into the form of (10.36) which involves the Jaumann rate. Hence, we can find a relationship between the constitutive tensor D_{tTK} and D_{tJK}. This issue will be discussed further in Section 12.4.

In order to find equivalent relationships to (10.55) for the Cauchy stresses, it is necessary to differentiate $\tau = J\boldsymbol{\sigma}$ with $J = \det(\mathbf{F})$. This leads to

$$\dot{\tau} = J\dot{\boldsymbol{\sigma}} + \dot{J}\boldsymbol{\sigma} = J(\dot{\boldsymbol{\sigma}} + \mathrm{tr}(\dot{\varepsilon})\boldsymbol{\sigma}) \tag{10.57}$$

[†]Truesdell rate, $\dot{\tau}_{\mathrm{T}} = \mathbf{F}\dot{\mathbf{S}}\mathbf{F}^{\mathrm{T}}$ can also be considered as the Lie derivative of the Kirchhoff strees [M1]. With such a notation, the Kirchhoff strees, τ would firstly be 'pulled back' from the 'spatial' to the 'material configuration' to give $\mathbf{S} = \mathbf{F}^{-1}\tau\mathbf{F}^{-\mathrm{T}}$ and then differentiated (to obtain $\dot{\mathbf{S}}$) before being 'pushed forward' to the real configuration.

In deriving the final relationship in (10.57), we used the expression

$$\dot{J} = J \operatorname{tr}(\dot{\boldsymbol{\varepsilon}}) \tag{10.58}$$

This relationship can be obtained by writing $J = \det(\mathbf{F})$ in terms of principal stretches (see Sections 4.8 and 10.1) so that, with $\mathbf{F} = \mathbf{RU}$ and $\mathbf{R}$ being an orthogonal rotation matrix, via (10.1a), we have:

$$J = \det(\mathbf{F}) = \det(\mathbf{RU}) = \det(\mathbf{U}) = \lambda_1\lambda_2\lambda_3 \tag{10.59}$$

so that

$$\dot{J} = \frac{\mathrm{d}}{\mathrm{d}t}(\det(\mathbf{F})) = \dot{\lambda}_1\lambda_2\lambda_3 + \dot{\lambda}_2\lambda_1\lambda_3 + \dot{\lambda}_3\lambda_1\lambda_2 = J\left(\frac{\dot{\lambda}_1}{\lambda_1} + \frac{\dot{\lambda}_2}{\lambda_2} + \frac{\dot{\lambda}_3}{\lambda_3}\right) = J \operatorname{tr}(\dot{\boldsymbol{\varepsilon}}) \tag{10.60}$$

The last relationship in (10.60) follows directly from equation (10.109) which will be derived in Section 10.6.5. For the present, we may simply note that, in the principal directions, the stretches are (see 4.131) $\lambda = l_n/l_o$ with l_n as the new length of an element and l_o the original length of an element. Hence:

$$\dot{\lambda} = \frac{\dot{l}_n}{l_o}; \qquad \dot{\varepsilon} = \frac{\dot{l}_n}{l_n} = \frac{\dot{\lambda}}{\lambda} \tag{10.61}$$

The relationship in (10.61) for the Eulerian strain rate corresponds with the relationship given in (3.14) for truss elements and discussed further in Sections 3.2.1 and 4.6.

Substituting from (10.57) into (10.55) gives

$$\dot{\boldsymbol{\sigma}} = \frac{1}{J}\dot{\boldsymbol{\tau}} - \boldsymbol{\sigma} \operatorname{tr}(\dot{\boldsymbol{\varepsilon}}) = \frac{1}{J}\mathbf{D}_{tTK}:\dot{\boldsymbol{\varepsilon}} + \mathbf{L}\boldsymbol{\sigma} + \boldsymbol{\sigma}\mathbf{L}^{\mathrm{T}} - \boldsymbol{\sigma} \operatorname{tr}(\dot{\boldsymbol{\varepsilon}}) \tag{10.62}$$

or:

$$\dot{\boldsymbol{\sigma}} = \dot{\boldsymbol{\sigma}}_{\mathrm{T}} + \mathbf{L}\boldsymbol{\sigma} + \boldsymbol{\sigma}\mathbf{L}^{\mathrm{T}} - \operatorname{tr}(\dot{\boldsymbol{\varepsilon}})\boldsymbol{\sigma} \tag{10.63}$$

with

$$\dot{\boldsymbol{\sigma}}_{\mathrm{T}} = \mathbf{D}_{tTC}:\dot{\boldsymbol{\varepsilon}} = \frac{1}{J}\dot{\boldsymbol{\tau}}_{\mathrm{T}} = \frac{1}{J}\mathbf{D}_{tTK}:\dot{\boldsymbol{\varepsilon}} \tag{10.64}$$

Again, it can be shown (see Section 10.8) that $\dot{\boldsymbol{\sigma}}_{\mathrm{T}}$ is objective in the sense of (10.30)-(10.32). This applies even if the Truesdell rate in (10.64) is related to $\dot{\boldsymbol{\varepsilon}}$ via a tangent constitutive tensor, $\mathbf{D}_{tTC}$, that does not follow that in (10.64) and (10.56); in other words, if a hypoelastic relationship is adopted. However (assuming an elastic material), unless the constitutive tensor is derived from some hyperelastic relationship, stresses may be generated as a result of a closed strain cycle [K1]. Also one may obtain bizarre oscillatory stresses when the strains are large (see Section 10.8).

There are a range of objective stress rates other than the Jaumann and Truesdell rates. Two such alternatives will be discussed in Section 10.8.

10.5 CONJUGATE STRESS AND STRAIN MEASURES WITH EMPHASIS ON ISOTROPIC CONDITIONS

In Section 10.1, we introduced a number of strain measures. The current section will lead to the definition of the equivalent work-conjugate stress measures. We will often simplify the analysis by considering isotropic conditions. The derivation of some of the

relationships can be found in Section 10.6 which is fairly complex and may be skipped at a first reading.

From the work of Sections 4.6 and 4.7, the power per unit initial volume can be expressed as

$$\mathbf{V} = J\boldsymbol{\sigma}:\dot{\boldsymbol{\varepsilon}} = \boldsymbol{\tau}:\dot{\boldsymbol{\varepsilon}} = \mathbf{S}:\dot{\mathbf{E}} = \mathbf{P}:\dot{\mathbf{F}} = \mathbf{B}:\dot{\boldsymbol{E}}_{\mathrm{b}} = \mathbf{O}:(\log_{\mathrm{e}}\dot{\mathbf{U}}) = \bar{\mathbf{S}}:\dot{\bar{\mathbf{A}}} \tag{10.65}$$

where the last three sets of stress measures, **B**, **O** and $\bar{\mathbf{S}}$, have not yet been defined. However, their corresponding strains are the Biot strain of (10.14), the log strain of (10.12) and the Almansi strain defined by Hill [H1] and discussed at the end of Section 10.1 (where it was referred to as **A(N)**). The latter is given by a combination of (10.2a) and (10.7) so that

$$\bar{\mathbf{A}} = \mathbf{Q}(\mathbf{N})\mathrm{Diag}\left(\frac{\lambda^2 - 1}{2\lambda^2}\right)\mathbf{Q}(\mathbf{N})^{\mathrm{T}} = \tfrac{1}{2}(\mathbf{I} - \mathbf{F}^{-1}\mathbf{F}^{-\mathrm{T}}) \tag{10.66}$$

(Note the more usual Almansi strain of (4.91) and (10.11), has **Q(n)**'s instead of **Q(N)**'s. i.e. (10.11) is related to the Eulerian triad while (10.66) is related to the Lagrangian triad—see also Section 4.7).

The fundamental measures can be considered as the Cauchy stress, $\boldsymbol{\sigma}$, and the velocity strain tensor, $\dot{\boldsymbol{\varepsilon}}$. However, because we are relating everything to the initial volume, we begin with the Kirchhoff stresses, $\boldsymbol{\tau}$ instead of the Cauchy stresses, $\boldsymbol{\sigma}$.

As a starting-point in the definition of a particular conjugate-stress measure it is necessary to find the relationship between the equivalent strain-rate terms in (10.65) and the velocity strain tensor, $\dot{\boldsymbol{\varepsilon}}$. This procedure was adopted in Section 4.6 in order to obtain the relationship between the second Piola–Kirchhoff stress, **S** and the Cauchy stress (see (4.105)). It will now be extended to the other strain measures in (10.65).

We will start with the Biot stress which is work conjugate to the Biot strain measure which was introduced in Section 10.1 (see 10.14) as

$$\boldsymbol{E}_{\mathrm{b}} = \mathbf{U} - \mathbf{I} \tag{10.67}$$

Clearly, in conjunctions with (10.65), the Biot stress, **B**, is defined by

$$V = \mathbf{B}:\dot{\boldsymbol{E}}_{\mathrm{b}} = \mathbf{B}:\dot{\mathbf{U}} = \boldsymbol{\tau}:\dot{\boldsymbol{\varepsilon}} \tag{10.68}$$

Hence we require a relationship between $\dot{\boldsymbol{\varepsilon}}$ and $\dot{\mathbf{U}}$. From (4.108), $\dot{\boldsymbol{\varepsilon}}$ is a function of **L** which in turn, from (4.109) is a function of $\dot{\mathbf{F}}$. Therefore, we start by differentiating the polar decomposition, $\mathbf{F} = \mathbf{RU}$ (see 4.126) to give

$$\dot{\mathbf{F}} = \mathbf{R}\dot{\mathbf{U}} + \dot{\mathbf{R}}\mathbf{U} \tag{10.69}$$

Hence, from (4.109) and (10.22),

$$\mathbf{L} = (\dot{\boldsymbol{\varepsilon}} + \dot{\boldsymbol{\Omega}}) = \frac{\partial \mathbf{v}}{\partial \mathbf{x}} = \frac{\partial \mathbf{v}}{\partial \mathbf{X}}\frac{\partial \mathbf{X}}{\partial \mathbf{x}} = \dot{\mathbf{F}}\mathbf{F}^{-1} = (\dot{\mathbf{R}}\mathbf{R}^{\mathrm{T}} + \mathbf{R}\dot{\mathbf{U}}\mathbf{U}^{-1}\mathbf{R}^{\mathrm{T}}) = (\mathbf{W} + \mathbf{R}\dot{\mathbf{U}}\mathbf{U}^{-1}\mathbf{R}^{\mathrm{T}}) \tag{10.70}$$

where $\mathbf{W} = \dot{\mathbf{R}}\mathbf{R}^{\mathrm{T}}$ is antisymmetric (see also Section 16.11 (and particularly equation (16.81c)) of Chapter 16 on large rotations). Substituting from (10.70) into (4.108) gives

$$\dot{\boldsymbol{\varepsilon}} = \frac{\mathbf{L} + \mathbf{L}^{\mathrm{T}}}{2} = \frac{\mathbf{R}}{2}(\dot{\mathbf{U}}\mathbf{U}^{-1} + \mathbf{U}^{-1}\dot{\mathbf{U}})\mathbf{R}^{\mathrm{T}} \tag{10.71}$$

Substitution into (10.68) gives

$$V = \boldsymbol{\tau}:\dot{\boldsymbol{\varepsilon}} = \boldsymbol{\tau}:\frac{\mathbf{R}}{2}(\dot{\mathbf{U}}\mathbf{U}^{-1} + \mathbf{U}^{-1}\dot{\mathbf{U}})\mathbf{R}^{\mathrm{T}} = \mathbf{R}^{\mathrm{T}}\boldsymbol{\tau}\mathbf{R}:\dot{\mathbf{U}}\mathbf{U}^{-1} = \mathbf{R}^{\mathrm{T}}\boldsymbol{\tau}\mathbf{R}\mathbf{U}^{-\mathrm{T}}:\dot{\mathbf{U}} = \mathbf{B}:\dot{\mathbf{U}} \quad (10.72)$$

Hence,

$$\mathbf{B} = \mathbf{R}^{\mathrm{T}}\boldsymbol{\tau}\mathbf{R}\mathbf{U}^{-\mathrm{T}} = \mathbf{R}^{\mathrm{T}}\boldsymbol{\tau}\mathbf{F}^{-\mathrm{T}} = \mathbf{R}^{\mathrm{T}}\mathbf{P} = \mathbf{R}^{\mathrm{T}}\mathbf{F}\mathbf{S} = \mathbf{U}\mathbf{S} \quad (10.73)$$

In general **B**, like **P** (see 4.119), is non-symmetric. However, for isotropic conditions, the principal directions of stress ad strain coincide (see Section 5.4.2). As a consequence both **E** (see (10.10)), **U** (see (10.1a)) and **S** can be written in the form:

$$\mathbf{X} = a_1\mathbf{N}_1\mathbf{N}_1^{\mathrm{T}} + a_2\mathbf{N}_2\mathbf{N}_2^{\mathrm{T}} + a_3\mathbf{N}_3\mathbf{N}_3^{\mathrm{T}} \quad (10.74)$$

with different values, in each case, for a_1–a_3. Hence, in these circumstances, **U** and **S** are coaxial and from the last term in (10.73), **B** is symmetric.

In relation to (10.74), the strains, **E**, $\boldsymbol{E}_{\mathrm{B}}$, $\log_{\mathrm{e}}\mathbf{U}$ and $\bar{\mathbf{A}}$ in (10.65) can all be written in the form:

$$\boldsymbol{E} = E_1\mathbf{N}_1\mathbf{N}_1^{\mathrm{T}} + E_2\mathbf{N}_2\mathbf{N}_2^{\mathrm{T}} + E_3\mathbf{N}_3\mathbf{N}_3^{\mathrm{T}} = f(\lambda_1)\mathbf{N}_1\mathbf{N}_1^{\mathrm{T}} + f(\lambda_2)\mathbf{N}_2\mathbf{N}_2^{\mathrm{T}} + f(\lambda_3)\mathbf{N}_3\mathbf{N}_3^{\mathrm{T}} \quad (10.75)$$

where (see Section 4.8) $\mathbf{N}_1$–$\mathbf{N}_3$ are the eigenvectors of **U**, E_1–E_3 are the principal strains and λ_1–λ_3 the principal stretches. From (10.5) to (10.8), $f(\lambda)$ in (10.75) are given by

$$f(\lambda) = \begin{cases} (\lambda^2 - 1)/2 & \text{Green strain } (\mathbf{E});\ \text{stress} = \mathbf{S} \quad \text{(a)} \\ (1 - \lambda^{-2})/2 & \text{Almansi's strain } (\bar{\mathbf{A}});\ \text{stress} = \bar{\mathbf{S}} \quad \text{(b)} \\ (\lambda - 1) & \text{Biot strain } (\boldsymbol{E}_{\mathrm{b}});\ \text{stress} = \mathbf{B} \quad \text{(c)} \\ \log_{\mathrm{e}}\lambda & \text{log strain } (\text{'}\log_{\mathrm{e}}\mathbf{U}\text{'});\ \text{stress} = \mathbf{O} \quad \text{(d)} \end{cases} \quad (10.76)$$

In order to derive appropriate conjugate stress measures to the strains in (10.75), we must find the relationship between a general strain rate $\dot{\boldsymbol{E}}$ and $\dot{\boldsymbol{\varepsilon}}$. This task will be tackled in Section 10.6. However, for the remainder of this section, we will concentrate on isotropic conditions. In these circumstances, because the principal directions of stress and strain coincide, corresponding to the strains of (10.75) and (10.76), we can write a general stress as

$$\boldsymbol{\kappa} = \kappa_1\mathbf{N}_1\mathbf{N}_1^{\mathrm{T}} + \kappa_2\mathbf{N}_2\mathbf{N}_2^{\mathrm{T}} + \kappa_3\mathbf{N}_3\mathbf{N}_3^{\mathrm{T}} = \mathbf{Q}(\mathbf{N})\mathbf{Diag}(\kappa_i)\mathbf{Q}(\mathbf{N})^{\mathrm{T}} \quad (10.77)$$

To obtain the relationship between the particular stress measures corresponding to the strain measures of (10.76), we merely need to ensure that

$$\kappa_i\delta E_i = \kappa_i\frac{\partial f(\lambda_i)}{\partial\lambda_i}\delta\lambda_i = \text{constant} \quad (10.78)$$

It follows from (10.76) and (10.78) that

$$S_i = \frac{1}{\lambda_i}B_i; \qquad O_i = \lambda_i B_i; \qquad \bar{S}_i = \lambda_i^3 B_i \quad (10.79)$$

Clearly, for small strains, when the strains are small so that $\lambda_i \simeq 1$, the stress measures **S**, **O** and **B** coincide.

Combining (10.79) and (10.77) and using (10.1a) for **U**, we can write

$$\mathbf{O} = \mathbf{Q}(\mathbf{N})\mathbf{Diag}(O_i)\mathbf{Q}(\mathbf{N})^{\mathrm{T}} = \mathbf{B}\mathbf{U} = \mathbf{Q}(\mathbf{N})\mathbf{Diag}(\lambda_i B_i)\mathbf{Q}(\mathbf{N})^{\mathrm{T}} \quad (10.80)$$

If we wish to find the Kirchhoff stress, which relates to the Eulerian triad, in terms of one of the stress measures of (10.77) relating to the Lagrangian triad, we can use $\boldsymbol{\tau} = \mathbf{F}\mathbf{S}\mathbf{F}^{\mathrm{T}}$. The latter must be combined with the polar decomposition $\mathbf{F} = \mathbf{R}\mathbf{U}$ (see (4.126)), $\mathbf{R} = \mathbf{Q}(\mathbf{n})\mathbf{Q}(\mathbf{N})^{\mathrm{T}}$ (see (4.147)) and (10.77) with S's instead of κ's and (10.1a) for $\mathbf{U}$. This leads to

$$\boldsymbol{\tau} = \mathbf{R}\mathbf{U}\mathbf{Q}(\mathbf{N})\mathbf{D}\mathrm{iag}(S_i)\mathbf{Q}(\mathbf{N})^{\mathrm{T}}\mathbf{U}\mathbf{R}^{\mathrm{T}} = \mathbf{Q}(\mathbf{n})\mathbf{D}\mathrm{iag}(\lambda_i^2 S_i)\mathbf{Q}(\mathbf{n})^{\mathrm{T}} = \mathbf{Q}(\mathbf{n})\mathbf{D}\mathrm{iag}(\tau_i)\mathbf{Q}(\mathbf{n})^{\mathrm{T}} \tag{10.81}$$

where τ_i are the principal Kirchhoff stresses. Combining (10.81) with (10.79), we can write

$$O_i = \tau_i = \lambda_i^2 S_i \tag{10.82}$$

where it must be emphasised that O_i and S_i relate to $\mathbf{Q}(\mathbf{N})$ while τ_i relates to $\mathbf{Q}(\mathbf{n})$. Using $\mathbf{R} = \mathbf{Q}(\mathbf{n})\mathbf{Q}(\mathbf{N})^{\mathrm{T}}$ (see (4.147)), we can write

$$\mathbf{O} = \mathbf{Q}(\mathbf{N})\mathbf{D}\mathrm{iag}(O_i)\mathbf{Q}(\mathbf{N})^{\mathrm{T}} = \mathbf{Q}(\mathbf{N})\mathbf{Q}(\mathbf{n})^{\mathrm{T}}\mathbf{Q}(\mathbf{n})\mathbf{D}\mathrm{iag}(\tau_i)\mathbf{Q}(\mathbf{n})^{\mathrm{T}}\mathbf{Q}(\mathbf{n})\mathbf{Q}(\mathbf{N})^{\mathrm{T}} = \mathbf{R}^{\mathrm{T}}\boldsymbol{\tau}\mathbf{R} \tag{10.83}$$

and hence, from (10.80):

$$\mathbf{B}\mathbf{U} = \mathbf{R}^{\mathrm{T}}\boldsymbol{\tau}\mathbf{R} \tag{10.84}$$

It will be shown in Sections 10.7 and 10.8 that, for isotropic conditions, we can add to the power expressions of (10.65), the relationships:

$$V = \boldsymbol{\tau} : (\log_{\mathrm{e}}\mathbf{V})^{\cdot} \tag{10.85a}$$

where $\log_{\mathrm{e}}\mathbf{V}$ was given in (10.13) and

$$V = \bar{\mathbf{B}} : \dot{\mathbf{V}} = \tfrac{1}{2}(\boldsymbol{\tau}\mathbf{V}^{-1} + \mathbf{V}^{-1}\boldsymbol{\tau}) : \dot{\mathbf{V}} = \mathbf{R}\mathbf{B}\mathbf{R}^{\mathrm{T}} : \dot{\mathbf{V}} \tag{10.85b}$$

where $\mathbf{B}$ is the Biot stress of (10.73) which is work conjugate to $\dot{\mathbf{U}}$.

For much of the future work in this book, the remaining sections of this chapter can be omitted, certainly at a first reading.

10.6 FURTHER WORK ON CONJUGATE STRESS AND STRAIN MEASURES

In this section, we will give a more detailed analysis of the relationship between the various stress and strain measures. The work will not be restricted to isotropic materials but will lead to proofs of some of the relationships given in the previous section for isotropic materials. It will also lead to some developments to follow in later chapters. The work is closely related to previous work by Hill [H1] and Atluri [A1]. As previously discussed, in Section 10.1, unless stated otherwise, it will be assumed that the principal stretches are distinct. The case with non-distinct stretches has been considered by Hoger [H2, H3] and Ogden [O1] and will also be discussed here in Section 13.8.

The aim of the present section will be to establish relationships between the stress measures (which are conjugate to the strains of (10.75) and (10.76)) and the Kirchhoff stress, $\boldsymbol{\tau}$ (and hence the Cauchy stress, $\boldsymbol{\sigma} = \boldsymbol{\tau}/J$). In order to establish these relationships, we will require the relationships between the rates of the strain measures in (10.75) and (10.76) and the velocity strain tensor, $\dot{\boldsymbol{\varepsilon}}$. This is easiest to achieve for the Biot strain $\boldsymbol{E}_{\mathrm{b}}$

which, from (10.15) is equal to $\mathbf{U}-\mathbf{I}$ so that $\dot{\boldsymbol{E}}_b=\dot{\mathbf{U}}$ and we only need to find the relationship between $\dot{\boldsymbol{\varepsilon}}$ and $\dot{\mathbf{U}}$. This exercise has already been completed in (10.71) but we will now work in principal directions in order to obtain an alternative expression.

As a starting-point, we follow Hill [H1] and introduce notations of the form:

$$\mathbf{T}_L=(\mathbf{T})_L=\mathbf{Q}(\mathbf{N})^T\mathbf{T}\mathbf{Q}(\mathbf{N}) \tag{10.86}$$

and

$$\mathbf{T}_E=(\mathbf{T})_E=\mathbf{Q}(\mathbf{n})^T\mathbf{T}\mathbf{Q}(\mathbf{n}) \tag{10.87}$$

where $\mathbf{T}$ is any tensor and the subscript L relates to the Lagrangian (material) triad and the subscript E to the Eulerian triad (see Section 4.8). Hence, $(\mathbf{T})_L$ is the tensor, $\mathbf{T}$, with components related to the Lagrangian frame while, $(\mathbf{T})_E$ is the same tensor related to the Eulerian frame (see Section 4.3.1 and (4.35) and (4.36)). We will then apply (10.65) in the form:

$$V=\boldsymbol{\tau}_E:\dot{\boldsymbol{\varepsilon}}_E=\boldsymbol{\kappa}_L:\dot{\boldsymbol{E}}_L \tag{10.88}$$

where $\dot{\boldsymbol{E}}$ are the rates of the strains $\boldsymbol{E}$ of (10.75) and (10.76) and $\boldsymbol{\kappa}$ are the corresponding stress measures. Only for isotropic materials can we assume that the latter take the form of (10.77).

10.6.1 Relationship between $\dot{\varepsilon}$ and $\dot{\mathbf{U}}$

Using (10.1a) and its inverse:

$$\mathbf{U}^{-1}=\mathbf{Q}(\mathbf{N})\mathbf{Diag}\left(\frac{1}{\lambda}\right)\mathbf{Q}(\mathbf{N})^T \tag{10.89}$$

with the aid of (10.86) and (10.87) and the relationship $\mathbf{R}=\mathbf{Q}(\mathbf{n})\mathbf{Q}(\mathbf{N})^T$ (see (4.147)), (10.71) can be re-expressed as

$$(\dot{\boldsymbol{\varepsilon}})_E=\tfrac{1}{2}(\dot{\mathbf{U}}\mathbf{U}^{-1}+\mathbf{U}^{-1}\dot{\mathbf{U}})_L=\tfrac{1}{2}(\dot{\mathbf{U}}_L\mathbf{Diag}(\lambda^{-1})+\mathbf{Diag}(\lambda^{-1})\dot{\mathbf{U}}_L) \tag{10.90}$$

In the two-dimensional case, (10.90) can be expanded as

$$\begin{aligned}(\dot{\boldsymbol{\varepsilon}})_E&=\frac{1}{2}\begin{bmatrix}\dot{U}_{11} & \dot{U}_{12}\\ \dot{U}_{21} & \dot{U}_{22}\end{bmatrix}_L\begin{bmatrix}1/\lambda_1 & 0\\ 0 & 1/\lambda_2\end{bmatrix}+\frac{1}{2}\begin{bmatrix}1/\lambda_1 & 0\\ 0 & 1/\lambda_2\end{bmatrix}\begin{bmatrix}\dot{U}_{11} & \dot{U}_{12}\\ \dot{U}_{21} & \dot{U}_{22}\end{bmatrix}_L\\ &=\begin{bmatrix}\dot{U}_{11L}/\lambda_1 & \dfrac{(\lambda_1+\lambda_2)}{2\lambda_1\lambda_2}\dot{U}_{12L}\\ \dfrac{(\lambda_1+\lambda_2)}{2\lambda_1\lambda_2}\dot{U}_{21L} & \dot{U}_{12L}/\lambda_2\end{bmatrix}\end{aligned} \tag{10.91}$$

Equation (10.91) can be generalised to three-dimensional case as

$$(\dot{\varepsilon}_{rs})_E=\frac{\lambda_r+\lambda_s}{2\lambda_r\lambda_s}(\dot{U}_{rs})_L \tag{10.92}$$

10.6.2 Relationship between the Biot stress, B and the Kirchhoff stress, τ

For the Biot stress and strain, (10.88) becomes

$$V = \tau_E : \dot{\varepsilon}_E = \mathbf{B}_L : (\dot{E}_b)_L = \mathbf{B}_L : \dot{\mathbf{U}}_L \tag{10.93}$$

Combining (10.92) and (10.93) leads to

$$(\tau_{rs})_E = \begin{cases} \lambda_r (B_{rr})_L & (r = s) \text{ (a)} \\ \dfrac{2\lambda_s \lambda_r}{\lambda_r + \lambda_s} (B_{rs})_L & (r \neq s) \text{ (b)} \end{cases} \tag{10.94}$$

This equation is equivalent to (10.73). For isotropic materials, (10.77) applies and we can write

$$\mathbf{B} = \mathbf{Q}(\mathbf{N}) \mathbf{Diag}(B_i) \mathbf{Q}(\mathbf{N})^T \tag{10.95}$$

so that, from (10.86),

$$\mathbf{B}_L = \mathbf{Diag}(B_i) \tag{10.96}$$

and hence with $r \neq s$, $(B_{rs})_L = 0$ and, from (10.94), we have

$$\tau_E = \mathbf{Diag}(\lambda_i B_i) = \mathbf{Q}(\mathbf{N})^T \mathbf{B} \mathbf{U} \mathbf{Q}(\mathbf{N}) \tag{10.97}$$

where for the last relationship in (10.97) we have used (10.1a) and (10.95). Using (10.87) for τ_E and the relationship $\mathbf{R} = \mathbf{Q}(\mathbf{n})\mathbf{Q}(\mathbf{N})^T$ (see (4.147)), it follows that

$$\mathbf{B}\mathbf{U} = \mathbf{R}^T \tau \mathbf{R} \tag{10.98}$$

This relationship was previously established in (10.84).

10.6.3 Relationship between $\dot{\mathbf{U}}$, the $\dot{\lambda}$'s and the spin of the Lagrangian triad, $\mathbf{W}_N$

To establish the relationship between τ and the other stress measures conjugate to the strain, E of (10.75) and (10.76), we require firstly the relationship between the strain rates, $\dot{E}$ and $\dot{\varepsilon}$. By studying (10.75), we can see that, as a first step, we will require the relationship between $\dot{E}$ and the principal stretch rates, $\dot{\lambda}$. We will find that we also involve the spin of the Lagrangian triad which we will write as $\mathbf{W}_N$ (in contrast to $\mathbf{W} = \dot{\mathbf{R}}\mathbf{R}^T$ of (10.70) which defines the spin of the Eulerian triad relative to the Lagrangian triad). In the next section (Section 10.6.4), we will obtain the equivalent relationships for $\dot{E}$ and finally, in Section 10.6.5, we derive the relationships between $\dot{E}$ and $\dot{\varepsilon}$.

As a starting-point, equation (10.1a) can be differentiated to give

$$\dot{\mathbf{U}} = \dot{\mathbf{Q}} \mathbf{Diag}(\lambda) \mathbf{Q}^T + \mathbf{Q} \mathbf{Diag}(\lambda) \dot{\mathbf{Q}}^T + \mathbf{Q} \mathbf{Diag}(\dot{\lambda}) \mathbf{Q}^T \tag{10.99}$$

where we have written $\mathbf{Q}$ as short for $\mathbf{Q}(\mathbf{N})$. Combining (10.99) with (10.86),

$$(\dot{\mathbf{U}})_L = \mathbf{Diag}(\dot{\lambda}) + \mathbf{Q}^T \dot{\mathbf{Q}} \mathbf{Diag}(\lambda) + \mathbf{Diag}(\lambda) \dot{\mathbf{Q}}^T \mathbf{Q} \tag{10.100}$$

Now, just as the matrix $\mathbf{W} = \dot{\mathbf{R}}\mathbf{R}^{\mathrm{T}}$ in (10.70) is antisymmetric, so is the matrix:

$$\mathbf{W}_{\mathrm{N}} = \dot{\mathbf{Q}}(\mathbf{N})\mathbf{Q}(\mathbf{N})^{\mathrm{T}} \tag{10.101}$$

The latter is the spin of the Lagrangian triad and can itself be related to the Lagrangian triad to give

$$(\mathbf{W}_{\mathrm{N}})_{\mathrm{L}} = \mathbf{Q}^{\mathrm{T}}(\dot{\mathbf{Q}}\mathbf{Q}^{\mathrm{T}})\mathbf{Q} = \mathbf{Q}^{\mathrm{T}}\dot{\mathbf{Q}} \tag{10.102}$$

and hence, from (10.100),

$$(\dot{\mathbf{U}})_{\mathrm{L}} = \mathbf{Diag}(\dot{\lambda}) + (\mathbf{W}_{\mathrm{N}})_{\mathrm{L}}\mathbf{Diag}(\lambda) - \mathbf{Diag}(\lambda)(\mathbf{W}_{\mathrm{N}})_{\mathrm{L}} \tag{10.103}$$

Expanding the above for the two-dimensional case, gives

$$(\dot{\mathbf{U}})_{\mathrm{L}} = \begin{bmatrix} \dot{U}_{11} & \dot{U}_{12} \\ \dot{U}_{21} & \dot{U}_{22} \end{bmatrix}_{\mathrm{L}} = \begin{bmatrix} \dot{\lambda}_1 & 0 \\ 0 & \dot{\lambda}_2 \end{bmatrix} + \begin{bmatrix} 0 & w_{12}^{\mathrm{NL}} \\ w_{21}^{\mathrm{NL}} & 0 \end{bmatrix}\begin{bmatrix} \lambda_1 & 0 \\ 0 & \lambda_2 \end{bmatrix} - \begin{bmatrix} \lambda_1 & 0 \\ 0 & \lambda_2 \end{bmatrix}\begin{bmatrix} 0 & w_{12}^{\mathrm{NL}} \\ w_{21}^{\mathrm{NL}} & 0 \end{bmatrix} \tag{10.104}$$

where w_{12}^{NL} and w_{21}^{NL} are components from $(\mathbf{W}_{\mathrm{N}})_{\mathrm{L}}$. Because the latter is antisymmetric, $w_{21}^{\mathrm{NL}} = -w_{12}^{\mathrm{NL}}$. Equation (10.104) can be rewritten as

$$(\dot{\mathbf{U}})_{\mathrm{L}} = \begin{bmatrix} \dot{\lambda}_1 & (\lambda_2 - \lambda_1)w_{12}^{\mathrm{NL}} \\ (\lambda_1 - \lambda_2)w_{21}^{\mathrm{NL}} & \dot{\lambda}_2 \end{bmatrix} \tag{10.105}$$

Expanding the previous expression to three dimensions and introducing a suffix notation:

$$(\dot{U}_{rs})_{\mathrm{L}} = \begin{cases} \dot{\lambda}_r & (r = s) \\ (\lambda_s - \lambda_r)w_{rs}^{\mathrm{NL}} & (r \neq s) \end{cases} \tag{10.106}$$

10.6.4 Relationship between $\dot{E}$, the $\dot{\lambda}$'s and the spin, $\mathbf{W}_{\mathrm{N}}$

Equation (10.106) relates $(\dot{\mathbf{U}})_{\mathrm{L}}$ to λ and $\dot{\lambda}$. Because (10.75), for a general strain, $\boldsymbol{E}$, of the same form as $\mathbf{U}$ in (10.1a), we can derive a similar relationship to (10.105), for $(\dot{\boldsymbol{E}})_{\mathrm{L}}$. In particular, differentiation of (10.75) leads to

$$\dot{\boldsymbol{E}} = \dot{\mathbf{Q}}\mathbf{Diag}(f(\lambda))\mathbf{Q}^{\mathrm{T}} + \mathbf{Q}\mathbf{Diag}(f(\lambda))\dot{\mathbf{Q}}^{\mathrm{T}} + \mathbf{Q}\mathbf{Diag}(\dot{f}(\lambda))\mathbf{Q}^{\mathrm{T}} \tag{10.107}$$

and eventually, in place of (10.106) we obtain:

$$(\dot{E}_{rs})_{\mathrm{L}} = \begin{cases} \dfrac{\partial f(\lambda_r)}{\partial \lambda_r}\dot{\lambda}_r & (r = s) \\ (f(\lambda_s) - f(\lambda_r))w_{rs}^{\mathrm{NL}} & (r \neq s) \end{cases} \tag{10.108}$$

We can make (10.108) specific to the particular strain measures of (10.75) and (10.76) by adopting (10.76) for the specific $f(\lambda)$'s. This exercise will be undertaken in Section 10.6.6.1. For the present, we note that with $f(\lambda) = \lambda - 1$, and with $\dot{\mathbf{U}} = \dot{\boldsymbol{E}}$, we recover (10.106).

It remains to relate the $\dot{\lambda}$'s and spin components, w_{rs}^{NL} to $\dot{\boldsymbol{\varepsilon}}$.

10.6.5 Relationship between $\dot{\varepsilon}$, the $\dot{\lambda}$'s and the spin, $\mathbf{W}_N$

Equation (10.92) relates $\dot{\boldsymbol{\varepsilon}}_E$ to $\dot{\mathbf{U}}_L$ while (10.106) relates $\dot{\mathbf{U}}_L$ to the $\dot{\lambda}$'s and the spin $(\mathbf{W}_N)_L$. From these two equations, for $r = s$, it follows that

$$(\dot{\varepsilon}_{rr})_E = \dot{\lambda}_r/\lambda_r; \qquad r = s \tag{10.109}$$

which shows that the diagonal components of the velocity strain tensor, $\dot{\boldsymbol{\varepsilon}}$, when related to the Eulerian triad are equal to the rates of the logarithms of the principal stretches. Provided $\lambda_s \neq \lambda_r$, we can use (10.106) to obtain the components of the spin $(\mathbf{W}_N)_L$ in terms of the stretches and components of $\dot{\mathbf{U}}_L$ while, from (10.92), we can further relate the latter to the components of $\dot{\boldsymbol{\varepsilon}}_E$ so that

$$w_{rs}^{NL} = \frac{1}{(\lambda_s - \lambda_r)}(\dot{U}_{rs})_L = \frac{2\lambda_r\lambda_s}{\lambda_s^2 - \lambda_r^2}(\varepsilon_{rs})_E; \qquad r \neq s \tag{10.110}$$

10.6.6 Relationship between $\dot{E}$ and $\dot{\varepsilon}$

We can now substitute from (10.109) and (10.110) into (10.108) to obtain:

$$(\dot{E}_{rs})_L = \begin{cases} \lambda_r \dfrac{\partial f(\lambda_r)}{\partial \lambda_r}(\dot{\varepsilon}_{rr})_E & (r = s) \\ \dfrac{2\lambda_r\lambda_s}{\lambda_r^2 - \lambda_s^2}(f(\lambda_r) - f(\lambda_s))(\dot{\varepsilon}_{rs})_E & (r \neq s) \end{cases} \tag{10.111}$$

10.6.6.1 Specific strain measures

Substitution from (10.76) into (10.111) leads to

$$(\dot{E}_{rs}(\text{Green}))_L = (\dot{E}_{rs})_L = \lambda_r\lambda_s(\dot{\varepsilon}_{rs})_E \tag{10.112a}$$

$$(\dot{E}_{rs}(\text{Almansi}))_L = (\dot{\bar{A}}_{rs})_L = (\dot{\varepsilon}_{rs})_E/\lambda_r\lambda_s \tag{10.112b}$$

$$(\dot{E}_{rs}(\log))_L = ((\log_e U)^{\cdot}_{rs})_L$$

$$= \begin{cases} (\dot{\varepsilon}_{rs})_E & (r = s) \quad (a) \\ \dfrac{2\lambda_r\lambda_s}{\lambda_r^2 - \lambda_s^2}\log_e\left(\dfrac{\lambda_r}{\lambda_s}\right)(\dot{\varepsilon}_{rs})_E = g(\lambda)(\dot{\varepsilon}_{rs})_E & (r \neq s) \quad (b) \end{cases} \tag{10.112c}$$

as well as

$$(\dot{E}_{rs}(\text{Biot}))_L = \begin{cases} \lambda_r(\dot{\varepsilon}_{rr})_E & (r = s) \quad (a) \\ \dfrac{2\lambda_s\lambda_r}{\lambda_r + \lambda_s}(\dot{\varepsilon}_{rs})_E & (r \neq s) \quad (b) \end{cases} \tag{10.112d}$$

Equation (10.112c) applies only if $\lambda_r \neq \lambda_s$.

In conjuction with $\dot{\mathbf{U}} = \dot{\boldsymbol{E}}(\text{Biot})$, the last relationship coincides with (10.92). For the log strain, by using series expansions, it can be shown [H1] that $g(\lambda)$ from (10.112c) can

be expressed as

$$g(\lambda) = \frac{2\lambda_r\lambda_s}{\lambda_r^2 - \lambda_s^2}\log_e\left(\frac{\lambda_r}{\lambda_s}\right) = 1 - \frac{1}{6}\left(\frac{\lambda_r}{\lambda_s} - 1\right)^2 + \cdots \tag{10.113}$$

and hence, from (10.112c), if $\lambda_r \simeq \lambda_s$,

$$(\dot{E}_{rs}(\log))_L \simeq (\dot{e}_{rs})_E \tag{10.114}$$

Using $\mathbf{R} = \mathbf{Q}(\mathbf{n})\mathbf{Q}(\mathbf{N})^T$ (see (4.147)) in conjunction with (10.86) and (10.87), (10.114) can be re-expressed as

$$\dot{\boldsymbol{E}}(\log) = (\log_e \mathbf{U})^{\cdot} \simeq \mathbf{R}^T\dot{\boldsymbol{\varepsilon}}\mathbf{R} = \mathbf{R}^T\dot{\boldsymbol{\varepsilon}}\mathbf{R} + O(E^2) \tag{10.115}$$

and hence

$$\dot{\boldsymbol{\varepsilon}} \simeq \mathbf{R}(\log_e \mathbf{U})^{\cdot}\mathbf{R}^T \tag{10.116}$$

10.6.7 Conjugate stress measures

The conjugate stress measures can be obtained by applying (10.93) in conjunction with (10.111) or (10.112). Considering, first, the second Piola–Kirchhoff stresses and Green strains, from (10.93) and (10.112a),

$$(\tau_{rs})_E = \lambda_r\lambda_s(S_{rs})_L \tag{10.117}$$

which can be rewritten as:

$$(\boldsymbol{\tau})_E = \mathbf{D}\mathrm{iag}(\lambda)(\mathbf{S})_L\mathbf{D}\mathrm{iag}(\lambda) \tag{10.118}$$

Using (10.86) and (10.87), the latter becomes

$$\boldsymbol{\tau} = \mathbf{Q}(\mathbf{n})\mathbf{Q}(\mathbf{N})^T\mathbf{Q}(\mathbf{N})\mathbf{D}\mathrm{iag}(\lambda)\mathbf{Q}(\mathbf{N})^T\mathbf{S}\mathbf{Q}(\mathbf{N})\mathbf{D}\mathrm{iag}(\lambda)\mathbf{Q}(\mathbf{N})^T\mathbf{Q}(\mathbf{N})\mathbf{Q}(\mathbf{n})^T \tag{10.119}$$

With the aid of the polar decomposition $\mathbf{F} = \mathbf{RU}$ (see (4.126)), the relationship $\mathbf{R} = \mathbf{Q}(\mathbf{n})\mathbf{Q}(\mathbf{N})^T$ (see (4.147)), and the relationship in (10.1a) for the symmetric, $\mathbf{U}$, (10.119) gives the standard relationship $\boldsymbol{\tau} = \mathbf{FSF}^T$.

Considering, now, the Almansi strain, $\bar{\mathbf{A}}$ of (10.66) or (10.75) with (10.76b), from (10.93) and (10.112b),

$$(\tau_{rs})_E = \frac{1}{\lambda_r\lambda_s}(\bar{S}_{rs})_L \tag{10.120}$$

where $\bar{S}_{rs}$ are components of the stress tensor, $\bar{\mathbf{S}}$, that is conjugate to the Almansi strain $\bar{\mathbf{A}}$. Equation (10.120) can be developed to give

$$\boldsymbol{\tau} = \mathbf{F}^{-T}\bar{\mathbf{S}}\mathbf{F}^{-1} \tag{10.121}$$

The Biot stress, $\mathbf{B}$, has already been considered in Section 10.6.2. Equations (10.93) and (10.112d) can be used to re-establish (10.94) with subsequent developments leading to (10.95)–(10.98).

Considering the log strain of (10.12) or (10.75) with (10.76d), by combining (10.93) with (10.112c), the conjugate stress, $\mathbf{O}$, is found to be related to $\boldsymbol{\tau}$ by

$$(\tau_{rs})_E = \begin{cases} (O_{rs})_L & (r = s) \quad \text{(a)} \\ \dfrac{2\lambda_r\lambda_s}{\lambda_r^2 - \lambda_s^2}\log_e\left(\dfrac{\lambda_r}{\lambda_s}\right)(O_{rs})_L & (r \neq s) \quad \text{(b)} \end{cases} \tag{10.122}$$

Equations (10.122), which were derived by Hill [H1], apply only if none of the principal stretches coincide.

A good approximation to (10.122) can be obtained by combining (10.93) with (10.115) to give

$$\mathbf{O} \simeq \mathbf{R}^{\mathrm{T}}\boldsymbol{\tau}\mathbf{R} \tag{10.123}$$

Indeed, as established in (10.83), this relationship is exact for an isotropic response.

10.7 USING $\log_e$V WITH ISOTROPY

It can be shown [O1, H2, H3] that for a general material, there is no equivalent to (10.122) when we use $\log_e\mathbf{V}$ rather than $\log_e\mathbf{U}$. In other words we cannot find a stress measure that is work conjugate to $\log_e\mathbf{V}$. However, as indicated at the end of Section 10.5, for isotropic conditions we can write the power/unit initial volume as $V = \boldsymbol{\tau}:(\log_e\mathbf{V})^{\cdot}$. This follows if we can show that

$$V = \boldsymbol{\tau}:(\log_e\mathbf{V})^{\cdot} = \boldsymbol{\tau}:\dot{\boldsymbol{\varepsilon}} \tag{10.124}$$

In (10.69), was differentiated $\mathbf{F} = \mathbf{RU}$ to obtain the expression (10.71) for $\dot{\boldsymbol{\varepsilon}}$ which involves $\dot{\mathbf{U}}$ and $\mathbf{U}$. Instead we now differentiate $\mathbf{F} = \mathbf{VR}$ to obtain:

$$\mathbf{L} = \dot{\mathbf{F}}\mathbf{F}^{-1} = [\dot{\mathbf{V}}\mathbf{R} + \mathbf{V}\dot{\mathbf{R}}]\mathbf{R}^{\mathrm{T}}\mathbf{V}^{-1} = \dot{\mathbf{V}}\mathbf{V}^{-1} + \mathbf{V}\mathbf{W}\mathbf{V}^{-1} \tag{10.125}$$

where $\mathbf{W} = \dot{\mathbf{R}}\mathbf{R}^{\mathrm{T}}$ (see (10.170)). It follows that

$$\dot{\boldsymbol{\varepsilon}} = \frac{\mathbf{L} + \mathbf{L}^{\mathrm{T}}}{2} = \tfrac{1}{2}[\dot{\mathbf{V}}\mathbf{V}^{-1} + \mathbf{V}^{-1}\dot{\mathbf{V}} + \mathbf{V}\mathbf{W}\mathbf{V}^{-1} - \mathbf{V}^{-1}\mathbf{W}\mathbf{V}] \tag{10.126}$$

and hence:

$$\boldsymbol{\tau}:\dot{\boldsymbol{\varepsilon}} = \boldsymbol{\tau}:\tfrac{1}{2}[\dot{\mathbf{V}}\mathbf{V}^{-1} + \mathbf{V}^{-1}\dot{\mathbf{V}}] + [\mathbf{V}\boldsymbol{\tau}\mathbf{V}^{-1} - \mathbf{V}^{-1}\boldsymbol{\tau}\mathbf{V}]:\frac{\mathbf{W}}{2} \tag{10.127}$$

If the material is isotropic $\mathbf{V}$ (see (10.1b)), $\mathbf{V}^{-1}$ and $\boldsymbol{\tau}$ (see (10.81)) are coaxial and hence the second term in brackets in (10.127) vanishes and we are left with

$$\boldsymbol{\tau}:\dot{\boldsymbol{\varepsilon}} = \boldsymbol{\tau}:\tfrac{1}{2}[\dot{\mathbf{V}}\mathbf{V}^{-1} + \mathbf{V}^{-1}\dot{\mathbf{V}}] \tag{10.128}$$

To proceed further, we differentiate [10.1b] to obtain:

$$\dot{\mathbf{V}} = \mathbf{Q}(\mathbf{n})\mathbf{Diag}(\dot{\lambda}\Omega\mathbf{Q}(\mathbf{n})^{\mathrm{T}} + \dot{\mathbf{Q}}(\mathbf{n})\mathbf{Diag}(\lambda)\mathbf{Q}(\mathbf{n})^{\mathrm{T}} + \mathbf{Q}(\mathbf{n})\mathbf{Diag}(\lambda)\dot{\mathbf{Q}}(\mathbf{n})^{\mathrm{T}} \tag{10.129}$$

so that

$$\dot{\mathbf{V}}\mathbf{V}^{-1} = \mathbf{Q}(\mathbf{n})\mathbf{Diag}\left(\frac{\dot{\lambda}}{\lambda}\right)\mathbf{Q}(\mathbf{n})^{\mathrm{T}} + \dot{\mathbf{Q}}(\mathbf{n})\mathbf{Q}(\mathbf{n})^{\mathrm{T}} + \mathbf{Q}(\mathbf{n})\mathbf{Diag}(\lambda)\mathbf{Q}(\mathbf{n})^{\mathrm{T}}\mathbf{Q}(\mathbf{n})\dot{\mathbf{Q}}(\mathbf{n})^{\mathrm{T}}\mathbf{Q}(\mathbf{n})\mathbf{Diag}\left(\frac{1}{\lambda}\right)\mathbf{Q}(\mathbf{n})^{\mathrm{T}}$$

or

$$\dot{\mathbf{V}}\mathbf{V}^{-1} = Q(\mathbf{n})\mathbf{Diag}\left(\frac{\dot{\lambda}}{\lambda}\right)\mathbf{Q}(\mathbf{n})^{\mathrm{T}} + \mathbf{W}_n - \mathbf{V}\mathbf{W}_n\mathbf{V}^{-1} \tag{10.130}$$

where

$$\mathbf{W}_n = \dot{\mathbf{Q}}(\mathbf{n})\mathbf{Q}(\mathbf{n})^{\mathrm{T}} \tag{10.131}$$

is the antisymmetric spin of the Eulerian triad (see (10.101) for the spin of the Lagrangian triad).

Substituting from (10.130) and a similar expression for $\mathbf{V}^{-1}\dot{\mathbf{V}}$ into (10.128) gives

$$\boldsymbol{\tau}:\dot{\boldsymbol{\varepsilon}} = \boldsymbol{\tau}:\mathbf{Q}(\mathbf{n})\mathbf{Diag}\left(\frac{\dot{\lambda}}{\lambda}\right)\mathbf{Q}(\mathbf{n})^{\mathrm{T}} + [\mathbf{V}^{-1}\boldsymbol{\tau}\mathbf{V} - \mathbf{V}\boldsymbol{\tau}\mathbf{V}^{-1}]:\frac{\mathbf{W}_n}{2} \tag{10.132}$$

Once again, assuming isotropic conditions, the square-bracketed term vanishes and we are left with

$$\boldsymbol{\tau}:\dot{\boldsymbol{\varepsilon}} = \boldsymbol{\tau}:\mathbf{Q}(\mathbf{n})\mathbf{Diag}\left(\frac{\dot{\lambda}}{\lambda}\right)\mathbf{Q}(\mathbf{n})^{\mathrm{T}} \tag{10.133}$$

We will now apply a similar exercise with $V = \boldsymbol{\tau}:(\log_e \mathbf{V})^{\cdot}$ and differentiate (10.1b) to obtain

$$(\log_e \mathbf{V})^{\cdot} = \mathbf{Q}(\mathbf{n})\mathbf{Diag}\left(\frac{\dot{\lambda}}{\lambda}\right)\mathbf{Q}(\mathbf{n})^{\mathrm{T}} + \mathbf{W}_n\log_e \mathbf{V} - \log_e \mathbf{V}\mathbf{W}_n \tag{10.134}$$

so that

$$\boldsymbol{\tau}:(\log_e \mathbf{V})^{\cdot} = \boldsymbol{\tau}:\mathbf{Q}(\mathbf{n})\mathbf{Diag}\left(\frac{\dot{\lambda}}{\lambda}\right)\mathbf{Q}(\mathbf{n})^{\mathrm{T}} + [\boldsymbol{\tau}\log_e \mathbf{V} - \log_e \mathbf{V}\boldsymbol{\tau}]:\mathbf{W}_n \tag{10.135}$$

which again, for isotropic conditions degenerates to (10.133) and the relationship (10.124) is established. Hence, for isotropic conditions $\boldsymbol{\tau}$ is work-conjugate to the strain measure $\log_e \mathbf{V}$.

10.8 OTHER STRESS RATES AND OBJECTIVITY

In Section 10.4, we derived the Truesdell rate of Kirchhoff stress by differentiating $\boldsymbol{\tau} = \mathbf{FSF}^{\mathrm{T}}$. If we apply a similar procedure to $\boldsymbol{\tau} = \mathbf{R}O\mathbf{R}^{\mathrm{T}}$ as obtained from (10.83) (with $\mathbf{O}$ as the stress that is work-conjugate to $\log_e \mathbf{U}$), in place of (10.53), we obtain:

$$\dot{\boldsymbol{\tau}} = \mathbf{R}\dot{\mathbf{O}}\mathbf{R}^{\mathrm{T}} + \mathbf{W}\boldsymbol{\tau} + \boldsymbol{\tau}\mathbf{W}^{\mathrm{T}} = \dot{\boldsymbol{\tau}}_{\mathrm{GN}} + \mathbf{W}\boldsymbol{\tau} + \boldsymbol{\tau}\mathbf{W}^{\mathrm{T}} \tag{10.136}$$

where $\mathbf{W} = \dot{\mathbf{R}}\mathbf{R}^{\mathrm{T}}$. The use of $\dot{\boldsymbol{\tau}}_{\mathrm{GN}}$ was proposed by Dienes [D1]. It is often called the Green–Nagdhi [G1] rate of Kirchhoff stress. For a hyperelastic material it stems from the relationship for $\mathbf{O}$. However, when used with a hypoelastic material it provides another objective stress rate and it was in this context that its use was advocated by Dienes [D1]. He suggested its use in preference to the Jaumann rate because of the oscillatory stresses that resulted with the latter rate when analysing a body subject to shear (see Section 13.10.3). However, the oscillations were associated with large elastic strains, and for such large elastic strains it can be argued that one should use a hyperelastic constitutive relationship (Chapters 13 and 19).

In order to compare the Green–Naghdi rate with the Jaumann rate, we need to establish a relationship between $\mathbf{W} = \dot{\mathbf{R}}\mathbf{R}^{\mathrm{T}}$ and $\boldsymbol{\Omega} = \frac{1}{2}(\mathbf{L} - \mathbf{L}^{\mathrm{T}})$. To this end, from (10.70),

we can obtain:

$$\dot{\boldsymbol{\Omega}} = \frac{\mathbf{L} - \mathbf{L}^{\mathrm{T}}}{2} = \mathbf{W} + \frac{\mathbf{R}}{2}(\dot{\mathbf{U}}\mathbf{U}^{-1} - \mathbf{U}^{-1}\dot{\mathbf{U}})\mathbf{R}^{\mathrm{T}} \tag{10.137}$$

so that using (10.86) and (10.87) in conjunction with the relationship $\mathbf{R} = \mathbf{Q}(\mathbf{n})\mathbf{Q}(\mathbf{N})^{\mathrm{T}}$ we obtain:

$$[\dot{\boldsymbol{\Omega}} - \mathbf{W}]_{\mathrm{E}} = [\dot{\mathbf{U}}\mathbf{U}^{-1} - \mathbf{U}^{-1}\dot{\mathbf{U}}]_{\mathrm{L}} \tag{10.138}$$

and following a similar procedure to that adopted in Section 10.6.1, we arrive at the relationship:

$$(\omega_{rs} - w_{rs})_{\mathrm{E}} = \frac{\lambda_r - \lambda_s}{2\lambda_r\lambda_s}(\dot{U}_{rs})_{\mathrm{L}} \tag{10.139}$$

so that with the aid of (10.92), we have

$$(\omega_{rs} - w_{rs})_{\mathrm{E}} = \frac{\lambda_r - \lambda_s}{\lambda_r + \lambda_s}(\dot{\varepsilon}_{rs})_{\mathrm{E}} \tag{10.140}$$

Clearly, when the stretches are nearly of the same magnitude, $\omega_{rs} \simeq w_{rs}$ and there will be very little difference between the Green–Naghdi rate and the Jaumann rate. These issued have been explored in more detail by Peric [P1].

Among the Lagrangian strain measures discussed in Sections 10.1 and 10.5, was the Almansi strain, $\bar{\mathbf{A}}$ (in the form used by Hill [H1]) as defined in (10.66). If we defined the stress tensor that is work conjugate to $\bar{\mathbf{A}}$ as $\bar{\mathbf{S}}$ where (see (10.121)), $\boldsymbol{\tau} = \mathbf{F}^{-\mathrm{T}}\bar{\mathbf{S}}\mathbf{F}^{-1}$, differentiation (following a very similar procedure to that adopted in Section 10.4 for the Truesdell rate) would lead to the relationship:

$$\dot{\boldsymbol{\tau}} = \mathbf{F}^{-\mathrm{T}}\dot{\bar{\mathbf{S}}}\mathbf{F}^{-1} - \boldsymbol{\tau}\mathbf{L} - \mathbf{L}^{\mathrm{T}}\boldsymbol{\tau} = \dot{\boldsymbol{\tau}}_{\mathrm{O}} - \boldsymbol{\tau}\mathbf{L} - \mathbf{L}^{\mathrm{T}}\boldsymbol{\tau} \tag{10.141}$$

where $\dot{\boldsymbol{\tau}}_{\mathrm{O}}$ is sometimes known [P1] as the Oldroyd [O2] rate of Kirchhoff stress. It is also sometimes known as the Cotter–Rivlin rate or as the 'convected rate'. The stress rate that we have called the Truesdell rate, Lubliner [L4.14] also calls the 'Oldroyd rate' although, in relation to the rate of Cauchy stress, with the Oldroyd rate, Lubliner would omit the $\mathrm{tr}(\dot{\boldsymbol{\varepsilon}})$ that is included in (10.62).

We have derived all of the rates except the Jaumann rate by taking time derivatives of stresses that were defined in the Lagrangian frame. It was implied that these rates might then relate to a hyperlastic relationship. However, as pointed out in Section 10.4, even if these rates are used in conjunction with a hypoelastic relationship, they are still 'objective' (issues regarding the integration of the rates are discussed in Section 19.5). The issue of objectivity was discussed in Section 10.2 (see equations (10.30)–(10.33)), although the proof that the Jaumann rate was objective was not completed. We will complete it now.

As in Section 10.2, we will consider a rigid body rotation superimposed on top of the current state so that (repeating (10.30)):

$$\mathrm{d}\mathbf{x}' = \mathbf{R}\,\mathrm{d}\mathbf{x} \tag{10.142}$$

where, in the above and for the rest of this chapter, $\mathbf{R}$ is a general rotation matrix and is not the rotation matrix associated with a polar decomposition. From (10.142), it

follows that

$$\frac{\partial \mathbf{x}'}{\partial \mathbf{X}} = \mathbf{F}' = \mathbf{R}\frac{\partial \mathbf{x}}{\partial \mathbf{X}} = \mathbf{RF} \tag{10.143}$$

Time differentiation of (10.143) leads to the relationship:

$$\dot{\mathbf{F}} = \mathbf{R}\dot{\mathbf{F}} + \dot{\mathbf{R}}\mathbf{F} = \mathbf{R}\dot{\mathbf{F}} + \dot{\mathbf{R}}\mathbf{R}^{\mathrm{T}}\mathbf{RF} = \mathbf{R}\dot{\mathbf{F}} + \mathbf{WRF} \tag{10.144}$$

It follows that

$$\mathbf{L}' = \dot{\mathbf{F}}'\mathbf{F}'^{-1} = (\mathbf{R}\dot{\mathbf{F}} + \mathbf{WRF})\mathbf{F}^{-1}\mathbf{R}^{\mathrm{T}} = \mathbf{RLR}^{\mathrm{T}} + \mathbf{W} \tag{10.145}$$

and hence:

$$\dot{\boldsymbol{\varepsilon}}' = \frac{\mathbf{L}' + \mathbf{L}'^{\mathrm{T}}}{2} = \mathbf{R}\left(\frac{\mathbf{L} + \mathbf{L}^{\mathrm{T}}}{2}\right)\mathbf{R}^{\mathrm{T}} + \left(\frac{\mathbf{W} + \mathbf{W}^{\mathrm{T}}}{2}\right) = \mathbf{R}\dot{\boldsymbol{\varepsilon}}\mathbf{R}^{\mathrm{T}} \tag{10.146}$$

(so that $\dot{\boldsymbol{\varepsilon}}$ is objective) and

$$\dot{\boldsymbol{\Omega}}' = \frac{\mathbf{L}' - \mathbf{L}'^{\mathrm{T}}}{2} = \mathbf{R}\left(\frac{\mathbf{L} - \mathbf{L}^{\mathrm{T}}}{2}\right)\mathbf{R}^{\mathrm{T}} + \left(\frac{\mathbf{W} - \mathbf{W}^{\mathrm{T}}}{2}\right) = \mathbf{R}\dot{\boldsymbol{\Omega}}\mathbf{R}^{\mathrm{T}} + \mathbf{W} \tag{10.147}$$

(which is not objective). We now differentiate $\boldsymbol{\tau}' = \mathbf{R}\boldsymbol{\tau}\mathbf{R}^{\mathrm{T}}$ (where we are using the Kirchhoff stress although we could have used the Cauchy stress) to obtain

$$\dot{\boldsymbol{\tau}}' = \mathbf{R}\boldsymbol{\tau}\mathbf{R}^{\mathrm{T}} + \dot{\mathbf{R}}\boldsymbol{\tau}\mathbf{R}^{\mathrm{T}} + \mathbf{R}\boldsymbol{\tau}\dot{\mathbf{R}}^{\mathrm{T}} = \boldsymbol{\tau}' + \mathbf{W}\boldsymbol{\tau}' + \boldsymbol{\tau}'\mathbf{W}^{\mathrm{T}} \tag{10.148}$$

We are now in a position to express the Jaumann rate of Kirchhoff stress (see (10.36)) in the rotated configuration as

$$\dot{\boldsymbol{\tau}}'_{\mathrm{J}} = \dot{\boldsymbol{\tau}}' - \dot{\boldsymbol{\Omega}}'\boldsymbol{\tau}' + \boldsymbol{\tau}'\dot{\boldsymbol{\Omega}}' = \boldsymbol{\tau}' + \mathbf{W}\boldsymbol{\tau}' + \boldsymbol{\tau}'\mathbf{W}^{\mathrm{T}} - (\mathbf{R}\dot{\boldsymbol{\Omega}}\mathbf{R}^{\mathrm{T}} + \mathbf{W})\boldsymbol{\tau}' + \boldsymbol{\tau}'(\mathbf{R}\dot{\boldsymbol{\Omega}}\mathbf{R}^{\mathrm{T}} + \mathbf{W}) \tag{10.149}$$

so that in conjunction with the relationship, $\boldsymbol{\tau}' = \mathbf{R}\boldsymbol{\tau}\mathbf{R}^{\mathrm{T}}$, we can write

$$\dot{\boldsymbol{\tau}}'_{\mathrm{J}} = \mathbf{R}(\dot{\boldsymbol{\tau}} - \dot{\boldsymbol{\Omega}}\boldsymbol{\tau} + \boldsymbol{\tau}\dot{\boldsymbol{\Omega}})\mathbf{R}^{\mathrm{T}} = \mathbf{R}\dot{\boldsymbol{\tau}}_{\mathrm{J}}\mathbf{R}^{\mathrm{T}} \tag{10.150}$$

which demonstrates the objectivity of the Jaumann rate, $\dot{\boldsymbol{\tau}}_{\mathrm{J}}$. Very similar procedures can be used to demonstrate the objectivity of the other stress rates that have been discussed.

10.9 SPECIAL NOTATION

Scalars

$B_1 - B_3$ = principal values of $\mathbf{B}$
J = det($\mathbf{F}$)
$S_1 - S_3$ = principal values of $\mathbf{S}$
V = power/initial unit volume
$\tau_1 - \tau_3$ = principal values of $\boldsymbol{\tau}$
$\mathbf{E}_1 - \mathbf{E}_3$ = principal values of $\mathbf{E}$
$E_1 - E_3$ = principal values of $\boldsymbol{E}$
μ = shear modulus
ϕ = strain energy

λ = stretch
$\bar{\lambda}$ = Lamé constant

Vectors

$\mathbf{E}$ = Green strains
$\mathbf{n}$ = unit principal vector in current (Eulerian or spatial) configuration
$\mathbf{N}$ = unit principal vector in original (Lagrangian) configuration
$\mathbf{u}$ = displacements
$\mathbf{v}$ = velocities
$\mathbf{X}$ = position vector in original configuration
$\mathbf{x}$ = position vector in current configuration

Matrices or tensors

$\mathbf{1}$ = second-order unit tensor
$\mathbf{A}$ = Almansi strain (related to Eulerian triad)
$\bar{\mathbf{A}}$ = alternative Almansi strain related to Lagrangian triad
$\mathbf{b} = \mathbf{F}\mathbf{F}^{\mathrm{T}}$ = left Cauchy Green tensor
$\mathbf{B}$ = Biot stresses (conjugate to Biot strains, $\boldsymbol{E}_{\mathrm{b}}$)
$\bar{\mathbf{B}} = \mathbf{R}\mathbf{B}\mathbf{R}^{\mathrm{T}}$ (see 10.85b)
$\mathbf{C} = \mathbf{F}^{\mathrm{T}}\mathbf{F}$ = (right) Cauchy Green tensor
$\mathbf{D}$ = constitutive (stress–strain moduli) matrices or tensors
$\mathbf{E}$ = Green strains
$\boldsymbol{E}$ = General strain measure related to Lagrangian triad
$\boldsymbol{E}_{\mathrm{b}}$ = Biot strain (related to Lagrangian triad)
$\mathbf{F}$ = deformation gradient
$\mathbf{I}$ = identity matrix
$\mathbf{I}_4$ = fourth order unit tensor
$\mathbf{L}$ = velocity gradient, $\partial\mathbf{v}/\partial\mathbf{x}$
$\mathbf{O}$ = stress conjugate to '$\log_{\mathrm{e}}\mathbf{U}$'
$\mathbf{P}$ = first Piola–Kirchhoff stress (or 'nominal stress')
$\mathbf{Q}$ = orthogonal matrix containing principal directions ($\mathbf{N}$'s or $\mathbf{n}$'s)
$\mathbf{Q}(\mathbf{N})$ = contains the Lagrangian triad
$\mathbf{Q}(\mathbf{n})$ = contains the Eulerian or spatial triad
$\mathbf{R}$ = rotation matrix
$\mathbf{S}$ = second Piola–Kirchhoff stresses
$\bar{\mathbf{S}}$ = stresses conjugate to $\bar{\mathbf{A}}$
$\mathbf{U}$ = right-stretch
$\mathbf{V}$ = left-stretch
$\mathbf{W} = \dot{\mathbf{R}}\mathbf{R}^{\mathrm{T}}$ (antisymmetric) = spin of the Eulerian triad relative to the Lagrangian trial
$\mathbf{W}_n$ = (antisymmetric) spin of the Eulerian triad = $\dot{\mathbf{Q}}(\mathbf{n})\mathbf{Q}(\mathbf{n})^{\mathrm{T}}$
$\mathbf{W}_N$ = (antisymmetric) spin of the Lagrangian triad = $\dot{\mathbf{Q}}(\mathbf{N})\mathbf{Q}(\mathbf{N})^{\mathrm{T}}$
δ_{ij} = Kronecker delta ($= 1, i = j; \quad = 0, i \neq j$)

$\dot{\boldsymbol{\varepsilon}}$ = velocity strain tensor (also, loosely, $\delta\boldsymbol{\varepsilon}$) (note $\dot{\boldsymbol{\varepsilon}}$ is not the rate of $\boldsymbol{\varepsilon}$)
$\boldsymbol{\sigma}$ = Cauchy stress
$\boldsymbol{\kappa}$ = General stress conjugate to general strain, $\boldsymbol{E}$
$\boldsymbol{\tau}$ = Kirchhoff or nominal stress ($= J\boldsymbol{\sigma}$)
$\dot{\boldsymbol{\Omega}}$ = spin $= \frac{1}{2}(\mathbf{L} - \mathbf{L}^{\mathrm{T}})$ (also, loosely, $\delta\boldsymbol{\Omega}$) (note $\dot{\boldsymbol{\Omega}}$ is not the rate of $\boldsymbol{\Omega}$)

Subscripts

E = Eulerian, signifies a tensor rotated into the Eulerian triad (see (10.87))
GN = Green–Naghdi rate
J = Jaumann rate
L = Lagrangian, signifies a tensor rotated into the Lagrangian triad (see (10.86))
O = Oldroyd rate
T = Truesdell rate

Superscripts

$\cdot$ = time derivative

10.10 REFERENCES

[A1] Atluri, S. N., Alternate stress and conjugate strain measures and mixed variational formulations involving rigid rotations, for computational analysis of finitely deformed solids, with application to plates and shells—I, *Theory*, *Computers and Structures*, **18**, (1), 93–116 (1983).

[B1] Bathe, K.-J., *Finite Element Procedures*, Prentice-Hall, Englewood Cliffs, New Jersey (1996).

[D1] Dienes, J. K., On the analysis of rotation and stress rate in deforming bodies, *Acta Mechanica*, **32**, 217–232 (1979).

[G1] Green. A. E. & Nagdhi, P. M., A general theory of elastic-plastic continuum, *Arch. Rat. Mech. Anal.*, **18**, 251–281 (1965).

[H1] Hill, R., Aspects of invariance, *Advances in Applied Mechanics*, Vol. 18, Academic Press, New York, pp. 1–75 (1978).

[H2] Hoger, A., The stress conjugate to log strain, *Int. J. Solids & Struct* **23**, 1645–1656 (1987).

[H3] Hoger, A., The material time derivative of logarithmic strain, *Int. J. Solids & Struct.* **22**, (9), 1019–1032 (1986).

[K1] Kojic, M. & Bathe, K.-J., Studies of finite element procedures—stress solution of a closed elastic strain path with stretching and shearing using the updated Lagrangian Jaumann formulation, *Computers & Structs.*, **26**, 175–179 (1987).

[M1] Marsden, J. E. & Hughes, T. J. R., *Mathematical Foundations of Elasticity*, Prentice-Hall, Englewood Cliffs, New Jersey (1983).

[N1] Nemat-Nasser, S., On finite deformation elasto-plasticity, *Int. J. Solids & Structs.*, **18**, 857–872 (1982).

[O1] Ogden, R. W., *Non-linear Elastic Deformations*, Ellis Horwood, Chichester (1984).

[O2] Oldroyd, J. G., On the formulation of rheological equations of state, *Proc. Roy. Soc. London*, **A200**, 523–541 (1950).

[P1] Peric, D., On consistent stress rates in solid mechanics: Computational implications, *Int. J. for Num. Meth. in Engng.*, **33**, 799–817 (1992).
[T1] Truesdell, C., *Rational Thermodynamics*, Springer-Verlag, New York (1984).
[T2] Truesdell, C. & Toupin, R. A., The classical field theories, *Handbuch der Physik*, ed. S. Flugge, Vol. III/1, Springer-Verlag, Berlin (1960).
[T3] Truesdell, C. & Noll, W., The nonlinear field theories, *Handbuch der Physik*, ed. S. Flugge, Vol. III/3, Springer-Verlag, Berlin (1965).

11 Non-orthogonal coordinates and co- and contravariant tensor components

In all of the previous chapters we have, at the stress–strain level, worked in rectangular orthogonal coordinates. In Chapter 8, on shells, when we need to apply the plane stress hypothesis (Section 8.2.1), we set up a local (Gauss-point level) orthogonal system, before transforming the material properties to the global orthogonal system via (4.55). However, for most finite element work, the shape functions are written with respect to a set of non-orthogonal curvilinear coordinates and we use the inverse Jacobian, to transform differentials with respect to these coordinates to differentials with respect to the global cartesian system (see (5.7) or (5.8)).

An alternative is to work directly with stress and strain components related to the non-orthogonal curvilinear system which is used, in any case, for the shape functions. To do this we can use co- and contravariant components of the stresses and strains which relate to the non-orthogonal curvilinear coordinates. With a view to such analyses, we will initially describe non-orthogonal coordinates and the transformations that use these co-ordinates and will introduce concepts such as the 'reciprocal basis' and the 'metric'. We will also develop expressions for the Green strain and second Piola–Kirchhoff stresses in relation to such coordinates.

For a more thorough grounding, the reader should refer to [S1, Y1]. Before commencing, it should be emphasised that, while some of the later work in this book is based on the concepts developed in this chapter, this is not generally the case. Consequently, with a view to subsequent chapters, the present chapter can initially be skipped if the reader is not particularly interested in the topic.

11.1 NON-ORTHOGONAL COORDINATES

Figures 11.1 and 11.2 introduce four sets of coordinates and three sets of base vectors. In Figure 11.1, we can see two of the latter; the rectangular (global) base system with vectors $\mathbf{i}_1$–$\mathbf{i}_3$ and a non-orthogonal system with vectors $\mathbf{e}_1$–$\mathbf{e}_3$ that are tangential at

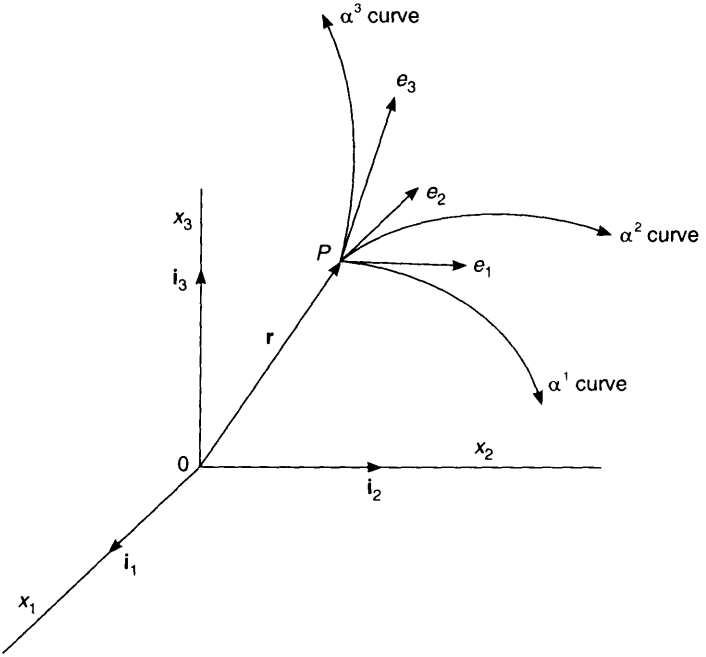

Figure 11.1 Local base vectors.

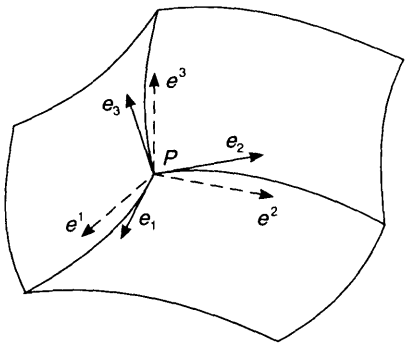

Figure 11.2 Local reciprocal basis.

point P to the curvilinear coordinates, α^i. These could be the standard finite element 'natural coordinates' so that

$$\alpha^1 = \xi; \qquad \alpha^2 = \eta; \qquad \alpha^3 = \zeta \tag{11.1}$$

(The reason for the use of superscripts rather than subscripts will be explained later.) To obtain the base vectors, $\mathbf{e}_1$–$\mathbf{e}_3$, we have

$$\mathbf{e}_i = \frac{\partial \mathbf{r}}{\partial \alpha^i}; \qquad i = 1, 3 \tag{11.2}$$

Given these (co-variant or natural) base vectors (which may not be of unit length), it is useful to obtain the 'reciprocal basis' composed of a set of (contravariant) vectors $\mathbf{e}^1$–$\mathbf{e}^3$ (Figure 11.2). These vectors are such that $\mathbf{e}^1$ is orthogonal to $\mathbf{e}_2$ and $\mathbf{e}_3$; $\mathbf{e}^2$ is orthogonal to $\mathbf{e}_3$ and $\mathbf{e}_1$; $\mathbf{e}^3$ is orthogonal to $\mathbf{e}_1$ and $\mathbf{e}_2$. In addition, we require that $\mathbf{e}^1$–$\mathbf{e}^3$ forms a right-handed system (as does $\mathbf{e}_1$–$\mathbf{e}_3$) and that $\mathbf{e}_1^{\mathrm{T}}\mathbf{e}^1 = \mathbf{e}_2^{\mathrm{T}}\mathbf{e}^2 = \mathbf{e}_3^{\mathrm{T}}\mathbf{e}^3 = 1$. Clearly, if the original system $\mathbf{e}_1$–$\mathbf{e}_3$ is orthonormal (orthogonal and with each vector of unit length), then the reciprocal basis $\mathbf{e}^1$–$\mathbf{e}^3$ will coincide with the original basis. The previous conditions can be expressed as

$$\mathbf{e}_i^{\mathrm{T}}\mathbf{e}^j = \mathbf{e}_i \cdot \mathbf{e}^j = \delta_i^j = 1 \qquad (i = j) = 0\ (i \neq j) \tag{11.3}$$

In equation (11.3) we have introduced the notation that will be used throughout this chapter whereby a dot is used for the 'dot product' rather than using the transpose symbol, 'T'. (This procedure is used to avoid cluttering, as we are now adopting superscripts as well as subscripts.) Using the cyclic (1, 2, 3) system, we can, from the above, obtain the vectors, $\mathbf{e}^i$ via

$$\mathbf{e}^i = \frac{\mathbf{e}_j \times \mathbf{e}_k}{v} \tag{11.4}$$

where v is the volume of the parallelepiped with edges along the base vectors $\mathbf{e}_i$. This positive scalar (with a right-handed system) is given by

$$v = \mathbf{e}_1 \cdot (\mathbf{e}_2 \times \mathbf{e}_3) = \mathbf{e}_2 \cdot (\mathbf{e}_3 \times \mathbf{e}_1) = \mathbf{e}_3 \cdot (\mathbf{e}_1 \times \mathbf{e}_2) \tag{11.5}$$

Any vector, can now be expressed either in terms of the (global) orthonormal base vectors $\mathbf{i}_1$–$\mathbf{i}_3$ or the base vectors $\mathbf{e}_1$–$\mathbf{e}_3$ or the reciprocal base vectors, $\mathbf{e}^1$–$\mathbf{e}^3$. In particular, we can write

$$\mathbf{x} = x^1\mathbf{e}_1 + x^2\mathbf{e}_2 + x^2\mathbf{e}_3 = x^i\mathbf{e}_i \tag{11.6a}$$

or as

$$\mathbf{x} = x_1\mathbf{e}^1 + x_2\mathbf{e}^2 + x_3\mathbf{e}^3 = x_i\mathbf{e}^i \tag{11.6b}$$

The components x^i in (11.6a) are known as the contravariant components of $\mathbf{x}$, while the components x_i in (11.6b) are known as the covariant components of $\mathbf{x}$. By multiplying (11.6a) by $\mathbf{e}^i$ and using (11.3), we can obtain the contravariant components of $\mathbf{x}$ as

$$x^i = \mathbf{x} \cdot \mathbf{e}^i \tag{11.7a}$$

while a similar multiplication of (11.6b) by $\mathbf{e}_i$ leads to

$$x_i = \mathbf{x} \cdot \mathbf{e}_i \tag{11.7b}$$

11.2 TRANSFORMING THE COMPONENTS OF A VECTOR (FIRST-ORDER TENSOR) TO A NEW SET OF BASE VECTORS

In Section 4.3.1, we considered the issue of transforming both vectors and tensors to a new set of orthonormal axes. In the present section, we will consider the similar

transformation for the components of a first-order tensor (or vector) using non-orthogonal bases. To this end, the vector $\mathbf{x}$ of (11.6a) and (11.6b) is re-expressed in relation to a new set of non-orthogonal basis vectors $\bar{\mathbf{e}}_1 - \bar{\mathbf{e}}_3$ and $\bar{\mathbf{e}}^1 - \bar{\mathbf{e}}^3$ so that

$$\mathbf{x} = \bar{x}^1\bar{\mathbf{e}}_1 + \bar{x}^2\bar{\mathbf{e}}_2 + \bar{x}^3\bar{\mathbf{e}}_3 = x^i\bar{\mathbf{e}}_1 \tag{11.8a}$$

$$\mathbf{x} = \bar{x}_1\bar{\mathbf{e}}^1 + \bar{x}_2\bar{\mathbf{e}}^2 + \bar{x}_3\bar{\mathbf{e}}^3 = x_i\bar{\mathbf{e}}^l \tag{11.8b}$$

Consequently, referring to this new system, in place of (11.7), we have:

$$\bar{x}^i = x \cdot \bar{\mathbf{e}}^i \tag{11.9a}$$

$$\bar{x}_i = x \cdot \bar{\mathbf{e}}_1 \tag{11.9b}$$

Substitution from (11.6a) into (11.9a) gives

$$\bar{x}^l = (x^j\mathbf{e}_j) \cdot \bar{\mathbf{e}}^i = (\bar{\mathbf{e}}^l \cdot \mathbf{e}_j)x^j = (\bar{\mathbf{e}}^l \cdot \mathbf{e}_1)x^l + (\bar{\mathbf{e}}^i \cdot \mathbf{e}_2)x^2 + (\bar{\mathbf{e}}^i \cdot \mathbf{e}_3)x^3 \tag{11.10a}$$

while substitution from (11.6b) into (11.9a) gives

$$\bar{\mathbf{x}}^i = (\bar{\mathbf{e}}^i \cdot \mathbf{e}^j)x_j \tag{11.10b}$$

with substitution from (11.6a) into (11.9b) giving

$$\bar{x}_i = (\bar{\mathbf{e}}_i \cdot \mathbf{e}_j)x^j \tag{11.10c}$$

and substitution from (11.6b) into (11.9b) giving

$$\bar{x}_l = (\bar{\mathbf{e}}_l \cdot \mathbf{e}^j)x_j \tag{11.10d}$$

In terms of the components, we can adopt a matrix notation so that, for example from (11.10a), we have

$$[\bar{x}^i] = [\bar{\mathbf{e}}^i \cdot \mathbf{e}_j][x^j] \tag{11.11}$$

where the vector $\{\bar{x}^i\}$ is the vector containing the three contravariant components with respect to the barred base vectors, and the vector $\{x^j\}$ contains the three contravariant components with respect to the unbarred base vectors while the matrix $[\bar{\mathbf{e}}^l \cdot \mathbf{e}_j]$ contains, for example, the scalar $\bar{e}^1 \cdot \mathbf{e}_3$ in the position (1, 3).

If we consider orthonormal bases, there is no distinction between co- and contravariant components so that we can use subscripts throughout and (11.10a) would become

$$\bar{x}_i = \bar{\mathbf{e}}_l \cdot \mathbf{e}_j x_j; \qquad [\bar{x}_l] = [\bar{\mathbf{e}}_i \cdot \mathbf{e}_j][x_j] \tag{11.12}$$

In Section 4.3.1, equation (4.41) transformed an 'old' vector, $\mathbf{r}_o$ to a ' new' vector $\mathbf{r}_n$ using (see (4.41)):

$$\mathbf{r}_n = \mathbf{T}\mathbf{r}_o = \mathbf{T}_n\mathbf{T}_o^T\mathbf{r}_o \tag{11.13}$$

where, strictly, we were working with components so that, in relation to the new terminology:

$$\mathbf{r}_o = \{\mathbf{x}_i\}; \qquad \mathbf{r}_n = \{\bar{x}_i\} \tag{11.14}$$

following for this switch of notation, (11.13) (or (4.41)) with (4.49) coincides with (11.12).

11.3 SECOND-ORDER TENSORS IN NON-ORTHOGONAL COORDINATES

In (11.6a) we expressed a vector (or first-order tensor) in terms of its contravariant components using the covariant, non-orthogonal base vectors, $\mathbf{e}_1$–$\mathbf{e}_3$ while in (11.6b) we used the covariant components and the reciprocal, contravariant, base vectors $\mathbf{e}^1$–$\mathbf{e}^2$. The same procedure will now be applied to a second-order tensor, $\mathbf{A}$ (such as stress or strain). This process leads to

$$\mathbf{A} = A^{ij}\mathbf{e}_i\mathbf{e}_j = A^{11}\mathbf{e}_1\mathbf{e}_1 + A^{12}\mathbf{e}_1\mathbf{e}_2 + A^{13}\mathbf{e}_1\mathbf{e}_3 + A^{21}\mathbf{e}_2\mathbf{e}_1 + \cdots \tag{11.15a}$$

$$\mathbf{A} = A_{ij}\mathbf{e}^i\mathbf{e}^j = A_{11}\mathbf{e}^1\mathbf{e}^1 + A_{12}\mathbf{e}^1\mathbf{e}^2 + A_{13}\mathbf{e}^1\mathbf{e}^3 + A_{12}\mathbf{e}^2\mathbf{e}^1 + \cdots \tag{11.15b}$$

(Note that $\mathbf{A} \neq [A_{ij}]$ and that, in this chapter, we are changing our normal notation whereby the matrix $\mathbf{ab}^{\mathrm{T}}$ or $\mathbf{a} \otimes \mathbf{b}$ is the outer product of the vectors $\mathbf{a}$ and $\mathbf{b}$ so that, instead, the matrix is given by $\mathbf{ab}$).

Equation (11.15a) involves the nine contravariant components of $\mathbf{A}$, namely A^{ij} while equation (11.15b) involves the nine covariant components, namely A_{ij}. In order to obtain an expression for A^{ij}, we can multiply both sides of (11.15a) by $\mathbf{e}^j$ and use (11.3) so that

$$[\mathbf{A}:\mathbf{e}^j] = A^{1j}\mathbf{e}_1 + A^{2j}\mathbf{e}_2 + A^{3j}\mathbf{e}_3 = A^{ij}\mathbf{e}_i \tag{11.16}$$

This operation is followed by the premultiplication of both sides of (11.16) by $\mathbf{e}^{iT}$ to obtain:

$$A^{ij} = \mathbf{e}^{iT}(\mathbf{A}:\mathbf{e}^j) = \mathbf{e}^i \cdot (\mathbf{A}:\mathbf{e}^j) \tag{11.17a}$$

In a similar fashion we can obtain

$$A_{ij} = \mathbf{e}_i \cdot (\mathbf{A}:\mathbf{e}_j) \tag{11.17b}$$

11.4 TRANSFORMING THE COMPONENTS OF A SECOND-ORDER TENSOR TO A NEW SET OF BASE VECTORS

For a different set of base vectors, $\bar{\mathbf{e}}_1$–$\bar{\mathbf{e}}_3$ and $\bar{\mathbf{e}}^1$–$\bar{\mathbf{e}}^3$, (11.15a) and (11.15b) can be replaced with

$$\mathbf{A} = \bar{A}^{ij}\bar{\mathbf{e}}_i\bar{\mathbf{e}}_j \tag{11.18a}$$

$$\mathbf{A} = \bar{A}_{ij}\bar{\mathbf{e}}^i\bar{\mathbf{e}}^j \tag{11.18b}$$

while in place of (11.17a) and (11.17b), we have

$$\bar{A}^{ij} = \bar{\mathbf{e}}^i \cdot (\mathbf{A}:\bar{\mathbf{e}}^j) \tag{11.19a}$$

and

$$\bar{A}_{ij} = \bar{\mathbf{e}}_i \cdot (\mathbf{A}:\bar{\mathbf{e}}_j) \tag{11.19b}$$

Substituting from (11.15a) into (11.19a) gives

$$\bar{A}^{ij} = \bar{\mathbf{e}}^i \cdot (A^{ab}\mathbf{e}_a\mathbf{e}_b \cdot \bar{\mathbf{e}}^j) = (\bar{\mathbf{e}}^i \cdot \mathbf{e}_a)(\bar{\mathbf{e}}^j \cdot \mathbf{e}_b)A^{ab} \tag{11.20a}$$

or

$$\bar{A}^{ij} = (\bar{\mathbf{e}}^i \cdot \mathbf{e}_1)(\bar{\mathbf{e}}^j \cdot \mathbf{e}_1)A^{11} + (\bar{\mathbf{e}}^i \cdot \mathbf{e}_1)(\bar{\mathbf{e}}^j \cdot \mathbf{e}_2)A^{12} + (\bar{\mathbf{e}}^i \cdot \mathbf{e}_1)(\bar{\mathbf{e}}^j \cdot \mathbf{e}_3)A^{13} + (\bar{\mathbf{e}}^i \cdot \mathbf{e}_2)(\bar{\mathbf{e}}^j \cdot \mathbf{e}_1)A^{21} + \cdots \tag{11.20b}$$

In a similar fashion, by substituting from (11.15b) into (11.19b), we obtain:

$$\bar{A}_{ij} = (\bar{\mathbf{e}}_i \cdot \mathbf{e}^a)(\bar{\mathbf{e}}_\lambda \cdot \mathbf{e}^b)A_{ab} \tag{11.20c}$$

We could also substitute from (11.15a) into (11.19b) to get a similar relationship between a term $\bar{A}_{ij}$ and the nine components A^{ab} or from (11.15b) into (11.19a) to get a relationship between a term $\bar{A}^{ij}$ and the nine components A_{ab}.

A matrix expression that is equivalent to, say, (11.20c) can easily be obtained as

$$[\bar{A}] = [T][A][T]^{\mathrm{T}} \tag{11.21}$$

where $[\bar{A}]$ is a 3×3 matrix containing the nine components $\bar{A}_{ij}$ and $[A]$ an equivalent-matrix containing the nine components A_{ij} while the transformation matrix $[T]$ contains the nine components of $\bar{\mathbf{e}}_i \cdot \mathbf{e}^j$, i.e.

$$[\bar{A}] = [\bar{A}_{ij}]; \qquad [A] = [A_{ij}]; \qquad [T] = [\bar{\mathbf{e}}_i \cdot \mathbf{e}_j] \tag{11.22}$$

If we consider orthogonal axes so that subscripts can be used everywhere, equations (11.20a) and (11.20b) are equivalent to the transformations of (4.51) and (4.50) derived in Section 4.3.1. In addition, the matrix form in (11.21) and (11.22) is equivalent to the combination of (4.42) with (4.49).

11.5 THE METRIC TENSOR

Substituting from (11.7) into (11.6) gives:

$$\mathbf{x} = (\mathbf{x} \cdot \mathbf{e}_j)\mathbf{e}^j \tag{11.23a}$$

$$\mathbf{x} = (\mathbf{x} \cdot \mathbf{e}^j)\mathbf{e}_j \tag{11.23b}$$

If, in 11.23a), we set $x = \mathbf{e}_i$, we obtain

$$\mathbf{e}_i = (\mathbf{e}_i \cdot \mathbf{e}_j)\mathbf{e}^j = e_{ij}\mathbf{e}^j \tag{11.24a}$$

while if we set $\mathbf{x} = \mathbf{e}^i$ in (11.23b), we obtain

$$\mathbf{e}^i = (\mathbf{e}^i \cdot \mathbf{e}^j)\mathbf{e}_j = e^{ij}\mathbf{e}_j \tag{11.24b}$$

The nine scalar coefficients e_{ij} (often written with the letter g) are known as the covariant components of the metric tensor while the nine scalar coefficients e^{ij} are known as the contravariant components of the metric tensor. The former are given by

$$e_{ij} = \mathbf{e}_i \cdot \mathbf{e}_j \tag{11.25a}$$

while the latter are given by

$$e^{ij} = \mathbf{e}^i \cdot \mathbf{e}^j \tag{11.25b}$$

By taking the dot product of both sides of (11.24a) with $\mathbf{e}^k$ and making use o (11.3), it can be shown that

$$\mathbf{e}_i \cdot \mathbf{e}^k = \delta_i^k = e_{ij}\mathbf{e}^j \cdot \mathbf{e}^k = e_{ij}e^{jk} \tag{11.26}$$

Consequently the matrix $[e_{ij}]$ containing the nine components e_{ij} is the inverse of the matrix, $[e^{ij}]$ containing the nine components of e^{ij}, i.e.:

$$[e^{ij}] = [e_{ij}]^{-1} \tag{11.27}$$

Equations (11.24a) and (11.24b) allow the components of the metric tensor to be used to transform from the original basis, ($\mathbf{e}_1$–$\mathbf{e}_3$) to the reciprocal basis, ($\mathbf{e}^1$–$\mathbf{e}^3$). These components can also be used to transform between co- and contravariant components of a tensor (such as stress and strain). To this end, if we substitute from (11.24b) into (11.15b) and compare the result with (11.15a), we obtain

$$A^{ij} = e^{ik}e^{jl}A_{kl} \tag{11.28a}$$

A similar manipulation can be used to obtain

$$A_{ij} = e_{ik}e_{jl}A^{kl} \tag{11.28b}$$

11.6 WORK TERMS AND THE TRACE OPERATION

In all of the previous chapters, we have used work expressions in relation to an orthonormal cartesian system so that the work per unit volume is given by (see (4.76))

$$W = \boldsymbol{\sigma}:\delta\boldsymbol{\varepsilon} = \sigma_{ij}\delta\varepsilon_{ij} = \sigma_{11}\delta\varepsilon_{11} + \sigma_{22}\delta\varepsilon_{12} + \cdots \tag{11.29}$$

where $\boldsymbol{\sigma}$ are some stresses and $\delta\boldsymbol{\varepsilon}$ the equivalent work-conjugate strain changes. Equation (11.29) involves the tensors $\boldsymbol{\sigma}$ and $\delta\boldsymbol{\varepsilon}$. We will now generalise the operation in relation to general tensors $\mathbf{A}$ and $\mathbf{B}$ which may be related to non-orthogonal bases. We then have

$$W = \mathbf{A}:\mathbf{B} = \mathbf{B}:\mathbf{A} = \mathbf{A}^{\mathrm{T}}:\mathbf{B}^{\mathrm{T}} = A_{ij}B^{ij} = A^{ij}B_{ij} = \bar{A}^{ij}\bar{B}_{ij} \tag{11.30}$$

Clearly, with a rectangular, cartesian system, using subscripts throughout, (11.30) will be consistent with (11.29).

In order to demonstrate the validity of (11.30), it is useful to note that, while in cartesian coordinates, the identity matrix, $\mathbf{I}$, can be written as

$$\mathbf{I} = \mathbf{e}_i\mathbf{e}_i = \mathbf{e}_1\mathbf{e}_1 + \mathbf{e}_2\mathbf{e}_2 + \mathbf{e}_3\mathbf{e}_3 \tag{11.31}$$

with non-orthonormal bases, we have

$$\mathbf{I} = \mathbf{e}_i\mathbf{e}^i = \mathbf{e}^i\mathbf{e}_i \tag{11.32}$$

To show that $A_{ij}B^{ij} = A^{ij}B_{ij}$, we can use (11.3), (11.25), (11.28) and (11.32) so that

$$\begin{aligned} A_{ij}B^{ij} &= (\mathbf{e}_i\cdot\mathbf{e}_a)(\mathbf{e}_j\cdot\mathbf{e}_b)A^{ab}(\mathbf{e}^i\cdot\mathbf{e}^c)(\mathbf{e}^j\cdot\mathbf{e}^d)B_{cd} \\ &= (\mathbf{e}_a\cdot\mathbf{e}_i\mathbf{e}^i\mathbf{e}^c)(\mathbf{e}_b\cdot\mathbf{e}_j\mathbf{e}^j\mathbf{e}^d)A^{ab}B_{cd} \\ &= (\mathbf{e}_a\cdot\mathbf{e}^c)(\mathbf{e}_b\cdot\mathbf{e}^d)A^{ab}B_{cd} = A^{ab}B_{ab} = A^{ij}B_{ij} \end{aligned} \tag{11.33}$$

To show that any set of bases can be used and, for example, that $\bar{A}_{ij}\bar{B}^{ij} = A_{ij}B^{ij}$, we can use (11.3), (11.20) and (11.32) so that:

$$\begin{aligned} \bar{A}_{ij}\bar{B}^{ij} &= (\bar{\mathbf{e}}_i\cdot\mathbf{e}^a)(\bar{\mathbf{e}}_j\cdot\mathbf{e}^b)A^{ab}(\bar{\mathbf{e}}^i\cdot\mathbf{e}_c)(\bar{\mathbf{e}}^j\cdot\mathbf{e}_d)B_{cd} \\ &= (e^a\cdot\bar{\mathbf{e}}_i\mathbf{e}^i\mathbf{e}_c)(\mathbf{e}^b\cdot\mathbf{e}_j\bar{\mathbf{e}}^j\mathbf{e}_d)A^{ab}B_{cd} \\ &= (\mathbf{e}^a\cdot\mathbf{e}_c)(\mathbf{e}^b\cdot\mathbf{e}_d)A^{ab}B_{cd} = A^{ab}B_{ab} = A^{ij}B_{ij} = A_{ij}B^{ij} \end{aligned} \tag{11.34}$$

11.7 COVARIANT COMPONENTS, NATURAL COORDINATES AND THE JACOBIAN

In most finite element analyses, to obtain the strains, we initially use the shape function to express the displacements in terms of natural (curvilinear coordinates). We later use the Jacobian matrix to express the derivatives with respect to the natural coordinates in terms of derivatives with respect to the base orthonormal system. With a view to later work (Section 18.11) on 'enhanced' or 'assumed' strains, it turns out to be very useful to consider the strains in terms of these 'natural coordinates'.

In the following, to reduce the number of terms, we will often work in two dimensions, although the concepts are easily extended to three dimensions and indeed some of the equations will be given in the full three-dimensional form. Following on from (11.1), in two dimensions, the natural coordinates will be written as

$$\xi = \alpha^1; \quad \eta = \alpha^2 \tag{11.35}$$

The 'natural strains' can be considered as the covariant strain components, $\bar{\varepsilon}_{ij}$, where

$$\varepsilon = \bar{\varepsilon}_{ij}\mathbf{G}^i\mathbf{G}^j = \bar{\varepsilon}_{11}\mathbf{G}^1\mathbf{G}^1 + \bar{\varepsilon}_{12}\mathbf{G}^1\mathbf{G}^2 + \cdots \tag{11.36}$$

With $\mathbf{G}^1-\mathbf{G}^3$ as the contravariant base vectors (previously $\mathbf{e}^1-\mathbf{e}^3$) while the covariant base vectors are (see (11.12))

$$\mathbf{G}_i = \frac{\partial \mathbf{X}}{\partial \alpha^i} \tag{11.37}$$

(Capital $\mathbf{X}$ is being used because this will relate to the initial configuration, while in the next section we will also consider the current configuration for which a small x will be adopted). In a two-dimensional setting, the conventional Jacobian matrix is

$$\mathbf{J} = \begin{bmatrix} \dfrac{\partial X}{\partial \xi} & \dfrac{\partial Y}{\partial \xi} \\ \dfrac{\partial X}{\partial \eta} & \dfrac{\partial Y}{\partial \eta} \end{bmatrix} = \begin{bmatrix} \mathbf{G}_1^{\mathrm{T}} \rightarrow \\ \mathbf{G}_2^{\mathrm{T}} \rightarrow \end{bmatrix} = \begin{bmatrix} \mathbf{G}_1(1)\mathbf{G}_1(2) \\ \mathbf{G}_2(1)\mathbf{G}_2(2) \end{bmatrix} = [J_{rs}] = [\mathbf{G}_r \cdot \mathbf{i}^s] \tag{11.38}$$

where $\mathbf{i}^s = \mathbf{i}_s$ are the unit normal vectors defining the rectangular orthogonal base system. (Note: some authors define $\mathbf{J}$ as the transpose of the current $\mathbf{J}$.)

Rather than starting with the strains, we will firstly consider the displacement derivatives (see (4.72)) and will write:

$$D = \bar{D}_{rs}\mathbf{G}^r\mathbf{G}^s = \bar{D}_{rs}\,\mathbf{i}^r\mathbf{i}^s \tag{11.39}$$

where $\bar{D}_{rs}$ are the covariant components and $\hat{D}_{rs}$ are the conventional cartesian components. With the aid of (11.21) and (11.22), it follows that

$$[\bar{D}_{rs}] = [\mathbf{G}_r \cdot \mathbf{i}^s][\bar{D}_{rs}][\mathbf{G}_r \cdot \mathbf{i}^s]^{\mathrm{T}} \tag{11.40}$$

or, using (11.38),

$$\bar{\mathbf{D}} = \mathbf{J}\hat{\mathbf{D}}\mathbf{J}^{\mathrm{T}} \tag{11.41}$$

where $\bar{\mathbf{D}}$ is the matrix containing the covariant components $\bar{D}$ and $\hat{\mathbf{D}}$ is the matrix

containing the cartesian components $\bar{D}$. Using a vector notation, (11.41) can be re-expressed as

$$v(\bar{D}) = \begin{bmatrix} \bar{D}_{11} \\ \bar{D}_{12} \\ \bar{D}_{21} \\ \bar{D}_{22} \end{bmatrix} = \begin{bmatrix} J_{11}^2 & J_{11}J_{12} & J_{11}J_{12} & J_{12}^2 \\ J_{11}J_{21} & J_{11}J_{22} & J_{12}J_{21} & J_{12}J_{22} \\ J_{11}J_{21} & J_{12}J_{21} & J_{11}J_{22} & J_{12}J_{22} \\ J_{21}^2 & J_{22}J_{21} & J_{22}J_{21} & J_{22}^2 \end{bmatrix} \begin{bmatrix} \hat{D}_{11} \\ \hat{D}_{12} \\ \hat{D}_{21} \\ \hat{D}_{22} \end{bmatrix} = \mathbf{J}_4 v(\hat{\mathbf{D}}) \tag{11.42}$$

In relation to strains, the equivalent of (11.41) is

$$\bar{\varepsilon} = \mathbf{J}\hat{\varepsilon}\,\mathbf{J}^{\mathrm{T}} \tag{11.43}$$

while the equivalent of (11.42) is

$$v(\bar{\varepsilon}) = \begin{bmatrix} \bar{D}_{11} \\ \bar{D}_{22} \\ \bar{D}_{12} + \bar{D}_{21} \end{bmatrix} = \begin{bmatrix} J_{11}^2 & J_{12}^2 & J_{11}J_{12} \\ J_{12}^2 & J_{22}^2 & J_{22}J_{21} \\ 2J_{11}J_{21} & 2J_{12}J_{22} & J_{12}J_{21} + J_{11}J_{22} \end{bmatrix} \begin{bmatrix} \hat{D}_{11} \\ \hat{D}_{22} \\ \hat{D}_{12} + \hat{D}_{21} \end{bmatrix} = \mathbf{J}_3 v(\hat{\boldsymbol{\varepsilon}}) \tag{11.44}$$

In component from (see (11.20c)), (11.43) is written as

$$\bar{\varepsilon}_{cd} = (\mathbf{G}_c \cdot \mathbf{i}^k)(\mathbf{G}_d \cdot \mathbf{i}^l)\hat{\varepsilon}_{kl} \tag{11.45}$$

Using the previous, notation, we can write:

$$\hat{\mathbf{D}} = \begin{bmatrix} \dfrac{\partial u}{\partial X} & \dfrac{\partial u}{\partial Y} \\ \dfrac{\partial v}{\partial X} & \dfrac{\partial v}{\partial Y} \end{bmatrix} \tag{11.46}$$

and if we define

$$\mathbf{D}_\xi = \begin{bmatrix} \dfrac{\partial u}{\partial \xi} & \dfrac{\partial u}{\partial \eta} \\ \dfrac{\partial v}{\partial \xi} & \dfrac{\partial v}{\partial \eta} \end{bmatrix} = \begin{bmatrix} \dfrac{\partial \mathbf{d}}{\partial \xi} & \dfrac{\partial \mathbf{d}}{\partial \eta} \end{bmatrix} = \begin{bmatrix} \dfrac{\partial \mathbf{d}}{\partial \alpha^1} & \dfrac{\partial \mathbf{d}}{\partial \alpha^2} \end{bmatrix} \tag{11.47}$$

then the conventional procedure for obtaining the cartesian derivatives would involve

$$\hat{\mathbf{D}}^{\mathrm{T}} = \mathbf{J}^{-1}\mathbf{D}_\xi^{\mathrm{T}} \tag{11.48}$$

so that substitution into (11.41) gives the equivalent matrix of covariant components as

$$\bar{\mathbf{D}} = \mathbf{J}\mathbf{D}_\xi \tag{11.49}$$

Directly in terms of these components, (11.49) can be written as

$$\bar{D}_{ij} = \mathbf{G}_i \cdot \frac{\partial \mathbf{d}}{\partial \alpha^j} \tag{11.50}$$

It is worth noting that while the Jacobian matrix is given by (11.38), the inverse Jacobian can be written as

$$\mathbf{J}^{-1} = [\mathbf{G}^1\mathbf{G}^2] = \begin{bmatrix} \mathbf{G}^1(1)\,\mathbf{G}^2(1) \\ \mathbf{G}^1(2)\,\mathbf{G}^2(2) \end{bmatrix} = [J_{rs}^{-1}] = [\mathbf{i}_r \cdot G^s] \tag{11.51}$$

11.8 GREEN'S STRAIN AND THE DEFORMATION GRADIENT

We will adopt convected curvilinear coordinates (Figure 11.1) so that the equivalent point in the original and final configurations is still referred to by the same convected coordinates, α^i. For an element in the initial configuration, we then obtain

$$d\mathbf{X} = \frac{\partial \mathbf{X}}{\partial \alpha^i} d\alpha^i = G_i \, d\alpha^i \tag{11.52a}$$

where $\mathbf{G}_1 - \mathbf{G}_3$ are the covariant (or natural) base vectors (in Sections 11.1–11.6, the latter were written as $\mathbf{e}_1 - \mathbf{e}_3$). In the current configuration:

$$d\mathbf{x} = \frac{\partial \mathbf{x}}{\partial \alpha^i} d\alpha^i = \mathbf{g}_i \, d\alpha^i \tag{11.52b}$$

The conventional relationship $d\mathbf{x} = \mathbf{F} d\mathbf{X}$ is recovered from (11.52a) and (11.52b) with

$$\mathbf{F} = \mathbf{g}_i \mathbf{G}^I = \mathbf{g}_1 \mathbf{G}^1 + \mathbf{g}_2 \mathbf{G}^2 + \mathbf{g}_3 \mathbf{G}^3 \tag{11.53}$$

With the aid of (11.32), we can also write

$$\mathbf{F}^{\mathrm{T}} = \mathbf{G}^i \mathbf{g}_i; \qquad \mathbf{F}^{-\mathrm{t}} = \mathbf{G}_I \mathbf{g}^i : \mathbf{F}^{-\mathrm{T}} = \mathbf{g}^i \mathbf{G}_i \tag{11.54}$$

and

$$\mathbf{g}_I = \mathbf{F}\mathbf{G}_I; \quad \mathbf{G}^i = \mathbf{F}^{\mathrm{T}} \mathbf{g}^i; \qquad \mathbf{G}_I = \mathbf{F}^{-1} \mathbf{g}_i; \qquad \mathbf{g}^i = \mathbf{F}^{-\mathrm{T}} \mathbf{G}^I \tag{11.55}$$

Following the approach of Section 4.4 (but now in non-orthogonal coordinates), we can use (11.52) to write

$$\begin{aligned} E_{ij} \, d\alpha^i \, d\alpha^j &= \tfrac{1}{2}(d\mathbf{x} \cdot d\mathbf{x} - d\mathbf{X} \cdot d\mathbf{X}) = \tfrac{1}{2}[\mathbf{g}_I \mathbf{g}_j - \mathbf{G}_I \cdot \mathbf{G}_j] d\alpha^I d\alpha^j \\ &= \tfrac{1}{2}[g_{ij} - G_{ij}] d\alpha^I d\alpha^j \end{aligned} \tag{11.56}$$

where E_{ij} are the covariant components of the Green strain tensor, $\mathbf{E}$, with respect to the base-vectors $\mathbf{G}^1 - \mathbf{G}^3$. In addition:

$$\mathbf{E} = E_{ij} \mathbf{G}^i \mathbf{G}^j = E_{11} \mathbf{G}^1 \mathbf{G}^1 + E_{12} \mathbf{G}^1 \mathbf{G}^2 + \cdots = \tfrac{1}{2}[g_{ij} - G_{ij}] \mathbf{G}^i \mathbf{G}^j \tag{11.57a}$$

which could be obtained more directly from (4.74) (11.24a), (11.32) and (11.36) so that

$$\mathbf{E} = \tfrac{1}{2}[\mathbf{F}^{\mathrm{T}} \mathbf{F} - \mathbf{I}] = \tfrac{1}{2}[(\mathbf{G}^i \mathbf{g}_i) \cdot (\mathbf{g}_j \mathbf{G}^j) - \mathbf{G}_i \mathbf{G}^i] = \tfrac{1}{2}[g_{ij} - G_{ij}] \mathbf{G}^i \mathbf{G}^j \tag{11.57b}$$

11.8.1 Recovering the standard cartesian expressions

Before proceeding further, it is useful to show how a similar procedure to that of Section 11.8 may be used with the Cartesian base vectors to recover the standard expression for the Green strain:

$$\mathbf{E} = \tfrac{1}{2}(\mathbf{F}^{\mathrm{T}} \mathbf{F} - \mathbf{I}); \qquad E_{ij} = \frac{1}{2}\left(\frac{\partial \mathbf{x}_k}{\partial \mathbf{X}_i} \frac{\partial \mathbf{x}_k}{\partial \mathbf{X}_j} - \delta_{ij}\right) \tag{11.58}$$

to this end, we use the cartesian base vector $\mathbf{i}_1 - \mathbf{i}_3$ so that the initial vector to a point

P is

$$\mathbf{X} = X_i \mathbf{i}_i = X_2 \mathbf{i}_1 + X_2 \mathbf{i}_2 + X_3 \mathbf{i}_3 \tag{11.59}$$

Also, the coordinates α^I in (11.52a) would simply be X, so that:

$$\mathbf{G}_i = \frac{\partial \mathbf{X}}{\partial X_i} = \mathbf{i}_i \tag{11.60}$$

Still using the cartesian base vectors, the position vector of the final point P′, would be

$$\mathbf{x} = x_i \mathbf{i}_i = x_1 \mathbf{i}_1 + x_2 \mathbf{i}_2 + x_3 \mathbf{i}_3 \tag{11.61}$$

so that using (11.52b):

$$\mathbf{g}_i = \frac{\partial \mathbf{x}}{\partial X_i} = \frac{\partial x_1}{\partial X_i}\mathbf{i}_1 + \frac{\partial x_2}{\partial X_i}\mathbf{i}_2 + \frac{\partial x_3}{\partial X_i}\mathbf{i}_3 \tag{11.62}$$

and, using (11.25a) (but with g's instead of e's):

$$\begin{aligned} g_{ij} = \mathbf{g}_i \cdot \mathbf{g}_j &= \left(\frac{\partial x_1}{\partial X_i}\mathbf{i}_1 + \frac{\partial x_2}{\partial X_i}\mathbf{i}_2 + \frac{\partial x_3}{\partial X_i}\mathbf{i}_3\right) \cdot \left(\frac{\partial x_1}{\partial X_j}\mathbf{i}_1 + \frac{\partial x_2}{\partial X_j}\mathbf{i}_2 + \frac{\partial x_3}{\partial X_j}\mathbf{i}_3\right) \\ &= \frac{\partial x_1}{\partial X_I}\frac{\partial x_1}{\partial X_j} + \frac{\partial x_2}{\partial X_I}\frac{\partial x_2}{\partial X_j} + \frac{\partial x_3}{\partial X_i}\frac{\partial x_3}{\partial X_j} = \frac{\partial x_k}{\partial X_I}\frac{\partial x_k}{\partial X_j} \end{aligned} \tag{11.63}$$

while, using (11.25a) with G's instead of e's:

$$G_{ij} = \mathbf{G}_i \cdot \mathbf{G}_j = \mathbf{i}_i \cdot \mathbf{i}_j = \delta_{ij} \tag{11.64}$$

Hence, substituting from (11.63) and (11.64) into (11.56) gives as expression for E_{ij} that coincides with the component form in (11.58).

If, following the approach of Section 11.7, we use hats to represent the components with respect to the cartesian system and bars to represent the covariant components, we can use (11.21) and (11.22) (see also (11.43)) so that:

$$\bar{\mathbf{E}} = \mathbf{J}\hat{\mathbf{E}}\mathbf{J}^{\mathrm{T}} \tag{11.65}$$

or, in component form (see (11.20c)):

$$\bar{E}_{cd} = (G_c \cdot \mathbf{i}^k)(G_d \cdot \mathbf{i}^l)\hat{E}_{kl} \tag{11.66}$$

11.9 THE SECOND PIOLA-KIRCHHOFF STRESSES AND THE VARIATION OF THE GREEN'S STRAIN

The second Piola-Kirchhoff stresses are work-conjugate to the Green strain so that (see 4.118), with an orthonormal cartesian system, (11.29) would give:

$$W = \mathbf{S} : \delta\mathbf{E} = \hat{S}_{ij}\delta\hat{E}_{ij} \tag{11.67}$$

(As in Sections 11.7 and 11.8, the hats are introduced for components related to the cartesian base vectors). It has already been shown in Section 11.8 that it is convenient to work with the covariant components of the Green strain. In these circumstances, from (11.30), we should adopt the contravariant components of the second Piola-Kirchhoff

stress so that:

$$W = \mathbf{S}:\delta\mathbf{E} = \hat{S}_{ij}\delta\hat{E}_{ij} = \bar{S}^{ij}\delta\bar{E}_{ij} \tag{11.68}$$

where the bars indicate covariant components for strains (or strain variations) and contravariant components for stresses. Consequently to complement the Green strain in the form of (11.38), we require to express the second Piola–Kirchhoff stresses via:

$$\mathbf{S} = \bar{S}^{ij}\mathbf{G}_i\mathbf{G}_j = \bar{S}^{11}\mathbf{G}_1\mathbf{G}_1 + \bar{S}^{12}\mathbf{G}_1\mathbf{G}_2 + \cdots \tag{11.69}$$

To complete the work definition (see (11.68)), we require the variations of the Green strain, $\delta\mathbf{E}$. From (11.57), the variations of the covariant components are given by

$$\delta\bar{E}_{ij} = \tfrac{1}{2}\delta g_{ij} = \tfrac{1}{2}\delta(\mathbf{g}_i\cdot\mathbf{g}_j) = \tfrac{1}{2}(\mathbf{g}_i\cdot\delta\mathbf{g}_j + \delta\mathbf{g}_i\cdot\mathbf{g}_j) \tag{11.70}$$

Using (11.52b) for $\mathbf{g}_i$, we have:

$$\delta\mathbf{g}_j = \delta\left(\frac{\partial\mathbf{x}}{\partial\alpha^j}\right) = \frac{\partial\delta\mathbf{x}}{\partial\alpha^j} = \frac{\partial\delta\mathbf{d}}{\partial\alpha^j} \tag{11.71}$$

where $\delta\mathbf{d}$ are the changes in displacements (with $\mathbf{x} = \mathbf{X}$ (initial) + $\mathbf{d}$).

11.10 TRANSFORMING THE COMPONENTS OF THE CONSTITUTIVE TENSOR

Suppose we have a constitutive tensor, $\mathbf{C}$, related to the orthonormal, cartesian system (with base vectors $\mathbf{i}_1$–$\mathbf{i}_3$) so that:

$$\hat{S}_{ab} = \hat{C}_{abcd}\hat{E}_{cd} \tag{11.72}$$

(Similar developments can apply to the tangent form of (11.72) with $\delta\hat{S}_{ab}$ instead of $\hat{S}_{ab}$ and $\delta\hat{E}_{cd}$ instead of $\hat{E}_{cd}$.) The tensor, $\mathbf{S}$ can be expressed as

$$\mathbf{S} = \hat{S}_{ij}\mathbf{i}_i\mathbf{i}_j = \bar{S}^{ij}\mathbf{G}_i\mathbf{G}_j \tag{11.73}$$

while, for work conjugacy (i.e. with the work being expressed via (11.68)), the Green strain $\mathbf{E}$ should be expressed as

$$\mathbf{E} = \hat{E}_{ij}\mathbf{i}_i\mathbf{i}_j = \bar{E}_{ij}\mathbf{G}^i\mathbf{G}^j \tag{11.74}$$

We now wish to modify $\hat{C}_{abcd}$ so as to relate $\bar{S}^{ij}$ to $\bar{E}_{ij}$. To this end, we can use (11.20a) to provide:

$$\bar{S}^{ij} = (\mathbf{G}^i\cdot\mathbf{i}_a)(\mathbf{G}^j\cdot\mathbf{i}_b)\hat{S}_{ab} \tag{11.75}$$

where we have used the fact that in relation to the base vectors, $\mathbf{i}_1$–$\mathbf{i}_3$, there are no differences between co- and contravariant vectors or components so that subscripts can always be used. Applying a similar process to (11.20c) leads to

$$\hat{E}_{cd} = (\mathbf{i}_c\cdot\mathbf{G}^k)(\mathbf{i}_d\cdot\mathbf{G}^l)\bar{E}_{kl} \tag{11.76}$$

In matrix form, the latter involves:

$$\hat{\mathbf{E}} = \mathbf{J}^{-1}\bar{\mathbf{E}}\mathbf{J}^{-\mathrm{T}} \tag{11.77}$$

Substitution from (11.66) into (11.69) is followed by the substitution of (11.76) into the result and gives:

$$\bar{S}^{ij} = (\mathbf{G}^i \cdot \mathbf{i}_a)(\mathbf{G}^j \cdot \mathbf{i}_b)(\mathbf{G}^k \cdot \mathbf{i}_c)(\mathbf{G}^l \cdot \mathbf{i}_d)\hat{C}_{abcd}\bar{E}_{kl} = \bar{C}^{ijkl}\bar{E}_{kl} \tag{11.78}$$

where

$$\bar{C}^{ijkl} = (\mathbf{G}^i \cdot \mathbf{i}_a)(\mathbf{G}^j \cdot \mathbf{i}_b)(\mathbf{G}^k \cdot \mathbf{i}_c)(\mathbf{G}^l \cdot \mathbf{i}_d)\hat{C}_{abcd} \tag{11.79}$$

Suppose the system $\mathbf{G}_1$–$\mathbf{G}_3$ was, in fact orthonormal so that $\mathbf{G}_i = \mathbf{G}^i$, then equation (11.79) represents the transformation of the components of a constitutive tensor from one orthonormal system to another. Such transformations were considered in Section 4.3.1, where the components of the transformation matrix were written in (4.50) as

$$T_{ij} = (\mathbf{e}_{in} \cdot \mathbf{e}_{jo}) = (\mathbf{G}_i \cdot \mathbf{i}_j) \tag{11.80}$$

where the first relationship uses the notation of Section 4.3.1 and the last relationship uses the present notation. It follows that, in these circumstances, (11.57) coincides with (4.55).

In the special case of a linear isotropic material, in relation to the system $\mathbf{i}_1$–$\mathbf{i}_3$, we have (see (4.30))

$$\hat{C}_{abcd} = \lambda\delta_{ab}\delta_{cd} + \mu(\delta_{ac}\delta_{bd} + \delta_{ad}\delta_{bc}) \tag{11.81}$$

hence, in relation to co- and contra-variant components, we can, via (11.57), write:

$$\bar{C}^{ijkl} = \lambda(\mathbf{G}^i \cdot \mathbf{G}^j)(\mathbf{G}^k \cdot \mathbf{G}^l) + \mu((\mathbf{G}^i \cdot \mathbf{G}^k)(\mathbf{G}^j \cdot \mathbf{G}^l) + (\mathbf{G}^i \cdot \mathbf{G}^l)(\mathbf{G}^j \cdot \mathbf{G}^k)) \tag{11.82a}$$

or

$$\bar{C}^{ijkl} = \lambda(G^{ij})(G^{kl}) + \mu((G^{ik})(G^{jl}) + (G^{il})(G^{jk})) \tag{11.82b}$$

11.11 A SIMPLE TWO-DIMENSIONAL EXAMPLE INVOLVING SKEW COORDINATES

The objective of this example is to work through the various stress, strain and work expressions using both conventional orthogonal base vectors and non-orthogonal base vectors and to highlight the equivalence of the two systems. The objective is not to use the most efficient formulation.

The developments can be assumed to relate to a parallelogram element as shown in Figure 11.3. In relation to this figure, any point in the initial configuration can be represented using the orthogonal unit base vectors, $\mathbf{i}_1, \mathbf{i}_2$ via

$$\mathbf{X} = \begin{pmatrix} X \\ Y \end{pmatrix} = X\mathbf{i}_1 + Y\mathbf{i}_2 \tag{11.83}$$

Here X and Y can also be mapped using the standard isoparametric shape functions in terms of the non-dimensional coordinates, ξ and η which, in the present context, are special forms of 'convected curvilinear coordinates', α^i $(i = 1, 2)$. Hence, from (11.52a) and Figure 11.3, the covariant base vectors $\mathbf{G}_i$ can be found as

$$\mathbf{G}_1 = \frac{\partial \mathbf{X}}{\partial \alpha^1} = \frac{\partial \mathbf{X}}{\partial \xi} = \frac{\partial X}{\partial \xi}\mathbf{i}_1 + \frac{\partial Y}{\partial \xi}\mathbf{i}_2 = a\mathbf{i}_1 = a\begin{pmatrix} 1 \\ 0 \end{pmatrix} \tag{11.84a}$$

$$\mathbf{G}_2 = \frac{\partial \mathbf{X}}{\partial \alpha^2} = \frac{\partial \mathbf{X}}{\partial \eta} = \frac{\partial X}{\partial \eta}\mathbf{i}_1 + \frac{\partial Y}{\partial \eta}\mathbf{i}_2 = \begin{pmatrix} b\cos\theta \\ b\sin\theta \end{pmatrix} \tag{11.84b}$$

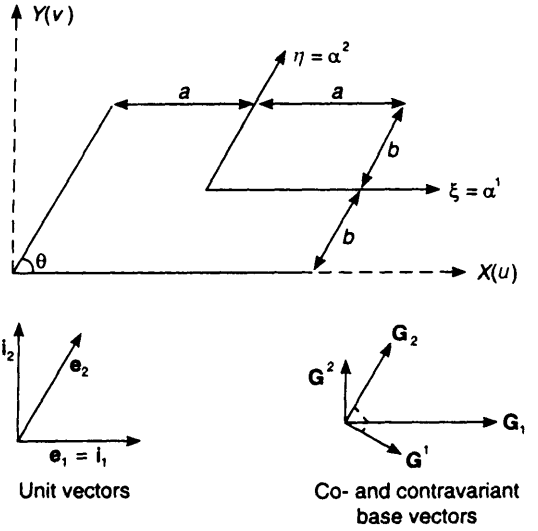

Figure 11.3 Skew coordinate system.

(If equations (11.84a) and (11.84b) cannot be accepted by inspection, one may simply obtain them by expressing the initial coordinates X and Y in terms of a, b and θ using the usual bilinear isoparametric shape functions.) Hence, from (11.25) (but with G's instead of e's):

$$G_{11} = \mathbf{G}_1 \cdot \mathbf{G}_1 = a^2, \qquad G_{22} = \mathbf{G}_2 \cdot \mathbf{G}_2 = b^2, \qquad G_{12} = \mathbf{G}_1 \cdot \mathbf{G}_2 = ab\cos\theta \tag{11.85}$$

so that the matrix containing the four covariant components of the metric tensor is

$$[G_{ij}] = \begin{bmatrix} a^2 & ab\cos\theta \\ ab\cos\theta & b^2 \end{bmatrix} \tag{11.86}$$

and the determinant is

$$\det[G_{ij}] = a^2 b^2 \sin^2\theta \tag{11.87}$$

Hence, using (11.27) (again with G's instead of e's):

$$[G^{ij}] = [G_{ij}]^{-1} = \frac{1}{a^2 b^2 \sin^2\theta}\begin{bmatrix} b^2 & -ab\cos\theta \\ -ab\cos\theta & a^2 \end{bmatrix} \tag{11.88}$$

so that, using (11.24b):

$$\mathbf{G}^1 = G^{11}\mathbf{G}_1 + \mathbf{G}^{12}\mathbf{G}_2 = \frac{1}{a}\begin{pmatrix} 1 \\ -\cot\theta \end{pmatrix} \tag{11.89a}$$

$$\mathbf{G}^2 = G^{21}\mathbf{G}_1 + \mathbf{G}^{22}\mathbf{G}_2 = \frac{1}{b\sin\theta}\begin{pmatrix} 0 \\ 1 \end{pmatrix} \tag{11.89b}$$

For the Green strains, we require the base vectors, $\mathbf{g}_i$, which are given by

$$\mathbf{g}_i = \frac{\partial \mathbf{x}}{\partial \alpha^i} = \frac{\partial(\mathbf{X} + \mathbf{d})}{\partial \alpha^i} = \mathbf{G}_i + \frac{\partial \mathbf{d}}{\partial \alpha^i} \tag{11.90}$$

where $\mathbf{d}$ are the displacements with $\mathbf{d}^{\mathrm{T}} = (u, v)^{\mathrm{T}}$. For the current example:

$$\mathbf{g}_1 = \mathbf{G}_1 + \begin{pmatrix} u_\xi \\ v_\xi \end{pmatrix} = \begin{pmatrix} a + u_\xi \\ v_\xi \end{pmatrix} \tag{11.91a}$$

$$\mathbf{g}_2 = \mathbf{G}_2 + \begin{pmatrix} u_\eta \\ v_\eta \end{pmatrix} = \begin{pmatrix} b\cos\theta + u_\eta \\ b\sin\theta + v_\eta \end{pmatrix} \tag{11.91b}$$

where $u_\xi = \partial u/\partial\xi$, etc. and, from (11.91) and (11.25a):

$$g_{11} = \mathbf{g}_1 \cdot \mathbf{g}_1 = (a + u_\xi)^2 + v_\xi^2 \tag{11.92a}$$

$$g_{22} = \mathbf{g}_2 \cdot \mathbf{g}_2 = (bc + u_\eta)^2 + (bs + v_\eta)^2 \tag{11.92b}$$

$$g_{12} = \mathbf{g}_1 \cdot \mathbf{g}_2 = (a + u_\xi)(bc + u_\eta) + v_\xi(bs + v_\eta) \tag{11.92c}$$

where we are adopting the shorthand,

$$s = \sin\theta, \quad c = \cos\theta \tag{11.93}$$

The covariant components of the Green strain, E_{ij}, can be found using (11.56), (11.88) and (11.92). Also, from (11.64), (11.65) and (11.91):

$$\delta E_{11} = \mathbf{g} \cdot \delta\mathbf{g}_1 = (a + u_\xi)\delta u_\xi + v_\xi \delta v_\xi \tag{11.94a}$$

$$\delta E_{22} = \mathbf{g}_2 \cdot \delta\mathbf{g}_2 = (bc + u_\eta)\delta u_\eta + (bs + v_\eta)\delta v_\eta \tag{11.94b}$$

$$\begin{aligned} 2\delta E_{12} = 2\delta E_{21} &= \mathbf{g}_1 \cdot \delta\mathbf{g}_2 + \mathbf{g}_2 \cdot \delta\mathbf{g}_1 \\ &= (a + u_\xi)\delta u_\eta + v_\xi \delta v_\eta + (bc + u_\eta)\delta u_\xi + (bs + v_\eta)\delta v_\xi \end{aligned} \tag{11.94c}$$

If we wish to relate the covariant strain components to a set of 'hatted' strains relating to a rectangular system, with base vectors, $\mathbf{i}_1, \mathbf{i}_2$ (see Figure 11.3), we note that from the first relationship in (11.68):

$$\mathbf{E} = \hat{E}_{11}\mathbf{i}_1\mathbf{i}_1 + \hat{E}_{12}\mathbf{i}_1\mathbf{i}_2 + \hat{E}_{21}\mathbf{i}_2\mathbf{i}_1 + \hat{E}_{22}\mathbf{e}_2\mathbf{e}_2 \tag{11.95}$$

while from the second relationship in (11.68):

$$\mathbf{E} = \bar{E}_{11}\mathbf{G}^1\mathbf{G}^1 + \bar{E}_{12}\mathbf{G}^1\mathbf{G}^2 + \bar{E}_{21}\mathbf{G}^2\mathbf{G}^1 + \bar{E}_{22}\mathbf{G}^2\mathbf{G}^2 \tag{11.96}$$

and using (11.70):

$$\begin{bmatrix} \hat{E}_{11} & \hat{E}_{12} \\ \hat{E}_{21} & \hat{E}_{22} \end{bmatrix} = \begin{bmatrix} \mathbf{i}_1 \cdot \mathbf{G}^1 & \mathbf{i}_1 \cdot \mathbf{G}^2 \\ \mathbf{i}_2 \cdot \mathbf{G}^1 & \mathbf{i}_2 \cdot \mathbf{G}^2 \end{bmatrix} \begin{bmatrix} \bar{E}_{11} & \bar{E}_{12} \\ \bar{E}_{21} & \bar{E}_{22} \end{bmatrix} \begin{bmatrix} \mathbf{i}_1 \cdot \mathbf{G}^1 & \mathbf{i}_2 \cdot \mathbf{G}^1 \\ \mathbf{i}_1 \cdot \mathbf{G}^2 & \mathbf{i}_2 \cdot \mathbf{G}^2 \end{bmatrix} \tag{11.97}$$

where we have used the matrix form of (11.21). From (11.84):

$$\mathbf{G}^1 \cdot \mathbf{i}_1 = \frac{1}{a}; \qquad \mathbf{G}^2 \cdot \mathbf{i}_2 = \frac{1}{b\sin\theta}; \qquad \mathbf{G}^1 \cdot \mathbf{i}_2 = \frac{-\cot\theta}{a}; \qquad \mathbf{G}^2 \cdot \mathbf{i}_1 = 0 \tag{11.98}$$

and hence, from (11.97):

$$\hat{E}_{11} = \frac{\bar{E}_{11}}{a^2} \tag{11.99a}$$

$$\hat{E}_{22} = \bar{E}_{11}\frac{\cot^2\theta}{a^2} - 2\bar{E}_{12}\frac{c}{abs^2} + \frac{\bar{E}_{22}}{b^2 s^2} \tag{11.99b}$$

$$\hat{E}_{12} = \hat{E}_{21} = -\hat{E}_{11}\frac{\cot\theta}{a^2} + \frac{\hat{E}_{12}}{abs} \tag{11.99c}$$

We could obtain these relationships using the Jacobian matrix by noting (see also (11.77)) that (11.97) can be written as $\hat{\mathbf{E}} = \mathbf{J}^{-1}\hat{\mathbf{F}}\mathbf{J}^{-\mathrm{T}}$ where

$$\mathbf{J} = \begin{bmatrix} \dfrac{\partial X}{\partial \xi} & \dfrac{\partial Y}{\partial \xi} \\ \dfrac{\partial X}{\partial \eta} & \dfrac{\partial Y}{\partial \eta} \end{bmatrix} = \begin{bmatrix} \mathbf{G}_1^{\mathrm{T}} \rightarrow \\ \mathbf{G}_2^{\mathrm{T}} \rightarrow \end{bmatrix} = \begin{bmatrix} a & 0 \\ bc & bs \end{bmatrix} \tag{11.100}$$

while the inverse Jacobian is

$$\mathbf{J}^{-1} = \frac{1}{abs}\begin{bmatrix} bs & 0 \\ -bc & a \end{bmatrix} \tag{11.101}$$

which could be obtained using the contravariant base vectors of (11.89) in conjunction with (11.51).

The previous relationships (11.99) also apply to the δE_{ij}'s so that, from (11.99) and (11.94):

$$\delta\hat{E}_{11} = \frac{1}{a^2}((a + u_\xi)\delta u_\xi + v_\xi \delta v_\xi) \tag{11.102a}$$

$$\begin{aligned}\delta\hat{E}_{22} = \frac{1}{a^2b^2s^2}&((b^2c^2u_\xi - abcu_\eta)\delta u_\varepsilon + (b^2c^2v_\xi - ab^2sc - absv_\eta)\delta v_\xi \\ &+ (-abcu_\xi + a^2u_\eta)\delta u_\eta + (a^2bs - abcv_\xi + a^2v_\eta)\delta v_\eta)\end{aligned} \tag{11.102b}$$

$$\begin{aligned}2\delta\hat{E}_{12} = \frac{1}{a^2bs}&(((-abc - 2bcu_\xi + au_\eta)\delta u_\xi + (abs - sbcu\xi + av_\eta)\delta v_\xi \\ &+ (a^2 + au_\xi)\delta u_\eta + av_\xi \delta v_\eta))\end{aligned} \tag{11.102c}$$

The latter strain variations can, of course, be obtained in a more conventional manner using (4.79) ($2\delta\mathbf{E} = \mathbf{F}^{\mathrm{T}}\delta\mathbf{D} + \delta\mathbf{D}\mathbf{F}^{\mathrm{T}}$) in conjunction with terms such as

$$\begin{bmatrix} \dfrac{\partial \delta u}{\partial X} \\ \dfrac{\partial \delta u}{\partial Y} \end{bmatrix} = \mathbf{J}^{-1}\begin{bmatrix} \dfrac{\partial \delta u}{\partial \xi} \\ \dfrac{\partial \delta u}{\partial \eta} \end{bmatrix} = \mathbf{J}^{-1}\begin{pmatrix} \delta u_\xi \\ \partial u_\eta \end{pmatrix}; \qquad \begin{bmatrix} \dfrac{\partial u}{\partial X} \\ \dfrac{\partial u}{\partial Y} \end{bmatrix} = \mathbf{J}^{-1}\begin{pmatrix} u_\xi \\ u_\eta \end{pmatrix} \tag{11.103}$$

or using (11.48):

$$\delta\hat{\mathbf{D}}^{\mathrm{T}} = \mathbf{J}^{-1}\delta\mathbf{D}_\xi^{\mathrm{T}} = \mathbf{J}^{-1}\begin{bmatrix} \delta u_\xi & \delta v_\xi \\ \delta u_\eta & \delta v_\eta \end{bmatrix}; \qquad \hat{\mathbf{D}} = \mathbf{J}^{-1}\mathbf{D}_\xi^{\mathrm{T}} \tag{11.104}$$

In conjunction with $\mathbf{F} = \mathbf{I} + \hat{\mathbf{D}}$ or with (11.53) whereby $\mathbf{F} = \mathbf{g}_1\mathbf{G}^1 + \mathbf{g}_2\mathbf{G}^2$. The reader can easily demonstrate that this route also leads to the strain variation terms in (11.102).

The stresses can be expressed via:

$$\mathbf{S} = \hat{S}_{11}\mathbf{i}_1\mathbf{i}_1 + \hat{S}_{12}\mathbf{i}_1\mathbf{i}_2 + \hat{S}_{21}\mathbf{i}_2\mathbf{i}_1 + \hat{S}_{22}\mathbf{i}_2\mathbf{i}_2 \tag{11.105}$$

or alternatively, from (11.69), we can write:

$$\mathbf{S} = \bar{S}^{11}\mathbf{G}_1\mathbf{G}_1 + \bar{S}^{12}\mathbf{G}_1\mathbf{G}_2 + \bar{S}^{21}\mathbf{G}_2\mathbf{G}_1 + \bar{S}^{22}\mathbf{G}_2\mathbf{G}_2 \tag{11.106}$$

so that, from (11.20a) or the matrix equivalent:

$$\begin{bmatrix} \hat{S}_{11} & \hat{S}_{12} \\ \hat{S}_{21} & \hat{S}_{22} \end{bmatrix} = \begin{bmatrix} \mathbf{i}_1\cdot\mathbf{G}_1 & \mathbf{i}_1\cdot\mathbf{G}_2 \\ \mathbf{i}_2\cdot\mathbf{G}_1 & \mathbf{i}_2\cdot\mathbf{G}_2 \end{bmatrix} \begin{bmatrix} \bar{S}^{11} & \bar{S}^{12} \\ \bar{S}^{21} & \bar{S}^{22} \end{bmatrix} \begin{bmatrix} \mathbf{i}_1\cdot\mathbf{G}_1 & \mathbf{i}_2\cdot\mathbf{G}_1 \\ \mathbf{i}_1\cdot\mathbf{G}_2 & \mathbf{i}_2\cdot\mathbf{G}_2 \end{bmatrix} \tag{11.107}$$

Hence, using (11.84):

$$\hat{S}_{11} = \bar{S}^{11}a^2 + 2\bar{S}^{12}abc + \bar{S}^{22}b^2c^2 \tag{11.108a}$$

$$\hat{S}_{22} = b^2s^2\bar{S}^{22} \tag{11.108b}$$

$$\hat{S}_{12} = \hat{S}_{21} = \bar{S}^{12}abs + \bar{S}^{22}b^2sc \tag{11.108c}$$

It is left to the reader to demonstrate that:

$$\begin{aligned} \mathbf{S}:\delta\mathbf{E} &= \hat{S}^{ij}\delta\hat{E}_{ij} = \hat{S}_{11}\delta\hat{E}_{11} + \hat{S}_{22}\delta\hat{E}_{22} + 2\hat{S}_{12}\delta\hat{E}_{12} \\ &= \bar{S}^{ij}\delta\bar{E}_{ij} = \bar{S}^{11}\delta\bar{E}_{11} + \bar{S}^{22}\delta\bar{E}_{22} + 2\bar{S}^{12}\delta\bar{E}_{12} \end{aligned} \tag{11.109}$$

11.12 SPECIAL NOTATION

Scalars and components of vectors and tensors

a, b = scalar dimensions (Figure 11.3)
A_{ij} = covariant components of **A** (also $\bar{A}_{ij}$'s of $\bar{\mathbf{A}}$)
A^{ij} = contravariant components of **A** (also $\bar{A}^{ij}$'s of $\bar{\mathbf{A}}$
$c = \cos\theta$ (Section 11.11)
$\hat{C}_{abcd}$ = components of fourth-order constitutive tensor, **C**, with respect to orthonormal base vectors, $\mathbf{i}_1$–$\mathbf{i}_3$
$\bar{C}^{ijkl}$ = contravariant components of fourth-order constitutive tensor, **C**
e_{ij} = covariant components of metric tensor
e^{ij} = contravariant components of metric tensor
E_{ij} (sometimes $\bar{E}_{ij}$) = covariant components of Green strain, **E**
$\hat{E}_{ij}$ = components of Green strain, **E**, with respect to orthonormal base vectors, $\mathbf{i}_1$–$\mathbf{i}_3$
g_{ij} = covariant components of metric tensor in final configuration (from Section 11.8 onwards)
G_{ij} = covariant components of metric tensor in initial configuration (from Section 11.7 onwards)
ξ, η = natural co-ordinates (Section 11.11)
$s = \sin\theta$ (Section 11.10)
S_{ij} (sometimes $\bar{S}_{ij}$) = covariant components of second Piola–Kirchhoff stress, **S**
$\hat{S}_{ij}$ = components of second Piola–Kirchhoff stress, **S** with respect to orthonormal base vectors, $\mathbf{i}_1$–$\mathbf{i}_3$
S^{ij} = contravariant components of second Piola–Kirchhoff stress, **S**
u, v = displacement components (Section 11.11)

u_ξ = differential of u with respect to ξ (similar for u_η) (Section 11.11)
v_ξ = differential of v with respect to ξ (similar for v_η) (Section 11.11)
v = volume of parallelepiped (Section 11.1)
x_i = covariant components of $\mathbf{x}$ (also $\bar{x}_i$'s of $\bar{\mathbf{x}}$)
x^i = contravariant components of $\mathbf{x}$ (also $\bar{x}^i$'s of $\mathbf{x}$)
μ = shear modulus
α^1–α^3 = convected curvilinear coordinates (natural coordinates)
ξ, η, ζ = natural coordinates
λ = Lamé constant
θ = angle (Figure 11.3)

Vectors

$\mathbf{d}$ = displacement vector
$\mathbf{e}_1$–$\mathbf{e}_3$ = covariant base vectors (also $\bar{\mathbf{e}}_i$'s)
$\mathbf{e}^1$–$\mathbf{e}^3$ = contravariant base vectors (also $\bar{\mathbf{e}}^i$'s)
$\mathbf{G}_1$–$\mathbf{G}_3$ = covariant base vectors of initial configuration
$\mathbf{g}_1$–$\mathbf{g}_3$ = covariant base vectors of final configuration
$\mathbf{i}_1$–$\mathbf{i}_3$ = orthonormal base vectors
$\mathbf{r}$ = position vector
$\mathbf{x}$ = position vector (from Section 11.7 in final configuration)
$\mathbf{X}$ = position vector in initial configuration

Matrices and tensors

$\mathbf{A}$ = second-order tensor (also $\bar{\mathbf{A}}$)
$\mathbf{C}$ = fourth-order constitutive tensor
$\mathbf{D}$ = displacement derivatives
$\hat{\mathbf{D}} = [\hat{D}_{ij}]$-matrix of displacement derivatives with respect to orthonormal cartesian base vectors
$\bar{\mathbf{D}} = [\bar{D}_{ij}]$-matrix of covariant components of the displacement derivatives.
$\mathbf{D}_\xi$ = matrix derivatives with respect to natural co-ordinates (see (11.47))
$[\mathbf{e}_{ij}]$ = matrix of covariant components of metric tensor
$[\mathbf{e}^{ij}]$ = matrix of contravariant components of metric tensor
$\mathbf{E}$ = Green strain
$\mathbf{F}$ = deformation gradient
$[G_{ij}]$ = matrix of covariant components of metric tensor in initial configuration
$[G^{ij}]$ = matrix of contravariant components of metric tensor in initial configuration
$\mathbf{I}$ = unit matrix (second-order tensor)
$\mathbf{J}$ = Jacobian matrix (see Section 11.7)

$\mathbf{S}$ = second Piola–Kirchhoff stresses
$\mathbf{T}$ = transformation matrix
δ_i^j = Kronector delta (see (11.3))
$\boldsymbol{\sigma}$ = general stress tensor
$\delta\boldsymbol{\varepsilon}$ = general strain variation tensor

11.13 REFERENCES

[S1] Sokolnikov, I. S., *Tensor Analysis*, Wiley, New York, London, Sydney (1964).
[Y1] Young, E. C., *Vector and Tensor Analysis*, Marcel Dekker, New York (1978).

12 More finite element analysis of continua

In this chapter, we will apply some of the theory of Chapters 10 and 11 to the finite element analysis of continua. The developments of Chapter 5 were all based on the Green strain and the second Piola–Kirchhoff stresses. To this end, they used the total Lagrangian system in which the stress and strain measures are related to the 'initial' configuration. An updated Lagrangian system was also discussed in which these measures were related to some (temporarily fixed) new updated 'initial' configuration (Sections 5.3 and 5.4).

An alternative that is often adopted in large-strain analysis is to relate all measures to the current configuration. A finite element formulation using this approach was initially given by McMeeking and Rice [M1] and used the Jaumann rate introduced in Section 10.2. McMeeking and Rice called this approach 'Eulerian' and used it for large-strain elasto-plastic analysis. The details of the elasto-plastic side of the analysis will be discussed in Chapter 19 (with the related topic of hyperelasticity being considered at an earlier stage in Chapter 13). For the present we will concentrate on the development of the finite element equations—in particular the internal force vector and the tangent stiffness matrix.

We will follow McMeeking and Rice in calling this formulation 'Eulerian', but will include the parentheses because the terminology has a debatable origin. Indeed the method is not Eulerian in the sense that the latter is often used in relation to computational fluid dynamics in which the material moves through a mesh. In the current 'Eulerian procedure' the progress of a specific material particle is traced and in that sense the method is Lagrangian. Indeed it could be termed as a form of updated Lagrangian technique whereby the reference configuration is the current configuration. However, in this book we will continue to consider the updated Lagrangian technique as being a total Lagrangian technique in which the reference configuration is periodically updated but is held fixed while the equilibrium iterations are performed (Sections 5.3 and 5.4). In contrast in our Eulerian formulation, the reference configuration is continuously changing and we must account for this change.

It will be shown in Chapter 13, that in conjunction with a hyperelastic material behaviour (Section 10.3 and Chapter 13), the Eulerian formulation can be exactly equivalent to one based on the Green strain and second Piola–Kirchhoff stresses using the total Lagrangian approach. In describing the tangent stiffness matrix for the Eulerian formulation, we will use various rate forms (particularly the Truesdell rate

(Section 10.4) and Jaumann rate (Section 10.2). It should again be emphasised that with a hyperelastic material it makes no difference which rate form is used.

The total Lagrangian formulations of Chapter 5, were all based on a rectangular cartesian coordinate system. In Section 12.6, we will reformulate some of these developments using the convected coordinates and co- and contravariant base vectors discussed in Chapter 11.

Because of the limited objectives within this chapter, there will be little discussion of other finite element work in the wide area of non-linear analysis of continua. Instead, such discussion will be postponed to the later related Chapter 13 (on hyperelasticity), Chapter 18 (on continua and shell elements) and Chapter 19 (on large-strain elasto-plastic analysis).

12.1 A SUMMARY OF THE KEY EQUATIONS FOR THE TOTAL LAGRANGIAN FORMULATION

Some of the equations for the Eulerian formulation take a very similar form to those derived in Chapter 5 for the total Lagrangian formulation. Consequently, we will start by summarising the latter. To save space, throughout this chapter, we will concentrate on the two-dimensional formulation. As shown in Section 5.1.3, for the total Lagrangian formulation, the three-dimensional procedure takes a very similar form.

12.1.1 The internal force vector

The internal force vector (5.19) is given by

$$\mathbf{q}_i = \int \mathbf{B}_{nl}^{\mathrm{T}} \mathbf{S}\, \mathrm{d}V_0 = \int \mathbf{G}(\mathbf{X})^{\mathrm{T}} [\mathbf{H} + \mathbf{A}(\boldsymbol{\theta})] \mathbf{S}\, \mathrm{d}V_0 \tag{12.1}$$

where $\mathbf{S}$ is the vector of second Piola–Kirchhoff stresses while

$$\mathbf{H} = \begin{bmatrix} 1 & 0 & 0 & 0 \\ 0 & 0 & 0 & 1 \\ 0 & 1 & 1 & 0 \end{bmatrix} \tag{12.2}$$

and the displacement derivatives, $\boldsymbol{\theta}$ (vector equivalent of $\mathbf{D}$ – (4.71)) are obtained from

$$\boldsymbol{\theta} = \begin{bmatrix} \dfrac{\partial u}{\partial X} \\ \dfrac{\partial u}{\partial Y} \\ \dfrac{\partial v}{\partial X} \\ \dfrac{\partial v}{\partial Y} \end{bmatrix} = \begin{bmatrix} \mathbf{J}^{-1}(1,1)\mathbf{h}_\xi^{\mathrm{T}} + \mathbf{J}^{-1}(1,2)\mathbf{h}_\eta^{\mathrm{T}} & \mathbf{0}^{\mathrm{T}} \\ \mathbf{J}^{-1}(2,1)\mathbf{h}_\xi^{\mathrm{T}} + \mathbf{J}^{-1}(2,2)\mathbf{h}_\eta^{\mathrm{T}} & \mathbf{0}^{\mathrm{T}} \\ \mathbf{0}^{\mathrm{T}} & \mathbf{J}^{-1}(1,1)\mathbf{h}_\xi^{\mathrm{T}} + \mathbf{J}^{-1}(1,2)\mathbf{h}_\eta^{\mathrm{T}} \\ \mathbf{0}^{\mathrm{T}} & \mathbf{J}^{-1}(2,1)\mathbf{h}_\xi^{\mathrm{T}} + \mathbf{J}^{-1}(2,2)\mathbf{h}_\eta^{\mathrm{T}} \end{bmatrix} \begin{bmatrix} \mathbf{u} \\ \mathbf{v} \end{bmatrix} = \mathbf{G}(\mathbf{X})\mathbf{p} \tag{12.3}$$

where $\mathbf{h}_\xi$ and $\mathbf{h}_\eta$ are derivatives of the shape functions with respect to the non-dimensional coordinates while $\mathbf{J}$ is the 2×2 Jacobian matrix (see (5.6)) which is here

a function of the initial coordinates, **X**. (With a different ordering for the nodal variables, the matrix **G**(**X**) would take a different from but the concepts would be the same.) In contrast to the work in Chapter 5, we will here keep rigorously to the convention whereby capital X's and Y's relate to the initial coordinates while small x's and y's relate to the current coordinates. The matrix $\mathbf{A}(\boldsymbol{\theta})$ in (12.1) is given (see (5.10)) by

$$\mathbf{A}(\boldsymbol{\theta}) = \begin{bmatrix} \dfrac{\partial u}{\partial X} & 0 & \dfrac{\partial v}{\partial X} & 0 \\ 0 & \dfrac{\partial u}{\partial Y} & 0 & \dfrac{\partial v}{\partial Y} \\ \dfrac{\partial u}{\partial Y} & \dfrac{\partial u}{\partial X} & \dfrac{\partial v}{\partial Y} & \dfrac{\partial v}{\partial X} \end{bmatrix} \tag{12.4}$$

while the variation of Green strain is given by (see (5.15) and (5.19))

$$\delta\mathbf{E} = [\mathbf{H} + \mathbf{A}(\boldsymbol{\theta})]\delta\mathbf{p} = \mathbf{B}_{nl}(\mathbf{p})\delta\mathbf{p} \tag{12.5}$$

The three-dimensional forms of **H** and $\mathbf{A}(\boldsymbol{\theta})$ are given in (5.33) and (5.34).

12.1.2 The tangent stiffness matrix

The tangent stiffness matrix takes the form (see (5.26)):

$$\mathbf{K}_t = \mathbf{K}_{t1} + \mathbf{K}_{t\sigma} = \int \mathbf{B}_{nl}^{\mathrm{T}}\mathbf{C}_{t\mathrm{K}2}\mathbf{B}_{nl}\mathrm{d}V_{\mathrm{o}} + \int \mathbf{G}(\mathbf{X})^{\mathrm{T}}\hat{\mathbf{S}}\mathbf{G}(\mathbf{X})\mathrm{d}V_{\mathrm{o}} \tag{12.6}$$

with:

$$\hat{\mathbf{S}} = \begin{bmatrix} \begin{bmatrix} S_{11} & S_{12} \\ S_{12} & S_{22} \end{bmatrix} & \begin{bmatrix} 0 & 0 \\ 0 & 0 \end{bmatrix} \\ \begin{bmatrix} 0 & 0 \\ 0 & 0 \end{bmatrix} & \begin{bmatrix} S_{11} & S_{12} \\ S_{12} & S_{22} \end{bmatrix} \end{bmatrix} \tag{12.7}$$

The three-dimensional form of $\hat{\mathbf{S}}$ is given in (5.36).

In (12.6), we have included the subscript tK2 on the tangential constitutive modular matrix to indicate that the latter relates to the second Piola–Kirchhoff stresses. As originally indicated in Sections 3.1 and 3.2, once large strains are introduced it is important to specify the types of stress and strain measure when considering the constitutive relationships.

12.2 THE INTERNAL FORCE VECTOR FOR THE 'EULERIAN FORMULATION'

We will take as a starting-point, the last form of the internal virtual power in (4.118) whereby:

$$\dot{V}_i = \int \boldsymbol{\sigma}:\dot{\boldsymbol{\varepsilon}}_{\mathrm{v}}\mathrm{d}V_{\mathrm{n}} = \int \boldsymbol{\tau}:\dot{\boldsymbol{\varepsilon}}_{\mathrm{v}}\mathrm{d}V_{\mathrm{o}} \tag{12.8}$$

with $\boldsymbol{\sigma}$ as the Cauchy stresses and $\boldsymbol{\tau}$ as the Kirchhoff stresses (see 4.122) given by $\boldsymbol{\tau} = J\boldsymbol{\sigma} = \det(\mathbf{F})\boldsymbol{\sigma}$. The final integral in (12.8) relates to the initial volume while the first integral relates to the current volume. In (12.8), $\dot{\boldsymbol{\varepsilon}}_v$ are the virtual strains following from the virtual velocities (or, effectively—see Section 4.6—virtual displacement changes). From (4.108) and (4.109) (see also (10.21) and (10.22)), we can write:

$$\dot{\boldsymbol{\varepsilon}}_v = \frac{1}{2}\left[\frac{\partial \mathbf{v}_v}{\partial \mathbf{x}} + \frac{\partial \mathbf{v}_v^T}{\partial \mathbf{x}}\right] = \tfrac{1}{2}[\mathbf{L}_v + \mathbf{L}_v^T] = \mathbf{H}\dot{\boldsymbol{\theta}}_v = \mathbf{H}\mathbf{G}(\mathbf{x})\dot{\mathbf{p}}_v = \mathbf{B}(\mathbf{x})\dot{\mathbf{p}}_v \tag{12.9}$$

where we have, rather loosely, mixed tensor and matrix and vector notation. The matrix $\mathbf{H}$ was defined in (12.2) while $\mathbf{G}(\mathbf{x})$ takes precisely the same form as $\mathbf{G}(\mathbf{X})$ in (12.3), although now the included terms from the Jacobian matrix $\mathbf{J}$ relate to $\mathbf{J}(\mathbf{x})$ rather than $\mathbf{J}(\mathbf{X})$. Using a pure matrix and vector notation, we can write:

$$\dot{\boldsymbol{\varepsilon}} = \begin{bmatrix} \dfrac{\partial \dot{u}}{\partial x} \\ \dfrac{\partial \dot{v}}{\partial y} \\ \dfrac{\partial \dot{u}}{\partial y} + \dfrac{\partial \dot{v}}{\partial x} \end{bmatrix} = \begin{bmatrix} 1 & 0 & 0 & 0 \\ 0 & 0 & 0 & 1 \\ 0 & 1 & 1 & 0 \end{bmatrix} \begin{bmatrix} \dfrac{\partial \dot{u}}{\partial x} \\ \dfrac{\partial \dot{u}}{\partial y} \\ \dfrac{\partial \dot{v}}{\partial x} \\ \dfrac{\partial \dot{v}}{\partial y} \end{bmatrix} = \mathbf{H}\dot{\boldsymbol{\theta}} = \mathbf{H}\mathbf{G}(\mathbf{x})\dot{\mathbf{p}} = \mathbf{B}(\mathbf{x})\dot{\mathbf{p}} \tag{12.10}$$

where

$$\dot{\boldsymbol{\theta}}(\mathbf{x}) = \begin{bmatrix} \dfrac{\partial \dot{u}}{\partial x} \\ \dfrac{\partial \dot{u}}{\partial y} \\ \dfrac{\partial \dot{v}}{\partial x} \\ \dfrac{\partial \dot{v}}{\partial y} \end{bmatrix} = \begin{bmatrix} \mathbf{J}^{-1}(1,1)\mathbf{h}_\xi^T + \mathbf{J}^{-1}(1,2)\mathbf{h}_\eta^T & \mathbf{0}^T \\ \mathbf{J}^{-1}(2,1)\mathbf{h}_\xi^T + \mathbf{J}^{-1}(2,2)\mathbf{h}_\eta^T & \mathbf{0}^T \\ \mathbf{0}^T & \mathbf{J}^{-1}(1,1)\mathbf{h}_\xi^T + \mathbf{J}^{-1}(1,2)\mathbf{h}_\eta^T \\ \mathbf{0}^T & \mathbf{J}^{-1}(2,1)\mathbf{h}_\xi^T + \mathbf{J}^{-1}(2,2)\mathbf{h}_\eta^T \end{bmatrix} \begin{bmatrix} \dot{\mathbf{u}} \\ \dot{\mathbf{v}} \end{bmatrix}$$

$$= \mathbf{G}(\mathbf{x})\dot{\mathbf{p}} \tag{12.11}$$

and $\dot{\mathbf{p}}$ contains the vector of nodal displacement changes (or velocities). (Note, the three-dimensional ordering of $\dot{\boldsymbol{\theta}}(\mathbf{x})$ follows the form given in (5.29).)

Substitution from (12.9) into (12.8) gives:

$$\dot{V} = \dot{\mathbf{p}}_v^T \mathbf{q}_i = \dot{\mathbf{p}}_v^T \int \mathbf{B}(\mathbf{x})^T \boldsymbol{\sigma}\, dV_n = \dot{\mathbf{p}}_v^T \int \mathbf{B}(\mathbf{x})^T \boldsymbol{\tau}\, dV_o \tag{12.12}$$

Knowing the stresses $\boldsymbol{\sigma}$ (or $\boldsymbol{\tau}$), the internal force vector, $\mathbf{q}_i$ is easily computed from (12.19) as

$$\mathbf{q}_i = \int \mathbf{B}(\mathbf{x})^T \boldsymbol{\sigma}\, dV_n = \int \mathbf{B}(\mathbf{x})^T \boldsymbol{\tau}\, dV_o = \int \mathbf{G}(\mathbf{x})^T \mathbf{H}^T \boldsymbol{\tau}\, dV_o \tag{12.13}$$

12.3 THE TANGENT STIFFNESS MATRIX IN RELATION TO THE TRUESDELL RATE OF KIRCHHOFF STRESS

We have chosen to start with the Truesdell rate of Kirchhoff stress because this choice gives the simplest form of the tangent stiffness equations. We will start by writing down the solution (which is remarkably simple) and will later give the derivation (which is not so simple).

In place of (12.6) for the total Lagrangian formulation, we obtain:

$$\mathbf{K}_t = \mathbf{K}_{t1} + \mathbf{K}_{t\sigma} = \int \mathbf{B}(\mathbf{x})^T \mathbf{C}_{tTK} \mathbf{B}(\mathbf{x}) dV_o + \int \mathbf{G}(\mathbf{x})^T \hat{\boldsymbol{\tau}} \mathbf{G}(\mathbf{x}) dV_o \tag{12.14}$$

where $\hat{\boldsymbol{\tau}}$ takes precisely the same form as $\hat{\mathbf{S}}$ in (12.7), i.e.

$$\hat{\boldsymbol{\tau}} = \begin{bmatrix} \begin{bmatrix} \tau_{11} & \tau_{12} \\ \tau_{12} & \tau_{22} \end{bmatrix} & \begin{bmatrix} 0 & 0 \\ 0 & 0 \end{bmatrix} \\ \begin{bmatrix} 0 & 0 \\ 0 & 0 \end{bmatrix} & \begin{bmatrix} \tau_{11} & \tau_{12} \\ \tau_{12} & \tau_{22} \end{bmatrix} \end{bmatrix} \tag{12.7}$$

In three dimensions, $\hat{\boldsymbol{\tau}}$ takes the same form as $\hat{\mathbf{S}}$ in (5.36), i.e.

$$\hat{\boldsymbol{\tau}} = \begin{bmatrix} \bar{\boldsymbol{\tau}} & \mathbf{0} & \mathbf{0} \\ \mathbf{0} & \bar{\boldsymbol{\tau}} & \mathbf{0} \\ \mathbf{0} & \mathbf{0} & \bar{\boldsymbol{\tau}} \end{bmatrix}; \qquad \bar{\boldsymbol{\tau}} = \begin{bmatrix} \tau_{11} & \tau_{12} & \tau_{13} \\ \tau_{12} & \tau_{22} & \tau_{23} \\ \tau_{13} & \tau_{23} & \tau_{33} \end{bmatrix} \tag{12.15b}$$

The subscript tTK on the tangential constitutive modular matrix in (12.14) indicates that the latter relates to the Truesdell rate of Kirchhoff stress. The transformation between the coefficients of $\mathbf{C}_{tT2}$ for use in (12.6) and the coefficients of $\mathbf{C}_{tTK}$ for use in (12.14) has been given in (10.56). It is worth restressing that if such transformations are made and if a consistent hyperelastic formulation is used (more in the next chapter), the current 'Eulerian formulation' should give identical results (including an identical tangent stiffness matrix) to the previous 'total Lagrangian formulation'. Because of the relationship between $\mathbf{B}(\mathbf{x})$ and $\mathbf{G}(\mathbf{x})$ in (12.10), (12.14) can be expressed in the more efficiently programmable form:

$$\mathbf{K}_t = \int \mathbf{G}(\mathbf{x})^T [\mathbf{H}^T \mathbf{C}_{tTK} \mathbf{H} + \hat{\boldsymbol{\tau}}] \mathbf{G}(\mathbf{x}) dV_o \tag{12.16}$$

12.3.1 Continuum derivation of the tangent stiffness matrix

The variation of (12.8) leads to

$$\delta \dot{V} = \delta \mathbf{q}_i^T \dot{\mathbf{p}}_v = \int \boldsymbol{\tau} : \delta \dot{\boldsymbol{\varepsilon}}_v dV_o + \int \dot{\boldsymbol{\tau}} : \boldsymbol{\varepsilon}_v dV_o = I_1 + I_2 \tag{12.17}$$

To compute I_1 from (12.17), we need the variation of (12.9) which is given by

$$\delta \dot{\boldsymbol{\varepsilon}}_v = \frac{1}{2} \delta \left[\frac{\partial \mathbf{v}_v}{\partial \mathbf{x}} + \frac{\partial \mathbf{v}_v^T}{\partial \mathbf{x}} \right] = \tfrac{1}{2} \delta [\mathbf{L}_v + \mathbf{L}_v^T] \tag{12.18}$$

and hence require

$$\frac{\partial \mathbf{v}_v}{\partial \mathbf{x}} = \mathbf{L}_v = \frac{\partial \mathbf{v}_v}{\partial \mathbf{X}} \frac{\partial \mathbf{X}}{\partial \mathbf{x}} = \frac{\partial \mathbf{v}_v}{\partial \mathbf{X}} \mathbf{F}^{-1} \tag{12.19}$$

Also because $\mathbf{X}$ is fixed,

$$\delta\left(\frac{\partial \mathbf{v}_v}{\partial \mathbf{X}}\right) = \mathbf{0} = \delta\left(\frac{\partial \mathbf{v}_v}{\partial \mathbf{x}}\right)\mathbf{F} + \frac{\partial \mathbf{v}_v}{\partial \mathbf{x}}\delta\mathbf{F} = \delta\left(\frac{\partial \mathbf{v}_v}{\partial \mathbf{x}}\right)\mathbf{F} + \frac{\partial \mathbf{v}_v}{\partial \mathbf{x}}\dot{\mathbf{F}} \tag{12.20}$$

In the previous equation and throughout this chapter we will loosely switch between δ's and rates ('s) as it appears convenient to do so. A stricter formulation would involve the introduction of certain δt's — see Section 4.6.

From (12.20) we can write:

$$\delta\left(\frac{\partial \mathbf{v}_v}{\partial \mathbf{x}}\right) = \delta\mathbf{L}_v = -\frac{\partial \mathbf{v}_v}{\partial \mathbf{x}}\dot{\mathbf{F}}\mathbf{F}^{-1} = -\mathbf{L}_v\mathbf{L} \tag{12.21}$$

where the last relationship follows from the non-virtual equivalent of (4.112). Substituting from (12.21) into (12.18) gives:

$$\delta\dot{\boldsymbol{\varepsilon}}_v = -\frac{1}{2}\left[\frac{\partial \mathbf{v}_v}{\partial \mathbf{x}}\frac{\partial \mathbf{v}}{\partial \mathbf{x}} + \frac{\partial \mathbf{v}^T}{\partial \mathbf{x}}\frac{\partial \mathbf{v}_v^T}{\partial \mathbf{x}}\right] = -\tfrac{1}{2}[\mathbf{L}_v\mathbf{L} + \mathbf{L}^T\mathbf{L}_v^T] \tag{12.22}$$

Using (12.22) and the fact that $\boldsymbol{\tau}$ is symmetric, the I_1 term in (12.17) is found to be given by

$$I_1 = \int \boldsymbol{\tau} : \delta\dot{\boldsymbol{\varepsilon}}_v \mathrm{d}V_0 = -\int \boldsymbol{\tau} : \mathbf{L}_v\,\mathbf{L}\,\mathrm{d}V_0 = -\int \boldsymbol{\tau} : \frac{\partial \mathbf{v}_v}{\partial \mathbf{x}}\frac{\partial \mathbf{v}}{\partial \mathbf{x}}\mathrm{d}V_0 \tag{12.23}$$

In order to compute the I_2 term from (12.17), we adopt the Truesdell rate of Kirchhoff stress so that from (10.53):

$$\dot{\boldsymbol{\tau}} = \dot{\boldsymbol{\tau}}_T + \mathbf{L}\boldsymbol{\tau} + \boldsymbol{\tau}\mathbf{L}^T = \mathbf{C}_{\tau TK} : \dot{\boldsymbol{\varepsilon}} + \mathbf{L}\boldsymbol{\tau} + \boldsymbol{\tau}\mathbf{L}^T \tag{12.24}$$

Substituting from (12.9) and (12.24) into I_2 from (12.17) leads to

$$I_2 = \int \dot{\boldsymbol{\tau}} : \dot{\boldsymbol{\varepsilon}}_v \mathrm{d}V_0 = \int ((\mathbf{C}_{\tau TK} : \dot{\boldsymbol{\varepsilon}}) : \dot{\boldsymbol{\varepsilon}}_v + \tfrac{1}{2}(\mathbf{L}\boldsymbol{\tau} + \boldsymbol{\tau}\mathbf{L}^T) : (\mathbf{L}_v + \mathbf{L}_v^T))\mathrm{d}V_0 \tag{12.25}$$

Using the relationship

$$\mathbf{AB} : \mathbf{C}^T = \mathbf{CA} : \mathbf{B}^T = \mathbf{BC} : \mathbf{A}^T \tag{12.26}$$

and noting that $\boldsymbol{\tau}$ is symmetric, we obtain:

$$I_2 = \int ((\mathbf{C}_{\tau TK}\dot{\boldsymbol{\varepsilon}}) : \dot{\boldsymbol{\varepsilon}}_v + \mathbf{L}_v^T\mathbf{L} : \boldsymbol{\tau} + \mathbf{L}_v\mathbf{L} : \boldsymbol{\tau})\mathrm{d}V_0 \tag{12.27}$$

Substituting for I_1 from (12.23) and for I_2 from (12.27) into (12.17) gives the expression

$$\delta\dot{V} = \int ((\mathbf{C}_{\tau TK}\dot{\boldsymbol{\varepsilon}}) : \dot{\boldsymbol{\varepsilon}}_v + \mathbf{L}_v^T\mathbf{L} : \boldsymbol{\tau})\mathrm{d}V_0 \tag{12.28}$$

Substituting for $\dot{\boldsymbol{\varepsilon}}$ as $\mathbf{B}(\mathbf{x})\dot{\mathbf{p}}$ (see (12.9)) and using a similar expression for the virtual

equivalent leads to the first term on the right-hand side of (12.28) being expressed as

$$\int (\mathbf{C}_{\mathrm{tTK}}:\dot{\boldsymbol{\varepsilon}}):\dot{\boldsymbol{\varepsilon}}_{\mathrm{v}}\,\mathrm{d}V_{\mathrm{o}} = \dot{\mathbf{p}}_{\mathrm{v}}^{\mathrm{T}}\mathbf{K}_{\mathrm{t1}}\dot{\mathbf{p}} = \dot{\mathbf{p}}_{\mathrm{v}}^{\mathrm{T}}\int \mathbf{B}(\mathbf{x})^{\mathrm{T}}\mathbf{C}_{\mathrm{tTK}}\mathbf{B}(\mathbf{x})\mathrm{d}V_{\mathrm{o}}\dot{\mathbf{p}} \tag{12.29}$$

which established the matrix $\mathbf{K}_{\mathrm{t1}}$ defined in (12.14).

The second term in (12.28) can be expressed as

$$\dot{\mathbf{p}}_{\mathrm{v}}^{\mathrm{T}}\mathbf{K}_{\mathrm{t}\sigma}\dot{\mathbf{p}} = \int \boldsymbol{\tau}:\mathbf{L}_{\mathrm{v}}^{\mathrm{T}}\mathbf{L}\,\mathrm{d}V_{\mathrm{o}} = \int \begin{bmatrix} \tau_{11} & \tau_{12} \\ \tau_{12} & \tau_{22} \end{bmatrix} : \begin{bmatrix} \dfrac{\partial \dot{u}}{\partial x} & \dfrac{\partial \dot{v}}{\partial x} \\ \dfrac{\partial \dot{u}}{\partial y} & \dfrac{\partial \dot{v}}{\partial y} \end{bmatrix}_{\mathrm{v}} \begin{bmatrix} \dfrac{\partial \dot{u}}{\partial x} & \dfrac{\partial \dot{u}}{\partial y} \\ \dfrac{\partial \dot{v}}{\partial x} & \dfrac{\partial \dot{v}}{\partial y} \end{bmatrix} \mathrm{d}V_{\mathrm{o}} \tag{12.30}$$

where $\mathbf{K}_{\mathrm{t}\sigma}$ is the 'geometric' or 'initial stress' contribution to the tangent stiffness matrix. Using (12.11), equation (12.30) can be re-expressed as

$$\dot{\mathbf{p}}_{\mathrm{v}}^{\mathrm{T}}\mathbf{K}_{\mathrm{t}\sigma}\dot{\mathbf{p}} = \int \begin{bmatrix} \dfrac{\partial \dot{u}}{\partial x} \\ \dfrac{\partial \dot{u}}{\partial y} \\ \dfrac{\partial \dot{v}}{\partial x} \\ \dfrac{\partial \dot{v}}{\partial y} \end{bmatrix}_{\mathrm{v}}^{\mathrm{T}} \begin{bmatrix} \begin{bmatrix} \tau_{11} & \tau_{12} \\ \tau_{12} & \tau_{22} \end{bmatrix} & \begin{bmatrix} 0 & 0 \\ 0 & 0 \end{bmatrix} \\ \begin{bmatrix} 0 & 0 \\ 0 & 0 \end{bmatrix} & \begin{bmatrix} \tau_{11} & \tau_{12} \\ \tau_{12} & \tau_{22} \end{bmatrix} \end{bmatrix} \begin{bmatrix} \dfrac{\partial \dot{u}}{\partial x} \\ \dfrac{\partial \dot{u}}{\partial y} \\ \dfrac{\partial \dot{v}}{\partial x} \\ \dfrac{\partial \dot{v}}{\partial y} \end{bmatrix} \mathrm{d}V_{\mathrm{o}} = \dot{\mathbf{p}}_{\mathrm{v}}^{\mathrm{T}}\int \mathbf{G}(\mathbf{x})^{\mathrm{T}}\hat{\boldsymbol{\tau}}\mathbf{G}(\mathbf{x})\mathrm{d}V_{\mathrm{o}}\dot{\mathbf{p}} \tag{12.31}$$

which establishes the 'initial stress' matrix $\mathbf{K}_{\mathrm{t}\sigma}$ defined in (12.14). (A very similar derivation will lead to the three-dimensional form of $\hat{\boldsymbol{\tau}}$ given in (12.15b)).

12.3.2 Discretised derivation of the tangent stiffness matrix

In the previous section, we derived the tangent stiffness equations by starting with the continuum expressions and only substituted in for the discretised (finite element) relationships at the final stage. In Section 5.1.2, it was shown that, for the total Lagrangian formulation, we could alternatively start with the discretised form for the internal force vector. We will now follow this route for the 'Eulerian formulation' and will differentiate (12.13) so that

$$\delta\mathbf{q}_{\mathrm{i}} = \int \delta\mathbf{G}(\mathbf{x})^{\mathrm{T}}\mathbf{H}^{\mathrm{T}}\boldsymbol{\tau}\mathrm{d}V_{\mathrm{o}} + \int \mathbf{G}(\mathbf{x})^{\mathrm{T}}\mathbf{H}^{\mathrm{T}}\delta\boldsymbol{\tau}\mathrm{d}V_{\mathrm{o}} = I_{\mathrm{a}} + I_{\mathrm{b}} \tag{12.32}$$

To obtain the integral I_{a}, a relationship must first be found between $\dot{\boldsymbol{\theta}}(\mathbf{X})$ and $\dot{\boldsymbol{\theta}}(\mathbf{x})$ which is given by

$$\dot{\boldsymbol{\theta}}(\mathbf{X}) = \begin{bmatrix} \dfrac{\partial \dot{u}}{\partial X} \\ \dfrac{\partial \dot{u}}{\partial Y} \\ \dfrac{\partial \dot{v}}{\partial X} \\ \dfrac{\partial \dot{v}}{\partial Y} \end{bmatrix} = \begin{bmatrix} \begin{bmatrix} \dfrac{\partial x}{\partial X} & \dfrac{\partial y}{\partial X} \\ \dfrac{\partial x}{\partial Y} & \dfrac{\partial y}{\partial Y} \end{bmatrix} \begin{bmatrix} 0 & 0 \\ 0 & 0 \end{bmatrix} \\ \begin{bmatrix} 0 & 0 \\ 0 & 0 \end{bmatrix} \begin{bmatrix} \dfrac{\partial x}{\partial X} & \dfrac{\partial y}{\partial Y} \\ \dfrac{\partial x}{\partial Y} & \dfrac{\partial y}{\partial Y} \end{bmatrix} \end{bmatrix} \begin{bmatrix} \dfrac{\partial \dot{u}}{\partial x} \\ \dfrac{\partial \dot{u}}{\partial y} \\ \dfrac{\partial \dot{v}}{\partial x} \\ \dfrac{\partial \dot{v}}{\partial y} \end{bmatrix} = \bar{\mathbf{F}}^{\mathrm{T}}\dot{\boldsymbol{\theta}}(\mathbf{x}) \tag{12.33}$$

from which, knowing that $\dot{\boldsymbol{\theta}}(\mathbf{X}) = \mathbf{G}(\mathbf{X})\dot{\mathbf{p}}$ and $\dot{\boldsymbol{\theta}}(\mathbf{x}) = \mathbf{G}(\mathbf{x})\dot{\mathbf{p}}$, we can write:

$$\mathbf{G}(\mathbf{X}) = \bar{\mathbf{F}}^{\mathrm{T}}\mathbf{G}(\mathbf{x}) \tag{12.34}$$

This equation can be differentiated to give:

$$\mathbf{0} = \bar{\mathbf{F}}^{\mathrm{T}}\delta\mathbf{G}(\mathbf{x}) + \dot{\bar{\mathbf{F}}}^{\mathrm{T}}\mathbf{G}(\mathbf{x}) \tag{12.35}$$

so that:

$$\delta\mathbf{G}(\mathbf{x})^{\mathrm{T}} = -\mathbf{G}(\mathbf{x})^{\mathrm{T}}\dot{\bar{\mathbf{F}}}\bar{\mathbf{F}}^{-1} = -\mathbf{G}(\mathbf{x})^{\mathrm{T}}\left[\begin{bmatrix}\dfrac{\partial\dot{u}}{\partial x} & \dfrac{\partial\dot{u}}{\partial y}\\ \dfrac{\partial\dot{v}}{\partial y} & \dfrac{\partial\dot{v}}{\partial y}\end{bmatrix}\begin{bmatrix}0 & 0\\ 0 & 0\end{bmatrix}\right.$$
$$\left.\begin{bmatrix}0 & 0\\ 0 & 0\end{bmatrix}\begin{bmatrix}\dfrac{\partial\dot{u}}{\partial x} & \dfrac{\partial\dot{u}}{\partial y}\\ \dfrac{\partial\dot{v}}{\partial x} & \dfrac{\partial\dot{v}}{\partial y}\end{bmatrix}\right] = -\mathbf{G}(\mathbf{x})^{\mathrm{T}}\bar{\mathbf{L}} \tag{12.36}$$

Consequently, the integral I_a in (12.32) can be expressed as

$$I_a = \int \delta\mathbf{G}(\mathbf{x})^{\mathrm{T}}\mathbf{H}^{\mathrm{T}}\boldsymbol{\tau}\,\mathrm{d}V_0 = \int \delta\mathbf{G}(\mathbf{x})^{\mathrm{T}}\begin{bmatrix}\tau_{11}\\ \tau_{12}\\ \tau_{12}\\ \tau_{22}\end{bmatrix}\mathrm{d}V_0 = \int \delta\mathbf{G}(\mathbf{x})^{\mathrm{T}}\boldsymbol{\tau}_4\,\mathrm{d}V_0 = -\int \mathbf{G}(\mathbf{x})^{\mathrm{T}}\bar{\mathbf{L}}\boldsymbol{\tau}_4\,\mathrm{d}V_0 \tag{12.37}$$

Further manipulations lead to

$$I_a = -\int \mathbf{G}(\mathbf{x})^{\mathrm{T}}\left[\begin{bmatrix}\tau_{11} & \tau_{12}\\ 0 & 0\end{bmatrix}\begin{bmatrix}0 & 0\\ \tau_{11} & \tau_{12}\end{bmatrix}\right.$$
$$\left.\begin{bmatrix}\tau_{12} & \tau_{22}\\ 0 & 0\end{bmatrix}\begin{bmatrix}0 & 0\\ \tau_{12} & \tau_{22}\end{bmatrix}\right]\dot{\boldsymbol{\theta}}(\mathbf{x})\,\mathrm{d}V_0 = -\int \mathbf{G}(\mathbf{x})^{\mathrm{T}}\dot{\boldsymbol{\tau}}\mathbf{G}(\mathbf{x})\,\mathrm{d}V_0\dot{\mathbf{p}} \tag{12.38}$$

Substitution from (12.24) into I_b in (12.32) gives:

$$I_b = \int \mathbf{G}(\mathbf{x})^{\mathrm{T}}[\mathbf{H}^{\mathrm{T}}\mathbf{C}_{t\mathrm{TK}}\mathbf{H}]\mathbf{G}(\mathbf{x})\,\mathrm{d}V_0\delta\mathbf{p} + \int \mathbf{G}(\mathbf{x})^{\mathrm{T}}\mathbf{H}^{\mathrm{T}}v(\mathbf{L}\boldsymbol{\tau} + \boldsymbol{\tau}\mathbf{L}^{\mathrm{T}})\,\mathrm{d}V_0 = I_{b1} + I_{b2} \tag{12.39}$$

where $v(\ )$ indicates the vector equivalent. From (12.39),

$$I_{b1} = \int \mathbf{B}(\mathbf{x})^{\mathrm{T}}\mathbf{C}_{t\mathrm{TK}}\mathbf{B}(\mathbf{x})\,\mathrm{d}V_0\delta\mathbf{p} = \mathbf{K}_{t1}\delta\mathbf{p} \tag{12.40}$$

which gives $\mathbf{K}_{t1}$ from (12.14) while

$$I_{b2} = \int \mathbf{G}(\mathbf{x})^{\mathrm{T}}\dot{\hat{\boldsymbol{\tau}}}\dot{\boldsymbol{\theta}}(\mathbf{x})\,\mathrm{d}V_0 + \int \mathbf{G}(\mathbf{x})^{\mathrm{T}}\hat{\boldsymbol{\tau}}\dot{\boldsymbol{\theta}}(\mathbf{x})\,\mathrm{d}V_0 \tag{12.41}$$

with $\hat{\boldsymbol{\tau}}$ from (12.15) and $\dot{\hat{\boldsymbol{\tau}}}$ from (12.38). Substitution from (12.11) into (12.41) leads to

$$I_{b2} = \int \mathbf{G}(\mathbf{x})^{\mathrm{T}}\dot{\hat{\boldsymbol{\tau}}}\mathbf{G}(\mathbf{x})\,\mathrm{d}V_0\dot{\mathbf{p}} + \int \mathbf{G}(\mathbf{x})^{\mathrm{T}}\hat{\boldsymbol{\tau}}\mathbf{G}(\mathbf{x})\,\mathrm{d}V_0\dot{\mathbf{p}} \tag{12.42}$$

Substitution from (12.38), (12.40) and (12.42) into (12.32) leads to the tangential stiffness equations:

$$\delta \mathbf{q}_i = \dot{\mathbf{q}}_i = \mathbf{K}_t \delta \mathbf{p} = \mathbf{K}_t \dot{\mathbf{p}} \tag{12.43}$$

with $\mathbf{K}_t$ from (12.14).

12.4 THE TANGENT STIFFNESS MATRIX USING THE JAUMANN RATE OF KIRCHHOFF STRESS

Following the work in Section 12.3, we will first write down the solution and then give the derivation which stems from the use of the Jaumann rate form (see 10.36):

$$\dot{\boldsymbol{\tau}} = \dot{\boldsymbol{\tau}}_J + \dot{\boldsymbol{\Omega}}\boldsymbol{\tau} + \boldsymbol{\tau}\dot{\boldsymbol{\Omega}}^T = \mathbf{C}_{tTK} : \dot{\boldsymbol{\varepsilon}} + \dot{\boldsymbol{\Omega}}\boldsymbol{\tau} + \boldsymbol{\tau}\dot{\boldsymbol{\Omega}}^T \tag{12.44}$$

and leads to a tangent stiffness matrix given by

$$\begin{aligned}
\mathbf{K}_t &= \mathbf{K}_{t1} + \mathbf{K}_{t\sigma 2} + \mathbf{K}_{t\sigma 1} \\
&= \int \mathbf{B}(\mathbf{x})^T \mathbf{C}_{tTK} \mathbf{B}(\mathbf{x}) \mathrm{d}V_0 - \int \mathbf{B}(\mathbf{x})^T \tilde{\boldsymbol{\tau}} \mathbf{B}(\mathbf{x}) \mathrm{d}V_0 + \int \mathbf{G}(\mathbf{x})^T \hat{\boldsymbol{\tau}} \mathbf{G}(\mathbf{x}) \mathrm{d}V_0 \\
&= \int \mathbf{B}(\mathbf{x})^T (\mathbf{C}_{tTK} - \tilde{\boldsymbol{\tau}}) \mathbf{B}(\mathbf{x}) \mathrm{d}V_0 + \int \mathbf{G}(\mathbf{x})^T \hat{\boldsymbol{\tau}} \mathbf{G}(\mathbf{x}) \mathrm{d}V_0
\end{aligned} \tag{12.45}$$

with $\hat{\boldsymbol{\tau}}$ as given previously in (12.15) and, in two dimensions, $\tilde{\boldsymbol{\tau}}$ being given by

$$\tilde{\boldsymbol{\tau}} = \begin{bmatrix} 2\tau_{11} & 0 & \tau_{12} \\ 0 & 2\tau_{22} & \tau_{12} \\ \tau_{12} & \tau_{12} & \dfrac{\tau_{11} + \tau_{22}}{2} \end{bmatrix} \tag{12.46}$$

while, in three dimensions, it is given by

$$\tilde{\boldsymbol{\tau}} = \begin{bmatrix} 2\tau_{11} & 0 & 0 & 0 & \tau_{13} & \tau_{12} \\ 0 & 2\tau_{22} & 0 & \tau_{23} & 0 & \tau_{21} \\ 0 & 0 & 2\tau_{33} & \tau_{32} & \tau_{31} & 0 \\ 0 & \tau_{32} & \tau_{23} & \tau_{23} & \tau_{21} & \tau_{31} \\ \tau_{31} & 0 & \tau_{13} & \tau_{12} & \tilde{\tau}_{13} & \tau_{32} \\ \tau_{21} & \tau_{12} & 0 & \tau_{13} & \tau_{23} & \tau_{12} \end{bmatrix} \tag{12.47}$$

where

$$\tilde{\tau}_{ij} = \tfrac{1}{2}(\tau_{ii} + \tau_{jj}) \tag{12.48}$$

For the same hyperelastic material, the tangent stiffness matrix in (12.45) should be identical to that given earlier for the Truesdell rate in (12.14) (or (12.16)). To show this relationship, we have to take account of the differences in the tangent $\mathbf{C}_t$ tensors. In particular, comparing (12.24) with (12.44) leads to the relationship

$$\dot{\boldsymbol{\tau}}_T + \mathbf{L}\boldsymbol{\tau} + \boldsymbol{\tau}\mathbf{L}^T = \dot{\boldsymbol{\tau}}_J + \dot{\boldsymbol{\Omega}}\boldsymbol{\tau} + \boldsymbol{\tau}\dot{\boldsymbol{\Omega}}^T \tag{12.49}$$

or allowing for the fact that $\mathbf{L} = \dot{\boldsymbol{\varepsilon}} + \dot{\boldsymbol{\Omega}}$ (see (10.22)) and noting the symmetry of $\dot{\boldsymbol{\varepsilon}}$,

$$\dot{\boldsymbol{\tau}}_T = \mathbf{C}_{tTK}:\dot{\boldsymbol{\varepsilon}} = \dot{\boldsymbol{\tau}}_J - \dot{\boldsymbol{\varepsilon}}\boldsymbol{\tau} - \boldsymbol{\tau}\dot{\boldsymbol{\varepsilon}} = \mathbf{C}_{tJK}\dot{\boldsymbol{\varepsilon}} - \dot{\boldsymbol{\varepsilon}}\boldsymbol{\tau} - \boldsymbol{\tau}\dot{\boldsymbol{\varepsilon}} \tag{12.50}$$

Using suffix notation, from (12.50), the two modular matrices are related by

$$C^{tTK}_{ijkl} = C^{tJK}_{ijkl} - \tfrac{1}{2}[\tau_{il}\delta_{jk} + \tau_{jl}\delta_{ik} + \tau_{ik}\delta_{jl} + \tau_{jk}\delta_{il}] \tag{12.51}$$

Hence, writing $\mathbf{C}_{tTK}$ from (12.51) in terms of $\mathbf{C}_{tJK}$ and substituting into (12.14) leads directly to (12.45) and indeed, $\tilde{\boldsymbol{\tau}}$ from (12.48) and (12.49) is the matrix equivalent of the second fourth-order tensor term in (12.51).

12.4.1 Alternative derivation of the tangent stiffness matrix

Because of the relationships that were established at the end of the last section, a derivation of the tangent stiffness matrix in (12.45) has already been given. In this section, we will give an alternative derivation following the lines of Section 12.3.1 for the Truesdell rate.

The I_1 term in (12.17) remains unaltered in the form given in (12.23) while, using (12.44), the I_2 term in (12.17) now becomes

$$I_2 = \int \dot{\boldsymbol{\tau}}:\dot{\boldsymbol{\varepsilon}}_v \mathrm{d}V_o = \int ((\mathbf{C}_{tJK}\dot{\boldsymbol{\varepsilon}}):\dot{\boldsymbol{\varepsilon}}_v + (\dot{\boldsymbol{\Omega}}\boldsymbol{\tau} + \boldsymbol{\tau}\dot{\boldsymbol{\Omega}}^T)\dot{\boldsymbol{\varepsilon}}_v)\mathrm{d}V_o = \int ((\mathbf{C}_{tJK}\dot{\boldsymbol{\varepsilon}}):\dot{\boldsymbol{\varepsilon}}_v + 2\dot{\boldsymbol{\Omega}}\boldsymbol{\tau}\dot{\boldsymbol{\varepsilon}}_v)\mathrm{d}V_o \tag{12.52}$$

In deriving the last term in (12.52), we have used the fact that $\dot{\boldsymbol{\Omega}}$ is skew-symmetric while $\boldsymbol{\tau}$ and $\dot{\boldsymbol{\varepsilon}}_v$ are symmetric. We can now use the relationship (see (10.22)), $\dot{\boldsymbol{\Omega}} + \dot{\boldsymbol{\varepsilon}} = \mathbf{L}$, to obtain:

$$I_2 = \int ((\mathbf{C}_{tJK}\dot{\boldsymbol{\varepsilon}}):\dot{\boldsymbol{\varepsilon}}_v + 2\mathbf{L}\boldsymbol{\tau}:\dot{\boldsymbol{\varepsilon}}_v - 2\dot{\boldsymbol{\varepsilon}}\boldsymbol{\tau}:\dot{\boldsymbol{\varepsilon}}_v)\mathrm{d}V_o \tag{12.53}$$

Using (12.26), (12.53) reduces to

$$I_2 = \int ((\mathbf{C}_{tJK}\dot{\boldsymbol{\varepsilon}}):\dot{\boldsymbol{\varepsilon}}_v + 2\dot{\boldsymbol{\varepsilon}}_v\mathbf{L}:\boldsymbol{\tau} - 2\dot{\boldsymbol{\varepsilon}}_v\dot{\boldsymbol{\varepsilon}}:\boldsymbol{\tau})\mathrm{d}V_o \tag{12.54}$$

and substituting from (12.18) for $\dot{\boldsymbol{\varepsilon}}_v$ in the second term on the right-hand-side of (12.54), we arrive at

$$I_2 = \int ((\mathbf{C}_{tJK}:\dot{\boldsymbol{\varepsilon}}):\dot{\boldsymbol{\varepsilon}}_v + \mathbf{L}_v^T\mathbf{L}:\boldsymbol{\tau} + \mathbf{L}_v\mathbf{L}:\boldsymbol{\tau} - 2\dot{\boldsymbol{\varepsilon}}_v\dot{\boldsymbol{\varepsilon}}:\boldsymbol{\tau})\mathrm{d}V_o \tag{12.55}$$

Substitution for I_1 from (12.23) and I_2 from (12.55) into (12.17) leads to the relationship

$$\delta\dot{V} = \delta\mathbf{q}_i^T\dot{\mathbf{p}}_v = \dot{\mathbf{p}}_v^T\mathbf{K}_t\dot{\mathbf{p}} = \dot{\mathbf{p}}_v^T[\mathbf{K}_{t1} + \mathbf{K}_{t\sigma 2} + \mathbf{K}_{t\sigma 1}]\dot{\mathbf{p}} \tag{12.56}$$

with $\mathbf{K}_{t1}$, $\mathbf{K}_{t\sigma 1}$ and $\mathbf{K}_{t\sigma 2}$ as given in (12.45) and, in particular with

$$\dot{\mathbf{p}}_v^T\mathbf{K}_{t\sigma 2}\dot{\mathbf{p}} = -2\int \dot{\boldsymbol{\varepsilon}}_v\dot{\boldsymbol{\varepsilon}}:\boldsymbol{\tau}\,\mathrm{d}V_o = -\dot{\boldsymbol{\varepsilon}}_v^T\tilde{\boldsymbol{\tau}}\dot{\boldsymbol{\varepsilon}}\,\mathrm{d}V_o = -\dot{\mathbf{p}}_v^T\int \mathbf{B}(\mathbf{x})^T\tilde{\boldsymbol{\tau}}\mathbf{B}(\mathbf{x})\mathrm{d}V_o\dot{\mathbf{p}} \tag{12.57}$$

12.5 THE TANGENT STIFFNESS MATRIX USING THE JAUMANN RATE OF CAUCHY STRESS

In first deriving, the tangent stiffness equations for the 'Eulerian formulation', McMeeking and Rice [M1] used the Jaumann rate of Cauchy stress. Following the work in the previous sections, we will first write down the solution and then give the derivation which stems from the use of the Jaumann rate form (see 10.36):

$$\dot{\boldsymbol{\sigma}} = \dot{\boldsymbol{\sigma}}_J + \dot{\boldsymbol{\Omega}}\boldsymbol{\sigma} + \boldsymbol{\sigma}\dot{\boldsymbol{\Omega}}^T = \mathbf{C}_{tJC}:\dot{\boldsymbol{\varepsilon}} + \dot{\boldsymbol{\Omega}}\boldsymbol{\sigma} + \boldsymbol{\sigma}\dot{\boldsymbol{\Omega}}^T \tag{12.58}$$

and leads to a tangent stiffness matrix given by

$$\begin{aligned}\mathbf{K}_t &= \mathbf{K}_{t1} + \mathbf{K}_{t\sigma 2} + \mathbf{K}_{t\sigma 1} + \mathbf{K}_{tns} \\ &= \int \mathbf{B}(\mathbf{x})^T \mathbf{C}_{tJC} \mathbf{B}(\mathbf{x}) \mathrm{d}V_n - \int \mathbf{B}(\mathbf{x})^T \tilde{\boldsymbol{\sigma}} \mathbf{B}(\mathbf{x}) \mathrm{d}V_n \\ &\quad + \int \mathbf{G}(\mathbf{x})^T \hat{\boldsymbol{\sigma}} \mathbf{G}(\mathbf{x}) \mathrm{d}V_n + \int \mathbf{B}(\mathbf{x})^T \check{\boldsymbol{\sigma}} \mathbf{B}(\mathbf{x}) \mathrm{d}V_n \\ &= \int \mathbf{B}(\mathbf{x})^T (\mathbf{C}_{tJC} - \tilde{\boldsymbol{\sigma}} + \check{\boldsymbol{\sigma}}) \mathbf{B}(\mathbf{x}) \mathrm{d}V_n + \int \mathbf{G}(\mathbf{x})^T \hat{\boldsymbol{\sigma}} \mathbf{G}(\mathbf{x}) \mathrm{d}V_n\end{aligned} \tag{12.59}$$

with $\hat{\boldsymbol{\sigma}}$ taking precisely the same form as given previously in (12.15) for $\hat{\boldsymbol{\tau}}$ (although of course now involving components of the Cauchy stress tensor) while, in a similar fashion, $\tilde{\boldsymbol{\sigma}}$ is given by equations of the same form as (12.46) in two dimensions or (12.47) in three dimensions. In two dimensions, for plane strain, the non-symmetric matrix $\check{\boldsymbol{\sigma}}$ is given by

$$\check{\boldsymbol{\sigma}} = \begin{bmatrix} \sigma_{11} & \sigma_{11} & 0 \\ \sigma_{22} & \sigma_{22} & 0 \\ \sigma_{12} & \sigma_{12} & 0 \end{bmatrix} \tag{12.60}$$

while, in three dimensions the equivalent term is

$$\check{\boldsymbol{\sigma}} = \begin{bmatrix} \sigma_{11} & \sigma_{11} & \sigma_{11} & 0 & 0 & 0 \\ \sigma_{22} & \sigma_{22} & \sigma_{22} & 0 & 0 & 0 \\ \sigma_{33} & \sigma_{33} & \sigma_{33} & 0 & 0 & 0 \\ \sigma_{12} & \sigma_{12} & \sigma_{12} & 0 & 0 & 0 \\ \sigma_{23} & \sigma_{23} & \sigma_{23} & 0 & 0 & 0 \\ \sigma_{31} & \sigma_{31} & \sigma_{31} & 0 & 0 & 0 \end{bmatrix} \tag{12.61}$$

The simplest way of deriving equation (12.59) is to initially find the relationship between $\mathbf{C}_{tJC}$ and $\mathbf{C}_{tJK}$. To this end, we can substitute from (12.44) and (12.58) into (10.57) to obtain

$$\dot{\boldsymbol{\tau}} = \mathbf{C}_{tJK}:\dot{\boldsymbol{\varepsilon}} + \dot{\boldsymbol{\Omega}}\boldsymbol{\tau} + \boldsymbol{\tau}\dot{\boldsymbol{\Omega}}^T = J(\dot{\boldsymbol{\sigma}} + \boldsymbol{\sigma}\,\mathrm{tr}(\dot{\boldsymbol{\varepsilon}})) = J\mathbf{C}_{tJC}:\dot{\boldsymbol{\varepsilon}} + \dot{\boldsymbol{\Omega}}\boldsymbol{\tau} + \boldsymbol{\tau}\dot{\boldsymbol{\Omega}}^T + \boldsymbol{\tau}\,\mathrm{tr}(\dot{\boldsymbol{\varepsilon}}) \tag{12.62}$$

so that:

$$\mathbf{C}_{tJK}:\dot{\boldsymbol{\varepsilon}} = J(\mathbf{C}_{tJC}:\dot{\boldsymbol{\varepsilon}} + \boldsymbol{\sigma}\,\mathrm{tr}(\dot{\boldsymbol{\varepsilon}})) \tag{12.63}$$

Adopting suffix notation and moving the subscripts in (12.63) to superscripts (purely

for printing convenience), it follows that:

$$C^{tJK}_{ijkl} = J(C^{tJC}_{ijkl} + \sigma_{ij}\delta_{kl}) \tag{12.64}$$

Substitution from (12.64) into (12.45) along with the relationships $\boldsymbol{\tau} = J\boldsymbol{\sigma}$ and $dV_n = J\,dV_o$ leads directly to (12.59) and indeed, $\tilde{\boldsymbol{\sigma}}$ from (12.61) is the matrix equivalent of the second fourth-order tensor term in (12.64).

In (12.59), we have labelled the term in $\mathbf{K}_t$ associated with $\check{\boldsymbol{\sigma}}$ as $\mathbf{K}_{tns}$ (with ns for non-symmetric) leaving the implication that the other terms are symmetric. However, this does not necessarily follow. For example when using a hyperelastic formulation the natural starting-point is the symmetric $\mathbf{C}_{tTK}$ (more details in the next chapter). Using (12.51) this would, in turn, lead to a symmetric $\mathbf{C}_{tJK}$ while, from (12.64), we would obtain a non-symmetric $\mathbf{C}_{tJC}$. If, for some reason, one wished to use a formulation involving the Jaumann rate of Cauchy stress, the resulting tangent stiffness matrix via (12.59) would be symmetric, and indeed it would be identical to that obtained more directly from (12.14) (or (12.16)). However, if one were to postulate a symmetric (possibly hypoelastic) $\mathbf{C}_{tJC}$, then from (12.59), the total tangent stiffness matrix would be non-symmetric.

12.5.1 Alternative derivation of the tangent stiffness matrix

Following on from (12.64), we have already effectively given one derivation of the tangent stiffness matrix of (12.59). As an alternative, we can consider the variation of the first expression in (12.8) which leads to

$$\delta\dot{V} = \delta\mathbf{q}_i^T\dot{\mathbf{p}}_v = \int \boldsymbol{\tau}:\delta\dot{\boldsymbol{\varepsilon}}_v\,dV_o + \int \dot{\boldsymbol{\sigma}}:\dot{\boldsymbol{\varepsilon}}_v\,dV_n + \int \boldsymbol{\sigma}:\dot{\boldsymbol{\varepsilon}}_v\delta(dV_n) = I_1 + I_2' + I_3 \tag{12.65}$$

The I_1 term in the above is identical to that previously derived in Section 12.3.1 (see (12.23)) while substitution from (12.58) into I_2' in (12.65), followed by some manipulation following the lines of that in Section 12.4.1, eventually leads to the relationship

$$I_2' = \int ((\mathbf{C}_{tJC}:\dot{\boldsymbol{\varepsilon}}):\dot{\boldsymbol{\varepsilon}}_v\,dV_n + \int \mathbf{L}_v^T\mathbf{L}:\boldsymbol{\tau} + \mathbf{L}_v\mathbf{L}:\boldsymbol{\tau} - 2\dot{\boldsymbol{\varepsilon}}_v\dot{\boldsymbol{\varepsilon}}:\boldsymbol{\tau})dV_0 \tag{12.66}$$

so that, using (12.23) for I_1:

$$I_1 + I_2' = \int ((\mathbf{C}_{tJC}:\dot{\boldsymbol{\varepsilon}}):\dot{\boldsymbol{\varepsilon}}_v\,dV_n + \int (\mathbf{L}_v^T\mathbf{L}:\boldsymbol{\sigma} - 2\dot{\boldsymbol{\varepsilon}}_v\dot{\boldsymbol{\varepsilon}}:\boldsymbol{\sigma})dV_n \tag{12.67}$$

Following the work in Section 12.4.1, these three terms provide the tangent stiffness contributions $\mathbf{K}_{t1}$, $\mathbf{K}_{t\sigma 1}$ and $\mathbf{K}_{t\sigma 2}$ of (12.59) so that we are left with I_3 in (12.65). To evaluate this term, we will use (10.88) whereby $\dot{J} = \mathrm{tr}(\dot{\boldsymbol{\varepsilon}})$ so that:

$$\delta(dV_n) = \delta(J\,dV_o) = \dot{J}\,dV_o = J\,\mathrm{tr}(\dot{\boldsymbol{\varepsilon}})dV_o = \mathrm{tr}(\dot{\boldsymbol{\varepsilon}})dV_n \tag{12.68}$$

Substitution into I_3 from (12.65) gives:

$$I_3 = \int \boldsymbol{\sigma}:\dot{\boldsymbol{\varepsilon}}_v\delta(dV_n) = \int \dot{\boldsymbol{\varepsilon}}_v:\boldsymbol{\sigma}\,\mathrm{tr}(\dot{\boldsymbol{\varepsilon}})dV_n \tag{12.69}$$

Considering the two-dimensional plane-strain case, we can write:

$$I_3 = \dot{\mathbf{p}}_v \mathbf{K}_{tns} \dot{\mathbf{p}} = \int \dot{\boldsymbol{\varepsilon}}_v : \boldsymbol{\sigma}\, \mathrm{tr}(\dot{\boldsymbol{\varepsilon}}) \mathrm{d}V_n = \int \begin{bmatrix} \dot{\varepsilon}_{11} & \dot{\varepsilon}_{12} \\ \dot{\varepsilon}_{12} & \dot{\varepsilon}_{22} \end{bmatrix}_v : \begin{bmatrix} \sigma_{11} & \sigma_{12} \\ \sigma_{12} & \sigma_{22} \end{bmatrix} (\dot{\varepsilon}_{11} + \dot{\varepsilon}_{22}) \mathrm{d}V_n \tag{12.70}$$

or

$$\dot{\mathbf{p}}_v \mathbf{K}_{tns} \dot{\mathbf{p}} = \int \begin{bmatrix} \dot{\varepsilon}_{11} \\ \dot{\varepsilon}_{22} \\ 2\dot{\varepsilon}_{12} \end{bmatrix}_v \check{\boldsymbol{\sigma}} \begin{bmatrix} \dot{\varepsilon}_{11} \\ \dot{\varepsilon}_{22} \\ 2\dot{\varepsilon}_{12} \end{bmatrix} \mathrm{d}V_n = \dot{\mathbf{p}}_v^{\mathrm{T}} \int \mathbf{B}(\mathbf{x})^{\mathrm{T}} \check{\boldsymbol{\sigma}} \mathbf{B}(\mathbf{x}) \mathrm{d}V_n \dot{\mathbf{p}} \tag{12.71}$$

A very similar development can be shown to lead to the equivalent three-dimensional form with $\check{\boldsymbol{\sigma}}$ from (12.61).

12.6 CONVECTED COORDINATES AND THE TOTAL LAGRANGIAN FORMULATION

In Section 11.8, we used convected curvilinear coordinates to obtain the covariant components of the Green strain and in Section 11.9, we considered the work-conjugate contravariant components of the second Piola–Kirchhoff stress tensor. In Section 5.1, the governing finite element equations were derived for a total Lagrangian formulation using orthonormal cartesian coordinates. In the present section, we will work directly with the convected curvilinear coordinates in order to obtain equivalent expressions.

12.6.1 Element formulation

Following the work of Section 5.1.1, a two-dimensional formulation will initially be considered using the convected coordinates,

$$\alpha^1 = \xi; \qquad \alpha^2 = \eta \tag{12.72}$$

corresponding to the non-dimensional coordinates ξ, η of Section 5.1. In place of (5.8) or (12.3), we now have

$$\boldsymbol{\theta} = \begin{bmatrix} \dfrac{\partial u}{\partial \xi} \\ \dfrac{\partial u}{\partial \eta} \\ \dfrac{\partial v}{\partial \xi} \\ \dfrac{\partial v}{\partial \eta} \end{bmatrix} = \begin{bmatrix} \mathbf{h}_\xi^{\mathrm{T}} & \mathbf{0}^{\mathrm{T}} \\ \mathbf{h}_\eta^{\mathrm{T}} & \mathbf{0}^{\mathrm{T}} \\ \mathbf{0}^{\mathrm{T}} & \mathbf{h}_\xi^{\mathrm{T}} \\ \mathbf{0}^{\mathrm{T}} & \mathbf{h}_\eta^{\mathrm{T}} \end{bmatrix} \begin{pmatrix} \mathbf{u} \\ \mathbf{v} \end{pmatrix} = \bar{\mathbf{G}} \mathbf{p} \tag{12.73}$$

where $\mathbf{p}$ contains the full vector of nodal displacements which relate to the usual fixed orthogonal coordinates. (In this section, the usual $\mathbf{G}$ matrix (as in (5.8)) will be written as $\bar{\mathbf{G}}$ to avoid confusion with the initial contravariant base vectors, $\mathbf{G}_i$ that will be defined shortly). A similar equation to (12.73) relates $\delta\boldsymbol{\theta}$ (vector equivalent to $\delta\mathbf{D}$—see

Chapter 5) to $\delta\mathbf{p}$ so that:

$$\delta\boldsymbol{\theta} = \bar{\mathbf{G}}\delta\mathbf{p} \tag{12.74}$$

From (11.56), we can write the covariant components of the Green strain as

$$E_{ij} = \tfrac{1}{2}(\mathbf{g}_i^{\mathrm{T}}\mathbf{g}_i - \mathbf{G}_i^{\mathrm{T}}\mathbf{G}_j) \tag{12.75}$$

where $\mathbf{G}_i$ and $\mathbf{g}_i$ are the initial and final covariant base vectors. From (11.52a) and (11.52b), the latter are given by

$$\mathbf{G}_i = \frac{\partial \mathbf{X}}{\partial \alpha^i}; \qquad \mathbf{g}_i = \frac{\partial \mathbf{x}}{\partial \alpha^i} = \mathbf{G}_i + \frac{\partial \mathbf{d}}{\partial \alpha^i} \tag{12.76}$$

where the vector $\mathbf{d}$ contains the displacements (i.e. $(\mathbf{d}^{\mathrm{T}} = (u, v)^{\mathrm{T}}$ — in standard cartesian coordinates). Using (12.76), (12.75) can be rewritten as

$$E_{ij} = \frac{1}{2}\left(\mathbf{G}_i^{\mathrm{T}}\frac{\partial \mathbf{d}}{\partial \alpha^j} + \mathbf{G}_j^{\mathrm{T}}\frac{\partial \mathbf{d}}{\partial \alpha^i}\right) + \frac{1}{2}\frac{\partial \mathbf{d}^{\mathrm{T}}}{\partial \alpha^i}\frac{\partial \mathbf{d}}{\partial \alpha^j} \tag{12.77}$$

which involves linear and non-linear terms as in (5.10). Noting that, with $\alpha^1 = \xi$, $\alpha^2 = \eta$, the terms from $\partial\mathbf{d}/\partial\alpha^i$ are the components of the vector $\boldsymbol{\theta}$ in (12.73), using vector and matrix notation, we can now replace (5.11) and (5.12) by

$$\mathbf{E} = \begin{bmatrix} E_{11} \\ E_{22} \\ 2E_{12} \end{bmatrix} = \mathbf{E}_l \rightarrow \mathbf{E}_{\mathrm{nl}} = \mathbf{H}\boldsymbol{\theta} + \frac{1}{2}\begin{bmatrix} \dfrac{\partial u}{\partial \xi} & 0 & \dfrac{\partial v}{\partial \xi} & 0 \\ 0 & \dfrac{\partial u}{\partial \eta} & 0 & \dfrac{\partial v}{\partial \eta} \\ \dfrac{\partial u}{\partial \eta} & \dfrac{\partial u}{\partial \xi} & \dfrac{\partial v}{\partial \eta} & \dfrac{\partial v}{\partial \xi} \end{bmatrix}\begin{bmatrix} \dfrac{\partial u}{\partial \xi} \\ \dfrac{\partial u}{\partial \eta} \\ \dfrac{\partial v}{\partial \xi} \\ \dfrac{\partial v}{\partial \eta} \end{bmatrix} = [\mathbf{H} + \tfrac{1}{2}\mathbf{A}(\boldsymbol{\theta})]\boldsymbol{\theta} \tag{12.78}$$

where

$$\mathbf{H} = \begin{bmatrix} G_1(1) & 0 & G_1(2) & 0 \\ 0 & G_2(1) & 0 & G_2(2) \\ G_2(1) & G_1(1) & G_2(2) & G_1(2) \end{bmatrix} \tag{12.79}$$

Following a very similar procedure to that of (5.13)–(5.16), the change in the covariant components of the Green strain can be expressed as

$$\delta\mathbf{E} = (\mathbf{B}_l + \mathbf{A}(\boldsymbol{\theta})\bar{\mathbf{G}})\delta\mathbf{p} = \mathbf{B}_{nl}\delta\mathbf{p} = (\mathbf{H} + \mathbf{A}(\boldsymbol{\theta}))\bar{\mathbf{G}}\,\delta\mathbf{p} \tag{12.80}$$

where all higher-order terms have been considered as negligible.

Using virtual work (see (11.62)) with the contravariant components of the second Piola–Kirchhoff stresses:

$$V_i = \delta\mathbf{p}_v^{\mathrm{T}}\mathbf{q}_i = \int S^{ij}\delta E_{ij}\,\mathrm{d}V_o = \delta\mathbf{p}_v^{\mathrm{T}}\int \mathbf{B}_{nl}^{\mathrm{T}}(\mathbf{p})\mathbf{S}\,\mathrm{d}V_o \tag{12.81}$$

from which the internal force vector is given by

$$\mathbf{q}_i = \int \mathbf{B}_{nl}^{\mathrm{T}}(\mathbf{p})\mathbf{S}\,\mathrm{d}V_o \tag{12.82}$$

where **S** contains the contravariant components of the second Piola–Kirchhoff stresses so that

$$\mathbf{S}^{\mathrm{T}} = (S^{11}, S^{22}, S^{12}) \tag{12.83}$$

For constant thickness, t, the element of volume $\mathrm{d}V_0$ in (12.82) is given by

$$\mathrm{d}V_0 = t(G_1 \times G_2)\mathrm{d}\xi\mathrm{d}\eta \tag{12.84}$$

12.6.2 The tangent stiffness matrix

Apart from the new definition of $\mathbf{B}_{nl}$ in (12.80) which includes the new **G** (now $\bar{\mathbf{G}}$) in (12.73), the new $\mathbf{A}(\theta)$ in (12.78) and the new **H** in (12.79), the working of Section 5.1.2 remains virtually unchanged so that (see (5.26) or(12.6)) the tangent stiffness matrix is

$$\mathbf{K}_t = \mathbf{K}_{t1} + \mathbf{K}_{t\sigma} = \int (\mathbf{B}_{nl}^{\mathrm{T}}(\mathbf{p})\mathbf{C}_t\mathbf{B}_{nl}(\mathbf{p}) + \bar{\mathbf{G}}^{\mathrm{T}}\hat{\mathbf{S}}\bar{\mathbf{G}})\mathrm{d}V_0 \tag{12.85}$$

However, the $\hat{\mathbf{S}}$ matrix now involves the contravariant components of the second Piola–Kirchhoff stresses so that (see (5.24) or (12.7)):

$$\hat{\mathbf{S}} = \begin{bmatrix} \begin{bmatrix} S^{11} & S^{12} \\ S^{12} & S^{22} \end{bmatrix} & \begin{bmatrix} 0 & 0 \\ 0 & 0 \end{bmatrix} \\ \begin{bmatrix} 0 & 0 \\ 0 & 0 \end{bmatrix} & \begin{bmatrix} S^{11} & S^{12} \\ S^{12} & S^{22} \end{bmatrix} \end{bmatrix} \tag{12.86}$$

12.6.3 Extension to three dimensions

The extension to three dimensions is straightforward and follows very closely the developments of Section 5.1.3. In particular, in (5.29) for $\boldsymbol{\theta}$ and (5.34) for $\mathbf{A}(\boldsymbol{\theta})$, we need simply replace x, y and z with ξ, η and ζ respectively. Also the **H** matrix is such that the linear strain vector, $\mathbf{E}_l$ is given by

$$E_l = \begin{bmatrix} E_{11} \\ E_{22} \\ E_{33} \\ 2E_{12} \\ 2E_{13} \\ 2E_{23} \end{bmatrix}_l = \mathbf{H}\boldsymbol{\theta}$$

$$= \begin{bmatrix} G_1(1) & 0 & 0 & G_1(2) & 0 & 0 & G_1(3) & 0 & 0 \\ 0 & G_2(1) & 0 & 0 & G_2(2) & 0 & 0 & G_2(3) & 0 \\ 0 & 0 & G_3(1) & 0 & 0 & G_3(2) & 0 & 0 & G_3(3) \\ G_2(1) & G_1(1) & 0 & G_2(2) & G_1(2) & 0 & G_2(3) & G_1(3) & 0 \\ G_3(1) & 0 & G_1(1) & G_3(2) & 0 & G_1(2) & G_3(3) & 0 & G_1(3) \\ 0 & G_3(1) & G_2(1) & 0 & G_3(2) & G_2(2) & 0 & G_3(3) & G_2(3) \end{bmatrix} \boldsymbol{\theta} \tag{12.87}$$

with the element of volume, dV_o being given by

$$dV_o = \mathbf{G}_1^T(\mathbf{G}_2 \times \mathbf{G}_3)d\xi d\eta d\zeta \tag{12.88}$$

For a linear isotropic material, the tangent and secant modular tensors are the same and, from (11.82a), are given by:

$$C^{ijkl} = \lambda(\mathbf{G}^i \cdot \mathbf{G}^j)(\mathbf{G}^k \cdot \mathbf{G}^l) + \mu((\mathbf{G}^i \cdot \mathbf{G}^k)(\mathbf{G}^j \cdot \mathbf{G}^l) + (\mathbf{G}^i \cdot \mathbf{G}^l)(\mathbf{G}^j \cdot \mathbf{G}^k)) \tag{12.89}$$

where to avoid clashes with the superscripts, we have temporarily reverted to the notation of Section 11 in using a dot to represent the inner product.

12.7 SPECIAL NOTATION

Scalars

$J = \det(\mathbf{F})$
V_o = initial volume
V_n = final volume
$\dot{V}_i$ = internal virtual power
μ = shear modulus
λ = Lamé constant
α^i = convected coordinate components

Vectors

$\mathbf{d}$ = displacements
$\mathbf{h}_\xi, \mathbf{h}_\eta$ = vectors containing derivatives with respect to ξ and η of shape-function vector, h.
$\mathbf{G}_i$ = covariant base vectors for initial configuration (Section 12.6)
$\mathbf{g}_i$ = covariant base vectors for final configuration (Section 12.6)
$\mathbf{p}$ = nodal displacements ($\dot{\mathbf{p}}$ = nodal velocities (or changes in dispalcement—$\delta\mathbf{p}$)
ordering for two-dimensional elements, $\mathbf{p}^T = (\mathbf{u}^T, \mathbf{v}^T)$
ordering for three-dimensional elements $\mathbf{p}^T = (\mathbf{u}^T, \mathbf{v}^T, \mathbf{w}^T)$
$\mathbf{u}$ = x-direction nodal displacements
$\mathbf{v}$ = y-direction nodal displacements
$\mathbf{w}$ = z-direction nodal displacements
$\mathbf{x}$ = current coordinates
$\mathbf{X}$ = initial coordinates
$\mathbf{v}$ = velocities
$\dot{\boldsymbol{\varepsilon}}$ = Eulerian strain rate (note $\dot{\boldsymbol{\varepsilon}}$ is not the rate of $\boldsymbol{\varepsilon}$)
$\boldsymbol{\theta}$ = vector of displacement derivatives (see (12.73))
$\dot{\boldsymbol{\theta}}$ = velocity derivatives in vector form (see (12.11))

Matrices and tensors

$\mathbf{A}(\boldsymbol{\theta})$ = matrix containing displacement derivatives (see (12.78))
$\mathbf{B}(\mathbf{x})$ = in Section 12.2–12.3, matrix (function of current co-ordinates, $\mathbf{x}$) connecting $\dot{\boldsymbol{\varepsilon}}$ to $\dot{\mathbf{p}}$
$\mathbf{C}$ = constitutive tensor

$\mathbf{E}$ = Green strain
$\mathbf{F}$ = deformation gradient
$\mathbf{G}$ = in Sections 12.2–12.3, matrix connecting $\dot{\boldsymbol{\theta}}$ to $\dot{\mathbf{p}}$ (see (12.11))
$\bar{\mathbf{G}}$ = in Section 12.6, matrix connecting $\boldsymbol{\theta}$ to $\mathbf{p}$ or $\delta\boldsymbol{\theta}$ ti $\delta\mathbf{p}$
$\mathbf{H}$ = in Sections 12.2–12.3, Boolean matrix (see (12.10))
$\mathbf{H}$ = in Section 12.6, matrix involving components of $\mathbf{G}$ (see (12.79))
$\mathbf{J}$ = Jacobian matrix (with respect to current configuration)
$\mathbf{L}$ = velocity gradient
$\mathbf{S}$ = second Piola–Kirchhoff stresses
$\hat{\mathbf{S}}$ = matrix containing contravariant components of $\mathbf{S}$
$\boldsymbol{\sigma}$ = Cauchy stresses
$\check{\boldsymbol{\sigma}}$ = matrix of Cauchy stresses (see (12.60) and (12.61))
$\dot{\boldsymbol{\varepsilon}}$ = Eulerian strain-rate (note $\dot{\boldsymbol{\varepsilon}}$ is not the rate of $\boldsymbol{\varepsilon}$)
$\boldsymbol{\tau}$ = Kirchhoff stresses
$\hat{\boldsymbol{\tau}}$ = matrix of Kirchhoff stresses (see (12.13))
$\dot{\boldsymbol{\Omega}}$ = spin (note, $\dot{\boldsymbol{\Omega}}$ is not the rate of $\boldsymbol{\Omega}$)

Subscripts

J = Jaumann
t = tangent
T = Truesdell
tJC = tangent for Jaumann rate of Cauchy stress
tTK = tangent for Truesdell rate of Kirchhoff stress
tJK = tangent for Jaumann rate of Kirchhoff stress
v = virtual

12.8 REFERENCES

[M1] McMeeking, R. M. & Rice, J. R., Finite-element formulations for problems of large elastic-plastic deformation, *Int. J. Solids & Structs.*, 601–616 (1975).

13 Large strains, hyperelasticity and rubber

13.1 INTRODUCTION TO HYPERELASTICITY

The theoretical analysis of hyperelastic or rubberlike materials has been investigated by many authors since the first half of the century (see Treloar [T1] and Mullins and Thomas [M3] for an overview of pioneering work in the field and [G2, F1] and for reviews). Important early work was due to Mooney [M2] and Rivlin [R1]. Another important development was due to Valanis and Landel [V1] who separated the strain energy function into a separable form relating to the principal directions. This approach led to the Ogden model [O1.10, O4, O5] which is much used today. Early finite element applications were due to Oden [O2, O3] who emphasised the difficulties associated with modelling 'incompressibility'. Other work in this area was due to Malkus and Hughes [M1] (see also Hughes [H3] and Zienkiewciz and Taylor [Z1]. Further work involving finite elements can be found in [D1, D3, D4, G1, H1, O1, P1, S1–S6, W1].

Hyperelasticity has already been briefly introduced in Section 4.12 and discussed in a little more detail in Section 10.3. In the present chapter, we will concentrate on materials for which the stresses are derivable from a scalar elastic potential. (There is a wider class of materials not necessarily restricted in this manner called 'Cauchy elastic materials' [D2].)

In Section 10.3, we introduced the simplest isotropic, linear, strain-energy function as (see (10.37))

$$\varphi = 2\mu \bar{I}_2 + \frac{\bar{\lambda}}{2} I_1^2 \tag{13.1}$$

where

$$I_1 = \mathrm{tr}(\boldsymbol{\varepsilon}) = \varepsilon_{ii} = \varepsilon_{11} + \varepsilon_{22} + \varepsilon_{33} \tag{13.2a}$$

$$\bar{I}_2 = \tfrac{1}{2}\,\mathrm{tr}(\boldsymbol{\varepsilon}^2) = \tfrac{1}{2}\varepsilon_{ij}\varepsilon_{ij} \tag{13.2b}$$

For a more general approach, with a view to invariance, we first note that the principal values of strain, ε_p, satisfy the eigenvalue relationship:

$$\boldsymbol{\varepsilon}\mathbf{z} = \varepsilon_p \mathbf{z} \tag{13.3}$$

where **z** are the directions of principal strain or eigenvectors of $\boldsymbol{\varepsilon}$. Non-trivial solutions to (13.3) only exist if

$$\det(\boldsymbol{\varepsilon} - \varepsilon_p \mathbf{I}) = 0 \tag{13.4}$$

The latter equation can be re-expressed as

$$\varepsilon_p^3 - I_1 \varepsilon_p^2 + I_2 \varepsilon_p - I_3 = 0 \tag{13.5}$$

where I_1 has been given in (13.2a) and

$$I_2 = \varepsilon_{11}\varepsilon_{22} + \varepsilon_{22}\varepsilon_{33} + \varepsilon_{11}\varepsilon_{33} - \varepsilon_{12}^2 - \varepsilon_{23}^2 - \varepsilon_{13}^2 = \tfrac{1}{2}(\mathrm{tr}(\boldsymbol{\varepsilon})^2 - \mathrm{tr}(\boldsymbol{\varepsilon}^2))$$
$$= \tfrac{1}{2} I_1^2 - \bar{I}_2 \tag{13.6a}$$

$$I_3 = \det(\boldsymbol{\varepsilon}) \tag{13.6b}$$

Using these invariants, it is possible to construct a range of higher-order material models [D2]. However, if we wish to consider materials for which the strains are large (i.e. rubber) we know, from the work of Chapter 2, that we must define the type of stress and strain measure that we are using. Indeed, this observation applies even if the rotations are large and the strains are small. We have shown at the end of the Section 4.4 that, if the standard linear, engineering strain measures are adopted, strains are produced as a result of a rigid-body rotation. In these circumstances, the strain invariants would also be non-zero and hence if the energy function, φ, was related to these invariants we would incorrectly accumulate strain energy as a result of a rigid-body rotation.

For the remainder of this chapter, we will assume that we are working with an isotropic material. In these circumstances, from the work of Section 10.1, it is best to start with the principal stretch ratios.

13.2 USING THE PRINCIPAL STRETCH RATIOS

The principal stretch ratios (λ_1–λ_3) are clearly invariant with respect to both the coordinate system and the strain measure. Hence, we can produce strain energy functions for isotropic materials by using the principal stretch ratios (λ_1–λ_3) and by ensuring that:

1. The energy function, φ is zero for the 'ground state', $\lambda_1 = \lambda_2 = \lambda_3 = 1$;
2. The energy function is symmetric in λ_1–λ_3;
3. The energy function is always $\geqslant 0$. (13.7)

However, from the discussions of Section 4.8, it is easier to compute the right Cauchy–Green tensor **C**:

$$\mathbf{C} = \mathbf{F}^T\mathbf{F} \tag{13.8}$$

or the left Cauchy–Green tensor, **b**:

$$\mathbf{b} = \mathbf{F}\mathbf{F}^T \tag{13.9}$$

which have eigenvalues of λ_1^2–λ_3^2, rather than the stretches **U** or **V**. Hence, work in hyperelasticity has often involved the principal invariants of **C** and **b**. (Note, that in this

chapter, having used **C** for the right Cauchy–Green tensor, we will use **D** for the constitutive tensor.)

Following a similar procedure to that in the previous section, we note that non-trivial solutions to (4.136) and (4.144) only exist if

$$\det[\mathbf{C} - \lambda_p^2 \mathbf{I}] = \det[\mathbf{b} - \lambda_p^2 \mathbf{I}] = 0 \tag{13.10}$$

which can be re-expressed as

$$\lambda_p^6 - I_1 \lambda_p^4 + \lambda_p^2 I_2 - I_3 = 0 \tag{13.11}$$

where the invariants of **C** and **b** are given by

$$I_1 = \lambda_1^2 + \lambda_2^2 + \lambda_3^2 = C_{11} + C_{22} + C_{33} = \mathrm{tr}(\mathbf{C}) = \mathbf{I}:\mathbf{C} = \mathrm{tr}(\mathbf{b}) = \mathbf{I}:\mathbf{b} \tag{13.12a}$$

$$\begin{aligned} I_2 &= \lambda_2^2\lambda_3^2 + \lambda_3^2\lambda_1^2 + \lambda_1^2\lambda_2^2 \\ &= C_{11}C_{22} + C_{22}C_{33} + C_{33}C_{11} - C_{12}C_{21} - C_{23}C_{32} - C_{13}C_{31} \\ &= \tfrac{1}{2}(I_1^2 - \mathrm{tr}(\mathbf{C}^2)) = \tfrac{1}{2}(I_1^2 - \mathrm{tr}(\mathbf{b}^2)) \end{aligned} \tag{13.12b}$$

$$\begin{aligned} I_3 &= \lambda_1^2\lambda_2^2\lambda_3^2 \\ &= C_{11}C_{22}C_{33} + 2C_{12}C_{23}C_{13} - C_{11}C_{23}C_{32} - C_{22}C_{13}C_{31} - C_{33}C_{12}C_{21} \\ &= J^2 = \det(\mathbf{C}) = \tfrac{1}{3}(\mathrm{tr}(\mathbf{C}^3) - I_1\mathrm{tr}(\mathbf{C}^2) - I_2\mathrm{tr}\,\mathbf{C}) = \det(\mathbf{b}) \end{aligned} \tag{13.12c}$$

where, from (4.96):

$$J = \det(\mathbf{F}) = I_3^{1/2} \tag{13.12d}$$

The invariants used here and for the remainder of the chapter are given by (13.12) and differ from those used in the previous section. It can be seen from the final forms in (13.12) that I_1–I_3 can be computed without the direct computation of λ_1–λ_3.

When the body is unloaded, λ_1–λ_3 are each unity and hence the initial values of the invariants I_1–I_3 are 3, 3 and 1 respectively. Hence a strain energy function that satisfies (13.7) is

$$\varphi = \sum_{p,q,r=0}^{\infty} C_{pqr}(I_1 - 3)^p(I_2 - 3)^q(I_3 - 1)^r: \qquad \text{with } C_{000} = 0 \tag{13.13}$$

For incompressible materials, $J = \det(\mathbf{F}) = \lambda_1\lambda_2\lambda_3 = 1$ (see (10.59)) and hence, from (13.12c), $I_3 = 1$. Consequently, (13.13) becomes

$$\varphi = \sum_{p,q=0}^{\infty} C_{pq}(I_1 - 3)^p(I_2 - 3)^q: \qquad \text{with } C_{00} = 0 \tag{13.14}$$

Special truncated forms of (13.13), which are much used in the analysis of rubber are the Mooney–Rivlin function (valid for strains up to about 100%):

$$\varphi = C_{10}(I_1 - 3) + C_{01}(I_2 - 3) = C_1(I_1 - 3) + C_2(I_2 - 3) \tag{13.15}$$

and the simpler 'neo-Hookean' function (valid for strains up to about 30%):

$$\varphi = C_{10}(I_1 - 3) = C_1(I_1 - 3) \tag{13.16}$$

Unfortunately, pure incompressibility leads to severe numerical difficulties (except for conditions of plane stress—see Section 13.4.2). In any event, rubber is to some extent

compressible and it can be important to consider this compressibility. Hence, in the following, we will generally work with the compressible form and introduce a strain energy contribution involving the bulk modulus, K. The incompressible form can be recovered by letting K tend to infinity.

The mean value theorem can be used to show [F2] that functions of the form:

$$F(a,b,c) = a + b + c - 3(abc)^{1/3} \tag{13.17}$$

are positive unless $a = b = c$. Hence with $a = \lambda_1^r$, $b = \lambda_2^r$, etc., we can devise functions of the form:

$$\varphi_r/c = \lambda_1^r + \lambda_2^r + \lambda_3^r - 3(\lambda_1\lambda_2\lambda_3)^{r/3} \tag{13.18}$$

so that with $r = 2$, we obtain:

$$\varphi/c = \lambda_1^2 + \lambda_2^2 + \lambda_3^2 - 3(\lambda_1\lambda_2\lambda_3)^{2/3} = I_1 - 3I_3^{1/3} \tag{13.19}$$

which is the compressible form of the neo-Hookean form of (13.16). By combining $r = 2$ with $r = -2$, we can obtain:

$$\varphi = c_1\varphi_2 + c_2'\varphi_{-2} = c_1(I_1 - 3I_3^{1/3}) + c_2'\left(\frac{I_2}{I_3} - 3I_3^{-1/3}\right)$$

$$= c_1(I_1 - 3I_3^{1/3}) + c_2(I_2 - 3I_3^{2/3}) \tag{13.20}$$

which can be considered as a compressible form of the Mooney–Rivlin relationship of (13.15). Both (13.19) and (13.20) have the drawback of being zero at $\lambda_1 = \lambda_2 = \lambda_3$. To overcome this difficulty, we may add a compressible term, φ_b, involving the bulk modulus, K (see Section 4.2.2) so that

$$\varphi_b = K[\log_e(\lambda_1\lambda_2\lambda_3)]^2/2 = K[\log_e J]^2/2 \tag{13.21a}$$

or

$$\varphi_b = K(J-1)^2/2 \tag{13.21b}$$

which are each zero for the initial conditions when $J = 1$. In most of the following we will adopt (13.21b), but (13.21a) will sometimes be used instead.

13.3 SPLITTING THE VOLUMETRIC AND DEVIATORIC TERMS

A convenient way to split the volumetric and deviatoric terms is to define modified stretches:

$$\bar{\lambda} = J^{-1/3}\lambda \tag{13.22}$$

which are such that

$$\bar{J} = \bar{\lambda}_1\bar{\lambda}_2\bar{\lambda}_3 = 1 \tag{13.23}$$

Hence these modified stretches are 'volume preserving'. In Section 13.8 and 13.10, we will work directly with the stretches, while in the present section we will work with the

invariants. From the work of Sections 4.8 and 10.1, it follows that:

$$\bar{\mathbf{F}} = J^{-1/3}\mathbf{F} = I_3^{-1/6}\mathbf{F} \tag{13.24a}$$

$$\bar{\mathbf{C}} = \bar{\mathbf{F}}^{\mathrm{T}}\bar{\mathbf{F}} = J^{-2/3}\mathbf{C} = I_3^{-1/3}\mathbf{C} \tag{13.24b}$$

$$\bar{\mathbf{b}} = \bar{\mathbf{F}}\bar{\mathbf{F}}^{\mathrm{T}} = J^{-2/3}\mathbf{b} = I_3^{-1/3}\mathbf{b} \tag{13.24c}$$

while, from (13.12),

$$\bar{I}_1 = I_1 I_3^{-1/3} = I_1 J^{-2/3} \tag{13.25a}$$

$$\bar{I}_2 = I_2 I_3^{-2/3} = I_2 J^{-4/3} \tag{13.25b}$$

Hence, using these modified invariants, with φ_{b} from (13.21b) and adapting φ_{d} (deviatoric) from (13.20), the modified Mooney–Rivlin function might involve

$$\varphi = \varphi_{\mathrm{d}} + \varphi_{\mathrm{b}} = C_1(\bar{I}_1 - 3) + C_2(\bar{I}_2 - 3) + \tfrac{1}{2}K(J-1)^2 \tag{13.26}$$

For a pure uniform pressure (with $\lambda_1 = \lambda_2 = \lambda_3$), $\bar{I}_1$ and $\bar{I}_2$ are each equal to 3 so that $\varphi = \varphi_{\mathrm{b}}$.

In Sections 13.5 and 13.7, we will develop finite element formulations based on (13.26). The neo-Hookean law can be considered as a special case with $C_2 = 0$.

13.4 DEVELOPMENT USING SECOND PIOLA–KIRCHHOFF STRESSES AND GREEN'S STRAINS

Because (see (4.74)), the Green strain, $\mathbf{E}$, is given by $\frac{1}{2}(\mathbf{C} - \mathbf{I})$, using equation (13.26), the stress–strain relationship can easily be computed using:

$$\mathbf{S} = \frac{\partial \varphi}{\partial \mathbf{E}} = 2\frac{\partial \varphi}{\partial \mathbf{C}} = 2\left(A_1\frac{\partial I_1}{\partial \mathbf{C}} + A_2\frac{\partial I_2}{\partial \mathbf{C}} + A_3\frac{\partial I_3}{\partial \mathbf{C}}\right) = \frac{\partial \varphi_{\mathrm{d}}}{\partial \mathbf{C}} + \frac{\partial \varphi_{\mathrm{b}}}{\partial \mathbf{C}} \tag{13.27}$$

where

$$A_1 = C_1 I_3^{-1/3}$$

$$A_2 = C_2 I_3^{-2/3}$$

$$A_3 = -\tfrac{1}{3}C_1 I_3^{-4/3} I_1 - \tfrac{2}{3}C_2 I_3^{-5/3} I_2 + K\frac{(J-1)}{2J} \tag{13.28}$$

and we can obtain $\partial I_1/\partial \mathbf{C}$, $\partial I_2/\partial \mathbf{C}$ and $\partial I_3/\partial \mathbf{C}$ from (13.12) via:

$$\delta I_1 = \frac{\partial I_1}{\partial \mathbf{C}} : \delta \mathbf{C} = \mathbf{I} : \delta \mathbf{C} = \mathrm{tr}(\delta \mathbf{C})$$

$$\delta I_2 = \frac{\partial I_2}{\partial \mathbf{C}} : \delta \mathbf{C} = (I_1 \mathbf{I} - \mathbf{C}) : \delta \mathbf{C}$$

$$\delta I_3 = \frac{\partial I_3}{\partial \mathbf{C}} : \delta \mathbf{C} = I_3 \mathbf{C}^{-1} : \delta \mathbf{C} = J^2 \mathbf{C}^{-1} : \delta \mathbf{C} \tag{13.29}$$

Under pure uniform pressure, with $\lambda_1 = \lambda_2 = \lambda_3 = \lambda$, we have

$$I_1 = 3\lambda^2; \qquad I_2 = 3\lambda^4; \qquad I_3 = \lambda^6; \qquad J = \lambda^3 \tag{13.30a}$$

$$\mathbf{C} = \mathbf{F}^{\mathrm{T}}\mathbf{F} = \lambda^2\mathbf{I}; \qquad \mathbf{C}^{-1} = \lambda^{-2}\mathbf{I} \tag{13.30b}$$

and, it follows from (13.27) to (13.29) that, in these circumstances:

$$\mathbf{S} = KJ(J-1)\mathbf{C}^{-1} = K(J-1)\lambda\mathbf{I} \tag{13.31}$$

Transforming to a Cauchy stress, via (4.121) (or (10.50)) gives:

$$\boldsymbol{\sigma} = \frac{1}{J}\mathbf{F}(KJ(J-1)\mathbf{C}^{-1})\mathbf{F}^{\mathrm{T}} = K(J-1)\mathbf{I} = K\frac{\mathrm{d}V - \mathrm{d}V_{\mathrm{o}}}{\mathrm{d}V_{\mathrm{o}}}\mathbf{I} = -p\mathbf{I} \tag{13.32}$$

where p is the pressure (positive for compression). It follows that

$$p = -K(J-1) \tag{13.33}$$

Substituting from (13.29) and (13.33) into (13.28) and (13.27) gives:

$$\mathbf{S} = (B_1\mathbf{I} + B_2\mathbf{C} + B_3\mathbf{C}^{-1}) - pI_3^{1/2}\mathbf{C}^{-1} = \frac{\partial\varphi_{\mathrm{d}}}{\partial\mathbf{E}} + \frac{\partial\varphi_{\mathrm{b}}}{\partial\mathbf{E}} \tag{13.34}$$

where

$$\begin{aligned} B_1 &= 2C_1I_3^{-1/3} + 2C_2I_3^{-2/3}I_1 \\ B_2 &= -2C_2I_3^{-2/3} \\ B_3 &= -\tfrac{2}{3}C_1I_3^{-1/3}I_1 - \tfrac{4}{3}C_2I_3^{-2/3}I_2 \end{aligned} \tag{13.34a}$$

Given the strain energy function, φ (via the three material constants, C_1, C_2 and K—which would be obtained from experimental results), we can now, via (13.34), obtain the second Piola–Kirchhoff stresses, $\mathbf{S}$ from the Green strains $\mathbf{E} = \frac{1}{2}(\mathbf{C} - \mathbf{I})$. For the neo-Hookean model, with $C_2 = 0$ and $2C_1 = \mu$, (13.34a) becomes

$$\mathbf{S} = \mu J^{-2/3}[\mathbf{I} - \tfrac{1}{3}I_1\mathbf{C}^{-1}] - pJ\mathbf{C}^{-1} = \mu\,\mathrm{dev}(\bar{\mathbf{C}})\mathbf{C}^{-1} - pJ\mathbf{C}^{-1} \tag{13.35}$$

with $\bar{\mathbf{C}}$ from (13.24b).

If we were to work with a genuinely incompressible material (with $J = I_3 = 1$), we could use the simpler energy function of (13.15) to obtain $\mathbf{S} = 2\partial\varphi/\partial\mathbf{C}$ and then add the pressure contribution $-p\mathbf{C}^{-1}$ (see (13.35)). The latter can only be obtained by considering the kinematics. In the following, it can be obtained by treating 'nodal' p's as Lagrangian multipliers or, effectively, letting K tend to infinity in the following compressible formulation. In this approach, we will often keep the pressure as a separate variable and in Section 13.5, we will describe the resulting finite element procedure. However, in some circumstances (see Sections 18.12 and 18.13), it is possible to work directly with a pure displacement-based formulation. It is a simple matter to modify the following 'split equations' to avoid the separate treatment of the pressure.

In a conventional total Lagrangian finite element formulation, we could now obtain the internal force vector. However, to find the tangent stiffness matrix, we require the differentiation of (13.35) whereby, using (13.29), we obtain:

$$\delta\mathbf{S} = D_1\mathbf{I} + D_2\mathbf{C} + D_3\mathbf{C}^{-1} + D_4\delta\mathbf{C} + D_5(\mathbf{C}^{-1}\delta\mathbf{C}\mathbf{C}^{-\mathrm{T}}) - I_3^{1/2}\mathbf{C}^{-1}\delta p \tag{13.36}$$

with

$$
\begin{aligned}
D_1 &= -\tfrac{2}{3}C_1 I_3^{-1/3}(\mathbf{C}^{-1}{:}\delta\mathbf{C}) + 2C_2 I_3^{-2/3} I_1(\mathbf{I}{:}\delta\mathbf{C}) - \tfrac{4}{3}C_2 I_3^{-2/3} I_1(\mathbf{C}^{-1}{:}\delta\mathbf{C}) \\
D_2 &= \tfrac{4}{3}C_2 I_3^{-2/3}(\mathbf{C}^{-1}{:}\delta\mathbf{C}) \\
D_3 &= -\tfrac{2}{3}C_1 I_3^{-1/3}(\mathbf{I}{:}\delta\mathbf{C}) + \tfrac{2}{9}C_1 I_3^{-1/3} I_1(\mathbf{C}^{-1}{:}\delta\mathbf{C}) \\
&\quad + \tfrac{8}{9}C_2 I_3^{-2/3} I_2(\mathbf{C}^{-1}{:}\delta\mathbf{C}) - \tfrac{4}{3}C_2 I_3^{-2/3}(I_1(\mathbf{I}{:}\delta\mathbf{C}) - (\mathbf{C}^{-1}{:}\delta\mathbf{C})) \\
&\quad - \tfrac{1}{2}pI_3^{1/2}(\mathbf{C}^{-1}{:}\delta\mathbf{C}) \\
D_4 &= -2C_2 I_3^{-2/3} \\
D_5 &= \tfrac{2}{3}C_1 I_3^{-1/3} I_1 + \tfrac{4}{3}C_2 I_3^{-2/3} I_2 + pI_3^{1/2}
\end{aligned}
\tag{13.37}
$$

It will be shown that (13.36) can be re-expressed as

$$
\delta\mathbf{S} = \mathbf{D}_{\mathrm{tK2}}{:}\delta\mathbf{E} + \mathbf{G}_{\mathrm{tK2}}\delta p \tag{13.38}
$$

where $\mathbf{D}_{\mathrm{tK2}}$ is a fourth-order constitutive tensor and $\mathbf{G}_{\mathrm{tK2}}$ is a second-order constitutive tensor. The subscript K2 shows that the tensors relate to the second Piola–Kirchhoff stresses (and Green strains). To devise expressions for the constitutive tensor, it is best to apply suffix notation to (13.36)–(13.37) and obtain:

$$
\delta S_{ij} = D^{\mathrm{tK2}}_{ijkl}\delta E_{kl} + G^{\mathrm{tK2}}_{ij}\delta p \tag{13.39}
$$

where the use of superscripts for the tK2 in (13.39) in place of the subscripts in (13.38) is purely for space considerations. The tensor components in (13.39) are given by

$$
\begin{aligned}
D^{\mathrm{tK2}}_{ijkl} &= F_1 C^{-1}_{ij} C^{-1}_{kl} + F_2(\delta_{ij} C^{-1}_{kl} + C^{-1}_{ij}\delta_{kl}) \\
&\quad + F_3(C^{-1}_{ik} C^{-1}_{jl} + C^{-1}_{il} C^{-1}_{jk}) + F_4\delta_{ij}\delta_{kl} + F_5(\delta_{ik}\delta_{jl} + \delta_{il}\delta_{jk}) \\
&\quad + F_6(C_{ij} C^{-1}_{kl} + C^{-1}_{ij} C_{kl})
\end{aligned}
\tag{13.40}
$$

where a term such as C^{-1}_{ij} is the ijth component of $\mathbf{C}^{-1}$ not $1/C_{ij}$, but is written as C^{-1}_{ij} to save space. The coefficients in (13.40) are given by

$$
\begin{aligned}
F_1 &= \tfrac{4}{9}C_1 I_3^{-1/3} I_1 + \tfrac{16}{9}C_2 I_3^{-2/3} I_2 - pI_3^{1/2} \\
F_2 &= -\tfrac{4}{9}C_1 I_3^{-1/3} - \tfrac{8}{3}C_2 I_3^{-2/3} I_1 \\
F_3 &= \tfrac{2}{3}C_1 I_3^{-1/3} I_1 + \tfrac{4}{3}C_2 I_3^{-2/3} I_2 + pI_3^{1/2} \\
F_4 &= 4C_2 I_3^{-2/3} \\
F_5 &= -2C_2 I_3^{-2/3} \\
F_6 &= \tfrac{8}{3}C_2 I_3^{-2/3}
\end{aligned}
\tag{13.41}
$$

while (see (13.38) and (13.39) the pressure connection term is

$$
\mathbf{G}_{\mathrm{tK2}} = -I_3^{-1/2}\frac{\partial I_3}{\partial \mathbf{C}}; \qquad G^{\mathrm{tK2}}_{ij} = -I_3^{1/2} C^{-1}_{ij} \tag{13.42}
$$

Equation (13.39) has been aimed at a finite element formulation in which the displacements and pressure variables are separate. Without such a separation, we can modify (13.39) to directly relate δS_{ij} to δE_{ij} by first obtaining δp from (13.33) as

$$
\delta p = -KJ\mathbf{C}^{-1}{:}\delta\mathbf{E} \tag{13.43}
$$

where use has been made of (13.29). Substitution of (13.43) into (13.38) and (13.42) shows that the tangent coefficients (D_{ijkl}) of (13.40) would, in these circumstances be

enhanced by the terms

$$KJ^2C_{ij}^{-1}C_{kl}^{-1}$$

13.4.1 Plane strain

Many of the previous formulae simplify considerably for the special case of plane strain. In these circumstances, we have:

$$C_{33} = \lambda_3 = 1; \qquad C_{13} = C_{31} = C_{23} = C_{32} = 0 \tag{13.44a}$$

so that:

$$\mathbf{C} = \begin{bmatrix} C_{11} & C_{12} & 0 \\ C_{21} & C_{22} & 0 \\ 0 & 0 & 1 \end{bmatrix} \tag{13.44b}$$

and

$$\begin{aligned} I_1 &= 1 + \lambda_1^2 + \lambda_2^2 = 1 + C_{11} + C_{22} \\ I_2 &= \lambda_1^2 + \lambda_2^2 + \lambda_1^2\lambda_2^2 = C_{11}C_{22} + C_{11}^2 + C_{22}^2 - C_{12}^2 \\ I_3 &= \lambda_1^2\lambda_2^2 = C_{11}C_{22} - C_{12}^2 \end{aligned} \tag{13.45}$$

while

$$\mathbf{C}^{-1} = \frac{1}{I_3}\begin{bmatrix} C_{22} & -C_{21} & 0 \\ -C_{12} & C_{11} & 0 \\ 0 & 0 & I_3 \end{bmatrix} \tag{13.46}$$

13.4.2 Plane stress with incompressibility

For states of plane stress, the incompressibility condition does not impose any significant difficulties and we can set:

$$J = \lambda_1\lambda_2\lambda_3 = I_3 = \lambda_1^2\lambda_2^2\lambda_3^2 = 1 \tag{13.47}$$

We can now use (13.47) to eliminate λ_3 and directly use the deviatoric energy function, φ_d. However, this is not obvious and so we will first keep all three stretches as well as the pressure term, p. Because of (13.47), $\bar{I}_1 = I_1$, $\bar{I}_2 = I_2$ and from (13.26), we can write the deviatoric Mooney–Rivlin function as

$$\varphi_d = C_1(\lambda_1^2 + \lambda_2^2 + \lambda_3^2 - 3) + C_2\left(\frac{1}{\lambda_1^2} + \frac{1}{\lambda_2^2} + \frac{1}{\lambda_3^2} - 3\right) \tag{13.48}$$

From (13.47) and (13.34),

$$\mathbf{S} = \frac{\partial\varphi_d}{\partial\mathbf{E}} - p\mathbf{C}^{-1} = 2\frac{\partial\varphi_d}{\partial\mathbf{C}} - p\mathbf{C}^{-1} \tag{13.49}$$

Working in the principal directions so that $\mathbf{F} = \mathbf{Diag}(\lambda)$, $\mathbf{C} = \mathbf{Diag}(\lambda^2)$ and using the

relationship:

$$E_i = \tfrac{1}{2}(\lambda_i^2 - 1) \tag{13.50}$$

we can use (13.48)–(13.50) to obtain:

$$S_i = \frac{\partial \varphi_d}{\partial \lambda_i}\frac{\partial \lambda_i}{\partial E_i} - \frac{1}{\lambda_i^2}p = \frac{1}{\lambda_i}\frac{\partial \varphi_d}{\partial \lambda_i} - \frac{1}{\lambda_i^2}p = \frac{1}{\lambda_i}(2C_1\lambda_i - 2C_2\lambda_i^3) - \frac{1}{\lambda_i^2}p \tag{13.51}$$

With a view to eliminating p via the plane stress hypothesis, we can use $\boldsymbol{\sigma} = \mathbf{F}\mathbf{S}\mathbf{F}^{\mathrm{T}}$ (with $J = 1$) to change (13.51) to give:

$$\sigma_i = \lambda_i \frac{\partial \varphi_d}{\partial \lambda_i} - p = \lambda_i(2C_1\lambda_i - 2C_2\lambda_i^3) - p \tag{13.52}$$

from which, via $\sigma_3 = 0$, we can obtain:

$$p = \lambda_3(2C_1\lambda_3 - 2C_2\lambda_3^{-3}) = \frac{2C_1}{\lambda_1^2\lambda_2^2} - 2C_2\lambda_1^2\lambda_2^2 \tag{13.53}$$

where, for the last relationship in (13.53), we have used the incompressibility condition of (13.47). We can now substitute from this last expression in (13.53) into (13.52) for $i = 1, 2$ and can also use (13.47) to obtain:

$$S_1 = 2C_1(1 - \lambda_1^{-4}\lambda_2^{-2}) + 2C_2(-\lambda_1^{-4} + \lambda_2^2) \tag{13.54a}$$

$$S_2 = 2C_1(1 - \lambda_2^{-4}\lambda_1^{-2}) + 2C_2(-\lambda_2^{-4} + \lambda_1^2) \tag{13.54b}$$

If we directly incorporated the incompressibility condition of (13.47) into (13.48), we would obtain:

$$\varphi(\lambda_1, \lambda_2) = C_1\left(\lambda_1^2 + \lambda_2^2 + \frac{1}{\lambda_1^2\lambda_2^2} - 3\right) + C_2\left(\frac{1}{\lambda_1^2} + \frac{1}{\lambda_2^2} + \lambda_1^2\lambda_2^2 - 3\right) \tag{13.55}$$

If we now use (13.50) and (13.55) to obtain:

$$S_i = \frac{\partial \varphi(\lambda_1, \lambda_2)}{\partial \lambda_i}\frac{\partial \lambda_i}{\partial E_i} \tag{13.56}$$

we recover (13.54) without directly considering the pressure term.

From (13.54), the tangential constitutive relationships can be obtained as

$$\begin{pmatrix} \dot{S}_1 \\ \dot{S}_2 \end{pmatrix} = \begin{bmatrix} D_{11} & D_{12} \\ D_{21} & D_{22} \end{bmatrix}\begin{pmatrix} \dot{E}_1 \\ \dot{E}_2 \end{pmatrix} \tag{13.57}$$

where

$$D_{11} = \frac{\partial S_1}{\partial E_1} = \frac{\partial S_1}{\partial \lambda_1}\frac{\partial \lambda_1}{\partial E_1} = 8\lambda_1^{-6}(C_1\lambda_2^{-2} + C_2)$$

$$D_{21} = D_{12} = \frac{\partial S_1}{\partial E_2} = \frac{\partial S_1}{\partial \lambda_2}\frac{\partial \lambda_2}{\partial E_2} = 4(C_1\lambda_1^{-4}\lambda_2^{-4} + C_2) \tag{13.58}$$

with a similar relationship to D_{11} for D_{22}.

Equations (13.57) suffice if the principal directions do not change. Such a situation occurs for an axisymmetric membrane for which a total Lagrangian finite element

formulation was discussed in Section 5.1.4. An instructive computer exercise involves modifying that formulation to allow for a Mooney–Rivlin material by incorporating (13.54) for the second Piola–Kirchhoff stresses and (13.57) and (13.58) for the tangential modular matrix. The procedure can also be easily extended [W1] to account for the Ogden material model that will be discussed in Section 13.10.2.

If the principal directions do change (as with a general plane-stress membrane [G3]), one can adopt a method that will be discussed in Section 13.8. Alternatively, one could use (13.35) for **S** with p from (13.53) with the differential giving the tangential modular matrix. In this case, we also have:

$$D_{13} = D_{31} = D_{23} = D_{32} = 0 \tag{13.59a}$$

$$\lambda_3^2 = C_{33} = \lambda_1^{-2}\lambda_2^{-2} = (D_{11}D_{22} - D_{12}^2)^{-1} \tag{13.59b}$$

while in (13.12):

$$I_1 = \lambda_1^2 + \lambda_2^2 + \lambda_1^{-2}\lambda_2^{-2} = D_{11} + D_{22} + (D_{11}D_{22} - D_{12}^2)^{-1} \tag{13.60a}$$

$$\begin{aligned} I_2 &= \lambda_1^{-2} + \lambda_2^{-2} + \lambda_1^2\lambda_2^2 \\ &= D_{11}D_{22} - D_{12}^2 + (D_{11} + D_{22})(D_{11}D_{22} - D_{12}^2)^{-1} \end{aligned} \tag{13.60b}$$

13.5 TOTAL LAGRANGIAN FINITE ELEMENT FORMULATION

We have now established both total ((13.34) and (13.35)) and tangential ((13.38)–(13.42)) stress/strain laws using the second Piola–Kirchhoff stress and the Green strain. Hence, with one reservation, we can simply insert these into a total Lagrangian formulation using the procedure described in Section 5.1 of Chapter 5. The reservation relates to the pressure and the difficulty of satisfying (13.33) as the bulk modulus, K, becomes large. The linear form of (13.33) is

$$p = -K\left(\frac{\partial u}{\partial x} + \frac{\partial v}{\partial y} + \frac{\partial w}{\partial z}\right) \tag{13.61}$$

from which one can conclude that the pressure p should take a lower variation than the displacements u, v and w (see also [H3, Z1]). For this reason, in the previous developments, we have kept the pressure term separate so that we can introduce separate pressure variables into the finite element formulation. This leads naturally to two of the methods that are advocated for dealing with the 'incompressibility problem'. Both 'near incompressibility' and 'effective incompressibility' need to be considered. For the latter, we can simply give the bulk modulus, K, a high number so that we obtain a form of penalty procedure to enforce the incompressibility condition. Alternatively, the pressure variables can be considered to act as a Lagrange multipliers to enforce the incompressibility condition. In some circumstances (Section 18.12 and 18.13), it is possible to work directly with a displacement formulation. The following developments can easily be modified to relate to this simpler formulation.

13.5.1 A mixed formulation

We will first consider a mixed formulation with displacements and pressures as variables at the structural level. To this end, we adopt different shape functions for the displacement and pressure variables with the latter taking a lower order variation. The precise form of the shape functions will be discussed later, but with $h_p \neq h$, we can write

$$p = \sum h_{pi} p_i; \qquad u = \sum h_i u_i; \qquad v = \sum h_i v_i; \qquad w = \sum h_i w_i \tag{13.62}$$

where collectively p_i become the nodal pressure variables, $\boldsymbol{p}$ and u_i, v_i and w_i become the nodal displacement variables, $\mathbf{p}$. The first equation of (13.62) can be rewritten as

$$p = \mathbf{h}_p^{\mathrm{T}} \boldsymbol{p}; \qquad \delta p = \mathbf{h}_p^{\mathrm{T}} \delta \boldsymbol{p} \tag{13.63}$$

where the second form (for δp and $\delta \boldsymbol{p}$) follows the first (total form) because the pressure shape functions, $\mathbf{h}_p$, are functions of the initial geometry.

Using identical procedures to those of Chapter 5, the virtual Green strains can be expressed as

$$\delta \mathbf{E}_{\mathrm{v}} = \mathbf{B}_{nl}(\boldsymbol{p}) \delta \mathbf{p}_{\mathrm{v}} \tag{13.64}$$

where we are now adopting vector and matrix notation (see Chapter 5) so that $\delta \mathbf{E}_{\mathrm{v}}$ is a vector and $\mathbf{B}_{nl}$ is a matrix. Again using the procedures of Chapter 5, virtual work can be used to find the out-of-balance force vector, $\mathbf{g}$ where

$$\mathbf{g} = \mathbf{q}_{\mathrm{i}} - \mathbf{q}_{\mathrm{e}} = \int B_{nl}^{\mathrm{T}} \mathbf{S} \, \mathrm{d}V_{\mathrm{o}} - \mathbf{q}_{\mathrm{e}} \tag{13.65}$$

with $\mathbf{S}$ as the second Piola–Kirchhoff stresses, $\mathbf{q}_{\mathrm{i}}$ the internal forces and $\mathbf{q}_{\mathrm{e}}$ the external forces (In this chapter, these will be considered to be of a non-follower type although for many hyperelastic problems we require follower forces. The latter are considered in Section 17.5 of Chapter 17.)

Assuming exact equilibrium from a previous increment, $\mathbf{g} = \mathbf{0}$ and differentiation of (13.65) leads to

$$\delta \mathbf{q}_{\mathrm{e}} = \delta \mathbf{q}_{\mathrm{i}} = \int \mathbf{B}_{nl}^{\mathrm{T}} \delta \mathbf{S} \, \mathrm{d}V_{\mathrm{o}} + \int \delta \mathbf{B}_{nl}^{\mathrm{T}} \mathbf{S} \, \mathrm{d}V_{\mathrm{o}} \tag{13.66}$$

To proceed further, we require the matrix and vector equivalent of (13.38) which we can write as

$$\delta \mathbf{S} = \mathbf{D}_{\mathrm{t}K2} \delta \mathbf{E} + \mathbf{g}_{\mathrm{t}K2} \delta p \tag{13.67}$$

where $\mathbf{D}_{\mathrm{t}K2}$ is a matrix and $\mathbf{g}_{\mathrm{t}K2}$ a (column) vector. Substitution from (13.67) for $\delta \mathbf{S}$ into (13.66) (and the application of the techniques of Section 5.1.2 for the second term in (13.66) which gives the 'geometric' stiffness matrix, $\mathbf{K}_{\mathrm{t}\sigma}$), then leads to

$$\delta \mathbf{q}_{\mathrm{e}} = \frac{\partial \mathbf{q}_{\mathrm{i}}}{\partial \mathbf{p}} \delta \mathbf{p} = \mathbf{K}_{\mathrm{t}} \delta \mathbf{p} + \mathbf{a} \tag{13.68}$$

where

$$\mathbf{K}_{\mathrm{t}} = \frac{\partial \mathbf{q}_{\mathrm{i}}}{\partial p} = \frac{\partial \mathbf{G}}{\partial p} = \int \mathbf{B}_{nl}^{\mathrm{T}} \mathbf{D}_{\mathrm{t}K2} \mathbf{B}_{nl} \, \mathrm{d}V_{\mathrm{o}} + \mathbf{K}_{\mathrm{t}\sigma} \tag{13.69}$$

with (5.26) for $\mathbf{K}_{t\sigma}$. The load/pressure variable coupling vector, $\mathbf{a}$ in (13.68) is given by

$$\mathbf{a} = \int \mathbf{B}_{nl}^{\mathrm{T}} \mathbf{g}_{\mathrm{tK}2} \delta p \, \mathrm{d}V_{\mathrm{o}} = \mathbf{P} \delta \boldsymbol{p} \tag{13.70}$$

where the derivation of the matrix $\mathbf{P}$ will follow.

Substituting from (13.63) for the pressure change δp in terms of its nodal variables, $\delta \boldsymbol{p}$, gives:

$$\mathbf{a} = \mathbf{P} \, \delta \boldsymbol{p} = \int \mathbf{B}_{nl}^{\mathrm{T}} \mathbf{g}_{\mathrm{tK}2} \mathbf{h}_p^{\mathrm{T}} \mathrm{d}V_{\mathrm{o}} \delta \boldsymbol{p} \tag{13.71}$$

from which:

$$\mathbf{P} = \frac{\partial \mathbf{q}_{\mathrm{i}}}{\partial \boldsymbol{p}} = \frac{\partial \mathbf{g}}{\partial \boldsymbol{p}} = \int \mathbf{B}_{nl}^{\mathrm{T}} \mathbf{g}_{\mathrm{tK}2} \mathbf{h}_p^{\mathrm{T}} \mathrm{d}V_{\mathrm{o}} \tag{13.72}$$

We have yet to apply the pressure-displacement relationship of (13.33). This can be achieved using a Galerkin-type procedure to obtain a 'weak form' [Z1] of (13.33) by multiplying it by δp (with the latter obtained from (13.63)) and integrating over the element; i.e.

$$\int \left((J-1) + \frac{1}{K} p \right) \delta p \, \mathrm{d}V_{\mathrm{o}} = \delta \boldsymbol{p}^{\mathrm{T}} \int \mathbf{h}_p \left((J-1) + \frac{1}{K} p \right) \mathrm{d}V_{\mathrm{o}} = \delta \boldsymbol{p}^{\mathrm{T}} \mathbf{f} = 0 \tag{13.73}$$

This relationship should hold for any $\delta \boldsymbol{p}$ so that with $\mathbf{f}$ representing the lack of pressure compatibility:

$$\mathbf{f} = - \int \mathbf{h}_p \left((J-1) + \frac{1}{K} p \right) \mathrm{d}V_{\mathrm{o}} = \mathbf{0} \tag{13.74}$$

Equations (13.65) and (13.74) represent the governing equations for the 'nodal' displacement ($\mathbf{p}$) and pressure (p) variables. For full incompressibility, the p/K term in (13.74) would vanish and this equation could be used to provide a weak form of the incompressibility constraint.

Assuming continued satisfaction of (13.74) from an 'equilibrium state',

$$\delta \mathbf{f} = \frac{\partial \mathbf{f}}{\partial \mathbf{p}} \delta \mathbf{p} + \frac{\partial \mathbf{f}}{\partial \boldsymbol{p}} \delta \boldsymbol{p} = \mathbf{P}^{\mathrm{T}} \delta \mathbf{p} + \mathbf{H} \, \delta \boldsymbol{p} = \mathbf{0} \tag{13.75}$$

where

$$\mathbf{H} = \frac{\partial \mathbf{f}}{\partial \boldsymbol{p}} = \frac{\partial \mathbf{f}}{\partial p} \frac{\partial p}{\partial \boldsymbol{p}} = - \int \frac{1}{K} \mathbf{h}_p \mathbf{h}_p^{\mathrm{T}} \mathrm{d}V_{\mathrm{o}} \tag{13.76}$$

and $\mathbf{P}$ has already been given in (13.72). It is not obvious that $\partial \mathbf{f}/\partial \mathbf{p}$ in (13.75) is equal to $\mathbf{P}^{\mathrm{T}}$ with $\mathbf{P}$ from (13.72). However, from (13.74) we have:

$$\frac{\partial \mathbf{f}}{\partial \mathbf{p}} = \frac{\partial \mathbf{f}}{\partial J} \frac{\partial J}{\partial \mathbf{E}} \frac{\partial \mathbf{E}}{\partial \mathbf{p}} = \int \mathbf{h}_p \mathbf{g}_{\mathrm{tK}2}^{\mathrm{T}} \mathbf{B}_{nl} \mathrm{d}V_{\mathrm{o}} \tag{13.77}$$

where we have used (13.64) and, with $J = I_3^{1/2}$, the relationship:

$$\frac{\partial J}{\partial \mathbf{E}} = \frac{1}{2} I_3^{-1/2} \frac{\partial I_3}{\partial \mathbf{E}} = I_3^{-1/2} \frac{\partial I_3}{\partial \mathbf{C}} = I_3^{1/2} \mathbf{C}^{-1} = - \mathbf{G}_{\mathrm{tK}2} \tag{13.78}$$

with $\partial I_3/\partial \mathbf{C}$ from (13.29) and $\mathbf{G}_{tK2}$ from (13.42) ($\mathbf{g}_{tK2}$ is simply the vector equivalent of G_{tK2}).

With $\delta \mathbf{f} = \mathbf{0}$, the combination of equations (13.68), (13.70) and (13.75) gives the tangential governing equations as

$$\begin{pmatrix} \delta \mathbf{q}_c \\ \mathbf{0} \end{pmatrix} = \begin{bmatrix} \mathbf{K}_t & \mathbf{P} \\ \mathbf{P}^T & \mathbf{H} \end{bmatrix} \begin{pmatrix} \delta \mathbf{p} \\ \delta p \end{pmatrix} \tag{13.79}$$

which can be solved in a combined manner for $\delta \mathbf{p}$ and δp. Alternatively, the second set of equations can be solved first and then substituted into the first set to give:

$$\delta \mathbf{q}_c = [\mathbf{K}_t - \mathbf{P}\mathbf{H}^{-1}\mathbf{P}^T]\delta \mathbf{p} = \bar{\mathbf{K}}_t \delta \mathbf{p} \tag{13.80}$$

where $\bar{\mathbf{K}}_t$ is the effective tangent stiffness matrix. For full incompressibility, the $\mathbf{H}$ matrices in (13.76) and (13.79) would be zero, and hence one could not apply the two-stage solution implied in (13.80). Instead, one would have to solve (13.79) directly by using, say, Gaussian elimination, starting from the top (assuming $\mathbf{K}_t$ was non-singular).

To form the basis of a Newton–Raphson iteration, we expand (13.65) and (13.74) using truncated Taylor series. Hence, with subscript n meaning 'new' and subscript o meaning 'old', we have, from (13.65):

$$\mathbf{g}_n = \mathbf{0} = \mathbf{g}_o + \frac{\partial \mathbf{g}}{\partial \mathbf{p}} \delta \mathbf{p} + \frac{\partial \mathbf{g}}{\partial p} \delta p \tag{13.81}$$

while from (13.74), we have:

$$\mathbf{f}_n = \mathbf{0} = \mathbf{f}_o + \frac{\partial \mathbf{f}}{\partial \mathbf{p}} \delta \mathbf{p} + \frac{\partial \mathbf{f}}{\partial p} \delta p \tag{13.82}$$

Droping the subscript o, equations (13.81) and (13.82) can be combined to give:

$$-\begin{pmatrix} \mathbf{g} \\ \mathbf{f} \end{pmatrix} = \begin{bmatrix} \mathbf{K}_t & \mathbf{P} \\ \mathbf{P}^T & \mathbf{H} \end{bmatrix} \begin{pmatrix} \delta \mathbf{p} \\ \delta p \end{pmatrix} \tag{13.83}$$

Using a mixed formulation, equations (13.83) can be solved directly as part of a Newton–Raphson loop. Alternatively, the second set of equations can be solved first and then substituted into the first set to give:

$$-\bar{\mathbf{g}} = -(\mathbf{g} - \mathbf{P}\mathbf{H}^{-1}\mathbf{f}) = [\mathbf{K}_t - \mathbf{P}\mathbf{H}^{-1}\mathbf{P}^T]\delta \mathbf{p} = \bar{\mathbf{K}}_T \delta \mathbf{p} \tag{13.84}$$

In a plane strain environment, an appropriate form of element [Z1] might involve nine nodes for the displacements and four for the pressure (see Figure 13.1).

13.5.2 A hybrid formulation

Because the governing equations (13.74) involving the pressure and not its derivative, there is no need for the pressure to be continuous between elements. Hence, if the pressure variables, p, are internal (see Fig. 13.2), they can be eliminated at the element level. For such elements, equations of the form of (13.79) and (13.83), can be formed at the element level prior to the merging process to form the structural matrix, $\bar{\mathbf{K}}_t$, and

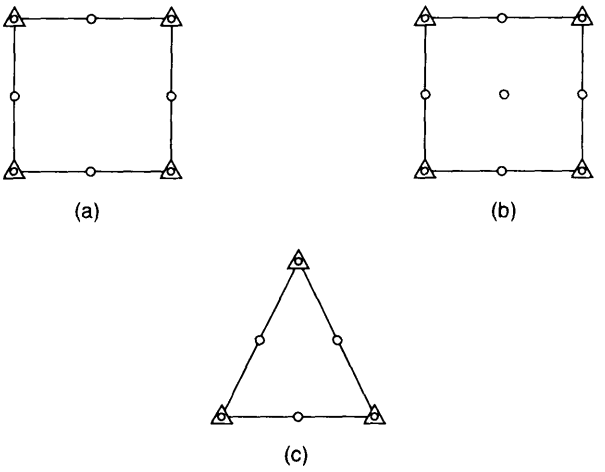

Figure 13.1 Possible configurations for mixed elements. (○) Displacement node; (△) pressure node.

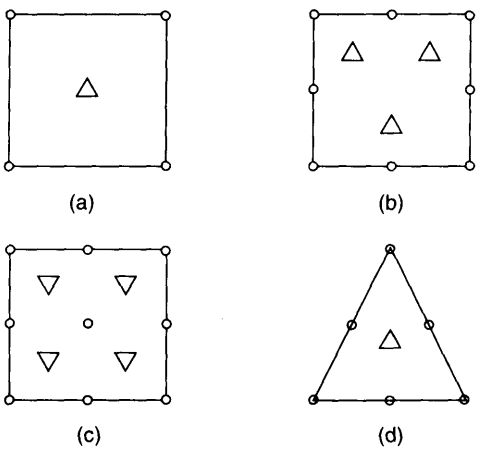

Figure 13.2 Possible configurations for hybrid elements. (○) Displacement node (△) pressure point.

out-of-balance force vector, $\bar{\mathbf{g}}$. We will refer to the resulting element as a 'hybrid element' although it is really a different form of 'mixed element'. Figure 13.2, gives some possible configurations for the displacement and pressure variables appropriate to a hybrid formulation. In fact, the configurations in Figures 13.1a, 13.2a and 13.2b do not pass the 'incompressible patch test' or LBB (Babuska–Brezzi) condition [H3, S7, Z1, Z2] but, none the less, often give very reasonable results. More detail on this topic can be found in [H3], [S7] and [Z1].

Incompressibility is also an important issue for plasticity and, in relation to small-strain elasto-plasticity, for a plane-strain environment, Zienkiewicz *et al.* [Z3]

have reported good results using the element configurations shown in Figures 13.1c, 13.2a and 13.2d. In contrast, when certain mesh orientations were adopted, completely unreliable results were obtained with the equivalent displacement models (without the pressure variables).

In some circumstances, instead of using the formulation of (13.79), (13.83) and (13.84), it is possible to introduce a modified $\mathbf{B}$ (here $\mathbf{B}_{nl}$) matrix which allows the final stiffness matrix to be formed more simply using the form of (13.69) but with modified $\bar{\mathbf{B}}$'s instead of $\mathbf{B}$'s. Details of this 'B-bar method' are given in [H3, Z1]. A non-linear implementation has been described by Simo *et al.* [S5].

13.6 DEVELOPMENTS USING THE KIRCHHOFF STRESS

The previous developments have used the second Piola–Kirchhoff stress and Green strain and have led to a total Lagrangian finite element formulation. We can, instead, adopt the Kirchhoff stress and a 'Eulerian' finite element formulation (similar to that described in Chapter 12). In order to ease the arithmetic, we will start by adopting the simpler modified neo-Hookean energy function rather than the modified Mooney–Rivlin function in (13.26). This can be simply achieved by setting C_2 in the latter to zero and, for convenience, then equating $2C_1$ to the shear modulus, μ. We will later show that it is very easy, using the methods of Section 10.4, to simply transform the relationships of Section 13.4 which adopted the second Piola–Kirchhoff stresses and Green strains. However, we will firstly apply a more direct (but lengthier) approach with the 'neo-Hookean' model, for which, from (13.35), we have:

$$\mathbf{S} = \mu I_3^{-1/3}\left[\mathbf{I} - \frac{I_1}{3}\mathbf{C}^{-1}\right] - pI_3^{1/2}\mathbf{C}^{-1} \tag{13.85}$$

With the aid of (10.50) or (4.122), this can be converted to a Kirchhoff stress so that:

$$\boldsymbol{\tau} = \mathbf{F}\mathbf{S}\mathbf{F}^{\mathrm{T}} = \mu I_3^{-1/3}\left[\mathbf{b} - \frac{I_1}{3}\mathbf{I}\right] - pI_3^{1/2}\mathbf{I} \tag{13.86}$$

where $\mathbf{b} = \mathbf{F}\mathbf{F}^{\mathrm{T}}$ (see (13.9)). By noting from (13.24c) that $\bar{\mathbf{b}} = I_3^{-1/3}\mathbf{b}$ and, using (13.12a) for I_1 so that $\mathrm{tr}(\bar{\mathbf{b}}) = I_3^{-1/3}I_1$, we can re-express (13.86) as

$$\boldsymbol{\tau} = \mu\,\mathrm{dev}(\bar{\mathbf{b}}) - pJ\mathbf{I} = \mu\,\mathrm{dev}(\bar{\mathbf{b}}) + KJ(J-1)\mathbf{I} \tag{13.87}$$

where we have used (13.33) for the pressure, p. For a genuinely incompressible material, we would obtain (13.86) with $I_3 = 1$.

In order to differentiate (13.87), we require:

$$\delta\mathbf{b} = \mathbf{F}\delta\mathbf{F}^{\mathrm{T}} + \delta\mathbf{F}\mathbf{F}^{\mathrm{T}} = \mathbf{F}\mathbf{F}^{\mathrm{T}}\mathbf{F}^{-\mathrm{T}}\delta\mathbf{F}^{\mathrm{T}} + \delta\mathbf{F}\mathbf{F}^{-1}\mathbf{F}\mathbf{F}^{\mathrm{T}} = \mathbf{b}\mathbf{L}^{\mathrm{T}} + \mathbf{L}\mathbf{b} \tag{13.88}$$

where, from (4.112) and (10.20):

$$\mathbf{L} = \delta\mathbf{F}\mathbf{F}^{-1} = \delta\boldsymbol{\varepsilon} + \delta\boldsymbol{\Omega} \tag{13.89}$$

Using the second relationship in (13.89), (13.88) can be re-expressed as

$$\delta\mathbf{b} = \mathbf{b}(\delta\boldsymbol{\varepsilon} + \delta\boldsymbol{\Omega})^{\mathrm{T}} + (\delta\boldsymbol{\varepsilon} + \delta\boldsymbol{\Omega})\mathbf{b} \tag{13.90}$$

where $\delta\boldsymbol{\varepsilon}$ is symmetric and $\delta\boldsymbol{\Omega}$ is antisymmetric (so that $\delta\boldsymbol{\Omega}^{\mathrm{T}} = -\delta\boldsymbol{\Omega}$).

As well as needing $\delta\mathbf{b}$, to differentiate (13.87), we require δI_3 and δI_1 in terms of $\delta\boldsymbol{\varepsilon}$. From (13.29) and (13.90), we have:

$$\delta I_1 = 2(\mathbf{I}{:}\mathbf{b}\delta\boldsymbol{\varepsilon}) = 2\mathrm{tr}(\mathbf{b}\delta\boldsymbol{\varepsilon}) = 2(\mathbf{b}{:}\delta\boldsymbol{\varepsilon}) \tag{13.91}$$

where we have used the symmetries of $\delta\boldsymbol{\varepsilon}$ and $\mathbf{b}$ and the antisymmetry of $\delta\boldsymbol{\Omega}$. (The last step in (13.91) can easily be confirmed using a simple two-dimensional example). Also from (13.29), we can obtain δI_3 as

$$\begin{aligned}\delta I_3 &= 2\lambda_1\lambda_2^2\lambda_3^2\delta\lambda_1 + 2\lambda_1^2\lambda_2\lambda_3^2\delta\lambda_2 + 2\lambda_1^2\lambda_2^2\lambda_3\delta\lambda_3 \\ &= 2\lambda_1^2\lambda_2^2\lambda_3^2\left(\frac{\delta\lambda_1}{\lambda_1} + \frac{\delta\lambda_2}{\lambda_2} + \frac{\delta\lambda_3}{\lambda_3}\right) = 2I_3\,\mathrm{tr}(\delta\boldsymbol{\varepsilon}) = 2I_3(\mathbf{I}{:}\delta\boldsymbol{\varepsilon})\end{aligned} \tag{13.92}$$

which is equivalent to (10.60). We can now differentiate (13.87) to obtain:

$$\begin{aligned}\delta\boldsymbol{\tau} = {} & \mu I_3^{-1/3}(\mathbf{b}\delta\boldsymbol{\varepsilon} + \delta\boldsymbol{\varepsilon}\mathbf{b}) + \mu I_3^{-1/3}(-\mathbf{b}\delta\boldsymbol{\Omega} + \delta\boldsymbol{\Omega}\mathbf{b}) \\ & - \tfrac{2}{3}\mu I_3^{-1/3}(\mathbf{b}{:}\delta\boldsymbol{\varepsilon})\mathbf{I} - \tfrac{2}{3}\mu I_3^{-1/3}(\mathbf{I}{:}\delta\boldsymbol{\varepsilon})\left(\mathbf{b} - \frac{I_1}{3}\mathbf{I}\right) \\ & - pI_3^{-1/2}(\mathbf{I}{:}\delta\boldsymbol{\varepsilon})\mathbf{I} - I_3^{1/2}\delta p\mathbf{I}\end{aligned} \tag{13.93a}$$

From which, with the aid of indicial notation, we can write:

$$\delta\tau_{ij} = D^{\mathrm{tJK}}_{ijkl}\delta\varepsilon_{kl} + \mu I_3^{-1/3}(-b_{ik}\delta\Omega_{kj} + \delta\Omega_{ik}b_{kj}) + G^{\mathrm{tK}}_{ij}\delta p \tag{13.93b}$$

where we have added superscripts 'tJK' for 'tangential Jaumann rate of Kirchhoff stress' (see Section 10.2 and equation (10.36)) to the constitutive terms D_{ijkl} and 'tK' for 'tangential Kirchhoff' to the G_{ij} terms. The reasoning behind the superscripts will be amplified later. The components of the constitutive tensors are given by

$$\begin{aligned}D^{\mathrm{tJK}}_{ijkl} = {} & (\tfrac{2}{9}\mu I_3^{-1/3}I_1 - I_3^{-1/2}p)\delta_{ij}\delta_{kl} \\ & - \tfrac{2}{3}\mu I_3^{-1/3}(b_{ij}\delta_{kl} + \delta_{ij}b_{kl}) + \mu I_3^{-1/3}(\delta_{ik}b_{jl} + b_{ik}\delta_{jl})\end{aligned} \tag{13.94}$$

and

$$G^{\mathrm{tK}}_{ij} = -I_3^{1/2}\delta_{ij} \tag{13.95}$$

Using (13.87) for $\boldsymbol{\tau}$ and noting the symmetry of $\mathbf{b}$, we can rewrite (13.93b) as

$$\delta\tau_{ij} = D^{\mathrm{tJK}}_{ijkl}\delta\varepsilon_{kl} + G^{\mathrm{tK}}_{ij}\delta p - \tau_{ik}\delta\Omega_{kj} + \delta\Omega_{ik}\tau_{kj} \tag{13.96a}$$

which can be written, without suffix notation, as

$$\delta\boldsymbol{\tau} = \mathbf{D}_{\mathrm{tJK}}{:}\delta\boldsymbol{\varepsilon} + \mathbf{G}_{\mathrm{tK}}\delta p - \boldsymbol{\tau}\delta\boldsymbol{\Omega} + \delta\boldsymbol{\Omega}\boldsymbol{\tau} \tag{13.96b}$$

Apart from the pressure term, equation (13.96b) is identical to (10.36) of Section 10.2, derived in relation to the 'Jaumann rate of Kirchhoff stress' hence, the sub- or superscripts tJK in (13.89). From the work of Sections 10.4 and 12.4, we would expect to be able to transform (13.96) to involve the Truesdell rate of Kirchhoff stress (see (12.51)). Indeed by using (13.89) to write $\delta\boldsymbol{\Omega}$ as $\delta\boldsymbol{\varepsilon} - \mathbf{L}$, we can change (13.96) to give:

$$\delta\boldsymbol{\tau} = \mathbf{D}_{\mathrm{tTK}}{:}\delta\boldsymbol{\varepsilon} + \mathbf{G}_{\mathrm{tK}}\delta p + \mathbf{L}\boldsymbol{\tau} + \boldsymbol{\tau}\mathbf{L}^{\mathrm{T}} \tag{13.97}$$

where, in place of (13.94), we have

$$D^{\mathrm{tTk}}_{ijkl} = (\tfrac{2}{9}\mu I_3^{-1/2} I_1 - I_3^{-1/2} p)\delta_{ij}\,\delta_{kl} - \tfrac{2}{3}\mu I_3^{-1/3}(b_{ij}\,\delta_{kl} + \delta_{ij}\,b_{kl}) + \left(\frac{\mu}{3} I_1 I_3^{-1/3} + p I_3^{1/2}\right)(\delta_{ik}\delta_{jl} + \delta_{il}\delta_{jk}) \tag{13.98}$$

From the work of Section 10.4, we would expect that the above relationship could be derived more simply by transforming it directly from the equivalent relationships involving the second Piola-Kirchhoff stresses and Green strains or, in the present case, from (13.39)–(13.41) with $2C_1 = \mu$ and $C_2 = 0$. To this end, we can simply apply (10.56) or

$$D^{\mathrm{tTK}}_{ijkl} = F_{ia}F_{jb}F_{kc}F_{id}D^{\mathrm{tT2}}_{abcd} \tag{13.99}$$

to (13.40) and (13.41). With $\mathbf{b} = \mathbf{F}\mathbf{F}^{\mathrm{T}}$ and $\mathbf{C} = \mathbf{F}^{\mathrm{T}}\mathbf{F}$, it is not difficult to show that this involving changing (13.40) and (13.41) so that:

$$C^{-1}_{ij} \Rightarrow \delta_{ij}; \qquad \delta_{ij} \Rightarrow b_{ij} \tag{13.100}$$

(Note that in (13.40) and (13.41), C^{-1}_{ij} is the ijth component of $\mathbf{C}^{-1}$). Application of this process to (13.40) and (13.41), can be shown (with $2C_1 = \mu$, $C_2 = 0$) to lead directly to (13.98). (More details on the application of (13.99) are given in Section 13.8.3.) It follows that this same process could be very simply applied to (13.40) and (13.41) to obtain the C^{iTK}_{ijkl} terms for the Mooney–Rivlin energy function (with $C_2 \neq 0$). Using (12.51), we could (if wished) find the equivalent terms in relation to the Jaumann rate of Kirchhoff stress.

13.7 A 'EULERIAN' FINITE ELEMENT FORMULATION

'Eulerian' finite element formulations have been considered in the previous chapter where we used either the Jaumann rate of Kirchhoff stress (Section 12.4) or the Truesdell rate (Section 12.3). We have just shown how to obtain, for our hyperelastic materials, the constitutive laws in relation to the latter. Hence we could use either of these formulations although we now have to consider the pressure terms separately. To this end, we can adopt a similar approach to that of Section 13.5. We will now briefly outline the procedure.

Our starting-point will as usual be the principal of virtual work so that we can obtain the internal force vector via:

$$\mathbf{q}_I^{\mathrm{T}}\delta \mathrm{p}_r = \int \sigma : \delta\varepsilon_v \mathrm{d}V_{\mathrm{n}} = \int \tau : \delta\varepsilon_v \mathrm{d}V_{\mathrm{o}} \tag{13.101}$$

which leads to

$$\mathbf{q}_I = \int \mathbf{B}(\mathbf{x})^{\mathrm{T}} \tau dV_{\mathrm{o}} \tag{13.102}$$

where $\mathbf{B}(\mathbf{x})$ is the linear strain-displacement matrix which is a function of the current coordinates, $\mathbf{x}$, as detailed in Section 12.2. Following the approach of Section 13.5, from

(13.74), the other 'equilibrium equation' will be

$$\mathbf{f} = -\int \mathbf{h}_p \left((J-1) + \frac{1}{K} p \right) \mathrm{d}V_0 = \mathbf{0} \tag{13.103}$$

where $\mathbf{h}_p$ contains the shape function for the pressure. To obtain the tangent stiffness relationships, from (13.101), we have:

$$\delta \mathbf{q}_i^{\mathrm{T}} \delta \mathbf{p}_v = \int \delta \boldsymbol{\tau} : \delta \boldsymbol{\varepsilon}_v \mathrm{d}V_0 + \int \boldsymbol{\tau}\, \mathrm{d}\delta \boldsymbol{\varepsilon}_v \mathrm{d}V_0 \tag{13.104}$$

If we use (13.97) for $\delta\boldsymbol{\tau}$ and adopt the techniques of Section 12.3, we obtain:

$$\mathbf{q}_i^{\mathrm{T}} \delta \mathbf{p}_v = \int (\mathbf{D}_{tTK} : \delta \boldsymbol{\varepsilon} + \mathbf{G}_{tK} \delta p) : \delta \boldsymbol{\varepsilon}_v + \mathbf{L}_v^{\mathrm{T}} \mathbf{L} : \boldsymbol{\tau}) \mathrm{d}V_0 \tag{13.105}$$

which, apart form the pressure term $+\mathbf{G}_{tK}\delta p$, is identical to (12.28). Combining the techniques of Section 12.3 with those of Section 13.5, we can obtain the 'tangent stiffness' equation of (13.79), i.e.

$$\begin{pmatrix} \delta \mathbf{q}_e \\ \mathbf{0} \end{pmatrix} = \begin{bmatrix} \mathbf{K}_t & \mathbf{P} \\ \mathbf{P}^{\mathrm{T}} & \mathbf{H} \end{bmatrix} \begin{pmatrix} \delta \mathbf{p} \\ \delta p \end{pmatrix} \tag{13.106}$$

with $\mathbf{K}_t$ being given by (12.45) if the Jaumann rate of Kirchhoff stress is adopted or by (12.16) if the Truesdell rate of Kirchhoff stress is used (as emphasised in Chapter 12, provided the appropriate tangent constitutive terms are adopted, both formulations lead to the same stiffness matrix). The pressure connection matrix $\mathbf{P}$, is given by

$$\mathbf{P} = \int \mathbf{B}(\mathbf{x})^{\mathrm{T}} \mathbf{g}_{tK} \mathbf{h}_p^{\mathrm{T}} \mathrm{d}V_0 \tag{13.107}$$

while the $\mathbf{H}$ matrix in (13.106) is given by (13.76). The solution procedure would closely follow that outlined in Section 13.5 for the total Lagrangian formulation.

13.8 WORKING DIRECTLY WITH THE PRINCIPAL STRETCH RATIOS

Although in Section 13.2, we did begin by working in terms of the principal stretches, the invariants, $I_1 - I_3$ of (13.12) were eventually expressed in terms of $\mathbf{C} = \mathbf{F}^{\mathrm{T}}\mathbf{F}$ or $\mathbf{b} = \mathbf{F}\mathbf{F}^{\mathrm{T}}$ and for most developments, we used the latter. However, in Section 13.4.2, most of the work related directly to the principal stretches and we indicated there that, for later developments, such as the Ogden model (Section 13.10.2), we would return to working directly with the principal stretches and principal directions.

The basis for such formulations is closely related to the work on conjugate stress and strain measures previously developed in Section 10.5. We start by considering a general potential function $\varphi(\lambda_1, \lambda_2, \lambda_3)$. Because, the Biot stresses are conjugate to the stretch $\mathbf{U}$ (see (10.67) and (10.68)), it is simplest to obtain the principal Biot stresses from φ using:

$$\begin{aligned} \boldsymbol{B} &= b_1 \mathbf{N}_1 \mathbf{N}_1^{\mathrm{T}} + b_2 \mathbf{N}_2 \mathbf{N}_2^{\mathrm{T}} + b_3 \mathbf{N}_3 \mathbf{N}_3^{\mathrm{T}} \\ &= \frac{\partial \varphi}{\partial \lambda_1} \mathbf{N}_1 \mathbf{N}_1^{\mathrm{T}} + \frac{\partial \varphi}{\partial \lambda_2} \mathbf{N}_2 \mathbf{N}_2^{\mathrm{T}} + \frac{\partial \varphi}{\partial \lambda_3} \mathbf{N}_3 \mathbf{N}_3^{\mathrm{T}} \end{aligned} \tag{13.108}$$

For isotropic conditions, the Kirchhoff (and hence Cauchy) stresses can then be obtained from the Biot stresses using (10.84) so that, with $\boldsymbol{B}$ and $\mathbf{U}$ coaxial:

$$\mathbf{R}^{\mathrm{T}}\boldsymbol{\tau}\mathbf{R} = \boldsymbol{B}\mathbf{U} = \lambda_1 \frac{\partial \varphi}{\partial \lambda_1}\mathbf{N}_1\mathbf{N}_1^{\mathrm{T}} + \lambda_2 \frac{\partial \varphi}{\partial \lambda_2}\mathbf{N}_2\mathbf{N}_2^{\mathrm{T}} + \lambda_3 \frac{\partial \varphi}{\partial \lambda_3}\mathbf{N}_3\mathbf{N}_3^{\mathrm{T}} \tag{13.109}$$

Hence, from (4.147), using the relationship, $\mathbf{R} = \mathbf{Q}(\mathbf{n})\mathbf{Q}(\mathbf{N})^{\mathrm{T}}$:

$$\boldsymbol{\tau} = \lambda_1\lambda_2\lambda_3\boldsymbol{\sigma} = \lambda_1 \frac{\partial \varphi}{\partial \lambda_1}\mathbf{n}_1\mathbf{n}_1^{\mathrm{T}} + \lambda_2 \frac{\partial \varphi}{\partial \lambda_2}\mathbf{n}_2\mathbf{n}_2^{\mathrm{T}} + \lambda_3 \frac{\partial \varphi}{\partial \lambda_3}\mathbf{n}_3\mathbf{n}_3^{\mathrm{T}} \tag{13.110}$$

The second Piola–Kirchhoff stresses can be obtained from (13.27) as

$$\mathbf{S} = \frac{\partial \varphi}{\partial \mathbf{E}} = 2\frac{\partial \varphi}{\partial \mathbf{C}} \tag{13.111}$$

or more directly using the principal stretches, from (10.6), we have:

$$\frac{\partial \varphi}{\partial E_{\mathrm{i}}} = \frac{\partial \varphi}{\partial \lambda_{\mathrm{i}}}\frac{\partial \lambda_{\mathrm{i}}}{\partial E_{\mathrm{i}}} = \frac{1}{\lambda_{\mathrm{i}}}\frac{\partial \varphi}{\partial \lambda_{\mathrm{i}}} \tag{13.112}$$

and hence with coaxiality of the second Piola–Kirchhoff stresses and the Green strains, from (10.75) and (10.77):

$$\mathbf{S} = \frac{1}{\lambda_1}\frac{\partial \varphi}{\partial \lambda_1}\mathbf{N}_1\mathbf{N}_1^{\mathrm{T}} + \frac{1}{\lambda_2}\frac{\partial \varphi}{\partial \lambda_2}\mathbf{N}_2\mathbf{N}_2^{\mathrm{T}} + \frac{1}{\lambda_3}\frac{\partial \varphi}{\partial \lambda_3}\mathbf{N}_3\mathbf{N}_3^{\mathrm{T}} \tag{13.113}$$

Using a similar approach, the 'log-stress', $\mathbf{O}$, which is conjugate to $\log_{\mathrm{e}}\mathbf{U}$ (see (10.65) and (10.79)) is given by

$$\mathbf{O} = \lambda_1 \frac{\partial \varphi}{\partial \lambda_1}\mathbf{N}_1\mathbf{N}_1^{\mathrm{T}} + \lambda_2 \frac{\partial \varphi}{\partial \lambda_2}\mathbf{N}_2\mathbf{N}_2^{\mathrm{T}} + \lambda_3 \frac{\partial \varphi}{\partial \lambda_3}\mathbf{N}_3\mathbf{N}_3^{\mathrm{T}} \tag{13.114}$$

Equations (13.108), (13.113) and (13.114) are special cases of (10.77).

13.8.1 The compressible 'neo-Hookean model'

The previous compressible Mooney–Rivlin and compressible neo-Hookean models can be developed directly in terms of principal stretches. Before considering more sophisticated models will reconsider the latter. From (13.26) with $C_1 = \mu/2$ and $C_2 = 0$, in terms of principal stretches we have:

$$\begin{aligned}\varphi &= \frac{\mu}{2}(I_1 J^{-2/3} - 3) + \tfrac{1}{2}K(J-1)^2 \\ &= \frac{\mu}{2}((\lambda_1^2 + \lambda_2^2 + \lambda_3^2)(\lambda_1\lambda_2\lambda_3)^{-2/3} - 3) + \tfrac{1}{2}K(\lambda_1\lambda_2\lambda_3 - 1)^2\end{aligned} \tag{13.115}$$

From the above

$$\frac{\partial \varphi}{\partial \lambda_{\mathrm{i}}} = \mu J^{-2/3}\left(\lambda_i - \frac{I_1}{3\lambda_{\mathrm{i}}}\right) + K\frac{(J-1)J}{\lambda_{\mathrm{i}}} \tag{13.116}$$

From which, with the aid of (13.113),

$$\mathbf{S} = \mu J^{-2/3}\mathbf{Q(N)Diag}\left(1 - \frac{I_1}{3\lambda_i^2}\right)\mathbf{Q(N)}^{\mathrm{T}} + KJ(J-1)(\mathbf{Q(N)Diag}\left(\frac{1}{\lambda_i^2}\right)\mathbf{Q(N)}^{\mathrm{T}} \quad (13.117a)$$

or:

$$\mathbf{S} = \mu J^{-2/3}\mathbf{Q(N)Diag}\left(1 - \frac{I_1}{3\lambda_i^2}\right)\mathbf{Q(N)}^{\mathrm{T}} - pJ\mathbf{Q(N)Diag}\left(\frac{1}{\lambda_i^2}\right)\mathbf{Q(N)}^{\mathrm{T}} \quad (13.117b)$$

with p from (13.33). Equation (13.117b) coincides with (13.35). Clearly, we could also use (13.116) with (13.110) to obtain an equivalent relationship for τ which would correspond with (13.86).

In the derivations leading to (13.117), it has been assumed that the stretches are distinct. However, if two of the stretches coincide (say λ_1 and λ_2), we can still write such an expression although the $\mathbf{N}_1$ and $\mathbf{N}_2$ are only defined to within an arbitrary rotation about $\mathbf{N}_3$. If all of the stretches coincide, equation (13.117b) degenerates to

$$\mathbf{S} = -p\lambda\mathbf{I} = K\lambda(\lambda^3 - 1) \quad (13.118)$$

where the last expressions follow from (13.33).

For a general energy function of the form $\varphi = \varphi(\lambda_1, \lambda_2, \lambda_3)$, we can write:

$$S_i = \frac{1}{\lambda_i}\frac{\partial\varphi}{\partial\lambda_i} \quad (13.119)$$

where S_i are the principal stress and

$$\mathbf{S} = \mathbf{Q(N)Diag}(S_i)\mathbf{Q(N)}^{\mathrm{T}} \quad (13.120)$$

We will now consider the issue of obtaining the tangential relationships initially in relation to the second Piola–Kirchhoff stresses and Green strains.

13.8.2 Using the Green strain relationships in the principal directions

To this end, we note that because of isotropy, the directions of principal stress and strain coincide and hence we can complement (13.120) with:

$$\mathbf{E} = \mathbf{Q(N)Diag}(E_i)\mathbf{Q(N)}^{\mathrm{T}} \quad (13.121)$$

Differentiation of (13.120) and (13.121) leads to

$$\dot{\mathbf{S}} = \mathbf{Q(N)}\dot{\mathbf{D}}\mathbf{iag}(S_i)\mathbf{Q(N)}^{\mathrm{T}} + \dot{\mathbf{Q}}\mathbf{(N)Diag}(S_i)\mathbf{Q(N)}^{\mathrm{T}} + \mathbf{Q(N)Diag}(S_i)\dot{\mathbf{Q}}\mathbf{(N)}^{\mathrm{T}} \quad (13.122a)$$

$$\dot{\mathbf{E}} = \mathbf{Q(N)}\dot{\mathbf{D}}\mathbf{iag}(E_i)\mathbf{Q(N)}^{\mathrm{T}} + \dot{\mathbf{Q}}\mathbf{(N)Diag}(E_i)\mathbf{Q(N)}^{\mathrm{T}} + \mathbf{Q(N)Diag}(E_i)\dot{\mathbf{Q}}\mathbf{(N)}^{\mathrm{T}} \quad (13.122b)$$

where E_i are the principal Green strains. Relating the above to the Lagrangian frame (see also Sections 4.3, 4.8 and 10.6), gives

$$\dot{\mathbf{S}}_{\mathrm{L}} = \mathbf{Q(N)}^{\mathrm{T}}\dot{\mathbf{S}}\mathbf{Q(N)} = \dot{\mathbf{D}}\mathbf{iag}(S_i) + \mathbf{Q(N)}^{\mathrm{T}}\dot{\mathbf{Q}}\mathbf{(N)Diag}(S_i) + \mathbf{Diag}(S_i)\dot{\mathbf{Q}}\mathbf{(N)}^{\mathrm{T}}\mathbf{Q(N)} \quad (13.123a)$$

$$\dot{\mathbf{E}}_{\mathrm{L}} = \mathbf{Q(N)}^{\mathrm{T}}\dot{\mathbf{E}}\mathbf{Q(N)} = \dot{\mathbf{D}}\mathbf{iag}(E_i) + \mathbf{Q(N)}^{\mathrm{T}}\dot{\mathbf{Q}}\mathbf{(N)Diag}(E_i) + \mathbf{Diag}(E_i)\dot{\mathbf{Q}}\mathbf{(N)}^{\mathrm{T}}\mathbf{Q(N)} \quad (13.123b)$$

From (10.101), the spin of the Lagrangian triad is given by the antisymmetric $\mathbf{W}_{\mathrm{N}}$,

where

$$\mathbf{W}_N = \dot{\mathbf{Q}}(\mathbf{N})\mathbf{Q}(\mathbf{N})^T \tag{13.124a}$$

while in relation to the Lagrangian triad (see also (10.102)), we have:

$$(\mathbf{W}_N)_L = \mathbf{Q}(\mathbf{N})^T\mathbf{W}_N\mathbf{Q}(\mathbf{N}) = \mathbf{Q}(\mathbf{N})^T\dot{\mathbf{Q}}(\mathbf{N}) \tag{13.124b}$$

and we can write (13.123) as

$$\dot{\mathbf{S}}_L = \mathbf{Q}(\mathbf{N})\dot{\mathbf{S}}\mathbf{Q}(\mathbf{N})^T = \dot{\mathbf{D}}\mathrm{iag}(S_i) + (\mathbf{W}_N)_L\mathbf{D}\mathrm{iag}(S_i) - \mathbf{D}\mathrm{iag}(S_i)(\mathbf{W}_N)_L \tag{13.125a}$$

$$\dot{\mathbf{E}}_L = \mathbf{Q}(\mathbf{N})\dot{\mathbf{E}}\mathbf{Q}(\mathbf{N})^T = \dot{\mathbf{D}}\mathrm{iag}(E_i) + (\mathbf{W}_N)_L\mathbf{D}\mathrm{iag}(E_i) - \mathbf{D}\mathrm{iag}(E_i)(\mathbf{W}_N)_L \tag{13.125b}$$

Following closely the developments of Section 10.6, we can, for the two-dimensional case, re-write (13.125b) as:

$$\dot{\mathbf{E}}_L = \begin{bmatrix} \dot{E}_1 & 0 \\ 0 & \dot{E}_2 \end{bmatrix} + \begin{bmatrix} 0 & w_{12}^{NL} \\ w_{21}^{NL} & 0 \end{bmatrix}\begin{bmatrix} E_1 & 0 \\ 0 & E_2 \end{bmatrix} - \begin{bmatrix} E_1 & 0 \\ 0 & E_2 \end{bmatrix}\begin{bmatrix} 0 & w_{12}^{NL} \\ w_{21}^{NL} & 0 \end{bmatrix} \tag{13.126}$$

where $w_{12}^{NL} = -w_{21}^{NL}$. It follows that:

$$\dot{\mathbf{E}}_L = \begin{bmatrix} \dot{E}_1 & (E_2 - E_1)w_{12}^{NL} \\ (E_2 - E_1)w_{12}^{NL} & \dot{E}_2 \end{bmatrix} \tag{13.127}$$

from which (provided $E_1 \neq E_2$):

$$w_{12}^{NL} = \frac{\dot{E}_{12L}}{(E_2 - E_1)} \tag{13.128}$$

and, in the general three-dimensional case (provided $E_r \neq E_s$)

$$w_{rs}^{NL} = \frac{\dot{E}_{rsL}}{(E_s - E_r)} \tag{13.129}$$

(The latter equations could be derived directly from (10.108).) Equation (13.127) was derived from (13.125b). An equivalent expression can be derived for $\dot{\mathbf{S}}_L$ from (13.125a). Substituting into this expression from (13.128) for the spin component w_{12}^{NL} gives:

$$\dot{\mathbf{S}}_L = \begin{bmatrix} \dot{S}_1 & \dfrac{(S_2 - S_1)}{(E_2 - E_1)}\dot{E}_{12L} \\ \dfrac{(S_2 - S_1)}{(E_2 - E_1)}\dot{E}_{12L} & \dot{S}_2 \end{bmatrix} \tag{13.130}$$

Considering first the diagonal terms in the above and extending to the three-dimensional case we can write:

$$\begin{bmatrix} \dot{S}_{11} \\ \dot{S}_{22} \\ \dot{S}_{33} \end{bmatrix} = \begin{bmatrix} \dot{S}_1 \\ \dot{S}_2 \\ \dot{S}_3 \end{bmatrix} = \begin{bmatrix} \dfrac{\partial S_1}{\partial E_1} & \dfrac{\partial S_1}{\partial E_2} & \dfrac{\partial S_1}{\partial E_3} \\ \dfrac{\partial S_2}{\partial E_1} & \dfrac{\partial S_2}{\partial E_2} & \dfrac{\partial S_2}{\partial E_3} \\ \dfrac{\partial S_3}{\partial E_1} & \dfrac{\partial S_3}{\partial E_2} & \dfrac{\partial S_3}{\partial E_3} \end{bmatrix}\begin{bmatrix} \dot{E}_1 \\ \dot{E}_2 \\ \dot{E}_3 \end{bmatrix} = \begin{bmatrix} \dfrac{\partial S_1}{\partial E_1} & \dfrac{\partial S_1}{\partial E_2} & \dfrac{\partial S_1}{\partial E_3} \\ \dfrac{\partial S_2}{\partial E_1} & \dfrac{\partial S_2}{\partial E_2} & \dfrac{\partial S_2}{\partial E_3} \\ \dfrac{\partial S_3}{\partial E_1} & \dfrac{\partial S_3}{\partial E_2} & \dfrac{\partial S_3}{\partial E_3} \end{bmatrix}\begin{bmatrix} \dot{E}_{11} \\ \dot{E}_{22} \\ \dot{E}_{33} \end{bmatrix}_L \tag{13.131}$$

where the terms such as $\partial S_1/\partial E_1$ come from the differentiation of (13.119) in conjunction with the relationship $E_i = \frac{1}{2}(\lambda_i^2 - 1)$. An example with plane stress and the Mooney–Rivlin energy function has already been given in Section 13.4.2 (see (13.54) and (13.56)).

Extending (13.130) to the three-dimensional case for the off-diagonal shear components, we have:

$$\begin{bmatrix} \dot{S}_{12} \\ \dot{S}_{13} \\ \dot{S}_{23} \end{bmatrix}_L = \begin{bmatrix} \dfrac{(S_1 - S_2)}{(E_1 - E_2)} & & \\ & \dfrac{(S_1 - S_3)}{(E_1 - E_3)} & \\ & & \dfrac{(S_2 - S_3)}{(E_2 - E_3)} \end{bmatrix} \begin{bmatrix} \dot{E}_{12} \\ \dot{E}_{13} \\ \dot{E}_{23} \end{bmatrix}_L \tag{13.132}$$

The stiffness in (13.132) is caused by the change of direction of the principal axes. In the case that E_r and E_s coincide, (13.132) cannot be used but a limiting process results in terms such as

$$\lim\left(\frac{(S_1 - S_2)}{(E_1 - E_2)}\right) = \frac{\partial S_1}{\partial E_1} - \frac{\partial S_2}{\partial E_1} \tag{13.133}$$

where the latter relates to the case $E_1 = E_2$ (or $\lambda_1 = \lambda_2$). Equation (13.133) can be derived by noting that with $E_1 = E_2$, it follows that $S_1 = S_2$ and, to ensure isotropy:

$$\frac{\partial S_1}{\partial E_1} = \frac{\partial S_2}{\partial E_2}; \qquad \frac{\partial S_1}{\partial E_2} = \frac{\partial S_2}{\partial E_1} \tag{13.134}$$

so that, in these circumstances, the application of Taylor series to S_1, S_2, E_1 and E_2 leads to:

$$\frac{S_1 - S_2}{E_1 - E_2} = \frac{\left(\dfrac{\partial S_1}{\partial E_1} - \dfrac{\partial S_2}{\partial E_1}\right)(\dot{E}_1 - \dot{E}_2) + \left(\dfrac{\partial S_1}{\partial E_3} - \dfrac{\partial S_2}{\partial E_3}\right)\dot{E}_3}{(\dot{E}_1 - \dot{E}_2)} \tag{13.135}$$

and hence, as $\dot{E}_1$, $\dot{E}_2$ and $\dot{E}_3$ tend to zero, we obtain the limit in (13.133).

Equations (13.131)–(13.132) allow us to define the tangential constitutive matrix or tensor in the Lagrangian frame such that:

$$\dot{S}_{ij}^{L} = D_{ijkl}^{tK2L} \dot{E}_{kl}^{L} \tag{13.136}$$

We can then transform back to the 'base frame' using standard matrix transformations of (4.55) which here give:

$$D_{ijkl}^{tK2} = Q_{ia} Q_{jb} Q_{kc} Q_{ld} D_{abcd}^{tK2L} \tag{13.137}$$

where the Q terms are components from $\mathbf{Q}(\mathbf{N})$.

If all of the principal Green strains coincide, in place of (13.134), we have:

$$\frac{\partial S_1}{\partial E_1} = \frac{\partial S_2}{\partial E_2} = \frac{\partial S_3}{\partial E_3} = A \tag{13.138a}$$

$$\frac{\partial S_1}{\partial E_2} = \frac{\partial S_1}{\partial E_3} = \frac{\partial S_2}{\partial E_1} = \frac{\partial S_1}{\partial E_3} = \frac{\partial S_3}{\partial E_1} = \frac{\partial S_3}{\partial E_2} = B \tag{13.138b}$$

and (13.131) becomes:

$$\begin{bmatrix} \dot{S}_{11} \\ \dot{S}_{22} \\ \dot{S}_{33} \end{bmatrix} = \begin{bmatrix} A & B & B \\ B & A & B \\ B & B & A \end{bmatrix} \begin{bmatrix} \dot{E}_{11} \\ \dot{E}_{22} \\ \dot{E}_{33} \end{bmatrix} \tag{13.139a}$$

while (13.132) gives:

$$\begin{bmatrix} \dot{S}_{12} \\ \dot{S}_{13} \\ \dot{S}_{23} \end{bmatrix} = \begin{bmatrix} (A-B) & 0 & 0 \\ 0 & (A-B) & 0 \\ 0 & 0 & (A-B) \end{bmatrix} \begin{bmatrix} \dot{E}_{12} \\ \dot{E}_{13} \\ \dot{E}_{23} \end{bmatrix} \tag{13.139b}$$

where we have dropped the subscript L for 'Lagrangian' because the same tangential properties now apply with respect to any orthogonal set of axes. Equations (13.139) can be re-expressed as

$$\dot{S}_{ij} = B\dot{E}_{kk}\delta_{ij} + (A-B)\dot{E}_{ij} \tag{13.140}$$

so that, allowing for the symmetry between $\dot{E}_{ij}$ and $\dot{E}_{ji}$:

$$D^{\mathrm{tK2}}_{ijkl} = B\delta_{ij}\delta_{kl} + \frac{(A-B)}{2}(\delta_{ik}\delta_{jl} + \delta_{il}\delta_{jk}) \tag{13.141}$$

In this section, we have not yet considered keeping the pressure term as a separate variable. If we wish to adopt such an approach, we could still apply the previous techniques to obtain the tensor $\mathbf{D}_{\mathrm{tK2}}$ in (13.38) or (13.39) provided the terms $\partial S_i/\partial E_j$ are computed (from say (13.117b)) with p kept constant. The pressure connection matrix ($\mathbf{G}_{\mathrm{tK2}}$ in (13.38)) would follow, as before, from (13.42).

Before moving on to consider, the equivalent relationships with respect to the Eulerian triad, we can summarise the previous relationships as follows. Provided all of the principal stretch ratios (or principal Green strains) are distinct, the only non-zero components of D_{tK2L} are (from (13.131) and (13.132)):

$$D^{\mathrm{tK2L}}_{iijj} = \frac{\partial S_i}{\partial E_j} = \frac{1}{\lambda_j}\frac{\partial S_i}{\partial \lambda_j} \tag{13.142a}$$

$$D^{\mathrm{tK2L}}_{ijij} = D^{\mathrm{tK2L}}_{ijji} = D^{\mathrm{tK2L}}_{jiij} = D^{\mathrm{tK2L}}_{ijji} = \frac{S_i - S_j}{2(E_i - E_j)} = \frac{S_i - S_j}{\lambda_i^2 - \lambda_j^2} \qquad (i \neq j) \tag{13.142b}$$

If $E_i = E_j$ (and $S_i = S_j$), from (13.133), (13.142b) is replaced by

$$D^{\mathrm{tK2L}}_{ijij} = \frac{1}{2}\left(\frac{\partial S_i}{\partial E_i} - \frac{\partial S_j}{\partial E_j}\right) = \frac{1}{2\lambda_i}\left(\frac{\partial S_i}{\partial \lambda_i} - \frac{\partial S_i}{\partial \lambda_j}\right) \qquad (i \neq j) \tag{13.142c}$$

13.8.3 Transforming the tangent constitutive relationships for a 'Eulerian formulation'

If we adopt a 'Eulerian formulation' (Chapter 12 and Section 13.7), we can simply use (13.99) to transform the material constitutive tensor on the left-hand side of (13.137) so as to involve the Truesdell rate of Kirchhoff stress. However, following Chadwick and

Ogden [C1, C2], it is simpler to work from the material tensor in the Lagrangian frame (as in (13.136)) and initially obtain the equivalent spatial constitutive tensor in relation to the Eulerian frame.

To this end, we can write:

$$\mathrm{d}\mathbf{x} = \mathbf{Q}(\mathbf{n})\mathrm{d}\mathbf{x}_{\mathrm{E}}; \qquad \mathrm{d}\mathbf{X} = \mathbf{Q}(\mathbf{N})\mathrm{d}\mathbf{X}_{\mathrm{L}} \tag{13.143a}$$

so that $\mathrm{d}\mathbf{x}$ can be expressed in terms of its components $\mathrm{d}\mathbf{x}_{\mathrm{E}}$ with respect to the Eulerian frame while $\mathrm{d}\mathbf{X}$ can be expressed in terms of its components with respect to the Lagrangian frame. Substitution from (13.143a) into the relationship $\mathrm{d}\mathbf{x} = \mathbf{F}\,\mathrm{d}\mathbf{X}$ then leads to

$$\mathrm{d}\mathbf{x}_{\mathrm{E}} = \mathbf{Q}(\mathbf{n})^{\mathrm{T}}\mathbf{F}\mathbf{Q}(\mathbf{N})\mathrm{d}\mathbf{X}_{\mathrm{L}} = \mathbf{D}\mathrm{iag}(\lambda)\mathrm{d}\mathbf{X}_{\mathrm{L}} = \mathbf{F}'\mathrm{d}\mathbf{X}_{\mathrm{L}} \tag{13.144a}$$

$$F'_{ij} = \lambda_i\delta_{ij} \tag{13.144b}$$

which gives the expected result that $\mathrm{d}x_{\mathrm{iE}} = \lambda_i \mathrm{d}X_{\mathrm{iL}}$. In moving from the second to the third expressions in (13.144a), we have used the relationship (see (4.148)):

$$\mathbf{Q}(\mathbf{n})^{\mathrm{T}}\mathbf{F}\mathbf{Q}(\mathbf{N}) = \mathbf{D}\mathrm{iag}(\lambda) \tag{13.144c}$$

With respect to the Eulerian and Lagrangian coordinate systems, (13.99) can now be directly applied using $\mathbf{F}'$ instead of $\mathbf{F}$. This leads to the transformation:

$$D^{\mathrm{tTKe}}_{ijkl} = \lambda_i\lambda_j\lambda_k\lambda_l D^{\mathrm{tK2L}}_{ijkl} \tag{13.145}$$

In addition, the relationship $\boldsymbol{\tau} = \mathbf{F}\mathbf{S}\mathbf{F}^{\mathrm{T}}$ gives:

$$S_i = \frac{1}{\lambda_i^2}\tau_i \tag{13.146}$$

so that:

$$\frac{\partial S_i}{\partial \lambda_j} = \frac{1}{\lambda_i^2}\frac{\partial \tau_i}{\partial \lambda_j} - \frac{2}{\lambda_i^3}\tau_i\frac{\partial \lambda_i}{\partial \lambda_j} = \frac{1}{\lambda_i^2}\frac{\partial \tau_i}{\partial \lambda_j} - \frac{2}{\lambda_i^3}\tau_i\delta_{ij} \tag{13.147}$$

Substitution from (13.145)–(13.147) into (13.142a)–(13.142c) gives the non-zero components of $\mathbf{D}_{\mathrm{tTKE}}$ as

$$D^{\mathrm{tTKE}}_{iijj} = \lambda_j\frac{\partial \tau_i}{\partial \lambda_j} - 2\frac{\lambda_j}{\lambda_i}\tau_i\delta_{ij} = \lambda_j\frac{\partial \tau_i}{\partial \lambda_j} - 2\tau_i\delta_{ij} \tag{13.148a}$$

$$D^{\mathrm{tTKE}}_{ijij} = D^{\mathrm{tTKE}}_{ijji}D^{\mathrm{tTKE}}_{jiij} = D^{\mathrm{tTKE}}_{ijji} = \frac{\lambda_j^2\tau_i - \lambda_i^2\tau_j}{\lambda_i^2 - \lambda_j^2} \qquad (i \neq j) \tag{13.148b}$$

If $\lambda_i = \lambda_j$ and $(\tau_i = \tau_j)$, we have:

$$D^{\mathrm{tTKE}}_{ijij} = D^{\mathrm{tTKE}}_{ijji} = D^{\mathrm{tTKE}}_{jiij} = D^{\mathrm{tTKE}}_{ijji} = \frac{\lambda_i}{2}\left(\frac{\partial \tau_i}{\partial \lambda_i} - \frac{\partial \tau_i}{\partial \lambda_j}\right) - \tau_i \qquad (i \neq j) \tag{13.148c}$$

If all three principal stretch ratios coincide, we can directly compute $\mathbf{D}_{\mathrm{tK2}}$ from the equivalent of (13.141) whereby:

$$D^{\mathrm{tTK}}_{ijkl} = B\delta_{ij}\delta_{kl} + \frac{(A-B)}{2}(\delta_{ik}\delta_{jl} + \delta_{il}\delta_{jk}) \tag{13.149}$$

although, in place of (13.138) we now have

$$\lambda\frac{\partial\tau_1}{\partial\lambda_1}-2\tau=\lambda\frac{\partial\tau_2}{\partial\lambda_2}-2\tau=\lambda\frac{\partial\tau_3}{\partial\lambda_3}-2\tau=A \tag{13.150a}$$

$$\lambda\frac{\partial\tau_1}{\partial\lambda_2}=\lambda\frac{\partial\tau_1}{\partial\lambda_3}=\lambda\frac{\partial\tau_2}{\partial\lambda_1}=\lambda\frac{\partial\tau_1}{\partial\lambda_3}=\lambda\frac{\partial\tau_3}{\partial\lambda_1}=\lambda\frac{\partial\tau_3}{\partial\lambda_2}=B \tag{13.150b}$$

In this section, we have not kept the pressure term separate. However, if we wish to apply such a technique, we can simply apply the previous procedures to obtain the tensor $\mathbf{D}_{\mathrm{tTK}}$ in (13.97) provided the terms $\partial\tau_i/\partial\lambda_j$ etc. are computed with p kept constant. The pressure connection matrix $\mathbf{G}_{\mathrm{tK}}$ would be given by (13.95).

13.9 EXAMPLES

In this section, we will give some examples relating to specific hyperelastic models. The objective is to link earlier work in Sections 13.4 and 13.6 with the work of Section 13.8 involving the principal stretches.

13.9.1 A simple example

Before moving on to the compressible neo-Hookean model, to ease the algebra, we will start with an even simpler (conceptual) hyperelastic model for which we assume that:

$$\varphi=\frac{\mu}{2}(I_1-2\log_{\mathrm{e}}J-3)=\frac{\mu}{2}(\lambda_1^2+\lambda_2^2+\lambda_3^2-2\log_{\mathrm{e}}(\lambda_1\lambda_2\lambda_3)-3) \tag{13.151}$$

From (13.119), we obtain:

$$S_i=\frac{1}{\lambda_i}\frac{\partial\varphi}{\partial\lambda_i}=\mu\left(1-\frac{1}{\lambda_i^2}\right)=\mu\left(1-\frac{1}{2E_i+1}\right) \tag{13.152}$$

or, from (13.146):

$$\tau_i=\mu(\lambda_i^2-1) \tag{13.153}$$

From (13.120) and the expression for S_i in (13.152) involving λ_i, we obtain:

$$\mathbf{S}=\mu[\mathbf{I}-\mathbf{C}^{-1}] \tag{13.154}$$

and from (13.110) and (13.153):

$$\boldsymbol{\tau}=\mu[\mathbf{b}-\mathbf{I}] \tag{13.155}$$

with $\mathbf{b}=\mathbf{F}\mathbf{F}^{\mathrm{T}}$.

Following the approach of Section 13.4 (see (13.36)), differentiation of (13.154) gives:

$$\dot{\mathbf{S}}=\mu\mathbf{C}^{-1}\dot{\mathbf{C}}\mathbf{C}^{-1}=2\mu\mathbf{C}^{-1}\dot{\mathbf{E}}\mathbf{C}^{-1} \tag{13.156}$$

from which

$$D_{ijkl}^{\mathrm{tKT}2}=\mu(C_{ik}^{-1}C_{jl}^{-1}+C_{il}^{-1}C_{jk}^{-1}) \tag{13.157}$$

while using the approach of Section 13.6 (see (13.93b)), from (13.155) we obtain:

$$\dot{\boldsymbol{\tau}} = \mu\dot{\mathbf{b}} = \mu(\mathbf{b}\dot{\boldsymbol{\varepsilon}} + \dot{\boldsymbol{\varepsilon}}\mathbf{b}) - \mu\mathbf{b}\dot{\boldsymbol{\Omega}} + \mu\boldsymbol{\Omega}\mathbf{b} = \mu(\mathbf{b}\dot{\boldsymbol{\varepsilon}} + \dot{\boldsymbol{\varepsilon}}\mathbf{b}) - \boldsymbol{\tau}\dot{\boldsymbol{\Omega}} + \dot{\boldsymbol{\Omega}}\boldsymbol{\tau} \tag{13.158}$$

from which

$$D^{\mathrm{tJK}}_{ijkl} = \mu(\delta_{ik}b_{jl} + b_{il}\delta_{jk}) \tag{13.159}$$

Setting $\dot{\boldsymbol{\Omega}} = \dot{\boldsymbol{\varepsilon}} - \mathbf{L}$ in (13.158) gives:

$$\dot{\boldsymbol{\tau}} = \mu\dot{\mathbf{b}} = 2\mu\dot{\boldsymbol{\varepsilon}} + \boldsymbol{\tau}\mathbf{L}^{\mathrm{T}} + \mathbf{L}\boldsymbol{\tau} \tag{13.160}$$

which is of the form for a Truesdell rate (see (10.55)) so that:

$$D^{\mathrm{tTK}}_{ijkl} = \mu(\delta_{ik}\delta_{jl} + \delta_{il}\delta_{jk}) \tag{13.161}$$

The latter could also be obtained from (13.159) via (12.51).

We have not yet applied the procedure of 13.8.2 to obtain the tangential constitutive relationships. To this end, we can differentiate (13.152) to obtain:

$$\dot{S}_i = \dot{S}^{\mathrm{L}}_{ii} = \frac{\partial S_i}{\partial \lambda_i}\dot{\lambda}_i = 2\mu\frac{\dot{\lambda}_i}{\lambda_i^3} = 2\mu\frac{\dot{E}_i}{\lambda_i^4} = 2\mu\frac{\dot{E}^{\mathrm{L}}_{ii}}{\lambda_i^4} \tag{13.162}$$

and with respect to the Lagrangian triad, non-zero constitutive terms are given by

$$D^{\mathrm{tK\,2L}}_{iiii} = \frac{2\mu}{\lambda_i^4} \tag{13.163}$$

which could also be obtained from (13.142a).

For the shear terms, via (13.132) and (13.152), we have:

$$\dot{S}^{\mathrm{L}}_{ij} = \frac{(S_i - S_j)}{(E_i - E_j)}\dot{E}^{\mathrm{L}}_{ij} = \frac{2\mu}{\lambda_i^2\lambda_j^2}\dot{E}^{\mathrm{L}}_{ij} \tag{13.164}$$

so that (allowing for the symmetry between $\dot{E}_{ij}$ and $\dot{E}_{ji}$).

$$D^{\mathrm{tK\,2L}}_{ijij} = \frac{\mu}{\lambda_i^2\lambda_j^2} \tag{13.165}$$

The latter could also be obtained directly from (13.142b).

If λ_i and λ_j coincide, from (13.142c) and differentiation of (13.152):

$$D^{\mathrm{tK\,2L}}_{ijij} = \frac{1}{2\lambda_i}\left(\frac{\partial S_i}{\partial \lambda_i} - \frac{\partial S_i}{\partial \lambda_j}\right) = \frac{\mu}{\lambda_i^4} \tag{13.166}$$

Equations (13.164) and (13.165) can be combined to give:

$$D^{\mathrm{tK\,2L}}_{ijkl} = \frac{\mu}{\lambda_i^2\lambda_j^2}(\delta_{ik}\delta_{jl} + \delta_{il}\delta_{jk}) = \mu\left(\frac{\delta_{ik}}{\lambda_i\lambda_j}\frac{\delta_{jl}}{\lambda_j\lambda_l} + \frac{\delta_{il}}{\lambda_i\lambda_l}\frac{\delta_{jk}}{\lambda_j\lambda_k}\right) \tag{13.167}$$

The latter can be transformed back from the Lagrangian triad using (13.137) (with the Q's as the components of $\mathbf{Q}(\mathbf{N})$) so that:

$$D^{\mathrm{tK\,2}}_{ijkl} = \mu Q_{ia}Q_{jb}Q_{kc}Q_{ld}\left(\frac{\delta_{ac}}{\lambda_a\lambda_c}\frac{\delta_{bd}}{\lambda_b\lambda_d} + \frac{\delta_{ad}}{\lambda_a\lambda_d}\frac{\delta_{bc}}{\lambda_b\lambda_c}\right) \tag{13.168}$$

If we note that:

$$\mathbf{C}^{-1} = \mathbf{Q}(\mathbf{N})\mathbf{Diag}(\lambda^{-2})\mathbf{Q}(\mathbf{N})^{\mathrm{T}} \tag{13.169a}$$

or

$$C_{ik}^{-1} = \frac{\delta_{ac}}{\lambda_a \lambda_c} Q_{ia} Q_{kc} \tag{13.169b}$$

we can see that (13.168) is equivalent to (13.157).

If all the principal stretch ratios coincide (at say λ), from (13.138a) and (13.152):

$$A = \frac{\partial S_i}{\partial E_i} = \lambda_i \frac{\partial S_i}{\partial \lambda_i} = \frac{2\mu}{\lambda^2} \tag{13.170}$$

while $B = 0$. Hence, from (13.141):

$$D_{ijkl}^{\mathrm{IK}2} = \frac{\mu}{\lambda^2}(\delta_{ik}\delta_{jl} + \delta_{il}\delta_{jk}) \tag{13.171}$$

Again, with the stretch ratios coinciding:

$$\mathbf{C}^{-1} = \frac{1}{\lambda^2}\mathbf{I}; \qquad C_{ik}^{-1} = \frac{1}{\lambda^2}\delta_{ik} \tag{13.172}$$

If we work with the Kirchhoff stress, τ, then from (13.148a) and (13.153), we have:

$$D_{iiii}^{\mathrm{tTKE}} = \lambda_i \frac{\partial \tau_i}{\partial \lambda_i} - 2\tau_i = 2\mu\lambda_i^2 - 2\mu(\lambda_i^2 - 1) = 2\mu \tag{13.173}$$

with $D_{iijj} = 0$ while from (13.148b) and (13.153), we obtain:

$$D_{ijij}^{\mathrm{tTKE}} = \mu \frac{(\lambda_j^2(\lambda_i^2 - 1) - \lambda_i^2(\lambda_j^2 - 1))}{\lambda_i^2 - \lambda_j^2} = \mu \tag{13.174}$$

If the stretch ratios λ_i and λ_j coincide, via (13.148c), we obtain the same result.

Combining (13.173) and (13.174) gives:

$$D_{ijkl}^{\mathrm{tTKE}} = \mu(\delta_{ik}\delta_{jl} + \delta_{il}\delta_{jk}) \tag{13.175}$$

Strictly we should now transform back from the Eulerian triad using the equivalent of (13.137) (obtained via (4.55)) with the Q's now relating to $\mathbf{Q}(\mathbf{n})$'a with the n's defining the Eulerian triad. However, because of the isotropy, this is not necessary and we can simply remove the superscript E in (13.175) so as to obtain (13.161). We will now labour the point by demonstrating this relationship.

The transformations lead to

$$D_{ijkl}^{\mathrm{tTK}} = Q_{ia}Q_{jb}Q_{kc}Q_{ld}D_{abcd}^{\mathrm{tTKE}} = \mu Q_{ia}Q_{jb}Q_{kc}Q_{ld}(\delta_{ac}\delta_{bd} + \delta_{ad}\delta_{bc}) \tag{13.176}$$

However because $\mathbf{QQ}^{\mathrm{T}} = \mathbf{QIQ}^{\mathrm{T}} = \mathbf{I}$, we can write:

$$Q_{ia}\delta_{ak}Q_{kc} = \delta_{ik} \tag{13.177}$$

so that $D_{ijkl}^{\mathrm{tTK}} = D_{ijkl}^{\mathrm{tTKE}}$.

13.9.2 The compressible neo-Hookean model

In Section 13.8.1, we showed that the compressible neo-Hookean model could be (but need not be) expressed directly in terms of principal stretch ratios. In this section, we will briefly outline the application of the method of Section 13.8.3, so as to directly obtain the constitutive tensor in relation to the Truesdell rate of Kirchhoff stress. To this end, we start by applying (13.110) and (13.116) so as to obtain the principal Kirchhoff stresses as

$$\tau_i = \lambda_i \frac{\partial \varphi}{\partial \lambda_i} = \mu J^{-2/3}\left(\lambda_i^2 - \frac{I_1}{3}\right) - pJ = \mu J^{-2/3}\left(\lambda_i^2 - \frac{I_1}{3}\right) + KJ(J-1) \tag{13.178}$$

In order to obtain the constitutive tensor, we now require:

$$\lambda_j \frac{\partial \tau_i}{\partial \lambda_j} = -\frac{2}{3}\mu J^{-2/3}\left(\lambda_i^2 + \lambda_j^2 - \frac{I_1}{3}\right) - pJ + 2\mu J^{-2/3}\lambda_j^2 \delta_{ij} \tag{13.179a}$$

$$\lambda_j \frac{\partial \tau_i}{\partial \lambda_j} = -\frac{2}{3}\mu J^{-2/3}\left(\lambda_i^2 + \lambda_j^2 - \frac{I_1}{3}\right) + KJ(2J-1) + 2\mu J^{-2/3}\lambda_j^2 \delta_{ij} \tag{13.179b}$$

where in (13.179a) we have kept the pressure, p, constant while in (13.179b) we give the equivalent combined relationship.

Application of (13.148a) now leads to

$$D_{iijj}^{[\mathrm{TKE}]} = -\frac{2}{3}\mu J^{-2/3}\left(\lambda_i^2 + \lambda_j^2 - \frac{I_1}{3}\right) - pJ + (2\mu J^{-2/3}\lambda_j^2 - 2\tau_i)\delta_{ij} \tag{13.180a}$$

$$D_{iijj}^{[\mathrm{TKE}]} = -\frac{2}{3}\mu J^{-2/3}\left(\lambda_i^2 + \lambda_j^2 - \frac{I_1}{3}\right) + KJ(2J-1) + (2\mu J^{-2/3}\lambda_j^2 - 2\tau_i)\delta_{ij} \tag{13.180b}$$

where, again, we have kept p constant in the first relationship.

From (13.178) and (13.148b), the 'shear terms' are given by

$$D_{ijij}^{[\mathrm{TKE}]} = D_{ijji}^{[\mathrm{TKE}]} = D_{jiij}^{[\mathrm{TKE}]} = D_{ijji}^{[\mathrm{TKE}]} = \frac{\mu}{3} J^{-2/3} I_1 + pJ \tag{13.181a}$$

$$D_{ijij}^{[\mathrm{TKE}]} = D_{ijji}^{[\mathrm{TKE}]} = D_{jiij}^{[\mathrm{TKE}]} = D_{ijji}^{[\mathrm{TKE}]} = \frac{\mu}{3} J^{-2/3} I_1 - KJ(J-1) \tag{13.181b}$$

Equations (13.180) and (13.181) are directly compatible with (13.98).

12.10 FURTHER WORK WITH PRINCIPAL STRETCH RATIOS

There are a number of energy functions which, unlike the neo-Hookean and Mooney–Rivlin models, can only be formulated in terms of the principal stretch ratios (and therefore require a polar decomposition—see Chapter 4). Such functions are based on the 'Valanis–Landel hypothesis' (of separability into principal directions [V1]) and we will now consider some examples.

13.10.1 An energy function using the principal log strains (the Hencky model [H2])

Consider the potential function:

$$\varphi = \mu \sum_{i=1}^{3} (\log_e \lambda_i)^2 + \tfrac{1}{2}(K - \tfrac{2}{3}\mu)(\log_e J)^2 \tag{13.182}$$

where again μ is the shear modulus and K the bulk modulus. Differentiation of (13.182) leads to

$$\frac{\partial \varphi}{\partial \lambda_i} = 2\mu\left(\frac{\log_e \lambda_i}{\lambda_i}\right) + [K - \tfrac{2}{3}\mu]\frac{\log_e J}{\lambda_i} = 2\mu\left(\frac{\log_e \lambda_i}{\lambda_i} - \frac{1}{3}\frac{\log_e J}{\lambda_i}\right) + K\frac{\log_e J}{\lambda_i} \tag{13.183}$$

Hence, from (13.110), the principal Kirchhoff stresses are

$$\tau_i = \lambda_i \frac{\partial \varphi}{\partial \lambda_i} = 2\mu \log_e \lambda_i - \tfrac{2}{3}\mu \log_e J - pJ \tag{13.184}$$

where

$$p = \frac{-K \log_e J}{J} \tag{13.185}$$

so that from (13.110):

$$\boldsymbol{\tau} = 2\mu \sum (\log_e \lambda_i - \tfrac{1}{3}\log_e J)\mathbf{n}_i \mathbf{n}_i^{\mathrm{T}} - pJ\mathbf{I} \tag{13.186a}$$

or

$$\boldsymbol{\tau} = 2\mu\, \mathrm{dev}(\log_e \mathbf{V}) - pJ\mathbf{I} \tag{13.186b}$$

If (13.185) is assumed, (13.186b) can be re-expressed as $\boldsymbol{\tau} = \mathbf{C}{:}\log_e \mathbf{V}$, where $\mathbf{C}$ is the standard linear constitutive tensor. From (13.186a), it is easy to show that when the principal stretches coincide, the coefficient of μ vanishes so that we have complete 'separability'. If we wish to work in the 'material frame' from (13.114), we can write the stress that is conjugate to $\log_e \mathbf{U}$ as

$$\mathbf{O} = 2\mu\, \mathrm{dev}(\log_e \mathbf{U}) - pJ\mathbf{I} \tag{13.187}$$

Alternatively, we could use (13.113) to obtain the second Piola–Kirchhoff stresses, $\mathbf{S}$. The procedure of Section 13.8.2 could then be used to obtain the tangent constitutive tensor. Instead, we will now apply the technique of Section 13.8.3 to obtain the constitutive tensor in relation to the Truesdell rate of Kirchhoff stress. To this end, we require (see (13.148)):

$$\lambda_j \frac{\partial \tau_i}{\partial \lambda_j} = -\tfrac{2}{3}\mu - pJ + 2\mu\delta_{ij} \tag{13.188a}$$

$$\lambda_j \frac{\partial \tau_i}{\partial \lambda_j} = -\tfrac{2}{3}\mu + K + 2\mu\delta_{ij} \tag{13.188b}$$

where, following the approach of Section 13.8.5, we have kept the pressure term constant in the first equation.

Application of (13.148a) now leads to

$$D_{iijj}^{\mathrm{tTKE}} = -\tfrac{2}{3}\mu - pJ + (2\mu - 2\tau_i)\delta_{ij} \tag{13.189a}$$

$$D_{iijj}^{\mathrm{tTKE}} = -\tfrac{2}{3}\mu + K + (2\mu - 2\tau_i)\delta_{ij} \tag{13.189b}$$

where, again, we have kept p constant in the first relationship.

Provided, $\lambda_i \neq \lambda_j$, the shear terms can be obtained directly from (13.148b). However, if $\lambda_i = \lambda_j$, we can use (13.148c) to obtain:

$$D_{ijij}^{\mathrm{tJKE}} = D_{ijji}^{\mathrm{tTKE}} = D_{jiij}^{\mathrm{tTKE}} = D_{ijji}^{\mathrm{tTKE}} = \mu - \tau_i \tag{13.190a}$$

It is instructive to apply (12.51) to these tangential moduli in order to relate them to the Jaumann rate rather than the Truesdell rate. In these circumstances, from (13.189b), we obtain:

$$D_{iijj}^{\mathrm{tJKE}} = -\tfrac{2}{3}\mu + K + 2\mu\delta_{ij} \tag{13.190b}$$

while from (13.148b) we have:

$$\begin{aligned} D_{ijij}^{\mathrm{tJKE}} &= D_{ijji}^{\mathrm{tJKE}} = D_{jiij}^{\mathrm{tJKE}} = D_{ijji}^{\mathrm{tJKE}} \\ &= \frac{\lambda_i^2\tau_i - \lambda_j^2\tau_j}{\lambda_i^2 - \lambda_j^2} + \frac{1}{2}(\tau_i + \tau_j) = \frac{(\lambda_i^2 + \lambda_j^2)}{2(\lambda_i^2 - \lambda_j^2)}(\tau_i - \tau_j) \quad i \neq j \end{aligned} \tag{13.190c}$$

Substitution from (13.184) and (13.185) into the latter, leads to the relationship:

$$D_{ijij}^{\mathrm{tJKE}} = D_{ijji}^{\mathrm{tJKE}} = D_{jiij}^{\mathrm{tJKE}} = D_{ijji}^{\mathrm{tJKE}} = \mu\frac{(\lambda_i^2 + \lambda_j^2)}{(\lambda_i^2 - \lambda_j^2)}\log_{\mathrm{e}}\left(\frac{\lambda_i}{\lambda_j}\right) \qquad i \neq j \tag{13.190d}$$

Using series expansions, we can obtain the approximation:

$$D_{ijij}^{\mathrm{tJKE}} = D_{ijji}^{\mathrm{tJKE}} = D_{jiij}^{\mathrm{tJKE}} = D_{ijji}^{\mathrm{tJKE}} = \mu\left(1 + \frac{1}{3}\left(\frac{\lambda_i}{\lambda_j}\right)^2 + \cdots\right) \simeq \mu \tag{13.190e}$$

Because (13.190b) and (13.190e) give an isotropic relationship, the transformation from the Eulerian triad is trivial (see Section 13.8.4) and we can combine these equations to obtain the linear isotropic relationship (see also (10.43)):

$$D_{ijkl}^{\mathrm{tJK}} \simeq \mu(\delta_{ik}\delta_{jl} + \delta_{il}\delta_{jk}) + (K - \tfrac{2}{3}\mu)\delta_{ij}\delta_{kl} \tag{13.190f}$$

It follows that provided the stretches are reasonably close to each other, instead of using Hencky's hyperelastic potential we could obtain effectively the same results using a hypoelastic formulation with a fixed linear elastic tangential modular tensor in conjunction with the Jaumann rate of Kirchhoff stress. (This is not to imply that the latter procedure is simpler.) Issues involving the integration of such a hypoelastic approach will be discussed in Chapter 19.

13.10.2 Ogden's energy function [O1.14, O4, O5]

This function has been found to be effective for very large strains. It can be considered to follow from (13.18) and can be written as

$$\varphi = \sum_{p=1}^{N} \mu_p(\lambda_1^{\alpha_p} + \lambda_2^{\alpha_p} + \lambda_3^{\alpha_p} - 3)/\alpha_p \tag{13.191}$$

where typical values of α_p and μ_p, for a three-term expansion ($N = 3$) are

$$\mu_1 = 6.0; \qquad \mu_2 = 0.01; \qquad \mu_3 = -0.1\ \mathrm{N/mm^2} \tag{13.192a}$$

$$\alpha_1 = 1.3; \qquad \alpha_2 = 5.0; \qquad \alpha_3 = -2.0 \tag{13.192b}$$

If a two-term expansion is applied with $\alpha_1 = 2$ and $\alpha_2 = -2$, (13.191) coincides with the Mooney–Rivlin function. Typical values for μ_1 (previously $2C_1$) and μ_2 (previously $-2C_2$) might be

$$\mu_1 = 4.0\ \mathrm{N/mm^2}; \qquad \mu_2 = -0.07\ \mathrm{N/mm^2} \tag{13.193}$$

It follows from (13.191) that:

$$\frac{\partial \varphi}{\partial \lambda_i} = \sum \mu_p \lambda_i^{\alpha_p - 1} \tag{13.194}$$

and from (13.110) that:

$$\tau_i = \sum \mu_p \lambda_i^{\alpha_p} \tag{13.195}$$

If we wish to adopt a compressible form, we can apply the approach of Section 13.3 and replace λ_i with $\bar{\lambda}_i = J^{-1/3}\lambda$ and, in addition, introduce a term for the volumetric energy (say (13.121a)) so that we have:

$$\varphi = \sum_{p=1}^{N} \left(\frac{\mu_p}{\alpha_p} (J^{-\alpha_p/3}(\lambda_1^{\alpha_p} + \lambda_2^{\alpha_p} + \lambda_3^{\alpha_p}) - 3) \right) + \frac{K}{2} (\log_e J)^2 \tag{13.196a}$$

or

$$\varphi = \sum_{p=1}^{N} \left(\frac{\mu_p}{\alpha_p} (J^{-\alpha_p/3} a_p - 3) + \frac{K}{2} (\log_e J)^2 \right. \tag{13.196b}$$

with

$$a_p = \lambda_1^{\alpha_p} + \lambda_2^{\alpha_p} + \lambda_3^{\alpha_p} \tag{13.197}$$

It follows from (13.110) that:

$$\tau_i = \lambda_i \frac{\partial \varphi}{\partial \lambda_i} = \sum_{p=1}^{N} \mu_p J^{-\alpha_p/3} (\lambda_i^{\alpha_p} - \tfrac{1}{3} a_p) - pJ \tag{13.198}$$

with the pressure p being given by

$$p = -K(\log_e J)/J \tag{13.199}$$

Knowing the principal stresses, τ_i, the stress tensor $\boldsymbol{\tau}$ can be simply obtained from (13.110).

To obtain the constitutive tensor, from (13.148a), we require:

$$\lambda_j \frac{\partial \tau_i}{\partial \lambda_j} = \sum \frac{\mu_p \alpha_p}{3} J^{-\alpha_p/3} (\tfrac{1}{3} a_p + 3\lambda_i^{\alpha_p} \delta_{ij} - \lambda_i^{\alpha_p} - \lambda_j^{\alpha_p}) - pJ \tag{13.200a}$$

$$\lambda_j \frac{\partial \tau_i}{\partial \lambda_j} = \sum \frac{\mu_p \alpha_p}{3} J^{-\alpha_p/3} (\tfrac{1}{3} a_p + 3\lambda_i^{\alpha_p} \delta_{ij} - \lambda_i^{\alpha_p} - \lambda_j^{\alpha_p}) + K \tag{13.200b}$$

where we have kept the pressure, p, fixed in the former equation. Hence the terms

D_{iijj}^{tTKE} can be obtained directly from (13.148a). Provided $\lambda_i \neq \lambda_j$, the terms D_{ijij}^{tTKE} (and equivalents—see (13.142b)) can be obtained directly from (13.148b) while if $\lambda_i = \lambda_j$, from (13.148c), we obtain:

$$D_{ijij}^{\mathrm{tTKE}} = \frac{\lambda_i}{2}\left(\frac{\partial \tau_i}{\partial \lambda_i} - \frac{\partial \tau_i}{\partial \lambda_j}\right) - \tau_i = \sum_{p=1}^{N} \frac{\mu_p \alpha_p}{2} J^{-\alpha_p/3} \lambda_i^{\alpha_p}(1 - \delta_{ij}) - \tau_i \qquad (13.201)$$

If N is set to 1 in the above, α_p is set to 2 and $\mu_p = \mu = 2C_1$, the previous equations coincide with those given in Section 13.8.5 for the 'neo-Hookean' model (apart from differences due to the use of different terms for φ_b). In particular, equation (13.200a) above coincides with (13.179a).

13.10.3 An example using Hencky's model

In this section, we will apply Hencky's model (Section 13.10.1) to the shear deformation of an initially square block (Fig. 13.3) under plane strain. The imposed displacements are given by

$$u = Ye; \qquad v = 0 \qquad (13.202)$$

so that the displacement derivative matrix is

$$\mathbf{D} = \begin{bmatrix} 0 & e \\ 0 & 0 \end{bmatrix} \qquad (13.203)$$

and the deformation gradient is given by

$$\mathbf{F} = \mathbf{I} + \mathbf{D} = \begin{bmatrix} 1 & e \\ 0 & 1 \end{bmatrix} \qquad (13.204)$$

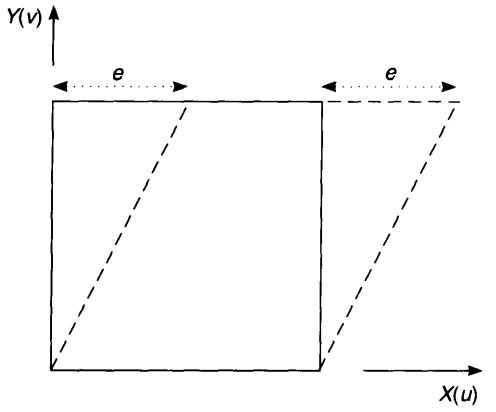

Figure 13.3 Shearing a block.

while the left Cauchy–Green tensor is given by:

$$\mathbf{b} = \begin{bmatrix} 1+e^2 & e \\ e & 1 \end{bmatrix} \tag{13.205}$$

The eigenvalues of (13.205) give the squares of the principal stretches so that:

$$\lambda_1 = \frac{e+\sqrt{e^2+4}}{2}; \qquad \lambda_2 = \frac{-e+\sqrt{e^2+4}}{2} \tag{13.206}$$

(Because of the plane-strain condition, $\lambda_3 = 1$). Using (13.184) and noting that $J = 1$ and $p = 0$, we obtain:

$$\tau_1 = 2\mu \log_e \lambda_1; \qquad \tau_2 = 2\mu \log_e \lambda_2 = -2\mu \log_e \lambda_1 \tag{13.207}$$

The second expression in (13.207) can be obtained by noting that $\lambda_2 = \lambda_1^{-1}$.

We now require the principal directions of the Eulerian frame in order to transform the principal Kirchhoff stresses into the base system. To this end, if we define the displacement e in Figure 13.3 as

$$e = 2\tan\beta \tag{13.208}$$

we can redefine (13.206) with

$$\lambda_1 = \frac{1+s}{c}; \qquad \lambda_2 = \frac{1-s}{c} \tag{13.209}$$

where

$$s = \sin\beta; \qquad c = \cos\beta \tag{13.210}$$

and the principal directions of $\mathbf{b}$ from (13.205) are

$$\mathbf{n}_1^{\mathrm{T}} = \frac{1}{\sqrt{2(1+s)}}(1+s, c)$$

$$\mathbf{n}_2^{\mathrm{T}} = \frac{1}{\sqrt{2(1+s)}}(-c, 1+s) \tag{13.211}$$

Using (13.186a), the Kirchhoff stress tensor is now given by

$$\boldsymbol{\tau} = 2\mu \log_e \lambda_1 \begin{bmatrix} s & c \\ c & -s \end{bmatrix} \tag{13.212}$$

while the rotation matrix $\mathbf{R}$ is given by

$$\mathbf{R} = \begin{bmatrix} c & s \\ -s & c \end{bmatrix} \tag{13.213}$$

The normalised components of the Kirchhoff stress are plotted against e in Figure 13.4. Dienes [D1.10] considered this example and showed that one obtained oscillatory shear stresses when using a hypoelastic formulation with a fixed tangential modular matrix in conjunction with a Jaumann rate formulation, but no such oscillatory stresses

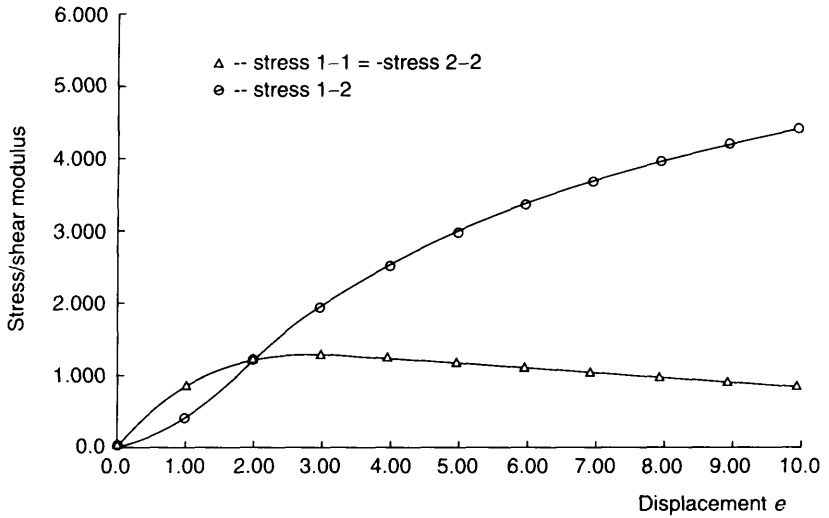

Figure 13.4 Normalised Kirchhoff stresses.

when applying a similar procedure using the Green–Nagdhi rate (Section 10.8). Of course, no such oscillatory stresses are obtained with the current hyperelastic formulation.

13.11 SPECIAL NOTATION

B_1–B_3 = scalars—see (13.34a)
$\mathbf{b} = \mathbf{F}\mathbf{F}^{\mathrm{T}}$ (left Cauchy–Green tensor)
$\bar{\mathbf{B}} = \bar{\mathbf{F}}\bar{\mathbf{F}}^{\mathrm{T}}$ ('volume preserving' left Cauchy–Green tensor)
$\mathbf{B}_{nl}$ = matrix connecting $\delta\mathbf{E}$ to $\delta\mathbf{p}$ (Section 13.5.1)
$\mathbf{B}(\mathbf{x})$ = matrix connecting $\delta\boldsymbol{\varepsilon}$ to $\delta\boldsymbol{p}$ (Section 13.7)
$\boldsymbol{B}$ = Biot stress (Section 13.8)
C_1, C_2 = constants for Mooney–Rivlin strain energy function
$\mathbf{C} = \mathbf{F}^{\mathrm{T}}\mathbf{F}$ (right Cauchy–Green tensor)
$\bar{\mathbf{C}} = \bar{\mathbf{F}}^{\mathrm{T}}\bar{\mathbf{F}}$ ('volume preserving' right Cauchy–Green tensor)
C_{ij}^{-1} = ijth component from $\mathbf{C}^{-1}$
$\mathbf{D}$ = fourth-order constitutive tensor
D_1–D_5 = scalars—see (13.37)
$\mathbf{E}$ = Green strain
$\mathbf{f}$ = nodal quantities representing lack of pressure compatibility (see (13.74))
F_1–F_6 = scalars—see (13.41)
$\mathbf{F}$ = deformation gradient
$\bar{\mathbf{F}}$ = 'volume preserving' deformation gradient (see (13.24a)
$\mathbf{G}$ = second-order pressure connection tensor
$\mathbf{g}$ = vector form of $\mathbf{G}$
h = shape function coefficients (for displacements)

$\mathbf{h}$ = shape function vector (for displacements)
h_p = shape function coefficients (for pressure)
$\mathbf{h}_p$ = shape function vector (for pressure)
$\mathbf{H}$ = pressure term in tangent stiffness matrix—see (13.79)
I_1–I_3 = in Section 13.1, invariants of $\boldsymbol{\varepsilon}$
I_1–I_3 = in other sections, invariants of $\mathbf{C}$ and $\mathbf{b}$ (see (13.12))
$\bar{I}_2$ = modified invariant (see (13.3)) in Section 13.1
$\bar{I}_1$–$\bar{I}_2$ = second invariants (see (13.26)) in Sections 13.3–13.10
$\mathbf{I}$ = identify matrix
J = $\det(\mathbf{F}) = I_3^{1/2}$
K = bulk modulus
$\mathbf{L}$ = velocity gradient
$\mathbf{N}_1$–$\mathbf{N}_3$ = unit principal vectors in initial (Lagrangian) configuration
$\mathbf{n}_1$–$\mathbf{n}_3$ = unit principal vectors in current (Eulerian or spatial) configuration
$\mathbf{O}$ = stress conjugate to '$\log_e \mathbf{U}$'
$\mathbf{U}$ = right stretch tensor
$\mathbf{p}$ = nodal displacements; changes, $\delta\mathbf{p}$
$\mathbf{P}$ = pressure-displacement connectivity part of tangent stiffness matrix (see (13.72))
p = pressure (positive for compression)
$\boldsymbol{p}$ = nodal pressure variables; changes, $\delta\boldsymbol{p}$
$\mathbf{Q}(\mathbf{N})$ = orthogonal matrix containing the Lagrangian triad of $\mathbf{N}$'s
$\mathbf{Q}(\mathbf{n})$ = orthogonal matrix containing the Eulerian traid of $\mathbf{n}$'s
$\mathbf{R}$ = rotation matrix
$\mathbf{S}$ = second Piola–Kirchhoff stresses
$\mathbf{W}_n$ = Section 13.8.2 spin of the Lagrangian triad—see (13.124a)
$\mathbf{z}$ = eigenvectors of $\boldsymbol{\varepsilon}$ (Section 13.1)
$\boldsymbol{\varepsilon}$ = small-strain tensor (Section 13.1)
$\dot{\boldsymbol{\varepsilon}}$ = Eulerian strain rate (or $\delta\boldsymbol{\varepsilon}$)
ε_p = principal values of $\boldsymbol{\varepsilon}$ (Section 13.1)
φ = strain energy function; φ_d—distortional, φ_b—volumetric or 'bulk'
$\boldsymbol{\Omega}$ = spin (or $\delta\boldsymbol{\Omega}$)
$\boldsymbol{\tau}$ = Kirchhoff stresses
λ_1–λ_3 = principal stretches
$\bar{\lambda}_1$–$\bar{\lambda}_3$ = 'volume preserving' principal stretches (see (13.22))
μ = shear modulus

Subscripts or superscripts

$\dot{\mathrm{L}}$ = (only in Section 13.8.2) implies a tensor related to the Lagrangian triad
t = tangential
v = virtual
tJK = tangential for Jaumann rate of Kirchhoff stress
tTK = tangential for Truesdell rate of Kirchhoff stress
tK = tangential for Kirchhoff stress
tK2 = tangential for second Piola–Kirchhoff stress

13.12 REFERENCES

[C1] Chadwick, P. & Ogden, R. W., A theorem of tensor calculus and its application to isotropic elasticity, *Archive for Rational Mechanics and Analysis*, **44**, 54–68 (1971).

[C2] Chadwick, P. & Ogden, R. W., On the definition of elastic moduli, *Archive for Rational Mechanics and Analysis*, **44**, 41–53 (1971).

[D1] De Borst, R., Van den Bogert, P. A. J. & Zeilmaker, J., Modelling and analysis of rubberlike materials, *Heron*, **33**(1), (1988).

[D2] Desai, C. S. & Siriwardane, H. J., *Constitutive Laws for Engineering Materials with Emphasis on Geological Materials*, Prentice-Hall, Englewood Cliffs (1984).

[D3] Dobrowlski, M. A., A mixed finite element method for approximating incompressible materials, *SAIM J. Numer. Anal.*, **29**(2), 365–389 (1992).

[D4] Duffett, G. & Reddy, B. D., The analysis of incompressible hyperelastic bodies by the finite element method, *Comp. Meth. in Appl. Mech. & Engng.*, **41**(1), 105–120 (1983).

[F1] Freakley, P. K. & Payne, A. R., *Theory and Practice of Engineering with Rubber*, Applied Science Publishers, London (1978).

[F2] Fried, I. & Johnson, A. R., A note on elastic energy density functions for largely deformed compressible rubber solids, *Comp. Meth. in Appl. Mech. & Engng.*, **69**, 53–64 (1988).

[G1] Gadala, M. S., Alternative methods for the solution of hyperelastic problems with incompressibility, *Computers & Structures*, **42** (1), 1–10 (1992).

[G2] Gent, A. N., Rubber and rubber elasticity; a review, *Journal of Polymer Science; Polymer Symposia, No. 48*, ed. A. S. Dunn, Interscience, pp 1–17 (1974).

[G3] Gruttman, F. & Taylor, R. L., Theory and finite element formulation of rubber-like membrane shells using principal stretches, *Int. J. for Num. Meth. in Engng.*, **35**, 1111–1126 (1992).

[H1] Haggblad, B. & Sundberg, J. A., Large strain solutions of rubber components, *Comp. & Struct.*, **17** (6/6), 835–843 (1983).

[H2] Hencky, H., The elastic behaviour of vulcanised rubber. *J. of Appl. Mech.*, **1**, 45–53 (1933).

[H3] Hughes, T. J. R., *The Finite Element Method; Linear Static and Dynamic Finite Element Analysis*, Prentice-Hall, Englewood Cliffs, New Jersey (1987).

[M1] Malkus, D. S. & Hughes, T. J. R., Mixed finite element methods – reduced and selective integration techniques: a unification of concepts, *Comp. Meth. in Appl. Mech. & Engng.*, **15**, 68–81 (1978).

[M2] Mooney, M., A theory of large elastic deformations, *J. of Appl. Mech.*, **11**, 582–592 (1940).

[M3] Mullins, L. & Thomas, A. G., A theory of rubber-like elasticity, *The Chemistry and Physics of Rubber-like Substances*, Chapter 7 ed. L. Bateman, Maclaren, London, 1963.

[O1] Ochi, M., Nato, S. & Abe, T., Numerical analysis of deformation of rubber composite materials, *JSME Int. Journal, Series I*, **35**, 4 (1992).

[O2] Oden, J. T., *Finite Elements of Nonlinear Continua*, McGraw-Hill, New York (1972).

[O3] Oden, J. T. & Kikuchi, N., Finite element methods for constrained problems in elasticity, *Int. J. for Num. Meth. in Engng.*, **18**, 701–725 (1982).

[O4] Ogden, R. W., Large deformation isotropic elastic – on the correlation of theory and experiment for incompressible rubberlike solids, *Proc. Roy. Soc. London*, **A326**, 565–584 (1972).

[O5] Ogden, R. W., *Elastic Deformation of Rubberlike Solids*, Mechanics of Solids, the Rodney Hill 60th Anniversary Volume, ed. H. G. Hopkins & M. J. Sewell, Pergamon, Oxford (1982).

[P1] Peeken, H., Dopper, R. & Orschall, B., A 3-D rubber material model verified in a user supplied subroutine, *Comp. & Struct.*, **1/2**, 181–189 (1987).

[R1] Rivlin, R. S., Large elastic deformations of isotropic materials, IV, Further developments of the general theory, *Phil. Trans. Roy. Soc.*, **A241**, 379–397 (1948).

[S1] Saleed, A. F., Change, T. Y. P. & Arnol, S. M., On the development of explicit robust schemes for implementation of a class of hyperelastic models in large-strain analysis of rubber, *Int. J. for Num. Meth. in Engng.*, **33**, 1237–1249 (1992).

[S2] Simo, J. C. & Taylor, R. L., Quasi-incompressible elasticity in principal stretches; continuum basis and numerical algorithms, *Comp. Meth. in Appl. Mech. & Engng.*, **85**, 273–310 (1991).

[S3] Simo, J. C. & Ortiz, M., A unified approach to finite deformation elastoplastic analysis based on the use of hyperelastic constitutive equations, *Comp. Meth. in Appl. Mech. & Engng.*, **49**, 221–245 (1985).

[S4] Simo, J. C. & Pister, K. S., Remarks on rate constitutive equations for finite deformation problems: computational implications, *Comp. Meth. in Appl. Mech. & Engng.*, **46**, 201–215 (1874).

[S5] Simo, J. C., Taylor, R. L. & Pister, K. S., Variational and projection methods for the volume constraint in finite deformation elastoplasticity, *Comp. Meth. in Appl. Mech. & Engng.*, **51**, 177–208 (1985).

[S6] Sussman, T. & Bathe, K.-J., A finite element formulation for nonlinear incompressible elastic and inelastic analysis, *Computers & Structs.*, **26** (1/2), 357–409 (1987).

[S7] Szabo, B. & Babuska, I., *finite Element Analysis*, Wiley, 1991.

[T1] Treloar, L. R. G., *The Physics of Rubber Elasticity*, 3rd edn., Oxford Univ. Press, 1975.

[V1] Valanis, K. C. & Landel, R. F., The strain energy function of a hyperelastic material in terms of the extension ratios, *J. of Appl. Phys.*, **38**, 2997–3002 (1967).

[W1] Wriggers, P. & Taylor, R. L., A fully nonlinear axisymmetrical membrane element for rubberlike materials, *Engng. Computations*, **7**, 303–310 (1990).

[Z1] Zienkiewicz, O. C. & Taylor, R. L., *The Finite Element Method*, 4th edn, Vol. 1, *Basic Formulation and Linear Problems*, McGraw-Hill (1989).

[Z2] Zienkiewicz, O. C., Qu, S., Taylor, R. L. & Nakazawa, S., The patch test for mixed formulation, *Int. J. for Num. Meth. in Engng.*, **23**, 1873–1883 (1986).

[Z3] Zienkiewciz, O. C., Maosong Huang & M. Pastor, Localization problems in plasticity using finite element with adaptive remeshing, *Int. J. for Num. Meth. in Engng.*, **19**, 127–148 (1995).

14 More plasticity and other material non-linearity—I

14.1 INTRODUCTION

In Chapter 6, we introduced plasticity and concentrated on the von Mises (J2) yield criterion. Although many of the concepts and, indeed, the algorithms in that chapter are relevant to other criteria, no details were provided. The present chapter will consider a range of other yield criteria. Initially, we will concentrate on those criteria which involve a 'volumetric component' and can be used for geomechanical materials. We will also introduce criteria which involve corners in the yield surface and will discuss some special algorithms required for their numerical treatment. Details are given for both the Mohr–Coulomb yield criterion and the Ilyushin yield criterion for shells, which works directly with the stress resultants. Later in the chapter, we will consider criteria than can be used for anisotropic plasticity. As a by-product, methods will be introduced for the backward-Euler return that are computationally more efficient than some of the methods introduced in Chapter 6.

Towards the end of the chapter, we will consider softening and fracturing materials, with emphasis on concrete. Some of the suggested procedures also fall into the 'plasticity' category while others do not. Among the latter is 'damage mechanics' which is briefly discussed in the final section of this chapter. A further chapter on plasticity is Chapter 16 which concentrates on various forms of hardening and also considers viscoplasticity.

Both the current and the next chapter will follow Chapter 6 in concentrating on 'algorithmic aspects'. References to more general reading were given in Chapter 6. More recent books covering plasticity are due to Lemaitre and Chaboche [L3], Lubliner [L4] and Simo and Hughes [S5]. Also, in relation to finite elements, the new editions of the books by Bathe [B1.4] and Zienkiewicz and Taylor [Z1] give chapters devoted to the topic and a report by Waszczyszyn [W1] covers a range of issues. Both the current and the following chapters are limited to small strains. Large strains will be considered in Chapter 19.

14.2 OTHER ISOTROPIC YIELD CRITERIA

The von Mises yield criterion is a function of the second deviatoric stress invariant (J_2—see (6.26)) and, in principal stress space, can be depicted as a cylinder

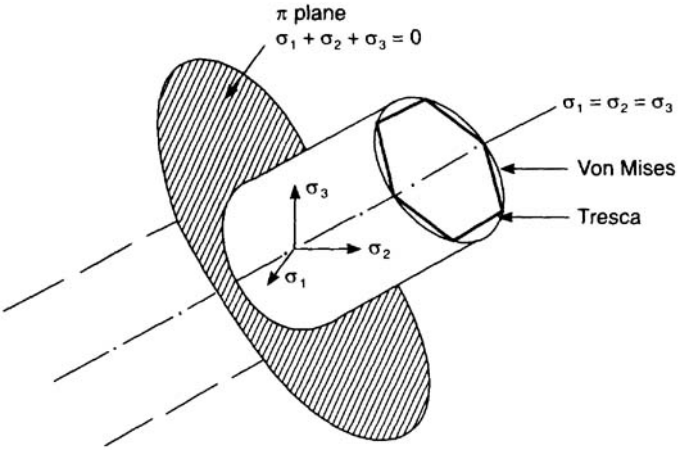

Figure 14.1 Von Mises and Tresca yield functions.

(Figure 14.1). In order to make the magnitude of the yield surface cross-section change with volumetric or mean stress, we must make the yield criterion a function of the first invariant, $I_1 = J_1$ where

$$I_1 = (\sigma_1 + \sigma_2 + \sigma_3) = 3\sigma_m \tag{14.1}$$

With $f = f(I_1, J_2)$, we can produce the Drucker–Prager yield criterion [D6] (Figure 14.2) where

$$f = (DI_1 + J_2^{1/2}) - \sigma_o \tag{14.2}$$

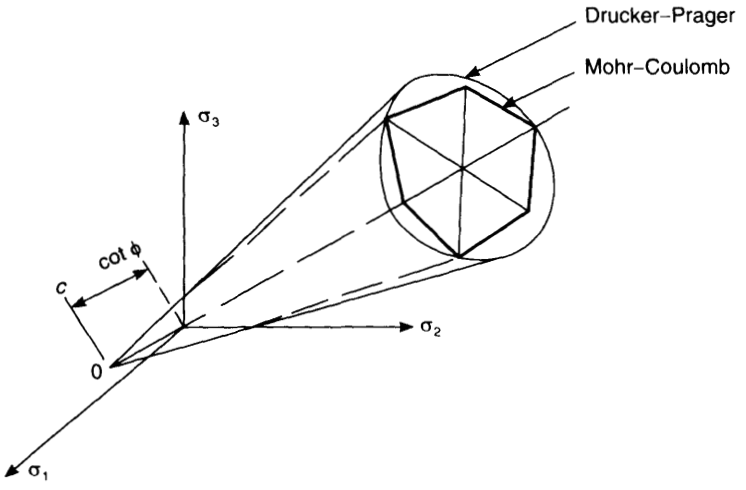

Figure 14.2 Drucker–Prager and Mohr–Coulomb yield functions.

Details will be given later, and an alternative form for the Drucker–Prager criterion will be given in Section 14.9.

A well-Known alternative to the von Mises yield criterion is the Tresca yield criterion (Figure 14.1). In terms of principal stresses, this crterion is given by

$$f = (\sigma_1 - \sigma_3) - \sigma_o = 0 \tag{14.3a}$$

$$\sigma_1 > \sigma_2 > \sigma_3 \tag{14.3b}$$

In order to express this yield criterion in terms of stress invariants, we can follow Nayak and Zienkiewicz [N1] and Owen and Hinton [O2] and use the relationship:

$$\begin{bmatrix} \sigma_1 \\ \sigma_2 \\ \sigma_3 \end{bmatrix} = \frac{2J_2^{1/2}}{\sqrt{3}} \begin{bmatrix} \sin(\theta + 2\pi/3) \\ \sin\theta \\ \sin(\theta - 2\pi/3) \end{bmatrix} + \frac{I_1}{3} \begin{bmatrix} 1 \\ 1 \\ 1 \end{bmatrix} \tag{14.4}$$

where J_2 was defined in (6.26) and the (Lode) angle θ (see Figure 14.3) is related to the third deviatoric invariant:

$$J_3 = \det[\mathbf{s}] \tag{14.5}$$

where $\mathbf{s}$ are the deviatoric stresses (see Section 4.2.2 and (6.28)) via:

$$-\pi/6 \leqslant \theta = \tfrac{1}{3}\sin^{-1}\left(\frac{-3\sqrt{3}J_3}{2J_2^{3/2}}\right) \leqslant \pi/6 \tag{14.6}$$

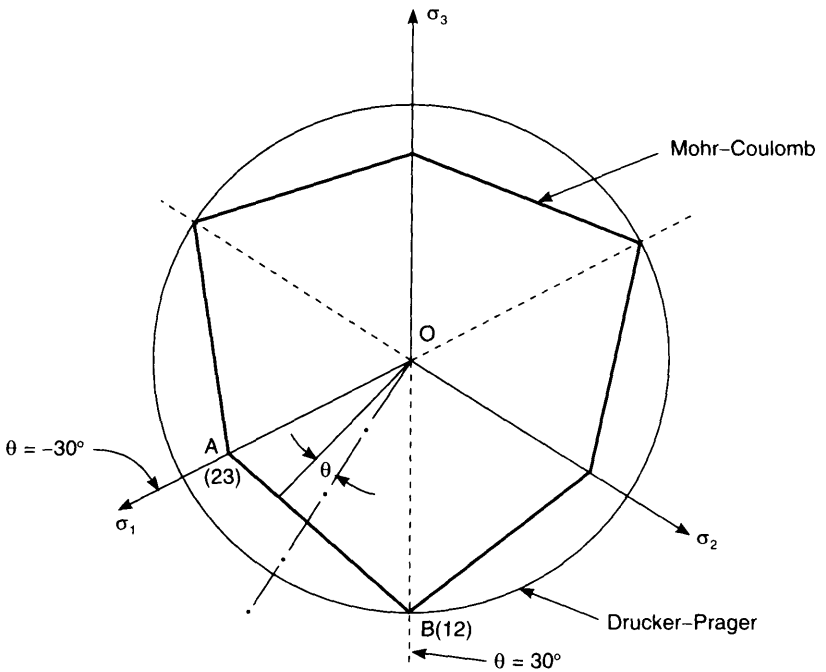

Figure 14.3 The Pl-plane.

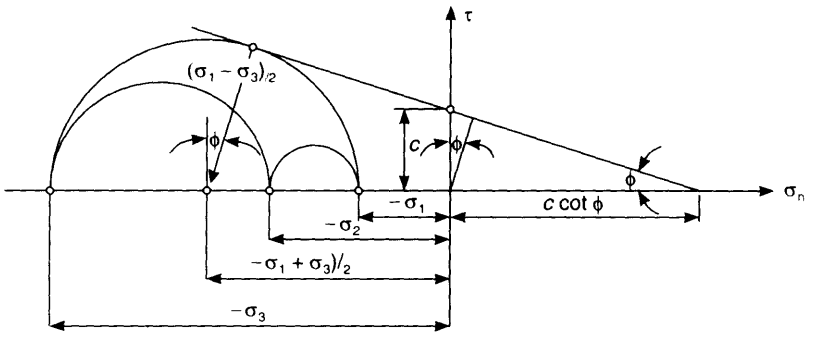

Figure 14.4 τ/σ_n and Mohr's circle representations of Mohr–Coulomb yield function.

For 'two-dimensional' applications, J_3 can be expressed as

$$J_3 = s_z(s_z^2 - J_2) \tag{14.7}$$

In relation to Figure 14.3, if we impose the restriction of (14.3b) on the ordering of the principal stresses, we need only work in the sextent OAB.

Using (14.4), the Tresca yield criterion of (14.3) can be re written as

$$f = 2(J_2)^{1/2} \cos\theta - \sigma_o = \sigma_e - \sigma_o \tag{14.8}$$

The Mohr-Coulomb yield criterion [M4, C15] is a generalisation of the cohesive-frictional relationship (Figure 14.4):

$$f = \tau \cos\varphi + \sigma_n \sin\varphi - c \cos\varphi = 0 \tag{14.9a}$$

where σ_n is the normal stress on the 'slip-plane' at which the shear stress is τ. The constant c is the cohesion and φ is the angle of friction. Assuming $\sigma_1 > \sigma_2 > \sigma_3$, (14.9a) generalises to

$$f = \tfrac{1}{2}(\sigma_1 - \sigma_3) + \tfrac{1}{2}(\sigma_1 + \sigma_3)\sin\varphi - c\cos\varphi \tag{14.9b}$$

and using (14.4), (14.9b) can be rewritten as

$$f = (\tfrac{1}{3} I_1 \sin\varphi + J_2^{1/2} A(\theta)) - c\cos\varphi = \sigma_e - \sigma_o \tag{14.9c}$$

with

$$A(\theta) = \left(\cos\theta - \frac{\sin\theta \sin\varphi}{\sqrt{3}} \right) \tag{14.10}$$

where θ was defined in (14.6). The Mohr–Coulomb criterion is illustrated in principal stress space in Figure 14.2.

The Drucker–Prager criterion of (14.2) (see also Figures 14.2 and 14.3) can be considered as a smoothed approximation to the Mohr–Coulomb relationship of (14.9c) (see Figure 14.5) and can be expressed via (14.2) which is reproduced here for convenience as

$$f = (DI_1 + J_2^{1/2}) - \sigma_o \tag{14.11}$$

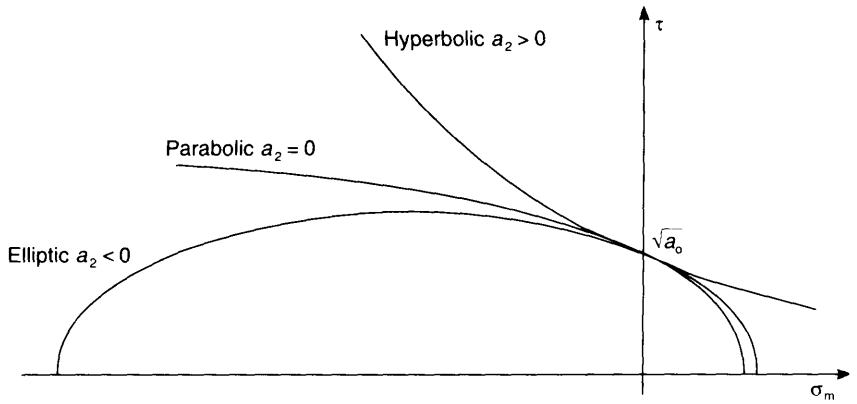

Figure 14.5 τ/σ_m relationships for 'crushable foam' model.

where

$$D = \frac{2\sin\varphi}{\sqrt{3}(3 \pm \sin\varphi)} \tag{14.12a}$$

$$\sigma_0 = \frac{6c\cos\varphi}{\sqrt{3}(3 \pm \sin\varphi)} \tag{14.12b}$$

with the plus sign being adopted if the yield surface is made to coincide with the inner corners of the Mohr–Coulomb surface while the minus sign applies if the surface is fitted to the outer corners (as in Figures 14.2 and 14.3).

Before moving on to the numerical implementation of the various yield criteria, we note that they can all be expressed in the form:

$$f = \sigma_e(I_1, J_2, \theta) - \sigma_0 = 0 \tag{14.13}$$

where the precise forms are given in Table 14.1.

Before moving on to consider the previous yield criteria in detail, we will very briefly discuss some further yield criteria involving a pressure contribution. From Figure 14.2,

Table 14.1 Yield criteria: $f = \sigma_e(I_1, J_2, \theta) - \sigma_0$.

	σ_e	σ_0
Von Mises	$\sqrt{3}J_2^{1/2}$	σ_0
Tresca	$2J_2^{1/2}\cos\theta$	σ_0
Drucker–Prager	$DI_1 + J_2^{1/2}$ (see (14.12a) for D)	σ_0 (see (14.12b))
Mohr–Coulomb	$(\frac{1}{3}I_1\sin\varphi + J_2^{1/2}A(\theta))$ (see (14.10) for $A(\theta)$)	$c\cos\varphi$

it can be seen that the previous yield criteria are open at the compressive end. One way of closing the yield criterion is to apply a 'cap' to the Drucker–Prager model [R2]. An alternative is provided by the 'crushable foam model' of Key [K2] (see also Duffet *et al.* [D7]). In describing this criterion, we will use the mean stress σ_m from (14.1) and $\tau = J_2^{1/2}$. The yield criterion is then given by

$$f = \tau^2 - a_0 + a_1\sigma_m - a_2\sigma_m^2 = 0 \tag{14.14}$$

If $a_1 = a_2 = 0$ and $3a_0 = \sigma_0^2$, we recover the von Mises yield criterion, while with $a_2 = 0$, we obtain the modified von Mises yield criterion of Raghava *et al.* [R1]. In particular, we can then set:

$$a_0 = -\sigma_c\sigma_t/3; \qquad a_1 = -(\sigma_c + \sigma_t) \tag{14.15}$$

where σ_c (a negative number) and σ_t (a positive number) are the effective yield stresses in tension and compression respectively.

If $a_2 \neq 0$, we can obtain an elliptical ($a_2 < 0$), parabolic ($a_2 = 0$) or hyperbolic ($a_2 > 0$) shape (see Figure 14.5). The elliptical criterion takes the shape of the modified Cam clay model [R3]. A similar shape can be obtained by Tvergaard's modification [T1] of Gurson's model [G1] for porous materials which takes the form:

$$f = \tau^2 - a_0 + a_1 \cosh(a_2\sigma_m) \tag{14.16}$$

Here a_0 and a_1 are related to the void volume fractions.

14.2.1 The flow rules

In the following, it will be assumed that an associative flow rule is being adopted. (In practice, for many applications with soils, a non-associative flow rule may be used so that the flow direction is governed by a plastic potential, $Q \neq f$ (see Section 6.3.1 where the symbol g was used rather than the current symbol Q). To reduce the 'dilation' effects, a non-pressure-dependent function, such as the von Mises function, may be used for Q.

As a first step in any numerical formulation, we require expressions for the flow vectors, $\mathbf{a}$ which were written in Chapter 6 as

$$\mathbf{a} = \frac{\partial f}{\partial \boldsymbol{\sigma}} \tag{14.17}$$

with $\partial f/\partial \boldsymbol{\sigma}$ being defined throughout this chapter (as in Chapter 6) as a column vector. In order to obtain this vector ($\mathbf{a}$) via differentiation of (14.13), we require from (14.6):

$$\frac{\partial \theta}{\partial \boldsymbol{\sigma}} = \frac{-\sqrt{3}}{2\cos 3\theta}\left(J_2^{-3/2}\frac{\partial J_3}{\partial \boldsymbol{\sigma}} - \frac{3}{2}J_3 J_2^{-5/2}\frac{\partial J_2}{\partial \boldsymbol{\sigma}}\right) \tag{14.18}$$

The various yield functions can now be differentiated to give

$$\mathbf{a} = C_1\mathbf{a}_1 + C_2\mathbf{a}_2 + C_3\mathbf{a}_3 \tag{14.19}$$

Table 14.2 Constants C_1–C_3 for different yield functions.

Yield function	C_1	C_2	C_3
von Mises	0	$\sqrt{\frac{3}{4}}J_2^{-1/2}$	0
Tresca	0	$\cos\theta(1+\tan\theta\tan 3\theta)J_2^{-1/2}$	$\dfrac{\sqrt{3}\sin\theta}{J_2\cos 3\theta}$
Drucker–Prager	D (equation (14.14a))	$\frac{1}{2}J_2^{-1/2}$	0
Mohr–Coulomb	$\sin\varphi/3$	$\frac{1}{2}J_2^{-1/2}\left(A(\theta)-\tan 3\theta\dfrac{\mathrm{d}A}{\mathrm{d}\theta}\right)$	$\dfrac{-\sqrt{3}}{2J_2\cos 3\theta}\dfrac{\mathrm{d}A}{\mathrm{d}\theta}$

Note: The terms $\mathrm{d}A/\mathrm{d}\theta$ in Table 14.2 are simply obtained by differentiation of equation (14.10).

where

$$\mathbf{a}_1^{\mathrm{T}} = \left(\frac{\partial I_1}{\partial \boldsymbol{\sigma}}\right)^{\mathrm{T}} = \{1,1,1,0,0,0\} \tag{14.20}$$

$$\mathbf{a}_2^{\mathrm{T}} = \left(\frac{\partial J_2}{\partial \boldsymbol{\sigma}}\right) = \{s_x, s_y, s_z, 2\tau_{xy}, 2\tau_{yz}, 2\tau_{zx}\} \tag{14.21}$$

$$\mathbf{a}_3^{\mathrm{T}} = \left(\frac{\partial J_3}{\partial \boldsymbol{\sigma}}\right)^{\mathrm{T}}$$
$$= ((s_y s_z - \tau_{yz}^2 + J_2/3), (s_x s_z - \tau_{xz}^2 + J_2/3), (s_x s_y - \tau_{xy}^2 + J_2/3), 2(\tau_{yz}\tau_{xz} - s_z\tau_{xy}),$$
$$2(\tau_{xz}\tau_{xy} - s_x\tau_{yz}), 2(\tau_{xy}\tau_{yz} - s_y\tau_{xz})) \tag{14.22}$$

To fully defined the flow vector, $\mathbf{a}$, we also require the constants, C_1–C_3 in (14.19) which are given in Table 14.2.

14.2.2 The matrix $\partial\mathbf{a}/\partial\boldsymbol{\sigma}$

The previous definitions are sufficient to enable the forward-Euler method to be applied to the different yield criteria so as to produce, the tangent modular matrix via (6.9). However, if the backward-Euler method (Section 6.6.6) is to be applied and a consistent tangent modular matrix (Section 6.7) is to be used, the matrix $\partial\mathbf{a}/\partial\boldsymbol{\sigma}$ (see Section 6.6.6) must be formed. This matrix has already been derived for the von Mises yield criterion in (6.47). More generally, (14.19) must be differentiated so that:

$$\frac{\partial \mathbf{a}}{\partial \boldsymbol{\sigma}} = C_2\frac{\partial \mathbf{a}_2}{\partial \boldsymbol{\sigma}} + C_3\frac{\partial \mathbf{a}_3}{\partial \boldsymbol{\sigma}} + C_{22}\mathbf{a}_2\mathbf{a}_2^{\mathrm{T}} + C_{23}\mathbf{a}_2\mathbf{a}_3^{\mathrm{T}} + C_{32}\mathbf{a}_3\mathbf{a}_2^{\mathrm{T}} + C_{33}\mathbf{a}_3\mathbf{a}_3^{\mathrm{T}} \tag{14.23}$$

where

$$\frac{\partial \mathbf{a}_2}{\partial \boldsymbol{\sigma}} = \frac{1}{3}\begin{bmatrix} 2 & -1 & -1 & & & \\ -1 & 2 & -1 & & & \\ -1 & -1 & 2 & & & \\ & & & 6 & & \\ & & & & 6 & \\ & & & & & 6 \end{bmatrix} \tag{14.24}$$

$$\frac{\partial \mathbf{a}_3}{\partial \boldsymbol{\sigma}} = \frac{2}{3}\begin{bmatrix} s_x & & & & & \\ s_z & s_y & & & & \\ s_y & s_x & s_z & & & \\ \tau_{xy} & \tau_{xy} & -2\tau_{xy} & -3s_z & & \\ -2\tau_{yz} & \tau_{yz} & \tau_{yz} & 3\tau_{xz} & -3s_x & \\ \tau_{xz} & 2\tau_{xz} & \tau_{xz} & 3\tau_{yz} & 3\tau_{xy} & -3s_y \end{bmatrix} \tag{14.25}$$

and the constants C_{22}–C_{33} are given in Table 14.3. In relation to Table 14.3, $A(\theta)$ is given by (14.10) and $\mathrm{d}A/\mathrm{d}\theta$ and $\mathrm{d}^2A/\mathrm{d}\theta^2$ are the first and second derivatives of (14.10) with respect to θ. Table 14.3 does not give a specific relationship for the Tresca yield criterion because this criterion can be considered as a special case of the Mohr–Coulomb criterion with the angle of friction, φ, being set to zero.

For the Tresca and Mohr–Coulomb yield criteria and others that involve corners, special procedures are required. These will be discussed in the next section and in Section 14.5. However, with this reservation, many of the techniques of Chapter 6 can be applied now that we have defined the **a** vector and $\partial\mathbf{a}/\partial\boldsymbol{\sigma}$ matrices. (If non-associative plasticity is considered (Section 6.3.1), we require $\mathbf{b}' = \partial Q/\partial\boldsymbol{\sigma}$ and $\partial\mathbf{b}'/\partial\boldsymbol{\sigma}$, where Q is the plastic potential. The derivation of the backward-Euler return procedure and related

Table 14.3 Coefficients required for $\partial\mathbf{a}/\partial\boldsymbol{\sigma}$.

von Mises:

$$C_{22} = -\tfrac{\sqrt{3}}{4}J_2^{-3/2}, \qquad C_{23} = C_{32} = C_{33} = 0$$

Drucker–Prager:

$$C_{22} = -\tfrac{1}{4}J_2^{-3/2}, \qquad C_{23} = C_{32} = C_{33} = 0$$

Mohr-Coulomb:

$$C_{23} = C_{32} = \left(\frac{1}{2}\tan 3\theta\, C_4 + \frac{\mathrm{d}A}{\mathrm{d}\theta}\right)\frac{\sqrt{3}}{2J_2^2\cos 3\theta}$$

$$C_{22} = -\left(A(\theta) - \tan^2 3\theta\, C_4 - 3\tan 3\theta\frac{\mathrm{d}A}{\mathrm{d}\theta}\right)\Big/ 4J_2^{3/2}$$

$$C_{33} = \frac{3C_4}{4J_2^{5/2}\cos^2 3\theta}, \qquad C_4 = \frac{d^2A}{\mathrm{d}\theta^2} + 3\tan 3\theta\frac{\mathrm{d}A}{\mathrm{d}\theta}$$

consistent tangent matrix for the non-associative case follows a straightforward modification of the associative development and hence will not be specifically detailed here.) In particular, we can apply the backward-Euler procedures of Section 6.6.6 and can derive the consistent tangent modular matrix of (6.110). Alternative methods for applying the backward-Euler return will be discussed in Section 14.7.

14.3 YIELD FUNCTIONS WITH CORNERS

Various attempts have been made to approximate yield functions with corners either using a smooth rounding [Z2] or a very local rounding [S7]. However, Koiter [K4] has devised a theory that is applicable to yield functions with corners and the author has found that this technique is numerically far more effective [C3, C4] than attempts at local rounding. Other work on yield criteria with corners has been given by Owen *et al.* [O3], Marques [M1], Pankaj & Bicanic [P1], de Borst *et al.* [D1, D2], Pramono & Willam [P4] and Simo *et al.* [S3].

As a first step, we will, in general terms, extend the backward-Euler technique of Section 6.6.6 to cover the case where the return is being made to the corner region at which two yield surfaces are active (the procedure can be extended to cover more than two yield surfaces). We will then derive an equivalent consistent tangent modular matrix by extending the approach of Section 6.7.2.

For the first practical application, we will consider the Ilyushin yield function [I1] which is a stress-resultant approach that can be applied to shells [I1, I2, C5–C9] (see Section 14.4). Later, in Section 14.5, we will consider the Mohr–Coulomb yield criterion in some detail.

14.3.1 A backward-Euler return with two active yield surfaces

It will be assumed that we know that the return will take us to a corner where two yield surfaces are active (Figure 14.6). The equivalent yield functions will be $f = 0$ and $g = 0$ with the normal to the first surface being $\mathbf{a}$ (as with our conventional use for a single yield surface) and $\mathbf{b}$ will be the normal to the second surface. Consequently $\mathbf{a} = \partial f/\partial \boldsymbol{\sigma}$ and $\mathbf{b} = \partial g/\partial \boldsymbol{\sigma}$. In place of (6.78), the backward-Euler return is given by

$$\boldsymbol{\sigma}_C = \boldsymbol{\sigma}_B - \Delta\lambda \mathbf{C}\mathbf{a}_C - \Delta\eta \mathbf{C}\mathbf{b}_C \tag{14.26}$$

where the subscripts B and C have the same meaning as they did in Chapter 6 (see Figure 6.12) with B being the 'trial' elastic position and C the final return point (now on a corner). If we have some initial estimates for $\boldsymbol{\sigma}_C$ (and hence $\mathbf{a}_C$ and $\mathbf{b}_C$), $\Delta\lambda$ and $\Delta\eta$ (see Sections 14.4.4 and 1.5 for details), these will in general not satisfy (14.26) and, following the approach of Section 6.6.6, we can set up a residual, $\mathbf{r}$, where

$$\mathbf{r} = \boldsymbol{\sigma}_C - (\boldsymbol{\sigma}_B - \Delta\lambda \mathbf{C}\mathbf{a}_C - \Delta\eta \mathbf{C}\mathbf{b}_C) \tag{14.27}$$

With a view to a Newton–Raphson iteration, the application of a Taylor series expansion leads to (compare (6.81))

$$\mathbf{r}_n = \mathbf{r}_o + \dot{\boldsymbol{\sigma}} + \dot{\lambda}\mathbf{C}\mathbf{a} + \dot{\eta}\mathbf{C}\mathbf{b} + \Delta\lambda \mathbf{C}\frac{\partial \mathbf{a}}{\partial \boldsymbol{\sigma}}\dot{\boldsymbol{\sigma}} + \Delta\eta \mathbf{C}\frac{\partial \mathbf{b}}{\partial \boldsymbol{\sigma}}\dot{\boldsymbol{\sigma}} \tag{14.28}$$

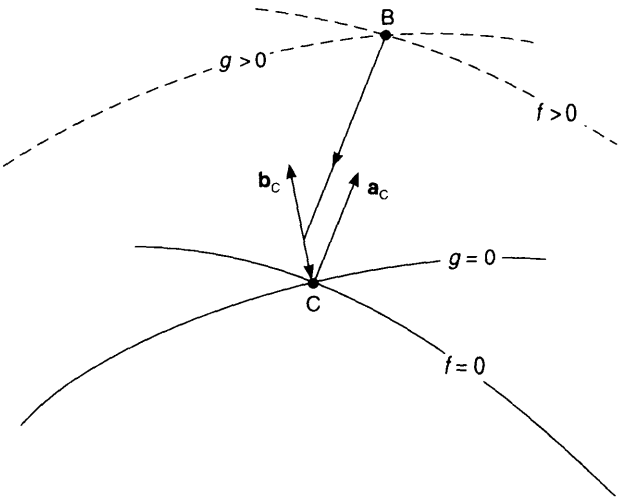

Figure 14.6 Backward-Euler return to a corner with two active yield surfaces.

Setting $\mathbf{r}_n$ to zero leads (in place of (6.80)) to

$$\begin{aligned}\dot{\boldsymbol{\sigma}} &= -\left(\mathbf{I} + \Delta\lambda\mathbf{C}\frac{\partial \mathbf{a}}{\partial \boldsymbol{\sigma}} + \Delta\eta\mathbf{C}\frac{\partial \mathbf{b}}{\partial \boldsymbol{\sigma}}\right)^{-1}(\mathbf{r}_o + \dot{\lambda}\mathbf{C}\mathbf{a} + \dot{\eta}\mathbf{C}\mathbf{b}) \\ &= -\mathbf{Q}^{-1}\mathbf{r}_o - \dot{\lambda}\mathbf{Q}^{-1}\mathbf{C}\mathbf{a} - \dot{\eta}\mathbf{Q}^{-1}\mathbf{C}\mathbf{b}. \end{aligned} \tag{14.29}$$

For simplicity, we will omit hardening so that, in conjunction with (14.29), the application of truncated Taylor series to the two yield functions leads to

$$\begin{aligned} f_{Cn} &= f_{Co} + \mathbf{a}_C^T\dot{\boldsymbol{\sigma}} + = f_{Co} - \mathbf{a}_C^T\mathbf{Q}^{-1}\mathbf{r}_o - \dot{\lambda}\mathbf{a}_C^T\mathbf{Q}^{-1}\mathbf{C}\mathbf{a}_C - \dot{\eta}\mathbf{a}_C^T\mathbf{Q}^{-1}\mathbf{C}\mathbf{b}_C = 0 \\ g_{Cn} &= g_{Co} + \mathbf{b}_C^T\dot{\boldsymbol{\sigma}} + = g_{Co} - \mathbf{b}_C^T\mathbf{Q}^{-1}\mathbf{r}_o - \dot{\lambda}\mathbf{b}_C^T\mathbf{Q}^{-1}\mathbf{C}\mathbf{a}_C - \dot{\eta}\mathbf{b}_C^T\mathbf{Q}^{-1}\mathbf{C}\mathbf{b}_C = 0 \end{aligned} \tag{14.30}$$

Equations (14.30) provide two simultaneous scalar equations in $\dot{\lambda}$ and $\dot{\eta}$ and can easily be solved so that $\Delta\lambda$ and $\Delta\eta$ can be updated after which the updated stress can be obtained by adding $\dot{\boldsymbol{\sigma}}$ from (14.29) to the previous values of $\boldsymbol{\sigma}_C$.

14.3.2 A consistent tangent modular matrix with two active yield surfaces

In Chapter 6, with one active yield surface, the backward-Euler return of Section 6.6.6 was followed by an equivalent consistent tangent modular matrix in Section 6.7.2. We will now extend these ideas to cover the case where there are two active yield surfaces. In these circumstances, noting that $\boldsymbol{\sigma}_B$ in (14.26) is no longer constant, differentiation of (14.26) leads to

$$\dot{\boldsymbol{\sigma}} = \mathbf{C}\dot{\boldsymbol{\varepsilon}} - \dot{\lambda}\mathbf{C}\mathbf{a} - \dot{\eta}\mathbf{C}\mathbf{b} - \Delta\lambda\mathbf{C}\frac{\partial \mathbf{a}}{\partial \boldsymbol{\sigma}}\dot{\boldsymbol{\sigma}} - \Delta\eta\mathbf{C}\frac{\partial \mathbf{b}}{\partial \boldsymbol{\sigma}}\dot{\boldsymbol{\sigma}} \tag{14.31}$$

so that we can obtain:

$$\dot{\boldsymbol{\sigma}} = \mathbf{Q}^{-1}\mathbf{C}(\dot{\boldsymbol{\varepsilon}} - \dot{\lambda}\mathbf{a} - \dot{\eta}\mathbf{b}) = \mathbf{R}(\dot{\boldsymbol{\varepsilon}} - \dot{\lambda}\mathbf{a} - \dot{\eta}\mathbf{b}) \tag{14.32}$$

where the matrix $\mathbf{Q}$ has been defined in (14.29) and the matrix $\mathbf{R}$ is the equivalent of that in (6.108). In order to remain on both yield surfaces, $\dot{f}$ and $\dot{g}$ should be zero so that:

$$\dot{f}_{Cn} = \mathbf{a}_C^T\dot{\boldsymbol{\sigma}} = a_C^T\mathbf{R}\dot{\boldsymbol{\varepsilon}} - \dot{\lambda}\mathbf{a}_C^T\mathbf{R}\mathbf{a}_C - \dot{\eta}\mathbf{a}_C^T\mathbf{R}\mathbf{b}_C = \mathbf{a}_C^T\mathbf{R}\dot{\boldsymbol{\varepsilon}} - \dot{\lambda}a_{11} - \dot{\eta}a_{12} = 0 \tag{14.33}$$

$$\dot{g}_{Cn} = \mathbf{b}_C^T\dot{\boldsymbol{\sigma}} = \mathbf{b}_C^T\mathbf{R}\dot{\boldsymbol{\varepsilon}} - \dot{\lambda}\mathbf{b}_C^T\mathbf{R}\mathbf{a}_C - \dot{\eta}\mathbf{b}_C^T\mathbf{R}\mathbf{b}_C = \mathbf{b}_C^T\mathbf{R}\dot{\boldsymbol{\varepsilon}} - \dot{\lambda}a_{21} - \dot{\eta}a_{22} = 0$$

where (dropping from here on the subscript C):

$$a_{11} = \mathbf{a}^T\mathbf{R}\mathbf{a}; \qquad a_{12} = a_{21} = \mathbf{a}^T\mathbf{R}\mathbf{b}; \qquad a_{22} = \mathbf{b}^T\mathbf{R}\mathbf{b} \tag{14.34}$$

From (14.33), we can obtain:

$$\begin{pmatrix}\dot{\lambda}\\ \dot{\eta}\end{pmatrix} = \frac{1}{q}\begin{pmatrix} a_{22} & -a_{12}\\ -a_{12} & a_{22}\end{pmatrix}\begin{pmatrix}\mathbf{a}^T\mathbf{R}\dot{\boldsymbol{\varepsilon}}\\ \mathbf{b}^T\mathbf{R}\dot{\boldsymbol{\varepsilon}}\end{pmatrix} \tag{14.35}$$

with

$$q = a_{11}a_{22} - a_{12}^2 \tag{14.36}$$

so that substitution into (14.32) leads to

$$\dot{\boldsymbol{\sigma}} = \mathbf{C}_{ct}\dot{\boldsymbol{\varepsilon}} = \left[\mathbf{R} - \frac{a_{22}}{q}\mathbf{R}\mathbf{a}\mathbf{a}^T\mathbf{R}^T + \frac{a_{12}}{q}\mathbf{R}\mathbf{a}\mathbf{b}^T\mathbf{R}^T + \frac{a_{12}}{q}\mathbf{R}\mathbf{b}\mathbf{a}^T\mathbf{R}^T - \frac{a_{11}}{q}\mathbf{R}\mathbf{b}\mathbf{b}^T\mathbf{R}\right]\dot{\boldsymbol{\varepsilon}} \tag{14.37}$$

14.4 YIELD FUNCTIONS FOR SHELLS THAT USE STRESS RESULTANTS

In Sections 7.1.2 and 8.1.2, we considered the issue of integrating through the thickness of beams, plates and shells. For shells with plasticity, a typical procedure would then involve the application within each layer (or at each integration point through the thickness—see Section 7.1.2) of the plane stress von Mises conditions (see Section 6.8.2)). However, more approximate procedures can be used which work directly with the stress resultants $\mathbf{N}$ and $\mathbf{M}$ and thereby avoid the through-thickness integration.

14.4.1 The one-dimensional case

So that the reader can understand the limitations of these resultant techniques, it is worth quickly deriving such a criterion for the 'one-dimensional case' in which there are two stress resultants, N and M (Figure 14.7c). In this case the strain which takes the form of Figure 14.7a) is assumed to be such that the yield stress has been reached at all sections through the depth so that, assuming a perfectly plastic stress–strain relationship, the stress distribution takes the form of the stress blocks shown in Figure 14.7b). In these circumstances resolving horizontally, one can obtain:

$$n = \frac{N}{N_o} = \frac{N}{\sigma_o t} = 1 - 2\eta \tag{14.38}$$

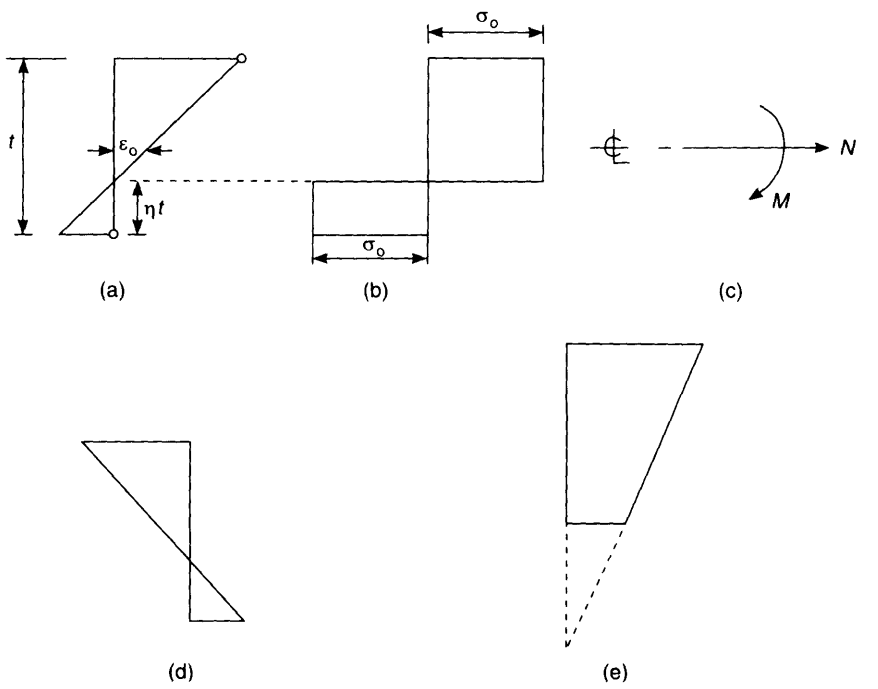

Figure 14.7 Stress and strain profiles for uniaxial case. (a) Strain profile; (b) stress profile; (c) stress resultants; (d) reverse strain profile; (e) in-plane dominant strain profile.

and, taking moments about the centre of the beam:

$$m = \frac{M}{M_0} = \frac{4M}{\sigma_0 t^2} = 4(\eta - \eta^2) \tag{14.39}$$

From which one can eliminate the non-dimensional depth, η (Figure 14.7a and b) and obtain:

$$f = n^2 + m - 1 = 0 \tag{14.40}$$

With the reversed strain profile in Figure 14.7d, one obtains:

$$f = n^2 - m - 1 = 0 \tag{14.41}$$

so that a combined yield surface is given (see Figure 14.8) by

$$f = n^2 + |m| - 1 = n^2 + sm - 1 = 0 \tag{14.42}$$

where

$$s = \frac{m}{|m|} \tag{14.43}$$

Equation (14.42) also covers the 'in-plane dominant' situation which corresponds to the situations in which the neutral point lies outside the section (as illustrated in Figure 14.7e) for which $m = 0$ and $n^2 = 1$.

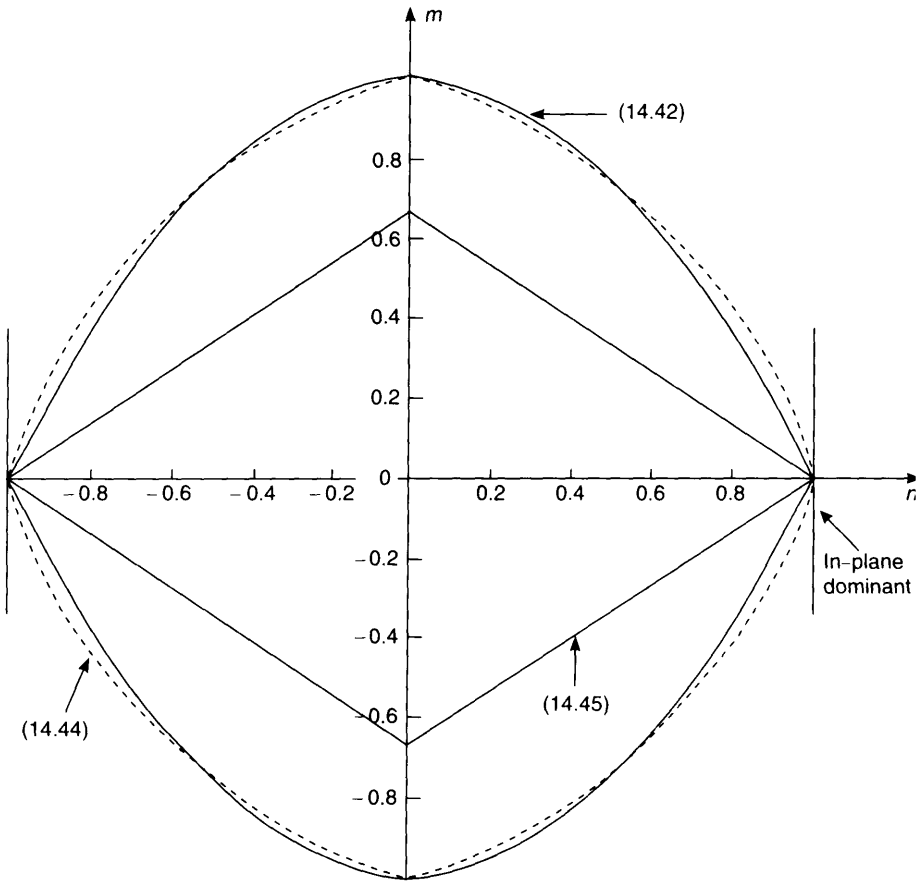

Figure 14.8 Yield functions for uniaxial case.

With regard to later developments, it is useful to consider the approximation to (14.42) given by

$$f = m^2 + \frac{s}{\sqrt{3}}mn + m^2 - 1 = 0 \tag{14.44}$$

The various yield functions are plotted in Figure 14.8.

Before turning to the two-dimensional case (with six generalised stress resultants), one should note that, instead of using the non-dimensional depth, η, the previous derivation of (14.42) can be made by working with the ratio ε_o/χ where ε_o is the plastic strain at the centre-line and χ is the plastic curvature. For bending dominant situations, the stress blocks in Figure 14.7b strictly require both infinite plastic curvature and a perfectly plastic stress–strain relationship without hardening. We should also point out the yield surface represents a state of 'full-section yield' and takes no account of the earlier fibre yield that occurs (Figure 14.8) when

$$f = \tfrac{9}{4}m^2 + 3smn + n^2 - 1 = 0 \tag{14.45}$$

To make some allowance for this 'fibre yield', the author proposed [C8] a procedure whereby (14.44) was modified to

$$f = \frac{m^2}{\alpha^2} + \frac{s}{\alpha\sqrt{3}}mn + n^2 - 1 = 0 \tag{14.46}$$

with α moving from 2/3 to 1 with increasing plastic curvature.

However, on reflection, the author now believes that it is best to reserve full-section yield criteria for quick approximate analyses with a full through thickness integration(Sections 7.1.2 and 8.1.2) being reserved for final detailed analyses. In particular, it is unwise (especially if the basic yield criteria are used without the α's) to use a full-section yield approach for the collapse analysis of structure that is very imperfection-sensitive, because in this case, loss of stability is often associated with the early loss of stiffness induced by fibre-yield.

14.4.2 The two-dimensional case

Ilyushin [I1] described a complex yield function which involves the quadratic 'stress intensities':

$$Q_t = \frac{1}{N_o^2}(N_x^2 + N_y^2 - N_x N_y + 3N_{xy}^2) = \frac{\bar{N}}{N_o^2} \tag{14.47a}$$

$$Q_m = \frac{1}{M_o^2}(M_x^2 + M_y^2 - M_x M_y + 3M_{xy}^2) = \frac{\bar{M}}{N_o^2} \tag{14.47b}$$

$$Q_{tm} = \frac{1}{N_o M_o}(N_x M_x + N_y M_y - \tfrac{1}{2}N_x M_y - \tfrac{1}{2}N_y M_x + 3N_{xy}M_{xy}) = \frac{P}{N_o M_o} \tag{14.47c}$$

by means of the strain ratios parameters:

$$\varphi = \frac{e_{i2}}{e_{i1}}; \qquad \mu = \frac{e_{io}}{e_{i1}} \tag{14.48}$$

where e_{i1} is the equivalent plastic strain on the top surface, e_{i2} is the equivalent plastic strain off the bottom surface and e_{io} is the minimum value of e_i. The stress intensities intensities in (14.47) were made functions of these strain ratios, with two relationship being given, one for the 'bending dominant case (with e_{io} inside the section) and one for the 'in-plane dominant case' (with e_{io} lying outside the section). For bending dominant situations, he suggested the approximation:

$$f = Q_t + Q_m + \frac{1}{\sqrt{3}}|Q_{tm}| - 1 = 0 \tag{14.49a}$$

A more accurate approximation has been given by Ivanov [12] as

$$f = Q_t + \tfrac{1}{2}Q_m + \sqrt{\tfrac{1}{4}Q_m^2 + Q_{tm}^2} - \frac{1(Q_t Q_m - Q_{tm}^2)}{4(Q_t + 0.48Q_m)} \tag{14.49b}$$

Both yield surfaces have been used by the author [C5–C8], in each case both with and without the previous α parameter designed to give some allowance for 'fibre yield'. The

latter is simply achieved by replacing M_o in (14.47) with αM_o, where α is a 'pseudo-hardening parameter' which increases from 2/3 to 1 as the equivalent plastic curvature increases from zero to infinity. The relationship was made to give a close fit to the uniaxial moment/plastic curvature relationship via

$$\alpha = 1 - 0.4\exp\left(-2.6\sqrt{\frac{Et\chi_{ps}}{3\sigma_o}}\right) \tag{14.50a}$$

with

$$\dot{\chi}_{ps}^2 = \tfrac{4}{3}(\chi_{px}^2 + \chi_{py}^2 + \chi_{px}\chi_{py} + \tfrac{1}{4}\chi_{pxy}^2) \tag{14.50b}$$

However, following the earlier discussions and with a view to the development of a backward-Euler procedure with a consistent tangent modular matrix, we will here concentrate on the simpler function of (14.49a) without the introduction of the α parameter.

14.4.3 A backward-Euler return with the Ilyushin yield function

For subsequent developments, we will re-express (14.50a) directly in terms of the quadratic resultant terms, $\bar{N}$, $\bar{M}$ and P of (14.47). We will also adopt a square-rooted form so that:

$$f = \sigma_e - \sigma_o = \left(\frac{\bar{N}}{t^2} + \frac{4sP}{t^3\sqrt{3}} + \frac{16\bar{M}}{t^4}\right)^{1/2} - \sigma_o = 0 \tag{14.51}$$

where

$$s = \frac{P}{|P|} \tag{14.52}$$

Assuming normality, we will write the plastic 'strains' as

$$\bar{\varepsilon}_p = \begin{pmatrix}\varepsilon_p \\ \chi_p\end{pmatrix} = \Delta\lambda\mathbf{a} = \Delta\lambda\frac{1}{2t^4\sigma_e}\begin{bmatrix} t^2\bar{N}_{,N} + \dfrac{2st}{\sqrt{3}}\bar{M}_{,M} \\ \dfrac{2st}{\sqrt{3}}\bar{N}_{,N} + 16\bar{M}_{,M}\end{bmatrix} \tag{14.53}$$

where we have adopted the convention whereby, for example, $\bar{N}_{,N}$ is the three-dimensional vector containing the derivative of $\bar{N}$ in (14.87a) with regard to the three stress resultants N_x, N_y and N_{xy}. We have added a bar on the 'strains' on the left-hand side of (14.53), to indicate that they are 'generalised' strains which include the curvatures. In the following, we will often omit the bar and it will be assumed that we are working with six 'strains' and six 'stress resultants'.

Considering, first, the situation in which we have a single active yield function, in order to apply the backward-Euler procedure of Section 6.6.6, the only additional

information we require is the matrix $\partial \mathbf{a}/\partial \boldsymbol{\sigma}$. This is given by

$$\frac{\partial \mathbf{a}}{\partial \boldsymbol{\sigma}} = \frac{1}{2t^4\sigma_e}\begin{bmatrix} t^2\mathbf{A} & + & \dfrac{2st}{\sqrt{3}}\mathbf{A} \\ \dfrac{2st}{\sqrt{3}}\mathbf{A} & + & 16\mathbf{A} \end{bmatrix} - \frac{1}{\sigma_e}\mathbf{a}\mathbf{a}^{\mathrm{T}} \tag{14.54}$$

where $\mathbf{A}$ is the matrix of (6.47) which is reproduced here, for convenience as

$$\mathbf{A} = \begin{bmatrix} 2 & -1 & -1 & & & \\ -1 & 2 & -1 & & & \\ -1 & -1 & 2 & & & \\ & & & 6 & & \\ & & & & 6 & \\ & & & & & 6 \end{bmatrix} \tag{14.55}$$

We are now in a position to apply the single surface backward-Euler return of 6.6.6 (and predictor from the second method of Section 6.6.2) although, we should note that the elastic consitutive matrix, $\mathbf{C}$, is now of dimension 6×6 and contains the standard in-plane matrix in the upper 3×3 quadrant and the standard bending matrix in the lower 3×3 quadrant. We can also derive the consistent tangent modular matrix by following the procedure of Section 6.7.2.

14.4.4 A backward-Euler return and consistent tangent matrix for the Ilyushin yield criterion when two yield surfaces are active

We have already indicated that the yield surface of (14.51) has a 'corner region' (because of the choice of s in (14.52)). In this corner region, we can consider there to be two active yield surfaces, one with $s = +1$ and with $s = -1$ and we can then apply the method of Section 14.3.1. However, as a first step, we need to know that we are in the corner region. The author and co-worker [C9] have adopted the following procedure.

We start with the predictor discussed in the second half of Section 6.6.2 whereby a first estimate for the stresses at C are given by

$$\sigma_C = \boldsymbol{\sigma}_B - \Delta\lambda \mathbf{C}\mathbf{a}_B \tag{14.56}$$

where $\mathbf{a}_B$ is the normal at the 'elastic trial position', B, and the first estimate for $\Delta\lambda$ is given by (6.59) so that:

$$\Delta\lambda = \frac{f_B}{\mathbf{a}_B^{\mathrm{T}}\mathbf{C}\mathbf{a}_B} \tag{14.57}$$

with f_B as the value of the yield function at B. In computing the latter, we use s_B with s from (14.52). We now apply a standard single vector return with s_B fixed. Having returned to the yield surface, we compute s_C. If $s_C = s_B$, the yield function will be (effectively) zero and we will have completed a successful single vector return. However, if $s_C \neq s_B$, we have crossed the corner.

Let us assume that $s_B = 1$ (and hence $s_C = -1$). We can now define the two active yield surfaces as $f = f(s = +1)$ and $g = f(s = -1)$. The stresses resulting from the previous single vector return can be used as a starting estimate for the iteration of Section 14.3.1 with $\Delta\lambda$ as the valued previously calculated and $\Delta\eta$ starting as zero. The starting values of the yield functions will then be $f = 0, g \neq 0$. Throughout the iteration, the scalar s is maintained at 1 for the yield function f and at -1 for the yield function g. If $s_B = -1$ (and hence $s_C = +1$), we simply reverse the definitions of f and g. In very rare circumstances, the trial position B will also be on a corner so that s in (14.52) is undefined. In these circumstances one can simply make an arbitrary choice between ± 1 for s at B and still apply the previous method.

Having returned to the corner, we can simply compute the consistent tangent modular matrix using the procedure of Section 14.3.2.

14.5 IMPLEMENTING A FORM OF BACKWARD-EULER PROCEDURE FOR THE MOHR–COULOMB YIELD CRITERION

From the work of Section 14.1, we know that the Morh–Coulomb yield criterion has corners. (So does the Tresca yield criterion which can be considered as a special case of the Mohr–Coulomb function.) For this function, we can again apply the method of Section 14.3.1. However, the author used a slightly different technique which will be described in this section.

Earlier work on the Mohr–Coulomb yield criterion has been given by Marques [M1] and Owen *et al.* [O3] and who have detailed some of the limitations of the sub-incremented, forward-Euler procedure (Section 6.6.4) with its associated 'crossing of the yield surface' (Section 6.6.1). Early work on the Tresca yield criterion has been given by Runnesson and Booker [R5]. Sloan [S7] has advocated a local rounding of the corners. The author tried a similar procedure [C3, C4], but found that the adoption of the 'two-vectored return' and associated consistent tangent was numerically more effective. Other work in the latter category can be found in [D1, P1]. The introduction of hardening (or softening) has been considered by Simo *et al.* [S3] and Pramono and Willam [P4]. The present work will be restricted to perfect plasticity.

We will assume that, as in the previous section, we start with a predictor as given by (14.56) and (14.57). In relation to Figure 14.9a, this return is exact for the Mohr–Coulomb yield criterion because $\mathbf{a}_B = \mathbf{a}_C$. However, in relation to Figure 14.9(b), the stresses $\boldsymbol{\sigma}_D$ lie above the yield surface, $g = 0$. If we proceeded in the standard manner with the single-vector 'iterative return' of Section 6.6.3, we would return the stresses to point E (Figure 14.9b). In contrast, a tightly sub-incremented forward-Euler technique would return the stresses to the corner, C, on the corner. We could obtain this solution by means of the two-vector iterative return of Section 14.3.1 using two active yield surfaces which eventually involve the flow directions $\mathbf{a}_C$ and $\mathbf{b}_C$. However, for the Mohr–Coulomb yield surface, we can modify the procedure and use the directions $\mathbf{a}_B$ and $\mathbf{b}_B$ (Figure 14.9c). In either case, we need to know that we are in the 'corner region'. A number of authors have suggested procedures for identifying this situation. Following the predictor of (14.56) and (14.57), the author [C3, C4] computed the normal at the

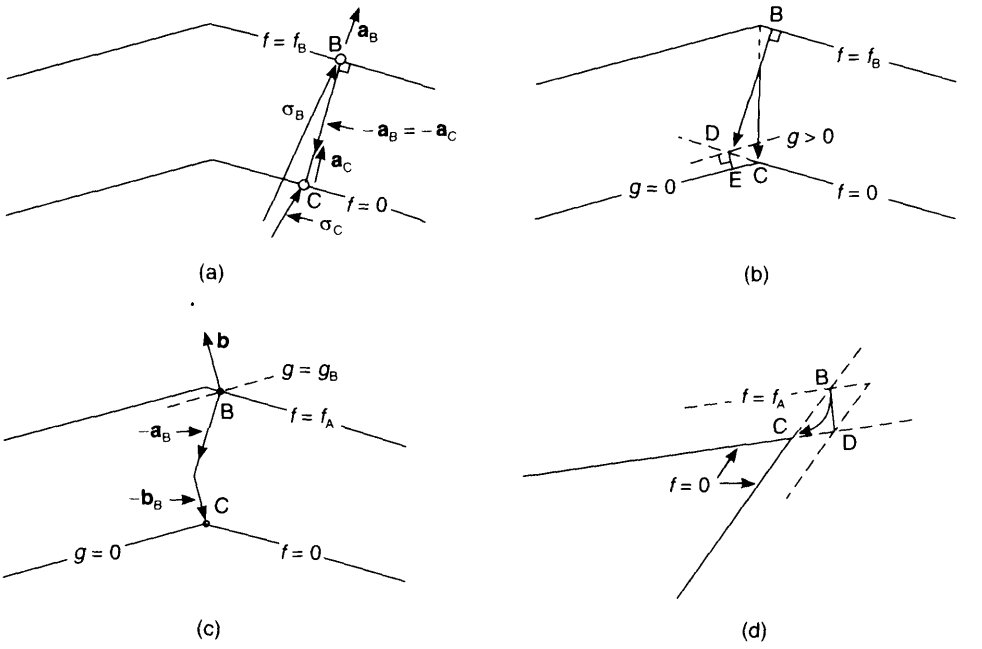

Figure 14.9 Various returns with the Mohr–Coulomb yield surface. (a) Simple return; (b) return crossing the corner line; (c) two-vectored return; (d) return to the apex.

resulting point D (Figure 14.9b) and then the angle, β, between $\mathbf{a}_B$ and $\mathbf{a}_D$, which is given by

$$\cos\beta = \frac{\mathbf{a}_B^T \mathbf{a}_D}{\|\mathbf{a}_B\| \, \|\mathbf{a}_D\|} \tag{14.58}$$

If this angle is zero or nearly zero (say, less than one degree), the simple return is valid and relates to Figure 14.9a. If the angle is greater than 90°, the stresses are being returned to a point beyond the apex and, consequently, one should return directly to the apex (see Figure 14.9d and Section 14.5.2). If the angle is significant but less than 90°, a two-vector return is applied (Figure 14.9c)) with

$$\boldsymbol{\sigma}_C = \boldsymbol{\sigma}_B - \Delta\lambda \mathbf{C}\mathbf{a}_B - \Delta\eta \mathbf{C}\mathbf{b}_B \tag{14.59}$$

where $\mathbf{b}_B$ is the normal to the 'second yield surface at B', which following the work of Section 14.3, we will designate as g. However, we need to know which of the second yield functions is relevant. This information follows if we know which type of corner (Figure 14.3 and 14.10), we have crossed. To ths end, the author [C3, C4] computed the first-order estimate for the change in θ from point B to point D (Figure 14.9b) which can be obtained as

$$\Delta\theta = \frac{\partial\theta^T}{\partial\boldsymbol{\sigma}} \Delta\boldsymbol{\sigma} = -\Delta\lambda \mathbf{c}_B^T \mathbf{C}\mathbf{a}_B \tag{14.60}$$

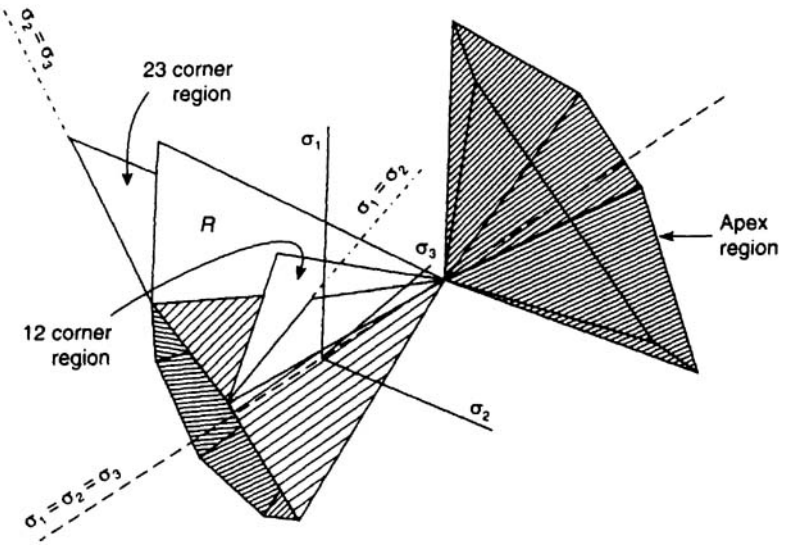

Figure 14.10 Mohr–Coulomb yield surfaces with corner and apex regions.

where the vector $\mathbf{c}$ is given by

$$\mathbf{c} = \frac{\partial \theta}{\partial \boldsymbol{\sigma}} = D_2 \mathbf{a}_2 + D_3 \mathbf{a}_3 \tag{14.61}$$

with

$$D_2 = \frac{-\tan 3\theta}{2J_2}, \qquad D_3 = \frac{-\sqrt{3}}{2J_2^{3/2} \cos 3\theta} \tag{14.62}$$

and $\mathbf{a}_2$ and $\mathbf{a}_3$ being given by (14.21) and (14.22) as computed at point B. If $\Delta\theta$ is positive, the corner being crossed is at $\theta = +30^\circ$ (the '12' corner—see Fig. 14.3 because at this corner $\sigma_1 = \sigma_2$). If $\Delta\theta$ is negative, the corner is at $\theta = -30^\circ$ (the '23' corner—see Figure 14.3 because at this corner $\sigma_2 = \sigma_3$).

An alternative approach has been given by Pankaj and Bicanic [P1] (see also [D1]). They also start by applying a single-vector return using (15.56) and (14.57), but operate in principal stress space so that, referring to the yield function of (14.9b), the normal vector is given by

$$\mathbf{a}^{\mathrm{T}} = \tfrac{1}{2}(s + 1, 0, s - 1) \tag{14.63}$$

with

$$s = \sin \varphi \tag{14.64}$$

Using the upper 3 × 3 submatrix from (4.10) for **C**, (14.56) and (14.57) then lead to

$$\begin{pmatrix}\sigma_1\\ \sigma_2\\ \sigma_3\end{pmatrix}_C = \begin{pmatrix}\sigma_1\\ \sigma_2\\ \sigma_3\end{pmatrix}_B - \frac{f_B}{E'(1-2\nu+s^2)}\begin{pmatrix}1-2\nu+s\\ 2\nu s\\ -1+2\nu+s\end{pmatrix} \tag{14.65}$$

where

$$E' = \frac{E}{(1+\nu)(1-2\nu)} \tag{14.66}$$

In relation to Figures 14.3 and 14.10, if the '12' corner has been crossed, instead of the usual $\sigma_1 > \sigma_2 > \sigma_3$, we would be in a region where $\sigma_2 > \sigma_1 > \sigma_3$ and hence $\sigma_{2C} > \sigma_{1C}$ and, from (14.65), we would obtain:

$$\mu_{12} = f_B + \frac{(1-2\nu+s^2)}{(1-2\nu)(s+1)}(\sigma_{B2} - \sigma_{B1}) > 0 \tag{14.67a}$$

or, using (14.4):

$$\mu_{12} = f_B - 2\frac{(1-2\nu+s^2)}{(1-2\nu)(s+1)}J_2^{1/2}\sin(30-\theta) > 0 \tag{14.67b}$$

where, in the latter, J_2 and θ would be computed at the predictor state 'B'.

In a similar fashion (Figures 14.3 and 14.9), if the corner '23' has been crossed, $\sigma_{3C} > \sigma_{2C}$ and we have:

$$\mu_{23} = f_B + \frac{(1-2\nu+s^2)}{(1-2\nu)(s+1)}(\sigma_{B3} - \sigma_{B2}) > 0 \tag{14.68a}$$

or

$$\mu_{23} = f_B - 2\frac{(1-2\nu+s^2)}{(1-2\nu)(s+1)}J_2^{1/2}\sin(30+\theta) > 0 \tag{14.68b}$$

Hence, if both μ_{12} and μ_{23} are negative, the single-vector return of (14.56) and (14.57) will be exact while, if μ_{12} is positive and μ_{23} is negative, the corner '12' has been crossed and if μ_{12} is negative and μ_{23} is positive, the corner '23' has been crossed.

14.5.1 Implementing a two-vectored return

If, using either of the two previous indicators, it is concluded that a corner has been crossed, the two-vectored return of (14.59) can be used. At this stage, we also need to know which type of corner has been crossed. If the '12' corner has been crossed, the 'second yield function' is

$$g = \tfrac{1}{2}(\sigma_2 - \sigma_3) + \tfrac{1}{2}(\sigma_2 + \sigma_3)\sin\varphi - c\cos\varphi = 0 \tag{14.69a}$$

while if the '23' corner has been crossed, the 'second yield function' is

$$g = \tfrac{1}{2}(\sigma_1 - \sigma_2) + \tfrac{1}{2}(\sigma_1 + \sigma_2)\sin\varphi - c\cos\varphi = 0 \tag{14.69b}$$

These yield criteria can, using (14.4), be re-expressed in the form of (14.9c) provided the

$A(\theta)$ term of (14.10) is redefined as

$$\text{With corner '12'} \quad A(\theta) = \tfrac{1}{2}\cos\theta(1 - \sin\varphi) + \frac{\sin\theta}{2\sqrt{3}}(3 + \sin\varphi) \tag{14.70a}$$

$$\text{With corner '23'} \quad A(\theta) = \tfrac{1}{2}\cos\theta(1 + \sin\varphi) + \frac{\sin\theta}{2\sqrt{3}}(\sin\varphi - 3) \tag{14.70b}$$

The second normal vector, $\mathbf{b}_B$ at the trial position, B, can now be simply computed from (14.19) with the coefficients C_1–C_3 from Table 14.2 although we must use $A(\theta)$ and its derivative $dA/d\theta$ from (14.70).

Using (14.59), the return is now completely defined apart from the scalars, $\Delta\lambda$ and $\Delta\eta$. To obtain these scalars, we now apply Taylor expansions of the form of (6.15) (but here without hardening) to both the yield function f (see 14.9c) and (14.10) and the second yield function from (14.9c) and (14.70). This leads to

$$0 = f_B - (\mathbf{a}_B^T\mathbf{C}\mathbf{a}_B)\Delta\lambda - (\mathbf{a}_B^T\mathbf{C}\mathbf{b}_B)\Delta\eta = f_B - a_{11}\Delta\lambda - a_{12}\Delta\eta \tag{14.71a}$$

$$0 = g_B - (\mathbf{b}_B^T\mathbf{C}\mathbf{a}_B)\Delta\lambda - (\mathbf{b}_B^T\mathbf{C}\mathbf{b}_B)\Delta\eta = g_B - a_{21}\Delta\lambda - a_{22}\Delta\eta \tag{14.71b}$$

and hence

$$\Delta\lambda = \frac{1}{q}(a_{22}f_B - a_{12}g_B); \qquad \Delta\eta = \frac{1}{q}(a_{11}g_B - a_{12}f_B) \tag{14.72}$$

with:

$$a_{11} = \mathbf{a}_B^T\mathbf{C}\mathbf{a}_B; \qquad a_{22} = \mathbf{b}_B^T\mathbf{C}\mathbf{b}_B; \qquad a_{12} = a_{21} = \mathbf{a}_B^T\mathbf{C}\mathbf{b}_B; \qquad q = ab - d^2 \tag{14.73}$$

14.5.2 A return from a corner or to the apex

The previous two-vectored return cannot be applied if the trial point B is exactly on a corner so that the modulus of θ is 30° (this will very rarely happen). The return cannot be applied because in these circumstances one cannot compute the coefficients C_2 and C_3 from Table 14.2 because $\tan 3\theta$ and $1/\cos 3\theta$ are each infinite. The solution is simply to use the coefficients C_1–C_3 for the Drucker—Prager return and use it in conjunction with a single-vector return. The author used such a procedure whnever $|\theta| > 29.99°$ [C3, C4].

In some circumstances, the trial position will be such that the return will be directly to the apex (Figures 14.9d and 14.10). In these circumstances, one might apply a multi-vectored return. However, if the return is from the 'apex region', one can (without hardening) simply return the stresses to the vertex given by

$$\boldsymbol{\sigma}^T = c\cot\varphi(1, 1, 1, 0, 0, 0) \tag{14.74}$$

Pankaj and Bicanic [P1] have given relationships for assessing whether or not an 'apex return' is required. As discussed in Section 14.3, the author used the angle β from (14.58) which can be obtained following a trial 'single-vector return' [C3, C4]. An 'apex return' is required if β is greater than 90°.

14.5.3 A consistent tangent modular matrix following a single-vector return

The single-vector return (see Figure 14.9a) can be written in either of the two forms:

$$\boldsymbol{\sigma}_C = \boldsymbol{\sigma}_B - \Delta\dot{\lambda}\mathbf{C}\mathbf{a}_C \tag{14.75a}$$

or

$$\boldsymbol{\sigma}_C = \boldsymbol{\sigma}_B - \Delta\dot{\lambda}\mathbf{C}\mathbf{a}_B \tag{14.75b}$$

where (14.75b) is of the form of the 'predictor' of (14.56) and (14.57). Because $\mathbf{a}_C = \mathbf{a}_B$, we can also use (14.75a) which is in the conventional form of a 'backward-Euler return'. Hence, the conventional method of Section 6.7.3 can be applied to (14.75a) and will result in the use of (6.110) for the 'consistent tangent modular matrix' with $\mathbf{a}$ (at the final position, C) being taken from (14.19) and $\partial\mathbf{a}/\partial\boldsymbol{\sigma}$ (again at C) being taken from Section 14.2.2).

With a view to the formation of the consistent tangent modular matrix for the two-vectored return, it is worth considering an alternative form for the modular matrix for the single-vectored return that stems from (14.75b) rather than (14.75a). To this end, the variation of (14.75b) leads to

$$\dot{\boldsymbol{\sigma}}_C = \mathbf{C}\dot{\boldsymbol{\varepsilon}} - \dot{\lambda}\mathbf{C}\mathbf{a}_B - \Delta\lambda\mathbf{C}\left.\frac{\partial\mathbf{a}}{\partial\boldsymbol{\sigma}}\right|_B \dot{\boldsymbol{\sigma}}_B = \mathbf{C}\mathbf{T}\dot{\boldsymbol{\varepsilon}} - \dot{\lambda}\mathbf{C}\mathbf{a}_B \tag{14.76}$$

where

$$\mathbf{T} = \left(I - \Delta\lambda\left.\frac{\partial\mathbf{a}}{\partial\boldsymbol{\sigma}}\right|_B \mathbf{C}\right) \tag{14.77}$$

Because the consistency condition can be expressed as

$$\dot{f} = \mathbf{a}_C^{\mathrm{T}}\dot{\boldsymbol{\sigma}}_C = \mathbf{a}_B^{\mathrm{T}}\dot{\boldsymbol{\sigma}}_C = \mathbf{a}^{\mathrm{T}}\dot{\boldsymbol{\sigma}} = 0 \tag{14.78}$$

we can obtain $\dot{\lambda}$ as

$$\dot{\lambda} = \frac{\mathbf{a}^{\mathrm{T}}\mathbf{C}\mathbf{T}\dot{\boldsymbol{\varepsilon}}}{\mathbf{a}^{\mathrm{T}}\mathbf{C}\mathbf{a}} \tag{14.79}$$

from which:

$$\dot{\boldsymbol{\sigma}}_C = \mathbf{C}\left[\mathbf{I} - \frac{\mathbf{a}\mathbf{a}^{\mathrm{T}}\mathbf{C}}{\mathbf{a}^{\mathrm{T}}\mathbf{C}\mathbf{a}}\right]\mathbf{T}\dot{\boldsymbol{\varepsilon}} = \mathbf{C}_t\mathbf{T}\dot{\boldsymbol{\varepsilon}} = \mathbf{C}_{ct}\dot{\boldsymbol{\varepsilon}} \tag{14.80}$$

where $\mathbf{C}_t$ is the standard tangent modular matrix of equation (6.18). The consistent tangent matrix, $\mathbf{C}_{ct}$ of (14.80), will be found to coincide with that obtained from (14.75a) (leading to (6.110)) and can be shown to be symmetric on account of the relationship:

$$\left.\frac{\partial\mathbf{a}}{\partial\boldsymbol{\sigma}}\right|_B \mathbf{C}\mathbf{a} = 0 \tag{14.81}$$

The form of (14.80) (involving $\partial \mathbf{a}/\partial \boldsymbol{\sigma}|_B$) has an advantage for the rare occasions when the single-vector return from B exactly reaches the corner at C. In these circumstances, there would be difficulties in the computation of $\partial \mathbf{a}/\partial \boldsymbol{\sigma}|_C$.

14.5.4 A consistent tangent matrix following a two-vectored return

In contrast to the previous situation, when a two-vectored return is adopted, we will always return to a corner (Figure 14.9c). Hence, following the work of the previous section, it is best to derive a consistent tangent modular matrix from the two-vector equivalent of (14.45b) and thus avoid the difficulties in computing $\partial \mathbf{a}/\partial \boldsymbol{\sigma}$ at the corner. Differentiation of (14.59) then leads to

$$\dot{\boldsymbol{\sigma}}_C = \mathbf{C}\mathbf{T}\dot{\boldsymbol{\varepsilon}} - \dot{\lambda}\mathbf{C}\mathbf{a} - \dot{\eta}\mathbf{C}\mathbf{b} \tag{14.82}$$

where

$$\mathbf{T} = \left(\mathbf{I} - \Delta\lambda \left.\frac{\partial \mathbf{a}}{\partial \boldsymbol{\sigma}}\right|_B \mathbf{C} - \Delta\eta \left.\frac{\partial \mathbf{b}}{\partial \boldsymbol{\sigma}}\right|_B \mathbf{C} \right) \tag{14.83}$$

The consistency conditions are then obtained from $\dot{f} = \dot{g} = 0$ which lead to

$$\mathbf{a}^T\dot{\boldsymbol{\sigma}}_C = \mathbf{b}^T\dot{\boldsymbol{\sigma}}_C = 0 \tag{14.84}$$

from which, using (14.82), we can obtain:

$$\begin{pmatrix} \dot{\lambda} \\ \dot{\eta} \end{pmatrix} = \frac{1}{q} \begin{pmatrix} a_{22} & -a_{12} \\ -a_{12} & a_{11} \end{pmatrix} \begin{pmatrix} \mathbf{a}^T\mathbf{C}\mathbf{T}\dot{\boldsymbol{\varepsilon}} \\ \mathbf{b}^T\mathbf{C}\mathbf{T}\dot{\boldsymbol{\varepsilon}} \end{pmatrix} \tag{14.85}$$

where a_{11}, a_{12}, a_{22} and q have been given in equation (14.73). Substitution from (14.85) into (14.82) gives:

$$\dot{\boldsymbol{\sigma}}_C = \mathbf{C}\left[\mathbf{I} - \frac{a_{22}}{q}\mathbf{a}\mathbf{a}^T\mathbf{C} + \frac{a_{12}}{q}\mathbf{a}\mathbf{b}^T\mathbf{C} + \frac{a_{12}}{q}\mathbf{b}\mathbf{a}^T\mathbf{C} - \frac{a_{11}}{q}\mathbf{b}\mathbf{b}^T\mathbf{C} \right]\mathbf{T}\,\delta\boldsymbol{\varepsilon} = \mathbf{C}_{ct}\dot{\boldsymbol{\varepsilon}} \tag{14.86}$$

which with

$$\left.\frac{\partial \mathbf{a}}{\partial \boldsymbol{\sigma}}\right|_B \mathbf{C}\mathbf{a} = \left.\frac{\partial \mathbf{b}}{\partial \boldsymbol{\sigma}}\right|_B \mathbf{C}\mathbf{b} = \mathbf{0} \tag{14.87}$$

can be shown to be symmetric.

14.5.5 A consistent tangent modular matrix following a return from a corner or an apex

We have already indicated, in Section 14.3.2, that a possible way to deal with the unusual case of a return from a corner is to use the Drucker Prager version of the flow vector $\mathbf{a}$ and its derivative $\partial \mathbf{a}/\partial \boldsymbol{\sigma}$. Using these parameters, one can then use the single-vectored consistent tangent modular matrix of Section 14.5.3.

For the structural 'predictor solution', at the beginning of a load step, there is normally no issue of a 'return' when the first modular matrix is formed. In these

circumstances, one might again use the 'Drucker–Prager' form for those stress points on a corner. There will be many more such points than there will be points returning from a corner trial predictor (at the Gauss-point level) once the structural iterations have commenced. There would seem to be scope in this area for changing the conventional Euler tangent predictor (at the structural level). One simple possibility is to use the tangent matrix obtained at the end of the previous load step (assuming full Newton–Raphson iterations have been used).

The issue of a return from the apex is more problematic. One possibility for the tangent modular matrix is to use a flow rule based on (14.19) with $C_2 = C_3 = 0$ thus implying only volumetric flow. However, following a return to the apex during the equilibrium iterations, one could argue that the changes in stress should be zero, since the stresses will remain at the apex. This implies a null tangent modular matrix at such Gauss point [C3, C4]! The author conducted preliminary investigations using such a strategy with encouraging results [C3, C4]. However, there are obvious dangers with mechanisms. Clearly this is an area requiring further work.

14.6 YIELD CRITERIA FOR ANISOTROPIC PLASTICITY

In this section, we will consider two yield criteria that can be used for anisotropic plasticity: the Hill criterion [H1, H2] and the Hoffman criterion [H4]. The former can be considered as an anisotropic version of the von Mises yield criterion and will be considered first. Numerical applications have been described by de Borst [D3] and Schellekens and de Borst [S1] and some of the following developments relate to work in these papers. Other work on anisotropic plasticity is due to Bicanic *et al.* [B3] and Owen and Figueras [O4].

14.6.1 Hill's yield criterion

Hill expressed his yield criterion in the form:

$$f_h = F(\sigma_{22} - \sigma_{33})^2 + G(\sigma_{33} - \sigma_{11})^2 + H(\sigma_{11} - \sigma_{22})^2 + 2L\sigma_{23}^2 + 2M\sigma_{31}^2 + 2N\sigma_{12}^2 - 1 = 0 \tag{14.88}$$

where the 1–2–3 system relates to the principal axes of anisotropy. For future developments, we will sometimes adopt an equivalent form similar to (6.51), whereby

$$f_2 = \sigma_e^2 - \sigma_o^2 \tag{14.89a}$$

so that, instead of using (6.26), the effective stress, σ_e, can be expressed as

$$2\sigma_e^2 = \alpha_{12}(\sigma_{11} - \sigma_{22})^2 + \alpha_{23}(\sigma_{22} - \sigma_{33})^2 + \alpha_{31}(\sigma_{33} - \sigma_{11})^2 + 6\alpha_{44}\sigma_{12}^2 + 6\alpha_{55}\sigma_{23}^2 + 6\alpha_{66}\sigma_{31}^2 \tag{14.89b}$$

where the relationship between the coefficients F, G, H, L, M, N in (14.88) and the coefficients α_{ij} in (14.89b) is straightforward. To recover the von Mises yield criterion, each of the coefficients, α_{ij}, (14.89b) is set to unity (see (6.26)). To obtain the coefficients, α_{ij}, experiments can be conducted to obtain the yield stresses in the 1–3 directions, $\bar{\sigma}_{11}$,

$\bar{\sigma}_{22}$ and $\bar{\sigma}_{33}$ and the three shear yield stresses, $\bar{\sigma}_{12}$, $\bar{\sigma}_{23}$ and $\bar{\sigma}_{31}$. It then follows from (14.88) and (14.89) that:

$$\tfrac{1}{2}\alpha_{12} = H\sigma_o^2 = (\sigma_o/\bar{\sigma}_{11})^2 + (\sigma_o/\bar{\sigma}_{22})^2 - (\sigma_o/\bar{\sigma}_{33})^2 \tag{14.90a}$$

$$\tfrac{1}{2}\alpha_{23} = F\sigma_o^2 = (\sigma_o/\bar{\sigma}_{22})^2 + (\sigma_o/\bar{\sigma}_{33})^2 - (\sigma_o/\bar{\sigma}_{11})^2 \tag{14.90b}$$

$$\tfrac{1}{2}\alpha_{31} = G\sigma_o^2 = (\sigma_o/\bar{\sigma}_{11})^2 + (\sigma_o/\bar{\sigma}_{33})^2 - (\sigma_o/\bar{\sigma}_{22})^2 \tag{14.90c}$$

$$3\alpha_{44} = 2N\sigma_o^2 = (\sigma_o/\bar{\sigma}_{12})^2 \tag{14.90d}$$

$$3\alpha_{55} = 2L\sigma_o^2 = (\sigma_o/\bar{\sigma}_{23})^2 \tag{14.90e}$$

$$3\alpha_{66} = 2M\sigma_o^2 = (\sigma_o/\bar{\sigma}_{31})^2 \tag{14.90f}$$

If we now let the 'yield stress', σ_o, be one of the uniaixal yield stresses such as $\bar{\sigma}_{11}$, we can obtain the coefficients, α_{ij}, from (14.90).

Equations (14.88) and (14.89) can be re-expressed in the matrix and vector form:

$$f_2 = \sigma_e^2 - \sigma_o^2 = \tfrac{1}{2}\boldsymbol{\sigma}^{\mathrm{T}}\mathbf{P}\boldsymbol{\sigma} - \sigma_o^2 \tag{14.91}$$

where

$$\mathbf{P} = \begin{bmatrix} \alpha_{12}+\alpha_{31} & -\alpha_{12} & -\alpha_{31} & & & \\ -\alpha_{12} & \alpha_{12}+\alpha_{23} & -\alpha_{23} & & & \\ -\alpha_{31} & -\alpha_{23} & \alpha_{31}+\alpha_{23} & & & \\ & & & 6\alpha_{44} & & \\ & & & & 6\alpha_{55} & \\ & & & & & 6\alpha_{66} \end{bmatrix} \tag{14.92}$$

The von Mises yield criterion is recovered by setting each of the coefficients α_{ij} in (14.92) to unity so that:

$$\mathbf{P}_{J2} = \begin{bmatrix} 2 & -1 & -1 & & & \\ -1 & 2 & -1 & & & \\ -1 & -1 & 2 & & & \\ & & & 6 & & \\ & & & & 6 & \\ & & & & & 6 \end{bmatrix} \tag{14.93}$$

For the von Mises yield criterion, equation (14.91) corresponds with equation (6.51) with $\mathbf{P}$ from (14.93) corresponding to $\mathbf{A}$ from (6.47).

The flow rules for Hill's yield criterion can be obtained from (14.88) as

$$\dot{\boldsymbol{\varepsilon}}_{\mathrm{p}} = \begin{bmatrix} \dot{\varepsilon}_{11} \\ \dot{\varepsilon}_{22} \\ \dot{\varepsilon}_{33} \\ \dot{\gamma}_{12} \\ \dot{\gamma}_{23} \\ \dot{\gamma}_{31} \end{bmatrix} = \dot{\lambda}_{\mathrm{h}} \frac{\partial f_{\mathrm{h}}}{\partial \boldsymbol{\sigma}} = 2\dot{\lambda}_{\mathrm{h}} \begin{bmatrix} H(\sigma_{11}-\sigma_{22}) + G(\sigma_{11}-\sigma_{33}) \\ F(\sigma_{22}-\sigma_{33}) + H(\sigma_{22}-\sigma_{11}) \\ G(\sigma_{33}-\sigma_{11}) + F(\sigma_{33}-\sigma_{22}) \\ 2N\sigma_{12} \\ 2L\sigma_{23} \\ 2M\sigma_{31} \end{bmatrix} \tag{14.94}$$

or from (14.91) as

$$\dot{\boldsymbol{\varepsilon}}_p = \begin{bmatrix} \dot{\varepsilon}_{11} \\ \dot{\varepsilon}_{22} \\ \dot{\varepsilon}_{33} \\ \dot{\gamma}_{12} \\ \dot{\gamma}_{23} \\ \dot{\gamma}_{31} \end{bmatrix} = \dot{\lambda}_2 \mathbf{P}\boldsymbol{\sigma} = \dot{\lambda}_2 \begin{bmatrix} \alpha_{12}(\sigma_{11}-\sigma_{22}) + \alpha_{31}(\sigma_{11}-\sigma_{33}) \\ \alpha_{23}(\sigma_{22}-\sigma_{33}) + \alpha_{12}(\sigma_{22}-\sigma_{11}) \\ \alpha_{31}(\sigma_{33}-\sigma_{11}) + \alpha_{23}(\sigma_{33}-\sigma_{22}) \\ 6\alpha_{44}\sigma_{12} \\ 6\alpha_{55}\sigma_{23} \\ 6\alpha_{66}\sigma_{31} \end{bmatrix} \tag{14.95}$$

One need not adopt the squared yield form of (14.91) but, instead, could write the yield function as

$$f = \sigma_e - \sigma_o = (\tfrac{1}{2}\boldsymbol{\sigma}^T \mathbf{P}\boldsymbol{\sigma})^{1/2} - \sigma_o \tag{14.96a}$$

or, using a notation involving tensor components,

$$f = (\tfrac{1}{2} P_{ijkl}\sigma_{ij}\sigma_{km})^{1/2} - \sigma_o \tag{14.96b}$$

and the flow rule then follows as

$$\dot{\varepsilon}_p = \dot{\lambda}\frac{\partial f}{\partial \boldsymbol{\sigma}} = \frac{1}{2\sigma_e}\mathbf{P}\boldsymbol{\sigma} = \dot{\lambda}\mathbf{a} \tag{14.97}$$

The relationship between the plastic strain-rate multipliers in (14.94), (14.95) and (14.97) is given by:

$$\dot{\lambda} = 2\sigma_e \dot{\lambda}_2 = 2\frac{\dot{\lambda}_h}{\sigma_e} \tag{14.98}$$

14.6.2 Hardening with Hill's yield criterion

The concept of hardening with an anisotropic yield criterion is not straightforward. Here we will only discuss the simplest approach in which it is assumed that the yield criterion does not change in shape as the material hardens. We will start by deriving and expression for the equivalent plastic strain rate, $\dot{\varepsilon}_{ps}$, that is the equivalent of that given in (6.29) for isotropic hardening of the von Mises isotropic yield criterion. To this end, from (14.95), we can obtain relationships of the form:

$$\alpha_{31}\dot{\varepsilon}_{22} - \alpha_{12}\dot{\varepsilon}_{33} = \dot{\lambda}_2 A(\sigma_{22} - \sigma_{33}) \tag{14.99}$$

where

$$A = \alpha_{12}\alpha_{23} + \alpha_{12}\alpha_{31} + \alpha_{23}\alpha_{31} \tag{14.100}$$

and in (14.99) and throughout this section, we will omit the subscript p for 'plastic' on the strain rates.

With a view to substitution into the yield function of (14.89), we can obtain from (14.99) the relationship:

$$\alpha_{23}(\sigma_{22} - \sigma_{33})^2 = \frac{\alpha_{23}}{\dot{\lambda}_2^2 A^2}(\alpha_{31}\dot{\varepsilon}_{22} - \alpha_{12}\dot{\varepsilon}_{33})^2 \tag{14.101}$$

while for the shear terms, from (14.95), we have

$$6\alpha_{44}\sigma_{12}^2 = \frac{1}{6\dot{\lambda}_2^2\alpha_{44}}\dot{\gamma}_{12}^2 \tag{14.102}$$

Summing terms such as (14.101) and (14.102), leads, in conjunction with (14.89) to

$$2\sigma_e^2 = \frac{1}{\dot{\lambda}_2^2}B^2 \tag{14.103}$$

where

$$B^2 = \frac{1}{A^2}(\alpha_{12}(\alpha_{23}\dot{\varepsilon}_{11} - \alpha_{31}\dot{\varepsilon}_{22})^2 + \alpha_{23}(\alpha_{31}\dot{\varepsilon}_{22} - \alpha_{12}\dot{\varepsilon}_{33})^2 + \alpha_{31}(\alpha_{12}\dot{\varepsilon}_{33} - \alpha_{23}\dot{\varepsilon}_{11})^2)$$
$$+\left(\frac{\dot{\gamma}_{12}^2}{6\alpha_{44}} + \frac{\dot{\gamma}_{23}^2}{6\alpha_{55}} + \frac{\dot{\gamma}_{31}^2}{6\alpha_{66}}\right) \tag{14.104}$$

Using (14.98) and (14.103), we can now obtain:

$$\dot{\lambda} = \dot{\varepsilon}_{ps} = 2\sigma_e\dot{\lambda}_2 = \sqrt{2}B \tag{14.105}$$

where we have anticipated a step to follow where we show that, as with the von Mises yield criterion, $\dot{\lambda} = \dot{\varepsilon}_{ps}$. An exercise for the reader might be to derive equivalent expressions to (14.99)–(14.105) for the isotropic case when each of α_{ij} is unity. In there circumstances, A from (14.100) $= 3$ and noting that for the isotropic case, $\varepsilon_{11p} + \varepsilon_{22p} + \varepsilon_{33p} = 0$, we recover (6.29).

To justify the step whereby $\dot{\lambda} = \dot{\varepsilon}_{ps}$, we must resort, as in Section 6.4.2 to the concept of plastic work which leads to the relationship:

$$\dot{W} = \boldsymbol{\sigma}^T\dot{\boldsymbol{\varepsilon}}_p = \sigma_o\dot{\varepsilon}_{ps} \tag{14.106}$$

Using (14.91), (14.95) and (14.98), it follows that:

$$\boldsymbol{\sigma}^T\dot{\boldsymbol{\varepsilon}}_p = \dot{\lambda}_2\boldsymbol{\sigma}^T\mathbf{P}\boldsymbol{\sigma} = 2\dot{\lambda}_2\sigma_o^2 = \sigma_o\dot{\lambda} \tag{14.107}$$

From (14.106) and (14.107), we can see the equality between $\dot{\lambda}$ and $\dot{\varepsilon}_{ps}$.

As with an isotropic yield criterion, we can use a uniaxial test to obtain the relationship between σ_o and $\varepsilon_{ps} = \int\dot{\varepsilon}_{ps}$. Suppose such a test is applied in the 1-direction. Then, from (14.89), the relationship between σ_{11} and σ_o is given by

$$\frac{1}{\sqrt{2}}(\alpha_{12} + \alpha_{31})^{1/2}\sigma_{11} = \sigma_o \tag{14.108}$$

It was mentioned in Section 14.6.1 that the definition of σ_o in (14.89) was arbitrary. If we had defined σ_o as the yield stress in the 1-direction (i.e. $\bar{\sigma}_{11}$ in (14.90)), then in defining the coefficients, α_{ij}, we would have set:

$$\frac{1}{\sqrt{2}}(\alpha_{12} + \alpha_{31})^{1/2} = 1 \tag{14.109}$$

While (14.108) gives the relationship between σ_{11} and σ_o, we also require the relationship between ε_{11p} and ε_{ps}. To this end, we note from (14.95), that the plastic strain $\dot{\varepsilon}_{11p}$

would be accompanied by

$$\dot{\varepsilon}_{22p} = \frac{-\alpha_{12}}{\alpha_{12}+\alpha_{31}}\dot{\varepsilon}_{11p}; \qquad \dot{\varepsilon}_{33p} = \frac{-\alpha_{31}}{\alpha_{12}+\alpha_{31}}\dot{\varepsilon}_{11p} \tag{14.110}$$

from which after substitution into (14.104) and (14.105), tedious algebra leads to

$$\dot{\varepsilon}_{ps} = \frac{\sqrt{2}}{(\alpha_{12}+\alpha_{31})^{1/2}}\dot{\varepsilon}_{11p} \tag{14.111}$$

(For the isotropic case, the equivalent of (14.110) leads to $\dot{\varepsilon}_{22p} = \dot{\varepsilon}_{33p} = -\dot{\varepsilon}_{11p}/2$.) As before, if we have set $\sigma_o = \bar{\sigma}_{11}$, equation (14.109) applies and, as a consequence, the relationship between σ_o and $\int \dot{\varepsilon}_{ps}$ is obtained directly from the relationship between σ_{11} and $\int \dot{\varepsilon}_{11p}$.

In order to test the validity of the assumption regarding a yield function that maintains its shape, equivalent relationships to those in (14.108)) and (14.111) could be derived for tests in the 2- and 3-directions (although with σ_o being equivalent to $\bar{\sigma}_{11}$, the equivalent to (14.109) would not apply). The resulting relationships between σ_o and $\int \dot{\varepsilon}_{ps}$ could then be compared to that obtained from the test in the 1-direction and strictly they should coincide.

14.6.3 Hill's yield criterion with plane stress

For rolled sheet, we can write the yield criterion in the plane-stress form as

$$f_h = (G+H)\sigma_{11}^2 + (F+H)\sigma_{22}^2 - 2H\sigma_{11}\sigma_{22} + 2N\sigma_{12}^2 - 1 = 0 \tag{14.112}$$

or

$$f_2 = \frac{(\alpha_{31}+\alpha_{12})}{2}\sigma_{11}^2 + \frac{(\alpha_{23}+\alpha_{12})}{2}\sigma_{22}^2 - \alpha_{12}\sigma_{11}\sigma_{22} + 3\alpha_{44}\sigma_{12}^2 - \sigma_o^2 = 0 \tag{14.113}$$

where, traditionally, the 1-direction will be taken to coincide with the direction of rolling, the 2-direction will be transverse to the direction of rolling while the 3-direction will be the 'through-thickness' direction.

For this situation, the equivalent plastic strain can be degenerated from (14.104) and (14.105) by setting $\dot{\varepsilon}_{33p} = -\dot{\varepsilon}_{11p} - \dot{\varepsilon}_{22p}$ to obtain:

$$\dot{\varepsilon}_{ps} = \sqrt{2}\left(\frac{1}{A^2}(a_{11}\dot{\varepsilon}_{11}^2 + a_{22}\dot{\varepsilon}_{22}^2 + a_{12}\dot{\varepsilon}_{11}\dot{\varepsilon}_{22}) + \frac{\dot{\gamma}_{12}^2}{6\alpha_{44}}\right)^{1/2} \tag{14.114}$$

with

$$a_{11} = \alpha_{12}A + \alpha_{23}^2(\alpha_{12}+\alpha_{31}) + \alpha_{12}\alpha_{23}\alpha_{31} \tag{14.115a}$$

$$a_{22} = \alpha_{12}A + \alpha_{31}^2(\alpha_{12}+\alpha_{31}) + \alpha_{12}\alpha_{23}\alpha_{31} \tag{14.115b}$$

$$a_{12} = 2\alpha_{12}A \tag{14.115c}$$

The simplest anisotropic situation then involves out-of-plane anisotropy while the in-plane response is isotropic. In this situation, we can write:

$$G = F; \qquad \alpha_{23} = \alpha_{31} \tag{14.116}$$

$$N = F + 2H; \qquad 3\alpha_{44} = \alpha_{23} + 2\alpha_{12}$$

so that (14.112) can be re-expressed as

$$f_h = (F+H)\sigma_{11}^2 + (F+H)\sigma_{22}^2 - 2H\sigma_{11}\sigma_{22} + 2(F+2H)\sigma_{12}^2 - 1 = 0 \quad (14.117)$$

while, if we use (14.91) or (14.96), the matrix $\mathbf{P}$ is given by

$$\mathbf{P} = \begin{bmatrix} \alpha_{12}+\alpha_{23} & -\alpha_{12} & 0 \\ -\alpha_{12} & \alpha_{12}+\alpha_{23} & 0 \\ 0 & 0 & 2(\alpha_{23}+\alpha_{12}) \end{bmatrix} \quad (14.118)$$

From a uniaxial test in the 1-direction we can obtain:

$$G+H = F+H = \frac{1}{2\sigma_o^2}(\alpha_{23}+\alpha_{12}) = \frac{1}{\sigma_o^2} = \frac{1}{\bar{\sigma}_{11}^2} \quad (14.119)$$

from which we can define $\sigma_o = \bar{\sigma}_{11}$ and

$$(\alpha_{23}+\alpha_{12}) = 2 \quad (14.120)$$

To obtain separate expressions for F and H, we could, in addition perform a test to obtain the through-thickness yield stress, $\bar{\sigma}_{33}$, and use (14.90a)–(14.90c). Alternatively, we could use the ratio of plastic strains as obtained from the original uniaxial test in the 1-direction. In particular, from (14.94) and (14.95), we then obtain:

$$R = \frac{\dot{\varepsilon}_{22p}}{\dot{\varepsilon}_{33p}} = \frac{H}{F} = \frac{H}{G} = \frac{\alpha_{12}}{\alpha_{23}} = \frac{\alpha_{12}}{\alpha_{31}} \quad (14.121)$$

which is the Lankford anisotropy coefficient [L2]. From (14.90), (14.120) and (14.121), it follows that:

$$H = \frac{\alpha_{12}}{2\sigma_o^2} = \frac{1}{\sigma_o^2}\left(\frac{R}{1+R}\right) \quad (14.122)$$

while using (14.90d), (14.116) and (14.122),

$$N = F+2H = \frac{3\alpha_{44}}{2\sigma_o^2} = \frac{(\alpha_{23}+2\alpha_{12})}{2\sigma_o^2} = \frac{1}{\sigma_o^2}\left(\frac{2R+1}{1+R}\right) \quad (14.123)$$

Hence, from (14.119), (14.122) and (14.123), we can write the yield function in the form of (14.117) using $\sigma_o = \bar{\sigma}_{11}$ and R. Alternatively, we can use the form of (14.91) of (14.96), again with σ_o as the yield stress in the 11-direction. From (14.118), (14.120), (14.122) and (14.123) we then obtain:

$$\mathbf{P} = \begin{bmatrix} 2 & \text{symmetric} & \\ \dfrac{-2R}{1+R} & 2 & \\ 0 & 0 & \dfrac{4(1+2R)}{1+R} \end{bmatrix} \quad (14.124)$$

With hardening, we also require an expression for the equivalent plastic strain. Substitution from (14.121) to (14.123) into (14.114)–(14.115) leads to the relationship:

$$\dot{\varepsilon}_{ps} = \frac{(1+R)}{\sqrt{(1+2R)}}\left(\dot{\varepsilon}_{11}^2 + \dot{\varepsilon}_{22}^2 + \frac{2R}{(1+R)}\dot{\varepsilon}_{11}\dot{\varepsilon}_{22} + \frac{\dot{\gamma}_{12}^2}{2(1+R)}\right)^{1/2} \quad (14.125)$$

which coincides with the isotropic form in (6.12) when $R = 1$.

In general, we can supplement data from the yield strength tests as inserted into (14.90) with data from plastic strain-rate ratios as obtained from (14.94) or (14.95) in order to check the derived coefficients. For a thin sheet with in-plane as well as through-thickness anisotropy, we need to obtain the coefficients F, G, H and N in (14.112) (or the equivalent α_{ij} quantities in (14.113)). These could be obtained from three uniaxial strength tests in the 1-, 2- and 3-directions (leading to F, G and H) and one shear strength test in the 1–2 plane (leading to N). Instead of conducting a through-thickness test, we could conduct an "off-axis test' at 45° to the 1-direction leading to a yield strength of $\bar{\sigma}_\theta$. From Mohr's circle, the other stresses are then:

$$\sigma_{11} = \sigma_{22} = \sigma_{12} = \bar{\sigma}_\theta/2 \tag{14.126}$$

so that, in (14.112), we obtain:

$$(G + F + 2N) = \frac{(\alpha_{31} + \alpha_{23} + 6\alpha_{44})}{2\sigma_o^2} = \frac{2}{\bar{\sigma}_\theta^2} \tag{14.127}$$

As an alternative, we could conduct a uniaxial test in the 1-direction to obtain:

$$G + H = \frac{1}{2\sigma_o^2}(\alpha_{31} + \alpha_{12}) = \frac{1}{\sigma_o^2} = \frac{1}{\bar{\sigma}^2} \tag{14.128}$$

and supplement this with a strain ratio resulting from this test so that using (14.94) or (14.95):

$$R_0 = \frac{\dot{\varepsilon}_{22p}}{\dot{\varepsilon}_{33p}} = \frac{H}{G} = \frac{\alpha_{12}}{\alpha_{31}} \tag{14.129}$$

From an equivalent test in the 2-direction, we could obtain:

$$R_{90} = \frac{\dot{\varepsilon}_{11p}}{\dot{\varepsilon}_{33p}} = \frac{H}{F} = \frac{\alpha_{12}}{\alpha_{23}} \tag{14.130}$$

Equations (14.128)–(14.130) could provide F, G and H (or the equivalent α_{23}, α_{31} and α_{12}), while to obtain the coefficient, N, we could again conduct an 'off-axis' test at 45 and either use (14.127) or one of the strain ratios:

$$R_{45} = \frac{\dot{\varepsilon}_p(\theta = 135^\circ)}{\dot{\varepsilon}_{33p}} = \frac{(0.5(\dot{\varepsilon}_{11p} + \dot{\varepsilon}_{22p}) + \dot{\varepsilon}_{12p})}{\dot{\varepsilon}_{33p}} = -\frac{1}{2} - \frac{N}{G+H} = -\frac{1}{2} - \frac{\alpha_{44}}{\alpha_{31} + \alpha_{12}} \tag{14.131a}$$

or

$$R'_{45} = \frac{\dot{\varepsilon}_p(\theta = 45^\circ)}{\dot{\varepsilon}_{33p}} = \frac{(0.5(\dot{\varepsilon}_{11p} + \dot{\varepsilon}_{22p}) - \dot{\varepsilon}_{12p})}{\dot{\varepsilon}_{33p}} = -\frac{1}{2} + \frac{N}{G+H} = -\frac{1}{2} + \frac{\alpha_{44}}{\alpha_{31} + \alpha_{12}} \tag{14.131b}$$

Equations (4.131) were obtained with the aid of Mohr's circle for the strains (or via (4.52)) and (14.126) for the stresses.

14.7 POSSIBLE RETURN ALGORITHMS AND CONSISTENT TANGENT MODULAR MATRICES

In this section we will consider some backward-Euler return algorithms for yield criteria which can be expressed in the form of (14.96) which is reproduced here as

$$f = \sigma_e - \sigma_o = (\tfrac{1}{2}\boldsymbol{\sigma}^T\mathbf{P}\boldsymbol{\sigma})^{1/2} - \sigma_o \tag{14.132}$$

If $\mathbf{P}$ is taken from (14.92), we have Hill's yield criterion, while if $\mathbf{P}$ taken from (14.93) we have the von Mises yield criterion. The latter was considered in Chapter 6 of Volume 1, and clearly, the backward-Euler return algorithm of Section 6.6.6 can be applied to either of the two previous yield criteria. To apply the return, we merely need to define the flow vector, $\mathbf{a}$, and the matrix $\partial\mathbf{a}/\partial\boldsymbol{\sigma}$. From (14.132), we have:

$$\mathbf{a} = \frac{\partial f}{\partial \boldsymbol{\sigma}} = \frac{1}{2\sigma_e}\mathbf{P}\boldsymbol{\sigma} \tag{14.133}$$

with further differentiation leading to:

$$\frac{\partial \mathbf{a}}{\partial \boldsymbol{\sigma}} = \frac{1}{2\sigma_e}\mathbf{P} - \frac{1}{\sigma_e}\mathbf{a}\mathbf{a}^T \tag{14.134}$$

which, for the von Mises yield criterion with $\mathbf{P}$ (see (14.92)) $= \mathbf{P}_{J2}$ (see (14.93)) and $\mathbf{A}$ from (6.47) coincides with (6.47).

With $\mathbf{a}$ and $\partial\mathbf{a}/\partial\boldsymbol{\sigma}$ defined, we can simply apply the method of Section 6.6.6. However, for yield criteria that can be written in the form of (14.96), other return procedures are possible. They follow by noting that one can write the stresses following from the backward-Euler return as

$$\boldsymbol{\sigma}_C = \boldsymbol{\sigma}_B - \frac{\Delta\lambda}{2\sigma_{eC}}\mathbf{C}\mathbf{P}\boldsymbol{\sigma}_C = \boldsymbol{\sigma}_B - \Delta\lambda_2\mathbf{C}\mathbf{P}\boldsymbol{\sigma}_C \tag{14.135}$$

where $\boldsymbol{\sigma}_B$ are the fixed 'trial stresses', $\boldsymbol{\sigma}_B$. Instead of setting up the residual as in Section 6.6.6 (see (6.79)), we can use (14.135) to obtain an expression for the required stresses $\boldsymbol{\sigma}_C$ with $\Delta\lambda$ as the only unknown. In particular, we have:

$$\boldsymbol{\sigma}_C = \left[\mathbf{I} + \frac{\Delta\lambda}{2\sigma_{eC}}\mathbf{C}\mathbf{P}\right]^{-1}\boldsymbol{\sigma}_B = [\mathbf{I} + \Delta\lambda_2\mathbf{C}\mathbf{P}]^{-1}\boldsymbol{\sigma}_B = \mathbf{B}^{-1}\boldsymbol{\sigma}_B \tag{14.136}$$

Consequently, the yield function of (14.132) can be expressed as

$$f = \sigma_{eC} - \sigma_o = (\tfrac{1}{2}\boldsymbol{\sigma}_B^T\mathbf{B}^{-T}\mathbf{P}\mathbf{B}^{-1}\boldsymbol{\sigma}_B)^{1/2} - \sigma_o = 0 \tag{14.137}$$

Hence, in principle we have a non-linear scalar equation in one unknown ($\Delta\lambda$ which is hidden within $\mathbf{B}$—see (14.136)). Application of a truncated Taylor series to (14.137) leads to

$$f_n = f_o + \dot{\sigma}_{eC} - \dot{\sigma}_o = f_o + \dot{\sigma}_{eC} - A'\dot{\lambda} = 0 \tag{14.138}$$

where A' is the hardening parameter. From (14.137),

$$\dot{\sigma}_{eC} = -\frac{1}{2\sigma_{eC}}K\dot{\lambda}_2 \tag{14.139a}$$

with

$$K = \boldsymbol{\sigma}_C^T \mathbf{P}\mathbf{B}^{-1}\mathbf{C}\mathbf{P}\boldsymbol{\sigma}_C = \boldsymbol{\sigma}_B^T \mathbf{B}^{-T}\mathbf{P}\mathbf{B}^{-1}\mathbf{C}\mathbf{P}\mathbf{B}^{-1}\boldsymbol{\sigma}_B = \boldsymbol{\sigma}_B \mathbf{B}^{-T}\mathbf{P}\mathbf{B}^{-2}\mathbf{C}\mathbf{P}\boldsymbol{\sigma}_B \quad (14.139b)$$

Without hardening (with $A' = 0$), one can simply iterate using (14.138) and (14.139) to obtain the $\Delta\lambda_2$ that is required in (14.136) to define $\boldsymbol{\sigma}_C$ fully. With hardening, we must work directly to obtain $\Delta\lambda$ and therefore need the relationship between $\dot{\lambda}_2$ and $\dot{\lambda}$. From the definition of $\Delta\lambda_2$ in (14.135),

$$2\sigma_{eC}\dot{\lambda}_2 = \dot{\lambda} - 2\Delta\lambda_2\dot{\sigma}_{eC} \quad (14.140)$$

and hence in (14.139a),

$$\dot{\sigma}_{eC} = \frac{-K\dot{\lambda}}{(4\sigma_{eC}^2 - 2K\Delta\lambda_2)} \quad (14.141)$$

so that (14.138) provides the iterative change $\dot{\lambda}$ in $\Delta\lambda$.

While, in principle, this procedure involves a scalar iteration, in practice, because of the definition of K in (14.139), the procedure involves some quite complex matrix and vector manipulations and it is debatable whether it is more efficient than the method of Section 6.6.6. In Section 6.8.2, it was shown how a special, economic, form of the return algorithm could be developed for conditions of plane stress. These ideas will be extended in Section 14.10.

Before leaving this section, we should note that one could work directly with the squared yield criterion, f_2, of (14.91) and use the incremental form of the flow rule from (14.95), so that the relationship for $\boldsymbol{\sigma}_C$ directly involves $\Delta\lambda_2$ in the form given in (14.136) while, from (14.91), the yield function can be expressed as

$$f_2 = \sigma_{eC}^2 - \sigma_{oC}^2 = \tfrac{1}{2}\boldsymbol{\sigma}_B^T \mathbf{B}^{-T}\mathbf{P}\mathbf{B}^{-1}\boldsymbol{\sigma}_B - \sigma_{oC}^2 = 0 \quad (14.142)$$

and a truncated Taylor series leads to

$$f_{2n} = f_{2o} + 2\sigma_{eC}\dot{\sigma}_e - 2\sigma_{oC}A'\dot{\varepsilon}_{ps} = f_{2o} + 2\sigma_{eC}\dot{\sigma}_{eC} - 4\sigma_{oC}\sigma_{eC}A'\dot{\lambda}_2 = 0 \quad (14.145)$$

where we have used (14.105). From (14.145), $\dot{\sigma}_{eC}$ can be obtained in precisely the same form as in (14.139). The combination of the latter equation with (14.145) allows the computation of the iterative change, $\dot{\lambda}_2$.

De Borst [D2] argues that there are advantages in using the former, square-rooted form of the yield criterion (14.96) rather than (14.91). An example in which there are difficulties with the squared formulation will be discussed in Section 14.11.4.

14.7.1 The consistent tangent modular matrix

If we adopt the yield criterion in the square-rooted form of (14.96), the development of the consistent tangent modular matrix directly follows the procedure of Section 6.7.2 with the flow vector $\mathbf{a}$ from (14.133) and the matrix $\partial\mathbf{a}/\partial\boldsymbol{\sigma}$ from (14.134). Using the notation of that section, the iterative change in stresses is given by

$$\dot{\boldsymbol{\sigma}} = \left[\mathbf{I} + \Delta\lambda\mathbf{C}\frac{\partial\mathbf{a}}{\partial\boldsymbol{\sigma}}\right]^{-1}\mathbf{C}(\dot{\boldsymbol{\varepsilon}} - \dot{\lambda}\mathbf{a}) = \mathbf{R}(\dot{\boldsymbol{\varepsilon}} - \dot{\lambda}\mathbf{a}) \quad (14.146)$$

and application of the consistency condition (6.109) then leads to

$$\dot{\boldsymbol{\sigma}} = \mathbf{C}_{ct}\dot{\boldsymbol{\varepsilon}} = \left[\mathbf{R} - \frac{\mathbf{R}\mathbf{a}\mathbf{a}^{\mathrm{T}}\mathbf{R}^{\mathrm{T}}}{a}\right]\dot{\boldsymbol{\varepsilon}} \tag{14.147}$$

where

$$a = \mathbf{a}^{\mathrm{T}}\mathbf{R}\mathbf{a} + A' \tag{14.148}$$

Equation (14.148) is of the same form as (6.110).

If we work with the yield function in the squared form of (14.91), we again obtain (14.147) although we now have:

$$\mathbf{a} = \mathbf{P}\boldsymbol{\sigma}; \qquad \frac{\partial \mathbf{a}}{\partial \boldsymbol{\sigma}} = \mathbf{P} \tag{14.149}$$

The consistency condition then gives (see (14.145)):

$$\dot{f} = \mathbf{a}^{\mathrm{T}}\dot{\boldsymbol{\sigma}} - 4\sigma_0^2 A'\dot{\lambda}_2 = 0 \tag{14.150}$$

(with the yield criterion being fully satisfied, there is no difference between the σ_e and σ_0). Hence, with the new definitions of $\mathbf{a}$ and $\partial\mathbf{a}/\partial\boldsymbol{\sigma}$ from (14.149), the consistent tangent modular matrix is again given by (14.147) although, in place of (14.148), the scalar a is given by

$$a = \mathbf{a}^{\mathrm{T}}\mathbf{R}\mathbf{a} - 4\sigma_0^2 A' \tag{14.151}$$

14.8 HOFFMAN'S YIELD CRITERION

The Hoffman yield criterion [H4] can be written as an extension of the Hill criterion of (14.89) with

$$\begin{aligned} f_2 = {} & \frac{\alpha_{12}}{2}(\sigma_{11} - \sigma_{22})^2 + \frac{\alpha_{23}}{2}(\sigma_{22} - \sigma_{33})^2 \\ & + \frac{\alpha_{31}}{2}(\sigma_{33} - \sigma_{11})^2 + 3\alpha_{44}\sigma_{12}^2 + 3\alpha_{55}\sigma_{23}^2 + 3\alpha_{66}\sigma_{31}^2 \\ & + \alpha_{11}\sigma_{11} + \alpha_{22}\sigma_{22} + \alpha_{33}\sigma_{33} \end{aligned} \tag{14.152}$$

(It should be noted that not all of the α terms have the same units.) The new terms involve α_{11}, α_{22} and α_{33} and relate to the volumetric stresses.

From (14.152), the von Mises criterion is recovered with

$$\alpha_{12} = \alpha_{23} = \alpha_{31} = \alpha_{44} = \alpha_{55} = \alpha_{66} = 1 \tag{14.153a}$$

$$\alpha_{11} = \alpha_{22} = \alpha_{33} = 0 \tag{14.153b}$$

while the Drucker–Prager relationship is another degenerate case which will be explored further in Section 14.9.

For the general case, the nine coefficients, α_{ij}, can be obtained from nine experiments relating to the principal axes of anisotropy (see also Section 14.6.2). These tests involve three unixial compressive tests (leading to $\bar{\sigma}_{11}$, $\bar{\sigma}_{22}$ and $\bar{\alpha}_{33}$), three uniaxial tensile tests

(leading to $\hat{\sigma}_{11}$, $\hat{\sigma}_{22}$ and $\hat{\sigma}_{33}$) as well as three shear tests (leading to magnitudes $\bar{\sigma}_{12}$, $\bar{\sigma}_{13}$ and $\bar{\sigma}_{23}$). From the uniaxial tests in the '1'-direction, one can obtain from (14.152) the relationship:

$$\left(\frac{\alpha_{12}+\alpha_{13}}{2}\right)\hat{\sigma}_{11}^2+\alpha_{11}\hat{\sigma}_{11}=\sigma_o^2 \tag{14.154a}$$

and

$$\left(\frac{\alpha_{12}+\alpha_{13}}{2}\right)\bar{\sigma}^2-\alpha_{11}\bar{\sigma}=\sigma_o^2 \tag{14.154b}$$

Four similar relationships follows from the tests in the '2'- and '3'-directions and in addition, the shear tests yield (14.90d)–(14.90f). From these equations, we can obtain the coefficients α_{ij} from equations such as

$$\alpha_{11}=\sigma_o^2\left(\frac{\bar{\sigma}_{11}-\hat{\sigma}_{11}}{\hat{\sigma}_{11}\bar{\sigma}_{11}}\right) \tag{14.155a}$$

$$\alpha_{23}=\sigma_o^2\left(\frac{1}{\hat{\sigma}_{33}\bar{\sigma}_{33}}+\frac{1}{\hat{\sigma}_{22}\bar{\sigma}_{22}}-\frac{1}{\hat{\sigma}_{33}\bar{\sigma}_{33}}\right) \tag{14.155b}$$

$$\alpha_{44}=\frac{1}{3}\left(\frac{\sigma_o}{\bar{\sigma}^{12}}\right)^2 \tag{14.155c}$$

(The relationships for the remaining coefficients can be very easily deduced from those given above.) Alternatively (or additionally), one can use plastic strain ratios as discussed for the Hill criterion in Section 14.6.1.

For the purposes of finite element analysis, it is best to rewrite (14.152) in a form that is similar to (14.91) so that:

$$f_2=\tfrac{1}{2}\boldsymbol{\sigma}^{\mathrm{T}}\mathbf{P}\boldsymbol{\sigma}+\mathbf{p}^{\mathrm{T}}\boldsymbol{\sigma}-\sigma_o^2=0 \tag{14.156}$$

where the matrix $\mathbf{P}$ is taken from (14.92) and the vector $\mathbf{p}$ is given by

$$\mathbf{p}^{\mathrm{T}}=(\alpha_{11},\alpha_{22},\alpha_{33},0,0,0) \tag{14.157}$$

It should be noted that the vector $\mathbf{p}$ has units of stress.

The Hill criterion can be recovered from (14.156) by setting $\mathbf{p}=\mathbf{0}$. In order the derive an effective 'return procedure', we can now follow closely the approach of Section 14.7 and write the flow rule as

$$\dot{\boldsymbol{\varepsilon}}_{\mathrm{p}}=\dot{\lambda}_2\frac{\partial f_2}{\partial\boldsymbol{\sigma}}=\dot{\lambda}_2(\mathbf{P}\boldsymbol{\sigma}+\mathbf{p}) \tag{14.158}$$

The backward-Euler return follows as

$$\boldsymbol{\sigma}_{\mathrm{C}}=\boldsymbol{\sigma}_{\mathrm{B}}-\Delta\lambda_2\mathbf{C}[\mathbf{P}\boldsymbol{\sigma}_{\mathrm{C}}+\mathbf{p}] \tag{14.159}$$

so that, in place of (14.136), we have:

$$\boldsymbol{\sigma}_{\mathrm{C}}=[\mathbf{I}+\Delta\lambda_2\mathbf{CP}]^{-1}\{\boldsymbol{\sigma}_{\mathrm{B}}-\Delta\lambda\mathbf{Cp}\}=\mathbf{B}(\Delta\lambda_2)^{-1}\{\boldsymbol{\sigma}_{\mathrm{B}}-\Delta\boldsymbol{\lambda}_2\mathbf{b}\}=\mathbf{B}(\Delta\lambda_2)^{-1}\bar{\boldsymbol{\sigma}}_{\mathrm{B}} \tag{14.160}$$

As a consequence, the yield criterion of (14.156) can be written as

$$f_2=\sigma_{e\mathrm{C}}^2-\sigma_{o\mathrm{C}}^2=\tfrac{1}{2}\boldsymbol{\sigma}_{\mathrm{B}}^{\mathrm{T}}\mathbf{B}^{-\mathrm{T}}\mathbf{P}\mathbf{B}^{-1}\bar{\boldsymbol{\sigma}}_{\mathrm{B}}+\mathbf{p}^{\mathrm{T}}\mathbf{B}^{-1}\bar{\boldsymbol{\sigma}}_{\mathrm{B}}-\sigma_{o\mathrm{C}}^2 \tag{14.161}$$

Equation (14.161) provides a scalar equation in $\Delta\dot{\lambda}_2$, for which a truncated Taylor series leads to

$$f_{2n} = f_{2o} + 2\sigma_{eC}\dot{\sigma}_{eC} - 4\sigma_{oC}\sigma_{eC}A'\dot{\lambda}_2 = f_{2o} + K\dot{\lambda}_2 - 4\sigma_{oC}\sigma_{eC}A'\dot{\lambda}_2 = 0 \quad (14.162)$$

with

$$K = -\{\mathbf{p} + \mathbf{P}\mathbf{B}^{-1}\bar{\boldsymbol{\sigma}}_B\}^T\{\mathbf{B}^{-1}\mathbf{b} + \mathbf{B}^{-2}\mathbf{C}\mathbf{P}\bar{\sigma}_B\} \quad (14.163)$$

which allows us to obtain the iterative change, $\dot{\lambda}_2$ to $\Delta\dot{\lambda}_2$. In deriving (14.162), it has been assumed that an equation of the form of (14.105) can again be obtained for the rate of equivalent plastic strain. In contrast to the work of Section 14.6.2 we have not, in this section, defined the latter. As previously discussed, in relation to a complicated anisotropic yield criterion such as that of Hoffman, the issue of hardening is complex. Schellekens and de Borst [S1] recommend a sublayer approach (see Section 15.10).

14.8.1 The consistent tangent modular matrix

The derivation of the consistent tangent modular matrix follows closely the developments of Section 14.7.1—in particular, those relating to the squared form of the yield criterion. It is easy to show that we again arrive at a consistent tangent modular matrix in the form of (14.147) and (14.151) although now the vector $\mathbf{a}$ and matrix $\partial\mathbf{a}/\partial\boldsymbol{\sigma}$ are given by

$$\mathbf{a} = \mathbf{P}\boldsymbol{\sigma} + \mathbf{p}; \qquad \frac{\partial\mathbf{a}}{\partial\boldsymbol{\sigma}} = \mathbf{P} \quad (14.164)$$

However, with hardening, there can be difficulties in using the yield criterion in the form of f_2 from (14.156). This issue will be discussed further in Section 14.11.4.

14.9 THE DRUCKER–PRAGER YIELD CRITERION

It has already been indicated that the Drucker–Prager yield criterion can be obtained as a special (isotropic) case of the Hoffman yield criterion. We will now explore the two alternative forms of the former criterion. In particular, we will consider the relationship between the form of (14.2) from which we can obtain:

$$J_2 = \sigma_o^2 - 2DI_1\sigma_o + DI_1^2 \quad (14.165)$$

and the form of (14.156). To this end we note (see (6.51)) that we can write:

$$J_2 = \tfrac{1}{2}\boldsymbol{\sigma}^T\mathbf{P}_{J2}\boldsymbol{\sigma} \quad (14.166)$$

with $\mathbf{P}_{J2}$ from (14.93) and, using (14.1):

$$I_1 = \mathbf{p}_{J2}^T\boldsymbol{\sigma} = (1, 1, 1, 0, 0, 0)\boldsymbol{\sigma} \quad (14.167)$$

so that, from (14.165), we have:

$$f_2 = \tfrac{1}{2}\boldsymbol{\sigma}^T\mathbf{P}_{J2}\boldsymbol{\sigma} - D\boldsymbol{\sigma}^T\mathbf{p}_{J2}\mathbf{p}_{J2}^T\boldsymbol{\sigma} + 2D\sigma_o\mathbf{p}_{J2}^T\boldsymbol{\sigma} - \sigma_o^2 = \tfrac{1}{2}\sigma^T\mathbf{P}\boldsymbol{\sigma} + \mathbf{p}^T\boldsymbol{\sigma} - \sigma_o^2 = 0 \quad (14.168)$$

which allows $\mathbf{P}$ to be expressed in terms of D and $\mathbf{P}_{J2}$ and $\mathbf{p}$ in terms of D (see Section 14.2), σ_o and $\mathbf{p}_{J2}$.

14.10 USING AN EIGENVECTOR EXPANSION FOR THE STRESSES

Matthies [M2] has proposed a method for the solution of the backward-Euler return of Section 14.7 which involves making use of an eigenvector expansion. It will be shown in Section 14.10.1 that this method has close links with the procedure used in Section 6.8.2 for plane-stress plasticity with the von Mises yield criterion.

The process can be applied to any yield criterion which can be expressed in the form of (14.156). In relation to the previous developments, a starting-point for Matthies' procedure can be found by multiplying through (14.160) by $\mathbf{A} = \mathbf{C}^{-1}$ so as to obtain:

$$[\mathbf{A} + \Delta\lambda\mathbf{P}]\boldsymbol{\sigma}_C = \mathbf{A}\boldsymbol{\sigma}_B - \Delta\lambda\mathbf{p} = \mathbf{c} - \Delta\lambda\mathbf{p} \tag{14.169}$$

where, in (14.169) and for the remainder of this section, we are using $\Delta\lambda$ instead of the previous (Section 14.6.1) $\Delta\lambda_2$. Now $\boldsymbol{\sigma}_C$ can be expressed in terms of the eigenvectors of φ_i with eigenvalues μ_i which satisfy the relationship:

$$\mathbf{P}\boldsymbol{\varphi}_i = \mu_i\mathbf{A}\boldsymbol{\varphi}_i \tag{14.170}$$

and are normalised such that

$$\boldsymbol{\varphi}_i^{\mathrm{T}}\mathbf{A}\boldsymbol{\varphi}_j = \delta_{ij} \tag{14.171}$$

For a given set of material parameters which are defined by $\mathbf{C}$ (or $\mathbf{A}$) and $\mathbf{P}$, this eigenvalue problem need only be solved once.

Matthies shows [M2] that the solution to (14.169) can be expressed as

$$\boldsymbol{\sigma}_C = \sum \alpha_i\boldsymbol{\varphi}_i \tag{14.172}$$

so that substitution into (14.169) leads to

$$[\mathbf{A} + \Delta\lambda\mathbf{P}]\sum \alpha_i\boldsymbol{\varphi}_i = \mathbf{c} - \Delta\lambda\mathbf{p} \tag{14.173}$$

Pre-multiplying (14.173) by $\boldsymbol{\varphi}_j$ and making use of (14.170) and (14.171) leads to

$$\alpha_i = \frac{(c - \Delta\lambda\mathbf{p})^{\mathrm{T}}\boldsymbol{\varphi}_i}{(1 + \mu_i\Delta\lambda_i)} \tag{14.174}$$

Substitution from (14.172) into (14.156) and making use of (14.170) and (14.171) gives:

$$f_2 = \tfrac{1}{2}\sum \mu_i\alpha_i^2 + \sum \alpha_i(\mathbf{p}^{\mathrm{T}}\boldsymbol{\varphi}_i) - \sigma_o^2 = 0 \tag{14.175}$$

so that, assuming perfect plasticity, a truncated Taylor series leads to a relationship of the form:

$$f_{2n} = f_{2o} + \tfrac{1}{2}\sum \mu_i\alpha_i\frac{\partial a_i}{\partial\Delta\lambda}\dot{\lambda} - \sum \frac{\partial\alpha_i}{\partial\Delta\lambda}(\mathbf{p}^{\mathrm{T}}\boldsymbol{\varphi}_i) = 0 \tag{14.176}$$

where, from (14.174), we have:

$$\frac{\partial\alpha_i}{\partial\Delta\lambda} = \frac{-\mathbf{p}^{\mathrm{T}}\boldsymbol{\varphi}_i}{(1 + \mu_i\Delta\lambda)} - \frac{\mu_i\alpha_i}{(1 + \mu_i\Delta\lambda)} \tag{14.177}$$

Equations (14.176) and (14.177) provide a relationship for the iterative change, $\dot{\lambda}$, in $\Delta\lambda$ and allows a scalar Newton–Raphson iteration to obtain $\Delta\lambda$.

14.10.1 An example involving plane-stress plasticity and the von Mises yield criterion

Matthies has shown [M2] that, for the von Mises yield criterion, the previous method can be used to recover the radial return method of Section 6.6.6. Simo *et al.* have applied a similar procedure to plane-stress plasticity [S4]. We will now investigate the latter case with reference to the von Mises yield criterion which, using the form of (14.91), can be expressed as

$$f_2 = \tfrac{1}{2}\boldsymbol{\sigma}^{\mathrm{T}}\mathbf{P}\boldsymbol{\sigma} - \sigma_{\mathrm{o}}^2 \tag{14.178}$$

where

$$\boldsymbol{\sigma}^{\mathrm{T}} = (\sigma_{xx}, \sigma_{yy}, \tau_{xy}) \tag{14.179}$$

$$\mathbf{P} = \begin{bmatrix} 2 & -1 & 0 \\ -1 & 2 & 0 \\ 0 & 0 & 6 \end{bmatrix} \tag{14.180}$$

$$\mathbf{C} = \frac{E}{(1-\nu)^2}\begin{bmatrix} 1 & \nu & 0 \\ \nu & 1 & 0 \\ 0 & 0 & (1-\nu)/2 \end{bmatrix}; \qquad \mathbf{A} = \mathbf{C}^{-1} = \frac{1}{E}\begin{bmatrix} 1 & -\nu & 0 \\ -\nu & 1 & 0 \\ 0 & 0 & 2(1+\nu) \end{bmatrix} \tag{14.181}$$

and the solution to the eigenvalue problem of (14.170) and (14.171) is

$$\mu_1 = \frac{E}{(1-\nu)}; \qquad \mu_2 = \mu_3 = \frac{3E}{(1+\nu)} \tag{14.181}$$

$$\boldsymbol{\varphi}_1 = \frac{1}{\sqrt{2}}\mu_1^{1/2}\begin{bmatrix} 1 \\ 1 \\ 0 \end{bmatrix}; \qquad \boldsymbol{\varphi}_2 = \frac{1}{\sqrt{6}}\mu_2^{1/2}\begin{bmatrix} 1 \\ -1 \\ 0 \end{bmatrix}; \qquad \boldsymbol{\varphi}_3 = \frac{1}{\sqrt{6}}\mu_2^{1/2}\begin{bmatrix} 0 \\ 0 \\ 1 \end{bmatrix} \tag{14.182}$$

Given these relationships one can simply apply the method of the previous section to produce a backward-Euler return that coincides with that of Section 6.8.2.

14.11 CRACKING, FRACTURING AND SOFTENING MATERIAL

In concept, the previous plasticity procedures can be applied to 'softening materials', by simply introducing a softening rather than a hardening equivalent stress-equivalent plastic strain relationship. In practice, there are many difficulties a number of which are still unresolved. Some of these problems will now be briefly discussed.

14.11.1 Mesh dependency and alternative equilibrium states

We will begin by discussing the difficulties with a 'stress-based' failure criterion for a 'purely brittle material' such as concrete. (In fact, carefully controlled experiments

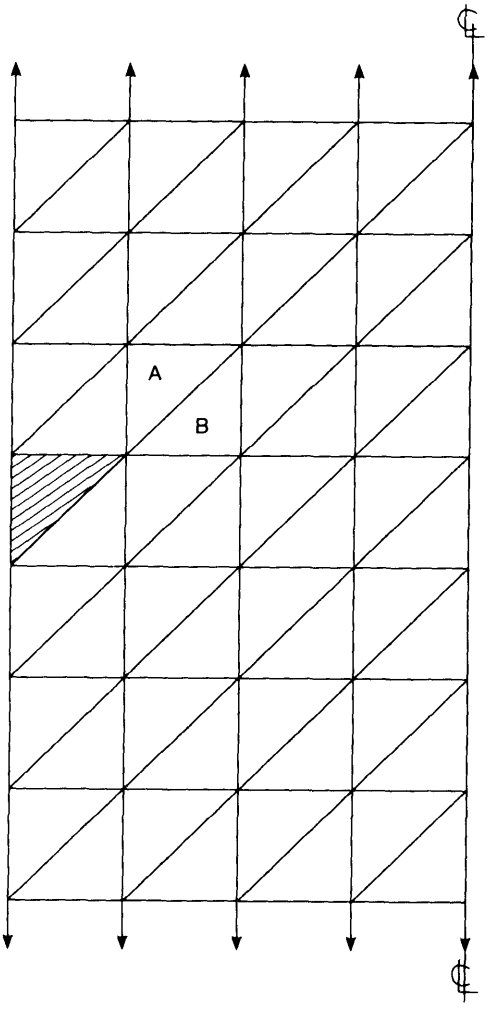

Figure 14.11 Uniaxial uniform tension and mesh dependency.

[P2, E1] indicate that cracking in concrete is a softening phenomenon and that the material exhibits a fracture energy). Bazant [B1] and Bazant and Cedolin [B2] used a model that was similar to that of Figure 14.11 to illustrate the problem of mesh dependency. The shaded (constant stress) element at the edge can be assumed to represent a notch or flaw. Assuming that the maximum stress is now in element A, once this has cracked, a brittle model would simply reduce the stiffness of this element to zero. However, because of the flaw, there is a stress concentration and, for a more refined mesh, the load to reach the critical stress in the first element (equivalent to element A) would be reduced.

This problem does not simply apply to the first cracking, it also applies to the crack propagation. With a refined mesh, the load for the next cracking (after A) in the current most highly stressed element (say element B) will also be reduced. As pointed out by

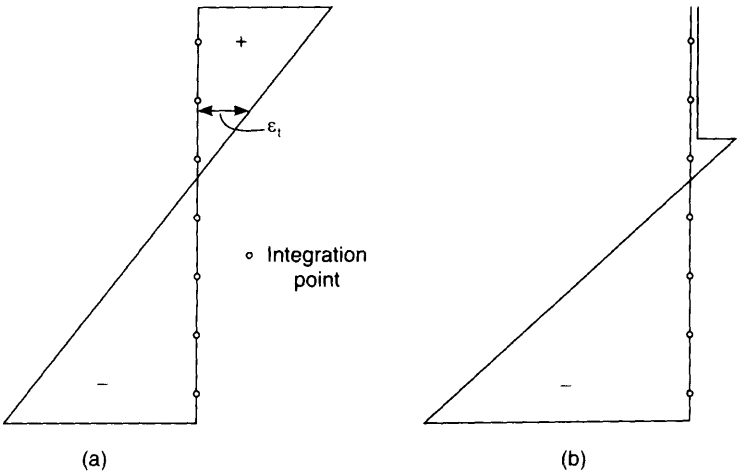

Figure 14.12 Benign stress concentration with plane sections remaining plane. (a) Strain; (b) stress.

Bazant [B1], and Bazant and Cedolin [B2], by continually refining the mesh, we can make the crack propagate through the plate at lower and lower loads. The concept does not only apply to constant stress elements but would also relate to Gauss point cracking in higher-order elements.

It is worth noting that there is one class of problem that does not suffer very severely from these difficulties. In some analyses of beams or plates, we may have integration points through the depth (see Sections 7.1.2 and 8.1.2). In these circumstances, we can degrade the properties to zero and, while there would be a stress concentration in a full three-dimensional or even two-dimensional analysis, no such concentration occurs in relation to the adopted strain assumption that 'plane sections remain plane' (Figure 14.12).

Having recognised the serious limitation of stress-based failure criteria, we could move to methods directly involving 'fracture mechanics' [R4]. An alternative procedure, pioneered by Hilleborg *et al.* [H3], is to introduce a softening stress–strain relationship (possibly within a plasticity setting), with the latter being related to the 'fracture energy'. In this way, fracture mechanics is indirectly introduced. We will discuss this method later but will first point out the mesh dependency and alternative equilibrium states associated with a softening stress–strain relationship.

The author [C10] used the simple model of Figure 14.13 to illustrate these effects. It will be assumed that each constant stress (and strain) element in Figure 14.13b is given the softening stress–strain relationship of Figure 14.13a. A 'displacement-controlled' solution will be considered which is controlled by the displacement Δ in Figure 14.13b. At the maximum load, P, the stress in the elements would each have reached the point B in Figure 14.13a so that each stress is at σ_1. Following this stage, a possible equilibrium path in the load/deflection space is given by the falling curve 1 in Figure 14.13c. For this path, it is assumed that each of the elements follows the softening stress–strain line BC. On the other hand, the falling line 2 in Figure 14.13c could be obtained if three of the elements softened down BC in Figure 14.13a, while one

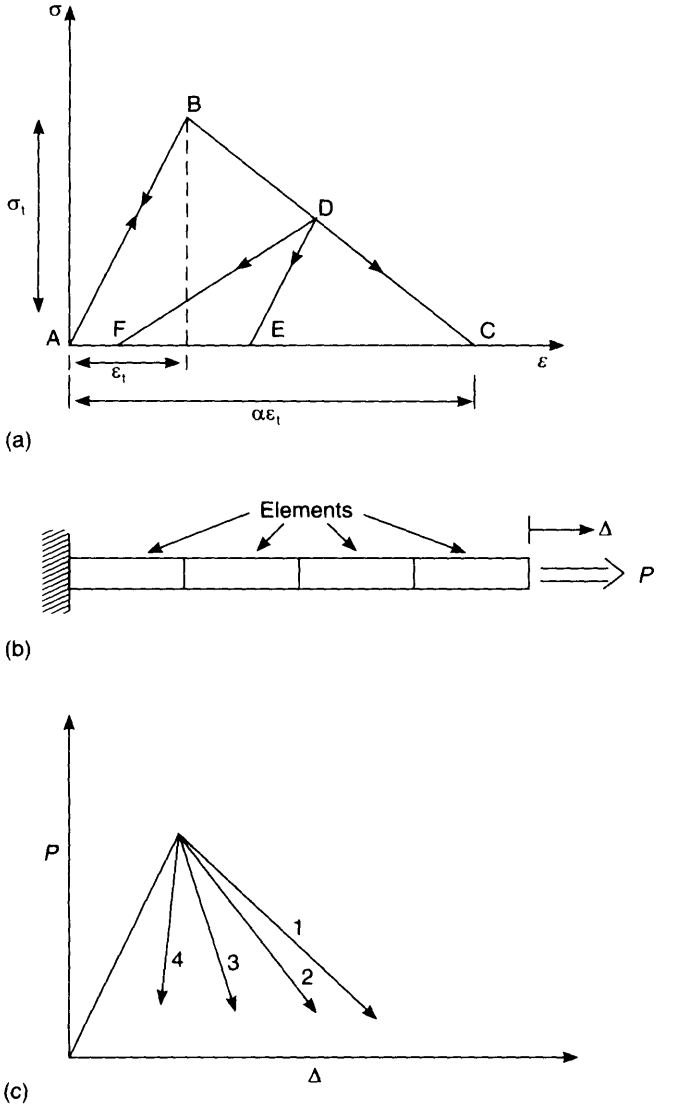

Figure 14.13 Strain localisation and alternative equilibrium states for a simple model. (a) Uniaxial strain-softening model; (b) simple tie-bar; (c) structural response.

of them unloaded elastically down BA. In relation to the adopted model, the only 'stable path' would be path 4, for which only one element softened while the others all unloaded elastically. If the mesh were refined, this 'stable path' would be a line doubling back directly on the elastic loading line.

We consider the latter path as 'stable', because, if the strength of each element was fractionally perturbed, the model structure would reach its maximum load when the

weakest of the elements first reached its σ_t value and, beyond this level, only the weakest element would soften. Clearly, the situation in Figure 14.13c involves a form of 'material bifurcation'. For the situation in Figure 14.13c, the 'curve', 4, would be associated with one negative pivot in the tangent stiffness matrix (associated with the snap-back) while in moving from 'curves' 3 to 2 to 1 we would one each occasion add a further negative pivot for having passed 'material bifurcation points'.

While, with a 'material imperfection', there would strictly be only one attainable equilibrium curve, with finite steps, a finite element solution procedure can easily converge on to a 'higher unstable state' (see Section 2.6.4 for an equivalent situation with 'geometric imperfections'). It is true that these problems are at their most severe for 'constant stress states' such as depicted in Figure 14.13. None the less, equivalent problems can plague finite element solutions even in other circumstances with a varying stress gradient [C11].

We will now turn to the technique of relating the stress–strain curve to the fracture energy. (For concrete, the latter is $G_c \simeq 100\,\text{N/mm}$ [B1, B2].) In relation to Figure 14.13a, we set the area under the stress/strain curve to G_c so that:

$$G_c = 0.5c\alpha\sigma_t\varepsilon_t \tag{14.183}$$

where c is the 'effective length' of the element and, for the simple constant stress/strain elements of Figure 14.13, would be the actual length of the element. In these circumstances, if a material perturbation was provided so that only the 'materially stable' solution was obtained (with one softening element), the adopted load deflection curve would be independent of the mesh. In a two-dimensional plane-stress environment, the author extended this concept by defining the effective length, c, using the interaction of the principle tensile strength direction with a skewed ellipse derived from the Jacobian at the Gauss point [C11].

Before leaving Figure 13, it is worth noting that the unloading line DE might relate to a 'plastic model', while if point F coincided with the orgin at point A, we would have an 'elastic damage model' [L3]. In this case, we could write:

$$\sigma = (1 - d)E_o\varepsilon \tag{14.184}$$

where E_0 is the initial elastic stiffness (slope of AB) and d is the scalar damage parameter given by

$$\begin{aligned} &d = 0, && \varepsilon < \varepsilon_t \\ &d = \frac{\alpha}{\alpha - 1}\frac{\varepsilon_{max} - \varepsilon_t}{\varepsilon_{max}} && \alpha\varepsilon_t > \varepsilon > \varepsilon_t \\ &d = 1 && \varepsilon > \varepsilon_t \end{aligned} \tag{14.185}$$

Equation (14.184) applies with loading ($\varepsilon = \varepsilon_{max}$), where ε_{max} is the maximum strain so far experienced, or unloading ($\varepsilon < \varepsilon_{max}$). If point F is distinct from point A (as in the figure), the unloading line DF would define an 'elastic–plastic damage model'. 'Damage mechanics' is discussed further is Section 14.12.

It is worth mentioning that the previous 'softening stress/strain' approach can also be applied to delamination in composites using 'interface elements' so that the fracture energy is now the area under the traction (load/unit area)—'relative opening (assuming mode 1) displacement' relationship [S2, C13, C14]. In these circumstances there is no need to introduce the length parameter c.

Returning to continuum rather than interface modelling, the difficulties that have been described have led a number of workers to turn to various forms 'of non-local continuum approach' [B2, P3, D5]. These formulations, which often lead to non-standard finite element procedures, fall outside the scope of this book. Before considering the detail of some 'concrete models', it is worth mentioning an analytical 'trick' that can be quite helpful with a softening or fracturing material such as concrete. The trick involves superimposing on the model of the structure another linear elastic structure (with the same nodes and elements) with a very small elastic stiffness. The latter is meant to stop the model structure falling 'totally apart'.

14.11.2 'Fixed' and 'rotating' crack models in concrete

While the earliest finite element involved 'discrete cracks', the 'smeared cracking' procedure soon became more popular [A1]. Interestingly, there is now some interest in methods that merge the two procedures by embedding localised discontinuities within the element [K3, O1, L5]. In the 'fixed crack model', the direction of the crack would be related to the first occurrence of a principle tensile stress of magnitude equal to the 'cracking stress', σ_t. In relation to the resulting fixed directions (1 and 2 in Figure 14.14), tangential stiffnesses would be provided involving some softening stress–strain curve in the fixed principal tensile direction (σ_{11} and ε_{11}) while for shear stresses (τ_{12}), the shear modulus would be reduced by the 'shear retention factor'. A major disadvantage of this method was that it allowed new principal tensile stresses to arise at some oblique angle which exceeded σ_t. Generally, these were not monitored and no new reduction in stiffness was applied. As a result, the method tended to give solutions that were over-stiff (and unsafe) [C12]. De Borst and Nauta [D4] proposed a solution which allowed a set of cracks at a Gauss point. However, the models were very complex and severe difficulties were often encountered with the 'threshold angle'. Earlier, Cope *et al.* [C14] had introduced the 'rotating' or 'swinging' crack method, in which the crack direction relates to the current direction of the principal tensile strain and hence rotates or swings. Objections to this model related to its 'unphysical aspects'—cracks cannot move. However, these objections are reduced if one thinks of the 'swinging crack direction' as representing the 'current most active crack' (remembering that a Gauss point represents an area (or volume)).

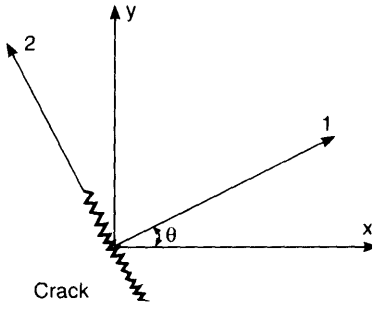

Figure 14.14 1–2 and x–y directions.

Variants of the 'rotating crack model' are still being developed and, as will be shown, are closely related to 'plasticity models'. In describing the method (and the subsequent plasticity methods) we will concentrate on the two-dimensional plane-stress situation.

In relation to Figure 14.14, it will be assumed that θ defines the directions of the current principal tensile strain direction so that:

$$\tan 2\theta = \frac{\gamma_{xy}}{\varepsilon_x - \varepsilon_y} \tag{14.186}$$

and we can write:

$$\boldsymbol{\sigma} = \begin{bmatrix} \sigma_x \\ \sigma_y \\ \tau_{xy} \end{bmatrix} = \begin{bmatrix} c^2 & s^2 & -2sc \\ s^2 & c^2 & 2sc \\ sc & -sc & c^2 - s^2 \end{bmatrix} \begin{bmatrix} \sigma_1(\varepsilon_1(\theta)) \\ \sigma_2(\varepsilon_2(\theta)) \\ 0 \end{bmatrix}$$

$$= \mathbf{T}^{\mathrm{T}} \boldsymbol{\sigma}_{12} = \begin{bmatrix} c^2 & s^2 \\ s^2 & c^2 \\ sc & -sc \end{bmatrix} \begin{pmatrix} \sigma_1 \\ \sigma_2 \end{pmatrix} = \bar{\mathbf{T}}^{\mathrm{T}} \bar{\boldsymbol{\sigma}}_{12} \tag{14.187}$$

where $c = \cos\theta$ and $s = \sin\theta$. Having computed the principal strains ε_1 and ε_2, the analyst can simply look up σ_1 and σ_2 on the input uniaxial stress strain curve (which will probably involve softening in the tensile regime) and then compute the stress vector with respect to the fixed cartesian axes from (14.187).

To obtain the tangential constitutive relationship, differentiation of (14.187) leads to

$$\delta\boldsymbol{\sigma} = \bar{\mathbf{T}}^{\mathrm{T}} \begin{bmatrix} \frac{\partial\sigma_1}{\partial\varepsilon_1} & \frac{\partial\sigma_2}{\partial\varepsilon_2} \\ \frac{\partial\sigma_2}{\partial\varepsilon_1} & \frac{\partial\sigma_2}{\partial\varepsilon_2} \end{bmatrix} \bar{\mathbf{T}}\delta\boldsymbol{\varepsilon} + \frac{\partial\bar{\mathbf{T}}^{\mathrm{T}}}{\partial\theta}\bar{\boldsymbol{\sigma}}_{12}\frac{\partial\theta}{\partial\boldsymbol{\varepsilon}}\delta\boldsymbol{\varepsilon} \tag{14.188}$$

which can be further manipulated [C12] to give:

$$\delta\boldsymbol{\sigma} = \bar{\mathbf{T}}^{\mathrm{T}} \begin{bmatrix} \frac{\partial\sigma_1}{\partial\varepsilon_1} & \frac{\partial\sigma_2}{\partial\varepsilon_2} \\ \frac{\partial\sigma_2}{\partial\varepsilon_1} & \frac{\partial\sigma_2}{\partial\varepsilon_2} \end{bmatrix} \bar{\mathbf{T}}\delta\boldsymbol{\sigma} + \frac{(\sigma_1 - \sigma_2)}{2(\varepsilon_1 - \varepsilon_2)}\mathbf{z}\mathbf{z}^{\mathrm{T}}\delta\boldsymbol{\varepsilon} \tag{14.189}$$

where

$$\mathbf{z}^{\mathrm{T}} = (\sin 2\theta, -\sin 2\theta, -\cos 2\theta) \tag{14.190}$$

Resolving (14.189) into the 12 directions gives:

$$\delta\boldsymbol{\sigma}_{12} = \begin{bmatrix} \frac{\partial\sigma_1}{\partial\varepsilon_1} & \frac{\partial\sigma_1}{\partial\varepsilon_2} & 0 \\ \frac{\partial\sigma_2}{\partial\sigma_1} & \frac{\partial\sigma_2}{\partial\sigma_2} & 0 \\ 0 & 0 & \frac{(\sigma_1 - \sigma_2)}{2(\varepsilon_1 - \varepsilon_2)} \end{bmatrix} \delta\boldsymbol{\varepsilon}_{12} \tag{14.191}$$

The shear stiffness term is closely related to that given in (13.142b) of Section 13.8.2 for

a hyperelastic material and the procedure discussed in that section can be used to find a solution when $\varepsilon_1 = \varepsilon_2$.

In the simplest implementation, the stress σ_1 would only be related to ε_1 so that terms such as $\partial\sigma_1/\partial\varepsilon_2$ in (14.189) would be zero. However other implementations are possible [C12] although they may lead to a non-symmetric tangent stiffness matrix.

14.11.3 Relationship between the 'rotating crack model' and a 'deformation theory' plasticity approach using the 'square yield criterion'

Figure 14.15 shows the 'square yield criterion' that is often used in 'limit analysis' [N2]. (The tensile part of the yield criterion is also referred to as the Rankine yield criterion.) The yield criterion can be expressed as

$$f_2 = (\sigma_1 - \sigma_t)(\sigma_2 - \sigma_t) = (\sigma_1 - \sigma_c)(\sigma_2 - \sigma_c) = 0 \tag{14.192}$$

where σ_t is the tensile yield stress and σ_c is the compressive yield stress. In limit analysis, the former would usually be set to zero so that we would have a 'no-tension material'. A conservative value would usually be provided for the compressive yield stress to make an allowance for the limited ductility in compression.

By expressing the principal stresses σ_1 and σ_2 in terms of the cartesian components, (14.192) can be re-expressed as

$$f_2 = (\sigma_x - \sigma_t)(\sigma_y - \sigma_t) - \tau_{xy}^2 = (\sigma_x - \sigma_c)(\sigma_y - \sigma_c) - \tau_{xy}^2 = 0 \tag{14.193}$$

For future developments, it will be useful to express (14.193) in a similar form to (14.168)

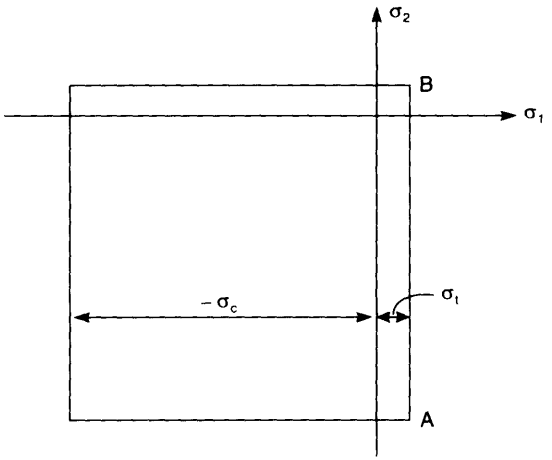

Figure 14.15 The 'square yield criterion' in principal stress space.

so that:

$$f_2 = \tfrac{1}{2}\begin{bmatrix}\sigma_x\\ \sigma_y\\ \tau_{xy}\end{bmatrix}^{\mathrm{T}}\begin{bmatrix}0 & 1 & 0\\ 1 & 0 & 0\\ 0 & 0 & -2\end{bmatrix}\begin{bmatrix}\sigma_x\\ \sigma_y\\ \tau_{xy}\end{bmatrix} - \sigma_o\begin{bmatrix}1\\ 1\\ 0\end{bmatrix}^{\mathrm{T}}\begin{bmatrix}\sigma_x\\ \sigma_y\\ \tau_{xy}\end{bmatrix} + \sigma_o^2 = \tfrac{1}{2}\boldsymbol{\sigma}^{\mathrm{T}}\mathbf{P}\boldsymbol{\sigma} + \mathbf{p}(\sigma_o)^{\mathrm{T}}\boldsymbol{\sigma} + \sigma_o^2 = 0 \tag{14.194}$$

In (14.194), σ_o is either σ_t or σ_c depending on which part of the yield function is active (both should be checked).

Suppose we apply a 'deformation theory' form of plasticity to (14.194) with an associated flow rule. In these circumstances, the plastic strains can be expressed as

$$\boldsymbol{\varepsilon}_p = \begin{bmatrix}\varepsilon_x\\ \varepsilon_y\\ \gamma_{xy}\end{bmatrix}_p = \lambda\frac{\partial f_2}{\partial \boldsymbol{\sigma}} = \lambda\begin{bmatrix}\sigma_y - \sigma_o\\ \sigma_x - \sigma_o\\ -2\tau_{xy}\end{bmatrix} = \lambda[\mathbf{P}\boldsymbol{\sigma} + \mathbf{p}] \tag{14.195}$$

so that, for simplicity, considering the case with $\nu = 0$, we have:

$$\begin{aligned}\sigma_x &= E(\varepsilon_x - \lambda(\sigma_y - \sigma_o))\\ \sigma_y &= E(\varepsilon_y - \lambda(\sigma_x - \sigma_o))\\ \tau_{xy} &= \frac{E}{2}(\gamma_{xy} + 2\lambda\tau_{xy})\end{aligned} \tag{14.196}$$

Equations (14.196) can be used to show that:

$$\tan 2\theta = \frac{\gamma_{xy}}{\varepsilon_x - \varepsilon_y} = \frac{\tau_{xy}}{\sigma_x - \sigma_y} \tag{14.197}$$

and hence, as with the rotating crack model of the previous section, the directions of principal stress and strain coincide. Indeed, if elastic/perfectly-plastic stress–strain curves of the form of Figure 14.16 are used, the deformation theory plasticity model and the rotating crack models are equivalent [C13].

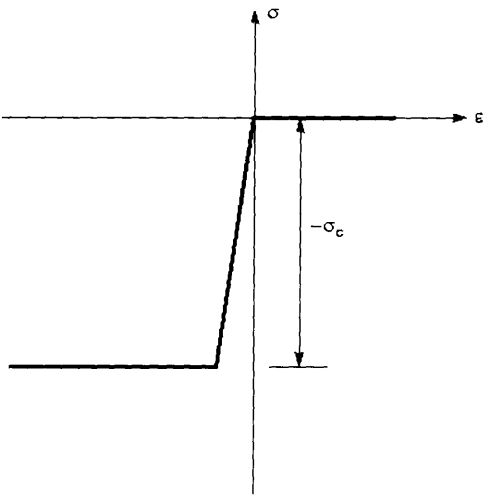

Figure 14.16 Idealised uniaxial stress–strain relationship.

14.11.4 A flow theory approach for the 'square yield criterion'

We will now consider the application of a flow-theory form of plasticity. The work is closely related to that described earlier by Feenstra *et al.* [F1]. We will initially consider a simple elastic/perfectly-plastic model with no hardening or softening. In these circumstances, if we wished to introduce a 'no tension model', we would set $\sigma_0 = \sigma_1 = 0$. In addition, we may or may not wish to constrain the compressive behaviour. In either case, we can use the yield criterion of (14.194) with σ_0 being assumed fixed.

To apply a backward-Euler return, we could use the general method of Section 6.6.6 which would involve an iteration with three stress variables and the incremental plastic strain rate multiplier, $\Delta\lambda$. Alternatively, we could apply the method of Section 14.10, where with the current form of the matrix $\mathbf{P}$ (see (14.194)), the eigenvalues μ_i of (14.170) turn out to be given by

$$\mu_1 = \frac{E}{(1-\nu)}; \qquad \mu_2 = \mu_3 = \frac{-E}{(1+\nu)} \tag{14.198}$$

while the eigenvectors, $\boldsymbol{\varphi}_i$ are given by

$$\boldsymbol{\varphi}_1 = \frac{1}{\sqrt{2}}\mu_1^{1/2}\begin{bmatrix}1\\1\\0\end{bmatrix}; \qquad \boldsymbol{\varphi}_2 = \frac{1}{\sqrt{2}}(-\mu_2)^{1/2}\begin{bmatrix}1\\-1\\0\end{bmatrix}; \qquad \boldsymbol{\varphi}_2 = \frac{1}{\sqrt{2}}(-\mu_2)^{1/2}\begin{bmatrix}0\\0\\1\end{bmatrix} \tag{14.199}$$

Hence we can express the required stresses, $\boldsymbol{\sigma}_C$, using (14.172) with the coefficients α_i being related to the single unknown, $\Delta\lambda$, via (14.174). In place of (14.175), the current yield function is expressed in the form:

$$f_2 = \frac{1}{2}\sum \mu_i \alpha_i^2 + \sum \alpha_i(\mathbf{p}^{\mathrm{T}}\boldsymbol{\varphi}_i) + \sigma_0^2 = 0 \tag{14.200}$$

where there is now a plus sign in front of the σ_0^2 term. With the α_i coefficients being given by (14.174), equation (14.200) provides a non-linear scalar equation in $\Delta\lambda$ and we can directly use the method of Section 14.10 to use the Newton–Raphson method to solve the scalar equation in $\Delta\lambda$.

We will now consider the inclusion of hardening or softening. Before considering the detail of the particular hardening or softening rule, we will consider an alternative form for the yield criterion of (14.194) and will also point out some possible pitfalls in using the former.

We will continue to concentrate on the tensile regime and, instead of starting from (14.192), we will consider the yield criterion as

$$f_1 = \sigma_1 - \sigma_0 = 0 \tag{14.201}$$

where σ_1 is the principal tensile stress. Using Mohr's circle, we can re-express the above in terms of the cartesian stress components so that:

$$f_1 = (\tfrac{1}{2}\boldsymbol{\sigma}^{\mathrm{T}}\bar{\mathbf{P}}\boldsymbol{\sigma})^{1/2} + \tfrac{1}{2}\boldsymbol{\pi}^{\mathrm{T}}\boldsymbol{\sigma} - \sigma_0 = \sigma_{c1} + \sigma_{c2} - \sigma_0 = 0 \tag{14.202}$$

with

$$\bar{\mathbf{P}} = \frac{1}{2}\begin{bmatrix} 1 & -1 & 0 \\ -1 & 1 & 0 \\ 0 & 0 & 4 \end{bmatrix} \tag{14.203}$$

$$\boldsymbol{\pi}^{\mathrm{T}} = (1, 1, 0) \tag{14.204}$$

Using these terms, the earlier yield criterion of (14.194) can be expressed as

$$f_2 = \tfrac{1}{2}\boldsymbol{\sigma}^{\mathrm{T}}\mathbf{P}\boldsymbol{\sigma} - \sigma_0\boldsymbol{\pi}^{\mathrm{T}}\boldsymbol{\sigma} + \sigma_0^2 = 0 \tag{14.205}$$

where

$$\mathbf{P} = \begin{bmatrix} 0 & 1 & 0 \\ 1 & 0 & 0 \\ 0 & 0 & -2 \end{bmatrix} = \frac{1}{2}\begin{bmatrix} 1 & 1 & 0 \\ 1 & 1 & 0 \\ 0 & 0 & 0 \end{bmatrix} - \frac{1}{2}\begin{bmatrix} 1 & -1 & 0 \\ -1 & 1 & 0 \\ 0 & 0 & 4 \end{bmatrix} = \tfrac{1}{2}\boldsymbol{\pi}\boldsymbol{\pi}^{\mathrm{T}} - \bar{\mathbf{P}} \tag{14.206}$$

For future developments, it is worth noting that (14.205) can also be expressed in the form:

$$\bar{f}_2 = f_1^2 - 2\sigma_{c1}f_1 = 0 \tag{14.207}$$

where we have added the bar to f_2 because we will now distinguish between the results obtained by using f_2 from (14.205) and $\bar{f}_2$ from (14.207).

In the following we will concentrate on the consistent tangent modular matrix having assumed that we have obtained $\Delta\lambda$ and σ_0. Using the approach of Section 6.7.2, we obtain the solution as

$$\mathbf{C}_t = \left[\mathbf{R} - \frac{\mathbf{R}\mathbf{a}\mathbf{a}^{\mathrm{T}}\mathbf{R}^{\mathrm{T}}}{\mathbf{a}^{\mathrm{T}}\mathbf{R}\mathbf{a} + A'}\right] \tag{14.208}$$

with

$$\mathbf{R} = \mathbf{Q}^{-1}\mathbf{C} = \left[\mathbf{I} + \Delta\lambda\frac{\partial\mathbf{a}}{\partial\boldsymbol{\sigma}}\right]^{-1}\mathbf{C} \tag{14.209}$$

For $\mathbf{C}_t$ to be symmetric, we require $\partial\mathbf{a}/\partial\boldsymbol{\sigma}$ to be symmetric.

We will now derive the latter matrix starting from various assumptions regarding the yield criterion and will initially consider f_1 of (14.202) for which we can write:

$$\mathbf{a}_1 = \frac{\partial f_1}{\partial\sigma} = \frac{\bar{\mathbf{P}}\sigma}{2\sigma_{c1}} + \frac{1}{2}\boldsymbol{\pi} \tag{14.210}$$

and

$$\frac{\partial\mathbf{a}_1}{\partial\boldsymbol{\sigma}} = \frac{\bar{\mathbf{P}}}{2\sigma_{c1}} - \frac{1}{4\sigma_{c1}^2}(\bar{\mathbf{P}}\boldsymbol{\sigma})(\bar{\mathbf{P}}\boldsymbol{\sigma})^{\mathrm{T}} \tag{14.211}$$

which is clearly symmetric.

If we now start from (14.205), we obtain:

$$\mathbf{a}_2 = \frac{\partial f_2}{\partial\boldsymbol{\sigma}} = \mathbf{P}\boldsymbol{\sigma} - \sigma_0\boldsymbol{\pi} \tag{14.212}$$

and

$$\frac{\partial \mathbf{a}_2}{\partial \boldsymbol{\sigma}} = \mathbf{P} - \boldsymbol{\pi}\frac{\partial \sigma_o}{\partial \boldsymbol{\sigma}} \tag{14.213}$$

If there is no hardening or softening, $\partial \mathbf{a}_2/\partial \boldsymbol{\sigma} = \mathbf{P}$ which is symmetric and there are no problems with using f_2 from (14.205). However, with hardening or softening, from (14.205), we obtain:

$$\dot{f}_2 = \mathbf{a}_2^{\mathrm{T}}\dot{\boldsymbol{\sigma}} + (2\sigma_o - \boldsymbol{\pi}^{\mathrm{T}}\boldsymbol{\sigma})\dot{\sigma}_o = 0 \tag{14.214}$$

so that substitution into (14.212) gives:

$$\frac{\partial \mathbf{a}_2}{\partial \boldsymbol{\sigma}} = \mathbf{P} - \frac{1}{(\boldsymbol{\pi}^{\mathrm{T}}\boldsymbol{\sigma} - 2\sigma_o)}\boldsymbol{\pi}\mathbf{a}^{\mathrm{T}} \tag{14.215}$$

which is non-symmetric. The source of the anomaly can be revealed by starting from (14.207) without assuming that $f_1 = 0$. In these circumstances, we obtain:

$$\bar{\mathbf{a}}_2 = (2f_1 - 2\sigma_{e1})\mathbf{a}_1 - \left(\frac{f_1}{\sigma_{e1}}\right)\bar{\mathbf{P}}\boldsymbol{\sigma} \tag{14.216}$$

If we set $f_1 = 0$, and use (14.206) and (14.210), we recover $\mathbf{a}_2$ from (14.212). Further differential of (14.216) leads to the relationship:

$$\left.\frac{\partial \bar{\mathbf{a}}_2}{\partial \boldsymbol{\sigma}}\right|_{f_1=0} = 2\mathbf{a}_1\mathbf{a}_1^{\mathrm{T}} - 2\sigma_{e1}\frac{\partial \mathbf{a}_1}{\partial \boldsymbol{\sigma}} - \frac{1}{\sigma_{e1}}[\mathbf{a}_1(\bar{\mathbf{P}}\boldsymbol{\sigma})^{\mathrm{T}} - (\bar{\mathbf{P}}\boldsymbol{\sigma})\mathbf{a}_1] \tag{14.127}$$

which is symmetric. It should be emphasised that in obtaining (14.217), we substitute in the relationship $f_1 = 0$ *after* the differentiation of $\bar{\mathbf{a}}_2$.

The previous workings have indicated that, with hardening (or softening), while it may be possible to use a yield function in the form of (14.205), there are potential pitfalls. Consequently, in the following, we will use f_1 from (14.202) although the subscript 1 will now be dropped.

We will concentrate on a simple form of softening with an assumed uniaxial stress–strain curve of the form of Figure 14.17. (With a view to minimising the mesh dependency, the degree of softening could be related to the fracture energy via the 'size' of the element or Gauss point—see Section 14.11.1.) We will therefore consider the situation whereby σ_o is σ_t, the tensile strength which softens to zero from $\bar{\sigma}_t$. In relation to Figure 14.17, we can write:

$$\varepsilon_m < \varepsilon < \varepsilon_1$$

$$\sigma_o = \bar{\sigma}_t\frac{(\varepsilon_m - \varepsilon)}{(\varepsilon_m - \varepsilon_1)} = \bar{\sigma}_t\frac{\varepsilon_m}{(\varepsilon_m - \varepsilon_1)} - \bar{\sigma}_t\frac{\varepsilon_{ps}}{(\varepsilon_m - \varepsilon_1)} - \sigma_o\frac{\varepsilon_1}{(\varepsilon_m - \varepsilon_1)} = \bar{\sigma}_t\frac{(\varepsilon_m - \varepsilon_{ps})}{\varepsilon_m} \tag{14.218}$$

so that

$$\frac{\partial \sigma_o}{\partial \varepsilon_{ps}} = -\frac{\bar{\sigma}_t}{\varepsilon_m} = \mathrm{H}' \tag{14.219}$$

We now require the relationship between the 'equivalent plastic strain rate', $\dot{\varepsilon}_{ps}$ and the 'plastic strain rate multiplier', $\dot{\lambda}$. To this end we equate the work rate (see Section 6.4.2)

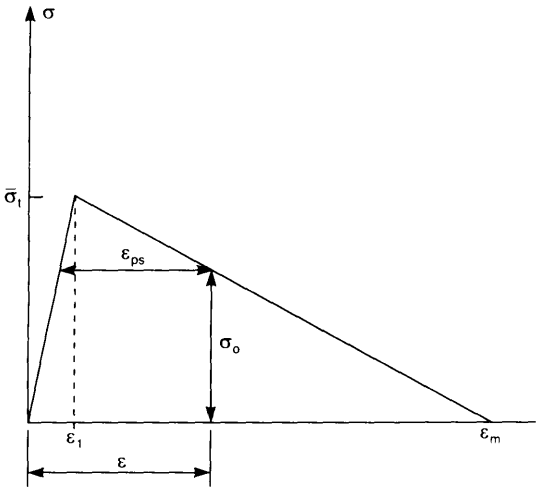

Figure 14.17 Simple softening stress–strain relationship.

so that:

$$\dot{W} = \boldsymbol{\sigma}^T \dot{\boldsymbol{\varepsilon}}_p = \dot{\lambda}(\mathbf{a}^T \boldsymbol{\sigma}) = \sigma_o \dot{\varepsilon}_{ps} \tag{14.220}$$

and using a from (14.210) and $f = 0$ from (14.202), it is easy to show that $(\mathbf{a}^T\boldsymbol{\sigma}) = \sigma_o$ and $\dot{\varepsilon}_{ps} = \dot{\lambda}$ and using the notation of Chapter 6, we now have $A' = H'$.

It is possible to use eigenvalue expansions, even when adopting a yield function in the form of f_1 from (14.202) [F1, F2]. However, the equations get rather complex and, as an alternative, we will here outline the use of a similar procedure to that originally described in Section 6.6.1. We start by defining the following equations which must be satisfied:

$$\mathbf{r} = \boldsymbol{\sigma}_C - (\boldsymbol{\sigma}_B - \Delta\lambda \mathbf{C}\mathbf{a}_C) = \boldsymbol{\sigma}_C - \left(\boldsymbol{\sigma}_B - \Delta\lambda C\left(\frac{1}{2\sigma_{eC}}\bar{\mathbf{P}}\boldsymbol{\sigma}_C + \frac{1}{2}\boldsymbol{\pi}\right)\right) = 0 \tag{14.221}$$

$$s = \sigma_{oC} - f(\varepsilon_{psold} + \Delta\lambda A'_C) = 0 \tag{14.222}$$

$$f = (\tfrac{1}{2}\boldsymbol{\sigma}_C^T \bar{\mathbf{P}} \boldsymbol{\sigma}_C)^{1/2} + \tfrac{1}{2}\boldsymbol{\pi}^T \boldsymbol{\sigma}_C - \sigma_{oC} = \sigma_{e1C} + \sigma_{e2C} - \sigma_{oC} = 0 \tag{14.223}$$

In (14.222), $f(\varepsilon_{psold} + \Delta\lambda A'_C)$ is the stress obtained from the adopted unixial stress–strain relationship (i.e. Figure 14.17).

With a view to iteratively improving an initial solution to the above we can apply truncated Taylor expansions so that:

$$\mathbf{r}_{new} = \mathbf{r}_{old} + \left[\mathbf{I} + \Delta\lambda \mathbf{C} \left.\frac{\partial \mathbf{a}}{\partial \boldsymbol{\sigma}}\right|_C\right] \dot{\boldsymbol{\sigma}}_C + \dot{\lambda}\mathbf{C}\mathbf{a}_C = \mathbf{r}_{old} + \mathbf{Q}\dot{\sigma}_C + \dot{\lambda}\mathbf{C}\mathbf{a}_C \tag{14.224}$$

$$s_{new} = s_{old} + \dot{\sigma}_{oC} + A'_C \dot{\lambda} \tag{14.225}$$

$$f_{new} = f_{old} + \mathbf{a}_C^T \dot{\boldsymbol{\sigma}}_C + \dot{\sigma}_{oC} \tag{14.226}$$

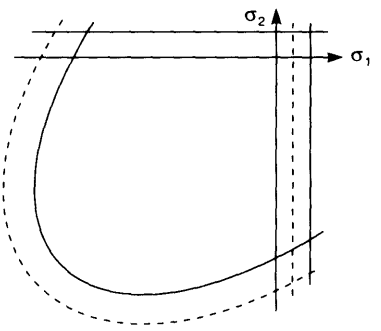

Figure 14.18 Combined yield criteria for concrete.

Setting $\mathbf{r}_{new}$ to zero, we obtain:

$$\dot{\boldsymbol{\sigma}}_C = -\mathbf{Q}^{-1}\mathbf{r}_{old} - \dot{\lambda}\mathbf{Q}^{-1}\mathbf{C}\mathbf{a}_C \tag{14.227}$$

Substitution from (14.227) and (14.225) (with $s_{new} = 0$) into (14.226) (with $f_{new} = 0$) leads to the relationship:

$$\dot{\lambda} = \frac{f_{old} - \mathbf{a}^T\mathbf{Q}^{-1}\mathbf{r} - s_{old}}{\mathbf{a}^T\mathbf{Q}^{-1}\mathbf{C}\bar{\mathbf{a}} + A'} \tag{14.228}$$

which allows $\Delta\lambda$ to be updated while substitution for $\dot{\lambda}$ into (14.225) (with $s_{new} = 0$) allows σ_{oC} to be updated.

So far we have only considered the tensile behaviour. We could also apply the 'square yield criterion' to the compressive behaviour (Figures 14.15 and 14.16) and introduce a hardening/softening relationship. In these circumstances, in place of (14.202), we would have:

$$f_1 = -(\tfrac{1}{2}\boldsymbol{\sigma}^T\bar{\mathbf{P}}\boldsymbol{\sigma})^{1/2} + \tfrac{1}{2}\boldsymbol{\pi}^T\boldsymbol{\sigma} - \sigma_o = -\sigma_{e1} + \sigma_{e2} - \sigma_o = 0 \tag{14.229}$$

where σ_o would now be σ_c, the compressive yield strength. Special difficulties would relate to the 'corner regions', such as A in Figure 14.15. In these regions, one should apply a procedure similar to those discussed in Sections 14.3–14.5 which involve a 'two-vectored return'. There are, of course, added complexities if both of the separate yield criteria are hardening or softening [F2]. Care must also be taken, in relation to the 'corners' such as B in Figure 14.15 [F2].

One need not be restricted to a square form of yield criterion in the compressive regime. Instead one could use a von Mises criterion [F1, F2] or a form of Drucker–Prager criterion [C11]. The latter (from [C11]) is depicted in Figure 14.18.

14.12 DAMAGE MECHANICS

The concept of damage as a 'load-bearing area reduction' was apparently first introduced by Kachanov [K1]. Since then, the terminology 'damage mechanics' has been used in many different ways but the main theme is a reduction in the secant

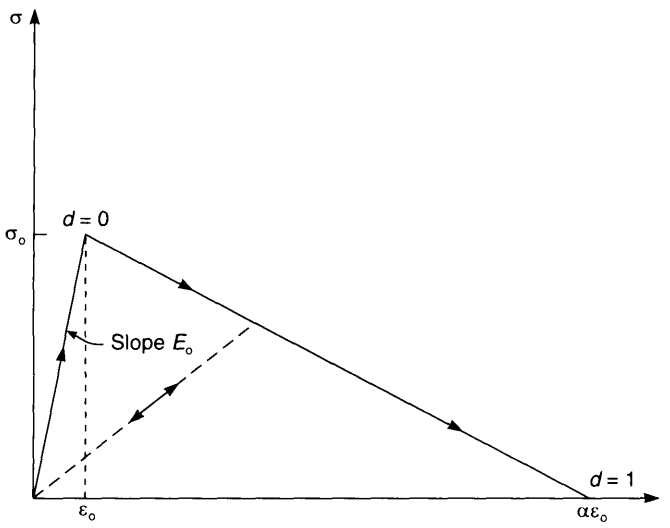

Figure 14.19 Simple tensile damaging relationship.

stiffness, as originally discussed in Section 14.11.1. Important work in the area has been given in the book by Lemaitre and Chaboche [L3] and in papers by Simo and Ju [S6], Mazars and Lemaitre [M3], Ladeveze *et al.* [L1] and Carol *et al.* [C1] among many others. In the following, we will give a brief outline and will concentrate on the simplest, 'scalar damage'. We will start with the one-dimensional, softening model that was introduced in Section 14.11.1 in Figure 14.13a which is reproduced here as Figure 14.19 using slightly different notation. It is assumed that the relationships in this figure are measured stress–strain relationships with the unloading taking the simple form which returns through the origin. (The link with fracture mechanics will be discussed later.)

We will start with the relationships defined in (14.184) and (14.185) so that we can write:

$$\sigma = (1-d)E_o\varepsilon = (1-d)\bar{\sigma} \tag{14.230}$$

where

$$d = \frac{\alpha}{\alpha-1}\left(1-\frac{\varepsilon_o}{\varepsilon}\right) = \frac{\alpha}{\alpha-1}\left(1-\frac{\tau_o}{\tau}\right) \qquad \alpha\varepsilon_o > \varepsilon > \varepsilon_o \tag{14.231}$$

and we have introduced an auxiliary parameter, τ, which will now be related to the energy of the undamaged material so that:

$$\tau = g(\varepsilon) = (\tfrac{1}{2}E_o\varepsilon^2)^{1/2} = \left(\frac{1}{2E_o}\bar{\sigma}^2\right)^{1/2} = \sqrt{\frac{E_o}{2}}\varepsilon \tag{14.232}$$

In fact, for the present simple model, there is no need to introduce this energy term, although it will be useful for later extension

We will also introduce a 'damage function':

$$f = \tau - \max\{\tau_{old}, \tau_o\} \leqslant 0 \tag{14.233a}$$

$$f = \varepsilon - \max\{\varepsilon_{old}, \varepsilon_o\} \leqslant 0 \tag{14.233b}$$

where in (14.233b) we have introduced the straightforward form without the auxiliary energy term. With $\varepsilon < \varepsilon_o$ (here, the subscript o does not mean 'old'), there is no damage and $f < 0$. Once $\varepsilon > \varepsilon_o$, the material damages until at $\varepsilon \geqslant \alpha\varepsilon_o$, it is fully damaged and $d = 1$.

From (14.230) and (14.231), we can write:

$$\dot{\sigma} = (1 - d)E_o\dot{\varepsilon} - \dot{d}E_o\varepsilon \tag{14.234}$$

with

$$\dot{d} = \frac{\mathrm{d}d}{d\varepsilon}\dot{\varepsilon} = \frac{\alpha}{\alpha - 1}\frac{\varepsilon_o}{\varepsilon^2}\dot{\varepsilon} = \tag{14.235a}$$

$$\dot{d} = \frac{\alpha}{\alpha - 1}\frac{\tau_o}{\tau^2}\frac{\mathrm{d}\tau}{\mathrm{d}\varepsilon} \qquad \dot{\varepsilon} = \frac{\alpha}{\alpha - 1}\frac{\tau_o}{\tau^2}\sqrt{\frac{E_o}{2}}\dot{\varepsilon} \tag{14.235b}$$

so that

$$\dot{\sigma} = (1 - d)E_o\dot{\varepsilon} - \frac{\alpha}{\alpha - 1}\frac{\varepsilon_o}{\varepsilon}E_o\dot{\varepsilon} = \frac{1}{1 - \alpha}E_o\dot{\varepsilon} = E_t\dot{\varepsilon} \tag{14.236a}$$

or

$$\dot{\sigma} = (1 - d)E_o\dot{\varepsilon} - \frac{\alpha}{\alpha - 1}\frac{\tau_0}{\tau^2}\sqrt{\frac{E_o}{2}}E_o\dot{\varepsilon} = E_t\dot{\varepsilon} \tag{14.236b}$$

where E_t is the tangent modulus. Having set $\tau_{old} = \varepsilon_{old} = d_{old} = 0$, an algorithm for updating the stresses and damage and producing the tangent modulus, E_t, could then be written as

$$\sigma = (1 - d_{old})E_o\varepsilon; \qquad E_t = (1 - d)E_o$$

$$\tau = \sqrt{\frac{E_o}{2}}\varepsilon$$

$$f = \tau - \max(\tau_{old}, \tau_o) \qquad (\text{or } f = \varepsilon - \max(\varepsilon_{old}, \varepsilon_o))$$

If $f \geqslant 0$,

$$\tau_{old} = \tau \qquad (\text{or } \varepsilon_{old} = \varepsilon) \qquad (\text{so that } f \text{ now} = 0)$$

$$d = \frac{\alpha}{\alpha - 1}\left(1 - \frac{\tau_o}{\tau}\right) \qquad \left(\text{or } d = \frac{\alpha}{\alpha - 1}\left(1 - \frac{\varepsilon_o}{\varepsilon}\right)\right)$$

$$d_{old} = d$$

$$\sigma = (1 - d)E_o\varepsilon$$

$$E_t = (1 - d)E_o - \frac{\alpha}{\alpha - 1}\frac{\tau_o}{\tau^2}\sqrt{\frac{E_o}{2}}E_o \qquad \left(\text{or } E_t = \frac{1}{1 - \alpha}E_o\right)$$

Algorithm 14.1 One dimensional scalar damage.

In the above, we have not considered the case where $\varepsilon > \alpha\varepsilon_o$, but this is easily included.

We will now directly generalise the concepts in the following algorithm.

$$\boldsymbol{\sigma} = (1 - d_{\text{old}})\mathbf{C}_o\boldsymbol{\varepsilon} = (1 - d_{\text{old}})\bar{\boldsymbol{\sigma}}; \quad \mathbf{C}_t = (1 - d)\mathbf{C}_o \tag{14.237}$$

$$\tau = (\tfrac{1}{2}\boldsymbol{\varepsilon}^T\mathbf{C}_o\boldsymbol{\varepsilon})^{1/2} = (\tfrac{1}{2}\bar{\boldsymbol{\sigma}}^T\mathbf{C}_o^{-1}\bar{\boldsymbol{\sigma}})^{1/2} \tag{14.238}$$

$$f = \tau - \max(\tau_{\text{old}}, \tau_o)$$

If $f \geqslant 0$,

$$\tau_{\text{old}} = \tau \text{ (so that } f \text{ now} = 0)$$

$$d = g(\tau, \tau_o)$$

$$d_{\text{old}} = d$$

$$\boldsymbol{\sigma} = (1 - d)\mathbf{C}_o\boldsymbol{\varepsilon}$$

$$\mathbf{C}_t = (1 - d)\mathbf{C}_o - \frac{1}{\tau}\frac{dg}{d\tau}\Big(\mathbf{C}_o\boldsymbol{\varepsilon}\Big)\Big(\mathbf{C}_o\boldsymbol{\varepsilon}\Big)^T = (1 - d)\mathbf{C}_o - \frac{1}{\tau}\frac{dg}{d\tau}\bar{\boldsymbol{\sigma}}\bar{\boldsymbol{\sigma}}^T \tag{14.239}$$

Algorithm 14.2 Multidimensional scalar damage.

In deriving the tangential modular matrix, $\mathbf{C}_t$, in (14.239), we have used the relationship:

$$\dot{d} = \frac{dg}{d\tau}\dot{\tau} = \frac{1}{\tau}\frac{dg}{d\tau}\boldsymbol{\varepsilon}^T\mathbf{C}_o\dot{\boldsymbol{\varepsilon}} \tag{14.240}$$

In Algorithm 14.2, the precise form of the 'damage relationship' between d and τ has been undefined. Clearly, it should be related to experiments. Cervera *et al.* [C2] use:

$$d = 1 - \frac{\tau_o}{\tau}\exp\left(A\left(1 - \frac{\tau}{\tau_o}\right)\right) \tag{14.241}$$

in place of (14.231) for the tensile behaviour of concrete. The constant A is chosen to make the area under the stress–strain curve equal to the fracture energy. The concept is similar to the approach discussed in Section 14.11.1 whereby the parameter α in (14.231) is related to the critical fracture energy via (14.183). As discussed earlier, some length parameter (related to the element of Gauss point) is also required.

Clearly, one cannot directly use (14.231) or (14.241) in conjunction with Algorithm 14.2, because the complete material would then degrade in this 'tensile softening manner'. One solution, is to introduce two damage parameters, d^+ for the tensile behaviour (say from (14.231) or (14.241)) and d^- for the compressive behaviour (see [C2]). In fact this is effectively the approach adopted by the author in the 'rotating crack model' [C12] (see Section 14.11.2) where in relation to the tensile behaviour, Algorithm 14.1 was effectively applied in relation to the continuously rotating principal tensile strain direction. For the compressive response, a different relationship was used for the stress in the direction of the principal compressive strain [C12]. Cervera *et al.* [C2] (who apply a three-dimensional model), split the 'effective stress', $\bar{\boldsymbol{\sigma}}$ (see (14.237)) into

$$\bar{\boldsymbol{\sigma}}^+ = \langle\bar{\boldsymbol{\sigma}}\rangle = \sum_{i=1}^{3}\langle\bar{\sigma}_i\rangle\mathbf{a}_i\mathbf{a}_i^T \tag{14.242a}$$

and

$$\boldsymbol{\sigma}^- = \rangle \bar{\sigma} \langle = \sum_{i=1}^{3} \rangle \bar{\sigma}_i \langle \mathbf{a}_i \mathbf{a}_i^{\mathrm{T}} \tag{14.242b}$$

where $\langle \bar{\sigma}_i \rangle$ is $\bar{\sigma}_i$ if the latter is tensile or zero otherwise. Also $\mathbf{a}_i$ define the (unit) principal directions of $\bar{\boldsymbol{\sigma}}$ (or assuming an isotropic $\mathbf{C}_0$, of $\boldsymbol{\varepsilon}$). The symbols $\rangle \langle$ in (14.242b) are such that $\langle x \rangle + \rangle x \langle = x$. Cervera *et al.* [C2] then degrade the stresses via:

$$\boldsymbol{\sigma} = (1 - d^+)\bar{\boldsymbol{\sigma}}^+ + (1 - d^-)\bar{\boldsymbol{\sigma}}^- \tag{14.243}$$

where d^+ was defined in (14.241) and an alternative relationship was used for the 'compressive damage', d^-.

Clearly, the latter model is closely related to the earlier 'rotating crack model' and, as with the latter, account must be taken of the changes in the principal directions in defining the tangent modular matrix (as it is with hyperelasticity—see Chapter 13).

14.13 SPECIAL NOTATION

$\mathbf{a} = \partial f / \partial \boldsymbol{\sigma}$ (flow vector) which is defined as a column vector
$\mathbf{a}_1 - \mathbf{a}_3$ = vectors from $\mathbf{a}$ (see (14.19))
α = pseudo-hardening parameter in Section 14.4 (see (14.50))
$\alpha_{12}, \alpha_{23}, \alpha_{31}, \alpha_{44}, \alpha_{55}, \alpha_{66}$ = constants for Hill's yield criterion (Section 14.6.1) or for Hoffman yield criterion (see Section 14.8)
$\alpha_{11}, \alpha_{22}, \alpha_{33}$ = constants for Hoffman yield criterion (Section 14.8)
$\mathbf{b} = \partial g / \partial \boldsymbol{\sigma}$ (flow vector) which is defined as a column vector
$\mathbf{b}' = \partial Q / \partial \boldsymbol{\sigma}$ (flow vector) which is defined as a column vector
A = constant for use with Hill's yield function (see (14.100))
A' = hardening parameter
$A(\theta)$ = function of θ (see (14.12))
$\mathbf{A}$ = special matrix within $\partial \mathbf{a} / \partial \boldsymbol{\sigma}$ (see (14.55))
$\mathbf{A} = \mathbf{C}^{-1}$ in Section 14.10
B = constant for use with Hill's yield function (see 14.104))
$\mathbf{B}$ = special matrix (see (14.136))
c = cohesion
C_1, C_2, C_3 = constants for flow vector (see 14.19))
$C_{22}, C_{23}, C_{32}, C_{33}$ = constants for $\partial \mathbf{a} / \partial \boldsymbol{\sigma}$ (see (14.23))
$\mathbf{C}$ = constitutive matrix
$\mathbf{C}_t$ = tangential constitutive tensor (or matrix)
$\mathbf{C}_{tc}$ = consistent tangential constitutive tensor (or matrix)
D = matrial constant for Drucker–Prager yield function
$E' = E/(1 + \nu)(1 - 2\nu)$
f = yield function, f_2 = yield function in 'squared form'
f_h = particular form of Hill's yield function (see (14.88))
F, H, H, L, M, N = constants for Hill's yield criterion (Section 14.6.1)
g = second yield function when two functions are active
I_1 = first stress invariant

J_2 = second stress deviator invariant
J_3 = third stress deviator invariant
K = constant in Section 14.7 (see (14.139b)
M = bending moment (stress resultant)
$\bar{M}$ = quadratic stress intensity with M's
M_o = yield moment M
m = non-dimensional bending moment (see (14.39)
N = axial force (stress resultant)
$\bar{N}$ = quadratic stress intensity with N's
n = non-dimensional axial force (see (14.38))
N_o = yield value of N
P = quadratic stress intensity with N's and M's
Q_t, Q_m, Q_{tm} = non-dimensional quadratic stress intensities (see 14.47)
$\mathbf{P}$ = matrix for yield function in quadratic form (see (14.91))
$\mathbf{p}$ = vector for pressure contributions with yield function in (14.156)
Q = plastic potential
$\mathbf{Q}$ = special matrix (see (14.29))
$\mathbf{r}$ = residual vector (see (14.27))
R = Lankford anisotropy coefficient in Section 14.6.3
$\mathbf{R}$ = special matrix (see (14.32))
s = constant for stress resultant yield criteria (± 1 – see (14.43) and (14.52))
s = $\sin \varphi$ in Section 14.5
$\mathbf{s}$ = devitoric stresses
t = thickness
$\mathbf{T}$ = special matrix (see (14.83))
$\dot{W}_p$ = plastic work rate
$\dot{\chi}_p$ = plastic curvature rates
χ_{ps} = equivalent plastic curvature
$\dot{\varepsilon}_{ps}$ = equivalent plastic strain rate
$\boldsymbol{\varepsilon}$ = vector or tensor of strains
$\dot{\boldsymbol{\varepsilon}}$ = strain rate
$\dot{\boldsymbol{\varepsilon}}_t$ = total strain rate (the subscript t is often dropped)
$\dot{\boldsymbol{\varepsilon}}_p$ = plastic strain rate
$\dot{\lambda}$ or $\Delta\lambda$ = plastic strain rate multiplier
$\dot{\eta}$ or $\Delta\eta$ = plastic strain rate multiplier for second yield function, g
$\dot{\lambda}_2$ or $\Delta\lambda_2$ = plastic strain rate multiplier for yield function in squared form
τ_{xy}, etc. = shear stress
μ = shear modulus
μ_i = eigenvalue in Section 14.10
σ_e = effective stress
σ_o = yield stress
σ_m = mean stress
$\boldsymbol{\sigma}$ = stress (as vector or tensor)
$\dot{\boldsymbol{\sigma}}$ = stress rate

θ = angle (see (14.6))
φ = angle of friction
$\boldsymbol{\varphi}_i$ = eigenvector in Section 14.10

14.14 REFERENCES

[A1] ASCE, *Finite Element Analysis of Reinforced Concrete; State of the Art Report*, Struct. Div. Committee on Conc. & Masonry Structures, ASCE, New York (1982).

[B1] Bazant, Z. P., Instability, ductility and size-effect in strain-softening concrete, ASCE, *J. Eng. Mech.*, **102**, 331–344 (1976).

[B2] Bazant, Z. P. & Cedolin, L., *Stability of Structures*, Oxford University Press, 1991.

[B3] Bicanic, N., Pearce, C. J. & Owen, D. R. J., Failure predictions of concrete like materials using a softening Hoffman plasticity model, *Computational Modelling of Concrete Structures*, ed. H. Mang *et al.*, Cromwell Press, Melksham, pp. 199–208 (1994).

[C1] Carol, I., Rizzi, E. & Willam, K., Towards a general formulation of elastic degradation and damage based on a loading surface, *Computational Modelling of Concrete Structures*, ed. H. Mang *et al.*, Cromwell Press, Melksham, pp. 199–208 (1994).

[C2] Cervera, M., Oliver, J. & Galindo, M., Seismic evaluation of concrete dams using continuum damage models, *Computational Modelling of Concrete Structures*, ed. H. Mang *et al.*, Cromwell Press, Melksham, pp. 629–638 (1994).

[C3] Crisfield, M. A., Plasticity computations using the Mohr Coulomb yield criterion, *Engineering Computations*, 4, 300–308 (1987).

[C4] Crisfield, M. A., Consistent schemes for plasticity computation with the Newton Raphson method, *Computational Plasticity: Models, Software & Applications*, ed. D. R. J. Owen *et al.*, Part 1, Pineridge Press, Swansea, pp. 133–159 (1987).

[C5] Crisfield, M. A., *Large-deflection Elasto-plastic Buckling Analysis of Plates Using Finite Elements*, Transport & Road Res. Lab. Report LR 593, Crowthorne, Berks., England (1973).

[C6] Crisfield M. A. *Some Approximations in the Non-linear Analysis of Rectangular Plates Using Finite Elements*, Transport & Road Res. Lab. Report SR 51UC, Crowthorne, Berks., England (1974).

[C7] Crisfield, M. A., *Ivanov's Yield Criterion for Thin Plates and Shells Using Finite Elements*, Transport & Road Res. Lab. Report LR 919, Crowthorne, Berks., England (1979).

[C8] Crisfield, M. A., *On an Approximate Yield Criterion for Thin Steel Shells*, Transport & Road Res. Lab. Report LR 658, Crowthorne, Berks., England (1974).

[C9] Crisfield, M. A. & Peng, X., Efficient nonlinear shell formulations with large rotations and plasticity, *Computational Plasticity: Models, Software & Applications*, ed. D. R. J. Owen *et al.*, Part 1, Pineridge Press, Swansea, pp. 1979–1997 (1992).

[C10] Crisfield, M. A., Local instabilities in the non-linear analysis of reinforced concrete beams and slabs, *Proc. Instn. Civ. Engrs.*, Part 2, **73**, 135–145 (1982).

[C11] Crisfield, M. A., Difficulties with current numerical models for reinforced concrete and some tentative solutions, *Computer Aided Analysis and Design of Concrete Structures*, ed. F. Damjanic *et al.*, Pineridge Press, Swansea, pp. 331–358 (1984).

[C12] Crisfield, M. A. & Wills, J., Analysis of R/C panels using different concrete models, *J. Eng. Mech. Div., ASCE*, 578–597, (1989).

[C13] Crisfied, M. A. & Hellweg, H.-B., Some recent work with reinforced concrete and other composite materials *FEMSA 95*, ed. D. Langksch, Univ. of Cape Town Printing Dept., Vol. 1, pp 106–122 (1995)

[C14] Cope, R. J., Rao, P. V., Clark, L. A. & Norris, P., Modelling of reinforced concrete behaviour for finite element analysis of slabs, ed. C. Taylor *et al.*, Pineridge Press, Swansea, Vol. 1, pp. 457–470 (1980).

[C14] Corigliano, A., Formulation, identification and use of interface models in the numerical analysis of composite delamination, *Int. J. Solids & Structs.*, **30**, 2779–2811 (1993).

[C15] Coulomb, C. A., Essai sur une application de règles de maximis et minimis à quelques problèmes de statiques relatifs à l'architecture, *Mem. de Math. et de Phys. Pres à l'Acad. Roy. des Sci. par divers savants*, **7**, 343 (1773).

[D1] De Borst, R., Pankaj & Bicanic, N., A note on singularity indicators for Mohr–Coulomb type yield criteria, *Comp. & Struct.*, **39**, 219–220 (1991).

[D2] De Borst, R., Integration of plasticity equations for singular yield functions, *Comp. & Struct.* **26**, 823–829 (1987).

[D3] De Borst, R. & Feenstra, P. H., Studies in anisotropic plasticity with reference to the Hill criterion, *Int. J. for Num. Meth. in Engng.*, **29**, 315–336 (1990).

[D4] de Borst, R. & Nauta, P., Non-orthogonal cracks in a smeared finite element model, *Engineering Computations*, **2**, 35–46 (1985).

[D5] de Borst, R. & Mulhaus, Gradient dependant plasticity: formulation and algorithmic aspects, *Int. J. for Num. Meth. in Engng.*, **35**, 521–539.

[D6] Drucker, D.C. & Prager, W., Soil mechanics and plastic analysis or limit design, *Quart. Appl. Math.*, **10**, 157–165 (1952).

[D7] Duffett, G., Jelenic, G. & Lyons, P., A study of the material models in LUSAS for the analysis of geotechnical materials, *Computational Plasticity: Models, Software & Applications*, ed. D. R. J. Owen *et al.*, Part 2, Pineridge Press, Swansea, pp. 1737–1749 (1995).

[E1] Evans, R. H. & Marathe, M. S., Microcracking and stress–strain curves for concrete in tension, *Materiaux et Constructions*, **1**, 61–64 (1968).

[F1] Feenstra, P. H., de Borst, R. & Rots, J. G., An energy-based model for concrete, *Comput. Models of Concrete Structures*, ed. H. Mang *et al.*, Cromwell Press, Melksham, pp. 83–92 (1994).

[F2] Feenstra, P. H., Computational aspects of biaxial stress in plain and reinforced concrete, PhD. dissertation, Delft Univ., The Netherlands (1993).

[G1] Gurson A. L., Continuum theory of ductile fracture void nucleation and growth: Part 1—yield criteria and flow rules for porous ductile materials, *J. Eng. Mat. Tech.*, **99**, 2–15 (1977).

[H1] Hill, R., *The Mathematical Theory of Plasticity*, Oxford University Press (1950).

[H2] Hill, R., A theory of the yielding and plastic flow of anisotropic materials, *Proc. Roy. Soc.*, **A193**, 281–297 (1947).

[H3] Hilleborg, A., Modeer, M. & Petersson, P. E., Analysis of crack formation and growth in concrete by means of fracture mechanics and finite elements, *Cement and Concrete Res.*, **6**, 773–782 (1976).

[H4] Hoffman, O., The brittle strength of orthotropic materials, *J. Comp. Mater.*, **1**, 200–206 (1967).

[I1] Ilyushin, A. A., *Plasticité*, Editions Eyrolles, Paris (1956).

[I2] Ivanov, G. V., *Inzhenernyi Zhurnal Mekhanika Tverdogo Tela*, **6**, 74–75 (1967).

[K1] Kachanov, L. M., Time rupture under creep conditions, *Izv., A. Rad. Nauk. SSSR otd Tekh. Nauk.*, **8**, 26–31 (1958).

[K2] Key, S. W., *HONDO—a Finite Element Computer Program for the Large Deformation Dynamic Response of Axisymmetric Solids*, Sandia Nat. Labs., Albuquerque, USA, Report 74-0039 (1974).

[K3] Klisinski, M, Runesson, K & Sture, S., Finite elements with inner softening band, *J. of Eng. Mech.*, **3**, 575–587 (1991).

[K4] Koiter, W. T., Stress strain relations, uniqueness and variational theorems for elastic-plastic materials with a singular yield surface, *Quarterly of Appl. Math.*, **11**, 350 354 (1953).

[L1] Ladeveze, P., Gasser, A. & Allix, O., Damage mechanisms modelling for ceramic composites, *J. of Engineering Mat. & Tech.*, **116**, 331 336 (1994).

[L2] Lankford, W. T., Loww, R. J. & Gensamer, M., *Trans. Am. Inst. Min. Met. Eng.*, **171**, 574, (1947).

[L3] Lemaitre, J. & Chaboche, J.-L., *Mechanics of Solid Materials*, Cambridge Univ. Press, Cambridge (1990).

[L4] Lubliner, J., *Plasticity Theory*, Macmillan, New York (1990).

[L5] Larsson, R. & Runesson, K., Element-embedded localisation band based on regularised displacement discontinuity, *Proc. ASCE, J. of Eng. Mech. Div.*, **122**, 402 411 (1996).

[M1] Marques, J. M. M. C., Stress computations in elastoplasticity, *Eng. Comp.*, **1**, 42 51 (1984).

[M2] Matthies, H. G., A decomposition method for integration of the elastic plastic rate problem, *Int. J. for Num. Meth. in Engng.*, **28**, 1 11 (1989).

[M3] Mazars, J. & Lemaitre, J., Application of continuous damage mechanics to strain and fracture behaviour of concrete, *Application of Fracture Mech. to Cementitious Composites, NATO Adv. Res. Workshop*, ed. S. P. Shah., Northwestern Univ., Evanston, Illinous, pp. 375 378 (1984).

[M4] Mohr, O., Welche Umstande Bedingen die Elastizitatsgrenze und den Bruch Eines Materials, *Z. Veriens Dtsch. Ing.*, **44**, 1525 1572 (1900).

[N1] Nayak, G. C. & Zinekiewicz, O. C., Elastoplastic stress analysis: a generalisation for various constitutive laws including strain softening, *Int. J. for Num. Meth. in Engng.*, **5**, 113 135 (1972).

[N2] Neilson, M. P., Yield conditions for reinforced concrete shells in the membrane state, in Non-classical shell problems, *Proc. IASS Symp.*, North-Holland, Amsterdam, pp. 1030 1040 (1963).

[O1] Oliver, J. & Simo, J. C., Modelling strong discontinuities by means of strain softening constitutive equations, in: *Comput. Models of Concrete Structures*, ed. H. Mang *et al.*, Cromwell Press, Melksham, pp. 363 372 (1994).

[O2] Owen, D. R. J. & Hinton, E., *Finite Elements in Plasticity Theory and Practice*, Pineridge Press, Swansea (1980).

[O3] Owen, D. R. J., Marques, J. M. M. C. & Cesae de Sa, J. M. A., Reliability considerations in the numerical solution of elasto-plastic, visco-plastic and flow problems, *Reliability of Methods for Engineering Analysis*, ed. K.-J. Bathe & D. R. J. Owen, Pineridge Press, Swansea, pp. 221 254 (1986).

[O4] Owen, D. R. J. & Figueras, J. A., Anisotropic elasto-plastic finite element analysis of thick and thin plates and shells, **19**, 541 566 (1983).

[P1] Pankaj & Bicanic, N., On multivector stress returns in Mohr Coulomb yield functions, *Proc. 2nd Int. Conf. Computational Plasticity: Models, Software & Applications*, ed. D. R. J. Owen *et al.*, Part 1, pp. 421 436, Pineridge Press, Swansea (1989).

[P2] Petersson, P. E., *Crack Growth and Development of Fracture Zones in Plain Concrete and Similar Materials*, Report TVBM-1006, Div. of Building Materials, Lund Inst. of Tech., Lund, Sweden (1981).

[P3] Pijaudier-Cabot, G. & Bazant, Z. P., Non-local damage theory, *ASCE, J. of Engng. Mech. Div.*, **113**, 1512 1533 (1987).

[P4] Pramono, E. & Willam, K., Implicit integration of composite yield surfaces with corners, *Engng. Comp.*, **6**, 186 197 (1989).

[R1] Raghava, R., Caddekk, R. M. & Yeh, G. S. Y., The macroscopic yield behaviour of polymers, *J. Material Science*, **8**, 225 232 (1973).

[R2] Resende, L. & Martin, J. B., Formulation of Drucker–Prager cap model, *Proc. ASCE, J. Engng. Mech. Div.*, **111**, 855–881 (1980).

[R3] Roscoe, K. H. & Burland, J. B., On the generalised stress strain behaviour of 'wet' clay, *Engineering Plasticity*, ed. J. Heyman & F. A. Leckie, Cambridge Univ. Press, Cambridge, (1968).

[R4] Rybicki, E. F. & Bentley, S. E. (eds), *Computational Fracture Mechanics*, ASME Special Publication (1975).

[R5] Runesson, K. & Booker, J. R., On mixed and displacement finite element methods in perfect plasticity, *Proc. 4th Int. Conf. in Australia on Finite Elements, Melbourne*, pp. 85–89 (1982).

[S1] Schellekens, J. C. J. & de Borst, R., The use of the Hoffman yield criterion in finite element analysis of anisotropic composites, *Comp. & Struct.*, **37**, 1087–1096 (1990).

[S2] Schellekens, J. C. & de Borst, R., Free edge delamination in carbon-epoxy laminates; a novel numerical/experimental approach, *Composite Structures*, **28**, 357–373 (1994).

[S3] Simo, J. C., Kennedy, J. G. & Govindee, S., Non-smooth multisurface plasticity and viscoplasticity. Loading/unloading conditions and numerical algorithms, *Int. J. for Num. Meth. in Engng.*, **26**, 2161–2186 (1988).

[S4] Simo, J. C. & Taylor, R. L., A return mapping algorithm for plane stress elastoplasticity, *Int. J. for Num. Meth. in Engng.*, **22**, 649–670 (1986).

[S5] Simo, J. C. & Hughes, T. J. R., Elastoplasticity and viscoplasticity computational aspects, Springer-Verlag, to be published.

[S6] Simo, J. C., Ju, J. W., Strain- and stress-based continuum damage models, I. Formulation, *Int. J. Solids & Structs.*, **23**, 821–840 (1987).

[S7] Sloan, S. W. & Booker, J. R., Removal of singularities in Tresca and Mohr–Coulomb yield functions, *Comm. in Appl. Num. Meth.*, **2**, 173–179 (1986).

[T1] Tvergaard, V., Influence of voids on shear band instabilities under plane strain conditions, *Int. Fract. Mech.*, **17**, 389–407 (1981).

[W1] Waszczyszyn, Z., *Computational Methods and Plasticity*, Report LR-583, Faculty of Aerospace Engineering, TU Delft, 1989.

[Z1] Zienkiewicz, O. C. & Taylor, R. L., *The Finite Element Method*, 4th edn, Vol. 2, McGraw-Hill, London (1991).

[Z2] Zienkiewicz, O. C. & Pande, G. N., Some useful forms of isotropic yield surfaces for soil and rock mechanics, *Finite Elements in Geomechanics*, ed. G. Gudehus, Wiley, Chichester, pp. 171–190 (1977).

15 More plasticity and other material non-linearity—II

15.1 INTRODUCTION

In this chapter, we will firstly extend the work of Chapter 6 of Volume 1 to include kinematic, mixed and other forms of hardening. Because the work is closely related to that of Chapter 6, we will often refer to equations in that chapter. However, for convenience, we will sometimes reproduce them here. As a conclusion to the Chapter, we will briefly consider viscoplasticity. As in Chapter 6, the present emphasis will be on backward-Euler schemes which can be used in conjunction with a consistent tangent modular matrix. Much of this work relates to papers that were referenced in Chapter 6, such as that of Simo and Taylor [S1].

Apart from a very brief introduction in Section 6.4.2, all of the work in Chapter 6 of Volume 1 related to isotropic hardening. However, for seismic problems or low-cycle fatigue, the induced cyclic loading may involve relatively small plastic strains. In these circumstances, the Bauschinger effect [B1] may be significant. Assuming a linear hardening, this effect is illustrated for a one-dimensional problem in Figure 15.1. Here, the yielding in tension has lowered the compressive strength so that:

$$(\sigma - \alpha) = \sigma_c = \pm\sigma_o \tag{15.1}$$

where α is the 'kinematic shift' of the centre of the yield surface. As a result of this shift, with σ_o being fixed (see Figure 15.1), the uniaxial strees σ 'hardens'.

The Bauschinger effect cannot be treated by the methods of Section 6.4.1 and 6.4.2 which involve 'isotropic hardening'. Consequently, Prager [P5, P6] derived a 'kinematic model' which assumed, for the von Mises yield criterion, a translation of the cylindrical yield surface (see Figure 15.2). It follows that the yield function can be written by simply replacing the stresses $\boldsymbol{\sigma}$ in the standard von Mises function by $\tilde{\boldsymbol{\sigma}} = \boldsymbol{\sigma} - \boldsymbol{\alpha}$ where the tensor $\boldsymbol{\alpha}$ defined the origin of the yield surface in its current configuration. Consequently:

$$f = \sigma_e(\boldsymbol{\sigma}) = \sigma_o(\boldsymbol{\sigma} - \boldsymbol{\alpha}) - \sigma_o = \sqrt{\tfrac{3}{2}}((\mathbf{s} - \boldsymbol{\alpha}') : (\mathbf{s} - \boldsymbol{\alpha}'))^{1/2} - \sigma_o \tag{15.2}$$

The form on the right-hand side of (15.2) relates specifically to the von Mises yield criterion with $\mathbf{s}$ as the deviatoric part of σ and $\boldsymbol{\alpha}'$ the deviatoric part of $\boldsymbol{\alpha}$ (compare (6.26)

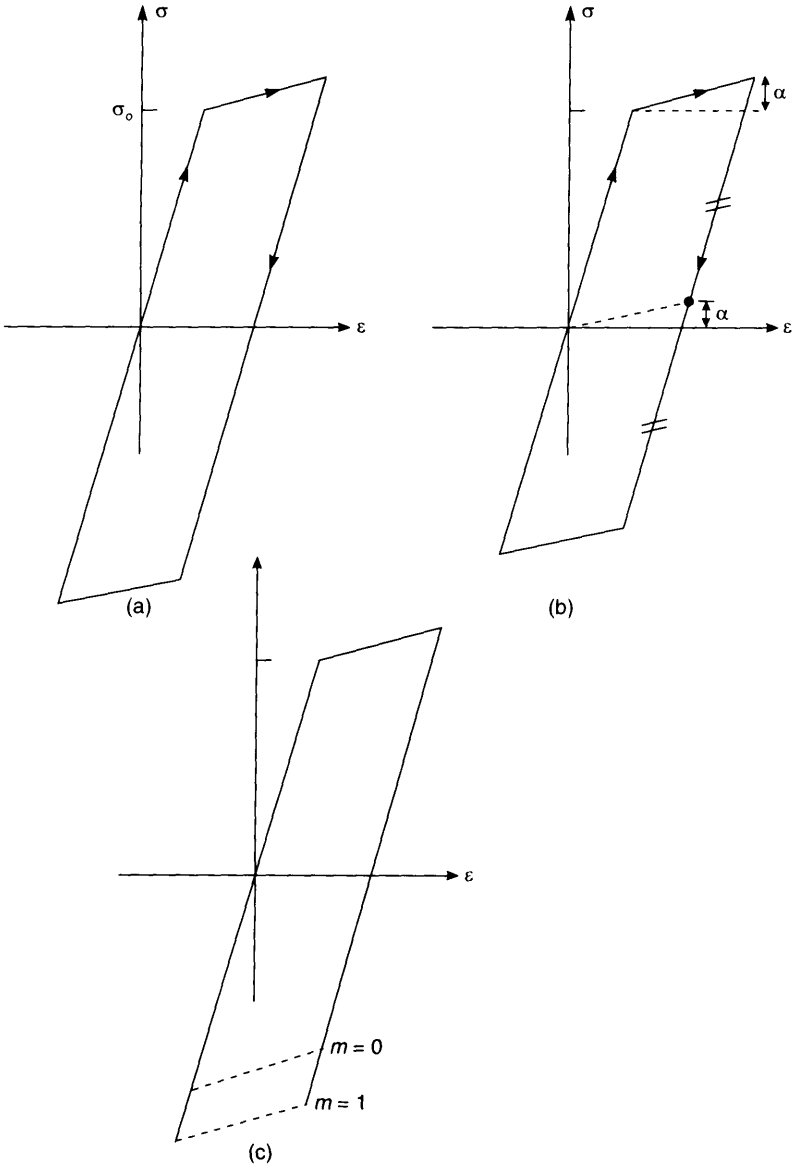

Figure 15.1 (a) Isotropic, (b) kinematic and (c) mixed hardening.

without kinematic hardening). The tensor $\boldsymbol{\alpha}$ is known as the back stresses, $\boldsymbol{\alpha}$ (and is related to the scalar α in (15.1)).

Prager assumed that the yield surface moved in the direction of the plastic strain so

$$\dot{\boldsymbol{\alpha}} = C_{\mathrm{p}}\dot{\boldsymbol{\varepsilon}}_{\mathrm{p}} = C_{\mathrm{p}}\dot{\lambda}\frac{\partial f}{\partial \boldsymbol{\sigma}} = C_{\mathrm{p}}\dot{\lambda}\mathbf{a} = C_{\mathrm{p}}\frac{3\dot{\lambda}}{2\sigma_{\mathrm{o}}}(\mathbf{s} - \boldsymbol{\alpha}') \tag{15.3a}$$

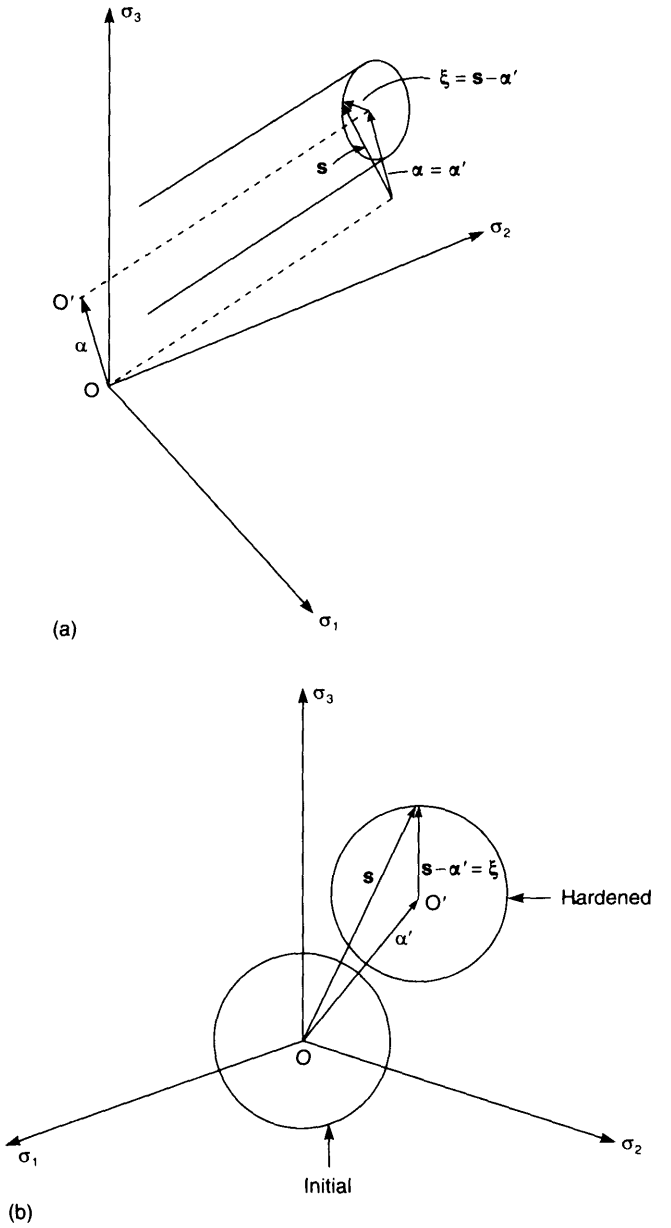

Figure 15.2 Kinematic hardening with von Mises. (a) Shifted von Mises cylinder; (b) end section.

where the final relationship applies specifically to the von Mises yield surface. In (15.3a), we have used the standard flow rule for $\dot{\boldsymbol{\varepsilon}}_p$ and have followed the convention of Chapter 6 (see 6.4), in writing $\mathbf{a} = \partial f/\partial \boldsymbol{\sigma}$. From (15.2), $\mathbf{a}$ is also equal to $-\partial f/\partial \boldsymbol{\alpha}$. Because, for the von Mises yield function, the plastic strains, $\dot{\boldsymbol{\varepsilon}}_p$ has no volumetric component, from

(15.3a), for the Prager evolution law, $\dot{\boldsymbol{\alpha}} = \dot{\boldsymbol{\alpha}}'$. Consequently, the centre of the yield surface, moves from O to O′ (Figure 15.2) with no movement in the direction of the mean stress.

The Prager model can lead to inconsistencies when working in a stress subspace such as that of plane stress [H2] unless (15.3a) is specifically reformulated for the relevant subspace. This will be illustrated in Section 15.3 for plane stress.

The inconsistencies can be avoided by adopting Ziegler's model [Z1] whereby:

$$\dot{\boldsymbol{\alpha}} = C_z \dot{\lambda}(\boldsymbol{\sigma} - \boldsymbol{\alpha}) \tag{15.3b}$$

For three-dimensional von Mises plasticity, it will be shown later in this section that the two formulations lead to the same results. However, using (15.3b) with the von Mises criterion, the centre of the yield surface will have a component of movement in the direction of the mean stress. None the less, because the yield surface is a cylinder, this does not effect the results. For the general, case, the relationship between the two formulations will become clearer following the specific application to plane stress in Section 15.3.

From (15.1), the consistency condition is

$$\dot{f} = \frac{\partial f}{\partial \boldsymbol{\sigma}} : \dot{\boldsymbol{\sigma}} + \frac{\partial f}{\partial \boldsymbol{\alpha}} : \dot{\boldsymbol{\alpha}} = 0 = \mathbf{a} : \dot{\boldsymbol{\sigma}} - \mathbf{a} : \dot{\boldsymbol{\alpha}} = 0 \tag{15.4}$$

For the von Mises yield function, the tensor $\mathbf{a} = \partial f / \partial \boldsymbol{\sigma}$ takes the same form as it does without hardening. For example, in vector form, one would simply replace the $\boldsymbol{\sigma}$ components in (6.32) with $\bar{\boldsymbol{\sigma}}$ components ($\bar{\boldsymbol{\sigma}} = \boldsymbol{\sigma} - \boldsymbol{\alpha}$). Using the Prager evolution law for $\dot{\boldsymbol{\alpha}}$, combining (15.3a) and (15.4) leads to

$$\dot{f} = \mathbf{a} : \dot{\boldsymbol{\sigma}} - C_p \dot{\lambda} \mathbf{a} : \mathbf{a} = \mathbf{a} : \dot{\boldsymbol{\sigma}} - \tfrac{3}{2} C_p \dot{\lambda} = 0 \tag{15.5a}$$

The last relationship in (15.5a) applies specifically to the von Mises yield function. (Note that, for von Mises, $\mathbf{a} : \mathbf{a} = 3/2$—see (6.34).) If we combine the Ziegler evolution law of (15.3b) with (15.4), we obtain:

$$\dot{f} = \mathbf{a} : \dot{\boldsymbol{\sigma}} - C_z \dot{\lambda} \mathbf{a} : (\boldsymbol{\sigma} - \boldsymbol{\alpha}) = \mathbf{a} : \dot{\boldsymbol{\sigma}} - C_z \dot{\lambda} \sigma_o \tag{15.5b}$$

where again the final expression relates specifically to the von Mises criterion.

In order to relate the multidimensional state to the uniaxial state, we must degenerate (15.5a) and (15.5b) to the uniaxial case. But first we must show that, for such a uniaxial case, the uniaxial plastic strain rate, say $\dot{\varepsilon}_{px}$, is equal to $\dot{\lambda}$. To this end, we can apply an identical procedure to that used for isotropic strain hardening and define the equivalent plastic strain rate, $\dot{\varepsilon}_{ps}$ via (6.29). We can then show that $\dot{\varepsilon}_{ps} = \dot{\lambda}$ (see (6.34)) and that, for the uniaxial case, $\dot{\varepsilon}_{ps} = \dot{\varepsilon}_{px}$.

We will now degenerate (15.5a) and (15.5b) to the uniaxial (say x-direction) case. Considering, first, (15,5a), we have:

$$\dot{f} = \dot{\sigma}_x - \tfrac{3}{2} C_p \dot{\lambda} = H' \dot{\varepsilon}_{px} - \tfrac{3}{2} C_p \dot{\varepsilon}_{px} = 0 \tag{15.6a}$$

where H' is the slope of the uniaxial stress/plastic–strain relationship (see (6.13) and Figure 6.5). On the other hand, from (15.5b), we have:

$$\dot{f} = \dot{\sigma}_x - C_z \dot{\lambda} \sigma_o = H' \dot{\varepsilon}_{px} - C_z \sigma_o \dot{\varepsilon}_{px} = 0 \tag{15.6b}$$

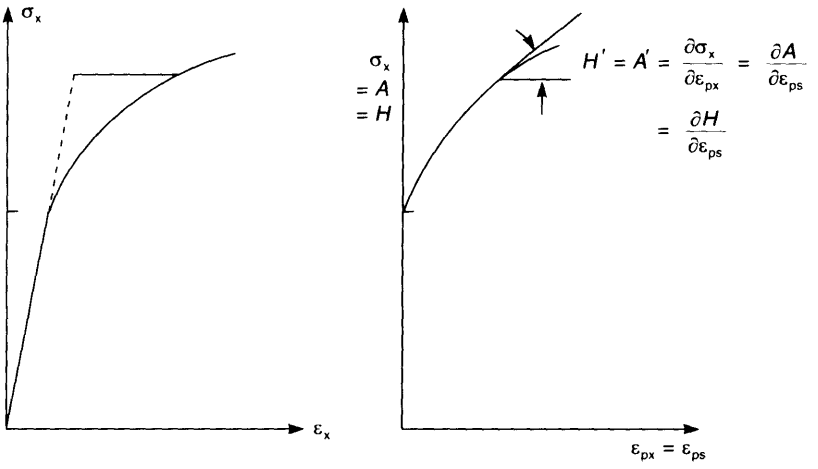

Figure 15.3 Uniaxial stress–strain relationships and 'plastic slopes' H' and A' (for von Mises). (a) Uniaxial (x-direction) stress strain relationship; (b) relationship of stress and equivalent stress with equivalent plastic strain.

It follows from (15.6a) that:

$$C_p = \tfrac{2}{3}H' \tag{15.7a}$$

On the other hand, from (15.6b), we obtain:

$$C_z = \frac{H'}{\sigma_o} \tag{15.7b}$$

Substitution from either (15.3a) (with Prager) or (15.3b) (with Ziegler) into (15.4) leads, in conjunction with (15.7a) or (15.7b) for Prager and Ziegler respectively to

$$\dot{f} = \mathbf{a}:\dot{\boldsymbol{\sigma}} - A'\dot{\lambda} = 0 \tag{15.8}$$

where

$$A'_p = C_p\mathbf{a}:\mathbf{a} = \tfrac{3}{2}C_p = H' = \frac{\partial\sigma_x}{\partial\varepsilon_{px}} \tag{15.9}$$

$$A'_z = C_z\mathbf{a}:(\boldsymbol{\sigma} - \boldsymbol{\alpha}) = C_z\sigma_e = H' = \frac{\partial\sigma_x}{\partial\varepsilon_{px}} \tag{15.10}$$

The last relationships in (15.9) and (15.10) relate specifically to the von Mises yield criterion. It follows that for the von Mises yield criterion, no difference results from the use of the different hardening rules (provided we work in the full stress and strain space—see Section 15.3).

Equation (15.8) is identical to the relationship (6.16) obtained with linear isotropic hardening. It follows that with the A' terms being given by (15.9) or (15.10), the standard tangent modular matrix (or tensor) will also be the same and will take the form of (6.18). However, in this chapter, we will be more concerned with a 'consistent tangent modular matrix' (see Section 6.7, 15.8 and 15.9) that follows on from a backward-Euler return (see Sections 6.6.6, 6.6.7 and 15.4–15.7).

In order to apply non-linear hardening, we can assume that C_p or C_z are functions of the equivalent plastic strain, ε_{ps}. Considering, the von Mises yield criterion, we can then use the uniaxial initial loading curve (Figure 15.3) of $\sigma_x = H = A$ against ε_{px} to obtain $A' = H' = \partial\sigma_x/\partial\varepsilon_{px}$ for a given value of the equivalent plastic strain, ε_{ps}. The latter equals the one-dimensional, ε_{px}, for the uniaxial initial loading curve (in the x-direction).

15.2 MIXED HARDENING

A more general hardening, which was suggested by Hodge [H2] and developed by Mroz [M1–M3] and others [A1], involves a combination of kinematic hardening, which moves the centre of the yield surface, and isotropic hardening which expands the yield surface. To introduce such a hardening, we can introduce a scalar m which represents the ratio of plastic strain associated with the isotropic response while the ratio $(1 - m)$ is left for the kinematic response. It follows that:

$$\dot{\boldsymbol{\varepsilon}}_p = \dot{\boldsymbol{\varepsilon}}_{pi} + \dot{\boldsymbol{\varepsilon}}_{pk} = m\dot{\boldsymbol{\varepsilon}}_p + (1 - m)\dot{\boldsymbol{\varepsilon}}_p \tag{15.11}$$

with the isotropic equivalent plastic strain rate being given by (see also (6.29) and (6.34)):

$$\dot{\varepsilon}_{psi} = m\dot{\varepsilon}_{ps} = m\sqrt{\tfrac{3}{2}}(\dot{\boldsymbol{\varepsilon}}_p{:}\dot{\boldsymbol{\varepsilon}}_p)^{1/2} = m\dot{\lambda} \tag{15.12}$$

With specific reference to J_2 plasticity, the yield function becomes:

$$f = \sigma_e(\boldsymbol{\sigma} - \boldsymbol{\alpha}) - \sigma_o = \sqrt{\tfrac{3}{2}}((\mathbf{s} - \boldsymbol{\alpha}'){:}(\mathbf{s} - \boldsymbol{\alpha}'))^{1/2} - \sigma_o(\varepsilon_{psi}) \tag{15.13}$$

where now σ_o changes with the isotropic equivalent plastic strain, ε_{psi}. In place of (15.3a) and (15.3b), the change in $\boldsymbol{\alpha}$ are now given by

$$\dot{\boldsymbol{\alpha}}_p = C_p(1 - m)\dot{\boldsymbol{\varepsilon}}_p = C_p(1 - m)\dot{\lambda}\mathbf{a} \tag{15.14a}$$

and:

$$\dot{\boldsymbol{\alpha}}_z = C_z(1 - m)(\boldsymbol{\sigma} - \boldsymbol{\alpha}) = C_z(1 - m)\bar{\boldsymbol{\sigma}} \tag{15.14b}$$

Also, in place of (15.8), the consistency condition becomes

$$\dot{f} = \mathbf{a}{:}\dot{\boldsymbol{\sigma}} - \frac{\partial\sigma_o}{\partial\varepsilon_{psi}}\dot{\boldsymbol{\varepsilon}}_{psi} = \mathbf{a}{:}\dot{\boldsymbol{\sigma}} - \mathbf{a}{:}\dot{\boldsymbol{\alpha}} - \bar{H}'m\dot{\lambda} \tag{15.15}$$

where $\bar{H}'$ is the plastic 'slope' related to isotropic hardening. For Prager and Ziegler respectively, we obtain, in place of (15.5a) and (15.5b):

$$\begin{aligned}\dot{f} &= \mathbf{a}{:}\dot{\boldsymbol{\sigma}} - C_p\dot{\lambda}(1 - m)\mathbf{a}{:}\mathbf{a} - \bar{H}'m\dot{\lambda} \\ &= \mathbf{a}{:}\dot{\boldsymbol{\sigma}} - \tfrac{3}{2}C_p\dot{\lambda}(1 - m) - \bar{H}'m\dot{\lambda} = 0\end{aligned} \tag{15.16a}$$

and

$$\begin{aligned}\dot{f} &= \mathbf{a}{:}\dot{\boldsymbol{\sigma}} - C_z\dot{\lambda}(1 - m)\mathbf{a}{:}(\boldsymbol{\sigma} - \boldsymbol{\alpha}) - \bar{H}'m\dot{\lambda} \\ &= \mathbf{a}{:}\dot{\boldsymbol{\sigma}} - C_z\sigma_e\dot{\lambda}(1 - m) - \bar{H}'m\dot{\lambda} = 0\end{aligned} \tag{15.16b}$$

where the last relationships in (15.16a) and (15.16b) relate specifically to the von Mises yield criterion.

For uniaxial condition (and the von Mises criterion), equations (15.16) become (in place of (15.6a) and (15.6b)):

$$\dot{f} = \dot{\sigma}_x - \tfrac{3}{2}C_p(1-m)\dot{\varepsilon}_{px} - \bar{H}'m\dot{\varepsilon}_{px} = H'\dot{\varepsilon}_{px} - \tfrac{3}{2}C_p(1-m)\dot{\varepsilon}_{px} - \bar{H}'m\dot{\varepsilon}_{px} = 0 \tag{15.17a}$$

$$\dot{f} = \dot{\sigma}_x - C_z\sigma_e(1-m)\dot{\varepsilon}_{px} - \bar{H}'m\dot{\varepsilon}_{px} = H'\dot{\varepsilon}_{px} - C_z\sigma_e(1-m)\dot{\varepsilon}_{px} - \bar{H}'m\dot{\varepsilon}_{px} = 0 \tag{15.17b}$$

These relationships must apply irrespective of m, and consequently we obtain:

$$C_p = \tfrac{2}{3}H' = \tfrac{2}{3}\bar{H}' \tag{15.18a}$$

$$C_z = \frac{H'}{\sigma_e} = \frac{\bar{H}'}{\sigma_e} \tag{15.18b}$$

where, even for linear hardening, with $\sigma_e = \sigma_o$ varying with ε_{psi}, C_z is not a constant. Equations (15.16) can be rewritten in the more general form:

$$\dot{f} = \mathbf{a}:\dot{\boldsymbol{\varepsilon}} - A'_k\dot{\lambda} - A'_i\dot{\lambda} = \mathbf{a}:\dot{\boldsymbol{\sigma}} - A'\dot{\lambda} \tag{15.19}$$

where $A' = A'_i + A'_k$ and

$$A'_{pk} = C_p(1-m)\mathbf{a}:\mathbf{a} = \tfrac{3}{2}C_p = H'(1-m) = \bar{H}'(1-m) = A'(1-m) \tag{15.20a}$$

$$A'_{zk} = C_z(1-m)\mathbf{a}:(\boldsymbol{\sigma}-\boldsymbol{\alpha}) = C_z(1-m)\sigma_o = H'(1-m) = \bar{H}'(1-m) = A'(1-m) \tag{15.20b}$$

$$A'_i = \bar{H}'m = H'm \tag{15.20c}$$

where the final relationships in (15.20a) and (15.20b) again relate specifically to the von Mises yield criterion. In this case, as with pure kinematic hardening ($m = 0$), the hardening parameters, A'_{zk} and A'_{pk} are the same. Consequently, provided we work in the full three-dimensional space (or apply plane strain or axial symmetry), it does not matter which evolution law we apply. Also, because (15.19) is in the standard form of (15.8) and (6.16), (6.18) again applies for the standard tangent modular matrix (or tensor).

With the von Mises yield criterion, we can (as in Section 15.1), for a given equivalent plastic strain, ε_{ps}, obtain A' from the initial uniaxial plastic strain relationship (Figure 15.3).

15.3 KINEMATIC HARDENING FOR PLANE STRESS

By assuming that:

$$\sigma_{13} = s_{13} = \alpha_{13} = \alpha'_{13} = \alpha_{23} = s_{23} = \alpha_{23} = \alpha'_{23} = \sigma_{33} = \alpha_{33} = 0 \tag{15.21}$$

the yield function of (15.2), which we rewrite here as

$$f_6 = \sqrt{\tfrac{2}{3}}((\mathbf{s}-\boldsymbol{\alpha}'):(\mathbf{s}-\boldsymbol{\alpha}')) - \sigma_o = f_6(\mathbf{s}-\boldsymbol{\alpha}') = f_6(\boldsymbol{\xi}) = \sigma_e - \sigma_o \tag{15.22}$$

where $\boldsymbol{\xi}$ is the 'reduced stress', becomes (see (6.3)):

$$f_3 = \bar{\sigma}_x^2 + \bar{\sigma}_y^2 - \bar{\sigma}_x\bar{\sigma}_y + 3\bar{\sigma}_{xy}^2 = f_3(\bar{\boldsymbol{\sigma}}-\boldsymbol{\alpha}) = f_3(\bar{\boldsymbol{\sigma}}) = \sigma_e - \sigma_o \tag{15.23}$$

where it is now convenient to use matrix and vector notation so that:

$$\bar{\boldsymbol{\sigma}}^T = (\sigma_x - \alpha_x,\ \sigma_y - \alpha_y,\ \tau_{xy} - \alpha_{xy}) \tag{15.24}$$

In the full three dimensional case, the plastic flow rules are

$$\dot{\boldsymbol{\varepsilon}}_{p6} = \dot{\lambda}\frac{\partial f}{\partial \boldsymbol{\sigma}} = \dot{\lambda}\mathbf{a} = \dot{\lambda}\frac{\partial f}{\partial \mathbf{s}} = \frac{3}{2\sigma_e}\dot{\lambda}(\mathbf{s}-\boldsymbol{\alpha}') = \frac{3}{2\sigma_e}\dot{\lambda}\boldsymbol{\xi} \tag{15.25}$$

where the subscript implies six components (having allowed for symmetry).

For the plane-stress case, using vector notation, (15.25) degenerates to

$$\dot{\boldsymbol{\varepsilon}}_{p4} = \begin{bmatrix} \dot{\varepsilon}_x \\ \dot{\varepsilon}_y \\ \dot{\varepsilon}_z \\ \dot{\gamma}_{xy} \end{bmatrix}_p = \dot{\lambda}\frac{\partial f}{\partial \boldsymbol{\sigma}} = \dot{\lambda}\mathbf{a} = \frac{1}{2\sigma_e}\dot{\lambda}\begin{bmatrix} 2\bar{\sigma}_x - \bar{\sigma}_y \\ -\bar{\sigma}_x + 2\bar{\sigma}_y \\ -\bar{\sigma}_x - \bar{\sigma}_y \\ 6\bar{\tau}_{xy} \end{bmatrix} \tag{15.26}$$

where, for the present, we have kept the $\dot{\varepsilon}_z$ term so that we have four components. However, the aim will be to investigate the possibility of discarding the third, z, component in order to arrive at the usual plane stress procedure of using only three components (see also Section 6.8.2). In writing (15.26), we have also accounted for the fact the engineering strain $\dot{\gamma}_{xy}$ is twice the tensor strain (see Section 4.1). Considering four components, the Prager relationship of (15.3a) for $\dot{\boldsymbol{\alpha}}$ can, in conjunction with (15.9) for C_p be written as

$$\dot{\boldsymbol{\alpha}}_4 = \tfrac{2}{3}A'\dot{\lambda}\mathbf{a}_4 = \frac{A'\dot{\lambda}}{3\sigma_o}\begin{bmatrix} 2\bar{\sigma}_x - \bar{\sigma}_y \\ -\bar{\sigma}_x + 2\bar{\sigma}_y \\ -\bar{\sigma}_x - \bar{\sigma}_y \\ 3\bar{\tau}_{xy} \end{bmatrix} \tag{15.27}$$

On the other hand, for the Ziegler rule of (15.3b) in conjunction with (15.10) for C_z, we obtain:

$$\dot{\boldsymbol{\alpha}}_4 = \frac{A'}{\sigma_o}\dot{\lambda}\begin{bmatrix} \bar{\sigma}_x \\ \bar{\sigma}_y \\ \bar{\sigma}_z = 0 \\ \bar{\sigma}_{xy} \end{bmatrix} = \frac{A'}{\sigma_o}\dot{\lambda}\bar{\boldsymbol{\sigma}}_4 \tag{15.28}$$

In this case, it is easy to verify that, for the four-component case (as with the six-component case), with the Prager rule of (15.27), the consistency condition becomes:

$$\dot{f}_{4p} = \mathbf{a}_4^T\dot{\boldsymbol{\sigma}}_4 - \mathbf{a}_4^T\dot{\boldsymbol{\alpha}}_4 = \mathbf{a}^T\dot{\boldsymbol{\sigma}}_4 - \tfrac{2}{3}A'\dot{\lambda}\mathbf{a}_4^T\mathbf{a}_4 = \mathbf{a}_4^T\dot{\boldsymbol{\sigma}}_4 - A'\dot{\lambda} = 0 \tag{15.29a}$$

and that with the Ziegler rule of (15.28), we obtain the same result, i.e.

$$\dot{f}_{4z} = \mathbf{a}_4^T\dot{\boldsymbol{\sigma}}_4 - \mathbf{a}_4^T\dot{\boldsymbol{\alpha}}_4 = \mathbf{a}_4^T\dot{\boldsymbol{\sigma}}_4 - \frac{A'}{\sigma_o}\dot{\lambda}\mathbf{a}_4^T(\boldsymbol{\sigma}_4 - \mathbf{a}_4) = \mathbf{a}_4^T\dot{\boldsymbol{\sigma}}_4 - A'\dot{\lambda} = 0 \tag{15.29b}$$

Noting that the third component of $\dot{\boldsymbol{\sigma}}_4$ and $\dot{\boldsymbol{\alpha}}_4$ (see (15.28)) is zero, we can remove the third (z-direction) component with no effect on (15.29b) and obtain:

$$\dot{f}_{4z} = \mathbf{a}_4^T\dot{\boldsymbol{\sigma}}_4 - A'\dot{\lambda} = f_{3z} = \mathbf{a}_3^T\dot{\boldsymbol{\sigma}}_3 - A'\dot{\lambda} = 0 \tag{15.30}$$

and, for this hardening law, we can therefore avoid considering the z-component terms and, instead, work in a three-component space. On the other hand, if we adopt the Prager evolution law of (15.27), we cannot apply a similar reduction, because the third component in (15.27) is not zero (nor is the corresponding component from $\mathbf{a}$) and we

have:

$$\mathbf{a}_4^{\mathrm{T}}\dot{\boldsymbol{\alpha}}_4 \neq \mathbf{a}_3^{\mathrm{T}}\dot{\boldsymbol{\alpha}}_3 \tag{15.31}$$

It follows that, while we can (for von Mises) obtain the same solution for plane stress using either Prager or Ziegler, in the former case, we would have to work with (at least) four components.

15.4 RADIAL RETURN WITH MIXED LINEAR HARDENING

We will now extent the radial-return procedure of Section 6.6.7 to include kinematic hardening in conjunction with the Prager evolution law. To this end, we will use the notation of Chapter 6, whereby point A is on or inside the yield surface and refers to the position at the beginning of the increment, point B is the elastic trial position and point C is the final position. A backward-Euler procedure then involves (see also (6.85)):

$$\mathbf{s}_{\mathrm{C}} = \mathbf{s}_{\mathrm{B}} - 2\mu\Delta\boldsymbol{\varepsilon}_{\mathrm{pc}} \tag{15.32}$$

and using (15.14a) and (15.20a) for $\dot{\boldsymbol{\alpha}}$ and applying a backward-Euler incremental form, we can write:

$$\boldsymbol{\alpha}_{\mathrm{C}} = \boldsymbol{\alpha}_{\mathrm{B}} + \tfrac{2}{3}A'_{\mathrm{k}}\Delta\boldsymbol{\varepsilon}_{\mathrm{pC}} = \boldsymbol{\alpha}_{\mathrm{A}} + \tfrac{2}{3}A'_{\mathrm{k}}\Delta\boldsymbol{\varepsilon}_{\mathrm{pC}} \tag{15.33}$$

where (see (15.25)):

$$\Delta\boldsymbol{\varepsilon}_{\mathrm{pC}} = \Delta\lambda\mathbf{a}_{\mathrm{C}} = \Delta\lambda\left.\frac{\partial f}{\partial\boldsymbol{\sigma}}\right|_{\mathrm{C}} = \frac{3\Delta\lambda}{2\sigma_{\mathrm{eC}}}\boldsymbol{\xi}_{\mathrm{C}} = \frac{3\Delta\lambda}{2\sigma_{\mathrm{eB}}}\boldsymbol{\xi}_{\mathrm{B}} \tag{15.34}$$

The last relationship in (15.34) stems from the cylindrical nature of the von Mises yield function. In particular, if $\boldsymbol{\xi}_{\mathrm{C}} = \theta\boldsymbol{\xi}_{\mathrm{B}}$, the same relationship applies for the equivalent stresses so that $\sigma_{\mathrm{eC}} = \theta\sigma_{\mathrm{eB}}$ and

$$\frac{1}{\theta_{\mathrm{eC}}}\boldsymbol{\xi}_{\mathrm{C}} = \frac{1}{\theta_{\mathrm{eB}}}\boldsymbol{\xi}_{\mathrm{B}} \tag{15.35}$$

From (15.32) to (15.34),

$$\boldsymbol{\xi}_{\mathrm{C}} = \mathbf{s}_{\mathrm{C}} - \boldsymbol{\alpha}_{\mathrm{C}} = \theta\boldsymbol{\xi}_{\mathrm{B}} = \left(1 - \frac{\Delta\lambda(3\mu + A'_{\mathrm{k}})}{\sigma_{\mathrm{eB}}}\right)\boldsymbol{\xi}_{\mathrm{B}} \tag{15.36}$$

so that

$$\sigma_{\mathrm{eC}} = \theta\sigma_{\mathrm{eB}} = \left(1 - \frac{\Delta\lambda(3\mu + A'_{\mathrm{k}})}{\sigma_{\mathrm{eB}}}\right)\sigma_{\mathrm{eB}} \tag{15.37}$$

The 'stresses', $\boldsymbol{\xi}_{\mathrm{C}}$, in (15.36) should satisfy the yield criterion:

$$f = \sqrt{\tfrac{3}{2}}\,\|\boldsymbol{\xi}_{\mathrm{C}}\| - \sigma_{\mathrm{oC}} = \sigma_{\mathrm{eC}} - \sigma_{\mathrm{oC}} = \sigma_{\mathrm{eB}} - (3\mu + A'_{\mathrm{k}})\Delta\lambda - (\sigma_{\mathrm{oB}} + \Delta\lambda A'_{\mathrm{i}}) \tag{15.38}$$

For the last relationship in (15.38), we have used (15.37) for σ_{eC}. In equation (15.38), the

scalar A'_i is the isotropic hardening parameter (see (15.20c)). From (15.38),

$$\Delta\lambda = \frac{\sigma_{eB} - \sigma_{oB}}{(3\mu + A'_i + A'_k)} = \frac{f_B}{(3\mu + A'_i + A'_k)} \tag{15.39}$$

From (15.33), (15.34) and (15.39),

$$\boldsymbol{\alpha}_C = \boldsymbol{\alpha}_A + \frac{A'_k \Delta\lambda}{\sigma_{eB}} \boldsymbol{\xi}_B = \boldsymbol{\alpha}_A + \frac{A'_k f_B}{(3\mu + A'_k + A'_i)\sigma_{eB}} \boldsymbol{\xi}_B \tag{15.40}$$

so that using (15.36) for $\boldsymbol{\xi}_C$ and the first relationship in (15.40) for $\boldsymbol{\alpha}_C$, we obtain:

$$\mathbf{s}_C = \boldsymbol{\xi}_C + \boldsymbol{\alpha}_C = \theta\boldsymbol{\xi}_B + \boldsymbol{\alpha}_C = \gamma\boldsymbol{\xi}_B + \boldsymbol{\alpha}_A = \left(1 - \frac{3\mu\Delta\lambda}{\sigma_{eB}}\right)\boldsymbol{\xi}_B + \boldsymbol{\alpha}_A \tag{15.41a}$$

or using (15.39) for $\Delta\lambda$,

$$\mathbf{s}_C = \gamma\boldsymbol{\xi}_B + \boldsymbol{\alpha}_A = \left(1 - \frac{3\mu f_B}{(3\mu + A'_i + A'_k)\sigma_{eB}}\right)\boldsymbol{\xi}_B + \boldsymbol{\alpha}_A \tag{15.41b}$$

Equations (15.39)–(15.41a) (or (15.40) and (15.41b)) define the complete return. (Note that the scalar γ in (15.41) is equivalent to the scalar α used in (6.67) when we only considered isotropic hardening. We are here using γ rather than α because the latter symbol is now used for the 'back stress'.)

Readers interested in the derivation of a consistent tangent relationship to follow the above 'return' might like to move directly to Section 15.8.

15.5 RADIAL RETURN WITH NON-LINEAR HARDENING

At the end of Section 6.6.7, we showed how a scalar Newton–Raphson iteration could be used to apply the radial return method with non-linear isotropic hardening. Such a technique can also be applied with kinematic or mixed hardening.

To this end, we can replace (15.40) with

$$\boldsymbol{\alpha}_C = \boldsymbol{\alpha}_A + \frac{A_{k'_{mean}} \Delta\lambda}{\sigma_{eB}} \boldsymbol{\xi}_B = \boldsymbol{\alpha}_A + (A_k(\varepsilon_{psC}) - A_k(\varepsilon_{psA}))\frac{\boldsymbol{\xi}_B}{\sigma_{eB}}$$

$$= \boldsymbol{\alpha}_A + (A_{k_C} - A_{k_A})\frac{\boldsymbol{\xi}_B}{\sigma_{eB}} \tag{15.42}$$

where

$$A_k(\varepsilon_{psA}) = A_{K_A} = (1-m)A_A \quad \text{and} \quad A_k(\varepsilon_{psC}) = A_{k_C} = (1-m)A_C$$

are the 'kinematic hardening stresses' respectively at the beginning and end of the increment. Knowing the equivalent plastic strains at these positions, A_A and A_C can be obtained from the uniaxial stress/strain relationship (see (Figure 15.3). In deriving (15.42), we have used the relationship:

$$A_{k'_{mean}} \Delta\lambda = A_{k'_{mean}} \Delta\varepsilon_{ps} \simeq A_k(\varepsilon_{psC}) - A_k(\varepsilon_{psA}) \tag{15.43}$$

Hence, replacing $A'_k\Delta\lambda$ by the right-hand side of (15.43) in (15.38) gives:

$$f_C = \sigma_{eB} - 3\mu\Delta\lambda - A_{k_C} + A_{k_A} - \sigma_{oC}(\varepsilon_{psC}) \tag{15.44}$$

which is a non-linear equation in $\Delta\lambda$ which can be solved using a Newton–Raphson iteration based on the truncated Taylor series:

$$f_{Cn} = f_{Co} + \left.\frac{\partial f}{\partial \lambda}\right|_{Co} \dot{\lambda} = f_{Co} - (3\mu + A'_k + A'_i)_{Co}\dot{\lambda} \tag{15.45}$$

On setting the new value of the yield function, f_{Cn} to zero, (15.45) gives an iterative change, $\dot{\lambda}$ in $\Delta\lambda$.

15.6 A GENERAL BACKWARD-EULER RETURN WITH MIXED LINEAR HARDENING

In this section, we will extend the general backward-Euler method of Section 6.6.6 to include mixed hardening. We will adopt the Ziegler evolution law. Following the procedure of Section 6.6.6, we start by defining a residual between the current stress and the correct backward-Euler return, i.e. (see (6.79)):

$$\mathbf{r}_\sigma = \boldsymbol{\sigma}_C - (\boldsymbol{\sigma}_B - \Delta\lambda \mathbf{C}\mathbf{a}_C) = \mathbf{0} \tag{15.46}$$

The **C** matrix in (15.46a) is the elastic constitutive matrix while the symbols A, B and C in (15.46a) follow those adopted in Section 15.4 and originally introduced in Sections 6.6.2, 6.6.5 and 6.6.6. In equation (15.46a) and throughout this section, we will work with matrices and vectors. Such an approach is directly applicable to plane strain and axisymmetric configurations (using four components) or to plane stress using three components. However for the full three-dimensional situation, we would either need to adopt the device of Section 4.2 and work with nine-component vectors or alternatively introduce the **L** matrix of Section 6.5.

In conjunction with (15.46a), we require a residual between the current back stress and the backward-Euler form so that, using (15.14b) and (15.20b) but with Δ's instead of rates:

$$\mathbf{r}_\alpha = \boldsymbol{\alpha}_C - \left(\boldsymbol{\alpha}_A + \frac{A'_k}{\sigma_{eC}} \Delta\lambda \bar{\boldsymbol{\sigma}}_C\right) = \mathbf{0} \tag{15.46b}$$

In addition, we must satisfy the yield function (15.38) which we will re-write here as:

$$f = \sigma_{eC} - \sigma_{oC} = 0 \tag{15.46c}$$

Equations (15.46a)–(15.46c) define the complete set of equations which must be satisfied.

As a starting-point for the iterative solution of these equations, we can obtain $\Delta\lambda$ from (6.59) (see also (15.19)) so that:

$$\Delta\lambda = \frac{f_B}{\mathbf{a}_B^T \mathbf{C}\mathbf{a}_B + A'_B} \tag{15.47a}$$

where all quantities are computed at the elastic trial position B. The hardening parameter A' in (15.47a) would be the sum of the kinematic and isotropic terms (see (15.19)) and would equal the hardening parameter at the initial position A (see Figure 15.4). The first estimate for $\boldsymbol{\sigma}_C$ would then be $\boldsymbol{\sigma}_B - \Delta\lambda \mathbf{C}\mathbf{a}_B$, which the first

estimate for $\boldsymbol{\alpha}_C$ would be obtained as

$$\boldsymbol{\alpha}_C = \boldsymbol{\alpha}_A + \frac{A'_k \Delta\lambda}{\sigma_{eB}} \bar{\boldsymbol{\sigma}}_B = \boldsymbol{\alpha}_A + \frac{A'_k \Delta\lambda}{\sigma_{eB}} (\boldsymbol{\sigma}_B - \boldsymbol{\alpha}_A) \tag{15.47b}$$

In order to solve iteratively (15.46a)–(15.46c), we apply truncated the Taylor series so that:

$$\mathbf{r}_{\sigma n} = \mathbf{r}_{\sigma o} + \dot{\boldsymbol{\sigma}} + \dot{\lambda}\mathbf{C}\mathbf{a} + \Delta\lambda \mathbf{C} \frac{\partial \mathbf{a}}{\partial \boldsymbol{\sigma}} (\dot{\boldsymbol{\sigma}} - \dot{\boldsymbol{\alpha}}) \tag{15.48a}$$

$$\mathbf{r}_{\alpha n} = \mathbf{r}_{\alpha o} + \dot{\boldsymbol{\alpha}} - \frac{A'_k}{\sigma_e} \dot{\lambda} \bar{\boldsymbol{\sigma}} + A'_k \frac{\Delta\lambda'}{\sigma_e} \bar{\boldsymbol{\sigma}} \dot{\sigma}_e - A'_k \Delta\lambda' (\dot{\boldsymbol{\sigma}} - \dot{\boldsymbol{\alpha}}) \tag{15.48b}$$

$$f_n = f_o + \dot{\sigma}_e - \dot{\sigma}_o = f_o + \dot{\sigma}_e - A'_i \dot{\lambda} \tag{15.48c}$$

where we are following the convention whereby the subscript n means 'new' and the subscript o means 'old'. We have also set:

$$\Delta\lambda' = \frac{\Delta\lambda}{\sigma_e} \tag{15.49}$$

and have dropped the subscript C. For the von Mises yield criterion, the matrix $\partial\mathbf{a}/\partial\boldsymbol{\sigma}$ has been given in (6.47) (Note that the $\mathbf{a}$ vectors involves $\bar{\boldsymbol{\sigma}}$ components rather than σ components).

By setting the left-hand sides of equations (15.48a–15.48c) to zero, we can provide the basis for a Newton–Raphson iteration. In particular, substituting into (15.48b) from (15.48c) for $\dot{\sigma}_e$

$$\dot{\boldsymbol{\alpha}} = -D_1 \mathbf{r}_{\alpha o} + D_2 \bar{\boldsymbol{\sigma}} + D_3 \dot{\lambda} \bar{\boldsymbol{\sigma}} + D_4 \dot{\boldsymbol{\sigma}} \tag{15.50}$$

where

$$d = A'_k \Delta\lambda' \tag{15.51a}$$

$$D_1 = \frac{1}{1+d}; \qquad D_2 = \frac{df_o}{(1+d)\sigma_e}; \qquad D_3 = \frac{A'_k(1 - A'_i \Delta\lambda')}{\sigma_e(1+d)}; \qquad D_4 = 1 - D_1 \tag{15.51b}$$

Substitution from (15.50) into (15.48a) then leads to

$$\mathbf{Q}\dot{\boldsymbol{\sigma}} = -\mathbf{r}_{\sigma o} - D_1 \Delta\lambda \mathbf{C} \frac{\partial \mathbf{a}}{\partial \boldsymbol{\sigma}} \mathbf{r}_{\alpha o} + \Delta\lambda D_2 \mathbf{C} \frac{\partial \mathbf{a}}{\partial \boldsymbol{\sigma}} \bar{\boldsymbol{\sigma}} - \dot{\lambda} \left(\mathbf{C}\mathbf{a} - D_3 \Delta\lambda \mathbf{C} \frac{\partial \mathbf{a}}{\partial \boldsymbol{\sigma}} \bar{\boldsymbol{\sigma}} \right) \tag{15.52}$$

with (compare (6.81)):

$$\mathbf{Q} = \left[\mathbf{I} + D_1 \Delta\lambda \mathbf{C} \frac{\partial \mathbf{a}}{\partial \boldsymbol{\sigma}} \right] \tag{15.53}$$

For the von Mises yield criterion, it can be shown (see (6.47) for $\partial\mathbf{a}/\partial\boldsymbol{\sigma}$) that:

$$\frac{\partial \mathbf{a}}{\partial \boldsymbol{\sigma}} \bar{\boldsymbol{\sigma}} = 0 \tag{15.54}$$

and hence, we can simplify (15.52) to give:

$$\dot{\boldsymbol{\sigma}} = -\mathbf{Q}^{-1} \bar{\mathbf{r}} - \dot{\lambda} \mathbf{Q}^{-1} \mathbf{C}\mathbf{a} = -\mathbf{Q}^{-1} \bar{\mathbf{r}} - \dot{\lambda} \mathbf{R}\mathbf{a} \tag{15.55}$$

where

$$\bar{\mathbf{r}} = \mathbf{r}_{\sigma o} + D_1 \Delta\lambda \mathbf{C} \frac{\partial \mathbf{a}}{\partial \boldsymbol{\sigma}} \mathbf{r}_{\alpha o} \tag{15.56}$$

and (see also (6.108)):

$$\mathbf{R} = \mathbf{Q}^{-1}\mathbf{C} \tag{15.57}$$

Substituting from (15.50) and (15.55) into (15.48c) allows one to obtain (for von Mises):

$$(A_i' + D_1 \mathbf{a}^T \mathbf{R} \mathbf{a} + D_3 \sigma_e)\dot{\lambda} = f_o - D_1 \mathbf{a}^T \mathbf{Q}^{-1} \bar{\mathbf{r}} + D_1 \mathbf{a}^T \mathbf{r}_{\alpha o} - D_2 \sigma_e \tag{15.58}$$

Having obtained $\dot{\lambda}$ from (15.58), we can obtain $\dot{\boldsymbol{\sigma}}$ from (15.55) and $\dot{\boldsymbol{\alpha}}$ from (15.50).

In Section 15.9, we derive a consistent tangent modular matrix that is consistent with this return. Readers might prefer to move directly to that section.

15.7 A BACKWARD-EULER PROCEDURE FOR PLANE STRESS WITH MIXED LINEAR HARDENING

We could use the general approach of the last section, which uses Ziegler's evolution law for plane stress. However, a simpler procedure can be derived by modifying the procedure of Section 6.8.2 to include mixed hardening. To this end we will adopt the equations of Section 15.3. In particular, we will use the mixed version (via the factor $(1 - m)$—see Section 15.2)) of the three-component form of (15.28) for $\dot{\boldsymbol{\alpha}}$ (although here using increments instead of rates). The backward-Euler stresses, $\boldsymbol{\sigma}_C$ are then given by

$$\boldsymbol{\sigma}_C = \bar{\boldsymbol{\sigma}}_C + \boldsymbol{\alpha}_C = \bar{\boldsymbol{\sigma}}_C + \left(\boldsymbol{\alpha}_B + \frac{\Delta\lambda A_k'}{\sigma_{eC}} \bar{\boldsymbol{\sigma}}_C\right) = \bar{\boldsymbol{\sigma}}_B - \Delta\lambda \mathbf{C}\mathbf{a}_C(\bar{\boldsymbol{\sigma}}_C) \tag{15.59}$$

or

$$\left(1 + \frac{\Delta\lambda A_k'}{\sigma_{eC}}\right)\bar{\boldsymbol{\sigma}}_C = \bar{\boldsymbol{\sigma}}_B - \Delta\lambda \mathbf{C}\mathbf{a}_C \tag{15.60}$$

Following closely the procedure of Section 6.8.1, in place of (6.124)–(6.126), we now obtain:

$$\left(1 + \frac{\Delta\lambda A_k'}{\sigma_{eC}} + \frac{\Delta\lambda E}{2\sigma_{eC}(1-\nu)}\right)(\bar{\sigma}_x - \bar{\sigma}_y)_C = (\bar{\sigma}_x + \bar{\sigma}_y)_B \tag{15.62}$$

$$\left(1 + \frac{\Delta\lambda A_k'}{\sigma_{eC}} + \frac{3\Delta\lambda\mu}{\sigma_{eC}}\right)(\bar{\sigma}_x - \bar{\sigma}_y)_C = (\bar{\sigma}_x - \bar{\sigma}_y)_B \tag{15.63}$$

$$\left(1 + \frac{\Delta\lambda A_k'}{\sigma_{eC}} + \frac{3\Delta\lambda\mu}{\sigma_{eC}}\right)\bar{\tau}_{xyC} = \bar{\tau}_{xyB} \tag{15.64}$$

where $\bar{\sigma}_{xB}$, $\bar{\sigma}_{yB}$ and $\bar{\tau}_{xyB}$ are known and (see (15.49)), $\Delta\lambda' = \Delta\lambda/\sigma_{eC}$. With kinematic hardening, in place of (6.128), we can write the equivalent stress as

$$\sigma_c^2 = \tfrac{1}{4}((\bar{\sigma}_x + \bar{\sigma}_y)^2 + 3(\bar{\sigma}_x - \bar{\sigma}_y)^2 + 12\bar{\tau}_{xy}^2) \tag{15.65}$$

Substitution from (15.62) to (15.64) for $(\bar{\sigma}_x + \bar{\sigma}_y)_C$, etc. gives the following expression for the yield function, $f_2 = \sigma_e^2 - \sigma_o^2$ (see also (6.129)):

$$f_2 = \frac{1}{4}\left(\frac{C_1}{(1 + \Delta\lambda' A_k' + \Delta\lambda' \mu r)^2} + \frac{C_2}{(1 + \Delta\lambda' A_k' + 3\Delta\lambda' \mu)^2}\right)^2 - \sigma_{oC}^2 = \sigma_{aC}^2 - \sigma_{oC}^2 = 0 \quad (15.66)$$

where r is given (see also (6.130)) by

$$r = \frac{(1 + v)}{(1 - v)} \quad (15.67)$$

and (compare (6.131))

$$C_1 = (\bar{\sigma}_x + \bar{\sigma}_y)_B^2; \qquad C_2 = 3(\bar{\sigma}_x - \bar{\sigma}_y)_B^2 + 12\bar{\tau}_{xyB}^2 \quad (15.68)$$

We have introduced a new 'effective stress', σ_{aC}, in (15.66) because σ_{aC} is itself a function of σ_{eC} (via $\Delta\lambda' = \Delta\lambda/\sigma_{eC}$). Hence, we must supplement (15.66) with

$$g = \sigma_{eC}^2 - \sigma_{oC}^2 = 0 \quad (15.69)$$

Equations (15.66) and (15.69) provide two non-linear equations in two unknowns, $\Delta\lambda$ and σ_{eC}. To solve these equations, we could use the method of Section 15.6 (i.e. equation 15.47a) to obtain a starting value for $\Delta\lambda$ and, in addition, start with $\sigma_{oC} = \sigma_{oA}$ and $\sigma_{eC} = \sigma_{eB}$. Application of truncated Taylor series to (15.66) now leads to

$$f_{2n} = f_{2o} + C_1\dot{\lambda}' - 2\sigma_o\dot{\sigma}_o = f_{2o} + C_3\left(\frac{\dot{\lambda}}{\sigma_e} - \frac{\Delta\lambda'\dot{\sigma}_e}{\sigma_e}\right) - 2\sigma_o A_i'\dot{\lambda} = 0 \quad (15.70)$$

where

$$C_3 = -\frac{1}{2}\left(\frac{C_1(A_k' + \mu r)}{(1 + \Delta\lambda' A_k' + \Delta\lambda' \mu r)^3} + \frac{C_2(A_k' + 3\mu)}{(1 + \Delta\lambda' A_k' + 3\Delta\lambda' \mu)^3}\right) \quad (15.71)$$

while a similar application to (15.69) leads to:

$$g_n = g_o + 2\sigma_e\dot{\sigma}_e - 2\sigma_{oC}\dot{\sigma}_{oC} = g_o + 2\sigma_e\dot{\sigma}_e - 2\sigma_{oC}A_i'\dot{\lambda} \quad (15.72)$$

As usual, we can derive an iterative process by setting the left-hand sides of (15.70) and (15.72) to zero. Substitution from (15.72) into (16.70) then leads to

$$\left(\frac{C_3}{\sigma_e} - A_i'\sigma_o\left(2 + \frac{\Delta\lambda'\sigma_o}{\sigma_e^2}\right)\right)\dot{\lambda} = -f_o - C_3\frac{\Delta\lambda'}{2\sigma_e^2}g_o \quad (15.73)$$

from which we can obtain $\dot{\lambda}$ and hence, via (15.72) (with $g_n = 0$) $\dot{\sigma}_e$. When the iterative process has converged, we know $\Delta\lambda$ and σ_e and via (15.62)–(15.64) can obtain $\bar{\boldsymbol{\sigma}}_C$. Also (see (15.59)), we can obtain:

$$\boldsymbol{\alpha}_C = \boldsymbol{\alpha}_A + \frac{\Delta\lambda A_k'}{\sigma_{eC}}\bar{\boldsymbol{\sigma}}_c \quad (15.74)$$

and hence $\boldsymbol{\sigma}_C = \bar{\boldsymbol{\sigma}}_C + \boldsymbol{\alpha}_C$.

In Section 6.8.2.1, we derived, a special form for the consistent tangent modular matrix which followed on from the special return of Section 6.8.2. The latter return corresponds with the present return when the kinematic hardening term A_k' is set to

zero. However, with kinematic hardening there does not seem to be any major advantages stemming from a special derivation of the consistent tangent modular matrix and, instead, one may use the general method to be outlined in Section 15.9.

15.8 A CONSISTENT TANGENT MODULAR TENSOR FOLLOWING THE RADIAL RETURN OF SECTION 15.4

Differentiation of (15.41a) gives

$$\dot{\mathbf{s}}_C = \gamma\dot{\boldsymbol{\xi}}_B + \dot{\gamma}\boldsymbol{\xi}_B = 2\mu\gamma\dot{\mathbf{e}} + \dot{\gamma}\boldsymbol{\xi}_B \tag{15.75}$$

where γ is given in (15.41a) as $1 - 3\mu\Delta\lambda/\sigma_{eB}$ so that:

$$\dot{\gamma} = -\frac{3\mu}{\sigma_{eB}}\dot{\lambda} + 3\Delta\lambda\mu\frac{\dot{\sigma}_{eB}}{\sigma_{eB}^2} = -(1-\gamma)\frac{\dot{\lambda}}{\Delta\lambda} + (1-\gamma)\frac{\dot{\sigma}_{eB}}{\sigma_{eB}} \tag{15.76}$$

The term $\dot{\sigma}_{eB}$ can be obtained by differentiating $\dot{\sigma}_{eB} = \sqrt{\frac{3}{2}}\,\|\,\xi_B\,\|$ to obtain:

$$\dot{\sigma}_{eB} = \sqrt{\frac{3}{2}}\frac{\boldsymbol{\xi}_B:\dot{\boldsymbol{\xi}}_B}{\|\,\boldsymbol{\xi}_B\,\|} = \frac{3}{\sigma_{eB}}\boldsymbol{\xi}_B:\dot{\mathbf{e}}_B = \frac{3}{\sigma_{eB}}\boldsymbol{\xi}_B:\dot{\mathbf{e}}_C \tag{15.77}$$

The consistency condition is obtained by differentiating the yield function:

$$f = \sigma_{eC} - \sigma_{oC} = \theta\sigma_{eB} - \sigma_{oC} \tag{15.78}$$

where θ was given in (15.37) as

$$1 - \frac{\Delta\lambda(3\mu + A_k')}{\sigma_{eB}}$$

so that:

$$\dot{f} = \theta\dot{\sigma}_{eB} + \dot{\theta}\sigma_{eB} - \dot{\sigma}_{oC} = \theta\dot{\sigma}_{eB} + \dot{\theta}\sigma_{eB} - A_i'\dot{\lambda} = 0 \tag{15.79}$$

where:

$$\dot{\theta} = -(1-\theta)\frac{\dot{\lambda}}{\Delta\lambda} + (1-\theta)\frac{\dot{\sigma}_{eB}}{\sigma_{eB}} \tag{15.80}$$

Consequently, we can obtain $\dot{\lambda}$ from (15.79) via:

$$\left(A_i' + \frac{(1-\theta)}{\Delta\lambda}\sigma_{eB}\right)\dot{\lambda} = \dot{\sigma}_{eB} = \frac{3}{\sigma_{eB}}\boldsymbol{\xi}_B:\dot{\mathbf{e}}_C \tag{15.81}$$

where, for the last relationship in (15.81), we have used (15.77) for $\dot{\sigma}_{eB}$. Substituting into (15.76) from (15.81) for $\dot{\lambda}$ and from (15.77) for $\dot{\sigma}_{eB}$ leads to

$$\dot{\gamma} = 2\mu\beta\boldsymbol{\xi}_B:\dot{\mathbf{e}}_C \tag{15.82}$$

where

$$\beta = \frac{3}{2\sigma_{eB}^2}(1-\gamma)\left(1 - \frac{\sigma_{eB}}{\Delta\lambda A_i' + (1-\theta)\sigma_{eB}}\right) = \frac{3}{2\sigma_{eB}^2}(1-\gamma)\left(1 - \frac{\sigma_{eB}}{\Delta\lambda(3\mu + A_i' + A_k')}\right) \tag{15.83}$$

where we have used (15.37) for θ. (Noting that γ from (15.41a) equals α from (6.87), equation (15.83) coincides with (6.101) once $A_i' + A_k'$ is replaced by A'.) Substituting from (15.82) for $\dot{\gamma}$ into (15.75) now leads to

$$\dot{\mathbf{s}} = 2\mu(\gamma \mathbf{I} + \beta \boldsymbol{\xi}_B \otimes \boldsymbol{\xi}_B)\dot{\mathbf{e}} \tag{15.84}$$

where β is given by (15.83) and γ by (15.41). Knowing, from (15.36), that $\boldsymbol{\xi}_B = \boldsymbol{\xi}_C/\theta$, equation (15.84) can easily be changed to involve $\boldsymbol{\xi}_C$. Apart from the replacement of $\mathbf{s}$ by $\boldsymbol{\xi}$, (15.84) takes an identical form to (6.102) derived in Section 6.7.1 for isotropic hardening. The latter chapter indicated how to modify (15.84) to relate to total rather than deviatoric terms.

15.9 GENERAL FORM OF THE CONSISTENT TANGENT MODULAR TENSOR

Following the backward-Euler procedure of Section 15.6, a consistent tangent can be derived by differentiating $\boldsymbol{\sigma}_C$ in (15.46a) (with $\mathbf{r}_\sigma = \mathbf{0}$) to give

$$\dot{\boldsymbol{\sigma}} = \mathbf{C}\dot{\boldsymbol{\varepsilon}} - \dot{\lambda}\mathbf{C}\mathbf{a} - \Delta\lambda\mathbf{C}\frac{\partial \mathbf{a}}{\partial \boldsymbol{\sigma}}\dot{\boldsymbol{\sigma}} + \Delta\lambda\mathbf{C}\frac{\partial \mathbf{a}}{\partial \boldsymbol{\sigma}}\dot{\boldsymbol{\alpha}} \tag{15.85}$$

We can now substitute into (15.85) from (15.50) for $\dot{\boldsymbol{\alpha}}$. In the following, we will assume that we are adopting the von Mises yield criterion so that (15.54) applies and we can therefore simplify the resulting expression to give:

$$\mathbf{Q}\dot{\boldsymbol{\sigma}} = \mathbf{C}\dot{\boldsymbol{\varepsilon}} - \dot{\lambda}\mathbf{C}\mathbf{a} \tag{15.86}$$

where $\mathbf{Q}$ was given in (15.53) (with D_1 from (15.51)). It follows that:

$$\dot{\boldsymbol{\sigma}} = \mathbf{Q}^{-1}\mathbf{C}\dot{\boldsymbol{\varepsilon}} - \dot{\lambda}\mathbf{Q}^{-1}\mathbf{C}\mathbf{a} = \mathbf{R}\dot{\boldsymbol{\varepsilon}} - \dot{\lambda}\mathbf{R}\mathbf{a} \tag{15.87}$$

To obtain $\dot{\lambda}$, we apply the consistency condition:

$$\dot{f} = \dot{\sigma}_e - \dot{\sigma}_o = \mathbf{a}^T\dot{\boldsymbol{\sigma}} - \mathbf{a}^T\dot{\boldsymbol{\alpha}} - A_i'\dot{\lambda} = 0 \tag{15.88}$$

where $\dot{\boldsymbol{\sigma}}$ from (15.87) and $\dot{\boldsymbol{\alpha}}$ from (15.50). Again restricting the solution to the von Mises yield criterion (via (15.54) and the relationship $\mathbf{a}^T\bar{\boldsymbol{\sigma}} = \sigma_e$), we obtain:

$$\dot{\lambda} = \frac{D_1\mathbf{a}^T\mathbf{R}\dot{\boldsymbol{\varepsilon}}}{(A_i' + D_3\sigma_e + D_1\mathbf{a}^T\mathbf{R}\mathbf{a})} = \frac{\mathbf{a}^T\mathbf{R}\dot{\boldsymbol{\varepsilon}}}{(\mathbf{a}^T\mathbf{R}\mathbf{a} + A_i' + A_k')} \tag{15.89}$$

In the first relationship in (15.89) D_1 and D_3 are from (15.51). The final relationship, which is obtained after some algebraic manipulation is of an identical form to that in (6.109) once $A_i' + A_k'$ are replaced by A'. Substitution from (15.89) into (15.87) then leads to the consistent tangential relationship whereby:

$$\dot{\boldsymbol{\sigma}} = \mathbf{C}_{ct}\dot{\boldsymbol{\varepsilon}} = \mathbf{R}\left[\mathbf{I} - \frac{\mathbf{a}^T\mathbf{a}\mathbf{R}}{\mathbf{a}^T\mathbf{R}\mathbf{a} + A_i' + A_k'}\right]\dot{\boldsymbol{\varepsilon}} \tag{15.90}$$

Equation (15.90) takes the same form as (6.110) once $A_i' + A_k'$ is replaced by A'. However, one should note that the $\mathbf{Q}$ matrix entering the $\mathbf{R}$ matrix via (15.57) (or see (15.87)) differs from the $\mathbf{Q}$ matrix of (6.109) because of the D_1 terms (see (15.51)) in (15.53).

15.10 OVERLAY AND OTHER HARDENING MODELS

Instead of using 'conventional' kinematic hardening, one may use some form of 'overlay' model [B2, M3, O1, H1, Z2] in which each 'overlay' has elastic/perfectly plastic material properties. The ideas are illustrated in Figures 15.4 and 15.5. The first of these figures relates to the simplest two-overlay model which can effectively reproduce pure linear kinematic hardening. This is achieved by allowing the first overlay (1) to yield at the yield stress σ_o^1 (Figure 15.4b) which is also set to the yield stress, σ_1 of the equivalent kinematic model (Figure 15.4c). The second overlay (2) is given linear elastic material properties. In relation to a conventional kinematic model with linear hardening, the E value E_2 in Figure 15.4c is related to the kinematic hardening parameter,

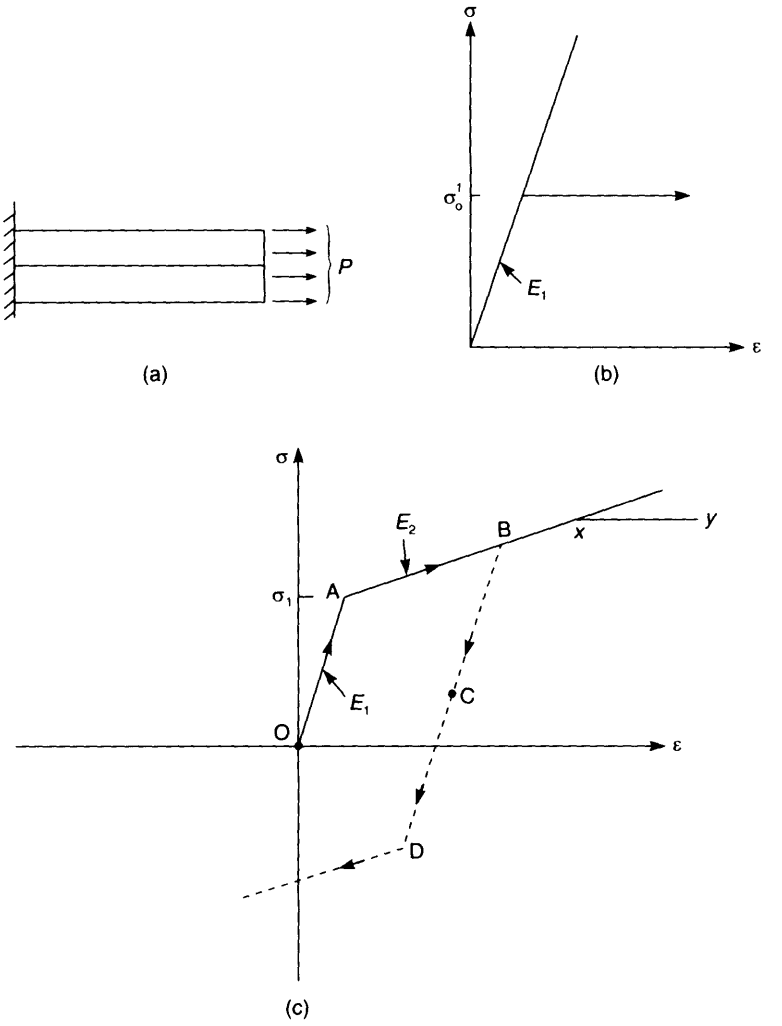

Figure 15.4 Two-layer overlay. (a) Overlay model; (b) stress–strain relationships for constituent overlays; (c) stress–strain relationship for 'overlay model'.

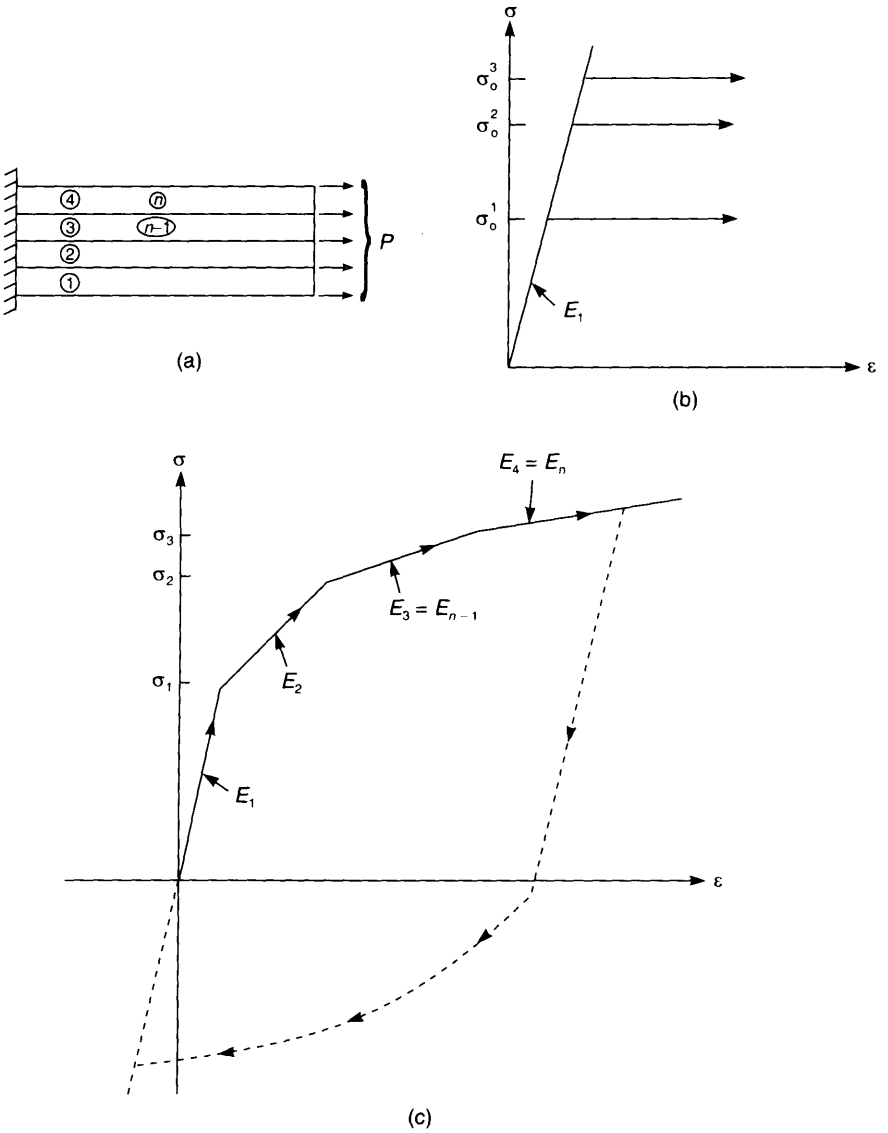

Figure 15.5 Four-layer overlay. (a) Overlays; (b) stress–strain relationships for constituent overlays; (c) stress–strain relationship for 'overlay model'.

A'_k via (see (6.13)):

$$A' = \frac{E_2}{1 - E_2/E_1} \tag{15.91}$$

On unloading, the composite will follow the line BC (Figure 15.4c) until at C (with CB = OA), the stress in the yield layer 1 will be zero (Figure 15.4b) and at D (with BC = CD) will have again reached the yield surface. The resulting composite stress–strain relationship (Figure 15.4c) displays the main features of kinematic hardening. By

giving the second layer (2) a higher yield stress, we can produce a form of piecewise linear, non-linear hardening as indicated by the horizontal line XY in Figure 15.4c). To produce a more general piecewise linear, non-linear hardening, we can introduce more layers (Figure 15.5).

Returning to the simple, two-overlay model, we have not yet indicated how the layer areas can be chosen to ensure the desired composite stress–strain relationship. From Figure 15.4a, equilibrium ensures that:

$$P = A\sigma = A_1\sigma^1 + A_2\sigma^2 = A(\omega_1\sigma^1 + \omega_2\sigma^2) \tag{15.92}$$

where A_1 and A_2 are the 'areas' of overlays 1 and 2 respectively and σ^1 and σ^2 are the equivalent stresses while σ is the 'composite stress'. In (15.92), we have also introduced the weighting parameters ω_1 and ω_2 which we will generally use rather than 'areas'. In order to ensure that the composite has the desired effective E value, E_2 (Figure 15.4c), we need merely ensure that following the yielding of overlay 1:

$$\dot{P} = A\dot{\sigma} = AE_2\dot{\varepsilon} = A_2\sigma^2 = A_2E_1\dot{\varepsilon} \tag{15.93}$$

where (see Figures (15.4b) and (15.4c)), E_1 is the elastic E value. From (15.93), it follows that:

$$\omega_2 = \frac{A_2}{A} = \frac{E_2}{E} = \frac{E_2}{E_1} \tag{15.94a}$$

$$\omega_1 = \frac{A_1}{A} = \frac{(E_1 - E_2)}{E_1} \tag{15.94b}$$

Readers might have noted an inconsistency in this model which relates to the effect of Poisson's ratio and the multiaxial/uniaxial relationships. We will address this issue in Section 15.10.1, but in the meantime, will consider the extension of the previous model to give a more sophisticated hardening relationship (Figure 15.5c).

We will assume that we have n overlays. Then to obtain, the slope E_n for the nth segment of the composite curve (Figure 15.5c), we obtain, in place of (15.94a):

$$\omega_n = \frac{E_n}{E_1} \tag{15.95}$$

while for the segment, $n-1$, the stress–strain relationships provide:

$$\frac{\dot{P}}{A} = E_{n-1}\dot{\varepsilon} = (\omega_n + \omega_{n-1})E_1\dot{\varepsilon} \tag{15.96}$$

from which:

$$\omega_n + \omega_{n-1} = \frac{E_{n-1}}{E_1} \tag{15.97a}$$

or

$$\omega_{n-1} = \frac{E_{n-1} - E_n}{E_1}; \qquad n = 2, n = 1 \tag{15.97b}$$

The previous relationships are tabulated (under simple weighting) for a four-layer model in Table 15.1.

Table 15.1 Table of properties for four-layer model.

Layer, k	Simple weighting, ω_k	Complex weighting, ω_k	Yield stress, σ_0^k
4	$\dfrac{E_4}{E_1}$	$\dfrac{2E_4(1+\nu)}{3E_1 - E_4(1-2\nu)}$	$\dfrac{\sigma_4 - \omega_3\sigma_3}{\omega_4}$
3	$\dfrac{E_3 - E_4}{E_1}$ or $\omega_3 + \omega_4 = \dfrac{E_3}{E_1}$	$\omega_3 + \omega_4 = \dfrac{2E_3(1+\nu)}{3E_1 - E_3(1-2\nu)}$	$\dfrac{\sigma_3 - \omega_2\sigma_2}{\omega_3 + \omega_4}$
2	$\dfrac{E_2 - E_3}{E_1}$ or $\omega_2 + \omega_3 + \omega_4 = \dfrac{E_2}{E_1}$	$\omega_2 + \omega_3 + \omega_4 = \dfrac{2E_2(1+\nu)}{3E_1 - E_2(1-2\nu)}$	$\dfrac{\sigma_2 - \omega_1\sigma_1}{\omega_2 + \omega_3 + \omega_4}$
1	$\dfrac{E_1 - E_2}{E_1}$ or $\omega_1 + \omega_2 + \omega_3 + \omega_4 = 1$	$\omega_1 + \omega_2 + \omega_3 + \omega_4 = 1$	σ_1

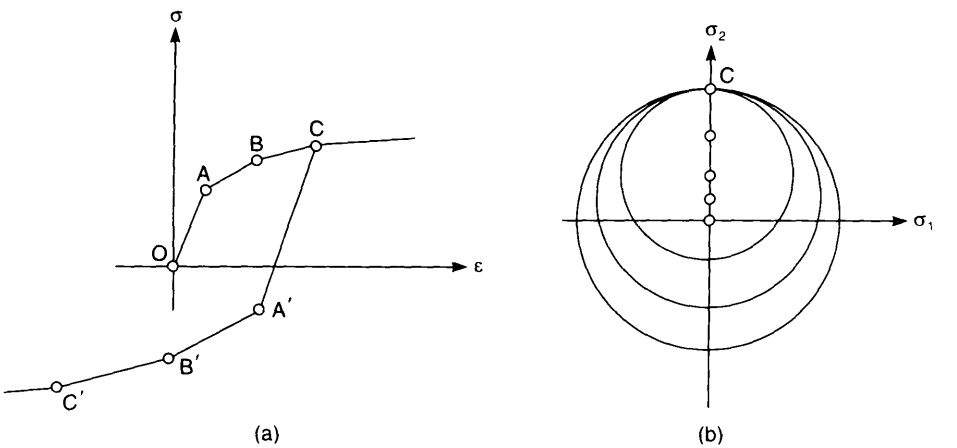

Figure 15.6 Mroz's overlay model. (a) Uniaxial relationship; (b) initially concentric yield surface after reaching point C in Figure 15.6(a).

We will now consider the computation of the yield stresses in the layers (σ_o^k) for the different layers. For the first layer to yield, we clearly have (see Figure 15.6), $\sigma_o^1 = \sigma_1$. For the second layer, we must note that in the model the first layer has already yielded so that equilibrium relationships provide:

$$\frac{P}{A} = \sigma_2 = (1 - \omega_1)\sigma_o^2 \tag{15.98}$$

(The last term in (15.98) is not σ_o squared.) We can continue in this manner to computer all of the σ_o^k. These relationships have been tabulated for a four-layer model in Table 15.1.

15.10.1 Sophisticated overlay model

We can refine the previous model so that the response for (the initial) monotonic, uniaxial loading corresponds with that of a conventional model with non-linear (piecewise linear) hardening. We will assume that this uniaxial loading occurs in the x-direction and that the strains in the y- and z-directions are equal. As a starting-point it is useful to compute the tangent stiffnesses following first yielding for such a uniaxial loading. These are tabulated in Table 15.2 for linear-elastic materials, elastic/perfectly plastic materials and elastic/hardening-plastic materials. These relationships have been expressed in terms of the bulk modulus, k and shear modulus μ (see (4.23)). For the elastic materials, the stiffnesses can be obtained from (4.27) (or (4.30) or (4.31)). For elasto-plastic materials, all the shear stresses are zero and we are left with

$$\sigma^T = (\sigma_x, \sigma_y = 0, \sigma_z = 0); \qquad \mathbf{s}^T = (\tfrac{2}{3}\sigma_x, -\tfrac{1}{3}\sigma_x, -\tfrac{1}{3}\sigma_x) \tag{15.99}$$

where $\sigma_x = \sigma_e = \sigma_o$. The elasto-plastic stiffnesses in Table 15.2 can then be obtained from (6.45) with:

$$\mu_{ef} = \frac{\mu A'}{3\mu + A'}; \qquad \bar{A} = \frac{A'}{3\mu} \tag{15.100}$$

Applying the relationships in Table 15.2 to the uniaxial loading and noting that

Table 15.2 Tangent stiffnesses for uniaxial (x-direction loading)

Stiffness	Elastic	Perfectly plastic	Plastic with hardening
C_{xx}	$k + \frac{4}{3}\mu$	k	$k + \frac{4}{3}\mu_{ef}$
$C_{xy} = C_{xz}$	$k - \frac{2}{3}\mu$	k	$k - \frac{2}{3}\mu_{ef}$
C_{yy}	$k + \frac{4}{3}\mu$	$k + \mu$	$k + \frac{\mu}{1+\bar{A}} + \frac{4}{3}\mu_{ef}$
C_{yz}	$k - \frac{2}{3}\mu$	$k - \mu$	$k - \frac{\mu}{1+\bar{A}} - \frac{4}{3}\mu_{ef}$

$\dot{\varepsilon}_y = \dot{\varepsilon}_z$, we can obtain:

$$\dot{\sigma}_x = k(\dot{\varepsilon}_x + 2\dot{\varepsilon}_y) + \tfrac{4}{3}\mu_{ef}(\dot{\varepsilon}_x - \dot{\varepsilon}_y) \tag{15.101a}$$

$$\dot{\sigma}_y = k(\dot{\varepsilon}_x + 2\dot{\varepsilon}_y) - \tfrac{2}{3}\mu_{ef}(\dot{\varepsilon}_x - \dot{\varepsilon}_y) \tag{15.101b}$$

Equations (15.101) can be applied to the elastic case by setting $\mu_{ef} = \mu$. If we assume that $\dot{\sigma}_y = 0$ and substitute from (15.101b) into (15.101a), we obtain:

$$\dot{\sigma}_x = 2\mu_{ef}(\dot{\varepsilon}_x - \dot{\varepsilon}_y) \tag{15.102}$$

while, from (15.101b), we can obtain (with $\dot{\sigma}_y = 0$)

$$\dot{\varepsilon}_y = -g\dot{\varepsilon}_x \tag{15.103a}$$

$$g = \frac{3k - 2\mu_{ef}}{6k + 2\mu_{ef}} = \frac{1}{2}\left(1 - \frac{E_2}{E_1}\right) + \mu\frac{E_2}{E_1} \tag{15.103b}$$

In deriving the last relationship in (15.103b), we have used (4.23) for k and μ (with $E = E_1$), (15.100) for μ_{ef} and (15.91) for A'. Substitution from (15.103) into (15.102) gives the desired relationship $\dot{\sigma}_x = E_2\dot{\varepsilon}_x$ (see Figure 15.5c). For perfect plasticity, $E_2 = \mu_{ef} = 0$ and g in (15.103) is 1/2. For elasticity, $E_2 = E_1$ and $\mu_{ef} = \mu$ and g in (14.103) is found to equal ν.

We will first consider the two-layer composite of Figure 15.5a) and following the yielding of layer 1 at $\sigma_o^1 = \sigma_1$, will require that $\dot{\varepsilon}_y = -g\dot{\varepsilon}_x$ with g from (15.103b). To make the following developments easier to follow, we will temporarily refer to layer 1 as the 'elastic layer' (with a subscript e) and layer 2 as the 'plastic layer' (with a subscript p). With the imposed strain rates, for the tangential relationships for these two layers can be obtained from Table 15.2 as

$$\dot{\sigma}_{xe} = (k(1 - 2g) + \tfrac{4}{3}\mu(1 + g))\dot{\varepsilon}_x \tag{15.104a}$$

$$\dot{\sigma}_{ye} = (k(1 - 2g) - \tfrac{2}{3}\mu(1 + g))\dot{\varepsilon}_x \tag{15.104b}$$

$$\dot{\sigma}_{xp} = \dot{\sigma}_{yp} = k(1 - 2g)\dot{\varepsilon}_x \tag{15.105}$$

For the combined composite, we require that:

$$\dot{\sigma}_y = \omega_e\dot{\sigma}_{ye} + \omega_p\dot{\sigma}_{yp} \tag{15.106}$$

Substitution from (15.104b) and (15.105) into (15.106), then leads to

$$\omega_e = \omega_2 = \frac{(1 + \nu)(1 - 2g)}{(1 - 2\nu)(1 + g)} = \frac{2E_2(1 + \nu)}{3E_1 + E_2(1 - 2\nu)} = \frac{A'}{3\mu + A'} \tag{15.107a}$$

so that:

$$\omega_p = \omega_1 = 1 - \omega_2 = \frac{3(E_1 - E_2)}{3E_1 + E_2(1 - 2\nu)} = \frac{3\mu}{3\mu + A'} \tag{15.107b}$$

As a check, we can show that, with ω_e and ω_p from (15.107), we obtain:

$$\dot{\sigma}_x = \omega_e\dot{\sigma}_{xe} + \omega_p\dot{\sigma}_{xp} = E_2\dot{\varepsilon}_x \tag{15.108}$$

with $\dot{\sigma}_{xe}$ from (15.104a) and $\dot{\sigma}_{xp}$ from (15.105).

It is not difficult to extend the previous concepts to relate to more layers. Considering, for example, four layers (as considered in Table 15.1), we can consider the situation in which the third layer has just yielded (previously the first layer had just yielded) to obtain an equivalent expression to (15.107a), but with the subscript 4 in place of the subscript 2 (see Table 15.1). Considering next the situation immediately following the yielding of layer two (so that the combined elastic weighting equals $\omega_3 + \omega_4$), we obtain the relationship given in Table 15.1, for $k = 3$. The procedure continues until the weightings for all the layers have been obtained.

15.10.2 Relationship with conventional kinematic hardening

We will now briefly explore the relationship between the conventional linear kinematic hardening of Section 15.1 and the present two-layered model. By the very definition of the sophisticated weighting parameters, the two formulations coincide for uniaxial loading. We will now write down the key equations for the two procedures with the (a) equations relating to the standard kinematic approach and the (b) equations relating to the layers model. We will concentrate on the deviatoric components since the mean stresses are clearly given by the same relationship in each model.

for the yield criterion, we have

$$f = \tfrac{3}{2} \| \boldsymbol{\xi} \| - \sigma_o; \qquad \boldsymbol{\xi} = \mathbf{s} - \boldsymbol{\alpha} \tag{15.109a}$$

$$f_p = \tfrac{3}{2} \| \mathbf{s}_p \| - \sigma_o; \qquad \mathbf{s}_p = \frac{1}{\omega_p} (\mathbf{s} - 2\mu\omega_e \mathbf{e}) \tag{15.109b}$$

For the (basic) tangent relationships, we have

$$\dot{\mathbf{s}} = 2\mu \left[\mathbf{1} - \frac{3\mu}{3\mu + A'} \frac{\boldsymbol{\xi} \otimes \boldsymbol{\xi}}{\boldsymbol{\xi} : \boldsymbol{\xi}} \right] : \dot{\mathbf{e}} \tag{15.110a}$$

$$\dot{\mathbf{s}} = \omega_p \dot{\mathbf{s}}_p + 2\mu\omega_e \dot{\mathbf{e}} = 2\mu \left[\mathbf{1} - \frac{3\mu}{3\mu + A'} \frac{\mathbf{s}_p \otimes \mathbf{s}_p}{\mathbf{s}_p : \mathbf{s}_p} \right] : \dot{\mathbf{e}} \tag{15.110b}$$

Equation (15.110a) can be simply obtained from (15.84) with $\gamma = 1$, while (15.110b) involves the standard relationship for $\dot{\mathbf{s}}$ given in (6.43).

In conjunction with the above, the evolution of the back stress and its equivalent for the two-layered model are given by

$$\dot{\boldsymbol{\alpha}} = \tfrac{2}{3} A' \dot{\mathbf{e}}_p = \frac{A'}{\sigma_e} \dot{\lambda} \boldsymbol{\xi} = \frac{2\mu A'}{(3\mu + A')} \frac{\boldsymbol{\xi} \otimes \boldsymbol{\xi}}{\boldsymbol{\xi} : \boldsymbol{\xi}} : \dot{\mathbf{e}} \tag{15.111a}$$

$$(2\mu\omega_e \mathbf{e})^{\cdot} = 2\mu\omega_e \dot{\mathbf{e}} = \frac{2\mu A'}{(3\mu + A')} \dot{\mathbf{e}} \tag{15.111b}$$

15.10.3 Other models

The previous model involved a set of sublayers in each of which the response was assumed to follow that of an elastic/perfectly plastic material. Mroz [M2, M3] has introduced a related model in which the response of each sublayer is governed by

conventional kinematic hardening. As with the previous sublayer model, a piecewise linear uniaxial loading curve can be specified (Figure 15.6a). In the multiaxial space (represented, for convenience, via the circles in (Figure 15.6b)), the initially concentric surfaces have translated. The inner surface which represents point A in Figure 15.8a, has on reaching the next surface (representing point B in Figure 15.6a)), moved in an outward direction so that the two surfaces touch each other but do not intersect. Related approaches have been applied by Krieg [K1] and Dafialas and Popov [D1, D2] with their two-surface and bounding-surface models.

15.11 COMPUTER EXERCISES

In Section 6.9, we gave a set of numerical examples illustrating the application of the various numerical strategies. These examples all involved plane stress with only two stress variables (by setting τ and γ to zero). They also involved no hardening. Once hardening, and especially kinematic hardening, is introduced, it becomes more difficult to obtain the solution 'by hand'. However, it is a simple exercise to write simple computer programs, illustrating the methods—particularly if the restriction to two stress variables are introduced. This exercise (which has been completed by the author) involves the following.

1. Write a computer program whereby the material properties are input as E, ν, A' and m (the mixed hardening parameter—see Section 15.2); the initial 'stresses' are input as $\boldsymbol{\sigma}_A$ (with $\boldsymbol{\alpha}_A$ assumed zero) and the strain increment is input as $\Delta\boldsymbol{\varepsilon}$. The program should then obtain the plastic strain-rate multiplier, $\Delta\lambda$ and the final 'stresses' $\boldsymbol{\sigma}_C$ and $\boldsymbol{\alpha}_C$ at C. The general method of Section 15.6 should first be used, and second the special method of Section 15.7. (Both methods should give (effectively) the same answers.)
2. Following on from these returns, apply the method of Section 15.9 to obtain the consistent tangent modular matrix.

The author has written the above computer programs and has adopted the input data of Section 6.9 with (see (6.141)):

$$E = 200\,000\ \text{N/mm}^2; \qquad \nu = 0.0; \qquad \sigma_o = 200\ \text{N/mm}^2 \tag{15.112}$$

and (see (6.142)):

$$\boldsymbol{\sigma}_A^T = (120, -80) \tag{15.113}$$

while (see (6.156)):

$$\Delta\boldsymbol{\varepsilon}^T = (0.0014, 0.0014) \tag{15.114}$$

For the first analyses, no hardening was considered so that $A' = 0$. In these circumstances, we obtained:

$$\boldsymbol{\sigma}_C^T = (226.2, 153.3); \qquad \Delta\lambda = 0.001\,62 \tag{15.115}$$

which corresponds with the solutions given in (6.171) and (6.172).

For this case, the consistent tangent matrix was that previously given in (6.177) and (6.180).

To apply hardening, A' was set to 20 000 N/mm^2. Isotropic hardening was initially considered so that $m = 1$. The following results were then obtained:

$$\boldsymbol{\sigma}_C^{\mathrm{T}} = (249.6,\ 164.4); \qquad \Delta\lambda = 0.000\,987; \qquad \sigma_e = \sigma_o = 219.7 \tag{15.116}$$

The consistent tangent modular matrix was then found to be

$$C_t = \begin{bmatrix} 0.290\,40\mathrm{e}5 & -0.105\,90\mathrm{e}5 \\ -0.105\,90\mathrm{e}5 & -0.950\,10\mathrm{e}5 \end{bmatrix} \tag{15.117}$$

(This matrix could be obtained by the method of Section 15.9 which, corresponds for isotropic hardening with that of Section 6.7.2 or by the method of Section 6.8.2.1.)

With pure kinematic hardening, so that $m = 0$, the following results were obtained:

$$\boldsymbol{\sigma}_C^{\mathrm{T}} = (249.6,\ 164.4); \qquad \boldsymbol{\alpha}_C^{\mathrm{T}} = (22.43,\ 15.77); \ \Delta\lambda = 0.000\,9873 \tag{15.118}$$

The resulting consistent tangent modular matrix was

$$C_t = \begin{bmatrix} 0.286\,8\mathrm{e}05 & -9353.0 \\ -9353.0 & 0.9077\mathrm{e}5 \end{bmatrix} \tag{15.119}$$

When mixed hardening was considered, with $m = 0.5$, we obtained:

$$\boldsymbol{\sigma}_C^{\mathrm{T}} = (249.6,\ 164.4); \qquad \boldsymbol{\alpha}_C^{\mathrm{T}} = (11.21,\ 7.39); \qquad \Delta\lambda = 0.000\,987; \qquad \sigma_e = \sigma_o = 209.9 \tag{15.120}$$

The resulting consistent tangent modular matrix was

$$\mathbf{C}_t = \begin{bmatrix} 0.288\,6\mathrm{e}05 & -9982.0 \\ -9982.0 & 0.9294\mathrm{e}5 \end{bmatrix} \tag{15.121}$$

15.12 VISCOPLASTICITY

Work on viscoplasticity can be found in [P1–P4, Z1.14]. Having introduced a time-dependent response, we can replace the flow rule:

$$\dot{\boldsymbol{\varepsilon}}_p = \dot{\lambda}\frac{\partial f}{\partial \boldsymbol{\sigma}} = \dot{\lambda}\mathbf{a} \tag{15.122}$$

with

$$\dot{\boldsymbol{\varepsilon}}_{vp} = \gamma\langle\phi\rangle\frac{\partial f}{\partial \boldsymbol{\sigma}} = \dot{\lambda}\mathbf{a} \tag{15.123}$$

where γ is a 'viscosity parameter' and

$$\langle\phi\rangle = 0 \quad \text{if} \quad f \leqslant 0 \tag{15.124a}$$

$$\langle\phi\rangle = \phi \quad \text{if} \quad f > 0 \tag{15.124b}$$

(If a non-associated law was adopted we would simply replace $\mathbf{a}$ in (15.123) with $\mathbf{b} = \partial g/\partial\boldsymbol{\sigma}$, where g is the plastic potential.) In practice, instead of expressing ϕ as a function of the yield function f, we might use a power law to express it in terms of the

effective stress, σ_e and the yield stress, σ_o, so that either:

$$\phi = \left(\frac{\sigma_e}{\sigma_o}\right)^N - 1 \tag{15.125a}$$

or

$$\phi = \left(\frac{\sigma_e}{\sigma_o} - 1\right)^N \tag{15.125b}$$

where, as usual, σ_e is a function of the stresses $\boldsymbol{\sigma}$ while σ_o is a function of some hardening parameter (here in an 'isotropic manner'). Equation (15.125b) is often known as the Perzyna model [P3, P4] while (15.125a) has been used by Pierce *et al.* [P1] and Peric and Owen [P2]. Using either (15.125a) or (15.125b), we could replace (15.124) with:

$$\langle\phi\rangle = 0 \quad \text{if} \quad \sigma_e \leqslant \sigma_o \tag{15.126a}$$

$$\langle\phi\rangle = \phi \quad \text{if} \quad \sigma_e > \sigma_o \tag{15.126b}$$

With time-independent plasticity, in the one-dimensional case, we would have $\sigma_e = \sigma_o = \sigma$ and

$$\sigma = \text{fn}(\varepsilon_p) \tag{15.127}$$

For the equivalent viscoplastic formulation, from (15.125a)

$$\sigma = \sigma_e = \sigma_o(\phi + 1)^{1/N} = \text{fn}(\varepsilon_{vp})(\phi + 1)^{1/N} = \text{fn}(\varepsilon_{vp})\left(1 + \left(\frac{\dot{\varepsilon}_{vp}}{\gamma}\right)\right)^{1/N} \tag{15.128a}$$

where we have also used (15.123) with $\mathbf{a} = 1$ in the one-dimensional case. From (15.125b) we would obtain:

$$\sigma = \sigma_e = \sigma_o(\phi^{1/N} + 1) = \text{fn}(\varepsilon_{vp})(\phi^{1/N} + 1) = \text{fn}(\varepsilon_{vp})\left(1 + \left(\frac{\dot{\varepsilon}_{vp}}{\gamma}\right)\right)^{1/N} \tag{15.128b}$$

As $\dot{\varepsilon}_{vp}$ tends to zero or γ tends to infinity, both (15.128a) and (15.128b) tend to the 'static solution' of (15.127). Also, as N tends to infinity (15.128) tends to the static solution. However, as pointed out by Peric and Owen [P2], the latter is not the case for (15.128b).

In order to integrate the flow rules, we can, as with time-independent plasticity, introduce a forward-Euller procedure, a backward-Euler procedure or some generalised mid-point rule (see Section 6.6.5 and Z1.14). With viscoplasticity, the forward-Euler procedure leads to a particularly simple formulation (see Z1.14). However, we will here follow the techniques that we have usually used for time-independent plasticity and will introduce a backward-Euler procedure which allows the use of relatively large time steps. The method turns out to be very similar to that previously described for the rate-independant case. Adopting such a backward-Euler procedure and following a very similar procedure to that of Section 6.6.6, we would attempt to satisfy the equations:

$$\mathbf{r} = \boldsymbol{\sigma}_c - (\boldsymbol{\sigma}_b - \Delta\lambda \mathbf{a}_C) = 0 \tag{15.129}$$

$$g = \Delta\lambda - \Delta t \gamma \langle\phi\rangle_C = 0 \tag{15.130}$$

In (15.130) we have introduced the time increment Δt, because we are now dealing with a genuinely time-dependent problem. In contrast, for the time-independent problem,

time was only conceptual (see comments below (6.4) in Section 6.3) and there was therefore no need to directly introduce Δt although it was implicitly contained within the previous $\Delta\lambda$. To satisfy (15.129) and (15.130), we would apply the truncated Taylor series to both (15.129) and (15.130) so that:

$$\begin{aligned}\dot{\boldsymbol{\sigma}}_C &= -\left[\mathbf{I}+\Delta\lambda\left.\frac{\partial \mathbf{a}}{\partial \boldsymbol{\sigma}}\right|_C\right]^{-1}\mathbf{r}_{old}-\dot{\lambda}\left[\mathbf{I}+\Delta\lambda\left.\frac{\partial \mathbf{a}}{\partial \boldsymbol{\sigma}}\right|_C\right]^{-1}\mathbf{C}\mathbf{a}_C \\ &= -\mathbf{Q}^{-1}\mathbf{r}_{old}-\dot{\lambda}\mathbf{Q}^{-1}\mathbf{C}\mathbf{a}_C=-\mathbf{Q}^{-1}\mathbf{r}_{old}-\dot{\lambda}\mathbf{R}\mathbf{a}_C\end{aligned} \tag{15.131}$$

and

$$-g_{old}=\dot{\lambda}-\Delta t\gamma\phi'_e\mathbf{a}^T\dot{\boldsymbol{\sigma}}_C-\Delta t\gamma\phi'_oA'_C\dot{\lambda} \tag{15.132}$$

where

$$\phi'_e=\frac{\partial\phi}{\partial\sigma_e};\qquad \phi'_o=\frac{\partial\phi}{\partial\sigma_o} \tag{15.133}$$

so that, using (15.131), we could obtain:

$$\dot{\lambda}=\frac{-g_{old}-\Delta t\gamma\phi'_e\mathbf{a}^T\mathbf{Q}^{-1}\mathbf{r}_{old}}{(1+\Delta t\gamma\phi'_e\mathbf{a}^T\mathbf{R}\mathbf{a}-\Delta t\gamma\phi'_oA')}=\frac{1}{a}(-g_{old}-\Delta t\gamma\phi'_e\mathbf{a}^T\mathbf{Q}^{-1}\mathbf{r}_{old}) \tag{15.134}$$

and hence we can update $\Delta\lambda$ and, via (15.131), we can update $\boldsymbol{\sigma}_C$.

15.12.1 The consistent tangent matrix

Differentiation of (15.129), with $\mathbf{r}$ zero and $\boldsymbol{\sigma}_B$ now free, we obtain:

$$\dot{\boldsymbol{\sigma}}=\mathbf{R}\dot{\boldsymbol{\varepsilon}}-\dot{\lambda}\mathbf{R}\mathbf{a}=\mathbf{Q}^{-1}\mathbf{C}\dot{\boldsymbol{\varepsilon}}-\dot{\lambda}\mathbf{Q}^{-1}\mathbf{C}\mathbf{a} \tag{15.135}$$

while substituting from (15.135) into (15.132) (with $g_{old}=0$), we have:

$$\dot{\lambda}=\frac{\gamma\Delta t\phi'_e}{a}\mathbf{a}^T\mathbf{R}\dot{\boldsymbol{\varepsilon}} \tag{15.136}$$

with the scalar a having been defined in (15.134). Substitution into (15.135) then leads to the relationship:

$$\dot{\boldsymbol{\sigma}}=\left[\mathbf{R}-\frac{\gamma\Delta t\phi'_e}{a}\mathbf{R}\mathbf{a}\mathbf{a}^T\mathbf{R}\right]\dot{\boldsymbol{\varepsilon}}=\mathbf{C}_t\dot{\boldsymbol{\varepsilon}} \tag{15.137}$$

which can be re-expressed as

$$\dot{\boldsymbol{\sigma}}=\left[\mathbf{R}-\frac{1}{\dfrac{1}{\gamma\Delta t\phi'_e}+\mathbf{a}^T\mathbf{R}\mathbf{a}-\dfrac{\phi'_o}{\phi'_e}A'}\mathbf{R}\mathbf{a}\mathbf{a}^T\mathbf{R}\right]\dot{\boldsymbol{\varepsilon}} \tag{15.138}$$

The term $1/(\gamma\Delta t\phi'_e)$ tends to zero as $\gamma\to\infty$ or as $\Delta t\to\infty$, while in these circumstances $\phi\to 0$ so that $\sigma_e\to\sigma_o$ and assuming either (15.125a) or (15.125b):

$$\frac{\phi'_o}{\phi'_e}=-\left(\frac{\sigma_e}{\sigma_o}\right)=-1 \tag{15.139}$$

so that (15.128) then corresponds with the rate independent form of (6.110).

15.12.2 Implementation

Peric and Owen [P2], who used (15.125a), reported numerical difficulties as N became large and the system became stiff. They considered the latter to occur when $N > 5$. In these circumstances, they first applied the backward Euler return to the underlying, static or rate-independent problem. To this end the yield function would be defined by $f = \phi$ from (15.125a). They then used the one-dimensional relationship of (15.128a) to scale the resulting 'static stresses', $\boldsymbol{\sigma}_{C,static}$, so that:

$$\boldsymbol{\sigma}_C = \left(1 + \frac{\Delta\varepsilon_{ps}}{\gamma\Delta t}\right)\boldsymbol{\sigma}_{C,static} \tag{15.140}$$

These stresses would then provide a starting-point for the previous viscoplastic, backward-Euler return (Section 15.12).

15.13 SPECIAL NOTATION

$\mathbf{a} = \partial f/\partial\sigma = -\partial f/\partial\boldsymbol{\alpha}$ which is defined as a column vector
A' = hardening parameter, A'_k = isotropic parameter, A'_i = isotropic parameter
A_1, A_2 = scalars for plane-stress analysis (see (6.124) and (6.125))
C_p, C_z = Respectively Prager and Ziegler coefficients for kinematic hardening
C_1, C_2 = stress parameters for plane-stress analysis (see (15.68))
$\mathbf{C}$ = elastic constitutive matrix (or tensor)
$\mathbf{C}_t$ = tangential constitutive tensor (or matrix)
$\mathbf{C}_{tc}$ = consistent tangential constitutive tensor (or matrix)
$\mathbf{C}_3$ = constitutive matrix with three stress components; $\mathbf{C}_4$ = constitutive matrix with four stress components (Section 6.8)
D_1–D_4 = scalar (15.51b) in Section 15.6
$\mathbf{e}$ = deviatoric strains
f = yield function; f_2 = squared form (see (15.66))
g = yield function as given by (15.69)
H' = hardening parameter (slope of uniaxial stress/plastic–strain relationship); $\bar{H}' = H'$ for isotropic hardening
k = bulk modulus
m = ratio of plastic strain for isotopic response
$\mathbf{Q}$ = special matrix (see (15.53))
$r = (1 + \nu)/(1 - \nu)$ (Section 15.7)
$\mathbf{r}$ = residual vector; $\mathbf{r}_\sigma$ for stresses (15.46a); $\mathbf{r}_\alpha$ for back stresses (15.46b)
$\mathbf{R}$ = special matrix (see (15.57))
$\mathbf{s}$ = deviatoric stresses
$\boldsymbol{\alpha}$ = back stress
$\boldsymbol{\alpha}'$ = deviatoric back stress
β = scalar for consistent tangent (see (15.83))
ε_{ps} = equivalent plastic strain; ε_{psi} = isotropic ε_{ps}
$\boldsymbol{\varepsilon}$ = vector or tensor of strains

$\dot{\boldsymbol{\varepsilon}}$ = strain rate
$\dot{\boldsymbol{\varepsilon}}_t$ = total strain rate (the subscript t is often dropped)
$\dot{\boldsymbol{\varepsilon}}_p$ = plastic strain rate; $\dot{\boldsymbol{\varepsilon}}_{pk}$—kinematic, $\dot{\boldsymbol{\varepsilon}}_{pi}$—isotropic
$\mathbf{e}$ = deviatoric strains
$\dot{\gamma}$ = scalar for radial return
$\dot{\lambda}$ = plastic strain rate multiplier
$\Delta\lambda$ = incremental plastic strain rate multiplier, $\Delta\lambda' = \Delta\lambda/\sigma_e$
μ = shear modulus
σ_e = effective stress
σ_o = yield stress
σ = stress
$\bar{\boldsymbol{\sigma}} = \boldsymbol{\sigma} - \boldsymbol{\alpha}$
θ = scalar for radial return (Section 15.4)
$\boldsymbol{\xi} = \mathbf{s} - \boldsymbol{\alpha}'$

Subscripts

e = elastic
n = new
o = old
p = plastic

Superscripts

$\dot{\cdot}$ = rate (or change)

15.14 REFERENCES

[A1] Axelsson, K., *On Constitutive Modelling in Metal Plasticity*, Pub. 79:2, Chalmers Univ. of Tech., Goteborg, Sweden (1979).
[B1] Bauschinger, J., Uber die Weranderung der Elasticitatsgrenze und des Elasticitatsmoduls Verschiedener Metalle, *Zivilingenieur*, **27**, 289–349 (1881).
[B2] Besseling, J. F., A theory of elastic, plastic and creep deformations of an initially isotropic material showing anisotropic strain-hardening, creep recovery and secondary creep, *JAM*, 529–536 (1958).
[D1] Dafialis, Y. F. & Popov, E. P., A model of nonlinearly hardening materials for complex loadings, *Acta Mechanica*, **21** (21), 173–192 (1975).
[D2] Dafialis, Y. F. & Popov, E. P., Plastic internal variables formalism of cyclic plasticity, *JAM*, **32**, 645–651 (1976).
[H1] Harper, P. G., *An Analysis of the Sublayer Model for Plasticity under Multiaxial Stress*, Report No. RD/B/N4270, CEGB, Berkeley Nuclear Laboratories (1978).
[H2] Hodge, P. G., Jr, Discussion to Prager's paper, *JAM*, **23**, 482–483 (1957).
[K1] Krieg, R. D., A practical two surface plasticity theory, *JAM*, **31**, 641–646 (1975).
[M1] Mroz, Z., On the description of anisotropic workhardening, *Journal Mech. Phys. Sol.*, **15**, 163–175 (1967).

[M2] Mroz, Z., An attempt to describe the behaviour of metals under cyclic loads using a more general workhardening model, *Acta Mechanica*, **7**, 199–212, (1969).

[M3] Mroz, Z., *Mathematical Models of Inelastic Material Behaviour*, Solid Mechanics Div., University of Waterloo, Ontario, Canada (1973).

[O1] Owen, D. R. J., Prakash, A. & Zienkiewicz, O. C., Finite element analysis of nonlinear composite materials by use of overlay systems, *Comp. & Struct.*, **4**, 1251–1267 (1974).

[P1] Peirce, D., Shih, C. F. & Needleman, A., A tangent modulus method for rate dependent solids, *Comp. & Struct.*, **33**, 799–815 (1984).

[P2] Peric, D. & Owen, D. R. J., A model for large deformations of elasto-viscoplastic solids at finite strains: computational issues, *Finite Inelastic Deformations: Theory and Applications*, Springer-Verlag, Berlin (1992).

[P3] Perzyna, P., Fundamental problems in viscoplasticity, *Advances in Applied Mechanics*, 9, Academic Press, New York, pp. 243–377 (1968).

[P4] Perzyna, P. Thermodynamic theory of plasticity, *Advances in Applied Mechanics*, *11*, Academic Press, New York, pp. 313–354 (1971).

[P5] Prager, W., The theory of plasticity: a survey of recent achievements, *Proc. Instn. of Mech. Engrs.*, **169**, 41–57 (1955).

[P6] Prager, W., A new method for analysing stress and strain in workhardening, plastic solids, *J. Appl. Mech.*, **23**, 493 (1956).

[S1] Simo, J. C. & Taylor, R. L., Consistent tangent operators for rate independent plasticity, *Comp. Meth. in Appl. Mech. & Engng.*, **48**, 101–118 (1985).

[Z1] Ziegler, H., A modification of Prager's hardening rule, *Quart. of Appl. Mech.*, **17**, 55–65 (1959).

[Z2] Zienkiewicz, O. C., Nayak, G. C. & Owen, D. R. J., Composite and overlay models in numerical analysis of elasto-plastic continua, *Foundations of Plasticity*, ed. A. Sawczuk, Noordhoff, Leiden, pp. 107–123 (1973).

16 Large rotations

Basic reading on 'large rotations' can be found in [A1, A2, B1–B3, G1, P1, R1, R2, S1, S6]. The main aim of the present Chapter is to pave the way for the work in the next chapter on three-dimensional beams and some of the work in Chapter 18 on shells. The original intention was to avoid, in the present chapter, any direct mention of finite elements and the associated concepts such as 'nodes'. This has largely been achieved in Sections 16.1–16.13, but the work in Section 6.14 on curvature is fairly closely linked to the developments in Section 17.3 of Chapter 17. Rather than attempt to digest the complete chapter in one sitting, the reader might prefer to read Sections 16.1–16.10 as a general introduction and then move on to Chapter 17 before returning to the later sections of the present chapter as and when they are required.

16.1 NON-VECTORIAL LARGE ROTATIONS

Figure 16.1 shows that the result of a set of large rotations depends on the order in which they are applied. Hence, such rotations cannot be treated as vectors. This phenomenon has important implications for the finite element analysis of space frames and shells.

16.2 A ROTATION MATRIX FOR SMALL (INFINITESIMAL) ROTATIONS

In Figure 16.2b, a vector $\mathbf{r}_o$ is rotated in the 1–2 plane through $\Delta\theta$ to become a vector $\mathbf{r}_n$. We could therefore write:

$$\mathbf{r}_n^T = r_o\{\cos(\theta_o + \Delta\theta), \sin(\theta_o + \Delta\theta), 0\} \tag{16.1}$$

Alternatively, an approximation would involve:

$$\mathbf{r}_n = \mathbf{r}_o + \Delta\mathbf{r} = r_o\mathbf{t} + r_o\Delta\theta\mathbf{n} \tag{16.2}$$

where $r_o = \|\mathbf{r}_o\|$, $\mathbf{n}$ is the unit vector orthogonal to both $\mathbf{r}_o$ and the z-direction (or $\mathbf{e}_3$) so that $\mathbf{t}^T\mathbf{n} = \mathbf{e}_3^T\mathbf{n} = 0$ and hence:

$$\mathbf{n}^T = \{-\sin\theta_o, \cos\theta_o, 0\} \tag{16.3}$$

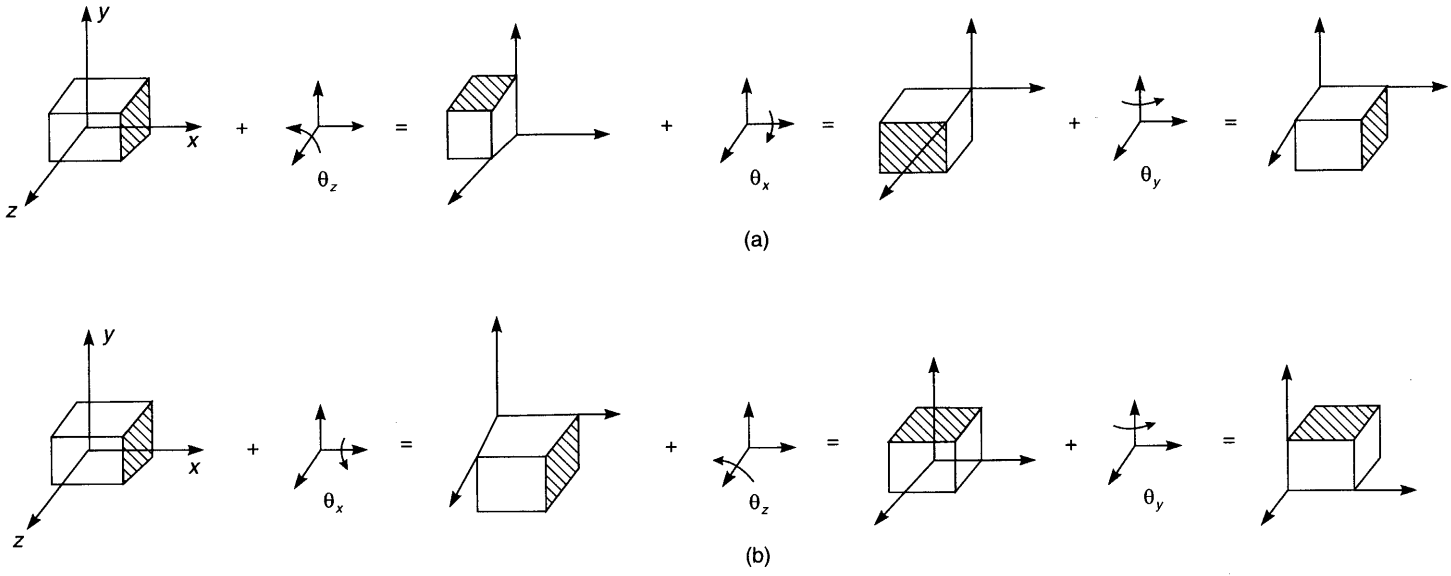

Figure 16.1 The non-commutativity of vector rotations. (a) $\theta_z, \theta_x, \theta_y$; (b) $\theta_x, \theta_z, \theta_y$.

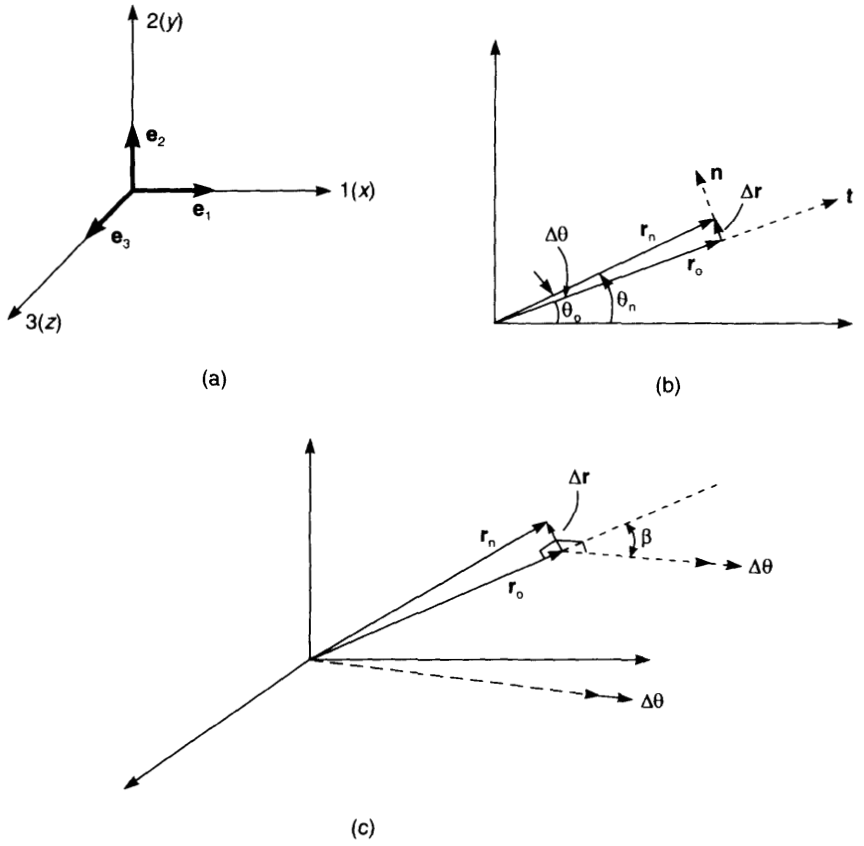

Figure 16.2 Axes and two- and three-dimensional rotations. (a) Axes and unit base vectors; (b) two-dimensional rotation; (c) small three-dimensional rotation.

Hence, (16.2) can be rewritten as

$$\mathbf{r}_n = \left[\begin{bmatrix} 1 & 0 & 0 \\ 0 & 1 & 0 \\ 0 & 0 & 1 \end{bmatrix} + \begin{bmatrix} 0 & -\Delta\theta & 0 \\ \Delta\theta & 0 & 0 \\ 0 & 0 & 0 \end{bmatrix}\right]\mathbf{r}_0 \tag{16.4}$$

or

$$\mathbf{r}_n = \mathbf{R}\mathbf{r}_o = [\mathbf{I} + \mathbf{S}(\Delta\boldsymbol{\theta})]\mathbf{r}_o \tag{16.5}$$

This relationship can be accompanied by

$$\boldsymbol{\theta}_n = \boldsymbol{\theta}_o + \Delta\boldsymbol{\theta} = \theta_o\mathbf{e}_3 + \Delta\theta\mathbf{e}_3 = (\theta_o + \Delta\theta)\mathbf{e}_3 \tag{16.6}$$

because in two dimensions rotations are additive. For the effectively two-dimensional problem of Figure 16.2b, there is little point in adopting (16.4) rather than the simpler exact form of (16.1). However, (16.2) can be generalised (Figure 16.2c) to

$$\mathbf{r}_n = \mathbf{r}_o + \Delta\mathbf{r} = \mathbf{r}_o + (\Delta\boldsymbol{\theta} \times \mathbf{r}_o) \tag{16.7}$$

where the symbol $\times$ denotes a cross-product so that $(\Delta\boldsymbol{\theta} \times \mathbf{r}_o)$ is orthogonal to both $\Delta\boldsymbol{\theta}$ and $\mathbf{r}_o$ and is of magnitude $\Delta\theta r_o \sin\beta$, where (Figure 16.2c) β is the angle between $\Delta\boldsymbol{\theta}$ and $\mathbf{r}_o$. Equation (16.7) can be recast in the form of (16.5) with

$$\mathbf{S}(\Delta\boldsymbol{\theta}) = \begin{bmatrix} 0 & -\Delta\theta_3 & \Delta\theta_2 \\ \Delta\theta_3 & 0 & -\Delta\theta_1 \\ -\Delta\theta_2 & \Delta\theta_1 & 0 \end{bmatrix} \tag{16.8}$$

With infinitesimal rotations, $\Delta\boldsymbol{\theta}$ represents the 'spin'.

16.3 A ROTATION MATRIX FOR LARGE ROTATIONS (RODRIGUES FORMULA [R2])

In this section we will derive equivalent expressions to (16.5) and (16.8) that apply even when the rotations are large. To this end, we will assume that rotation from $\mathbf{r}_o$ to $\mathbf{r}_n$ involves a 'pseudo-vector' [A1],

$$\boldsymbol{\theta} = \begin{bmatrix} \theta_1 \\ \theta_2 \\ \theta_3 \end{bmatrix} = \theta_1\mathbf{e}_1 + \theta_2\mathbf{e}_2 + \theta_3\mathbf{e}_3 = \theta\mathbf{e} \tag{16.9}$$

whre $\mathbf{e}$ is a unit vector about which the rotation occurs and (Figure 16.3):

$$\theta = \|\boldsymbol{\theta}\| = (\theta_1^2 + \theta_2^2 + \theta_3^2)^{1/2} = (\boldsymbol{\theta}^T\boldsymbol{\theta})^{1/2} \tag{16.10}$$

From Figure 16.3b,

$$\Delta\mathbf{r} = \Delta\mathbf{a} + \Delta\mathbf{b} \tag{16.11}$$

where $\Delta\mathbf{b}$ is orthogonal to $\Delta\mathbf{a}$. Also from Figure 16.3b, the length of $\Delta\mathbf{b}$ (Δb) is given by

$$\Delta b = R\sin\theta \tag{16.12}$$

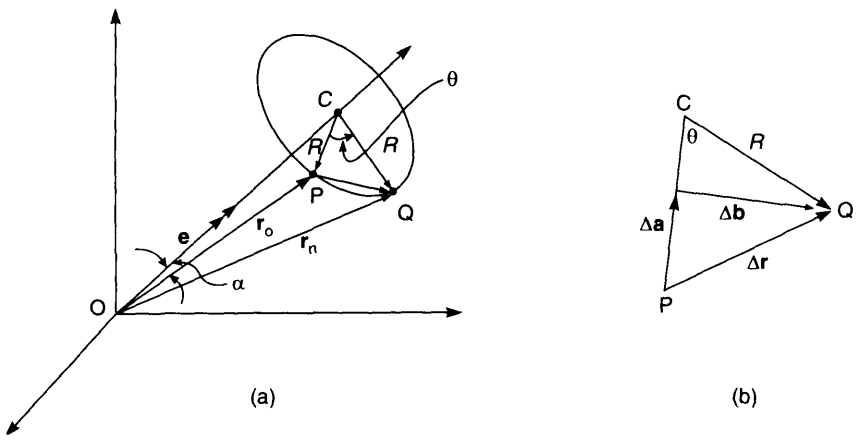

Figure 16.3 Three-dimensional rotation. (a) Rotation about OC; (b) detail.

so that:

$$\Delta\mathbf{b} = \frac{\Delta b}{\|\mathbf{r}_o \times \mathbf{e}\|}(\mathbf{e} \times \mathbf{r}_o) = \frac{R \sin\theta}{\|\mathbf{r}_o \times \mathbf{e}\|}(\mathbf{e} \times \mathbf{r}_o) \tag{16.13}$$

But (see Figure 16.3a):

$$\|\mathbf{e} \times \mathbf{r}_o\| = r_o \sin\alpha = R \tag{16.14}$$

so that (16.13) can be ex-expressed as

$$\Delta\mathbf{b} = \sin\theta(\mathbf{e} \times \mathbf{r}_o) = \frac{\sin\theta}{\theta}(\boldsymbol{\theta} \times \mathbf{r}_o) \tag{16.15}$$

From Figure 16.3, the vector $\Delta\mathbf{a}$ is orthogonal to both $\mathbf{e}$ and $\Delta\mathbf{b}$. Hence:

$$\Delta\mathbf{a} = \frac{\Delta a}{\|\mathbf{e} \times \mathbf{r}_o\|}(\mathbf{e} \times (\mathbf{e} \times \mathbf{r}_o)) = \frac{\Delta a}{R}(\mathbf{e} \times (\mathbf{e} \times \mathbf{r}_o)) \tag{16.16}$$

But, from Figure 16.3b,

$$\Delta a = R(1 - \cos\theta) \tag{16.17}$$

so that (16.16) can be re-expressed as

$$\Delta\mathbf{a} = (1 - \cos\theta)(\mathbf{e} \times (\mathbf{e} \times \mathbf{r}_o)) = \frac{(1 - \cos\theta)}{\theta^2}(\boldsymbol{\theta} \times (\boldsymbol{\theta} \times \mathbf{r}_o)) \tag{16.18}$$

Hence, from (16.11), (16.15) and (16.18):

$$\mathbf{r}_n = \mathbf{r}_o + \Delta\mathbf{r} = \mathbf{r}_o + \frac{\sin\theta}{\theta}(\boldsymbol{\theta} \times \mathbf{r}_o) + \frac{(1 - \cos\theta)}{\theta^2}(\boldsymbol{\theta} \times (\boldsymbol{\theta} \times \mathbf{r}_o) \tag{16.19}$$

But, from (16.7) and (16.8), we know that:

$$\boldsymbol{\theta} \times \mathbf{r}_o = \mathbf{S}(\boldsymbol{\theta})\mathbf{r}_o \tag{16.20}$$

and therefore:

$$\mathbf{r}_n = \mathbf{R}\mathbf{r}_o \tag{16.21}$$

where

$$\mathbf{R} = \left[\mathbf{I} + \frac{\sin\theta}{\theta}\mathbf{S}(\boldsymbol{\theta}) + \frac{(1 - \cos\theta)}{\theta^2}\mathbf{S}(\boldsymbol{\theta})\mathbf{S}(\boldsymbol{\theta})\right]$$

$$= [\mathbf{I} + \sin\theta\mathbf{S}(\mathbf{e}) + (1 - \cos\theta)\mathbf{S}(\mathbf{e})\mathbf{S}(\mathbf{e})] \tag{16.22}$$

and $\mathbf{e}$ is the unit vector obtained from the pseudo-vector $\boldsymbol{\theta}$ (see (16.9)).

An alternative derivation involves the rotation and transformation relationships of Sections 4.3.1 and 4.3.2. In particular, we will first define a triad of 'local' unit vectors (Figure 16.4) with $\mathbf{i}_1$ as the principal axis of rotation, $\mathbf{i}_1$ being equal to the previous $\mathbf{e}$, so that:

$$\boldsymbol{\theta} = \theta\mathbf{i}_1 \tag{16.23}$$

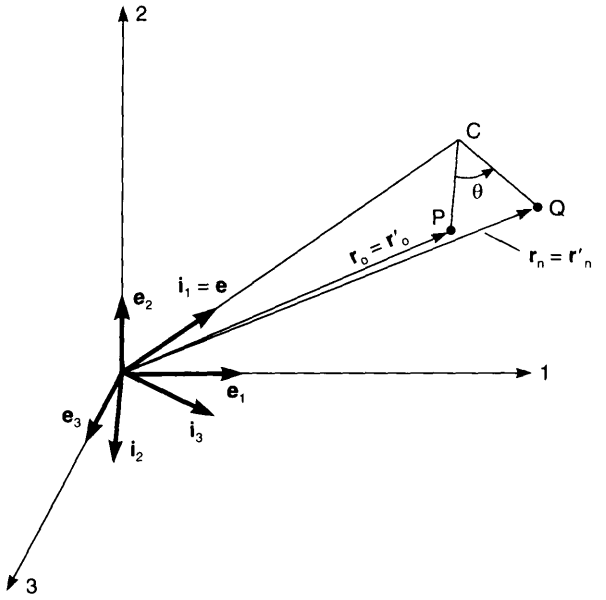

Figure 16.4 Three-dimensional rotation using the auxiliary triad, $\mathbf{i}_1$–$\mathbf{i}_3$

Possible solutions for the two vectors $\mathbf{i}_2$ and $\mathbf{i}_3$ that make up the triad are:

$$\mathbf{i}_2^{\mathrm{T}} = \left(\frac{\mathbf{i}_1(2)}{\alpha}, \frac{-\mathbf{i}_1(1)}{\alpha}, 0 \right) \tag{16.24}$$

$$\mathbf{i}_3^{\mathrm{T}} = \left(\frac{-\mathbf{i}_1(1)\mathbf{i}_1(3)}{\alpha}, \frac{\mathbf{i}_1(2)\mathbf{i}_1(3)}{\alpha}, -\alpha \right) \tag{16.25}$$

where $\mathbf{i}_1(2)$, for example, is the second component of $\mathbf{i}_1$ and

$$\alpha^2 = \mathbf{i}_1(1)^2 + \mathbf{i}_1(2)^2 \tag{16.26}$$

The unit vectors $\mathbf{i}_1$ and $\mathbf{i}_2$–$\mathbf{i}_3$ from (16.24) and (16.25) satisfy the orthogonality conditions, $\mathbf{i}_1^{\mathrm{T}}\mathbf{i}_2 = \mathbf{i}_1^{\mathrm{T}}\mathbf{i}_3 = \mathbf{i}_2^{\mathrm{T}}\mathbf{i}_3 = 0$.

By Euler's theorem, we can now rotate the vector $\mathbf{r}_o$ about the principal axis i_1 so that (see (Figure 16.4)):

$$\mathbf{r}'_n = \mathbf{R}'\mathbf{r}'_o = \begin{bmatrix} 1 & 0 & 0 \\ 0 & \cos\theta & -\sin\theta \\ 0 & \sin\theta & \cos\theta \end{bmatrix} \mathbf{r}'_o \tag{16.27}$$

and the prime indicates that $\mathbf{r}'_o$ and $\mathbf{r}'_n$ are expressed in 'local' $\mathbf{i}_1$–$\mathbf{i}_3$ coordinates. However, from (4.36) we can transform $\mathbf{R}'$ from 'local' to 'global' coordinates so that:

$$\mathbf{r}_n = \mathbf{R}\mathbf{r}_o = \mathbf{T}^{\mathrm{T}}\mathbf{R}'\mathbf{T}\,\mathbf{r}_o \tag{16.28}$$

where from (4.35):

$$\mathbf{T}^{\mathrm{T}} = [\mathbf{i}_1, \mathbf{i}_2, \mathbf{i}_3] \tag{16.29}$$

If (16.23)–(16.26) are substituted into (16.29) and (16.29) and (16.27) are substituted into (16.28), the rotation matrix $\mathbf{R}$ in (16.28) will be found to coincide with the expression previously obtained in (16.22).

In the last derivation, we used Euler's theorem which states that 'if a rigid body is rotated into a new configuration about a fixed point then there is only one line passing through the point which remains invariant during the motion' (the unit vector $\mathbf{e}$ in Figures 16.3 and 16.4). It follows that the rotation matrix, $\mathbf{R}$, rotates $\mathbf{e}$ on to itself. Consequently,

$$\mathbf{R}(\mathbf{e}, \boldsymbol{\theta})\mathbf{e} - \mathbf{e} = \mathbf{R}(\boldsymbol{\theta})\boldsymbol{\theta} - \boldsymbol{\theta} = \mathbf{0} \tag{16.30}$$

so that $\mathbf{e}$ is an eigenvector of $\mathbf{R}$ (with positive unit eigenvalue).

16.4 THE EXPONENTIAL FORM FOR THE ROTATION MATRIX

The rotation matrix of (16.22) can be expressed in an exponential form as

$$\mathbf{R} = \exp(\mathbf{S}(\boldsymbol{\theta})) = \mathbf{I} + \mathbf{S}(\boldsymbol{\theta}) + \frac{\mathbf{S}(\boldsymbol{\theta})^2}{2!} + \frac{\mathbf{S}(\boldsymbol{\theta})^3}{3!} + \cdots \tag{16.31}$$

This relationship can be established by expanding the $\sin\theta$ and $\cos\theta$ terms in (16.22) as

$$\sin\theta = \theta - \frac{\theta^3}{3!} + \frac{\theta^5}{5!} \tag{16.32a}$$

$$\cos\theta = 1 - \frac{\theta^2}{2!} + \cdots \tag{16.32b}$$

and making use of the relationships:

$$\mathbf{S}(\boldsymbol{\theta})^3 = -\theta^2\mathbf{S}(\boldsymbol{\theta}); \qquad \mathbf{S}(\boldsymbol{\theta})^4 = -\theta^2\mathbf{S}(\boldsymbol{\theta})^2, \text{ etc.} \tag{16.33a}$$

or

$$\mathbf{S}(\boldsymbol{\theta})^{2n-1} = (-1)^{n-1}\theta^{2(n-1)}\mathbf{S}(\boldsymbol{\theta}); \qquad \mathbf{S}(\boldsymbol{\theta})^{2n} = (-1)^{n-1}\theta^{2(n-1)}\mathbf{S}(\boldsymbol{\theta})^2 \tag{16.33b}$$

16.5 ALTERNATIVE FORMS FOR THE ROTATION MATRIX

Particularly with regard to compound rotations (Section 5.10.3), it can be useful to re-express (16.22) in slightly different forms that relate to modified forms of the pseudo-vector. As an example, instead of using $\boldsymbol{\theta}$ (16.9), we can use $\boldsymbol{\omega}$ where:

$$\boldsymbol{\omega} = \omega\mathbf{e} = 2\tan(\theta/2)\mathbf{e} = \frac{2\tan(\theta/2)}{\theta}\boldsymbol{\theta} \tag{16.34}$$

and has components which are sometimes known as Rodrigues parameters [R2].

Substitution from (16.34) into (16.22) gives:

$$\mathbf{R} = \mathbf{I} + \frac{1}{1 + \frac{1}{4}\boldsymbol{\omega}^{\mathrm{T}}\boldsymbol{\omega}}\left[\mathbf{S}(\boldsymbol{\omega}) + \tfrac{1}{2}\mathbf{S}(\boldsymbol{\omega})^2\right] \tag{16.35}$$

where $\mathbf{S}(\boldsymbol{\omega})$ is of the same form as $\mathbf{S}(\boldsymbol{\theta})$ — see (16.8). The reader will note that the pseudo-vector, $\boldsymbol{\omega}$, in (16.34), becomes infinite at $\theta = \pm 180°$ (and multiples thereof) while, simultaneously, $\mathbf{R}$ of (16.35) becomes singular. Equation (16.35) was used by Hughes and Winger [H2] in relation to large-strain analysis (see (19.60) of Section 19.5).

Rankin and Brogean [R1] have given a further alternative form for $\mathbf{R}$ that does not become singular (although, as will be shown in Section 16.7, there are problems of uniqueness). To this end, they replace (16.34) with

$$\boldsymbol{\psi} = \psi \mathbf{e} = 2\sin(\theta/2)\mathbf{e} = \frac{2\sin(\theta/2)}{\theta}\boldsymbol{\theta} \tag{16.36}$$

so that substitution into (16.22) leads to

$$\mathbf{R} = \mathbf{I} + \left(1 - \tfrac{1}{4}\boldsymbol{\psi}^{\mathrm{T}}\boldsymbol{\psi}\right)^{1/2}\mathbf{S}(\boldsymbol{\psi}) + \tfrac{1}{2}\mathbf{S}(\boldsymbol{\psi})^2 \tag{16.37}$$

where $\mathbf{S}(\boldsymbol{\psi})$ is of the same form as $\mathbf{S}(\boldsymbol{\theta})$ — see (16.8). From (16.34) and (16.36), the relationships between the pseudo-vectors, $\boldsymbol{\omega}$ and $\boldsymbol{\psi}$ are

$$\boldsymbol{\omega} = \left(1 - \tfrac{1}{4}\boldsymbol{\psi}^{\mathrm{T}}\boldsymbol{\psi}\right)^{-1/2}\boldsymbol{\psi}; \qquad \boldsymbol{\psi} = \left[1 + \tfrac{1}{4}\boldsymbol{\psi}^{\mathrm{T}}\boldsymbol{\omega}\right]^{-1/2} \tag{16.38}$$

16.6 APPROXIMATIONS FOR THE ROTATION MATRIX

The lowest-order approximation to $\mathbf{R}$ is $[\mathbf{I} + \mathbf{S}(\boldsymbol{\theta})$ (see (16.5)). A better approximation can be obtained by replacing $\sin\theta$ by θ and $\cos\theta$ by $1 - \frac{1}{2}\theta^2$ in (16.22). This leads to:

$$\mathbf{R} \simeq \mathbf{I} + \mathbf{S} + \tfrac{1}{2}\mathbf{S}^2 \tag{16.39}$$

From (16.34):

$$\frac{\theta}{2} = \tan^{-1}\left(\frac{\omega}{2}\right) = \frac{\omega}{2} - \frac{\omega^3}{24} + \frac{\omega^5}{160} - \cdots \tag{16.40}$$

so that

$$\theta = \omega - \frac{\omega^3}{12} + \cdots \tag{16.41}$$

and ω is a close approximation to θ for angles up to 30° and consequently $\mathbf{S}(\theta)$ is a good approximation to $\mathbf{S}(\boldsymbol{\omega})$ and hence, from (16.35):

$$\mathbf{R} \simeq \mathbf{I} + \frac{1}{(1 + \frac{1}{4}\boldsymbol{\theta}^{\mathrm{T}}\boldsymbol{\theta})}[\mathbf{S}(\boldsymbol{\theta}) + \tfrac{1}{2}\mathbf{S}(\boldsymbol{\theta}))^2] \tag{16.42}$$

is a better approximation to (16.22) than (16.39) and yet, unlike (16.22), does not require trignometric functions.

16.7 COMPOUND ROTATIONS

In a non-linear beam or shell analysis, we may have:

$$\boldsymbol{\theta}_0^{\mathrm{T}} = \{\theta_1, \theta_2, \theta_3\} \tag{16.43}$$

for which,

$$\mathbf{r}_1 = \mathbf{R}(\boldsymbol{\theta})\mathbf{r}_o \tag{16.44}$$

followed by an incremental rotation,

$$\Delta\boldsymbol{\theta}^T = \{\Delta\theta_1, \Delta\theta_2, \Delta\theta_3\} \tag{16.45}$$

for which:

$$\mathbf{r}_n = \Delta\mathbf{R}(\Delta\boldsymbol{\theta})\mathbf{r}_1 \tag{16.46}$$

where $\Delta\mathbf{R}(\Delta\boldsymbol{\theta})$ could be obtained from (16.22) (or (16.35) or (16.37)) and we could† then obtain

$$\mathbf{r}_n = \Delta\mathbf{R}(\Delta\boldsymbol{\theta})\mathbf{R}(\boldsymbol{\theta})\mathbf{r}_o \tag{16.47}$$

It should be emphasised that the $\Delta\boldsymbol{\theta}$ pseudo-vector in (16.45) is non-additive to $\boldsymbol{\theta}$ even in the limit as $\delta\boldsymbol{\theta}$ tends to zero. This point will be explored further in Section 16.11.

A more general compound rotation involves:

$$\mathbf{r}_1 = \mathbf{R}(\boldsymbol{\omega}_1)\mathbf{r}_o; \qquad \mathbf{r}_2 = \mathbf{R}(\boldsymbol{\omega}_2)\mathbf{r}_1 \tag{16.48}$$

so that:

$$\mathbf{r}_2 = \mathbf{R}_2(\boldsymbol{\omega}_2)\mathbf{R}_1(\boldsymbol{\omega}_1)\mathbf{r}_o \tag{16.49}$$

where we have used the $\boldsymbol{\omega}$ rather than $\boldsymbol{\theta}$ form of 'pseudo-vector' (related by a constant involving $\tan(\theta/2)$—see (16.34)) because the latter form will turn out to be more convenient. In particular, time and storage can be saved if (16.49) is replaced by an equivalent:

$$\mathbf{r}_2 = \mathbf{R}_{12}(\boldsymbol{\omega}_{12})\mathbf{r}_o \tag{16.50}$$

where $\boldsymbol{\omega}_{12}$ is the 'pseudo-vector' resulting from $\boldsymbol{\omega}_1$ followed by $\boldsymbol{\omega}_2$. Using (16.35) for $\mathbf{R}(\boldsymbol{\omega})$, one can show [A1, R1] that:

$$\boldsymbol{\omega}_{12} = \frac{\boldsymbol{\omega}_1 + \boldsymbol{\omega}_2 - \frac{1}{2}\boldsymbol{\omega}_1 \times \boldsymbol{\omega}_2}{1 - \frac{1}{4}\boldsymbol{\omega}_1^T\boldsymbol{\omega}_2} \tag{16.51}$$

Alternatively, if $\boldsymbol{\psi}$ (see (16.36)) is used as the 'pseudo-vector', substitution from (16.38) into (16.51), followed by algebraic manipulation gives:

$$\boldsymbol{\psi}_{12} = \pm((1 - \tfrac{1}{4}\boldsymbol{\psi}_2^T\boldsymbol{\psi}_2)^{1/2}\boldsymbol{\psi}_1 + (1 - \tfrac{1}{4}\boldsymbol{\psi}_1^T\boldsymbol{\psi}_1)^{1/2}\boldsymbol{\psi}_2 - \tfrac{1}{2}\boldsymbol{\psi}_1 \times \boldsymbol{\psi}_2) \tag{16.52}$$

where the sign in (16.52) follows that of:

$$(1 - \tfrac{1}{4}\boldsymbol{\psi}_2^T\boldsymbol{\psi}_2)^{1/2}(1 - \tfrac{1}{4}\boldsymbol{\psi}_1^T\boldsymbol{\psi}_1)^{1/2} - \tfrac{1}{4}\boldsymbol{\psi}_1^T\boldsymbol{\psi}_2 \tag{16.53}$$

With a view to subsequent work on 'normalised quanternions' or Euler parameters, (Section 16.9), it is interesting to look at the two-dimensional form of (16.49), which involves a rotation about a fixed axis. In this case, from (16.36),

$$\psi_1 = 2\sin(\theta_1/2); \qquad \psi_2 = 2\sin(\theta_2/2) \tag{16.54}$$

†Both here and later in the chapter we are adopting the notation $\Delta\mathbf{R}$ $(\Delta\boldsymbol{\theta})$ to indicate that $\Delta\mathbf{R}$ is the rotation matrix obtained from the pseudo-vector, $\Delta\boldsymbol{\theta}$, with the Δ indicating that $\Delta\boldsymbol{\theta}$ is of an incremental form. We need not have introduced the Δ in front of the $\mathbf{R}$ and could instead have written $\mathbf{R}(\Delta\boldsymbol{\theta})$. However, the introduction of the Δ turns out to be useful for future shorthand. Nonetheless, it should be emphasised that $\Delta\mathbf{R}(\Delta\boldsymbol{\theta})$ would be computed by inserting $\Delta\boldsymbol{\theta}$ for $\boldsymbol{\theta}$ in the right-hand side of (16.22).

and hence, (16.52) gives:

$$\psi_{12} = 2\sin\left(\frac{\theta_1 + \theta_2}{2}\right) = \pm 2(c(\theta_1/2)\sin(\theta_2/2) + c(\theta_2/2)\sin(\theta_1/2)) \tag{16.55}$$

with:

$$c(\theta_1) = (1 - \sin^2\theta_1)^{1/2} \tag{16.56}$$

and with the sign in (16.55) following that of:

$$c\left(\frac{\theta_1 + \theta_2}{2}\right) = c(\theta_1/2)c(\theta_2/2) - \sin(\theta_1/2)\sin(\theta_2/2) \tag{16.57}$$

The reader will recognise the sine and cosine addition formulae in (16.55) and (16.57). In these equations, the terminology $c(\theta)$ has been used rather than $\cos(\theta)$ because of the issue of the signs associated with the square root in (16.56). The latter has led to the introduction of the alternative signs in (16.52) and (16.55). However, at least for the two-dimensional case, the reader will be able to verify that the proposed procedure only works for $|(\theta_1 + \theta_2)| < 180°$. However, if we actually stored both $\sin(\theta/2)$ and $\cos(\theta/2)$, the formula (16.55) with $\cos(\theta/2)$ instead of $c(\theta/2)$ and without the $\pm$ would work irrespective of the quadrant in which the vectors lay. Such a procedure has close relationships with quaternions and Euler parameters which will be discussed in Section 16.9.

16.8 OBTAINING THE PSEUDO-VECTOR FROM THE ROTATION MATRIX, R

From (16.22), the antisymmetric part of $\mathbf{R}$ is given by

$$\mathbf{R}^a = \tfrac{1}{2}(\mathbf{R} - \mathbf{R}^T) = \sin\theta\mathbf{S}(\mathbf{e}) = \frac{\sin\theta}{\theta}\mathbf{S}(\boldsymbol{\theta}) \tag{16.58}$$

from which, knowing the anti-symmetric form of $\mathbf{S}$ (see (16.8)). $\mathbf{e}$ or $\boldsymbol{\theta}$ can be obtained via:

$$\sin\theta\mathbf{e} = \frac{\sin\theta}{\theta}\boldsymbol{\theta} = \frac{1}{2}\begin{bmatrix} R_{32} - R_{23} \\ R_{13} - R_{31} \\ R_{21} - R_{12} \end{bmatrix} \tag{16.59}$$

This equation can be used provided $0 < |\theta| < \pi$. A more general procedure will be given in Section 16.10.

If we adopt the approximation in (16.39) for $\mathbf{R}$, the skew-symmetrix matrix $\mathbf{S}(\boldsymbol{\theta})$ can be simply obtained as

$$\mathbf{S}(\boldsymbol{\theta}) = \mathbf{R}^a = \tfrac{1}{2}(\mathbf{R} - \mathbf{R}^T) \tag{16.60}$$

which coincides with (16.58) if $\sin\theta \simeq \theta$.

Using the approximation of (16.42), the antisymmetric part of $\mathbf{R}$ is given by

$$\mathbf{R}^a = \tfrac{1}{2}[\mathbf{R} - \mathbf{R}^T] = \frac{\mathbf{S}(\boldsymbol{\theta})}{1 + \frac{1}{4}\boldsymbol{\theta}^T\boldsymbol{\theta}} \tag{16.61}$$

By taking the trace of both sides of (16.42),

$$1 + \tfrac{1}{4}\boldsymbol{\theta}^{\mathrm{T}}\boldsymbol{\theta} = \frac{4}{1 + \mathrm{Tr}(\mathbf{R})} \tag{16.62}$$

where $\mathrm{Tr}(\mathbf{R})$ is the trace of $\mathbf{R}$ so that:

$$\mathrm{Tr}(\mathbf{R}) = R_{11} + R_{22} + R_{33} \tag{16.63}$$

From (16.61) and (16.62), a more accurate approximation than (16.60) can be obtained as

$$\mathbf{S}(\boldsymbol{\theta}) = \frac{4\mathbf{R}^{\mathrm{a}}}{1 + \mathrm{Tr}(\mathbf{R})} = \frac{2(\mathbf{R} - \mathbf{R}^{\mathrm{T}})}{1 + \mathrm{Tr}(\mathbf{R})} \tag{16.64}$$

16.9 QUATERNIONS AND EULER PARAMETERS

In Sections 16.5 and 16.7, we pointed out some limitations that stem from the use of pseudo-vectors. Of the various pseudo-vector updates, that associated with the sine scaling (16.36) has certain advantages but it is non-unique for angles greater than 180°. This issue was discussed in Section 16.7 where it was shown that for the two-dimensional situation, the problem could be overcome by working with both $\sin(\theta/2)$ and $\cos(\theta/2)$. A similar approach can be adopted in three dimensions with the cost that we now have to work with four parameters (normalised quaternions or Euler parameters) rather than, as hitherto, three (pseudo-vector components). Further reading on quaternions can be found in [H1, S5, W1].

With such a process in mind, taking a lead from the work of Section 16.7, we can re-express (16.22) using half-angles so that:

$$\mathbf{R} = (\cos^2(\theta/2) - \sin^2(\theta/2))\mathbf{I} + 2\cos(\theta/2)\sin(\theta/2)\mathbf{S}(\mathbf{e}) + 2\sin^2(\theta/2)\mathbf{e}\mathbf{e}^{\mathrm{T}} \tag{16.65}$$

In deriving (16.65) from (16.22), use has not only been made of half-angle formulae, but also the relationship (easily verified with the aid of (16.8)):

$$\mathbf{S}(\mathbf{e})\mathbf{S}(\mathbf{e}) = \mathbf{S}(\mathbf{e})^2 = \mathbf{e}\mathbf{e}^{\mathrm{T}} - \mathbf{I} \tag{16.66}$$

A unit quaternion will now be defined using four Euler parameters, q_{o}–q_3, so that:

$$\hat{\mathbf{q}} = \cos(\theta/2) + \sin(\theta/2)\mathbf{e} = \begin{pmatrix} \mathbf{q} \\ q_{\mathrm{o}} \end{pmatrix} = \begin{pmatrix} \sin(\theta/2)\mathbf{e} \\ \cos(\theta/2) \end{pmatrix} = \begin{pmatrix} \boldsymbol{\psi}/2 \\ \cos(\theta/2) \end{pmatrix} \tag{16.67}$$

where $\boldsymbol{\psi}$ is the sine-scaled pseudo-vector of (16.36). From (16.67), the 'length' of $\hat{\mathbf{q}}$ is clearly unity with:

$$\hat{\mathbf{q}}^{\mathrm{T}}\hat{\mathbf{q}} = q_{\mathrm{o}}^2 + q_1^2 + q_2^2 + q_3^2 = 1 \tag{16.68}$$

Referring back to the two-dimensional example of Section 16.7, it will be noted that (16.67) now contains explicitly the required $\cos(\theta/2)$. Substitution from (16.67) into (16.65) leads to the relationship:

$$\mathbf{R} = 2\begin{bmatrix} q_{\mathrm{o}}^2 + q_1^2 - 1/2 & q_1q_2 - q_3q_{\mathrm{o}} & q_1q_3 + q_2q_{\mathrm{o}} \\ q_2q_1 + q_3q_{\mathrm{o}} & q_{\mathrm{o}}^2 + q_2^2 - 1/2 & q_2q_3 - q_1q_{\mathrm{o}} \\ q_3q_1 - q_2q_{\mathrm{o}} & q_3q_2 + q_1q_{\mathrm{o}} & q_{\mathrm{o}}^2 + q_3^2 - 1/2 \end{bmatrix} \tag{16.69}$$

The latter equation can be re-expressed as

$$\mathbf{R} = (q_o^2 - \mathbf{q}^T\mathbf{q})\mathbf{I} + 2\mathbf{q}\mathbf{q}^T + 2q_o\mathbf{S}(\mathbf{q}) \tag{16.70}$$

In place of (16.51) or (16.52), the quaternion compound rotation is given by [S5]

$$\hat{\mathbf{q}}_{12} = \hat{\mathbf{q}}_2\hat{\mathbf{q}}_1 \tag{16.71}$$

where $\hat{\mathbf{q}}_2\hat{\mathbf{q}}_1$ involves the quaternion product whereby:

$$\mathbf{ba} = a_o b_o - \mathbf{a}^T\mathbf{b} + a_o\mathbf{b} + b_o\mathbf{a} - \mathbf{a} \times \mathbf{b} \tag{16.72}$$

which is non-commutative because the inverse product is

$$\mathbf{ab} = a_o b_o - \mathbf{a}^T\mathbf{b} + a_o\mathbf{b} + b_o\mathbf{a} + \mathbf{a} \times \mathbf{b} \tag{16.73}$$

The reader can explore the close similarity between the relationship (16.71) (using (16.67)) and the pseudo-vector updates in (16.52) and (16.53). Unlike the latter, (16.71) can be used for any angles.

16.10 OBTAINING THE NORMALISED QUATERNION FROM THE ROTATION MATRIX

In Section 16.8, we discussed the computation of the pseudo-vector from its rotation matrix. A more general approach involves the computation of the Euler parameters, q_o–q_3. This can be achieved via algebraic manipulations on the components of $\mathbf{R}$ as expressed in (16.69). Spurrier's algorithm [S4] (which can be simply checked by working with the components in (16.69)) then involves:

$$a = \max(\mathrm{Tr}(\mathbf{R}), R_{11}, R_{22}, R_{33}) \tag{16.74}$$

and

$$\text{if } a = \mathrm{tr}(\mathbf{R}) = R_{11} + R_{22} + R_{33} \tag{16.75}$$

(16.76) applies where:

$$q_o = \tfrac{1}{2}(1 + a)^{1/2} \tag{16.76a}$$

$$q_i = (R_{kj} - R_{jk})/4q_o; \qquad i = 1, 3 \tag{16.76b}$$

with i, j, k as the cyclic combination of 1, 2, 3.

$$\text{If, } a \neq \mathrm{tr}(\mathbf{R}) \text{ but instead} = R_{ii} \tag{16.77}$$

(16.78) applies with:

$$q_i = (\tfrac{1}{2}a + \tfrac{1}{4}(1 - \mathrm{tr}(\mathbf{R})))^{1/2} \tag{16.78a}$$

$$q_o = \tfrac{1}{4}(R_{kj} - R_{jk})/q_i \tag{16.78b}$$

$$q_l = \tfrac{1}{4}(R_{li} + R_{il})/q_i; \qquad l = j, k \tag{16.78c}$$

Allowing for the definition of q_o–q_3 in (16.67), equations (16.76) coincide with the earlier relationship for $\mathbf{e}$ (or $\boldsymbol{\theta}$) in (16.59). Having obtained q_o–q_3, for rotations of magnitude less than 180°, the tangent-scaled pseudo-vector of (16.34) can then be obtained from (16.67) as

$$\boldsymbol{\omega} = 2\tan\left(\frac{\theta}{2}\right)\mathbf{e} = \frac{2}{q_o}\mathbf{q} \tag{16.79}$$

16.11 ADDITIVE AND NON-ADDITIVE ROTATION INCREMENTS

We have already discussed compound rotations in Section 16.7 and have shown that we cannot simply add components of a pseudo-vector. We also implied that this restriction also applies when the second rotation involved a very small change. This point will now be amplified and the relationship between additive and non-additive (spin) changes will be established.

Suppose that following the rotation $\mathbf{r}_n = \mathbf{R}\mathbf{r}_o$ (see (16.21)), $\mathbf{r}_n$ is rotated further to $\mathbf{r}_{nn}$ via a new small rotation relating to a small non-additive pseudo-vector (or spin), $\delta\bar{\boldsymbol{\theta}}$ (Note that the bar is added to emphasise that $\delta\bar{\boldsymbol{\theta}}$ cannot be added to $\boldsymbol{\theta}$. Also $\delta\boldsymbol{\theta}$ is not the change in $\bar{\boldsymbol{\theta}}$.) The rotation matrix associated with the new change is (see (16.5)

$$\mathbf{R}(\delta\bar{\boldsymbol{\theta}}) = [\mathbf{I} + \mathbf{S}(\delta\bar{\boldsymbol{\theta}})] \tag{16.80}$$

From (16.44):

$$\mathbf{r}_{nn} = \mathbf{R}(\delta\bar{\boldsymbol{\theta}})\mathbf{r}_n = \mathbf{R}(\delta\bar{\boldsymbol{\theta}})\mathbf{R}(\boldsymbol{\theta})\mathbf{r}_o = [\mathbf{I} + \mathbf{S}(\delta\bar{\boldsymbol{\theta}})]\mathbf{R}(\boldsymbol{\theta})\mathbf{r}_o = \mathbf{R}(\boldsymbol{\theta} + \delta\boldsymbol{\theta}_a)\mathbf{r}_o \tag{16.81a}$$

where the last term in (16.81a) include the additive pseudo-vector, $\delta\boldsymbol{\theta}_a$. From (16.81a), we can obtain:

$$\mathbf{R}(\delta\bar{\boldsymbol{\theta}})\mathbf{R}(\boldsymbol{\theta}) = \mathbf{R}(\boldsymbol{\theta}) + \delta\mathbf{R} = \mathbf{R}(\boldsymbol{\theta}) + \mathbf{S}(\delta\bar{\boldsymbol{\theta}})\mathbf{R}(\boldsymbol{\theta}) \tag{16.81b}$$

so that:

$$\delta\mathbf{R} = \mathbf{S}(\delta\bar{\boldsymbol{\theta}})\mathbf{R} \tag{16.81c}$$

This relationship will be required later.

For some future developments we will need a relationship between the non-additive $\delta\bar{\boldsymbol{\theta}}$ (spin) and the additive $\delta\boldsymbol{\theta}_a$. With this in mind, we will now apply (16.51), with $\boldsymbol{\omega}_1$ as the tangent scaled $\boldsymbol{\theta}$ (16.34), $\boldsymbol{\omega}_2$ as the tangent scaled $\delta\bar{\boldsymbol{\theta}}$ which, with $\delta\bar{\boldsymbol{\theta}}$ small is equal to $\delta\bar{\boldsymbol{\theta}}$ and $\boldsymbol{\omega}_{12}$ as $\boldsymbol{\omega} + \delta\boldsymbol{\omega}_a$ with the subscript a implying additive. This leads to

$$\boldsymbol{\omega} - \tfrac{1}{4}(\boldsymbol{\omega}^T\delta\bar{\boldsymbol{\theta}})\boldsymbol{\omega} + \delta\boldsymbol{\omega}_a - \tfrac{1}{4}(\boldsymbol{\omega}^T\delta\bar{\boldsymbol{\theta}})\delta\boldsymbol{\omega}_a = \boldsymbol{\omega} + \delta\bar{\boldsymbol{\theta}} - \tfrac{1}{2}\boldsymbol{\omega} \times \delta\bar{\boldsymbol{\theta}} \tag{16.82}$$

as $\delta\bar{\boldsymbol{\theta}}$ and $\delta\boldsymbol{\omega}_a$ tend to zero, we can neglect the final term on the left-hand side of (16.82) so that:

$$\delta\boldsymbol{\omega}_a = \delta\bar{\boldsymbol{\theta}} - \tfrac{1}{2}\boldsymbol{\omega} \times \delta\bar{\boldsymbol{\theta}} + \tfrac{1}{4}(\boldsymbol{\omega}^T\delta\bar{\boldsymbol{\theta}})\boldsymbol{\omega} \tag{16.83}$$

The $\delta\boldsymbol{\omega}_a$ terms in (16.82) and (16.83) are obtained by differentiation of the tangent scaling in (16.34) whereby:

$$\delta\boldsymbol{\omega}_a = \frac{2\tan(\theta/2)}{\theta}\left[\mathbf{I} - \left(1 - \frac{\theta}{\sin\theta}\right)\mathbf{e}\mathbf{e}^T\right]\delta\boldsymbol{\theta}_a \tag{16.84}$$

where (see (16.9) and (16.10)) $\mathbf{e}$ is the unit vector obtained from $\boldsymbol{\theta}$.

Equation (16.83) can be re-expressed as

$$\delta\boldsymbol{\omega}_a = [\mathbf{I} - \tfrac{1}{2}\mathbf{S}(\boldsymbol{\omega}) + \tfrac{1}{4}\boldsymbol{\omega}\boldsymbol{\omega}^T]\delta\bar{\boldsymbol{\theta}} = \mathbf{C}(\boldsymbol{\omega})^{-1}\delta\bar{\boldsymbol{\theta}} \tag{16.85}$$

Using the relationship:

$$\mathbf{S}(\mathbf{a})\mathbf{S}(\mathbf{b}) = \mathbf{b}\mathbf{a}^T - (\mathbf{a}^T\mathbf{b})\mathbf{I} \tag{16.86}$$

the inverses of (16.83) and (16.85) can easily be shown to be

$$\delta\bar{\boldsymbol{\theta}} = \frac{1}{1+\frac{1}{4}\boldsymbol{\omega}^{\mathrm{T}}\boldsymbol{\omega}}(\delta\boldsymbol{\omega}_{\mathrm{a}} + \tfrac{1}{2}\boldsymbol{\omega}\times\delta\boldsymbol{\omega}_{\mathrm{a}}) \tag{16.87}$$

and

$$\delta\bar{\boldsymbol{\theta}} = \frac{1}{1+\frac{1}{4}\boldsymbol{\omega}^{\mathrm{T}}\boldsymbol{\omega}}[\mathbf{I} + \tfrac{1}{2}\mathbf{S}(\boldsymbol{\omega})]\delta\boldsymbol{\omega}_{\mathrm{a}} = \mathbf{C}(\boldsymbol{\omega})\delta\boldsymbol{\omega}_{\mathrm{a}} \tag{16.88}$$

Substituting from (16.84) into (16.88) leads to the following relationship between the non-additive ($\delta\bar{\boldsymbol{\theta}}$) and additive ($\delta\boldsymbol{\theta}_{\mathrm{a}}$) pseudo-vector changes:

$$\delta\bar{\boldsymbol{\theta}} = \mathbf{H}(\boldsymbol{\theta})\delta\boldsymbol{\theta}_{\mathrm{a}} \tag{16.89}$$

where:

$$\mathbf{H}(\boldsymbol{\theta}) = \left[\frac{\sin\theta}{\theta}\mathbf{I} + \frac{1}{\theta^2}\left(1-\frac{\sin\theta}{\theta}\right)\boldsymbol{\theta}\boldsymbol{\theta}^{\mathrm{T}} + \frac{1}{2}\left(\frac{\sin(\theta/2)}{(\theta/2)}\right)^2\mathbf{S}(\boldsymbol{\theta})\right] \tag{16.90}$$

From (16.90), $\mathbf{H}(\boldsymbol{\theta})$ is equal to the identity matrix when $\boldsymbol{\theta}$ tends to zero. In these circumstances, $\delta\bar{\boldsymbol{\theta}}$ is equal to $\delta\boldsymbol{\theta}_{\mathrm{a}}$.

In order to obtain the inverse of (16.90), we first find the inverse of (16.84) using the relationship:

$$[\mathbf{I} + \alpha\mathbf{e}\mathbf{e}^{\mathrm{T}}]^{-1} = \left[I - \frac{\alpha}{1+\alpha}\mathbf{e}\mathbf{e}^{\mathrm{T}}\right] \tag{16.91}$$

where $\mathbf{e}$ is a unit vector. This process leads to

$$\delta\boldsymbol{\theta}_{\mathrm{a}} = \frac{\theta}{2}\cot\left(\frac{\theta}{2}\right)\left[\mathbf{I} - \left(1-\frac{\sin\theta}{\theta}\right)\mathbf{e}\mathbf{e}^{\mathrm{T}}\right]\delta\boldsymbol{\omega}_{\mathrm{a}} \tag{16.92}$$

A direct relationship between $\delta\boldsymbol{\theta}_{\mathrm{a}}$ and $\delta\bar{\boldsymbol{\theta}}$ can now be obtained by substituting from (16.85) into (16.92) so that:

$$\delta\boldsymbol{\theta}_{\mathrm{a}} = \mathbf{H}(\boldsymbol{\theta})^{-1}\delta\bar{\boldsymbol{\theta}} \tag{16.93}$$

where

$$\mathbf{H}(\boldsymbol{\theta})^{-1} = \left[\frac{\theta}{2}\cot\left(\frac{\theta}{2}\right)\mathbf{I} - \mathbf{S}\left(\frac{\boldsymbol{\theta}}{2}\right) + \left(1-\frac{\theta}{2}\cot(\theta/2)\right)\frac{\boldsymbol{\theta}\boldsymbol{\theta}^{\mathrm{T}}}{\theta^2}\right] \tag{16.94}$$

For some future developments (in particular, the work in Section 17.4), it is useful to obtain the derivative of $\mathbf{H}(\boldsymbol{\theta})$ in (16.90). This follows via:

$$\begin{aligned}\delta\mathbf{H}(\boldsymbol{\theta}) = {} & \left(\cos\theta - \frac{\sin\theta}{\theta}\right)\frac{\boldsymbol{\theta}^{\mathrm{T}}\delta\boldsymbol{\theta}_{\mathrm{a}}}{\theta^2}\mathbf{I} + \left(1-\frac{\sin\theta}{\theta}\right)\left(\frac{\boldsymbol{\theta}\delta\boldsymbol{\theta}_{\mathrm{a}}^{\mathrm{T}} + \delta\boldsymbol{\theta}_{\mathrm{a}}\boldsymbol{\theta}^{\mathrm{T}}}{\theta^2}\right) \\ & + \left(3\frac{\sin\theta}{\theta} - \cos\theta - 2\right)\frac{\boldsymbol{\theta}^{\mathrm{T}}\delta\boldsymbol{\theta}_{\mathrm{a}}}{\theta^2}\left(\frac{\boldsymbol{\theta}\boldsymbol{\theta}^{\mathrm{T}}}{\theta^2}\right) \\ & - \left(\left(\frac{\sin(\theta/2)}{(\theta/2)}\right)^2 - \frac{\sin\theta}{2}\right)\frac{\boldsymbol{\theta}^{\mathrm{T}}\delta\boldsymbol{\theta}_{\mathrm{a}}}{\theta^2}\mathbf{S}(\boldsymbol{\theta}) + \frac{1}{2}\left(\frac{\sin(\theta/2)}{(\theta/2)}\right)^2\mathbf{S}(\delta\boldsymbol{\theta}_{\mathrm{a}})\end{aligned} \tag{16.95}$$

which is dramatically simplified when $\boldsymbol{\theta} = \mathbf{0}$ to give:

$$\delta\mathbf{H}(\boldsymbol{\theta})|_{\boldsymbol{\theta}=0} = \tfrac{1}{2}\mathbf{S}(\delta\boldsymbol{\theta}_{\mathrm{a}}) \tag{16.96}$$

16.12 THE DERIVATIVE OF THE ROTATION MATRIX

To obtain $\delta\mathbf{R} = \mathbf{R}(\delta\boldsymbol{\theta})$ which we will write as $\delta\mathbf{R}(\delta\boldsymbol{\theta}_a)$ to emphasise that the $\delta\boldsymbol{\theta}$ term is additive to $\boldsymbol{\theta}$, we could directly differentiate (16.22). Alternatively, we can use the previous developments to find the relationship between $\delta\mathbf{R}(\delta\boldsymbol{\theta}_a)$ and $\delta\bar{\boldsymbol{\theta}}$. Adopting the latter approach, (16.81a) can be used to obtain:

$$\begin{aligned}\delta\mathbf{r}_n = \mathbf{r}_{nn} - \mathbf{r}_n = \mathbf{S}(\delta\bar{\boldsymbol{\theta}})\mathbf{r}_n = [\mathbf{R}(\boldsymbol{\theta} + \delta\boldsymbol{\theta}_a) - \mathbf{R}(\boldsymbol{\theta})]\mathbf{r}_o \\ = [\mathbf{R}(\boldsymbol{\theta} + \delta\boldsymbol{\theta}_a) - \mathbf{R}(\boldsymbol{\theta})]\mathbf{R}_o^T\mathbf{r}_n \end{aligned} \tag{16.97a}$$

or

$$\mathbf{S}(\delta\bar{\boldsymbol{\theta}})\mathbf{r}_n = [\mathbf{R}(\boldsymbol{\theta} + \delta\boldsymbol{\theta}_a) - \mathbf{R}(\boldsymbol{\theta})]\mathbf{R}_o^T\mathbf{r}_n = \delta\mathbf{R}(\delta\boldsymbol{\theta}_a)\mathbf{R}_o^T\mathbf{r}_n \tag{16.97b}$$

which shows that $\delta\mathbf{R}\mathbf{R}^T$ is the skew-symmetric matrix $(\mathbf{S}(\delta\bar{\boldsymbol{\theta}}))$. This can be proved more quickly from a straight differentiation of the relationship $\mathbf{R}\mathbf{R}^T = \mathbf{I}$ from which:

$$\delta\mathbf{R}\mathbf{R}^T = -\mathbf{R}\delta\mathbf{R}^T = -(\delta\mathbf{R}\mathbf{R}^T)^T \tag{16.98}$$

From (16.97b) and making use of (16.87) for $\delta\bar{\boldsymbol{\theta}}$,

$$\begin{aligned}\delta\mathbf{R}(\delta\boldsymbol{\omega}_a)\mathbf{R}(\boldsymbol{\omega})^T = \mathbf{S}(\delta\bar{\boldsymbol{\theta}}) = \frac{1}{1 + \frac{1}{4}\boldsymbol{\omega}^T\boldsymbol{\omega}}[\mathbf{S}(\delta\boldsymbol{\omega}_a) + \tfrac{1}{2}\mathbf{S}(\boldsymbol{\omega} \times \delta\boldsymbol{\omega}_a)] \\ = \frac{1}{1 + \frac{1}{4}\boldsymbol{\omega}^T\boldsymbol{\omega}}[\mathbf{S}(\delta\boldsymbol{\omega}_a) - \tfrac{1}{2}\boldsymbol{\omega}\delta\boldsymbol{\omega}_a^T + \tfrac{1}{2}\delta\boldsymbol{\omega}_a\boldsymbol{\omega}^T] \end{aligned} \tag{16.99}$$

In deriving the last expression in (16.99), use has been made of the relationship:

$$\mathbf{S}(\mathbf{a} \times \mathbf{b}) = \mathbf{b}\mathbf{a}^T - \mathbf{a}\mathbf{b}^T \tag{16.100}$$

With the aid of (16.86), equation (16.99) can be re-expressed as

$$\delta\mathbf{R}(\delta\boldsymbol{\omega}_a)\mathbf{R}(\boldsymbol{\omega})^T = \mathbf{S}(\delta\bar{\boldsymbol{\theta}}) = \frac{1}{1 + \frac{1}{4}\boldsymbol{\omega}^T\boldsymbol{\omega}}[\mathbf{S}(\delta\boldsymbol{\omega}_a) + \tfrac{1}{2}\mathbf{S}(\boldsymbol{\omega})\mathbf{S}(\delta\boldsymbol{\omega}_a) - \tfrac{1}{2}\mathbf{S}(\delta\boldsymbol{\omega}_a)\mathbf{S}(\boldsymbol{\omega})] \tag{16.101}$$

16.13 ROTATING A TRIAD SO THAT ONE UNIT VECTOR MOVES TO A SPECIFIED UNIT VECTOR VIA THE 'SMALLEST ROTATION'

For the work in Chapter 17 on three-dimensional beams and Chapter 18 on shells, we will need to rotate a unit triad on to another triad in such a manner that one of the original unit vectors is rotated on to another (known) unit vector via the 'smallest rotation'. In relation to Figure 16.3, this rotation would be such that its axis (given by the unit vector, $\mathbf{e}$) is orthogonal to the original vector $\mathbf{r}_o$ and the final vector, $\mathbf{r}_n$. In relation to Figure 16.3 and equation (16.22), it follows that, in these circumstances:

$$\boldsymbol{\theta} = \mathbf{e}\theta = \theta\frac{\mathbf{r}_o \times \mathbf{r}_n}{\|\mathbf{r}_o \times \mathbf{r}_n\|} \tag{16.102}$$

where

$$\cos\theta = \mathbf{r}_o^T\mathbf{r}_n \tag{16.103a}$$

$$\mathbf{r}_o \times \mathbf{r}_n = \frac{\sin\theta}{\theta}\boldsymbol{\theta} \tag{16.103b}$$

Equations (16.102) and (16.103) can be used in conjunction with (16.22) to give:

$$\mathbf{R}(\mathbf{r}_o, \mathbf{r}_n) = \left[\mathbf{I} + \mathbf{S}(\mathbf{r}_o \times \mathbf{r}_n) + \frac{1}{(1+\mathbf{r}_o^T\mathbf{r}_n)}\mathbf{S}(\mathbf{r}_o \times \mathbf{r}_n)^2\right] \tag{16.104}$$

which, with the aid of (16.86) can be written in the alternative form:

$$\mathbf{R}(\mathbf{r}_o, \mathbf{r}_n) = (\mathbf{r}_o^T\mathbf{r}_n)\mathbf{I} + \mathbf{S}(\mathbf{r}_o \times \mathbf{r}_n) + \frac{1}{(1+\mathbf{r}_o^T\mathbf{r}_n)}(\mathbf{r}_o \times \mathbf{r}_n)(\mathbf{r}_o \times \mathbf{r}_n)^T \tag{16.105}$$

Suppose we now have an initial unit triad $\mathbf{P} = [\mathbf{p}_1, \mathbf{p}_2, \mathbf{p}_3]$ which we wish to rotate to a new unit triad $\mathbf{Q} = [\mathbf{q}_1, \mathbf{q}_2, \mathbf{q}_3]$ such that the vector $\mathbf{p}_2$ is rotated on to $\mathbf{q}_2$ through an axis that is orthogonal to both. Using (16.104) with $\mathbf{r}_o = \mathbf{p}_2$ and $\mathbf{r}_n = \mathbf{q}_2$, with the aid of the relationship:

$$\mathbf{S}(\mathbf{a} \times \mathbf{b}) = (\mathbf{a} \times \mathbf{b}) \times \mathbf{c} = (\mathbf{a}^T\mathbf{c})\mathbf{b} - (\mathbf{b}^T\mathbf{c})\mathbf{a} \tag{16.106}$$

we obtained the desired result that $\mathbf{q}_2 = \mathbf{R}(\mathbf{p}_2, \mathbf{q}_2)\mathbf{p}_2$ while:

$$\mathbf{q}_1 = \mathbf{p}_1 - \frac{b_1}{1+b_2}(\mathbf{p}_2 + \mathbf{q}_2) \tag{16.107a}$$

$$\mathbf{q}_3 = \mathbf{p}_3 - \frac{b_3}{1+b_2}(\mathbf{p}_2 + \mathbf{q}_2) \tag{16.107b}$$

where

$$b_k = \mathbf{p}_k^T\mathbf{q}_2; \qquad k = 1, 2, 3 \tag{16.108}$$

In later work (Chapters 17 and 18) we will need the differentials of the expressions in (16.107). In the work of Chapter 17 on beams, the rotations between the two triads will involve only moderate rotations. In these circumstances, with a view to the subsequent differentials, it is useful to approximate equations (16.107) by

$$\mathbf{q}_1 = \mathbf{p}_1 - \frac{b_1}{2}(\mathbf{p}_2 + \mathbf{q}_2) \tag{16.109a}$$

$$\mathbf{q}_3 = \mathbf{p}_3 - \frac{b_3}{2}(\mathbf{p}_2 + \mathbf{q}_2) \tag{16.109b}$$

which can also be obtained geometrically from a mid-point rule (Figure 16.5). As a result of the approximation, the triad $\mathbf{Q} = [\mathbf{q}, \mathbf{q}_2, \mathbf{q}_3]$ is no longer exactly orthogonal. In particular,

$$\mathbf{q}_1^T\mathbf{q}_2 = \tfrac{1}{2}\mathbf{p}_1^T\mathbf{q}_2(1 - \mathbf{p}_2^T\mathbf{q}_2) \tag{16.110}$$

If the triads are reasonably close, this quantity will be very small while, using (16.109), it can be shown that $\mathbf{q}_1^T\mathbf{q}_3$ will be even smaller. In the special situation where $\mathbf{p}_3 = \mathbf{q}_3$,

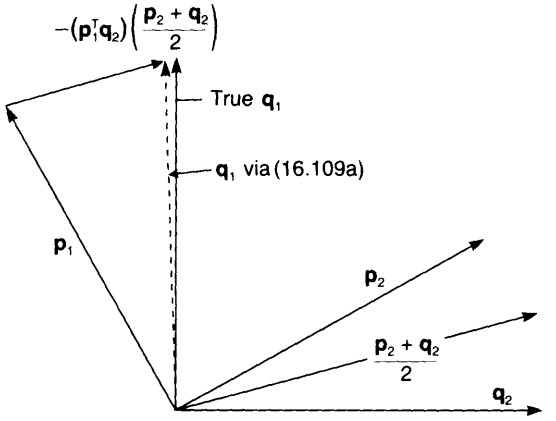

Figure 16.5 Special case illustration of equation (16.109a).

equation (16.109a) can be illustrated graphically as in Figure 16.5. With the angle between $\mathbf{p}_2$ and $\mathbf{q}_2$ being 30°, the lack of orthogonality in (16.110) is 1.9°. For angles of 15°, this lack of orthogonality is reduced to 0.25°.

16.14 CURVATURE

In Section 16.14.1, we will discuss some methods for obtaining the curvature that could be appropriate for co-rotational three-dimensional beam formulations such as those that will be considered in Sections 17.1 and 17.2. In Section 16.14.2, we will use the developments of Section 16.14.2 to introduce some more general expressions for curvature. The latter will be used in Section 17.2 for a three-dimensional beam formulation that is closely related to that of Simo [S2] and Simo and Vu-Quoc [S3].

16.14.1 Expressions for curvature that directly use nodal triads

Figure 16.6 shows a beam element with a nodal triad **T** at the left-hand node, A and a nodal triad **U** at the right-hand node, B. The figure also shows a triad, **E**, that represents the 'local frame'. (Details on the derivation of the latter will be given in Section 17.1.2.)

In relation to Figure 16.6, we can use (16.47) and (16.31) to obtain the rotation between the left and right-hand triads as

$$\exp(\mathbf{S}(\Delta\boldsymbol{\theta}_g)) = \mathbf{U}\mathbf{T}^T \tag{16.111}$$

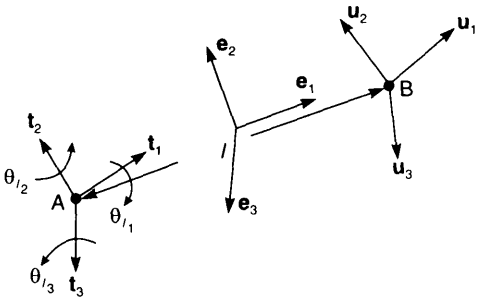

Figure 16.6 Nodal triads **U** and **T** and element triad **E**.

so that, using the approximation in (16.60):

$$\mathbf{S}(\Delta\boldsymbol{\theta}_g) \simeq \frac{(\mathbf{U}\mathbf{T}^T - \mathbf{T}\mathbf{U}^T)}{2} \tag{16.112}$$

from which the pseudo-vector, $\Delta\boldsymbol{\theta}_g$, could be obtained. Assuming a constant curvature, one could obtain:

$$\mathbf{R}(\boldsymbol{\chi}_g) = \exp(\mathbf{S}(\boldsymbol{\chi}_g) = \frac{\exp(\mathbf{S}(\Delta\boldsymbol{\theta}_g)}{l} = \frac{\mathbf{U}\mathbf{T}^T}{l} \tag{16.113}$$

with

$$\mathbf{S}(\boldsymbol{\chi}_g) \simeq \frac{\mathbf{U}\mathbf{T}^T - \mathbf{T}\mathbf{U}^T}{2l} \tag{16.114}$$

so that the 'global' curvature vector is

$$\boldsymbol{\chi}_g = \frac{\Delta\boldsymbol{\theta}_g}{l} \tag{16.115}$$

With the **E** triad in Figure 16.6 defining the local frame, the local curvature vector, $\boldsymbol{\chi}_l$, is then given by

$$\boldsymbol{\chi}_l = \mathbf{E}^T\boldsymbol{\chi}_g = \mathbf{E}^T\frac{\Delta\boldsymbol{\theta}_g}{l} = \Delta\boldsymbol{\theta}_l/l \tag{16.116}$$

For later use, we can directly transform $\mathbf{S}(\boldsymbol{\chi}_g)$ to local coordinates so that, using (16.112):

$$\mathbf{S}(\boldsymbol{\chi}_l) = \frac{1}{l}\mathbf{E}^T\mathbf{S}(\Delta\boldsymbol{\theta}_g)\mathbf{E} \simeq \frac{\mathbf{E}^T\mathbf{U}\mathbf{T}^T\mathbf{E} - \mathbf{E}^T\mathbf{T}\mathbf{U}^T\mathbf{E}}{2l} \tag{16.117}$$

An alternative procedure, that will be used in Section 17.1 involves first obtaining the global rotation from **U** to **E** as

$$\mathbf{S}(\Delta\boldsymbol{\theta}_{gB}) \simeq \frac{(\mathbf{U}\mathbf{E}^T - \mathbf{E}\mathbf{U}^T)}{2} \tag{16.118}$$

and then the global rotation from **E** to **T** as

$$\mathbf{S}(\Delta\boldsymbol{\theta}_{gA}) = \frac{(\mathbf{T}\mathbf{E}^T - \mathbf{E}\mathbf{T}^T)}{2} \tag{16.119}$$

From which the local rotations with respect to the **E** frame are given by

$$\mathbf{S}(\boldsymbol{\theta}_{lB}) = \mathbf{E}^T\mathbf{S}(\Delta\boldsymbol{\theta}_{gB})\mathbf{E} \simeq \frac{(\mathbf{E}^T\mathbf{U} - \mathbf{U}^T\mathbf{E})}{2} \tag{16.120}$$

and

$$\mathbf{S}(\boldsymbol{\theta}_{lA}) = \mathbf{E}^T\mathbf{S}(\Delta\boldsymbol{\theta}_{gA})\mathbf{E} \simeq \frac{(\mathbf{E}^T\mathbf{T} - \mathbf{T}^T\mathbf{E})}{2} \tag{16.121}$$

Having obtained $\boldsymbol{\theta}_{lB}$ and $\boldsymbol{\theta}_{lA}$ from (16.120) and (16.121), assuming a constant curvature, the latter would be given by

$$\boldsymbol{\chi}_l = \frac{1}{l}\,(\boldsymbol{\theta}_{lB} - \boldsymbol{\theta}_{lA}) \tag{16.122}$$

In relation to (16.122), we also have (using (16.120) and (16.121)):

$$\mathbf{S}(\boldsymbol{\chi}_l) = \frac{1}{l}\,(\mathbf{S}(\boldsymbol{\theta}_{lB}) - \mathbf{S}(\boldsymbol{\theta}_{lA})) = \frac{1}{2l}\,(\mathbf{E}^T\mathbf{U} - \mathbf{U}^T\mathbf{E} - \mathbf{E}^T\mathbf{T} + \mathbf{T}^T\mathbf{E}) \tag{16.123}$$

As the differences between the triads become small, we could assume that rotation from **T** to **U** is the sum of the rotation from **T** to **E** and that from **E** to **U** and write:

$$\mathbf{U}\mathbf{T}^T \simeq \mathbf{U}\mathbf{E}^T + \mathbf{E}\mathbf{T}^T \tag{16.124}$$

Substitution from (16.124) into (16.117) then leads to (16.123).

Having used (16.120) and (16.121) to obtain $\boldsymbol{\theta}_{lB}$ and $\boldsymbol{\theta}_{lA}$, there is no need to assume a constant curvature, but rather one can use these local rotations to define, say a linear curvature for a corotational Kirchhoff element (see Section 17.1).

The derivations leading to (16.120) and (16.121) required the approximations in (16.118) and (16.119). In particular, (16.118) was used to obtain the skew-symmetric matrix $\mathbf{S}(\boldsymbol{\theta}_{gB})$ from the rotation matrix $\mathbf{U}\mathbf{E}^T$. Instead, we could express $\mathbf{U}\mathbf{E}^T$ with respect to the local (**E**) frame as

$$\mathbf{R}_{lB} = \mathbf{E}^T(\mathbf{U}\mathbf{E}^T)\mathbf{E} = \mathbf{E}^T\mathbf{U} = \begin{bmatrix} \mathbf{e}_1^T\mathbf{u}_1 & \mathbf{e}_1^T\mathbf{u}_2 & \mathbf{e}_1^T\mathbf{u}_3 \\ \mathbf{e}_2^T\mathbf{u}_1 & \mathbf{e}_2^T\mathbf{u}_2 & \mathbf{e}_2^T\mathbf{u}_3 \\ \mathbf{e}_3^T\mathbf{u}_1 & \mathbf{e}_3^T\mathbf{u}_2 & \mathbf{e}_3^T\mathbf{u}_3 \end{bmatrix} \tag{16.125}$$

We could then obtain $\mathbf{S}(\boldsymbol{\theta}_{lB})$ from $\mathbf{R}_{lB}$. A similar approach could be used to obtain $\mathbf{S}(\theta_{lA})$. If we used the approximation in (16.60) to obtain the skew-symmetric matrix (and hence the pseudo-vector) from the rotation matrix, this would lead to the previous result (i.e. (16.122)). However, we could use the expression in (16.59) so that:

$$\sin\theta_{lB}\mathbf{e} \cong \begin{bmatrix} \sin\theta_{l1} \\ \sin\theta_{l2} \\ \sin\theta_{l3} \end{bmatrix} = \frac{1}{2}\begin{bmatrix} \mathbf{e}_3^T\mathbf{u}_2 - \mathbf{e}_2^T\mathbf{u}_3 \\ \mathbf{e}_1^T\mathbf{u}_3 - \mathbf{e}_3^T\mathbf{u}_1 \\ \mathbf{e}_2^T\mathbf{u}_1 - \mathbf{e}_1^T\mathbf{u}_2 \end{bmatrix} \tag{16.126}$$

(Note that there is a slight conflict of notation here and that the vectgor, **e**, on the left-hand side of (16.126) is quite separate from the vectors $\mathbf{e}_1$–$\mathbf{e}_3$ appearing on the

right-hand side). Equation (16.126) can be derived directly [C1] using the geometry of the configuration in Figure 16.6. With $\sin\theta$ being approximated by θ, (16.126) becomes consistent with (16.120).

16.14.2 Curvature without nodal triads

From the work of the previous section, if we have two triads **U** and **T** that are a distance l apart, we can write:

$$\mathbf{S}(\chi_g) \simeq \frac{\mathbf{U}\mathbf{T}^T - \mathbf{T}\mathbf{U}^T}{2l} \tag{16.127}$$

If l is now replaced by an infinitesimal distance of arc, ds (ds is the initial arc length—see Section 17.3.6 for details) and **U** is replaced by $\mathbf{T} + (d\mathbf{T}/ds)ds$, we obtain:

$$\mathbf{S}(\chi_g) = \frac{1}{2ds}\left(\left(\mathbf{T} + \frac{d\mathbf{T}}{ds}ds\right)\mathbf{T}^T - \mathbf{T}\left(\mathbf{T} + \frac{d\mathbf{T}}{ds}ds\right)^T\right) = \frac{1}{2}\left(\frac{d\mathbf{T}}{ds}\mathbf{T}^T - \frac{d\mathbf{T}^T}{ds}\right) \tag{16.128}$$

It has already been shown in (16.98) that $\delta\mathbf{R}\mathbf{R}^T$ is antisymmetric. In a similar manner, it can be shown that $(\partial\mathbf{T}/\partial s)\mathbf{T}^T$ is antisymmetric and so, for future developments, replacing **T** by **R** in (16.128), leads to

$$\mathbf{S}(\chi_g) = \frac{d\mathbf{R}}{ds}\mathbf{R}^T \tag{16.129}$$

For the work in Section 17.3 we will use (16.129) to obtain the curvature with **R** and $d\mathbf{R}/ds$ being related to a particular Gauss point. However, we will eventually require the local curvature, χ_l rather than the global curvature, χ_g. Having obtained χ_g from (16.129), χ_l can be obtained as

$$\chi_l = \mathbf{R}^T\chi_g \tag{16.130}$$

(Here **R** is the equivalent of the previous **E**—see (16.116).)

For the work in Section 17.3 we first need to know how to update χ_g (or χ_l) and, second, how to obtain $\delta\chi_l$ for use with the virtual work. We will now deal with the latter.

Intuitively, one might simply write:

$$\delta\chi_l = \mathbf{R}^T\frac{d\delta\bar{\boldsymbol{\theta}}}{ds} \tag{16.131}$$

which, for a two-noded element, gives:

$$\delta\chi_l = \frac{1}{l}\mathbf{R}^T(\delta\bar{\boldsymbol{\theta}}_2 - \delta\bar{\boldsymbol{\theta}}_1) \tag{16.132}$$

In the above, the terms $\delta\bar{\boldsymbol{\theta}}_1$, etc. are non-additive spins as discussed in Section 16.11. (The delta symbol on the $\delta\bar{\boldsymbol{\theta}}$'s merely means that the quantities are infinitesimally small. The $\delta\bar{\boldsymbol{\theta}}$'s are not changes in $\bar{\boldsymbol{\theta}}$.) We will now show that (16.131) does indeed follow from (16.129) and (16.130).

From (16.129), we can obtain:

$$\delta \mathbf{S}(\boldsymbol{\chi}_g) = \mathbf{S}(\delta \boldsymbol{\chi}_g) = \delta\left(\frac{d\mathbf{R}}{ds}\right)\mathbf{R}^T + \frac{d\mathbf{R}}{ds}\delta\mathbf{R}^T \tag{16.133}$$

The $\delta\mathbf{R}$ term in (16.133) can be obtained from (16.81c) so that:

$$\delta\mathbf{R} = \mathbf{S}(\delta\bar{\boldsymbol{\theta}})\mathbf{R}; \qquad \delta\mathbf{R}^T = -\mathbf{R}^T\mathbf{S}(\delta\bar{\boldsymbol{\theta}}) \tag{16.134}$$

and, in addition, with a view to the first term on the right-hand side of (16.133), one can write:

$$\delta\left(\frac{d\mathbf{R}}{ds}\right) = \frac{d}{ds}(\delta\mathbf{R}) = \frac{d}{ds}(\mathbf{S}(\delta\bar{\boldsymbol{\theta}})\mathbf{R}) = \mathbf{S}(\delta\bar{\boldsymbol{\theta}})\frac{d\mathbf{R}}{ds} + \frac{d\mathbf{S}}{ds}\mathbf{R} = \mathbf{S}(\delta\bar{\boldsymbol{\theta}})\frac{d\mathbf{R}}{ds} + \mathbf{S}\left(\frac{d\delta\bar{\boldsymbol{\theta}}}{ds}\right)\mathbf{R} \tag{16.135}$$

Combining (16.133)–(16.135) and making use of (16.129), leads to

$$\mathbf{S}(\delta\boldsymbol{\chi}_g) = \mathbf{S}\left(\frac{d\delta\bar{\boldsymbol{\theta}}}{ds}\right) + \mathbf{S}(\delta\bar{\boldsymbol{\theta}})\mathbf{S}(\boldsymbol{\chi}_g) - \mathbf{S}(\boldsymbol{\chi}_g)\mathbf{S}(\delta\bar{\boldsymbol{\theta}}) \tag{16.136}$$

or

$$\mathbf{S}(\delta\boldsymbol{\chi}_g) = \mathbf{S}\left(\frac{d\delta\bar{\boldsymbol{\theta}}}{ds}\right) + \boldsymbol{\chi}_g\delta\bar{\boldsymbol{\theta}}^T - \delta\bar{\boldsymbol{\theta}}\boldsymbol{\chi}_g^T \tag{16.137}$$

where, in moving from (16.136) to (16.137), we have used (16.86) which is reproduced here, for convenience as

$$\mathbf{S}(\mathbf{a})\mathbf{S}(\mathbf{b}) = \mathbf{b}\mathbf{a}^T - (\mathbf{a}^T\mathbf{b})\mathbf{I}$$

The pseudo-vector from (16.137) is given by

$$\delta\boldsymbol{\chi}_g = \frac{d\delta\bar{\boldsymbol{\theta}}}{ds} + \mathbf{S}(\delta\bar{\boldsymbol{\theta}})\boldsymbol{\chi}_g = \frac{d\delta\bar{\boldsymbol{\theta}}}{ds} + \delta\bar{\boldsymbol{\theta}} \times \boldsymbol{\chi}_g \tag{16.138}$$

This can be checked by making use of (16.100).

To obtain $\delta\boldsymbol{\chi}_l$, we can now differentiate (16.130) to obtain:

$$\delta\boldsymbol{\chi}_l = \mathbf{R}^T\delta\boldsymbol{\chi}_g + \delta\mathbf{R}^T\boldsymbol{\chi}_g \tag{16.139}$$

With $\delta\boldsymbol{\chi}_g$ from (16.138) and $\delta\mathbf{R}^T$ from (16.135), this procedure leads to the relationship in (16.131) which was originally based on intuition.

The previous relationships apply for very small (infinitesimal) rotations and are therefore relevant to the virtual work. However, we would expect errors if we applied them to the finite 'incremental' values obtained from the finite element analysis. In particular, errors would result from updating $\boldsymbol{\chi}_l$ using (16.131) so that:

$$\boldsymbol{\chi}_l = \boldsymbol{\chi}_l \rightarrow \Delta\boldsymbol{\chi}_l = \boldsymbol{\chi}_l + \mathbf{R}_{old}^T\frac{d\Delta\boldsymbol{\theta}}{ds} \tag{16.140}$$

where the $\Delta\boldsymbol{\theta}$'s were obtained from the finite element analysis. (Strictly, we should have written $\Delta\bar{\boldsymbol{\theta}}$ rather than $\Delta\boldsymbol{\theta}$ in the above because the finite element variables that will be used in Sections 17.1–17.4 are non-additive (even in the limit). However, the developments that will follow involve differentials with respect to s, and the distinction is not

important.) Naively, one might modify (16.140) to give:

$$\chi_l = \chi_l + \Delta\chi_l = \chi_l + \mathbf{R}_{\text{mid}}^{\mathrm{T}} \frac{\mathrm{d}\Delta\boldsymbol{\theta}}{\mathrm{d}s} \tag{16.141}$$

with, say,

$$\mathbf{R}_{\text{mid}} = \Delta\mathbf{R}(\Delta\boldsymbol{\theta}/2)\mathbf{R}_{\text{old}} \tag{16.142}$$

where the footnote on page 196 applies in relation to the Δ in front of $\mathbf{R}(\Delta\boldsymbol{\theta}/2)$. However, following Simo [S2] and Simo and Vu-Quoc [S3] a more accurate update can be obtained. In particular, from (16.129), we can write:

$$\begin{aligned}\mathbf{S}_{\mathrm{n}}(\boldsymbol{\chi}_{\mathrm{gn}}) &= \frac{\mathrm{d}\mathbf{R}_{\mathrm{n}}}{\mathrm{d}s}\mathbf{R}_{\mathrm{n}}^{\mathrm{T}} = \frac{\mathrm{d}\mathbf{R}_{\mathrm{n}}}{\mathrm{d}s}\mathbf{R}_{\mathrm{o}}^{\mathrm{T}}\Delta\mathbf{R}(\Delta\boldsymbol{\theta})^{\mathrm{T}} = \frac{\mathrm{d}}{\mathrm{d}s}(\Delta\mathbf{R}\mathbf{R}_{\mathrm{o}})\mathbf{R}_{\mathrm{o}}^{\mathrm{T}}\Delta\mathbf{R}(\Delta\boldsymbol{\theta})^{\mathrm{T}} \\ &= \left(\frac{\mathrm{d}\Delta\mathbf{R}}{\mathrm{d}s}\mathbf{R}_{\mathrm{o}} + \Delta\mathbf{R}\frac{\mathrm{d}\mathbf{R}_{\mathrm{o}}}{\mathrm{d}s}\right)\mathbf{R}_{\mathrm{o}}^{\mathrm{T}}\Delta\mathbf{R}^{\mathrm{T}} = \frac{\mathrm{d}\Delta\mathbf{R}}{\mathrm{d}s}\Delta\mathbf{R}^{\mathrm{T}} + \Delta\mathbf{R}\mathbf{S}(\boldsymbol{\chi}_{\mathrm{go}})\Delta\mathbf{R}^{\mathrm{T}}\end{aligned} \tag{16.143}$$

(In the above and below, the subscript o is being used as short for old, and n as short for new.) Equation (16.143) can be rewritten as

$$\mathbf{S}_{\mathrm{n}}(\boldsymbol{\chi}_{\mathrm{g}}) = \frac{\mathrm{d}\Delta\mathbf{R}}{\mathrm{d}s}\Delta\mathbf{R}^{\mathrm{T}} + \Delta\mathbf{R}\mathbf{S}(\boldsymbol{\chi}_{\mathrm{go}})\Delta\mathbf{R}^{\mathrm{T}} = \mathbf{S}(\boldsymbol{\chi}_{\mathrm{gn1}}) + \mathbf{S}(\boldsymbol{\chi}_{\mathrm{gn2}}) \tag{16.144}$$

where, knowing $\Delta\mathbf{R}$, the last term is easily computed. Hence, to obtain $\mathbf{S}_{\mathrm{n}}$, we require $\mathbf{S}(\boldsymbol{\chi}_{\mathrm{gn1}}) = \mathrm{d}\Delta\mathbf{R}/\mathrm{d}s\,(\Delta\mathbf{R}^{\mathrm{T}})$.

In Section 16.12, we obtain the differential of the Rodrigues formula in (16.101). In the current context (with differentiation with respect to s which we will denote by adding a prime) an equivalent relationship can be obtained as

$$\mathbf{S}(\boldsymbol{\chi}_{\mathrm{gn1}}) = \frac{\mathrm{d}\Delta\mathbf{R}}{\mathrm{d}s}\mathbf{R}(\boldsymbol{\omega})^{\mathrm{T}} = \frac{1}{1+\frac{1}{4}\boldsymbol{\omega}^{\mathrm{T}}\boldsymbol{\omega}}\left[\mathbf{S}(\boldsymbol{\omega}') + \tfrac{1}{2}\mathbf{S}(\boldsymbol{\omega})\mathbf{S}(\boldsymbol{\omega}') - \tfrac{1}{2}\mathbf{S}(\boldsymbol{\omega}')\mathbf{S}(\boldsymbol{\omega})\right] \tag{16.145}$$

In the above, $\boldsymbol{\omega}$ is the tangent scaled pseudo-vector (here from $\Delta\boldsymbol{\theta}$) so that (see (16.34)):

$$\boldsymbol{\omega} = \frac{2\tan(\Delta\theta/2)}{\Delta\theta}\Delta\boldsymbol{\theta} = 2\tan(\Delta\theta/2)\mathbf{e} \tag{16.146}$$

and, via differentiation of (16.146) with respect to s (see also (16.84)):

$$\boldsymbol{\omega}' = \frac{\mathrm{d}\boldsymbol{\omega}}{\mathrm{d}s} = \frac{2\tan(\Delta\theta/2)}{\Delta\theta}\left[\mathbf{I} - \left(1 - \frac{\Delta\theta}{\sin\Delta\theta}\right)\mathbf{e}\mathbf{e}^{\mathrm{T}}\right]\frac{\mathrm{d}\Delta\boldsymbol{\theta}}{\mathrm{d}s} \tag{16.147}$$

Hence, knowing $\Delta\boldsymbol{\theta}$ and $\mathrm{d}\Delta\boldsymbol{\theta}/\mathrm{d}s$, (16.145)–(16.147) can be used to obtain $\mathbf{S}(\boldsymbol{\chi}_{\mathrm{gn1}})$ and hence $\boldsymbol{\chi}_{\mathrm{gn1}}$. Indeed the latter is given directly (see also (16.87)) as

$$\boldsymbol{\chi}_{\mathrm{gn1}} = \frac{1}{1+\frac{1}{4}\boldsymbol{\omega}^{\mathrm{T}}\boldsymbol{\omega}}\left[\boldsymbol{\omega}' + \tfrac{1}{2}(\boldsymbol{\omega}\times\boldsymbol{\omega}')\right] \tag{16.148}$$

(with $\boldsymbol{\omega}$ from (16.146) and $\boldsymbol{\omega}'$ from (16.147)).

At a particular Gauss point, we would know $\mathbf{R}_{\mathrm{o}}$ and $\boldsymbol{\chi}_{\mathrm{go}}$ and, as a result of an increment or iteration in the finite element analysis, we could obtain $\Delta\boldsymbol{\theta}$ and $\mathrm{d}\Delta\boldsymbol{\theta}/\mathrm{d}s$, using the nodal 'rotations' and the interpolations (see Section 17.2 for details). The

updating procedure at a Gauss point could then involve:

1. Computer $\Delta\mathbf{R}(\Delta\boldsymbol{\theta})$ via the Rodrigues formula;
2. Compute $\mathbf{R}_n = \Delta\mathbf{R}\mathbf{R}_o$;
3. Compute $\mathbf{S}(\boldsymbol{\chi}''_{gn}) = \Delta\mathbf{R}\mathbf{S}(\boldsymbol{\chi}_{go})\Delta\mathbf{R}^T$ (see (16.144));
4. Compute $\boldsymbol{\chi}_{gn1}$ from (16.148) (with (16.146) and (16.147));
5. Compute $\boldsymbol{\chi}_{gn} = \boldsymbol{\chi}_{gn1} + \boldsymbol{\chi}_{gn2}$ (see (16.144));
6. Compute $\boldsymbol{\chi}_{ln}$ from $\mathbf{R}_n^T\boldsymbol{\chi}_{gn}$ (see (16.130)).

If the objective is simply the computation of $\boldsymbol{\chi}_{ln}$ (as in Section 17.3.3), the previous algorithm can be simplified. To this end, we first rewrite the last step (6) in the previous algorithm as

$$\boldsymbol{\chi}_{ln} = \boldsymbol{\chi}_{ln} + \boldsymbol{\chi}_{ln} = \mathbf{R}_n^T\boldsymbol{\chi}_{gn1} + \mathbf{R}_n^T\boldsymbol{\chi}_{gn2} \tag{16.149}$$

From the relationships in (16.144), we can write:

$$\boldsymbol{\chi}_{gn2} = \Delta\mathbf{R}\boldsymbol{\chi}_{go} \tag{16.150}$$

so that

$$\boldsymbol{\chi}_{ln2} = \mathbf{R}_n^T\boldsymbol{\chi}_{gn2} = \mathbf{R}_n^T\Delta\mathbf{R}\boldsymbol{\chi}_{go} = \mathbf{R}_o^T\boldsymbol{\chi}_{go} = \boldsymbol{\chi}_{lo} \tag{16.151}$$

and hence (16.149) reduces to

$$\boldsymbol{\chi}_{ln} = \boldsymbol{\chi}_{lo} + \mathbf{R}_o^T\boldsymbol{\chi}_{gn1} \tag{16.152}$$

Hence, the previous algorithm can be simplified to avoid $\boldsymbol{\chi}_{gn2}$ and to involve:

1. Computer $\Delta\mathbf{R}(\Delta\boldsymbol{\theta})$ via the Rodrigues formula;
2. Compute $\mathbf{R}_n = \Delta\mathbf{R}\mathbf{R}_o$;
3. Compue $\boldsymbol{\chi}_{gn1}$ from (16.148) (with (16.146) and (16.147));
4. Compute $\boldsymbol{\chi}_{ln} = \boldsymbol{\chi}_{lo} + \mathbf{R}_n^T\boldsymbol{\chi}_{gn1}$.

It will now be shown that, in the limit, (16.152) corresponds with (16.130) as $\Delta\boldsymbol{\theta}$ (or $\Delta\bar{\boldsymbol{\theta}}$—see discussion below (16.140)) tends to $\delta\bar{\boldsymbol{\theta}}$ which tends to zero. For this to be true, we require:

$$\delta\boldsymbol{\chi}_l \sim \lim[\mathbf{R}_n^T\boldsymbol{\chi}_{gn1}] = \mathbf{R}_o^T\frac{d\delta\bar{\boldsymbol{\theta}}}{ds} \tag{16.153}$$

From (16.146) and (16.147) in the limiting case, we have

$$\boldsymbol{\omega} = \delta\bar{\theta}\mathbf{e} = \gamma\bar{\boldsymbol{\theta}}; \qquad \delta\boldsymbol{\omega}_a = \frac{d\delta\bar{\boldsymbol{\theta}}}{ds} \tag{16.154}$$

so that in (16.148):

$$\boldsymbol{\chi}_{gn1} = \frac{d\delta\bar{\boldsymbol{\theta}}}{ds} + \frac{1}{2}\left(\delta\bar{\boldsymbol{\theta}} \times \frac{d\delta\bar{\boldsymbol{\theta}}}{ds}\right) \tag{16.155}$$

Also, in the limit, one can write (see (16.5), (16.80) and (16.81)):

$$\mathbf{R}_n = [\mathbf{I} + \mathbf{S}(\delta\bar{\boldsymbol{\theta}})]\mathbf{R}_o; \quad \mathbf{R}_n^T = \mathbf{R}_0^T[\mathbf{I} - \mathbf{S}(\delta\bar{\boldsymbol{\theta}})] \tag{16.156}$$

and consequently, in (16.153):

$$\delta\boldsymbol{\chi}_l \sim \mathbf{R}_o^T \frac{d\delta\bar{\boldsymbol{\theta}}}{ds} + \left(\frac{1}{2}\mathbf{R}_o^T\left(\delta\bar{\boldsymbol{\theta}} \times \frac{d\delta\bar{\boldsymbol{\theta}}}{ds}\right) - \mathbf{R}_o^T\mathbf{S}(\delta\bar{\boldsymbol{\theta}})\frac{d\delta\bar{\boldsymbol{\theta}}}{ds}\right)_h$$

$$= \mathbf{R}_o^T \frac{d\delta\bar{\boldsymbol{\theta}}}{ds} - \left(\frac{1}{2}\mathbf{R}_o^T\mathbf{S}(\delta\bar{\boldsymbol{\theta}})\frac{d\delta\bar{\boldsymbol{\theta}}}{ds}\right)_h \tag{16.157}$$

where the higher-order terms vanish in the limit and (16.153) is confirmed.

We can also justify the approximation intuitively put forward in (16.141). For, with

$$\mathbf{R}_{mid} \simeq [\mathbf{I} + \tfrac{1}{2}\mathbf{S}(\Delta\bar{\boldsymbol{\theta}})]\mathbf{R}_o \tag{16.158}$$

and δ's changed to Δ's, (16.141) coincides with (16.157) with the higher-order terms included.

16.15 SPECIAL NOTATION

$\mathbf{C}$ = matrix connection $\delta\bar{\boldsymbol{\theta}}$ to $\delta\boldsymbol{\omega}_a$ (see (16.88))
$\mathbf{E}$ = in Section 16.14, triad defining 'local' element frame
$\mathbf{e}$ = unit vector in direction of axis of rotation
$\exp(\mathbf{S}(\boldsymbol{\theta}))$ = exponential form of rotation matrix (see (16.31))
$\mathbf{H}$ = matrix connecting $\delta\bar{\boldsymbol{\theta}}$ to $\delta\boldsymbol{\theta}_a$ (see (16.90))
$\mathbf{p}$ = unit vector
$\hat{\mathbf{q}}$ = unit quaternion (see (16.67))
$\mathbf{q}$ = in Section 16.9, part of $\hat{\mathbf{q}}$ (see (16.67))
$\mathbf{q}$ = in Section 16.13, unit vector
q_0, q_1, q_2, q_3 = components of $\hat{\mathbf{q}}$
$\mathbf{r}$ = unit vector
$\mathbf{R}$ = rotation matrix
$\mathbf{S}$ = skew symmetric matrix (see (16.8))
s = arc length (Section 16.14.2)
$\mathbf{T}$ = 'left-hand' nodal triad with components $\mathbf{t}_1$–$\mathbf{t}_3$ (Section 16.14.1)
$\mathbf{U}$ = 'right-hand' nodal triad with components $\mathbf{u}_1$–$\mathbf{u}_3$ (Section 16.14.1)
$\delta\bar{\boldsymbol{\theta}}$ = spin vector
$\boldsymbol{\theta}$ = pseudo-vector = $\theta\mathbf{e}$
θ = magnitude of $\boldsymbol{\theta}$ such that $\theta^2 = \boldsymbol{\theta}^T\boldsymbol{\theta}$
$\boldsymbol{\omega}$ = tangent scaled-pseudo-vector (see (16.35))
ω = magnitude of $\boldsymbol{\omega}$ such that $\omega^2 = \boldsymbol{\omega}^T\boldsymbol{\omega}$
$\boldsymbol{\psi}$ = sine scaled pseudo-vector (see (16.36))
ψ = magnitude of $\boldsymbol{\psi}$ such that $\psi^2 = \boldsymbol{\psi}^T\boldsymbol{\psi}$
$\boldsymbol{\chi}$ = curvature vector (Section (16.14))

Subscripts

a = additive
g = global

l = local
n = new
o = old

16.16 REFERENCES

[A1] Argyris, J., An excursion into large rotations, *Comp. Meth. in Appl. Mech. & Engng.*, **32**, 85–155 (1982).

[A2] Atluri, S. N. & Cazzani, A., Rotations in computational solid mechanics, *Archives of Computational Methods in Engineering*, **2**, 49–138 (1995).

[B1] Bates, D. N., The mechanics of thin walled structures with special reference to finite rotations, Ph.D. thesis, Dept. of Civil Engng., Imperial College, London (1987).

[B2] Besseling, J. F., Large rotations in problems of structural mechanics, *Finite Element Methods for Nonlinear Problems*, ed. P. G. Bergan *et al.*, Springer-Verlag, Berlin, 25–39 (1986).

[B3] Bottema, O. & Roth, B., *Theoretical Kinematics*, North-Holland, Amsterdam (1979).

[C1] Crisfield, M. A., A consistent co-rotational formulation for non-linear three-dimensional beam elements, *Comp. Meth. in Appl. Mech. & Engng.*, **81**, 131–150 (1990).

[G1] Geradin, M., Park, K. C. & Cardona, A., *On the Representation of Finite Rotations in Spatial Kinematics*, Report No. VA-51, Dept. of Mech. Engng., Univ. of Colorado, Boulder Colorado (1988).

[H1] Hamilton, W. R., *Elements of Quaternions*, Cambridge Univ. Press., Cambridge (1899).

[H2] Hughes, T. J. R. & Winget, J., Finite rotation effects in numerical integration of rate constitutive equations arising in large deformation analysis, *Int. J. for Num. Meth. in Engng.*, **15**, 1862–1867 (1980).

[P1] Pars, L. A., A treatise on analytical dynamics, Ch. 7: *The Theory of Rotations*, Heinemann, London, pp. 90–107 (1965).

[R1] Rankin, C. C. & Brogan, F. A., An element independent corotational procedure for the treatment of large rotations *Collapse Analysis of Structures*, ed. L. H. Sobel & K. Thomas, ASME, New York, pp. 85–100 (1984).

[R2] Rodrigues, O., Des lois géométriques qui régissent les déplacements d'un système solide dans l'espace et de la variation des coordinnées provenant de ces déplacements considéres indépendment des causes qui peuvent les produire, *J. Math. Pures Appl.*, **5**, 380–440 (1840).

[S1] Shabena, A. A., *Dynamics of Multi-body Systems*, Wiley, New York (1989).

[S2] Simo, J. C., A finite strain beam formulation—the three-dimensional dynamic problem Part 1, *Comp. Meth. in Appl. Mech. & Engng.*, **49**, 55–70 (1985).

[S3] Simo, J. C. & Vu-Quoc, L., A three-dimensional finite-strain rod model. Part II: Computational aspects, *Comp. Meth. in Appl. Mech. Mech. & Engng.*, **58**, 79–116 (1986).

[S4] Spurrier, R. A., Comment on 'singularity-free extraction of a quaternion from direction cosine matrix', *J. Spacecraft*, **15** (4), 255 (1978).

[S5] Spring, K. W., Euler parameters and the use of quaternion algebra in the manipulation of finite rotations: a review, *Mechanism and Mechine Theory*, **21** (5), 365–373 (1986).

[S6] Stuelpnagel, J., On the parametrisation of the three-dimensional rotation group, *SIAM Review*, **6** (4), 422–430 (1964).

[W1] Wehage, R. A., Quaternions and Euler parameters—a brief exposition, *Computer Aided Analysis and Optimisation of Mechanical System Dynamics*, NATO ASI Series, Vol. F9, ed. E. J. Haug, Springer-Verlag, Heidelberg, pp. 147–180 (1984).

17 Three-dimensional formulations for beams and rods

Finite element methods for three-dimensional beams have been described in [B1, B3, B4, C1, C3, C5, C1.16, D1, E1, H2, J2, K1, K2, N1, O1, O2, S2.16, S3.16, W1–W3]. In the present chapter, we will extend some of the work of Chapter 7, which covered two-dimensional beams, to encompass three-dimensional beams. To this end, the main difficulty relates to the non-vectorial nature of large rotations which was discussed in the previous chapter. We will start by describing a co-rotational formulation related to earlier work by the author [C1.16, C3] and Cole [C5] which can be considered as a three-dimensional extension of the two-dimensional work in Sections 7.2 and 7.3. We will then give an interpretation of a three-dimensional beam element due to Simo and Vu-Quoc [S3.16] which can be considered as an extension of the two-dimensional work in Section 7.4 and is related to Reissner's theory [R2].

In Section 7.5, we described a degenerate continuum approach for two-dimensional beams based on the total Lagrangian approach. In Section 17.3 of the present Chapter, we describe a related three-dimensional formulation due to Dvorkin *et al.* [D1]. Unconventionally, some of the finite-element formulations lead to non-symmetric tangent stiffness matrices, even for conservative loadings. However, symmetry is recovered at equilibrium (or almost so—see Section 17.4) and the quadratic convergence properties are maintained when the stiffness matrices are artificially symmetrised. These issues are discussed in Section 17.4 where it is shown that the symmetry or non-symmetry is related to the choice of rotation variables.

Finally, in Section 17.5, we consider various forms of conservative and non-conservative loading, while in Section 17.6, we consider a method for introducing joints into non-linear beams. The work on conservative and non-conservative loading has relevance to structures other than beams.

17.1 A CO-ROTATIONAL FRAMEWORK FOR THREE-DIMENSIONAL BEAM ELEMENTS

A brief history of the co-rotational technique was given in conjunction with a set of appropriate references in Section 7.2. These include Argyris's work on the 'natural

approach' [A3] and the early work of Belytschko *et al.* [B3, B4]. In reference [C1.16], the author developed a three-dimensional co-rotational element based on Kirchhoff (or Euler–Bernoulli) theory. In conjunction with Cole, this work was later adapted to cover a Timoshenko element (with shear deformation) in reference [C3]. In the present section, we will follow the approach of Rankin and Brogan [R1.16] and will take the co-rotational procedure outside the algorithm for the linear element computations. In this way the concepts should be applicable to any beam element which has two nodes and six degrees of freedom at each node. Indeed, one could cover higher-order elements with internal nodes provided the internal variables are eliminated at the element level (this should be very simple for a beam). The procedure that will be described follows Rankin and Brogan [R1.16] in totally divorcing the co-rotational procedure from the linear element computations, but differs in other respects; in particular the precise definition of the local element frame (but see Section 17.1.6) and the computation of the 'initial stress matrix' (not considered by Rankin and Brogan in [R1.16], but considered later by Rankin and co-workers in [R1, N1]).

Following the two-dimensional work of Section 7.2, we will initially assume that the 'internal element' is linear and that all of the non-linearity is introduced via the co-rotational technique. In Section 7.2, we indicated how this approach could later be extended to include higher-order non-linear axial terms. In relation to the present formalism, this would mean that one could later embed a 'locally shallow' beam element (for example, based on von Karman theory) within the co-rotational framework. This aspect will be considered in Section 17.5.

Some of the detail associated with the current co-rotational procedures becomes a little cumbersome and an alternative approach will be outlined in Section 18.10. The latter work has strong links with the techniques advocated by Nour-Omid and Rankin [N1].

Figure 17.1 shows the element which has two nodes and six degrees of freedom. The 'local' degrees of freedom are

$$\mathbf{p}_l^{\mathrm{T}} = (\mathbf{d}_{l1}^{\mathrm{T}}, \boldsymbol{\theta}_{l1}^{\mathrm{T}}, \mathbf{d}_{l2}^{\mathrm{T}}, \boldsymbol{\theta}_{l2}) \tag{17.1}$$

where

$$\mathbf{d}_{l1}^{\mathrm{T}} = (u_{l1}, v_{l1}, w_{l1}) \tag{17.1a}$$

and

$$\boldsymbol{\theta}_{l1}^{\mathrm{T}} = (\theta_{l1}, \theta_{l2}, \theta_{l3}) \tag{17.1b}$$

relate respectively to the translations and rotations at node 1 (Figure 17.1). The displacements u_l, v_l and w_l relate to the local element axes defined by unit base vector $\mathbf{e}_1$, $\mathbf{e}_2$ and $\mathbf{e}_3$ respectively where $\mathbf{e}_1$ lies along the element between nodes 1 and 2. In the current configuration, $\mathbf{e}_1$ can be computed from:

$$\mathbf{e}_1 = (\mathbf{x}_{21} + \mathbf{d}_{21})/l_2 \tag{17.2}$$

where the subscript '21' takes the same form as in Chapters 3 and 7 so that, for example, $\mathbf{x}_{21} = \mathbf{x}_2 - \mathbf{x}_1$ (with $\mathbf{x}$ being the *initial* vector—see Figure 17.1a). The term l_n in (17.2) is the current length between the two nodes (without accounting for any non-straightness). The precise definition for the vectors $\mathbf{e}_2$ and $\mathbf{e}_3$, which make up the local element triad, will be given later.

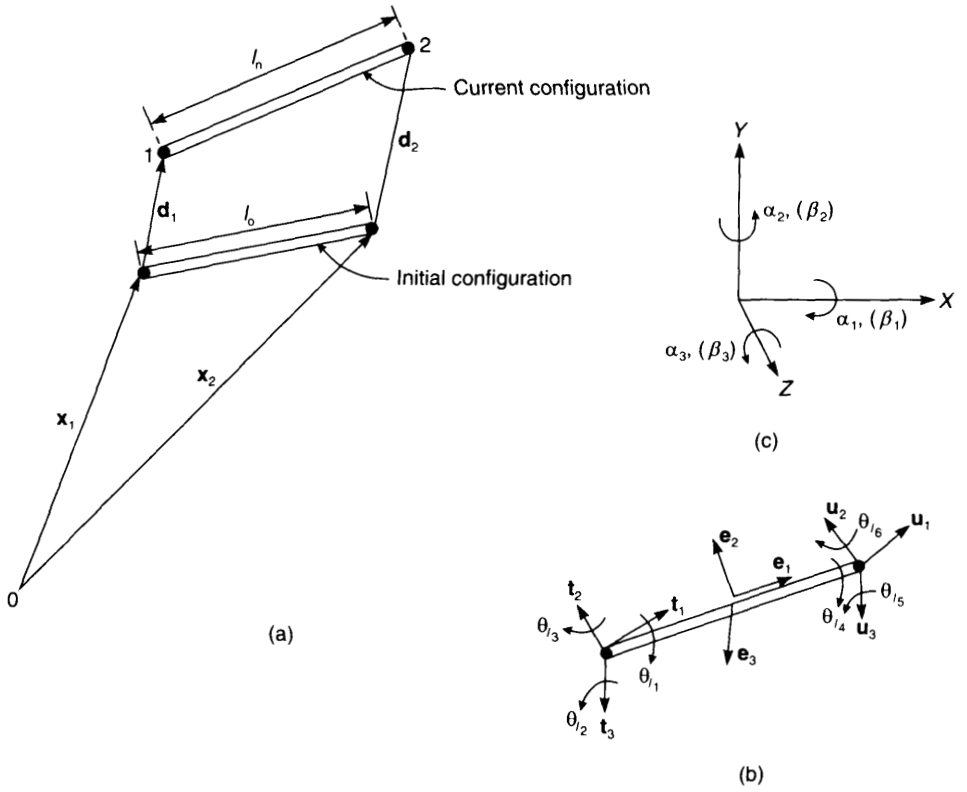

Figure 17.1 Two-noded, three-dimensional beam element. (a) Geometry; (b) current base vectors and local slopes; (c) global rotation variables.

The ordering and sign convention for the local rotation variables is given in Figure 17.1b. These variables may be slopes (as with a Kirchhoff or Euler–Bernoulli element) or rotations of the normal (as with a Timoshenko element). All that is required, is that we have access to the linear stiffness matrix, $\mathbf{K}_l$ which relates the local nodal forces, $\mathbf{q}_l$ to the local nodal displacements, $\mathbf{p}_l$ of (17.1) so that:

$$\mathbf{q}_l = \mathbf{K}_l \mathbf{p}_l \tag{17.3}$$

(In practice, because some of the local variables are zero, we do not need to fill in all the terms in $\mathbf{K}_l$. Indeed, we can condense some of the following equations to allow for zero rows and columns. However, this will be considered as a programming detail and will not be directly considered here.) In order to apply the co-rotational approach we first need some way of computing the local variables from the global variables ($\mathbf{p}$ without a subscript) and second we require the equivalent tangential relationship whereby:

$$\delta \mathbf{p}_l = \mathbf{F} \delta \mathbf{p} \tag{17.4}$$

(We have adopted the notation $\mathbf{F}$ rather than the $\mathbf{T}$ adopted in Chapter 3 or the $\mathbf{B}$ in Chapter 7 because the latter symbols are now being used for other purposes.) Following

the approach of Section 7.2.4, we can now equate the virtual work in the local and global systems so that $\mathbf{q}_{li}^{\mathrm{T}}\delta\mathbf{p}_{lv} = \mathbf{q}_{i}\delta\mathbf{p}_{v}$ and hence we can obtain the global internal force vector as

$$\mathbf{q}_{i} = \mathbf{F}^{\mathrm{T}}\mathbf{q}_{li} = \mathbf{F}^{\mathrm{T}}\mathbf{K}_{l}\mathbf{p}_{l} \tag{17.5}$$

and the tangent stiffness equations as

$$\delta\mathbf{q}_{i} = \mathbf{F}^{\mathrm{T}}\delta\mathbf{q}_{li} + \delta\mathbf{F}^{\mathrm{T}}\mathbf{q}_{li} = \mathbf{F}^{\mathrm{T}}\mathbf{K}_{l}\mathbf{F}\delta\mathbf{p} + \mathbf{K}_{i\sigma}\delta\mathbf{p} \tag{17.6}$$

17.1.1 Computing the local 'displacements'

Following the work of Section 7.2, we consider the axial deformation as being completely defined by the local strain producing extension which is given by

$$u_{l} = l_{\mathrm{n}} - l_{\mathrm{o}} = ((\mathbf{x}_{21} + \mathbf{d}_{21})^{\mathrm{T}}(\mathbf{x}_{21} + \mathbf{d}_{21}))^{1/2} - (\mathbf{x}_{21}^{\mathrm{T}}\mathbf{x}_{21})^{1/2} \tag{17.7}$$

Apart from the fact that there are now three rather than two displacement components, the procedure is essentially identical to that of Sections 7.2.1 and 7.2.3. Because the local co-rotating frame is effectively attached to node 1, and passes through node 2, we now have:

$$\mathbf{d}_{l1} = \mathbf{0} \tag{17.8a}$$

$$\mathbf{d}_{l2}^{\mathrm{T}} = (u_{l}, 0, 0) \tag{17.8b}$$

For the local rotations, we turn to Figure 17.1c which shows two 'nodal triads' $\mathbf{T} = [\mathbf{t}_1, \mathbf{t}_2, \mathbf{t}_3]$ and $\mathbf{U} = [\mathbf{u}_1, \mathbf{u}_2, \mathbf{u}_3]$ as well as the local element base frame $\mathbf{E} = [\mathbf{e}_1, \mathbf{e}_2, \mathbf{e}_3]$. If, for the present, we assume that we know these triads, from the work of Section 16.14.1 (and in particular equations (16.126)) we can obtain the 'local rotations' as

$$\begin{aligned}
2\sin(\mathbf{p}_{l}(4)) &= 2\sin\theta_{l1} = -\mathbf{t}_3^{\mathrm{T}}\mathbf{e}_2 + \mathbf{t}_2^{\mathrm{T}}\mathbf{e}_3 \\
2\sin(\mathbf{p}_{l}(5)) &= 2\sin\theta_{l2} = -\mathbf{t}_2^{\mathrm{T}}\mathbf{e}_1 + \mathbf{e}_2^{\mathrm{T}}\mathbf{t}_1 \\
2\sin(\mathbf{p}_{l}(6)) &= 2\sin\theta_{l3} = -\mathbf{t}_3^{\mathrm{T}}\mathbf{e}_1 + \mathbf{e}_3^{\mathrm{T}}\mathbf{t}_1 \\
2\sin(\mathbf{p}_{l}(10)) &= 2\sin\theta_{l4} = -\mathbf{u}_3^{\mathrm{T}}\mathbf{e}_2 + \mathbf{u}_2^{\mathrm{T}}\mathbf{e}_3 \\
2\sin(\mathbf{p}_{l}(11)) &= 2\sin\theta_{l5} = -\mathbf{u}_2^{\mathrm{T}}\mathbf{e}_1 + \mathbf{e}_2^{\mathrm{T}}\mathbf{u}_1 \\
2\sin(\mathbf{p}_{l}(12)) &= 2\sin\theta_{l6} = -\mathbf{u}_3^{\mathrm{T}}\mathbf{e}_1 + \mathbf{e}_3^{\mathrm{T}}\mathbf{u}_1
\end{aligned} \tag{17.9}$$

(Note the different ordering and sign convention for the local rotations in comparison with those considered in Section 16.4.1.) The complete set of local rotations, θ_{l1}–θ_{l6} will sometimes be collectively referred to via the vector, $\boldsymbol{\theta}_{l}$.

In equations (17.9), a term such as $\mathbf{p}_{l}(6)$ means the scalar that is the sixth component of the vector $\mathbf{p}_{l}$ (defined in (17.1)). To obtain (17.9) one need not resort to the formal approach in Section 16.4.1, but rather can appeal directly to geometry and Figure 17.1c. It should be noted that, with only small deformations at the local element level, it may not be necessary to include the trigonometric terms and, as a reasonable approximation, one could replace the $\sin\theta_{l}$'s by θ_{l}'s.

We have so far assumed that the triads **T**, **U** and **E** are available, but have not described how they would be computed. We will first consider the triad, **T** at node

1 (Figure 17.1b). The initial configuration for this triad can be obtained from the initial geometry, while subsequently it can be updated using a relationship of the form (see (16.47))

$$\mathbf{T}_n = \Delta\mathbf{T}(\Delta\boldsymbol{\alpha})\mathbf{T}_0 = \exp\mathbf{S}(\Delta\boldsymbol{\alpha})\mathbf{T}_0 \tag{17.10}$$

where $\mathbf{T}_0$ is the old triad (with an associated pseudo-vector, $\boldsymbol{\alpha}_0$) and $\Delta\mathbf{T}(\Delta\boldsymbol{\alpha})$ could be computed from one of the various form sof Rodrigues formula (see (16.22) or (16.31) or (16.35)). (In practice, it is better to use unit quaternions as will be described in Section 17.1.4.) The vector $\Delta\boldsymbol{\alpha}$ contains the three components of the pseudo-vector for node 1. These are usually the finite element variables for the iteration and, in the current formulation, are not additive (even in the limit as $\Delta\boldsymbol{\alpha}$ tend to $\delta\boldsymbol{\alpha}$ as discussed in Section 16.11). The variables $\Delta\boldsymbol{\alpha}$ are therefore effectively 'iterative spins'. (We will later, in Section 17.4, consider the possibility of using other rotation variables that are additive in the limit.)

A similar formula to (17.10) can be used to update the triad $\mathbf{U}$ at node 2 (Figure 17.1b). To complete the definition of the local slopes in (17.9), we require the local element triad $\mathbf{E} = [\mathbf{e}_1, \mathbf{e}_2, \mathbf{e}_3]$. The computation of the unit vector, $\mathbf{e}_1$ (Figure 17.1b) has already been described (see (17.2)) and is straightforward. The following describes the procedure for evaluating the $\mathbf{e}_2$ and $\mathbf{e}_3$ vectors that was adopted by the author in [C1.16]. An alternative procedure due to Rankin and Brogan [R1.16] is described in Section 17.1.6.

In order to compute the vectors $\mathbf{e}_2$ and $\mathbf{e}_3$, we first compute a triad, $\bar{\mathbf{R}}$, that is intermediate between $\mathbf{U}$ and $\mathbf{T}$ so that:

$$\bar{\mathbf{R}} = \Delta\mathbf{R}_m\left(\frac{\boldsymbol{\gamma}}{2}\right)\mathbf{T} \tag{17.11}$$

where

$$\Delta\mathbf{R}(\boldsymbol{\gamma}) = \mathbf{U}\mathbf{T}^{\mathrm{T}} \tag{17.12}$$

and $\boldsymbol{\gamma}$ is the pseudo-vector associated with the rotation from $\mathbf{T}$ to $\mathbf{U}$. Although pseudo-vectors are not additive, $\boldsymbol{\gamma}$ will only be moderately large and hence $\Delta\mathbf{R}_m(\boldsymbol{\gamma}/2)$ can be used as a reasonable representation of the rotation from $\mathbf{T}$ to the 'average or mean configuration'. (Further details on the precise method for the computation of $\bar{\mathbf{R}}$ will be given in Section 17.1.4.)

The mean rotation matrix, $\bar{\mathbf{R}}$, must now be 'rotated' on to $\mathbf{e}_1$ to obtain $\mathbf{e}_2$ and $\mathbf{e}_3$. To this end, we adopt the 'mid-point procedure' of (16.109) which is valid for moderate rotations (here between the $\bar{\mathbf{R}}$ and $\mathbf{E}$ triads). Using the present notation, this process leads to

$$\mathbf{e}_2 = \mathbf{r}_2 - \frac{\mathbf{r}_2^{\mathrm{T}}\mathbf{e}_1}{2}(\mathbf{e}_1 + \mathbf{r}_1) \tag{17.13}$$

$$\mathbf{e}_3 = \mathbf{r}_3 - \frac{\mathbf{r}_3^{\mathrm{T}}\mathbf{e}_1}{2}(\mathbf{e}_1 + \mathbf{r}_1) \tag{17.14}$$

where $\bar{\mathbf{R}} = [\mathbf{r}_1, \mathbf{r}_2, \mathbf{r}_3]$. (We could have used the exact procedure of equations (16.107) which would involve replacing the 2's with the expressions $(1 + \mathbf{e}_1^{\mathrm{T}}\mathbf{r}_1)$), but this would have led to a more complicated differentiation when we consider the virtual work.

None the less, to ensure an exact orthogonal triad we could use the exact form for the actual up date and yet maintain the following developments related to the simpler form for the virtual work and tangent stiffness matrix. When the strains are small, the difference will be negligible.)

17.1.2 Computation of the matrix connecting the infinitesimal local and global variables

The finitesimal global displacement variables can be expressed as

$$\delta \mathbf{p}^{\mathrm{T}} = (\delta \mathbf{d}_1^{\mathrm{T}}, \delta \boldsymbol{\alpha}^{\mathrm{T}}, \delta \mathbf{d}_2^{\mathrm{T}}, \delta \boldsymbol{\beta}^{\mathrm{T}}) \tag{17.15}$$

where the rotations $\boldsymbol{\alpha}$ and $\boldsymbol{\beta}$ are indicated in Figure 17.1c. They are the components of the pseudo-vector that can be used to define the nodal triads $\mathbf{T}$ and $\mathbf{U}$ respectively. In the present section, we will detail the computation of the transformation matrix $\mathbf{F}$ of (17.4) which relates $\delta \mathbf{p}_l$ of (17.1) to $\delta \mathbf{p}$ of (17.15). In Section 17.1.3 we will describe the differentiation of $\mathbf{F}^{\mathrm{T}}\mathbf{q}_{li}$ which leads to the initial stress matrix. The work of both sections becomes rather detailed and those readers only interested in an overview could skip these two sections and move directly to Section 17.1.4. Indeed, a rather neater derivation (including some approximations) of the transformation matrix and initial stress matrix will be given later in Section 18.10. However, this work requires an earlier reading of the co-rotational formulations for continua in Sections 18.2 and 18.3.

The matrix $\mathbf{F}$ of (17.4) will be written as

$$\mathbf{F} = \begin{bmatrix} \mathbf{f}_1^{\mathrm{T}} \\ \mathbf{f}_2^{\mathrm{T}} \\ \vdots \\ \mathbf{f}_{12}^{\mathrm{T}} \end{bmatrix} \tag{17.16}$$

where $\mathbf{f}_3^{\mathrm{T}}$ is the third row of $\mathbf{F}$. Because of the definitions in (17.1) and (17.8), we can write:

$$\mathbf{f}_1 = \mathbf{f}_2 = \mathbf{f}_3 = \mathbf{f}_8 = \mathbf{f}_9 = \mathbf{O} \tag{17.17}$$

The seventh row of $\mathbf{F}$ involves the connection between δu_l and the global nodal displacement changes and can be obtained via differentiation of (17.7), while the remaining rows of $\mathbf{F}$ are obtained via differentiation of (17.9). Details will now be given, but those readers interested in the concepts, without the detail, could jump straight to the text which follows equation (17.38).

Either via differentiation of (17.7) or via geometric arguments (see Section 7.2.3) one obtains:

$$\delta u_l = \delta \mathbf{p}_l(7) = \mathbf{e}_1^{\mathrm{T}} \delta \mathbf{d}_{21} = \mathbf{f}_7^{\mathrm{T}} \delta \mathbf{p} \tag{17.18}$$

where

$$\mathbf{f}_7^{\mathrm{T}} = (-\mathbf{e}_1^{\mathrm{T}}, \mathbf{0}^{\mathrm{T}}, \mathbf{e}_1^{\mathrm{T}}, \mathbf{0}^{\mathrm{T}}) \tag{17.19}$$

In order to compute the other non-zero rows of $\mathbf{F}$, we need to obtain expressions for the $\delta\theta_l$'s stemming from the variation of the terms in (17.9). To this end we require terms such as $\delta \mathbf{t}_1$. These are obtained using (see (16.7) and (16.8)):

$$\delta \mathbf{t}_i = \delta \boldsymbol{\alpha} \times \mathbf{t}_i = \mathbf{S}(\delta \boldsymbol{\alpha}) \mathbf{t}_i = -\mathbf{S}(\mathbf{t}_i) \delta \boldsymbol{\alpha} \tag{17.20}$$

with a similar expression relating $\delta \mathbf{u}_i$ to the nodal variables $\delta\boldsymbol{\beta}$ at node 2 (Figure 17.1). The matrices $\mathbf{S}$ in (17.20) are skew symmetric (see (16.8)).

We also require $\delta\mathbf{e}_1$, $\delta\mathbf{e}_2$ and $\delta\mathbf{e}_3$ which are the variations of the local element frame. From the definition of $\mathbf{e}_1$ in (17.2) and of u_l and l_n in (17.7),

$$\delta\mathbf{e}_1 = \frac{\delta\mathbf{d}_{21}}{l_n} - \frac{(\mathbf{x}_{21} + \mathbf{d}_{21})}{l_n^2}\,\delta u_l = \mathbf{A}\,\delta\mathbf{d}_{21} \tag{17.21}$$

where

$$\mathbf{A} = \frac{1}{l_n}[\mathbf{I} - \mathbf{e}_1\mathbf{e}_1^{\mathrm{T}}] \tag{17.22}$$

(Note that $\mathbf{A}$ is symmetric.) In order to obtain $\delta\mathbf{e}_2$ and $\delta\mathbf{e}_3$, we must differentiate (17.13) and (17.14). This will require the variation of the unit vectors $\mathbf{r}_1$, $\mathbf{r}_2$ and $\mathbf{r}_3$ which make up the 'average triad', $\bar{\mathbf{R}}$ which is computed from (17.11). Intuitively, the latter can be related to the nodal variables by

$$\delta\mathbf{r}_i = \mathbf{S}\left(\frac{\delta\boldsymbol{\alpha} + \delta\boldsymbol{\beta}}{2}\right)\mathbf{r}_i = -\mathbf{S}(\mathbf{r}_i)\left(\frac{\delta\boldsymbol{\alpha} + \delta\boldsymbol{\beta}}{2}\right) \tag{17.23}$$

The following set of equations ((17.24)–(17.31)) attempt to justify the intuitive step in (17.23). They may be ignored by those readers who are not too concerned with rigour.

More strictly, the variation of the vectors $\mathbf{r}_i$ ($i = 2$ and 3) involve:

$$\delta\mathbf{r}_i = \mathbf{S}(\delta\boldsymbol{\eta})\mathbf{r}_i \tag{17.24}$$

where, using (16.97b) and (17.11):

$$\mathbf{S}(\delta\boldsymbol{\eta}) = \delta\bar{\mathbf{R}}\mathbf{R}^{\mathrm{T}} = \delta(\Delta\mathbf{R}_m\mathbf{T})(\Delta\mathbf{R}_m\mathbf{T})^{\mathrm{T}} \tag{17.25}$$

Equation (17.25) can be expanded as

$$\mathbf{S}(\delta\boldsymbol{\eta}) = \delta\Delta\mathbf{R}_m\mathbf{R}_m^{\mathrm{T}} + \Delta\mathbf{R}_m\delta\mathbf{T}\mathbf{T}^{\mathrm{T}}\delta\mathbf{R}_m^{\mathrm{T}} = \delta\Delta\mathbf{R}_m\mathbf{R}_m^{\mathrm{T}} + \Delta\mathbf{R}_m\mathbf{S}(\delta\boldsymbol{\alpha})\Delta\mathbf{R}_m^{\mathrm{T}} \tag{17.26}$$

Assuming that the pseudo-vector of $\Delta\mathbf{R}_m$ is reasonably small, there is no difference between the tangent scaled and unscaled forms (see (16.34)) and hence, for the first terms on the right-hand sides of (17.26), we can use (16.101) (assuming also that $\boldsymbol{\gamma}^{\mathrm{T}}\boldsymbol{\gamma}/4 \ll 1$) to obtain:

$$\delta\Delta\mathbf{R}_m\mathbf{R}_m^{\mathrm{T}} = \mathbf{S}\left(\frac{\delta\boldsymbol{\gamma}}{2}\right) + \tfrac{1}{4}\mathbf{S}(\boldsymbol{\gamma})\mathbf{S}(\delta\boldsymbol{\gamma}) - \tfrac{1}{4}\mathbf{S}(\delta\boldsymbol{\gamma})\mathbf{S}(\boldsymbol{\gamma}) \tag{17.27}$$

with pseudo-vector:

$$\delta\boldsymbol{\eta}' = \tfrac{1}{2}\delta\boldsymbol{\gamma} + \tfrac{1}{4}\boldsymbol{\gamma} \times \delta\boldsymbol{\gamma} \tag{17.28}$$

(The latter can be confirmed using (16.86) and (16.100).) The axial vector from the second term in (17.25) can be written as

$$\delta\boldsymbol{\eta}'' = \Delta\mathbf{R}_m\boldsymbol{\alpha} \simeq \left[\mathbf{I} + \mathbf{S}\left(\frac{\delta\boldsymbol{\gamma}}{2}\right)\right]\delta\boldsymbol{\alpha} \simeq \delta\boldsymbol{\alpha} \tag{17.29}$$

where, in the limit, it is reasonable to neglect the higher-order term so that we can write the axial vector, $\delta\boldsymbol{\eta}$, as

$$\delta\boldsymbol{\eta} = \delta\boldsymbol{\eta}' + \delta\boldsymbol{\eta}'' = \tfrac{1}{2}\delta\boldsymbol{\gamma} + \delta\boldsymbol{\alpha} + \tfrac{1}{4}\boldsymbol{\gamma} \times \delta\boldsymbol{\gamma} \simeq \tfrac{1}{2}\delta\boldsymbol{\gamma} + \delta\boldsymbol{\alpha} \tag{17.30}$$

The neglecting of the higher-order term in (17.30) is justified by noting that not only is γ small (a local difference after the removal of the rigid body rotation) but so, of course is $\delta\gamma$. In addition, the two terms are often nearly parallel, thus making the cross-product even smaller.

Because γ is the pseudo-vector associated with the rotation between the triads, $\delta\gamma = \delta\beta - \delta\alpha$ and hence we obtain:

$$\delta\eta \simeq \tfrac{1}{2}(\delta\alpha + \delta\beta) \tag{17.31}$$

which when combined with (17.24) leads to the original equation (17.23) which was intuitively derived.

Using (17.21) for $\delta\mathbf{e}_1$ and (17.23) for $\delta\mathbf{r}_i$ as well as (17.20) for $\delta\mathbf{t}_i$ (and the equivalent for $\delta\mathbf{u}_i$), we can find the variations of (17.13) and (17.14) as

$$\delta\mathbf{e}_2 = \mathbf{L}(\mathbf{r}_2)^{\mathrm{T}}\delta\mathbf{p}; \qquad \delta\mathbf{e}_3 = \mathbf{L}(\mathbf{r}_3)^{\mathrm{T}}\delta\mathbf{p} \tag{17.32}$$

where

$$\mathbf{L}^{\mathrm{T}} = [\mathbf{L}_1^{\mathrm{T}}, \mathbf{L}_2^{\mathrm{T}}, -\mathbf{L}_1^{\mathrm{T}}, \mathbf{L}_2^{\mathrm{T}}] \tag{17.33}$$

$$\mathbf{L}_1(\mathbf{r}_i) = \frac{\mathbf{r}_i^{\mathrm{T}}\mathbf{e}_1}{2}\mathbf{A} + \tfrac{1}{2}\mathbf{A}\mathbf{r}_i(\mathbf{e}_1 + \mathbf{r}_1)^{\mathrm{T}} \tag{17.34}$$

$$\mathbf{L}_2(\mathbf{r}_i) = \frac{\mathbf{S}(\mathbf{r}_i)}{2} - \frac{\mathbf{r}_i^{\mathrm{T}}\mathbf{e}_1}{4}\mathbf{S}(\mathbf{r}_1) - \tfrac{1}{4}\mathbf{S}(\mathbf{r}_i)\mathbf{e}_1(\mathbf{e}_1 + \mathbf{r}_1)^{\mathrm{T}} \tag{17.35}$$

The variations of the local rotations in (17.9) can now be obtained so that a typical term will take the form:

$$\delta\mathbf{p}_l(4) = \delta\theta_{l1} = \mathbf{f}_4^{\mathrm{T}}\delta\mathbf{p} = \frac{1}{2\cos\theta_{l1}}\bar{\mathbf{f}}_4^{\mathrm{T}}\delta\mathbf{p} = \frac{1}{2\cos(\mathbf{p}_4(4))}\bar{\mathbf{f}}_4^{\mathrm{T}}\delta\mathbf{p} \tag{17.36}$$

where the $\mathbf{f}_4$ vector is the fourth row of the transformation matrix $\mathbf{F}$ of (17.4) (see also (17.16)). In (17.36) and, for future work, we have introduced a set of scaled vectors $\bar{\mathbf{f}}$ for the local rotation terms. The $\mathbf{f}$ vectors associated with these local rotations are given by

$$\begin{aligned}
\bar{\mathbf{f}}_4 &= 2\cos(\mathbf{p}_l(4))\,\mathbf{f}_4 = 2\cos\theta_{l1}\,\mathbf{f}_4 = \mathbf{L}(\mathbf{r}_3)\mathbf{t}_2 - \mathbf{L}(\mathbf{r}_2)\mathbf{t}_3 + \mathbf{h}_1\\
\bar{\mathbf{f}}_5 &= 2\cos(\mathbf{p}_l(5))\,\mathbf{f}_5 = 2\cos\theta_{l2}\,\mathbf{f}_5 = \mathbf{L}(\mathbf{r}_2)\mathbf{t}_1 + \mathbf{h}_2\\
\bar{\mathbf{f}}_6 &= 2\cos(\mathbf{p}_l(6))\,\mathbf{f}_6 = 2\cos\theta_{l3}\,\mathbf{f}_6 = \mathbf{L}(\mathbf{r}_3)\mathbf{t}_1 + \mathbf{h}_3\\
\bar{\mathbf{f}}_{10} &= 2\cos(\mathbf{p}_l(10))\,\mathbf{f}_{10} = 2\cos\theta_{l4}\,\mathbf{f}_{10} = \mathbf{L}(\mathbf{r}_3)\mathbf{u}_2 - \mathbf{L}(\mathbf{r}_2)\mathbf{u}_3 + \mathbf{h}_4\\
\bar{\mathbf{f}}_{11} &= 2\cos(\mathbf{p}_l(11))\,\mathbf{f}_4 = 2\cos\theta_{l5}\,\mathbf{f}_{11} = \mathbf{L}(\mathbf{r}_2)\mathbf{u}_1 - \mathbf{h}_5\\
\bar{\mathbf{f}}_{12} &= 2\cos(\mathbf{p}_l(12))\,\mathbf{f}_{12} = 2\cos\theta_{l6}\,\mathbf{f}_{12} = \mathbf{L}(\mathbf{r}_3)\mathbf{u}_1 - \mathbf{h}_6
\end{aligned} \tag{17.37}$$

and

$$\begin{aligned}
\mathbf{h}_1^{\mathrm{T}} &= \{\mathbf{0}^{\mathrm{T}}, (-\mathbf{S}(\mathbf{t}_3)\mathbf{e}_2 + \mathbf{S}(\mathbf{t}_2)\mathbf{e}_3)^{\mathrm{T}}, \mathbf{0}^{\mathrm{T}}, \mathbf{0}^{\mathrm{T}}\}\\
\mathbf{h}_2^{\mathrm{T}} &= \{(\mathbf{A}\mathbf{t}_2)^{\mathrm{T}}, (-\mathbf{S}(\mathbf{t}_2)\mathbf{e}_1 + \mathbf{S}(\mathbf{t}_1)\mathbf{e}_2)^{\mathrm{T}}, -(\mathbf{A}\mathbf{t}_2)^{\mathrm{T}}, \mathbf{0}^{\mathrm{T}}\}\\
\mathbf{h}_3^{\mathrm{T}} &= \{(\mathbf{A}\mathbf{t}_3)^{\mathrm{T}}, (-\mathbf{S}(\mathbf{t}_3)\mathbf{e}_1 + \mathbf{S}(\mathbf{t}_1)\mathbf{e}_3)^{\mathrm{T}}, -(\mathbf{A}\mathbf{t}_3)^{\mathrm{T}}, \mathbf{0}^{\mathrm{T}}\}\\
\mathbf{h}_4^{\mathrm{T}} &= \{\mathbf{0}^{\mathrm{T}}, \mathbf{0}^{\mathrm{T}}, \mathbf{0}^{\mathrm{T}}, (-\mathbf{S}(\mathbf{u}_3)\mathbf{e}_2 + \mathbf{S}(\mathbf{u}_2)\mathbf{e}_3)^{\mathrm{T}}\}\\
\mathbf{h}_5^{\mathrm{T}} &= \{(\mathbf{A}\mathbf{u}_2)^{\mathrm{T}}, \mathbf{0}^{\mathrm{T}}, -(\mathbf{A}\mathbf{u}_2)^{\mathrm{T}}, (-\mathbf{S}(\mathbf{u}_2)\mathbf{e}_1 + \mathbf{S}(\mathbf{u}_1)\mathbf{e}_2)^{\mathrm{T}}\}\\
\mathbf{h}_6^{\mathrm{T}} &= \{(\mathbf{A}\mathbf{u}_3)^{\mathrm{T}}, \mathbf{0}^{\mathrm{T}}, -(\mathbf{A}\mathbf{u}_3)^{\mathrm{T}}, (-\mathbf{S}(\mathbf{u}_3)\mathbf{e}_1 + \mathbf{S}(\mathbf{u}_1)\mathbf{e}_3)^{\mathrm{T}}\}
\end{aligned} \tag{17.38}$$

Having computed the transformation matrix $\mathbf{F}$, the global internal force vector can be simply computed from (17.5) (i.e. $\mathbf{q}_i = \mathbf{F}^T\mathbf{q}_{li} = \mathbf{F}^T\mathbf{K}_l\mathbf{p}_l$).

17.1.3 The tangent stiffness matrix

Differentiation of the expression for the internal force vector (in (17.5)) leads to the tangent stiffness equations of (17.6) so that:

$$\delta\mathbf{q}_i = \mathbf{K}_t\delta\mathbf{p} = (\mathbf{K}_{t1} + \mathbf{K}_{t\sigma})\delta\mathbf{p} \tag{17.39}$$

where

$$\mathbf{K}_{t1} = \mathbf{F}^T\mathbf{K}_l\mathbf{F} \tag{17.40}$$

and

$$\mathbf{K}_{t\sigma}\delta\mathbf{p} = \delta\mathbf{F}^T\mathbf{q}_{li}\delta\mathbf{p} = \sum_{j=1}^{12} \mathbf{q}_{li}(j)\delta\mathbf{f}_j \tag{17.41}$$

Because of (17.17), we only have to consider the variations of the vectors $\mathbf{f}_4$, $\mathbf{f}_5$, $\mathbf{f}_6$, $\mathbf{f}_7$, $\mathbf{f}_{10}$, $\mathbf{f}_{11}$ and $\mathbf{f}_{12}$.

At this stage we will detail the computation of $\mathbf{K}_{t\sigma}$ via the computation of the variations of the $\mathbf{f}$ vectors. Those readers not concerned with this detail would be advised to jump to the text immediately following equation (17.55b).

In forming the geometric stiffness matrix, $\mathbf{K}_{t\sigma}$, it is useful to define a set of scaled internal forces relating to the rotational variables as

$$\bar{q}_{li}(j) = \frac{1}{2\cos\theta_{lj}}\, q_{li}(j) \qquad \text{for } j = 4, 5, 6, 10, 11, 12 \tag{17.42}$$

All the other components of $\bar{\mathbf{q}}_{li}$ will be assumed zero.

The geometric stiffness matrix, $\mathbf{K}_{t\sigma}$ is now obtained from (17.41) as

$$\begin{aligned}\mathbf{K}_{t\sigma} = \mathbf{K}_{\sigma 1} &+ \mathbf{F}\,\mathrm{Diag}(\bar{\mathbf{q}}_{li}\tan\theta_{li})\mathbf{F}^T + \mathbf{q}_{li}(10)[\mathbf{K}_{\sigma 2}(\mathbf{r}_2, \mathbf{t}_3 - \mathbf{u}_3) + \mathbf{K}_{\sigma 2}(\mathbf{r}_3, \mathbf{u}_2 - \mathbf{t}_2)] \\ &+ \bar{\mathbf{q}}_{li}(5)\mathbf{K}_{\sigma 2}(\mathbf{r}_2, \mathbf{t}_1) + \bar{\mathbf{q}}_{li}(6)\mathbf{K}_{\sigma 2}(\mathbf{r}_3, \mathbf{t}_1) + \bar{\mathbf{q}}_{li}(11)\mathbf{K}_{\sigma 2}(\mathbf{r}_2, \mathbf{u}_1) \\ &+ \bar{\mathbf{q}}_{li}(12)\mathbf{K}_{\sigma 2}(\mathbf{r}_3, \mathbf{u}_1) + \mathbf{K}_{\sigma 3} + \mathbf{K}_{\sigma 3}^T + \mathbf{K}_{\sigma 4} + \mathbf{K}_{\sigma 5}\end{aligned} \tag{17.43}$$

In describing the various matrices, it is useful to work with submatrices, so that:

$$\mathbf{K} = \begin{bmatrix} \mathbf{K}_{11} & \mathbf{K}_{12} & \mathbf{K}_{13} & \mathbf{K}_{14} \\ \mathbf{K}_{21} & \mathbf{K}_{22} & \mathbf{K}_{23} & \mathbf{K}_{24} \\ \mathbf{K}_{31} & \mathbf{K}_{32} & \mathbf{K}_{33} & \mathbf{K}_{34} \\ \mathbf{K}_{41} & \mathbf{K}_{42} & \mathbf{K}_{43} & \mathbf{K}_{44} \end{bmatrix} \tag{17.44}$$

and to adopt the convention that, if a submatrix is unmentioned, it is zero.

The matrix $\mathbf{K}_{\sigma 1}$ in (17.43) comes from the differentiation of $\mathbf{f}_7$ (see (17.19)) and involves:

$$\mathbf{K}_{11} = \mathbf{K}_{33} = -\mathbf{K}_{13} = -\mathbf{K}_{31} = \mathbf{q}_{li}(7)\mathbf{A} \tag{17.45}$$

where $\mathbf{A}$ has been defined in (17.22). The $\mathbf{K}_{\sigma 2}(\mathbf{r}_i, \mathbf{z})$ terms come from the variation of the

$\mathbf{L}(\mathbf{r}_i)\mathbf{z}$ terms in (17.37) with $\mathbf{z}$ being fixed. $\mathbf{K}_{\sigma 2}(\mathbf{r}_i, \mathbf{z})$ involves the submatrices:

$$\mathbf{K}_{11} = -\mathbf{K}_{13} = -\mathbf{K}_{31} = \mathbf{K}_{33} = \mathbf{X} + \mathbf{X}^{\mathrm{T}} + \frac{\mathbf{r}_i^{\mathrm{T}}\mathbf{e}_1}{2l_n}(2(\mathbf{e}_1^{\mathrm{T}}\mathbf{z}) + \mathbf{z}^{\mathrm{T}}\mathbf{r}_1)\mathbf{A} \tag{17.46}$$

where

$$\mathbf{X} = -\tfrac{1}{2}\mathbf{A}\mathbf{z}\mathbf{r}_i^{\mathrm{T}}\mathbf{A} + \frac{\mathbf{r}_i^{\mathrm{T}}\mathbf{e}_1}{2l_n}\mathbf{A}\mathbf{z}\mathbf{e}_1^{\mathrm{T}} + \frac{\mathbf{z}^{\mathrm{T}}(\mathbf{e}_1 + \mathbf{r}_1)}{2l_n}\mathbf{A}\mathbf{r}_i\mathbf{e}_1^{\mathrm{T}} \tag{17.47}$$

$$\begin{aligned} 4\mathbf{K}_{12} &= 4\mathbf{K}_{14} = -4\mathbf{K}_{32} = -4\mathbf{K}_{34} \\ &= -\mathbf{A}\mathbf{z}\mathbf{e}_1^{\mathrm{T}}\mathbf{S}(\mathbf{r}_i) - \mathbf{A}\mathbf{r}_i\mathbf{z}^{\mathrm{T}}\mathbf{S}(\mathbf{r}_1) - \mathbf{z}^{\mathrm{T}}(\mathbf{e}_1 + \mathbf{r}_1)\mathbf{A}\mathbf{S}(\mathbf{r}_i) \end{aligned} \tag{17.48}$$

$$\mathbf{K}_{21} = \mathbf{K}_{41} = -\mathbf{K}_{23} = -\mathbf{K}_{43} = \mathbf{K}_{12}^{\mathrm{T}} \tag{17.49}$$

$$\begin{aligned} 8\mathbf{K}_{22} &= 8\mathbf{K}_{24} = 8\mathbf{K}_{42} = 8\mathbf{K}_{44} \\ &= -(\mathbf{r}_i^{\mathrm{T}}\mathbf{e}_i)\mathbf{S}(\mathbf{z})\mathbf{S}(\mathbf{r}_1) + \mathbf{S}(\mathbf{r}_1)\mathbf{z}\mathbf{e}_1^{\mathrm{T}}\mathbf{S}(\mathbf{r}_i) + \mathbf{S}(\mathbf{r}_i)\mathbf{e}_1\mathbf{z}^{\mathrm{T}}\mathbf{S}(\mathbf{r}_1) \\ &\quad -(\mathbf{e}_1 + \mathbf{r}_1)^{\mathrm{T}}\mathbf{z}\mathbf{S}(\mathbf{e}_1)\mathbf{S}(\mathbf{r}_i) + 2\mathbf{S}(\mathbf{z})\mathbf{S}(\mathbf{r}_i) \end{aligned} \tag{17.50}$$

Note that the sub-matrices $\mathbf{K}_{22}$, etc. are non-symmetric. We will return to this issue later in Section 17.4.

The $\mathbf{K}_{\sigma 3}$ terms in (17.43) come from (17.37) via terms such as $\mathbf{L}(\mathbf{r}_2)\delta\mathbf{t}_1$ and involve:

$$\mathbf{K}_{\sigma 3} = [\mathbf{0}, \bar{\mathbf{K}}_2, \mathbf{0}, \bar{\mathbf{K}}_4] \tag{17.51}$$

with

$$\bar{\mathbf{K}}_2 = -\mathbf{L}(\mathbf{r}_2)[\bar{\mathbf{q}}_{li}(10)\mathbf{S}(\mathbf{t}_3)] + \bar{\mathbf{q}}_{li}(5)\mathbf{S}(\mathbf{t}_1)] + \mathbf{L}(\mathbf{r}_3)[\bar{\mathbf{q}}_{li}(10)\mathbf{S}(\mathbf{t}_2) - \bar{\mathbf{q}}_{li}(6)\mathbf{S}(\mathbf{t}_1)] \tag{17.52}$$

$$\bar{\mathbf{K}}_4 = \mathbf{L}(\mathbf{r}_2)[\bar{\mathbf{q}}_{li}(10)\mathbf{S}(\mathbf{u}_3) - \bar{\mathbf{q}}_{li}(11)\mathbf{S}(\mathbf{u}_1)] - \mathbf{L}(\mathbf{r}_3)[\bar{\mathbf{q}}_{li}(10)\mathbf{S}(\mathbf{u}_2) + \bar{\mathbf{q}}_{li}(12)\mathbf{S}(\mathbf{u}_1)] \tag{17.53}$$

The matrix $\mathbf{K}_{\sigma 3}^{\mathrm{T}}$ comes from the terms such as $\mathbf{S}(\mathbf{t}_i)\delta\mathbf{e}_2$ from $\delta\mathbf{h}_1$ in (17.38).

The matrix $\mathbf{K}_{\sigma 4}$ comes from terms such as $\mathbf{S}(\delta\mathbf{t}_3)\mathbf{e}_2$ which stem from $\delta\mathbf{h}_1$ (see (17.38)) and, in relation to (17.44), has only non-zero $\mathbf{K}_{22}$ and $\mathbf{K}_{44}$ (non-symmetric) submatrices where

$$\begin{aligned} \mathbf{K}_{22} &= \bar{\mathbf{q}}_{li}(10)[\mathbf{S}(\mathbf{e}_2)\mathbf{S}(\mathbf{t}_3) - \mathbf{S}(\mathbf{e}_3)\mathbf{S}(\mathbf{t}_2)] + \mathbf{q}_{li}(5)[-\mathbf{S}(\mathbf{e}_1)\mathbf{S}(\mathbf{t}_2) + \mathbf{S}(\mathbf{e}_2)\mathbf{S}(\mathbf{t}_1)] \\ &\quad + \bar{\mathbf{q}}_{li}(6)[-\mathbf{S}(\mathbf{e}_1)\mathbf{S}(\mathbf{t}_3) + \mathbf{S}(\mathbf{e}_3)\mathbf{S}(\mathbf{t}_1)] \end{aligned} \tag{17.54a}$$

$$\begin{aligned} \mathbf{K}_{44} &= -\bar{\mathbf{q}}_{li}(10)[\mathbf{S}(\mathbf{e}_2)\mathbf{S}(\mathbf{u}_3) - \mathbf{S}(\mathbf{e}_3)\mathbf{S}(\mathbf{u}_2)] + \bar{\mathbf{q}}_{li}(11)[-\mathbf{S}(\mathbf{e}_1)\mathbf{S}(\mathbf{u}_2) + \mathbf{S}(\mathbf{e}_2)\mathbf{S}(\mathbf{u}_1)] \\ &\quad + \bar{\mathbf{q}}_{li}(12)[-\mathbf{S}(\mathbf{e}_1)\mathbf{S}(\mathbf{u}_3) + \mathbf{S}(\mathbf{e}_3)\mathbf{S}(\mathbf{u}_1)] \end{aligned} \tag{17.54b}$$

The matrix $\mathbf{K}_{\sigma 5}$ in (17.43) has

$$\begin{aligned} \mathbf{K}_{12} &= -\mathbf{K}_{32} = -(\bar{\mathbf{q}}_{li}(5)\mathbf{A}\mathbf{S}(\mathbf{t}_2) + \bar{\mathbf{q}}_{li}(6)\mathbf{A}\mathbf{S}(\mathbf{t}_3)] \\ \mathbf{K}_{14} &= -\mathbf{K}_{34} = -(\bar{\mathbf{q}}_{li}(11)\mathbf{A}\mathbf{S}(\mathbf{u}_2) + \bar{\mathbf{q}}_{li}(12)\mathbf{A}\mathbf{S}(\mathbf{u}_3)] \\ \mathbf{K}_{21} &= -\mathbf{K}_{23} = \mathbf{K}_{12}^{\mathrm{T}} \\ \mathbf{K}_{41} &= -\mathbf{K}_{43} = \mathbf{K}_{14}^{\mathrm{T}} \end{aligned} \tag{17.54c}$$

Rows 1 and 3 come from terms as $\mathbf{A}\,\delta\mathbf{t}_2$ from $\delta\mathbf{h}_2$ (see (17.38)) while rows 2 and 4 come from terms such $-\mathbf{S}(\mathbf{t}_2)\delta\mathbf{e}_1$ in $\delta\mathbf{h}_2$ (see (17.38)).

Other sub-matrices in the matrix $\mathbf{K}_{\sigma 5}$ in (17.43) come from terms such as $\mathbf{A}\mathbf{t}_2$ in $\mathbf{h}_2$ (see (17.38)) and involve:

$$\mathbf{K}_{11} = \mathbf{K}_{33} = -\mathbf{K}_{13} = -\mathbf{K}_{31} = = \mathbf{A}\mathbf{v}\mathbf{e}_1^{\mathrm{T}} + \mathbf{e}_1\mathbf{v}^{\mathrm{T}}\mathbf{A} + (\mathbf{e}_1^{\mathrm{T}}\mathbf{v})\mathbf{A} \tag{17.55a}$$

with

$$\mathbf{v} = = \frac{1}{l_n}\{\bar{\mathbf{q}}_{li}(5)\mathbf{t}_2 + \bar{\mathbf{q}}_{li}(6)\mathbf{t}_3 + \bar{\mathbf{q}}_{li}(11)\mathbf{u}_2 + \bar{\mathbf{q}}_{li}(12)\mathbf{u}_3\} \tag{17.55b}$$

It will be noted that the 'geometric stiffness matrix', $\mathbf{K}_{t\sigma}$ is non-symmetric. This observation is consistent with that of Simo and Vu-Quoc [12, 13] who adopted a different formulation which will be discussed in Section 17.2. The issue will be discussed further in Section 17.4. In the meantime, we note that numerical experiments have shown that, for conservative problems, the tangent stiffness matrix becomes almost symmetric as the iterative procedure reaches equilibrium (see Section 17.4.3 and the observation by Simo and Vu-Quoc [S3.16]). The numerical results [C1.16] show that the excellent (quadratic) convergence characteristics exhibited by the method (when used in conjunction with the full Newton–Raphson procedure) are not impaired if the tangent stiffness matrix is artificially symmetrised.

17.1.4 Numerical implementation of the rotational updates

Equation (17.10) described the conceptual manner in which the nodal triad $\mathbf{T}$ could be updated. Instead, one could update the pseudo-vector, $\boldsymbol{\alpha}$, using one of the 'compound updates' such as (16.51) or (16.52) with (16.53). However, following the arguments in Section 16.9, it is better to use (and store) unit quaternions and then use the quaternion product of (16.71).

For the computation of the 'mean nodal triad', $\bar{\mathbf{R}}$ of (17.11), the following algorithm was adopted in [C1.16].

1. Obtain $\Delta\mathbf{R}(\gamma) = \mathbf{U}\mathbf{T}^{\mathrm{T}}$ (see (17.12))
2. Use the method of Section 16.10 (equations (16.74)–(16.79)) to obtain the tangent-scaled γ from $\Delta\mathbf{R}$.
3. Obtain the unscaled γ using (16.34).
4. Compute $\gamma/2$.
5. Compute $\Delta\mathbf{R}_{\mathrm{m}}(\gamma/2)$ from (16.34) and (16.35).
6. Compute $\bar{\mathbf{R}}$ from (17.11).

17.1.5 Overall solution strategy with a non-linear 'local element' formulation

The previous formulation can be very simply modified to account for both geometric and material non-linearity within an existing beam element in which the geometric non-linearities are only valid for 'moderated rotations'. In these circumstances, the existing element should give both the internal force vector, $\mathbf{q}_{li}$, and the local tangent stiffness matrix, $\mathbf{K}_{ll}$. Given an iterative change of the global displacement variables, $\delta\mathbf{p}$,

the following procedure would be applied in order to compute the global internal force vector, $\mathbf{q}_i$ and the global tangent stiffness matrix, $\mathbf{K}_t$.

1. Update the translational displacements via $\mathbf{d} = \mathbf{d} + \delta\mathbf{d}$.
2. Update the nodal triads $\mathbf{T}$ and $\mathbf{U}$ (or their pseudo-vectors $\boldsymbol{\alpha}$ and $\boldsymbol{\beta}$) using $\boldsymbol{\alpha}$ and $\delta\boldsymbol{\beta}$ and the procedure discussed in Section 17.1.4.
3. Compute the $\bar{\mathbf{R}}$ triad using the procedure discussed in Section 17.1.4.
4. Compute the $\mathbf{e}_1$ vector using (17.2).
5. Compute the $\mathbf{e}_2$ and $\mathbf{e}_3$ vectors using (17.13) and (17.14).
6. Compute the local rotations $\boldsymbol{\theta}_l$ comprising $(\theta_{l1} \rightarrow \theta_{l6})$ or $(\mathbf{p}_l(4), \mathbf{p}_l(5), \mathbf{p}_l(6), \mathbf{p}_l(10), \mathbf{p}_l(11), \mathbf{p}_l(12))$ using (17.9).
7. Compute the local axial displacement $u_l = \mathbf{p}_l(7)$ via (17.7).
8. Enter the existing element routines with the local 'displacements' from (6) and (7) (with the other terms zero) and
   (a) compute or update the local stresses (or stress resultants);
   (b) compute the local internal force vector, $\mathbf{q}_{li}$.
   (c) compute the local tangent stiffness matrix, $\mathbf{K}_{tl}$.
9. Compute the transformation matrix $\mathbf{F}$ (where $\delta\mathbf{p}_l = \mathbf{F}\delta\mathbf{p}$).
10. Compute the global internal force vector, $\mathbf{q}_i = \mathbf{F}^T\mathbf{q}_{li}$.
11. Compute the global tangent stiffness matrix $\mathbf{K}_t = \mathbf{F}^T\mathbf{K}_{tl}\mathbf{F} + \mathbf{K}_{t\sigma}$ with $\mathbf{K}_{t\sigma}$ from (17.43).

It is not essential for the co-rotational procedure that the local element computations of step (8) above should account for 'local non-linearity'. However, more accurate solutions would be expected with coarse meshes if such local non-linearity were to be included.

An appropriate two-dimensional shallow arch formulation was discussed in Section 7.1 and the idea of including the 'higher-order terms' in the co-rotational formulation was considered in Section 7.2.7. In three dimensions, we might follow these approaches and modify an existing linear beam element to account for local non-linearity by adopting the axial strain term:

$$\varepsilon_{xl} = \frac{\partial u_l}{\partial x_l} + \frac{1}{2}\left(\frac{\partial v_l}{\partial x_l}\right)^2 + \frac{1}{2}\left(\frac{\partial w_l}{\partial x_l}\right)^2 = \frac{1}{l_o}\{\mathbf{p}_l(7)\} + \tfrac{1}{60}\boldsymbol{\theta}_l^T\mathbf{X}\boldsymbol{\theta}_l \tag{17.56a}$$

where

$$\mathbf{X} = \begin{bmatrix} 0 & 0 & 0 & 0 & 0 & 0 \\ 0 & 4 & 0 & 0 & -1 & 0 \\ 0 & 0 & 4 & 0 & 0 & -1 \\ 0 & 0 & 0 & 0 & 0 & 0 \\ 0 & -1 & 0 & 0 & 4 & 0 \\ 0 & 0 & -1 & 0 & 0 & 4 \end{bmatrix} \tag{17.56b}$$

with the second term in (17.56a) containing the 'higher-order terms' and being the three-dimensional equivalent of the term in (7.90). It can be obtained by assuming cubics for v_l and w_l and integrating over the length of the element (see Section 7.2.7). The

modification of the linear local element formulation to account for the these 'higher-order' terms would then follow conventional lines. Equation (17.56a) assumes that the beam element is initially straight. It is a relatively simple matter to modify the theory to allow for initial curvature by including terms involving the 'initial local rotations'. To this end, (17.56a) would be replaced by

$$\varepsilon_{xl} = \frac{1}{l_o}\{\mathbf{p}_l(7)\} + \tfrac{1}{60}\boldsymbol{\theta}_l^{\mathrm{T}}\mathbf{X}\boldsymbol{\theta}_l - \tfrac{1}{60}\boldsymbol{\theta}_{lo}^{\mathrm{T}}\mathbf{X}\boldsymbol{\theta}_{lo} \tag{17.56c}$$

where $\boldsymbol{\theta}_{lo}$ contains the initial local rotations and $\boldsymbol{\theta}_l$ contains the current total rotations, so that initially $\boldsymbol{\theta}_l = \boldsymbol{\theta}_{lo}$.

17.1.6 Possible simplifications

There is considerable scope for simplifying the expressions used with the previous co-rotational formulation. The full formulation has been given because it has been coded by the author (and in relation to a Timoshenko beam formulation by Cole [C5]) and excellent results have been obtained. None the less, we will now outline a few possibilities for simplification that are based on the assumption that, at the local element, we have small strains and moderate deformations.

It has already been noted that, in these circumstances, it would be reasonable to replace the sin θ_l's by θ_l's in (17.9). As a further simplification, one might replace (17.13) by the lower-order approximation:

$$\mathbf{e}_2 = \mathbf{r}_2 - (\mathbf{r}_2^{\mathrm{T}}\mathbf{e}_1)\mathbf{e}_1 \tag{17.57}$$

However, in these circumstance, it would be sensible to define $\mathbf{e}_3$ in a different manner and force it to given by $\mathbf{e}_3 = \mathbf{e}_1 \times \mathbf{e}_2 = \mathbf{e}_1 \times \mathbf{r}_2$.

The procedure would then have strong similarities with the approach of Rankin and Brogan [R1.16] which leads to an alternative simpler formulation. Using their approach, one defines an intermediate nodal triad at node 1, $\bar{\mathbf{T}}$, which is obtained from the triad at node 1, $\mathbf{T}$, via rotation with a *fixed* rotation matrix $(\mathbf{E}_o\mathbf{T}_o^{\mathrm{T}})$ so that:

$$\bar{\mathbf{T}} = (\mathbf{E}_o\mathbf{T}_o^{\mathrm{T}})\mathbf{T} \tag{17.58}$$

The rotation matrices $\mathbf{E}_o$ and $\mathbf{T}_o$ in (17.58) are simply the initial values of the matrices $\mathbf{E} = [\mathbf{e}_1, \mathbf{e}_2, \mathbf{e}_3]$ and $\mathbf{T} = [\mathbf{t}_1, \mathbf{t}_2, \mathbf{t}_3]$. Using this approach, in the initial configuration, $\bar{\mathbf{T}}$ coincides with $\mathbf{E}_o$. In the current configuration, $\mathbf{e}_1$ is defined as in (17.2) while having computed the $\bar{\mathbf{T}}$ matrix, $\mathbf{e}_3$ is computed via

$$\mathbf{e}_3 = \mathbf{e}_1 \times \bar{\mathbf{t}}_2 \tag{17.59a}$$

and $\mathbf{e}_2$ is computed so as to make up an orthogonal element triad, i.e. via

$$\mathbf{e}_2 = -\mathbf{e}_1 \times \mathbf{e}_3 = \bar{\mathbf{t}}_2 - (\bar{\mathbf{t}}_2^{\mathrm{T}}\mathbf{e}_1)\mathbf{e}_1 \tag{17.59b}$$

(The latter can be compared with (17.57).) As noted by Rankin and Brogan, this procedure will ensure that rotations about the axis of the beam will remain of the same order as those which produce torsion [R1, R6]. Having adopted this alternative definition for the $\mathbf{E}$ frame, one could proceed by following closely the previous

developments. In particular the variations of (17.59a) and (17.59b) turn out to be

$$\delta \mathbf{e}_2 = -\{(\bar{\mathbf{t}}_2^{\mathrm{T}}\mathbf{e}_1)\mathbf{A} + \mathbf{e}_1\bar{\mathbf{t}}_2^{\mathrm{T}}\mathbf{A}\}\delta \mathbf{d}_{21} - [\mathbf{I} - \mathbf{e}_1\mathbf{e}_1^{\mathrm{T}}]\mathbf{S}(\bar{\mathbf{t}}_2)\delta\boldsymbol{\alpha} \tag{17.60a}$$

$$\delta \mathbf{e}_3 = -\mathbf{S}(\bar{\mathbf{t}}_2)\mathbf{A}\,\delta \mathbf{d}_{21} - \mathbf{S}(\mathbf{e}_1)\mathbf{S}(\bar{\mathbf{t}}_2)\delta\boldsymbol{\alpha} \tag{17.60b}$$

While under the topic of simplification, it is worth noting, that in relation to a computer implementation, it can be convenient to re-express the key equation (17.4) whereby $\delta \mathbf{p}_l = \mathbf{F}\delta \mathbf{p}$ in the form:

$$\delta \mathbf{p}_l = \mathbf{F}_1\delta \mathbf{p} + \mathbf{F}_2\begin{bmatrix}\delta \mathbf{e}_1\\ \delta \mathbf{e}_2\\ \delta \mathbf{e}_3\end{bmatrix} = \mathbf{F}_1\delta \mathbf{p} + \mathbf{F}_2\delta\bar{\mathbf{e}} \tag{17.61}$$

in conjunction with an extra equation which, with the earlier formulation would be obtained from (17.21) and (17.32), so that:

$$\delta\bar{\mathbf{e}} = \mathbf{F}_3\delta \mathbf{p} = \begin{bmatrix}-\mathbf{A} & \mathbf{0} & \mathbf{A} & \mathbf{0}\\ \mathbf{L}(\mathbf{r}_2)^{\mathrm{T}}\rightarrow & & & \\ \mathbf{L}(\mathbf{r}_3)^{\mathrm{T}}\rightarrow & & & \end{bmatrix}\delta \mathbf{p} \tag{17.62}$$

Using Rankin and Brogan's approach, the last two blocks in (17.62) would be obtained from (17.60). In relation to the earlier formulation, the split in (17.61) is most easily achieved in conjunction with the approximation whereby the $\sin\theta_l$'s are replaced by θ_l's.

Terms from the matrix $\mathbf{F}_3$ turn out to be very useful in relation to various forms of follower loading (see Section 17.5).

17.2 AN INTERPRETATION OF AN ELEMENT DUE TO SIMO AND VU-QUOC

Simo and Vu-Quoc have described a finite element formulation for a three-dimensional beam with finite strains [S3.16]. The present section will describe the author's interpretation of this formulation. Readers should note the emphasis of the word 'interpretation' because the description will take a rather different form to that given in the original paper. None the less, in conjunction with Cole [C5], the author has programmed the formulation and the numerical results seem to be identical to those given in the original papers.

In the present description, the formulation will be quite closely related to the previous co-rotational techniques although now, instead of updating nodal triads, the configuration of the Gauss points is updated. The conventional co-rotational approach is often thought of as involving and $\mathbf{F} = \mathbf{VR}$ split (see Section 4.8), with the straining being induced by the stretch $\mathbf{V}$. In order to understand the links with the approach of Simo and Vu-Quoc [S3.16], it is better to think of the co-rotational approach as involving an $\mathbf{F} = \mathbf{RU}$ split with the stress inducing stretches relating to the material frame and preceding the rotation. More on this topic will be given in Chapter 18.

In the first place, we will describe a two-noded element and will effectively use a 'one-point integration scheme' which does not introduce shape functions. However,

later in Section 17.2.6, we will consider the extension to a general isoparametric formulation. The current three-dimensional procedure can be considered as an extension of the two-dimensional formulation of Section 7.4.

17.2.1 The finite element variables

The element has precisely the same variables as those for the previous elements so that the vector of nodal 'displacement changes' is given by (17.15). The displacement variables, $\mathbf{d}$, at the nodes are simply updated as with the previous elements using:

$$\mathbf{d}_n = \mathbf{d}_o + \delta\mathbf{d} \tag{17.63}$$

(with 'n' meaning 'new' and 'o' mean 'old'). However, having obtained 'spin variables', $\delta\boldsymbol{\alpha}$, at node 1 and $\delta\boldsymbol{\beta}$ at node 2, these are not now used to update nodal triads. Instead they are interpolated to the Gauss point (here the centre of the element) so that:

$$\delta\boldsymbol{\alpha}_c = \tfrac{1}{2}(\delta\boldsymbol{\alpha} + \delta\boldsymbol{\beta}) \tag{17.64}$$

Following this, the triad at the centre, which we will now call $\mathbf{T}$, is conceptually updated using the equivalent of (17.10) so that:

$$\mathbf{T}_n = \Delta\mathbf{T}(\delta\boldsymbol{\alpha}_c)\mathbf{T}_o \tag{17.65}$$

As discussed in Section 17.1.4, in practice, it is best to perform the update using quaternions. Hence, at the end of an increment or iteration, both the current coordinates of the nodes ($\mathbf{x}_1 + \mathbf{d}_1$ and $\mathbf{x}_2 + \mathbf{d}_2$) are available as is the current configuration of the central triad ($\mathbf{T} = [\mathbf{t}_1, \mathbf{t}_2, \mathbf{t}_3]$).

17.2.2 Axial and shear strains

The axial and shear strains can be directly computed using the three-dimensional equivalent of the strain measures discussed in Section 7.4 and can be related to Figure 7.9. As an extension of the work in Section 7.4 (based on Reissner's theory [R2]), we have:

$$\varepsilon_{xl} = \frac{1}{l_o}\mathbf{t}_1^{\mathrm{T}}(\mathbf{x}_{21} + \mathbf{d}_{21}) - 1 = \frac{1}{l_o}\mathbf{t}_1^{\mathrm{T}}\mathbf{x}'_{21} - 1 \tag{17.66a}$$

$$\gamma_{l2} = \frac{1}{l_o}\mathbf{t}_2^{\mathrm{T}}\mathbf{x}'_{21} \tag{17.66b}$$

$$\gamma_{l3} = \frac{1}{l_o}\mathbf{t}_3^{\mathrm{T}}\mathbf{x}'_{21} \tag{17.66c}$$

The superscript, ', indicates that the values are current so that $\mathbf{x}' = \mathbf{x} + \mathbf{d}$ (see 17.66a)).

Equations (17.66a)–(17.66c) can be combined to give:

$$\boldsymbol{\varepsilon}_l = \begin{bmatrix} \varepsilon_x \\ \gamma_2 \\ \gamma_3 \end{bmatrix}_l = \frac{1}{l_o}\mathbf{T}^{\mathrm{T}}\mathbf{x}'_{21} - \begin{bmatrix} 1 \\ 0 \\ 0 \end{bmatrix} \tag{17.67}$$

With a view to the virtual work, we will require the variations of these strains which can be obtained as

$$\delta\boldsymbol{\varepsilon}_l = \delta\boldsymbol{\varepsilon}_{la} + \delta\boldsymbol{\varepsilon}_{lb} = \frac{1}{l_o}\mathbf{T}^T\delta\mathbf{d}_{21} + \frac{1}{l_o}\delta\mathbf{T}^T\mathbf{x}'_{21} \tag{17.68}$$

The matrix $\delta\mathbf{T}$ in (17.68) can be obtained by combining equations of the type given in (17.20) so that:

$$\delta\mathbf{T} = \mathbf{S}(\delta\boldsymbol{\alpha}_c)\mathbf{T} = \mathbf{S}\left(\frac{\delta\boldsymbol{\alpha} + \delta\boldsymbol{\beta}}{2}\right)\mathbf{T} \tag{17.69}$$

where we should note that $\delta\boldsymbol{\alpha}_c$ are 'non-additive spin variables' (see Section 16.11) and that the interpolation of (17.64) has been used for $\delta\boldsymbol{\alpha}_c$. Using (17.69), we can re-express $\delta\boldsymbol{\varepsilon}_{lb}$ in (17.68) as

$$\begin{aligned}\delta\boldsymbol{\varepsilon}_{lb} &= \frac{1}{l_o}\mathbf{T}^T\mathbf{S}(\delta\boldsymbol{\alpha}_c)^T\mathbf{x}'_{21} = -\frac{1}{l_o}\mathbf{T}^T\mathbf{S}(\delta\boldsymbol{\alpha}_c)\mathbf{x}'_{21} \\ &= \frac{1}{l_o}\mathbf{T}^T\mathbf{S}(\mathbf{x}'_{21})\delta\boldsymbol{\alpha}_c = \frac{1}{2l_o}\mathbf{T}^T\mathbf{S}(\mathbf{x}'_{21})(\delta\boldsymbol{\alpha} + \delta\boldsymbol{\beta})\end{aligned} \tag{17.70}$$

Equations (17.68) and (17.70) allow the strain variations, $\delta\boldsymbol{\varepsilon}_l$ to be directly related to the nodal changes, $\delta\mathbf{d}_1$, $\delta\mathbf{d}_2$, $\delta\boldsymbol{\alpha}$ and $\delta\boldsymbol{\beta}$.

17.2.3 Curvature

A detailed discussion relating to the curvature of the current element has been given in Section 16.4.2. Here, we will simply restate the main findings.

For the purposes of the virtual work, we can express the local curvature changes (see (16.132)) as

$$\delta\boldsymbol{\chi}_l = \begin{bmatrix}\delta\chi_1 \\ \delta\chi_2 \\ \delta\chi_3\end{bmatrix}_l = \mathbf{T}^T\frac{\mathrm{d}\delta\boldsymbol{\alpha}_c}{\mathrm{d}s} = \frac{1}{l_o}\mathbf{T}^T(\delta\boldsymbol{\beta} - \delta\boldsymbol{\alpha}) \tag{17.71}$$

Without nodal triads, we do not have a direct expression for the full curvature, but only expressions for updating the curvature (Section 16.14.2). An approximate mid-point relationship for such an update could be taken (see (16.141)) as

$$\boldsymbol{\chi}_{ln} = \boldsymbol{\chi}_{lo} + \mathbf{T}^T_{\text{mid}}\frac{\mathrm{d}\Delta\boldsymbol{\alpha}_c}{\mathrm{d}s} = \boldsymbol{\chi}_{lo} + \frac{1}{l_o}\mathbf{T}^T_{\text{mid}}(\Delta\boldsymbol{\beta} - \Delta\boldsymbol{\alpha}) \tag{17.72}$$

where (see (16.158)) we might write:

$$\mathbf{T}_{\text{mid}} \simeq [\mathbf{I} + \tfrac{1}{2}\mathbf{S}(\Delta\boldsymbol{\alpha}_c)]\mathbf{T}_o \tag{17.73}$$

An exact procedure for updating the curvature, based on the procedure of Simo and Vu-Quoc [S3.16] has been given in Section 16.14.2.

17.2.4 Virtual work and the internal force vector

From (17.68), (17.70) and (17.71), we can write the combined 'strain' variations at the Gauss point (centre) as

$$\delta\bar{\boldsymbol{\varepsilon}}_l = \begin{pmatrix} \delta\boldsymbol{\varepsilon} \\ \delta\boldsymbol{\chi} \end{pmatrix}_l = \frac{1}{l_o}\begin{bmatrix} \mathbf{T}^T & \mathbf{0} \\ \mathbf{0} & \mathbf{T}^T \end{bmatrix} \begin{bmatrix} -\mathbf{I} & \dfrac{\mathbf{S}(\mathbf{x}'_{21})}{2} & \mathbf{I} & \dfrac{\mathbf{S}(\mathbf{x}'_{21})}{2} \\ \mathbf{0} & -\mathbf{I} & \mathbf{0} & \mathbf{I} \end{bmatrix} \delta\mathbf{p} = \frac{1}{l_o}\bar{\mathbf{T}}^T\mathbf{X}^T\delta\mathbf{p} \tag{17.74}$$

where the ordering of the nodal variables, $\delta\mathbf{p}$ has been given in (17.15).

With a view to the principle of virtual work, the internal virtual work can be written as

$$V_i = l_o(\mathbf{N}^T\delta\boldsymbol{\varepsilon}_{lv} + \mathbf{M}^T\delta\boldsymbol{\chi}_{lv}) = \mathbf{q}_i^T\delta\mathbf{p}_v \tag{17.75}$$

where the subscript 'v' means virtual and the local (or material) stress resultants, $\mathbf{N}$ and $\mathbf{M}$ are obtained from the local (or material) strains and curvatures via:

$$\begin{pmatrix} \mathbf{N} \\ \mathbf{M} \end{pmatrix} = \mathbf{C}\begin{pmatrix} \boldsymbol{\varepsilon} \\ \boldsymbol{\chi} \end{pmatrix}_l = \mathbf{C}\bar{\boldsymbol{\varepsilon}}_l = \begin{bmatrix} EA & & & & & & \\ & GA_2 & & & & & \\ & & GA_3 & & & & \\ & & & GJ & & & \\ & & & & EI_2 & & \\ & & & & & EI_3 & \end{bmatrix} \bar{\boldsymbol{\varepsilon}}_l$$

$$= \begin{bmatrix} \mathbf{C}_m & \\ & \mathbf{C}_b \end{bmatrix} \bar{\boldsymbol{\varepsilon}}_l \tag{17.76}$$

Equation (17.76) assumes a linear constitutive relationship. Other material characteristics could be considered.

Using the relationships for $\delta\boldsymbol{\varepsilon}_l$ and $\delta\boldsymbol{\chi}_l$ in (17.74) (although now virtual so that a subscript v is added) equation (17.75) can be re-expressed as

$$V_i = \mathbf{n}^T(\delta\mathbf{d}_{21} + \tfrac{1}{2}\mathbf{S}(\mathbf{x}'_{21})(\delta\boldsymbol{\alpha} + \delta\boldsymbol{\beta})) + \mathbf{m}^T(\delta\boldsymbol{\beta} - \delta\boldsymbol{\alpha}) = \mathbf{q}_i^T\delta\mathbf{p}_v \tag{17.77}$$

where

$$\mathbf{n} = \mathbf{TN}; \qquad \mathbf{m} = \mathbf{TM} \tag{17.78}$$

From (17.77), the internal force vector, $\mathbf{q}_i$, is obtained as

$$\mathbf{q}_i = \mathbf{X}\bar{\mathbf{T}}\begin{pmatrix} \mathbf{N} \\ \mathbf{M} \end{pmatrix} = \mathbf{X}\begin{pmatrix} \mathbf{n} \\ \mathbf{m} \end{pmatrix} \tag{17.79}$$

where the matrix $\mathbf{X}$ has been given in (17.74).

17.2.5 The tangent stiffness matrix

From (17.76) and (17.74):

$$\begin{pmatrix} \delta\mathbf{N} \\ \delta\mathbf{M} \end{pmatrix} = \frac{1}{l_o}\mathbf{C}\bar{\mathbf{T}}^T\mathbf{X}^T\delta\mathbf{p} \tag{17.80}$$

so that differentiation of (17.79) leads to

$$\delta \mathbf{q}_i = \frac{1}{l_o}\mathbf{X}\bar{\mathbf{T}}\mathbf{C}\bar{\mathbf{T}}^T\mathbf{X}^T\delta\mathbf{p} + \begin{bmatrix} -\delta\mathbf{T} & \mathbf{0} \\ \mathbf{0} & -\delta\mathbf{T} \\ \delta\mathbf{T} & \mathbf{0} \\ \mathbf{0} & \delta\mathbf{T} \end{bmatrix} \begin{pmatrix} \mathbf{N} \\ \mathbf{M} \end{pmatrix} - \frac{1}{2}\begin{bmatrix} \mathbf{0} \\ \delta(\mathbf{S}(\mathbf{x}'_{21})\mathbf{T} \\ \mathbf{0} \\ \delta(\mathbf{S}(\mathbf{x}'_{21})\mathbf{T}) \end{bmatrix} \mathbf{N} \tag{17.81}$$

where the last two terms will contribute to the initial stress matrix.

Consider the term $\delta\mathbf{TN}$. From (17.69):

$$\delta\mathbf{TN} = \mathbf{S}(\delta\boldsymbol{\alpha}_c)\mathbf{TN} = \mathbf{S}(\delta\boldsymbol{\alpha}_c)\mathbf{n} = -\mathbf{S}(\mathbf{n})\delta\boldsymbol{\alpha}_c = \frac{-\mathbf{S}(\mathbf{n})}{2}(\delta\boldsymbol{\alpha} + \delta\boldsymbol{\beta}) \tag{17.82}$$

and a similar expression can be obtained for $\delta\mathbf{T}\,\mathbf{M}$. Hence, the second term in (17.81) gives:

$$\mathbf{K}_{\sigma 1}\delta\mathbf{p} = \frac{1}{2}\begin{bmatrix} \mathbf{0} & \mathbf{S}(\mathbf{n}) & \mathbf{0} & \mathbf{S}(\mathbf{n}) \\ \mathbf{0} & \mathbf{S}(\mathbf{m}) & \mathbf{0} & \mathbf{S}(\mathbf{m}) \\ \mathbf{0} & -\mathbf{S}(\mathbf{n}) & \mathbf{0} & -\mathbf{S}(\mathbf{n}) \\ \mathbf{0} & -\mathbf{S}(\mathbf{m}) & \mathbf{0} & -\mathbf{S}(\mathbf{m}) \end{bmatrix} \delta\mathbf{p} \tag{17.83}$$

For the last term in (17.81), we require:

$$\delta(\mathbf{S}(\mathbf{x}'_{21})\mathbf{T})\mathbf{N} = \delta\mathbf{S}(\mathbf{x}_{21})\mathbf{n} + \mathbf{S}(\mathbf{x}'_{21})\delta\mathbf{TN} \tag{17.84}$$

Using (17.69), it follows that:

$$\delta(\mathbf{S}(\mathbf{x}'_{21})\mathbf{T})\mathbf{N} = \mathbf{S}(\delta\mathbf{d}_{21})\mathbf{n} - \tfrac{1}{2}\mathbf{S}(\mathbf{x}_{21})\mathbf{S}(\mathbf{n})(\delta\boldsymbol{\alpha} + \delta\boldsymbol{\beta}) \tag{17.85}$$

Using (16.86), the above equation can be re-expressed as

$$\delta(\mathbf{S}(\mathbf{x}'_{21})\mathbf{T})\mathbf{N} = -\mathbf{S}(\mathbf{n})\delta\mathbf{d}_{21} - \tfrac{1}{2}(\mathbf{n}\mathbf{x}'^{T}_{21} - \mathbf{n}^T\mathbf{x}'_{21}\mathbf{I})(\delta\boldsymbol{\alpha} + \delta\boldsymbol{\beta}) \tag{17.86}$$

and hence from (17.81)

$$\mathbf{K}_{\sigma 2}\delta\mathbf{p} = \frac{1}{2}\begin{bmatrix} \mathbf{0} & \mathbf{0} & \mathbf{0} & \mathbf{0} \\ -\mathbf{S}(\mathbf{n}) & \mathbf{Y} & \mathbf{S}(\mathbf{n}) & \mathbf{Y} \\ \mathbf{0} & \mathbf{0} & \mathbf{0} & \mathbf{0} \\ -\mathbf{S}(\mathbf{n}) & \mathbf{Y} & \mathbf{S}(\mathbf{n}) & \mathbf{Y} \end{bmatrix} \delta\mathbf{p} \tag{17.87}$$

where:

$$\mathbf{Y} = \tfrac{1}{2}\mathbf{S}(\mathbf{x}'_{21})\mathbf{S}(\mathbf{n}) = (\tfrac{1}{2}(\mathbf{n}\mathbf{x}'^{T}_{21} - \mathbf{n}^T\mathbf{x}'_{21}\mathbf{I}) \tag{17.88}$$

Combining (17.81) with (17.83) and (17.86) gives the complete tangent stiffness matrix as

$$\mathbf{K}_t = \frac{1}{l_o}\mathbf{X}\bar{\mathbf{T}}\mathbf{C}\bar{\mathbf{T}}^T\mathbf{X}^T + \mathbf{K}_{\sigma 1} + \mathbf{K}_{\sigma 2} \tag{17.89}$$

where $\mathbf{K}_{\sigma 1}$ and $\mathbf{K}_{\sigma 2}$ have been given in (17.83) and (17.87) respectively.

It will be noted that there is a non-symmetric component of the tangent stiffness matrix given by

$$\mathbf{K}_{\text{tns}} = \frac{1}{2}\begin{bmatrix} \mathbf{0} & \mathbf{0} & \mathbf{0} & \mathbf{0} \\ \mathbf{0} & \mathbf{Z}+\mathbf{S(m)} & \mathbf{0} & \mathbf{Z} \\ \mathbf{0} & \mathbf{0} & \mathbf{0} & \mathbf{0} \\ \mathbf{0} & \mathbf{Z} & \mathbf{0} & \mathbf{Z}-\mathbf{S(m)} \end{bmatrix} \tag{17.90}$$

where

$$\mathbf{Z} = \tfrac{1}{2}[\mathbf{Y} - \mathbf{Y}^{\mathrm{T}}] = \tfrac{1}{4}[\mathbf{n}\mathbf{x}'^{\mathrm{T}}_{21} - \mathbf{x}'_{21}\mathbf{n}^{\mathrm{T}}] = \tfrac{1}{4}\mathbf{S}(\mathbf{x}'_{21} \times \mathbf{n}) \tag{17.91}$$

with (16.100) being used for the last relationship in (17.91).

It is argued in [S3.16] that this term vanishes (for conservative loadings) as the iterations reach equilibrium, and in [S3] that an alternative formulation leads to exactly the same symmetric stiffness matrix as would be obtained by artificially symmetrising the stiffness matrix. These issues will be discussed further in Section 17.4. Numerical experiments by the author and co-worker [C5] have indeed shown that, for the current element and the elements of Section 17.1 and 17.2, the excellent numerical (quadratic) convergence is maintained when such as artificial symmetrising process is adopted.

17.2.6 An isoparametric formulation

The previous formulation need not be restricted to a 'linear' two-noded element but can be extended to take a general isoparametric form using shape functions [S3.16]. In these circumstances, the coordinates, $\mathbf{x}$, and displacements, $\mathbf{d}$, can each be expressed in terms of nodal values using a non-dimensional coordinate, ζ so that:

$$\mathbf{x}(\zeta) = \sum h_i(\zeta)\mathbf{x}_i; \qquad \mathbf{d}(\zeta) = \sum h_i(\zeta)\mathbf{d}_i \tag{17.92}$$

where h_i is the standard isoparametric shape function. The 'rotation changes' can be expanded in a similar manner so that:

$$\delta\boldsymbol{\theta} = \sum h_i(\zeta)\delta\boldsymbol{\theta}_i \tag{17.93}$$

where $\delta\boldsymbol{\theta}_i$ are the nodal values. (In relation to the work in Sections 17.2.1–17.2.5, $\delta\boldsymbol{\theta}_1 = \delta\boldsymbol{\alpha}$, $\delta\boldsymbol{\theta}_2 = \delta\boldsymbol{\beta}$.)

Instead of using the length l_o, we now work with the element of length, ds, where

$$\mathrm{d}s = \alpha \mathrm{d}\zeta \tag{17.94}$$

and

$$\alpha^2 = \frac{\mathrm{d}\mathbf{x}^{\mathrm{T}}}{\mathrm{d}\zeta}\frac{\mathrm{d}\mathbf{x}}{\mathrm{d}\zeta} \tag{17.95}$$

with

$$\frac{\mathrm{d}\mathbf{x}}{\mathrm{d}\zeta} = \sum h_{\zeta i}\mathbf{x}_i \tag{17.96}$$

where $h_{\zeta i}$ is the derivative with respect to ζ of the ith shape function term.

Using this approach, equation (17.67) would be replaced by

$$\frac{d\mathbf{x}}{ds} + \boldsymbol{\varepsilon}_l(\zeta) = \mathbf{T}(\zeta)^T \frac{d\mathbf{x}'}{ds} = \frac{1}{\alpha(\zeta)} \mathbf{T}(\zeta)^T \frac{d\mathbf{x}'}{d\zeta} = \frac{1}{\alpha(\zeta)} \mathbf{T}(\zeta)^T \mathbf{x}'_\zeta \tag{17.97}$$

where $\mathbf{x}' = \mathbf{x} + \mathbf{d}$ has the current position vector, while, for the change, $\delta\boldsymbol{\varepsilon}_l$, in place of (17.68) and (17.70), we would have:

$$\delta\boldsymbol{\varepsilon}_l(\zeta) = \frac{1}{\alpha(\zeta)} \mathbf{T}(\zeta)^T \delta\mathbf{d}_\zeta + \frac{1}{\alpha(\zeta)} \mathbf{T}(\zeta)^T \mathbf{S}(\mathbf{x}'_\zeta)\delta\boldsymbol{\theta}(\zeta) \tag{17.98}$$

Also, in place of (17.71), the variation in the curvature would be written as

$$\delta\boldsymbol{\chi}_l(\zeta) = \mathbf{T}(\zeta)^T \frac{d\delta\boldsymbol{\theta}}{ds} = \frac{1}{\alpha(\zeta)} \mathbf{T}(\zeta)^T \delta\boldsymbol{\theta}_\zeta \tag{17.99}$$

so that, in place of (17.74), the relationship for the combined 'strain change' would be

$$\delta\boldsymbol{\varepsilon}_l(\zeta) = \begin{pmatrix} \delta\boldsymbol{\varepsilon} \\ \delta\boldsymbol{\chi} \end{pmatrix}_l = \frac{1}{\alpha(\zeta)} \begin{bmatrix} \mathbf{T}(\zeta)^T & \mathbf{0} \\ \mathbf{0} & \mathbf{T}(\zeta)^T \end{bmatrix} \begin{bmatrix} \mathbf{h}_{\zeta 1}\mathbf{I} & \mathbf{h}_1\mathbf{S}(\mathbf{x}'_\zeta) & \mathbf{h}_{\zeta 2}\mathbf{I} & \mathbf{h}_2\mathbf{S}(\mathbf{x}'_\zeta) \cdots \\ \mathbf{0} & \mathbf{h}_{\zeta 1}\mathbf{I} & \mathbf{0} & \mathbf{h}_{\zeta 2}\mathbf{I} \end{bmatrix} \delta\mathbf{p}$$

$$= \frac{1}{\alpha(\zeta)} \bar{\mathbf{T}}(\zeta)^T \mathbf{X}^T \delta\mathbf{p} \tag{17.100}$$

where

$$\delta\mathbf{p}^T = (\delta\mathbf{d}_1^T, \delta\boldsymbol{\theta}_1^T, \delta\mathbf{d}_2^T, \delta\boldsymbol{\theta}_2^T, \ldots) \tag{17.101}$$

Virtual work then leads to

$$\mathbf{q}_i = \int \mathbf{X}\bar{\mathbf{T}}(\zeta) \begin{pmatrix} \mathbf{N}(\zeta) \\ \mathbf{M}(\zeta) \end{pmatrix} d\zeta = \int \mathbf{X} \begin{pmatrix} \mathbf{n}(\zeta) \\ \mathbf{m}(\zeta) \end{pmatrix} d\zeta \tag{17.102}$$

which replaces (17.79) for the two-noded element.

The tangent stiffness equations are found by differentiating (17.102) sot that:

$$\delta\mathbf{q}_i = \int \frac{1}{\alpha} \mathbf{X}\bar{\mathbf{T}}\mathbf{C}\bar{\mathbf{T}}^T\mathbf{X}^T d\zeta \delta\mathbf{p} + \int \begin{bmatrix} h_{\zeta 1}\delta\mathbf{T} & \mathbf{0} \\ \mathbf{0} & h_{\zeta 1}\delta\mathbf{T} \\ h_{\zeta 2}\delta\mathbf{T} & \mathbf{0} \\ \mathbf{0} & h_{\zeta 2}\delta\mathbf{T} \\ \vdots & \vdots \end{bmatrix} \begin{pmatrix} \mathbf{N} \\ \mathbf{M} \end{pmatrix} d\zeta - \int \begin{bmatrix} \mathbf{0} & \\ h_1\delta(\mathbf{S}(\mathbf{x}'_\zeta)\mathbf{T}) & \\ \mathbf{0} & (\mathbf{N})d\zeta \\ h_2\delta(\mathbf{S}(\mathbf{x}'_\zeta)\mathbf{T}) & \\ \vdots & \vdots \end{bmatrix} \tag{17.103}$$

with

$$\mathbf{h}_{\zeta 1}\delta\mathbf{T}\mathbf{N} = -h_{\zeta 1}\mathbf{S}(\mathbf{n}) \sum h_i \delta\boldsymbol{\theta}_i \tag{17.104}$$

where, for brevity, we have omitted the (ζ)'s. From (17.103), the tangent stiffness matrix follows as

$$\mathbf{K}_t = \int \frac{1}{\alpha} \mathbf{X}\bar{\mathbf{T}}\mathbf{C}\bar{\mathbf{T}}^T\mathbf{X}^T d\zeta + \mathbf{K}_{t\sigma 1} + \mathbf{K}_{t\sigma 2} \tag{17.105}$$

where

$$\mathbf{K}_{\sigma 1} = \int \begin{bmatrix} \mathbf{0} & -\mathbf{S}(\mathbf{n})h_{\zeta 1}h_1 & \mathbf{0} & -\mathbf{S}(\mathbf{n})h_{\zeta 1}h_2 \\ \mathbf{0} & -\mathbf{S}(\mathbf{m})h_{\zeta 1}h_1 & \mathbf{0} & -\mathbf{S}(\mathbf{m})h_{\zeta 1}h_2 \\ \mathbf{0} & -\mathbf{S}(\mathbf{n})h_{\zeta 2}h_1 & \mathbf{0} & -\mathbf{S}(\mathbf{n})h_{\zeta 2}h_2 \\ \vdots & & \vdots & \end{bmatrix} \cdots \mathrm{d}\zeta \tag{17.106}$$

$$\mathbf{K}_{\sigma 2} = \int \begin{bmatrix} 0 & 0 & 0 & 0 \\ \mathbf{S}(\mathbf{n})h_1h_{\zeta 1} & \mathbf{Y}h_1h_1 & \mathbf{S}(\mathbf{n})h_1h_{\zeta 2} & \bar{\mathbf{Y}}h_1h_2 \\ 0 & 0 & 0 & 0 \\ \mathbf{S}(\mathbf{n})h_2h_{\zeta 1} & \mathbf{Y}h_2h_1 & \mathbf{S}(\mathbf{n})h_2h_{\zeta 2} & \bar{\mathbf{Y}}h_2h_2 \\ \vdots & \vdots & \vdots & \vdots \end{bmatrix} \cdots \mathrm{d}\zeta \tag{17.107a}$$

where

$$\bar{\mathbf{Y}} = \mathbf{S}(\mathbf{x}'_\zeta)\mathbf{S}(\mathbf{n}) \tag{17.107b}$$

The present results only coincide with those of Sections 17.2.4 and 17.2.5 if a two-noded element is evaluated using 'one-point integration' and the integrals are evaluated numerically at $\zeta = 0$.

17.3 AN ISOPARAMETRIC TIMOSHENKO BEAM APPROACH USING THE TOTAL LAGRANGIAN FORMULATION

A degenerate continuum approach for two-dimensional beams has been given in Section 7.5 and for shells in Section 8.2. In this section we will describe a Timoshenko beam approach for three-dimensional beams that has much in common with these earlier formulations. The method is largely based on the work of Dvorkin *et al.* [D1], but also uses some of the procedures developed in the earlier sections of this chapter. As a consequence, in contrast to the work in [D1], in the first instance, the present formulation leads to a non-symmetric stiffness matrix. This issue will be discussed further in Sections 17.4.2 and 17.5 with the links with and differences from the formulation of Dvorkin *et al.* [D1] being explored in the former section.

In common with the work in [D1], we will use convected coordinates with co- and contravariant stress and strain components (although an equivalent formulation could be devised without using this approach). The formulation therefore has close links with the continuum formulation of Section 12.4.

As a starting-point, the geometry is expressed using the standard isoparametric form (see also (8.32) and Figure 17.2) as

$$\mathbf{x} = \bar{\mathbf{x}} + \Delta\mathbf{r} = \sum h(r)_i \bar{\mathbf{x}}_i + \frac{s}{2}\sum h(r)_i a_i \mathbf{v}_{io} + \frac{t}{2}\sum h(r)_i b_i \mathbf{w}_{io} \tag{17.108}$$

where $\bar{\mathbf{x}}_i$ contains the coordinates of node i while $\mathbf{v}_{io}$, $\mathbf{w}_{io}$ are the initial pseudo-normal vectors (see Figure 17.2) and a_i and b_i are the nodal thicknesses (fixed) in the directions of the pseudo-normals. The shape functions $\mathbf{h}$ (with components h) are only functions of the non-dimensional centre-line coordinate, r. Hence, in future, the (r) on h will be

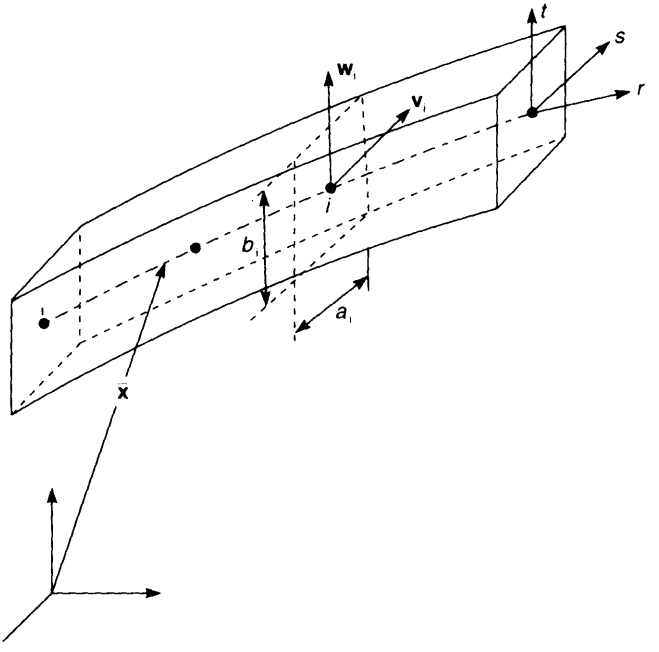

Figure 17.2 Isoparametric degenerate-continuum beam element.

omitted. The terms s and t in (17.108) are the non-dimensional coordinates of width and height.

From (17.108), the displacements $\mathbf{d}$ can be expressed as

$$\mathbf{d} = \bar{\mathbf{d}} + \Delta\mathbf{d} = \sum h_i \bar{\mathbf{d}}_i + \frac{s}{2}\sum h_i a_i(\mathbf{v}_i - \mathbf{v}_{io}) + \frac{t}{2}\sum h_i b_i(\mathbf{w}_i - \mathbf{w}_{io}) \tag{17.109}$$

where $\mathbf{v}_i$ and $\mathbf{w}_i$ are the current pseudo-normal vectors which are forced to remain of unit length. Since $\mathbf{v}_i$ and $\mathbf{v}_{io}$ have the same origin and are of the same length, their motion can be described as a pure rotation, which from Chapter 16 involves:

$$\mathbf{v} = \mathbf{R}(\boldsymbol{\alpha})\mathbf{v}_o \tag{17.110}$$

Hence, (17.109) can be re-expressed as

$$\mathbf{d} = \sum h_i \bar{\mathbf{d}}_i + \frac{s}{2}\sum h_i(\mathbf{R}(\boldsymbol{\alpha}_i) - \mathbf{I})a_i\mathbf{v}_{io} + \frac{t}{2}\sum h_i(\mathbf{R}(\boldsymbol{\alpha}_i) - \mathbf{I})b_i\mathbf{w}_{io} \tag{17.111}$$

For the fundamental expression of virtual work, we need the variation of (17.111). To this end, from (16.97b) and (17.111) we have:

$$\delta\mathbf{R}\mathbf{v}_{io} = \mathbf{S}(\delta\boldsymbol{\alpha}_i)\mathbf{R}\mathbf{v}_{io} = \mathbf{S}(\delta\boldsymbol{\alpha}_i)\mathbf{v}_i = -\mathbf{S}(\mathbf{v}_i)\delta\boldsymbol{\alpha}_i \tag{17.112}$$

where $\delta\boldsymbol{\alpha}_i$ are nodal 'spin variables' that are not additive to $\boldsymbol{\alpha}_i$ even in the limit as $\delta\boldsymbol{\alpha}$ tends to zero (see Section 16.11). (In Section 16.11, we adopted the notation, $\delta\bar{\boldsymbol{\theta}}$, to emphasise this point but, here, will omit the bar.)

Using (17.112), the variation of $\mathbf{d}$ in (17.111) can be expressed as

$$\delta\mathbf{d} = \sum h_i \delta\bar{\mathbf{d}}_i - \frac{s}{2}\sum h_i \mathbf{S}(\mathbf{v}_i) a_i \delta\boldsymbol{\alpha}_i - \frac{t}{2}\sum h_i b_i \mathbf{S}(\mathbf{w}_i)\delta\boldsymbol{\alpha}_i \tag{17.113}$$

At this stage, we introduce the covariant components of the Green strain (see 11.56) and (12.75)) as

$$\begin{aligned} \varepsilon_{rr} &= \tfrac{1}{2}(\mathbf{g}_r^{\mathrm{T}}\mathbf{g}_r - \mathbf{G}_r^{\mathrm{T}}\mathbf{G}_r) \\ \gamma_{rs} &= 2\varepsilon_{rs} = \mathbf{g}_r^{\mathrm{T}}\mathbf{g}_s - \mathbf{G}_r^{\mathrm{T}}\mathbf{G}_s \\ \gamma_{rt} &= 2\varepsilon_{rt} = \mathbf{g}_r^{\mathrm{T}}\mathbf{g}_t - \mathbf{G}_r^{\mathrm{T}}\mathbf{G}_t \end{aligned} \tag{17.114}$$

where $\mathbf{G}_r$–$\mathbf{G}_t$ are the covariant base vectors in the initial configuration and $\mathbf{g}_r$–$\mathbf{g}_t$ are the equivalent vectors in the current configuration. Consequently (see Section 11.7):

$$\mathbf{G}_r = \frac{\partial\mathbf{x}}{\partial r}, \mathbf{G}_s = \frac{\partial\mathbf{x}}{\partial s}, \mathbf{G}_t = \frac{\partial\mathbf{x}}{\partial t}; \qquad \mathbf{g}_r = \frac{\partial(\mathbf{x}+\mathbf{d})}{\partial r}, \mathbf{g}_s = \frac{\partial(\mathbf{x}+\mathbf{d})}{\partial s}, \mathbf{g}_t = \frac{\partial(\mathbf{x}+\mathbf{d})}{\partial t} \tag{17.114a}$$

The variations of the covariant components in (17.114) are given (see (11.70) and (11.71)) by

$$\begin{aligned} \delta\varepsilon_{rr} &= \mathbf{g}_r^{\mathrm{T}}\frac{\partial\delta\mathbf{d}}{\partial r} = \mathbf{g}_r^{\mathrm{T}}\delta\mathbf{d}_r = \left(\mathbf{G}_r + \frac{\partial\mathbf{d}}{\partial r}\right)^{\mathrm{T}}\delta\mathbf{d}_r = (\mathbf{G}_r + \mathbf{d}_r)\delta\mathbf{d}_r \\ \delta\gamma_{rs} &= \mathbf{g}_r^{\mathrm{T}}\delta\mathbf{d}_s + \mathbf{g}_s^{\mathrm{T}}\delta\mathbf{d}_r \\ \delta\gamma_{rt} &= \mathbf{g}_r^{\mathrm{T}}\delta\mathbf{d}_t + \mathbf{g}_t^{\mathrm{T}}\delta\mathbf{d}_r \end{aligned} \tag{17.115}$$

where the subscripts r and s and t or $\mathbf{d}$ represent partial differentiation. It is worth emphasising that the equivalent subscripts on $\mathbf{G}$ and $\mathbf{g}$ do not indicate partial differentiation on $\mathbf{G}$ or $\mathbf{g}$ but rather on $\mathbf{x}$ or $(\mathbf{x}+\mathbf{d})$—see (17.114a). From (17.113) and (17.115), we can produce the standard matrix expression (see also Section 5.1.1 and (12.80)) for the changes in Green strain, whereby

$$\delta\boldsymbol{\varepsilon} = \begin{bmatrix} \delta\varepsilon_{rr} \\ \delta\gamma_{rs} \\ \delta\gamma_{rt} \end{bmatrix} = [\mathbf{H}(\mathbf{G}) + \mathbf{A}(\boldsymbol{\theta})]\delta\boldsymbol{\theta} = \mathbf{H}(\mathbf{g})\delta\boldsymbol{\theta} \tag{17.116}$$

where we are now writing:

$$\delta\boldsymbol{\theta}^{\mathrm{T}} = (\delta\mathbf{d}_r^{\mathrm{T}}, \delta\mathbf{d}_s^{\mathrm{T}}, \delta\mathbf{d}_t^{\mathrm{T}}) \tag{17.117}$$

so that a different ordering has been introduced for the components of $\delta\boldsymbol{\theta}$ to the orderings adopted in Chapter 5 (see (5.29)), Chapter 7 (see (7.160)), Chapter 8, (see (8.44)) and Chapter 12 (see (12.78)). The matrices $\mathbf{H}(\mathbf{G})$ and $\mathbf{A}(\boldsymbol{\theta})$ in (17.116) are given by

$$\mathbf{H}(\mathbf{G}) = \begin{bmatrix} \mathbf{G}_r^{\mathrm{T}} & \mathbf{0}^{\mathrm{T}} & \mathbf{0}^{\mathrm{T}} \\ \mathbf{G}_s^{\mathrm{T}} & \mathbf{G}_r^{\mathrm{T}} & \mathbf{0}^{\mathrm{T}} \\ \mathbf{G}_t^{\mathrm{T}} & \mathbf{0}^{\mathrm{T}} & \mathbf{G}_r^{\mathrm{T}} \end{bmatrix} \tag{17.118}$$

and

$$\mathbf{A}(\boldsymbol{\theta}) = \begin{bmatrix} \mathbf{d}_r^{\mathrm{T}} & \mathbf{0}^{\mathrm{T}} & \mathbf{0}^{\mathrm{T}} \\ \mathbf{d}_s^{\mathrm{T}} & \mathbf{d}_r^{\mathrm{T}} & \mathbf{0}^{\mathrm{T}} \\ \mathbf{d}_t^{\mathrm{T}} & \mathbf{0}^{\mathrm{T}} & \mathbf{d}_r^{\mathrm{T}} \end{bmatrix} \tag{17.119}$$

We will now order the nodal variables as

$$\delta \mathbf{p}^{\mathrm{T}} = (\delta \mathbf{d}_1^{\mathrm{T}}, \delta \boldsymbol{\alpha}_1^{\mathrm{T}}, \delta \mathbf{d}_2^{\mathrm{T}}, \delta \boldsymbol{\alpha}_2^{\mathrm{T}}, \ldots) \tag{17.120}$$

This ordering differs from the orderings in Chapters 5 (see (5.8)), Chapter 7 (see (7.160)), Chapter 8, (see (8.43)) and Chapter 12 (see (12.73)). Using this ordering and with the aid of (17.113), the components of the $\delta\boldsymbol{\theta}$ vector of (17.117) are given by

$$\delta \mathbf{d}_r = \mathbf{B}_r \delta \mathbf{p}; \qquad \delta \mathbf{d}_s = \mathbf{B}_s \delta \mathbf{p}; \qquad \delta \mathbf{d}_t = \mathbf{B}_t \delta \mathbf{p} \tag{17.121}$$

where

$$\mathbf{B}_r = [\mathbf{A}_{rd1}\mathbf{A}_{r\alpha 1}\mathbf{A}_{rd2}\mathbf{A}_{r\alpha 2} \cdots \mathbf{A}_{rdi}\mathbf{A}_{r\alpha i} \cdots] \tag{17.122}$$

and

$$\mathbf{A}_{rdi} = h_r(i)\mathbf{I} \tag{17.123}$$

$$\mathbf{A}_{r\alpha i} = -h_r(i)\left(\frac{s}{2} a_i \mathbf{S}(\mathbf{v}_i) + \frac{t}{2} b_i \mathbf{S}(\mathbf{w}_i)\right) \tag{17.124}$$

where $h_r(i)$ is the ith component of the vector obtained via partial differentiation of the shape function $\mathbf{h}$ with respect to r.

The matrices $\mathbf{B}_s$ and $\mathbf{B}_t$ take an identical form to (17.122) although now:

$$\mathbf{A}_{sdi} = \mathbf{A}_{tdi} = 0 \tag{17.125}$$

while

$$\mathbf{A}_{s\alpha i} = -\frac{h(i)}{2} a_i \mathbf{S}(\mathbf{v}_i) \tag{17.126}$$

$$\mathbf{A}_{t\alpha i} = -\frac{h(i)}{2} b_i \mathbf{S}(\mathbf{w}_i) \tag{17.127}$$

Equations (17.121) can now be combined to give an expression of the form:

$$\delta\boldsymbol{\theta} = \begin{bmatrix} \delta \mathbf{d}_r \\ \delta \mathbf{d}_s \\ \delta \mathbf{d}_t \end{bmatrix} = \bar{\mathbf{G}}\,\delta \mathbf{p} = \begin{bmatrix} \mathbf{B}_r \\ \mathbf{B}_s \\ \mathbf{B}_t \end{bmatrix} \delta \mathbf{p} \tag{17.128}$$

Application of the principle of virtual work leads to the standard form (see (12.80) and (12.82)):

$$\mathbf{q}_i = \int \bar{\mathbf{G}}^{\mathrm{T}}[\mathbf{H}(\mathbf{G}) + \mathbf{A}(\boldsymbol{\theta})]^{\mathrm{T}} \mathbf{S}\, \mathrm{d}V = \int \bar{\mathbf{G}}^{\mathrm{T}}[\mathbf{H}(\mathbf{g})]^{\mathrm{T}} \mathbf{S}\, \mathrm{d}V_0 \tag{17.129}$$

where the vector $\bar{\mathbf{S}}$ contains the contravariant components of the second Piola Kirchhoff stress with:

$$\bar{\mathbf{S}}^{\mathrm{T}} = (\bar{S}^{rr}, \bar{S}^{rs}, \bar{S}^{rt}) \tag{17.130}$$

The bar has been put on top of these stresses to avoid confusion with the $\mathbf{S}$ used for the skew-symmetric matrix. The element of initial volume $\mathrm{d}V_0$ is given (see (11.5)) by

$$\mathrm{d}V_0 = \mathbf{G}_r^{\mathrm{T}}(\mathbf{G}_s \times \mathbf{G}_t) \tag{17.131}$$

17.3.1 The tangent stiffness matrix

The variation of (17.129) leads to the tangent stiffness equations so that:

$$\delta \mathbf{q}_i = (\mathbf{K}_{t1} + \mathbf{K}_{\sigma 1} + \mathbf{K}_{\sigma 2})\delta \mathbf{p} = \mathbf{K}_{t1}\delta \mathbf{p} + \int \bar{\mathbf{G}}^{\mathrm{T}} \delta(\mathbf{A}(\boldsymbol{\theta}))^{\mathrm{T}} \mathbf{S}\, \mathrm{d}V_0 + \int \delta \bar{\mathbf{G}}^{\mathrm{T}} \mathbf{H}(\mathbf{g})^{\mathrm{T}} \mathbf{S}\, \mathrm{d}V_0 \tag{17.132}$$

where $\mathbf{K}_{t1}$ is the standard tangent stiffness matrix, given by

$$\mathbf{K}_{t1} = \int \bar{\mathbf{G}}^{\mathrm{T}} \mathbf{H}(\mathbf{g})^{\mathrm{T}} \mathbf{C} \mathbf{H}(\mathbf{g}) \bar{\mathbf{G}}\, \mathrm{d}V_0 \tag{17.133}$$

The **C** matrix in (17.133) relates the changes in the contravariant components of the second Piola–Kirchhoff stress (17.130) to the covariant components of Green strain increment (17.116) or in terms of tensor components (see (11.78)):

$$\bar{S}^{ij} = C^{ijkl} \delta \varepsilon_{kl} \tag{17.134}$$

If we know the components of the constitutive tensor in an orthonormal system with unit base vectors, $\mathbf{i}_1$–$\mathbf{i}_3$ as $\hat{C}_{ijkl}$, then from (11.79), we have:

$$C^{ijkl} = (\mathbf{G}^i \cdot \mathbf{i}_a)(\mathbf{G}^j \cdot \mathbf{i}_b)(\mathbf{G}^k \cdot \mathbf{i}_c)(\mathbf{G}^l \cdot \mathbf{i}_d)\hat{C}_{abcd} \tag{17.135}$$

According to [D1], with constant nodal thickness, an orthonormal system can be defined from the initial covariant base vectors, $\mathbf{G}_r$, $\mathbf{G}_s$, $\mathbf{G}_t$ via:

$$\mathbf{i}_i = \mathbf{G}_i / \| \mathbf{G}_i \|, \qquad i = r, s, t \tag{17.136}$$

with the constitutive matrix in the orthonormal system being defined by

$$\hat{\mathbf{C}} = \begin{bmatrix} E & 0 & 0 \\ 0 & kG & 0 \\ 0 & 0 & kG \end{bmatrix} \tag{17.137}$$

with E as Young's modulus, G as the shear modulus and k as the shear correction factor.

The second term in (17.132) leads to the conventional geometric stiffness matrix:

$$\mathbf{K}_{\sigma 1} = \int (\bar{S}^{rr} \mathbf{B}_r^{\mathrm{T}} \mathbf{B}_r + \bar{S}^{rs}(\mathbf{B}_r^{\mathrm{T}} \mathbf{B}_s + \mathbf{B}_s^{\mathrm{T}} \mathbf{B}_r) + \bar{S}^{rt}(\mathbf{B}_r^{\mathrm{T}} \mathbf{B}_t + \mathbf{B}_t^{\mathrm{T}} \mathbf{B}_r))\mathrm{d}V_0 \tag{17.138}$$

while the last term in (17.132) gives rise to

$$\mathbf{K}_{\sigma 2}\delta \mathbf{p} = \int [\delta \mathbf{B}_r^{\mathrm{T}}\, \delta \mathbf{B}_s^{\mathrm{T}} \delta \mathbf{B}_t^{\mathrm{T}}] \begin{bmatrix} \bar{S}^{rr}\mathbf{g}_r + \bar{S}^{rs}\mathbf{g}_s + \bar{S}^{rt}\mathbf{g}_t \\ \bar{S}^{rs}\mathbf{g}_r \\ \bar{S}^{rt}\mathbf{g}_r \end{bmatrix} \mathrm{d}V_0 \tag{17.139}$$

Consider, first, the terms involving $\bar{S}^{rr}$. From (17.122) to (17.124), these involve 3×3 submatrices, $\mathbf{P}_{rr}(i)$ on the diagonal of the tangent stiffness matrix associated with the $\delta\alpha$ terms for the ith node, i.e.:

$$\mathbf{P}_{rr}(i)\delta \boldsymbol{\alpha}_i = \int \bar{S}^{rr} \delta \mathbf{A}_{r\alpha i}^{\mathrm{T}} \mathbf{g}_r \mathrm{d}V_0 \tag{17.140}$$

and, using (17.124):

$$\delta \mathbf{A}_{r\alpha i}^{\mathrm{T}} \mathbf{g}_r = -h_r(i)\left(\frac{s}{2} a_i \delta \mathbf{S}^{\mathrm{T}}(\mathbf{v}_i) + \frac{t}{2} b_i \delta \mathbf{S}^{\mathrm{T}}(\mathbf{w}_i)\right)\mathbf{g}_r \tag{17.141}$$

For the following two equations, it is more convenient to drop the nodal subscript, i and we can note that:

$$\delta \mathbf{S}^{\mathrm{T}}(\mathbf{v})\mathbf{g}_r = -\delta \mathbf{S}(\mathbf{v})\mathbf{g}_r = \mathbf{S}(\mathbf{g}_r)\delta(\mathbf{v}) \tag{17.142}$$

while:

$$\delta \mathbf{v} = -\mathbf{v} \times \delta \boldsymbol{\alpha} = -\mathbf{S}(\mathbf{v})\delta \boldsymbol{\alpha} \tag{17.143}$$

Equivalent expressions to (17.142)–(17.143) can be obtained involving $\mathbf{w}$. Substituting from these expressions and from (17.141) to (17.143) into (17.140) an reintroducing the subscript i leads to the relationship:

$$\begin{aligned}\mathbf{P}_{rr}(i)\delta \boldsymbol{\alpha}_i &= \int \bar{S}^{rr} \delta \mathbf{A}_{r\alpha i} \mathbf{g}_r \mathrm{d}V_{\mathrm{o}} \\ &= \int h_r(i)\bar{S}^{rr}\left[\mathbf{S}(\mathbf{g}_r)\left[\frac{s}{2} a_i \mathbf{S}(\mathbf{v}_i) + \frac{t}{2} b_i \mathbf{S}(\mathbf{w}_i)\right]\right]\mathrm{d}V_{\mathrm{o}}\delta \boldsymbol{\alpha}_i\end{aligned} \tag{17.144}$$

Using (16.86), we can rewrite the 3×3 diagonal submatrix for the ith node as

$$\mathbf{P}_{rr}(i) = \int h_r(i)\bar{S}^{rr}\left[\frac{s}{2} a_i [\mathbf{v}_i \mathbf{g}_r^{\mathrm{T}} - \mathbf{g}_r^{\mathrm{T}} \mathbf{v}_i \mathbf{I}] + \frac{t}{2} b_i [\mathbf{w}_i \mathbf{g}_r^{\mathrm{T}} - \mathbf{g}_r^{\mathrm{T}} \mathbf{w}_i \mathbf{I}]\right]\mathrm{d}V_{\mathrm{o}} \tag{17.145}$$

For the $\delta \mathbf{B}_r$ term in (17.139), we also require:

$$\mathbf{P}_{rs}(i)\delta \boldsymbol{\alpha}_i = \int \bar{S}^{rs} \delta \mathbf{A}_{r\alpha i} \mathbf{g}_s \mathrm{d}V_{\mathrm{o}}; \qquad \mathbf{P}_{rt}(i)\delta \boldsymbol{\alpha}_i = \int \bar{S}^{rt} \delta \mathbf{A}_{r\alpha i} \mathbf{g}_t \mathrm{d}V_{\mathrm{o}} \tag{17.146}$$

which leads to

$$\mathbf{P}_{rs}(i) = \int \bar{S}^{rs} h_r(i)\left[\frac{s}{2} a_i [\mathbf{v}_i \mathbf{g}_s^{\mathrm{T}} - \mathbf{g}_s^{\mathrm{T}} \mathbf{v}_i \mathbf{I}] + \frac{t}{2} b_i [\mathbf{w}_i \mathbf{g}_s^{\mathrm{T}} - \mathbf{g}_s^{\mathrm{T}} \mathbf{w}_i \mathbf{I}]\right]\mathrm{d}V_{\mathrm{o}} \tag{17.147a}$$

$$\mathbf{P}_{rt}(i) = \int \bar{S}^{rt} h_i(i)\left[\frac{s}{2} a_i [\mathbf{v}_i \mathbf{g}_t^{\mathrm{T}} - \mathbf{g}_t^{\mathrm{T}} \mathbf{v}_i \mathbf{I}] + \frac{t}{2} b_i [\mathbf{w}_i \mathbf{g}_t^{\mathrm{T}} - \mathbf{g}_t^{\mathrm{T}} \mathbf{w}_i \mathbf{I}]\right]\mathrm{d}V_{\mathrm{o}} \tag{17.147b}$$

For the $\delta \mathbf{B}_s$ and $\delta \mathbf{B}_t$ terms in (17.139), we require:

$$\mathbf{Q}_{rs}(i)\delta \boldsymbol{\alpha}_i = \int \bar{S}^{rs} \delta \mathbf{A}_{s\alpha i} \mathbf{g}_r \mathrm{d}V_{\mathrm{o}}; \qquad Q_{rt}(i)\delta \boldsymbol{\alpha}_i = \int \bar{S}^{rt} \delta \mathbf{A}_{t\alpha i} \mathbf{g}_r \mathrm{d}V_{\mathrm{o}} \tag{17.148}$$

which leads to

$$\mathbf{Q}_{rs}(i) = \frac{1}{2}\int \bar{S}^{rs} h(i) a_i [\mathbf{v}_i \mathbf{g}_r^{\mathrm{T}} - \mathbf{g}_r^{\mathrm{T}} \mathbf{v}_i \mathbf{I}]\mathrm{d}V_{\mathrm{o}} \tag{17.149a}$$

$$\mathbf{Q}_{rt}(i) = \frac{1}{2}\int \bar{S}^{rt} h(i) b_i [\mathbf{w}_i \mathbf{g}_r^{\mathrm{T}} - \mathbf{g}_r^{\mathrm{T}} \mathbf{w}_i \mathbf{I}]\mathrm{d}V_{\mathrm{o}} \tag{17.149b}$$

Finally, from (17.139), the geometric tangent stiffness matrix, $\mathbf{K}_{\sigma 2}$, involves 3×3 submatrices on the $\delta\boldsymbol{\alpha}_i$ terms of the diagonal associated with the ith node where:

$$\text{`}\mathbf{K}_{\sigma 2}(i,i)\text{'} = \mathbf{P}_{rr}(i) + \mathbf{P}_{rs}(i) + \mathbf{Q}_{rs}(i) + \mathbf{P}_{rt}(i) + \mathbf{Q}_{rt}(i) \tag{17.150}$$

with $\mathbf{P}_{rr}(i)$ from (17.145), $\mathbf{P}_{rs}(i)$ and $\mathbf{P}_{rt}(i)$ from (17.147) and $\mathbf{Q}_{rs}(i)$ and $\mathbf{Q}_{rt}(i)$ from (17.149). From an inspection of the latter equations, it can be observed that $\mathbf{K}_{\sigma 2}$ is non-symmetric. If we artificially introduce symmetry, it is not difficult to show that:

$$\mathbf{K}_{s\sigma 2} = \tfrac{1}{2}[\mathbf{K}_{\sigma 2} + \mathbf{K}_{\sigma 2}^{\mathrm{T}}] \tag{17.151}$$

corresponds with the expression derived by Dvorkin *et al.* [D1].

17.3.2 Outline of the relationship with the formulation of Dvorkin *et al.* [D1]

The previous formulation has introduced an initial stress (or geometric stiffness) matrix, $\mathbf{K}_{\sigma 2}$, that is non-symmetric. In contrast, the formulation of Dvorkin *et al.* [D1] led to a symmetric stiffness matrix. The latter was based on an 'incremental formulation' which only differs from the formulation of Sections 17.3.1 and 17.3.2 in relation to the rotation terms and hence we will now only consider the latter. In addition, we will only consider the key elements and so will let the thicknesses, a_i and b_i be unity with the work being concentrated on a typical term involving the unit pseudo-normal, $\mathbf{v}$.

The basis of the incremental formulation is to write the incremental displacement due to a rotation as

$$\Delta\mathbf{d}_i = \mathbf{R}(\boldsymbol{\alpha}_i)\mathbf{v}_i - \mathbf{v}_i \tag{17.152}$$

so that, adopting the approximation in (16.39), we can write:

$$\begin{aligned}\Delta\mathbf{d}_i &= \Delta\mathbf{d}_{i1} + \Delta\mathbf{d}_{i2} = [\mathbf{S}(\Delta\boldsymbol{\alpha}_i) + \tfrac{1}{2}\mathbf{S}(\Delta\boldsymbol{\alpha}_i)^2]\mathbf{v}_i \\ &= \Delta\boldsymbol{\alpha}_i \times \mathbf{v}_i + \tfrac{1}{2}\Delta\boldsymbol{\alpha}_i \times (\Delta\boldsymbol{\alpha}_i \times \mathbf{v}_i)\end{aligned} \tag{17.153}$$

Using similar approximations, in place of the variation in the Green strain with $\delta\varepsilon_{rr}$ from (17.115), we could write the incremental change as

$$\Delta\varepsilon_{rr} = \Delta\varepsilon_{rr1} + \Delta\varepsilon_{rr2} + \Delta\varepsilon_{rr3} = \mathbf{g}_r^{\mathrm{T}}\Delta\mathbf{d}_{1r} + \mathbf{g}_r^{\mathrm{T}}\Delta\mathbf{d}_{2r} + \tfrac{1}{2}\Delta\mathbf{d}_{1r}^{\mathrm{T}}\Delta\mathbf{d}_{1r} \tag{17.154}$$

where the non-linear incremental terms are given by $\Delta\varepsilon_{rr2}$ and $\Delta\varepsilon_{rr3}$ and Δ's of third and fourth order have been neglected. The terms $\Delta\varepsilon_{rr2}$ and $\Delta\varepsilon_{rr3}$ in (17.154) lead to contributions to the initial stress matrices $\mathbf{K}_{\sigma 2}$ (17.150) and $\mathbf{K}_{\sigma 1}$ (17.138) respectively. In the latter case, the result is the same as before and so we will concentrate on the former and will consider only terms involving $\bar{S}^{rr}$ for which the initial stress matrix, $\mathbf{K}_{\sigma 2}$, is now given by [D1]

$$\delta\Delta\boldsymbol{\alpha}^{\mathrm{T}}\mathbf{K}_{\sigma 2}\delta\Delta\boldsymbol{\alpha} = \int \bar{S}^{rr}\delta\Delta\varepsilon_{rr2}\,\mathrm{d}V_0 \tag{17.155}$$

If we consider the term $S^{rr}\Delta\varepsilon_{rr2}$ with $\Delta\varepsilon_{rr2}$ from (17.154) and $\Delta\mathbf{d}_2$ from (17.153), we

obtain:

$$\bar{S}^{rr}\Delta\varepsilon_{rr2} = \tfrac{1}{2}\bar{S}^{rr}\mathbf{g}_r^{\mathrm{T}}\{\Delta\boldsymbol{\alpha} \times (\Delta\boldsymbol{\alpha} \times \mathbf{v})\} \tag{17.156}$$

and using the relationship:

$$\mathbf{a} \times (\mathbf{b} \times \mathbf{c}) = (\mathbf{a}^{\mathrm{T}}\mathbf{c})\mathbf{b} - (\mathbf{a}^{\mathrm{T}}\mathbf{b})\mathbf{c} \tag{17.157}$$

we arrive at

$$\bar{S}^{rr}\Delta\varepsilon_{rr2} = \tfrac{1}{2}\bar{S}^{rr}((\Delta\boldsymbol{\alpha}^{\mathrm{T}}\mathbf{g}_r)\mathbf{v}^{\mathrm{T}}\Delta\boldsymbol{\alpha} - (\mathbf{g}_r^{\mathrm{T}}\mathbf{v})\Delta\boldsymbol{\alpha}^{\mathrm{T}}\Delta\boldsymbol{\alpha}) = \tfrac{1}{2}\bar{S}^{rr}\Delta\boldsymbol{\alpha}^{\mathrm{T}}(\mathbf{g}_r\mathbf{v}^{\mathrm{T}} - [\mathbf{g}_r^{\mathrm{T}}\mathbf{v})\mathbf{I}]\Delta\boldsymbol{\alpha} \tag{17.158}$$

For (17.156), we require $\bar{S}^{rr}\delta\Delta\varepsilon_{rr2}$. Using (17.158), and substituting into (17.155) leads to

$$\delta\Delta\boldsymbol{\alpha}^{\mathrm{T}}\mathbf{K}_{\sigma 2}\Delta\boldsymbol{\alpha} = \delta\Delta\boldsymbol{\alpha}^{\mathrm{T}}[\tfrac{1}{2}\bar{S}^{rr}[\mathbf{g}_r\mathbf{v}^{\mathrm{T}} + \mathbf{v}\mathbf{g}_r^{\mathrm{T}}] - \bar{S}^{rr}(\mathbf{g}_r^{\mathrm{T}}\mathbf{v})\mathbf{I}]\Delta\boldsymbol{\alpha} \tag{17.159}$$

which contains the symmetric form (via (17.151)) of the $\mathbf{K}_{\sigma 2}$ term in (17.150) and (17.145).

17.4 SYMMETRY AND THE USE OF DIFFERENT 'ROTATION VARIABLES'

The main reason for the non-symmetric terms in the earlier tangent stiffness matrices relates to the use of spin variables, $\delta\bar{\boldsymbol{\theta}}$ (see Section 16.11) that are non-additive even in the limit as $\delta\bar{\boldsymbol{\theta}}$ tends to zero.*

For an 'additive system' one can write:

$$\mathbf{x}_{\mathrm{new}} = \mathbf{x}_{\mathrm{old}} + \delta\mathbf{x} \tag{17.160}$$

Using such variables, standard arguments relating to a potential can be used to show that $\mathbf{K}_{\mathrm{t}}$ must symmetric because:

$$\mathbf{K}_{\mathrm{t}}(x_1, x_2) = \frac{\partial^2\varphi}{\partial x_1 \partial x_2} = \mathbf{K}_{\mathrm{t}}(x_2, x_1) = \frac{\partial^2\varphi}{\partial x_2 \partial x_1} \tag{17.161}$$

However, with 'spin variables', (17.160) does not apply and hence neither does (17.161). We will show in Sections 17.4.2 and 17.4.3 that we can change the parametrisation of the rotations so as to ensure symmetry. We will also show that, at least in some cases, the resulting stiffness matrix is identical to that obtained by artificially symmetrising the stiffness matrix derived using 'spin variables'.

It was argued by Simo and Vu-Quoc [S3.16] that their stiffness matrix (see Section 17.2) became symmetric at equilibrium. The author and co-worker [C5] used numerical experiments to show that this also occurred for the co-rotational beam elements [C1.16, C3, C5] using the theory of Section 17.1. More recently, detailed numerical studies have shown that it is more correct to say that this symmetry is 'almost achieved' at equilibrium. This finding fits in with the theoretical arguments that will be given in Section 17.4.3.

* However, it is worth noting that the co-rotational three-dimensional continuum formultion of Section 18.3 (without rotational variables) also leads to a non-symmetric stiffness matrix although symmetry is recovered at equilibrium.

17.4.1 A simple model showing symmetry and non-symmetry

Suppose that a potential, φ, depends on a unit position vector, $\mathbf{r}$, that is a function of $\boldsymbol{\theta}$ and is free to rotate so that:

$$\varphi = \varphi(\mathbf{r}(\boldsymbol{\theta})) \tag{17.162}$$

From (16.97b), we can write:

$$\delta\mathbf{r} = \delta\bar{\boldsymbol{\theta}} \times \mathbf{r} = \mathbf{S}(\delta\bar{\boldsymbol{\theta}})\mathbf{r} = -\mathbf{S}(\mathbf{r})\delta\bar{\boldsymbol{\theta}} \tag{17.163}$$

where $\delta\bar{\boldsymbol{\theta}}$ is the (non-additive) 'spin vector'.

From (17.162) and (17.163):

$$\delta\varphi = \frac{\partial\varphi^{\mathrm{T}}}{\partial\mathbf{r}}\delta\mathbf{r} = -\frac{\partial\varphi^{\mathrm{T}}}{\partial\mathbf{r}}\mathbf{S}(\mathbf{r})\delta\bar{\boldsymbol{\theta}} = \delta\bar{\boldsymbol{\theta}}^{\mathrm{T}}\left(\mathbf{S}(\mathbf{r})\frac{\partial\varphi}{\partial\mathbf{r}}\right) = \delta\bar{\boldsymbol{\theta}}^{\mathrm{T}}\left(\mathbf{r} \times \frac{\partial\varphi}{\partial\mathbf{r}}\right) = \delta\bar{\boldsymbol{\theta}}^{\mathrm{T}}\bar{\mathbf{g}} \tag{17.164}$$

so that for equilibrium:

$$\bar{\mathbf{g}} = \mathbf{r} \times \frac{\partial\varphi}{\partial\mathbf{r}} = \mathbf{0} \tag{17.165}$$

The latter could also be obtained using virtual work.

To obtain the tangent stiffness matrix, we have:

$$\begin{aligned}\delta^2\varphi = \delta\bar{\boldsymbol{\theta}}^{\mathrm{T}}\delta\bar{\mathbf{g}} &= \delta\bar{\boldsymbol{\theta}}^{\mathrm{T}}\bar{\mathbf{K}}_{\mathrm{t}}\delta\bar{\boldsymbol{\theta}} = \delta\bar{\boldsymbol{\theta}}^{\mathrm{T}}(\bar{\mathbf{K}}_{\mathrm{t}1} + \bar{\mathbf{K}}_{\mathrm{t}2})\delta\bar{\boldsymbol{\theta}} \\ &= \delta\bar{\boldsymbol{\theta}}^{\mathrm{T}}\left(\delta\mathbf{r} \times \frac{\partial\varphi}{\partial\mathbf{r}} + \mathbf{r} \times \frac{\partial^2\varphi}{\partial\mathbf{r}\,\partial\mathbf{r}}\delta\mathbf{r}\right)\end{aligned} \tag{17.166}$$

where use has been made of (17.165). With the aid of (17.163), the second term in the last expression in (17.166) is

$$\bar{\mathbf{K}}_{\mathrm{t}2}\delta\bar{\boldsymbol{\theta}} = -\mathbf{S}(\mathbf{r})\frac{\partial^2\varphi}{\partial\mathbf{r}\partial\mathbf{r}}\mathbf{S}(\mathbf{r})^{\mathrm{T}}\delta\bar{\boldsymbol{\theta}} \tag{17.167}$$

where $\bar{\mathbf{K}}_{\mathrm{t}2}$ is symmetric. The first term gives:

$$\bar{\mathbf{K}}_{\mathrm{t}1}\delta\bar{\boldsymbol{\theta}} = (\delta\bar{\boldsymbol{\theta}} \times \mathbf{r}) \times \frac{\partial\varphi}{\partial\mathbf{r}} = -\frac{\partial\varphi}{\partial\mathbf{r}} \times (\delta\bar{\boldsymbol{\theta}} \times \mathbf{r}) \tag{17.168a}$$

Using (17.157), (17.168a) can be re-expressed as

$$\bar{\mathbf{K}}_{\mathrm{t}1}\delta\bar{\boldsymbol{\theta}} = \left[-\left(\frac{\partial\varphi^{\mathrm{T}}}{\partial\mathbf{r}}\mathbf{r}\right)\mathbf{I} + \mathbf{r}\frac{\partial\varphi^{\mathrm{T}}}{\partial\mathbf{r}}\right]\delta\bar{\boldsymbol{\theta}} \tag{17.168b}$$

where the second term in (17.168b) is non-symmetric.

However, at equilibrium, from (17.165), it follows that $\mathbf{r}$ and $\partial\varphi/\partial\mathbf{r}$ will be co-linear so that this term will become symmetric. It will be shown in Section 17.4.3 that, in contrast to this simple 'model', for a finite element formulation, the result is less clear.

17.4.2 Using additive rotation components

For the elements of Sections 17.1–17.3, we have adopted 'spin variables' whereby given $\mathbf{r}_n = \mathbf{R}(\boldsymbol{\theta}_0)\mathbf{r}_0$, the finite element variables are $\Delta\bar{\boldsymbol{\theta}}$ (not additive to $\boldsymbol{\theta}$) for which, using the notation of Section 16.11 (see (16.81a)):

$$\mathbf{r}_{nn} = \mathbf{R}(\Delta\bar{\boldsymbol{\theta}})\mathbf{R}(\boldsymbol{\theta}_0)\mathbf{r}_0 = \exp(\mathbf{S}(\Delta\bar{\boldsymbol{\theta}}))\mathbf{R}(\boldsymbol{\theta}_0)\mathbf{r}_0 = \mathbf{R}(\theta)\mathbf{r}_0 \tag{17.169}$$

with $\boldsymbol{\theta} \neq \boldsymbol{\theta}_0 + \Delta\bar{\boldsymbol{\theta}}$ and

$$\delta\mathbf{r} = \delta\bar{\boldsymbol{\theta}} \times \mathbf{r} = \mathbf{S}(\delta\bar{\boldsymbol{\theta}})\mathbf{r} \tag{17.170}$$

An alternative procedure would involve always working with the total relationship:

$$\mathbf{r}_n = \mathbf{R}(\boldsymbol{\theta}_0)\mathbf{r}_0; \qquad \mathbf{r}_{nn} = \mathbf{R}(\boldsymbol{\theta}_n)\mathbf{r}_0 = \mathbf{R}(\boldsymbol{\theta}_0 + \Delta\boldsymbol{\theta})\mathbf{r}_0 \tag{17.171}$$

where the finite element variables would be $\Delta\boldsymbol{\theta}$ which can be added to $\boldsymbol{\theta}_0$. In these circumstances, we must apply:

$$\delta\mathbf{r} = \delta\mathbf{R}(\delta\boldsymbol{\theta})\mathbf{R}^{\mathrm{T}}\mathbf{r} = \mathbf{S}(\delta\bar{\boldsymbol{\theta}})\mathbf{r} \tag{17.172}$$

where $\delta\mathbf{R}$ is the variation of the Rodrigues formula (see (16.101)) and the relationship between the spin, $\delta\boldsymbol{\theta}$, and the additive $\delta\boldsymbol{\theta}$ is given in (16.89). Such an approach has been adopted by Parisch [P1] for shells and (apart from approximations induced by the interpolation) should lead to a symmetric stiffness matrix.

We will now investigate a procedure whereby we introduce transformations between the non-additive $\delta\bar{\boldsymbol{\theta}}$ (spin) variables and the additive $\delta\boldsymbol{\theta}$ variables. From (16.89) we can relate the former to the latter via:

$$\delta\bar{\boldsymbol{\theta}} = \mathbf{H}(\boldsymbol{\theta})\delta\boldsymbol{\theta} \tag{17.173}$$

where (see (16.90)):

$$\mathbf{H}(\boldsymbol{\theta}) = \frac{\sin\theta}{\theta}\mathbf{I} + \left(1 - \frac{\sin\theta}{\theta}\right)\frac{\boldsymbol{\theta}\boldsymbol{\theta}^{\mathrm{T}}}{\theta^2} + \frac{1}{2}\left(\frac{\sin(\theta/2)}{(\theta/2)}\right)^2 \mathbf{S}(\boldsymbol{\theta}) \tag{17.174}$$

Applying (17.173) to (17.164) gives:

$$\delta\varphi = \delta\boldsymbol{\theta}^{\mathrm{T}}\mathbf{H}(\boldsymbol{\theta})^{\mathrm{T}}\bar{\mathbf{g}} = \delta\boldsymbol{\theta}^{\mathrm{T}}\mathbf{g} = 0 \tag{17.175}$$

so that with these modified variables, the equilibrium equations are

$$\mathbf{g} = \mathbf{H}(\boldsymbol{\theta})^{\mathrm{T}}\bar{\mathbf{g}} = \mathbf{0} \tag{17.176}$$

with $\bar{\mathbf{g}}$ as in (17.165). It follows that:

$$\begin{aligned}\delta\mathbf{g} = \mathbf{K}_{\mathrm{t}}\delta\boldsymbol{\theta} &= \mathbf{H}(\boldsymbol{\theta})^{\mathrm{T}}\delta\bar{\mathbf{g}} + \delta\mathbf{H}(\boldsymbol{\theta})^{\mathrm{T}}\bar{\mathbf{g}} = \mathbf{H}(\boldsymbol{\theta})^{\mathrm{T}}\bar{\mathbf{K}}_{\mathrm{t}}\delta\bar{\boldsymbol{\theta}} + \delta\mathbf{H}(\boldsymbol{\theta})^{\mathrm{T}}\bar{\mathbf{g}} \\ &= \mathbf{H}(\boldsymbol{\theta})^{\mathrm{T}}\bar{\mathbf{K}}_{\mathrm{t}}\mathbf{H}(\boldsymbol{\theta})\delta\boldsymbol{\theta} + \delta\mathbf{H}(\boldsymbol{\theta})^{\mathrm{T}}\bar{\mathbf{g}}\end{aligned} \tag{17.177}$$

The term $\delta\mathbf{H}(\boldsymbol{\theta})$ involves a complicated expression that is given in (16.95). Subsequent developments are considerably simplified by setting $\boldsymbol{\theta} = \mathbf{0}$. (It will be shown later in Section 17.4.4 how this can be applied.) In these circumstances, from (16.96):

$$\delta\mathbf{H}(\boldsymbol{\theta})_{\boldsymbol{\theta}=\mathbf{0}} = \tfrac{1}{2}\mathbf{S}(\delta\boldsymbol{\theta}) \tag{17.178}$$

while, from (17.174):

$$\mathbf{H}(\boldsymbol{\theta})_{\boldsymbol{\theta}=\mathbf{0}} = \mathbf{I} \tag{17.179}$$

Substitution from (17.178) and (17.179) into (17.177) leads to:

$$\mathbf{K}_t \delta\boldsymbol{\theta} = \bar{\mathbf{K}}_t \delta\boldsymbol{\theta} + \mathbf{K}_{tex} \delta\boldsymbol{\theta} = \bar{\mathbf{K}}_t \delta\boldsymbol{\theta} - \tfrac{1}{2}\mathbf{S}(\delta\boldsymbol{\theta})\bar{\mathbf{g}} = [\bar{\mathbf{K}}_t + \tfrac{1}{2}\mathbf{S}(\bar{\mathbf{g}})]\delta\boldsymbol{\theta} \tag{17.180}$$

with $\bar{\mathbf{g}}$ from (17.165). It follows that:

$$\mathbf{K}_{tex}\delta\boldsymbol{\theta} = \tfrac{1}{2}\mathbf{S}(\bar{\mathbf{g}})\delta\boldsymbol{\theta} = -\tfrac{1}{2}\delta\boldsymbol{\theta} \times \left(\mathbf{r} \times \frac{\partial \varphi}{\partial \mathbf{r}}\right) \tag{17.181a}$$

and using (17.157):

$$\mathbf{K}_{tex}\delta\boldsymbol{\theta} = -\tfrac{1}{2}\mathbf{r}\frac{\partial \varphi^{\mathrm{T}}}{\partial \mathbf{r}}\delta\boldsymbol{\theta} + \frac{1}{2}\frac{\partial \varphi}{\partial \mathbf{r}}\mathbf{r}^{\mathrm{T}}\delta\boldsymbol{\theta} \tag{17.181b}$$

From (17.180), $\mathbf{K}_t$ is obtained by adding $\mathbf{K}_{tex}$ from (17.181b) to $\bar{\mathbf{K}}_t$ in (17.166). The latter is the sum of $\bar{\mathbf{K}}_{t1}$ from (17.168b) and $\bar{\mathbf{K}}_{t2}$ from (17.167). The addition process leads to

$$\mathbf{K}_t = -\mathbf{S}(\mathbf{r})\frac{\partial^2 \varphi}{\partial \mathbf{r}\partial \mathbf{r}}\mathbf{S}(\mathbf{r})^{\mathrm{T}} + \frac{1}{2}\mathbf{r}\frac{\partial \varphi^{\mathrm{T}}}{\partial \mathbf{r}} + \frac{1}{2}\frac{\partial \varphi}{\partial \mathbf{r}}\mathbf{r}^{\mathrm{T}} - \frac{\partial \varphi^{\mathrm{T}}}{\partial \mathbf{r}}\mathbf{r}\,\mathbf{I} = \frac{\bar{\mathbf{K}}_t + \bar{\mathbf{K}}_t^{\mathrm{T}}}{2} \tag{17.182}$$

Consequently, the stiffness matrix is symmetric and corresponds exactly with the artificially symmetrised $\bar{\mathbf{K}}_t$ which was obtained using 'spin variables'. In Section 17.4.4, a similar procedure will be applied to a finite element formulation.

17.4.3 CONSIDERING SYMMETRY AT EQUILIBRIUM FOR THE ELEMENT OF SECTION 17.2

While, in Section 17.4.1, we indicated that a 'spin-based' formulation would become symmetric at equilibrium, the arguments were applied to a simple model that does not account for all the features of a finite element formulation. In order to consider the latter, we must consider the contributions to a single node from two adjacent element (Figure 17.3). We will also concentrate on the rotation terms since the non-symmetry lies in the 3×3 submatrices associated with these terms.

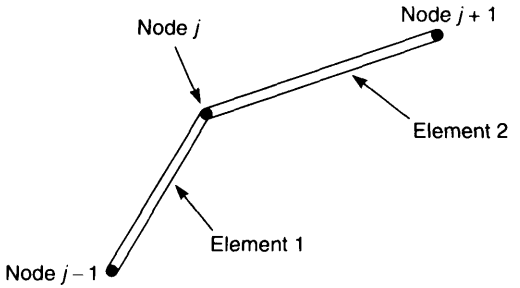

Figure 17.3 Two elements meeting at a common node.

We will concentrate here on the element of Simo and Vu-Quoc [S3.16] which was considered in Section 17.2 and, in particular, on the linear version, which uses reduced integration, of Sections 17.2.1–17.2.5. Using the expression for $\mathbf{q}_i$ in (17.79), we can write down the equilibrium equations corresponding to the rotation variables at the centre node in Figure 17.3 as

$$\mathbf{g} = \mathbf{q}_i = -\tfrac{1}{2}\mathbf{S}(\mathbf{x}^1_{2\,1})\mathbf{n}^1 + \mathbf{m}^1 - \tfrac{1}{2}\mathbf{S}(\mathbf{x}^2_{2\,1})\mathbf{n}^2 - \mathbf{m}^2 = \mathbf{0} \tag{17.183}$$

In (17.183), the superscripts relate to the element number. Also, it has been assumed that there are no applied external moments at the common node (The issue of applied external moments will be considered in Section 17.5.2.)

Using (17.90) and (17.91), the submatrices that contribute to the non-symmetric stiffness matrix associated with this variable are

$$\begin{aligned}\mathbf{K}_{\text{tns}}(j,j) &= \tfrac{1}{2}[\mathbf{Z}^1 - \mathbf{S}(\mathbf{m}^1) + \mathbf{Z}^2 + \mathbf{S}(\mathbf{m}^2)] \\ &= \tfrac{1}{2}[\tfrac{1}{4}\mathbf{S}(\mathbf{x}^1_{2\,1} \times \mathbf{n}^1) + \tfrac{1}{4}\mathbf{S}(\mathbf{x}^2_{2\,1} \times \mathbf{n}^2) + \mathbf{S}(\mathbf{m}^2) - \mathbf{S}(\mathbf{m}^1)]\end{aligned} \tag{17.184a}$$

and

$$\mathbf{K}_{\text{tns}}(j,j+1) = \tfrac{1}{2}[\mathbf{Z}^2] = \tfrac{1}{8}\mathbf{S}(\mathbf{x}^2_{2\,1} \times \mathbf{n}^2) \tag{17.184b}$$

and

$$\mathbf{K}_{\text{tns}}(j,j-1) = \tfrac{1}{2}[\mathbf{Z}^1] = \tfrac{1}{8}\mathbf{S}(\mathbf{x}^1_{2\,1} \times \mathbf{n}^1) \tag{17.184c}$$

It will be noted that the equilibrium equation of (17.183) cannot be used to demonstrate the vanishing of these submatrices. Indeed it can be inferred that non-diagonal contributions (as in (17.184b) and (17.184c)) can never be made to vanish as a result of the achievement of symmetry. This argument applies to any element and is valid because both the residual force (which we seek to vanish) and the stiffness are assembled in the same way only for those contributions belonging to the same node' [R3]. Interestingly, however, from (17.183)–(17.184), at equilibrium we have:

$$\mathbf{K}_{\text{tns}}(j,j-1) + \mathbf{K}_{\text{tns}}(j,j) + \mathbf{K}_{\text{tns}}(j,j+1) = \mathbf{0} \tag{17.185}$$

None the less, numerical experiments have indicated that the individual non-symmetric contributions do almost vanish at equilibrium.

Consider an off-diagonal block such as $\mathbf{K}_{\text{tns}}(j,j-1)$ in (17.184c). This term will vanish as $\mathbf{x}^1_{2\,1}$ becomes coaxial with $\mathbf{n}^1$. From (17.78):

$$\mathbf{n} = \mathbf{N}_1\mathbf{t}_1 + \mathbf{N}_2\mathbf{t}_2 + \mathbf{N}_3\mathbf{t}_3 \tag{17.186}$$

where $\mathbf{N}_1$ is the local axial force and $\mathbf{N}_2$ and $\mathbf{N}_3$ are the local shear forces. In general, at equilibrium, the shear forces will be small in comparison with the axial forces so that $\mathbf{n} \simeq \mathbf{N}_1\mathbf{t}_1$ and because $\mathbf{t}_1 \simeq k\mathbf{x}'_{2\,1}$, coaxiality of $\mathbf{x}'_{2\,1}$ and $\mathbf{n}$ will be nearly achieved at equilibrium and hence $\mathbf{K}_{\text{tns}}(j,j-1)$ and $\mathbf{K}_{\text{tns}}(j,j+1)$ will nearly vanish at equilibrium. If they do, from (17.183) and (17.184a), the diagonal block $\mathbf{K}_{\text{tns}}(j,j)$ will also vanish. The latter will also occur if the $\mathbf{n}$ terms in (17.183) and (17.184) are small in comparison with the $\mathbf{m}$ terms.

While the discussions have been related to the linear version of the element, with reduced integration, similar arguments can be related to the general isoparametric form (Section 17.2.6), although the algebra is a little more complex and integration

by parts is required. It would seem that Simo and Vu-Quoc's argument [S3.16] for symmetry at equilibrium was based on the equations prior to discretisation.

It should perhaps be re-emphasised that these discussions are somewhat academic because, in practice, the excellent quadratic performance of the element is maintained when the tangent stiffness matrix is symmetrised (with conservative loadings). A more theoretical justification will now be given (see also [N1]).

17.4.4 Using additive (in the limit) rotation components with the element of Section 17.2

We will now apply the method of Section 17.4.2 to the element of Section 17.2. In the first instance we will attempt a naive approach in which we merely change the rotation changes from barred spin variables to non-barred additive (in the limit) variables without considering the associated interpolations. Using the transformation of (17.173), we can rewrite the internal virtual work for a rotation component as:

$$V_i = \delta\bar{\boldsymbol{\theta}}_v^T \bar{\mathbf{q}}_i = \delta\boldsymbol{\theta}^T \mathbf{H}(\boldsymbol{\theta})^T \bar{\mathbf{q}}_i = \delta\boldsymbol{\theta}^T \mathbf{q}_i \tag{17.187}$$

so that:

$$\mathbf{q}_i = \mathbf{H}(\boldsymbol{\theta})^T \bar{\mathbf{q}}_i \tag{17.188}$$

and the barred terms would be those previously derived (although without bars) in Section 17.2. Equation (17.188) is the equivalent of (17.176).

The variation of (17.188) now leads to

$$\delta\mathbf{q}_i = \mathbf{H}(\boldsymbol{\theta})^T \delta\bar{\mathbf{q}} + \delta\mathbf{H}(\boldsymbol{\theta})^T \bar{\mathbf{q}}_i = \mathbf{K}_t \delta\boldsymbol{\theta} \tag{17.189}$$

where with spin variables, we would have obtained:

$$\delta\bar{\mathbf{q}}_i = \bar{\mathbf{K}}_t \delta\bar{\boldsymbol{\theta}} \tag{17.190}$$

Assuming $\boldsymbol{\theta} = \mathbf{0}$ and using (16.96), we now obtain as a parallel with (17.177), the relationship.

$$\delta\mathbf{q}_i = \mathbf{K}_t \delta\boldsymbol{\theta} = [\bar{\mathbf{K}}_t + \mathbf{K}_{tex}]\delta\boldsymbol{\theta} = [\bar{\mathbf{K}}_t + \tfrac{1}{2}\mathbf{S}(\bar{\mathbf{q}}_i)]\delta\boldsymbol{\theta} \tag{17.191}$$

In Section 17.2, we used the symbols $\delta\boldsymbol{\alpha}$ and $\delta\boldsymbol{\beta}$ for the rotation changes at the two nodes. The latter should now be considered as barred and the equivalents of (17.173) would be

$$\delta\bar{\boldsymbol{\alpha}} = \mathbf{H}(\boldsymbol{\alpha})\delta\boldsymbol{\alpha}; \qquad \delta\bar{\boldsymbol{\beta}} = \mathbf{H}(\boldsymbol{\beta})\delta\boldsymbol{\beta} \tag{17.192}$$

Hence after adopting (17.191), the 'extra' stiffness contribution is given by

$$\mathbf{K}_{tex} = \begin{bmatrix} 0 & 0 & 0 & 0 \\ 0 & \mathbf{K}_{22} & 0 & 0 \\ 0 & 0 & 0 & 0 \\ 0 & 0 & 0 & \mathbf{K}_{44} \end{bmatrix} \tag{17.193}$$

where

$$\mathbf{K}_{22} = \tfrac{1}{2}\mathbf{S}(\bar{\mathbf{q}}_\alpha); \qquad \mathbf{K}_{44} = \tfrac{1}{2}\mathbf{S}(\bar{\mathbf{q}}_\beta) \tag{17.194}$$

From (17.74) and (17.79),

$$\bar{\mathbf{q}}_\alpha = -\tfrac{1}{2}\mathbf{x}'_{2\,1} \times \mathbf{n} - \mathbf{m}; \qquad \bar{\mathbf{q}}_\beta = -\tfrac{1}{2}\mathbf{x}'_{2\,1} \times \mathbf{n} + \mathbf{m} \tag{17.195}$$

Using (16.100) whereby $\mathbf{S}(\mathbf{a} \times \mathbf{b}) = \mathbf{b}\mathbf{a}^{\mathrm{T}} - \mathbf{a}\mathbf{b}^{\mathrm{T}}$, it follows from (17.194) that:

$$\mathbf{K}_{2\,2} = \tfrac{1}{2}\mathbf{S}(\mathbf{m}) - \tfrac{1}{4}\mathbf{n}\mathbf{x}'^{\mathrm{T}}_{2\,1} + \tfrac{1}{4}\mathbf{x}'_{2\,1}\mathbf{n}^{\mathrm{T}} \tag{17.196}$$

$$\mathbf{K}_{4\,4} = -\tfrac{1}{2}\mathbf{S}(\mathbf{m}) - \tfrac{1}{4}\mathbf{n}\mathbf{x}'^{\mathrm{T}}_{2\,1} + \tfrac{1}{4}\mathbf{x}'_{2\,1}\mathbf{n}^{\mathrm{T}} \tag{17.197}$$

With our assumption that $\boldsymbol{\theta} = \mathbf{0}$ and $\mathbf{H}(\boldsymbol{\theta}) = \mathbf{I}$ (see (17.174) and (17.179), to obtain the new tangent stiffness matrix, from (17.191) and (17.193), we simply add $\mathbf{K}_{\mathrm{tex}}$ from (17.193) to the $\mathbf{K}_{\mathrm{t}}$ in (17.89) (with the latter now considered as barred). Although this process removes the non-symmetric $\mathbf{S}(\mathbf{m})$ terms in (17.90), it does not remove the non-symmetric $\mathbf{Z}$ terms in the same equation.

The reason relates to the averaging process involved in (17.64) whereby:

$$\delta\boldsymbol{\alpha}_{\mathrm{c}} = \tfrac{1}{2}(\delta\boldsymbol{\alpha} + \delta\boldsymbol{\beta}) \tag{17.198}$$

with $\delta\boldsymbol{\alpha}_{\mathrm{c}}$ as the rotation change at the central 'Gauss point'. In relation to an isoparametric formulation (Section 17.2.6) the latter equation involves the interpolation of (17.93).

In order to obtain a fully symmetric matrix we must be more rigorous and rewrite (17.71) as

$$\delta\boldsymbol{\chi}_l = \frac{\mathbf{T}^{\mathrm{T}}}{l_{\mathrm{o}}}(\delta\bar{\boldsymbol{\beta}} - \delta\bar{\boldsymbol{\alpha}}) = \frac{\mathbf{T}^{\mathrm{T}}}{l_{\mathrm{o}}}(\mathbf{H}(\boldsymbol{\beta})^{\mathrm{T}}\delta\boldsymbol{\beta} - \mathbf{H}(\boldsymbol{\alpha})^{\mathrm{T}}\delta\boldsymbol{\alpha}) \tag{17.199}$$

and (17.68) combined with (17.70) as

$$\begin{aligned}\delta\boldsymbol{\varepsilon}_l &= \frac{1}{l_{\mathrm{o}}}\left(\mathbf{T}^{\mathrm{T}}\delta\mathbf{d}_{2\,1} + \mathbf{T}^{\mathrm{T}}\mathbf{S}(\mathbf{x}'_{2\,1})\frac{\delta\bar{\boldsymbol{\alpha}} + \delta\bar{\boldsymbol{\beta}}}{2}\right) \\ &= \frac{1}{l_{\mathrm{o}}}\left(\mathbf{T}^{\mathrm{T}}\delta\mathbf{x}_{2\,1} + \mathbf{T}^{\mathrm{T}}\mathbf{S}(\mathbf{x}'_{2\,1})\mathbf{H}(\boldsymbol{\alpha}_{\mathrm{c}})\frac{\delta\boldsymbol{\alpha} + \delta\boldsymbol{\beta}}{2}\right)\end{aligned} \tag{17.200}$$

The virtual work can now be written (see also (17.75)) as

$$\mathbf{q}^{\mathrm{T}}_{\mathrm{d}\,1}\delta\mathbf{d}_1 + \mathbf{q}^{\mathrm{T}}_{\mathrm{d}\,2}\delta\mathbf{d}_2 + \mathbf{q}^{\mathrm{T}}_{\alpha}\delta\boldsymbol{\alpha} + \mathbf{q}^{\mathrm{T}}_{\beta}\delta\boldsymbol{\beta} = l_{\mathrm{o}}\mathbf{M}^{\mathrm{T}}\delta\boldsymbol{\chi}_1 + l_{\mathrm{o}}\mathbf{N}^{\mathrm{T}}\delta\boldsymbol{\varepsilon} \tag{17.201}$$

where, to avoid cluttering we have omitted the subscript v for virtual. The combination of (17.199)–(17.201) leads to

$$\mathbf{q}_\alpha = -\mathbf{H}(\boldsymbol{\alpha})^{\mathrm{T}}\mathbf{T}\mathbf{M} - \mathbf{H}(\boldsymbol{\alpha}_{\mathrm{c}})^{\mathrm{T}}\frac{\mathbf{S}(\mathbf{x}'_{2\,1})}{2}\mathbf{T}\mathbf{N} = -\mathbf{H}(\boldsymbol{\alpha})^{\mathrm{T}}\mathbf{m} - \mathbf{H}(\boldsymbol{\alpha}_{\mathrm{c}})^{\mathrm{T}}\frac{\mathbf{S}(\mathbf{x}'_{2\,1})}{2}\mathbf{n} \tag{17.202a}$$

$$\mathbf{q}_\beta = \mathbf{H}(\boldsymbol{\beta})^{\mathrm{T}}\mathbf{T}\mathbf{M} - \mathbf{H}(\boldsymbol{\alpha}_{\mathrm{c}})^{\mathrm{T}}\frac{\mathbf{S}(\mathbf{x}'_{2\,1})}{2}\mathbf{T}\mathbf{N} = \mathbf{H}(\boldsymbol{\beta})^{\mathrm{T}}\mathbf{m} - \mathbf{H}(\boldsymbol{\alpha}_{\mathrm{c}})^{\mathrm{T}}\frac{\mathbf{S}(\mathbf{x}'_{2\,1})}{2}\mathbf{n} \tag{17.202b}$$

In relation to the variations of (17.202), we require the equivalent of (17.82) with 'additive variables' for which:

$$\delta\mathbf{T}\mathbf{N} = -\mathbf{S}(\mathbf{n})\delta\boldsymbol{\alpha}_{\mathrm{c}} = -\mathbf{S}(\mathbf{n})\mathbf{H}(\boldsymbol{\alpha}_{\mathrm{c}})\left(\frac{\delta\boldsymbol{\alpha} + \delta\boldsymbol{\beta}}{2}\right) \tag{17.203}$$

with a similar expression for $\delta\mathbf{T}\mathbf{M}$. Using (17.76), (17.78), (17.86), (17.199), (17.200) and

(17.203), equation (17.202a) can be differentiated to give (see also (17.86) and (17.88)):

$$\delta\mathbf{q}_a = \frac{1}{l_o}\mathbf{H}(\boldsymbol{\alpha})^T\mathbf{T}\mathbf{C}_b\mathbf{T}^T\mathbf{H}(\boldsymbol{\alpha})\delta\boldsymbol{\alpha} - \frac{1}{l_o}\mathbf{H}(\boldsymbol{\alpha})^T\mathbf{T}\mathbf{C}_b\mathbf{T}^T\mathbf{H}(\boldsymbol{\beta})\delta\boldsymbol{\beta}$$
$$+ \tfrac{1}{2}\mathbf{H}(\boldsymbol{\alpha})^T\mathbf{S}(\mathbf{m})\mathbf{H}(\boldsymbol{\alpha}_c)\delta\boldsymbol{\alpha} + \tfrac{1}{2}\mathbf{H}(\boldsymbol{\alpha})^T\mathbf{S}(\mathbf{m})\mathbf{H}(\boldsymbol{\alpha}_c)\delta\boldsymbol{\beta} + \tfrac{1}{2}\mathbf{H}(\boldsymbol{\alpha}_c)^T\mathbf{S}(\mathbf{n})\delta\mathbf{d}_{21}$$
$$+ \tfrac{1}{2}\mathbf{H}(\boldsymbol{\alpha}_c)^T\frac{\mathbf{Y}}{2}\mathbf{H}(\boldsymbol{\alpha}_c)\delta\boldsymbol{\alpha} + \tfrac{1}{2}\mathbf{H}(\boldsymbol{\alpha}_c)^T\frac{\mathbf{Y}}{2}\mathbf{H}(\boldsymbol{\alpha}_c)\delta\boldsymbol{\beta} + \text{'extra'} \tag{17.204}$$

where the 'extra' terms come from the variations of $\mathbf{H}(\boldsymbol{\alpha})$ and $\mathbf{H}(\boldsymbol{\alpha}_c)$ in (17.202a) so that:

$$\text{'extra'} = -\delta\mathbf{H}(\boldsymbol{\alpha})^T\mathbf{m} - \tfrac{1}{2}\delta\mathbf{H}(\boldsymbol{\alpha}_c)^T(\mathbf{x}'_{21}) \times \mathbf{n}) \tag{17.205}$$

If we now set $\boldsymbol{\alpha} = \boldsymbol{\beta} = \mathbf{0}$ so that $\boldsymbol{\alpha}_c = \mathbf{0}$ and

$$\mathbf{H}(\boldsymbol{\alpha}) = \mathbf{H}(\boldsymbol{\beta}) = \mathbf{H}(\boldsymbol{\alpha}_c) = \mathbf{I} \tag{17.206}$$

the terms in (17.204) are found to coincide with those in (17.89) while, from (16.96) and (16.100), equation (17.205) can be re–expressed as

$$\text{'extra'} = -\tfrac{1}{2}\mathbf{S}(\mathbf{m})\delta\boldsymbol{\alpha} - \tfrac{1}{8}\mathbf{S}(\mathbf{x}'_{21} \times \mathbf{n})(\delta\boldsymbol{\alpha} + \delta\boldsymbol{\beta})$$
$$= \left[-\frac{\mathbf{S}(\mathbf{m})}{2} - \tfrac{1}{8}\mathbf{n}\mathbf{x}'^T_{21} + \tfrac{1}{8}\mathbf{x}'_{21}\mathbf{n}^T\right]\delta\boldsymbol{\alpha} + [-\tfrac{1}{8}\mathbf{n}\mathbf{x}'^T_{21} + \tfrac{1}{8}\mathbf{x}'_{21}\mathbf{n}^T]\delta\boldsymbol{\beta} \tag{17.207}$$

Combining (17.204) with (17.207), leads to the symmetric tangent stiffness matrix that would result from 'artificially symmetrising' the original non-symmetric matrix of (17.89) so that the non-symmetric matrix in (17.90) vanishes. This conclusion coincides with that of Simo [S3] who obtained the result by following a rather different route.

Having set $\boldsymbol{\alpha} = \boldsymbol{\beta} = \boldsymbol{\alpha}_c = 0$, from (17.206) and (17.192), there is no difference between $\Delta\boldsymbol{\alpha}$ and $\Delta\bar{\boldsymbol{\alpha}}$ and, provided that actual update on the mid-point triad is performed using (17.65), the former process will not effect the earlier formulation. Hence, we can simply use the procedure of symmetrising the previous non-symmetric stiffness matrix obtained via spin variables, although now we have some theoretical justification.

While the previous developments have related to the beam element of Simo and Vu-Quoc for which an interpretation was given in Section 17.2, it is believed that a similar justification for the symmetrising process could be applied to the corotational elements of Sections 17.1 (although the algebra would be more tedious). A similar process could also probably be applied to the derivation in Section 17.3 of an isoparametric Timoshenko beam element. In the latter case, certain aspects would be simpler because, as indicated in Section 17.3.1, for this element all the non-symmetry is confined to the 3×3 block diagonals associated with the rotation terms.

Cardona and Geradin [C1] have used similar arguments to develop symmetric formulations that, with respect to rotations, can be considered as total lagrangian or updated Lagrangian with the latter working with increments from the last converged equilibrium state. Buechter and Ramm [B5] appear to propose a method that is closer to the present, with $\boldsymbol{\theta}$ being set to zero at the start of the current iteration in order to generate a relatively simple symmetric tangent stiffness matrix. The issue of symmetry in relation to co-rotational beam elements has been discussed by Krenk [K3].

17.5 VARIOUS FORM OF APPLIED LOADING INCLUDING 'FOLLOWER LOADS'

The loading on three-dimensional beams can either be related to fixed global axes or can be related to local 'follower axes'. In some cases, these loadings lead to a conservative system with a symmetric tangent stiffness matrix; in other cases, the loading is 'non-conservative' and the tangent stiffness matrix will be non-symmetric [A4, H1, S1]. In some cases, we obtain an 'extra' contribution to the tangent stiffness matrix.

With conventional 'load control', the corrector phase of the Newton–Raphson process, can be derived via a truncated Taylor series of the form:

$$\mathbf{g}_n = \mathbf{q}_{in} - \mathbf{q}_{en} = \mathbf{g}_o + \frac{\partial \mathbf{g}}{\partial \mathbf{p}}\delta\mathbf{p} = \{\mathbf{q}_{io} - \mathbf{q}_{eo}\} + \left\{\frac{\partial \mathbf{q}_{io}}{\partial \mathbf{p}} - \frac{\partial \mathbf{q}_{eo}}{\partial \mathbf{p}}\right\}\delta\mathbf{p} = \mathbf{0} \tag{17.208}$$

Normally, with the load level fixed (the process is a little different with the arc-length methods, but can very easily be adapted), there is no contribution to the term $\partial \mathbf{q}_{eo}/\partial \mathbf{p}$. However, with certain types of loading, particularly those that depend on the current configuration of the structure, we do have such a contribution so that, dropping the subscript o for 'old', equation (17.208) becomes:

$$\mathbf{g} = \mathbf{q}_i - \mathbf{q}_e = \{\mathbf{K}_{t1} + \mathbf{K}_{t\sigma}(\mathbf{q}_i) - \mathbf{K}_{t\sigma}(\mathbf{q}_e)\}\delta\mathbf{p} \tag{17.209}$$

Loadings on beams can take the form of point loads or distributed loads. In the former case the loads can be 'distributed' to the nodes in the conventional manner (strictly via the shape functions). We will therefore start by considering various forms of point loading—initially via conventional forces (Section 17.5.1) and later via moments (Section 17.5.2).

17.5.1 Point loads applied at a node

Clearly if the point load is applied in a fixed global direction, then conventional procedures apply. Consequently, we will concentrate on various forms of follower load.

In relation to Figure 17.1, suppose that we have a load P that is to be applied at node 1 in one of the directions $\mathbf{t}_i$ ($i = 1, 3$), where $\mathbf{t}_i$ define the direction of the (moving) nodal triad. The external virtual work is then given by

$$\mathbf{V}_e = P(\delta\mathbf{d}_{1v}^{\mathrm{T}}\mathbf{t}_i) = \mathbf{q}_e^{\mathrm{T}}\delta\mathbf{d}_{1v} \tag{17.210}$$

so that the external force corresponding to the translational degrees of freedom at the node would be given by

$$\mathbf{q}_e = P\mathbf{t}_i \tag{17.211}$$

To obtain the associated stiffness relationships, with P fixed, the variation of (17.211) is given by

$$\delta\mathbf{q}_e = P\,\delta\mathbf{t}_i = -P\mathbf{S}(\mathbf{t}_i)\delta\boldsymbol{\alpha} = \mathbf{K}_{t\sigma}(\mathbf{q}_e)\delta\mathbf{p} \tag{17.212}$$

where use has been made of (17.20). It follows that we obtain a contribution to the stiffness matrix $\mathbf{K}_{t\sigma}(\mathbf{q}_e)$ in the $\mathbf{K}_{12}$ position of (17.44) of $-P\mathbf{S}(\mathbf{t}_i)$. The tangent stiffness matrix is non-symmetric and the loading is non-conservative.

As an alternative, follower loads might be applied in the direction of the unit vectors of the 'element frame', $\mathbf{e}_1$–$\mathbf{e}_3$ (Figure 17.1). The load might still be applied at the 'left-hand end' (node 1). In these circumstances (17.211) would be replaced by

$$\mathbf{q}_e = P_1\mathbf{e}_1 + P_2\mathbf{e}_2 + P_3\mathbf{e}_3 \tag{17.213}$$

and the variation would involve the terms $\delta\mathbf{e}_{1-3}$. Consequently, in relation to the translational variables at the first node, with the P's fixed, we would have:

$$\delta\mathbf{q}_e = P_1\mathbf{F}_3(1\text{–}3)^T + P_2\mathbf{F}_3(3\text{–}6)^T + P_3\mathbf{F}_3(6\text{–}9)^T = \mathbf{K}_{t\sigma}(\mathbf{q}_e)\delta\mathbf{p} \tag{17.124}$$

where $\mathbf{F}_3(3\text{–}6)$ for example has the third to sixth rows of the matrix $\mathbf{F}_3$ of (17.62).

For the two-noded element of Simo and Vu-Quoc [S3.16] (Section 17.2), a point load applied at node 1 which followed the 'element direction', $\mathbf{t}_i$, which have a load vector applied to node 1 as in (17.211). With the aid of (17.69), with $\mathbf{q}_e$ fixed, differentiation would lead to

$$\delta\mathbf{q}_e = P\,\delta\mathbf{t}_i = -\frac{P}{2}\mathbf{S}(\mathbf{t}_i)(\delta\boldsymbol{\alpha} + \delta\boldsymbol{\beta}) = \mathbf{K}_{t\sigma}(\mathbf{q}_e)\delta\mathbf{p} \tag{17.215}$$

so that stiffness contributions would be added to both $\mathbf{K}_{12}$ and $\mathbf{K}_{14}$ in (17.44).

17.5.2 Concentrated moments applied at a node

Ziegler [Z1] has shown that moments about fixed axes are non-conservative. The reasoning can be related to the system in Figure 17.4 in which a constant moment M is assumed to act about the fixed X_1 axis. The motion from the system in Figure 7.4a to the configuration in 7.4b then results in the work, $W = \pi M$, where a rotation of π radians has been applied about the X_1 axis. (The lower-case letters relate to the orientation of the rotated body.) On the other hand, the motion from the initial configuration in Figure 7.4c (which is identical to that in 7.4a) to the configuration in Figure 7.4e (which is identical to that in 7.4b) via the intermediate configuration in Figure 7.4d leads to no work. The latter process involves a rotation of π radians about the X_2 axis followed by a rotation of π radians about the X_3 axis, but none the less leads to the same final configuration as the earlier work-consuming process. Consequently, the work is path-dependent and the moment is non-conservative and will lead to a non-symmetric tangent stiffness matrix.

In relation to the element of Sections 17.1 and 17.2 which use 'spin rotation variables', conjugate to moments about fixed axes, we simply have external loadings that contribute to the rotation terms (i.e. for node 1 of the elements of Section 17.1, the moments would be applied to the third to the sixth terms in the load vector). Consequently, no contributions are added to the tangent stiffness matrices when variations are applied to these loads so that there are no terms $\mathbf{K}_{t\sigma}(\mathbf{q}_e)$. However, for such loadings, we can no longer use the arguments of Sections 17.4 justify artificially symmetrising the tangent stiffness matrices. Indeed, the tangent stiffness matrix will, in such cases, turn out to be non-symmetric and, if an artificial symmetry is imposed, a very poor convergence rate will be found [C5].

For the co-rotational elements of Section 17.1, it is not difficult to apply local 'follower moments' at the nodes. For example, if such moments were applied in relation

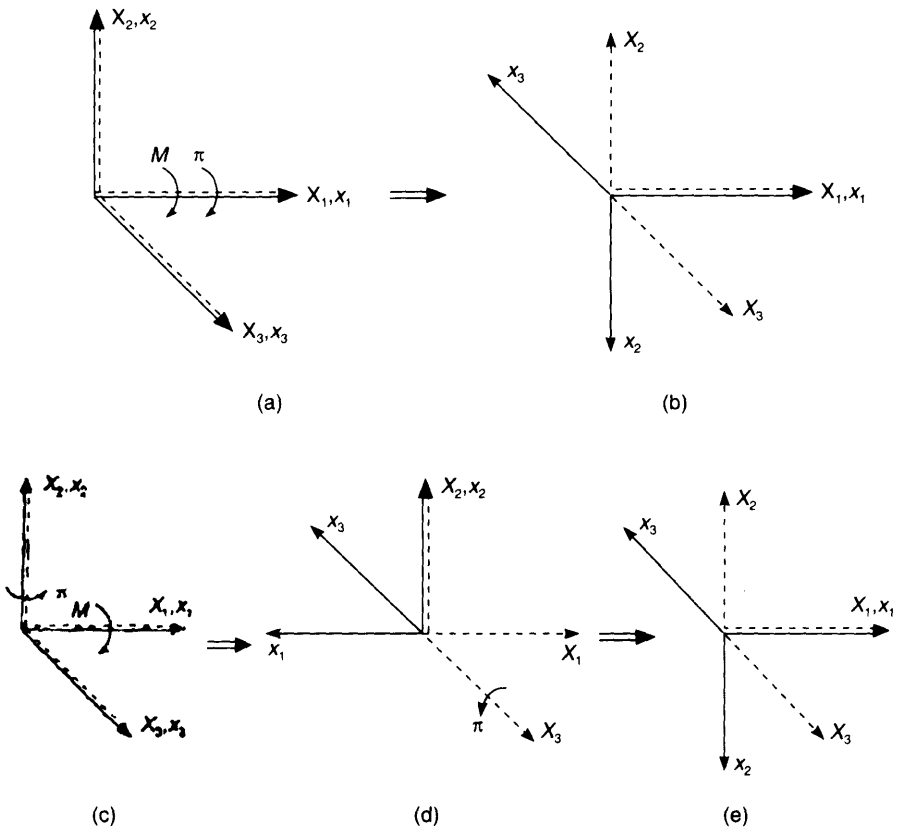

Figure 17.4 Illustration of the non-conservative nature of moments about fixed axes.

to the local element axes at node 1, one could consider the external work to be given by

$$V_e = M_{e1}\delta\theta_{l1} + M_{e2}\delta\theta_{l2} + M_{e3}\delta\theta_{l3} = \mathbf{q}_{el}^{\mathrm{T}}\delta\mathbf{p}_l \tag{17.216a}$$

where to avoid cluttering, we have omitted the subscript ν for virtual. The $\mathbf{q}_{el}$ term in (17.216a) would take the form:

$$\mathbf{q}_{el}^{\mathrm{T}} = (0,0,0,M_{el},M_{e2},M_{e3},0,0,0,0,0,0) \tag{17.216b}$$

so that using (17.4) whereby $\delta\mathbf{p}_l = \mathbf{F}\delta\mathbf{p}_1$, the global external forces could be obtained as

$$\mathbf{q}_e = \mathbf{F}^{\mathrm{T}}\mathbf{q}_{el} \tag{17.217}$$

and with $\mathbf{q}_{el}$ fixed, we would obtain:

$$\delta\mathbf{q}_e = \delta\mathbf{F}^{\mathrm{T}}\mathbf{q}_{el} = \mathbf{K}_{i\sigma}(\mathbf{q}_{il})\delta\mathbf{p} \tag{17.218}$$

where the tangent terms $\mathbf{K}_{i\sigma}(\mathbf{q}_{el})$ would take precisely the same form as the conventional initial stress terms, $\mathbf{K}_{i\sigma}(\mathbf{q}_{il})$ of Section 17.1.3.

17.5.3 Gravity loading with co-rotational elements

While gravity loading is normally considered to be a conventional, 'non-follower' loading, some anomalies arise with the co-rotational formulation.

Suppose a gravity loading is applied in the fixed unit direction $\mathbf{a}$, with a density, ρ. For a two-noded co-rotational Timoshenko element, we would conceptually derive an appropriate loading vector by considering shape functions of the form:

$$\bar{\mathbf{d}} = \tfrac{1}{2}(1-\zeta)\mathbf{d}_1 + \tfrac{1}{2}(1+\zeta)\mathbf{d}_2 \tag{17.219}$$

which relate to the centre-line translations using 'global measures'. The external virtual work would then follow as

$$V_e = \mathbf{q}_e^{\mathrm{T}}\delta\mathbf{p} = \int A_o\rho g(\mathbf{a}^{\mathrm{T}}\delta\mathbf{d}_v)\mathrm{d}x_{lo} \tag{17.220}$$

from which we would obtain a conventional lumped load vector:

$$\mathbf{q}_e^{\mathrm{T}} = \frac{A_o\rho g l_o}{2}(\mathbf{a}^{\mathrm{T}}, \mathbf{0}^{\mathrm{T}}\,\mathbf{a}^{\mathrm{T}}, \mathbf{0}^{\mathrm{T}}) \tag{17.221}$$

With $\mathbf{a}$ being fixed, we would find no contribution to $\mathbf{K}_{t\sigma}(\mathbf{q}_e)$.

Strictly, the situation with a two-noded Euler–Bernoulli element would be rather more complicated, because in place of (17.219) we would have:

$$\bar{\mathbf{d}} = \tfrac{1}{2}(1-\zeta)\mathbf{d}_1 + \tfrac{1}{2}(1+\zeta)\mathbf{d}_2 + \Delta\mathbf{d} \tag{17.222a}$$

with:

$$\Delta\mathbf{d} = \frac{l_o}{8}(\zeta^2-1)(\zeta-1)(\theta_{l2}\mathbf{e}_2 + \theta_{l3}\mathbf{e}_3) + \frac{l_o}{8}(\zeta^2-1)(\zeta+1)(\theta_{l5}\mathbf{e}_2 + \theta_{l6}\mathbf{e}_3) \tag{17.222b}$$

where the latter term relates to the cubic transverse shape functions. For a strict solution, we are forced to relate some of the shape functions to the moving local directions because the shape functions for the different displacement components are not the same. The first two terms on the right-hand side of (17.222a) will lead to the same external load vector as previously obtained for the Timoshenko element (see (17.221)). However, the term in (17.222b) will lead to some additional, more complicated, terms. The latter can be simplified to give 'fixed end-moments' which, in relation to the sign convention and ordering adopted for the element of Section 17.1, take the form:

$$\mathbf{q}_e^{\mathrm{T}} = \frac{A_o\rho g l_o^2}{12}(0,0,0,0,-(\mathbf{e}_3^{\mathrm{T}}\mathbf{a}),(\mathbf{e}_2^{\mathrm{T}}\mathbf{a}),0,0,0,0,-(\mathbf{e}_3^{\mathrm{T}}\mathbf{a}),(\mathbf{e}_2^{\mathrm{T}}\mathbf{a})) \tag{17.223}$$

The latter should be added to the terms in (17.221). Strictly, differentiation of (17.223) will lead to stiffness contributions, $\mathbf{K}_{t\sigma}(\mathbf{q}_e)$, which can be incorporated using terms from the matrix $\mathbf{F}_3$ of (17.62). It might, however, be better to use a Timoshenko-type formulation for such loadings even if a Euler–Bernoulli formulation is used for the stiffness. A similar approach is advocated in Section 24.11 for the treatment of inertia effects in dynamics.

17.6 INTRODUCING JOINTS

Many structures which are modelled with three-dimensional beam elements require joints at the nodes which follow the axes of the rotating system. Examples include deployable space structures, robots and rotating machinery. Joints can be modelled using Lagrangian multipliers (see Section 23.6 for the use of Lagrangian multipliers in relation to contact with continuum elements). Not only do such methods introduce extra variables but also Cardona and Geradin [C2] have shown that, in a non-linear dynamic environment, problems can sometimes arise with oscillations in the multipliers. As with continuum contact problems (see Section 23.7), various forms of augmented Lagrangian approach can be adopted [B2].

Perhaps the simplest approach is the penalty procedure, but convergence difficulties can then result [J2]. An alternative procedure involves the 'master–slave approach' [A1] in which certain subservient, slave variables, are expressed in terms of master variables. In the present section, we will describe a 'master–slave approach' that has been specifically geared to deal with large rotations [J2]. The description does not require the precise detail of the formulation adopted for the particular three-dimensional element, although it should have six degrees of freedom at each of the two (end) nodes. However, for the theory to be directly applied, the beam elements should use 'spin variables' (see Section 16.11) as the rotation variables. In describing the theory, we have also assumed an element with 'nodal triads' (such as the elements in Sections 17.1) rather than 'Gauss point triads' (as with the elements of Section 17.2). However, the concepts would still apply to the latter and it would not be difficult to modify the detail.

Figure 17.5 shows the basis of the proposed master–slave formulation. The deformations for the internal element are considered to be slave variables which are subservient to the master variables associated with adjoining nodes. These slave variables will be expressed in terms of the master variables and a set of 'relative variables' which will be eliminated at the element level so that, at the structural level, the only variables are the master variables. Generally, some of these 'relative variables' will be zero and only some of the local 'relative variables' will be released. However, in describing the theory, a full set of 'relative variables' will be assumed.

We will adopt a similar notation to that used for the beam element of Section 17.1 (see Figure 17.1). Hence, at node 1, the master variables involve a translation vector $\mathbf{d}_{m1}$, and a pseudo-vector $\boldsymbol{\alpha}_m$ associated with a nodal triad, $\mathbf{T}_m = [\mathbf{t}_{m1}, \mathbf{t}_{m1}, \mathbf{t}_{m1}]$. The slave variables takes a similar form, although now with a subscript s instead of m. For the relative variables, we will use the subscript sm. In relation to node 1, the following relationships connect the variables (Figure 17.5):

$$\mathbf{d}_{s1} = \mathbf{d}_{m1} + \mathbf{d}_{sm1} \tag{17.224a}$$

$$\mathbf{T}_s(\boldsymbol{\alpha}_s) = \mathbf{T}_{sm}(\boldsymbol{\alpha}_{sm})\mathbf{T}_m(\boldsymbol{\alpha}_m) \tag{17.224b}$$

Using the notation of Section 17.1 (see also Figures 17.1 and 17.5), the equivalent relationships for node 2 are

$$\mathbf{d}_{s2} = \mathbf{d}_{m2} + \mathbf{d}_{sm2} \tag{17.225a}$$

$$\mathbf{U}_s(\boldsymbol{\beta}_s) = \mathbf{U}_{sm}(\boldsymbol{\beta}_{sm})\mathbf{U}_m(\boldsymbol{\beta}_m) \tag{17.225b}$$

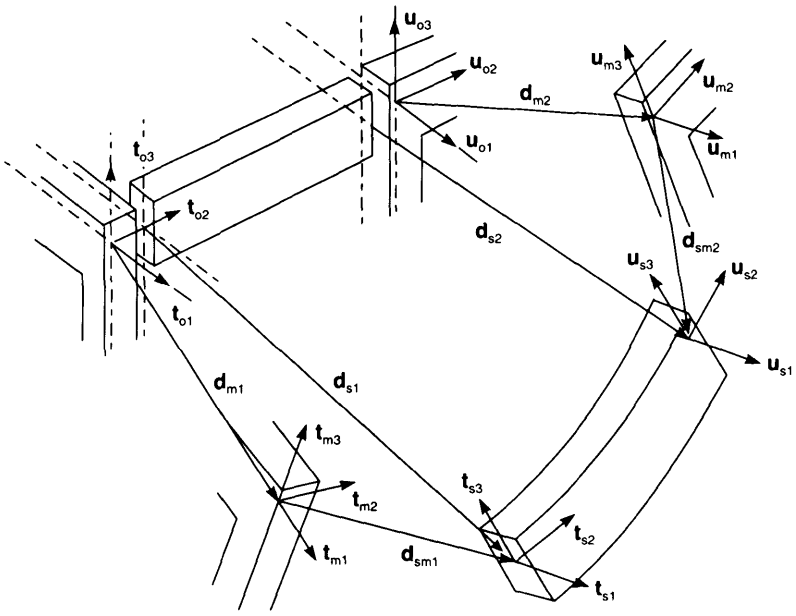

Figure 17.5 Master–slave relationships.

It will be assumed that the relative variables can be expressed in relation to the continuously rotating master triads and we will supply a superscript bar for the variables when they are expressed with respect to the latter so that at node 1, for example, we have:

$$\bar{\mathbf{d}}_{sm1} = \mathbf{T}_m^T \mathbf{d}_{sm1} \tag{17.226a}$$

$$\bar{\boldsymbol{\alpha}}_{sm} = \mathbf{T}_m^T \boldsymbol{\alpha}_{sm} \tag{17.226b}$$

Some of these variables will be constrained to zero and others will be released. For example, in Figure 17.6a, we only allow a sliding in the direction of the second component of $\bar{\mathbf{d}}_{sm1}$ (labelled as S in the figure) while in Figure 17.6b, we only allow a rotation (labelled as φ in the figure) about the continuously moving direction $\mathbf{t}_{m1} = \mathbf{t}_{s1}$ so that the first component of $\bar{\boldsymbol{\alpha}}_{sm}$ is free. The former is a 'prismatic joint' while the latter is a 'revolute joint' [A2].

The presented theory is based on the hypothesis that the master and slave triads are initially coincident (with an initial triad $[\mathbf{t}_{o1}, \mathbf{t}_{o2}, \mathbf{t}_{o3}]$ at node 1 and a triad $[\mathbf{u}_{o1}, \mathbf{u}_{o2}, \mathbf{u}_{o3}]$ at node 2—Figure 17.5) and that the required freedoms can be related to the former. The required kinematics will not always be consistent with this assumption. However, the problem could be overcome by defining an auxiliary triad, rigidly connected to either the master or slave triads. This approach would have similarities to the method that will be discussed in Section 18.6 for defining an 'element nodal triad' $\mathbf{U}_e$ that is always a fixed rotation from a surface triad $\mathbf{U}_s$).

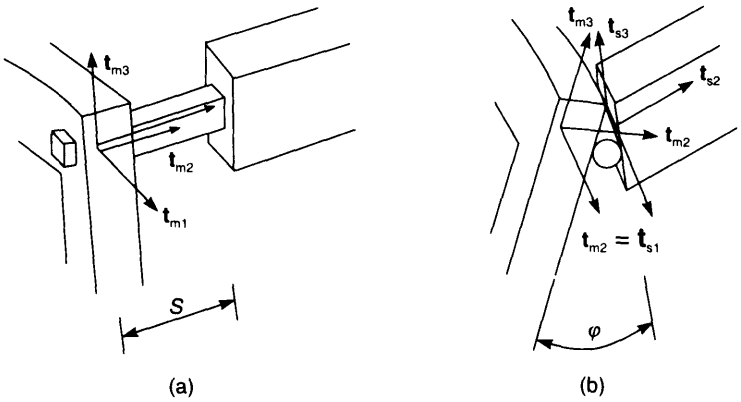

Figure 17.6 Examples of different joints. (a) Prismatic joint; (b) revolute joint.

As a result of the Newton–Raphson equilibrium iterations, we will obtain (details later) the variables:

$$\delta \mathbf{p}_m^T = (\delta \mathbf{d}_{m1}^T, \delta \boldsymbol{\alpha}_{m1}^T, \delta \mathbf{d}_{m2}^T, \delta \boldsymbol{\beta}_m^T) \tag{17.227a}$$

and

$$\delta \bar{\mathbf{p}}_{sm}^T = (\delta \bar{\mathbf{d}}_{sm1}^T, \delta \bar{\boldsymbol{\alpha}}_{sm1}^T, \delta \bar{\mathbf{d}}_{sm2}^T, \delta \bar{\boldsymbol{\beta}}_{sm}^T) \tag{17.227b}$$

Given the first of the vectors, the master variables would be updated in the standard way (as in Section 17.1), so that at node 1, for example, we would have:

$$\mathbf{d}_{m1,new} = \mathbf{d}_{m1,old} + \delta \mathbf{d}_{m1} \tag{17.228a}$$

$$\mathbf{T}_{m,new} = \Delta \mathbf{T}_m(\delta \boldsymbol{\alpha}_m)\mathbf{T}_{m,old} = \exp \mathbf{S}(\delta \boldsymbol{\alpha}_m)\mathbf{T}_{m,old} \tag{17.228b}$$

The slave variables are now updated via:

$$\mathbf{d}_{s1,new} = \mathbf{d}_{m1,new} + \mathbf{T}_{m,new}\bar{\mathbf{d}}_{sm1,new} = \mathbf{d}_{m1,new} + \mathbf{T}_{m,new}\{\bar{\mathbf{d}}_{sm1,new} + \delta \mathbf{d}_{sm1}\} \tag{17.229a}$$

$$\mathbf{T}_{s,new} = \mathbf{T}_{m,new}\bar{\mathbf{T}}_{sm,new} = \mathbf{T}_{m,new}[\exp \mathbf{S}(\delta \bar{\boldsymbol{\alpha}}_{sm})\bar{\mathbf{T}}_{sm,old}] \tag{17.229b}$$

where we have made use of (17.226) to convert back from the barred variables, which relate to the rotating master triad. The first relationship in (17.229b) needs further elaboration. It stems from the relationship:

$$\bar{\mathbf{T}}_{sm} = \mathbf{T}_m^T \mathbf{T}_{sm} \mathbf{T}_m \tag{17.230}$$

and hence, from (17.224b), we can write:

$$\mathbf{T}_s = \mathbf{T}_{sm}\mathbf{T}_m = \mathbf{T}_m \bar{\mathbf{T}}_{sm} \mathbf{T}_m^T \mathbf{T}_m = \mathbf{T}_m \bar{\mathbf{T}}_{sm} \tag{17.231}$$

For the application of the principle of virtual work, we require the variation of (17.229) which gives:

$$\begin{aligned} \delta \mathbf{d}_{s1} &= \delta \mathbf{d}_{m1} + \mathbf{T}_m \delta \bar{\mathbf{d}}_{sm1} + \mathbf{S}(\delta \boldsymbol{\alpha}_m)\mathbf{T}_m \bar{\mathbf{d}}_{sm1} = \delta \mathbf{d}_{m1} + \mathbf{T}_m \delta \bar{\mathbf{d}}_{sm1} + \mathbf{S}(\delta \boldsymbol{\alpha}_{sm1})\mathbf{d}_{sm1} \\ &= \delta \mathbf{d}_{m1} + \mathbf{T}_m \delta \bar{\mathbf{d}}_{sm1} - \mathbf{S}(\mathbf{d}_{sm1})\delta \boldsymbol{\alpha}_m \end{aligned} \tag{17.232a}$$

$$\delta \boldsymbol{\alpha}_s = \delta \boldsymbol{\alpha}_m + \mathbf{T}_m \delta \bar{\boldsymbol{\alpha}}_{5m} \tag{17.232b}$$

Equation (17.232b) is 'intuitively obvious', but a proof of its derivation is given in [J2]. By combining (17.232) with the equivalent relationships for the right-hand side node 2, we obtain:

$$\delta\mathbf{p}_s = \begin{bmatrix} \delta\mathbf{d}_{s1} \\ \delta\boldsymbol{\alpha}_s \\ \delta\mathbf{d}_{s2} \\ \delta\boldsymbol{\beta}_s \end{bmatrix} = \begin{bmatrix} \mathbf{T}_m & \mathbf{0} & \mathbf{0} & \mathbf{0} & \mathbf{I} & -\mathbf{S}(\mathbf{d}_{sm1}) & \mathbf{0} \\ \mathbf{0} & \mathbf{T}_m & \mathbf{0} & \mathbf{0} & \mathbf{0} & \mathbf{I} & \mathbf{0} \\ \mathbf{0} & \mathbf{0} & \mathbf{U}_m & \mathbf{0} & \mathbf{0} & \mathbf{0} & -\mathbf{S}(\mathbf{d}_{sm2}) \\ \mathbf{0} & \mathbf{0} & \mathbf{0} & \mathbf{U}_m & \mathbf{0} & \mathbf{0} & \mathbf{I} \end{bmatrix} \begin{pmatrix} \delta\mathbf{p}_m \\ \delta\bar{\mathbf{p}}_{sm} \end{pmatrix} = \mathbf{H}\delta\mathbf{p}_{mr} \tag{17.233}$$

where $\delta\mathbf{p}_m$ and $\delta\bar{\mathbf{p}}_{sm}$ were defined in (17.227) and the reader may need reminding that the triad $\mathbf{U}$ is the equivalent at node 2 to the triad $\mathbf{T}$ at node 1. The subscript 'mr' used for the combined displacement variation vector, on the right-hand side of (17.233), stands for 'master and released'.

Application of the principle of virtual work, now leads to the internal force vector $\mathbf{q}_{i,mr}$ corresponding to $\delta\mathbf{p}_{mr}$ as

$$\mathbf{q}_{i,mr} = \mathbf{H}_{i,s}^T\mathbf{q}_{i,s} \tag{17.234}$$

where $\mathbf{q}_{i,s}$ is the standard internal force vector relating to the 'slave element'.

To obtain the tangent stiffness matrix related to $\delta\mathbf{p}_{mr}$, we vary (17.234) to obtain:

$$\delta\mathbf{q}_{i,mr} = \mathbf{H}^T\mathbf{K}_{t,s}\mathbf{H}\delta\mathbf{p}_{mr} + \delta\mathbf{H}^T\mathbf{q}_{i,s} = \mathbf{H}^T\mathbf{K}_{t,s}\mathbf{H}\delta\mathbf{p}_{mr} + \mathbf{K}_{t\sigma}\delta\mathbf{p}_{mr} \tag{17.235}$$

(For simplicity, we have assumed no external forces associated with the slave variables but the developments are easily modified should the latter exist.)

In deriving the initial stress matrix, we use relationships such as

$$\mathbf{T}_m = \mathbf{S}(\delta\boldsymbol{\alpha}_m)\mathbf{T}_m \tag{17.236}$$

and

$$-\delta(\mathbf{S}(\mathbf{d}_{sm1})) = -\delta(\mathbf{S}(\mathbf{T}_m\bar{\mathbf{d}}_{sm1})) = \mathbf{S}(\mathbf{d}_{sm1} \times \delta\boldsymbol{\alpha}_m) - \mathbf{S}(\mathbf{T}_m\bar{\mathbf{d}}_{sm1}) \tag{17.237}$$

in conjunction with (16.86), (16.100) and (16.106). Finally, we obtain the initial stress matrix as:

$$\mathbf{K}_{t\sigma} = \begin{bmatrix} \mathbf{0} & \mathbf{0} & \mathbf{0} & \mathbf{0} & \mathbf{0} & \mathbf{T}_m^T\mathbf{S}(\mathbf{q}_1) & \mathbf{0} & \mathbf{0} \\ \mathbf{0} & \mathbf{0} & \mathbf{0} & \mathbf{0} & \mathbf{0} & \mathbf{T}_m^T\mathbf{S}(\mathbf{q}_2) & \mathbf{0} & \mathbf{0} \\ \mathbf{0} & \mathbf{0} & \mathbf{0} & \mathbf{0} & \mathbf{0} & \mathbf{0} & \mathbf{0} & \mathbf{U}_m^T\mathbf{S}(\mathbf{q}_3) \\ \mathbf{0} & \mathbf{0} & \mathbf{0} & \mathbf{0} & \mathbf{0} & \mathbf{0} & \mathbf{0} & \mathbf{U}_m^T\mathbf{S}(\mathbf{q}_4) \\ \mathbf{0} & \mathbf{0} & \mathbf{0} & \mathbf{0} & \mathbf{0} & \mathbf{0} & \mathbf{0} & \mathbf{0} \\ -\mathbf{S}(\mathbf{q}_1)\mathbf{T}_m & \mathbf{0} & \mathbf{0} & \mathbf{0} & \mathbf{0} & \mathbf{d}_{sm1}\mathbf{q}_1^T - (\mathbf{q}_1^T\mathbf{s}_{sm1})\mathbf{I} & \mathbf{0} & \mathbf{0} \\ \mathbf{0} & \mathbf{0} & \mathbf{0} & \mathbf{0} & \mathbf{0} & \mathbf{0} & \mathbf{0} & \mathbf{0} \\ \mathbf{0} & \mathbf{0} & -\mathbf{S}(\mathbf{q}_3)\mathbf{U}_m & \mathbf{0} & \mathbf{0} & \mathbf{0} & \mathbf{0} & \mathbf{d}_{sm2}\mathbf{q}_3^T - (\mathbf{q}_3^T\mathbf{d}_{sm2})\mathbf{I} \end{bmatrix} \tag{17.238}$$

where we have split $\mathbf{q}_{i,s}$ into subvectors such that:

$$\mathbf{q}_{i,s}^T = (\mathbf{q}_1^T, \mathbf{q}_2^T, \mathbf{q}_3^T, \mathbf{q}_4^T) \tag{17.239}$$

As discussed in Section 17.4, because we have used 'spin variables', non-symmetric terms are found in the tangent stiffness matrix. However, following the arguments of that section, in the absence of follower loads, there should be no deterioration in the convergence charateristics if we apply an aritificial symmetrisation. This theory is borne out by numerical experiments [J2].

Because the 'release variables', $\delta\bar{\mathbf{p}}_{sm}$, are only related to a particular node and element, they can be eliminated 'at the element level' using a similar procedure to that described in Section 18.12 for eliminating internal variables, such as 'enhanced strains', within continuum elements.

17.7 SPECIAL NOTATION

a_i, b_i = 'nodal thicknesses' in Section 17.4
$\mathbf{A}$ = matrix (see (17.22) in Sections 17.1 and 17.2
$\mathbf{A}$ = matrices in (17.23)–(17.27) in Section 17.3
$\mathbf{A}(\boldsymbol{\theta})$ = matrix defined in (17.114) in Section 17.2
$\mathbf{B}_i, \mathbf{B}_s, \mathbf{B}_t$ = matrices connecting $\mathbf{d}_i, \mathbf{d}_s, \mathbf{d}_t$ to $\delta\mathbf{p}$ in Section 17.3
$\mathbf{C}$ = constitutive matrix; $\mathbf{C}_m$—membrane, $\mathbf{C}_b$—bending
$\mathbf{d}$ = displacement vector ($\mathbf{d}_1$ at left-hand-side node, $\mathbf{d}_2$ at right-hand-side node in Sections (17.1–17.2)
$\bar{\mathbf{d}}$ = displacement vector at reference section in Section 17.3
$\bar{\mathbf{d}}_{sm}$ = relative displacement vector written with respect to current master triad in Section 17.6
$\mathbf{d}_r, \mathbf{d}_s, \mathbf{d}_t$ = partial derivatives of $\mathbf{d}$ with respect to r, s and t in Section 17.4
$\mathbf{e}_1$–$\mathbf{e}_3$ = element base vectors
$\mathbf{E}$ = triad containing $\mathbf{e}_1$–$\mathbf{e}_3$
$\mathbf{f}_i$ = columns of $\mathbf{F}$ in Section 17.1, vectors (see (17.16)) in Section 17.1
$\mathbf{F}$ = (Section 17.1) matrix connecting $\delta\boldsymbol{\theta}_t$ to $\delta\mathbf{p}$ (see (17.4))
$\mathbf{g}_r, \mathbf{g}_s, \mathbf{g}_t$ = covariant base vectors in current configuration in Section 17.3
$\mathbf{G}_r, \mathbf{G}_s, \mathbf{G}_t$ = covariant base vectors in initial configuration in Section 17.3
$\bar{\mathbf{G}}$ = matrix connecting $\delta\boldsymbol{\theta}$ to $\delta\mathbf{p}$ in Section 17.3
$\mathbf{h}_i$ = vectors (see (17.92)
$\mathbf{H}$ = matrix in (17.116) in Section 17.3
$\mathbf{H}$ = matrix in relating changes in slave variables, $\delta\mathbf{p}_s$, to changes in master and released variables, $\delta\underline{\mathbf{p}}_{mr}$ in Section 17.6
$\mathbf{H}(\boldsymbol{\theta})$ = matrix connecting $\delta\bar{\boldsymbol{\theta}}$ to $\delta\boldsymbol{\theta}$ (see (17.184)) in Section 17.5
$\mathbf{L}$ = matrix connecting $\delta\mathbf{e}$'s to $\delta\mathbf{p}$'s (see (17.32))
$\mathbf{m}$ = scaled local bending moments (see (17.78) in Section 17.2)
$\mathbf{M}$ = vector of local bending moments
$\mathbf{N}$ = axial force
$\mathbf{n}$ = scaled N's (see (17.78)) in Section 17.2
$\mathbf{N}$ = vector of local axial and shear stress-resultants in Section 17.2
$\mathbf{P}_{rr}$ etc. = 3×3 submatrices for tangent stiffness matrix in Section 17.3
$\mathbf{q}_i$ = internal force vector
$\bar{\mathbf{q}}_i$ = internal force vector work-conjugate to $\delta\bar{\boldsymbol{\theta}}$ in Section 17.4
$\mathbf{r}_1$–$\mathbf{r}_3$ = components of $\bar{\mathbf{R}}$ (Section 17.1)

r = non-dimensional coordinate along bar in Section 17.3
$\bar{\mathbf{R}}$ = intermediate triad (Section 17.1)
s, t = non-dimensional coordinates in 'pseudo-normal' directions in Section 17.3
$\mathbf{S}$ = skew-symmetric matrix
$\mathbf{S}$ = in Section 17.3, also vector with covariant components of second Piola–Kirchhoff stress (see (17.130))—with components S^{rr}, S^{rs}, S^{rt}
$\mathbf{T}$ = in Section 17.1, nodal triad for left-hand-side node, component vectors are $\mathbf{t}_1$–$\mathbf{t}_3$
$\mathbf{T}$ = in Section 17.2, mid-element triad (see (17.89))
$\bar{\mathbf{T}}$ = in Section 17.3, matrix in (17.74)
$\mathbf{U}$ = nodal triad for right-hand-side node, component vectors $\mathbf{u}_1$–$\mathbf{u}_3$
$\mathbf{v}$ = in Section 17.1, vector defined in (17.55b)
$\mathbf{v}_i, \mathbf{w}_i$ = nodal 'unit pseudo-normal vectors' in Section 17.3
$\mathbf{x}$ = initial coordinate vector
$\bar{\mathbf{x}}$ = initial coordinate vector of reference section in Section 17.3
$\mathbf{x}'$ = current coordinate vector
$\mathbf{X}$ = in Section 17.1.5, matrix—see (17.47); in Section 17.1.5, matrix—see (17.56b); in Section 17.2, matrix—see (17.100)
$\mathbf{Y}$ = in Section 17.2, matrix—see (17.88)
$\mathbf{z}$ = vector representing $\mathbf{t}_1$ or $\mathbf{u}_1$, etc. in (17.46)–(17.50)
$\mathbf{Z}$ = in Section 17.2 matrix—see (17.91)
u_l = local axial stretch displacement
l_o, l_n = old and new length of beam (straight between nodes)
α = length parameter (see (17.95)) in Section 17.2.6
$\Delta\boldsymbol{\alpha}$ = finite element rotation variables at left-hand-side node (Sections 17.1–17.2)
$\Delta\boldsymbol{\beta}$ = finite element rotation variables at right-hand-side node (Sections 17.1–17.2)
γ_2, γ_3 = local shear strains in Section 17.2
$\boldsymbol{\varepsilon}_l$ = local 'strain vector'; see (17.67) for Section 17.2 and (17.97) for Section 17.2.6
$\boldsymbol{\theta}_l$ = vector of local element rotations
$\Delta\mathbf{R}_m$ = rotation matrix defining rotation from $\mathbf{T}$ to 'mean configuration' (Section 17.1)
χ_{l1}–χ_{l3} = local curvatures (Sections 17.1 and 17.2)
$\boldsymbol{\chi}_l$ = vector of local curvatures (Section 17.2)
ζ = non-dimensional coordinate along beam in Section 17.5
$\delta\boldsymbol{\theta}$ = vector of variations in displacement derivatives in Section 17.4
$\delta\boldsymbol{\theta}$ = small changes in pseudo-vector in Section 17.3: also $\delta\boldsymbol{\theta}$—larger changes
$\delta\bar{\boldsymbol{\theta}}$ = spin variables in Section 17.4—also $\Delta\bar{\boldsymbol{\theta}}$
φ = potential in Section 17.4

17.8 REFERENCES

[A1] Abel, J. F. & Shepard, M. S., An algorithm for multipoint constraints in finite element analysis, *Int. J. for Num. Meth. in Engng.*, **14** (3), 464–467 (1979).

[A2] Angeles, J., *Spatial Kinematic Chains*, Springer-Verlag, Berlin, Heidelberg, New York (1982)

[A3] Argyris, J. H., Balmer, H., Doltsinis, J. St, Dunne, P. C., Haase, M., Klieber, M., Malejannakis, G. A., Mlejenek, J. P., Muller, M. & Scharpf, D. W., Finite element method the natural approach, *Comp. Meth. in Appl. Mech. & Engng.*, **17/18**, 1 106 (1979).

[A4] Argyris, J. H. & Symeonidis, Sp., Nonlinear finite element analysis of elastic systems under nonconservative loading natural formulation, Part 1. Quasistatic problems, *Comp. Meth. in Appl. Mech. & Engng.*, **26**, 75 123 (1981).

[B1] Bathe, K.-J. & Bolourchi, S., Large displacement analysis of three-dimensional beam structures, *Int. J. for Num. Meth. in Engng.*, **14**, 961 986 (1979).

[B2] Bayo, E., De Jalon, J. G. & Serna, M. A., A modified Lagrangian formulation for the dynamic analysis of constrained mechanical systems, *Comp. Meth. in Appl. Mech. & Engng.*, **71**, 183 195 (1988).

[B3] Belytschko, T. & Schwer, L., Large displacement, transient analysis of space frames, *Int. J. for Num. Meth. in Engng.*, **11**, 65 84 (1977).

[B4] Belytschko, T. & Glaum, L. W., Applications of higher order corotational stretch theories to nonlinear finite element analysis, *Computers & Structures*, **10**, 175 182 (1979).

[B5] Buechter, N. & Ramm, E., Shell theory versus degeneration. A comparison in large rotation shell theory, *Int. J. for Num. Meth. in Engng.*, **34**, 39 59 (1992).

[C1] Cardona, A. & Geradin, M., A beam finite element non-linear theory with finite rotations, *Int. J. for Num. Meth. in Engng.*, **26**, 2404 2438 (1988).

[C2] Cardona, A. & Geradin, M., Numerical integration of second-order differential- algebraic systems in flexible mechanism dynamics, Vol. 1, *Proc. NATO-ASI* on Computer Aided Analysis of Rigid and Flexible Systems, ed. M. S. Pereira *et al.*, July, 165 194 (1993).

[C3] Crisfied, M. A. & Cole, G., Co-rotational beam elements for two and three-dimensional non-linear analysis, *Discretisation Methods in Structural* mechanics, ed. G. Kuhn & H. Mang, Spring-Verlag, pp. 115 124 (1989).

[C4] Crisfield, M. A. & G. F. Moita, A unified co-rotational framework for solids, shells and beams, *Int. J. for Solids & Structs.*, **33**, 2969 2992 (1996).

[C5] Cole, G., Co-rotational beam elements consistently formulated for geometrically non-linear problems involving large rotations, Ph.D. thesis, Kingston Polytechnic (1990).

[D1] Dvorkin, E. N., Onate, E. & Oliver, J., On a non-linear formulation for curved Timoshenko beam elements considering large displacement/rotation increments, *Int. J. for Num. Meth. in Engng.*, **26**, 1597 1613 (1988).

[E1] Epstein, M. & Murray, D., Three-dimensional large deformation analysis of thin walled beams, *Int. J. Solids & Structs.*, **12**, 867 876 (1976).

[H1] Hibbitt, H. D., Some follower forces and load stiffness, *Int. J. for Num. Meth. in Engng.*, **14**, 937 941 (1979).

[H2] Hsiao, K. M. Horng, H.-J. & Chen, Y. R., A corotational procedure that handles large rotations of spatial beam structures, *Comp. & Struct.*, **27**, pp. 693 701 (1987).

[J1] Jelenic, G. & Crisfield, M. A., Non-linear 'master slave' relationships for joints in 3-D beams with large rotations, *Comp. Meth. in Appl. Mech. & Engng.*, **135**, 211 228 (1996).

[J2] Jelenic, G. & Saje, M., A kinematically exact space finite strain beam model finite element formulation by generalised virtual work pinciple, *Comp. Meth. in Appl. Mech. & Engng.*, **120**, 131 161 (1995).

[K1] Kassimali, A., Large deformation analysis of elasto-plastic beams, *ASCE J. of Struct. Div.*, **109** (8), 1869 1886 (1983).

[K2] Kani, I. M. & McConnel, R. E., Collapse of shallow lattice domes, *ASCE J. of Struct. Div.*, **113** (8), 1806 1819 (1987).

[K3] Krenk, S., Stiffness of elastic co-rotating beam elements, *Advances in Finite Element Technology*, ed. N.-E. Wiberg, CIMNE, Barcelona, pp. 237–253 (1995).

[N1] Nour-Omid, B. & Rankin, C. C., Finite rotation analysis and consistent linearisation using projectors, *Comp. Meth. in Appl. Mech. & Engng.*, **93**, 353–384 (1991).

[O1] Oran, C., Tangent stiffness in space frames, *J. of Engng. Mech. Div., ASCE*, **99**, 987–1001 (1973).

[O2] Oran, C. & Kassimali, A., Large deformations of framed structures under static and dynamic loads, *Computers & Structures*, **6**, 539–547 (1976).

[P1] Parisch, H., An investigation of a finite rotation four-node shell element, *Int. J. for Num. Meth. in Engng.*, **31**, 127–150 (1991).

[R1] Rankin, C. C. & Nour-Omid, B., The use of projectors to improve finite element performance, *Comp. & Struct.*, **30**, 257–267 (1988).

[R2] Reissner, E., On finite deformations in space-curved beams, *J. of Appl. Math. & Physics*, **32**, 734–744 (1981).

[R3] Rankin, C. C. Private communication.

[S1] Schweizerhof, K. & Ramm, E., Displacement dependent pressure loads in nonlinear finite element analysis, *Computers & Struct.*, **18**, 1099–1114 (1984).

[S2] Shi, G. & Atluri, S. N., Elasto-plastic large deformation analysis of space-frames: a plastic-hinge and stress-based explicit derivation of tangent stiffnesses, *Int. J. for Num. Meth. in Engng.*, **26**, 589–615.

[S3] Simo, J. C., The (symmetric) hessian for geometrically nonlinear models in solid analysis: intrinsic definition and geometric interpretation, *Comp. Meth. in Appl. Mech. & Engng.*, **96**, 189–200 (1992).

[W1] Wood, R. D. & Zienkiewicz, O. C., Geometrically nonlinear finite element analysis of beams, frames, arches and axisymmetric shells, *Comp. & Struct.*, **7**, 725–735 (1977).

[W2] Wen, R. K. & Rahimzadeh, J. Nonlinear elastic frame analysis by finite element, *ASCE, J. of Struct. Div.*, **109** (8), 1952–1971 (1983).

[W3] Wunderlich, W. & Obrecht, H., Large spatial deformations of rods using generalised variational principles, *Non-linear Finite Element Analysis* in *Structural Mechanics*, ed. W. Wunderlich, E. Stein, & K. J. Bathe, Springer-Verlag, Berlin, 185–216 (1981).

[Z1] Ziegler, H., *Principles of Structural Stability*, Blaisdell, Waltham, MA (1968).

18 More on continuum and shell elements

18.1 INTRODUCTION

In relation to specific finite element work rather than to the surrounding mechanics, the main developments on continua in this volume have involved the 'Eulerian formulation' of Chapter 12 and the various mixed or hybrid formulations introduced in Chapter 13 in relation to hyperelasticity so as to combat volumetric locking. In this chapter, an alternative technique is discussed (Section 18.12) in which 'incompatible modes' or 'enhanced strains' or 'assumed co-variant strains' are used to improve the performance of lower-order elements. This is achieved with the aid of an enhanced deformation gradient and leads directly to an enhanced Eulerian formulation which was originally introduced by Simo and co-workers [S5–S7].

The remainder of the chapter is primarily directly concerned with the co-rotational approach and starts with continua and then moves on to shells (with a short return to three-dimensional beams in Section 18.10). However, although the work on shells is based on the co-rotational approach, some of the concepts have a wider application. In particular, the treatment of large rotations is a also relevant to other formulations. In addition, three separate approaches are adopted for dealing with the 'drilling rotation'.

In the first (Section 18.6), the issue is effectively ignored and the problem is formulated directly in terms of nodes with three rotational variables. Because the method is based on the co-rotational procedure, the issue of the drilling rotation is left to the embedded linear element which is assumed to have an in-plane rotational stiffness. This stiffness may be 'real' if the element directly incorporates 'drilling variables' [A1, B3, F1, I1, K1, M1]. Alternatively the stiffness may be left as zero in which case singularities may arise as the curvature of the system approaches zero and the system becomes planar or as the mesh is refined. As a third alternative, the approach of Zienkiewicz *et al.* [Z1] may be adopted so that an artificial stiffness is introduced. However, in a non-linear environment, there are likely to be problems with such an approach in which the artificial stiffness is related to the real stiffness of the adjacent elements. In particular, these problems may arise when plasticity is involved.

An alternative way of dealing with the problem of the 'drilling variable' is to use no drilling variable and instead use a single rotation about an element side. This is

the procedure adopted in both the 'Morley triangle' [M4] (see also [B2, H1, H2, W4]) and in Irons's semi-loof elements [I2, I3]. A moderate rotation formulation involving the former has been given by Morley [M5] while large-rotation formulations have been given by Peng and Crisfield [P2], Peric *et al.* [P3] and by van Keulen *et al.* [V1] (see also Backlund [B1]). A similar (but simpler) approach is described in Section 18.7 while a possible extension to the semi-loof elements is discussed in Section 18.9.

Yet another procedure for handling the issue of the 'drilling rotation' is to only include such a rotations at branched intersections (In contrast to the previous technique, a more complex 'house-keeping' is required). Away from intersections, assuming the shell to be smooth, only two rotational variables are included. Such a formulation is described in Section 18.8. In a non-linear context, the method can be considered to have its origins in an important early paper by Horrigmoe and Bergan [H3]. However, in contrast to the latter work, the accuracy of the current work does not depend on the assumption of small increments. With respect to its treatment of the rotational variables, the current work has much in common with the procedure of Simo *et al.* [S1–S4] and Celicoj [C1]. Other work on shells which specifically deals with large rotations can be found in [B5.17, P1, P1.17, B4, H4, N1, W2]. It is worth adding that it is possible to derive a shell element formulation without considering rotations at all [O1, P4].

Many finite element formulations for shells have followed on from continuum formulations so that the finite element techniques take the form of 'degenerate continuum techniques' (Section 8.2). In the present chapter the co-rotational shell formulations also follow on from equivalent formulations for continua. This is much less conventional. Indeed at first sight there seems to be little to be gained by applying the co-rotational procedure to a continuum. However, we will attempt to show in Sections 18.2 and 18.3 that there are some benefits (apart from leading the way to a more elegant technique for handling shells). In particular, with small strains (but including plasticity), it is found to be a simple matter to include any (preferably lower-order) continuum element within a co-rotational framework in which the internal linear element formulation remains untouched. This procedure was described in Section 17.1 for three-dimensional beams and has its origins in the work of Rankin and Brogan [R1.16]. However, for continua, there remains the issue of how to choose the local element frame and we adopt an idea originally due to Jetteur and Cescotto [J1] which will be detailed in Sections 18.2 and 18.3. Once the co-rotational 'harness' has been generated, it is a simple matter to change the internal linear element. In this way, one can quickly incorporate the best new linear element. These ideas are illustrated in Section 18.11 where 'incompatible modes' or 'enhanced strains' are introduced.

It turns out that some of the concepts for a co-rotational continuum formulation help to introduce a more elegant formulation for shells (and indeed three-dimensional beams—Section 18.10). The concepts can again be traced back to the work of Rankin and Brogan [R1.16] and Nour-Omid and Rankin [N1.17].

In the final sections of this chapter, it is shown how both the Eulerian formulation (Chapter 12) and the co-rotational approach for continua can be extended to handle large (here elastic) strains in conjunction with extra internal variables such as incompatible modes or enhanced strains.

18.2 A CO-ROTATIONAL APPROACH FOR TWO-DIMENSIONAL CONTINUA

The current section describes the work originally described in [C3, M2]. As a first step, the initial co-rotating local coordinates are set equal to the initial co-ordinates minus those at node 1 so that at node j:

$$\mathbf{X}_l^j = \mathbf{X}^j - \mathbf{X}^1 \tag{18.1}$$

In this and in many subsequent equations, the node numbers have been placed as postscripts. This is purely for convenience to avoid a clash with the subscript l for local. However, where such a potential clash would not arise, we will sometimes revert to using subscripts for node numbers. If we assume, for the present, that the local rotating unit vectors, $\mathbf{e}_1$ and $\mathbf{e}_2$ are know, then from Figure 18.1, by writing the current position vector of node j in two separate ways, we can obtain:

$$\mathbf{x}_l^j = \mathbf{X}_l^j + \mathbf{d}_l^j = \begin{pmatrix} X_l \\ Y_l \end{pmatrix}^j + \begin{pmatrix} u_l \\ v_l \end{pmatrix}^j = \mathbf{E}^{\mathrm{T}}(\mathbf{x}^j - \mathbf{x}^1) = \mathbf{E}^{\mathrm{T}}\mathbf{x}^{j1} = \mathbf{E}^{\mathrm{T}}\begin{pmatrix} x \\ y \end{pmatrix}^{j1} \tag{18.2a}$$

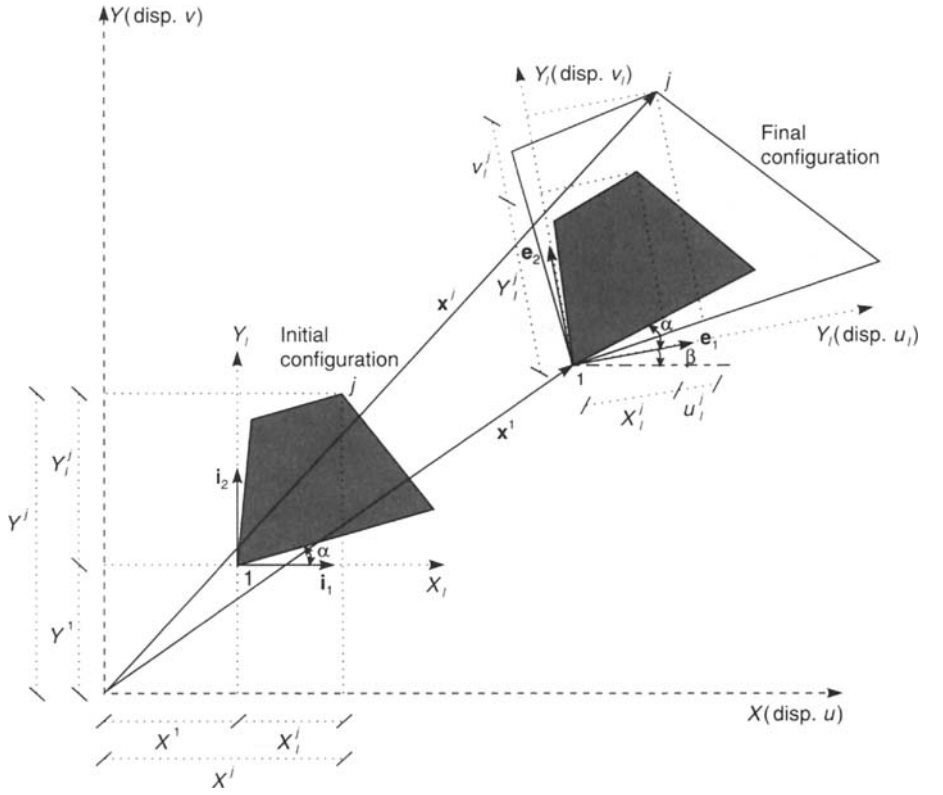

Figure 18.1 Initial and final configuration—rotation follower by stretch.

where

$$\mathbf{E} = [\mathbf{e}_1 \mathbf{e}_2] = \begin{bmatrix} \cos\beta & -\sin\beta \\ \sin\beta & \cos\beta \end{bmatrix} = \begin{bmatrix} c & -s \\ s & c \end{bmatrix} \tag{18.2b}$$

It would be possible to make the vector $\mathbf{e}_1$ coincide with one of the sides of the element. However, the element would not then pass the large-strain patch test [J1, S6] which was originally proposed by Jetteur and Cescotto [J1] and later defined by Simo and Armero [S6] as requiring 'the exact solution for homogeneous deformations with constant deformation gradient **F**. The concept is illustrated in Figure 18.2 for direct tension. No matter what hyperelastic model is chosen, the strains (of whatever type) should be the same for each integration point in each element. An equivalent test under shear could involve the example of Section 13.10.3 with a non-uniform mesh.

A procedure for successfully choosing the local axes was originally proposed by Jetteur and Cescotto [J1] and is illustrated in Figure 18.3 and ensures that the local

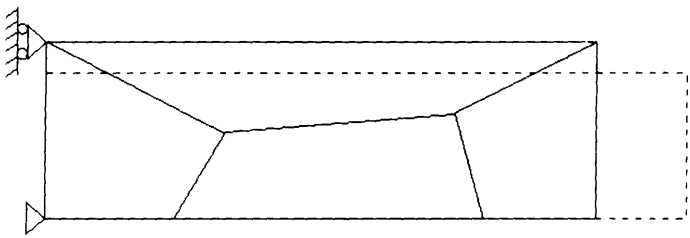

Figure 18.2 Large strain patch test (in uniaxial tension).

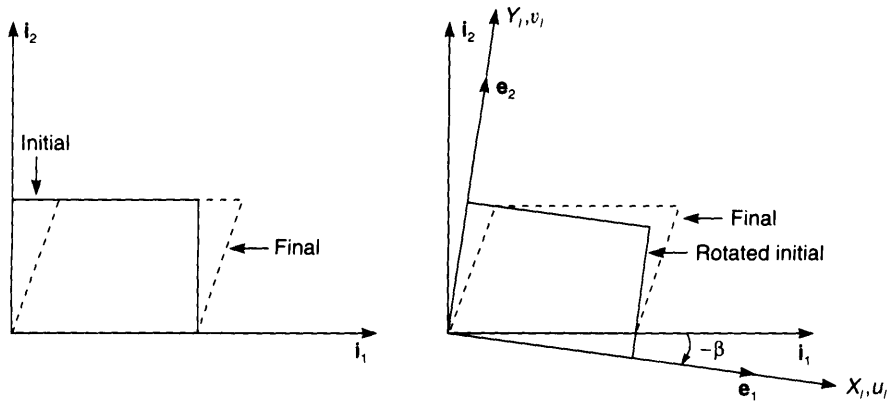

Figure 18.3 example with local axes $\mathbf{e}_1$ and $\mathbf{e}_2$.

'spin' at the centre of the element is zero. i.e.

$$\Omega_{lm} = \left(\frac{\partial u}{\partial Y} - \frac{\partial v}{\partial X} \right)_{lm} = \sum \mathbf{a}_l^{j\mathrm{T}} \mathbf{d}_l^j = 0 \tag{18.3}$$

Here the subscript m means 'middle' and the 2×1 vectors $\mathbf{a}_l^j$ are obtained from the conventional linear formulation using the derivatives of the shape functions evaluated at the centre of the element. The terms $\mathbf{a}_l^j$ (with $j = 1,4$ for a four-noded element) are functions of the initial coordinates $\mathbf{X}_l$. They can be obtained by first computing the displacement derivative matrix, $\mathbf{G}(\mathbf{X}_l)$ (see (5.8)) where:

$$\boldsymbol{\theta}_l = \begin{bmatrix} \dfrac{\partial u}{\partial X} \\ \dfrac{\partial u}{\partial Y} \\ \dfrac{\partial v}{\partial X} \\ \dfrac{\partial v}{\partial Y} \end{bmatrix}_l = \mathbf{G}(\mathbf{X}_l)\mathbf{p}_l \tag{18.4}$$

and the combined vector of nodal displacements takes the form:

$$\mathbf{p}^{\mathrm{T}} = (\mathbf{d}_1^{\mathrm{T}}, \mathbf{d}_2^{\mathrm{T}}, \mathbf{d}_3^{\mathrm{T}}, \mathbf{d}_4^{\mathrm{T}}) \tag{18.5}$$

with an equivalent expression for the local quantities.

Substitution from (18.2a) and (18.2b) into (18.3) leads to

$$\Omega_{lm} = \sum \mathbf{a}_l^{j\mathrm{T}} \left(c \begin{pmatrix} x^{j1} \\ y^{j1} \end{pmatrix} + s \begin{pmatrix} y^{j1} \\ -x^{j1} \end{pmatrix} \right) - \sum \mathbf{a}_l^{j\mathrm{T}} \mathbf{X}_l^j = 0 \tag{18.6}$$

However, from the standard properties of isoparametric linear elements, the last term is zero so that:

$$\Omega_{lm} = as + bc = 0 \tag{18.7}$$

where

$$a = \sum \mathbf{a}_l^{j\mathrm{T}} \begin{pmatrix} y^{j1} \\ -x^{j1} \end{pmatrix}; \qquad b = \sum \mathbf{a}_l^{j\mathrm{T}} \begin{pmatrix} x^{j1} \\ y^{j1} \end{pmatrix} \tag{18.8}$$

Clearly the angel β (Figures 18.1 and 18.3) which defines the local axes, in $\mathbf{E}$, can be obtained from the above equation.

A key step in the co-rotational procedure is the computation of the transformation matrix whereby,

$$\delta \mathbf{p}_l = \mathbf{T}\, \delta \mathbf{p} \tag{18.9}$$

(In contrast to Chapter 17, where $\mathbf{F}$ was used for the transformation matrix, we are now using $\mathbf{T}$ because $\mathbf{F}$ is being used for the deformation gradient.)

To obtain this matrix, differentiation of (18.2a) leads to

$$\delta \mathbf{d}_l^j = \mathbf{E}^{\mathrm{T}} \delta \mathbf{d}^{j1} + \delta \mathbf{E}^{\mathrm{T}} \mathbf{x}^{j1} = \mathbf{E}^{\mathrm{T}} \delta \mathbf{d}^{j1} + \mathbf{E}^{\mathrm{T}} \begin{pmatrix} y^{j1} \\ -x^{j1} \end{pmatrix} \delta \beta \tag{18.10a}$$

Equation (18.10a) will ensure that $\delta \mathbf{d}_l^1$ is zero. We could proceed with such an approach which would closely follow that of Sections 7.2 and 17.1. However, the equations turn out to be simpler if we work with a modified set of local displacement changes, $\delta \bar{\mathbf{d}}_l^j$, which are obtained by adding $\mathbf{E}^{\mathrm{T}} \delta \mathbf{d}_1$ to each local nodal displacement change vector. If the local element computations correctly satisfy the infinitesimal strain-free rigid body requirements, this modification should have no effect. As a result of the modification, (18.10a) is replaced by

$$\delta \bar{\mathbf{d}}_l^j = \mathbf{E}^{\mathrm{T}} \delta \mathbf{d}^j + \delta \mathbf{E}^{\mathrm{T}} \mathbf{x}^{j1} = \mathbf{E}^{\mathrm{T}} \delta \mathbf{d}^j + \mathbf{E}^{\mathrm{T}} \begin{pmatrix} y^{j1} \\ -x^{j1} \end{pmatrix} \delta \beta \tag{18.10b}$$

In the following (and for all of the co-rotational work in this chapter), we will use (18.10b) rather than (18.10a) although we will not bother to use the barred superscript.

In order to obtain $\delta \beta$ differentiation of (18.7) leads to

$$(ac - bs)\delta \beta = -s\,\delta a - c\,\delta b = \mathbf{f}^{\mathrm{T}} \delta \mathbf{p} \tag{18.11}$$

where the vector $\mathbf{f}$ stems from the differentiation of the terms in (18.8) (note the $\mathbf{a}_l^j$ vectors are fixed as they are functions of $\mathbf{X}_l$ and, for example, $\delta y^{j1} = \delta v_j - \delta v_1$). It is therefore a simple matter to obtain a vector $\mathbf{v}$ such that:

$$\delta \beta = \mathbf{v}^{\mathrm{T}} \delta \mathbf{p} \tag{18.12}$$

so that, via (18.10b), the transformation matrix $\mathbf{T}$ in (18.9) is given by

$$\mathbf{T} = \mathrm{Diag}(\mathbf{E}^{\mathrm{T}}) - \mathrm{Diag}(\mathbf{E}^{\mathrm{T}}) \mathbf{z} \mathbf{v}^{\mathrm{T}} \tag{18.13}$$

with

$$\mathbf{z}^{\mathrm{T}} = (0, 0, -y^{21}, x^{21}, -y^{31}, x^{31}, -y^{41}, x^{41}) \tag{18.14}$$

(For the first predictor solution on the first increment the matrix $\mathbf{T}$ can be taken as the identity matrix in order to obtain the global stiffness matrix from the local stiffness matrix.)

The equivalence of virtual work in the local and global systems leads to the relationship:

$$\mathbf{q}_{\mathrm{i}} = \mathbf{T}^{\mathrm{T}} \mathbf{q}_{l\mathrm{i}} \tag{18.15}$$

or

$$\mathbf{q}_{\mathrm{i}} = \mathrm{col}(\mathbf{E}\mathbf{q}_{l\mathrm{i}}^j) - \mathbf{v}\mathbf{z}^{\mathrm{T}} \mathrm{col}(\mathbf{E}\mathbf{q}_{l\mathrm{i}}^j) = \mathrm{col}(\bar{\mathbf{q}}_{l\mathrm{i}}^j) - \mathbf{v}\mathbf{z}^{\mathrm{T}} \mathrm{col}(\bar{\mathbf{q}}_{l\mathrm{i}}^j) \tag{18.16}$$

With a view to later developments, we will express the 2×1 vector for node j as

$$\bar{\mathbf{q}}_{l\mathrm{i}}^j = \mathbf{E}\mathbf{q}_{l\mathrm{i}}^j = \begin{pmatrix} \bar{U} \\ \bar{V} \end{pmatrix}^j \tag{18.17}$$

If $\mathbf{q}_{l\mathrm{i}}^j$ are the local internal forces at node j with respect to the axes $\mathbf{e}_1$ and $\mathbf{e}_2$, it is clear that $\bar{\mathbf{q}}_{l\mathrm{i}}^j$ are the equivalent forces with respect to the global axes. Equally, the scalar:

$$\mathbf{z}^{\mathrm{T}} \mathrm{col}(\bar{\mathbf{q}}_{l\mathrm{i}}^j) = \sum \begin{pmatrix} -y^{j1} \\ x^{j1} \end{pmatrix}^{\mathrm{T}} (\bar{\mathbf{q}}_{l\mathrm{i}}^j) \tag{18.18}$$

in (18.16) represents the total moment of the internal forces about the e_3 axis perpendicular to the paper) and is therefore zero once equilibrium is established.

The tangent stiffness matrix is obtained as usual by differentiation of (18.15) (or (18.16)) so that:

$$\delta \mathbf{q}_i = \mathbf{T}^T \mathbf{K}_l \mathbf{T}\, \delta \mathbf{p} + \text{col}(\delta \mathbf{E} \mathbf{q}_{li}^j) + \mathbf{v}\, \delta \mathbf{z}^T \text{col}(\bar{\mathbf{q}}_{li}^j) + \mathbf{v} \mathbf{z}^T \text{col}(\delta \mathbf{E} \mathbf{q}_{li}^j) \tag{18.19}$$

In deriving (18.19), it has been assumed that, with respect to the rotating base frame the local element stiffness matrix, $\mathbf{K}_l$, is fixxed and linear. (The introduction of large strains will be considered later in Section 18.13.) We have also omitted terms stemming from the variation of the 'spin vector' $\mathbf{v}$. The reasoning relates to the observation below (18.18) that the terms multiplying $\mathbf{v}$ in (18.17) will be zero at equilibrium. Away from equilibrium, therefore, the terms stemming from the variation of $\mathbf{v}$ should strictly be included. This can be done [C3, M2]. However, numerical experience has shown that almost nothing is gained in terms of any improvement in the convergence rate [C3, M2]. Consequently in the following (and throughout this chapter) we will neglect the variation of the 'spin vector (or later matrix)' so that, in the current case, the last three terms in (18.19) lead to the initial stress matrix and provide:

$$\mathbf{K}_{l\sigma} = \overset{*}{\mathbf{q}} \mathbf{v}^T + \mathbf{v} \overset{*}{\mathbf{q}}^T - \mathbf{v}(\mathbf{z}^T \overset{*}{\mathbf{q}}) \mathbf{v}^T \tag{18.20}$$

where

$$\overset{*}{\mathbf{q}}^T = (-\bar{V}_1, \bar{U}_1, -\bar{V}_2, \bar{U}_2, -\bar{V}_3, \bar{U}_3, -\bar{V}_4, \bar{U}_4) \tag{18.21}$$

with $\bar{U}$ and $\bar{V}$ having been defined in (18.17).

18.3 A CO-ROTATIONAL APPROACH FOR THREE-DIMENSIONAL CONTINUA

In order to extend the previous formulation to three dimensions [M2, M3, C4], it will be shown that the previous procedure for computing the local rotating base vectors $\mathbf{e}_1$ and $\mathbf{e}_2$ (now also $\mathbf{e}_3$), is equivalent to the computation of

$$\mathbf{E} = [\mathbf{e}_1\, \mathbf{e}_2\, \mathbf{e}_3] = \mathbf{R}_m \tag{18.22}$$

where

$$\mathbf{F}_m = \mathbf{R}_m \mathbf{U}_m \tag{18.23}$$

involves a polar decomposition at the centroid (or 'middle'—hence the subscript m) of the element. To demonstrate this assertion, we begin with the deformations shown in Figure 18.4. If we compare Figure 18.1 with Figure 18.4, we note that they are equivalent with the latter illustrating a process whereby the element is strained and later rotated while the former represents a rotation followed by a stretch.

From Figures 18.1 and 18.4, at the centroid of the element, we can write:

$$\mathbf{U}_m = \left[\frac{\partial \mathbf{x}_l}{\partial \mathbf{X}_l} \right]_m = \left[\mathbf{I} + \frac{\partial \mathbf{u}_l}{\partial \mathbf{X}_l} \right]_m = \mathbf{I} + \mathbf{D}_{lm} \tag{18.24}$$

Here $\mathbf{x}_l = \mathbf{X}_l + \mathbf{u}_l$ and $\mathbf{D}_{lm}$ is the local displacement derivative matrix (see (4.72)).

We can also write the local engineering strain (still at the centroid) as

$$\boldsymbol{\varepsilon}_{lm} = \tfrac{1}{2}(\mathbf{D}_{lm} + \mathbf{D}_{lm}^T) \tag{18.25}$$

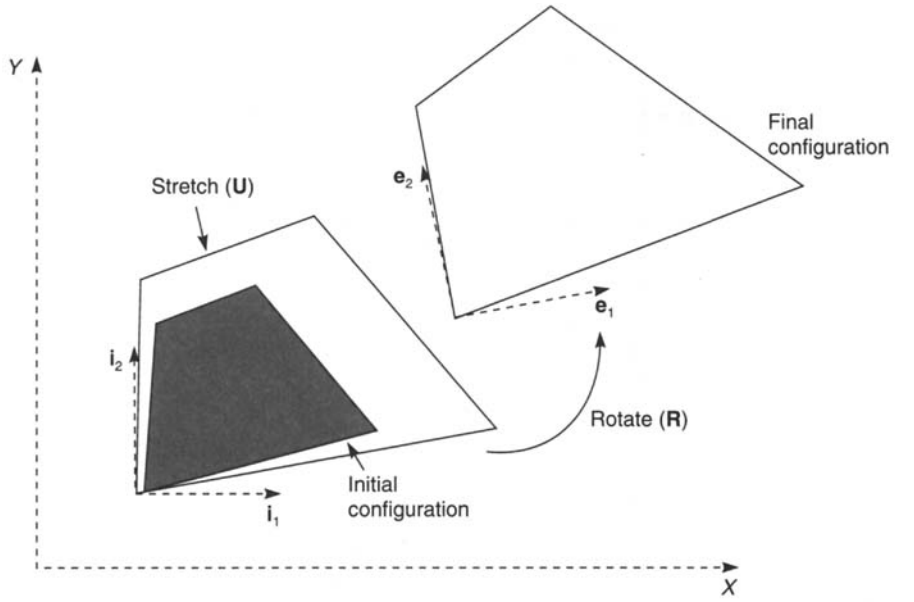

Figure 18.4 Polar decomposition—stretching preceding the rotation.

Equations (18.24) and (18.25) lead to an expression for the local engineering strain of the form:

$$\boldsymbol{\varepsilon}_{lm} = \tfrac{1}{2}\mathbf{U}_m + \tfrac{1}{2}\mathbf{U}_m^T - \mathbf{I} = \mathbf{U}_m - \mathbf{I} \tag{18.26}$$

which shows that $\boldsymbol{\varepsilon}_{lm}$ can be considered as a Biot strain (see also (10.14) and (10.64)). In (18.26) we have used the property of the symmetry of the right stretch matrix $\mathbf{U}$ so that $\mathbf{D}_{lm} = \mathbf{D}_{lm}^T$. In the two-dimensional case, the latter relationship is entirely equivalent to (18.3).

In practice, we do not compute the local strains from (18.26) but rather (at the Gauss points) from the local displacements $\mathbf{p}_l$ obtained from the $\mathbf{d}_l^j$ of (18.2a) with the aid of the $\mathbf{E}$ matrix previously computed from (18.22) and (18.23) using a polar decomposition at the centroid of the element.

To obtain the important transformation matrix $\mathbf{T}$, we differentiate (18.2a) and now also use the relationship (see (16.81c)):

$$\delta\mathbf{E} = \mathbf{S}(\delta\boldsymbol{\beta})\mathbf{E} \tag{18.27}$$

so that

$$\delta\mathbf{d}_l^j = \mathbf{E}^T\delta\mathbf{d} + \mathbf{E}^T\mathbf{S}(\mathbf{x}^{j1})\delta\boldsymbol{\beta} \tag{18.28}$$

To obtain an expression for $\delta\boldsymbol{\beta}$, we note that, as a parallel with (18.6), we can obtain:

$$\boldsymbol{\Omega}_{lm} = \sum \mathbf{A}_l^j \mathbf{d}_l^j = 0 \tag{18.29}$$

where the 3×1 vector $\boldsymbol{\Omega}_{lm}$ is the vector equivalent of $\mathbf{D}_{lm} - \mathbf{D}_{lm}^T$ (see (18.24)) and is obtained at the centroid of the element (possibly via the equivalent of (18.4)—see

(5.29)–(5.31)). Differentiation of (18.29) and substitution from (18.27) leads to

$$\delta\boldsymbol{\Omega}_{lm} = \sum \mathbf{A}_l^j \mathbf{E}^{\mathrm{T}} \delta\mathbf{d}_j + \sum \mathbf{A}_l^j \mathbf{E}^{\mathrm{T}} \mathbf{S}(\mathbf{x}^{j1}) \delta\boldsymbol{\beta} = \mathbf{0} \tag{18.30}$$

from which

$$\delta\boldsymbol{\beta} = -\left[\sum \mathbf{A}_l^j \mathbf{E}^{\mathrm{T}} \mathbf{S}(\mathbf{x}^{j1})\right]^{-1} \sum \mathbf{A}_l^j \mathbf{E}^{\mathrm{T}} \delta\mathbf{d}_j = \mathbf{V}^{\mathrm{T}} \delta\mathbf{p} \tag{18.31}$$

where the 'spin matrix' $\mathbf{V}^{\mathrm{T}}$ is of dimension 3×24 (assuming an eight-noded brick element) and is the equivalent of the vector $\mathbf{v}$ in (18.12).

Equation (18.31) can now be substituted into (18.28) so that:

$$\delta\mathbf{p}_l = \mathbf{T}\,\delta\mathbf{p} = [[\mathbf{Diag}\,\mathbf{E}^{\mathrm{T}}] + \mathrm{col}(\mathbf{E}^{\mathrm{T}}\mathbf{S}(\mathbf{x}^{j1}))\mathbf{V}^{\mathrm{T}}]\delta\mathbf{p} \tag{18.32}$$

and consequently, the global internal force vector, $\mathbf{q}_i = \mathbf{T}^{\mathrm{T}}\mathbf{q}_{li}$, can be expressed as

$$\mathbf{q}_i = \mathrm{col}(\mathbf{E}\mathbf{q}_{li}^j) - \mathbf{V}\mathrm{row}(\mathbf{S}(\mathbf{x}^{j1}))\mathrm{col}(\mathbf{E}\mathbf{q}_{li}^j) = \mathrm{col}(\bar{\mathbf{q}}_{li}^j) - \mathbf{V}\mathrm{row}(\mathbf{S}(\mathbf{x}^{j1}))\mathrm{col}(\bar{\mathbf{q}}_{li}^j) \tag{18.33}$$

As with the previous two-dimensional case, the terms following $\mathbf{V}$ in (18.33) represent rotational equilibrium equations (now three of them) for the element and will therefore vanish at equilibrium. Again as in the two-dimensional case, we will use this observation as a justification for ignoring the $\delta\mathbf{V}$ terms in the following derivation of the initial stress matrix. (It is, however, worth noting that while in the two-dimensional case, the full formulation (including terms from $\delta\mathbf{V}$) leads to a symmetric stiffness matrix [M2], this is not true of the three-dimensional formulation for which a non-symmetric tangent stiffness matrix results [M2, M3].)

As usual the tangent stiffness matrix is composed of a conventional term $\mathbf{T}^{\mathrm{T}}\mathbf{K}_l\mathbf{T}$ and an initial stress contribution, with the latter stemming from the differentiation of (18.33) with $\mathbf{q}_{li}$ fixed. This process leads to

$$\begin{aligned}\delta\mathbf{q}_i = \mathbf{T}^{\mathrm{T}}\mathbf{K}_l\mathbf{T}\,\delta\mathbf{p} &+ \mathrm{col}(\delta\mathbf{E}\mathbf{q}_{li}^j) - \mathbf{V}\mathrm{row}(\mathbf{S}(\delta\mathbf{x}^{j1}))\mathrm{col}(\mathbf{E}\mathbf{q}_{li}^j) \\ &- \mathbf{V}\mathrm{row}(\mathbf{S}(\mathbf{x}^{j1}))\mathrm{col}(\delta\mathbf{E}\mathbf{q}_{li}^j)\end{aligned} \tag{18.34}$$

With the aid of (18.27) and (18.31) we now obtain:

$$\mathbf{K}_{t\sigma} = -\mathrm{col}(\mathbf{S}(\bar{\mathbf{q}}_{li}^j))\mathbf{V}^{\mathrm{T}} + \mathbf{V}\mathrm{row}(\mathbf{S}(\bar{\mathbf{q}}_{li}^j)) + \mathbf{V}\mathrm{row}(\mathbf{S}(\mathbf{x}^{j1}))\mathrm{col}(\mathbf{S}(\bar{\mathbf{q}}_{li}^j))\mathbf{V}^{\mathrm{T}} \tag{18.35}$$

The first term is the transpose of the second term, but the third term is in general non-symmetric because the central 3×3 component can be written as

$$\sum \mathbf{S}(\mathbf{x}^{j1})\mathbf{S}(\bar{\mathbf{q}}_{li}^j) = \sum(\mathbf{x}^{j1}\bar{\mathbf{q}}_{li}^{j\mathrm{T}} - (\mathbf{x}^{j1\mathrm{T}}\bar{\mathbf{q}}_{li}^j)\mathbf{I}) \tag{18.36}$$

where use has been made of (16.86). The non-symmetric part of (18.36) is

$$\text{Non-sym} = \tfrac{1}{2}\sum(\mathbf{x}^{j1}\bar{\mathbf{q}}_{li}^{j\mathrm{T}} - \bar{\mathbf{q}}_{li}^j\mathbf{x}^{j1\mathrm{T}}) \tag{18.37}$$

However, as previously discussed, at equilibrium the term after V in the last term of (18.33) will be zero, i.e.

$$\mathbf{q} = \sum \mathbf{x}^{j1} \times \bar{\mathbf{q}}_{li}^j = \mathbf{0} \tag{18.38a}$$

and in addition:

$$\mathbf{S}(\mathbf{a}) = \sum \mathbf{S}(\mathbf{x}^{j1} \times \bar{\mathbf{q}}_{li}^j) = \sum(\mathbf{x}^{j1}\bar{\mathbf{q}}_{li}^{j\mathrm{T}} - \bar{\mathbf{q}}_{li}^j\mathbf{x}^{j1\mathrm{T}}) = \mathbf{0} \tag{18.38b}$$

where use has been made of (16.100). It follows that the non-symmetric term (18.37) will

vanish at equilibrium and we will be justified in using the symmetric part of the tangent stiffness matrix in (18.35) for our Newton–Raphson iterations so that:

$$\mathbf{K}_{t\sigma} = -\operatorname{col}(\mathbf{S}(\tilde{\mathbf{q}}_{fi}^{j}))\mathbf{V}^{\mathrm{T}} + \mathbf{V}\operatorname{row}(\mathbf{S}(\tilde{\mathbf{q}}_{fi}^{j})) + \mathbf{V}\operatorname{sym}\left(\sum\left(\mathbf{S}(\mathbf{x}^{j1})\mathbf{S}(\tilde{\mathbf{q}}_{fi}^{j})\right)\right)\mathbf{V}^{\mathrm{T}} \quad (18.39)$$

Numerical experiments support this contention and show that an excellent rate of convergence is achieved [M2, M3]. A theoretical justification has been given by Nour-Omid and Rankin [N1.17] who prove that a formulation which becomes symmetric at equilibrium will still exhibit 'quadratic convergence' if artificially symmetrised away from equilibrium.

18.4 A CO-ROTATIONAL APPROACH FOR A CURVED MEMBRANE USING FACET TRIANGLES

With a view to later work on shells, we will first consider a curved triangular membrane composed of simple constant strain triangles by means of facet approximation (Figure 18.5). Facet approximations to shells have been adopted by many authors (see [B1, C2, D1, H4, M6, Z1, Z1.13].

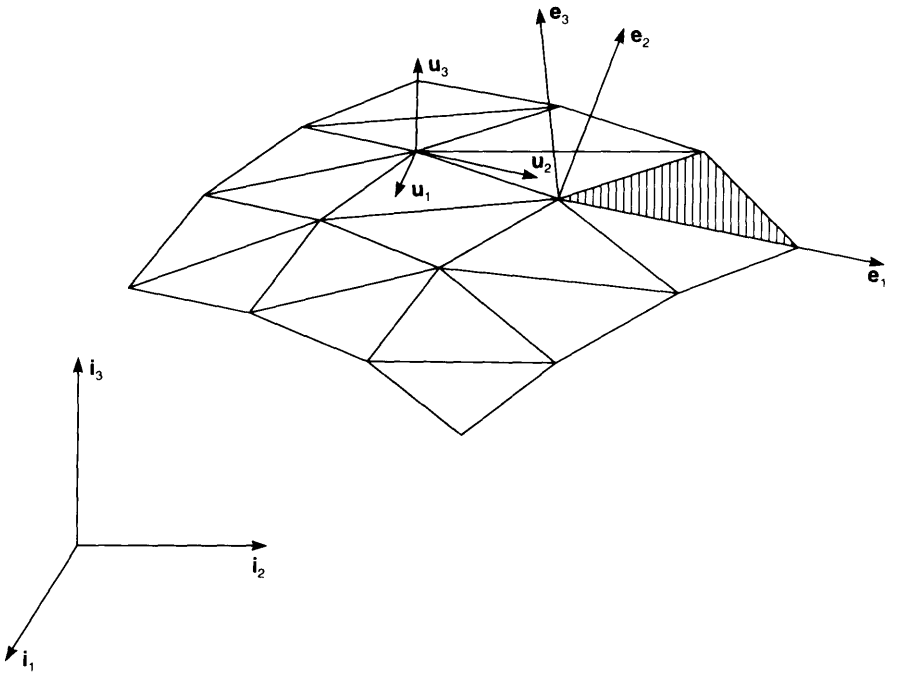

Figure 18.5 Triangular facet approximation to curved shell with first choice for local element frame ($\mathbf{e}_1$, $\mathbf{e}_2$, $\mathbf{e}_3$) and nodal surface triad $\mathbf{U}_s = (\mathbf{u}_1, \mathbf{u}_2, \mathbf{u}_3)$.

In the following, we will again choose the origin of the co-rotating system at node 1. The $\mathbf{e}_3$ vector is simply chosen as being orthogonal to the current facet (Figure 18.5). The simplest way to choose the two remaining vectors $\mathbf{e}_1$ and $\mathbf{e}_2$ would be to make one of them coincide with one of the current sides of the element so that:

$$\mathbf{e}_1 = \frac{\mathbf{x}_2 - \mathbf{x}_1}{\| \mathbf{x}_2 - \mathbf{x}_1 \|} = \frac{\mathbf{x}_{21}}{\| \mathbf{x}_{21} \|}; \qquad \mathbf{e}_3 = \frac{\mathbf{x}_{21} \times \mathbf{x}_{31}}{\| \mathbf{x}_{21} \| \, \| \mathbf{x}_{31} \|}; \qquad \mathbf{e}_2 = \mathbf{e}_3 \times \mathbf{e}_1 \tag{18.40}$$

In the initial configuration, the local initial nodal coordinates, $\mathbf{X}_l^j$, would then be computed with respect to this initial element frame and would be kept fixed as the co-rotating local initial coordinates. For the first predictor solution on the first increment, one could use the $\mathbf{E}$ matrix given by combining the $\mathbf{e}$ vectors in (18.40) and could ignore the $\mathbf{z}\mathbf{v}^{\mathrm{T}}$ term in (18.13) when forming the initial tangent stiffness matrix $\mathbf{K}_t = \mathbf{T}^{\mathrm{T}}\mathbf{K}_l\mathbf{T}$.

In the current configuration, with a view to possible later extensions to large strains, and also to produce a formulation that is independent of the nodal ordering, it is best to follow the approach of Sections 18.1 and 18.2. To this end, we could start with an initial set of current base vectors obtained from (18.40) in the current configuration and then use (18.2) to obtain intial values for the nodal displacements $\mathbf{d}_l^j$ at each of the nodes j and hence obtain initial estimates for the local nodal displacement vector $\mathbf{p}_l$. At which point the local displacements derivatives (4×1) can be obtained from (18.4) and hence the matrix equivalent $\mathbf{D}_l(2 \times 2)$. To obtain the new $\mathbf{e}_1$ and $\mathbf{e}_2$ with respect to the old ones (Figure 18.6) we can (via (18.23) and (18.24)) write:

$$\mathbf{U} = \mathbf{R}^{\mathrm{T}}\mathbf{F} = \begin{bmatrix} \cos\gamma & \sin\gamma \\ -\sin\gamma & \cos\gamma \end{bmatrix} [\mathbf{I} + \mathbf{D}_l] \tag{18.41}$$

so that the condition $\mathbf{U}(1,2) = \mathbf{U}(2,1)$ leads to

$$-\sin\gamma\left(1 + \left(\frac{\partial u}{\partial X}\right)_l\right) + \cos\gamma\left(\frac{\partial v}{\partial X}\right)_l = \cos\gamma\left(\frac{\partial u}{\partial Y}\right)_l + \sin\gamma\left(1 + \left(\frac{\partial v}{\partial Y}\right)_l\right) \tag{18.42}$$

from which we can obtain the angle γ and hence the new axes (Figure 18.6):

$$\begin{aligned} \mathbf{e}_{1\,\mathrm{new}} &= \cos\gamma\,\mathbf{e}_{1\,\mathrm{old}} + \sin\gamma\,\mathbf{e}_{2\,\mathrm{old}} \\ \mathbf{e}_{2\,\mathrm{new}} &= -\sin\gamma\,\mathbf{e}_{1\,\mathrm{old}} + \cos\gamma\,\mathbf{e}_{2\,\mathrm{old}} \end{aligned} \tag{18.43}$$

while the $\mathbf{e}_3$ vector is unaltered.

The local displacements can now be recomputed (via (18.2a)) using the new base vectors. In the future developments, we will not use the subscript 'new', but it will be implied whenever the base vectors are referred to. In order to proceed further, it is necessary to find an expression for the spin of the (new) base vectors. To this end, the key equations are

$$\begin{aligned} w_{l2} &= \mathbf{e}_3^{\mathrm{T}}\mathbf{x}_{21} = 0 \\ w_{l3} &= \mathbf{e}_3^{\mathrm{T}}\mathbf{x}_{31} = 0 \\ \Omega_{lm} &= \left(\frac{\partial u}{\partial Y} - \frac{\partial v}{\partial X}\right)_l = 0 \end{aligned} \tag{18.44}$$

The first two of the above equations (which are consistent with (18.2a) having noted

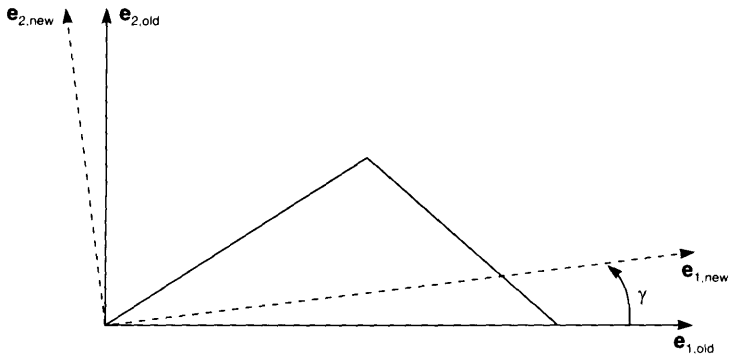

Figure 18.6 Modifying first-choice (old) element frame to new element frame.

that $Z_1 = Z_2 = Z_3 = 0$) ensure that the local base frame always passes through nodes 2 and 3 (as well as the origin at node 1). Differentiation of the first two of these equations leads to

$$\begin{aligned} \mathbf{e}_3^{\mathrm{T}}\delta\mathbf{d}_{21} - \mathbf{x}_{21}^{\mathrm{T}}(\mathbf{S}(\mathbf{e}_3)\delta\boldsymbol{\beta}) = 0 \\ \mathbf{e}_3^{\mathrm{T}}\delta\mathbf{d}_{31} - \mathbf{x}_{31}^{\mathrm{T}}(\mathbf{S}(\mathbf{e}_3)\delta\boldsymbol{\beta}) = 0 \end{aligned} \tag{18.45}$$

while differentiation of the last equation gives:

$$\delta\Omega_l = \sum \mathbf{a}_l^{j\mathrm{T}}\delta\mathbf{d}_l^j = 0 \tag{18.46}$$

where $\mathbf{a}_l^j$ and $\delta\mathbf{d}_l^j$ are here of dimension 2×1. With the aid of (18.28) we can obtain:

$$\delta\mathbf{d}_l^j = \begin{pmatrix} \mathbf{e}_1^{\mathrm{T}}\delta\mathbf{d}^j \\ \mathbf{e}_2^{\mathrm{T}}\delta\mathbf{d}^j \end{pmatrix} + \begin{pmatrix} \mathbf{e}_1^{\mathrm{T}}\mathbf{S}(\mathbf{x}^{j1})\delta\boldsymbol{\beta} \\ \mathbf{e}_2^{\mathrm{T}}\mathbf{S}(\mathbf{x}^{j1})\delta\boldsymbol{\beta} \end{pmatrix} \tag{18.47}$$

The combination of (18.46) and (18.47) provides one equation in the three unknown coefficients of $\delta\boldsymbol{\beta}$ while the two other equations are provided by (18.45). Hence we can use a similar procedure to that leading to (18.31) to obtain a relationship of the form:

$$\delta\boldsymbol{\beta} = \mathbf{V}^{\mathrm{T}}\delta\mathbf{p} \tag{18.48}$$

where for the current three-noded triangle, $\mathbf{V}^{\mathrm{T}}$ is of dimensions 3×9.

The transformation matrix $\mathbf{T}$ now takes precisely the same form as that previously given in (18.31) (although $\mathbf{T}$ is now of dimensions 9×9) while (18.33) again defines the global internal force vector and (18.39) defines the initial stress matrix.

18.5 A CO-ROTATIONAL APPROACH FOR A CURVED MEMBRANE USING QUADRILATERALS

Figure 18.7 illustrates the proposed procedure for obtaining a close fit to the curved surface (see also [R1.16]). Again as a starting-point, the initial $\mathbf{e}_1$ vector is chosen to lie

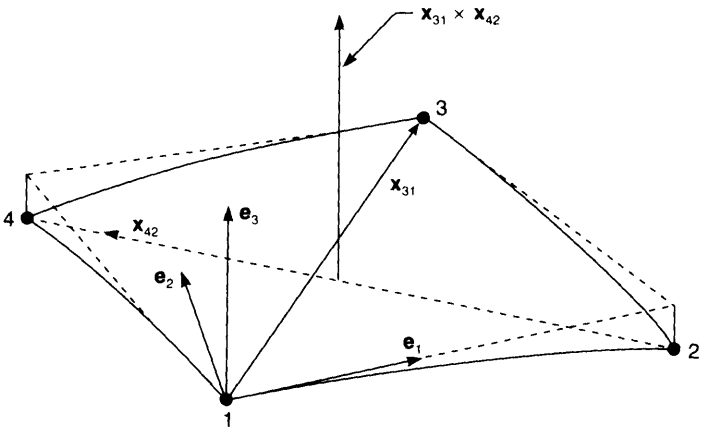

Figure 18.7 First-choice element frame for a curved quadrilateral.

(as closely as possible along a side). Hence the initial choice of base vectors is

$$\mathbf{e}_3 = \frac{\mathbf{x}_{13} \times \mathbf{x}_{24}}{\| \mathbf{x}_{13} \| \| \mathbf{x}_{24} \|}; \qquad \mathbf{e}_1 = \frac{\mathbf{x}_{21} - (\mathbf{x}_{21}^{\mathrm{T}} \mathbf{e}_3)\mathbf{e}_3}{\| \mathbf{x}_{21} - (\mathbf{x}_{21}^{\mathrm{T}} \mathbf{e}_3)\mathbf{e}_3 \|}; \qquad \mathbf{e}_2 = \mathbf{e}_3 \times \mathbf{e}_1 \tag{18.49}$$

As with the triangular element, a two-stage procedure is again applied with the second stage involving equations (18.41)–(18.43) (although we should now emphasise that the subscript l terms are really subscript lm, i.e. they are computed at the centroid of the element).

To obtain the current 3×12 spin matrix $\mathbf{V}^{\mathrm{T}}$, we again use the combination of (18.46) and (18.47) for one of the equations in the three components of $\delta\boldsymbol{\beta}$. For the other two, we first differentiate (18.49a) to obtain an equation of the form:

$$\delta \mathbf{e}_3 = \mathbf{A}\, \delta \mathbf{p} \tag{18.50}$$

where $\mathbf{A}$ is of dimension 3×12. However, we also know that:

$$\delta \mathbf{e}_3 = -\mathbf{S}(\mathbf{e}_3)\delta\boldsymbol{\beta} \tag{18.51}$$

so that

$$\mathbf{e}_1^{\mathrm{T}} \mathbf{A} \delta \mathbf{p} = -\mathbf{e}_1^{\mathrm{T}} \mathbf{S}(\mathbf{e}_3)\delta\boldsymbol{\beta} = \mathbf{e}_2^{\mathrm{T}} \delta\boldsymbol{\beta}$$

and

$$\mathbf{e}_2^{\mathrm{T}} \mathbf{A}\, \delta \mathbf{p} = -\mathbf{e}_2^{\mathrm{T}} \mathbf{S}(\mathbf{e}_3)\delta\boldsymbol{\beta} = -\mathbf{e}_1^{\mathrm{T}} \delta\boldsymbol{\beta} \tag{18.52}$$

provide the remaining two equations from which we can obtain (18.48) with $\mathbf{V}^{\mathrm{T}}$ now being of dimension 3×12. Apart from the different nature of the $\mathbf{V}$ matrix and the different number of nodes, the formation of the internal force vector and tangent stiffness matrix takes essentially the same form as it did for the three-noded facet membrane and again follows the continuum formulation in using (18.33) for $\mathbf{q}_i$ and (18.39) for $\mathbf{K}_{t\sigma}$.

18.6 A CO-ROTATIONAL SHELL FORMULATION WITH THREE ROTATIONAL DEGREES OF FREEDOM PER NODE

Figure 18.8 shows a faceted approximation for a shell with a typical surface triad, $\mathbf{U}_\theta$, and a typical element triad, $\mathbf{E}$ (drawn in relation to separate elements purely to avoid cluttering). Let us assume that these triads relate to the initial configuration and can therefore be found from the initial geometry of the shell. As a first stage, for each element, we conceptually relate these nodal triads to the element frame so that:

$$\mathbf{U}_e = \mathbf{U}_s[\mathbf{U}_s{}^T\mathbf{E}] = \mathbf{U}_s\bar{\mathbf{X}} \tag{18.53}$$

and hence in the initial configuration, $\mathbf{U}_e$ is simply $\mathbf{E}$. In the deformed configuration, we would again have:

$$\mathbf{U}_e = \mathbf{U}_s\bar{\mathbf{X}} \tag{18.54}$$

where $\bar{\mathbf{X}}$ is fixed and computed for the original configuration from $\mathbf{U}_e = \mathbf{U}_s{}^T\mathbf{E}$. In the deformed configuration, of course, $\mathbf{U}_e$ will not (as in the original configuration) coincide with the element $\mathbf{E}$ frame.

The membrane contribution to the element will be assumed to be identical to that of Section 18.4 as will the procedure for choosing the current $\mathbf{E}$ frame. Given some iterative pseudo-vector change $\delta\boldsymbol{\alpha}^j$ at node j (say, from the structural Newton–Raphson iterations), we can update $\mathbf{U}_s$ according to

$$\mathbf{U}_\theta = \mathbf{R}(\delta\alpha)\mathbf{U}_\theta \tag{18.55}$$

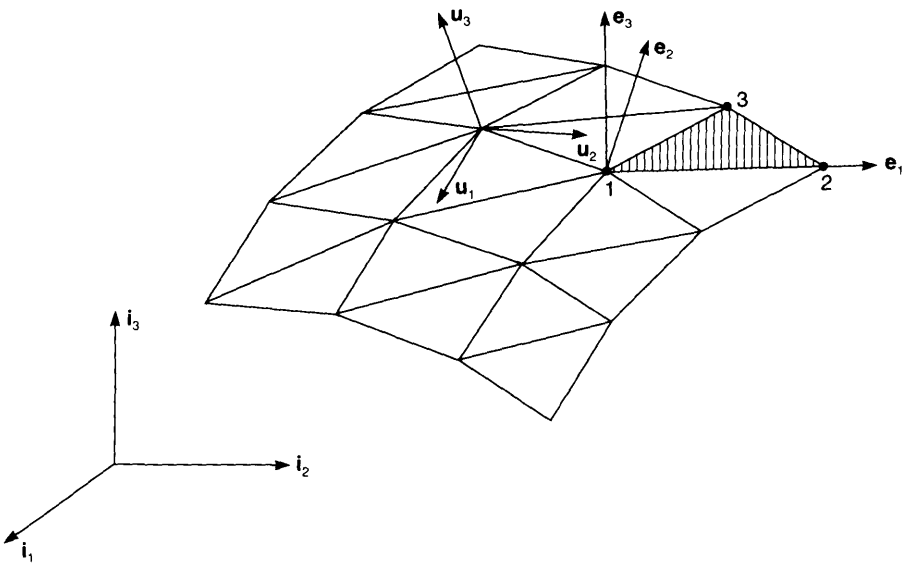

Figure 18.8 Triangular facet approximation to curved shell with first choice for local element frame ($\mathbf{e}_1, \mathbf{e}_2, \mathbf{e}_3$ and nodal surface triad $\mathbf{U}_s = (\mathbf{u}_1, \mathbf{u}_2, \mathbf{u}_3)$

with $\mathbf{R}(\delta\boldsymbol{\alpha})$ being computed from the Rodrigues formula (16.22). Given the new $\mathbf{U}_e$, the new $\mathbf{U}_e$ can be computed from (18.54) and (16.120) can now be used to obtain the local rotations, $\boldsymbol{\theta}_l$ (a the particular node) so that:

$$\mathbf{S}(\boldsymbol{\theta}_l) = \frac{\mathbf{E}^{\mathrm{T}}\mathbf{U}_e - \mathbf{U}_e^{\mathrm{T}}\mathbf{E}}{2} \tag{18.56}$$

In the following, we will drop the subscript e on $\mathbf{U}$ (and its components), but the subscript will be implied so that from (18.56) we can obtain:

$$2\boldsymbol{\theta}_l^j = \begin{bmatrix} \mathbf{e}_3^{\mathrm{T}}\mathbf{u}_2 - \mathbf{u}_3^{\mathrm{T}}\mathbf{e}_2 \\ \mathbf{e}_1^{\mathrm{T}}\mathbf{u}_3 - \mathbf{u}_1^{\mathrm{T}}\mathbf{e}_3 \\ \mathbf{e}_2^{\mathrm{T}}\mathbf{u}_1 - \mathbf{u}_2^{\mathrm{T}}\mathbf{e}_1 \end{bmatrix}^j \tag{18.57a}$$

For the virtual work, we will require the variation of (18.57a) which gives:

$$2\delta\boldsymbol{\theta}_l^j = \mathbf{E}^* \operatorname{col}\mathbf{S}(\mathbf{u}_k)^j \delta\boldsymbol{\alpha}^j - \mathbf{U}^{*j} \operatorname{col}\mathbf{S}(\mathbf{e}_k)\mathbf{V}^{\mathrm{T}}\delta\mathbf{p}_t \tag{18.57b}$$

where $\mathbf{p}_t$ contains the translational nodal variables and

$$\mathbf{E}^* = \begin{bmatrix} \mathbf{0}^{\mathrm{T}} & -\mathbf{e}_3^{\mathrm{T}} & \mathbf{e}_2^{\mathrm{T}} \\ \mathbf{e}_3^{\mathrm{T}} & \mathbf{0}^{\mathrm{T}} & -\mathbf{e}_1^{\mathrm{T}} \\ -\mathbf{e}_2^{\mathrm{T}} & \mathbf{e}_1^{\mathrm{T}} & \mathbf{0}^{\mathrm{T}} \end{bmatrix}$$

$$\mathbf{U}^{*j} = \begin{bmatrix} \mathbf{0}^{\mathrm{T}} & -\mathbf{u}_3^{\mathrm{T}} & \mathbf{u}_2^{\mathrm{T}} \\ \mathbf{u}_3^{\mathrm{T}} & \mathbf{0}^{\mathrm{T}} & -\mathbf{u}_1^{\mathrm{T}} \\ -\mathbf{u}_2^{\mathrm{T}} & \mathbf{u}_1^{\mathrm{T}} & \mathbf{0}^{\mathrm{T}} \end{bmatrix}^j \tag{18.58}$$

while

$$\operatorname{col}\mathbf{S}(\mathbf{e}_k) = \begin{bmatrix} \mathbf{S}(\mathbf{e}_1) \\ \mathbf{S}(\mathbf{e}_2) \\ \mathbf{S}(\mathbf{e}_3) \end{bmatrix}; \qquad \operatorname{col}\mathbf{S}(\mathbf{u}_k)^j = \begin{bmatrix} \mathbf{S}(\mathbf{u}_1) \\ \mathbf{S}(\mathbf{u}_2) \\ \mathbf{S}(\mathbf{u}_3) \end{bmatrix}^j \tag{18.59}$$

The part of the global internal force vector stemming from the 'rotational local forces', $\mathbf{q}_{li\mathrm{r}}$ is now obtained via the usual equivalence of virtual work in the two systems. Once this process is combined with the similar procedure for the translational internal forces, $\mathbf{q}_{li\mathrm{c}}$, (previously just $\mathbf{q}_{li}$ in (18.33)), we obtain:

$$\begin{aligned} \mathbf{q}_{i\mathrm{t}} &= \operatorname{col}(\mathbf{E}\mathbf{q}_{li\mathrm{t}}^j) - \mathbf{V}\left(\sum_j (\mathbf{S}(\mathbf{x}^{j1})\bar{\mathbf{q}}_{li\mathrm{t}}^j - \tfrac{1}{2}(\operatorname{row}\mathbf{S}(\mathbf{e}_k)\mathbf{U}^{*j\mathrm{T}}\mathbf{q}_{li\mathrm{r}}^j))\right) \\ &= \operatorname{col}(\bar{\mathbf{q}}_{li\mathrm{t}}^j) - \mathbf{V}\left(\sum_j (\mathbf{S}(\mathbf{x}^{j1})\bar{\mathbf{q}}_{li\mathrm{t}}^j - \tfrac{1}{2}(\operatorname{row}\mathbf{S}(\mathbf{e}_k)\mathbf{U}^{*j\mathrm{T}}\mathbf{q}_{li\mathrm{r}}^j))\right) \end{aligned} \tag{18.60}$$

Here, the first two terms are taken directly from (18.33) while the last term stems from the local rotational virtual work:

$$V_{\mathrm{r}} = \sum \mathbf{q}_{li\mathrm{r}}^{j\mathrm{T}} \delta\boldsymbol{\theta}_l^j \tag{18.61}$$

As in the previous developments, the terms following the $\mathbf{V}$ vector represent three rotational equilibrium equations for the element and will therefore vanish at equilibrium.

Stemming from the first term in (18.57b), we have global 'rotational forces' at each node j of the form:

$$\mathbf{q}_{\mathrm{ir}}^{j} = -\tfrac{1}{2}\,\mathrm{row}\,\mathbf{S}(\mathbf{u}_k)^j\mathbf{E}^{*\mathrm{T}}\mathbf{q}_{lir}^{j} = -\tfrac{1}{2}\,\mathrm{row}\,\mathbf{S}(\mathbf{u}_k)^j \begin{bmatrix} \mathbf{q}_{lir1}^{e} \\ \mathbf{q}_{lir2}^{e} \\ \mathbf{q}_{lir3}^{e} \end{bmatrix}^j \tag{18.62}$$

For the initial stress part of the tangent stiffness matrix, the translational-translational terms due to $\mathbf{q}_{lit}$ have already been given in (18.35) (where the current $\mathbf{q}_{lit}$ were simply $\mathbf{q}_{li}$). From (18.60), we now have an additional contribution stemming from:

$$\text{term} = \tfrac{1}{2}\mathbf{V}\sum_j (\mathrm{row}\,\mathbf{S}(\delta\mathbf{e}_k)\mathbf{U}^{*j\mathrm{T}}\mathbf{q}_{lir}^{j}) = \tfrac{1}{2}\mathbf{V}\sum_j \left(\mathrm{row}\,\mathbf{S}(\delta\mathbf{e}_k)\begin{pmatrix} \mathbf{q}_{lir1}^{u} \\ \mathbf{q}_{lir2}^{u} \\ \mathbf{q}_{lir3}^{u} \end{pmatrix}^j\right) \tag{18.63}$$

which gives an additional contribution of the form:

$$\mathbf{K}_{t\sigma}(t,t) = \tfrac{1}{2}\mathbf{V}\sum_j\sum_k \underset{k}{\mathrm{sum}}\,\mathbf{S}(\mathbf{q}_{lirk}^{uj})\mathbf{S}(c_k)\mathbf{V}^{\mathrm{T}} \tag{18.64}$$

This term can be combined with the last term in (18.35) to give a contribution of the form $\mathbf{VZV}^{\mathrm{T}}$, where following previous arguments, the $\mathbf{Z}$ term may be symmetrised because it will become symmetric at equilibrium when the term following the matrix $\mathbf{V}$ in (18.60) vanishes.

For the term coupling the translational and rotational variables, the variation of (18.60) leads to a term

$$\text{term} = \tfrac{1}{2}\mathbf{V}\left(\sum_j (\mathrm{row}\,\mathbf{S}(\mathbf{e}_k)\delta\mathbf{U}^{*j\mathrm{T}}\mathbf{q}_{lir}^{j})\right) \tag{18.65}$$

which in turn leads to a contribution coupling the translational forces to the rotational variables at node j of the form:

$$\mathbf{K}_{t\sigma}(t,\alpha^j) = \tfrac{1}{2}\mathbf{V}\,\mathrm{row}\,\mathbf{S}(\mathbf{e}_k)\begin{bmatrix} -\mathbf{q}_{lir}(2)\mathbf{S}(\mathbf{u}_3) & +\mathbf{q}_{lir}(3)\mathbf{S}(\mathbf{u}_2) \\ \mathbf{q}_{lir}(1)\mathbf{S}(\mathbf{u}_3) & -\mathbf{q}_{lir}(3)\mathbf{S}(\mathbf{u}_1) \\ -\mathbf{q}_{lir}(1)\mathbf{S}(\mathbf{u}_2) & +\mathbf{q}_{lir}(2)\mathbf{S}(\mathbf{u}_1) \end{bmatrix}^j \tag{18.66}$$

From the term involving the variation of (18.62) with:

$$\text{term} = -\tfrac{1}{2}\mathrm{row}\,\mathbf{S}(\mathbf{u}_k)\delta\mathbf{E}^{*\mathrm{T}}\mathbf{q}_{lir}^{j} \tag{18.67}$$

we obtain:

$$\mathbf{K}_{t\sigma}(\alpha^j,t) = -\tfrac{1}{2}\mathrm{row}\,\mathbf{S}(\mathbf{u}_k)\begin{bmatrix} -\mathbf{q}_{lir}(2)\mathbf{S}(\mathbf{e}_3) & +\mathbf{q}_{lir}(3)\mathbf{S}(\mathbf{e}_2) \\ \mathbf{q}_{lir}(1)\mathbf{S}(\mathbf{e}_3) & -\mathbf{q}_{lir}(3)\mathbf{S}(\mathbf{e}_1) \\ -\mathbf{q}_{lir}(1)\mathbf{S}(\mathbf{e}_2) & +\mathbf{q}_{lir}(2)\mathbf{S}(\mathbf{e}_1) \end{bmatrix}^j \mathbf{V}^{\mathrm{T}} \tag{18.68}$$

which can be shown to be the transpose of (18.66).

Finally, the rotational–rotational terms are obtained from the term involving the variation of (18.62) with:

$$\text{term} = \tfrac{1}{2}\mathrm{row}\,\mathbf{S}(\delta\mathbf{u}_k)^j\mathbf{E}^{*\mathrm{T}}\mathbf{q}_{lir}^{j} = -\tfrac{1}{2}\mathrm{row}\,\mathbf{S}(\delta\mathbf{u}_k)^j \begin{bmatrix} \mathbf{q}_{lir1}^{e} \\ \mathbf{q}_{lir2}^{e} \\ \mathbf{q}_{lir3}^{e} \end{bmatrix}^j \tag{18.69}$$

from which we obtain:

$$\mathbf{K}_{t\sigma}(\boldsymbol{\alpha}^j, \boldsymbol{\alpha}^j) = -\tfrac{1}{2}\sum_k \mathbf{S}(\mathbf{q}^e_{\text{lirk}})^j \mathbf{S}(\mathbf{u}_k)^j \tag{18.70}$$

This 3×3 submatrix is in general non-symmetric. However (for conservative loadings), we can probably justify taking the symmetric part by again resorting to the argument of a recovery of symmetry at equilibrium. However, a proof of such a contention would now be more complex as it would involve equilibrium with terms such as (18.62) now being summed over the element contributions to a particular node (as in Section 17.4.3).

At the beginning of this section, we specifically considered a triangular facet approximation (Figure 18.8). However, the developments could equally be applied to a quadrilateral-based facet approximation using the procedure of Section 18.4. Indeed, the same equations would apply although j would now range from one to four. In addition, there is no reason why the element level computations should be restricted to a facet. They could instead involve a shallow shell formulation. In these circumstances, it would be necessary to revise the procedure discussed at the beginning of this section to set up the element nodal frame, $\mathbf{U}_e$ from the surface nodal frame $\mathbf{U}_s$. Instead we could obtain the initial value of the $\mathbf{U}_e$ frame by rotating the initial element $\mathbf{E}$ frame through the vector angle, γ between $\mathbf{e}_3$ and $\mathbf{u}_{s3}$ where

$$\gamma = \cos^{-1}(\mathbf{e}_3^{\mathrm{T}}\mathbf{u}_{s3})\frac{\mathbf{e}_3 \times \mathbf{u}_{s3}}{\|\mathbf{e}_3 \times \mathbf{u}_{s3}\|} \tag{18.71a}$$

so that initially,

$$\mathbf{U}_e = \mathbf{R}(\gamma)\mathbf{E} \tag{18.71b}$$

with $\mathbf{R}(\gamma)$ being obtain via the Rodrigues formula (16.22). The initial local rotations could then be computed from (18.57a). In addition, the matrix $\bar{\mathbf{X}}$ of (18.54) could be computed in the initial configuration as $\bar{\mathbf{X}} = \mathbf{U}_e\mathbf{U}_s^{\mathrm{T}}$ and subsequently used in the current configuration in conjunction with (18.54) to obtain $\mathbf{U}_e$ from $\mathbf{U}_s$. It is worth re-emphasising that from (18.57a) onwards, the expressions for $\mathbf{U}$ have an implied subscript e (see the text below (18.56)).

Before leaving this section, it is worth mentioning that the formulation at the local element level can itself be non-linear. The resulting formulation was discussed in Section 17.1.5 for co-rotational beams and a very similar procedure can be applied for shells.

18.7 A CO-ROTATIONAL FACET SHELL FORMULATION BASED ON MORLEY'S TRIANGLE

As discussed in the Introduction to this chapter, the previous formulation (Section 18.6) has some serious drawbacks because of the need for a drilling rotation at the local element level. An alternative is to use a rotation about an element side as originally applied in a linear context by Morely [M4]. The following large-deformation formulation is closely related to that originally given by Peng and Crisfield [P2] and Crisfield and Peng [C9.14]. However, we now adopt the general framework originally developed for continuum elements and the resulting formulation turns out to be much neater.

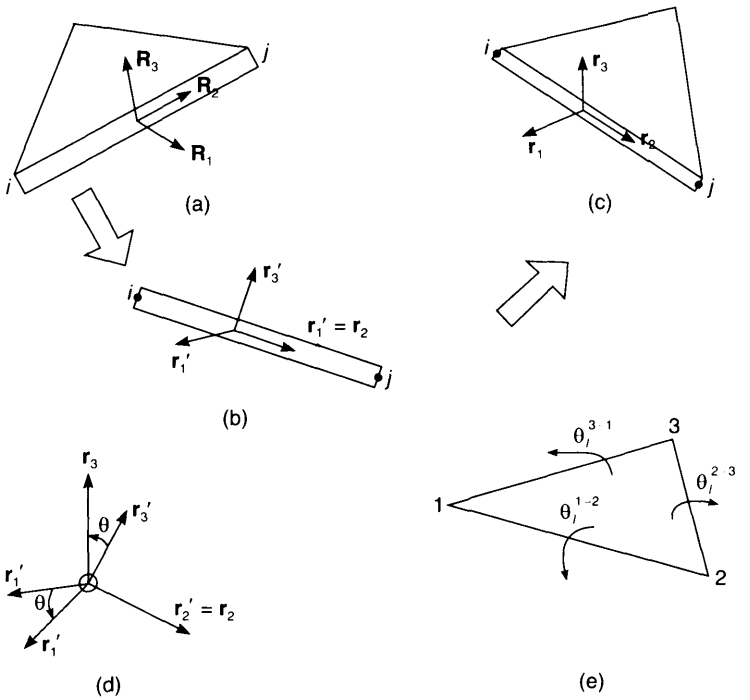

Figure 18.9 'Rotational variables and triads' for use with Morley's triangle. (a) Initial mid-side triad ($\mathbf{R}_1$, $\mathbf{R}_2$, $\mathbf{R}_3$) for side *ji* (initial configuration; (b) intermediate mid-side triad ($\mathbf{r}'_1$, $\mathbf{r}'_2$, $\mathbf{r}'_3$) in current configuration; (c) final mid-side triad in current configuration; (d) global mid-side rotation θ; (e) local mid-side rotation θ_l.

The element frame and equivalent spin matrix, $\mathbf{V}^{\mathrm{T}}$ can be taken to be identical to that for the facet membrane of Section 18.4. For the mid-side rotational variables, we will suppose a current triad composed of $\mathbf{r}_1, \mathbf{r}_2$ and $\mathbf{r}_3$ (Figure 18.9(c)) with $\mathbf{r}_2$ lying along a side with node *j* at the 'front' of $\mathbf{r}_2$ and node *i* at the 'tail'. For a simple facet formulation, the initial side triad $\mathbf{R}_1, \mathbf{R}_2$ and $\mathbf{R}_3$ can be found with $\mathbf{R}_3$ coinciding with the initial value of $\mathbf{e}_3$ (i.e. being perpendicular to the plane of the initial facet). To obtain the equivalent current triad, we first obtain $\mathbf{r}_2$ from:

$$\mathbf{r}_2 = \frac{\mathbf{x}_{ji}}{\| \mathbf{x}_{ji} \|} \tag{18.72}$$

and then rotate the initial triad $\mathbf{R}_1$–$\mathbf{R}_3$ in the plane formed by $\mathbf{R}_2$ and $\mathbf{r}_2$ through the vector angle:

$$\gamma = \cos^{-1}(\mathbf{R}_2^{\mathrm{T}}\mathbf{r}_2)\frac{\mathbf{R}_2 \times \mathbf{r}_2}{\| \mathbf{R}_2 \times \mathbf{r}_2 \|} \tag{18.73}$$

As a result of this exercise, the initial mid-side triad $\mathbf{R}_1$–$\mathbf{R}_3$ becomes the triad $\mathbf{r}'_1$–$\mathbf{r}'_3$ (Figure 18.9b) where $\mathbf{r}'_2 = \mathbf{r}_2$ but, in general, $\mathbf{r}'_1 \neq \mathbf{r}_1$ and $\mathbf{r}'_3 \neq \mathbf{r}_3$.

In order to reach the final configuration with the mid-side triad of $\mathbf{r}_1$–$\mathbf{r}_3$, we now apply the (positive clockwise) global rotation, θ, about the $\mathbf{r}_2 = \mathbf{r}'_2$ axis. This leads to the relationships:

$$\mathbf{r}_1 = \mathbf{r}'_1 \cos\theta - \mathbf{r}'_3 \sin\theta \tag{18.74a}$$

$$\mathbf{r}_2 = \mathbf{r}'_2 \tag{18.74b}$$

$$\mathbf{r}_3 = \mathbf{r}'_1 \sin\theta + \mathbf{r}'_3 \cos\theta \tag{18.74c}$$

Having computed the triad, $\mathbf{r}_1$–$\mathbf{r}_3$, the current (clockwise) local mid-side rotations (Figure 18.9e) can be obtained using:

$$\sin\theta_l = -\mathbf{e}_3^{\mathrm{T}}\mathbf{r}_1 \tag{18.75}$$

At this stage, we should note that the $\mathbf{r}'$ triad can be computed from:

$$[\mathbf{r}'_1, \mathbf{r}'_2, \mathbf{r}'_3] = \mathbf{R}(\gamma)[\mathbf{R}_1, \mathbf{R}_2, \mathbf{R}_3] \tag{18.76}$$

where $\mathbf{R}(\gamma)$ is obtained from the Rodrigues formula (16.22) or as an alternative equivalent form (see (16.107)):

$$\mathbf{r}'_1 = \mathbf{R}_1 - \frac{b_1}{1+b_2}(\mathbf{R}_2 + \mathbf{r}_2) \tag{18.77a}$$

$$\mathbf{r}'_2 = \mathbf{r}_2 \tag{18.77b}$$

$$\mathbf{r}'_3 = \mathbf{R}_3 - \frac{b_3}{1+b_2}(\mathbf{R}_2 + \mathbf{r}_2) \tag{18.77c}$$

where

$$b_k = \mathbf{R}_k^{\mathrm{T}}\mathbf{r}_2 \tag{18.78}$$

With a view to the use of virtual work, we require the variation of (18.75) so that:

$$\delta\theta_l = \frac{-1}{\cos\theta_l}(\mathbf{e}_3^{\mathrm{T}}\delta\mathbf{r}_1 + \delta\mathbf{e}_3^{\mathrm{T}}\mathbf{r}_1) \tag{18.79}$$

The change in the $\mathbf{e}_3$ vector is simply:

$$\delta\mathbf{e}_3 = -\mathbf{S}(\mathbf{e}_3)\delta\boldsymbol{\beta} = -\mathbf{S}(\mathbf{e}_3)\mathbf{V}^{\mathrm{T}}\delta\mathbf{p}_t \tag{18.80}$$

where we have used (18.48) for $\delta\boldsymbol{\beta}$ and $\delta\mathbf{p}_t$ relates to the translational nodal variables. With a view to the insertion of (18.80) into (18.79), we also note that:

$$\mathbf{e}_3 \times \mathbf{r}_1 = \mathbf{S}(\mathbf{e}_3)\mathbf{r}_1 = \mathbf{r}_2 \cos\theta_l \tag{18.81}$$

and hence for the last term in (18.79), we have:

$$\frac{-1}{\cos\theta_l}(\delta\mathbf{e}_3^{\mathrm{T}}\mathbf{r}_1) = -\mathbf{r}_2^{\mathrm{T}}\delta\boldsymbol{\beta} = -\mathbf{r}_2^{\mathrm{T}}\mathbf{V}^{\mathrm{T}}\delta\mathbf{p}_t \tag{18.82}$$

With a view to the first term in (18.79), differentiation of (18.74a) and (18.77) leads, after

some manipulation, to

$$\delta\mathbf{r}_1 = \frac{1}{(1+b_2)}[-(\mathbf{R}_2+\mathbf{r}_2)\mathbf{r}_1^{\mathrm{T}} + (\mathbf{R}_2^{\mathrm{T}}\mathbf{r}_1)\mathbf{I}]\delta\mathbf{r}_2 - \mathbf{r}_3\delta\theta$$

$$= \frac{-1}{(1+b_2)}\mathbf{S}(\mathbf{r}_1)\mathbf{S}(\mathbf{R}_2+\mathbf{r}_2)\delta\mathbf{r}_2 - \mathbf{r}_3\delta\theta \tag{18.83}$$

where the scalar b_2 comes from (18.78) and use has been made of (16.86). Substitution from (18.83) and (18.81) into (18.79) leads to

$$\delta\theta_l = \delta\theta + \frac{1}{(1+b_2)}\mathbf{r}_2^{\mathrm{T}}\mathbf{S}(\mathbf{R}_2+\mathbf{r}_2)\delta\mathbf{r}_2 - \mathbf{r}_2^{\mathrm{T}}\mathbf{V}^{\mathrm{T}}\delta\mathbf{p}_{\mathrm{t}} \tag{18.84}$$

To proceed further we can either express $\delta\mathbf{r}_2$ via:

$$\delta\mathbf{r}_2 = -\mathbf{S}(\mathbf{r}_2)\delta\boldsymbol{\beta} = -\mathbf{S}(\mathbf{r}_2)\mathbf{V}^{\mathrm{T}}\delta\mathbf{p}_{\mathrm{t}} \tag{18.85a}$$

which is strictly only valid for small strains or (see (17.21) and (17.22)) via:

$$\delta\mathbf{r}_2 = \frac{1}{s}[\mathbf{I} - \mathbf{r}_2\mathbf{r}_2^{\mathrm{T}}]\delta\mathbf{d}_{ji} \tag{18.85b}$$

where s is the current length of the side along which $\mathbf{r}_2$ lies.

While the former might seem the most direct, it turns out that there are some advantages in using the latter so that substitution into (18.84) leads to

$$\delta\theta_l = \delta\theta - \frac{1}{(1+b_2)s}(\mathbf{R}_2\times\mathbf{r}_2)^{\mathrm{T}}\delta\mathbf{d}_{ji} - \mathbf{r}_2^{\mathrm{T}}\mathbf{V}^{\mathrm{T}}\delta\mathbf{p}_{\mathrm{t}} \tag{18.86}$$

By equating the virtual work in the local and global systems, we now arrive at the translational internal forces as:

$$\mathbf{q}_{\mathrm{it}} = \mathrm{col}(\bar{\mathbf{q}}_{l\mathrm{it}}^{j}) - \mathbf{V}\left(\sum_j(\mathbf{S}(\mathbf{x}^{j1})\bar{\mathbf{q}}_{l\mathrm{it}}^{j}) + \sum_k(q_{l\mathrm{ir}}^{k}\mathbf{r}_2^{k})\right) + \mathbf{q}_{\mathrm{it}}^{*} \tag{18.87}$$

where the first two terms are related to local translations and take the same form as in (18.60), while the last two terms stem from the 'rotational local virtual work' via (18.86). In (18.87), the sum j is over the corner nodes and the sum k is over the mid-side nodes. For a particular corner node j, the contribution to $\mathbf{q}_{\mathrm{it}}^{*}$ (which stems from the second term in (18.86)) is

$$\mathbf{q}_{\mathrm{it}}^{*j} = \left(q_{l\mathrm{ir}}\frac{1}{(1+b_2)s}(\mathbf{R}_2\times\mathbf{r}_2)\right)^{j-} - \left(q_{l\mathrm{ir}}\frac{1}{(1+b_2)s}(\mathbf{R}_2\times\mathbf{r}_2)\right)^{j+} \tag{18.88}$$

where $j-$ is the mid-side node clockwise behind the node and $j+$ is the mid-side node clockwise ahead of the corner node.

For the 'rotational internal forces', using (18.86), the equivalence of virtual work in the local and global systems leads to the trivial relationship:

$$q_{\mathrm{ir}} = q_{l\mathrm{ir}} \tag{18.89}$$

at each of the mid-side nodes.

It is now useful to study the equilibrium relationships in (18.87) and (18.88). As in the previous developments, the terms following the $\mathbf{V}$ matrix in (18.87) can be identified as

three rotational equilibrium equations for the element and will therefore vanish at equilibrium. Noting the results in (18.89), if no external moments are applied, any particular mid-side local internal moment will, via (18.88) contribute terms to the translational forces of an adjacent corner node which will be exactly cancelled by the equivalent contributions from the adjacent element. Hence we can argue that at the structural level the $\mathbf{q}_{it}^{*}$ terms in (18.87) and (18.88) will vanish at equilibrium. These terms take the form of scalar, involving the local q_{lir} terms which will be zero, multiplied by terms which we would normally vary for the initial stress matrix. However, because the scalar will become zero at equilibrium, we can argue that there is no need to apply such variations. (It is possible to include all terms [P2], but the resulting equations are rather complex.)

The translational–translational terms in $\mathbf{K}_{t\sigma}$ due to $\mathbf{q}_{lit}$ in (18.87) have already been given in (18.35) (although the current $\mathbf{q}_{lit}$ were in (18.35) simply referred to as $\mathbf{q}_{li}$). From (18.87), we now have an additional contribution stemming from:

$$\text{term} = -\mathbf{V}\left(\sum_k (q_{lir}^k \delta \mathbf{r}_2^k)\right) \tag{18.90a}$$

which, using $\delta \mathbf{r}_2$ from (18.85a) gives an additional contribution of the form:

$$\mathbf{K}_{t\sigma}(t, t) = \mathbf{V}\sum_k (q_{lir}^k \mathbf{S}(\mathbf{r}_2^k))\mathbf{V}^{\mathrm{T}} \tag{18.90b}$$

When this term is combined with the last term in (18.35), it can be expressed in the form $\mathbf{VZV}^{\mathrm{T}}$ where following previous arguments, the $\mathbf{Z}$ term may be symmetrised because it will become symmetric at equilibrium when the term following $\mathbf{V}$ in (18.87) vanishes. Indeed, in these circumstances, because $\mathbf{S}(\mathbf{r}_2^k)$ is skew-symmetric, the term in (18.90b) vanishes.

The previous developments have followed the work in [P2] and have used a 'total formulation' in which the current mid-side triad $[\mathbf{r}_1, \mathbf{r}_2, \mathbf{r}_3]$ are up-dated directly from the initial triads $[\mathbf{R}_1, \mathbf{R}_2, \mathbf{R}_3]$ via the total global rotation, θ. Numerical experiments have shown that a more robust formulation can be devised by resetting $\mathbf{R}_{1\ 3} = \mathbf{r}_{1\ 3}$ and $\theta = 0$ at the end of each increment. The key equations remain unaltered and, in particular, the local rotations are still computed from (18.75). Van Keulen *et al.* [V1] go one stage further and apply this update at the end of each iteration. As a consequence (with $\mathbf{R}_2 = \mathbf{r}_2$), some of the previous expressions can be simplified further. These authors also include second-order memberane terms due to the curvature which effectively involves adding local shallow shell terms (see Section 17.1.5).

Numerical experiments have been conducted using the current formulation. These have shown that, for small strains, we achieve effectively the same solutions and convergence rate as those obtained via the earlier formulation [P2] although the current formulation is much simpler [C6].

18.8 A CO-ROTATIONAL SHELL FORMULATION WITH TWO ROTATIONAL DEGREES OF FREEDOM PER NODE

As indicated in the introduction to this chapter, two rotational variables would be used for those nodes associated with a smooth part of the shell while three rotational

variables (using the procedure of Section 18.6) would be used for those nodes associated with a branched junction.

Let us assume that in the initial configuration, we know the unit normal surface vector $\mathbf{u}_3$ (Figure 18.8) as well as the element triad $\mathbf{E} = [\mathbf{e}_1, \mathbf{e}_2, \mathbf{e}_3]$. In which case we can approximate the initial local rotations as

$$\theta_{I2} = -\mathbf{u}_3^{\mathrm{T}}\mathbf{e}_2; \qquad \theta_{I1} = \mathbf{u}_3^{\mathrm{T}}\mathbf{e}_1 \tag{18.91}$$

The directions $\mathbf{u}_1$ and $\mathbf{u}_2$ can be arbitrarily chosen with, say, $\mathbf{u}_2$ lying above a particular side. For the first load increment, we will keep this surface triad fixed as $\mathbf{U}_0$ (o for old) and will allow two rotations α_1 about $\mathbf{u}_{1o}$ and α_2 about $\mathbf{u}_{2o}$. We will now be concerned with the updating, within the increment, of $\mathbf{u}_{3o}$ to $\mathbf{u}_{3n}$. To this end we will operate in fixed surface coordinates (with components along $\mathbf{u}_{1o}$, $\mathbf{u}_{2o}$ and $\mathbf{u}_{3o}$). We will use a superimposed bar to denote that quantities are written with respect to these axes. Then we have:

$$\bar{\mathbf{u}}_{3o} = \begin{bmatrix} 0 \\ 0 \\ 1 \end{bmatrix} \tag{18.92}$$

and (see Figure 18.10)

$$\bar{\mathbf{u}}_{3n} = \cos\alpha\,\bar{\mathbf{u}}_{3o} + \frac{\sin\alpha}{\alpha}\boldsymbol{\alpha} \times \bar{\mathbf{u}}_{3o} \tag{18.93}$$

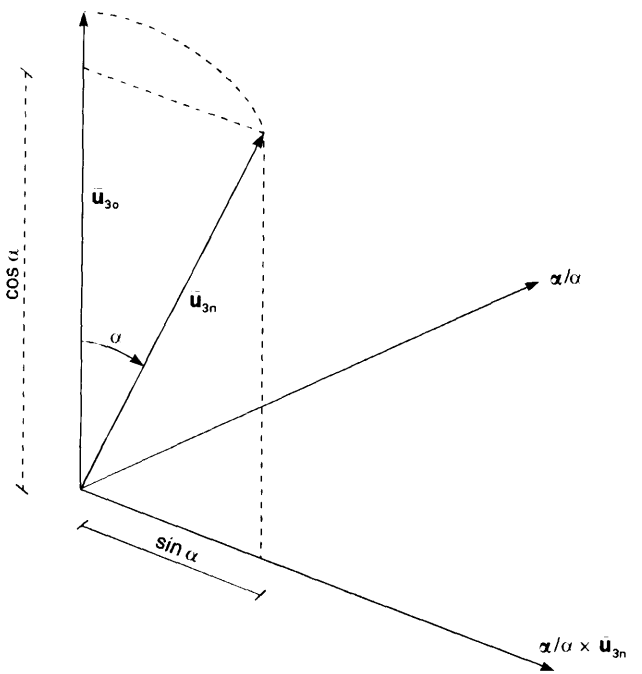

Figure 18.10 Rotating $\bar{\mathbf{u}}_{3o}$ to $\bar{\mathbf{u}}_{3n}$.

with

$$\boldsymbol{\alpha}^1 = (\alpha_1, \alpha_2, 0); \qquad \alpha = (\alpha_1^2 + \alpha_2^2)^{1/2} \tag{18.94}$$

With respect to the usual fixed cartesian coordinate frame, we can then compute:

$$\mathbf{u}_{3n} = \mathbf{U}_o \bar{\mathbf{u}}_{3n} \tag{18.95}$$

with the current local rotations then being obtained in a similar fashion to (18.91), i.e. with

$$\theta_{l2} = -\mathbf{u}_{3n}^{\mathrm{T}} \mathbf{e}_2; \qquad \theta_{l1} = \mathbf{u}_{3n}^{\mathrm{T}} \mathbf{e}_1 \tag{18.96}$$

where $\mathbf{e}_1$ and $\mathbf{e}_2$ now relate to the current (new) element frame. At this stage we have all the required local quantities to pass to the local element routines so as to compute $\mathbf{q}_{lit}$ and $\mathbf{q}_{lir}$ where, for a simple triangle, the latter will be of dimensions six.

With a view to the virtual work, we can write:

$$\delta \bar{\mathbf{u}}_{3n} = \delta \boldsymbol{\alpha} \times \bar{\mathbf{u}}_{3n} = -\mathbf{S}^*(\bar{\mathbf{u}}_{3n}) \delta \boldsymbol{\alpha}_2 \tag{18.97}$$

where we have introduced the $*$ on $\mathbf{S}$ to indicate that the current matrix is of dimensions 3×2, i.e. (see (16.8)):

$$\mathbf{S}^*(\mathbf{a}) = \begin{bmatrix} 0 & -a_3 \\ a_3 & 0 \\ -a_2 & a_1 \end{bmatrix} \tag{18.98}$$

and the subscript 2 on $\delta\boldsymbol{\alpha}$ implies that we have only two components, $\delta\alpha_1$ and $\delta\alpha_2$. For the future developments, we will drop this subscript on $\delta\boldsymbol{\alpha}$ (and on $\boldsymbol{\alpha}$) which will be assumed to be of dimensions 2×1.

Using (18.95) and (18.97), we can obtain the variation of (18.96) as

$$\delta\theta_{l1} = \mathbf{u}_{3n}^{\mathrm{T}} \mathbf{S}(\mathbf{e}_2) \delta\boldsymbol{\beta} + \mathbf{e}_2^{\mathrm{T}} \mathbf{U}_o \mathbf{S}^*(\bar{\mathbf{u}}_{3n}) \delta\boldsymbol{\alpha} \tag{18.99a}$$

$$\delta\theta_{l1} = \mathbf{u}_{3n}^{\mathrm{T}} \mathbf{S}(\mathbf{e}_1) \delta\boldsymbol{\beta} - \mathbf{e}_1^{\mathrm{T}} \mathbf{U}_o \mathbf{S}^*(\bar{\mathbf{u}}_{3n}) \delta\boldsymbol{\alpha} \tag{18.99a}$$

so that, in conjunction with the relationships of (18.33) and (18.48) we can construct the element $\mathbf{T}$ matrix and hence obtain the internal force vector for which the translational terms may be explicitly written as

$$\mathbf{q}_{it} = \mathrm{col}(\bar{\mathbf{q}}_{lit}^j) - \mathbf{V}\left(\sum_j (\mathbf{S}(\mathbf{x}^{j1}) \bar{\mathbf{q}}_{lit}^j + \mathbf{S}(\mathbf{e}_2)(q_{lir}(1)^j \mathbf{u}_{3n}^j) - \mathbf{S}(\mathbf{e}_1)(q_{lir}(2)^j \mathbf{u}_{3n}^j)) \right) \tag{18.100}$$

while at node j the rotational terms may be expressed as

$$\mathbf{q}_{ir}^j = q_{lir}(1) \mathbf{S}^*(\bar{\mathbf{u}}_{3n})^{\mathrm{T}} \mathbf{U}_o^{\mathrm{T}} \mathbf{e}_2 - q_{lir}(2) \mathbf{S}^*(\bar{\mathbf{u}}_{3n})^{\mathrm{T}} \mathbf{U}_o^{\mathrm{T}} \mathbf{e}_1 \tag{18.101}$$

where $\mathbf{q}_{ir}^j$ is of dimensions 2×1.

For the initial stress matrix, the translational–translational terms due to $\mathbf{q}_{lit}$ in (18.100) have already been given in (18.35) (although the current $\mathbf{q}_{lit}$ were in (18.35) simply referred to as $\mathbf{q}_{li}$). From (18.100), we now have an additional contribution stemming from:

$$\text{term} = -\mathbf{V}\left(\sum_j (\mathbf{S}(\delta\mathbf{e}_2)(q_{lir}(1)^j \mathbf{u}_{3n}^j) - \mathbf{S}(\delta\mathbf{e}_1)(q_{lir}(2)^j \mathbf{u}_{3n}^j)) \right) \tag{18.102}$$

which gives an additional contribution of the form:

$$\mathbf{K}_{t\sigma}(t,t) = \mathbf{V}\sum_j (q_{lir}(1)^j\mathbf{S}(u^j_{3n})\mathbf{S}(\mathbf{e}_2) - q_{lir}(2)^j\mathbf{S}(\mathbf{u}^j_{3n})\mathbf{S}(\mathbf{e}_1))\mathbf{V}^{\mathrm{T}} \tag{18.103}$$

Also stemming from (18.100), we have a translational coupling term stemming from:

$$\text{term} = -\mathbf{V}\left(\sum_j (\mathbf{S}(\mathbf{e}_2)(q_{lir}(1)^j\delta\mathbf{u}^j_{3n}) - \mathbf{S}(\delta\mathbf{e}_1)(q_{lir}(2)^j\delta\mathbf{u}^j_{3n}))\right) \tag{18.104}$$

which leads to a term coupling the translational forces to the rotational variables at node j of the form:

$$\mathbf{K}_{t\sigma}(t,\boldsymbol{\alpha}^j) = \mathbf{V}(-q_{lir}(1)^j\mathbf{S}(\mathbf{e}_2)\mathbf{U}^j_o\mathbf{S}^*(\bar{\mathbf{u}}^j_{3n}) + q_{lir}(2)^j\mathbf{S}(\mathbf{e}_1)\mathbf{U}^j_o\mathbf{S}^*(\bar{\mathbf{u}}^j_{3n})) \tag{18.105}$$

The transpose of the above is obtained from the variation of the terms $\mathbf{e}_1$ and $\mathbf{e}_2$ in (18.101) while we obtain a rotational–rotational term from:

$$\begin{aligned}\text{term} &= q_{lir}(1)\mathbf{S}^*(\delta\bar{\mathbf{u}}_{3n})^{\mathrm{T}}\mathbf{U}_o^{\mathrm{T}}\mathbf{e}_2 - q_{lir}(2)\mathbf{S}^*(\delta\bar{\mathbf{u}}_{3n})^{\mathrm{T}}\mathbf{U}_o^{\mathrm{T}}\mathbf{e}_1 \\ &= q_{lir}(1)\mathbf{S}^*(\delta\bar{\mathbf{u}}_{3n})^{\mathrm{T}}\mathbf{e}_2^u - q_{lir}(2)\mathbf{S}^*(\delta\bar{\mathbf{u}}_{3n})^{\mathrm{T}}\mathbf{e}_1^u\end{aligned} \tag{18.106a}$$

where we have introduced the vectors $\mathbf{e}_1^u = \mathbf{U}_o^{\mathrm{T}}\mathbf{e}_1$ and $\mathbf{e}_2^u = U_o^{\mathrm{T}}\mathbf{e}_2$ so that we can evaluate 18.106a) as leading to

$$\mathbf{K}_{t\sigma}(\boldsymbol{\alpha}^j,\boldsymbol{\alpha}^j) = q_{lir}(1)\mathbf{S}^*(\mathbf{e}_2^u)^{\mathrm{T}}\mathbf{S}^*(\bar{\mathbf{u}}_{3n}) - q_{lir}(2)\mathbf{S}^*(\mathbf{e}_1^u)^{\mathrm{T}}\mathbf{S}^*(\bar{\mathbf{u}}_{3n}) \tag{18.106b}$$

18.9 A CO-ROTATIONAL FRAMEWORK FOR THE SEMI-LOOF SHELLS

Irons's semi-loof shell elements [12,13] can be considered as higher-order versions of the Morley triangle (considered in Section 18.7). The nodal connectivity for the triangular element is illustrated in Figure 18.11. We will now outline one possible way of embedding such elements within a co-rotational framework. Following the earlier work, the objective will be to use existing element routines which may be linear or non-linear. (If the latter applies, the objective of the co-rotational harness would be to extend the range of the non-linearity.) We will concentrate on the triangular element although, using the concepts of Section 18.5, it should also be possible to consider the quadrilateral.

In the initial configuration, the element $\mathbf{E} = [\mathbf{e}_1, \mathbf{e}_2, \mathbf{e}_3]$ frame would be computed using the approach of Section 18.4 and, in particular, using (18.40) as illustrated in Figure 18.11 with $\mathbf{e}_3$ being orthogonal to both the straight lines between nodes 2 and 1 and nodes 3 and 1. Using this frame, the initial co-rotating coordinates of the nodes j can be obtained (and stored) as $\mathbf{X}_l^j$. Also we will assume that we know the initial $[\mathbf{R}_1, \mathbf{R}_2, \mathbf{R}_3]$ triads at the loof nodes (Figure 18.11). Knowing the normal to the surface, $\mathbf{R}_3$ at a loof node (Figure 18.11), one can obtain the vector angle between this vector and the element normal, $\mathbf{e}_3$ so that:

$$\gamma = \cos^{-1}(\mathbf{e}_3^{\mathrm{T}}\mathbf{R}_3)\frac{\mathbf{e}_3 \times \mathbf{R}_3}{\|\mathbf{e}_3 \times \mathbf{R}_3\|} \tag{18.107}$$

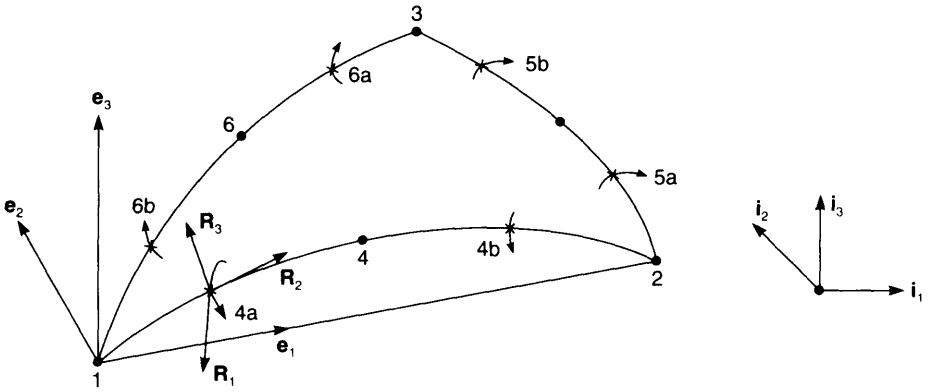

Figure 18.11 Nodal configuration, initial element and loof triads for semi-loof triangular shell element.

and

$$\mathbf{R}_3 = \mathbf{R}(\boldsymbol{\gamma})\mathbf{e}_3 \tag{18.108}$$

with $\mathbf{R}(\boldsymbol{\gamma})$ being obtained from the Rodrigues formula (16.22).

Having computed the first predictor solution (using the local coordinates $\mathbf{X}_l^j$ to define the geometry and with the transformation matrix $\mathbf{T}$ being given by Diag($\mathbf{E}^{\mathrm{T}}$) for the translational terms and with unity alone on the diagonals for the rotational terms), in the updated current configuration, the first estimate of the current element $\mathbf{E}$ frame can again be chosen using the procedure illustrated in Figure 18.6 which relates to equation (18.40) and is outlined in Section 18.4. A better estimate could then follow using the procedure contained in equations (18.41)–(18.43) with $\mathbf{D}_l$ in (18.41) being computed at the centre of the element using the shape functions for a six-noded plane triangle. The $\mathbf{V}^{\mathrm{T}}$ matrix of (18.48) would then be of dimensions 3×18 and would relate the spin vector $\delta\boldsymbol{\beta}$ to the 18 translational variables.

To obtain the local rotations at the loof nodes (designated (a) and (b) in Figure 18.11), instead of using (18.75) one would use:

$$\sin\theta_l = -\bar{\mathbf{R}}_3^{\mathrm{T}}\mathbf{r}_1 \tag{18.109}$$

where in the current configuration, $\bar{\mathbf{R}}_3$, would be computed from:

$$\bar{\mathbf{R}}_3 = \mathbf{R}(\boldsymbol{\gamma})\mathbf{e}_3 \tag{18.110}$$

with $\mathbf{e}_3$ being current and $\mathbf{R}(\boldsymbol{\gamma})$ being computed from the vector $\boldsymbol{\gamma}$ previously computed from (18.107) in the initial configuration.

The current loof triad $[\mathbf{r}_1, \mathbf{r}_2, \mathbf{r}_3]$ would be obtained from the current $\mathbf{r}_2$ vector and the global loof rotation θ, by essentially following the procedure of Section 18.7 and, in particular, using equations (18.73)–(18.78). However, rather than using (18.72), the current $\mathbf{r}_2$ vector would be computed from the quadratic shape functions and current nodal coordinates along the relevant side. In forming the translational internal forces, $\mathbf{q}_{\mathrm{it}}$, it would be better to follow the route of (18.85a) rather than that of (18.85b) so that

instead of being given by (18.88), the $\mathbf{q}_{it}^{*}$ vector in (18.87) would be given by

$$\mathbf{q}_{it}^{*} = \mathbf{V}\left(\sum_{k} \frac{q_{lir}^{k}}{(1+b_2^k)}(\mathbf{R}_2^k - b_2^k \mathbf{r}_2^k)\right) \tag{18.111}$$

18.10 AN ALTERNATIVE CO-ROTATIONAL FRAMEWORK FOR THREE-DIMENSIONAL BEAMS

The earlier developments in this chapter can be used to produce an alternative formulation to that of Section 17.1 for three-dimensional beams. The kinematics would basically remain the same, but a rather neater formulation can be derived and, in addition, the current procedure automatically neglects certain of the initial stress terms.

To use the earlier developments in this chapter, we need to follow closely the procedure of Section 18.6 for a shell element with three rotations at each node although now we have a beam with three rotations at each node. As with the shell, we will now define the pseudo-vector rotations at node j ($j = 1, 2$) as $\boldsymbol{\alpha}^j$ with the equivalent triad as $\mathbf{U}^j$ while the translations at node j will be $\mathbf{d}^j$ while the local rotations will be θ_i^j. In contrast to the work in Section 17.1, the latter will now be clockwise about $\mathbf{u}_1$, $\mathbf{u}_2$ and $\mathbf{u}_3$ respectively so they are given by (18.57a).

In order to obtain the important spin matrix, $\mathbf{V}^{\mathrm{T}}$, we can first apply the conditions that the local axes pass through the second node so that:

$$v_{l2} = \mathbf{e}_2^{\mathrm{T}}\mathbf{x}_{21} = 0; \qquad w_{l2} = \mathbf{e}_3^{\mathrm{T}}\mathbf{x}_{21} = 0 \tag{18.112}$$

Differentiation of the above gives:

$$\mathbf{x}_{21}^{\mathrm{T}}\delta\mathbf{e}_2 + \mathbf{e}_2^{\mathrm{T}}\delta\mathbf{d}_{21} = -\mathbf{x}_{21}^{\mathrm{T}}\mathbf{S}(\mathbf{e}_2)\delta\boldsymbol{\beta} + \mathbf{e}_2^{\mathrm{T}}\delta\mathbf{d}_{21} = 0 \tag{18.113}$$

$$\mathbf{x}_{21}^{\mathrm{T}}\delta\mathbf{e}_3 + \mathbf{e}_3^{\mathrm{T}}\delta\mathbf{d}_{21} = -\mathbf{x}_{21}^{\mathrm{T}}\mathbf{S}(\mathbf{e}_3)\delta\boldsymbol{\beta} + \mathbf{e}_3^{\mathrm{T}}\delta\mathbf{d}_{21} = 0 \tag{18.114}$$

Equations (18.113) and (18.114) provide two equations in the three components of $\delta\boldsymbol{\beta}$. If we use the procedure of Rankin and Brogan [R1.16] which was discussed at the beginning of Section 17.1.6, we can then differentiate equation (17.59a) to obtain the third equation:

$$\mathbf{e}_2^{\mathrm{T}}\mathbf{S}(\bar{t}_2)\delta\boldsymbol{\alpha}_1 = -(\bar{\mathbf{t}}_2^{\mathrm{T}}\mathbf{e}_1)\mathbf{e}_3^{\mathrm{T}}\delta\boldsymbol{\beta} \tag{18.115}$$

where $\delta\boldsymbol{\alpha}_1$ is the pseudo-vector change at the first node. Using equations (18.113)–(18.114) one can obtain (18.48) which is reproduced here for convenience as

$$\delta\boldsymbol{\beta} = \mathbf{V}^{\mathrm{T}}\delta\mathbf{p} \tag{18.116}$$

In contrast to the work of Section 18.6 on shells, $\delta\boldsymbol{\beta}$ is now coupled to the rotational variables (via (18.15)) and not just the translational variables.

With a view to the use of the procedure of Section 17.1.1 for defining the element triad, it is worth noting that equation (18.115) could equally have been obtained by taking the expression for $\delta\mathbf{e}_2$ in (17.60a) and substituting:

$$\mathbf{A}\,\delta\mathbf{d}_{21} = \delta\mathbf{e}_1 = -\mathbf{S}(\mathbf{e}_1)\delta\boldsymbol{\beta} \tag{18.117}$$

and premultiplying the resulting equation by $\mathbf{e}_2^{\mathrm{T}}$ before setting it to zero. The same

equation could be obtained by working in an equivalent manner with $\delta\mathbf{e}_3$ (from 17.60b) and $\mathbf{e}_3$.

Consequently, if we use the procedure of Section 17.1.1 for defining the element triad, we can adopt a similar approach. For example, equation (17.32a) gives an expression for $\delta\mathbf{e}_2$ involving $\mathbf{A}\,\delta\mathbf{d}_{21}$ for which we can substitute from (18.117) before premultiplication by $\mathbf{e}_2^{\mathrm{T}}$ and setting the result to zero. This process would provide an equation for $\delta\boldsymbol{\beta}$ which could be combined with equations (18.113) and (18.114) in order to obtain the spin matrix $\mathbf{V}^{\mathrm{T}}$ of (18.116). However, because the procedure of (17.13) and (17.14) does not lead to an exactly orthogonal $\mathbf{E} = [\mathbf{e}_1, \mathbf{e}_2, \mathbf{e}_3]$ frame, a slightly different third equation would be obtained if we worked with (17.32b) for $\delta\mathbf{e}_3$ instead of (17.32a) for $\delta\mathbf{e}_2$. One could take the average of the two equations.

Having obtain the 3×12 $\mathbf{V}^{\mathrm{T}}$ matrix, we are now in a position to apply a very similar procedure to that of Section 18.6 for shells. In particular from (18.28), we would have:

$$\delta\mathbf{d}_t^j = \mathbf{E}^{\mathrm{T}}\delta\mathbf{d}^j + \mathbf{E}^{\mathrm{T}}\mathbf{S}(\mathbf{x}^{j1})\mathbf{V}^{\mathrm{T}}\delta\mathbf{p} \tag{18.118}$$

while from (18.57b) we would obtain:

$$2\delta\boldsymbol{\theta}_t^j = \mathbf{E}^* \operatorname{col}\mathbf{S}(u_k)^j\delta\boldsymbol{\alpha}^j - \mathbf{U}^{*j}\operatorname{col}\mathbf{S}(\mathbf{e}_k)\mathbf{V}^{\mathrm{T}}\delta\mathbf{p} \tag{18.119}$$

from which the 12×12 transformation matrix $\mathbf{T}$ can be obtained and hence the global internal force vector.

The initial stress matrix would then follow by combining the last part of (18.35) with (18.64) to give a contribution:

$$\mathbf{K}_{\iota\sigma}(\mathbf{p},\mathbf{p}) = \mathbf{V}\sum_j\left(\mathbf{S}(\mathbf{x}^{j1})\mathbf{S}(\bar{\mathbf{q}}_{\mathrm{lit}}^j) + \frac{1}{2}\sum_k \mathbf{S}(\mathbf{q}_{\mathrm{lirk}}^{uj})\mathbf{S}(\mathbf{e}_k)\right)\mathbf{V}^{\mathrm{T}} \tag{18.120}$$

where following previous arguments, the central part could be symmetrised. Also, from (18.35) and (18.66), we would obtain a contribution connecting all of the variables ($\mathbf{p}$) to the pseudo-vector rotations at node j ($\boldsymbol{\alpha}^j$) of the form:

$$\mathbf{K}_{\iota\sigma}(\mathbf{p},\boldsymbol{\alpha}^j) = \mathbf{V}\left[\mathbf{S}(\bar{\mathbf{q}}_{\mathrm{lit}}^j) + \tfrac{1}{2}\operatorname{row}\mathbf{S}(\mathbf{e}_k)\begin{bmatrix} -q_{\mathrm{lir}}(2)\mathbf{S}(\mathbf{u}_3) & +q_{\mathrm{lir}}(3)\mathbf{S}(\mathbf{u}_2) \\ q_{\mathrm{lir}}(1)\mathbf{S}(\mathbf{u}_3) & -q_{\mathrm{lir}}(3)\mathbf{S}(\mathbf{u}_1) \\ -q_{\mathrm{lir}}(1)\mathbf{S}(\mathbf{u}_2) & +q_{\mathrm{lir}}(2)\mathbf{S}(\mathbf{u}_1)\end{bmatrix}^j\right] \tag{18.121a}$$

with equivalent transposed terms. Finally, from (18.70) we would obtain the rotation–rotation terms as

$$\mathbf{K}_{\iota\sigma}(\boldsymbol{\alpha}^j,\boldsymbol{\alpha}^j) = -\frac{1}{2}\sum_k \mathbf{S}(\mathbf{q}_{\mathrm{lirk}}^e)^j\mathbf{S}(\mathbf{u}_k)^j \tag{18.121b}$$

Following the previous arguments, it is likely that we could artificially symmetrise these terms without introducing any deterioration to the convergence characteristics. However, numerical evidence is required.

18.10.1 Two-dimensional beams

It is a useful exercise to apply the theory of this section to the simple two-dimensional beam formulation of Section 7.2. In contrast to this earlier approach, we are now

working with all of the local variables. As a consequence, we are eventually left with an expression for the tangent stiffness matrix that involves W_{l2}/l_n instead of $(\bar{M}_1 + \bar{M}_2)/l_n^2$ as the factor pre-multiplying the last term in (7.79). Here, W_{l2} is the local normal internal force (in the $\mathbf{e}_2$ direction) at node 2. The two terms can be shown to be identical once it is realised that the local nodal forces satisfy the equilibrium relationship:

$$\bar{M}_1 + \bar{M}_2 + l_n W_{l2} = \bar{M}_1 + \bar{M}_2 - l_n W_{l1} = 0 \tag{18.122}$$

Also, the vector $\mathbf{z}/l_n$ in (7.66) is the current 'spin vector', $\mathbf{v}$.

18.11 INCOMPATIBLE MODES, ENHANCED STRAINS AND SUBSTITUTE STRAINS FOR CONTINUUM ELEMENTS

The performance of the conventional lower-order isoparametric elements (four noded quadrilaterals and eight noded bricks) are in many respects deficient. In particular, they perform badly in bending due to shear locking (Figure 18.12a) and in the incompressible limit (as $\mu \to 0.5$ for a linear material) due to 'incompressible locking' (Figure 18.12b, which indicates that if the element sides are straight, point d cannot move in the direction of F without an increase in the volume). In a linear context, a number of different techniques have been proposed for improving the basic elements. If a co-rotational approach is adopted (as in Sections 18.2 and 18.3), these techniques can be very easily introduced into a non-linear formulation (details in Section (18.12). Alternatively, if a 'Eulerian formulation' is adopted (Chapter 12), the linear element formulations may be extended to the non-linear range with the aid of the enhanced deformation gradient, $\mathbf{F}$. This method was proposed by Simo and co-workers [S6, S7] and will be discussed in Section 18.13. In either case, the key building block is the linear enhancement.

Various options will be discussed here (a 'constant volume' approach related to the B-bar method [H3.13] has already been discussed in Section 13.5) with emphasis being placed on two-dimensional elements. Extensions to three dimensions are relatively straightforward, although there are additional complexities [A2, S7]. While the current developments will all be related to continua, it should be noted that many of the concepts can also be applied to shells [B4].

18.11.1 Incompatible modes

In a linear context, the method of 'incompatible modes' was originally formulated by Wilson *et al.* [W1] and later modified so that it passed the 'patch test' by Taylor *et al.* [T1]. If we start with the 'shear locking' of Figure 18.12a, a possible solution involves the addition of the mode (Figure 18.13):

$$v = (1 - \xi^2) v_1^* \tag{18.123}$$

This mode is clearly 'incompatible'. A more general procedure, proposed by Wilson

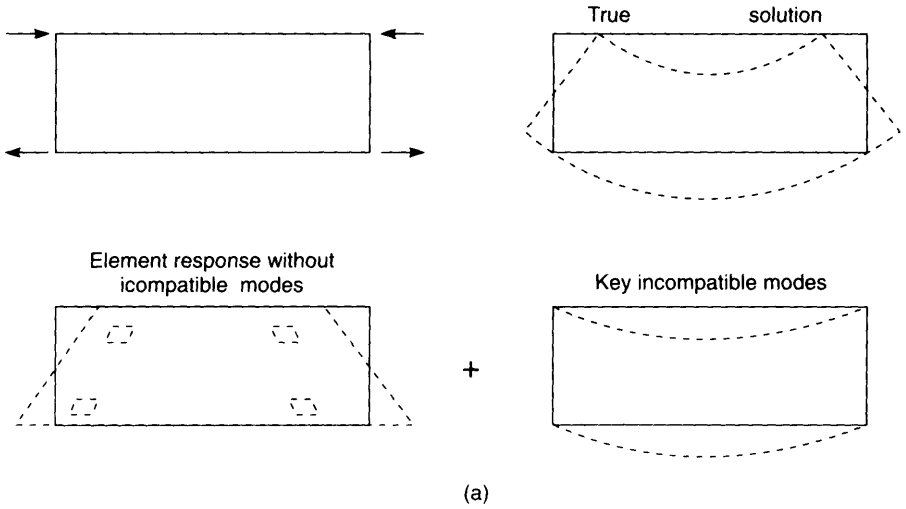

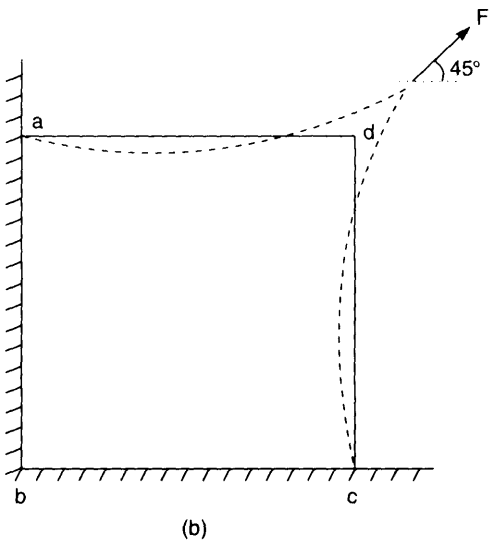

Figure 18.12 Locking behaviour. (a) Shear locking in bending; (b) incompressible locking.

et al. [W1], is to introduced the two incompatible modes:

$$\mathbf{h}^* = \begin{pmatrix} 1-\xi^2 \\ 1-\eta^2 \end{pmatrix} \tag{18.124}$$

so that the displacements u and v would be interpolated via:

$$\begin{aligned} u &= \mathbf{h}^{\mathrm{T}}\mathbf{u} + \mathbf{h}^{*\mathrm{T}}\mathbf{u}^* \\ v &= \mathbf{h}^{\mathrm{T}}\mathbf{v} + \mathbf{h}^{*\mathrm{T}}\mathbf{v}^* \end{aligned} \tag{18.125}$$

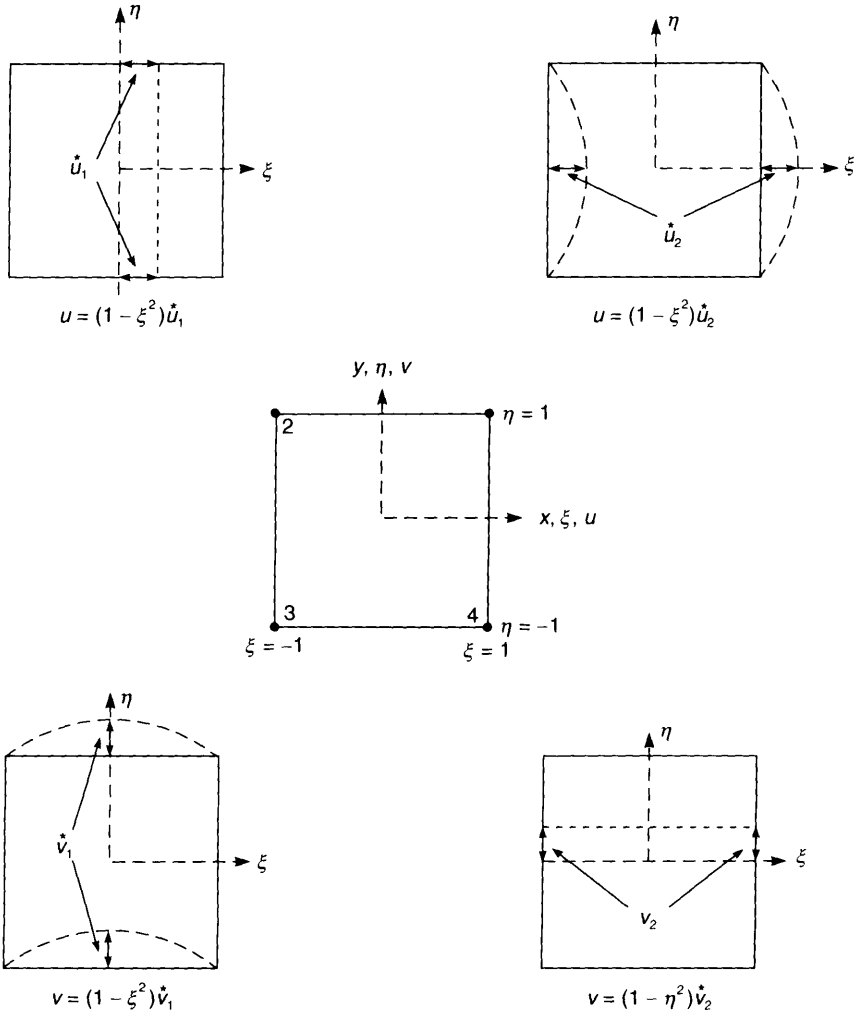

Figure 18.13 Incompatible modes.

with **h** containing the conventional, compatible, shape functions for the corner-nodes and **u** and **v** being the corresponding nodal variables (collectively $\mathbf{p}_1$) and **u*** and **v*** (collectively $\mathbf{p}_2$) containing the magnitudes of the incompatible modes (Figure 18.13).

In its basic form the resulting elements does not always pass the 'patch test'. The proposed modification, by Taylor *et al.* [T1], introduces the strain-displacement relationships:

$$\boldsymbol{\varepsilon} = \boldsymbol{\varepsilon}_1 + \boldsymbol{\varepsilon}_2 = \mathbf{B}_1\mathbf{p}_1 + \mathbf{B}_2\mathbf{p}_2 \tag{18.126}$$

with

$$\varepsilon_2 = \frac{J_o}{j}\begin{bmatrix} \mathbf{J}_o^{-1}(1,1)\mathbf{h}_\xi^{*\mathrm{T}} + \mathbf{J}_o^{-1}(1,2)\mathbf{h}_\eta^{*\mathrm{T}} & \mathbf{0}^{\mathrm{T}} \\ \mathbf{0}^{\mathrm{T}} & \mathbf{J}_o^{-1}(2,1)\mathbf{h}_\xi^{*\mathrm{T}} + \mathbf{J}_o^{-1}(2,2)\mathbf{h}_\eta^{*\mathrm{T}} \\ \mathbf{J}_o^{-1}(2,1)\mathbf{h}_\xi^{*\mathrm{T}} + \mathbf{J}_o^{-1}(2,2)\mathbf{h}_\eta^{*\mathrm{T}} & \mathbf{J}_o^{-1}(1,1)\mathbf{h}_\xi^{*\mathrm{T}} + \mathbf{J}_o^{-1}(1,2)\mathbf{h}_\eta^{*\mathrm{T}} \end{bmatrix}\begin{bmatrix} \mathbf{u}^* \\ \\ \mathbf{v}^* \end{bmatrix} \tag{18.127}$$

where $\mathbf{h}_\xi^*$ and $\mathbf{h}_\eta^*$ contain the derivatives of the incompatible shape functions of (18.124) with respect to ξ and η respectively and:

$$j = \det(\mathbf{J}); \qquad j_o = \det(\mathbf{J}_o) \tag{18.128}$$

where the Jacobian matrix $\mathbf{J}_o$ is computed at the centroid of the element. For future working, we will re-express (18.127) as

$$\varepsilon_2 = \mathbf{B}_2\mathbf{p}_2 = \frac{j_o}{j}\,\bar{\mathbf{B}}_2\mathbf{p}_2 \tag{18.129}$$

To show that the resulting element will pass the patch test, we note that the internal forces associated with the incompatible modes can be written as

$$\mathbf{q}_{i2} = \int\int \mathbf{B}_2^{\mathrm{T}}\boldsymbol{\sigma} j \mathrm{d}\xi\mathrm{d}\eta = \int\int \frac{j_o}{j}\bar{\mathbf{B}}_2^{\mathrm{T}}\boldsymbol{\sigma} j \mathrm{d}\xi\mathrm{d}\eta = j_o\int\int \bar{\mathbf{B}}_2^{\mathrm{T}}\boldsymbol{\sigma}\mathrm{d}\xi\mathrm{d}\eta \tag{18.130}$$

Under patch test conditions, the stresses are constant and hence for $\mathbf{q}_{i2}$ to vanish, we require that:

$$\int\int \bar{\mathbf{B}}_2 \mathrm{d}\xi\mathrm{d}\eta = 0 \tag{18.131}$$

Because of the form of $\bar{\mathbf{B}}_2$ in (18.127) and (18.129), which involves the constant terms from $\mathbf{J}_o$, (18.131) is satisfied if:

$$\int\int \mathbf{h}_\xi^* \mathrm{d}\xi\mathrm{d}\eta = \int\int \mathbf{h}_\eta^* \mathrm{d}\xi\mathrm{d}\eta = 0 \tag{18.132}$$

These conditions are clearly satisfied by the shape functions of (18.124).

The incompatible variables $\mathbf{p}_2$ can be eliminated at the element level (see Section 18.12) and the resulting element gives an excellent performance (see Section 18.11.4). We have already indicated why this is true for shear locking. With respect to incompressible locking, it is worth considering a square of side length 2 and noting that (for plane strain), the standard shape functions $\mathbf{h}$ head to a 'linear volumetric strain' of the form:

$$\varepsilon_{xx} + \varepsilon_{yy} = A + \tfrac{1}{4}\,(v_1 - v_2 + v_3 - v_4)\xi + \tfrac{1}{4}\,(u_1 - u_2 + u_3 - u_4)\eta \tag{18.133}$$

Hence, without 'incompatible' modes, we cannot, in general, recover a constant volumetric strain. Using the previous developments, the incompatible modes give:

$$\varepsilon_{2xx} + \varepsilon_{2yy} = -2\xi(u_1^* + v_1^*) - 2\eta(u_2^* + v_2^*) \tag{18.134}$$

so that coefficients of ξ and η in (18.133) can be neutralised by the additions of incompatible terms arising from (18.134). Further discussion on this topic is given in [A2].

18.11.2 Enhanced strains

The full derivation [S5] involves a mixed three-field variational approach. In the following we will be less rigorous and will start by deriving an 'enhanced strain formulation' that is exactly equivalent to the previous technique with two incompatible modes and four incompatible variables. Using (18.124) and (18.125)), we can use the incompatible shape functions in (11.47) to write:

$$\mathbf{D}_\xi = \begin{bmatrix} \overline{\frac{\partial u}{\partial \xi}} & \overline{\frac{\partial u}{\partial \eta}} \\ \overline{\frac{\partial v}{\partial \xi}} & \overline{\frac{\partial v}{\partial \eta}} \end{bmatrix} = -2\xi \begin{bmatrix} u_1^* & 0 \\ v_1^* & 0 \end{bmatrix} - 2\eta \begin{bmatrix} 0 & u_2^* \\ 0 & v_2^* \end{bmatrix} \tag{18.135}$$

So that, via (11.49) we can write the covariant (or natural) strains with respect to the contravariant base vectors at the centroid as

$$\bar{\mathbf{D}} = \mathbf{J}_o \left[-2\xi \begin{bmatrix} u_1^* & 0 \\ v_1^* & 0 \end{bmatrix} - 2\eta \begin{bmatrix} 0 & u_2^* \\ 0 & v_2^* \end{bmatrix} \right] \tag{18.136}$$

or, in vector form as

$$\begin{bmatrix} \bar{D}_{11} \\ \bar{D}_{12} \\ \bar{D}_{21} \\ \bar{D}_{22} \end{bmatrix} = -2 \begin{bmatrix} J_{o,11}\xi & J_{o,12}\xi & 0 & 0 \\ 0 & 0 & J_{o,11}\eta & J_{o,12}\eta \\ J_{o,21}\xi & J_{o,22}\xi & 0 & 0 \\ 0 & 0 & J_{o,21}\eta & J_{o,21}\eta \end{bmatrix} \begin{bmatrix} u_1^* \\ v_1^* \\ u_2^* \\ v_2^* \end{bmatrix} \tag{18.137}$$

or defining new variables so that:

$$\begin{pmatrix} \alpha_1 \\ \alpha_3 \end{pmatrix} = -2\mathbf{J}_o \begin{pmatrix} u_1^* \\ v_1^* \end{pmatrix}; \qquad \begin{pmatrix} \alpha_4 \\ \alpha_2 \end{pmatrix} = -2\mathbf{J}_o \begin{pmatrix} u_2^* \\ v_2^* \end{pmatrix} \tag{18.138}$$

we have:

$$\begin{bmatrix} \bar{D}_{11} \\ \bar{D}_{12} \\ \bar{D}_{21} \\ \bar{D}_{22} \end{bmatrix} = \begin{bmatrix} \xi & 0 & 0 & 0 \\ 0 & 0 & 0 & \eta \\ 0 & 0 & \xi & 0 \\ 0 & \eta & 0 & 0 \end{bmatrix} \begin{bmatrix} \alpha_1 \\ \alpha_2 \\ \alpha_3 \\ \alpha_4 \end{bmatrix} = \bar{\mathbf{G}}\boldsymbol{\alpha} \tag{18.139}$$

and the corresponding 'natural strains' are:

$$\begin{bmatrix} \bar{\varepsilon}_{11} \\ \bar{\varepsilon}_{22} \\ \bar{\varepsilon}_{12} + \bar{\varepsilon}_{21} \end{bmatrix} = \begin{bmatrix} \xi & 0 & 0 & 0 \\ 0 & \eta & 0 & 0 \\ 0 & 0 & \xi & \eta \end{bmatrix} \begin{bmatrix} \alpha_1 \\ \alpha_2 \\ \alpha_3 \\ \alpha_4 \end{bmatrix} = \bar{\mathbf{B}}\boldsymbol{\alpha} \tag{18.140}$$

With the aid of (11.44), we can now write:

$$\hat{\boldsymbol{\varepsilon}}_2 = \begin{bmatrix} \hat{\varepsilon}_{11} \\ \hat{\varepsilon}_{22} \\ \hat{\varepsilon}_{12} + \hat{\varepsilon}_{21} \end{bmatrix} = \frac{j_o}{j} \mathbf{J}_3 (J_o)^{-1} \bar{\mathbf{B}}_2 \boldsymbol{\alpha} = \mathbf{B}_2 \boldsymbol{\alpha} = \mathbf{B}_2 \mathbf{p}_2 \tag{18.141}$$

where $\mathbf{J}_3$ was defined in (11.44) and is here evaluated at the centroid (hence the J_o in

parenthesis). We have added a subscript 2 to the strains $\hat{\boldsymbol{\varepsilon}}$ for consistency with Section 18.11.1, where the 2 implies enhanced strains to be superimposed on the conventional strains. Equation (18.141) is now entirely equivalent to (18.127) and (18.129) which were obtained using incompatible modes.

Regarding the satisfaction of the patch test, following the approach of equation (18.130), the internal forces corresponding to the variables $\boldsymbol{\alpha}$ are:

$$\mathbf{q}_{i2} = \int\int \mathbf{B}_2^{\mathrm{T}} \boldsymbol{\sigma} j \, \mathrm{d}\xi \mathrm{d}\eta = \int\int \frac{j_o}{j} \bar{\mathbf{B}}^{\mathrm{T}} \mathbf{J}_3 (J_o)^{-\mathrm{T}} \boldsymbol{\sigma} j \, \mathrm{d}\xi \mathrm{d}\eta = j_o \int\int \bar{\mathbf{B}}^{\mathrm{T}} \mathbf{J}_3 (J_o)^{-\mathrm{T}} \boldsymbol{\sigma} \, \mathrm{d}\xi \mathrm{d}\eta \quad (18.142)$$

Under patch test conditions, the stresses are constant and hence for $\mathbf{q}_{i2}$ to vanish, we require that:

$$\int\int \bar{\mathbf{B}} \, \mathrm{d}\xi \mathrm{d}\eta = 0 \quad (18.143)$$

Clearly, from (18.140) this condition is satisfied.

Simo and Rifai [S5] proposed a 'fifth mode' whereby:

$$\begin{bmatrix} \bar{\varepsilon}_{11} \\ \bar{\varepsilon}_{22} \\ \bar{\varepsilon}_{12} + \bar{\varepsilon}_{21} \end{bmatrix} = \begin{bmatrix} \xi & 0 & 0 & 0 & \xi\eta \\ 0 & \eta & 0 & 0 & -\xi\eta \\ 0 & 0 & \xi & \eta & g \end{bmatrix} \begin{bmatrix} \alpha_1 \\ \alpha_2 \\ \alpha_3 \\ \alpha_4 \\ \alpha_5 \end{bmatrix} = \mathbf{B}^* \boldsymbol{\alpha} \quad (18.144)$$

with

$$g = \xi^2 - \eta^2 \quad (18.145)$$

(which is zero at the integration points if 2×2 Gaussian integration is adopted).

For a rectangular element of dimensions $2a \times 2b$, in relation to the method of Section 18.11.1, this is equivalent to adding an incompatible mode of the form:

$$u = -\frac{1}{2a}(1 - \xi^2)\eta\alpha_5; \qquad v = \frac{1}{2b}(1 - \eta^2)\xi\alpha_5 \quad (18.146)$$

if g in (18.144) is $(\xi^2 - \eta^2)/2$.

In relation to the enhanced **F** formulation which will be detailed in Section 18.13, it is useful to work with the enhanced displacement derivatives. In this situation, in place of (18.141) we have:

$$\hat{\mathbf{D}}_2 = \begin{bmatrix} \hat{D}_{11} \\ \hat{D}_{12} \\ \hat{D}_{21} \\ \hat{D}_{22} \end{bmatrix} = \frac{j_o}{j} \mathbf{J}_4 (J_o)^{-1} \bar{\mathbf{G}}_2 \boldsymbol{\alpha} = \mathbf{G}_2 \boldsymbol{\alpha} = \mathbf{G}_2 \mathbf{p}_2 \quad (18.147)$$

where the matrix $\mathbf{J}_4$ was given in (11.42) and $\bar{\mathbf{G}}$ was defined in (18.139). For this enhanced **F** method, the author and co-workers have shown [C4] (see also [W3, D3]) that when the either the full four or full five modes are introduced, there are difficulties with the incompatible mode or 'enhanced strain' formulations for large compressive strains. These problems are associated with eigenmodes involving the incompatible

modes which can propagate in an hour-glassing manner (see also Section 18.15). In relation to a rectangular element, the 'dangerous modes' are those involving v_1^* and u_2^* (Figure 18.13). For other shapes, it is difficult to visualise the incompatible modes but, with enhanced strains, we can associate the difficulties with the variables α_3 and α_4 (see (18.139), (18.140) and (18.144)). One possible remedy [D2] is to retain only the enhanced natural strains associated with α_1 and α_2. As will be shown in Section 18.11.4, this approach improves the performance of the basic element with respect to incompressible locking but still leads to a poor performance in near-rectangular configurations under bending. The problem is associated with shear locking and can be alleviated by the method of substitute functions.

18.11.3 Substitute functions

In relation to the poor bending performance of a rectangle, a well-known solution (particularly in the development of beam elements) is to use 'reduced integration' for the shear energy [Z1.13]. An equivalent technique is to use substitute functions or substitute strains so that:

$$\boldsymbol{\varepsilon} = [\mathbf{B} + \begin{bmatrix} 0 & 0 & 0 \\ 0 & 0 & 0 \\ 0 & 0 & 1 \end{bmatrix} [\mathbf{B}_0 - \mathbf{B}]]\mathbf{p} \tag{18.148}$$

Equation (18.148) effectively replaces the last row of the $\mathbf{B}$ matrix (associated with the shear) with the last row of the $\mathbf{B}$ matrix at the centroid ($\mathbf{B}_0$).

Bathe and Dvorkin [B5] have generalised the concept of substitute strain functions, in relation to the analysis of shells. More recently, the approach has been applied to continua by Dvorking and Vassolo [D5] who, in relation to Figure 18.14, use the following functions for the covariant strain components (with respect to the contravariant base vectors at the centroid):

$$\bar{\varepsilon}_{11} = \bar{\varepsilon}_{11}|_o + \frac{\sqrt{3}}{2}(\bar{\varepsilon}_{11}|_D - \bar{\varepsilon}_{11}|_B)\frac{j_o}{j}\xi + \frac{\sqrt{3}}{2}(\bar{\varepsilon}_{11}|_A - \bar{\varepsilon}_{11}|_C)\frac{j_o}{j}\eta$$

$$\bar{\varepsilon}_{22} = \bar{\varepsilon}_{22}|_o + \frac{\sqrt{3}}{2}(\bar{\varepsilon}_{22}|_D - \bar{\varepsilon}_{22}|_B)\frac{j_o}{j}\xi + \frac{\sqrt{3}}{2}(\bar{\varepsilon}_{22}|_A - \bar{\varepsilon}_{22}|_C)\frac{j_o}{j}\eta$$

$$\bar{\varepsilon}_{12} = \bar{\varepsilon}_{12}|_o \tag{18.149}$$

where all the terms on the right-hand side of the equal signs are evaluated at the specified points using the conventional isoparametric shape functions. Consequently, we could for example, compute:

$$\bar{\varepsilon}|_D = \mathbf{J}_3(J_o)\mathbf{B}|_D\mathbf{p} \tag{18.150}$$

where $\mathbf{J}_3$ was defined in (11.44) and $\mathbf{B}|_D$ is the conventional $\mathbf{B}$ matrix computed at point D. Equations (18.149) can be used to compute $\bar{\mathbf{B}}(\xi, \eta)$ where:

$$\bar{\boldsymbol{\varepsilon}}(\xi, \eta) = \bar{\mathbf{B}}(\xi, \eta)\mathbf{p} \tag{18.151}$$

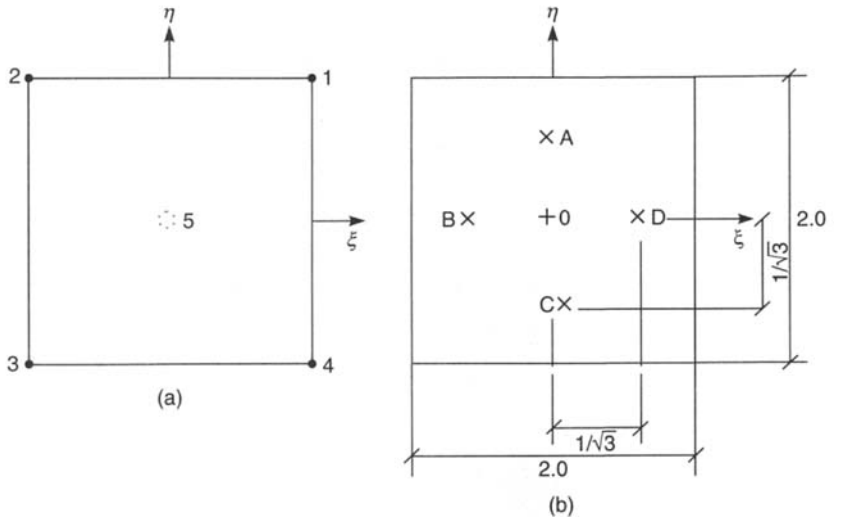

Figure 18.14 Assumed strain procedures. (a) Displacement nodes; (b) strain sampling points.

after which:

$$\hat{\boldsymbol{\varepsilon}}(\xi,\eta) = \mathbf{J}_3(J_o)^{-1}\bar{\mathbf{B}}(\xi,\eta)\mathbf{p} = \hat{\mathbf{B}}\mathbf{p} \tag{18.152}$$

where $\hat{\mathbf{B}}$ is the modified $\mathbf{B}$ matrix with respect to the conventional cartesian axes.

In relation to the patch test, we note that with the adopted functions (see (18.149) and (18.152)):

$$\int \hat{\mathbf{B}}\,\mathrm{d}V = \int \mathbf{J}_3(J_o)^{-1}\bar{\mathbf{B}}_o\,\mathrm{d}V = \int \mathbf{B}_o\,\mathrm{d}V = \int \mathbf{B}\,\mathrm{d}V \tag{18.153}$$

where $\mathbf{B}$ is the conventional $\mathbf{B}$ matrix computed directly from the isoparametric shape functions.

Dvorkin and Vassolo [D5] use the substitute strain functions in conjunction with a five-noded quadrilateral (Figure 18.14) so that the basic shape functions $\mathbf{h}$ of (18.125) include:

$$\mathbf{h}(5) = (1-\xi^2)(1-\eta^2) \tag{18.154}$$

The associated variables u_5 and v_5 are then eliminated at the element level using a very similar procedure to that adopted for the incompatible displacements or enhanced strain variables. In relation to a 'co-rotational formulation' details are given in Section 18.12.

In order to extend the method to an enhanced $\mathbf{F}$ formulation (details in Section 18.13), substitute functions must be found for the displacement derivatives. To this end, the author proposes the relationship:

$$\hat{\mathbf{D}} = \hat{\boldsymbol{\varepsilon}} + \tfrac{1}{2}[\mathbf{D}_o - \mathbf{D}_o^{\mathrm{T}}] \tag{18.155}$$

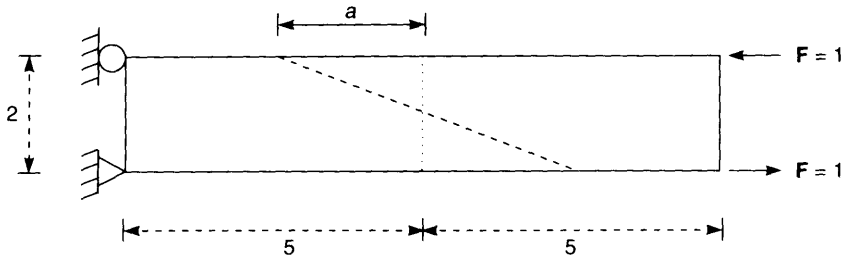

Figure 18.15 Cantilever for mesh distortion tests.

where $\hat{\boldsymbol{\varepsilon}}$ are the substitute strains and $\mathbf{D}_0$ are the conventional displacement derivatives at the centroid. Using this approach, for a linear formulation, the original substitute strain procedure of Dvorking and Vassolo [D5] will be recovered.

18.11.4 Numerical comparisons

In this section, we will compare the numerical performances obtained using a number of the previous algorithms when analysing (in a linear mode) the cantilever of Figure 18.15. To this end, we will define the following methods:

- I Conventional displacement based isoparametric formulation with no extra internal variables
- $\bar{\mathrm{B}}$ Conventional B-bar method [H3.13] or constant pressure approach.
- E2 Enhanced strain formulation using α_1 and α_2 from (18.140). The results obtained by adding α_5 from (18.144) were very similar.
- E4 Enhanced strain formulation using $\alpha_1, \alpha_2, \alpha_3$ and α_4 from (18.140). The results obtained by adding α_5 from (18.144) were very similar.
- D2 The substitute strain method of Dvorkin and Vassolo (Section 18.11.3) with two internal variables related to the 'bubble function'. The substitute strain procedure is also applied to the latter.
- D4 A modified version of the substitute strain procedure in which instead of adding the bubble functions, the four incompatible modes (or enhanced strains) are used as internal variables. These are directly added without resource to substitute strains.

All of the results were obtained with the aid of 2×2 Gaussian integration and relate to the average displacement at the tip. For methods E2 and E4, the same results could have been obtained using incompatible modes.

Figure 18.16a and 18.16b illustrates the very poor performance of the conventional formulation (I) particularly as $\nu \to 0.5$. At the other end of the spectrum, the best results are obtained for method E4. However, as noted at the end of Section 18.11.2 (see also Section 18.15), in a large strain context, problems can result from the use of the full four-moded enhancement. Consequently, we are also interested in the performance of the other methods.

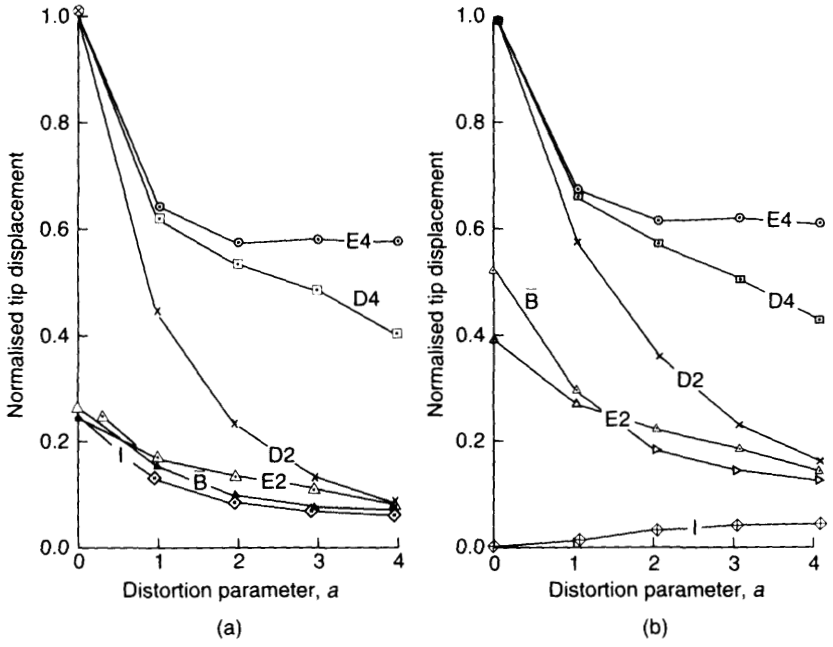

Figure 18.16 Sensitivity to mesh distortion. (a) $\nu = 0$; (b) $\nu = 0.499$.

As anticipated, the E2 method behaves badly when a rectangular elements are used ($a = 0$) although as $\nu \rightarrow 0.5$, the technique gives significantly better results than the conventional formulation (I) and gives solutions that are very similar to those obtained by the B-bar (or constant pressure) approach. The method of Dvorkin *et al.* (D2) behaves well when the element is of nearly rectangular shape and, even when distorted, is significantly better than the other formulations with two or less 'internal variables'. The proposed method D4 gives a response that is only a little worse than that of the element E4. However, as will be indicated in Section 18.15, it would seem to be less sensitive to instabilities than the latter in a non-linear environment when used with the 'enhanced **F**' formulation (Section 18.13).

18.12 INTRODUCING EXTRA INTERNAL VARIABLES INTO THE CO-ROTATIONAL FORMULATION

In Section 18.11, we discussed a number of methods for enhancing the linear performance of the standard 'isoparametric element' by introducing extra internal variables. Using the method of Section 18.11.1, the latter would be displacements relating to incompatible modes; with the method of Section 18.11.2, they would be enhanced strain multipliers, while with one of the methods of Section 18.11.3, they would be displacements related to the bubble function. In a co-rotational context, these variables would be added (and eliminated) at the local level where we could define them as $\mathbf{p}_{l2}$ with $\mathbf{p}_{l1}$

being the local nodal displacement variables associated with the corner nodes. In this section, we will indicate how these extra local internal variables would be treated in a small-strain (but possibly materially non-linear) context.

We will assume that the work is related to a continuum formulation (as in Sections 18.2, 18.3 and 18.11), but similar concepts could be applied to shells. Let us assume that we have some trial displacements, $\mathbf{p}$, related to the primary, corner-node variables. (We will not use specific subscripts or superscripts to indicate the difference between the structural and element level variables, but will rather assume that the distinction is obvious from the context.) The main steps would then involve:

1. Compute the element frame $\mathbf{E} = [\mathbf{e}_1, \mathbf{e}_2, \mathbf{e}_3]$ and hence obtain the local displacements, $\mathbf{p}_l$. In terms of the current terminology, these variables are $\mathbf{p}_{l1}$. We will assume we also have current estimates for $\mathbf{p}_{l2}$.
2. Enter existing linear element routines and compute:

   (a) $\boldsymbol{\sigma}_l$ (possibly accounting for plasticity);

   (b) $$\mathbf{q}_{li1} = \int \mathbf{B}_1(\mathbf{X}_l)^{\mathrm{T}} \boldsymbol{\sigma}_l \mathrm{d}V_0; \qquad \mathbf{q}_{li2} = \int \mathbf{B}_2(\mathbf{X}_l)^{\mathrm{T}} \boldsymbol{\sigma}_l \mathrm{d}V_0 \tag{18.156}$$

   Using the methods of 18.11.1 or 18.11.2, the matrix $\mathbf{B}_2$ would include the 'tricks' required to ensure satisfaction of the patch test. Using the methods of Section 18.11.3, $\mathbf{B}_1$ would also be modified.

   (c) $$\mathbf{K}_{l11} = \int \mathbf{B}_1(\mathbf{X}_l)^{\mathrm{T}} \mathbf{C}_t \mathbf{B}_1(\mathbf{X}_l) \mathrm{d}V_0; \qquad \mathbf{K}_{l12} = \int \mathbf{B}_1(\mathbf{X}_l)^{\mathrm{T}} \mathbf{C}_t \mathbf{B}_2(\mathbf{X}_l) \mathrm{d}V_0$$

   $$\mathbf{K}_{l22} = \int \mathbf{B}_2(\mathbf{X}_l)^{\mathrm{T}} \mathbf{C}_t \mathbf{B}_2(\mathbf{X}_l) \mathrm{d}V_0 \tag{18.157}$$

   These local stiffness matrices will generally be in the nature of local tangent stiffness matrices with $\mathbf{C}_t$ accounting for plasticity. (Indeed we could, in concept, also have local geometric non-linearity so that we might write $\mathbf{B}_1(\mathbf{X}_l + \mathbf{p}_{l1})$ – see Section 17.1.5.)
3. Exit from the existing linear element routines and prepare for static condensation for which truncated Taylor series on $\mathbf{q}_{li1}$ and $\mathbf{q}_{li2}$ give:

   $$\mathbf{q}_{li1} + \mathbf{K}_{l11}\delta\mathbf{p}_{l1} + \mathbf{K}_{l12}\delta\mathbf{p}_{l2} = \mathbf{0} \tag{18.158}$$

   $$\mathbf{q}_{li2} + \mathbf{K}_{l21}\delta\mathbf{p}_{l1} + \mathbf{K}_{l22}\delta\mathbf{p}_{l2} = \mathbf{0} \tag{18.159}$$

   Because there are no external local forces we can operate directly on (18.159) at the element level to obtain:

   $$\delta\mathbf{p}_{l2} = -\mathbf{K}_{l22}^{-1}\mathbf{K}_{l21}\delta\mathbf{p}_{l1} - \mathbf{K}_{l22}^{-1}\mathbf{q}_{li2} \tag{18.160}$$

   and hence substitute into (18.158) to obtain:

   $$\bar{\mathbf{q}}_{li} = \mathbf{q}_{li1} - \mathbf{K}_{l12}\mathbf{K}_{l22}^{-1}\mathbf{q}_{li2} = \bar{\mathbf{K}}_l \delta\mathbf{p}_{l1} \tag{18.161}$$

   where:

   $$\bar{\mathbf{K}} = \mathbf{K}_{l11} - \mathbf{K}_{l12}\mathbf{K}_{l22}^{-1}\mathbf{K}_{l21} \tag{18.162}$$

4. Form the transformation matrix, $\mathbf{T}$ and hence the effective internal global force vector:

$$\mathbf{q}_i = \mathbf{T}^T \bar{\mathbf{q}}_{li} \tag{18.163}$$

5. Form the (global) tangent stiffness matrix:

$$\mathbf{K}_t = \mathbf{T}\bar{\mathbf{K}}_l\mathbf{T}^T + \mathbf{K}_{t\sigma}(\mathbf{q}_{li1}) \tag{18.164}$$

6. Merge to the structural level and solve:

$$\delta\mathbf{p} = -\mathbf{K}_t^{-1}(\mathbf{q}_i - \mathbf{q}_e) \tag{18.165}$$

7. Update $\mathbf{p} = \mathbf{p} + \delta\mathbf{p}$
8. At the element level, recover:

$$\delta\mathbf{p}_{l1} = \mathbf{T}\,\delta p \tag{18.166}$$

and obtain $\delta\mathbf{p}_{l2}$ via (18.160) and update:

$$\mathbf{p}_{l2} = \mathbf{p}_{l2} + \delta\mathbf{p}_{l2} \tag{18.167}$$

18.13 INTRODUCING EXTRA INTERNAL VARIABLES INTO THE EULERIAN FORMULATION

The main developments of this section follow the work of Simo and co-workers [S6, S7] and will introduce a form of 'enhanced deformation gradient', $\mathbf{F}$ which these authors applied in conjunction with the method of enhanced strains (Section 18.11.2). Naturally, the method could also be applied to incompatible modes. Unconventionally, we will advocate here that the method could be applied to the method of substitute strains (Section 18.11.3).

We will adopt a similar notation to that of the previous sections so that subscript 1 relates to the basic (possibly corner-node) variables while subscript 2 relates to the extra internal variables (see the beginning of the previous section). The starting-point is to split the deformation gradient into parts associated with the primary corner-node variables and those associated with the extra internal variables so that:

$$\mathbf{F} = \mathbf{I} + \mathbf{D}_1 + \mathbf{D}_2 \tag{18.168}$$

where $\mathbf{D}$ contains the displacement derivatives $\partial\mathbf{u}/\partial\mathbf{X}$. The latter can be obtained from:

$$v(\mathbf{D}_1) = \mathbf{G}_1(\mathbf{X})\mathbf{p}_1; \qquad v(\mathbf{D}_2) = \mathbf{G}_2(\mathbf{X})\mathbf{p}_2 \tag{18.169}$$

where $v(\mathbf{D}_1)$ means the vector form of $\mathbf{D}_1$ (see for example (5.8) or (18.4)). For the method of enhanced strains, $\mathbf{G}_1$ would be conventional (see (5.8) or (12.3)) while $\mathbf{G}_2$ would involve the techniques discussed in Section 18.11.2 (see (18.147)). For the method of incompatible modes, $\mathbf{G}_1$ would again be conventional while $\mathbf{G}_2$ would follow a very similar procedure to that described in Section 18.11.1 for the generation of $\mathbf{B}_2$. Adapting the proposed modification of the method of Dvorking and Vassolo [D5], we could apply the procedure discussed in the latter part of Section 11.4.3, so that both $\mathbf{G}_1$ and $\mathbf{G}_2$ would be obtained as submatrices of $\hat{\mathbf{G}}$ obtained from $\hat{\mathbf{D}}$ as defined in (18.155). (It is worth noting that Dvorkin and co-workers adopted an alternative approach involving the 'rotated stress tensor' [D6] in order to introduce large strain.) To use the method D4 of Section 18.11.4, $\mathbf{G}_1$ would be obtained from $\hat{\mathbf{G}}$ via (18.155) without

considering any 'bubble function', while $\mathbf{G}_2$ would take the same form as it would with the method of incompatible modes or enhanced strains. Having obtained $\mathbf{F}$, the Kirchhoff stresses τ can be obtained using, for example, a hyperelastic model as in Chapter 13. In order to obtain the internal nodal force vector, with a conventional displacement-based procedure, one would simply compute (see (12.13)):

$$\mathbf{q}_i = \int \mathbf{B}(\mathbf{x})^T \tau \, dV_o \tag{18.170}$$

where $\mathbf{x}$ are the updated coordinates. However, if we adopt any of the modified techniques of Section 18.11, it is necessary to go back to the origins of the Eulerian formulation and compute the velocity gradient (see (12.19)):

$$\mathbf{L} = \mathbf{L}_1 + \mathbf{L}_2 = \mathbf{F}\mathbf{F}^{-1} = (\dot{\mathbf{D}}_1 + \dot{\mathbf{D}}_2)\mathbf{F}^{-1} \tag{18.171}$$

with

$$v(\dot{\mathbf{D}}_1) = \mathbf{G}_1(\mathbf{X})\dot{\mathbf{p}}_1; \qquad v(\dot{\mathbf{D}}_2) = \mathbf{G}_2(\mathbf{X})\dot{\mathbf{p}}_2 \tag{18.172}$$

Using (18.171) it is easy to modify $\mathbf{G}_1(\mathbf{X})$ and $\mathbf{G}_2(\mathbf{X})$ by multiplying terms by $\mathbf{F}^{-1}$ to obtain $\mathbf{G}_1(\text{`}\mathbf{x}\text{'})$ and $\mathbf{G}_2(\text{`}\mathbf{x}\text{'})$ such that:

$$v(\mathbf{L}_1) = \mathbf{G}_1(\text{`}\mathbf{x}\text{'})\dot{\mathbf{p}}_1; \qquad v(\mathbf{L}_2) = \mathbf{G}_2(\text{`}\mathbf{x}\text{'})\dot{\mathbf{p}}_2 \tag{18.173}$$

Again, with a conventional, pure displacement-based, formulation, $\mathbf{G}(\mathbf{x})$ could be directly computed from the current coordinates as in (12.11). Having obtained the matrices $\mathbf{G}_1(\text{`}\mathbf{x}\text{'})$ and $\mathbf{G}_2(\text{`}\mathbf{x}\text{'})$ it is a simple matter to compute the equivalent 'strain matrices' $\mathbf{B}_1(\text{`}\mathbf{x}\text{'})$ and $\mathbf{B}_2(\text{`}\mathbf{x}\text{'})$ (see (12.10)) and hence the two internal force vectors:

$$\mathbf{q}_{i1} = \int \mathbf{B}_1(\text{`}\mathbf{x}\text{'})^T \tau \, dV_o; \qquad \mathbf{q}_{i2} = \int \mathbf{B}_2(\text{`}\mathbf{x}\text{'})^T \tau \, dV_o \tag{18.174}$$

and the three tangent stiffness submatrices (see (12.14)):

$$\begin{aligned}
\mathbf{K}_{t11} &= \int \mathbf{B}_1(\text{`}\mathbf{x}\text{'})^T \mathbf{C}_t \mathbf{B}_1(\text{`}\mathbf{x}\text{'}) dV_o + \int \mathbf{G}_1(\text{`}\mathbf{x}\text{'})^T \hat{\tau} \mathbf{G}_1(\text{`}\mathbf{x}\text{'}) dV_o \\
\mathbf{K}_{t12} &= \int \mathbf{B}_1(\text{`}\mathbf{x}\text{'})^T \mathbf{C}_t \mathbf{B}_2(\text{`}\mathbf{x}\text{'}) dV_o + \int \mathbf{G}_1(\text{`}\mathbf{x}\text{'})^T \hat{\tau} \mathbf{G}_2(\text{`}\mathbf{x}\text{'}) dV_o \\
\mathbf{K}_{t22} &= \int \mathbf{B}_2(\text{`}\mathbf{x}\text{'})^T \mathbf{C}_t \mathbf{B}_2(\text{`}\mathbf{x}\text{'}) dV_o + \int \mathbf{G}_2(\text{`}\mathbf{x}\text{'})^T \hat{\tau} \mathbf{G}_2(\text{`}\mathbf{x}\text{'}) dV_o
\end{aligned} \tag{18.175}$$

The procedure for non-linear static condensation is very similar to that outlined in the previous section although there are now no distinctions between local and global quantities.

Simo *et al.* [S7] adopt a slightly different procedure for the enhanced $\mathbf{D}_2$ term in (18.168). Instead of directly applying (18.147) for $\mathbf{D}_2$, they use $\mathbf{D}_2 = \mathbf{F}_0\hat{\mathbf{D}}_2$ ((18.147) tensor), where $\mathbf{F}_0$ is the deformation gradient at the centroid computed from the conforming corner node variables, i.e. $\mathbf{F}_0 = [\mathbf{I} + \mathbf{D}_1]$. If the $\mathbf{F}_0$ term is omitted and $\mathbf{D}$ is computed from (18.139), the results will be unaltered although the enhanced variables, α_1–α_4, will be modified via a linear combination. However, if other interpolations are used for $\bar{\mathbf{D}}$, without the addition of the $\mathbf{F}_0$ term, the formulation may not be invariant to a rigid-body rotation (see Section 18.15). If the $\mathbf{F}_0$ term is included, the $\mathbf{G}_2$ matrix must be modified using a similar procedure to that discussed in (18.171)–(18.173).

In concept there are no problems in applying this enhanced **F** technique to hyperelastic materials. Indeed, because of the effectiveness of the modified methods or enhanced strains in overcoming 'volumetric locking', there is no need directly to introduce mixed of hybrid formulations (see Sections 13.5.1 and 13.5.2). However, as already discussed, it is sometimes found that there are difficulties with 'hour-glassing' when the four or more extra internal variables are adopted. These diffiulties particularly relate to constrained compressive environments when the strains are large [C4, D3, W3] (and see Section 18.15).

18.14 INTRODUCING LARGE ELASTIC STRAINS INTO THE CO-ROTATIONAL APPROACH

The key to the introduction of hyperelasticity into the co-rotational continuum approaches of Sections 18.2 and 18.3 is the observation drawn at the beginning of Section 18.3 that the local engineering strain is a close approximation to the Biot strain. In particular, under uniform strain states the local engineering strain is equal to the Biot strain (see (18.26)). It follows that it is only sensible to apply the co-rotational approach to large strains when using lower-order elements.

Let us work with a hyperelastic formulation using principal stretches (as in Section 13.8). In a strict formulation the Biot stresses could be obtained via (13.108) as:

$$\boldsymbol{B} = \sum \frac{\partial \varphi}{\partial \lambda_i} \mathbf{N}_i \mathbf{N}_i^{\mathrm{T}} = \sum B_i \mathbf{N}_i \mathbf{N}_i^{\mathrm{T}} \tag{18.176}$$

where φ is the elastic potential and the λ_i's are the principal stretch ratios while the $\mathbf{N}_i$'s are the equivalent principal directions of $\mathbf{U}$ of $\mathbf{F}^{\mathrm{T}}\mathbf{F}$. It follows that, for the co-rotational approach, a reasonable approximation is to replace (18.176) with:

$$\boldsymbol{\sigma}_l = \sum \frac{\partial \varphi}{\partial \lambda_i} \mathbf{a}_i \mathbf{a}_i^{\mathrm{T}} = \sum \sigma_{li} \mathbf{a}_i \mathbf{a}_i^{\mathrm{T}} \tag{18.177}$$

where $\mathbf{a}_i$ are the principal directions of the local engineering strain $\boldsymbol{\varepsilon}_l$, and the principal stretches can be approximated as

$$\lambda_i = 1 + \varepsilon_{li} \tag{18.178}$$

where ε_{li} are the principal values of the local engineering strain, $\boldsymbol{\varepsilon}_l$.

The local tangent stiffness matrix is simply computed using the local linear **B** matrix and the constitutive tangent modular matrix appropriate to a Biot formulation. Using a very similar procedure to that of Section 13.8.2, with respect to principal directions $\mathbf{N}_i$ (here approximated by $\mathbf{a}_i$), the components of the constitutive tensor are given by

$$\begin{aligned} C_{iijj} &= \frac{\partial B_i}{\partial \lambda_j} \\ C_{ijij} = C_{ijji} = C_{jiij} = C_{jiji} &= \frac{1}{2}\left(\frac{B_i - B_j}{\lambda_i - \lambda_j}\right) \qquad (i \neq j) \end{aligned} \tag{18.179}$$

which can be rotated back to the 'base frame' (here the local frame) using the standard transformations of (4.55) (or see (13.137)).

For output purpose, because the local stresses approximate the Biot stresses, using

(13.109), the Kirchhoff stresses can be obtained as

$$\tau = \mathbf{R}_m \sigma_l [\mathbf{I} + \varepsilon_l] \mathbf{R}_m^T \tag{18.180}$$

Probably because of the approximation whereby the rotation matrix **R** is held at its centroidal value (see Section 18.3), it is found that no hour-glassing difficulties are encountered with this method even when using (in a two-dimensional context) four or more enhanced strain variables (or equivalent incompatible modes)[C4]. However, the stress distribution has been found to be rather more oscillatory than that obtained from the enhanced **F** technique [C5]. These oscillations are reduced [C5] by using the 'fifth mode' α_5 of (18.144). In this context, it was noted at the end of Section 18.11 (see (18.133) and (18.134)), that the four incompatible modes (or equivalent enhanced strains) allowed a constant volumetric strain (see also [A2]). However, the arguments related to a linear volumetric strain. For hyperelasticity (see (13.21)), we instead use $(J-1)$ or $\log_e J$, where $J = \det(\mathbf{F})$. In a plane-strain context, with $J-1$, instead of $\varepsilon_{xx} + \varepsilon_{yy}$ (see (18.133)), we would have, in addition, the non-linear terms $\varepsilon_{xx}\varepsilon_{yy} + \gamma_{xy}^2$ and it is in this context that the fifth mode appears to help to reduce the oscillations in the volumetric strain and hence the stresses.

18.15 A SIMPLE STABILITY TEST AND ALTERNATIVE ENHANCED F FORMULATIONS

Following on form the work of Wriggers [W3], the author and co-workers used the single element example of Figure 18.17 to investigate the stability of various enhanced formulations under large compressive strains [C4]. The originally square element is initially of unit side and is uniformly compressed using displacement control. A Hencky hyperelastic model (Section 13.10.1) has been adopted with $\mu = 20$ and the bulk modulus $K = 10^5$.

Using the conventional enhanced **F** formulation, with four enhanced strains or incompatible modes (Sections 18.11 and 18.13), at an imposed deflection at nodes 1 and 2 of $\Delta = 0.377$, a zero pivot was encountered. For further deformations, factorisation of the tangent stiffness matrix introduced a negative pivot, indicating an instability. The eigenmode associated with the zero pivot is also plotted in Figure 18.17, with the

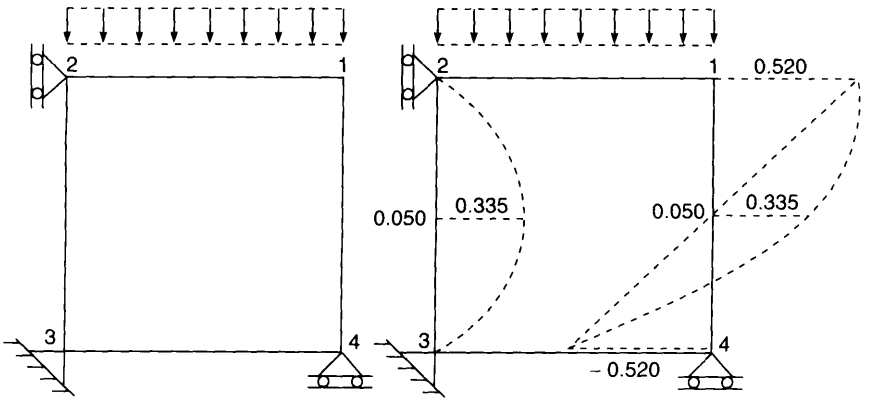

Figure 18.17 Single element instability test with eigenmode.

incompatible modes also being illustrated. For a multi-element formulation, this eigenmode can propagate [C4, W3].

For this problem, no negative pivots were encountered, up to a squash ratio of $\Delta = 0.95$, with any of the methods E2, D2 or D4 of Section 18.11.4 when they were embedded within an enhanced **F** framework (Section 18.13). The same observation applied to the co-rotational method of Section 18.14 when using the four conventional enhanced strains or incompatible modes.

As discussed in Section 18.13, the key to an enhanced **F** formulation is the specification of the displacement-derivative matrix, **D**. In addition to the previous methods D2 and D4 (see Sections 18.11.3 and 18.11.4), the author has found that a procedure to avoid 'hour-glassing' can be found by setting:

$$\mathbf{D} = \boldsymbol{\varepsilon}_1 + \tfrac{1}{2}[\mathbf{D}_{1o} - \mathbf{D}_{1o}^{\mathrm{T}}] + \boldsymbol{\varepsilon}_2 = \tfrac{1}{2}[\mathbf{D}_1 + \mathbf{D}_1^{\mathrm{T}}] + \tfrac{1}{2}[\mathbf{D}_{1o} - \mathbf{D}_{1o}^{\mathrm{T}}] + \boldsymbol{\varepsilon}_2 \quad (18.181)$$

where $\boldsymbol{\varepsilon}_1$ contains the conventional corner-node strains, $\mathbf{D}_{1o}$ contains the conventional corner-node displacement derivatives at the centroid and $\boldsymbol{\varepsilon}_2$ contains the conventional enhanced strains (see (18.140) and (18.141)).

Having studied the closed form solution for the instability problem of this section, Korelc and Wriggers [K2] have proposed an alternative technique that is more closely related to the original enhanced **F** procedure whereby (see (18.168)):

$$\mathbf{D} = \mathbf{D}_1 + \mathbf{D}_2 \quad (18.182)$$

with $\mathbf{D}_1$ relating to the corner nodes and for the usual enhanced **F** procedure (see Section 18.11.1 and (18.135)–(18.139)), we would use (18.147) for $\mathbf{D}_2$ with the associated $\bar{\mathbf{D}}$ (see (18.139)) being given by:

$$\bar{\mathbf{D}} = \begin{bmatrix} \xi\alpha_1 & \eta\alpha_4 \\ \xi\alpha_3 & \eta\alpha_2 \end{bmatrix} \quad (18.183)$$

Korelc and Wriggers propose a general form [K2]:

$$\bar{\mathbf{D}} = \begin{bmatrix} \xi\alpha_1 & P_{12}(\xi,\eta)\alpha_4 \\ P_{21}(\xi,\eta)\alpha_3 & \eta\alpha_2 \end{bmatrix} \quad (18.184)$$

and argue that, for stability, we should ensure that:

$$\int P_{12}(\xi,\eta)P_{21}(\xi,\eta)\mathrm{d}V = 0 \quad (18.185a)$$

$$\int P_{12}(\xi,\eta)\eta\,\mathrm{d}V = 0 \quad (18.185b)$$

$$\int P_{21}(\xi,\eta)\xi\,\mathrm{d}V = 0 \quad (18.185c)$$

The original formulation with $\bar{\mathbf{D}}$ from (18.183) does not satisfy (18.185b) and (18.185c) and so, instead, Korlec and Wriggers propose adopting:

$$\mathbf{D}_2 = \begin{bmatrix} \xi\alpha_1 & \xi\alpha_4 \\ \eta\alpha_3 & \eta\alpha_2 \end{bmatrix} \quad (18.186)$$

which is the transpose of the relationship in (18.184) and now does completely satisfy

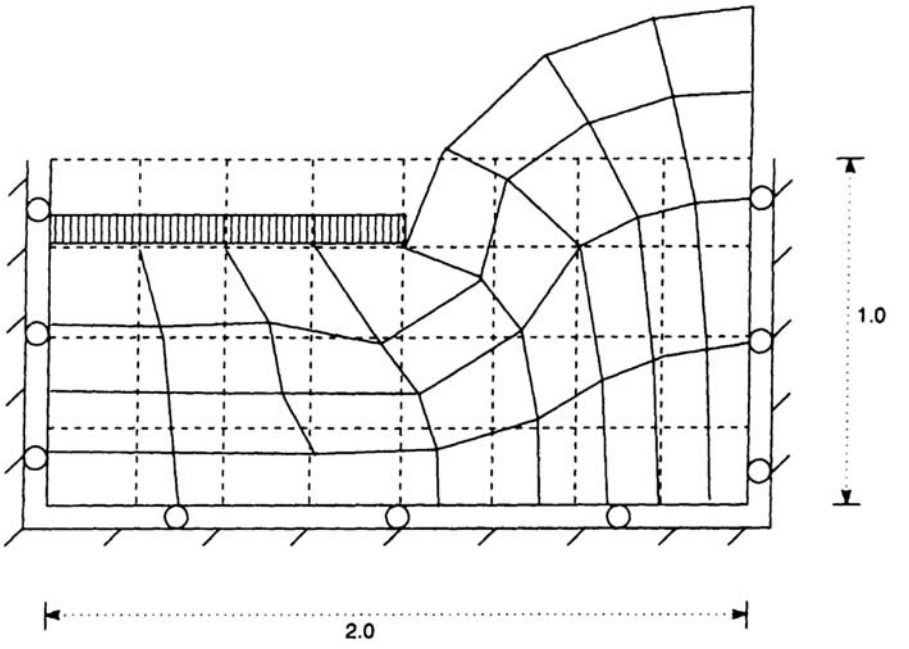

Figure 18.18 Indentation problem—Mooney–Rivlin material ($C_1 = 1.5$; $C_2 = 0.5$; $k = 1000$).

(18.185). For a linear problem, we are only interested in:

$$\boldsymbol{\varepsilon}_2 = \tfrac{1}{2}[\mathbf{D}_2 + \mathbf{D}_2^{\mathrm{T}}] \tag{18.187}$$

and, in this context, both (18.184) and (18.186) degenerate to the conventional enhanced strain formulation (E4) for linear problems. Glaser and Armero [G1] have pointed out that the formulation of Korelc and Wriggers [K2] is not invariant to a superimposed rigid-body rotation. They recommend a similar procedure using (18.186) but with the addition of the $\mathbf{F}_0$ term as discussed below (18.175).

From the numerical tests that have been conducted by Korelc and Wriggers [K2] (and those conducted by the author), this procedure would seem to be free of hour-glassing. In addition, it exhibits better convergence characteristics than those exhibited by the original enhanced **F** procedure. However, when analysing a particular hyperelastic indentation problem (see Figure 18.18 and [C3]), the author has found that all of the previous enhanced **F** procedures suffer from rather poor convergence characteristics. Better convergence characteristics were obtained with the co-rotational method (Section 18.14 and [C3]) and even better characteristics by the 'constant pressure approach' (Sections 13.5, 13.7 and 19.9). The latter procedure also gives a very similar distribution (and magnitude) for the reactions.

It would seem that for constrained problems, without significant bending, there can still be advantages in using the constant pressure (or mean dilatation) approach. In this context, de Souza Neto *et al.* [D4] advocate an constant **F** approach that is very similar to the constant pressure procedure (although leading to a non-symmetric tangent stiffness matrix). These authors point out some disadvantages of the enhanced **F**

procedures in relation to adaptivity when the enhanced strain variables must be mapped from one mesh to another. The overall issue is still not fully resolved. It is worth noting that in relation to large-strain elasto-plasticity (see Chapter 19 and, in particular, Section 19.9), Simo and Armero [S6] have reported hour-glassing with the constant pressure approach for axisymmetric and three-dimensional problems.

18.16 SPECIAL NOTATION

$\mathbf{B}$ = matrix relating strains to nodal displacements
$\mathbf{d}$ = translational displacement vector
$\mathbf{D}$ = displacement derivatives
$\hat{\mathbf{D}}$ = (Section 18.11.3) matrix of displacement derivatives with respect to orthonormal cartesian base vectors
$\bar{\mathbf{D}} = [\bar{D}_{ij}]$ matrix of covariant components of the displacement derivatives (Sections 18.11.2 and 18.15)
$\mathbf{D}_\xi$ = matrix derivatives with respect to natural coordinates (see (11.47))
$\mathbf{E}$ = element triad matrix containing unit orthogonal column vectors
$\mathbf{e}_1 - \mathbf{e}_3$ = which define the local coordinate axes
$\mathbf{F}$ = deformation gradient
$\mathbf{G}$ = matrix relating $\boldsymbol{\theta}$ to $\mathbf{p}$ (or $\delta\boldsymbol{\theta}$ to $\delta\mathbf{p}$)
h = shape functions
$\mathbf{J}$ = Jacobian matrix
j = det ($\mathbf{J}$)
$\mathbf{J}_o$ = Jacobian matrix computed at centroid
j_o = det ($\mathbf{J}_o$)
$\mathbf{p}$ = nodal 'displacements' (including rotations)
$\mathbf{q}$ = internal forces
$\bar{\mathbf{q}} = \mathbf{E}\mathbf{q}$
$\mathbf{r} = [\mathbf{r}_1, \mathbf{r}_2, \mathbf{r}_3]$ current values of mid-side triad in Section 18.7
$\mathbf{r}'_1, \mathbf{r}'_2, \mathbf{r}'_3$ = intermediate values of mid-side triad in Section 18.7
$\mathbf{R} = [\mathbf{R}_1, \mathbf{R}_2, \mathbf{R}_3]$ initial values of mid-side triad in Section 18.7
$\mathbf{S}$ = skew symmetric matrix
$\mathbf{T}$ = transformation matrix whereby $\delta\mathbf{p}_l = \mathbf{T}\,\delta\mathbf{p}$ (the latter is 'global')
$\mathbf{U}$ = right stretch tensor or
$\mathbf{U}$ = nodal triad matrix containing unit orthogonal column vectors $\mathbf{u}_1 - \mathbf{u}_3$ which define the nodal triad
$\mathbf{V}$ = 'spin matrix' whereby $\delta\boldsymbol{\beta} = \mathbf{V}^T\delta\mathbf{p}$ or $\delta\boldsymbol{\beta} = \mathbf{V}^T\delta\mathbf{p}_l$ (translational)
$\mathbf{v}$ = 'spin vector', whereby $\delta\beta = \mathbf{v}^T\delta\mathbf{p}$ or $\delta\beta = \mathbf{v}^T\delta\mathbf{p}_l$ (translational)
$\mathbf{x}$ = current coordinates or position vector
$\mathbf{X}$ = initial coordinates or position vector
$\delta\boldsymbol{\alpha}$ = pseudo-vector change for nodal rotations
β = angle defining direction of $\mathbf{e}_1$
$\delta\boldsymbol{\beta}$ = vector rotation change of element triad
$\boldsymbol{\varepsilon}$ = strains
θ = mid-side rotation in Section 18.7
$\boldsymbol{\theta}$ = vector of displacement derivatives i.e. vector form of $\mathbf{D}$
$\boldsymbol{\theta}_l$ = vector of local rotations
ξ, η = non-dimensional coordinates

Subscripts of superscripts

1 relates to primary 'corner node' variables in Sections 18.11–18.14
2 relates to secondary 'internal' variables in Sections 18.11–18.14
i = internal
l = local
r = rotational
t = translational or tangential
* = 'incompatible'—Section 18.11.1
$\hat{}$ relating to conventional cartesian axes (Sections 18.11–18.12)
$\bar{}$ relating to covariant components (Sections 18.11–18.12)

18.17 REFERENCES

[A1] Allman, D. J., Variational validation of membrane finite elements with drilling rotations, *Comm. in Num. Meth. in Engng.*, **9**, 345–351 (1993).

[A2] Anddelfinger, U., Ramm, E. & Roehl, D., 2D- and 3D-enhanced assumed strain elements and their application in plasticity, in plasticity, in *Computational Plasticity, Fundamentals & Applications*, Part 2, ed. D. R. J. Owen *et al.*, Pineridge Press, Swansea, 1997–2008 (1992)

[B1] Backlund, J., Finite element analysis of nonlinear structures, Ph.D. thesis, Chalmers Univ., Göteborg, Sweden (1973).

[B2] Batoz, J.-L. & Dhatt, G., *Modelisation des Structures par Eléments Finis*, Vol. 2, *Poutres et plaques*, Hermes, Paris (1990).

[B3] Bergan, P. G. & Felippa, C. A. Efficient implementation of a triangular membrane element with drilling freedoms, *Finite Element Methods for Plate and Shell Structures*, Vol. 1, ed. T. J. R. Hughes & E. Hinton, Pineridge Press, Swansea, pp. 128–152 (1986).

[B4] Buechter, N., Ramm, E. & Roehl, D., 3-D extensions of non-linear shell formulation based on the enhanced assumed strain concept, *Int. J. for Num. Meth. in Engng.*, **15**, 2551–2568 (1994).

[B5] Bathe, K.-J. & Dvorkin, E. N., A formulation of general shell elements—the use of mixed tensorial components, in *NUMETA 85, Numerical Methods in Engineering: Theory & Applications*, Vol. 2, ed. J. Middleton *et al.*, A. A. Balkema, Rotterdam, 551–563 (1985).

[C1] Celicoj, C. C., A strain and displacement based variational method applied to geometrically nonlinear shells, *Int. J. for Num. Meth. in Engng.*, **39**, 2231–2248 (1996).

[C2] Chen, K. K., A triangular plate finite element for large-displacement elastic-plastic analysis of automobile structural components, *Comp. & Struct.*, **10**, 203–215 (1979).

[C3] Crisfield, M. A. & Moita, G. F., A co-rotational formulation for 2-D continua including incompatible modes, *Int. J. for Num. Meth. in Engng.*, **39**, 2619–2633 (1996).

[C4] Crisfield, M. A., Moita, G. F., Jelenic, G. & Lyons, L. P. R., Enhanced lower-order element formulations for large strains, *Computational Plasticity, Fundamentals & Applications*, Part 1, ed. D. R. J. Owen *et al.*, Pineridge Press, Swansea, pp. 293–320 (1995) (and *Computational Mechanics*, **17**, 62–73 (1995)).

[C5] Crisfield, M. A. & Moita, G. F., Co-rotational and Biot-like formulations for the nonlinear analysis of continua, *FEMSA 95*, Vol. 1 ed. D. Langsch, Univ. of Cape Town Printing Dept., pp. 123–137 (1995).

[C6] Crisfield, M. A., Mi, Y., Jelenic, G. and Fan, F., Some applications of the nonlinear finite element method, *Finite Elements in Engineering and Design*, to be published.

[D1] Dawe, D. J., Shell analysis using a simple facet element, *J. Strain Anal.*, **7**, 266–270 (1972).

[D2] De Borst, R. & Groen, A. E., Some observations on element performance in isochoric and dilatant flow, *Int. J. for Num. Meth. in Engng.*, **36**, 2887–2906 (1995).

[D3] De Souza Neto, E. A., Peric, D., Huang, G. C. & D. R. J. Owen, Remarks on stability of

enhanced strain elements in finite elasticity and elastoplasticity, in *Computational Plasticity, Fundamentals & Applications*, Part 1, ed. D. R. J. Owen *et al.*, Pineridge Press, Swansea, pp. 361–372 (1995).

[D4] De Souza Neto, E. A., Peric, D., Dutko, M. & D. R. J. Owen, Design of simple lower-order finite elements for large-deformation analysis of nearly incompressible solids, *Int. J. of Solids & Structs.*, **33**, 3277–3296 (1996)

[D5] Dvorkin, E. N. & Vassolo, S. I., A quadrilateral 2-D finite element based on mixed interpolation of tensorial components, *Engineering Computations*, **6**, 217–224 (1989).

[D6] Dvorkin, E. N., Pantuso, D. & Repetto, E., A finite element formulation for finite strain elasto-plastic analysis based on mixed interpolation of tensorial components, *Comp. Meth. in Appl. Mech. & Engng.*, **114**, 35–54 (1994).

[F1] Fox, D. D. & Simo, J. C., Drill rotation formulation for geometrically exact shells, *Comp. Meth. in Appl. Mech. & Engng.*, **98**, 329–343 (1992).

[G1] Glaser, S. & Armero, F., On the formulation of enhanced strain elements in finite deformations, submitted to *Engineering Computations* (1996).

[H1] Herrmann, L. R. & Campbell, D. M., A finite element analysis of thin shells, *AIAA J.*, **6**, 1842–1846. (1968).

[H2] Herrmann, L. R., Finite element bending analysis of plates, *J. Engng. Mech. Div., ASCE*, **93** (EM5), 13–25. (1967).

[H3] Horrigmoe, G. & Bergan, P. G., Nonlinear analysis of free-form shells by flat finite elements, *Comp. Meth. in Appl. Mech. & Engng.*, **16**, 11–35 (1978).

[H4] Hsiao, K.-M., Nonlinear analysis of general shell structures by flat triangular shell element, *Comp. & Struct.*, **25**, 665–675 (1987).

[I1] Ibrahimbegovic, A. & Frey, F., Geometrically non-linear method of incompatible modes in application to finite elasticity with independent rotation field, *Int. J. for Num. Meth. in Engng.*, **36**, 4185–4200 (1993).

[I2] Irons, B. M. & Razzaque, A., Experiences with the patch test for convergence of finite elements, *Mathematical Foundations of the Finite Element Method with Applications to Partial Differential Equations*, ed. K. Aziz, Academic Press, New York (1972).

[I3] Irons, B. M., The semi-loof element, *Finite Elements for Thin Shells and Curved Members*, ed., D. G. Ashwell *et al.*, Wiley, New York, pp. 197–222 (1976).

[J1] Jetteur, P. H. & Cescotto, S., A mixed finite element for the analysis of large inelastic strains, *Int. J. for Num. Meth. in Engng.*, **31**, 229–239 (1991).

[K1] Kozar, I. & Ibrahimbegovic, A., Finite element formulation of the drilling rotation solid element, *Finite Elements in Analysis and Design*, **20**, 101–126 (1995).

[K2] Korelc, J. & Wriggers, P., Consistent gradient formulation for a stable enhanced strain method for large deformations, *Engineering Computations*, **13**, 103–123 (1996).

[M1] MacNeal, R. H. & Harter, R. L., A refined four-noded membrane element with rotational degrees of freedom, *Computers & Structures*, **28**, 75–88 (1988).

[M2] Moita, G. F., Nonlinear finite element analysis of continua with emphasis on hyperelasticity, Ph.D. thesis, Imperial College, London (1994).

[M3] Moita, G. F. & Crisfield, M. A., A finite element formulation for 3-D continua using the co-rotational technique, to be published in *Int. J. for Num. Meth. in Engng.*

[M4] Morley, L. S. D., The constant-moment plate-bending element, *J. Strain Analysis*, **6**, (1), 20–24 (1971).

[M5] Morley, L. S. D. Geometrically nonlinear constant moment triangle which passes the von Karman patch test, *Int. J. for Num. Meth. in Engng.*, **31**, 241–263 (1991).

[M6] Morley, L. S. D., Facet like shell theory, *Int. J. of Engng. Sci.*, **22**, 1315–1327, (1989).

[N1] Nygard, M. K. & Bergan, P. G. Advances in treating large rotations for nonlinear problems, *State of the Art Surveys on Computational Mechanics*, ed. A. K. Noor & T. J. Oden, ASME, New York (1989).

[O1] Onate, E. & Cervera, M., Derivation of thin plate bending elements with one degree of freedom per node: a simple three node triangle, *Engineering Computations*, **10**, 545–561(1993).

[P1] Parisch, H., Continuum based shell theory for non-linear applications, *Int. J. for Num. Meth. in Engng.*, **38**, 1855–1883 (1995).

[P2] Peng, X. & Crisfield, M. A., A consistent co-rotational formulation for shells using the constant stress/constant moment triangle, *Int. J. for Num. Meth. in Engng.*, **35**, 1829–1847 (1992).

[P3] Peric, D., Owen, D. R. J. & Honor, M. E., Simulation of thin sheet metal forming processes employing a thin shell element, *Proc. Int. Conf. on Finite Element Simulation of 3-D Metal Forming Processes in the Automotive Industry*, 000 Zurich, May 1991.

[P4] Phaal, R. & Calladine, C., Simple class of finite element for plate and shell problems, II: an element for thin shells with only translational degrees of freedom, *Int. J. for Num. Meth. in Engng.*, **35**, 979–996 (1992).

[S1] Simo, J. C., Fox, D. D. & Rifai, M. S., On a stress resultant geometrically exact shell model, Part 1: Formulation and parametrisation, *Comp. Meth. in Appl. Mech. & Engng.*, **72**, 267–304 (1989).

[S2] Simo, J. C., Fox, D. D. & Rifai, M. S., On a stress resultant geometrically exact shell model, Part 2: The linear theory; computational aspects, *Comp. Meth. in Appl. Mech. & Engng.*, **73**, 53–92 (1989).

[S3] Simo, J. C., Fox, D. D. & Rifai, M. S., On a stress resultant geometrically exact shell model, Part 3: Computational aspects of the non-linear theory, *Comp. Meth. in Appl. Mech. & Engng.*, 000 (1990).

[S4] Simo, J. C., On a stress resultant geometrically exact model, Part 7: Shell intersections with 5/6-DOF finite element formulation, *Comp. Meth. in Appl. Mech. & Engng.*, **108**, 319–339 (1993).

[S5] Simo, J. C. & Rifai, M. S. A class of assumed strain methods and the method of incompatible modes, *Int. J. for Num. Meth. in Engng.*, **29**, 1595–1638 (1990).

[S6] Simo, J. C., & Armero, F., Geometric non-linear enhanced strain mixed method and the method of incompatible modes, *Int. J. for Num. Meth. in Engng.*, **33**, 1413–1449 (1992).

[S7] Simo, J. C., Armero, F. & Taylor, R. L., Improved versions of assumed enhanced strain tri-linear elements for 3D finite deformation problems, *Comp. Meth. in Appl. Mech. & Engng.*, 110, 359–386 (1993).

[T1] Taylor, R. L., Beresford, P. J. & Wilson, E. L., A non-conforming element for stress analysis, *Int. J. for Num. Meth. in Engng.*, **10**, 1211–1219 (1976).

[V1] Van Keulen, F. Bout, A. & Ernst, L. J. (1993). Nonlinear thin shell analysis using a curved triangular element, *Comp. Meth. in Appl. Mech. & Engng.*, **103**, 315–343.

[W1] Wilson, E. L., Taylor, R. L., Doherty, W. P. & Ghaboussi, J., Incompatible displacement models, *Numerical and Computer Methods in Structural Mechanics*, ed. S. J. Fenves *et al.*, Academic Press, NewYork, 43–57 (1973).

[W2] Wriggers, P. & Gruttmann, F., Thin shells with finite rotations: theory and finite element formulation, in *Analytical and Computational Models of Shells*, Vol. 3 ed. A. K. Noor *et al.*, ASME, CED-, pp. 135–159 (1989).

[W3] Wriggers, P. & Reese, S., A note on enhanced strain method for large deformations, *Comp. Meth. in Appl. Mech. & Engng.*, **135**, 201–210 (1996).

[W4] Wood, A shape function routine for the constant moment triangular plate bending element, *Engng. Comp.*, **1**, pp. 189–197 (1984).

[Z1] Zienkiewicz, O. C., Parekh, C. J. & King, I. P. Arch dams analysed by a linear finite element shell solution program, in *Proc. Symp. on Arch Dams*, Institution of Civil Engineers, London (1968).

19 Large strains and plasticity

19.1 INTRODUCTION

Since the pioneering work of Hibbitt *et al.* in 1979 [H2] and of McKeeking and Rice [M1.12] in 1975, there have been very many publications of describing finite element analysis of plasticity with large strains. This work has included important contributions by Nagtegaal [N1] and Nagtegaal and de Jong [N2, N3] in 1981 and 1982. However, while certain trends have developed, the subject still invokes much controversy. This controversy relates as much to the underlying physics as it does to the numerical algorithms. For the former, the reader is referred to the work in [A1–A3, D1, N1.10, L1, L2, L4.14, M1, N5, N6, R1, S5.14]. In the present chapter, we will largely concentrate on the latter.

Most early finite element work was based on a Eulerian formulation (Section 12.2 and 12.3) using the Jaumann rate of Cauchy or Kirchhoff stress. This stage was followed by debates relating to the advantages or otherwise of using other rates (see Section 10.8 [A1.10, D1.10, N1.10, R3] and Section 13.10.3). However, no matter which rate form was used, the formulations were only 'objective' (see Section 10.2 and 19.4) as the step sizes tended to zero. Hence special measures were adopted to 'integrate' the rate relationships without leading to straining under rigid rotations. [F1, G1, H3, H4, K1–K3, P3]. In an 'explicit dynamics code' (Section 19.4), the time steps may be sufficiently small that these 'special measures' can be avoided.

More recently, one of the main trends has seen the increasing use of a multiplicative decomposition of the deformation gradient [C2, E1, M2, P1, P2, S1–S4] in conjunction with the elastic deformation being computed via a hyperelastic relationship (as in the previous references and B1, B2). The main objective has not necessarily been to consider large elastic strains but rather to avoid the issue of integrating the rate equations and linearising the resulting algorithms. (None the less, some of the resulting formulations can be used with elastic strains that are large or moderately large). In addition, following the work on small-strain plasticity, much work has been concentrated on the development of consistent tangent modular matrices.

In this chapter, we will start by outlining the basis of the multiplicative decomposition and will then show how the resulting equations can be simplified to lead to the conventional 'Jaumann-rate form'. We will then briefly indicate the difficulties with integration and mention some of the solutions that have been proposed. Finally, we will

consider a more modern approach based on a multiplicative decomposition which leads, for J_2 plasticity, to both a 'return algorithm' and a 'consistent tangent modular matrix' that is very similar to that previously described in Chapter 6 for small-strain plasticity. While emphasis is placed on J_2 plasticity, many of the concepts are relevant to other yield criteria.

19.2 THE MULTIPLICATIVE F_eF_p APPROACH

The $\mathbf{F}_e$, $\mathbf{F}_p$ multiplicative decomposition was originally introduced by Lee [L1]. In order to illustrate the procedure, we will assume (see Figure 19.1), that a line element $d\mathbf{X}$ is first moved plastically into an intermediate configuration $d\hat{\mathbf{x}}$ and then elastically into its final state $d\mathbf{x}$. For the first phase, we have:

$$d\hat{\mathbf{x}} = \frac{\partial \hat{\mathbf{x}}}{\partial \mathbf{X}} d\mathbf{X} = \mathbf{F}_p d\mathbf{X} \tag{19.1}$$

and for the second:

$$d\mathbf{x} = \frac{\partial \mathbf{x}}{\partial \hat{\mathbf{x}}} d\hat{\mathbf{x}} = \mathbf{F}_e d\hat{\mathbf{x}} \tag{19.2}$$

so that in total:

$$d\mathbf{x} = \frac{\partial \mathbf{x}}{\partial \mathbf{X}} d\mathbf{X} = \mathbf{F}\, d\mathbf{X} = \mathbf{F}_e \mathbf{F}_p d\mathbf{X} \tag{19.3}$$

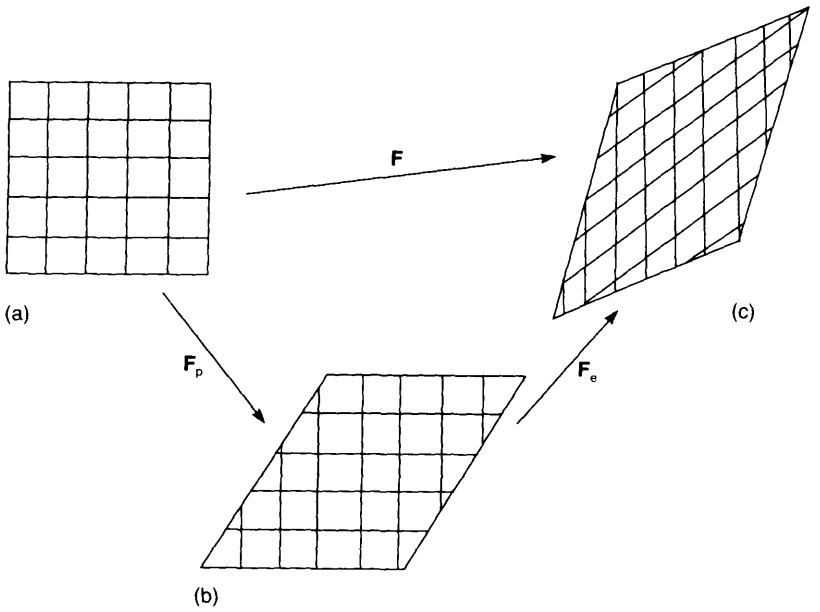

Figure 19.1 The $\mathbf{F}_e\mathbf{F}_p$ decomposition. (a) Initial ($d\mathbf{X}$); (b) intermediate ($d\hat{\mathbf{x}}$); (c) final ($d\mathbf{x}$).

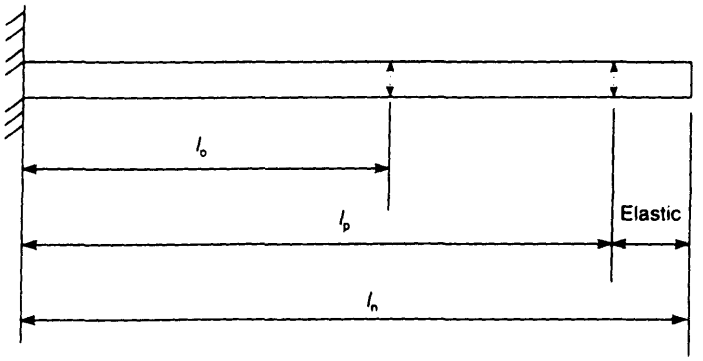

Figure 19.2 Multiplicative decomposition in one dimension.

with

$$\mathbf{F} = \mathbf{F}_e\mathbf{F}_p \tag{19.4a}$$

containing the multiplicative decomposition of the deformation gradient, $\mathbf{F}$. For a 'one-dimensional idealisation' (Figure 19.2), we can write:

$$\lambda = \frac{l_n}{l_o} = \frac{l_n}{l_p}\frac{l_p}{l_o} = \lambda_e\lambda_p \tag{19.4b}$$

where the λ's are 'stretch ratios' and in relation to Figure 19.2, l_o is the original length, l_n the final length and l_p the 'plastic length'.

As noted by Lee, the multiplicative decomposition is non-unique. In particular, following (19.1), we could rotate the intermediate configuration via:

$$d\check{\mathbf{x}} = \frac{\partial\check{\mathbf{x}}}{\partial\hat{\mathbf{x}}}d\hat{\mathbf{x}} = \mathbf{R}\,d\hat{\mathbf{x}} \tag{19.5}$$

so that

$$d\check{\mathbf{x}} = \mathbf{R}\mathbf{F}_p d\mathbf{X} = \mathbf{F}'_p d\mathbf{X} \tag{19.6}$$

after which, using (19.2),

$$d\mathbf{x} = \frac{\partial\mathbf{x}}{\partial\hat{\mathbf{x}}}\frac{\partial\hat{\mathbf{x}}}{\partial\check{\mathbf{x}}}d\check{\mathbf{x}} = \mathbf{F}'_e\mathbf{R}^T d\check{\mathbf{x}} = \mathbf{F}_e d\check{\mathbf{x}} \tag{19.7}$$

so that

$$d\mathbf{x} = \mathbf{F}_e\mathbf{F}_p d\mathbf{X} = \mathbf{F}'_e\mathbf{F}'_p d\mathbf{X} = \mathbf{F}d\mathbf{X} \tag{19.8}$$

Lee included the rotation in the plastic deformation gradient while, following micro-mechanical models involving a single slip crystal in crystalline plasticity [A1], Simo and Hughes [S5.14] consider $\mathbf{F}_e$ as involving the stretching and rotation of the crystal lattice with $\mathbf{F}_p$ characterising plastic flow (via dislocation—see Figure 19.1).

For a general material, there is a problem in relating the stresses on the intermediate configuration, say $\mathbf{S}$, to $\mathbf{E}_e$ because, following the procedure above, one can show [L4.14] that $\mathbf{E}_e$ is not invariant to a rotation of the intermediate configuration. In

particular, using (19.7), we would obtain:

$$\mathbf{E}'_e = \mathbf{R}\mathbf{E}_e\mathbf{R}^T \tag{19.9a}$$

However, if the material is isotropic, we would also obtain:

$$\mathbf{S}' = \mathbf{R}\mathbf{S}\mathbf{R}^T \tag{19.9b}$$

and hence the stress state would not be affected by the intermediate rotation.

From (4.112) and (19.4)

$$\mathbf{l} = \frac{\partial \mathbf{v}}{\partial \mathbf{x}} = \dot{\mathbf{F}}\mathbf{F}^{-1} = \dot{\mathbf{F}}_e\mathbf{F}_e^{-1} + \mathbf{F}_e\dot{\mathbf{F}}_p\mathbf{F}_p^{-1}\mathbf{F}_e^{-1} = \mathbf{l}_e + \mathbf{l}_p \tag{19.10}$$

where following Simo [S1, S2] and Oritz [O1], we have now used lower case l's for the velocity gradients because they are related to the final configuration. Equation (19.10) can be used to show that, although we started with a multiplicative decomposition (19.4), we have an additive decomposition of the strain rates [N1.10, N5, N6]. However, this depends on the definition of $\mathbf{l}_p$ taking the form in (19.10) (if we are referring to the current configuration) rather than the form:

$$\mathbf{L}_p = \dot{\mathbf{F}}_p\mathbf{F}_p^{-1} \tag{19.11}$$

Referring to the current configuration, we would then have:

$$\dot{\boldsymbol{\varepsilon}}_p = \text{sym}(\mathbf{l}_p) = \tfrac{1}{2}(\mathbf{F}_e\mathbf{L}_p\mathbf{F}_e^{-1} + \mathbf{F}_e^{-T}\mathbf{L}_p^T\mathbf{F}_e^T) \tag{19.12}$$

The equivalent relationship on the intermediate configuration can be obtained, using a transformation of the form of (4.101) so that:

$$\dot{\mathbf{E}}_p = \mathbf{F}_e^T\dot{\boldsymbol{\varepsilon}}_p\mathbf{F}_e = \tfrac{1}{2}(\mathbf{C}_e\mathbf{L}_p + \mathbf{L}_p^T\mathbf{C}_e) \tag{19.13}$$

Lubliner [L4.14] has observed that 'regarding the plastic deformation rate, (here $\dot{\boldsymbol{\varepsilon}}_p$ on the current configuration or $\dot{\mathbf{E}}_p$ on the intermediate configuration where the dot merely indicates a rate and does not imply that $\dot{\boldsymbol{\varepsilon}}_p$ is the differential of some $\boldsymbol{\varepsilon}_p$ nor the $\dot{\mathbf{E}}_p$ the differential of some $\mathbf{E}_p$) there is no unequivocal definition'. Among those that have been advocated, apart from (19.12) and (19.13), he also quotes:

$$\dot{\mathbf{E}}_p = \tfrac{1}{2}(\mathbf{L}_p + \mathbf{L}_p^T) \tag{19.14}$$

from which one might obtain:

$$\dot{\boldsymbol{\varepsilon}}_p = \mathbf{F}_e^{-T}\left(\frac{\mathbf{L}_p + \mathbf{L}_p^T}{2}\right)\mathbf{F}_e^{-1} \tag{19.15}$$

In more recent work, Simo [S4] uses (see also Section 19.7.1):

$$\dot{\boldsymbol{\varepsilon}}_p = -\tfrac{1}{2}L_v(\mathbf{b}_e)\mathbf{b}_e^{-1} = \mathbf{F}_e\left(\frac{\mathbf{L}_p + \mathbf{L}_p^T}{2}\right)\mathbf{F}_e^{-1} \tag{19.16}$$

where $L_v(\,)$ is the Lie derivative (see footnote in Section 10.4 and ref. [M1.10]) and $\mathbf{b}_e = \mathbf{F}_e\mathbf{F}_e^T$. For small elastic strains, $\mathbf{F}_e \simeq \mathbf{R}_e$ (see Section 4.10) and hence $\mathbf{F}_e \simeq \mathbf{F}_e^{-T}$ so that (19.15) and (19.16) would coincide. Also, for small elastic strains, $\mathbf{C}_e \simeq \mathbf{I}$ and (19.13) and (19.14) coincide. Indeed, in these circumstances, one can show an equivalence between (19.12) and (19.16).

19.3 USING THE F_eF_p APPROACH TO ARRIVE AT THE CONVENTIONAL 'RATE FORM'

As explained in the introduction to this chapter, most early finite element formulations started from a rate formulation (usually from the Jaumann rate). In this section, we will show that, given certain assumptions, such procedures (which we refer to as 'conventional' in the title to this section) are entirely consistent with an $\mathbf{F}_e\mathbf{F}_p$ approach. The work is largely based on that of Needleman [N4]. We start by assuming that the elastic behaviour is governed by some elastic energy potential (Chapter 13) so that the second Piola–Kirchhoff stresses with respect to the intermediate configuration can be obtained as

$$\mathbf{S} = \frac{\partial \varphi}{\partial \mathbf{E}_e} \tag{19.17}$$

where the elastic Green strains $\mathbf{E}$ are also taken with respect to the intermediate configuration, i.e.

$$\mathbf{E}_e = \tfrac{1}{2}(\mathbf{F}_e^T\mathbf{F}_e - \mathbf{I}) \tag{19.18}$$

If plastic straining is assumed to have no effect on the elastic moduli, further differentiation of (19.17) gives (see also (10.47) and Section 13.4):

$$\dot{\mathbf{S}} = \mathbf{D}_{tK2}\dot{\mathbf{E}}_e \quad \text{or} \quad \dot{S}_{ab} = D^{tK2}_{abcd}\,\dot{E}^e_{cd} \tag{19.19}$$

with

$$D^{tK2}_{abcd} = \frac{\partial^2 \varphi}{\partial E^e_{ab}\partial E^e_{cd}} \tag{19.20}$$

Given (19.17), the Kirchhoff stresses, τ, which relate to the final configuration can be obtained via (10.50) as

$$\tau = \mathbf{F}_e\mathbf{S}\mathbf{F}_e^T \tag{19.21}$$

Following very closely the approach in Section 10.4, we can now differentiate (19.21) to obtain:

$$\dot{\tau} = \dot{\tau}_T + \mathbf{l}_e\tau + \tau\mathbf{l}_e^T = \mathbf{D}_{tK2}:\dot{\boldsymbol{\varepsilon}}_e + \mathbf{l}_e\tau + \tau\mathbf{l}_e^T \tag{19.22}$$

where, via (10.56), the components of the tangential D_{rTK} tensor are related to those in (19.20) via:

$$D^{tTK}_{ijkl} = F^e_{ia}F^e_{jb}F^e_{kc}F^e_{ld}D^{tK2}_{abcd} \tag{19.23}$$

(There is no significance in the e for elastic now being a superscript, it is put there purely for considerations of space.)

Using the relationships in Section 12.4, equation (19.22) can be reworked to include the Jaumann rate so that

$$\dot{\tau} = \dot{\tau}_J + \dot{\boldsymbol{\Omega}}_e\tau + \tau\dot{\boldsymbol{\Omega}}_e^T = \mathbf{D}:_{tJK}\dot{\boldsymbol{\varepsilon}}_e + \dot{\boldsymbol{\Omega}}_e\tau + \tau\dot{\boldsymbol{\Omega}}_e^T \tag{19.24}$$

where the relation between the Jaumann-rate constitutive tensor, $\mathbf{D}_{tJK}$ and the Truesdell-rate tensor, $\mathbf{D}_{tTK}$ has been given in (12.51).

By assuming that stresses are small compared to any elastic moduli, the stress terms in (12.51) can be ignored so that we are left with the tansformations in (19.23) to relate $\mathbf{D}_{tTJ}$ to $\mathbf{D}_{tK2}$. Assuming small elastic strains, the F^e terms (from $\mathbf{F}_e$) in (19.23) may be approximated by terms from the rotation, $\mathbf{R}_e$ (see (Section 4.10)). Hence, assuming elastic isotropy, the latter has no effect so that:

$$\dot{\tau} = \dot{\tau}_J + \dot{\boldsymbol{\Omega}}_e\tau + \tau\dot{\boldsymbol{\Omega}}_e^T = \mathbf{D}:\dot{\boldsymbol{\varepsilon}}_e + \dot{\boldsymbol{\Omega}}_e\tau + \tau\dot{\boldsymbol{\Omega}}_e^T \tag{19.25}$$

where $\mathbf{D}$ in (19.25) would contain the tangent moduli stemming from (19.20). Using the simplest possible formulation, this would be a fixed linear-elastic modular matrix.

If, in addition, it is assumed that the plastic spin ($\dot{\boldsymbol{\Omega}}_p$) is zero (valid for a wide range, but not all plasticity [N4]), (19.25) is further replaced by

$$\dot{\tau} = \dot{\tau}_J + \dot{\boldsymbol{\Omega}}\tau + \tau\dot{\boldsymbol{\Omega}}^T = \mathbf{D}:\dot{\boldsymbol{\varepsilon}}_e + \dot{\boldsymbol{\Omega}}\tau + \tau\dot{\boldsymbol{\Omega}}^T \tag{19.26}$$

where $\dot{\boldsymbol{\Omega}}$ are the total spins. Equation (19.26) is the basis of the Eulerian finite element formulation already described in Section 12.4.

We must now introduce the yield criterion and plastic flow. The latter are strictly associated with the Cauchy stresses, $\boldsymbol{\sigma}$, rather than the Kirchhoff stresses $\tau = J\boldsymbol{\sigma}$. However, we have already shown in Section 12.5 that the use of the Jaumann rate of Cauchy stress (in conjunction with a fixed symmetric modular matrix $\mathbf{D}$) leads to a non-symmetric tangent stiffness matrix while this is not true (Section 12.4) of the Kirchhoff stresses. Luckily, the only difference between the two involves the J term which relates the current volume to the initial volume. For von Mises, J_2, plasticity, the volume change is only associated with elastic deformation and can therefore be considered as small. Hence, we can approximate J as 1 and effectively redefine the reference configuration as the current configuration.

Indeed, we can make such an approximation even if there are large plastic volume changes provided the elastic strains are small [N2]. This observation follows from (19.21) from which τ is related to $\boldsymbol{\sigma}$ by

$$\boldsymbol{\sigma} = \tau/J_e \tag{19.27}$$

where J_e is the elastic volume change from the intermediate to the current configuration.

To consider plasticity, we may therefore as a reasonable approximation, write the yield criterion etc. in terms of Kirchhoff stresses and apply (19.26). In order to apply the finite element formulation of Section 12.4, we need to be able to re-express (19.26) so as to involve the total strain rate ($\dot{\boldsymbol{\varepsilon}}$) rather than the elastic strain rate ($\dot{\boldsymbol{\varepsilon}}_e$) so that:

$$\dot{\tau} = \dot{\tau}_J + \dot{\boldsymbol{\Omega}}\tau + \tau\dot{\boldsymbol{\Omega}}^T = \mathbf{D}_{tep}:\dot{\boldsymbol{\varepsilon}} + \dot{\boldsymbol{\Omega}}\tau + \tau\dot{\boldsymbol{\Omega}}^T \tag{19.28}$$

Naively, one might simply use the small-strain procedures of Sections 6.3–6.5 to obtain $\mathbf{D}_{tep}$. It is, however, not obvious that such an approach is valid and hence we will outline the derivation which is closely related to that in Section 6.5.2.

As a start, we write the yield function in the form:

$$f = \tau_e - \tau_o = \sqrt{\tfrac{3}{2}}(\tau':\tau')^{1/2} - \tau_o \tag{19.29}$$

where, for the reasons given previously, we are working with Kirchhoff stresses rather than Cauchy stresses. Certainly for metal plasticity, there will be very little difference

between the two. In the following we will work with the first form in (19.29) with τ_e as the equivalent stress (equivalent to σ_e in Chapter 6) and τ_o as the yield stress.

We assume an additive decomposition of the strain rates (Section 19.2) so that:

$$\dot{\boldsymbol{\varepsilon}}_e = \dot{\boldsymbol{\varepsilon}} - \dot{\boldsymbol{\varepsilon}}_p \tag{19.30}$$

Assuming associative plasticity, the plastic strain rates are then given (see (6.33)) by

$$\dot{\boldsymbol{\varepsilon}}_p = \dot{\eta}\frac{\partial f}{\partial \boldsymbol{\tau}} = \dot{\eta}\mathbf{a} \tag{19.31}$$

so that (19.26) can be written as

$$\dot{\boldsymbol{\tau}} = \dot{\boldsymbol{\tau}}_J + \dot{\boldsymbol{\Omega}}\boldsymbol{\tau} - \boldsymbol{\tau}\dot{\boldsymbol{\Omega}} = \mathbf{D}(\dot{\boldsymbol{\varepsilon}} - \dot{\eta}\mathbf{a}) + \dot{\boldsymbol{\Omega}}\boldsymbol{\tau} - \boldsymbol{\tau}\dot{\boldsymbol{\Omega}} \tag{19.32}$$

The consistency condition is now given by

$$\dot{f} = \mathbf{a}:\dot{\boldsymbol{\tau}} + A'\dot{\eta} = 0 \tag{19.33}$$

(with A' as the hardening parameter—see Chapter 6). Substituting from (19.32) into (19.33) leads to

$$\mathbf{a}:\dot{\boldsymbol{\tau}}_J + A'\dot{\eta} = \mathbf{a}:\mathbf{D}:(\dot{\boldsymbol{\varepsilon}} - \dot{\eta}\mathbf{a}) = 0 \tag{19.34}$$

The validity of (19.34) depends on the relationship:

$$\mathbf{a}:(\dot{\boldsymbol{\Omega}}\boldsymbol{\tau} - \boldsymbol{\tau}\dot{\boldsymbol{\Omega}}) = 0 \tag{19.35}$$

This relationship is true if (as here) $\mathbf{a}$ and $\boldsymbol{\tau}$ are symmetric while $\dot{\boldsymbol{\Omega}}$ is antisymmetric. It is this step that will allow the direct use of the small-strain equations for $\mathbf{D}_{tep}$. It is also valid if, in (19.32), we used some other objective stress rate of the form:

$$\dot{\boldsymbol{\tau}}_o = \dot{\boldsymbol{\tau}} - \mathbf{A}\boldsymbol{\tau} + \boldsymbol{\tau}\mathbf{A} \tag{19.36}$$

with $\mathbf{A}$ as a skew matrix. For example, the Green-Nagdhi rate (Section 10.8) would be satisfactory in this respect while the Truesdell rate would not.

For completeness, we note that substitution for $\dot{\eta}$ from (19.33) into (19.32) leads in conjunction with (19.28) to the standard expression of (6.18), i.e.

$$\dot{\boldsymbol{\tau}}_J = \left(\mathbf{D} - \frac{1}{\mathbf{a}:\mathbf{D}:\mathbf{a} + A'}(\mathbf{D}:\mathbf{a}) \otimes \mathbf{D}:\mathbf{a})\right):\dot{\boldsymbol{\varepsilon}} \tag{19.37}$$

The issue of the use of different objective rates in relation to elastic analysis has been discussed in Sections 10.8 and 13.10.3 where the issue of oscillating stresses following a pure shear deformation [D1.10] was discussed. It was pointed out that the problem largely related to the use of a hypoelastic rather than a hyperelastic model for the elasticity and was associated with large elastic strains. The oscillations can be removed by adopting the Green–Nagdhi rate [D1.10]. However, other anomalies remain [A2]. Similar oscillating stresses can be obtained with plasticity and small elastic strains if kinematic hardening is introduced [N3, L4.14]. Needleman [N4], Atluri [A2] and Nemat–Nasser [N1.10] argue that the key issue is not the chosen rate but rather the evolution law used in a large-strain environment for the relevant internal variables (back stresses–Chapter 15).

In summary, in this section, we have shown that (with elastic isotropy and isotropic hardening), 'conventional' Jaumann-rate based solutions are consistent with $\mathbf{F}_e - \mathbf{F}_p$-

based solutions if the elastic strains are small. This will be illustrated numerically in Section 19.10.

19.4 USING THE RATE FORM WITH AN 'EXPLICIT DYNAMICS CODE'

In the previous section, we showed that, for small elastic strains, a Jaumann rate formulation was effectively equivalent to an $\mathbf{F}_e\mathbf{F}_p$ formulation (see also [N4]). But unless the increments are very small, there are considerable difficulties with the integration of the rate equations such as (19.26). However, for one important class of problem, the incremental steps are indeed very small. Algorithms for explicit dynamics are discussed in Section 24.5 and 24.6 of Chapter 24 on 'Non-linear Dynamics'. For such codes, a staggered system is usually applied so that the nodal velocities are known at the half time steps (i.e. $\dot{\mathbf{p}}_{n+1/2}$) and the stresses and displacements at the whole time steps (i.e. $\boldsymbol{\sigma}_{n+1}$ and $\mathbf{p}_{n+1}$).

We will assume that the Jaumann rate of Cauchy stress is being adopted so that, instead of starting from (19.26), our basic equation is

$$\dot{\boldsymbol{\sigma}} = \dot{\boldsymbol{\sigma}}_J + \dot{\boldsymbol{\Omega}}\boldsymbol{\sigma} + \boldsymbol{\sigma}\dot{\boldsymbol{\Omega}}^T \tag{19.38}$$

An appropriate updating procedure might then involve:

1. Given $\dot{\mathbf{p}}_{n+1/2}$, compute:

$$\dot{\boldsymbol{\theta}}_{n+1/2} = v(\mathbf{l}_{n+1/2}) = \mathbf{G}(\mathbf{x}_n)\dot{\mathbf{p}}_{n+1/2} \tag{19.39a}$$

   where the symbol $v(\mathbf{A})$ means vector form of $\mathbf{A}$ and $\mathbf{G}(\mathbf{x})$ has been described in Section 12.2 (see (12.11)).
2. Then use (10.22) to compute $\dot{\boldsymbol{\varepsilon}}_{n+1/2}$ and $\dot{\boldsymbol{\Omega}}_{n+1/2}$ from $\mathbf{l}_{n+1/2}$ i.e. with

$$\dot{\boldsymbol{\varepsilon}}_{n+1/2} = \tfrac{1}{2}(\mathbf{l}_{n+1/2} + \mathbf{l}^T_{n+1/2}); \qquad \dot{\boldsymbol{\Omega}} = \tfrac{1}{2}(\mathbf{l}_{n+1/2} - \mathbf{l}^T_{n+1/2}) \tag{19.39b}$$

3. Compute:

$$\dot{\boldsymbol{\sigma}}_{J,n+1/2} = \mathbf{D}_{tep}(\boldsymbol{\sigma}_n)\dot{\boldsymbol{\varepsilon}}_{n+1/2} \tag{19.40}$$

   where $\mathbf{D}_{tep}$ is the elasto-plastic modular matrix which is assumed to be a function of the known Cauchy stresses at n (and internal variables such as equivalent plastic strains at n).

4. Compute:

$$\boldsymbol{\sigma}_{n+1} = \boldsymbol{\sigma}_n + \Delta t\dot{\boldsymbol{\sigma}}_{J,n+1/2} + \Delta t(\dot{\boldsymbol{\Omega}}_{n+1/2}\boldsymbol{\sigma}_n + \boldsymbol{\sigma}_n\dot{\boldsymbol{\Omega}}^T_{n+1/2}) \tag{19.41}$$

5. Compute the (static) internal force vector via:

$$\mathbf{q}_i = \int \mathbf{B}(\mathbf{x}_{n+1})^T\boldsymbol{\sigma}_{n+1}\mathrm{d}V_{n+1} \tag{19.42}$$

   Steps 3 and 4 above could be replaced by

3a. Compute:

$$\boldsymbol{\sigma}_{\text{trial}} = \boldsymbol{\sigma}_{\text{B}} = \boldsymbol{\sigma}_{\text{n}} + \Delta t \mathbf{D}_{\text{e}} \dot{\boldsymbol{\varepsilon}}_{n+1/2} \tag{19.43}$$

where $\mathbf{D}_{\text{e}}$ is the elastic modular matrix.

3b. Apply a small strain 'radial return' or 'backward Euler procedure' (see Chapters 6, 14 and 15) to change $\boldsymbol{\sigma}_{\text{B}}$ to $\boldsymbol{\sigma}_{\text{C}}$.

4. Compute:

$$\boldsymbol{\sigma}_{n+1} = \boldsymbol{\sigma}_{\text{C}} + \Delta t (\dot{\boldsymbol{\Omega}}_{n+1/2} \boldsymbol{\sigma}_n + \boldsymbol{\sigma}_n \dot{\boldsymbol{\Omega}}^{\text{T}}_{n+1/2}) \tag{19.44}$$

Algorithm 19.1 A rate related update suitable for an explicit dynamics code.

19.5 INTEGRATING THE RATE EQUATIONS

While the method of the previous section may be valid for an explicit dynamics code using very small times steps, more generally we must address the issue of a more accurate 'integration of the rate equations'. (Alternatively, as in Sections 19.6–19.8, we may return to an $\mathbf{F}_{\text{e}}\mathbf{F}_{\text{p}}$ formulation using a hyperelastic relationship.) Part of this integration is related to the 'plasticity side' as in small strain plasticity (see Chapters 6, 14 and 15). However, with large strains, we also have the issue of the rotation. As originally discussed in Section 10.2, if we use the Jaumann rate and have a pure rotation there will be no straining. However, this is only true for infinitesimal rates and not for the 'increments' that will be obtained within the implicit finite element formulation. Hence we require some simple 'integration procedure' that, at the very least, ensures no straining with finite rigid rotations. Much work has centred on this issue [S3.14, F1, G1, H3, H4, K1–K3, P3]. One such integration algorithm was obtained by Hughes and Winget [H4] and involves an extension of the mid-point algorithm discussed in Section 3.8 for simple truss elements. The algorithm is obtained by starting from equation (10.17) from which we derived the Jaumann rate relationship, i.e.

$$\boldsymbol{\sigma}_n = \mathbf{R}\boldsymbol{\sigma}_{\text{o}}\mathbf{R}^{\text{T}} + \Delta t \mathbf{D}_{\text{t}} : \dot{\boldsymbol{\varepsilon}} \tag{19.45}$$

where subscript o means 'old' and subscript n means 'new'. The Hughes–Winget algorithm, involves replacing (19.45) with

$$\boldsymbol{\sigma}_{\text{n}} = \mathbf{Q}(\boldsymbol{\Omega}_{\text{m}})\boldsymbol{\sigma}_{\text{o}}\mathbf{Q}(\boldsymbol{\Omega}_{\text{m}})]^{\text{T}} + \mathbf{D}_{\text{tm}} : \Delta\boldsymbol{\varepsilon}_{\text{m}} \tag{19.46}$$

where subscript m relates to the 'mid-point' and $\mathbf{Q}$ is an approximation to $\mathbf{R}$ that coincides with $\mathbf{R}$ when the incremental motion involves a pure rotation; $\Delta\boldsymbol{\varepsilon}_{\text{m}}$ and $\boldsymbol{\Omega}_{\text{m}}$would be obtained from:

$$\mathbf{l}_{\text{m}} = \frac{\partial \Delta \mathbf{u}}{\partial \mathbf{x}_{\text{m}}} \tag{19.47}$$

where in a finite element context, $\mathbf{l}_{\text{m}}$ would be obtained from $\Delta\boldsymbol{\theta}$ which would be of the same form as (12.11) but given by

$$\Delta\boldsymbol{\theta} = \mathbf{G}(\mathbf{x}_{\text{m}})\Delta\mathbf{p} \tag{19.48}$$

The tensors $\boldsymbol{\Omega}_{\text{m}}$ and $\Delta\boldsymbol{\varepsilon}_{\text{m}}$ in (19.46) would be obtained from:

$$\Delta\boldsymbol{\varepsilon}_{\text{m}} = \tfrac{1}{2}(\mathbf{l}_{\text{m}} + \mathbf{l}_{\text{m}}^{\text{T}}); \qquad \boldsymbol{\Omega}_{\text{m}} = \tfrac{1}{2}(\mathbf{l}_{\text{m}} - \mathbf{l}_{\text{m}}^{\text{T}}) \tag{19.49}$$

To be incrementally objective, the algorithm must ensure that, for a pure rigid body rotation, both $\Delta\boldsymbol{\varepsilon}_m$ is zero and the stresses are correctly updated with $\mathbf{Q}(\boldsymbol{\Omega}_m) = \mathbf{R}$. For such a rigid rotation we have:

$$\mathbf{x}_n = \mathbf{R}\mathbf{x}_o = \mathbf{x}_o + \Delta\mathbf{u} \tag{19.50}$$

so that:

$$2\mathbf{x}_m = \mathbf{x}_n + \mathbf{x}_o = (\mathbf{I} + \mathbf{R})\mathbf{x}_o \tag{19.51}$$

and hence, from (19.50) and (19.51):

$$\Delta\mathbf{u} = (\mathbf{R} - \mathbf{I})\mathbf{x}_o = 2(\mathbf{R} - \mathbf{I})(\mathbf{R} + \mathbf{I})^{-1}\mathbf{x}_m \tag{19.52}$$

and

$$\frac{\partial \Delta\mathbf{u}}{\partial \mathbf{x}_m} = \mathbf{l}_m = 2(\mathbf{R} - \mathbf{I})(\mathbf{R} + \mathbf{I})^{-1} \tag{19.53}$$

Substitution into the first expression in (19.49) gives:

$$\Delta\boldsymbol{\varepsilon}_m = (\mathbf{R} - \mathbf{I})(\mathbf{R} + \mathbf{I})^{-1} + (\mathbf{R} + \mathbf{I})^{-T}(\mathbf{R} - \mathbf{I})^T \tag{19.54a}$$

$$= \mathbf{R}(\mathbf{R} + \mathbf{I})^{-1} - (\mathbf{R} + \mathbf{I})^{-T} - (\mathbf{R} + \mathbf{I})^{-1} + (\mathbf{R} + \mathbf{I})^{-T}\mathbf{R}^T \tag{19.54b}$$

The relationship:

$$(\mathbf{R} + \mathbf{I})^T = (\mathbf{I} + \mathbf{R})\mathbf{R}^T = \mathbf{R}^T(\mathbf{I} + \mathbf{R}) \tag{19.55}$$

which stems from the relationship $\mathbf{R}^T\mathbf{R} = \mathbf{R}\mathbf{R}^T = \mathbf{I}$, can be used to ensure that the first two terms and last two terms in (19.54b) each combine to be zero and hence, as required, $\Delta\boldsymbol{\varepsilon}_m$ is zero. In the following, we will also require the relationship:

$$(\mathbf{I} + \mathbf{A}^T)^{-1} = (\mathbf{I} + \mathbf{A})^{-1}\mathbf{A} = \mathbf{A}(\mathbf{I} + \mathbf{A})^{-1} \tag{19.56}$$

which applies when $\mathbf{A}$ is a skew-symmetric matrix.

With $\Delta\boldsymbol{\varepsilon}_m$ zero, from (19.49), we obtain:

$$\boldsymbol{\Omega}_m = \mathbf{l}_m = 2(\mathbf{R} - \mathbf{I})(\mathbf{R} + \mathbf{I})^{-1} \tag{19.57}$$

or:

$$\boldsymbol{\Omega}_m(\mathbf{R} + \mathbf{I}) = 2(\mathbf{R} - \mathbf{I}) \tag{19.58}$$

This equation can be solved for $\boldsymbol{\Omega}_m$ to obtain:

$$\mathbf{R} = [\mathbf{I} - \tfrac{1}{2}\boldsymbol{\Omega}_m]^{-1}[\mathbf{I} + \tfrac{1}{2}\boldsymbol{\Omega}_m] = [\mathbf{I} + \tfrac{1}{2}\boldsymbol{\Omega}_m][\mathbf{I} - \tfrac{1}{2}\boldsymbol{\Omega}_m]^{-1} = [\mathbf{I} + [\mathbf{I} - \tfrac{1}{2}\boldsymbol{\Omega}_m]^{-1}\boldsymbol{\Omega}_m] \tag{19.59}$$

The equivalence of the various expressions in (19.59) can be demonstrated with the aid of (19.56) (note that $\boldsymbol{\Omega}_m$ is skew-symmetric).

In summary, the algorithm involves the use of (19.46) with $\mathbf{Q}(\boldsymbol{\Omega}_m) = \mathbf{R}$ from (19.59). In practice, there is no need to introduce the matrix divisions in (19.59) because the solution to (19.58) can also be expressed as (now using the symbol $\mathbf{Q}$):

$$\mathbf{Q} = \mathbf{I} + \frac{1}{(1 + \frac{1}{4}\boldsymbol{\omega}_m^T\boldsymbol{\omega}_m)}[\boldsymbol{\Omega}_m + \tfrac{1}{2}\boldsymbol{\Omega}_m\boldsymbol{\Omega}_m] \tag{19.60}$$

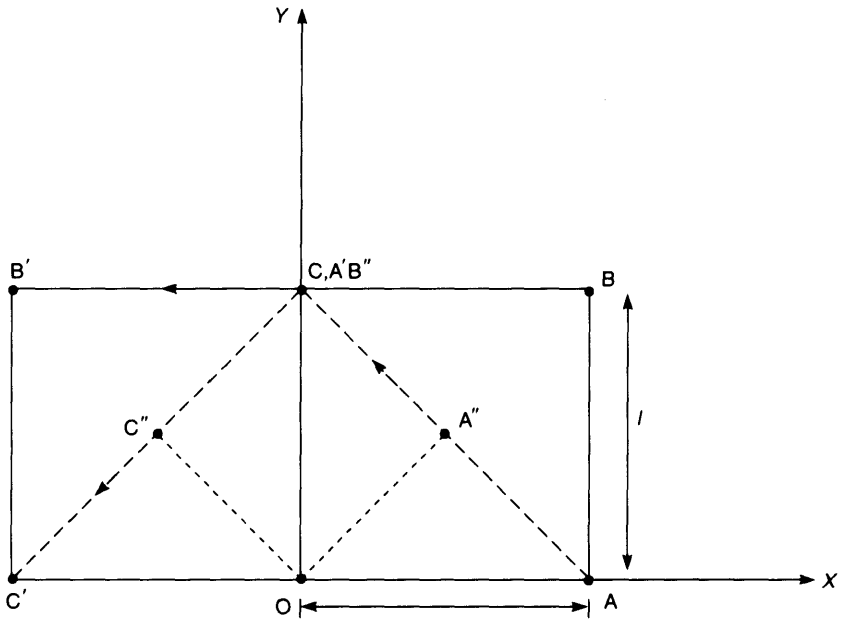

Figure 19.3 Illustrating the Hughes–Wingert algorithm.

where the antisymmetric mid-point spin matrix, $\mathbf{\Omega}_m$ from (19.49) can be written as:

$$\mathbf{\Omega}_m = \begin{bmatrix} 0 & -\omega_3 & \omega_2 \\ \omega_3 & 0 & -\omega_1 \\ -\omega_2 & \omega_1 & 0 \end{bmatrix} \tag{19.61}$$

and:

$$\boldsymbol{\omega}_m^T = (\omega_1, \omega_2, \omega_3) \tag{19.62}$$

is the vector equivalent of $\mathbf{\Omega}_m$. (In fact (19.60) is the form of the rotation matrix given in (16.35) while $\boldsymbol{\omega}_m$ is the tangent scaled pseudo vector.)

As a simple example, consider the square block in Figure 19.3 which is rotated through 90° about O from configuration OABC to configuration OA'B'C' via the intermediate configuration OA"B"C"D". The use of the standard bilinear shape functions will show that the mid-point Jacobian is given by

$$\mathbf{J}_m = \begin{bmatrix} \dfrac{\partial x}{\partial \xi} & \dfrac{\partial y}{\partial \xi} \\ \dfrac{\partial x}{\partial \eta} & \dfrac{\partial y}{\partial \eta} \end{bmatrix}_m = \frac{1}{4}\begin{bmatrix} 1 & 1 \\ -1 & 1 \end{bmatrix} \tag{19.63}$$

while the total displacement derivatives with respect to the non-dimensional

coordinates are:

$$\begin{bmatrix} \frac{\partial v}{\partial \xi} & \frac{\partial u}{\partial \eta} \\ \frac{\partial v}{\partial \xi} & \frac{\partial v}{\partial \eta} \end{bmatrix} = \frac{1}{2}\begin{bmatrix} -1 & -1 \\ 1 & -1 \end{bmatrix} \tag{19.64}$$

so that we obtain (with the ordering as in (4.72)):

$$\mathbf{l}_m = \frac{\partial \mathbf{u}}{\partial \mathbf{x}_m} = \begin{bmatrix} 0 & -2 & 0 \\ 2 & 0 & 0 \\ 0 & 0 & 0 \end{bmatrix} \tag{19.65}$$

from which with the aid of (19.49), $\Delta\boldsymbol{\varepsilon}_m = \mathbf{0}$ while (as anticipated) $\boldsymbol{\Omega}_m = \mathbf{l}_m$. We can now use either $\mathbf{Q} = \mathbf{R}$ from (19.59) or (19.60) (with (19.62)) to obtain:

$$\mathbf{Q}(\boldsymbol{\Omega}_m) = \begin{bmatrix} 0 & -1 & 0 \\ 1 & 0 & 0 \\ 0 & 0 & 0 \end{bmatrix} \tag{19.66}$$

which is the correct rotation matrix.

The reader can attempt to apply the same procedure with the block being rotated through 180°. He or she will find that graphically the mid-point configuration collapses to a point while numerically, $\mathbf{J}_m$ is singular. The rotation and stretch (here zero) could, of course, be obtained via a polar decomposition as in Section 4.8.

While the Hughes–Winget algorithm gives the correct solution for a pure rotation, it can introduce inaccuracies when the incremental motion involves stretching as well as a rotation. More sophisticated mid-point procedures have therefore been advocated by among others Key [K1–K3] and Hughes and Winget [H4] (see also Simo and Hughes [S5.14]). In essence, these techniques involve firstly rotating the stresses to the mid-point configuration, then applying the stress update (say via the conventional small-strain 'radial return'), then rotating on to the final configuration. The techniques therefore require the mid-point rotation matrix which may either be total or incremental. In either case, knowing $\mathbf{R}$ (either obtained approximately or exactly), one requires $\mathbf{R}^{1/2}$ where:

$$\mathbf{R}^{1/2}\mathbf{R}^{1/2} = \mathbf{R} \tag{19.67}$$

Considering, firstly the two-dimensional case, the rotation angle θ can easily be obtained from $\mathbf{R}$ which is then given by (see (16.27)):

$$\mathbf{R}(\theta) = \begin{bmatrix} 1 & 0 & 0 \\ 0 & \cos\theta & -\sin\theta \\ 0 & \sin\theta & \cos\theta \end{bmatrix} \tag{19.68}$$

so that we can simply obtain:

$$\mathbf{R}(\theta/2) = \begin{bmatrix} 1 & 0 & 0 \\ 0 & \cos(\theta/2) & -\sin(\theta/2) \\ 0 & \sin(\theta/2) & \cos(\theta/2) \end{bmatrix} \tag{19.69}$$

The three-dimensional equivalents of (19.68) and (19.69) are (see (16.22))

$$\mathbf{R}(\boldsymbol{\theta}) = \mathbf{R}(\theta\mathbf{e}) = \mathbf{I} + \frac{\sin\theta}{\theta}\mathbf{S}(\boldsymbol{\theta}) + \frac{(1-\cos\theta)}{\theta^2}\mathbf{S}(\boldsymbol{\theta})\mathbf{S}(\boldsymbol{\theta}) \tag{19.70}$$

$$\mathbf{R}^{1/2} = \mathbf{R}(\boldsymbol{\theta}/2) = \mathbf{R}\left(\frac{\theta}{2}\mathbf{e}\right) = \mathbf{I} + \frac{\sin(\theta/2)}{\theta}\mathbf{S}(\boldsymbol{\theta}) + \frac{(1-\cos(\theta/2))}{\theta^2}\mathbf{S}(\boldsymbol{\theta})\mathbf{S}(\boldsymbol{\theta}) \tag{19.71}$$

The simplest way to find $\mathbf{R}^{1/2}$ is to use the procedure of Section 16.10 to obtain the unit quaternion, $\hat{\mathbf{q}}$, from $\mathbf{R}$ where $\hat{\mathbf{q}}$ takes the form:

$$\hat{\mathbf{q}} = \begin{pmatrix} \sin(\theta/2)\mathbf{e} \\ \cos(\theta/2) \end{pmatrix} \tag{19.72}$$

after which $\mathbf{R}^{1/2}$ is easily computed from (19.71).

19.6 AN $\mathbf{F}_e\mathbf{F}_p$ UPDATE BASED ON THE INTERMEDIATE CONFIGURATION

A numer of workers have applied the $\mathbf{F}_e\mathbf{F}_p$ decomposition in conjunction with updates based on the intermediate configuration [C2, E1, H1, M2, O1, P1, P2, S1–S3, W1]. Such procedures are usually applied in conjunction with a hyperelastic constitutive law and thereby obviate the need for the integration of any rate equations. We will concentrate on a simple J_2 plasticity with isotropic hardening and will work with a hyperelastic model which uses principal log strains (Section 13.10.1). Such procedures have been applied in [E1, P1, P2, W1] and lead to an updated algorithm which turns out to be of a very similar form to the radial return algorithm (Section 6.6.7.) for small strains. The present work is largely based on that of Eterovic and Bathe [E1] but also includes elements from a similar procedure by Cuitino and Ortiz [C2].

The formulation for elasticity is based on the principal log strains and hence follows closely the development of Section 13.10.1. If we are working in fixed principal directions (as in an axisymmetric shell formulation [W2]), then, with respect to such a direction, if $\lambda = \lambda_e\lambda_p$ (see (19.4b)) and $\varepsilon_e = \log_e\lambda_e$ while $\varepsilon_p = \log_e\lambda_p$, then we have an additive decomposition in terms of these log strains so that $\varepsilon = \log_e\lambda = \log_e(\lambda_e\lambda_p) = \varepsilon_e + \varepsilon_p$. In the following we are also considering the changes of principal directions and we will initially concentrate on a formulation based on the stresses $\mathbf{O}$ which are work-conjugate to $\log_e\mathbf{U}$ (Section 10.5). Following the approach of Section 6.6.6 and 6.6.7, we apply a form of 'operator split' and first compute the stresses at the 'trial point', B, for which the plastic configuration ($\mathbf{F}_{pold}$) is assumed frozen in the form that it was at the end of the previous increment. In addition, we know the current total value of $\mathbf{F}$ ($\mathbf{F}_n$ with n for new). Via (19.4a), we can therefore compute the value of $\mathbf{F}$ at the 'trial point' B as

$$\mathbf{F}_B = \mathbf{F}_n\mathbf{F}_{po}^{-1} \tag{19.73}$$

and hence the principal directions of $\mathbf{C}_B = \mathbf{F}_B^T\mathbf{F}_B$ with equivalent stretches, λ_B so that (see (4.137) or (10.9)):

$$\mathbf{C}_B = \sum\lambda_{iB}^2\mathbf{N}_{iB}\otimes\mathbf{N}_{iB} \tag{19.74}$$

It follows that:

$$\log_e \mathbf{U}_B = \sum \log_e \lambda_{iB} \mathbf{N}_{iB} \otimes \mathbf{N}_{iB} \tag{19.75}$$

while the equivalent rotation (which will be required later) is given by

$$\mathbf{R}_B = \mathbf{F}_B \mathbf{U}_B^{-1} = \mathbf{F}_B \mathbf{Q}(\mathbf{N}_B)\, \mathbf{Diag}(\lambda_B^{-1})\, \mathbf{Q}(\mathbf{N}_B)^T \tag{19.76}$$

From (13.185) and (13.187), the equivalent 'log stresses', $\mathbf{O}_B$ (which are related to the intermediate configuration) are given by

$$\mathbf{O}_B = \sum O_{iB} \mathbf{N}_{iB} \otimes \mathbf{N}_{iB} = \sum O'_{iB} \mathbf{N}_{iB} \otimes \mathbf{N}_{iB} + K \log_e J_B \mathbf{I} \tag{19.77}$$

where the symbol ' denotes the deviatoric part and

$$O_{iB} = O'_{iB} + K \log_e J_B = O'_{iB} + K \sum \log_e(\lambda_{iB}) \tag{19.78}$$

with

$$O'_{iB} = 2\mu \log_e \lambda'_{iB} = 2\mu \log_e \lambda_{iB} - \tfrac{2}{3}\mu \log_e J_B \tag{19.79}$$

Regarding the yield function, we have already indicated in Section 19.3 that it is reasonable to write the function in terms of the kirchhoff stresses (see (19.29)) rather than the Cauchy stresses so that:

$$f = \tau_e - \tau_o = \sqrt{\tfrac{3}{2}}(\boldsymbol{\tau}' : \boldsymbol{\tau}')^{1/2} - \tau_o \tag{19.80}$$

From (10.83), the Kirchhoff stresses $\boldsymbol{\tau}$ are related to the 'rotated' stresses $\mathbf{O}$ (here with respect to the intermediate configuration) via a rotation so that:

$$\boldsymbol{\tau} = \mathbf{R}_B \mathbf{O} \mathbf{R}_B^T \tag{19.81}$$

can be obtained from Kirchhoff stresses. Equation (19.81) also applies with the deviatoric stresses. Hence the isotropic yield function of (19.80) transforms directly to

$$f = O_e - O_e = \sqrt{\tfrac{3}{2}}(\mathbf{O}' : \mathbf{O}')^{1/2} - \mathbf{O}_o \tag{19.82}$$

(The yield stress in (19.82) has been written as O_o; but $O_o = \tau_o \simeq \sigma_o$.) The flow rule then follows as

$$\dot{\mathbf{E}}_p = \mathbf{L}_p = \dot{\mathbf{F}}_p \mathbf{F}_p^{-1} = \dot{\eta}\mathbf{A} = \dot{\eta} \frac{\partial \mathbf{O}}{\partial \log_e \mathbf{U}} = \dot{\eta} \frac{3}{2O_e} \mathbf{O}' \tag{19.83}$$

In writing (19.83), (19.14) has been used for the 'plastic deformation rate', while the plastic spin (on the intermediate configuration) has been assumed to be zero. The plastic work rate, $\dot{W}_p$ (see (6.21)) can then be written as

$$\dot{W}_p = \mathbf{S} : \dot{\mathbf{E}}_p = \mathbf{F}_e^{-1} \boldsymbol{\tau} \mathbf{F}_e^{-T} : \dot{\mathbf{E}}_p = \mathbf{U}_e \mathbf{O} \mathbf{U}_e^{-1} : \dot{\mathbf{E}}_p = \mathbf{O} : \dot{\mathbf{E}}_p = O_e \dot{E}_{ps} \tag{19.84}$$

where we have used the fact that $\mathbf{O}$ and $\mathbf{U}_e$ are coaxial and (see (6.29) and (6.34)):

$$\dot{\eta} = \dot{E}_{ps} = \sqrt{\tfrac{2}{3}}(\dot{\mathbf{E}}_p : \dot{\mathbf{E}}_p) = \sqrt{\tfrac{2}{3}}(\mathbf{A} : \mathbf{A}) \tag{19.85}$$

is the equivalent plastic strain rate. The development in (19.84) remain valid even if an antisymmetric plastic spin term is added to the definition of $\dot{\mathbf{E}}_p$ in (19.83) because, with $\mathbf{S}$ symmetric, there will be no alteration to the work rate. If it is assumed that the plastic flow direction, $\mathbf{A}$, is fixed during the increment (say at $\mathbf{A}_B$) [C2], the solution to (19.83) in

moving from the 'trial elastic solution', B, to the final solution at C is

$$\mathbf{F}_{pn} = \mathbf{F}_{pC} = \exp(\Delta\eta \mathbf{A}_B)\mathbf{F}_{pB} = \exp(\Delta\eta \mathbf{A}_B)\mathbf{F}_{po} \tag{19.86}$$

Hence the final value of the elastic right Cauchy–Green tensor (at the 'return point', C) is given by

$$\mathbf{C}_C = (\mathbf{F}_B\mathbf{F}_{pC}^{-1})^T\mathbf{F}_B\mathbf{F}_{pC}^{-1} = \exp(-\Delta\eta \mathbf{A}_B^T)\mathbf{C}_B\exp(-\Delta\eta \mathbf{A}_B) \tag{19.87}$$

Having assumed that the flow direction is fixed at that at B, the principal directions of the flow direction coincide with those of $\mathbf{O}_B$ and $\log_e \mathbf{U}_B$—see (19.75) and (19.77) and of $\mathbf{C}_B$ (see (19.74)). It follows from (19.87) that the latter coincide with the principal directions of $\mathbf{C}_C$ (and hence of $\mathbf{O}_C$), i.e. $\mathbf{N}_C = \mathbf{N}_B$. Also from (19.87), it follows that:

$$\lambda_{iC}^2 = \exp(-2\Delta\eta A_{iB})\lambda_{iB}^2 \tag{19.88}$$

where A_{iB} are the principal values of the flow tensor $\mathbf{A}$ at B. Taking logs of both sides in (19.88) leads to the relationship:

$$\log_e \lambda_{iC} = \log_e \lambda_{iB} - \Delta\eta A_{iB} \tag{19.89}$$

In moving from B to C, the process has only involved plasticity and hence (with J_2 plasticity) no volume change would be expected. To check this, we note that via (19.89) we can write:

$$\mathbf{C}_C = \sum \lambda_{iC}^2 \mathbf{N}_{iB} \otimes \mathbf{N}_{iB} = \sum \lambda_{iB}^2 \exp(-2\Delta\eta A_{iB})\mathbf{N}_{iB} \otimes \mathbf{N}_{iB} \tag{19.90}$$

so that:

$$\begin{aligned} \det \mathbf{C}_C &= \lambda_{1B}^2\lambda_{2B}^2\lambda_{3B}^2\exp(-2\Delta\eta(A_{1B} + A_{2B} + A_{3B})) \\ &= \lambda_{1B}^2\lambda_{2B}^2\lambda_{3B}^2 = \det \mathbf{C}_B \end{aligned} \tag{19.91}$$

where we have used the fact that the flow direction $\mathbf{A}$ is deviatoric (proportional to $\mathbf{O}'$) so that:

$$A_{1B} + A_{2B} + A_{3B} = 0 \tag{19.92}$$

We can therefore write:

$$\log_e \lambda'_{iC} = \log_e \lambda'_{iB} - \Delta\eta A_{iB} \tag{19.93}$$

$$J_C = \det(\mathbf{F}_C) = J_B = \det(\mathbf{F}_B) \tag{19.94}$$

and finally:

$$\mathbf{O}_C = \sum O_{iC}\mathbf{N}_{iB} \otimes \mathbf{N}_{iB} = \sum O'_{iC}\mathbf{N}_{iB} \otimes \mathbf{N}_{iB} + K\log_e J_B \mathbf{I} \tag{19.95}$$

where

$$O_{iC} = O'_{iC} + K\log_e J_B = O'_{iC} + K\sum \log_e(\lambda_{iB}) \tag{19.96}$$

with the symbol ′ denoting the deviatoric part, and

$$\begin{aligned} O'_{iC} &= 2\mu\log_e \lambda'_{iC} = 2\mu(\log_e \lambda'_{iB} - \Delta\eta A_{iB}) \\ &= 2\mu\left(\log_e \lambda'_{iB} - \frac{3\Delta\eta}{2O_{eB}} O'_{iB}\right) = \alpha O'_{iB} \end{aligned} \tag{19.97}$$

with

$$\alpha = 1 - \frac{3\mu\Delta\eta}{O_{eB}} \tag{19.98}$$

Equation (19.98) is of an identical form to the small-strain expression in (6.90). To obtain the unknown scalar, $\Delta\eta$, we substitute (19.94)–(19.96) into the yield function f (from (19.82)) at C to obtain (compare (6.88)):

$$f_c = O_{eC}(O'_C) - O_{oC}(E_{psC}) \tag{19.99}$$

With linear hardening, we can apply an identical procedure to that in (6.89) to obtain:

$$\Delta\eta = \frac{f_B}{(3\mu + A')} \tag{19.100}$$

where f_B is the value of the yield function at the 'trial point', B. With non-linear hardening, we can apply a scalar Newton–Raphson iteration as described at the end of Section 6.6.7 (in particular, see (6.93)).

The complete algorithm can therefore be written as

1. Compute:

$$\mathbf{F}_B = \mathbf{F}\mathbf{F}_{po}^{-1} = \mathbf{F}\mathbf{F}_{pB}^{-1} \tag{19.101a}$$

2. Apply a polar decomposition on $\mathbf{C}_B = \mathbf{F}_B^T\mathbf{F}_B$ to obtain λ_{iB}, $\mathbf{N}_{iB}$ and $\mathbf{R}_B$ (via (19.76))
3. Obtain elastic trial stresses in the principal directions (at B) via:

$$O_{iB} = O'_{iB} + O_{imB} = O'_{iB} + K\log_e J_B \tag{19.101b}$$

$$O'_{iB} = 2\mu\log_e\lambda'_{iB} = 2\mu\log_e\lambda_{iB} - \tfrac{2}{3}\mu\log_e J_B \tag{19.101c}$$

4. Check for yielding, if no yielding, apply step (7) (with $\mathbf{O}_C = \mathbf{O}_B$) and then finish.
5. Apply a standard small-strain update to obtain:

$$O_{iC} = \alpha O'_{iB} + O_{imB} \tag{19.101d}$$

   where the α parameter is obtained using the same procedure as that for the small-strain update (via (19.98) and (19.100) with linear hardening).
6. Set $\mathbf{N}_{iC} = \mathbf{N}_{iB}$ and hence obtain:

$$\mathbf{O}_C = \sum O_{iC}\mathbf{N}_{iC} \otimes \mathbf{N}_{iC} \tag{19.101e}$$

7. Rotate the stresses so as to obtain Kirchhoff stresses for use in the finite element code via:

$$\tau_C = \mathbf{R}_B\mathbf{O}_C\mathbf{R}_B^T \tag{19.101f}$$

   where $\mathbf{R}_B$ has been obtained in step 2.
8. Update the plastic deformation gradient $\mathbf{F}_p$ via:

$$\mathbf{F}_{pC} = \mathbf{F}_{pn} = \exp(\Delta\eta\mathbf{A}_B)\mathbf{F}_{pB} = \exp(\Delta\eta\mathbf{A}_B)\mathbf{F}_{po} \tag{19.101g}$$

   where

$$\mathbf{A}_B = \sum \frac{3}{2O_{eB}} O'_{iB}\mathbf{N}_{iB} \otimes \mathbf{N}_{iB} = \frac{3}{2O_{eB}}\mathbf{O}'_B \tag{19.101h}$$

and

$$\exp(\Delta\eta \mathbf{A}_B) = \left[\sum \exp((1-\alpha)\log_e \lambda'_{iB}) \mathbf{N}_{iB} \otimes \mathbf{N}_{iB}\right] \tag{19.101i}$$

Algorithm 19.2 An update on the intermediate configuration.

It is worth noting that, having obtained the principal 'trial stresses' at point B in step 3 above, if these are converted back to full stresses using the principal directions $\mathbf{N}_{iB}$, we can then apply an entirely conventional small-strain plasticity algorithm on the resulting trial stresses $\mathbf{O}_B$ to obtain the 'returned stresses', $\mathbf{O}_C$ before rejoining the previous algorithm at step 7.

Cuitino and Ortiz [C2] have given a consistent tangent modular tensor for use with a very similar algorithm. Rather than pursue this line, we will now consider an update) that is performed directly on the current configuration (in terms of Kirchhoff stresses) from which a cnsistent tangent tensor will be obtained.

19.7 AN $\mathbf{F}_e\mathbf{F}_p$ UPDATE BASED ON THE FINAL (CURRENT) CONFIGURATION

Simo [S4] has described an updating procedure that is directly applied to Kirchhoff stresses in the current configuration. In the present section, we will derive an equivalent formulation largely by mapping directly from the previous update which was based on the intermediate configuration. The main assumptions are the same. In particular, an isotropic hyperelastic relationship is assumed which is again based on principal log strains. Also the formulation will be limited to J_2 plasticity with isotropic hardening.

As before, we assume that we know, $\mathbf{F}$ from the current displacements and also the old value of $\mathbf{F}_p$ and hence $\mathbf{C}_p = \mathbf{F}_p^T\mathbf{F}_p$ (at the last converged equilibrium state). We will write the latter as $\mathbf{C}_{po}$. Hence with $\mathbf{C}_{po}$ held fixed, we can compute the trial elastic configuration (at B) from:

$$\mathbf{b}_B = \mathbf{F}_B\mathbf{F}_B^T = \mathbf{F}\mathbf{C}_{po}^{-1}\mathbf{F}^T \tag{19.102}$$

and obtain the principal directions $\mathbf{n}_{iB}$ and principal stretches λ_{iB} (which will be identical to those obtained in (19.74)).

Hence we can write:

$$\mathbf{b}_B = \sum \lambda_{iB}^2 \mathbf{n}_{iB} \otimes \mathbf{n}_{iB} \tag{19.103}$$

The 'trial elastic' Kirchhoff stresses at B will be coaxial with $\mathbf{b}_B$ so that we can write:

$$\boldsymbol{\tau}_B = \sum \tau_{iB} \mathbf{n}_{iB} \otimes \mathbf{n}_{iB} = \sum \tau'_{iB} \mathbf{n}_{iB} \otimes \mathbf{n}_{iB} + K \log_e J_B \mathbf{I} \tag{19.104}$$

where

$$\tau_{iB} = \tau'_{iB} + K \log_e J_B = \tau'_{iB} + K \sum \log_e(\lambda_{iB}) \tag{19.105}$$

with the symbol $'$ again denoting the deviatoric part. The principal deviatoric stresses are given by

$$\tau'_{iB} = 2\mu \log_e \lambda'_{iB} = 2\mu \log_e \lambda_{iB} - \tfrac{2}{3}\mu \log_e J_B \tag{19.106}$$

A check for yielding is now made by inserting (19.104)–(19.106) into the yield function to obtain:

$$f_B = \tau_{eB} - \tau_o = \sqrt{\tfrac{3}{2}}(\boldsymbol{\tau}':\boldsymbol{\tau}')^{1/2} - \tau_o \tag{19.107}$$

If $f_B < 0$, the response is elastic and we simply set the final stresses $\boldsymbol{\tau}_C = \boldsymbol{\tau}_B$. If $f_B \geqslant 0$, we require a plastic return and adopt a similar 'operator split' to before so that in the movement from B to C the total displacements are fixed and only plastic straining occurs.

Using standard transformations between the intermediate and final configuration, we find that the previous coaxiality whereby the eigenvectors $\mathbf{N}_{iB} = \mathbf{N}_{iC}$ were shared by

$$\mathbf{O}_B, \mathbf{O}_C, \qquad \mathbf{F}_B^T\mathbf{F}_B \quad \text{and} \quad \mathbf{F}_C^T\mathbf{F}_C$$

now require that the eigenvectors $\mathbf{n}_{iB} = \mathbf{n}_{iC}$ are shared by

$$\boldsymbol{\tau}_B, \boldsymbol{\tau}_C, \qquad \mathbf{F}_B\mathbf{F}_B^T, \qquad \mathbf{F}_C\mathbf{F}_C^T$$

and hence Algorithm 19.2 can easily be adapted to give:

1. Compute:
$$\mathbf{F}_B = \mathbf{F}\mathbf{F}_{po}^{-1} = \mathbf{F}\mathbf{F}_{pB}^{-1}. \tag{19.108a}$$
2. Apply a polar decomposition on $\mathbf{b}_B = \mathbf{F}_B\mathbf{F}_B^T$ to obtain λ_{iB} and $\mathbf{n}_{iB}$ and
$$\mathbf{R}_B = \mathbf{Q}(\mathbf{n}_B)\mathbf{Diag}(\lambda_B^{-1})\mathbf{Q}(\mathbf{n}_B)^T\mathbf{F}_B \tag{19.108b}$$
3. Obtain elastic trial stresses in the principal directions (at B) via:
$$\tau_{iB} = \tau'_{iB} + \tau_{imB} = \tau'_{iB} + K\log_e J_B \tag{19.108c}$$
$$\tau'_{iB} = 2\mu\log_e\lambda'_{iB} = 2\mu\log_e\lambda_{iB} - \tfrac{2}{3}\mu\log_e J_B \tag{19.108d}$$
4. Check for yielding, if no yielding apply set $\boldsymbol{\tau}_C = \boldsymbol{\tau}_B$ and finish.
5. Apply a standard small strain update to obtain:
$$\tau_{iC} = \alpha\tau'_{iB} + \tau_{imB} \tag{19.108e}$$
where the α parameter is obtained using the procedure to the small-strain update (with linear hardening from (19.98) and (19.100) although with τ_{eB} instead of O_{eB}).
6. Set $\mathbf{n}_{iC} = \mathbf{n}_{iB}$ and hence obtain:
$$\boldsymbol{\tau}_C = \sum\tau_{iC}\mathbf{n}_{iC}\otimes\mathbf{n}_{iC} \tag{19.108f}$$
7. Update the plastic deformation gradient via:
$$\mathbf{F}_{pC} = \mathbf{F}_{pn} = \left[\sum\exp((1-\alpha)\log_e\lambda'_{iB})\mathbf{N}_{iB}\otimes\mathbf{N}_{iB}\right]\mathbf{F}_{pB} \tag{19.108g}$$
where the principal directions $\mathbf{N}_{iB}$ can be obtained (see (4.147) from:
$$\mathbf{Q}(\mathbf{N}_B) = \mathbf{R}_B^T\mathbf{Q}(\mathbf{n}_B) \tag{19.108h}$$

Algorithm 19.3 An update on the current configuration.

It is worth emphasising that, having obtained the principal 'trial stresses' at point B in step 3 above, if these are converted back to full stresses using the principal directions

$\mathbf{n}_{iB}$, we can then apply an entirely conventional small-strain plasticity algorithm on the resulting trial stresses τ_B to obtain the 'returned stresses', τ_C before rejoining the previous algorithm at step 7.

19.7.1 The flow rule

The previous return algorithm was obtained directly from an equivalent return on the 'intermediate configuration' given in Section 19.6. As previously indicated, Simo [S4] developed his return algorithm by working directly in the current configuration. To that end, he derived a flow rule of the form:

$$\dot{\boldsymbol{\varepsilon}}_p = -\tfrac{1}{2}L_v(\mathbf{b}_e)\mathbf{b}_e^{-1} = \dot{\eta}\mathbf{a} = \dot{\eta}\frac{\partial f}{\partial \boldsymbol{\tau}} \tag{19.109}$$

where $\mathbf{a}$ is the flow direction and was used by Simo to obtain the previous 'return algorithm'. Here, we merely show that (19.109) is equivalent to the expression previously given in Section 19.2 (see equation (19.16)). To this end, we note that the expression $L_v(.)$ is the Lie derivative (see footnote in Section 10.4 for the Lie derivative of the Kirchhoff stress and refs [M.10] for further elaboration) so that with $\mathbf{b}_e = \mathbf{F}_e\mathbf{F}_e^T$, via the decomposition $\mathbf{F} = \mathbf{F}_e\mathbf{F}_p$:

$$L_v(\mathbf{b}_e) = \mathbf{F}\frac{d}{dt}(\mathbf{F}^{-1}\mathbf{b}_e\mathbf{F}^{-T})\mathbf{F}^T = \mathbf{F}\frac{d}{dt}(\mathbf{C}_p^{-1})\mathbf{F}^T = -\mathbf{l}_p\mathbf{b}_e - \mathbf{b}_e\mathbf{l}_p^T \tag{19.110}$$

with $\mathbf{l}_p$ from (19.10). Consequently, from (19.109) and (19.110):

$$\dot{\boldsymbol{\varepsilon}}_p = \mathbf{F}_e\left(\frac{\mathbf{L}_p + \mathbf{L}_p^T}{2}\right)\mathbf{F}_e^{-1} \tag{19.111}$$

where $\mathbf{L}_p$ was given in (19.11) and is related to the intermediate configuration.

19.8 THE CONSISTENT TANGENT

The following is closely related to the work of Simo [S4], although the present derivations are different and the solution is expressed in a different form. We will first restate the equations that make up the return and must be differentiated to obtain the consistent tangent. From (19.108c) to (19.108f) they are

$$\boldsymbol{\tau}_C = \boldsymbol{\tau}'_C + \boldsymbol{\tau}_{mC} = \alpha\boldsymbol{\tau}'_B + \boldsymbol{\tau}_{mB} \tag{19.112}$$

where

$$\alpha = \left(1 - \frac{3\mu\Delta\eta}{\tau_{eB}}\right) = 1 - \frac{3\mu f_B}{(3\mu + A')\tau_{eB}} \tag{19.113}$$

Differentiation of (19.112) gives:

$$\dot{\boldsymbol{\tau}}_C = \alpha\dot{\boldsymbol{\tau}}'_B + \dot{\boldsymbol{\tau}}_{mB} + \dot{\alpha}\boldsymbol{\tau}'_B \tag{19.114}$$

We intend to adopt a Eulerian finite element formulation as discussed in Sections 12.2

and 12.3 and hence require the tangent modular tensor relating to the Truesdell rate of Kirchhoff stress. From (19.114), we have:

$$\dot{\tau}_C^{TK} = [\mathbf{D}^{1tTK}(\alpha\mu, K) + 2\mu\beta(\tau_{eB})\tau'_B \otimes \tau'_B]:\dot{\varepsilon} = [\mathbf{D}^{1tTK}(\alpha\mu, K) + \mathbf{D}^{2tTK}]:\dot{\varepsilon} \quad (19.115)$$

where the term TK means 'Truesdell rate' and the constant β is given by (see also (6.101))

$$\beta(\tau_{eB}) = \frac{3}{2\tau_{eB}^2}\frac{(1-\alpha)(3\mu + A') - 3\mu}{3\mu + A'} \quad (19.116)$$

The term $D^{1tTK}(\alpha\mu, K)$ in (19.115) stems from the first two terms in (19.114) and is derived from the hyperelastic relationships of Section (13.10.1) although, because of the α term in (19.114), the shear modulus μ is replaced by $\alpha\mu$. In relation to the principal directions $\mathbf{n}_{iB}$, from (13.189b) we have:

$$D_{iijj}^{1tTKE} = (K - \tfrac{2}{3}\alpha\mu) + 2\alpha\mu\delta_{ij} - 2\tau_{iC}\delta_{ij} \quad (19.117)$$

while via (13.148b):

$$D_{ijij}^{1tTKE} = \frac{\lambda_{jB}^2\tau_{iC} - \lambda_{iB}^2\tau_{jC}}{\lambda_{iB}^2 - \lambda_{jB}^2} \quad (19.118)$$

In (19.117) and (19.118), the indicial summation convention does not apply. The tensor components D_{ijij}^{1tTKE} must be transformed back from the principal directions $\mathbf{n}_{iB}$ using:

$$D_{ijkl}^{1tTK} = Q_{ia}Q_{jb}Q_{kc}Q_{ld}D_{abcd}^{1tTKE} \quad (19.119)$$

where the terms such as Q_{ia} are components of $\mathbf{Q} = [\mathbf{n}_{1B}, \mathbf{n}_{2B}, \mathbf{n}_{3B}]$.

The term D^{2tTK} in (19.115) stems from the last term in (19.114) and is computed with the important proviso that the principal directions remain fixed during the 'plastic return'. It is obtained in an almost identical manner to that given previously for the small-strain case in Section 6.7.1. In particular, differentiation of α from (19.113) combined with the consistency condition:

$$\dot{f}_C = \dot{\alpha}\tau_{eB} + \alpha\dot{\tau}_{eB} + A'_C\dot{\eta} = 0 \quad (19.120)$$

leads to:

$$\dot{\alpha} = \tfrac{2}{3}\beta(\tau_{eB})\tau_{eB}\dot{\tau}_{eB} = \beta(\tau_{eB})\tau'_B:\dot{\tau}'_B = 2\mu\beta(\tau_{eB})\tau'_B:\dot{\varepsilon} \quad (19.121)$$

with $\beta(\tau_{eB})$ being given by (19.116). Combining (19.121) with (19.114) leads to the expression for $\mathbf{D}^{2tTK}$ in (19.115). It is worth noting that this term can be re-expressed as

$$\mathbf{D}^{2tTK} = 2\mu\beta(\tau_{eC})\tau'_C \otimes \tau'_C \quad (19.122)$$

19.8.1 The limiting case

We would expect that, in the limit, as the step size tends to zero, we would obtain the same solution as that obtain in Section 19.3 using the Jaumann rate. In this situation, the parameters α (from 19.113) and β (from (19.116)) tend to unity and $-3/(2\tau_e^2)$ respectively. (For simplicity, we are here assuming perfect plasticity). Hence from

(19.115), (19.117) and (19.118), we obtain:

$$D_{iijj}^{\mathrm{tTKE}} = K - \tfrac{2}{3}\mu + 2\mu\delta_{ij} - 2\tau_i\delta_{ij} - \frac{3\mu}{\tau_e^2}\tau_i'\tau_j' \tag{19.123}$$

$$D_{ijij}^{\mathrm{tTKE}} = \left(\frac{\lambda_j^2\tau_i - \lambda_i^2\tau_j}{\lambda_i^2 - \lambda_j^2}\right)_{\mathrm{B}} \tag{19.124}$$

where the last term in (19.123) stems from $\mathbf{D}^{2\mathrm{tTK}}$ tensor. Following the approach of Section 13.10.1 (particularly equations (13.190b)–(13.190e)), we can transform the above to relate to the Jaumann rate so that:

$$D_{iijj}^{\mathrm{tJKE}} = K - \tfrac{2}{3}\mu + 2\mu\delta_{ij} - \frac{3\mu}{\tau_e^2}\tau_i'\tau_j' \tag{19.125a}$$

$$D_{ijij}^{\mathrm{tTKE}} \simeq \mu \tag{19.125b}$$

In deriving (19.125b), the assumption was made (see (13.190e)) that the elastic stretch ratios are close to unit. Rewriting the tensor components in (19.125) in relation to the 'base co-ordinate system results in the relationship:

$$D_{ijkl}^{\mathrm{tJK}} = 2\mu\left(\frac{\delta_{ik}\delta_{jl} + \delta_{il}\delta_{jk}}{2} - \frac{3}{2\tau_e^2}\tau_{ij}'\tau_{kl}'\right) + (K - \tfrac{2}{3}\mu)\delta_{ij}\delta_{kl} \tag{19.126a}$$

or

$$\mathbf{D}_{\mathrm{tJK}} = 2\mu\left(\mathbf{I} - \frac{3}{2\tau_e^2}\boldsymbol{\tau}'\otimes\boldsymbol{\tau}'\right) + (k - \tfrac{2}{3}\mu)\mathbf{1}\otimes\mathbf{1} \tag{19.126b}$$

with $\mathbf{I}$ as the unit fourth-order tensor and $\mathbf{1}$ as the unit second order tensor (see also (4.31)). Equation (19.126b) takes precisely the form that it had in the small-strain case (see (6.44)). This conclusion is the same as that proved at the end of Section 19.3.

19.9 INTRODUCING LARGE ELASTO-PLASTIC STRAINS INTO THE FINITE ELEMENT FORMULATION

The methods of Sections 19.7 and 19.8 can be directly applied using a Eulerian finite element formulation (Sections 12.2 and 12.3). In order to handle the incompressibility of metal plasticity, one may either use high-order elements (which are not very susceptible to incompressible locking [S5]) or introduce a mixed (or hybrid) formulation with pressure as a separate variable. Such techniques were discussed for hyperelasticity in Sections 13.5 and 13.7. The extension to large-strain elasto-plasticity is relatively straightforward. In this context, we will now give the key equations for a two-dimensional plane-strain formulation assuming a constant pressure over the element. In these circumstances, the 'equilibrium equations' take the form:

$$\mathbf{q}_i = \int \mathbf{B}(\mathbf{x})^{\mathrm{T}}\boldsymbol{\tau}_{\mathrm{C}}\,\mathrm{d}V_{\mathrm{o}} \tag{19.127}$$

$$f = -\int\left((J_{\mathrm{B}} - 1) + \frac{1}{K}p\right)\mathrm{d}V_{\mathrm{o}} \tag{19.128}$$

where the latter equation provides a weighted average satisfaction (over the element) of the relationship between the pressure (p) and the determinant of $\mathbf{F}_{\mathrm{B}}$, which is J_{B} (with

the plastic deformation gradient, $\mathbf{F}_p$, being frozen at the end of previous increment—see (19.108a)). In contrast to the work in Section 19.7 and 13.10.1, we are now using $p = -K(J-1)$ rather than $p = -K\log_e J/J$.

The current Kirchhoff stresses, τ_C, in (19.127) would be computed (see (19.108) and (13.186a)) from:

$$\tau_C = 2\mu\alpha\sum \log_e \lambda'_{iB}\mathbf{n}_i \otimes \mathbf{n}_i - pJ_B\mathbf{I} = \alpha\tau'_B - pJ_B\mathbf{I} \tag{19.129}$$

where the plastic return scalar, α, would be computed in the standard manner from the deviatoric stresses, τ'_B.

For the Newton–Raphson iterations, we require the variations of (19.127) and (19.128). The former gives:

$$\delta\mathbf{q}_i = \int \mathbf{B}(\mathbf{x})^T \mathbf{D}_t \mathbf{B}(\mathbf{x}) \mathrm{d}V_o \delta\mathbf{p} + \int \delta\mathbf{B}(\mathbf{x})^T \tau \mathrm{d}V_o - \int J_B \mathbf{B}(\mathbf{x})^T \begin{bmatrix} 1 \\ 0 \\ 1 \end{bmatrix} \mathrm{d}V_o \delta\rho \tag{19.130}$$

where the tangent modular matrix $\mathbf{D}_t$ is as given in (19.115)–(19.119), although the bulk modulus K in (19.117) would now be replaced by $-\rho J_B$.

The second term on the right-hand side of (19.130) gives the conventional initial stress contribution (associated with the Truesdell rate—see (12.14)). The variation of (19.128) gives:

$$\delta f = -\int J_B \begin{bmatrix} 1 \\ 0 \\ 1 \end{bmatrix} \mathbf{B}(\mathbf{x}) \mathrm{d}V_o \delta p - \int \frac{1}{K} \mathrm{d}V_o \delta\rho \tag{19.131}$$

where we have used (10.60) to obtain δJ.

Instead of using a presseure/displacement formulation, one may adopt one of the methods with extra internal variables discussed in Sections 18.11–18.13. The finite element algorithm for hyperelasticity (Section 18.13) is easily extended to introduce large-strain elasto-plasticity.

For plane-stress problems, there are no difficulties with the incompressibility issue. Consequently we may use a pure displacement-based approach coupled, for example, with the $\mathbf{F}_e\mathbf{F}_p$ 'Eulerian formulation' of Section 19.7. The trial stresses would be obtained from $\tau_B = \mathbf{C}:\log_e \mathbf{V}_B$ (see below (13.186b)) where $\mathbf{C}$ is the standard 3×3 plane-stress linear elastic constitutive matrix (see (4.17). A conventional small-strain backward-Euler return algorithm (as in Sections 6.8 or 14.10.1) would then return τ_B to τ_c.

Regarding the tangent modulus matrix, it is important to note the observations below (19.36) in relation to the consistency condition. It follows that, as input to the small-strain plasticity algorithm, in order to create the consistent tangent modular matrix, we should provide $\mathbf{C}$ relating to the Jaumann rather than the Truesdell rate. Hence, to enter this routine, the top 2×2 components of $\mathbf{C}$ would be standard while the shear term would be given by (13.190c) (with all terms computed at B). Assuming the finite element equations were based on the Truesdell rate so that the tangent stiffness matrix took the form of (12.14), one would now need to modify $\mathbf{C}_t$ by subtracting $\bar{\tau}$ from (12.46). The latter would be computed using τ_c.

Returning the conditions of plane strain, because of difficulties that were observed with the full enhanced strain formulation ([C4.18] and discussion in Section 18.11.2), the author and co-workers have extended the co-rotational technique to cover large elasto-plastic strains [C4.18]. The equivalent formulation for large elastic strains (hyperelasticity) has been discussed in Section 18.14. Unfortunately, the extension to

plasticity is not straightforward. However, in comparison with the enhanced **F** formulation using the full set of enhanced strains (four or five for plane strain), the method appears to be less prone to hour-glassing [C4.14] and consequently we will now briefly outline the adopted procedure.

By combining the approaches of Section 18.2, 18.3 and 19.6, the starting-point can be taken as the computation of the rotation matrix $\mathbf{R}_m$ at the centroid allowing for the old (stored) plastic deformation gradient, $\mathbf{F}_{po}$ at the centroid. To this end (see (18.23) and (19.73)), we compute:

$$\mathbf{F}_B = \mathbf{F}\mathbf{F}_{po}^{-1} = \mathbf{R}_m\mathbf{U}_m = \begin{bmatrix} \cos\beta & -\sin\beta \\ \sin\beta & \cos\beta \end{bmatrix}\mathbf{U}_m \tag{19.132}$$

where we have expanded $\mathbf{R}_m$ for the two-dimensional case which will now be studied. The matrix $\mathbf{F}_B$ would be computed from the global displacements **p**, by first computing:

$$\boldsymbol{\theta} = v(\mathbf{D}_1) = \mathbf{G}\mathbf{p} \tag{19.133}$$

so as to obtain $\mathbf{F} = \mathbf{I} + \mathbf{D}_1$. We are here adopting the notation of Sections 18.11–18.14 whereby the subscript 1 related to the primary (corner node) variables and the subscript 2 (to enter later) to the secondary variables. At the centroid, only the former are involved.

As in Section 18.3, the columns of $\mathbf{R}_m$ provide the base vectors for the local frame and hence, knowing $\mathbf{R}_m$, we can compute the local displacements $\mathbf{p}_{l1}$ (details in Sections 18.2 and 18.3). Before turning to the computations at the local element level, we will describe the procedure for computing the transformation matrix, **T**, which is used to transform the local internal forces to global internal forces (18.15). We will concentrate on the two-dimensional formulation and in this case (see Section 18.2), the key element is the computation of the spin vector, **v** which relates the change of angle of the local axes ($\delta\beta$) to the changes in (primary) nodal variables, $\delta\mathbf{p}_1$ (see (18.12)).

From the work of Sections 18.2 and 18.3, the angle β defining the local axes can be obtained from the condition:

$$\mathbf{U}_m(1,2) = \mathbf{U}_m(2,1) \tag{19.134}$$

which, from (19.132), leads to the condition:

$$\Omega_{lm} = as + bc = 0 \tag{19.135}$$

where $c = \cos\beta$ and $s = \sin\beta$, and

$$a = -\mathbf{F}_B(1,1) - \mathbf{F}_B(2,2); \qquad b = \mathbf{F}_B(2,1) - \mathbf{F}_B(1,2) \tag{19.136}$$

To proceed further (see also (18.11)), we must set the variation of (19.135) to zero so that:

$$(ac - bs)\delta\beta = -\begin{bmatrix} -s \\ -c \\ c \\ -s \end{bmatrix}^T \begin{bmatrix} \dot{F}_{11} \\ \dot{F}_{12} \\ \dot{F}_{21} \\ \dot{F}_{22} \end{bmatrix}_B = -\mathbf{d}^T\dot{\boldsymbol{\theta}}_B \tag{19.137}$$

Using conventional procedures (see (12.3)) we can compute:

$$\dot{\boldsymbol{\theta}} = \mathbf{G}_1\dot{\mathbf{p}}_1 \tag{19.138}$$

However, for (19.137), we require $\mathbf{G}_B$ where, via (19.132):

$$\dot{\theta}_B = v(\dot{\mathbf{F}}_B) = v(\dot{\mathbf{F}}\mathbf{F}_{po}^{-1}) = \mathbf{G}_B\dot{\mathbf{p}}_1 \tag{19.139}$$

and $v(\mathbf{A})$ implies the vector form of **A**. Knowing $\mathbf{F}_{po}^{-1}$ and $\mathbf{G}_1$, it is a simple matter to find $\mathbf{G}_B$ (see (18.171)–(18.173)) for similar manipulations). The combination of (19.137) and

(19.139) leads to the relationship:

$$\delta\beta = \frac{1}{(ac - bs)} \mathbf{d}^{\mathrm{T}} \mathbf{G}_{\mathrm{B}} \dot{\mathbf{p}}_1 = \mathbf{v}^{\mathrm{T}} \dot{\mathbf{p}}_1 \tag{19.140}$$

which gives the spin vector, $\mathbf{v}$ required for the generation of the transformation matrix, $\mathbf{T}$, using the method of Section 18.2. The initial stress matrix stemming from $\delta\mathbf{T}$ then follows without any additional complications.

We can now return to the local element computations for which, knowing $\mathbf{p}_{l1}$ and $\mathbf{p}_{l2}$, we can, at a typical Gauss point, compute the 'stretch', allowing for the old plastic deformation gradient, via:

$$\mathbf{U}_{\mathrm{B}} = [\mathbf{I} + \mathbf{D}_1(\mathbf{p}_{l1}) + \mathbf{D}_2(\mathbf{p}_{l2})]\mathbf{F}_{\mathrm{po}}^{-1} \tag{19.141}$$

where $\mathbf{F}_{\mathrm{po}}$ now relates to the particular Gauss point. For a uniform deformation gradient or with an element with a single Gauss point (and no incompatible modes, $\mathbf{p}_{l2}$), this $\mathbf{U}_{\mathrm{B}}$ would coincide with the $\mathbf{U}_{\mathrm{m}}$ from (19.132). However, this coincidence will generally not apply and, indeed $\mathbf{U}_{\mathrm{B}}$ will generally not be symmetric. Strictly therefore, we should not use the symbol $\mathbf{U}$ and indeed, without plasticity, using the earlier notation $\mathbf{U}_{\mathrm{B}}$ would be $\mathbf{I} + \boldsymbol{\varepsilon}_l$ where $\boldsymbol{\varepsilon}_l$ is the local engineering strain (see Section 18.3). However, we will continue to use $\mathbf{U}$ and indeed will use $\boldsymbol{B}$ for the Biot stresses (which were written as $\boldsymbol{\sigma}_l$ in Section 18.12) and $\mathbf{O}$ for the log stresses even although these definitions are not longer strictly valid (because we have applied the polar decomposition at the centroid rather than at the Gauss point). If the Gauss points were used, we would obtain a Biot stress formulation entirely equivalent to the earlier 'Eulerian formulation'.

We now obtain the principal directions and stretches from the symmetric part of $\mathbf{U}_{\mathrm{B}}$ so that:

$$\mathrm{sym}[\mathbf{U}_{\mathrm{B}}] = \sum \lambda_{\mathrm{iB}} \mathbf{N}_{\mathrm{iB}} \otimes \mathbf{N}_{\mathrm{iB}} \tag{19.142}$$

(Note in Section 18.14, we called these directions $\mathbf{a}_{\mathrm{i}}$ (see (18.177)) to draw the distinction between the co-rotational formulation and a pure Biot stress-based formulation.) For the yield criterion, we must use the $\mathbf{O}$ stresses and not the Biot stresses. The former are now obtained from (19.77) and will be designated $\mathbf{O}_{\mathrm{B}}$. After checking for yielding, we can apply a 'small strain return' via step 5 of algorithm 19.2 which involves the scalar α of (19.98) and (19.100) and returns the stresses $\mathbf{O}_{\mathrm{B}}$ to $\mathbf{O}_{\mathrm{C}}$. At which point, with the aid of (10.80), we can convert $\mathbf{O}_{\mathrm{C}}$ to 'Biot-like' stresses $\boldsymbol{B}_{\mathrm{C}}$ via:

$$\boldsymbol{B}_{\mathrm{C}} = \mathbf{O}_{\mathrm{C}}[\mathrm{sym}[\mathbf{U}_{\mathrm{B}}]]^{-1} \tag{19.143}$$

and the local internal force vectors can be computed from:

$$\mathbf{q}_{il1} = \int \mathbf{B}_{Bl1}^{\mathrm{T}} \boldsymbol{B}_{\mathrm{C}} \mathrm{d}V_{\mathrm{o}} \tag{19.144a}$$

$$\mathbf{q}_{il2} = \int \mathbf{B}_{Bl2}^{\mathrm{T}} \boldsymbol{B}_{\mathrm{C}} \mathrm{d}V_{\mathrm{o}} \tag{19.144b}$$

(In moving from (19.143) to (19.144) we have changed $\boldsymbol{B}_{\mathrm{C}}$ from a matrix or tensor to a vector.) The matrices $\mathbf{B}_{Bl1}$ and $\mathbf{B}_{Bl2}$ in (19.144) are not the 'conventional $\mathbf{B}$ matrices' but have to account for the old plastic $\mathbf{F}$'s. To this end (although now at the Gauss points), we can use a very similar procedure to that adopted in (19.138) to (19.139) so that (with $j = 1, 2$), using conventional procedures (see (12.3)) we can compute $\mathbf{G}_{lj}$

where:

$$\dot{\boldsymbol{\theta}}_{lj} = \mathbf{G}_{lj}\dot{\mathbf{p}}_{lj} \tag{19.145}$$

Knowing $\mathbf{G}_{lj}$ and $\mathbf{F}_{po}^{-1}$ it is a simple matter to compute $\mathbf{G}_{Blj}$ where:

$$\dot{\boldsymbol{\theta}}_{Blj} = v(\dot{\mathbf{D}}_{lj}\mathbf{F}_{po}^{-1}) = \mathbf{G}_{Blj}\dot{\mathbf{p}}_{lj} \tag{19.146}$$

and hence the required $\mathbf{G}_{Blj}$ which is easily modified to give the equivalent $\mathbf{B}_{Blj}$.

Because of the non-symmetry, the updating of $\mathbf{F}_p$ is not straightforward and instead of using (19.101g), the author and co-workers [C4.18] have adopted:

$$\mathbf{F}_{pn} = \Delta\bar{\mathbf{U}}_p\mathbf{F}_{po} = [\exp(-\Delta\eta\mathbf{A}_B)\mathrm{sym}(\mathbf{U}_B) + \mathrm{skew}(\mathbf{U}_B)]^{-1}\mathbf{U}_B\mathbf{F}_{po} \tag{19.147}$$

where $\exp(\Delta\eta\mathbf{A}_B)$ was defined in (19.101i). For homogeneous deformations, (19.147) coincides with (19.101g).

In relation to the principal directions $\mathbf{N}_{iB}$, the tangent modular terms are related to those for a hyperelastic Biot stress formulation and involve:

$$D_{iijj} = \left(k - \frac{2\mu\alpha}{3}\right)\frac{1}{\lambda_{iB}\lambda_{jB}} + (2\mu\alpha(1 - \log_e\lambda_{iB}) - (k - \tfrac{2}{3}\mu)\log_e J_B)\frac{\delta_{ij}}{\lambda_{iB}\lambda_{jB}} \tag{19.148a}$$

$$D_{ijij} = \frac{1}{2}\frac{(B_{iC} - B_{jC})}{(\lambda_{iB} - \lambda_{jB})} \tag{19.148b}$$

If $\alpha = 1$ (and point C is equal to point B), the above merely defines the conventional hyperelastic relationships stemming from (18.179) in conjunction with $\boldsymbol{B}_i = \partial\varphi/\partial\lambda_i$ with φ from (13.182). In (19.148a), the introduction of the α term that changes μ to $\alpha\mu$ follows the lines detailed in Section 19.8 for the 'Kirchhoff stress formulation'. The components in (19.148) must be transformed back to the base (local) directions before the addition of $2\mu\beta(\mathbf{O}_{eC})\boldsymbol{B}'_C \otimes \boldsymbol{B}'_C$ which is the counterpart of (19.122).

There is one additional complexity (and drawback). Via (19.147), we have updated $\mathbf{F}_p$ at the Gauss points. However, to commence the next increment, we require $\mathbf{F}_p$ at the centroid (see (19.132)). Consequently, at the end of an increment, we apply a least-squares fit to the $\Delta\bar{\mathbf{U}}_p$'s at the Gauss points (see (19.147)), with principal directions being dictated by those of $\mathbf{U}_m$ given by (19.132). Calling the resulting tensor $\Delta\mathbf{U}_{pm}$, we then updated the centroidal plastic deformation gradient via:

$$\mathbf{F}_{pn} = \Delta\mathbf{U}_{pm}\mathbf{F}_{po} \tag{19.149}$$

It should be noted that for uniform deformations, this co-rotational formulation gives identical results to those obtained using the method Section 19.7 [C4.18]. Indeed, when in addition the elastic strains are small, both methods give solutions [C14.18] that coincide with an exactly integrated Jaumann rate formulation due to Moss [M3] as the step size tends to zero. These observations will be amplified in the following section.

19.10 A SIMPLE EXAMPLE

In Sections 19.3 and 19.8.1, we have demonstrated the $\mathbf{F}_e\mathbf{F}_p$ formulations should coincide with the formulation based on the Jaumann rate if the elastic strains are small. We will now demonstrate this numerically in relation to the simple shearing example previously considered for hyperelasticity in Section 13.10.3. The example is reproduced here in Figure 19.4. Closed-form solutions to this problem have been derived by Moss

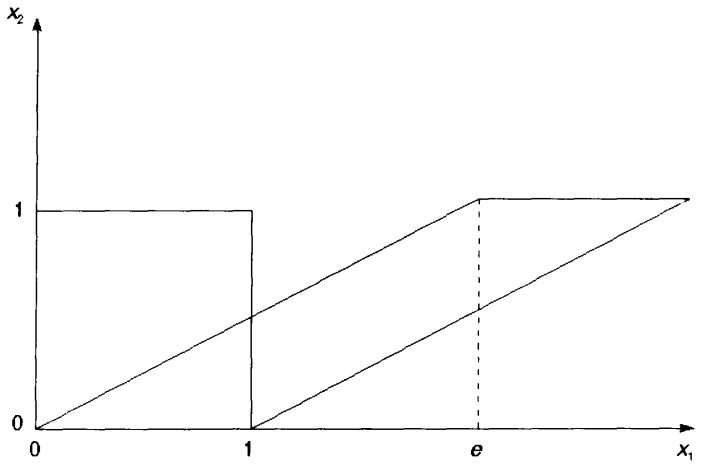

Figure 19.4 Simple shear.

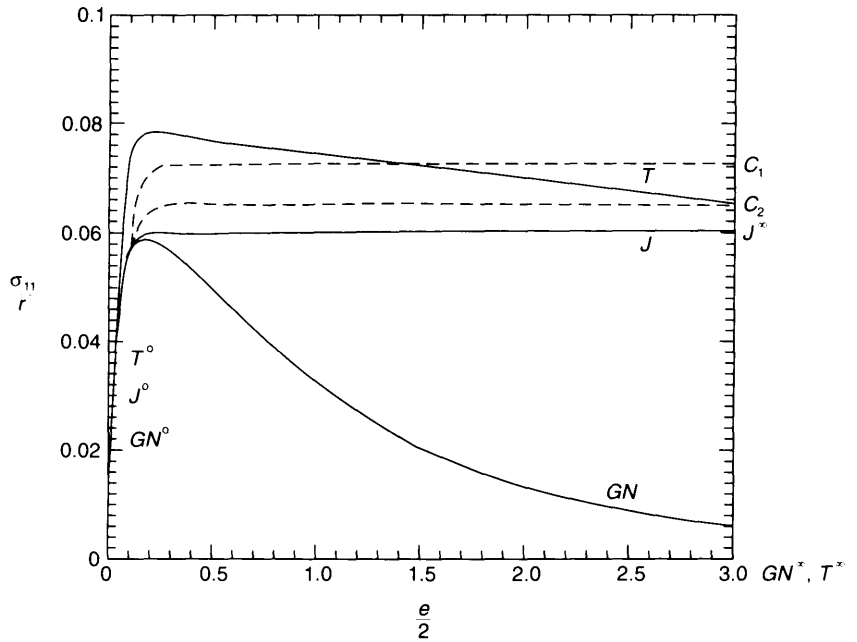

Figure 19.5 Normalised stress (σ_{11}/r) as a function of shear strain ($e/2$).

[M3]. In obtaining the solutions in Figures 19.5 and 19.6, the shear modulus, μ, has been set to unity and the yield stress, σ_0, has been set to 0.1 and it has been assumed that there is no hardening. Because the volume is exactly preserved, the solution should be independent of the bulk modulus, K. None the less for the numerical, $\mathbf{F}_e\mathbf{F}_p$-based, solutions, K was set to 2/3.

In presenting the graphs in Figures 19.5 and 19.6, the non-dimensionalising factor, r, is set to $1/\sqrt{3}$. In these figures, the stresses S_{11} and S_{12} are the Cauchy stresses which,

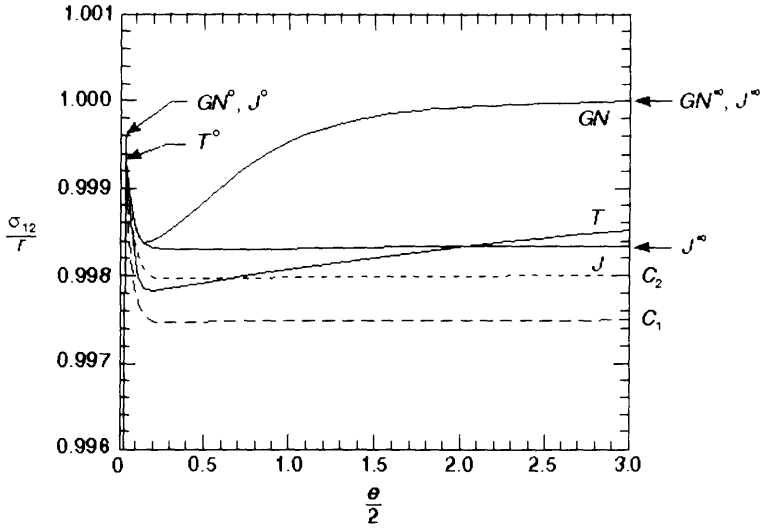

Figure 19.6 Normalised stress (σ_{12}/t) as a function of shear strain ($e/2$).

for the current problem, are equal to the Kirchhoff stresses. The solutions labelled T, J and GN are those obtained by Moss using Truesdell, Jaumann and Green–Nagdhi rates respectively.

While these 'rate-based' solutions were exactly integrated, the $\mathbf{F}_e\mathbf{F}_p$-based solutions were not and the solutions labelled C_1 and C_2 were obtained with steps of $\Delta e = 0.025$ and 0.01 respectively [C4.18]. The latter solutions could be obtained using either the current configuration formulation of Section 19.7 or the co-rotational formulation described in Section 19.9. Because the deformation is homogeneous, both formulations give identical results. It is clear from Figures 19.5 and 19.6 that as $\Delta e \to 0$, the $\mathbf{F}_e\mathbf{F}_p$-based solutions are tending towards the Jaumann-rate-based solutions. These observations coincide with those proved theoretically in Sections 19.3 and 19.8.1.

19.11 SPECIAL NOTATION

A' = hardening modulus
$\mathbf{b} = \mathbf{F}\mathbf{F}^{\mathrm{T}}$ (left Cauchy-Green tensor)
$\boldsymbol{B}$ = approximate Biot stresses (Section 19.9)
$\mathbf{C} = \mathbf{F}^{\mathrm{T}}\mathbf{F}$ (right Cauchy–Green tensor)
$\mathbf{D}$ = fourth-order constitutive tensor or displacement derivatives
f = yield function
$\mathbf{F}$ = deformation gradient
$\mathbf{F}_e$ = elastic deformation gradient
$\mathbf{F}_p$ = plastic deformation gradient
$\mathbf{G}$ = matrix connecting displacement or velocity derivatives to nodal displacement changes or velocities
$\mathbf{I}$ = identity matrix
$J = \det(\mathbf{F})$

k = bulk modulus
$\mathbf{l}$ = velocity gradient on the current configuration
$\mathbf{L}$ = velocity gradient on the intermediate configuration
$\mathbf{N}_1$–$\mathbf{N}_3$ = unit principal vectors in initial or intermediate configuration
$\mathbf{n}_1$–$\mathbf{n}_3$ = unit principal vectors in current (Eulerian or spatial) configuration
O = stress work conjugate to $\log_e \mathbf{U}$
$\mathbf{U}$ = right stretch tensor
$\mathbf{p}$ = nodal displacements; changes, $\delta\mathbf{p}$ or $\dot{\mathbf{p}}$
$\mathbf{Q}(\mathbf{N})$ = orthogonal matrix containing the triad of $\mathbf{N}$'s
$\mathbf{Q}(\mathbf{n})$ = orthogonal matrix containing the triad of $\mathbf{n}$'s
$\mathbf{R}$ = rotation matrix
$\mathbf{S}$ = second Piola–Kirchhoff stresses
α = scalar for 'plastic return'
$\dot{\boldsymbol{\varepsilon}}$ = Eulerian strain rate (or $\delta\boldsymbol{\varepsilon}$)
φ = strain energy function
$\boldsymbol{\Omega}$ = spin
$\boldsymbol{\tau}$ = Kirchhoff stresses
λ_1–λ_3 = principal stretches
μ = shear modulus
$\Delta\eta$ = plastic strain rate multiplier, change is $\dot{\eta}$

Subscript or superscripts

$'$ = deviatoric
B = at 'trial point'
C = at 'return point'
e = elastic (or equivalent)
f = yield function
J = Jaumann rate
m = mean
n = new
o = old
p = plastic
t = tangential
tJK = tangential for Jaumann rate of Kirchhoff stress
tTK = tangential for Truesdell rate of Kirchhoff stress
tK2 = tangential for second Piola–Kirchhoff stress
l = local

19.12 REFERENCES

[A1] Asaro, R. J., Crystal plasticity, *J. Appl. Mech.*, **50**, 921–934 (1983).

[A2] Atluri, S. N., On constitutive relations at finite strain: Hypo-elasticity and elasto-plasticity with isotropic or kinematic hardening, *Comp. Meth. in Appl. Mech. & Engng.*, **43**, 137–171 (1984).

[A3] Atluri, S. N., An endochronic approach and other topics in small and finite deformation computational elasto-plasticity, *Finite Element Methods for Nonlinear Problems*, ed. P. Bergan, *et al.*, Springer-Verlag, Berlin, pp. 201–215 (1986).

[B1] Bathe, K.-J., Slavkovic, R. and Kojic, M., On large strain elasto-plastic and creep analysis, in: *Finite Element Methods for Nonlinear Problems*, ed. P. Bergan, K.-J. Bathe and Wunderlich, Springer-Verlag, Berlin, pp. 175–189 (1986).

[C2] Cuitino, A. & Oritz, M., A material-independent method for extending stress update algorithms from small-strain plasticity to finite plasticity with multiplicative kinematics, *Engineering Computations*, **9**, 437–451 (1992).

[D1] Dafialis, Y. F., Issues on the constitutive formulation at large elastoplastic deformation, Part 1 Kinematics and Part 2 Kinematics, *Acta. Mech.*, **69**, 119–128 (1987) and **77**, 121–146 (1988).

[E1] Eterovic, A. L. & Bathe, K.-J., A hyperelastic based large strain elasto-plastic constitutive formulation with combined isotropic-kinematic hardening using logarithmic stress and strain measures, *Int. J. for Num. Meth. in Engng.*, **30**, 1099–1114 (1990).

[F1] Flanagan, D. P. and Taylor, L. M., An accurate numerical algorithm for stress integration with finite rotations, *Comp. Meth. in Appl. Mech. & Engng.*, **62**, 305–320 (1987).

[G1] Goudreau, G. L., Large scale computations, Chapter III of *Theoretical Foundation for Large-scale Computations for Nonlinear Material Behaviour*, ed. S. Nemat-Nasser *et al.*, Martinus Nijhoff, Dordrecht, The Netherlands, pp. 65–91 (1984).

[H1] Healey, B. E. & Dodds, R. H., A large strain plasticity model, *Computational Mechanics*, **9**, (1992).

[H2] Hibbitt, H. D., Marcal, P. V. & Rice, J. R., A finite element formulation for problems for large strain and large displacement, *Int. J. Solids & Structs.*, **6**, 1069–1086 (1970).

[H3] Hughes, T. J. R., Numerical implementation of constitutive models: rate-independent deviatoric plasticity, Chapter II of *Theoretical Foundation for Large-scale Computations for Nonlinear Material Behaviour*, ed. S. Nemat-Nasser *et al.*, Martinus Nijhoff, Dordrecht, The Netherlands, pp. 29–63 (1984).

[H4] Hughes, T. J. R. and Winget, J., Finite rotation effects in numerical integration of rate constitutive equations arising in large-deformation analysis, *Int. J. for Num. Meth. in Engng.*, **15**, 1862–1867 (1980).

[K1] Key, S. W. & Krieg, R. D., On the numerical implementation of inelastic time dependent and time independent, finite strain constitutive equations in structural mechanics, *Comp. Meth. in Appl. Mech. & Engng.*, **33**, 439–452 (1982).

[K2] Key, S. W., On an implementation of finite strain plasticity in transient dynamic large-deformation calculations, Chapter IV of *Theoretical foundation for large-scale Computations for Nonlinear Material Behaviour*, ed. S. Nemat-Nasser *et al.*, Martinus Nijhoff, Dordrecht, The Netherlands, pp. 99–108 (1984).

[K3] Krieg, R. D. & Key, S. W., Implementation of a time independent plasticity theory into structural computer programs, in *Constitutive Equations in Viscoplasticity: Computational and Engineering aspects*, ed. J. A. Stricklin and K. J. Saczalski, AMD-20, ASME, pp. 125–137 (1976).

[L1] Lee, E. H., Elastic-plastic deformation at finite strain, *J. Appl. Mech.*, **36**, 1–6, (1969).

[L2] Lee, E. H., Some comments on elastic-plastic analysis, *Int. J. for Solids & Structs.*, **17**, 859–872 (1981).

[M1] Mandel, J., Thermodynamics and plasticity, in *Foundations of Continuum Thermodynamics*, ed. J. J. Delgado Domingues, Macmillan, London, pp. 283–304 (1974).

[M2] Moran, B., Ortiz, M. & Shih, C. F., Formulation of implicit finite element methods for multiplicative finite deformation plasticity, *Int. J. for Num. Meth. in Engng.*, **29**, 483–514 (1990).

[M3] Moss, W. C., On instabilities in large deformation dimple shear loading, *Comp. Meth. in Appl. Mech. & Engng.*, **46**, 329–338 (1984).

[N1] Nagtegaal, J. C., On the implementation of inelastic onstitutive equations with special reference to large deformation problems, *Comp. Meth. in Appl. Mech. & Engng.*, **33**, 469–484 (1982).

[N2] Nagtegaal, J. C. & de Jong, J. E., Some computational aspects of elastic-plastic large strain analysis, *Int. J. for Num. Meth. in Engng.*, **17**, 15–41 (1981).

[N3] Nagtegaal, J. C. & de Jong, J. E., Some aspects of non-isotropic work-hardening in finite strain plasticity, *Plasticity of Metals at Finite Strain: Theory, Experiment and Computation*, ed. E. H. Lee and R. L. Mallett, Div. Appl. Mech. Stanford Univ. & Dept. of Mech. Engng., RPI, pp. 65–102 (1982).

[N4] Needleman, A., On finite element formulations for large elastic–plastic deformations, *Comp. & Struct.*, **20**, 247–257 (1985).

[N5] Nemat-Nasser, S., Theoretical foundations of plasticity, Chapter I of *Theoretical Foundation for Large-scale Computations for Nonlinear Material Behaviour*, ed. S. Nemat-Nasset *et al.*, Martinus Nijhoff, Dordrecht, The Netherlands, pp. 7–24 (1984).

[N6] Nemat-Nasser, S., On finite plastic flow of crystalline solids and geomaterials, *Trans. ASME*, **50**, 1114–1126 (1983).

[O1] Ortiz, M., Some computational aspects of finite deformation plasticity, in *Computational plasticity*, ed. D. R. J. Owen *et al.*, Pineridge Press, Swansea, pp. 1717–1756 (1987).

[P1] Peric, D. & Owen, D. R. J., A model for large deformations of elasto-viscoplastic solids at finite strain: computational issues, in *Proc. IUTAM Symp. on Finite Inelastic Deformations — Theory and Applications*, Hannover, Aug. (1991).

[P2] Peric, D., Owen, D. R. J. & Honnor, M. E., A model for finite strain elasto-plasticity based on logarithmic strains: computational issues, *Comp. Meth. in Appl. Mech. & Engng.*, **94**, 35–61 (1992).

[P3] Pinsky, P. M., Oritz, M. and Pister, K. S., Numerical integration of rate constitutive equations in finite deformation analysis, *Comp. Meth. in Appl. Mech. & Engng.*, **40**, 137–158 (1983).

[R1] Rice, J. R., Continuum mechanics and thermodynamics of plasticity in relation to microscale deformation mechanisms, *Constitutive Equations in Plasticity*, ed. A. S. Argon, MIT Press, Cambridge, Mass., 23–75 (1975).

[R2] Rolph III, W. D. and Bathe, K.-J., On a large strain finite element formulation for elasto-plastic analysis, in *Constitutive Equations: Macro and Computational Aspects*, ed. K. J. Williams, ASME, pp. 131–147 (1984?).

[R3] Rowe, G. W., Sturgess, C. E. N., Hartley, P. & Pillinger, I., *Finite Element Plasticity and Metal Forming*, Cambridge Univ. Press. (1991).

[S1] Simo, J. C., A framework for finite train elastoplasticity based on maximum plastic dissipation and the multiplicative decomposition: Part 1, Continuum formulation, *Comp. Meth. in Appl. Mech. & Engng.*, **66**, 199–219 (1988).

[S2] Simo, J. C., On the computational significance of the intermediate configuration and hyperelastic stress relations in finite deformation elastoplasticity, *Mechanics of Materials*, **4**, 439–451 (1985).

[S3] Simo, J. C. & Ortiz, M., A unified approach to finite deformation elastoplastic analysis based on the use of hyperelastic constitutive equations, *Comp. Meth. in Appl. Mech. & Engng.*, **49**, 221–245 (1985).

[S4] Simo, J. C., Algorithms for static and dynamic multiplicative plasticity that preserve the classical return mapping schemes of the infinitesimal theory, *Comp. Meth. in Appl. Mech. & Engng.*, **99**, 61–112 (1992).

[S5] Sloan, S. W. & Randolph, M. F., Numerical prediction of collapse loads using finite element methods, *Int. J. Num. & Analy. Meth. in Geomechanics*, **6**, 47–76 (1982).

[W1] Weber, G. & Anand, L., Finite deformation constitutive equations and a time integration procedure for isotropic hyperelastic–viscoplastic solids, *Comp. Meth. in Appl. Mech. & Engng.*, **79**, 173, 202 (1990).

[W2] Wriggers, P., Eberlain, R. & Gruttman, F., An axisymmetrical quasi-Kirchhoff-type shell element for large plastic strains, *Archive of Appl. Mech.*, **65**, 465–477 (1995).

20 Stability theory

20.1 INTRODUCTION

The work in this chapter will be strictly related to elastic systems. None the less, some of the theory can be useful in providing a framework for analysis procedures that include material non-linearity. The developments are closely related to those given by Koiter [K1, K2], Thompson and Hunt [T1], Sewell [S1, S2], Riks [R1] and, in particular, Allman [A1, A2]. A review has been given by Komarakul-Na-Nakorn and Arora [K3].

20.2 GENERAL THEORY WITHOUT 'HIGHER-ORDER TERMS'

As a starting-point, we will restate the energy functional of Section 9.1 as

$$\phi(\mathbf{p}, \lambda) = \varphi(\mathbf{p}) - \lambda \mathbf{p}^{\mathrm{T}} \mathbf{q} \tag{20.1}$$

where ϕ is the total potential energy, φ is the strain energy which is a function of the displacements, $\mathbf{p}$, $\mathbf{q}$ is a fixed load vector (previously $\mathbf{q}_{\mathrm{ef}}$) and λ a scalar load multiplier.

A small change in potential energy, $\delta\phi$ is found by applying a Taylor series to (20.1) (with λ fixed) to give:

$$\delta\phi = \frac{\partial \phi}{\partial \mathbf{p}} \delta\mathbf{p} + \frac{1}{2} \delta\mathbf{p}^{\mathrm{T}} \frac{\partial^2 \phi}{\partial \mathbf{p}^2} \delta\mathbf{p} + O(\delta\mathbf{p}^3) \tag{20.2}$$

or, using the relationships established in Section 9.1 for $\partial\phi/\partial\mathbf{p}$ and $\partial^2\phi/\partial\mathbf{p}^2$.

$$\delta\phi = \mathbf{g}^{\mathrm{T}} \delta\mathbf{p} + \tfrac{1}{2} \delta\mathbf{p}^{\mathrm{T}} K_{\mathrm{t}} \delta\mathbf{p} + O(\delta\mathbf{p}^3) \tag{20.3}$$

For the rest of this section, we will omit the higher-order terms in (20.2)–(20.3) and in similar expansions.

For equilibrium, the energy change in (20.3) should be stationary irrespective of $\delta\mathbf{p}$ and hence, the equilibrium equations are

$$\frac{\partial \phi^{\mathrm{T}}}{\partial \mathbf{p}} = \mathbf{g}(\mathbf{p}, \lambda) = \mathbf{0} \tag{20.4}$$

Also, for stable equilibrium, we would like the small change of energy to be positive for any small perturbation, $\delta\mathbf{p}$, about the equilibrium point. Hence, with equilibrium

from (20.4), in (20.3), we require:

$$\delta\mathbf{p}^{\mathrm{T}}\mathbf{K}_{\mathrm{t}}\delta\mathbf{p} > 0 \quad \text{for all} \quad \delta\mathbf{p} \tag{20.5a}$$

Hence $\mathbf{K}_{\mathrm{t}}$ should be positive definite (with only positive eigenvalues). For unstable equilibrium the change in energy will be negative, for a small perturbation, $\delta\mathbf{p}$, in a particular direction and consequently such a perturbation will move the system to another equilibrium state with a lower energy. Hence:

$$\delta\mathbf{p}^{\mathrm{T}}\mathbf{K}_{\mathrm{t}}\delta\mathbf{p} < 0 \quad \text{for some} \quad \delta\mathbf{p} \tag{20.5b}$$

In these circumstances, K_{t} will not be positive definite and will have at least one negative eigenvalue. A range of stable and unstable equilibrium states are illustrated in Figures 20.1 and 20.2.

Apart from stable and unstable states, we can also have a neutral state for which:

$$\delta\mathbf{p}^{\mathrm{T}}\mathbf{K}_{\mathrm{t}}\delta\mathbf{p} = 0 \quad \text{for some} \quad \delta\mathbf{p} \tag{20.5c}$$

and $\mathbf{K}_{\mathrm{t}}$ will have a zero eigenvalue. (In these circumstances, a full investigation of the stability will require higher-order terms—see Section 20.3.) Condition (20.5c) coincides with the condition:

$$\det(\mathbf{K}_{\mathrm{t}}) = 0 \tag{20.5d}$$

Given a solution at load level A, involving $\mathbf{p}_{\mathrm{A}}$ and λ_{A}, a Taylor expansion of the

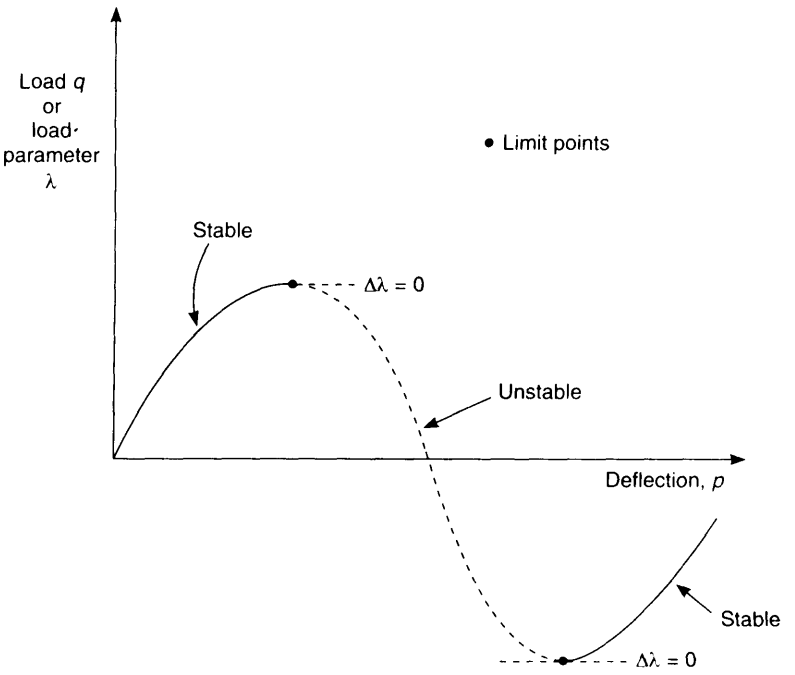

Figure 20.1 Limit points.

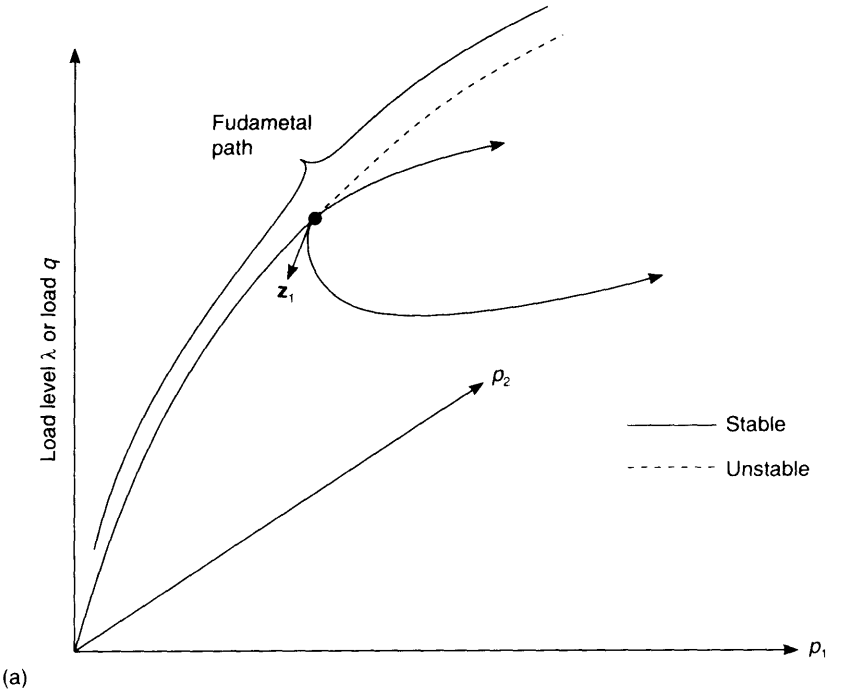

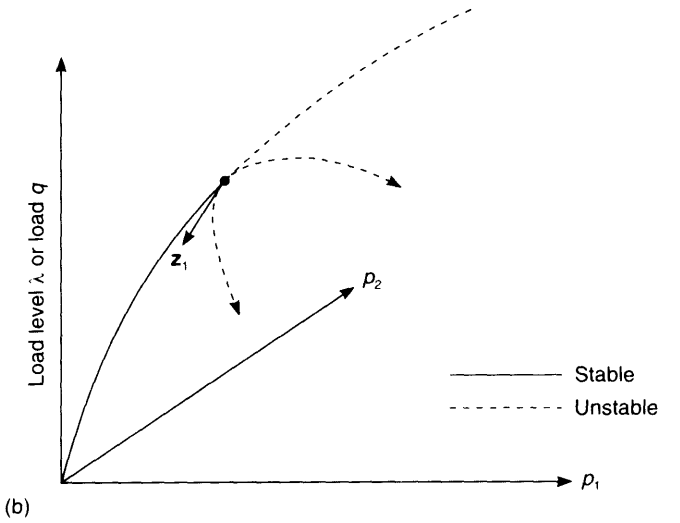

Figure 20.2 (*contd.*)

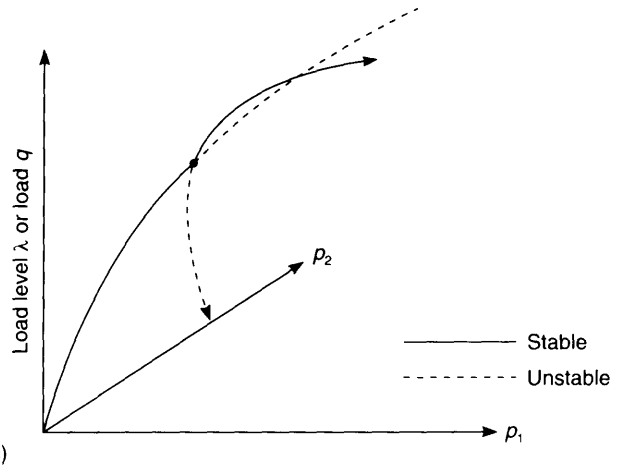

Figure 20.2 Various bifurcations. (a) Stable symmetric bifurcation; (b) unstable symmetric bifurcation; (c) unsymmetric bifurcation.

equilibrium equations (20.4) (with λ varying) gives:

$$\mathbf{g}(\mathbf{p}, \lambda)|_{\mathrm{B}} = \mathbf{g}(\mathbf{p}_{\mathrm{A}} + \Delta\mathbf{p}, \lambda_{\mathrm{A}} + \Delta\lambda) = \mathbf{g}(\mathbf{p}, \lambda)|_{\mathrm{A}} + \left.\frac{\partial \mathbf{g}}{\partial \mathbf{p}}\right|_{\mathrm{A}} \Delta\mathbf{p} + \left.\frac{\partial \mathbf{g}}{\partial \lambda}\right|_{\mathrm{A}} \Delta\lambda + O(\Delta\mathbf{p}^2, \Delta\lambda^2, \Delta\mathbf{p}\Delta\lambda). \tag{20.6}$$

where the symbol $|_{\mathrm{A}}$ means 'evaluated at A'. If point A is at equilibrium,

$$\mathbf{g}(\mathbf{p}, \lambda)|_{\mathrm{A}} = 0 \tag{20.7}$$

If point B is also to be at equilibrium,

$$\mathbf{g}(\mathbf{p}, \lambda)|_{\mathrm{B}} = \mathbf{0} \tag{20.8}$$

so that, neglecting the higher-order terms in (20.6),

$$\left.\frac{\partial \mathbf{g}}{\partial \mathbf{p}}\right|_{\mathrm{A}} \Delta\mathbf{p} + \left.\frac{\partial \mathbf{g}}{\partial \lambda}\right|_{\mathrm{A}} \Delta\lambda = \mathbf{K}_{\mathrm{t}}\Delta\mathbf{p} - \Delta\lambda\mathbf{q} = \mathbf{0} \tag{20.9}$$

from which, provided,

$$\det(\mathbf{K}_{\mathrm{t}}) \neq 0 \tag{20.10}$$

it follows that:

$$\Delta\mathbf{p} = \Delta\lambda\mathbf{K}_{\mathrm{t}}^{-1}\mathbf{q} \tag{20.11}$$

which is the standard tangential solution. The latter is only exact if the solution path is linear and there are no higher-order terms in (20.6).

If, (20.5d) applies, we cannot find $\Delta\mathbf{p}$ from (20.11) and we have a 'singular point' which may be either a limit point (Figure 20.1) or a bifurcation point (Figure 20.2). The former figure coincides with the load/deflection relationship for the simple bar considered in Section 1.2 (see Figures 1.1–1.2). To illustrate bifurcations, Figures 20.2a and 20.2b show possible responses for a system with two degrees of freedom, p_1 and p_2. These responses are closely related to the responses of Figure 3.15 that follow from the perfect

bar spring systems of Figure 3.12 (with $z = 0$). (These systems were discussed in Section 3.10.4.) However, for more generality, the non-linear fundamental paths have been illustrated in Figures 20.2a and 20.2b so that the paths are functions of p_1 and p_2 with the lowest eigenmode, $\mathbf{z}_1$ (Figure 20.2a) being another function of p_1 and p_2. The asymmetric bifurcation of Figure 20.2c will be discussed further in Section 20.4.4.

In order to proceed with the investigation, it is useful to introduce the eigenvalues, θ_i, and eigenvectors, $\mathbf{z}_i$, of $\mathbf{K}_t$ for which:

$$\mathbf{K}_t \mathbf{z}_i = \theta_i \mathbf{z}_i \tag{20.12}$$

where we will assume that the orthogonal $\mathbf{z}_i$ have been normalised so that:

$$\mathbf{z}_i^T \mathbf{z}_j = \delta_{ij} (= 1, \text{ if } i = j; = 0, \text{ if } i \neq j) \tag{20.13}$$

We will also assume an ordering of the θ_i's such that:

$$\theta_n > \theta_{n-1} > \cdots > \theta_1 \tag{20.14}$$

In the following, we will assume that the solution procedure is following the path from a stable state. In these circumstances, the lowest eigenvalue, θ_1, will be zero at the singular point. Consequently, at the singular point, from (20.12),

$$\mathbf{K}_t \mathbf{z}_1 = \mathbf{0} \tag{20.15}$$

This equation can be usefully applied with solution procedures that aim at the direct computation of 'singular points' (see Section 21.6). In the meantime, it is useful to multiply (20.9) by $\mathbf{z}_1$. This leads to

$$\Delta \mathbf{p}^T \mathbf{K}_t \mathbf{z}_1 - \Delta\lambda \mathbf{q}^T \mathbf{z}_1 = 0 \tag{20.16}$$

On account of (20.15), at the singular point, (20.16) leads to

$$\Delta\lambda \mathbf{q}^T \mathbf{z}_1 = 0 \tag{20.17}$$

At a limit point (Figure 20.1), (20.17) is satisfied via:

$$\Delta\lambda = 0; \qquad \mathbf{q}^T \mathbf{z}_1 \neq 0 \tag{20.18}$$

while, at a bifurcation point (Figures 20.2 and 20.3),

$$\mathbf{q}^T \mathbf{z}_1 = 0 \tag{20.19}$$

and (without considering higher-order terms), $\Delta\lambda$ is indeterminate. Equation (20.19) is illustrated for a very simple example, in Figure 20.3.

To proceed further, it is useful to express the displacement $\Delta\mathbf{p}$ in terms of the eigenvectors of $\mathbf{K}_t$ via:

$$\Delta \mathbf{p} = A_1 \mathbf{z}_1 + A_2 \mathbf{z}_2 + A_n \mathbf{z}_n \tag{20.20}$$

We now wish to find a typical coefficient in (20.20) such as A_2 which, using (20.13), can be expressed as $\mathbf{z}_2^T \Delta\mathbf{p}$. By multiplying (20.9) by $\mathbf{z}_2$ and substituting from (20.20) for $\Delta\mathbf{p}$, we obtain:

$$\mathbf{z}_2^T \mathbf{K}_t \Delta \mathbf{p} - \Delta\lambda \mathbf{q}^T \mathbf{z}_2 = \theta_2 \mathbf{z}_2^T \Delta \mathbf{p} - \Delta\lambda \mathbf{q}^T \mathbf{z}_2 = \theta_2 A_2 - \Delta\lambda \mathbf{q}^T \mathbf{z}_2 = 0 \tag{20.21}$$

where we have made use of (20.12) and (20.13).

Figure 20.3 Illustration of equation (20.19), $\mathbf{q}^T\mathbf{z}_1 = 0$.

20.2.1 Limit point

From (20.18), at a limit point, $\Delta\lambda = 0$, and hence, from (20.21), with $\theta_2 \neq 0$,

$$A_2 (\text{or } \mathbf{z}_2^T \Delta\mathbf{p}) = 0 \tag{20.22}$$

Similar developments can be used to show that $A_3 = A_4 = \cdots = A_n = 0$. Hence, from (20.20), at a limit point,

$$\Delta\mathbf{p} = A_1 \mathbf{z}_1 \tag{20.23}$$

Also, if we introduce the incremental arc length, Δs (Section 9.3.2), we have:

$$\Delta\mathbf{p}^T \Delta\mathbf{p} = \Delta s^2 = A_1^2 \tag{20.24}$$

so that A_1 can be equated to Δs.

20.2.2 Bifurcation point

At a bifurcation point, from (20.21), with $\Delta\lambda \neq 0$,

$$A_2 = \mathbf{z}_2^T \Delta\mathbf{p} = \frac{1}{\theta_2} \mathbf{q}^T \mathbf{z}_2 \Delta\lambda \tag{20.25}$$

Similar relationships can be derived for $A_3 - A_n$. Hence, (20.20) gives:

$$\Delta\mathbf{p} = A_1 \mathbf{z}_1 + \Delta\lambda \left[\frac{1}{\theta_2} (\mathbf{q}^T \mathbf{z}_2) \mathbf{z}_2 + \frac{1}{\theta_3} (\mathbf{q}^T \mathbf{z}_3) \mathbf{z}_3 + \cdots \frac{1}{\theta_n} (\mathbf{q}^T \mathbf{z}_n) \mathbf{z}_n) \right] = A_1 \mathbf{z}_1 + \Delta\lambda \mathbf{y} \tag{20.26}$$

Equation (20.26) applies to the limit point as well as the bifurcation point, although in the former case, from (20.18), $\Delta\lambda = 0$ and hence (20.26) coincides with (20.23). For a symmetric bifurcation (Figures 20.2a and 20.2b), ($\Delta\mathbf{p} = A_1 \mathbf{z}, \Delta\lambda = 0$) defines the bifurcated path while, for the fundamental path, A_1 is related to $\Delta\lambda$ in a manner to be discussed in the Section 20.3. Non-symmetric bifurcations will also be considered in that section.

An alternative formula for the $\mathbf{y}$ vector in (20.26) does not involve the eigenvectors, $\mathbf{z}_2 - \mathbf{z}_n$ and is given by

$$\mathbf{y} = \bar{\mathbf{K}}_t^{-1} \mathbf{q} = (\mathbf{K}_t + \beta \mathbf{z}_1 \mathbf{z}_1^T)^{-1} \mathbf{q} \tag{20.27}$$

where β is a positive scalar and the 'rank-one' modification $\beta \mathbf{z}_1 \mathbf{z}_1^T$ ensures that $\bar{\mathbf{K}}_T$ has

a non-zero determinant and can be inverted. The equivalence of the two expressions for $\mathbf{y}$ (in (20.26) and (20.27)) can be established using the relationship:

$$\mathbf{K}_t = \theta_1 \mathbf{z}_1 \mathbf{z}_1^T + \theta_2 \mathbf{z}_2 \mathbf{z}_2^T + \cdots + \theta_n \mathbf{z}_n \mathbf{z}_n^T \tag{20.28}$$

so that with $\theta_1 = 0$:

$$\bar{\mathbf{K}}_t = \beta \mathbf{z}_1 \mathbf{z}_1^T + \theta_2 \mathbf{z}_2 \mathbf{z}_2^T + \cdots + \theta_n \mathbf{z}_n \mathbf{z}_n^T \tag{20.29a}$$

and

$$\bar{\mathbf{K}}_t^{-1} = \frac{1}{\beta} \mathbf{z}_1 \mathbf{z}_1^T + \frac{1}{\theta_2} \mathbf{z}_2 \mathbf{z}_2^T + \cdots + \frac{1}{\theta_n} \mathbf{z}_n \mathbf{z}_n^T \tag{20.29b}$$

The use of (20.29b) with (20.19) and (20.27) gives the same vector $\mathbf{y}$ as in (20.26).

20.3 THE INTRODUCTION OF HIGHER-ORDER TERMS

In a finite element context, it is expensive to generate higher-order terms (involving differentials of the tangent stiffness matrix) and some progress with advanced path following can be made without such terms (Chapter 21). However, for a further development of the general theory, such terms are essential and they can be directly used in some finite element formulations (Sections 20.5 and 21.3).

In order to introduce the higher-order terms, we will write a fuller version of the Taylor expansion in (20.6) as

$$\mathbf{g}(\mathbf{p}, \lambda)|_B = \text{terms in (20.6)} + \frac{1}{2} \frac{\partial^2 \mathbf{g}}{\partial p_i \partial p_j}\bigg|_A \Delta p_i \Delta p_j + \frac{\partial^2 \mathbf{g}}{\partial p_i \partial \lambda}\bigg|_A \Delta p_i \Delta \lambda + \frac{1}{2} \frac{\partial^2 \mathbf{g}}{\partial \lambda^2}\bigg|_A \Delta \lambda^2 \tag{20.30}$$

(In order to clarify the notation and concepts, the reader might find it useful to turn to Section 20.5 in which, for truss elements, some of the higher derivatives are explicitly computed.) To make use of (20.30), we must be more rigorous about defining $\Delta \mathbf{p}$ and $\Delta \lambda$. To this end, we will expand the former using a Taylor expansion in terms of a path-length (see Section 9.3) parameter, Δs. Consequently,

$$\Delta \mathbf{p} = \dot{\mathbf{p}} \Delta s + \frac{\ddot{\mathbf{p}}}{2} \Delta s^2 \tag{20.31}$$

and for the latter:

$$\Delta \lambda = \dot{\lambda} \Delta s + \frac{\ddot{\lambda}}{2} \Delta s^2 \tag{20.32}$$

where the vector, $\dot{\mathbf{p}}$, contains the first order changes in $\mathbf{p}$ (with respect to s) and the vector $\ddot{\mathbf{p}}$ contains the second-order changes. Substituting from (20.31) and (20.32) into (20.30) gives:

$$\mathbf{g}(\mathbf{p}, \lambda)|_B = \mathbf{g}(\mathbf{p}, \lambda)|_A + \left\{ \frac{\partial \mathbf{g}}{\partial \mathbf{p}} \dot{\mathbf{p}} + \frac{\partial \mathbf{g}}{\partial \lambda} \dot{\lambda} \right\}\bigg|_A \Delta s + \frac{1}{2} \left\{ \frac{\partial \mathbf{g}}{\partial p_i \partial p_j} \dot{p}_i \dot{p}_j + 2 \frac{\partial \mathbf{g}}{\partial p_i \partial \lambda} \dot{p}_i \dot{\lambda} + \frac{\partial^2 \mathbf{g}}{\partial \lambda^2} \dot{\lambda}^2 + \frac{\partial \mathbf{g}}{\partial \mathbf{p}} \ddot{\mathbf{p}} + \frac{\partial \mathbf{g}}{\partial \lambda} \ddot{\lambda} \right\}\bigg|_A \Delta s^2 + \cdots \tag{20.33}$$

Setting the coefficient of Δs in (20.33) to zero (with a view to equilibrium) leads to

$$\frac{\partial \mathbf{g}}{\partial \mathbf{p}}\dot{\mathbf{p}} + \dot{\lambda}\frac{\partial \mathbf{g}}{\partial \lambda} = \mathbf{K}_t\dot{\mathbf{p}} - \dot{\lambda}\mathbf{q} = 0 \tag{20.34}$$

which is of a very similar form to (20.9). A similar development to that used in the previous section (leading to (20.26)) now leads to

$$\dot{\mathbf{p}} = A_1\mathbf{z}_1 + \dot{\lambda}\mathbf{y} \tag{20.35}$$

with $\mathbf{y}$ from (20.26). Also, in place of (20.17), we now have $\dot{\lambda}\mathbf{q}^T\mathbf{z}_1 = 0$ and hence in place of (20.18) and (20.19), we obtain:

$$\text{limit point;} \qquad \dot{\lambda} = 0; \qquad B_4 = -\mathbf{q}^T\mathbf{z}_1 \neq 0 \tag{20.36a}$$

$$\text{bifurcation point;} \qquad B_4 = -\mathbf{q}^T\mathbf{z}_1 = 0 \tag{20.36b}$$

From (20.33), for B to be an equilibrium point we also require the second-order terms (coefficients of Δs^2) to be zero. For the special case of proportional loading which is governed by (20.1), we have:

$$\frac{\partial \mathbf{g}}{\partial p_i \partial \lambda}\dot{p}_i\dot{\lambda} = \frac{\partial^2 \mathbf{g}}{\partial \lambda^2}\dot{\lambda}^2 = 0 \tag{20.37}$$

and are left with

$$\frac{\partial \mathbf{g}}{\partial p_i \partial p_j}\dot{p}_i\dot{p}_j + \mathbf{K}_t\ddot{\mathbf{p}} - \ddot{\lambda}\mathbf{q} = \mathbf{0} \tag{20.38}$$

Substitution from (20.35) into (20.38) and multiplication by the lowest eigenvector ($\mathbf{z}_1$) gives:

$$\mathbf{z}_1^T\left\{\frac{\partial^2 \mathbf{g}}{\partial p_i \partial p_j}A_1\mathbf{z}_1(i) + \dot{\lambda}\mathbf{y}(i)\right\}$$
$$\{A_1\mathbf{z}_1(j) + \dot{\lambda}\mathbf{y}(j)\} + \theta_1\mathbf{z}_1^T\ddot{\mathbf{p}} - \mathbf{q}^T\mathbf{z}_1\ddot{\lambda} = 0 \tag{20.39}$$

Note that we have used p_i as the ith component of p, but, $\mathbf{z}_1(i)$ as the ith component of $\mathbf{z}_1$. The latter notation is adopted because the subscript 1 has already been applied to $\mathbf{z}$ in order to indicate the first (lowest) eigenmode).

At the singular point, $\theta_1 = 0$, and (20.39) provides the following equation:

$$B_1A_1^2 + 2B_2A_1\dot{\lambda} + B_3\dot{\lambda}^2 + B_4\ddot{\lambda} = 0 \tag{20.40}$$

where

$$B_1 = \mathbf{z}_1^T\left\{\frac{\partial^2 \mathbf{g}}{\partial p_i \partial p_j}z_1(i)z_1(j)\right\} \tag{20.41}$$

$$B_2 = \mathbf{z}_1^T\left\{\frac{\partial^2 \mathbf{g}}{\partial p_i \partial p_j}z_1(i)y(j)\right\} \tag{20.42}$$

$$B_3 = \mathbf{z}_1^T\left\{\frac{\partial^2 \mathbf{g}}{\partial p_i \partial p_j}y(i)y(j)\right\} \tag{20.43}$$

$$B_4 = -\mathbf{q}^T\mathbf{z}_1 \tag{20.44}$$

where B_4 has already been introduced in (20.36b).

By multiplying equation (20.40) by Δs^2, we obtain:

$$B_1\Delta\bar{s}^2 + 2B_2\Delta\lambda\Delta\bar{s} + B_3\Delta\lambda^2 + B_4\Delta^2\lambda = 0 \tag{20.45}$$

where $\Delta\bar{s}$ is given by

$$\Delta\bar{s} = A_1\Delta s \tag{20.46}$$

and is the coefficient of $\mathbf{z}_1$ in the expansion for $\Delta\mathbf{p}$. From (20.31) and (20.35), the latter is

$$\Delta\mathbf{p} = \Delta\bar{s}\mathbf{z}_1 + \Delta\lambda\mathbf{y} + \left(\frac{1}{2}\ddot{\mathbf{p}} - \frac{\ddot{\lambda}}{2}\right)\Delta s^2 \tag{20.47a}$$

Close to the singular point, the Δs^2 term in (20.47a) may be neglected and we then have:

$$\Delta\mathbf{p} = \Delta\bar{s}\mathbf{z}_1 + \Delta\lambda\mathbf{y} \tag{20.47b}$$

In some circumstances, (i.e. at a limit point), $\Delta\lambda = 0$ and we have:

$$\Delta\mathbf{p} = \Delta\bar{s}\mathbf{z}_1 \tag{20.47c}$$

We can now classify various types of singular point. However, we will first find an expression for the change of energy (20.2) which will allow us to investigate the stability of the singular points. As indicated in Section 20.2, we need to investigate the change of energy with λ fixed. In these circumstances, close to the singular point, (20.47c) applies. Substitution into (20.3) (with higher-order terms), followed by the use of (20.4) and (20.15) then leads to [A1, A2]:

$$\delta\phi = \frac{B_1}{6}\Delta\bar{s}^3 + \frac{B_5}{24}\Delta\bar{s}^4 \tag{20.48}$$

where B_1 was given in (20.41) and B_5 is given by [A1, A2]

$$B_5 = \mathbf{z}_1^{\mathrm{T}}\left(\frac{\partial^3\mathbf{g}}{\partial\mathbf{p}_i\partial\mathbf{p}_j\partial\mathbf{p}_k}\mathbf{z}_1(i)\mathbf{z}_1(j)\mathbf{z}_1(k)\right) - \sum_{r=2}^{n}\frac{3}{\theta_r}\left(\mathbf{z}_1^{\mathrm{T}}\left(\frac{\partial^2\mathbf{g}}{\partial\mathbf{p}_i\partial\mathbf{p}_j}\mathbf{z}_1(i)\mathbf{z}_r(j)\right)\right)^2 \tag{20.49}$$

20.4 CLASSIFICATION OF SINGULAR POINTS

We can now classify the various type of singular points and derive some properties both in relation to their stability and to the tangential path directions.

20.4.1 Limit points

At a limit point, $\Delta\lambda = 0$ (see (20.18)), and we use (20.47c). Hence, (20.45) reduces to

$$B_1\Delta\bar{s}^2 + B_4\Delta^2\lambda = 0 \tag{20.50a}$$

From (20.50a), we have

$$\Delta\bar{s}^2 = \left(\frac{-B_4}{B_1}\right)\Delta^2\lambda; \qquad \Delta\bar{s} = \pm X\Delta^2\lambda \tag{20.50b}$$

from which, with (20.47c),

$$\Delta\mathbf{p} = \Delta\bar{s}\mathbf{z}_1 = \pm X\Delta^2\lambda\mathbf{z}_1 \tag{20.51}$$

which gives two solutions for Δs (of equal magnitude and opposite sign) in terms of $\Delta^2\lambda$ which are symmetrically placed about the limit point (Figure 20.1). Also, with $B_1 \neq 0$, from (20.48):

$$\delta\phi = \frac{B_1}{6}\Delta\bar{s}^3 + O(\Delta\bar{s})^4 \tag{20.52}$$

If B_1 is positive, the energy change is positive for positive $\Delta\bar{s}$ and negative for negative $\Delta\bar{s}$. Alternatively, if B_1 is negative, the energy change is negative for positive $\Delta\bar{s}$ and positive for negative $\Delta\bar{s}$. In either case, there is a direction in which negative energy results (Figure 20.1) and hence a limit point is unstable.

20.4.2 Bifurcation points

At a bifurcation point, from (20.36b) $B_4 = 0$ so that (20.45) gives:

$$B_1\Delta\bar{s}^2 + 2B_2\Delta\bar{s}\Delta\lambda + B_3\Delta\lambda^2 = 0 \tag{20.53}$$

while from (20.47b):

$$\Delta\mathbf{p} = \Delta\bar{s}\mathbf{z}_1 + \Delta\lambda\mathbf{y}$$

20.4.3 Symmetric bifurcations

At a symmetric bifurcation point, $B_1 = 0$ and hence (20.53) gives:

$$(2B_2\Delta\bar{s} + B_3\Delta\lambda)\Delta\lambda = 0 \tag{20.54}$$

with solutions:

$$\Delta\lambda = 0 \tag{20.55a}$$

or

$$\Delta\bar{s} = -\frac{1}{2}\left(\frac{B_3}{B_2}\right)\Delta\lambda = X\,\Delta\lambda \tag{20.55b}$$

Equation (20.55a) relates to the bifurcated path and in conjunction with (20.47b), we then have:

$$\Delta\mathbf{p}_b = \Delta\bar{s}\mathbf{z}_1 \tag{20.56}$$

where $\Delta\bar{s}$ may be positive or negative (Figures 20.2a or b). The fundamental path can be obtained by substituting from (20.55b) into (20.47b) and leads to

$$\Delta\mathbf{p}_f = \Delta\lambda(X\mathbf{z}_1 + \mathbf{y}) \tag{20.57}$$

with X from (20.55b). In (20.57) $\Delta\lambda$ may be positive or negative.

Because $B_1 = 0$, from (20.48), the stability of the symmetric bifurcation point (Figure 20.2a and b) is governed by the coefficient B_5 (see (20.49)).

20.4.4 Asymmetric bifurcations

At an asymmetric bifurcation (Figure 20.2c), $B_1 \neq 0$ and the solution of (20.53) is

$$\Delta\bar{s} = \frac{1}{B_1}(-B_2 \pm (B_2^2 - B_1B_3)^{1/2})\Delta\lambda; \qquad \Delta\bar{s} = X_i\Delta\lambda \tag{20.58}$$

where there are two possible values for X_i. By considering the limit of X_i as B_1 tends to zero and comparing the result with (20.55b), one can show that X_1, which corresponds to the use of the + sign from the $\pm$ in (20.58) relates to the fundamental path for which, via (20.47b), we have:

$$\Delta \mathbf{p}_f = \Delta\lambda(X_1\mathbf{z}_1 + \mathbf{y}) = \Delta\bar{s}\left(\mathbf{z}_1 + \frac{1}{X_1}\mathbf{y}\right) \tag{20.59}$$

while for the bifurcated path we adopt the $-$ sign from the $\pm$ in (20.58) which gives X_2 and, in place of (20.59) we have:

$$\Delta \mathbf{p}_b = \Delta\lambda(X_2\mathbf{z}_1 + \mathbf{y}) = \Delta\bar{s}\left(\mathbf{z}_1 + \frac{1}{X_2}\mathbf{y}\right) \tag{20.60}$$

Both the fundamental (20.59) and bifurcated (20.60) solutions have two equal and opposite directions because, considering the first forms in (20.59) and (20.60), $\Delta\lambda$ can be positive or negative.

If we know the fundamental path in the vicinity of the bifurcation point so that we can obtain $\Delta\mathbf{p}_f$ for a given $\Delta\lambda$, from (20.59) and (20.60), we can obtain:

$$\Delta \mathbf{p}_b = \Delta \mathbf{p}_f + \Delta\lambda(X_1 - X_2)\mathbf{z}_1 \tag{20.61}$$

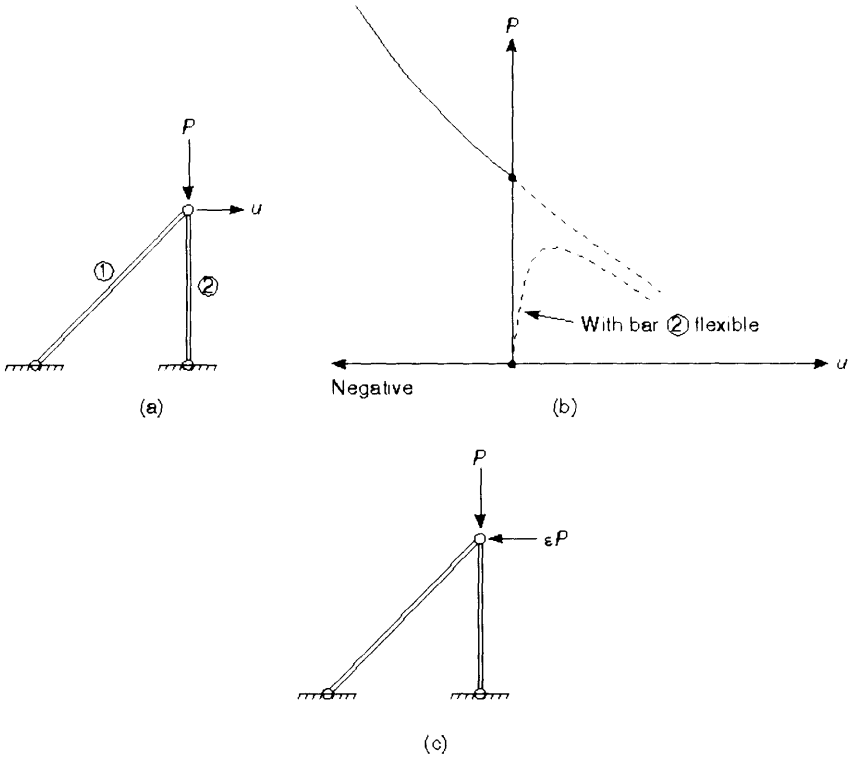

Figure 20.4 System and response for asymmetric bifurcation. (a) System; (b) response; (c) alternative loading.

The coefficient X_1 need not be obtained from (20.58), but rather could be obtained by multiplying (20.59) by $\mathbf{z}_1$ to obtain:

$$X_2 = \left(\frac{\Delta \mathbf{p}_f^T \mathbf{z}_l}{\Delta \lambda}\right) \tag{20.62}$$

so that the vector $\mathbf{y}$ can be obtained as

$$\Delta\lambda \mathbf{y} = \Delta \mathbf{p}_f - (\Delta \mathbf{p}_f^T \mathbf{z}_l)\mathbf{z}_l \tag{20.63}$$

However, there does not seem to be any way to obtaining X_1 without using second-order information. Without such information, there would seem to be no way of getting an estimate for the ratio between $\Delta \mathbf{p}_f$ and $\mathbf{z}_l$ in $\Delta \mathbf{p}_b$ in order to obtain a better predictor for the asymmetric bifurcation than (20.56) which applies for the symmetric bifurcation.

with $B_1 \neq 0$, the energy change is similar to that of a limit point (see (20.52)) and, following a similar argument to that given at the end of Section 20.4, it can be shown that an asymmetric bifurcation point is inevitably unstable (see Figure 20.2c).

Figure 20.4 shows a two-bar truss system that is closely related to the simple bar-spring systems of Chapters 1 and 3 (see also Figure 20.3). However, the vertical member 2 (Figure 20.4) is now rigid while the sideways, 'spring member' is inclined Croll and Walker [Cl] give a detailed analysis of this simple system which, when perfect, responds with an asymmetric bifurcation (Figure 20.4b). It should be noted that this bifurcation vanishes if the vertical member is made flexible (see Figure 20.4b). However, an asymmetric bifurcation from a non-linear fundamental path can be induced by adding a sideways load as illustrated in Figure 20.4c.

20.5 COMPUTATION OF HIGHER-ORDER DERIVATIVES FOR TRUSS ELEMENTS

Explicit computations for truss elements have been given by Wriggers *et al.* [W1]. Procedures using 'finite differences' have been described by Riks [R1], Eriksson [E1] and Wriggers and Simo [W2].

20.5.1 Amplification of notation

In the earlier sections of this chapter, we have introduced vectors of the form:

$$\mathbf{v} = \frac{\partial^2 \mathbf{g}}{\partial p_i \partial p_j} \delta p_i \delta p_j \tag{20.64}$$

(see, for example (20.30) which involves terms of the same form, although with Δ's instead of δ's). The vector $\mathbf{v}$ in (20.64) stems from the differentiation of the vector $(\partial \mathrm{g}/\partial \mathbf{p})\delta \mathbf{p}$ or $\mathbf{K}_t \delta \mathbf{p}$ with $\delta \mathbf{p}$ kept fixed. We can consider an individual term in the latter vector as

$$a_I = \frac{\partial g_I}{\partial p_i} \delta p_I = \frac{\partial g_1}{\partial p_1} \delta p_1 + \frac{\partial g_I}{\partial p_2} \delta p_2 + \cdots \tag{20.65}$$

Differentiation (with the δp's fixed) then leads to

$$v_I = \delta a_1 = \frac{\partial a_I}{\partial p_j} \delta p_j = \frac{\partial g_I}{\partial p_I \partial p_j} \delta p_i \delta p_j \tag{20.66}$$

Generally in this chapter, we have re-expressed the above in terms of the complete vector rather than in terms of an individual component, i.e. using (20.64) rather than (20.66). For further work, we will refer to the vector $\mathbf{v}$ as

$$\mathbf{v}(\delta\mathbf{p}, \delta\mathbf{p}) = \delta(\mathbf{K}_t\delta\mathbf{p})_{\delta\mathbf{p}=\text{const.}} = \frac{\partial^2 \mathbf{g}}{\partial p_i \partial p_j}\delta p_i \delta p_j \tag{20.67}$$

More generally, we require:

$$\mathbf{v}(\delta\mathbf{p}, \mathbf{a}) = \delta(\mathbf{K}_t\mathbf{a})_{\mathbf{a}=\text{const.}} = \mathbf{V}(\mathbf{a})\delta\mathbf{p} \tag{20.68}$$

where $\mathbf{V}(\mathbf{a})$ is a matrix. In most applications, we require the vector $\mathbf{v}$ and do not directly require this matrix (but see Section 21.5, for an application where the matrix $\mathbf{V}$ is required). The vector $\delta\mathbf{p}$ in (20.68) can be replaced by another vector $\mathbf{b}$ so that we would have:

$$\nabla_b(\mathbf{K}_t\mathbf{a}) = \mathbf{v}(\mathbf{b}, \mathbf{a}) = \mathbf{V}(\mathbf{a})\mathbf{b} \tag{20.69}$$

The expression on the very left of (20.69) denotes the directional derivative (in the direction $\mathbf{b}$). This form allows the computation of terms such as B_3 in (20.43).

20.5.2 Truss element using Green's strain

As a first example, we will consider the element of Section 3.3 for which the tangent stiffness matrix is

$$\mathbf{K}_t = c_1\mathbf{c}(\mathbf{x}')\mathbf{c}(\mathbf{x}')^T + \frac{A_o\sigma}{2\alpha_o}\bar{\mathbf{A}} \tag{20.70}$$

with

$$c_1 = \frac{EA_o}{8\alpha_o^3} \tag{20.71}$$

where α_o is half the length of the element. In relation to (20.70), for a two-dimensional element (as in Figure 3.6):

$$\mathbf{c}(\mathbf{x}')^T = (-x'_{21}, x'_{21}, -z'_{21}, z'_{21}) \tag{20.72}$$

where the primes indicate updated coordinates (see Section 3.3.5) and, for example, $x_{21} = x'_2 - x'_1$. Also, with the nodal variables ordered as in Chapter 3 (see Figure 3.6), the matrix $\bar{\mathbf{A}}$ is given by

$$\bar{\mathbf{A}} = \begin{bmatrix} 1 & -1 & 0 & 0 \\ -1 & 1 & 0 & 0 \\ 0 & 0 & 1 & -1 \\ 0 & 0 & -1 & 1 \end{bmatrix} \tag{20.73}$$

To differentiate (20.70), we require:

$$\delta\mathbf{c}(\mathbf{x}') = \bar{\mathbf{A}}\,\delta\mathbf{p} \tag{20.74}$$

and (see (3.65))

$$\delta\sigma = E\mathbf{b}(\mathbf{p})^T\delta\mathbf{p} = \frac{E}{4\alpha_o^2}\mathbf{c}(\mathbf{x}')^T\delta\mathbf{p} \tag{20.75}$$

In relation to (20.68), we can now obtain:

$$\mathbf{v}(\delta\mathbf{p}, \mathbf{a}) = \nabla_p(\mathbf{K}_t\mathbf{a}) = c_1\delta\mathbf{c}(\mathbf{x}')\mathbf{c}(\mathbf{x}')^T\mathbf{a} + c_1\mathbf{c}(\mathbf{x}')\delta\mathbf{c}(\mathbf{x}')^T\mathbf{a} + \frac{A_o\delta\sigma}{2\alpha_o}\bar{\mathbf{A}}\mathbf{a} \tag{20.76}$$

or

$$\mathbf{v}(\delta\mathbf{p}, \mathbf{a}) = \nabla_p(\mathbf{K}_t\mathbf{a}) = c_1\{(\mathbf{c}(\mathbf{x}')^T\mathbf{a})\bar{\mathbf{A}}\,\delta\mathbf{p} + (\mathbf{c}(\mathbf{x}')^T\delta\mathbf{p})\bar{\mathbf{A}}\mathbf{a} + (\delta\mathbf{p}^T\bar{\mathbf{A}}\mathbf{a})\mathbf{c}(\mathbf{x}')\} \tag{20.77}$$

The matrix $\mathbf{V}(\mathbf{a})$ of (20.68) follows as

$$\mathbf{V}(\mathbf{a}) = c_1\{(\mathbf{c}(\mathbf{x}')^T\mathbf{a})\bar{\mathbf{A}} + \bar{\mathbf{A}}\mathbf{a}\mathbf{c}(\mathbf{x}')^T + \mathbf{c}(\mathbf{x}')\mathbf{a}^T\bar{\mathbf{A}}\} \tag{20.78}$$

The vector $\mathbf{v}(\mathbf{b}, \mathbf{a}) = \nabla_b(\mathbf{K}_t\mathbf{a})$ of (20.69) can be simply obtained by replacing $\delta\mathbf{p}$ by $\mathbf{b}$ in (20.77).

Equations (20.77) and (20.78) remains valid for three-dimensional truss elements, provided the definitions of the vector $\mathbf{c}(\mathbf{x}')$ and the matrix $\bar{\mathbf{A}}$ are suitably modified (see Section 3.7).

20.5.3 Truss element using a rotated engineering strain

For this element (see Section 3.4), the stiffness matrix is

$$\mathbf{K}_t = c_1\lambda^2\mathbf{c}(\mathbf{x}')\mathbf{c}(\mathbf{x}')^T + \frac{A_o\sigma\lambda}{2\alpha_o}\bar{\mathbf{A}} \tag{20.79}$$

with c_1 being given by (20.71):

$$\lambda = \frac{\alpha_o}{\alpha_n} \tag{20.80}$$

with α_n as the current half-length of the element (see (3.53)). Using the relationship:

$$\delta\alpha_n = \frac{\lambda}{4\alpha_o}\delta\mathbf{p}^T\mathbf{c}(\mathbf{x}') \tag{20.81a}$$

so that:

$$\delta\lambda = \frac{-\lambda^3}{4\alpha_o^2}\delta\mathbf{p}^T\mathbf{c}(\mathbf{x}') \tag{20.81b}$$

one can show that in place of (20.77), we now arrive at:

$$\begin{aligned}\mathbf{v}(\delta\mathbf{p}, \mathbf{a}) = \nabla_p(\mathbf{K}_t\mathbf{a}) &= c_3\{(\mathbf{c}(\mathbf{x}')^T\mathbf{a})\bar{\mathbf{A}}\,\delta\mathbf{p} + (\mathbf{c}(\mathbf{x}')^T\delta\mathbf{p})\bar{\mathbf{A}}\mathbf{a} + (\delta\mathbf{p}^T\bar{\mathbf{A}}\mathbf{a})\mathbf{c}(\mathbf{x}')\} \\ &+ c_4\{(\delta\mathbf{p}^T\mathbf{c}(\mathbf{x}'))(\mathbf{a}^T\mathbf{c}(\mathbf{x}'))\mathbf{c}(\mathbf{x}')\}\end{aligned} \tag{20.82}$$

with

$$c_3 = \lambda^2 c_1 - c_2\lambda^3; \qquad c_4 = \frac{-\lambda^3}{4\alpha_o^2}(2c_1\lambda - 3\lambda^2 c_2) \tag{20.83}$$

and

$$c_2 = \frac{\sigma A_0}{8\alpha_o^2} \tag{20.84}$$

The matrix $\mathbf{V}(\mathbf{a})$ of (20.68) follows as

$$\begin{aligned}\mathbf{V}(\mathbf{a}) &= c_3\{(\mathbf{c}(\mathbf{x}')^T\mathbf{a})\bar{\mathbf{A}} + \bar{\mathbf{A}}\mathbf{a}\mathbf{c}(\mathbf{x}')^T + \mathbf{c}(\mathbf{x}')\mathbf{a}^T\bar{\mathbf{A}}\} \\ &+ c_4\{(\mathbf{a}^T\mathbf{c}(\mathbf{x}'))\mathbf{c}(\mathbf{x}')\mathbf{c}(\mathbf{x}')^T\}\end{aligned} \tag{20.85}$$

20.5.4 Computation of the stability coefficients B_1–B_3

In relation to the earlier work of Section 20.3, we can now compute the 'stability coefficients', B_1–B_3 of (20.41)–(20.43) (the stability coefficient B_4 of (20.44) does not need higher-order terms) by first using the notation of (20.68) to compute the vectors:

$$\mathbf{v}(\mathbf{z}_1, \mathbf{z}_1) = \mathbf{v}_1 = \frac{\partial^2 \mathbf{g}}{\partial p_i \partial p_j} \mathbf{z}_1(i)\mathbf{z}_1(j) \tag{20.86a}$$

$$\mathbf{v}(\mathbf{z}_1, \mathbf{y}) = \mathbf{v}_2 = \frac{\partial^2 \mathbf{g}}{\partial p_i \partial p_j} \mathbf{z}_1(i)\mathbf{y}(j) \tag{20.86b}$$

$$\mathbf{v}(\mathbf{y}, \mathbf{y}) = \mathbf{v}_3 = \frac{\partial^2 \mathbf{g}}{\partial p_i \partial p_j} \mathbf{y}(i)\mathbf{y}(j) \tag{20.86c}$$

For the truss elements, these vectors can be computed directly from (20.77) or (20.82). The coefficients B_1–B_3 of (20.41)–(20.43) then follow as

$$B_1 = \mathbf{z}_1^{\mathrm{T}} \mathbf{v}(z_1, \mathbf{z}_1) = \mathbf{z}_1^{\mathrm{T}} \mathbf{v}_1 = \mathbf{z}_1^{\mathrm{T}} \left(\frac{\partial^2 \mathbf{g}}{\partial p_i \partial p_j} \mathbf{z}_1(i)\mathbf{z}_1(j) \right) \tag{20.87a}$$

$$B_2 = \mathbf{z}_1^{\mathrm{T}} \mathbf{v}(\mathbf{z}_1, \mathbf{y}) = \mathbf{z}_1^{\mathrm{T}} \mathbf{v}_2 = \mathbf{z}_1^{\mathrm{T}} \left(\frac{\partial^2 \mathbf{g}}{\partial p_i \partial p_j} \mathbf{z}_1(i)\mathbf{y}(j) \right) \tag{20.87b}$$

$$B_3 = \mathbf{z}_1^{\mathrm{T}} \mathbf{v}(\mathbf{y}, \mathbf{y}) = \mathbf{z}_1^{\mathrm{T}} \mathbf{v}_3 = \mathbf{z}_1^{\mathrm{T}} \left(\frac{\partial^2 \mathbf{g}}{\partial p_i \partial p_j} \mathbf{y}(i)\mathbf{y}(j) \right) \tag{20.87c}$$

20.6 SPECIAL NOTATION

$A_1 - A_n$ = coefficients in eigenvector expansion of $\Delta\mathbf{p}$ (see (20.20))
B_1–B_5 = stability coefficients (see (20.36), (20.41)–(20.44) and (20.49))
$\mathbf{g}$ = gradient of total potential energy
$\mathbf{p}$ = displacement vector
$\mathbf{q}$ = load vector
$\mathbf{v}(\mathbf{b}, \mathbf{a})$ = related to directional derivative—see (20.69)
$\mathbf{y}$ = see (20.26) or (20.27)
$\mathbf{z}_i$ = eigenvectors of $\mathbf{K}_t$
θ_i = eigenvalues corresponding to eigenvectors $\mathbf{z}_i$
λ = load multiplier
φ = strain energy
ϕ = total potential energy
Δs = incremental length
$\nabla_{\mathbf{b}}$ = directional derivative (in direction $\mathbf{b}$)—see (20.69)

Subscripts

f = fundamental path
p = predictor

20.7 REFERENCES

[A1] Allman, D. J., On the general theory of the stability of equilibrium of discrete conservative systems, *The Aero Journal*, **93**, 29–35 (1989).

[A2] Allman, D. J., *Stability of Equilibrium of Singular Points in Discrete Conservative Systems*, Royal Aircraft Estab., Tech. Report 84022, Farnborough, Hants (1984).

[C1] Croll, J. G. A. & Walker, A. C., *Elements of Structural Stability*, Macmillan, London (1972).

[E1] Eriksson, A., Derivatives of tangential stiffness matrices for equilibrium path descriptions, *Int. J. for Num. Meth. in Engng.*, **32**, 1093–1113 (1991).

[K1] Koiter, W. T., *Over de Stabiliteit van het Elastisch Evenwicht*, H. J. Paris, Amsterdam (1945).

[K2] Koiter, W. T., English translation of [K1], NASA TT F-10833 (1967).

[K3] Komarakul-Na-Nakorn, A. & Arora, J. S., Stability criteria: a review, *Computers & Structures*, **37**, 35–49 (1990).

[R1] Riks, E., Bifurcation and stability—a numerical approach, *Innovative Methods for Nonlinear Problems*, ed. W. K. Liu *et al.*, Pineridge Press, Swansea, pp. 313–344 (1984).

[S1] Sewell, M. J., *Proc. Roy. Soc.*, **A306**, 201–223 (1968).

[S2] Sewell, M. J., *Proc. Roy. Soc.*, **A306**, 225–238. (1968).

[T1] Thompson, J. M. T. & Hunt, G. W., *A General Theory of Elastic Stability*, Wiley, London, 1973.

[W1] Wriggers, P., Wagner, W. & Miehe, C., A quadratically convergent procedure for the calculation of stability points in finite element analysis, *Comp. Meth. in Appl. Mech. & Engng.*, **70**, 329–347 (1988).

[W2] Wriggers, W. & Simo, J. C., A general procedure for the direct computation of turning and bifurcation points, *Int. J. for Num. Meth. in Engng.*, **30**, 1990, 155–176 (1990).

21 Branch switching and further advanced solution procedures

An extensive review of solution procedures for non-linear analysis was given in Chapter 9. In general, we will not repeat these references here. However, in the earlier volume, apart from the discussion in Section 9.10, we did not specifically consider either the computation of singular points or 'branch switching'. Because these matters will be directly addressed in this chapter, we will include here reference to papers on these topics, previously discussed in Section 9.10, which relate specifically to the finite element method. Reference to papers on the more general mathematical background can be found in Section 9.10 or in the review papers [C4, K2, S7].

In Section 21.1, we start by describing some simple bracketing procedures for the computation of singular points (limit points or bifurcations). Other work in this area is given in [B3, M1, S3, S4, W3]. Assuming that the bracketed point is a 'bifurcation point', we may then wish to switch on to the 'post-bifurcation path' instead of remaining on the fundamental path. Simple techniques for such branch switching [W2] only require the computation of the eigenmode associated with the lowest eigenvector and are considered in Section 21.2. Other work involving forms of 'eigenmode injection' has been given in [C3, D2, E1, M2].

In Section 21.3, we move on to consider more sophisticated branch switching techniques [E1.20, R1.20] that require second derivatives (of the total potential energy) and thus utilize some of the theory from Chapter 20. Sections 21.4 and 21.5 also consider implementations involving these higher-order derivatives for general predictor/corrector algorithms [W1]. In Section 21.4 the 'higher derivatives' are used to give better predictors, while in Section 21.5 they are used to give better 'correctors'. It should perhaps be emphasised that these techniques are not used in most current non-linear finite element programs and, indeed, that it has yet to be demonstrated that they are economically viable.

Further applications of the higher derivatives are considered in Section 21.5 which describes methods for directly computing singular points that can be considered as more sophisticated alternatives to the simple techniques discussed earlier in Section 21.1. Other work in this area is due to Wriggers *et al.* [W1.20, W2.20], Riks [R1.20] and Azrar *et al.* [A1].

In Section 21.7, we consider the extension of 'line search techniques' (Section 9.2) to various forms of 'arc-length method' [S2, S5, C1, C2]. While the technique often leads to an improvement in the basic method, with arc-length methods which may be used to converge to an unstable equilibrium state, some fundamental problems apply to 'line searches' which are aimed at a 'minimum energy' (see Section 21.7.3).

In Section 21.8, we describe some alternative arc-length methods using relative variables. This work is motivated by the problems with conventional arc-length methods that have been reported by a number of workers [D2, D3, S1] who suggest a possible solution that involves the implementation of a special form of generalised displacement control at a specific variable (see Section 9.3.2.3). In contrast to the conventional implementation of the latter methods, these techniques [D2, D3, S1] control the *relative* displacement at a particular point – for example the 'crack opening displacement'. These methods have considerable potential for use in conjunction with contact algorithms (Chapter 23).

For 'cracking problems', these techniques require a pre-knowledge of the crack position and its local topology. Particularly once multiple cracks are encountered, these methods may introduce considerable computational problems. Consequently, in Section 21.9, a modification is proposed to the cylindrical arc-length method ([H1]) that involves no such 'pre-knowledge and may extend the life of existing quadratic arc-length methods. Instead, the method is based on a new method for choosing the root for the cylindrical arc-length method (Section 9.4). The author and co-worker have found [H1] that this alternative technique (which is very easily to implement) gives a much better numerical performance for difficult path-following problems – particularly those involving the 'sharp snap-backs' that are often associated with cracking [C3].

Finally in Section 21.10, we will describe an alternative method for overcoming complex snap-throughs and snap-backs which involves a switch from statics to dynamics. Such procedures have been described by Riks *et al.* [R2] and by Skeie *et al.* [S8].

21.1 INDIRECT COMPUTATION OF SINGULAR POINTS

In the following, we will assume that the analyst is tracing a load/deflection equilibrium path using some form of predictor/corrector (or incremental/iterative) method. At some stage, the solution procedures converges on to an equilibrium point that is beyond the first singular point which may be a limit point or a bifurcation point. The computer code should give an indication as to which is likely (we can only say likely, because, from the work of Chapter 2 (see Figure 2.6) and Chapter 3 (see Figure 3.19), it is possible to converge on to a 'complementary equilibrium path'). To this end, if both the current stiffness parameter (Section 9.5.2) and the minimum pivot switch signs, it is likely that a limit point has been passed (further tests can be made with subsequent increments on the magnitude of the load parameter). On the other hand, if only the minimum pivot has switched signs, with no change in the sign of the current stiffness parameter, it is likely that a bifurcation point has been passed (see Figure 21.1). In these circumstances, the analyst might like to 'home in' on the singular point using some form of bracketing procedure. In the case of a 'bifurcation', this process could precede the activation of a 'branch switching' procedure. Such techniques will be discussed in Section 21.2.

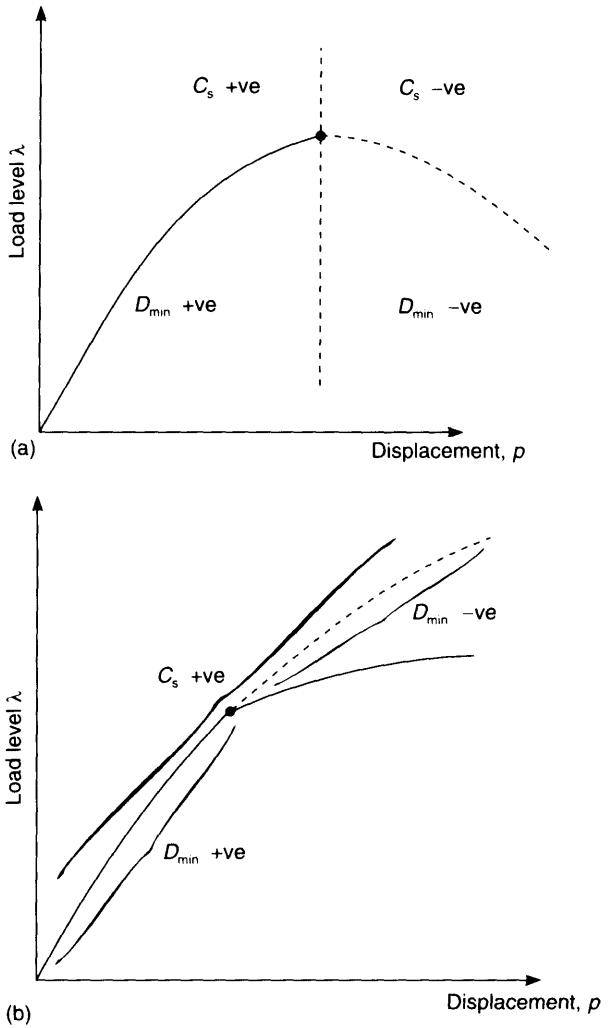

Figure 21.1 Response of current stiffness parameter C_s and minimum pivot, D_{min} to limit and bifurcation points. (a) Limit point; (b) bifurcation point.

The decision to implement the 'bracketing proces' may either be automatically activated, following the passing of a singular point (especially a bifurcation point), or may be introduced after 'a restart'. In the following we will briefly outline an algorithm to implement such a bracketing. We will concentrate on the situation in which the first singular point has been passed although the concepts can be applied to other situations.

The first issue to decide is the choice of 'test function', τ, which changes sign as the singular point is passed (see Figure 21.2). Possible choices are:

$$\begin{aligned} &\tau = \det(\mathbf{K}_t) && \text{(a)} \\ &\tau = \text{min. pivot from } \mathbf{K}_t, \text{ i.e. } D_{min} && \text{(b)} \\ &\tau = \text{product of } D_{max} \text{ and } D_{min} && \text{(c)} \\ &\tau = \text{min. eigenvalue of } \mathbf{K}_t && \text{(d)} \end{aligned} \qquad (21.1)$$

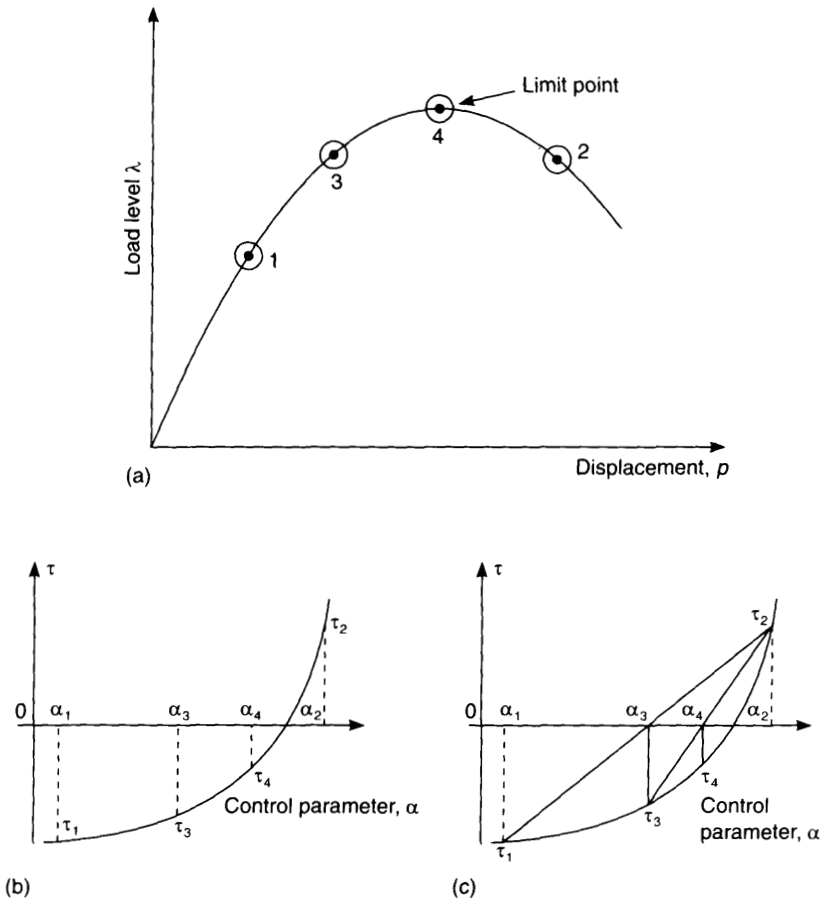

Figure 21.2 Bracketing procedure. (a) Bracketing points; (b) bisection for control parameter; (c) interpolation for control parameter.

where the D's are taken from the diagonal matrix, $\mathbf{D}$, from the $\mathbf{LDL}^{\mathrm{T}}$ factorisation (or equivalent) of $\mathbf{K}_{\mathrm{t}}$ (see Section 2.2.6). The test function in (d) above is potentially the most effective, but also requires the most work. The test function in (a) will not work with a multiple bifurcation. In the computer program for which results will be given in Chapter 22, we have included a range of bracketing options. In practice, it is best [S6] to use a normalised test function, $\bar{\tau}$ where:

$$\bar{\tau} = \tau/(|\tau_1 \tau_2|)^{1/2} \tag{21.2}$$

and τ_1 and τ_2 are the closest values of the test function on either side of the singular point once the bracketing procedure is started.

The bracketing process is very similar to that adopted for a line-search on the energy slopes (see Section 9.2). In particular, we always use the closest values on either side of the singular point so that in Figures 21.1b, τ_{i-2} would be positive, while τ_{i-1} would be

negative. The 'control parameter' in Figures 21.2b and 21.2c is α. This could be the 'load parameter' (λ elsewhere in the book) or it could be the arc length.

The simplest bracketing procedures involve bi-section or the golden section, but it is probably best to use interpolation so that:

$$\alpha_i = \alpha_{i-2} - \tau_{i-2}(\alpha_{i-1} - \alpha_{i-2})/(\tau_{i-1} - \tau_{i-2}) \tag{21.3}$$

where $\alpha_{i-1}, \alpha_{i-2}$ and τ_{i-1} and τ_{i-2} are the control parameters and test functions at the latest solutions that straddle the singular point (Figure 21.2). Equation (21.3) is applied with the proviso that close to the ends in Figure 21.2c, interpolation might lead to a very slow convergence rate. In these circumstances, one can overwrite (21.3) and introduce a minimum change so that:

$$\begin{aligned} &|\alpha_i - \alpha_{i-1}| = 0.8|\alpha_{i-1} - \alpha_{i-2}| \quad \text{if from (21.3)} \\ &|\alpha_i - \alpha_{i-1}| > 0.8|\alpha_{i-1} - \alpha_{i-2}| \end{aligned} \tag{21.4}$$

$$\begin{aligned} &|\alpha_i - \alpha_{i-1}| = 0.2|\alpha_{i-1} - \alpha_{i-2}| \quad \text{if from (21.3)} \\ &|\alpha_i - \alpha_{i-1}| < 0.2|\alpha_{i-1} - \alpha_{i-2}| \end{aligned}$$

In deciding on a suitable termination criterion for ending the bracketing, it is best to use both the value of the test function and the size of the bracket ($\Delta\alpha_i$). For example, one may use a small value (say 10^{-4}) on η where

$$\begin{aligned} &\eta = (|\bar{\tau}\,\Delta\alpha_i/\alpha_i|)^{1/2} = (|\bar{\tau}\,\Delta\lambda_i/\lambda_i|)^{1/2} \quad \text{for load control} \\ &\eta = (|\bar{\tau}\,\Delta\alpha_i/\alpha_o|)^{1/2} = (|\bar{\tau}\,\Delta l_i/\Delta l_o|)^{1/2} \quad \text{for arc-length control} \end{aligned} \tag{21.5}$$

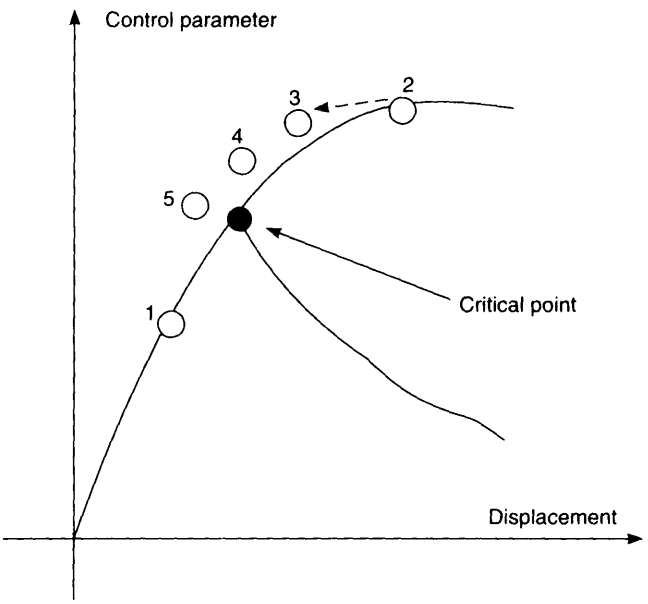

Figure 21.3 Semi-direct bracketing (without full iteration for intermediate points).

In the above, λ_t is the current value of the load parameter, while Δl_0 is the value of the arc-length increment just prior to the implementation of the bracketing procedure.

It has been assumed that we are allowed to move backwards along the solution path. Hence in relation to Figure 21.2a we would move sequentially through the points $1 \rightarrow 2 \rightarrow 3 \rightarrow 4$ (with the latter being assumed to be at the limit point). However, if we have a 'path-dependent material' and, for example, plasticity is involved, such a path reversal is invalid. However, the bracketing procedures can still be used but now, in relation to Figure 21.2a, we must apply the solutions:

(a) From point 1 to point 2
(b) From point 1 to point 3
(c) From point 3 to point 4

If the sole purpose of the analysis is to compute the singular point, it is possible to either eliminate the equilibrium iterations or, at least slacken the tolerance, for the intermediate points (see Fig. 21.3 and ref. [S6]).

21.2 SIMPLE BRANCH SWITCHING

Having computed the singular point with sufficient accuracy at say $(\overset{*}{\mathbf{p}}, \overset{*}{\lambda})$, we can compute $\mathbf{z}$, the lowest eigenmode corresponding to the lowest eigenvalue ($\theta \simeq 0$) of $\overset{*}{\mathbf{K}}_t$. To this end, it may be necessary to introduce a 'shift' [B1.10] for the eigenvalue calculation (because of the near-singular nature of $\overset{*}{\mathbf{K}}_t$). Having computed $\mathbf{z}$, we can compute the stability coefficient B_4 of (20.44) via:

$$B_4 = -\mathbf{q}_c^T \mathbf{z} \tag{21.6}$$

where $\mathbf{q}_c$ is the external load pattern. As indicated in Section 20.2 (see (20.19)), this quantity should be zero (or very nearly zero) for a bifurcation point. If we introduce, higher-order derivatives, it is possible to compute the coefficients B_1–B_3 of (20.41)–(20.43)) (and also B_5 of (20.49)) and hence to obtain additional information on the nature of the bifurcation. This information can also be useful for branch-switching. However, the higher derivatives are generally not available in standard finite element programs and, in any case, it is possible to branch switch without these terms.

Following standard predictor–corrector techniques, we will start with a predictor $\Delta \mathbf{p}_p$ relating to some new load level $\overset{*}{\lambda} + \Delta\lambda_p$. However, instead of using the usual Euler predictor, we will adopt:

$$\Delta \mathbf{p}_p = \Delta l \mathbf{z}; \qquad \Delta\lambda_p = 0 \tag{21.7}$$

At this stage we know $(\overset{*}{\mathbf{p}} + \Delta \mathbf{p}_p, \overset{*}{\lambda} + \Delta\lambda_p)$ and can, as usual, compute the out-of-balance force vector $\mathbf{g}$ and tangent stiffness matrix, $\mathbf{K}_t$. In the following algorithms, we will follow the procedures adopted for the various arc-length methods (Sections 9.3 and 9.4) and will implicitly calculate the standard Newton–Raphson iterative change at a new load level, $\lambda + \delta\lambda$ so that (see (9.23)):

$$\delta \mathbf{p} = -\mathbf{K}_t^{-1}(\mathbf{g}_o - \delta\lambda \mathbf{q}_c) = \delta \bar{\mathbf{p}} + \delta\lambda \delta \mathbf{p}_t \tag{21.8}$$

Given the iterative form of (21.8) and the predictor of (21.7), we can simply apply any of the methods of Section 9.3.2 based on 'generalised displacement control'

21.2.1 Corrector based on a linearised arc-length method

Conceptually the simplest algorithm is to adopte the 'two-vector' form of the Riks–Wempner algorithm (Section 9.3.2.2) so that, at each iteration, we force $\delta\mathbf{p}$ to be orthogonal to the predictor solution $\Delta\mathbf{p}_p$ and hence find $\delta\lambda$ as

$$\delta\lambda = \frac{-\Delta\mathbf{p}_p^T\delta\bar{\mathbf{p}}}{\Delta\mathbf{p}_p^T\delta\mathbf{p}_t} \tag{21.9}$$

Because, from (21.7), $\Delta\mathbf{p}_p$ is simply a multiple of $\mathbf{z}$, this procedure ensures that we obtain corrections that are orthogonal to $\mathbf{z}$ so that the final incremental solution (from $(\bar{\mathbf{p}})$) will be of the form

$$\Delta\mathbf{p} = \Delta\mathbf{p}_p + \delta\mathbf{p}_1 + \delta p_2 + \cdots = \Delta l\mathbf{z} + \mathbf{y} \quad \text{where} \quad \mathbf{y}^T\mathbf{z} = 0. \tag{21.10}$$

Geometrically (Figure 21.4), it follows that the solution is most unlikely to converge back on the unstable fundamental path. Kouhia [K1] has proposed using Fried's approah [F2] instead of (21.9). For this method (see Section 9.3.2.2), $\delta\bar{\mathbf{p}}$ is made orthogonal to $\delta\mathbf{p}_t$ so that the iterative change in λ ($\delta\lambda$) is as in (21.9) but with $\Delta\mathbf{p}_p$ being replaced by $\delta\mathbf{p}_t$.

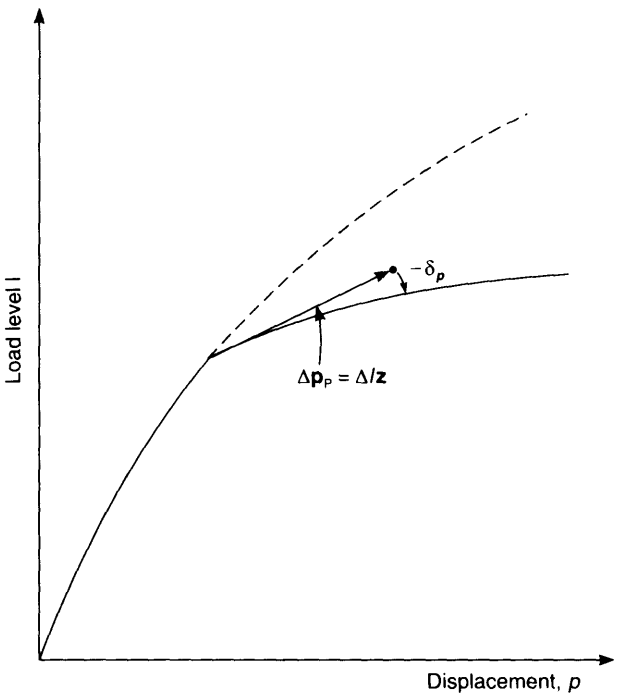

Figure 21.4 After branching, an iterative change $\delta\mathbf{p}$ that is orthogonal to the predictor $\Delta\mathbf{p}_p = \Delta l\mathbf{z}$.

21.2.2 Corrector using displacement control at a specified variable

In Section 9.3.2.3, we discussed Batoz's method [B2] (with enhancements by Rheinboldt [R1]) whereby the displacement increment at a specific variable was kept constant. Rheinboldt's modification was to choose the specific variable as the component with the maximum value in the predictor, $\Delta \mathbf{p}_p$, say, $\Delta \mathbf{p}_p(k)$. From (21.7) this corresponds to taking the displacement component (k) with the maximum value in $\mathbf{z}$. Also for future iterations $\Delta \mathbf{p}(k)$ must be kept fixed so that future iterative changes, $\delta \mathbf{p}$, must be such that the kth component is zero. From (21.8) it follows that:

$$\delta \lambda = \frac{-\delta \bar{p}(k)}{\delta p_t(k)} \tag{21.11}$$

21.2.3 Corrector using a 'cylindrical arc-length method'

In Section (9.4) we described a cylindrical arc-length method, which was a degenerate form (with $\Psi = 0$) of the 'spherical method' of Section 9.3.2.1. This method combined (21.8) with the constraint:

$$\Delta \mathbf{p}^T \Delta \mathbf{p} = \Delta l^2 \tag{21.12}$$

where Δl was a specified 'arc-length'. (Note the predictor solution of (21.7) satisfies this constraint.) When combined with the iterative change of (21.8), we can simply apply the standard arc-length method and find $\delta \lambda$ from the quadratic scalar equation (9.26).

21.3 BRANCH SWITCHING USING HIGHER-ORDER DERIVATIVES

From the work of Section 20.3, the stability coefficients $B_1 - B_4$ (see (20.41)–(20.44) and Section 20.5.4) can help by giving a better predictor than (21.7) only if we have an asymmetric bifurcation and from Section 20.4.4, $B_1 \neq 0$. In these circumstances we can solve the quadratic in (20.58) to find X_1 and X_2, with the former leading to a 'branching predictor',

$$\Delta \mathbf{p}_p = \Delta \lambda (X_1 \mathbf{z} + \mathbf{y}) = \Delta \lambda \delta \bar{\mathbf{p}}_t \tag{21.13}$$

where the final expression is taken from (9.38) and shows that, in contrast to the standard tangential direction:

$$\delta \mathbf{p}_t = \mathbf{K}_t^{-1} \mathbf{q} \tag{21.14}$$

where $\mathbf{q}$ is the load pattern, we now have an equivalent vector of $\delta \bar{\mathbf{p}}_t = X_1 \mathbf{z} + \mathbf{y}$ where the vector $\mathbf{y}$ is orthogonal to $\mathbf{z}$. In relation to (20.63) and (21.14), the predictor along the fundamental path, $\Delta \mathbf{p}_f$, would be $\Delta \lambda \delta \mathbf{p}_t$ and hence, from (20.63), the vector $\mathbf{y}$ can be obained from:

$$\mathbf{y} = \delta \mathbf{p}_t - (\delta \mathbf{p}_t^T \mathbf{z}) \mathbf{z} \tag{21.15}$$

Hence, we can completely define the vector $\delta \bar{\mathbf{p}}_t$ in (21.13). With a given arc-length Δl, $\Delta \lambda$

can be obtained from (9.39), but with $\delta\bar{\mathbf{p}}_t$ instead of $\delta\mathbf{p}_t$ so that:

$$\Delta\lambda = \pm \frac{\Delta l}{\sqrt{\delta\bar{\mathbf{p}}_t^T \delta\bar{\mathbf{p}}_t}} \tag{21.16}$$

The plus sign will lead to one branch and the minus sign to another asymmetric branch.

21.4 GENERAL PREDICTORS USING HIGHER-ORDER DERIVATIVES

In Section 21.6, we will return to bifurcations and will consider the use of higher-order derivatives to produce methods that directly iterate to the bifurcation point. However, we will firstly consider the use of higher-order derivatives for the computation of better (but, sadly, not cheaper) predictors for general predictor/corrector path-following techniques in the absence of bifurcation points (see also [W1]).

As a starting-point, we consider the Taylor expansion of the equilibrium conditions at some point where the control parameter has increased to Δs beyond the current equilibrium point. From (20.33) this leads to:

$$\{\mathbf{g}_p\dot{\mathbf{p}} + \mathbf{g}_\lambda\dot{\lambda}\}\Delta s + \tfrac{1}{2}\{\mathbf{g}_{pp}\dot{\mathbf{p}}\dot{\mathbf{p}} + 2\mathbf{g}_{p\lambda}\dot{\mathbf{p}}\dot{\lambda} + \mathbf{g}_{\lambda\lambda}\dot{\lambda}^2 + \mathbf{g}_p\ddot{\mathbf{p}} + \mathbf{g}_\lambda\ddot{\lambda}\}\Delta s^2 + \cdots = 0 \tag{21.17}$$

where the subscripts denote differentiation. In addition to (21.17), from (20.31) and (20.32), we have:

$$\Delta\mathbf{p} = \dot{\mathbf{p}}\,\Delta s + \frac{\ddot{\mathbf{p}}}{2}\Delta s^2 + \cdots \tag{21.18a}$$

$$\Delta\lambda = \dot{\lambda}\Delta s + \frac{\ddot{\lambda}}{2}\Delta s^2 + \cdots \tag{21.18b}$$

Setting the coefficient of Δs from (21.17) to zero leads to

$$\mathbf{g}_p\dot{\mathbf{p}} + \mathbf{g}_\lambda\dot{\lambda} = \mathbf{K}_t\dot{\mathbf{p}} - \dot{\lambda}\mathbf{q}_e = 0 \tag{21.19}$$

where the equilibrium equations are assumed to take the form:

$$\mathbf{g}(\mathbf{p}, \lambda) = \mathbf{q}_i(\mathbf{p}) - \lambda\mathbf{q}_e = 0 \tag{21.20}$$

where $\mathbf{q}_e$ is the fixed vector of the external loading pattern (referred to as $\mathbf{q}_{ef}$ in Chapter 9). In conjunction with (21.20), if we set the coefficient of Δs^2 to zero in (21.17), we obtain (assuming $\mathbf{q}_e$ is fixed so that $\mathbf{g}_{p\lambda} = \mathbf{g}_{\lambda\lambda} = 0$):

$$\mathbf{g}_{pp}\dot{\mathbf{p}}\dot{\mathbf{p}} + \mathbf{K}_t\ddot{\mathbf{p}} - \ddot{\lambda}\mathbf{q}_e = 0 \tag{21.21}$$

From (21.19), we can obtain:

$$\dot{\mathbf{p}} = \dot{\lambda}\mathbf{K}_t^{-1}\mathbf{q}_e = \dot{\lambda}\,\delta\mathbf{p}_t \tag{21.22}$$

where the 'tangential vector', $\delta\mathbf{p}_t$ is the same as in Chapter 9. Substituting from (21.22) into (21.21) leads to

$$\dot{\lambda}^2\mathbf{g}_{pp}\delta\mathbf{p}_t\delta\mathbf{p}_t + \mathbf{K}_t\ddot{\mathbf{p}} - \ddot{\lambda}\mathbf{q}_e = 0 \tag{21.23a}$$

Using the notation of Section 20.5.1 we can rewrite equation (21.23a) as

$$\dot{\lambda}^2 \mathbf{v}(\delta \mathbf{p}_t, \delta \mathbf{p}_t) + \mathbf{K}_t \ddot{\mathbf{p}} - \ddot{\lambda} \mathbf{q}_e = 0 \tag{21.23b}$$

where, we have shown in Sections 20.5.2 and 20.5.3 how to explicitly compute the vector $\mathbf{v}$ for a truss element and have also indicated how, for other elements, a finite difference form can be used [R1.20, E1.20, W2.20].

The solution of (21.23b) can be expressed as

$$\ddot{\mathbf{p}} = \ddot{\lambda} \mathbf{K}_t^{-1} \mathbf{q}_e - \dot{\lambda}^2 \mathbf{K}_t^{-1} \mathbf{v} = \ddot{\lambda} \delta \mathbf{p}_t - \dot{\lambda}^2 \mathbf{a} \tag{21.24a}$$

$$\mathbf{a} = \mathbf{K}_t^{-1} \mathbf{v} \tag{21.24b}$$

In order to proceed further, it is necessary to specify the control parameter, Δs.

21.4.1 Load control

In this case, we have:

$$\Delta s = \Delta \lambda; \qquad \dot{\lambda} = 1; \qquad \ddot{\lambda} = 0 \tag{21.25}$$

so that from (21.22) and (21.24a) we obtain:

$$\dot{\mathbf{p}} = \delta \mathbf{p}_t; \qquad \ddot{\mathbf{p}} = -\mathbf{a} \tag{21.26a}$$

and in (21.18a), we have:

$$\Delta \mathbf{p} = \Delta \lambda \delta \mathbf{p}_t - \frac{\Delta \lambda^2}{2} \mathbf{a} \tag{21.27}$$

Without the higher-order terms, the $\mathbf{a}$ vector would be zero and we would obtain the standard Euler predictor. With the higher-order terms, in order to compute (21.27), we must first obtain $\dot{\mathbf{p}} = \delta \mathbf{p}_t = \mathbf{K}_t^{-1} \mathbf{q}_e$ and then compute the vector $\mathbf{v}$ as a function of $\delta \mathbf{p}_t$ using the method discussed in Section 20.5 for truss elements (or using a finite difference approximation [E1.20, W2.20, R1.20] and then compute $\mathbf{a} = \mathbf{K}_t^{-1} \mathbf{v}$ (see (21.24b) using the previously factorised $\mathbf{K}_t$.

One can of course continue to use even higher derivatives so that the process is a form of 'perturbation technique' [A1, B1]. If we only consider second-order derivatives (of $\mathbf{g}$) as here, the extra work, in comparison with the first-order Euler predictor is of the same order as a modified Newton–Raphson iteration.

21.4.2 Displacement control at a specified variable

In this case, we have:

$$\Delta s = |\Delta p_k| = |\Delta \mathbf{p}(k)| = t \Delta \mathbf{p}(k) \tag{21.28a}$$

where Δs is a given positive scalar and the term k relates to the largest absolute value in $\delta \mathbf{p}_t$ (see Section 9.3.2.3). We are adopting the convention whereby, having added the term (k), the expression is a scalar (involving the kth term in the vector) despite the bold

character for the vector (here **p**). The scalar t in (21.28a) is given by

$$t = \pm 1 = \frac{\delta \mathbf{p}_t(k)}{|\delta \mathbf{p}_t(k)|} \tag{21.28b}$$

It follows from (21.28a) and (21.28b) that:

$$\dot{\mathbf{p}}(k) = \mathrm{t}; \qquad \ddot{\mathbf{p}}(k) = 0 \tag{21.28c}$$

From the first expression in (21.28c) in conjunction with (21.22), we can directly compute:

$$\dot{\lambda} = t/\delta \mathbf{p}_t(k) \tag{21.29}$$

Hence, with $\dot{\lambda}$ known, from the last expression in (21.28c) in conjunction with the (21.24a), we obtain:

$$\dddot{\lambda} = \frac{\dot{\lambda}^2 \mathbf{a}(k)}{\delta \mathbf{p}_t(k)} = \frac{\mathbf{a}(k)}{\{\delta \mathbf{p}_t(k)\}^3} \tag{21.30}$$

so that we can obtain $\Delta \mathbf{p}$ and $\Delta\lambda$ in terms of the prescribed $\Delta s = t\,\Delta \mathbf{p}(k)$ from (21.18). The final expressions take the form:

$$\Delta\lambda = \Delta\lambda_{\mathrm{E}} + \tfrac{1}{2} c \Delta\lambda_{\mathrm{E}}^2 \tag{21.31a}$$

$$\Delta \mathbf{p} = (1 + \tfrac{1}{2} c \Delta\lambda_{\mathrm{E}}) \Delta \mathbf{p}_{\mathrm{E}} - \tfrac{1}{2} \Delta\lambda_{\mathrm{E}}^2 \mathbf{a} \tag{21.31b}$$

$$\Delta \mathbf{p}_{\mathrm{E}} = \Delta\lambda_{\mathrm{E}} \delta \mathbf{p}_t \tag{21.31c}$$

where $\Delta\lambda_{\mathrm{E}}$ and $\Delta \mathbf{p}_{\mathrm{E}}$ are the Euler predictor's as given in Chapter 9 so that:

$$\Delta\lambda_{\mathrm{E}} = \pm \frac{t \Delta s}{\delta \mathbf{p}_t(k)} = \pm \frac{\Delta s}{|\delta \mathbf{p}_t(k)|} \tag{21.32}$$

The constant c in (21.31) is given by

$$c = \mathbf{a}(k)/\delta \mathbf{p}_t(k) \tag{21.33}$$

The plus or minus sign in (21.32) follows from the procedure described for the arc-length method in Section 9.4.3 and is related to either the minimum pivot of $\mathbf{K}_t$ or the current stiffness parameter. The algorithm for load control in Section 21.4.1 is also given by (21.31) but with $\Delta\lambda_{\mathrm{E}} = \Delta\lambda$ and $c = 0$.

21.4.3 The 'cylindrical arc-length method'

In this case, we have:

$$\Delta s^2 = \Delta \mathbf{p}^{\mathrm{T}} \Delta \mathbf{p} \tag{21.34}$$

so that substitution from (21.18a) leads to

$$\Delta s^2 = \{\dot{\mathbf{p}}^{\mathrm{T}} \dot{\mathbf{p}}\} \Delta s^2 + \{\dot{\mathbf{p}}^{\mathrm{T}} \ddot{\mathbf{p}}\} \Delta s^3 + \{\tfrac{1}{4} \ddot{\mathbf{p}}^{\mathrm{T}} \ddot{\mathbf{p}} + \tfrac{1}{3} \dddot{\mathbf{p}} \dot{\mathbf{p}}\} \Delta s^4 + \cdots \tag{21.35}$$

Equating the coefficients of Δs^2 and using (21.22) leads to

$$\dot{\lambda} = \pm \frac{1}{(\delta \mathbf{p}_t^{\mathrm{T}} \delta \mathbf{p}_t)^{1/2}} \tag{21.36}$$

and setting the coefficient of Δs^3 in (21.35) to zero leads, in conjunction with (21.24a), to:

$$\ddot{\lambda} = \frac{1}{\delta \mathbf{p}_t^T \delta \mathbf{p}_t} \dot{\lambda}^2 \mathbf{a}^T \delta \mathbf{p}_t = \frac{1}{(\delta \mathbf{p}_t^T \delta \mathbf{p}_t)^2} \mathbf{a}^T \delta \mathbf{p}_t \tag{21.37}$$

Hence, in conjunction with (21.18), $\Delta \mathbf{p}$ and $\Delta\lambda$ are completely defined for a given Δs. The solution is given by (21.31) in conjunction with:

$$\Delta\lambda_E = \pm \frac{1}{\sqrt{\delta \mathbf{p}_t^T \delta \mathbf{p}_t}} \tag{21.38}$$

$$c = \left(\frac{\mathbf{a}^T \delta \mathbf{p}_t}{\delta \mathbf{p}_t^T \delta \mathbf{p}_t} \right) \tag{21.39}$$

where the sign in (21.38) follows the procedures discussed in Section 9.4.3.

Because the Δs^4 terms in (21.35) have not been equated to zero, equation (21.31b) (in conjunction with (21.38) and (21.39)) will not exactly satisfy the constraint of (21.34). Two strategies are open. First, one may simply accept the solution and allow the subsequent 'corrector iterations' to automatically return to the required length. Alternatively, the length given following the higher-order predictor can be computed and this new length, which will be slightly different from the original intended length, can be employed for the corrector iterations.

21.5 CORRECTORS USING HIGHER-ORDER DERIVATIVES

In Section 1.3, the conventional Newton–Raphson method for load control was computed by expanding the residual $\mathbf{g}$ as a truncated Taylor series about some old (subscript o) configuration. A similar approach including second-order derivatives (of $\mathbf{g}$) leads to

$$\mathbf{g}_n = \mathbf{g}_o + \frac{\partial \mathbf{g}}{\partial \mathbf{p}} \delta \mathbf{p} + \frac{1}{2} \mathbf{g}_{pp} \delta \mathbf{p} \delta \mathbf{p} \tag{21.40}$$

where we can now set the 'new estimate', $\mathbf{g}_n$ to zero. If we set up a new residual vector, $\mathbf{f}$, which should be made zero, this leads to

$$\mathbf{f} = \mathbf{g}_o(\mathbf{p}_o) + \mathbf{K}_t(\mathbf{p}_o)\Delta \mathbf{p} + \tfrac{1}{2} \nabla_p (\mathbf{K}_t \Delta \mathbf{p}) = \mathbf{g}_o + \mathbf{K}_t \Delta \mathbf{p} + \tfrac{1}{2} \mathbf{v}(\Delta \mathbf{p}, \Delta \mathbf{p}) = 0 \tag{21.41}$$

where we are introducing the notation of Section 20.5.1 and have introduced Δ's instead of δ's because we will make iterative changes ($\delta \mathbf{p}$) to $\Delta \mathbf{p}$ with a view to the satisfaction of (21.41) as part of an inner loop. Equations (21.41) are to be solved for $\Delta \mathbf{p}$, with $\mathbf{p}_o$ kept fixed. A predictor to solve (21.41) would involve:

$$\Delta \mathbf{p} = -\mathbf{K}_t(\mathbf{p}_o)^{-1} \mathbf{g}_o(\mathbf{p}) \tag{21.42}$$

which is the standard first-order corrector from (21.40). We could now apply a corrector to (21.41) to give:

$$\delta \mathbf{p} = -\{\mathbf{K}_t(\mathbf{p}_o) + \mathbf{V}(\Delta \mathbf{p}_o)\}^{-1} \mathbf{f}_o(\mathbf{p}_o, \Delta \mathbf{p}_o) = -\bar{\mathbf{K}}_t^{-1} \mathbf{f}_o(\mathbf{p}_o, \Delta \mathbf{p}_o) \tag{21.43a}$$

with $\Delta \mathbf{p}_o$ as the predictor from (21.42). Having obtained $\delta \mathbf{p}$ from (21.43), the displacement change would be updated to give $\Delta \mathbf{p}_1 = \Delta \mathbf{p}_o + \delta \mathbf{p}$ and a second iteration would

produce a further change:

$$\delta\mathbf{p} = -\{\mathbf{K}_t(\mathbf{p}_0) + \mathbf{V}(\Delta\mathbf{p}_1)\}^{-1}\mathbf{f}_1(\mathbf{p}_0, \Delta\mathbf{p}_1) = -\bar{\mathbf{K}}_t^{-1}\mathbf{f}_1(\mathbf{p}_0, \Delta\mathbf{p}_1) \tag{21.43b}$$

until eventually $\mathbf{f}$ from (21.41) would be sufficiently near to zero. The algorithm involving (21.43) will be referred to as implicit.

To avoid the formation and factorisation of the new $\bar{\mathbf{K}}_t$, we could apply a modified Newton–Raphson iteration for the 'inner loop' and replace $\bar{\mathbf{K}}_t^{-1}$ in (21.43) with $\mathbf{K}_t(\mathbf{p}_0)^{-1}$ which would already be formed and factorised. This will be referred to as an explicit algorithm. There could be advantages in using the full implicit form near singular points when $\mathbf{K}_t$ may be nearly singular.

The techniques can easily be extended to encompass arc-length-like techniques by including terms that involve the change in load level so that (21.41) would be replaced by

$$\mathbf{f} = \mathbf{g}_0 + \mathbf{K}_t\Delta\mathbf{p} + \tfrac{1}{2}\mathbf{v}(\Delta\mathbf{p}, \Delta\mathbf{p}) - \Delta\lambda\mathbf{q}_e \tag{21.44}$$

with the predictor solution being given by

$$\Delta\mathbf{p} = -\mathbf{K}_t(\mathbf{p}_0)^{-1}\mathbf{g}_0(\mathbf{p}) + \Delta\lambda\mathbf{K}_t(\mathbf{p}_0)^{-1}\mathbf{q}_e = -\Delta\bar{\mathbf{p}} + \Delta\lambda\Delta\mathbf{p}_t \tag{21.45}$$

and $\Delta\lambda$ being chosen using standard arc-length techniques to satisfy the constraint. At this stage, $\Delta\mathbf{p}$ and $\Delta\lambda$ are the variables and, in place of (21.43a), we obtain:

$$\delta\mathbf{p} = -\{\mathbf{K}_t(\mathbf{p}_0) + \mathbf{V}(\Delta\mathbf{p}_0)\}^{-1}(\mathbf{f}_0 - \delta\lambda\mathbf{q}_e) = -\bar{\mathbf{K}}_t^{-1}\mathbf{f}_0(\mathbf{p}_0, \Delta\mathbf{p}_0) + \delta\lambda\bar{\mathbf{K}}_t^{-1}\mathbf{q}_e \tag{21.46}$$

which is split into two vectors with $\delta\lambda$ being found from the arc-length constraint in the standard way.

21.6 DIRECT COMPUTATION OF THE SINGULAR POINTS

In Section 21.1, we discussed indirect or bracketing methods for obtaining singular points on the equilibrium path. An alternative method using a form of 'secant formulation' has been proposed by Onate *et al.* [O1]. We will now consider a method [W1.20, W2.20] based on the solution of the 'extended system' composed first of the standard equilibrium equations:

$$\mathbf{g}(\mathbf{p}, \lambda) = \mathbf{0} \tag{21.47a}$$

and secondly of a set of equations:

$$\mathbf{K}_t\mathbf{z} = \mathbf{0} \tag{21.47b}$$

with $\mathbf{z}$ as the eigenmode corresponding to the lowest eigenvector of $\mathbf{K}_t$. This equation is only satisfied at singular points because at such points the eigenvalue is zero. The final equation puts some constraint on the size of the vector $\mathbf{z}$ and here we apply:

$$z_k = \mathbf{z}(k) = 1 \tag{21.47c}$$

where k is a particular component of $\mathbf{z}$. We could, instead have ensured that $\mathbf{z}$ was scaled to be of unit length. However, this would lead to a quadratic constraint and (21.47c) leads to an easier solution.

Because Newton's method has a finite bowl of convergence, it is probably best to start with a standard continuation method and to only introduce the direct computation once the first singular point has been passed and possibly after a few applications of the indirect bracketing approach of Section 21.1. In these circumstances, k can be chosen as the variable with the smallest pivot once the singular point has been passed. In order to start the process, an initial estimate is required for $\mathbf{z}$ at the singular point. For this purpose, one may compute the eigenmode, $\mathbf{z}$, corresponding to the lowest eigenvalue at the starting-point for the direct solution. Alternatively, one may use Seydel's approximation [S3]. This is obtained by prescribing the variable with the smallest pivot (here variable k) to unity and obtaining the predictor solution by firstly computing the equivalent load vector $\mathbf{q}'$ (see Section 2.2.5) and then obtaining $\mathbf{K}_t^{-1}\mathbf{q}'$ with the kth variable being treated (for this solution only) as prescribed.

Newton's solution procedure can be applied directly to (21.47a)–(21.47c) with the variables being $\mathbf{p}$, $\mathbf{z}$ and λ. However, as with the arc-length methods it is best to work in an indirect manner and apply Newton's method to (21.47a) to obtain the iterative change:

$$\delta\mathbf{p} = -\mathbf{K}_t^{-1}\mathbf{g} + \delta\lambda\mathbf{K}_t^{-1}\mathbf{q}_c = \delta\bar{\mathbf{p}} + \delta\lambda\delta\mathbf{p}_t \tag{21.48}$$

while the application of a truncated Taylor series to (21.47b) leads to

$$\{\mathbf{K}_t\mathbf{z}\}_n = \{\mathbf{K}_t\mathbf{z}\}_o + \mathbf{K}_t\delta\mathbf{z} + \nabla_p(\mathbf{K}_t\mathbf{z}) \tag{21.49}$$

with the subscript, n, meaning 'new' and the subscript, o, meaning 'old'. To compute the last term in (21.49), one can adopt the procedures of Section 20.5 to obtain:

$$\mathbf{v}(\delta\mathbf{p}, \mathbf{z}) = \nabla_p(\mathbf{K}_t\mathbf{z}) = \mathbf{v}_1(\delta\bar{\mathbf{p}}, \mathbf{z}) + \delta\lambda\mathbf{v}_2(\delta\mathbf{p}_t, \mathbf{z}) \tag{21.50}$$

where use has been made of (21.48). Setting the left-hand side of (21.49) to zero and using (21.50a) leads to:

$$\delta\mathbf{z} = -\mathbf{K}_t^{-1}(\mathbf{K}_t\mathbf{z} + \mathbf{v}_1 + \delta\lambda\mathbf{v}_2) = -\mathbf{z} + \mathbf{w}_1 + \delta\lambda\mathbf{w}_2 \tag{21.50b}$$

At this stage, the kth component of $\mathbf{z}$ can be updated to give:

$$\mathbf{z}_n(k) = \mathbf{z}_o(k) - \mathbf{z}_o(k) + \mathbf{w}_1(k) + \delta\lambda\mathbf{w}_2(k) = \mathbf{w}_1(k) + \delta\lambda\mathbf{w}_2(k) = 1 \tag{21.51}$$

where use has been made of (21.47c). The unknown $\delta\lambda$ is very simply obtained from (21.51) after which both $\delta\mathbf{p}$ (from (21.48)) and $\delta\mathbf{z}$ (from (21.50b)) are fully defined.

Wriggers and Simo [W2.20] have indicated that there may be numerical problems with the previous technique because of increasing ill-conditioning as $\mathbf{K}_t$ approaches singularity as the singular point is approached. They therefore propose the introduction of a penalty function (the concept being originally proposed in a different context by Felippa [F1]) whereby (21.47) is modified to give:

$$\mathbf{g}(\mathbf{p}, \lambda) + \gamma\mathbf{e}_k(\mathbf{e}_k^T\mathbf{p} - \mu) = \mathbf{0} \tag{21.52a}$$

$$\mathbf{K}_t\mathbf{z} + \gamma\mathbf{e}_k(\mathbf{e}_k^T\mathbf{z} - 1) = 0 \tag{21.52b}$$

$$z_k = \mathbf{z}(k) = \mathbf{e}_k^T\mathbf{z} = 1 \tag{21.52c}$$

$$\mathbf{e}_k^T\mathbf{p} - \mu = 0 \tag{21.52d}$$

where γ is a penalty parameter and the vector $\mathbf{e}_k$ is zero for all terms apart from the term k where it is unity. Applying a very similar procedure to that given previously starting

from (21.47), one may arrive at a 2×2 set of simultaneous equations for the two scalar variable changes $\delta\lambda$ and $\delta\mu$ [W2.20].

21.7 LINE-SEARCHES WITH ARC-LENGTH AND SIMILAR METHODS

In Section 9.2 of Volume 1, we described a simple bracketed line-search procedure which can be applied in a conjunction with iterative techniques such as the full or modified Newton–Raphson methods (or the quasi-Newton methods of Section 9.7). We also gave a set of references of which relatively few were specifically related to the finite element method (but see [L1]). Although the theoretical basis for these methods involve the minimisation of the total potential energy, they are particularly effective for problems involving plasticity in which there is no energy function. Indeed, line searches are especially rewarding for problems with sudden non-linearity such as those involving concrete cracking or contact (see Chapter 23).

In Sections 9.3 and 9.4, a range of arc length and similar techniques were considered with particular emphasis being given in Section 9.4 to the 'spherical' arc-length method and indeed to a sub set, the 'cylindrical method'. All these methods involve a form of indirect displacement control and we will in future refer to them as 'arc-length methods'. Such arc-length methods have been combined with line-search procedures in [C1, C2, S2, S5].

In introducing such a combination, two special difficulties are encountered. The first of these arises because the line searches are now aimed at finding the minimum energy configuration at a load level that is continuously varying as the iterations proceed. The second difficulty arises because these 'arc-length methods are often used to iterate to equilibrium points that do not coincide with minimum energy configurations because they are beyond limit points. For the present we will ignore this second problem (but later see Section 21.7.3) and will assume that we are analysing problems with a continuously rising stable equilibrium path.

21.7.1 Line-searches with the Riks/Wempner linear arc-length method

From Section 9.3.2.2 of Chapter 9, the adopted constraint is

$$\Delta\mathbf{p}_p^T\delta\mathbf{p} = \Delta\mathbf{p}_p^T(\delta\bar{\mathbf{p}} + \delta\lambda\delta\mathbf{p}_t) = 0 \tag{21.53}$$

where $\Delta\mathbf{p}_p$ is the 'predictor' incremental displacement. To introduce a line-search step-length, η, we have:

$$\mathbf{p} = \mathbf{p}_o + (\Delta\mathbf{p}_o + \eta\delta\mathbf{p}) \tag{21.54}$$

where $\mathbf{p}_o$ are the 'old' displacements at the end of the last increment, $\Delta\mathbf{p}_o$ are the 'old' incremental displacements, prior to the current iteration. It follows that, in place of (21.53), we now have:

$$\eta\delta\mathbf{p}^T\Delta\mathbf{p}_p = 0 = \eta(\delta\bar{\mathbf{p}} + \delta\lambda\delta\mathbf{p}_t)^T\Delta\mathbf{p}_p \tag{21.55}$$

which leads to precisely the same expression as (21.53) for $\delta\lambda$. Hence, the line-search and arc-length constraints are largely uncoupled so that at the end of the iteration, with an exact line search, we would aim to satisfy (see Section 9.2):

$$s(\eta) = \frac{\partial \phi}{\partial \eta} = \delta \mathbf{p}^{\mathrm{T}} \mathbf{g}(\eta, \lambda_{\mathrm{o}} + \delta\lambda) = 0 \tag{21.56}$$

where λ_{o} is the 'old' load level at the beginning of the iteration (and prior to the computation of $\delta\lambda$ from (21.53)).

In practice, a 'slack-line search' is applied so that one aims to satisfy (see Section 9.2):

$$r = |\frac{s(\eta)|}{|s(\eta = 0)|} = \frac{|s(\eta)|}{|s_{\mathrm{o}}|} \leqslant \varphi \tag{21.57}$$

With load-control, s_{o} is the energy slope at the beginning of the iteration with $\eta = 0$, so that:

$$s_{\mathrm{o}} = s(\eta = 0) = \frac{\partial \phi}{\partial \eta} = \delta \mathbf{p}^{\mathrm{T}} \mathbf{g}_{\mathrm{o}} = \delta \mathbf{p}^{\mathrm{T}} \mathbf{g}(\eta = 0) \tag{21.58}$$

Although the application of the line-search procedure or the Riks–Wempner arc-length method is relatively straightforward, we will outline the steps, partly as an introduction to the more complicated procedure required for the cylindrical arc-length method. Also, there is an important step (step 4 in Algorithm 21.1 below) that is not immediately obvious.

1. At the beginning of the iteration, compute:

$$\delta \bar{\mathbf{p}} = -\mathbf{K}_{\mathrm{t}}^{-1} \mathbf{g}_{\mathrm{o}}(\eta = 0, \lambda = \lambda_{\mathrm{o}})$$
$$\delta \mathbf{p}_{\mathrm{t}} = \mathbf{K}_{\mathrm{t}}^{-1} \mathbf{q}_{\mathrm{c}}$$

2. Apply the arc-length constraint to obtain:

$$\delta\lambda = -\Delta \mathbf{p}_{\mathrm{p}}^{\mathrm{T}} \delta \bar{\mathbf{p}} / \Delta \mathbf{p}_{\mathrm{p}}^{\mathrm{T}} \delta \mathbf{p}_{\mathrm{t}}$$
$$\delta \mathbf{p} = \delta \bar{\mathbf{p}} + \delta\lambda \delta \mathbf{p}_{\mathrm{t}}$$

3. Update with $\eta = 1$:

$$\eta = 1$$
$$\Delta \mathbf{p} = \Delta \mathbf{p}_{\mathrm{o}} + \eta \delta \mathbf{p}$$
$$\mathbf{p} = \mathbf{p}_{\mathrm{o}} + (\Delta \mathbf{p}_{\mathrm{o}} + \eta \delta \mathbf{p})$$
$$\lambda = \lambda_{\mathrm{o}} + \delta\lambda$$

4. Compute the inner product s_{o} so as to relate to the current load level.

$$s_{\mathrm{o}}(\eta = 0, \lambda_{\mathrm{o}} + \delta\lambda) = \delta \mathbf{p}^{\mathrm{T}}(\mathbf{g}_{\mathrm{o}}(\eta = 0, \lambda_{\mathrm{o}}) - \delta\lambda \mathbf{q}_{\mathrm{c}}) = \delta \mathbf{p}^{\mathrm{T}} \mathbf{g} - \delta\lambda \delta \mathbf{p}^{\mathrm{T}} \mathbf{q}_{\mathrm{c}}$$

5. Compute the residual with $\eta = 1$ (at $\lambda = \lambda_{\mathrm{o}} + \delta\lambda$); compute $\mathbf{g}_1(\eta_1 = 1, \lambda_{\mathrm{o}} + \delta\lambda)$.

6. Compute the current inner product,

$$s_1(\eta_1 = 1, \lambda = \lambda_{\mathrm{o}} + \delta\lambda) = \delta \mathbf{p}^{\mathrm{T}} \mathbf{g}_1(\eta_1 = 1, \lambda_{\mathrm{o}} + \delta\lambda)$$

7. If s_{o} is not sufficiently negative (downhill), abandon line search and accept the solution with $\eta = 1$ before moving to the next iteration.

8. If $r = |s_1/s_0| \leqslant \varphi$, accept the current solution with $\eta = 1$ before moving to the next iteration.
9. If the previous tolerance check is not satisfied, apply a bracketed line search (i.e. via subroutine SEARCH of Section 9.2.2.1) to obtain a new estimate η_2. The search requires the information:

$$(s_0, s_1) \text{ at } (\eta_0 = 0, \eta_1 = 1) \text{ all at load level } \lambda_0 + \delta\lambda$$

10. Recompute the current displacements via:

$$\mathbf{p} = \mathbf{p}_0 + (\Delta\mathbf{p}_0 + \eta_2\delta\mathbf{p})$$

11. Compute the residual with $\eta = \eta_2$ at $\lambda = \lambda_0 + \delta\lambda$), i.e. compute $\mathbf{g}_2(\eta_2, \lambda_0 + \delta\lambda)$
12. Compute the current inner product:

$$s_2(\eta_2, \lambda = \lambda_0 + \delta\lambda) = \delta\mathbf{p}^{\mathrm{T}}\mathbf{g}_2(\eta_2, \lambda_0 + \delta\lambda)$$

13. If $r = |s_2/s_0| \leqslant \varphi$, accept the current solution with η_2 before moving to the next iteration.
14. If the previous tolerance check is not satisfied, apply a bracketed line search (i.e. via subroutine SEARCH of Section 9.2.2.1) to obtain a new estimate η_3. The search require the information:

$$(s_0, s_1, s_2) \text{ at } (\eta_0 = 0, \eta_1 = 1, \eta_2) \text{ all at load level } \lambda_0 + \delta\lambda$$

Algorithm 21.1 Line-searches with the Riks–Wempner arc-length method.

It is a simple matter to modify Algorithm 21.1 to relate to any of the linearised arc-length methods (see Section 9.3.2.2) or to the method for generalised displacement control at a specific variable (see Section 9.3.2.3).

21.7.2 Line-searches with the cylindrical arc-length method

The cylindrical arc-length method can be considered as a special case of the spherical method (Section 9.4). Here we will only consider the cylindrical method, in which there are no load parameter terms in the constraint (see Section 9.4).

With the introduction of the line-search scalar, η, the cylindrical constraint becomes:

$$(\Delta\mathbf{p}_0 + \eta(\delta\bar{\mathbf{p}} + \delta\lambda\delta\mathbf{p}_1))^{\mathrm{T}}(\Delta\mathbf{p}_0 + \eta(\delta\bar{\mathbf{p}} + \delta\lambda\delta\mathbf{p}_1)) - \Delta l^2 = 0 \qquad (21.59)$$

where $\Delta\mathbf{p}_0$ contains the incremental displacements prior to the current iteration. In contrast to the linear constraint of (21.55), (21.59) involves a full coupling between $\delta\lambda$ and η. In other words, if (21.59) is initially solved with $\eta = 1$ to obtain $\delta\lambda$, the application of a line search to obtain a non-unit η, will lead to a violation of (21.59). Because the load level is continuously changing as the line search progresses, it will be useful to store the load level at each trial step length, η_j so that we have:

j	0	1	2
η_j	0	1.0	$\eta_2 \cdots$
λ_j	λ_0	λ_1	$\lambda_2 \cdots$

where j is the line-search number.

For the cylindrical arc-length method, the iterative direction, $\delta\mathbf{p}$, is itself changing as the line search proceeds because, from (21.48), we can write:

$$\delta\mathbf{p} = \delta\bar{\mathbf{p}} + (\lambda - \lambda_o)\delta\mathbf{p}_t \tag{21.60}$$

where λ_o is the load level at the end of the last iteration. Hence, we can express (21.56) as

$$s_j(\lambda, \eta_j) = (\delta\bar{\mathbf{p}} + (\lambda - \lambda_0)\delta\mathbf{p}_t)^T(\mathbf{g}_j(\lambda_j, \eta_j) - (\lambda - \lambda_j)\mathbf{q}_e) \tag{21.61}$$

Equation (21.61) is only strictly valid for $\lambda = \lambda_j$, where λ_j is the precise load level at which the residual $\mathbf{g}_j$ is computed. None the less, the approximation allows us to estimate the line-search inner product at other load levels. It will be convenient to re-express (21.61) as

$$s_j(\lambda, \eta_j) = e_{1,j} + (\lambda - \lambda_o)e_{2,j} + (\lambda - \lambda_j)d_5 + (\lambda - \lambda_o)(\lambda - \lambda_j)c_2 \tag{21.62}$$

where

$$\begin{aligned} e_{1,j} &= \delta\bar{\mathbf{p}}^T\mathbf{g}_j(\lambda_j, \eta_j) \\ e_{2,j} &= \delta\mathbf{p}_t^T\mathbf{g}_j(\lambda_j, \eta_j) \\ d_5 &= -\delta\bar{\mathbf{p}}^T\mathbf{q}_e \\ c_2 &= -\delta\mathbf{p}_t^T\mathbf{q}_e \end{aligned} \tag{21.63}$$

(Some of the notation follows from refs [C1, C2], but there are differences.)

In a similar fashion, we can express the inner product at the beginning of the iteration as

$$s_o(\lambda, \eta = 0) = d_6 + (\lambda - \lambda_o)(d_5 + d_7) + (\lambda - \lambda_o)^2 c_2 \tag{21.64}$$

where d_5 and c_2 have already been defined and

$$\begin{aligned} d_6 &= \delta\bar{\mathbf{p}}^T\mathbf{g}_o(\lambda_o, \eta = 0) \\ d_7 &= \delta\mathbf{p}_t^T\mathbf{g}_o(\lambda_o, \eta = 0) \end{aligned} \tag{21.65}$$

The inner products c_2, d_5, d_6 and d_7 can be computed at the beginning of each iteration, while the inner products $e_{1,j}$ and $e_{2,j}$ can be computed once the out-of-balance force vector, $\mathbf{g}$ at the trial step length is known. Equations (21.62) and (21.64) then allow the inner-product ratios of (21.57), which are required for to estimate a new step length, to be adjusted so as to relate to any modified load level.

The arc-length constraint of (21.59) can be rewritten with $\delta\lambda = (\lambda - \lambda_o)$ where λ_o is the load level prior to the application of the current iteration so that we have:

$$a_1(\lambda - \lambda_o)^2 + a_2(\lambda - \lambda_o) + a_3 = 0 \tag{21.66}$$

where

$$a_1 = \eta^2\delta\mathbf{p}_t^T\delta\mathbf{p}_t = \eta^2 c_1 \tag{21.67a}$$

$$a_2 = 2\delta\mathbf{p}_t^T\Delta\mathbf{p}_o + 2\eta\delta\mathbf{p}_t^T\delta\bar{\mathbf{p}} = 2\eta d_1 + 2\eta^2 d_2 \tag{21.67b}$$

$$\begin{aligned} a_3 &= \eta^2\delta\bar{\mathbf{p}}^T\delta\bar{\mathbf{p}} + 2\eta\delta\bar{\mathbf{p}}^T\Delta\mathbf{p}_o + [\Delta\mathbf{p}_o^T\Delta\mathbf{p}_o - \Delta l^2] \\ &= \eta^2 d_3 + 2\eta d_4 + [d_8 - \Delta l^2] \end{aligned} \tag{21.67c}$$

where the square-bracketed terms will be zero if the arc-length constraint was exactly satisfied at the previous iteration. In choosing the appropriate root from (21.66), we use the 'angles' (see 9.36):

$$\Delta l^2 \cos\theta_i = \Delta\mathbf{p}^T\Delta\mathbf{p}_o = d_8 + \eta(d_4 + (\lambda_i - \lambda_o)d_5) \tag{21.68}$$

where d_1, d_4, and d_8 have been defined in (21.67) and $\lambda_i - \lambda_o$ give the two possible solutions to (21.66), with $i = 1$ and 2.

The adopted solution procedure for each iteration now involves the following steps:

1. Compute $\delta\bar{\mathbf{p}} = -\mathbf{K}_t^{-1}\mathbf{g}_o(\lambda_o, \eta = 0)$ and $\delta\mathbf{p}_t = \mathbf{K}_t^{-1}\mathbf{g}_e$.
2. Compute the inner products $d_1 - d_8$ and c_1 and c_2.
3. Set $\eta_1 = 1$ and compute $(\lambda_1 - \lambda_o)$ to satisfy (21.66); set $\lambda_1 = \lambda_o + \lambda_1 - \lambda_o$ and store.
4. Set $\mathbf{p} = \mathbf{p}_o + \eta_1(\delta\bar{\mathbf{p}}_1 + (\lambda_1 - \lambda_o)\delta\mathbf{p}_t)$ and compute $\mathbf{g}_1(\eta_1, \lambda_1)$.
5. Compute $e_{1,1}$ and $e_{2,1}$ (see (21.63)).
8. Compute $s_1(\lambda_1, \eta_1)$ via (21.62) and $s_o(\lambda_1)$ via (21.64). Abandon the line searches and accept the solution with $\eta_1 = 1$ if s_o is not sufficiently negative (downhill).
9. Check $|s_1/s_o|$ against line-search tolerance, if the check is satisfied accept the solution with $\eta_1 = 1$ and proceed to the next iteration.
   The aim of this section (10) is to find λ_2, η_2.
10. Call SEARCH to apply a bracketed line search to estimate η_2. This search requires the information:

$$(s_o, s_1) \text{ at } (\eta = 0, \eta_1 = 1) \text{ all at load level } \lambda_1$$

10a. Solve (21.66) to obtain $(\lambda_2 - \lambda_o)$ and hence obtain λ_2.
10b. Compute $s_1(\lambda_2, \eta_1)$ via (21.62) and $s_o(\lambda_2)$ via (21.64).
10c. Recall SEARCH to apply a bracketed line search to estimate η_2. This search requires the information:

$$(s_o, s_1) \text{ at } (\eta = 0, \eta_1 = 1) \text{ all at load level } \lambda_2$$

10d. If current η_2 is close enough to the η_2 computed in (10) (or more generally to the last compute η_2) accept η_2 in (10) and λ_2 from 10a (or more generally the last comuted λ_2) which will exactly satisfy arc-length constraint. If not:
10e. Resolve (21.66) to obtain $(\lambda_2 - \lambda_o)$ and hence recompute λ_2, etc.
11. Assume we now have λ_2, η_2 then:
12. Set $\mathbf{p} = \mathbf{p}_o + \eta_2(\delta\bar{\mathbf{p}}_1 + (\lambda_2 - \lambda_o)\delta\mathbf{p}_t)$ and compute $\mathbf{g}_2(\eta_2, \lambda_2)$
13. Comute $e_{1,2}$ and $e_{2,2}$ (see (21.63)).
14. Compute $s_2(\lambda_2, \eta_2)$ and $s_1(\lambda_2, \eta_1)$ via (21.62) and $s_o(\lambda_2)$ via (21.64)
15. If s_o is not sufficiently negative, abandon the line search and accept the solution with $\eta_1 = 1$ and λ_1.
16. Check $|s_2/s_o|$ against the line-search tolerance, if satisfactory, terminate the line search and accept the solution with η_2 and λ_2. The aim of the next section (17) is to find λ_3, η_3.
17. Call SEARCH to apply a bracketed line-search to estimate η_3. This search requires the information:

$$(s_o, s_1, s_2) \text{ at } (\eta = 0, \eta_1 = 1, \eta_2) \text{ all at load level } \lambda_2$$

17a. Solve (21.66) to obtain $(\lambda_3 - \lambda_o)$ and hence compute λ_3.
17b. Compute $s_1(\lambda_3, \eta_1)$ and $s_2(\lambda_3, \eta_2)$ via (21.62) and $s_o(\lambda_3)$ via (21.64).
17c. Recall SEARCH to apply a bracketed line search to estimate η_3. This search requires the information:

$$(s_o, s_1, s_2) \text{ at } (\eta = 0, \eta_1 = 1, \eta_2) \text{ all at load level } \lambda_3$$

17d. If current η_3 is close enough to η_3 in (17) accept η_3 in (17) and λ_3 from 17a which will exactly satisfy arc-length constraint. If not:

17e. Resolve (21.66) to obtain $(\lambda_3 - \lambda_o)$ and hence recompute λ_3, etc.

Algorithm 21.2 Line searches with cylindrical arc-length method.

This algorithm is a lot more complicated than that for the linearised arc-length methods. However, the required computer time is very similar because the extra complexity largely involves scalar computations with previously computed inner products.

21.7.3 Uphill or downhill?

Conventionally, line-search procedures are aimed at problems with a stable equilibrium state, a positive definite $\mathbf{K}_t$, and hence a minimum energy configuration. However, as previously discussed, the arc-length methods are often used to converge on unstable equilibrium points. Such states will often be associated with a $\mathbf{K}_t$ with only one negative eigenvalue. This implies that, even for unstable equilibrium states, the iterative directions, $\delta\mathbf{p}$, will often be 'downhill' so that the previous line-search algorithms can still be applied [C1, C2]. Indeed, algorithms 21.1 and 21.2 specifically abandon the line searches (for the particular iteration in question), if the inner product, s_o, is found to be positive (or more strictly, insufficiently negative). However, this is clearly an area where further work is required.

21.8 ALTERNATIVE ARC-LENGTH METHODS USING RELATIVE VARIABLES

Suppose for a particular increment, we wish to constrain the difference between the displacements at variables a and b to a prescribed magnitude Δ. Such a procedure is clearly a simple extension of the technique of Sections 9.3.2.3 and 21.4.2 and involves a constraint:

$$\Delta\mathbf{p}(a) - \Delta\mathbf{p}(b) = \Delta \tag{21.69}$$

where $\Delta\mathbf{p}(a)$ is a scalar which is the ath component of the vector $\Delta\mathbf{p}$.

If the 'fixed load pattern' is $\mathbf{q}_c$ which is to be multiplied by a scalar loading parameter, λ, then the predictor displacement change is

$$\Delta\mathbf{p}_p = \Delta\lambda\delta\mathbf{p}_{to} = \Delta\lambda\mathbf{K}_{to}^{-1}\mathbf{q}_c \tag{21.70}$$

where $\mathbf{K}_{to}$ in the above is the predictor tangent. Substituting from (21.70) into (21.69), we obtain:

$$\Delta\lambda = \Delta/(\delta\mathbf{p}_{to}(a) - \delta\mathbf{p}_{to}(b)) \tag{21.71}$$

From (21.69), the iterative change is given by

$$\delta\mathbf{p}(a) - \delta\mathbf{p}(b) = \{\delta\bar{\mathbf{p}}(a) - \delta\bar{\mathbf{p}}(b)\} + \delta\lambda\{\delta\mathbf{p}_t(a) - \delta\mathbf{p}_t(b)\} = 0 \tag{21.72}$$

where we have used (21.48) for $\delta\mathbf{p}$. Equation (21.72) provides an expression for the change of load level, $\delta\lambda$.

In relation to contact algorithms (see Chapter 23), we might wish to prescribe a particular magnitude for the incremental gap, g, associated with a particular contact element, c. (This could be the magnitude required to close the gap.) In these circumstances, in place of (21.69), we would have:

$$\Delta g(\Delta \mathbf{p}_c) = \Delta \tag{21.73}$$

where the subscript c defines the nodal variables associated with the particular contact element (Chapter 23). The predictor load change would then be

$$\Delta\lambda = \Delta/(\Delta g(\delta \mathbf{p}_{toc})) \tag{21.74}$$

while, in place of (21.72), we would have:

$$\delta g = \frac{\partial g}{\partial \mathbf{p}_c}\delta\mathbf{p} = \mathbf{a}^T\delta\mathbf{p}_c = \mathbf{a}^T(\delta\bar{\mathbf{p}}_c + \delta\lambda\delta\mathbf{p}_{tc}) = 0 \tag{21.75}$$

where, considering a simple two-dimensional contact element, with a constraint on the normal gap, the vector $\mathbf{a}$ would be given by (23.7) and the vectors with subscripts c would be of dimension 6×1 (there being six displacement variables associated with the contact element). These vectors would simply be taken from the equivalent structural vectors (without the subscript c). Equation (21.74) provides the required change to the loading parameter, $\delta\lambda$.

21.9 AN ALTERNATIVE METHOD FOR CHOOSING THE ROOT FOR THE CYLINDRICAL ARC-LENGTH METHOD

When using the cylindrical arc-length method [C1] to analyse a double cantilever beam (DCB) subject to progressive delamination, the author and co-worder [H1] frequently experienced severe numerical difficulties that were associated with very sharp snap-backs. A careful analysis of the incremental/iterative behaviour showed that the problems were associated with an 'incorrect choice of root' from the two solutions to the quadratic equation in the load level change that is associated with the solution of the cylindrical constraint (see (9.26) and Section 9.4.1). The original strategy was to choose the root that gave the minimum angle between the old incremental displacement vector $\Delta\mathbf{p}_o$ and the new vector $\Delta\mathbf{p}_n$, where (see (9.35) and Figure 21.5) the two possibilities for $\Delta\mathbf{p}_n$ are updated from $\Delta\mathbf{p}_o$ via:

$$\Delta\mathbf{p}_{n1} = \Delta\mathbf{p}_o + \delta\bar{\mathbf{p}} + \delta\lambda_1\delta\mathbf{p}_t \tag{21.76a}$$

$$\Delta\mathbf{p}_{n2} = \Delta\mathbf{p}_o + \delta\bar{\mathbf{p}} + \delta\lambda_2\delta\mathbf{p}_t \tag{21.76b}$$

with

$$\delta\bar{\mathbf{p}} = -\mathbf{K}_t^{-1}\mathbf{g}(\lambda_o) \tag{21.77a}$$

and

$$\delta\mathbf{p}_t = K_t^{-1}\mathbf{q}_c \tag{21.77b}$$

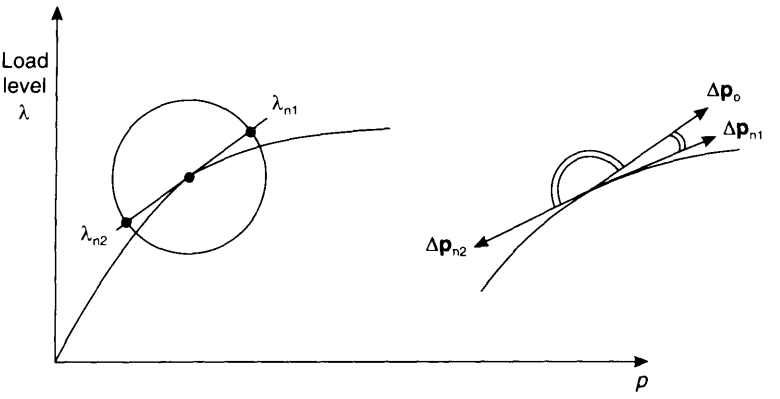

Figure 21.5 Avoiding a solution doubling back.

and $\delta\lambda_1$ and $\delta\lambda_2$ are the two roots of the quadratic equation:

$$a_1\delta\lambda^2 + a_2\delta\lambda + a_3 = 0 \tag{21.78}$$

with a_1–a_3 as given in (21.67) with $\eta = 0$.

The idea behind the choice of minimum angle is to avoid the solution 'doubling back' as illustrated in Figure 21.5. However, for a very sharp snap-back (Figure 21.6), one wants the solution to double back! The idea for the new choice of root is also illustrated in Figure 21.6 and is that, if one were to compute the new residual $\mathbf{g}(\lambda_{n1})$ having applied (21.76a) (with $\lambda_{n1} = \lambda_o + \delta\lambda_1$) and $\mathbf{g}(\lambda_{n2})$ having also applied (21.76b) (with $\lambda_{n2} = \lambda_o + \delta\lambda_2$) then the best root will be that leads to the smallest residual norm. In other words both options have to be tried and we compute both $\mathbf{g}(\mathbf{p}_o + \Delta\mathbf{p}_{n1}, \lambda_{n1})$ and $\mathbf{g}(\mathbf{p}_o + \Delta\mathbf{p}_{n2}, \lambda_{n2})$ where $\mathbf{p}_o$ are the displacements at the end of the last increment.

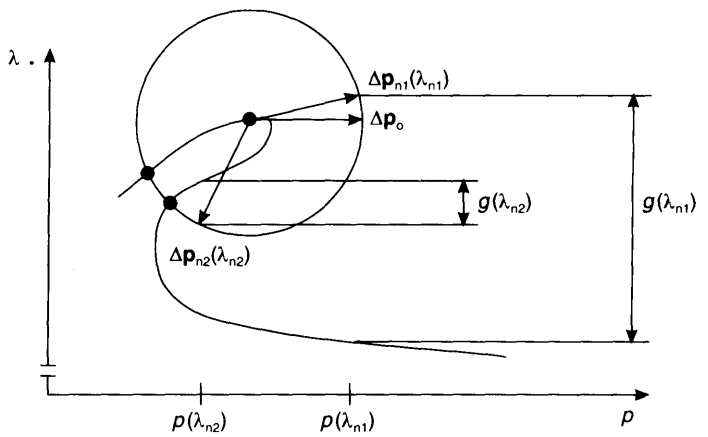

Figure 21.6 Illustration of the minimum residual criterion.

Naturally, this approach is more expensive than the conventional procedure. However, the extra expense is not large and is approximately of the same order as one step in a 'line search'. In addition, for most relatively smooth problems, this technique is not needed (although in such cases it should give the same answer as the 'conventional technique'). Consequently, an analyst need only turn on this option when he or she anticipates snap-backs or when he or she has had convergence difficulties. The author and co-worker found that for difficult problems this new method gave effective solutions where the conventional method failed [H1].

21.10 STATIC/DYNAMIC SOLUTION PROCEDURES

Despite the various improvements that can be made to the 'static solution procedure', it is worth re-emphasising that in many circumstances, the 'true solution' involves a combination of statics and dynamics. For example Figure 21.7a illustrates the dynamic snap, that would occur under load control for a simple 'snap-through' problem. When this observation is coupled with the difficulties that can accompany complex 'static path-following procedures', it is not surprising that a number of papers have recently considered a static/dynamic solution option [R2, S8]. Riks *et al.* [R2] also observe that, on some occasions, the real system will dynamically snap to a point that is statically separated from the original path. In other words, even if a static path-following technique could be used it would lead to the wrong equilibrium state.

Skeie *et al.* [S8] describe a dynamic procedure that they label as a 'Dynamic relaxation' algorithm with reference being made to the early work on dynamic relaxation by Day [D1]. The latter is a form of iterative method for the solution of equations which has a close relationship with the 'explicit dynamics' solution procedures (Section 24.5 and 24.6). However, Skeie *et al.* [S8] apply an 'implicit dynamics solution procedure' (Chapter 24) and hence the terminology may be a little confusing. The objective of the dynamic solution is to pass as quickly as possible to the next static solution and, to this end, Skeie *et al.* [S8] adjust the mass proportional coefficient appearing in the Rayleigh damping so that they solve the dynamic equations:

$$\mathbf{M}\ddot{\mathbf{p}} + \gamma\mathbf{M}\dot{\mathbf{p}} + \mathbf{g}(\mathbf{p}, \lambda) = 0 \tag{21.79}$$

where $\mathbf{g}(\mathbf{p}, \lambda)$ is the usual static term. The coefficient γ is obtained via:

$$\gamma = 2\omega; \quad \omega^2 = \frac{\Delta\mathbf{p}^{\mathrm{T}}\mathbf{K}_{\mathrm{diag}}\Delta\mathbf{p}}{\Delta\mathbf{p}^{\mathrm{T}}\mathbf{M}_{\mathrm{diag}}\Delta\mathbf{p}} \tag{21.80}$$

Here ω is considered to be an approximation to the lowest eigenfrequency of the structure. The calculation of ω is very similar to that described in more detail in Section 24.13 in relation to the computation of an automatically varying time-step for implicit dynamics.

Riks *et al.* [R2] give no detail on the damping procedure but do describe the technique for implementing a static/dynamic/static solution algorithm. The objective is to use existing static path-following techniques in combination with existing 'implicit dynamic solution procedures'. In relation to Figure 21.7b, the path-following technique would be used until the singular point (here limit point) had been passed, i.e. until point B at which point the displacements would be $\mathbf{p}_{\mathrm{B}}$. We could then 'home in' on the

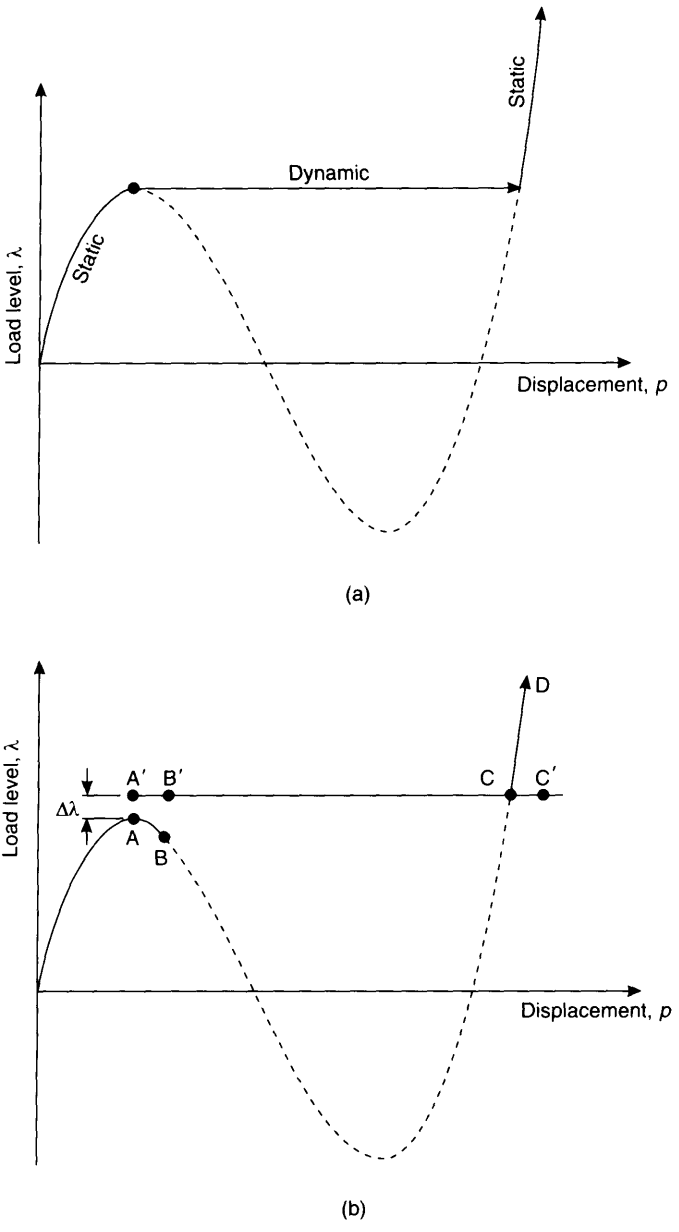

Figure 21.7 Static/dynamic solution procedure. (a) Static and dynamic paths; (b) solution strategy.

limit point using, for example, the 'bracketing technique of Section 21.1. The dynamic stage of the solution would now be instigated via a restart. The initial conditions, would involve:

$$\dot{\mathbf{p}}_A = \mathrm{O}; \qquad \mathbf{p}_A, \mathbf{p} \qquad \lambda_{A'} = \lambda_A + \Delta\lambda \tag{21.81}$$

For a limit point, there would seem to be no need to return to point A and one could replace the subscript A in the above by the subscript B relating to the point just beyond the limit point. In this way the bracketing procedure could be avoided. The dynamic algorithm would lead to a solution that oscillated, with decreasing amplitude due to the damping, about point C. Riks *et al.* [R2] recommend that this dynamic stage is terminated (at C′ in Figure 21.7b) when the kinetic energy is reduced below a certain quantity. At this stage, a restart would be used to implement a static-solution procedure with $(\lambda_{A'}, \mathbf{p}_{C'})$ as starting-points (i.e. the predictor) for a static Newton–Raphson iteration which should converge on point C. Further static path-following could not proceed up the path CD.

The previous technique can also be used for symmetric bifurcations [R1] although if we are restarting from an unstable point, it may be necessary to introduce a perturbation possibly via an initial velocity. Riks *et al.* [R1] suggest that this can be used to speed up the dynamic part of the algorithm. The initial velocity would then take the form, $\dot{\mathbf{p}}_A = \alpha \mathbf{z}$ where the $\mathbf{z}$ is the eigenvector associated with the zero eigenvalue at the singularity (see Section 21.2).

21.11 SPECIAL NOTATION (SEE ALSO SECTION 20.6)

a_1–a_3 see (21.67)
c_1, c_2 see (21.67a), (21.63)
d_1–d_4, d_8 see (21.67)
d_5–d_7 see (21.63), (21.64)
e_1, e_2 see (21.63)
α = control parameter
τ = test function
λ = load parameter scalar
η = line-search step length
Δs = incremental control parameter
s = energy slope—see (21.56)
Δl = incremental length parameter
$\mathbf{p}$ = nodal displacement vector
$\delta\mathbf{p}$ = iterative nodal displacement vector
$\delta\mathbf{p}_t$ = tangential displacement change—see (21.14)
$\delta\bar{\mathbf{p}}_t$ = modified tangential displacement change—see (21.13)
$\delta\bar{\mathbf{p}}$ see (21.48)
$\mathbf{q}$ external load vector
$\mathbf{v}(\mathbf{b}, \mathbf{a})$ related to directional derivative see (20.69)
$\mathbf{z}$ eigenvector of $\mathbf{K}_t$, corresponding to lowest eigenvalue

Subscripts

e = external
p = predictor or partial derivative in $\mathbf{p}$
λ = partial derivative λ.

21.12 REFERENCES

[A1] Azrar, L., Cochelin, B., Damil, N. & Poitier-Ferry, M., An asymptotic numerical method to compute the postbuckling behaviour of elastic plates and shells, *Int. J. for Num. Meth. in Engng.*, **26**, 1251–1278 (1993).

[B1] Batista, R. C., Antonini, R. C. & Alves, R. V., An asymptotic modal approach to nonlinear structural elastic stability, *Computers & Structures*, **38**, 475–484 (1991).

[B2] Batoz, J. L. & Dhatt, G., Incremental displacement algorithms for nonlinear problems, *Int. J. for Num. Meth. in Engng.*, 1262–1266 (1979).

[B3] Bergan, P. G., Horrigmoe, G., Krakeland, B. & Soreide, T. H., Solution techniques for non-linear finite element problems, *Int. J. for Num. Meth. in Engng.*, **12**, 1677–1696 (1978).

[C1] Crisfield, M. A., An arc-length method including line searches and accelerations, *Int. J. for Num. Meth. in Engng.*, 1269–1289 (1983).

[C2] Crisfied, M. A., *Variable Step-lengths for Non-linear Structural Analysis*, Transport & Road Res. Lab. Report LR1049, Crowthorne, Berks. (1982).

[C3] Crisfield, M. A. & Wills, J., Solution strategies and softening materials, *Comp. Meth. in Applied Mech. & Engng.*, **66**, 267–278 (1988).

[C4] Crisfield, M. A. & Shi, J., A review of solution procedures and path-following techniqes in relation to the nonlinear finite element analysis of structures, *Nonlinear Computational Mechanics – the State of the Art*, ed. P. Wriggers *et al.*, Springer-Verlag, pp. 47–68 (1990).

[D1] Day, A. S., An introduction to dynamic relaxation, *The Engineer*, **219**, 218–221 (1965).

[D2] De Borst, R., Computation of post-bifurcation and post-failure behaviour of strain-softening solids, *Computers and Structures*, **25**, 823–829 (1987).

[D3] Duan, Y. & May, I. M., A local arc-length procedure for strain softening, *Proc. Computational Mechanics in UK – 1994*, ed. Geotechnical Engineering Group, Dept. of Mech. Engng., Manchester, UK, 65–68 (1994).

[E1] Eriksson, A., Using eigenvector projections to improve convergence in non-linear finite element equilibrium iterations, *Int. J. for Num. Meth. in Engng.*, 497–512 (1987).

[F1] Felippa, C. A., Traversing critical points with penalty springs, *Transient/Dynamic Analysis and Constitutive Laws for Engineering Materials*, ed. Pande *et al.*, Martinus Nijhoff, Dordrecht, 1987, C2/1-C2/8.

[F2] Fried, I., Orthogonal trajectory accession to the nonlinear equilibrium curve, *Comp. Meth. in Appl. Mech. & Engng.*, **47**, 283–298 (1984).

[H1] Hellweg, H.-B. & Crisfield, M. A., A new arc-length method for handling sharp snap backs, submitted to *Computers & Structures* (1995).

[K1] Kouhia, R. & Mikkola, M., Tracing the equilibrium path beyond simple critical points, *Int. J. for Num. Meth. in Engng.*, **28**, 2923–2941 (1989).

[K2] Kouhia, R. & Mikkola, M., Strategies for structural stability analysis, *Advances in Finite Element Technology*, ed. N.-E. Wiberg, CIMNE, Barcelona, pp. 254–278 (1995).

[L1] Lee, S. H., Rudimentary considerations for effective line search method in nonlinear finite element analysis, *Computers & Structures*, **32**, 1287–1301 (1989).

[M1] Mang, H., On special points on load-displacement paths in the prebuckling domain of thin shells, *Int. J. for Num. Meth. in Engng.*, **31**, 207–228 (1991).

[M2] Meek, J. L. & Loganathan, S., Large displacement analysis of space frame structures, *Computer Methods in Applied Mechanics & Engng.*, **72**, 57–75 (1989).

[O1] Onate, E. & Matias, W. T., Enhanced prediction of structural points using a critical displacement method, *Advances in Finite Element Technology*, ed. N.-E. Wiberg, CIMNE, Barcelona, pp. 62–89 (1995).

[R1] Rheinboldt, W. C. Numerical analysis of continuation methods for nonlinear structural problems, Computers and Structures, **13**, 103–113 (1981).

[R2] Riks, E., Rankin, C. & Brogan, F. A., On the solution of mode jumping phenomena in thin walled shell structures, *Comp. Meth. in Appl. Mech. & Engng.*, **136**, 59–92 (1996).

[S1] Schellekens, J. C. J., Computational strategies for composite structures, Ph.D. thesis, Delft University, The Netherlands (1972).

[S2] Schweizerhof, K. H. & Wriggers, P., Consistent linearisation for path following methods in nonlinear f.e. analysis, *Comp. Meth. in Appl. Mech. & Engng.*, **59**, 261–279 (1986).

[S3] Seydel, R., *From equilibrium to Chaos*, Elsevier, Armsterdam 1988.

[S4] Shi, J. & Crisfield, M. A., A simple indicator and branch switching technique for hidden unstable equilibrium paths, *Finite Elements in Analysis & Design*, **12**, 1992, 303–312 (1992).

[S5] Shi, J. & Crisfield, M. A., Combining arc-length control and line searches in path following, *Communications in Appl. Num. Meth.*, **11**, 793–803 (1995).

[S6] Shi, J. & Crisfield, M. A., A semi-direct method for the computation of singular points, *Computers & Structures*, **51**, 107–115 (1994).

[S7] Shi, J., Computing critical points and secondary paths in nonlinear structural stability analysis by the finite element methods, *Computers & Structures*, **58**, 203–220 (1996).

[S8] Skeie, G., Astrup, O. C. & Bergan, P. G., Applications of adapted, nonlinear solution strategies, *Advances in Finite Element Technology*, ed. N.-E. Wiberg, CIMNE, Barcelona, pp. 212–236 (1995).

[W1] Wagner, W., A path-following algorithm with quadratic predictor, *Computers & Structures*, **39** (3/4), 1991; 339–348 (1991).

[W2] Wagner, W. & Wriggers, P., A simple method for the calculation of postcritical branches, *Engineering Computations*, **5**, 103–109 (1988).

[W3] Waszczyszyn, Z., Numerical problems of nonlinear stability analysis of elastic structures, *Computers & Structures*, **17**, 13–24 (1983).

22 Examples from an updated non-linear finite element computer program using truss elements

(written in conjunction with Dr Jun Shi)

In Chapters 2, 3 and 9 of Volume 1, we described a very simple non-linear finite element program involving a truss element and a linear spring which could be used to illustrate some of the fundamental structural problems including limit points and bifurcations. In addition, the programs incorporated not only the basic predictor–corrector algorithms but also more advanced concepts such as line searches and arc-length methods. Fortran routines were included in the text and were originally also available on floppy disks although in later editions they were instead made available on anonymous FTP. The author and co-worker (Dr Jun Shi) have now up-dated this computer program so that it firstly encompasses multiple elements and secondly includes some of the branch switching techniques and further advanced solution procedures of the previous chapter (as well as a few others).

While the resulting computer program is not large, it is inevitably significantly larger than that related to the initial volume. Consequently, we have decided not to include Fortran routines in the text, but rather to have them available on anomymous FTP (see the Preface). In addition to the Fortran routines, an input manual and a set of input files and a few sample output files are provided. These files relate directly to a set of examples which will be described in this chapter. Some of these problems have been taken from earlier analyses by other authors including (F1, P1, R1.21, S7.21, M2.21]. The labelling of the data and output files relates directly to the section headings in this chapter.

A number of the problems involve a range of singular points beyond the lowest point and, to that extent, are a little academic. The examples that illustrate the higher-order predictors and correctors of Sections 21.4 and 21.5 should be considered as preliminary

in that, although they illustrate the performance of the methods, no attempt has been made to properly assess their efficiency in comparison with more traditional techniques.

22.1 A TWO-BAR TRUSS WITH AN ASYMMETRIC BIFURCATION

Figure 22.1 shows a simple two-bar truss with two free degrees of freedom (variables 4 and 5) for which the response involves an asymmetric bifurcation (Figures 22.2 and

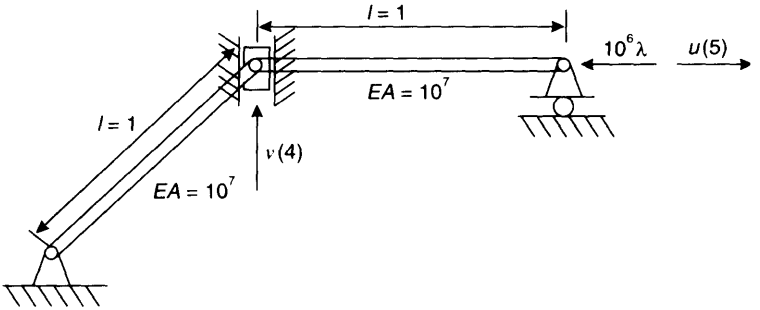

Figure 22.1 A simple asymmetrical bifurcation problem.

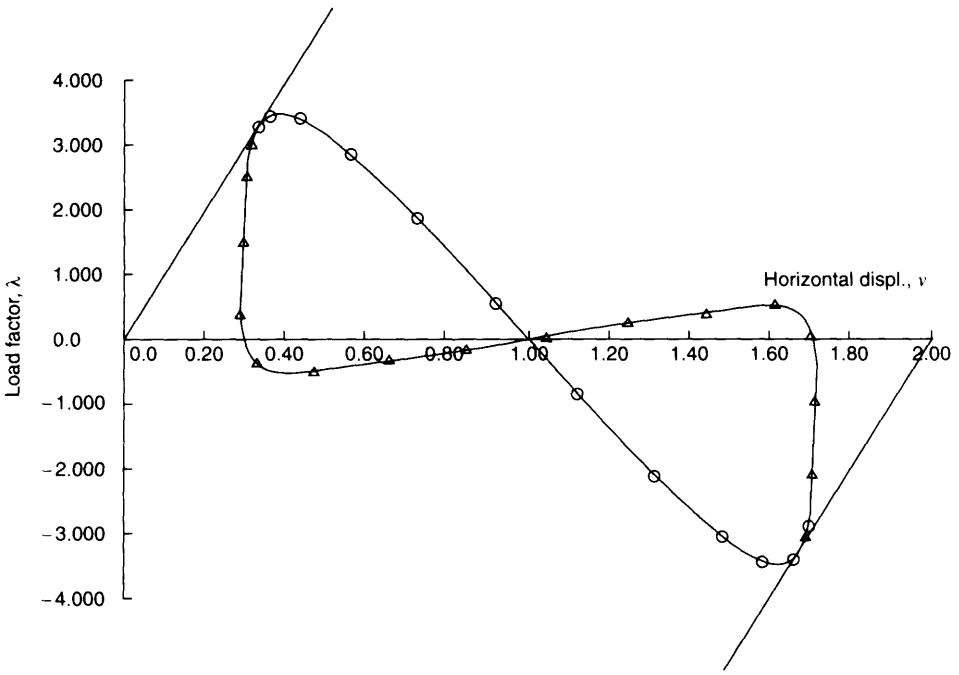

Figure 22.2 Structural response of the two-bar truss: load versus horizontal displacement.

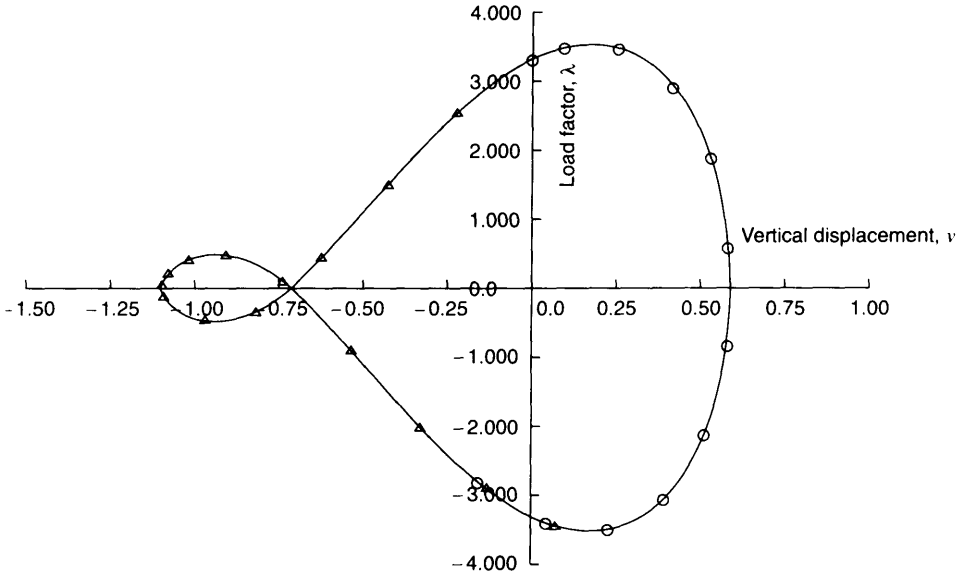

Figure 22.3 Structural response of the two-bar truss: load versus vertical displacement

22.3). Physically, the reason for the asymmetry is that the inclined bar gives a different response depending on whether the bar moves in an upward or downward direction.

22.1.1 Bracketing

The first stage is to use the bracketing techniques to identify and home in on the singular point. The type of bracketing technique is controlled by the input parameter IBRAC where the first five options relate to indirect methods as discussed in Section 21.1. The following options are available:

1. Bisection with the test function $\tau = D_{\min}$ (referred to as PMIN or PIVS in the computer program).
2. 0.618 Golden section with the test function $\tau = D_{\min}$.
3. Interpolation based on τ = determinant of $\mathbf{K}_t$.
4. Interpolation based on product of $D_{\max}$ (PIVB in the computer program) and $D_{\min}$ (i.e. test function c of (21.1)).
5. Interpolation based on $D_{\min}$ (i.e. test function b of (21.1)).

Alternatively, we can use the direct method of Section 21.6 or a combination of direct and indirect methods. In relation to the input parameter, IBRAC, these options are as follows:

—6—Direct method of Section 21.6—Direct 2.
6—Direct bracket using method 5 above until the first singular point is passed, followed by a switch to the direct method of Section 21.6—Direct 1.

Two alternative 'semi-direct methods' are available in which, as discussed in Section 21.1 and in more detail in [S6.21], once bracketing has started, the equilibrium iterations are initially omitted and then phased in as the singular point is approached.

7—A semi-direct method using bi-section with the test function $\tau = D_{\min}$.
−7—The same semi-direct method using interpolation with $\tau = D_{\min}$.

The data file for the current example is given below

Data input file 22.1.1

```
ANALYSIS TWO DIMENSIONAL
1
GENERAL DATA (NV,NE,NBCON,NLOAD,NMATE,NANIT,NDIM)
6 2 3 1 0 0 2
ITEYL,POSS,E,ANIT
2 0.0D0 1.0D7 0.0D0
NODAL COOR.
1,-0.7071067D0,-0.7071067D0  2,0.0D0,0.0D0  3,1.0D0,0.0D0
ELEM. CONN.
1,1,2  2,2,3
LOADINGS
3 -1.0D6 0.0D0
BOUNDARY COND.
1,1,1  2,1,0  3,0,1
OUTPUT VARIABLES
2 4 5
EARTHED SPRINGS
0
FACI, NINC,IWRIT,IAUTO,IARC,ILOAD
0.7D0 40  0      1      0     1
IACC,IRES,IBRAC,ICRIT,IBRSW,IROW
0    0    1      1      0     0
ICVCK,BETOK,ITERTY,NITMAX,NLSMX,EPSI,SHIF
1      1.0D-6 1      21      0     1.0D-4  0.0D0
IDES,FACMX,FACMN,ISWCH,ICORT,IPRED
3    1.0D0  0.1D0  1      0    0
CSTIFS
0.6D0
-------------------------------------------------
data file for two-flexual-bar bar asymmetric bifurcation problem
              ( 45 degrees inclination)
              pre-critical solution inl. bracketing
-------------------------------------------------
```

This file relates to the bracketing option, IBRAC = 1. The user can simply change IBRAC in the file to implement the other options although it should be emphasised that the current very simple example is not ideal for comparing the different methods. A truncated output file is given below.

Truncated output file 22.1.1

INPUT DATA SUMMARY

No. OF VARIABLES = 6
No. OF ELEMENTS = 2
POISSON RATIO = 0.00000E+00

ELEMENT TYPE = 2
1 = GREENS STRAIN;
2 = ENGNG. STRAIN;
3 = LOG STRAIN;
4 = LOG STRAIN WITH VOLUME CHANGES.

ELEMENT PROPERTIES

ELEM No.	NODAL No.		LENGTH	E	INITIAL FORCE	INITIAL AREA
1	1	2	0.1000E+01	0.1000E+08	0.0000E+00	0.1000E+01
2	2	3	0.1000E+01	0.1000E+08	0.0000E+00	0.1000E+01

NODAL PROPERTIES

NODAL No.	X	Y	Fx	Fy	BCx	BCy
1	-0.707E+00	-0.707E+00	0.000E+00	0.000E+00	1	1
2	0.000E+00	0.000E+00	0.000E+00	0.000E+00	1	0
3	0.100E+01	0.000E+00	-0.100E+07	0.000E+00	0	1

REPORT ON ERRORS IN INPUT DATA: PART 1

!!!! NO ERROR FOUND IN INPUT DATA: PART 1 !!!!

SOLUTION CONTROL PARAMETERS

INCREMENTAL LOAD FACTOR = 0.70000
NO. OF INCS. (NINC) = 40
IWRIT = 0; 0 = LIMITED ; 1 = FULL
IAUTO = 1; 0 = FIXED INCS., 1 = AUTOMATIC
IARC = 0; 0 = LOAD CONTROL 1 = Crisfield CYLINDRICAL ARC-LENGTH CONTROL
2 = Riks ORTHORGONAL PLANE ARC-LENGTH CONTROL
3 = Ramm UPDATED ORTHORGONAL PLANE ARC-LENGTH CONTROL
4 = Fried ORTHORGONAL TRAJECTORY ARC-LENGTH CONTROL
5 = Rheinboldt SPECIFIC DISPLACEMENT CONTROL
6 = Powell and Simon INCREMENTAL WORK CONTROL
ILOAD = 1; 1 = SLN. GUIDED BY CSTIFF.;
2 = SLN. GUIDED BY No. NEG. PIV.;

```
 IACC = 0;  0 = NO ACCEL,      1 = ACCEL WITH MOD. N-R
 IRES = 0;  0 = NOT A RE-START, 1 = IS A RE-START
 IBRAC = 1;  0 = NO BRACKETING,  1 =  ORIGINAL BISECTION
                      2 =  0.618 GOLDEN SECTION
                      3 =  INTERPOLATION BASED ON THE DETERMINENT
                      4 =  ..... PIVS*PIVB
                      5 =  ..... PMIN
                      6 =  AS 5; BUT ONCE ONLY THEN USE DIRECT COMP.
                     -6 =  DIRECT COMPUTATION OF SINGULAR PT
                      7 =  Riks's  SEMI-DIRECT with BI-SECTION
                     -7 =  .....with INTERPOLATION ON PMIN
 IBRSW = 0;  0 = NO BRANCHING,  1 = 1st EIGN-VECTOR INJECT.
                      2 =  USING 2nd ORDER TERMS
                      3 =  MULTIBIFUR WITH imulti LOWEST EIGEN-VEC.s
                      4 =  Seydel's APPROX. TO THE 1ST EIGN-VEC.
                      5 =  Riks's ORTHOGANAL TO PRIMARY TANGENT
 ICRIT = 1;  THE CRITICAL PT. No. TO BE BRACKETED
 IROW = 0;  ROW No. OF Kt REPLACED BY A UNIT VECTOR TO GET Seydel's
          PREDICTOR FOR BRANCHING IF ABS(IBRSW) = 4
        D.O.F. TO BE FIXED IN
          DIRECT COMP. OF SINGULAR PT. IF ABS(IBRAC) = 6

   CONV. CONTR. TYPE,ICVCK =   1
                1 = RESID-F SCALED BY EXTERNAL FORCE;
                2 = RESID-F SCALED BY REACTION;
                3 = ITER. DISP. SCALED BY TOTOAL DISP
   CONV. TOL FACTOR, BETOK =  0.10000E-05
ITERATIVE SOLN. TYPE, ITERTY =   1  ( 1 = FULL N-R; 2 = MOD. N-R )
    MAX NO OF ITERATIONS =  21
    MAX NO. OF L-SEARCHES =  0
BRACKETING TOLERENCE EPSILON =  0.10000E-03
SHIFT IN EIGEN ANALYSIS SHIF =  0.00000E+00

DATA FOR AUTOMATIC INCREMENTS
 DESIRED NO. OF ITERATIONS =  3
 MAX. LOAD INC.        =  1.000
 MIN. LOAD INC.        =  0.1000
 PARAM FOR ARC-L,  ISWCH =  1  ( 0=NO SWITCH, OTHER=SWITCH TO CORRP. A-L)
 CORRECTOR TYPE,  ICORT =  0  ( 0=NORMAL, 1=2ND ORDER EXPLICIT, 2=IMPLICIT)
 PREDICTOR TYPE,  IPRED =  0  ( 0=NORMAL, 1=2ND ORDER)

SWITCHES TO ARC-L WHEN CSTIF < CSTIFS =  0.6000


REPORT ON ERRORS IN INPUT DATA: PART 2

!!!! NO ERROR FOUND IN INPUT DATA: PART 2 !!!!


*********************************************************************************************

INCREMENT NO. =  1

*********************************************************************************************

CURR. STIFF. FACTOR = 0.1000E+01  NO. OF NEG. PIVOT =  0          PIVOT RATIO = 0.1000E+01
THE SMALLEST PIVOT = 0.5000E+07  THE LARGEST PIVOT = 0.1000E+08  DETERMINENT = 0.1000E+01
AT THE D.O.F.      =  4          AT THE D.O.F.    =  5           MINM PIV AT =  4
```

TOTAL LOAD FACTOR = 0.7000E+00 INC LOAD FACTOR = 0.7000E+00 INC LENGTH = 0.7000E-0

TOTAL DISPS. AFTER TANG. SOLN.

NODE No.	U	V	NODE No.	U	V
1	0.000E+00	0.000E+00	2	0.000E+00	0.000E+00

ITER. No.	CONV. FAC.	TOTAL POTENTIAL ENERGY	STRAIN ENERGY
0	0.1164E-21	-.2450E+05	0.2450E+05

ELEM. No.	AXIAL FORCE	ELEM. No.	AXIAL FORCE
1	0.000E+00	2	-0.700E+06

FINAL TOTAL DISPL. FINAL REACTION

NODE No.	U	V	Fx	Fy
1	0.000E+00	0.000E+00	0.000E+00	0.000E+00
2	0.000E+00	0.000E+00	0.700E+06	0.000E+00
3	-0.700E-01	0.000E+00	-0.700E+06	0.000E+00

****

INCREMENT NO. = 16

****

CURR. STIFF. FACTOR = 0.1000E+01 NO. OF NEG. PIVOT = 0 PIVOT RATIO = 0.3766E-04
THE SMALLEST PIVOT = 0.7382E+02 THE LARGEST PIVOT = 0.1000E+08 DETERMINENT = 0.7382E-01
AT THE D.O.F. = 4 AT THE D.O.F. = 5 MINM PIV AT = 4

SOLN. FOR THE LOWEST EIGNVALUES AND EIGNVECTORS :

THE 1st EIGENVALUE

ITER. NO	EIG. EST.	CONV. FACT.
1	0.738E+02	0.100E+03
2	0.738E+02	-0.738E-03
3	0.738E+02	-0.385E-13

X2 = -0.40221E-16

D.O.F.	YY VECTOR	EIGN. VECTOR(S)
1	0.000E+00	0.000E+00
2	0.000E+00	0.000E+00
3	0.000E+00	0.000E+00
4	0.402E-16	0.100E+01
5	-0.100E+00	0.402E-15
6	0.000E+00	0.000E+00

```
B1 = 0.1414E+08  B2 =-0.2250E+07  B3 =-0.1207E-09  B4 =-0.4022E-09

ASYMMETRIC BIFURCATION

X1 =  0.31819E+00   X2 =  -0.32927E-16

AT END OF RUN
 FACI =  -0.4883E-03 FACMX =  0.1000E+01 FACMN =  0.1000E+00 INBR =  11

!!!! NFEA EXECUTION COMPLETED !!!!
```

In the above, we have omitted the initial part of the file which simply 'echoes' the data input. At the beginning of each increment, information regarding the structure stiffness is written to the output file. This is followed by the tangential predictor and the iterative history. At the end of each increment, the converged displacements and corresponding internal forces are sent to the output file. If a more detailed output is required, this can be achieved by setting the input parameter IWRIT to 1. Because the bracketing flag (IBRAC) is non-zero, once a singular point has been found at the last increment, extra information regarding the type of singular point is output. In particular, the stability coefficients B_1–B_4 (equations (20.41)–(20.44)) are computed so that (see Section 20.4), we can specify a limit point if $B_4 \neq 0$, a bifurcation point if $B_4 = 0$ and an asymmetric bifurcation point if $B_1 \neq 0$. In the latter case (as here), we also output X_1 and X_2 from (20.58). In addition, the output file specifies the eigenvector ($\mathbf{z}_1$) associated with the lowest eigenvalue at the critical point and the number of bracketing increments (INBR).

Plotfile 22.1.1 contains the load factors (λ's) in the first column and the corresponding displacements at certain specified degrees of freedom (DOFs)—here 4 and 5 (see Figure 22.1)

Plotfile 22.1.1

```
 LOAD FACTOR   DISP AT D.O.F. =
                    4              5
0.70000000E+00 0.00000000E+00 -0.70000000E-01
0.17000000E+01 0.00000000E+00 -0.17000000E+00
0.27000000E+01 0.00000000E+00 -0.27000000E+00
0.37000000E+01 0.00000000E+00 -0.37000000E+00
0.32000000E+01 0.00000000E+00 -0.32000000E+00
0.34500000E+01 0.00000000E+00 -0.34500000E+00
0.33250000E+01 0.00000000E+00 -0.33250000E+00
0.33875000E+01 0.00000000E+00 -0.33875000E+00
0.33562500E+01 0.00000000E+00 -0.33562500E+00
0.33406250E+01 0.00000000E+00 -0.33406250E+00
0.33328125E+01 0.00000000E+00 -0.33328125E+00
0.33367188E+01 0.00000000E+00 -0.33367188E+00
0.33347656E+01 0.00000000E+00 -0.33347656E+00
0.33337891E+01 0.00000000E+00 -0.33337891E+00
0.33333008E+01 0.00000000E+00 -0.33333008E+00
```

Table 22.1 Number of bracketing increments for asymmetric bifurcation problem.

Method	Bisection on D_{min}	Interp. on determinant	Interp. on D_{min}	Direct 1	Direct 2
IBRAC	2	3	5	6	−6
No of increments	11	4	4	3	5

Despite the earlier reservation regarding the relevance of the current example, it is worth tabulating and discussing the bracketing performance with different bracketing options.

In Table 22.1, the number of increments are from the point when bracketing commenced. A number of additional increments (between two and three) were applied prior to this bracketing. In relation to the direct methods, the numbers given in the table are 'iterations' rather than increments. For the indirect methods, iterations are required during each increment, and it follows that the direct methods were more efficient at finding the asymmetric bifurcation point. We will see later that it is advantageous to adopt direct method 1 rather than direct method 2 (see Section 22.1) when the problems include more than one singular point.

Clearly, interpolation on either the determinant or the minimum pivot is more efficient than the bisection method. In general, interpolations are superior to the bisection method if the singular point is simple. It should be emphasised that the number of bracketing steps depends strongly on the specified bracketing tolerance (EPSI).

22.1.2 Branch switching

After bracketing, we can either use eigenmode injection (Section 21.2) or the tangents to the secondary path (Section 21.3). This is achieved by 'restarting' from the bifurcation point. The 'restart output file', REOUT, generated at the end of the bracketing takes the form:

Reout file 22.1.1

```
D0          PIVR0     PMIN0     STIFI          PIVMINI   CSTIFO    X1          FACT      NEGO IMULT
0.1000E11 0.5000E14 0.5000E07 0.1000E+08 0.1960E07 0.1000E01 0.3182E00 0.33333E01  1    1
NE   AN        ALN       ARN
 1 0.0000E+00 0.1000E+01 0.1000E+01
 2 -0.3333E+07 0.6667E+00 0.1000E+01
NODE   PT        YY        DT        Z1(s)
 1 0.0000E+00 0.0000E+00 0.0000E+00 0.0000E+00
 2 0.0000E+00 0.0000E+00 0.0000E+00 0.0000E+00
 3 0.0000E+00 0.0000E+00 0.0000E+00 0.0000E+00
 4 0.0000E+00 0.2030E-20 0.0000E+00 0.1000E+01
 5 -0.3333E+00 -0.1000E+00 -0.1000E+00 0.2030E-19
 6 0.0000E+00 0.0000E+00 0.0000E+00 0.0000E+00
```

```
 6 0.0000E+00 0.0000E+00 0.0000E+00 0.0000E+00
DERT          PIVR          PMIN          ALOD     NPIV
 1.425        0.2850E-03 -0.3003E-02 3.340        1
0.1425E-02 0.2850E-06 0.2850E-06 3.333        0
0.1425E-05 0.2850E-09 0.2850E-09 3.333        0
```

It contains all of the information from the last 'restart write'. The first line gives information regarding the stiffness at the initial (undeformed) and final loaded states. Here:

D0 = det($\mathbf{K}_0$)—at the initial state
PIVRPO = the product of the smallest and largest pivots (still at the initial state).
PMIN0 = the smallest pivot of $\mathbf{K}_0$ at the start of the solution.
STIF1 = the scaling factor for the current stiffness parameter (denominator in (9.43) of (9.44)).
PIVMINI = the smallest pivot just before bracketing starts.
CSTIFO = the initial current stiffness parameter.
X1 = coefficient for the tangent of the secondary path (from 20.58))
FACT = the total load factor (λ) at the end of the last run.
NEGO = the number of negative pivots at the end of the last run.
IMULTI = the multiplicity of the bracketed singular point (i.e. number of zero pivots).

For each member, the current internal force (AN), element length (ALN) and area (ARN) are also saved. In addition, we have the predictor tangential displacement vector, $\delta\mathbf{p}_1$ (see (21.14) and labelled DT), the eigenmode, $\mathbf{z}_1$, and the vector $\mathbf{y}$ (see (21.15) and labelled YY).

The last three lines of data in REOUT is provided for the last three increments so that it can be used to continue bracketing from a restart. To initiate such a 'restart', one first copies REOUT to REIN. In addition, one must provide a different control data in the input file. To branch switch for the current problem one can use the data file 22.1.2. The control data block is shown in Data Input file 22.1.2.

Data input file 22.1.2

```
.....
FACI, NINC,IWRIT,IAUTO,IARC,ILOAD
0.7D0 40   0      1      1   2
IACC,IRES,IBRAC,ICRIT,IBRSW,IROW
0    1   0      0      2     0
ICVCK,BETOK, ITERTY,NITMAX,NLSMX,EPSI,  SHIF
1      0.1D-8 1        21       0      1.0D-5 0.0D0
IDES,FACMX,FACMN,ISWCH,ICORT,IPRED
3    1.0D0  0.1D0  0      0      0
DLDES,DLDMX,DLDMN
1.0D-1 2.0D-1 1.0D-2
-------------------------------------------------
 data file for two-flexual-bar bar asymmetric bifurcation problem
                (post-critical solution)
-------------------------------------------------
```

Table 22.2 Branching residuals for asymmetric bifurcation problem.

Method	IBRSW	Predictor	First iteration
Eigenmode injection	1	0.3874E-1	0.2417E-4
Path tangents	2	0.2600E-1	0.6057E-5

The main difference from the previous pre-critical data file (22.1.1) is that now IBRAC = 0 and IBRSW ≠ 0. Also, IRES = 1 and IARC = 1. (Branch switching is always initiated with a restart using 'arc-length control'.) To follow the two parts of the secondary path (see Figure 22.2 and 22.3), one needs to use (separately) IBRSW as positive and negative. The last row of control data in file 22.1.2 is important for the success of the branching because too small a length Δl (DLDES) will lead to the solution reverting back to the primary path, while if the length is too large, convergence difficulties may result. This is particularly true for large systems.

Either eigenmode injection (IBRSW = 1 and Section 21.2) may be used, or alternatively one may utilise higher-order information regarding the tangent to the secondary path (IBRSW = 2 and Section 21.6). Although the present example involves an asymmetric bifurcation, for the current problem there is little difference in the resulting numerical performance between the two methods. Table 22.2 compares the residual force norm scaled by the external forces at the end of the predictor solution and the first iteration. Clearly these results depend on the selected length increment, Δl. The computed results for the post-bifurcation analyses are plotted in Figures 22.2 and 22.3.

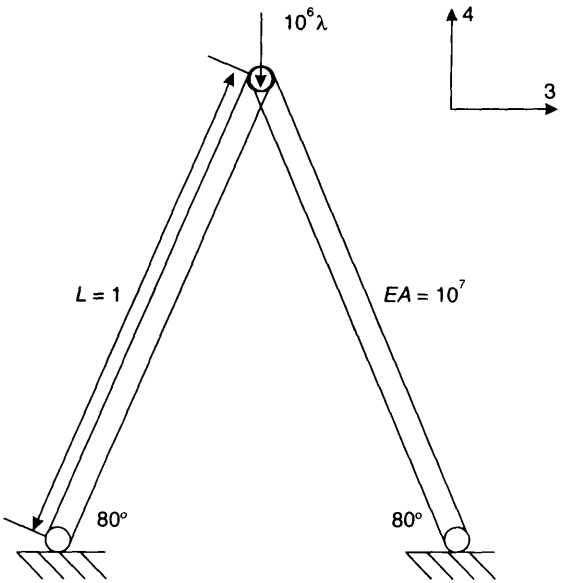

Figure 22.4 The von Mises truss.

22.2 THE VON MISES TRUSS

The truss is shown in Figure 22.4 and has two degrees of freedom (variables 3 and 4). The response involves both a limit and a bifurcation point (Figures 22.5 and 22.6) and the analytical results are obtained from [R1.21].

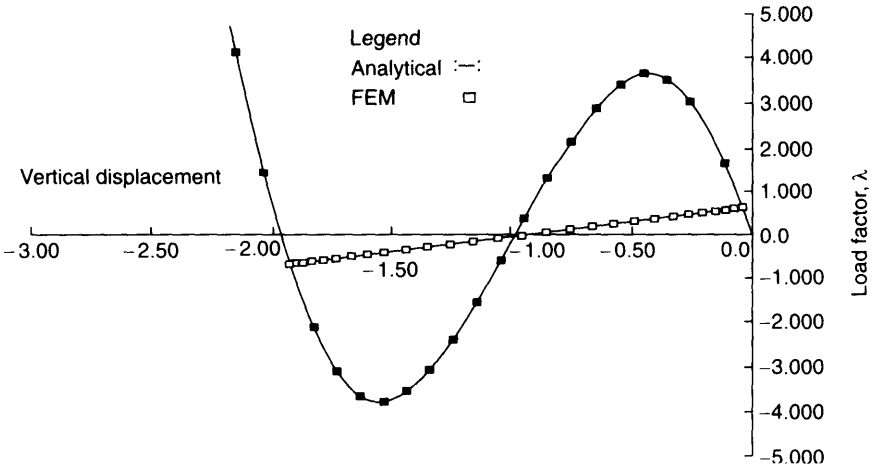

Figure 22.5 Structural response of the von Mises truss: load versus vertical displacement.

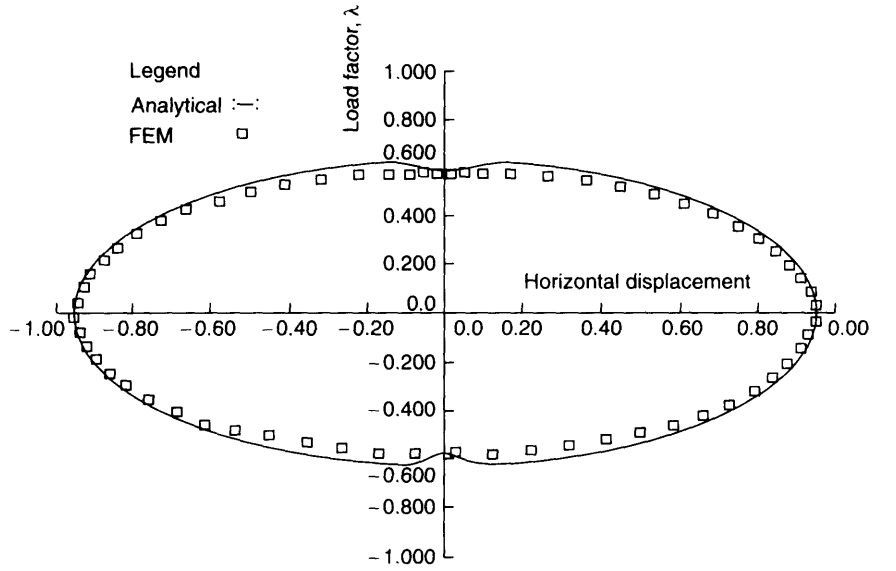

Figure 22.6 Structural response of the von Mises truss: load versus horizontal displacement.

22.2.1 Bracketing

The data file for bracketing on the first singular point (the bifurcation point) is given in Input Data file 22.2.1.

Input data file 22.2.1

```
ANALYSIS TWO DIMENSIONAL
1
GENERAL DATA (NV,NE,NBCON,NLOAD,NMATE,NANIT,NDIM)
6   2 2 1 0 0 2
ITEYL,POSS, E,   ANIT
1    0.0D0 1.0D7 0.0D0
NODAL COOR.
1,-0.1736481D0,0.0D0   2,0.0D0,0.9848077D0  3,0.1736481D0,0.0D0
ELEM. CONN.
1,1,2' 2,2,3
LOADINGS
2,0.0D0,-1.0D6
BOUNDARY COND.
1,1,1   3,1,1
OUTPUT VARIABLES
2,3,4
EARTHED SPRING
0
FACI,  NINC,IWRIT,IAUTO,IARC,ILOAD
0.2D0  40   0       1       0    1
IACC,IRES,IBRAC,ICRIT,IBRSW,IROW
0     0    1       1     0       3
ICVCK,BETOK, ITERTY,NITMAX,NLSMX,EPSI,  SHIF
1       1.0D-10 1       21        0    1.0D-4   0.0D0
IDES,FACMX,FACMN,ISWCH,IPRED,ICORT
3   5.0D-1 0.1D0  0    0    0
CSTIFFS
0.8D0
DLDES,DLDMX,DLDMN
5.0D-2 1.0D-1 1.0D-2
```

input datafile for 2D-two-bar-system (Von Mises' Truss)
pre-critical solution inl. bracketing
(80 degrees inclination)

If one wishes to home in on the second singular point (limit point), the input data parameter ICRIT would be changed from 1 to 2. To introduce bracketing on to singular points beyond the first, very simple changes have been made to the theory in Section 21.1. For these methods to work, the increments must be such that not more than one singular point is passed in a particular increment. Considering the first singular point, the number of bracketing increments is given in Table 22.3.

For this problem, the indirect bracketing results depended on the specified equilibrium convergence tolerance, BETOK. A loose tolerance (BETOK $= 10^{-6}$) led to

Table 22.3 Number of bracketing increments for von Mises truss.

Method	Bisection on D_{min}	Interp. on determinant	Interp. on D_{min}	Direct 1	Direct 2
IBRAC	2	3	5	6	−6
No. of increments	13	3	3	4	4

a failure in the bracketing procedure because the number of negative pivots was wrongly assessed. However, a tighter tolerance (10^{-10}) overcame this problem and gave the results shown in Table 22.3.

For direct bracketing, we can apply the constraint on the eigenmode (21.47c) with the parameter k being input as either 3 or 4 (Figure 22.4) as these are the only free variables. As anticipated, with $k=3$ we converge on to the bifurcation point while if $k=4$, we converge on to the limit point. Clearly some engineering pre-knowledge is very beneficial! (Note. If K is set to zero then the program implements the procedure discribed below (21.47c), where K corresponds to the variable with the smallest point once the singular point has been passed.)

22.2.2 Branch switching

To 'branch-switch' from the bifurcation point, file REOUT is copied to file REIN and the data file 22.2.2 (control section given in Input Data file 22.2.2) will lead to a successful switching using eigenmode injection (Section 21.2 and IBRSW = 1).

Input Data file 22.2.2

```
.....
FACI,  NINC,IWRIT,IAUTO,IARC,ILOAD
1.0D0 25   0      1      1    1
IACC,IRES,IBRAC,ICRIT,IBRSW,IROW
0     1    0      0     1      0
ICVCK,BETOK, ITERTY,NITMAX,NLSMX,EPSI,SHIF
1       1.0D-3 1         21       0       1.0D-5  0.0D0
IDES,FACMX,FACMN,ISWCH,IPRED,ICORT
4     1.0D0  0.1D0  0       0       0
DLDES, DLDMX,DLDMN
4.0D-2 1.5D-1 1.0D-3
-------------------------------------------------
input datafile for 2D-two-bar-system (Von Mises' Truss)
          post-critical solution inl. branching
          (80 degrees inclination)
-------------------------------------------------
```

Plots of the load parameter against the horizontal and vertical deflections are given in Figures 22.5 and 22.6 respectively.

22.3 A THREE-DIMENSIONAL DOME

The dome is shown in Figure 22.7 and is loaded with a set of point loads in the three directions (Figure 22.7). At the central node, this load is $-\frac{1}{2}$, while at each of the six nodes the circular ring of diameter 50 (Figure 22.7), the loads are -1. The response involves four singular points of which three are bifurcation points (including two double bifurcations) and a limit point on the primary path (Figure 22.8).

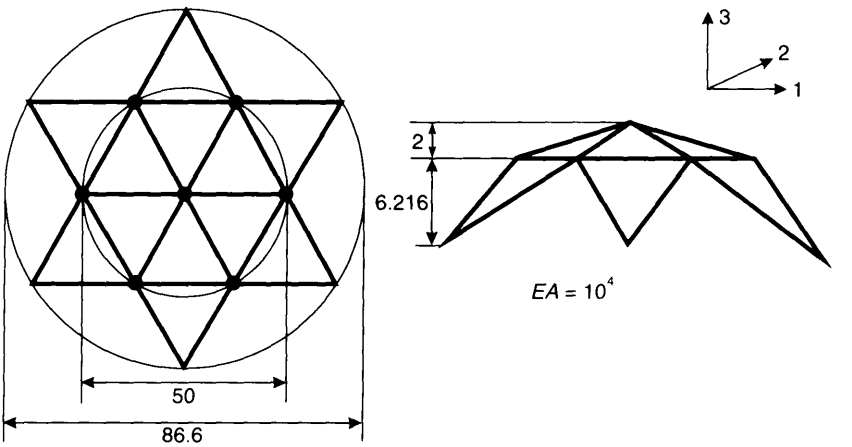

Figure 22.7 Three-dimensional dome.

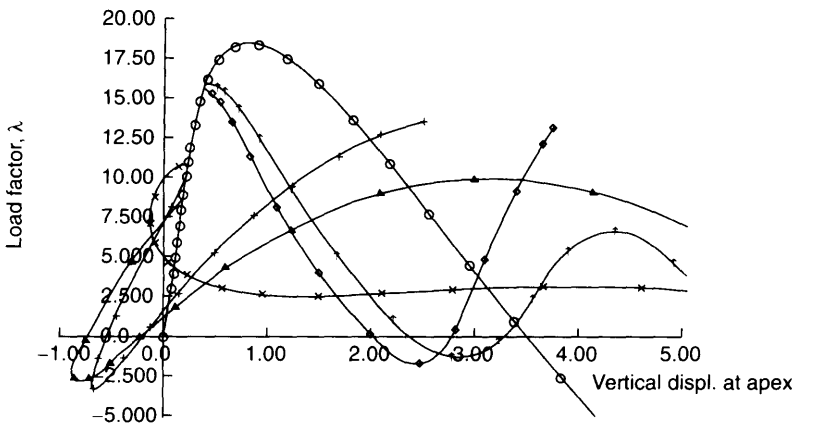

Figure 22.8 Structural response of the dome: load versus vertical displacement at the apex.

22.3.1 Bracketing

The singular points are fairly closely spaced ($\lambda_1 = 8.68$, λ_2, $= 10.26$, $\lambda_3 = 15.67$, $\lambda_4 = 18.40$). To avoid overstepping, the initial load step was taken as 3 and subsequent increments as 1. The input for the computation of the first critical point (a bifurcation point) is given in Input Data file 22.3.1.

Input data file 22.3.1

```
ANALYSIS THREE DIMENSIONAL
0
GENERAL DATA (NV,NE,NBCON,NLOAD,NMATE,NANIT,NDIM)
39 24 6 7 0 0,3
ITEYL,POSS,E,ANIT
2 0.0D0 1.0D4 0.0D0
NODAL COOR.
1     0.0D0,     0.0D0,8.216D0        2     2.5D1,     0.0D0,6.216D0
3     1.25D1,-2.1650635D1,6.216D0  4   -1.25D1,-2.1650635D1,6.216D0
5     -2.5D1,     0.0D0,6.216D0        6   -1.25D1, 2.1650635D1,6.216D0
7     1.25D1, 2.1650635D1,6.216D0  8  4.330127D1,     -2.5D1,0.0D0
9     0.0D0,     -5.0D1,0.0D0          10 -4.330127D1,     -2.5D1,0.0D0
11 -4.330127D1,     2.5D1,0.0D0    12     0.0D0,     5.0D1,0.0D0
13  4.330127D1,     2.5D1,0.0D0
ELEM. CONN.
 1,1,2   2,1,3  3,1,4   4,1,5   5,1,6    6,1,7
 7,2,3   8,3,4  9,4,5   10,5,6  11,6,7   12,7,2
13,3,8  14,3,9  15,9,4  16,10,4 17,10,5  18,5,11
19,11,6 20,6,12 21,12,7 22,7,13  23,13,2  24,2,8
LOADINGS
1,0.0D0,0.0D0,-0.5D0  2,0.0D0,0.0D0,-1.0D0  3,0.0D0,0.0D0,-1.0D0
4,0.0D0,0.0D0,-1.0D0  5,0.0D0,0.0D0,-1.0D0  6,0.0D0,0.0D0,-1.0D0
7,0.0D0,0.0D0,-1.0D0
BOUNDARY COND.
8,1,1,1  9,1,1,1  10,1,1,1  11,1,1,1  12,1,1,1  13,1,1,1
OUTPUT VARIABLES
1,3
EARTHED SPRING
0
FACI,  NINC,IWRIT,IAUTO,IARC,ILOAD
3.0D0   20 0      1        1    1
IACC,IRES,IBRAC,ICRIT,IBRSW,IROW
0    0    1       1      0       8
ICVCK,BETOK, ITERTY,NITMAX,NLSMX,EPSI,  SHIF
1       1.0D-6  1        40        0       1.0D-3 0.0D0
IDES,FACMX,FACMN,ISWCH,ICORT,IPRED
3      1.0D0 1.0D0    1       0       0
CSTIFFS
0.6D0
DLDES DLMAX DLMIN
0.5d0 1.0d0 0.1d0
```

input datafile for 3D-Truss-Dome
pre-critical solution

Table 22.3 Number of bracketing increments for first bifurcation point (ICRIT = 1) with three-dimensional dome.

Method	Bisection on D_{min}	Interp. on determinant	Interp. on D_{min}	Direct 1	Direct 2
IBRAC	2	3	5	6	−6
No. of increments	9	6	5	4	12 (limit pt)

Table 22.4 Number of bracketing increments for second bifurcation point (ICRIT = 2) with three-dimensional dome.

Method	Bisection on D_{min}	Interp. on determinant	Interp. on D_{min}	Direct 1	Direct 2
IBRAC	2	3	5	6	−6
No. of increments	5	Failed	6	5	12 (limit pt)

In Table 22.3, the number of bracketing increments is given. Here the direct method 2 (with no prior incrementation) iterates on to the limit point rather than the bifurcation point (when k is set to zero. For the same reason, one must ensure that the increment sizes are small enough to avoid an overstepping of two singular points in one increment.

When ICRIT is set to 2, we attempt to bracket the second bifurcation point (which is a double symmetric bifurcation point) and the response is summarised in Table 22.4.

Because of the double nature of the bifurcation point, the interpolation methods are not necessarily always interpolating on to the same (of the two) negative pivots and the interpolation methods turn out to be inferior to the bisection method. Because, for this example, the nullity is even, the determinant does not change sign so that the method using the determinant as the test function (IBRAC = 3) failed.

The performance of the interpolation methods deteriorated even further when we attempted to compute the third bifurcation point. There are now a maximum of five negative pivots and the program found this so confusing that indirect bracketing failed even for pivot-based interpolation. This third bifurcation point (ICRIT = 3) is also 'double in nature' so that determinant-based interpolation again failed. The direct method 2 always converges on the limit point if k in (21.47c) was set to 3. However, if k is set to any other value, we obtain different singular points and, in some cases, the third bifurcation point.

22.3.2 Branch switching

Branch switching at the first (single) bifurcation point is simple (IBRSW = ± 1). However, for the second and third double bifurcation points (IBRSW = ± 3), a lot of

Table 22.5 Branching inputs for three-dimensional dome.

	DLDES (Δl)	ζ_0	ζ_1	ζ_2
First bifurcation pt	2.0	0.0	1.0	0.0
Second bifurcation pt	1.0	0.0	1.0	5.0
	1.0	0.0	0.2	1.0
Third bifurcation pt	1.0	0.1	0.2	1.0
	1.0	0.0	0.1	5.0

'fine tuning' needs to be performed to find the weighting parameters ξ_i's (multiples of the eigenmodes) and step lengths, Δl. In these circumstance, instead of using (21.7) as the predictor, we set:

$$\Delta \mathbf{p}_p = \zeta_o \mathbf{y} + \zeta_1 \mathbf{z}_1 + \zeta_2 \mathbf{z}_2 + \cdots \tag{22.1}$$

with ζ_o, ζ_1, etc. are weighting factors and, following (22.1), $\Delta \mathbf{p}_p$ is then scaled to be of length Δl = DLDES.

For each of the double bifurcation points, two sets of constants are required for the two bifurcated branches. These constants should be added at the end of the REIN file in the form:

```
.....
AMPs FOR MULTIPLE BIFURCATION PUT BELOW: ζ0, ζ1, ζ2 ···
0.0D0   1.0D0   5.0D0
```

The employed constants are given in Table 22.5.

The response in terms of the load against the vertical displacement at the apex is given in Figure 22.8.

22.3.3 The higher-order predictor

We have also used this problem to try out the predictors using higher-order derivatives (Section 21.4). Considering the initial loading of the dome, with IBRAC = 0 (no bracketing), we could apply load control (IARC = 0) with the 'higher-order predictor' (IPRED = 1) via Data File 22.3.3a (only the control section is shown here).

Data file 22.3.3a

```
.....
FACI,  NINC,IWRIT,IAUTO,IARC,ILOAD
 3.0D0   2   0     1      0      1
IACC,IRES,IBRAC,ICRIT,IBRSW,IROW
0     0     0       4      0      8
ICVCK,BETOK, ITERTY,NITMAX,NLSMX,EPSI,  SHIF
1       1.0D-6 1      40    0       1.0D-3        0.0D0
IDES,FACMX,FACMN,ISWCH,ICORT,IPRED
3     1.0D0  1.0D0   1       0      1
```

```
CSTIFFS
0.6D0
DLDES DLMAX DLMIN
0.5d0 1.0d0 0.1d0
```

```
input datafile for 3D-Truss-Dome
        pre-critical solution
```

The conventional (Euler) predictor would be obtained by setting IPRED = 0. For the first step, the convergence history for the latter is given in Table 22.6. In contrast, if we set IPRED = 1, and use the method of Section 21.4, the convergence history is as given in Table 22.7. At the end of the predictor phase (iteration number 0), the higher-order predictor has led to a convergence factor (0.006846) that is significantly smaller than

Table 22.6 Convergence history for first step analysis of a three-dimensional dome using Euler predictor (load control).

Iteration no.	Convergence factor	Total potential energy	Strain energy
0 (predictor)	0.5879E-1	−1.733	1.626
1	0.6324E-3	−1.738	1.801
2	0.2895E-11	−1.738	1.801

Table 22.7 Convergence history for first step analysis of a three-dimensional dome using higher-order predictor (load control).

Iteration no.	Convergence factor	Total potential energy	Strain energy
0 (predictor)	0.6846E-2	−1.738	1.778
1	0.6324E-3	−1.738	1.801
2	0.2895E-11	−1.738	1.801

Table 22.8 Convergence history for first step analysis of a three-dimensional dome using Euler predictor (Arc-length control).

Iteration no.	Convergence factor	Total potential energy	Strain energy
0 (predictor)	0.6531E-1	−2.150	2.002
1	0.4647E-3	−1.922	1.997
2	0.6339E-7	−1.923	1.997

that at the end of the equivalent Euler predictor (0.05879). Instead, we may use arc-length control with the following data file relating to the higher-order predictor.

Data file 22.3.3b

```
.....
FACI,  NINC,IWRIT,IAUTO,IARC,ILOAD
3.0D0   2    0      1      1      1
IACC,IRES,IBRAC,ICRIT,IBRSW,IROW
0   0    1   4    0   8
ICVCK,BETOK, ITERTY,NITMAX,NLSMX,EPSI,  SHIF
1    1.0D-6 1     40    0    1.0D-3 0.0D0
IDES,FACMX,FACMN,ISWCH,ICORT,IPRED
3     1.0D0  1.0D0  0      0      1
DLDES DLMAX DLMIN
0.5d0 1.0d0 0.1d0
CSTIFFS
0.6D0
```

input datafile for 3D-Truss-Dome
pre-critical solution

With the Euler predictor (data as above, but with IPRED = 0), the convergence history is as given in Table 22.8, while with the higher-order predictor, it is as given in Table 22.9. Again, the higher-order predictor leads to a significantly lower convergence factor following the predictor solution.

22.3.4 The higher-order correctors

We have also used this example to apply the higher-order correctors (Section 21.5). Using load-control (IARC = 0), the data for the conventional Newton–Raphson iteration (ICORT = 0) was already given as Data file 22.3.3a and the iterative performance was given in Table 22.6. If we apply the 'explicit higher-order corrector' (see Section 21.5), we require Data file 22.3.4.

Table 22.9 Convergence history for first step analysis of a three-dimensional dome using higher-order predictor (Arc-length control).

Iteration no.	Convergence factor	Total potential energy	Strain energy
0 (predictor)	0.7780-2	−1.930	1.997
1	0.5010E-6	−1.923	1.997

Data file 22.3.4

```
.....
FACI, NINC,IWRIT,IAUTO,IARC,ILOAD
 3.0D0  1  0     1      0     1
IACC,IRES,IBRAC,ICRIT,IBRSW,IROW
 0   0   0   3   0   8
ICVCK,BETOK, ITERTY,NITMAX,NLSMX,EPSI,  SHIF
 1       1.0D-10  1      40    0          1.0D-2 0.0D0
IDES,FACMX,FACMN,ISWCH,ICORT,IPRED
 3     1.0D0 1.0D-1   0       1       0
DLDES DLMAX DLMIN
0.5d0 1.0d0 0.1d0
CSTIFFS
0.6D0
-------------------------------------
input datafile for 3D-Truss-Dome
          pre-critical solution
-------------------------------------
```

Here ICORT = 1 and we have also specified EPSI. This governs the convergence of the inner loop (Section 21.5) which is assumed to have converged when the Euclidean norm of $\delta\mathbf{p}$ from (21.43a) is less than EPSI times the Euclidean norm of $\Delta\mathbf{p}$ from (21.42). The current problems were run with EPSI = 10^{-2}, 10^{-4} and 10^{-6} and it was found that the outer convergence rate was not greatly affected by increasing EPSI above 10^{-2}, even although this led to a greater number of inner iterations. A conventional Euler predictor was used and, with EPSI set to 10^{-2}, only one iteration took place for each outer iteration and the performance of the outer iterations is detailed in Table 22.10.

When ICORT is changed to 2, we introduce the implicit higher-order corrector of Section 21.5. Again EPSI was set to 10^{-2} and there was one inner iteration per outer iteration. Table 22.11 details the convergence characteristics of the outer iteration. There is little difference between the performance of the explicit and implicit methods. However, the reader will find that if the inner loop tolerance (EPSI) is tightened, the implicit method gives a faster convergence rate. However, this is at the cost of significantly more work per inner iteration.

The arc-length method may be introduced by changing IARC to unity. Using the conventional Newton–Raphson method, the input data file has already been given (Data file 22.3.3b) and the convergence characteristics have been detailed in Table 22.8. For the explicit corrector (with ICORT = 1) the convergence characteristics (relating to

Table 22.10 Convergence history for first step analysis of a three-dimensional dome using explicit higher-order corrector (ICORT = 1) (load control).

Iteration no.	Convergence factor	Total potential energy	Strain energy
0 (predictor)	0.5879E-1	−1.733	1.626
1	0.1096E-4	−1.738	1.801
2	0.2899E-13	−1.738	1.801

Table 22.11 Convergence history for first step analysis of a three-dimensional dome using implicit higher-order corrector (ICORT = 2) (load control)

Iteration no.	Convergence factor	Total potential energy	Strain energy
0 (predictor)	0.5879E-1	−1.733	1.626
1	0.5739E-5	−1.738	1.801
2	0.4637E-14	−1.738	1.801

Table 22.12 Convergence history for first step analysis of a three-dimensional dome using explicit higher-order corrector (arc length).

Iteration no.	Convergence factor	Total potential energy	Strain energy
0 (predictor)	0.6531E-1	−2.150	2.002
1	0.1444E-4	−1.932	1.997
2	0.2927E-14	−1.923	1.997

Table 22.13 Convergence history for first step analysis of a three-dimensional dome using implicit higher-order corrector (arc length).

Iteration no.	Convergence factor	Total potential energy	Strain energy
0 (predictor)	0.6531E-1	−2.150	2.002
1	0.1594E-5	−1.923	1.997
2	0.1260E-14	−1.923	1.997

the outer iteration) are given in Table 22.12), while for the implicit corrector (with ICORT = 2), they are given in Table 22.13.

22.3.5 Line searches

Using load control with a very large load increment ($\Delta\lambda$ = FACI = 12), without line-searches (NITMAX = 0), the program fails to converge within the specified maximum number of iterations (15). (The relevant data is on Data File 22.3.5a.) As an exercise, we will introduce line searches, using a very tight tolerance (see the following section from the Data Inut file 22.3.5b).

Data input file 22.3.5b

```
FACI,  NINC,IWRIT,IAUTO,IARC,ILOAD
12.0D0 1  0     1    0   1
IACC,IRES,IBRAC,ICRIT,IBRSW,IROW
 0   0    0   4    0   8
ICVCK,BETOK, ITERTY,NITMAX,NLSMX,EPSI,  SHIF
1    1.0D-4 2     15    15    1.0D-3 0.0D0
IDES,FACMX,FACMN,ISWCH,ICORT,IPRED
3   4.0D0 4.0D0 1     0   0
DLDES DLDMAX DLMIN
0.D0  0.D0  0.D0
PERMLS AMPMX ETMXA ETMNA
0.5D-4  5.0D0  25.D0 0.01D0
CSTIFFS
0.6D0
-------------------------------------
input datafile for 3D-Truss-Dome
        testing of line search
-------------------------------------
```

Table 22.14 Extract of line-search response for analysis of three-dimensional dome (load control).

Line search no.	Potential energy	Strain energy	Energy change ratio	Step length
0	−31.90	39.35	−0.7486	1.0
1	−31.90	39.30	−0.435E-2	0.5719
2	−31.90	39.30	−0.251E-4	0.5694

The program now converges in eight iterations onto a point on the unstable primary path past the first two bifurcation points. To illustrate the line-search characteristics, in Table 22.14 we detail the line-search response for the third iteration.

The energy change ratio in Table 22.14 is $s(\eta)/s(\eta=0)$—see (9.8)–(9.11) and (21.57).

If the cylindrical arc-length method is applied and no line searches are introduced, we merely change IARC in Data File 23.3.5b to 1. This process leads to 13 iterations for convergence. A section of the input file is given below:

Data input file 22.3.5c

```
FACI,  NINC,IWRIT,IAUTO,IARC,ILOAD
12.0D0 1  0     1    1   1
IACC,IRES,IBRAC,ICRIT,IBRSW,IROW
0   0    0   4    0   8
ICVCK,BETOK, ITERTY,NITMAX,NLSMX,EPSI,  SHIF
1    1.0D-4 2     15    0    1.0D-3 0.0D0
IDES,FACMX,FACMN,ISWCH,ICORT,IPRED
3   4.0D0 4.0D0 1     0   0
DLDES DLDMAX DLMIN
0.D0  0.D0  0.D0
```

As an exercise, line searches are introduced with a very tight tolerance (PERMLS = 0.5×10^{-4}) in the Data Input file 22.3.5d of which the section relating to line searches is given below:

Data input file 22.3.5d

```
FACI, NINC,IWRIT,IAUTO,IARC,ILOAD
12.0D0 1  0     1   1   1
IACC,IRES,IBRAC,ICRIT,IBRSW,IROW
0   0    0   4    0   8
ICVCK,BETOK, ITERTY,NITMAX,NLSMX,EPSI,  SHIF
1    1.0D-4 2     15    15    1.0D-3 0.0D0
IDES,FACMX,FACMN,ISWCH,ICORT,IPRED
3    4.0D0 4.0D0 1     0    0
DLDES DLDMAX DLMIN
0.D0  0.D0  0.D0
PERMLS AMPMX ETMXA ETMNA
0.5D-4   5.0D0  25.D0 0.01D0
CSTIFFS
0.6D0
```

The number of iterations is now reduced from 13 to 4, but a lot of extra residual computations are required in relation to the line searches. None the less the exercise does show that the method of Section 21.7.2 will successfully apply the line-search concept. As an illustration, Table 22.15 details the line-search characteristics on the second iteration.

When a 'slack tolerance' is introduced with PERMLS = 0.4 (Data File 22.3.5e), the line searches are more usefully employed with the total number of iterations being five with only three extra residual calculations as a result of the line searches.

Table 22.15 Extract of line-search response for analysis of three-dimensional dome (arc-length control-IARC = 1).

Line search no.	Potential energy	Strain energy	Energy change ratio	Step length
0	−19.99	23.27	−0.5388	1.0
1	−19.99	23.27	0.215E-3	0.6498
2	−19.99	23.27	−0.1076	0.7199
3	−19.99	23.27	−0.213E-1	1.6639
4	−19.99	23.27	−0.409E-2	0.6526
5	−19.99	23.27	−0.647E-3	0.6504
6	−19.99	23.27	−0.234E-9	0.6500

22.4 A THREE-DIMENSIONAL ARCH TRUSS

Figure 22.9 shows the arch truss that has several singular points including four bifurcation points. There is a limit point at $\lambda = 99.26$ and two bifurcation points before the limit point ($\lambda = 12.28$ and $\lambda = 69.13$) and two bifurcation points beyond the limit point ($\lambda = 91.05$ and $\lambda = 22.94$). The computed relationships between the load and the three deflections at one of the top nodes under the vertical loading are shown in Figures 22.10, 22.11 and 22.12 where we have only plotted the post-buckling path for the first bifurcation point beyond the limit point ($\lambda = 91.05$). All of the bifurcation points are 'simple' and, as a result, there are no particular, difficulties either in 'bracketing' or 'branch switching' (except at the last bifurcation point ($\lambda = 22.94$) from where it is difficult to follow the whole secondary path).

As with the previous dome, care must be taken to ensure that the increment size is small enough so that no more than one singular point is passed in one increment. The adopted branching step lengths (Δl = DLDES) for the first three bifurcation points were 1.0, 2.0 and 0.5 respectively.

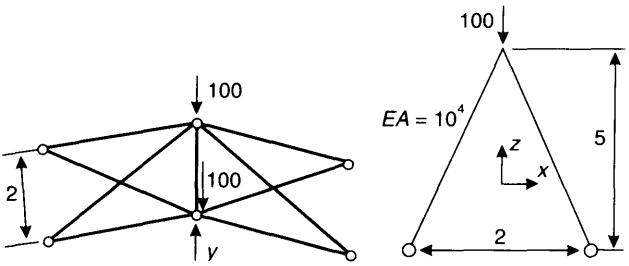

Figure 22.9 Three-dimensional arch truss.

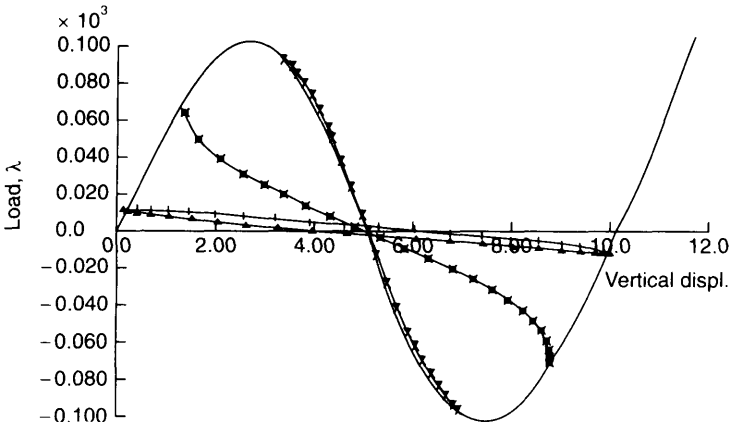

Figure 22.10 Structural response of the three-dimensional arch truss: load versus vertical displacement at the top.

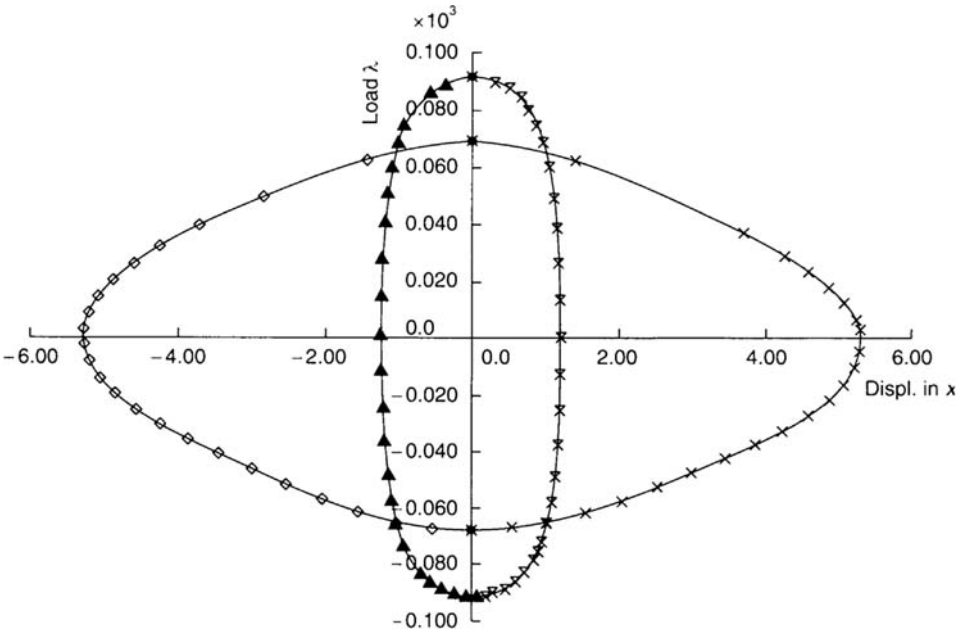

Figure 22.11 Structural response of the three-dimensional arch truss: load versus x displacement at the top.

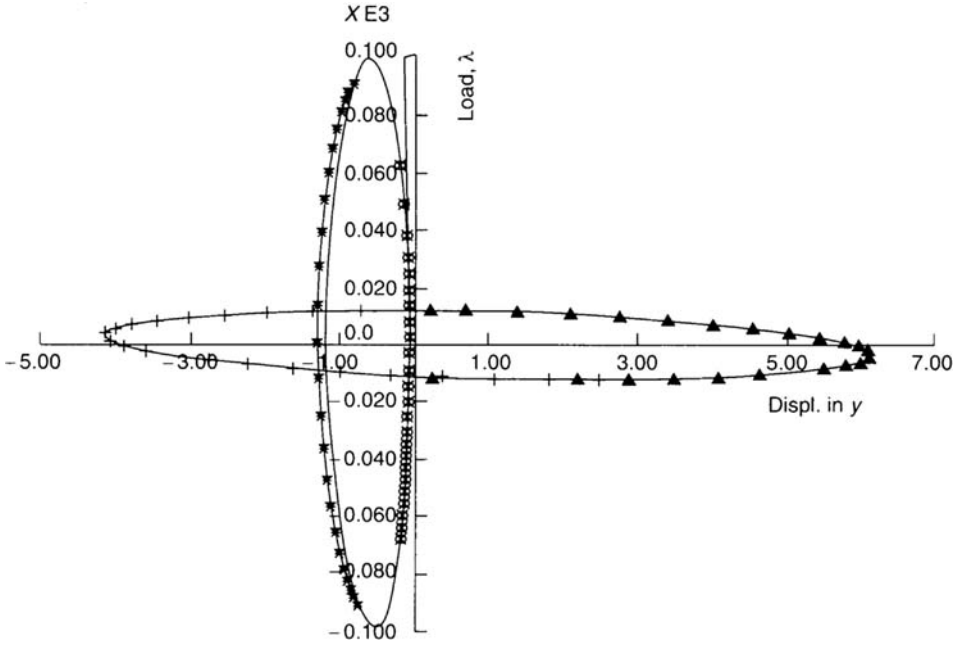

Figure 22.12 Structural response of the three-dimensional arch truss: load versus y displacement at the top.

At the first bifurcation points ($\lambda = 12.28$), the structure buckles in the yz plane (Figure 22.12) with no displacements in the x-direction: at the second ($\lambda = 69.13$) and third ($\lambda = 99.105$) bifurcation points, it buckles in the xz plane (Figure 22.11) so that the y-displacements are symmetric at the top nodes. In understanding Figures 22.11 and 22.12, it is worth noting that there are no x-direction displacements on the primary path while there are equivalent (non-linear) y-displacements.

A data file for 'bracketing' on to the first bifurcation point is given below:

Input data file 22.4a

```
ANALYSIS THREE DIMENSIONAL
1
GENERAL DATA (NV,NE,NBCON,NLOAD,NMATE,NANIT,NDIM)
18 9 4 2 0 0 3
ITEYL,POSS,E,ANIT
2 0.0D0 1.0D4 0.0D0
NODAL COOR.
 1,-2.0D0,0.0D0,0.0D0  2,0.0D0,0.0D0,5.0D0  3,2.0D0,0.0D0,0.0D0
 4,-2.0D0,2.0D0,0.0D0  5,0.0D0,2.0D0,5.0D0  6,2.0D0,2.0D0,0.0D0
ELEM. CONN.
 1,1,2  2,2,3  3,1,5  4,2,4  5,2,5  6,2,6  7,3,5  8,4,5  9,5,6
LOADINGS
 2,0.0D0,0.0D0,-1.0D2  5,0.0D0,0.0D0,-1.0D2
BOUNDARY COND.
 1,1,1,1  3,1,1,1  4,1,1,1  6,1,1,1
OUTPUT VARIABLES
 6,4,5,6,13,14,15
EARTHED SPRING
0
FACI, NINC,IWRIT,IAUTO,IARC,ILOAD
2.0D0 300 0     1     0     1
IACC,IRES,IBRAC,ICRIT,IBRSW,IROW
0     0     1    1     0     0
ICVCK,BETOK, ITERTY,NITMAX,NLSMX,EPSI, SHIF
1     1.0D-6  1     10     0     1.0D-5 5.0D0
IDES,FACMX,FACMN,ISWCH,ICORT,IPRED
1    1.0D1  1.0D0  1     0     ,0
CSTIFFS
0.7D0
```

input datafile for 3D-Truss-Arch

22.5 A TWO-DIMENSIONAL CIRCULAR ARCH

The arch is shown in Figure 22.13 with the response in Figure 22.14. The data to follow the unstable primary path is given in Input Data file 22.5a, while that to bracket on the bifurcation point (ICRIT = 1, $\lambda = 6.29$) is given in Input Data file 22.5b. The final set of data in Data Input file 22.5c relates to the 'branch switching'. In contrast to the response of the von Mises truss (Section 22.2), the current secondary paths do not rejoin the primary path.

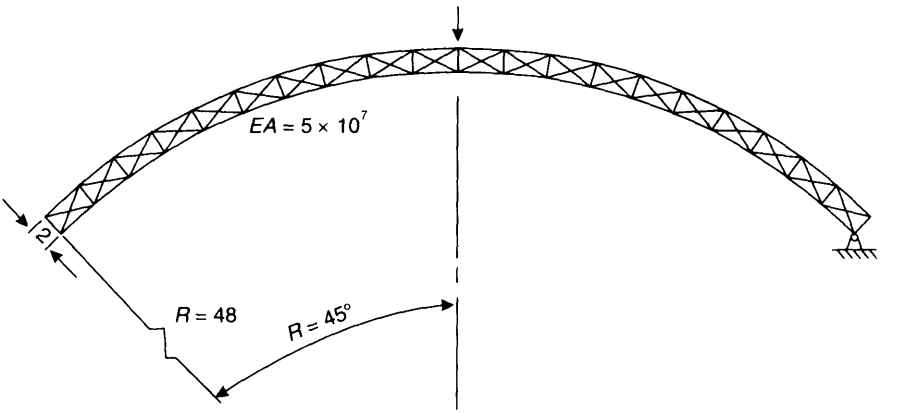

Figure 22.13 A two-dimensional circular arch.

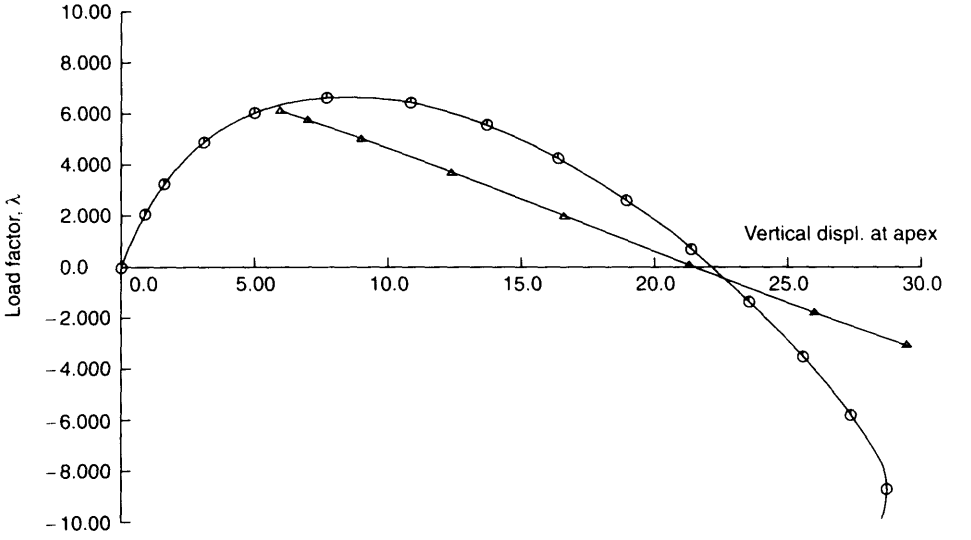

Figure 22.14 Structural response of the two-dimensional arch: load versus vertical displacement at the apex.

Truncated data input file 22.5b

```
ANALYSIS TWO DIMENSIONAL
 1
 GENERAL DATA (NV,NE,NBCON,NLOAD,NMATE,NANIT,NDIM)
          84 101 2   1    0    0    2
 ITEYL,POSS,E,ANIT
 2 0.0D0 5.0D7 0.0D0
 NODAL COOR.
              1  -33.9400       33.9400
              2  -35.3500       35.3500
             42   35.3500       35.3500
             41   33.9400       33.9400
              4  -32.4675       38.0146
              6  -29.3848       40.4447
              8  -26.1210       42.6256
             10  -22.6961       44.5436
             12  -19.1313       46.1870
             14  -15.4485       47.5456
             16  -11.6705       48.6112
             18  -7.82054       49.3770
             20  -3.92236       49.8383
             22  0.000000E+00   49.9924
             24   3.92236       49.8383
              "
              "
              "

 ELEM CONNECTION
        1      1      2
        6      3      4
       11      5      6
       16      7      8
       21      9     10
       26     11     12
       31     13     14
       36     15     16
       41     17     18
       46     19     20
       51     21     22
       56     23     24
       61     25     26
       66     27     28
       71     29     30
       76     31     32
       81     33     34
        "
        "
        "
       65     26     28
       70     28     30
       75     30     32
       80     32     34
       85     34     36
       90     36     38
       95     38     40
      100     40     42
```

```
LOADINGS
22  0.0D0 -1.0D5
BOUNDARY CONDITION
1  1  1      41  1  1
OUTPUT VARIABLES
2,43,44
EARTHED SPRINGS
0
FACI,NINC,IWRIT,IAUTO,IARC,ILOAD
0.5D0  100 0    1     0 1
IACC,IRES,IBRAC,ICRIT,IBRSW,IROW
0     0      -6      1      0       ,8
ICVCK,BETOK, ITERTY,NITMAX,NLSMX,EPSI, SHIF
1       1.0D-6 1          20     0  1.0D-4  1.0D2
IDES,FACMX,FACMN,ISWCH ICORT,IPRED
4   0.5D0 0.5D0 1       0  0
CSTIFF
0.2D0
DLDES,DLMAX,DLMIN
1.0D1,1.0D2,1.0D0
CSTIFS
0.8D0
```

input datafile for an 90 degrees' arch of radius 50

22.6 REFERENCES

[F1] Fujii, F. & Choong, K. K., Branch switching in simple spatial bifurcation models, *J. Engng. Mech. Div., ASCE*, 118 (1992).

[P1] Pecknold, A., Ghaboussi, J. & Healey, T. J., Snap-through and bifurcation in simple structures, *J. or Engng. Mech.*, **111**, 909–922 (1985).

23 Contact with friction

23.1 INTRODUCTION

Overview and review paper on contact have been given by Oden and Martins [O1] and Zong and Mackerle [Z3]. Early work [H5, B1, C2, F3] was largely related to a linear geometry and often involved node-to-node contact. Once significant non-linear contact deformations were introduced, methods tended to switch to node-on-segment or node-on surface contact [see, for example, H1–H3, J1, P3, W1]. Many of the latter methods directly involved nodal forces although it is possible to introduce contact pressure [S2, L1].

Two main methods of solution have been adopted; the penalty approach [P4, H1–H4, C5, M2, P1, W2] and the method of Lagrangian multipliers, see, for example [C3, G1, M2]. The former is closely related to techniques which attempt to introduce a genuine (although high and possibly non-linear) stiffness for the contact region [C4, K2, W5]. Thermomechanical coupling may then be involved [Z1]. One alternative procedure involves the elimination of degrees of freedom and can be considered as a form of non-linear master slave approach (see [J2.17] and Section 17.6).

There are important links between the finite element contact problem and mathematical programming techniques for constrained optimisation [F1, L4, V1]. Indeed, because the problems usually involves inequality constraints (varying contact areas), the mathematics can be related to the method of variational inequalities [K1]. However, in practice, the method is often treated using the engineering equivalent of the active set method [F1, L4, V1] whereby equality constraints are applied within the (changing) 'active set'. Many concepts from the mathematical programing literature have been incorporated within finite element algorithms—in particular the augmented Lagrangian technique [L1, L3, S1, W2, H4]. Other procedures such as the perturbed Lagrangian method [J1, S2] and a form of barrier method [Z2] can also be applied.

Within a finite element context, one of the most important recent developments has involve the 'consistent linearisation' of the changing geometrical contact relationships, see, for example, [W1, P3]. The latter has also been applied to friction [G2, L2, W5] often with the aid of a plasticity technique which follows from the observation of the close links between friction and plasticity made by Michalowski and Mroz [M2]. The resulting algorithm takes a very similar form to the procedures already discussed in Chapters 6, 14 and 15 although, generally, a non-associative flow rule is introduced [M1] so that the tangent stiffness matrix is non-symmetric.

Within a general non-linear finite element context, important issues are associated with contact detection [B2, H1–H3, O2]. The latter is simpler with lower order

elements and, partially for this reason these lower-order elements are still very popular and will be considered in the current chapter (although many of the concepts are more general). In a contact environment, there are clearly problems with lower-order faceted geometric approximations and, among others, Eterovic and Bathe [E1] have looked at higher-order interpolations aimed at introducing the necessary continuity for general quadratic convergence. (In this context, we should stress the importance of line searches in the early iterations which are inevitably non-smooth.)

Many of the lower-order contact formulations have origins in the non-linear 'slide-line procedure' pioneered by Hallquist *et al.* [H1–H3] (following on from linear geometric work by Chan and Tuba [C2]). In relation to these techniques, important issues are associated with the use of a one-pass or two-pass algorithm. In particular, Taylor and Papadopoulos have shown [T2] that a two-pass formulation is essential if the 'contact path test' (see Section 23.3) is to be passed. (A related, more general procedure, has been proposed by Papadopoulos *et al.* [P2]).

Although the previous discussion has been largely directed at implicit finite element codes, many of the issues (but clearly not the consistent linearisation) are common to explicit dynamic techniques. Additional special procedures have been developed for the latter [B2, C1, H1–H3, T1], including momentum-related techniques in which modifications are made to the accelerations, velocities and displacements, see [T1]. One of the aims of the latter, is to avoid the penalising effect on the time step of the explicit procedure which can be introduced by the high stiffnesses associated with penalty approaches.

In the present chapter, we will concentrate on the penalty approach, the Lagrangian multiplier approach and the augmented Lagrangian procedure. Both frictionless and frictional contact will be considered. For the latter, with 'sliding friction', we will describe a simple Coulomb friction technique which will be set within a 'plasticity framework'. Consistent tangent matrices will be derived. In the final two sections of the chapter, we will consider a modified penalty/barrier approach [Z2] and, in addition, will consider some possible modifications to the line-search and arc-length methods that are specifically geared towards contact.

23.2 A TWO-DIMENSIONAL FRICTIONLESS CONTACT FORMULATION USING A PENALTY APPROACH

For linear problems, penalty approaches conventionally lead to rank-one updates of the stiffness matrix [H5, O1]. However, for geometrically non-linear problems, a consistent approach should account for the change of geometry. In the two-dimensional case, such a formulations can be simply expressed in a co-rotational framework, with the contact zone (or element) rotating and translating and hence producing a local frame with respect to which the contact and friction relationships can be expressed. As with the co-rotational elements of Sections 7.2 and 7.3, the formulations then depend heavily on the variations of the base vectors that define the rotating element-frame. Consequently, we will adopt the earlier notation with the unit vector, $\mathbf{e}_1$, lying along the rotating tangent to the contact 'element' and the unit vector, $\mathbf{e}_2$, lying in the normal direction (Figure 23.1) so that:

$$\mathbf{e}_1^{\mathrm{T}} = (\cos\beta, \sin\beta); \qquad \mathbf{e}_2 = (-\sin\beta, \cos\beta) \tag{23.1}$$

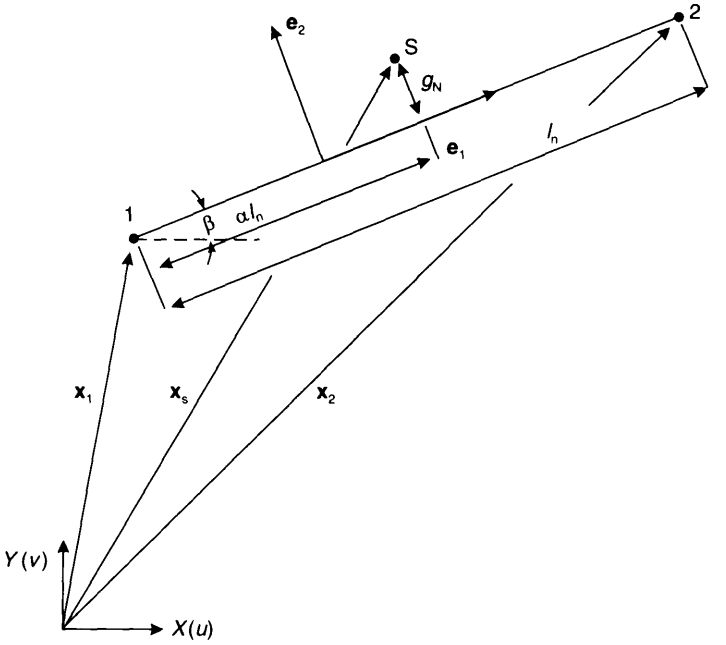

Figure 23.1 Two-dimensional 'contact element'

The contact element will take the form proposed by Hallquist [H1–H3] which involves a 'master' segment (with nodes 1 and 2) and a 'slave', impactor node (with node s). One may either adopt a 'one-pass' procedure or a 'two-pass' approach with the definition of master and slave being reversed for the second pass along the 'slide line' (or potential contact region). Here, we will concentrate on the single-pass procedure and will consider the two-pass technique as a fairly straightforward extension which will be discussed in more detail in Section 23.3. In the present section, we will consider normal contact with the tangential movement being considered as free (frictionless).

As a starting-point, we must define the normal gap, g_N (because there is a danger of a conflict of notation with our usual use of $\mathbf{g}$ for the residual vector, we are using an italic g for the 'gap'). From Figure 23.1, the gap is given by

$$g_N = (\mathbf{x}_s - \mathbf{x}_1)^T \mathbf{e}_2 = \mathbf{x}_{s1}^T \mathbf{e}_2 \tag{23.2}$$

which is negative with penetration and for the situation depicted in the figure there is a positive gap with no penetration.

The following developments could be introduced by starting form an energy functional (see Section 23.2.1) but, instead, we will here employ a virtual work approach. Following the previous work on co-rotational formulations, we require the relationship between the changes in the local variable (here g_N) and the changes in the global variables. The latter are given by

$$\mathbf{p}^T = (\mathbf{d}_s^T, \mathbf{d}_1^T, \mathbf{d}_2^T) \tag{23.3}$$

with, for example, $\mathbf{d}_1^T = (u_1, w_1)$. To obtain the change in g_N (see (23.2)), we require $\delta \mathbf{e}_2$.

Using the approach of Section 7.2.3, the latter is given by

$$\delta \mathbf{e}_2 = \begin{pmatrix} -\cos\beta \\ -\sin\beta \end{pmatrix} \delta\beta = -\frac{1}{l_n}\mathbf{e}_1\mathbf{e}_2^{\mathrm{T}}\delta\mathbf{d}_{21} = \frac{1}{l_n}\mathbf{e}_1\mathbf{b}^{\mathrm{T}}\delta\mathbf{p} \tag{23.4}$$

with

$$\mathbf{b}^{\mathrm{T}} = (\mathbf{0}^{\mathrm{T}}, \mathbf{e}_2^{\mathrm{T}} - \mathbf{e}_2^{\mathrm{T}}) \tag{23.5}$$

so that in (23.2):

$$\delta g_{\mathrm{N}} = \delta\mathbf{d}_{s1}^{\mathrm{T}}\mathbf{e}_2 + \mathbf{x}_{s1}^{\mathrm{T}}\delta\mathbf{e}_2 = \mathbf{a}^{\mathrm{T}}\delta\mathbf{p} \tag{23.6}$$

with

$$\mathbf{a}^{\mathrm{T}} = (\mathbf{e}_2^{\mathrm{T}}, -(1-\alpha)\mathbf{e}_2^{\mathrm{T}}, -\alpha\mathbf{e}_2^{\mathrm{T}}) \tag{23.7}$$

and

$$\alpha = \frac{1}{l_n}\mathbf{x}_{s1}^{\mathrm{T}}\mathbf{e}_1 \tag{23.8}$$

where l_n is the current length between nodes 1 and 2 (as in previous work on trusses and beams). From Figure 23.1, α can be interpreted as the non-dimensional tangential distance between node 1 and the projection of the contact node, s, on to $\mathbf{e}_1$. If the contact force is t_{N} (negative with penetration and zero otherwise), in relation to the nodes associated with the contact element, the virtual work is given by

$$V = V_{\mathrm{b}} + V_{\mathrm{c}} = V_{\mathrm{b}} + t_{\mathrm{N}}\delta g_{\mathrm{N}} = \mathbf{q}_{\mathrm{ib}}^{\mathrm{T}}\delta\mathbf{p} + \mathbf{q}_{\mathrm{ic}}^{\mathrm{T}}\delta\mathbf{p} = \mathbf{g}^{\mathrm{T}}\delta\mathbf{p} \tag{23.9}$$

where the subscript b relates to the two surrounding non-contact elements and the subscript c relastes to the contact element. (To avoid cluttering the subscript v for virtual has been omitted). The vector $\mathbf{q}_{\mathrm{ib}}$ is the standard internal force vector derived from the non-contact elements for nodes 1 and 2 for the master body and for node s for the slave body. For simplicity, it has been assumed in (23.9) that there are no external forces applied in the contact area.

The current objective is to find $\mathbf{q}_{\mathrm{ic}}$ which, via (23.6) and (23.9), is given by

$$\mathbf{q}_{\mathrm{ic}} = t_{\mathrm{N}}\mathbf{a} \tag{23.10}$$

With a conventional penalty approach, to complete the procedure, we would stipulate that:

$$t_{\mathrm{N}} = \varepsilon_{\mathrm{N}} g_{\mathrm{N}}; \qquad g_{\mathrm{N}} < 0 \tag{23.11a}$$

$$t_{\mathrm{N}} = 0, \qquad g_{\mathrm{N}} \geqslant 0 \tag{23.11b}$$

The positive scalar ε_{N} can either be interpreted as the penalty parameter or as the elastic stiffness of the contact area.

We now require the contribution to the tangent stiffness matrix that stems from the variation of (23.10). The latter is given by

$$\begin{aligned} \delta\mathbf{q}_{\mathrm{ic}} &= \mathbf{K}_{\mathrm{tc}}\delta\mathbf{p} = \delta t_{\mathrm{N}}\mathbf{a} + t_{\mathrm{N}}\delta\mathbf{a} = \varepsilon_{\mathrm{N}}\mathbf{a}\mathbf{a}^{\mathrm{T}}\delta\mathbf{p} + \mathbf{K}_{\mathrm{tc}\sigma}\delta\mathbf{p} \\ &= [\mathbf{K}_{\mathrm{tc1}} + \mathbf{K}_{\mathrm{tc}\sigma}]\delta\mathbf{p} \end{aligned} \tag{23.12}$$

where the matrix $\mathbf{K}_{\mathrm{tc}\sigma}$ can be interpreted as the initial stress matrix for the contact element. The term $\mathbf{K}_{\mathrm{tc1}}$ in (23.12) is the conventional linear rank-one contact stiffness.

With a view to the computation of the initial stress matrix, we use:

$$\delta \mathbf{e}_1 = \begin{pmatrix} -\sin\beta \\ \cos\beta \end{pmatrix} \delta\beta = \frac{1}{l_n} \mathbf{e}_2 \mathbf{e}_2^{\mathrm{T}} \delta \mathbf{d}_{21} = -\frac{1}{l_n} \mathbf{e}_2 \mathbf{b}^{\mathrm{T}} \delta \mathbf{p} \tag{23.13}$$

and (see Section 7.2.3):

$$\delta l_n = \mathbf{e}_1^{\mathrm{T}} \delta \mathbf{d}_{21} = -(\mathbf{0}^{\mathrm{T}}, \mathbf{e}_1^{\mathrm{T}}, -\mathbf{e}_1^{\mathrm{T}}) \delta \mathbf{p} = -\mathbf{b}_1^{\mathrm{T}}, \delta \mathbf{p} \tag{23.14}$$

so that the variation of the scalar α in (23.8) is given by

$$\delta\alpha = \frac{1}{l_n}(\mathbf{e}_1^{\mathrm{T}} \delta \mathbf{d}_{s1} - \alpha \mathbf{e}_1^{\mathrm{T}} \delta \mathbf{d}_{21}) + \frac{1}{l_n} \mathbf{x}_{s1}^{\mathrm{T}} \delta \mathbf{e}_1 = \frac{1}{l_n} \mathbf{c}^{\mathrm{T}} \delta \mathbf{p} - g_N \frac{1}{l_n^2} \mathbf{b}^{\mathrm{T}} \delta \mathbf{p} \tag{23.15}$$

with

$$\mathbf{c}^{\mathrm{T}} = (\mathbf{e}_1^{\mathrm{T}}, -(1-\alpha)\mathbf{e}_1^{\mathrm{T}}, -\alpha \mathbf{e}_1^{\mathrm{T}}) \tag{23.16}$$

Using (23.4) and (23.15), the variation of the vector $\mathbf{a}$ in (23.7) is given by

$$\delta \mathbf{a} = \frac{1}{l_n}[\mathbf{b}\mathbf{c}^{\mathrm{T}} + \mathbf{c}\mathbf{b}^{\mathrm{T}} - (g_N/l_n)\mathbf{b}\mathbf{b}^{\mathrm{T}}] \delta \mathbf{p} \tag{23.17}$$

and hence the initial stress matrix, $\mathbf{K}_{tc\sigma}$, in (23.12) is given by

$$\mathbf{K}_{tc\sigma}(t_N) = t_N \delta \mathbf{p} = \frac{t_N}{l_n}[\mathbf{b}\mathbf{c}^{\mathrm{T}} + \mathbf{c}\mathbf{b}^{\mathrm{T}} - (g_N/l_n)\mathbf{b}\mathbf{b}^{\mathrm{T}}] \delta \mathbf{p} \tag{23.18}$$

(The term t_N has been added in brackets to distinguish this term from a later term that will be derived for 'sticking friction' in Section 23.4.) Equation (23.18) agrees with the expression given by Wriggers and Simo [W1], although the derivation is different.

23.2.1 Some modifications

Some codes modify the previous formulation by making the stiffness parameter ε_N vary linearly between given nodal values. (Thereby aiming to reduce the jump in contact force as the contact point crosses a node and moves from one master element to another.) More detail regarding the contcact stiffness will be given in Section 23.7. For the present we will assume that:

$$\varepsilon_N(\alpha) = (1-\alpha)\varepsilon_1 + \alpha\varepsilon_2 = \varepsilon_1 + (\varepsilon_2 - \varepsilon_1)\alpha = \varepsilon_1 + \varepsilon_{21}\alpha \tag{23.19}$$

where α is the non-dimensional length parameter defined in (23.8). At a first inspection, one might simply introduce the modification by directly using the internal force vector of (23.10) with the contact force t_N now taking the form of (23.11) with $\varepsilon_N(\alpha)$ from (23.19) instead of the previous ε_N. However, the resulting formulation does not lead to a symmetric tangent stiffness matrix. With a view to achieving the latter, it is useful to start from an expression for the total potential energy whereby:

$$\phi = \phi_b + \tfrac{1}{2}\varepsilon_N(\alpha) g_N^2 = \phi_b + \varphi_c \tag{23.20}$$

where we have added the strain energy in the contact element, φ_c. Using (23.20), we can write:

$$\mathbf{q}_{ic} = \frac{\partial \varphi_c}{\partial \mathbf{p}} = \varepsilon_N(\alpha) g_N \frac{\partial g_N}{\partial \mathbf{p}} + \frac{1}{2} g_N^2 \varepsilon_{21} \frac{\partial \alpha}{\partial \mathbf{p}} \tag{23.21}$$

Using (23.6) and (23.15), we obtain:

$$\mathbf{q}_{ic} = \varepsilon_N(\alpha) g_N \mathbf{a} + \tfrac{1}{2} g_N^2 \varepsilon_{21} \left(\frac{1}{l_n} \mathbf{c} - \frac{g_N}{l_n} \mathbf{b} \right) \tag{23.22}$$

where **a**, **b** and **c** have already been defined in (23.7), (23.5) and (23.16) respectively. Apply variations to (23.22) leads [A1] to the tangent stiffness matrix:

$$\mathbf{K}_{tc} = \mathbf{K}_{tc1} + \mathbf{K}_{tc\sigma} + \mathbf{K}_{tc2} \tag{23.23}$$

where $\mathbf{K}_{tc1}$ is as previously defined in (23.12) (with $\varepsilon_N(\alpha)$ instead of ε_N) and $\mathbf{K}_{tc\sigma}$ is as previously defined in (23.18) while the new matrix $\mathbf{K}_{tc2}$ is given by [A1]

$$\begin{aligned} \mathbf{K}_{tc2} = {} & \varepsilon_{21} \left(\frac{g_N}{l_n} \right) [\mathbf{a}\mathbf{c}^T + \mathbf{c}\mathbf{a}^T] \\ & + \frac{\varepsilon_{21}}{2} \left(\frac{g_N}{l_n} \right)^2 \Big[-3\mathbf{a}\mathbf{b}^T - 3\mathbf{b}\mathbf{a}^T + 2\mathbf{c}\mathbf{b}_1^T \\ & + 2\mathbf{b}_1\mathbf{c}^T - 2 \left(\frac{g_N}{l_n} \right) [\mathbf{b}\mathbf{b}_1^T + \mathbf{b}_1\mathbf{b}^T] \Big] \end{aligned} \tag{23.24}$$

All of the vectors on right-hand side of (23.24) have been defined in the previous section.

Some detail has not yet been considered. This includes the numerical treatment of the corner region (see Figure 23.2). THe latter could be handled in a very similar manner to the 'two-vector return' used in plasticity (see Section 14.3 and Figure 14.6). Alternatively, in an approximate manned, one could apply an effective normal vector, $\mathbf{e}_2$ (Figure 23.1), which includes a contribution from the adjacent element as the corner is approached. However, as discussed earlier, the corner regions are always likely to introduce problems with a 'faceted dealisation'.

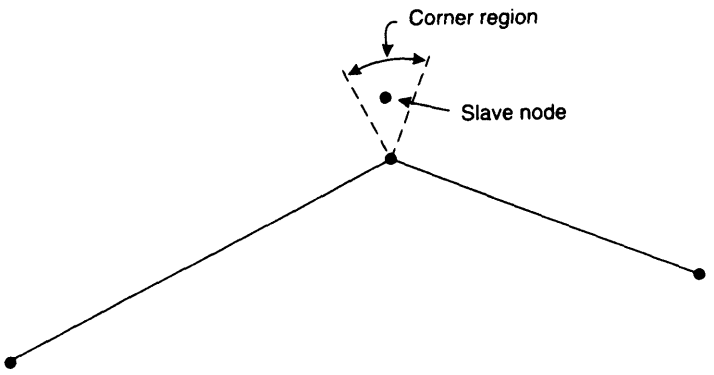

Figure 23.2 The 'corner-region'.

23.3 THE 'CONTACT PATCH TEST'

Taylor and Papadopoulos [T2] described a contact patch test which is illustrated in Figure 23.3. A uniform pressure is applied along the top surface with a frictionless interface being assumed between the two bodies. Irrespective of the mesh, we should obtain a uniform stress state. If the penalty approach of the Section 23.2 is applied, this will be true as the penalty stiffness parameter ε tends to infinity. (We can overcome this limitation by using the Lagrangian multiplier or the augmented Lagrangian technique which will be described in Sections 23.6 and (23.7.)

In the following (more details is given in [A1]), a linear formulation will be adopted and we will apply the previous penalty method using both single- and double-pass strategies. In relation to Figures 23.3 and 23.4, only the vertical forces need be considered and in these circumstances, from (23.10), the internal forces in the contact

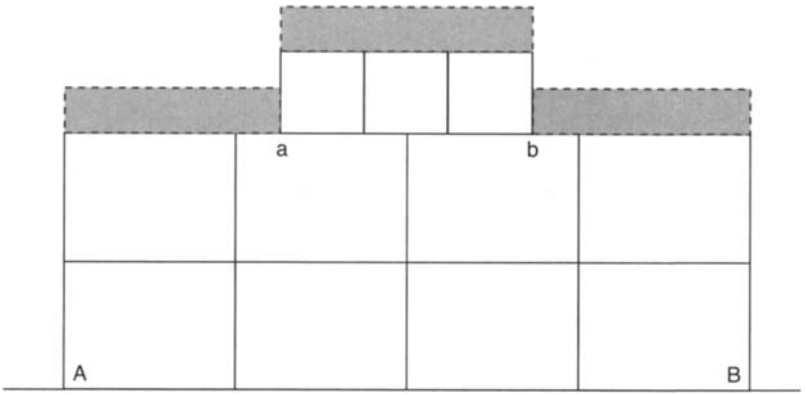

Figure 23.3 The 'contact patch test'.

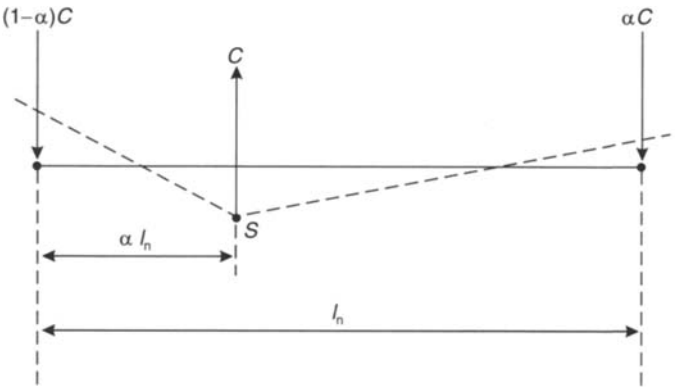

Figure 23.4 Contact internal forces.

element are given by

$$\mathbf{q}_i = \begin{bmatrix} q_{is} \\ q_{i1} \\ q_{i2} \end{bmatrix} = t_N \begin{bmatrix} 1 \\ \alpha - 1 \\ -\alpha \end{bmatrix} = \varepsilon g \begin{bmatrix} 1 \\ \alpha - 1 \\ -\alpha \end{bmatrix} = -C \begin{bmatrix} 1 \\ \alpha - 1 \\ -\alpha \end{bmatrix} \tag{23.25}$$

where we assume a negative gap (and hence penetration) with C as a positive force (Figure 23.4). The forces in (23.25) could, of course, have been obtained by simple statics.

We will now consider the application of uniform pressure to the mesh illustrated in Figure 23.5. The work-consistent external forces are given in Figure 23.5a while,

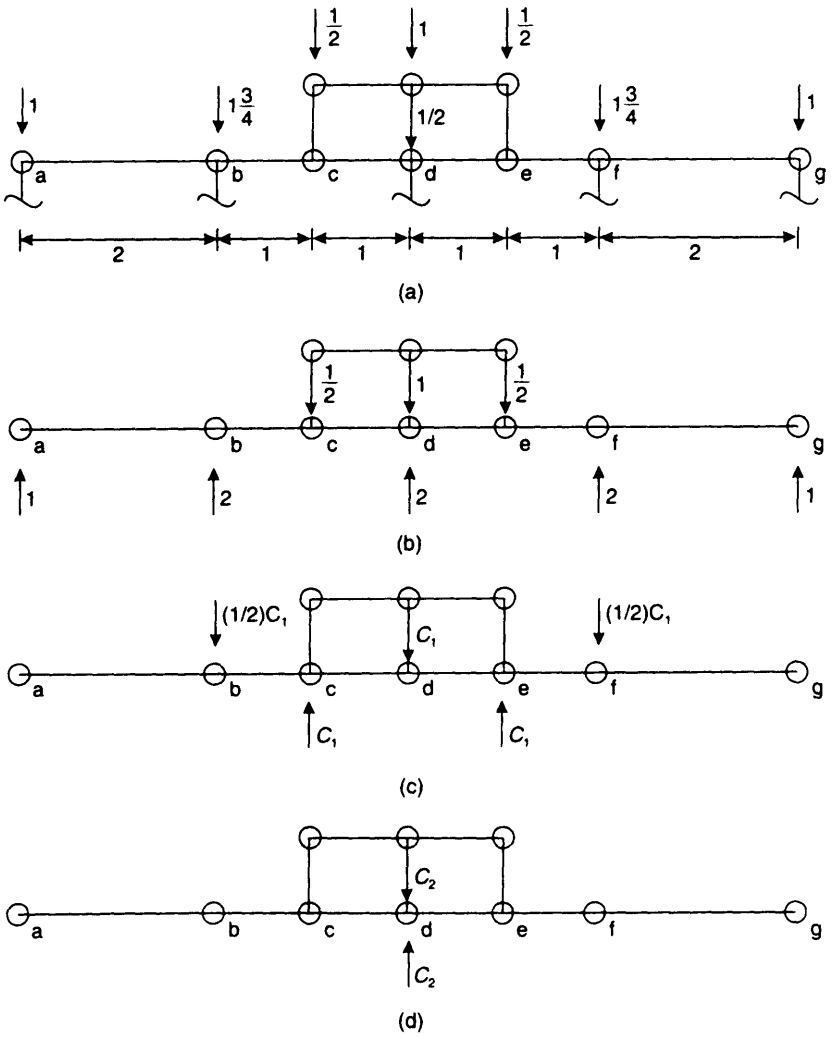

Figure 23.5 (a) External forces: (b) internal forces for non-contact elements; (c) one-pass solution—small surface into large surface—internal forces; (d) one-pass solution—large surface into small surface—internal forces.

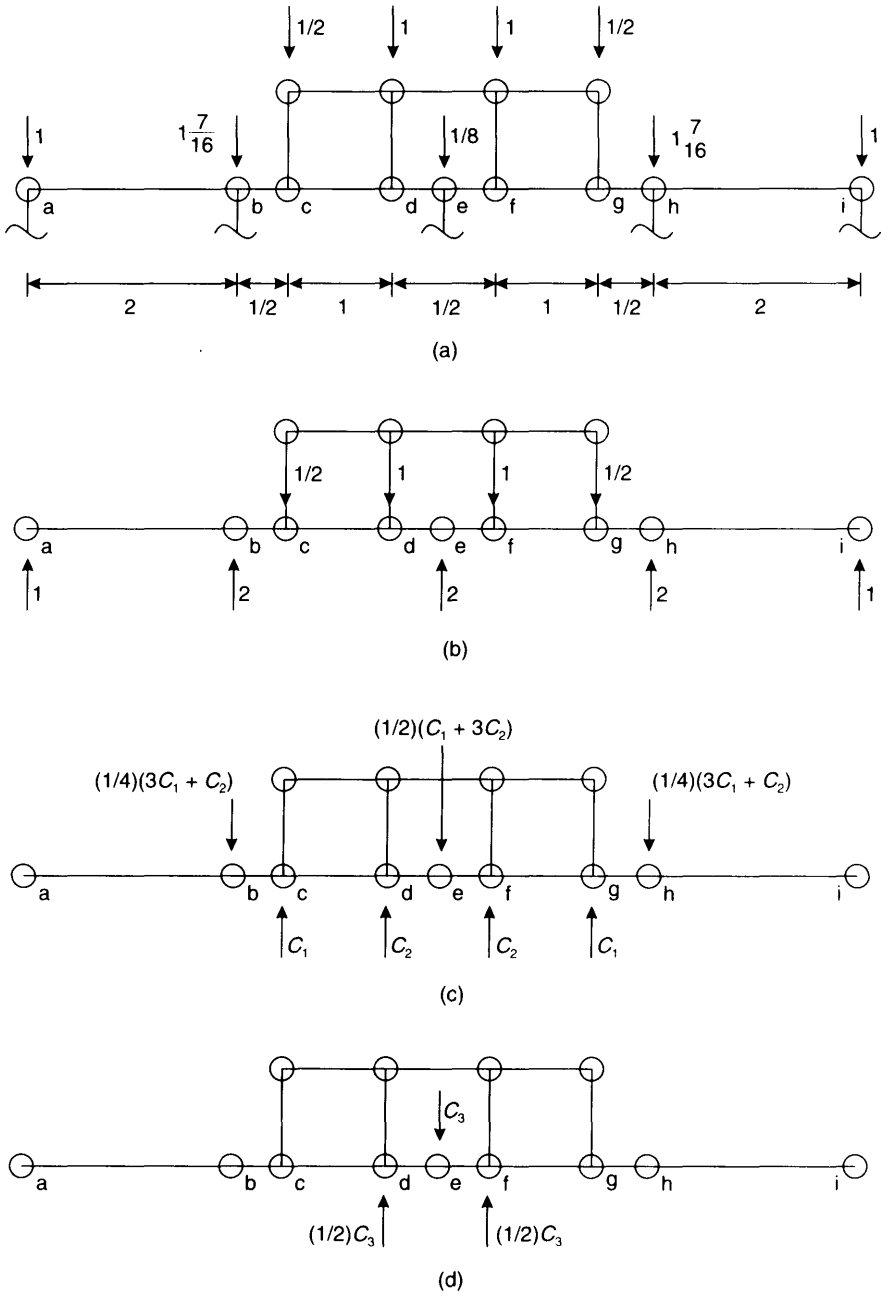

Figure 23.6 (a) External forces; (b) internal forces for non-contact elements: (c) one-pass solution—small surface into large surface—internal forces; (d) one-pass solution—large surface into small surface—internal forces.

assuming the desired solution of a uniform pressure within each parent element, the internal forces for the non-contact elements are illustrated in Figure 23.5b. Suppose we now introduce a single-pass penalty procedure with the large body as the master. In these circumstances, we have two contact elements (*bcd* and *def* in Figure 23.5a) and, using (23.25) the internal forces from the contact elements are as shown in Figure 23.5c where we have used C_1 for the force C in (23.25). (We could also consider node d as penetrating either element *bcd* or element *def* but, in either case this would lead to self-equilibrating forces at node d.) Clearly, if $C_1 = 1/2$, the combination of forces from Figures 23.5a,23.5b and 23.5c is in equilibrium.

Suppose we now consider the small body as the master body. In these circumstances, we have one contact element (either *cd* or *de* in Fig. 23.5a) and the internal forces are as shown in Figure 23.5d. It is now impossible to obtain an equilibrium solution by combining the forces from Figures 23.5a and 23.5b with those from Figure 23.5d. (This is not to say that the single-pass algorithm does not lead to equilibrium but rather that equilibrium is incompatible with a solution that correctly gives a uniform stress state.) However, the two-pass algorithm which combines Figure 23.5a, 23.5b, 23.5c and 23.5d will give equilibrium with $C_1 = 1/2$ and C_2 taking any value.

Now consider the mesh in Figure 23.6, for which the applied external forces are given in Figure 23.6a and the internal forces from the non-contact elements are as illustrated in Figure 23.6b. With the large body as the master body, we have four contact elements (*bce*, *bde*, *efh*, *egh* in Figure 23.6a). Using (23.25), the internal forces are as illustrated in Figure 23.6c (with C_1 relating to elements *bce* and *egh* and C_2 relating to elements *bde* and *efh*). It is impossible to choose values for C_1 and C_2 so that the combination of the forces in Figures 23.6a, 23.6b and 23.6c leads to equilibrium.

If we now take the small body as the master body, we have one contact element (*def* in Figure 23.6a) and, using (23.26), we arrive at the internal forces in Figure 23.6d. Again, the resulting one-pass algorithm cannot lead to equilibrium. However, if we combine the forces from all of the figures (as in a two-pass algorithm) we can obtain equilibrium with $C_1 = 1/2$, $C_2 = 3/4$ and $C_3 = 1/2$.

23.4 INTRODUCING 'STICKING FRICTION' IN TWO DIMENSIONS

A very similar procedure can be applied, for sticking friction, as has already been applied in Section 23.2 for normal contact. In this case, in place of (23.2), the *tangential* gap is defined (Figure 23.7) via:

$$g_T = \alpha l_o - \alpha_o l_o = \frac{l_o}{l_n}\mathbf{x}_{s1}^T \mathbf{e}_1 - \alpha_o l_o \tag{23.26}$$

where α_o is the value of the non-dimensional length parameter, α (see (23.8) and Figures 23.1 and 23.7) when the current phase of contact was first activated. One might think of defining g_T differently with l_n replacing l_o in (23.6). However, it turns out that the resulting tangent stiffness matrix is then non-symmetric.

With the aid of (23.15), we can now write:

$$\delta g_T = \frac{l_o}{l_n}\mathbf{e}_1^T \delta \mathbf{d}_{s1} - \alpha(\mathbf{e}_1^T \delta \mathbf{d}_{21}) + \frac{l_o}{l_n}\mathbf{x}_{s1}^T \delta \mathbf{e}_1 = \frac{l_o}{l_n}\mathbf{c}^T \delta \mathbf{p} - g_N \frac{l_o}{l_n^2}\mathbf{b}^T \delta \mathbf{p} = \mathbf{f}^T \delta \mathbf{p} \tag{23.27}$$

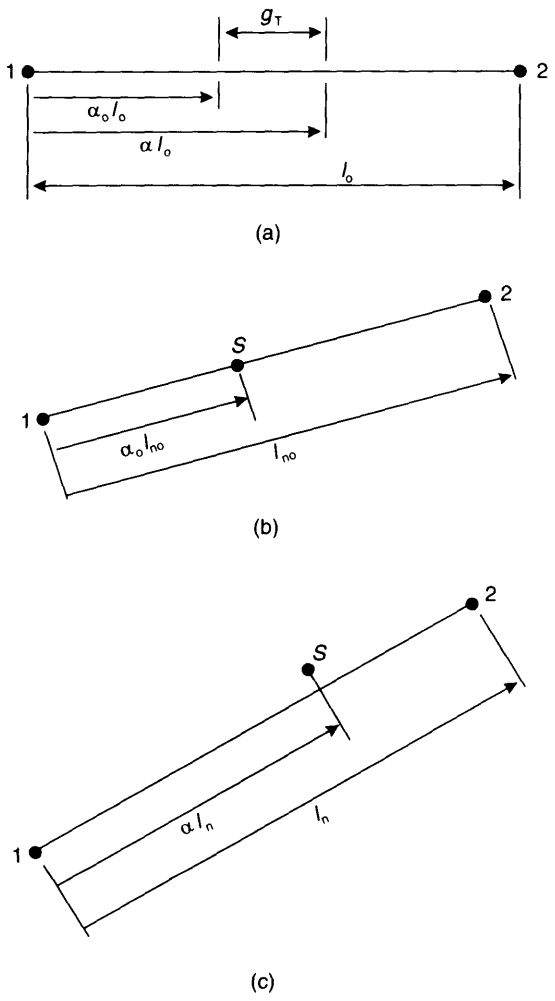

Figure 23.7 Two-dimensional contact and the tangential gap. (a) Initial configuration: (b) current configuration on first contact; (c) current 'current configuration'.

so that, using virtual work, the contribution to the internal force vector for the contact element is

$$\mathbf{q}_{ic} = t_T \mathbf{f} \tag{23.28}$$

where, to supplement (23.11), we now have:

$$t_T = \varepsilon_T g_T, \qquad g_N < 0 \tag{23.29a}$$

$$t_T = 0, \qquad g_N \geqslant 0 \tag{23.29b}$$

In the following, we will merely define the contributions from the 'sticking' component. The contributions from the normal component (via t_N) must also be added using the approach of Section 23.2. The two parts can be simply summed.

Again, following the approach of Section 23.2, we can write:

$$\delta \mathbf{q}_{ic} = \mathbf{K}_{tc}\delta \mathbf{p} = \delta t_T \mathbf{f} + t_T \delta \mathbf{f} = \varepsilon_T \mathbf{f}\mathbf{f}^T \delta \mathbf{p} + \mathbf{K}_{tc\sigma}\delta \mathbf{p} \tag{23.30}$$

For the initial stress matrix, variations must be applied to the vector $\mathbf{f}$ defined in (23.27). To this end, we use (23.14) for δl_n, (23.6) for δg_N, (23.13) for $\delta \mathbf{e}_1$ and (23.15) for $\delta\alpha$ (for the variation of the vector $\mathbf{c}$) and (23.4) for $\delta \mathbf{e}_2$ (for the variation of the vector $\mathbf{b}$— see (23.5)). This process eventually leads to the symmetric initial stress contribution:

$$\mathbf{K}_{tc\sigma}(t_T) = t_T \left[\frac{l_o}{l_n} [- \mathbf{a}\mathbf{b}^T - \mathbf{b}\mathbf{a}^T + \mathbf{b}_1\mathbf{c}^T + \mathbf{c}\mathbf{b}_1^T] - 2g_N \frac{l_o}{l_n^2} [\mathbf{b}\mathbf{b}_1^T + \mathbf{b}_1\mathbf{b}^T] \right] \tag{23.31}$$

Because 'sticking friction' is inevitably combined with 'normal contact', the combination of (23.10) and (23.28) leads to the relationship:

$$\mathbf{q}_{ic} = t_N \mathbf{a} + t_T \mathbf{f} = \mathbf{B}^T \begin{pmatrix} t_T \\ t_N \end{pmatrix} = \mathbf{B}^T \mathbf{t} \tag{23.32}$$

where

$$\delta \mathbf{g} = \begin{pmatrix} \delta g_T \\ \delta g_N \end{pmatrix} = \mathbf{B}\delta \mathbf{p} = \begin{pmatrix} \mathbf{f}^T \\ \mathbf{a}^T \end{pmatrix} \delta \mathbf{p} \tag{23.33}$$

Also the combined tangent stiffness matrix can be expressed as

$$\mathbf{K}_t = \mathbf{B}^T \mathbf{C}\mathbf{B} + \mathbf{K}_{tc\sigma}(t_T) + \mathbf{K}_{tc\sigma}(t_N) = \mathbf{B}^T \begin{bmatrix} \varepsilon_T & 0 \\ 0 & \varepsilon_N \end{bmatrix} \mathbf{B} + \mathbf{K}_{tc\sigma}(t_T) + \mathbf{K}_{tc\sigma}(t_N) \tag{23.34}$$

where $\mathbf{K}_{tc\sigma}(t_T)$ was defined in (23.31) while $\mathbf{K}_{tc\sigma}(t_N)$ was defined earlier in (23.18).

23.5 INTRODUCING COULOMB 'SLIDING FRICTION' IN TWO DIMENSIONS

Sliding friction is simply introduced with the aid of a 'plasticity algorithm' so that the yield function is given (see Figure 23.8) by

$$f = |t_T| + \mu t_N = 0 = s t_T + \mu t_N, \qquad (t_N < 0) \tag{23.35}$$

where

$$s = \frac{t_T}{|t_T|} \qquad (= \pm 1) \tag{23.36}$$

The contact forces are now given by

$$t_N = \varepsilon_N g_N \tag{23.37a}$$

$$t_T = t_{TA} + \varepsilon_T (\Delta g_T - \Delta g_{Tp}) = t_{TA} + \varepsilon_T (\Delta g_T - \Delta \eta s) \tag{23.37b}$$

In (23.37a), the normal gap, g_N, has previously been defined in (23.2) while the incremental tangential gap, Δg_T, is simply the current value of g_T from (23.26) minus the value of g_T at the end of the last increment. The term t_{TA} is the value of t_T at the end of the last increment while the 'plastic tangential slip', Δg_{Tp}, is related to a non-associative

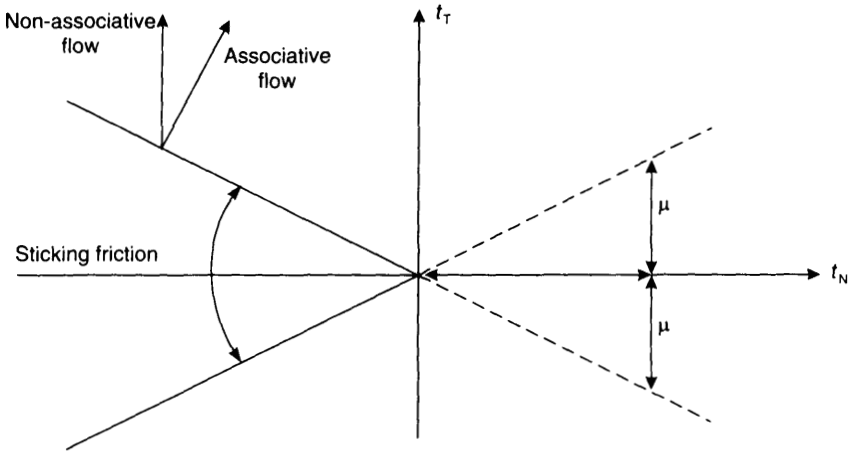

Figure 23.8 'Yield function' for coulomb friction in two dimensions.

plasticity law. To proceed further, we will write the yield function of (23.35) as

$$f = \bar{\mathbf{a}}^{\mathrm{T}}\mathbf{t} = \begin{pmatrix} s \\ \mu \end{pmatrix}^{\mathrm{T}} \begin{pmatrix} t_{\mathrm{T}} \\ t_{\mathrm{N}} \end{pmatrix} = 0 \tag{23.38}$$

while the non-associative flow rule (see Section 6.3.1) is given by

$$\dot{\boldsymbol{g}}_{\mathrm{p}} = \begin{pmatrix} \dot{g}_{\mathrm{T}} \\ \dot{g}_{\mathrm{N}} \end{pmatrix}_{\mathrm{p}} = \dot{\eta} \begin{pmatrix} \dfrac{\partial f}{\partial t_{\mathrm{T}}} \\ 0 \end{pmatrix} = \dot{\eta} \begin{pmatrix} s \\ 0 \end{pmatrix} = \dot{\eta}\bar{\mathbf{b}} \tag{23.39}$$

If an associative flow rule was adopted with $\bar{\mathbf{b}} = \partial f/\partial \mathbf{t} = \bar{\mathbf{a}}$, 'plastic slip' would occur in the normal direction (Figure 23.8). This would be physically unrealistic.

The scalar $\Delta\eta$ in (23.37b) is the incremental form of $\dot{\eta}$ in (23.39). As with the earlier developments in plasticity, we will adopt a backward-Euler formulation which turns out to give a very simple 'return mapping'. To this end, we will adopt the subscripts A, B and C of Chapters 6, 14 and 15 so that (23.37) can be expressed as

$$\begin{aligned} \mathbf{t}_{\mathrm{C}} &= \mathbf{t}_{\mathrm{A}} + \mathbf{C}(\Delta\mathbf{g} - \Delta\boldsymbol{g}_{\mathrm{p}}) = \boldsymbol{t}_{\mathrm{A}} + \mathbf{C}\left\{ \Delta\boldsymbol{g} - \Delta\eta \begin{pmatrix} s \\ 0 \end{pmatrix} \right\} \\ &= \mathbf{t}_{\mathrm{B}} - \Delta\eta\mathbf{C} \begin{pmatrix} s_{\mathrm{B}} \\ 0 \end{pmatrix} = \mathbf{t}_{\mathrm{B}} - \Delta\eta\mathbf{C}\bar{\mathbf{b}}_{\mathrm{B}} \end{aligned} \tag{23.40}$$

with $\mathbf{C}$ having been defined in (23.34). The forces $\mathbf{t}_{\mathrm{B}}$ are those computed at the elastic trial point. The simple nature of the adopted yield function allows the use of s_{B} instead of s_{C} in (23.40). Substitution from (23.40) into the yield function of (23.38) (or (23.35)) allows the scalar $\Delta\eta$ to be simply computed as

$$\Delta\eta = (s_{\mathrm{B}} t_{\mathrm{TB}} + \mu t_{\mathrm{NB}})/\varepsilon_{\mathrm{T}} = \frac{f_{\mathrm{B}}}{\varepsilon_{\mathrm{T}}} \tag{23.41}$$

where f_B is the value of the yield function computed at the trial point, B. By combining (23.37) with (23.41), the internal forces are completely defined.

A conventional return mapping procedure would be adopted so that we would first compute the elastic trial forces $\mathbf{t}_B$ and then check if the resulting yield function scalar $f_B \geqslant 0$. If not, the final forces, $\mathbf{t}_C$ would be set to $\mathbf{t}_B$ and we would have sticking friction. However, if $f_B \geqslant 0$, we would obtain the 'returned forces' from (23.40) combined with (23.41).

In order to obtain the tangent stiffness matrix, (23.40) can be differentiated to obtain:

$$\dot{\mathbf{t}}_C = \mathbf{C}\dot{\boldsymbol{g}} - \dot{\eta}\mathbf{C}\bar{\mathbf{b}}_B \tag{23.42}$$

where $\dot{\eta}$ is obtained by differentiating (23.41) so that:

$$\dot{\eta} = s_B \dot{g}_T + \frac{\mu}{\varepsilon_T}\varepsilon_N \dot{g}_N = \frac{1}{\bar{\mathbf{a}}^T\mathbf{C}\bar{\mathbf{b}}}\bar{\mathbf{a}}^T\mathbf{C}\dot{\boldsymbol{g}} \tag{23.43}$$

and (see also Section (6.3.1))

$$\dot{\mathbf{t}}_C = \mathbf{C}_t\dot{\boldsymbol{g}} = \mathbf{C}\left[\mathbf{I} - \frac{\bar{\mathbf{b}}\bar{\mathbf{a}}^T\mathbf{C}}{\bar{\mathbf{a}}^T\mathbf{C}\bar{\mathbf{b}}}\right]\dot{\boldsymbol{g}} = \varepsilon_N\begin{bmatrix}0 & -\mu s\\ 0 & 1\end{bmatrix}\dot{\boldsymbol{g}} \tag{23.44}$$

Because of the adopted non-associative law, $\mathbf{C}_t$ is non-symmetric.

In the previous 'plasticity developments', we have adopted 'rates' (dots) rather than the δ's used earlier. This approach has been adopted for consistency with the earlier work on plasticity. However, (see the earlier discussion in Section 6.3), the two are effectively equivalent and we will return to δ's in differentiating (23.32) (with the new definition of $\mathbf{t}$) to obtain:

$$\delta\mathbf{q}_{ic} = \mathbf{B}^T\delta\mathbf{t} + \delta\mathbf{B}^T\mathbf{t} = [\mathbf{B}^T\mathbf{C}_t\mathbf{B} + \mathbf{K}_{ic\sigma}(t_T) + \mathbf{K}_{ic\sigma}(t_N)]\delta\mathbf{p} \tag{23.45}$$

where $\mathbf{K}_{ic\sigma}(t_T)$ was defined in (23.31) while $\mathbf{K}_{ic\sigma}(t_N)$ was defined in (23.18). Consequently, to change from sticking to sliding friction we merely change $\mathbf{C}$ to $\mathbf{C}_t$ from (23.44) (thereby introducing non-symmetry). More sophisticated friction laws can be introduced. If these are related to plasticity, they will often involve some form of hardening and/or softening related to the plastic work [D1, H4]. A cohesion term can be added to the Coulomb friction of (23.35) [C4] by subtracting the 'initial shear yield term', t_{T0}.

23.6 USING LAGRANGIAN MULTIPLIERS INSTEAD OF THE PENALTY APPROACH

We will initially consider 'frictionless contact' for which the penalty approach was described earlier in Section 23.3. Using Lagrangian multipliers, we can adopt classical optimisation techniques and form the Lagrangian,

$$L = \phi + \sum \lambda_N g_N \tag{23.46}$$

where ϕ is the total potential energy, and the λ_N's are a set of Lagrangian multipliers relating to each of the contact elements. The variation of (23.46) gives:

$$\delta L = \bar{\mathbf{g}}^T\delta\mathbf{p} + \Sigma\,\lambda_N\delta g_N + \sum \delta\lambda_N g_N \tag{23.47}$$

where $\bar{\mathbf{g}}$ contains the gradient of the total potential energy for the 'non-contact

elements'. To satisfy the first-order conditions [F1, L4, V1], this variation must vanish for arbitrary $\delta\mathbf{p}$, δg_N (related to $\delta\mathbf{p}$) and $\delta\lambda_N$. In addition, the original contact constraints apply so that we have:

$$\bar{\mathbf{g}}\delta\mathbf{p} + \sum \lambda_N \delta g_N(\delta\mathbf{p}) = 0 \tag{23.48}$$

and

$$g_N \geqslant 0 \tag{23.49a}$$

$$\lambda_N \leqslant 0 \tag{23.49b}$$

$$g_N \lambda_N = 0 \tag{23.49c}$$

If we consider the δ quantities in (23.48) as virtual, and identify the λ's as the tractions across the interface, (23.48) can be recognised as a virtual work expression that takes a similar form to (23.9), although in the latter we had the (penalty) forces as t_N's rather than the current (Lagrangian multiplier) λ_N's. Equations (23.49), which apply to all the possible contact conditions, are the Kuhn–Tucker conditions [F1, L4, V1].

Equation (23.49a) ensures no penetration; equation (23.49b) ensures compressive contact forces while the complimentarity condition of (23.49c) ensures that, if there is no contact ($\lambda_N = 0$), the gaps are non-zero, while if there is contact ($g_N = 0$), the contact forces are non-zero. Because the λ's are zero away from the active contact zones, we can define an 'active set' which includes all of the current active contact elements and replace (23.46) with:

$$L = \phi + \sum_a \lambda_N g_N \tag{23.50}$$

where in relation to the active set we have:

$$g_N = 0 \qquad \text{over } a \tag{23.51}$$

At this stage we will introduce sticking friction and modify (23.48) to give:

$$\bar{\mathbf{g}}^T\delta\mathbf{p} + \sum_a \lambda_N \delta g_N(\delta\mathbf{p}) + \sum_a \lambda_T \delta g_T(\delta\mathbf{p}) = \bar{\mathbf{g}}^T\delta\mathbf{p} + \mathbf{q}_{ic}^T\delta\mathbf{p} = 0 \tag{23.52}$$

If we now consider a single contact element from the active set, we can define g_N and g_T in precisely the same manner as we did for the 'penalty approach' and, as before, obtain (23.33) which, for convenience, is reproduced below.

$$\delta\boldsymbol{g} = \begin{pmatrix} \delta\boldsymbol{g}_T \\ \delta g_N \end{pmatrix} = \mathbf{B}\delta\mathbf{p} = \begin{bmatrix} \mathbf{f}^T \\ \mathbf{a}^T \end{bmatrix}\delta\mathbf{p} \tag{23.53}$$

Using (23.53), the internal forces for the contact element can be derived as

$$\mathbf{q}_{ic} = \mathbf{B}^T\boldsymbol{\lambda} = \mathbf{B}^T\begin{pmatrix} \lambda_T \\ \lambda_N \end{pmatrix} \tag{23.54}$$

which takes a very similar form to (23.32). Again, considering a single contact element, the equilibrium equations of (23.54) must be supplemented by the contact constraints:

$$\boldsymbol{g} = \begin{pmatrix} g_T \\ g_N \end{pmatrix} = \mathbf{0} \tag{23.55}$$

For a general stage in the iterative solution process we will have the displacements

$\mathbf{p}$ and the Lagrangian multipliers, λ, but no satisfaction of either the equilibrium equations $\mathbf{g} = 0$ (including the $\mathbf{q}_{ic}$'s from the active contact elements) or the constraints of (23.55) (again at the active contact elements). To improve the solutions, we can apply a truncated Taylor series, so that for the equilibrium equations we have:

$$-\mathbf{g}_{\text{old}} = \bar{\mathbf{K}}_t \delta\mathbf{p} + \sum_a \delta\mathbf{q}_{ic} = \bar{\mathbf{K}}_t \delta\mathbf{p} + \sum_a \mathbf{B}^T \delta\lambda + \sum_a \delta\mathbf{B}^T \lambda \tag{23.56}$$

where $\bar{\mathbf{K}}_t$ has the tangent stiffness matrix from the non-contact elements. For an individual element, the last term in (23.56) produces precisely the same initial stress matrices as those obtained previously for the penalty approach (although now with λ's instead of t's). Hence we can rewrite (23.56) as

$$-\mathbf{g}_{\text{old}} = \bar{\mathbf{K}}_t \delta\mathbf{p} + \sum_a (\mathbf{K}_{tc\sigma}(\lambda_T) + \mathbf{K}_{tc\sigma}(\lambda_N))\delta\mathbf{p} + \sum_a \mathbf{B}^T \delta\lambda \tag{23.57}$$

In a similar manner, applying a truncated Taylor series to (23.55) and using (23.53), we have:

$$-\mathbf{g}_{\text{old}} = \mathbf{B}\delta\mathbf{p} \tag{23.58}$$

If we skip over the issue of 'merging' the different element contributions, the combination of (23.57) and (23.58) leads to a Newton-Raphson iteration of the form:

$$\begin{pmatrix} \delta\mathbf{p} \\ \delta\lambda \end{pmatrix} = -\begin{bmatrix} \mathbf{K}_t & \mathbf{B}^T \\ \mathbf{B} & \mathbf{O} \end{bmatrix}^{-1} \begin{pmatrix} \mathbf{g}_{\text{old}} \\ \mathbf{g}_{\text{old}} \end{pmatrix} \tag{23.59}$$

which can be solved to obtain the changes in displacements and changes in Lagrangian multipliers. For the contact elements, $\mathbf{K}_t$ in (23.59) contains the contributions from the earlier 'initial stress terms' (see (23.57).

In contrast to the previous penalty method, the new framework ensures exact satisfaction of the required constraints. However, in practice there are a number of disadvantages. First, there is the need to increase the number of variables via the Lagrangian multipliers, and secondly special care must be taken with the ordering of the equations during the solution process. (There can also be an increase in the band or front width.) However, it is possible to combine the penalty and Lagrangian multiplier methods with the aim of retaining the good points from each approach. The resulting procedures will be discussed in the next section.

23.7 THE AUGMENTED LAGRANGIAN METHODS

While in Sections 23.2 and 23.4, we used virtual work as the starting-point for the penalty method, we could have started with an 'energy functional':

$$\phi = \phi_b + \sum_a \frac{1}{2}\, g^T \mathbf{C} g \tag{23.60}$$

where we have added the strain energy in the active contact elements to the total potential energy of the rest of the body. In the following we will sometimes omit the summation sign. In these circumstances, using (23.60), we can write:

$$\begin{aligned} \delta\phi &= \delta\phi_b + \mathbf{g}^T \mathbf{C} \delta g = \delta\mathbf{p}^T \bar{\mathbf{g}} + \delta\mathbf{p}^T \mathbf{B}^T \mathbf{C} g \\ &= \delta\mathbf{p}^T \bar{\mathbf{g}} + \delta\mathbf{p}^T \mathbf{B}^T \mathbf{t} = \delta\mathbf{p}^T \bar{\mathbf{g}} + \delta\mathbf{p}^T \mathbf{q}_{ic} \end{aligned} \tag{23.61}$$

where we have used (23.53) for $\delta \boldsymbol{g}$. The internal force vector, $\mathbf{q}_{ic}$, from (23.61) is the same as that derived earlier for the penalty method.

For the augmented Lagrangian method, we augment the Lagrangian (see (23.46)) with the penalty (or contact strain energy terms) so that the starting-point is

$$A = L + \sum_a \frac{1}{2} \boldsymbol{g}^{\mathrm{T}} \mathbf{C} \boldsymbol{g} = \phi_{\mathrm{b}} + \sum_a \boldsymbol{g}^{\mathrm{T}} \boldsymbol{\lambda} + \sum_a \frac{1}{2} \boldsymbol{g}^{\mathrm{T}} \mathbf{C} \boldsymbol{g} \tag{23.62a}$$

Before proceeding with the development of the augmented Lagrangian procedure, we note that perturbed Lagrangian techniques can be developed [J1] from:

$$P = \phi_{\mathrm{b}} + \sum_a \boldsymbol{g}^{\mathrm{T}} \boldsymbol{\lambda} - \sum_a \frac{1}{2} \boldsymbol{\lambda}^{\mathrm{T}} \mathbf{C}^{-1} \boldsymbol{\lambda} \tag{23.62b}$$

Returning to the development of the augmented Lagrangian procedure, variations of (23.62a) give:

$$\delta A = \delta \mathbf{p}^{\mathrm{T}} \bar{\mathbf{g}} + \delta \mathbf{p}^{\mathrm{T}} \mathbf{B}^{\mathrm{T}} (\mathbf{C} \boldsymbol{g} + \boldsymbol{\lambda}) + \delta \boldsymbol{\lambda}^{\mathrm{T}} \boldsymbol{g} = \delta \mathbf{p}^{\mathrm{T}} \bar{\mathbf{g}} + \delta \mathbf{p}^{\mathrm{T}} \mathbf{B}^{\mathrm{T}} (\mathbf{t} + \boldsymbol{\lambda}) + \delta \boldsymbol{\lambda}^{\mathrm{T}} \boldsymbol{g} \tag{23.63}$$

where we have dropped the summation sign over the active set (but it is implied). When the first-order conditions are satisfied, δA vanishes for arbitrary $\delta \mathbf{p}$ and $\delta \boldsymbol{g}$ and hence:

$$\mathbf{g} = \bar{\mathbf{g}} + \mathbf{q}_{ic} = \bar{\mathbf{g}} + \mathbf{B}^{\mathrm{T}} (\mathbf{t} + \boldsymbol{\lambda}) = \bar{\mathbf{g}} + \mathbf{B}^{\mathrm{T}} (\mathbf{C} \boldsymbol{g} + \boldsymbol{\lambda}) = \mathbf{0} \tag{23.64}$$

and

$$\boldsymbol{g} = \mathbf{0} \tag{23.65}$$

When both (23.64) and (23.65) are satisfied, we obtain the conventional Lagrangian multiplier solution (see (23.54)) because the $\mathbf{C}\boldsymbol{g}$ in (23.63) will then vanish.

The first way of taking advantage of this fact is to add the penalty terms and retain the Lagrangian multipliers, thus effectively using a modified form of the procedure of Section 23.6. The key equations are now (23.64) and (23.65) and, following the approach leading to (23.59), the resulting Newton–Raphson iteration leads to

$$\begin{pmatrix} \delta \mathbf{p} \\ \delta \boldsymbol{\lambda} \end{pmatrix} = - \begin{bmatrix} \mathbf{K}_{\mathrm{t}} & \mathbf{B}^{\mathrm{T}} \\ \mathbf{B} & \mathbf{O} \end{bmatrix}^{-1} \begin{pmatrix} \mathbf{g}_{\mathrm{old}} \\ \boldsymbol{g}_{\mathrm{old}} \end{pmatrix} \tag{23.66}$$

where now the tangent stiffness contribution from the contact elements is

$$\mathbf{K}_{\mathrm{T}} = \mathbf{B}^{\mathrm{T}} \mathbf{C} \mathbf{B} + \mathbf{K}_{\mathrm{tc}\sigma} (\lambda_{\mathrm{T}} + \varepsilon_{\mathrm{t}} g_{\mathrm{T}}) + \mathbf{K}_{\mathrm{tc}\sigma} (\lambda_{\mathrm{N}} + \varepsilon_{\mathrm{N}} g_{\mathrm{N}}) \tag{23.67}$$

The first term in (23.67) stems from the variation of the $\boldsymbol{g}$ term in the last expression on the right-hand side of (23.64) while the $\mathbf{K}_{\mathrm{tc}\sigma}$ terms stem from the variation of $\mathbf{B}$ in the same expression. These 'initial stress matrices' take the same form as those derived earlier in Sections 23.2 and 23.4 (see (23.18) and (23.31)).

The advantage of adding these penalty terms is that by doing so, the difficulties associated with the 'solution ordering' in the Lagrangian multiplier approach are now effectively removed because $\mathbf{K}_{\mathrm{t}}$ on its own is now non-singular. (These advantages can also be obtained using the perturbed Lagrangian method.) Also, the adopted penalty parameters need not be very large because the contact conditions are effectively satisfied via the Lagrangian multipliers. None the less, we still have the disadvantages of the extra Lagrangian multiplier variables in the solution of the equations.

One way of overcoming this limitation is to use the 'method of multipliers' [B3, F1, L4, P5, R1, V1]. (There is some problem here with nomenclature because this new method is also known as the 'augmented Lagrangian technique'. However, it is clearly different from the augmented Lagrangian procedure that has just been described.) In the method of multipliers, the Lagrangian multipliers are retained as variables in the active contact elements, but they remain as element level variables and do not enter the global structural solution. The latter only involves the conventional displacement variables as it does with the penalty method. The solution process is described in the following algorithm.

1. Set $\boldsymbol{\lambda} = \boldsymbol{\lambda} + \mathbf{C}\boldsymbol{g}$ from the last increment (and $k = 0$) and define the active set from the last increment.
2. (Set $k = k + 1$) and use the Newton–Raphson method (or equivalent) to solve:

$$\bar{\mathbf{g}}_b + \mathbf{q}_{ic} = \mathbf{0} \tag{23.68}$$

with $\mathbf{p}$ as the variables and

$$\mathbf{q}_{ic} = \mathbf{B}^T(\mathbf{C}\boldsymbol{g}(\mathbf{p}) + \boldsymbol{\lambda}) \text{ (with } \lambda \text{ fixed)} \tag{23.69}$$

and $\mathbf{K}_t$ for the contact elements as in (23.67).

3. Within the active set, put

$$\boldsymbol{\lambda} = \boldsymbol{\lambda}_{old} + \mathbf{C}\boldsymbol{g} \tag{23.70}$$

and (optionally—see later) update the penalty parameters within $\mathbf{C}$, but if $\lambda > 0$, set $\lambda = 0$ and remove the element from the active set. Add into the active set any element for which $g_N \leqslant 0$ and store the α_0 value (see (23.26) and Figure 23.7).
4. Check for 'contact convergence' by ensuring that within the active set $|g_N| <$ tolerance. If O.K., start next increment and go to 1). If not go to 2) for a new Newton–Raphson loop.

Algorithm 23.1 The method of multipliers.

The justification for using (23.70) for the updating of the Lagrangian multipliers can be found in [F1, L4]. The technique that has been described is often called the Powell algorithm [P5] and seems to be the method favoured by Simo and Laursen [S1]. During the Newton–Raphson loop of stage 2), the λ's are fixed and so is the active set. Consequently, quadratic convergence can be expected for each of these stages. It would seem that, because the active set is fixed, the tangent stiffnesses should be computed even if the λ_N's are positive.

An alternative procedure is sometimes known as the 'Uzawa algorithm [see F2]. In this algorithm, which has been applied to frictionless contact by Wriggers *et al.* [W2], the active set is checked and changed during the Newton–Raphson stage 2). There would seem to a number of possibilities. First, checks could be made for new elements coming into contact and entering the active set with appropriate penalty terms then being added (as in the usual penalty approach). In this way, it would still be true to say that during the iterations, the λ's are fixed. One could allow a complete change of the active set by also checking for elements leaving the active set and putting the appropriate λ values to zero.

One of the main advantages of using the method of multipliers in contrast to the penalty procedure is the sensitivity of the latter to the selection of the penalty stiffnesses.

If the penalty parameter is too high, then a very poor convergence rate (or even no convergence rate) may result. Nour–Omid and Wriggers [N1] suggest that the penalty parameters should be limited according to

$$\varepsilon \leqslant \varepsilon_{\max} = \frac{k}{\sqrt{Nt}} \tag{23.71}$$

where k is a characteristic stiffness parameter of the adjoining elements, N is the total number of unknowns and t is the computer precision. While one can reduce the penalty parameter to avoid ill-conditioning, the inevitable consequence is penetration and hence a violation of the real physical situation. However, when using the method of multipliers, one need not start with a very large stiffness because the constraints will eventually be satisfied via the Lagrangian multipliers.

Equation (23.71) gives a guide to the maximum penalty stiffness that should be introduced. If the problem is sufficiently well conditioned that an efficient solution can be obtained with the penalty method, then clearly this will involve less work than an augmented Lagrangian solution. Consequently, the user would like to know when he or she should introduce 'augmentation'. In practice, it may be difficult to estimate the ill-conditioning effects of the high penalty stiffnesses because, although they will lead to poor convergence characteristics, this effect can also be introduced by other causes. For a linear 'tied slide-line solution', one can use the norm of the residual $\| \mathbf{g} \|$ as a guide to contamination by ill-conditioning [A1]. As part of a non-linear solution procedure, it may also be advisable to keep a periodic check on such a norm taken over the contact elements. To this end, a residual $\mathbf{g}_l$ should be computed with 'linear assumptions', i.e. without updating the geometry, etc.

The performance of the method of multipliers can be significantly improvement by incorporating the update of the penalty stiffnesses indicated in step (3) of the previous algorithm. Bertsekas [B3] proposes updating ε according to

$$\varepsilon^k = \beta \varepsilon^{k-1} \tag{23.72}$$

where k is the number of the equilibrium iteration loop (see previous algorithm) and

$$\beta = \bar{\beta} \quad \text{if } |\varepsilon^k| > \gamma |\varepsilon^{k-1}| \tag{23.73a}$$

$$\beta = 1 \quad \text{if } |\varepsilon^k| < \gamma |\varepsilon^{k-1}| \tag{23.73b}$$

In the above $\bar{\beta}$ might be 10 while γ might be 1/4. Wriggers [W4] adopted this approach, but also used (23.71) to apply a final limit to ε and only introduced (23.73b) if the gap was reducing.

23.8 AN AUGMENTED LAGRANGIAN TECHNIQUE WITH COULOMB 'SLIDING FRICTION'

Laursen and Simo [L2] have described methods for applying the method of multipliers in conjunction with Coulomb 'sliding friction'. The following description is closely related to their work.

For the penalty approach, the internal forces were defined by (23.32) coupled with the $\mathbf{t}$ vector from (23.40). For the augmented Lagrangian formulation, we modify these

equations to give:

$$\mathbf{q}_{ic} = \mathbf{B}^T \begin{pmatrix} \lambda_N + \varepsilon_N g_N \\ \lambda_T + \varepsilon_T(\Delta g_T - \Delta\eta s_B) \end{pmatrix} = \mathbf{B}^T \begin{pmatrix} t_N \\ t_T \end{pmatrix} = \mathbf{B}^T \mathbf{t} \tag{23.74a}$$

$$\mathbf{q}_{ic} = (\lambda_N + \varepsilon_N g_N)\mathbf{a} + (\lambda_T + \varepsilon_T(\Delta g_T - \Delta\eta s_B))\mathbf{f} = t_N \mathbf{a} + t_T \mathbf{f} \tag{23.74b}$$

In (23.74b), we have split the matrix $\mathbf{B}$ of (23.32) and (23.33) into its two constituent vectors $\mathbf{a}$ (see (23.7)) and $\mathbf{f}$ (see (23.27)). The unknown scalar $\Delta\eta$ in (23.74) is required to satisfy the yield criterion of (23.35) and is again given by (23.41) although now with the new definitions (see (23.74)) for the t's. Using these new definitions, the tangent stiffness matrix of (23.45) still applies and we can write the first few steps of an algorithm related to the method of multipliers as follows:

1. Set $\boldsymbol{\lambda} = \boldsymbol{\lambda}$ from the last increment (and $k = 0$) and define the active set from the last increment.
2. (Set $k = k + 1$) and use the Newton–Raphson method (or equivalent) to solve:

$$\bar{\mathbf{g}}_b + \mathbf{q}_{ic} = \mathbf{0} \tag{23.75}$$

   with $\mathbf{p}$ as the variables and $\mathbf{q}_{ic} = \mathbf{B}^T\mathbf{t}$ and $\Delta\eta$ from (23.41) and $\mathbf{K}_t$ for the 'contact elements' from (23.45) with $\mathbf{t}$ from (23.74) and $\boldsymbol{\lambda}$ fixed.
3. Within the active set, put

$$\lambda = t \tag{23.76}$$

   then continue with Algorithm 23.1

Algorithm 23.2 The method of multipliers with sliding friction

23.8.1 A symmetrised version

In the previous algorithm, the tangent stiffness matrix is non-symmetric because of the non-symmetric $\mathbf{C}_t$ in (23.45). Laursen and Simo (L3) have proposed a modified procedure to avoid this non-symmetry. In this case, equations (23.74) still apply, but no longer with $\Delta\eta$ from (23.42) with the new definitions of the t's from (23.74). Instead $\Delta\eta$ is chosen to satisfy the yield function (see (23.35)) as:

$$f = s_B(t_{TB} - \Delta\eta\varepsilon_T s_B) + \mu\lambda_N \tag{23.77}$$

The key difference is that we have now used λ_N instead of t_N. Consequently, when used with the 'method of multipliers', λ_N is fixed. As a result, we still obtain $\Delta\eta$ from (23.42) but now with:

$$f_B = s_B t_{TB} + \mu\lambda_N \tag{23.78}$$

Consequently, in obtaining the tangent modular matrix, $\mathbf{C}_t$, we use:

$$\dot{\eta} = s_B \dot{g}_T \tag{23.79}$$

in place of (23.43). It follows that, in place of (23.44), we now have:

$$\begin{aligned} \dot{t}_{TC} &= \varepsilon_T \dot{g}_T - \varepsilon_T \dot{g}_T = 0 \\ \dot{t}_{NC} &= \varepsilon_N \dot{g}_N \end{aligned} \tag{23.80}$$

and hence:

$$\mathbf{C}_t = \varepsilon_N \begin{bmatrix} 0 & 0 \\ 0 & 1 \end{bmatrix} \tag{23.81}$$

and the tangent stiffness matrix is now symmetric. However, we must now adopt a different procedure to (23.76) for updating the Lagrangian multipliers. To this end, we set:

$$\lambda_N^k = \lambda_N^{k-1} + \varepsilon_N g_N \tag{23.82a}$$

$$\lambda_T^k = \lambda_T^{k-1} + \varepsilon_T(\Delta g_T - \Delta\eta s_B) \tag{23.82b}$$

where $\Delta\eta$ in (23.82b) is no longer that obtained at the end of stage 2) of the 'multiplier algorithm', but is rather computed to satisfy:

$$f(\lambda_N^k, \lambda_T^k) = 0 \tag{23.83}$$

23.9 A THREE-DIMENSIONAL FRICTIONLESS CONTACT FORMULATION USING A PENALTY APPROACH

For three-dimensional contact, a frictionless formulation has been given by Parisch [P3] and a frictional formulation by Laursen and Simo [L2]. Both papers introduce co- and contravariant components. In the following, we will describe a frictionless formulation without introducing such components. The first stage, which leads to the precise location of the contact point and the definition of the associated normal vector was also described by Hallquist [H1].

For a general three-dimensional analysis, the contact surface is two-dimensional. In Figure 23.9, this surface is assumed to be a four-noded surface which can be mapped using the conventional isoparametric shape functions as

$$\mathbf{r}(\xi, \eta) = \sum h(\xi, \eta)_i \mathbf{x}_i \tag{23.84}$$

where the three-by-one vectors $\mathbf{x}_i$ contain the current coordinates of node i and h_i has the shape function (of ξ, η) associated with node i. (The modification to introduce a three-noded planar surface is straightforward.) In general, the contact surface does not lie in a plane. In relation to Figure 23.9, $\mathbf{x}_s$ is the three-by-one vector defining the slave node and the $\mathbf{x}_i$'s are assumed to be related to the master surface. For the contact-detecting algorithm, there are many issues associated with the full definition of the appropriate master surface for a particular slave node [H1–H3]. We will not consider these issues here; neither will we consider the issue of corner regions. Instead, we will takes as our starting-point the unambiguous definition of $\mathbf{x}_s$ and the associated $\mathbf{x}_i$'s. We will also assume that an intial estimate is available for the ξ, η values of the point $\mathbf{r}(\xi, \eta)$ in Figure 23.9 which lies immediately below (or above) $\mathbf{x}_s$ on the master surface.

In contrast to the previous two-dimensional case (with a one-dimensional contact zone), it is not a trivial matter to find the required ξ, η values. (For the two-dimensional problem, the equivalent issue is the calculation of α—equation (23.8), which is trivial.) We will now describe an iterative process to find (ξ, η) which also leads to data that will

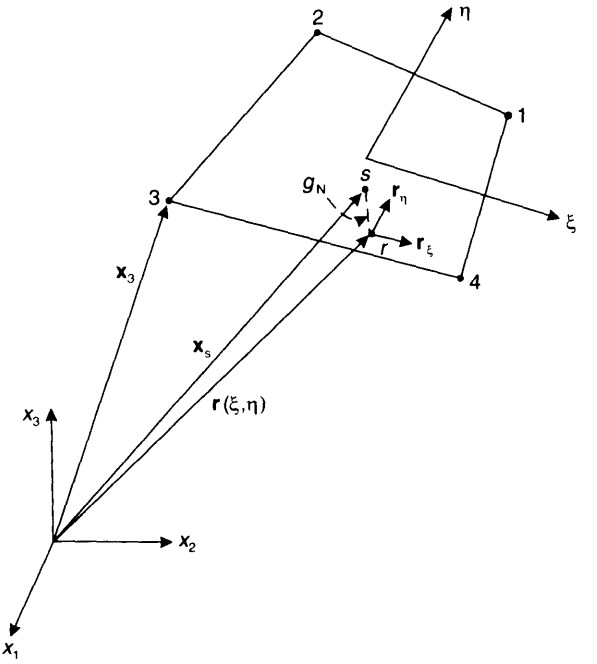

Figure 23.9 Current configuration for three-dimensional contact with 'normal gap', g_N.

later be relevant to the generation of the internal force vector and consistent tangent stiffness matrix. For the three-dimensional formulation, we will define $\mathbf{e}_3 = \mathbf{n}$ as the normal vector to the surface at the contact point (rather than the previous $\mathbf{e}_2$).

In relation to Figure 23.9, assuming we have an estimate for (ξ, η), we can compute the vector:

$$\mathbf{x}_{sr} = \mathbf{x}_s - \mathbf{r}(\xi, \eta) = \mathbf{x}_s - \sum h_i \mathbf{x}_i \tag{23.85}$$

Once the correct value of (ξ, η) is known, the vector $\mathbf{x}_{sr}$ will be orthogonal to the two vectors $\mathbf{r}_\xi, \mathbf{r}_\eta$ (Figure 23.9) which lie on the master surface. Hence the required equations to define (ξ, η) are

$$a = \mathbf{r}_\xi^{\mathrm{T}} \mathbf{x}_{sr} = \left(\frac{\partial \mathbf{r}}{\partial \xi} \right)^{\mathrm{T}} \mathbf{x}_{sr} \tag{23.86a}$$

$$b = \mathbf{r}_\eta^{\mathrm{T}} \mathbf{x}_{sr} = \left(\frac{\partial \mathbf{r}}{\partial \eta} \right)^{\mathrm{T}} \mathbf{x}_{sr} \tag{23.86b}$$

which can be combined to give:

$$\mathbf{a} = \begin{pmatrix} a \\ b \end{pmatrix} = [\mathbf{A}]^{\mathrm{T}} = [\mathbf{r}_\xi \ \mathbf{r}_\eta]^{\mathrm{T}} \mathbf{x}_{sr} = \mathbf{J} \mathbf{x}_{sr} \tag{23.86c}$$

where $\mathbf{J}$ is the Jacobian matrix at (ξ, η).

For future developments we will require $\delta\mathbf{r}$ which, from (23.84) is given by

$$\delta\mathbf{r} = \mathbf{A}\begin{pmatrix}\delta\xi\\ \delta\eta\end{pmatrix} + \sum h_i\mathbf{I}\delta\mathbf{d}_i = \mathbf{A}\delta\boldsymbol{\xi} + \sum h_i\mathbf{I}\delta\mathbf{d}_i \tag{23.87}$$

where $\mathbf{I}$ is a 3×3 unit matrix and $\delta\mathbf{d}_i$ is the displacement vector change at node i. In relation to the contact element, the displacement vector will be

$$\mathbf{p}^{\mathrm{T}} = = (\mathbf{d}_{\mathrm{s}}^{\mathrm{T}}, \mathbf{d}_1^{\mathrm{T}}, \mathbf{d}_2^{\mathrm{T}}, \mathbf{d}_3^{\mathrm{T}}, \mathbf{d}_4^{\mathrm{T}}) \tag{23.88}$$

while the equivalent current nodal coordinate vector is

$$\mathbf{x}^{\mathrm{T}} = = (\mathbf{x}_{\mathrm{s}}^{\mathrm{T}}, \mathbf{x}_1^{\mathrm{T}}, \mathbf{x}_2^{\mathrm{T}}, \mathbf{x}_3^{\mathrm{T}}, \mathbf{x}_4^{\mathrm{T}}) \tag{23.89}$$

We will require the variation of $\mathbf{x}_{\mathrm{sr}}$ in (23.85). Using (23.87), this is given by

$$\delta\mathbf{x}_{\mathrm{sr}} = [\mathbf{I}, -h_1\mathbf{I}, -h_2\mathbf{I}, -h_3\mathbf{I}, -h_4\mathbf{I}]\delta\mathbf{p} - \mathbf{A}\delta\boldsymbol{\xi} = \mathbf{F}\delta\mathbf{p} - \mathbf{A}\delta\boldsymbol{\xi} \tag{23.90}$$

We will also require $\delta\mathbf{r}_\xi$ and $\delta\mathbf{r}_\eta$. Via (23.84), the latter are given by

$$\begin{aligned}\delta\mathbf{r}_\xi &= [\mathbf{0}, h_{\xi 1}\mathbf{I}, h_{\xi 2}\mathbf{I}, h_{\xi 3}\mathbf{I}, h_{\xi 4}\mathbf{I}]\delta\mathbf{p} + \mathbf{r}_{\xi\eta}\delta\eta\\ &= \mathbf{C}_\xi\delta\mathbf{p} + \left(\sum h_{\xi\eta i}\mathbf{x}_i\right)\delta\eta\end{aligned} \tag{23.91a}$$

and

$$\begin{aligned}\delta\mathbf{r}_\eta &= [\mathbf{0}, h_{\eta 1}\mathbf{I}, h_{\eta 2}\mathbf{I}, h_{\eta 3}\mathbf{I}, h_{\eta 4}\mathbf{I}]\delta\mathbf{p} + \mathbf{r}_{\xi\eta}\delta\xi\\ &= \mathbf{C}_\eta\delta\mathbf{p} + \left(\sum h_{\xi\eta i}\mathbf{x}_i\right)\delta\xi\end{aligned} \tag{23.91b}$$

Assuming a four-noded contact surface (Figure 23.9), the shape functions and derivatives in (23.85) and (23.91) are

$$\mathbf{h}^{\mathrm{T}} = (h_1, h_2, h_3, h_4) = \tfrac{1}{4}\{(1+\xi)(1+\eta), (1-\xi)(1+\eta), (1-\xi)(1-\eta), (1+\xi)(1-\eta)\} \tag{23.92a}$$

$$\mathbf{h}_\xi^{\mathrm{T}} = (h_{\xi 1}, h_{\xi 2}, h_{\xi 3}, h_{\xi 4}) = \tfrac{1}{4}\{(1+\eta), -(1+\eta), -(1-\eta), (1-\eta)\} \tag{23.92b}$$

$$\mathbf{h}_\eta^{\mathrm{T}} = (h_{\eta 1}, h_{\eta 2}, h_{\eta 3}, h_{\eta 4}) = \tfrac{1}{4}\{(1+\xi), (1-\xi), -(1-\xi), -(1+\xi)\} \tag{23.92c}$$

$$\mathbf{h}_{\xi\eta}^{\mathrm{T}} = \mathbf{h}_{\eta\xi}^{\mathrm{T}} = (h_{\xi\eta 1}, h_{\xi\eta 2}, h_{\xi\eta 3}, h_{\xi\eta 4}) = \tfrac{1}{4}\{1, -1, 1, -1\} \tag{23.92d}$$

Returning to (23.86), we can now write:

$$\delta a = \mathbf{r}_\xi^{\mathrm{T}}[\mathbf{F}\delta\mathbf{p} - \mathbf{A}\delta\boldsymbol{\xi}] + \mathbf{x}_{\mathrm{sr}}^{\mathrm{T}}\mathbf{C}_\xi\delta\mathbf{p} + (\mathbf{x}_{\mathrm{sr}}^{\mathrm{T}}\mathbf{r}_{\xi\eta})\delta\eta \tag{23.93a}$$

$$\delta b = \mathbf{r}_\eta^{\mathrm{T}}[\mathbf{F}\delta\mathbf{p} - \mathbf{A}\delta\boldsymbol{\xi}] + \mathbf{x}_{\mathrm{sr}}^{\mathrm{T}}\mathbf{C}_\eta\delta\mathbf{p} + (\mathbf{x}_{\mathrm{sr}}^{\mathrm{T}}\mathbf{r}_{\xi\eta})\delta\xi \tag{23.93b}$$

Concentrating on the contact detection part of the algorithm, we have an estimate for (ξ, η) which we wish to improve. To this end the nodal coordinates are fixed so that $\delta\mathbf{p} = 0$ and hence we can use (23.86) and (23.93) to obtain a truncated Taylor series for $\mathbf{a}$ whereby:

$$\mathbf{0} = \mathbf{a}_{\mathrm{old}} + \mathbf{D}\delta\boldsymbol{\xi} \tag{23.94}$$

with

$$\mathbf{D} = -\mathbf{A}^{\mathrm{T}}\mathbf{A} + (\mathbf{x}_{\mathrm{sr}}^{\mathrm{T}}\mathbf{r}_{\xi\eta})\begin{bmatrix}0 & 1\\ 1 & 0\end{bmatrix} \tag{23.95}$$

which is a symmetric matrix. Equation (23.94) can then be used in a Newton–Raphson manner to find an improvement $\delta\boldsymbol{\xi}$ and hence to update the initial estimates for (ξ, η).

Many of the previous vectors and matrices will turn out to play a crucial role in the definition of the tangent stiffness matrix. With a view to the latter, as usual we first consider the internal force vector and, to this end, require the normal gap, g_N, which is given by

$$g_N^2 = \mathbf{x}_{sr}^T \mathbf{x}_{sr} \tag{23.96}$$

while the unit normal vector $\mathbf{e}_3 = \mathbf{n}$, is given by

$$\mathbf{e}_3 = \mathbf{n} = \frac{\mathbf{x}_{sr}}{\| \mathbf{x}_{sr} \|} \tag{23.97}$$

With a view to virtual work, we require the variation of (23.96) which is given by

$$\delta g_N = \left(\frac{1}{g_N} \mathbf{x}_{sr} \right)^T \delta \mathbf{x}_{sr} = \mathbf{n}^T [\mathbf{F} \delta \mathbf{p} - \mathbf{A} \delta \boldsymbol{\xi}] \tag{23.98}$$

where we have made use of (23.90) and (23.97). However, using (23.86) and (23.97), we can write:

$$\mathbf{A}^T \mathbf{n} = \mathbf{0} \tag{23.99}$$

and hence simplify (23.98) to give:

$$\delta g_N = \mathbf{n}^T \mathbf{F} \delta \mathbf{p} = \delta \mathbf{p}^T \mathbf{F}^T \mathbf{n} \tag{23.100}$$

As a consequence, the application of the principle of virtual work leads to the relationship:

$$\mathbf{q}_{ic} = t_N \mathbf{F}^T \mathbf{n} = \varepsilon_N g_N \mathbf{F}^T \mathbf{n} \tag{23.101}$$

where g_N, which must be negative, is taken from (23.96).

23.9.1 The consistent tangent matrix

In conjunction with (23.100), the variation of (23.101) leads to the relationship:

$$\delta \mathbf{q}_{ic} = \varepsilon_N \mathbf{F}^T \mathbf{n} \mathbf{n}^T \mathbf{F} \delta \mathbf{p} + \mathbf{K}_{t\sigma c} \delta \mathbf{p} = \mathbf{K}_{tc1} \delta \mathbf{p} + \mathbf{K}_{t\sigma c}(t_N) \delta \mathbf{p} \tag{23.102}$$

where

$$\mathbf{K}_{t\sigma c}(t_N) \delta \mathbf{p} = t_N \mathbf{F}^T \delta \mathbf{n} + t_N \delta \mathbf{F}^T \mathbf{n} \tag{23.103}$$

The variation of (23.97) gives:

$$\delta \mathbf{n} = \frac{1}{g_N} [\mathbf{I} - \mathbf{n}\mathbf{n}^T] \delta \mathbf{x}_{sr} \tag{23.104}$$

where $\delta \mathbf{x}_{sr}$ is given by (23.90). However, we wish to eliminate $\delta\boldsymbol{\xi}$ from the latter. To this end, we now apply the condition that $\delta\mathbf{a}$ (from (23.93)) is zero. Consequently we have:

$$[\mathbf{A}^T \mathbf{F} + g_N \boldsymbol{\alpha}(\mathbf{n})] \delta \mathbf{p} + \mathbf{D} \delta \boldsymbol{\xi} = \mathbf{0} \tag{23.105}$$

in conjunction with:

$$\boldsymbol{\alpha}(\mathbf{n}) = \begin{bmatrix} \boldsymbol{\alpha}_\xi^T \\ \boldsymbol{\alpha}_\eta \end{bmatrix}; \qquad \boldsymbol{\alpha}_\xi = \mathbf{C}_\xi^T \mathbf{n}, \qquad \boldsymbol{\alpha}_\eta = \mathbf{C}_\eta^T \mathbf{n} \tag{23.106}$$

Equation (23.105) can be solved to give:

$$\delta\boldsymbol{\xi} = -\mathbf{D}^{-1}[\mathbf{A}^{\mathrm{T}}\mathbf{F} + g_{\mathrm{N}}\boldsymbol{\alpha}(\mathbf{n})]\delta\mathbf{p} = \mathbf{D}^{-1}\mathbf{Y}^{\mathrm{T}}\delta\mathbf{p} \tag{23.107}$$

and substituting into (23.90), we obtain:

$$\delta\mathbf{x}_{\mathrm{sr}} = [\mathbf{F} + \mathbf{A}\mathbf{D}^{-1}[\mathbf{A}^{\mathrm{T}}\mathbf{F} + g_{\mathrm{N}}\boldsymbol{\alpha}(\mathbf{n})]]\delta\mathbf{p} = [\mathbf{F} - \mathbf{A}\mathbf{D}^{-1}\mathbf{Y}^{\mathrm{T}}]\delta\mathbf{p} \tag{23.108}$$

so that substitution into (23.104) gives:

$$\delta\mathbf{n} = \frac{1}{g_{\mathrm{N}}}[\mathbf{F} + \mathbf{A}\mathbf{D}^{-1}[\mathbf{A}^{\mathrm{T}}\mathbf{F} + g_{\mathrm{N}}\boldsymbol{\alpha}^{\mathrm{T}}]]\delta\mathbf{p} - \frac{1}{g_{\mathrm{N}}}\mathbf{n}\mathbf{n}^{\mathrm{T}}\mathbf{F}\delta\mathbf{p} \tag{23.109}$$

where we have made use of (23.99). Using (23.109), the first term on the right-hand side of (23.103) is given by

$$t_{\mathrm{N}}\mathbf{F}^{\mathrm{T}}\delta\mathbf{n} = \frac{t_{\mathrm{N}}}{g_{\mathrm{N}}}[\mathbf{F}^{\mathrm{T}}\mathbf{F} - \mathbf{F}^{\mathrm{T}}\mathbf{n}\mathbf{n}^{\mathrm{T}}\mathbf{F} + \mathbf{F}^{\mathrm{T}}\mathbf{A}\mathbf{D}^{-1}[\mathbf{A}^{\mathrm{T}}\mathbf{F} + g_{\mathrm{N}}\boldsymbol{\alpha}(\mathbf{n})]] \tag{23.110}$$

We will now consider the term $\delta\mathbf{F}^{\mathrm{T}}\mathbf{n}$ with $\mathbf{F}$ from (23.90). The definitions in (23.93) and (23.106) can be used to write:

$$\delta\mathbf{F}^{\mathrm{T}}\mathbf{n} = -\delta\xi\mathbf{C}_{\xi}^{\mathrm{T}}\mathbf{n} - \delta\eta\mathbf{C}_{\eta}^{\mathrm{T}}\mathbf{n} = -\boldsymbol{\alpha}(\mathbf{n})^{\mathrm{T}}\delta\boldsymbol{\xi} = \boldsymbol{\alpha}^{\mathrm{T}}\mathbf{D}^{-1}[\mathbf{A}^{\mathrm{T}}\mathbf{F} + g_{\mathrm{N}}\boldsymbol{\alpha}(\boldsymbol{n})]\delta\mathbf{p} \tag{23.111}$$

Finally, combining (23.93) with (23.110) and (23.111), we obtain the initial stress matrix as

$$\begin{aligned}\mathbf{K}_{t\sigma c}(t_{\mathrm{N}}) = \frac{t_{\mathrm{N}}}{g_{\mathrm{N}}}[&\mathbf{F}^{\mathrm{T}}\mathbf{F} - \mathbf{F}^{\mathrm{T}}\mathbf{n}\mathbf{n}^{\mathrm{T}}\mathbf{F} + \mathbf{F}^{\mathrm{T}}\mathbf{A}\mathbf{D}^{-1}\mathbf{A}^{\mathrm{T}}\mathbf{F} + g_{\mathrm{N}}\mathbf{F}^{\mathrm{T}}\mathbf{A}\mathbf{D}^{-1}\boldsymbol{\alpha}(n)\\ &+ g_{\mathrm{N}}\boldsymbol{\alpha}(\mathbf{n})^{\mathrm{T}}\mathbf{D}^{-1}\mathbf{A}^{\mathrm{T}}\mathbf{F} + g_{\mathrm{N}}^{2}\boldsymbol{\alpha}(\mathbf{n})^{\mathrm{T}}\mathbf{D}^{-1}\boldsymbol{\alpha}(\mathbf{n})]\end{aligned} \tag{23.112}$$

23.10 ADDING 'STICKING FRICTION' IN THREE DIMENSIONS

The following development for sticking friction, has strong links with the formulation of Laursen and Simo [L2] (although there are significant differences). As a start, we wish to define the tangential gaps, $\boldsymbol{g}_{\mathrm{T}}$ (2×1) using a similar procedure to that adopted in two dimensions (see (23.26) and Figure 23.7). In the latter case, we introduced αl_{o} which related to the initial configuration and we now apply a similar concept. In particular on first achieving contact (Figure 23.10), we have $\boldsymbol{\xi}_{\mathrm{o}}^{\mathrm{T}} = (\xi_{\mathrm{o}}, \eta_{\mathrm{o}})$ (as a counterpart to α_{o}—see Figure 23.7—in two dimensions). We also have $\mathbf{r}_{\xi\mathrm{o}}$ and $\mathbf{r}_{\eta\mathrm{o}}$ as well as $\mathbf{e}_{3\mathrm{o}} = \mathbf{n}_{\mathrm{o}}$. Using these three vectors, we can create an orthogonal triad:

$$\mathbf{E}_{\mathrm{o}} = [\mathbf{e}_{1\mathrm{o}}, \mathbf{e}_{2\mathrm{o}}, \mathbf{e}_{3\mathrm{o}}] \tag{23.113}$$

where we could set:

$$\mathbf{e}_{1\mathrm{o}} = \frac{\mathbf{r}_{\xi\mathrm{o}}}{\|\mathbf{r}_{\xi\mathrm{o}}\|}, \qquad \mathbf{e}_{2\mathrm{o}} = \mathbf{e}_{3\mathrm{o}} \times \mathbf{e}_{1\mathrm{o}} \tag{23.114}$$

We now define the initial coordinate vector of the contact point as

$$\mathbf{X}_{\mathrm{o}} = \sum h_i(\xi_{\mathrm{o}}, \eta_{\mathrm{o}})\mathbf{X}_i \tag{23.115}$$

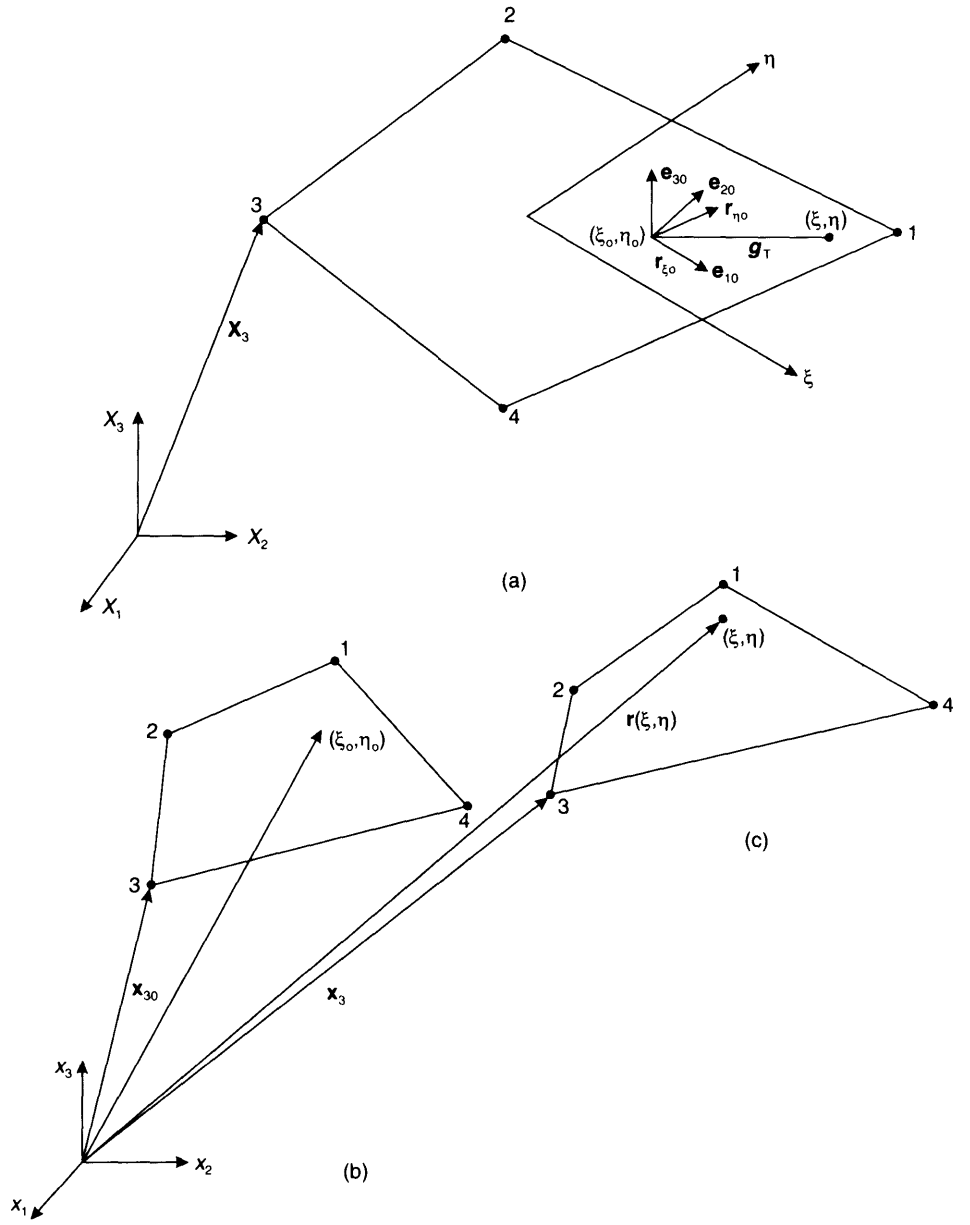

Figure 23.10 Three-dimensional contact and the tangential gap. (a) Initial configuration; (b) current configuration on first contact; (c) current 'current configuration'.

where the $\mathbf{X}_i$'s have the (master) initial nodal coordinates of the contact surface. For the current contact point (ξ, η), we can find the equivalent vector:

$$\mathbf{X} = \sum h_i(\xi, \eta)\mathbf{X}_i \tag{23.116}$$

Finally we define the tangential gaps as

$$\boldsymbol{g}_T = \begin{pmatrix} g_{T1} \\ g_{T2} \end{pmatrix} = [\mathbf{e}_{1o}, \mathbf{e}_{2o}]^T(\mathbf{X} - \mathbf{X}_o) \tag{23.117}$$

This is a two-dimensional equivalent to the scalar gap g_T of (23.26). (There are other possibilities [L2].)

With a view to virtual work, we now require the variation of (23.117) which is given by

$$\begin{aligned} \delta\mathbf{g}_T &= [\mathbf{e}_{1o}, \mathbf{e}_{2o}]^T[\mathbf{X}_\xi, \mathbf{X}_\eta]\mathrm{d}\xi = \bar{\mathbf{A}}_X\mathrm{d}\xi = -\bar{\mathbf{A}}_X\mathbf{D}^{-1}[\mathbf{A}^T\mathbf{F} + g_N\boldsymbol{\alpha}(\mathbf{n})]\delta\mathbf{p} \\ &= \bar{\mathbf{A}}_X\mathbf{D}^{-1}\mathbf{Y}^T\delta\mathbf{p} \end{aligned} \tag{23.118}$$

where we have made use of (23.107).

Applying the principle of virtual work, we obtain the internal force (related to the sticking friction forces) as

$$\mathbf{q}_{ic} = \mathbf{Y}\mathbf{D}^{-1}\bar{\mathbf{A}}_X^T\begin{pmatrix} t_{T1} \\ t_{T2} \end{pmatrix} = \mathbf{Y}\mathbf{D}^{-1}\bar{\mathbf{A}}_X^T\begin{pmatrix} \varepsilon_T g_{T1} \\ \varepsilon_T g_{T2} \end{pmatrix} = \mathbf{Y}\mathbf{D}^{-1}\bar{\mathbf{A}}_X^T\mathbf{t}_T = \mathbf{Y}\mathbf{D}^{-1}\bar{\mathbf{t}} = \mathbf{Y}\overset{*}{\mathbf{t}} \tag{23.119}$$

23.10.1 The consistent tangent matrix

The variation of (23.119) leads to the relationship:

$$\delta\mathbf{q}_{ic} = \varepsilon_T\mathbf{Y}\mathbf{D}^{-1}\bar{\mathbf{A}}_X^T\bar{\mathbf{A}}_X\mathbf{D}^{-1}\mathbf{Y}^T\delta\mathbf{p} + \mathbf{K}_{t\sigma c}(\mathbf{t}_T)\delta\mathbf{p} \tag{23.120}$$

where

$$[\delta\mathbf{Y}\overset{*}{\mathbf{t}}_T - \mathbf{Y}\mathbf{D}^{-1}\delta\mathbf{D}\overset{*}{\mathbf{t}}_T + \mathbf{Y}\mathbf{D}^{-1}\delta\mathbf{A}_X^T\mathbf{t}_T] = \mathbf{K}_{t\sigma c}(\mathbf{t}_T)\delta\mathbf{p} \tag{23.121}$$

In order to perform the variations in (23.121), it is useful to introduce the following auxiliary column vectors:

$$\overset{*}{t}_i = \begin{bmatrix} 0 & 1 \\ 1 & 0 \end{bmatrix}\overset{*}{\mathbf{t}}; \qquad \overset{*}{\mathbf{t}}_A = \mathbf{A}\overset{*}{\mathbf{t}}; \qquad \mathbf{t}_{eo} = [\mathbf{e}_{1o}, \mathbf{e}_{2o}]\mathbf{t}_T \tag{23.122}$$

and the following auxiliary matrices:

$$\mathbf{C}_{\xi\eta} = [\mathbf{0}, h_{\xi\eta 1}\mathbf{I}, h_{\xi\eta 2}\mathbf{I}, h_{\xi\eta 3}\mathbf{I}, h_{\xi\eta 4}\mathbf{I}] \tag{23.123}$$

$$\boldsymbol{\alpha}(\overset{*}{\mathbf{t}}_A) = \begin{bmatrix} \boldsymbol{\alpha}_\xi(\overset{*}{\mathbf{t}}_A)^T \\ \boldsymbol{\alpha}_\eta(\overset{*}{\mathbf{t}}_A)^T \end{bmatrix}; \qquad \boldsymbol{\alpha}_\xi(\overset{*}{\mathbf{t}}_A) = \mathbf{C}_\xi^T\overset{*}{\mathbf{t}}_A, \qquad \boldsymbol{\alpha}_\eta(\overset{*}{\mathbf{t}}_A) = \mathbf{C}_\eta^T\overset{*}{\mathbf{t}}_A \tag{23.124}$$

$$\mathbf{Z} = \overset{*}{\mathbf{t}}(1)\mathbf{C}_\xi + \overset{*}{\mathbf{t}}(2)\mathbf{C}_\eta \tag{23.125}$$

as well as the auxiliary row vector:

$$\boldsymbol{\alpha}_{\xi\eta}(\mathbf{n}) = \mathbf{n}^{\mathrm{T}}\mathbf{C}_{\xi\eta} \tag{23.126}$$

The matrix $\boldsymbol{\alpha}(\overset{*}{\mathbf{t}}_{\mathrm{A}})$ in (23.124) takes precisely the same form as the matrix, $\boldsymbol{\alpha}(\mathbf{n})$, previously defined in (23.106).

Given the previous definitions, the initial stress matrix, $\mathbf{K}_{\iota\sigma c}(\mathbf{t}_{\mathrm{T}})$, of (23.121) takes the following form:

$$\mathbf{K}_{\iota\sigma c}(\mathbf{t}_{\mathrm{T}}) = \mathbf{K}_1 + \mathbf{K}_1^{\mathrm{T}} + \mathbf{Y}\mathbf{D}^{-1}\mathbf{W}\mathbf{D}^{-1}\mathbf{Y}^{\mathrm{T}} \tag{23.127}$$

where

$$\mathbf{K}_1 = -\mathbf{F}^{\mathrm{T}}\mathbf{Z} + \mathbf{Y}\mathbf{D}^{-1}[\mathbf{A}^{\mathrm{T}}\mathbf{Z} + \boldsymbol{\alpha}(\overset{*}{\mathbf{t}}_{\mathrm{A}}) - \overset{*}{\mathbf{t}}_i\mathbf{r}_{\xi\eta}^{\mathrm{T}}\mathbf{F} - g_{\mathrm{N}}\overset{*}{\mathbf{t}}_i\boldsymbol{\alpha}_{\xi\eta}(\mathbf{n})^{\mathrm{T}}] \tag{23.128}$$

and

$$\mathbf{W} = A^{\mathrm{T}}\mathbf{r}_{\xi\eta}\overset{*}{\mathbf{t}}_i^{\mathrm{T}} + \overset{*}{\mathbf{t}}_i\mathbf{r}_{\xi\eta}^{\mathrm{T}}\mathbf{A} + ((\overset{*}{\mathbf{t}}_{\mathrm{A}}^{\mathrm{T}}\mathbf{r}_{\xi\eta}) + (\mathbf{t}_{\mathrm{eo}}^{\mathrm{T}}\mathbf{X}_{\xi\eta}))\begin{bmatrix} 0 & 1 \\ 1 & 0 \end{bmatrix} \tag{23.129}$$

The first term in (23.128) was obtained from the first term in (23.121), while the remaining terms in (23.128) were obtained from the second term in (23.121) as were the first three terms in (23.129), while the last term was obtained from the third term in (23.121).

23.11 COULOMB 'SLIDING FRICTION' IN THREE DIMENSIONS

To introduce sliding friction, the yield function of (23.38) must be altered to give:

$$f = \|\mathbf{t}_{\mathrm{T}}\| + \mu t_{\mathrm{N}} = 0 \tag{23.130a}$$

with:

$$\mathbf{t}_{\mathrm{T}}^{\mathrm{T}} = (t_{\mathrm{T}1}, t_{\mathrm{T}2}) \tag{23.130b}$$

where the components, $\mathbf{t}_{\mathrm{T}}, t_{\mathrm{N}}$ of the combined local force vector $\mathbf{t}$ are now given (see (23.40) in 2D)) by:

$$\begin{aligned}\mathbf{t}_{\mathrm{TC}} &= \mathbf{t}_{\mathrm{TA}} + \varepsilon_{\mathrm{T}}(\Delta\boldsymbol{g}_{\mathrm{T}} - \Delta\boldsymbol{g}_{\mathrm{pC}}) = \mathbf{t}_{\mathrm{TB}} - \varepsilon_{\mathrm{T}}\Delta\boldsymbol{g}_{\mathrm{pB}} \\ &= \left(1 - \frac{\varepsilon_{\mathrm{T}}\Delta\lambda}{\|\mathbf{t}_{\mathrm{TB}}\|}\right)\mathbf{t}_{\mathrm{B}} = \alpha\mathbf{t}_{\mathrm{TB}}\end{aligned} \tag{23.131a}$$

$$t_{\mathrm{NC}} = t_{\mathrm{NA}} + \varepsilon_{\mathrm{N}}\Delta g_{\mathrm{N}} \tag{23.131b}$$

In (23.131a), we have used a non-associative flow-rule so that $\Delta\boldsymbol{g}_{\mathrm{p}}$ is normal to the cylinder $\|\mathbf{t}_{\mathrm{T}}\| = \text{constant}$ and hence $\Delta\boldsymbol{g}_{\mathrm{pC}} = \Delta\boldsymbol{g}_{\mathrm{pB}}$. To completely define the forces, $\mathbf{t}_{\mathrm{C}}$, the scalar α (or the scalar $\Delta\lambda$) must be obtained via the satisfaction of the yield condition, $f_{\mathrm{C}} = 0$, from which:

$$\alpha = \frac{-\mu t_{\mathrm{NB}}}{\|\mathbf{t}_{\mathrm{TB}}\|} \tag{23.132}$$

The internal force vector now follows as:

$$\mathbf{q}_{ic} = \mathbf{B}^T \mathbf{t}_C \tag{23.133}$$

where $\mathbf{B}$ is found by combining (23.100) with (23.118) so that:

$$\delta g = \begin{pmatrix} \delta g_T \\ \delta g_N \end{pmatrix} = \begin{bmatrix} \bar{\mathbf{A}}_X \mathbf{D}^{-1} \mathbf{Y}^T \\ \mathbf{n}^T \mathbf{F} \end{bmatrix} \delta \mathbf{p} = \mathbf{B} \delta \mathbf{p} \tag{23.134}$$

To find the tangent modular relationships, variation of (23.131) and (23.132) leads to:

$$\dot{\mathbf{t}}_{TC} = \alpha \varepsilon_T \left[\mathbf{I} - \frac{\mathbf{t}_{TB} \mathbf{t}_{TB}^T}{\mathbf{t}_{TB}^T \mathbf{t}_{TB}} \right] \dot{\mathbf{g}}_T - \alpha \varepsilon_N \dot{g}_N \tag{23.135a}$$

$$\dot{\mathbf{t}}_{NC} = \varepsilon_N \dot{g}_N \tag{23.135b}$$

which can be combined to give $\dot{\mathbf{t}}_C = \mathbf{C}_t \dot{\mathbf{g}}$ where the modular matrix, $\mathbf{C}_t$, is non-symmetric.

The tangent stiffness matrix for the contact element can be obtained using a very similar procedure to that given earlier in Section 23.5 and we obtain the relationship:

$$\mathbf{K}_t = \mathbf{B}^T \mathbf{C}_t \mathbf{B} + \mathbf{K}_{tc\sigma}(t_N) + \mathbf{K}_{tc\sigma}(t_T) \tag{23.136}$$

with $\mathbf{K}_{tc\sigma}(t_N)$ being given by (23.112) and $\mathbf{K}_{tc\sigma}(t_T)$ being given by (23.118).

The developments in Sections 23.9–23.11 have involved a single slave node in contact with a four (or three noded) surface. Clearly the techniques could be extended to higher order elements. The framework for such a formulation has been given by Laursen and Simo [L2]. In such circumstances, one must add the concepts of area integration to the presented techniques which have all been developed in terms of contact forces rather than tractions.

23.12 A PENALTY/BARRIER METHOD FOR CONTACT

Apart from the issue of numerical conditioning, a further disadvantage of the earlier penalty approaches is that, in the early iterations, while a node is oscillating between being in and out of contact, the convergence characteristics can be very bad. In these circumstances, it is essential to use line searches or similar procedure. These issues will be discussed further in Section 23.13. One way of alleviating the numerical difficulties is to avoid the sudden change in stiffness that occurs when a previously contacting node moves out of contact. This can be achieved using a method proposed by Zavarise *et al.* [Z2] which combines elements from a penalty procedure with elements from a barrier method [F1, L4, V1]. In relation to Figure 23.11, the normal contact force, t_N, would be expressed as

$$t_N = \hat{t}_N + \varepsilon_N g_N; \qquad g_N < 0 \tag{23.137a}$$

$$t_N = \hat{t}_N \exp\left(\frac{\varepsilon_N}{\hat{t}_N} g_N \right); \qquad g_N \geqslant 0 \tag{23.137b}$$

where ε_N is the earlier penalty stiffness and $\hat{t}_N$ is an input estimate of the contact force. More details on $\hat{t}_N$ (which is a negative quantity) will be given later but from (23.137)

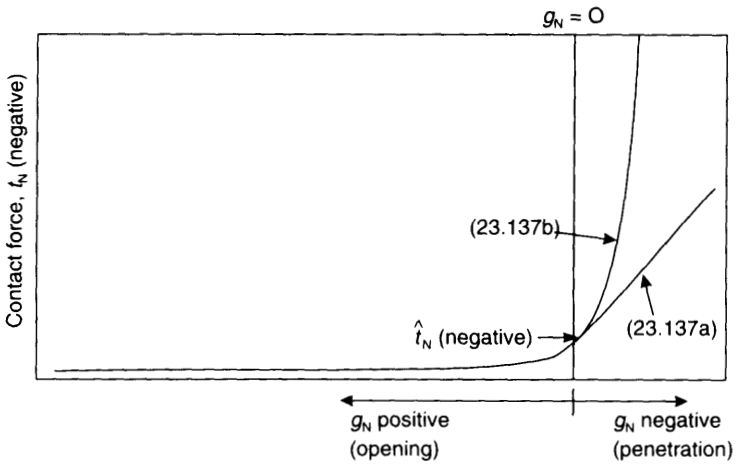

Figure 23.11 Contact force/gap relationship for penalty/barrier method.

and Figure 23.11, it is clear that $\hat{t}_N$ is the force when the gap is zero. When the gap is positive, the total force, t_N, rapidly decays to zero while, with penetration, it builds up from $\hat{t}_N$ via the penetration and the linear stiffness, ε_N. From (23.137), the tangential stiffnesses, are given by

$$\varepsilon_{tan} = \varepsilon_N g_N; \qquad g_N < 0 \tag{23.138a}$$

$$\varepsilon_{tan} = \varepsilon_N \exp\left(\frac{\varepsilon_N}{\hat{t}_N} g_N\right); \qquad g_N \geq 0 \tag{23.138b}$$

and there is no sudden jump.

If we assume for the moment that $\hat{t}_N$ is given, the necessary changes to an existing penalty formulation are trivial. Considering the simple two-dimensional normal contact formulation of Section 23.2, one would first replace (23.11) with (23.137) while the tangent stiffness matrices in (23.12) and (23.18) would be unchanged apart form the use of ε_{tan} from (23.138) in place of ε_N in $\mathbf{K}_{tc1}$ from (23.12).

Given reasonable estimates for $\hat{t}_N$, the author's work supports the claim in [Z2] that the method reduces the oscillations that plague the conventional penalty method so that, in some circumstances, the modified method will converge where the standard penalty procedure will not converge. However, the oscillation problems are not totally eliminated.

To obtain estimates for $\hat{t}_N$, one could use information from earlier increments and indeed from adjacent contact elements. The method can be used [Z2] in conjunction with a form of 'augmentation procedure' that has similarities with the earlier augmented Lagrangian methods (Sections 23.7 and 23.8). Having converged on a solution with t_N, one may simply set $\hat{t}_N = t_N$ and then proceed with a new iterative loop. Using this formulation, one can converge on a solution with 'no penetration'. As with the penalty and augmented Lagrangian methods, it can also be beneficial to iteratively increase the penalty parameter, ε_N (see the end of Section 23.7).

23.13 AMENDMENTS TO THE SOLUTION PROCEDURES

Although some of the earlier techniques involve some amendments to the solution procedures, the latter generally involve a cycle (or cycles) which are based on a Newton-like mode. For these cycles, one may use any of the enhancements of the earlier chapters (9 and 21) on solution techniques. However, some special considerations relate to problems with contact.

We have already emphasised the advantages to be gained by introducing line searches, particularly in the early iterations. However, with contact, there are sometimes some special characteristics which can be used to modify the earlier algorithms (Sections 9.2 and 21.7). We will initially consider a very simple problem with one contacting node.

Suppose that, at the end of the increment, this node will be in contact, but at the end of the current iteration it is out of contact. Consequently, for the next iteration there is no penalty stiffness and consequently, the iterative displacement vector, $\delta\mathbf{p}$, can be very large in comparison with the displacement change required to restore contact. As a result, the minimum step length, $\eta_{\min} = \text{ETMNA}$ (in subroutine SEARCH—Section 9.2.2) must be set to a very small number. Also the energy slope plot (see Figure 9.2) can take the form illustrated in Figure 23.12 so that, using the conventional algorithm, a large number of residual evaluations will be required before the line-search tolerance is obtained.

By using information relating to the gap size, one can reduce this work. Suppose that at $\eta = \eta_o = 0$, we have a positive gap, g_o, while at $\eta = 1$, we have $g_1(\eta_1)$ which is a large negative number (implying a large penetration because no penalty stiffness has been provided). We can easily estimate the step length to restore the gap to zero as

$$\eta_2 = \frac{-g_o}{g_1 - g_o} \tag{23.139}$$

which could be used to replace (9.13) which applies a similar interpolation on the energy slopes rather than the gaps. At this stage, if the energy slope, $s_2(\eta_2)$, is negative, we can simply proceed with the conventional method using the energy slopes. However, if $s_2(\eta_2)$ is positive, we still need a negative slope much closer to η_2 than $s_1(\eta_1 = 1)$. Consequently, we could set $\eta_3 = 2\eta_2$ and continue with doubling until we obtain a negative energy slope. Alternatively, we could interpolate between the values at η_1 and η_2. However, for this interpolation to be activated, we would need to temporarily suppress the part of the algorithm (see Figure 9.3) that would otherwise imposes a minimum change so that $\eta_3 = \eta_2 + 0.2(\eta_1 - \eta_2) \simeq 0.2$.

In reality there may be a large number of contacting nodes and one may then apply the previous technique, using the gap for the node with the maximum penetration at $\eta = 1$ and for which the gap is positive at $\eta = 0$. These ideas should be extendable to increments rather than iterations with the aid of a form of 'arc-length method'. In Section 21.8, it was demonstrated how such a technique could be introduced with the control constraint being a particular gap. It should be possible to introduce this procedure into a general algorithm whereby, at any increment, the chosen gap was that associated with the node for which, in the predictor solution, the penetration was a maximum while at the previous increment there was no contact.

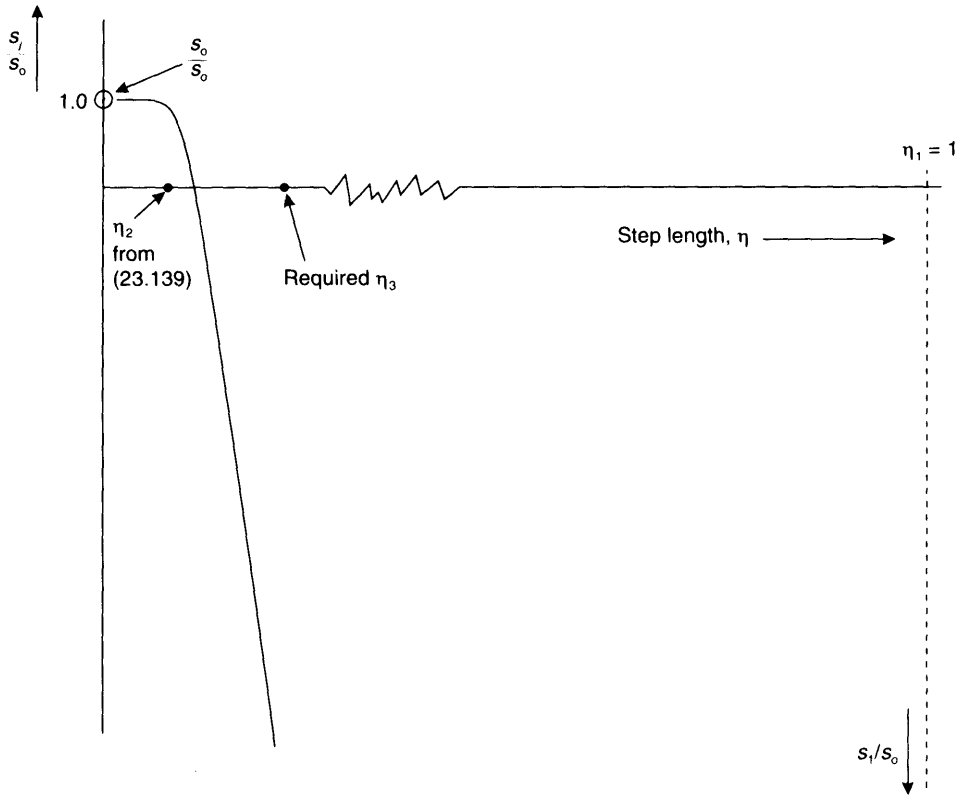

Figure 23.12 Line searches with contact.

23.14 SPECIAL NOTATION

Scalars

α = in two dimensions, non-dimensional coordinate of contact point
α_o = in two dimensions , value of α on first contact
ε = penalty or contact stiffness
ξ, η = in three dimensions, non-dimensional coordinates of contact point
ξ_o, η_o = in three dimensions, values of ξ, η on first contact
$\Delta\eta$ = plastic strain rate multiplier (incremental)
l_o = in two dimensions, initial length of contact segment
l_n = in two dimensions, current length of contact segment
s = plus or minus 1
t = force (usually related to penalty stiffness)
λ = Lagrangian multiplier
μ = coefficient of friction
g_N = normal gap
g_T, g_{T1}, g_{T2} = tangential gaps

Vectors

$\bar{\mathbf{a}}$ = flow vector (see (23.38))
$\bar{\mathbf{b}}$ = plastic direction vector (see (23.39))
$\mathbf{a}$ = in two dimensions, vector of (23.7)
$\mathbf{b}$ = in two dimensions, vector of (23.5)
$\mathbf{b}_1$ = in two dimensions, vector of (23.14)
$\mathbf{c}$ = in two dimensions, vector of (23.16)
$\mathbf{d}_i$ = global displacement vector for master node i
$\mathbf{f}$ = in two dimensions, vector of (23.37)
$\mathbf{e}_1, \mathbf{e}_2$ = in two dimensions, unit vectors in tangential and normal directions
$\mathbf{e}_1, \mathbf{e}_2$ = in three dimensions, unit vectors in two tangential directions
$\mathbf{e}_3 = \mathbf{n}$ = in three dimensions, unit normal vector
$\mathbf{p}$ = global nodal displacement vector with slave node first (see (23.3) and (23.88))
$\mathbf{r}$ = current position vector of point immediately below slave node
$\mathbf{t}$ = vector of local forces
$\bar{\mathbf{t}}, \overset{*}{\mathbf{t}}, \overset{*}{\mathbf{t}}_i, \overset{*}{\mathbf{t}}_A, \mathbf{t}_{co}$ = see (23.119) and (23.122)
$\mathbf{x}_i$ = current coordinate vector for master node i
$\mathbf{X}_i$ = current coordinate vector for master node i
$\mathbf{X}_o$ = initial initial coordinte vector of contact point (see (23.115))
$\mathbf{X}$ = current initial coordinate vector of contact point (see (23.116))
$\mathbf{x}_s$ = current coordinate vector of slave node
$\boldsymbol{\lambda}$ = vector of Lagrangian multipliers
$\boldsymbol{g}$ = vector of gaps

Matrices

$\mathbf{A}$ = in three dimensions matrix (related to Jacobian)—see (23.86c)
$\bar{\mathbf{A}}_X$ = in three dimensions, matrix—see (23.118)
$\mathbf{B}$ = matrix relating changes in gaps to changes in global nodal displacements
$\mathbf{C}$ = penalty or 'contact' elastic stiffnesses (diagonal)
$\mathbf{C}_t$ = elasto-plastic tangential equivalent to $\mathbf{C}$
$\mathbf{C}_\xi, \mathbf{C}_\eta, \mathbf{C}_{\xi\eta}$ = see (23.91) and (23.123)
$\mathbf{D}$ = see (23.95)
$\mathbf{E}_o = [\mathbf{e}_{1o}, \mathbf{e}_{2o}, \mathbf{e}_{3o}]$ orthogonal triad defined at first contact (see (23.113))
$\mathbf{F}$ = see (23.90)
$\mathbf{W}, \mathbf{Y}, \mathbf{Z}$ = see (23.129), (23.119) and (23.135) respectively
$\boldsymbol{\alpha}(\mathbf{n}), \boldsymbol{\alpha}(\overset{*}{\mathbf{t}}_A)$ = see (23.106) and (23.124) respectively

Subscripts

a = relates to 'active set'
b = relates to 'non-contact elements'

c = relates to 'contact element'
p = plastic
T = tangential
N = normal
s = related to slave node

23.15 REFERENCES

[A1] Asghar, M., Contact and the nonlinear finite element method, Ph.D. thesis, to be submitted, Dept. of Aeronautics, Imperial College, London.

[B1] Beer, G. Isoparametric joint/interface element for finite element analysis, *Int. J. for Num. Meth. in Engng.*, **21**, 585–600 (1985).

[B2] Belytschko, T. & Neal, M. O., Contact-impact by the pinball algorithm with penalty and Lagrangian methods, *Int. J. for Num. Meth. in Engng.*, 547–572 (1991).

[B3] Bertsekas, D. P., *Constrained Optimisation and Lagrange Multiplier Methods*, Academic Press, New York (1984).

[C1] Carpenter, N. J., Taylor, T. R. L. & Katona, M. G., Lagrange constraints for transient finite element surface contact, *Int. J. for Num. Meth. in Engng.*, **32**, 103–128 (1991).

[C2] Chan, S. K. & Tuba, I. S., A finite element method for contact problems of solid bodies Part 1, Theory & validation, *Int. J. for Num. Meth. in Engng.*, **13**, 615–625 (1971).

[C3] Chaudaray, A. B. & Bathe, K. J., A solution method for static and dynamic analysis of contact problems with friction, *Comp. & Struct.*, **24**, 855–873 (1986).

[C4] Curnier, A. A theory of friction, *Int. J. Solids & Structs.*, **20**, 637–647 (1984).

[C5] Curnier, A. & Alart, P., Generalisation of Newton type methods to contact problems with friction, *Journal de Mécanique Théorique et appliquée*,**7**, 67–82 (1988).

[D1] de Souza Neto, E. A., Hashimoto, K., Peric, D. & Owen, D. R. J., Phenomenological model for frictional contact of coated steel sheets, *J. of Materials Processing Tech.*, **50**, 252–263 (1995).

[E1] Eterovic, A. & Bathe, K. J., An interface interpolation scheme for quadratic convergence in the finite element analysis of contact problems, *Computational Methods in Nonlinear Mechanics*, ed. P. Wriggers and W. Wagner, Springer-Verlag, Berlin, pp. 703–715 (1991).

[F1] Fletcher, R., *Practical Methods of Optimisation*, 2nd edn, Wiley, New Delhi (1989).

[F2] Fortin, M. & Fortin, A., A generalisation of Uzawa's algorithm for the solution of the Navier–Stokes equations, *Commn. in Appl. Num. Meth.*, **1**, 205–208 (1985).

[F3] Fracavilla, A. & Zienkiewicz, O. C., A note on the numerical computation of elastic contact problems, *Int. J. for Num. Meth. in Engng.*, **9**, 913–924 (1975).

[G1] Gallego, F. J. & Anza, J. J., A mixed finite element for the elastic contact problem, *Int. J. for Num. Meth. in Engng.*, **28**, 1249–164 (1989).

[G2] Giannakopoulos, A. E., The return mapping method for the integration of friction constitutive relations, *Comp. & Struct.*, **32**, 157–167 (1989).

[H1] Hallquist, J. O., *An Implicit, Finite Deformation, Finite Element Code for Analysing Static and Dynamic Response of 2-D Solids*, Report UCID-19677, Lawrence Livermore Lab. (1983).

[H2] Hallquist, J. O., Goudreau, G. L. & Benson, D., Sliding interfaces with contact-impact in large-scale Lagrangian computations, *Comp. Meth. in Appl. Mech. & Engng.*, **51**, 107–137 (1985).

[H3] Hallquist, J. O., Schweizerhof, K. & Stillman, D., Efficiency refinements of contact strategies and algorithms in explicit F. E. programming, *Computational Plasticity: Fundamentals & Applications*, ed. D. R. J. Owen *et al.*, Pineridge Press, Swansea, pp. 457–481 (1992).

[H4] Heegard. J.-H. & Curnier, A., an augmented Lagrangian formulation for discrete large slip contact problems, *Int. J. for Num. Meth. in Engng.*, **36**, 569–593 (1993).

[H4] Heege, A., Alart, P. & Onate, E., Numerical modelling and simulation of frictional contact using a generalised Coulomb law, *Engineering Computations*, **12**, 641–656 (1995).

[H5] Hughes, T. J. R., Taylor, R. L., Sackman, J. L., Curnier, A. & Kanoknukulchai, W., A finite element method for a class of contact–impact problems, *Comp. Mech. in Appl. Meth. & Engng.*, **8**, 249–276 (1976).

[J1] Ju, Jiann-Wen, Taylor, R. L., Cheng, L. Y., A consistent finite element formulation of nonlinear frictional contact problems *NUMETA 87*, Vol. 1, ed. G. N. Pande & J. Middleton, Martinus Nijhoff Dordrecht, pp. D5/1-D5/13 (1987).

[K1] Kikuchi, N. & Oden, J. T., Contact problems in elasticity: a study of variational inequalities and finite element methods, *SIAM*, Philadelphia (1988).

[K2] Klarbring, A. & Bjorkman, G., Solution of large displacement contact problems with friction using Newton's method for generalised equations, *Int. J. for Num. Meth. in Engng.*, **34**, 249–269 (1992).

[L1] Laursen, T. A. & Simo, J. C., On the formulation and numerical treatment of finite deformation contact problems, *Computational Methods in Nonlinear Mechanics*, ed. P. Wriggers and W. Wagner, Springer-Verlag, Berlin, pp. 716–736 (1991).

[L2] Laursen, T. A. & Simo, J. C., A continuum-based finite element formulation for the implicit solution of multibody, large-deformation, frictional, contact problems, *Int. J. for Num. Meth. in Engng.*, **36**, 3451–3486 (1993).

[L3] Laursen, T. A. & Simo, J. C., Algorithmic symmetrization of Coulomb frictional problems using augmented Lagrangians, *Computer Methods in Appl. Mech. & Engng.*, **108**, 133–146 (1993).

[L4] Luenberger, D. G., *Linear and Nonlinear Programming*, 2nd edn, Addison-Wesley, Reading, Mass. (1984).

[M1] Mottershead, J. E., Pascoe, S. K. & English, R. G., A general finite element approach for contact stress analysis, *Int. J. for Num. Meth. in Engng.*, **33**, 767–779 (1992).

[M2] Michalowski, R. & Mroz, Z., Associated and non-associated sliding rules in contact friction problems, *Arch. Mech.*, **39**, 259–276 (1978).

[N1] Nour-Omid, B. & Wriggers, P., A note on the optimum choice for penalty parameters, *Comm. Appl. Num. Meth.*, **3**, 581–585 (1987).

[O1] Oden, J. T. & Martins, J. A. C., Models and computational methods for dynamic frictional phenomena, *Comp. Meth. in Appl. Mech. & Engng.*, **52**, 527–634 (1985).

[O2] Oldenburg, M. & Nilsson, The position code algorithm for contact searching, *Int J. for Num. Meth. in Engng.*, **37**, 359–386 (1994).

[P1] Papadopoulos, P. & Taylor, R. L., A mixed formulation for the finite element solution of contact problems, *Comp. Meth. in Appl. Mech. & Engng.*, **94**, 373–389 (1992).

[P2] Papadopoulos, P., Jones, R. E. & Solberg, J. M., A novel finite formulation for frictionless contact problems, *Int. J. for Num. Meth. in Engng.*, **38**, 2603–2617 (1995).

[P3] Parisch, H., A consistent tangent stiffness matrix for three-dimensional contact analysis, *Int. J. for Num. Meth. in Engng.*, **28**, 1803–1812 (1989).

[P4] Peric, D. & Owen, D. R. J., Computational model for 3-D contact problems with friction based on the penalty method, *Int. J. for Num. Mech. in Engng.*, **35**, 1289–1309 (1992).

[P5] Powell, M. J. D., A method for nonlinear constraints in minimisation, in *Optimisation*, ed. R. Fletcher, Academic Press, New York (1969).

[R1] Rockefellar, R. T., Augmented Lagrange multiplier functions and duality in non-convex programming, *SIAM J. Control*, **12**, 268–285 (1974).

[S1] Simo, J. C. & Laursen, T. A., An augmented Lagrangian treatment of contact problems involving friction, *Comp. & Struct.*, **42**(1), 97–116 (1992).

[S2] Simo, J. C., Wriggers, P. & Taylor, R. L., A perturbed Lagrangian formulation for the inite element solution of contact problems, *Comp. Meth. in Appl. Mech. & Engng.*, **51**, 163–180 (1985).

[T1] Taylor, L. M. & Flanagan, D. P., *PRONTO3D, a Three-dimensional Transient Solid Dynamics Program*, SAND87-1912, Sandia National Laboratories, Albuquerque, New Mexico, pp. 92–95 (1989).

[T2] Taylor, R. L. & Papadopoulos, P., On a patch test for contact problems in two dimensions, *Computational Methods in Nonlinear Mechanics*, ed. P. Wriggers and W. Wagner, Springer-Verlag, Berlin, pp. 690–702 (1991).

[V1] Vanderplaats, G. N., Numerical optimisation techniques for engineering design: with applications, McGraw-Hill, New York, 1984.

[W1] Wriggers, P. & Simo, J. C., A note on tangent stiffness for fully nonlinear contact problems, *Comm. Appl. Num. Meth.*, **1**, 199–203 (1985).

[W2] Wriggers, P., Simo, J. C. & Taylor, R. L., Penalty and augmented Lagrangian formulations for contact problems, *Proc. NUMETA '85 Conf., Swansea*, pp. 97–106 (1985).

[W3] Wriggers, P., Wagner, W. & Simo, J. C., Algorithms for non-linear contact constraints with application to stability problems of rods and shells, *Comp. Mechanics*, **2**, 215–230 (1987).

[W4] Wriggers, P. & Zavarise, G., On the application of augmented Lagrangian techniques for nonlinear constitutive laws in contact interfaces, *Comm. Appl. Num. Meth.*, **9**, 815–824 (1996).

[W5] Wriggers, P., Vu Van, T. & Stein, E., Finite element formulation of large deformation impact–contact problems with friction, *Comp. & Struct.*, **37**, 319–331 (1990).

[Z1] Zavarise, G., Schrefler, B. & Wriggers, P. Consistent formulation for thermomechanical contact based on microscopic interface laws, *Mechanics Research Communications*, **19**, 173–182 (1992).

[Z2] Zavarise, G., Wriggers, P. & Schrefler, B. A., A new method for solving contact problems, submitted to *Int. J. for Num. Meth. in Engng.* (1995).

[Z3] Zhong, Z.-H. & Mackerle, J., Static contact problems—a review, *Engineering Computations*, **9**, 3–37 (1992).

24 Non-linear dynamics

24.1 INTRODUCTION

Chapters on the application of the finite element method to dynamics can be found in the books by Hughes [H3.13], Zienkiewicz and Taylor [Z1.14], Bathe [B1.10] and Argyris and Mlejnek [A1]. The latter book also gives a good general introduction to dynamics. Conventional finite element solution procedures can be divided into two main types: explicit and implicit. The former is traditionally used for wave propagation and high-velocity impact problems, while the latter is more appropriate for structural applications dominated by the low-frequency response. In this chapter we will consider both techniques.

Conventional implicit techniques adopt very similar predictor/corrector procedures to those used for non-linear statics. However, the out-of-balance force vector is now augmented by the mass × acceleration terms while the conventional static tangent stiffness matrix is augmented by a factor × the mass matrix and another factor × the damping matrix. Dynamic equilibrium is usually enforced at the end of the time step. However, it will be shown in this chapter that there are alternative strategies including those that enforce a form of 'mid-point' dynamic equilibrium and, in some cases, are 'energy conserving'.

Various time-integration strategies can be used for updating the velocities and accelerations with the Newmark methods being very popular. In the present chapter these methods will provide a starting-point to introduce both 'implicit procedures' and 'explicit procedures'. The latter involve no real equation solving, but there are tight restrictions on the size of the time steps.

The initial sections will concentrate on continua or, more specifically, on finite element formulations in which the only variables are translations. As with statics (Chapters 16 and 17), considerable complexities are introduced once rotational variables are introduced in a three-dimensional context. These issues will be addressed in the latter sections (Section 24.14 onwards).

24.2 NEWMARK'S METHOD

It will be assumed that we are given a fixed 'mass matrix' $\mathbf{M}$ (more details in Section 24.9) and a fixed 'damping matrix' $\mathbf{C}$. In these circumstances, the dynamic equilibrium equations at the end of a step may be expressed as

$$\bar{\mathbf{g}}_{n+1} = \{\mathbf{q}_{i,n+1} - \mathbf{q}_{e,n+1}\} + \mathbf{M}\ddot{\mathbf{d}}_{n+1} + \mathbf{C}\dot{\mathbf{d}}_{n+1} = \mathbf{g}_{n+1} + \mathbf{M}\ddot{\mathbf{d}}_{n+1} + \mathbf{C}\dot{\mathbf{d}}_{n+1} = 0 \qquad (24.1)$$

where $\mathbf{g}_{n+1}$ are the 'static out-of balance forces' and $\bar{\mathbf{g}}_{n+1}$ the equivalent dynamic out-of-balance forces. If geometric non-linearity is present, the 'static internal forces', $\mathbf{q}_{i,n+1}$, in (24.1) can be computed using any of the methods that have been discussed earlier for statics. In particular, we may use a total Lagrangian formulation (Chapter 5), a 'Eulerian formulation' (Chapter 12) or a 'co-rotational formulation' (Chapters 17 and 18).

The $\mathbf{d}$'s in (24.1) are nodal displacements, the $\dot{\mathbf{d}}$'s are nodal velocities and the $\ddot{\mathbf{d}}$'s are nodal accelerations. We are not using our usual notation with $\mathbf{p}$'s as the nodal variables in order to emphasise that, at present, we are only considering nodal translations. The more complex issue of nodal rotations will be considered later in Section 24.14. In order to supplement (24.1), Newmark's time integration procedure [N1] involves:

$$\mathbf{d}_{n+1} = \mathbf{d}_n + \Delta t \dot{\mathbf{d}}_n + \frac{\Delta t^2}{2}\{(1-2\beta)\ddot{\mathbf{d}}_n + 2\beta\ddot{\mathbf{d}}_{n+1}\} \tag{24.2}$$

and

$$\dot{\mathbf{d}}_{n+1} = \dot{\mathbf{d}}_n + \Delta t\{(1-\gamma)\ddot{\mathbf{d}}_n + \gamma\ddot{\mathbf{d}}_{n+1}\} \tag{24.3}$$

where γ and β are the Newmark constants. By adopting certain choices for these constants, we can obtain either 'implicit methods' or 'explicit methods'. In the following, we will start by describing one of the best known implicit procedure and will show how it can be set within a 'predictor corrector framework' that is very similar to that conventionally applied with non-linear static analysis.

24.3 THE 'AVERAGE ACCELERATION METHOD' OR 'TRAPEZOIDAL RULE'

If we set $\beta = 1/4$ and $\gamma = 1/2$, then from (24.2) and (24.3), we obtain:

$$\mathbf{d}_{n+1} = \mathbf{d}_n + \Delta t \dot{\mathbf{d}}_n + \frac{\Delta t^2}{4}\{\ddot{\mathbf{d}}_n + \ddot{\mathbf{d}}_{n+1}\} \tag{24.4}$$

and

$$\dot{\mathbf{d}}_{n+1} = \dot{\mathbf{d}}_n + \frac{\Delta t}{2}\{\ddot{\mathbf{d}}_n + \ddot{\mathbf{d}}_{n+1}\} \tag{24.5}$$

Using (24.5), (24.4) can be re-expressed as.

$$\mathbf{d}_{n+1} = \mathbf{d}_n + \frac{\Delta t}{2}\{\dot{\mathbf{d}}_n + \dot{\mathbf{d}}_{n+1}\} \tag{24.6}$$

Equations (24.5) and (24.6) are both in the form of 'trapezoidal rules'.

24.4 THE 'IMPLICIT SOLUTION PROCEDURE'

If all of the required information is available at step n, we can use (24.5) and (24.6) to substitute for $\dot{\mathbf{d}}_{n+1}$ and $\ddot{\mathbf{d}}_{n+1}$ into the dynamics equilibrium equations (24.1). This process leads to a set of equations of the form:

$$\bar{\mathbf{g}}_{n+1}(\mathbf{d}_{n+1}) = \bar{\mathbf{g}}_{n+1}(\mathbf{q}_{i,n+1}(\mathbf{d}_{n+1}), \mathbf{d}_{n+1}) = \mathbf{0} \tag{24.7}$$

As with the equivalent static non-linear equilibrium equations, these equations are non-linear in $\mathbf{d}_{n+1}$ and, following the static procedure, we can solve them with the aid of a 'predictor-corrector technique'.

24.4.1 The 'predictor step'

Using a truncated Taylor series, let us assume that:

$$\mathbf{q}_{\mathrm{i},n+1} = \mathbf{q}_{\mathrm{i},n} + \left.\frac{\partial \mathbf{q}_{\mathrm{i}}}{\partial \mathbf{d}}\right|_n (\mathbf{d}_{n+1} - \mathbf{d}_n) = \mathbf{q}_{\mathrm{i},n} + \mathbf{K}_{\mathrm{t},n}\Delta\mathbf{d} \tag{24.8}$$

where $\mathbf{K}_{t,n}$ is the conventional 'static tangent stiffness matrix' computed at step n. Substitution from (24.8) for $\mathbf{q}_{\mathrm{i},n+1}$, from (24.5) for $\ddot{\mathbf{d}}_{n+1}$, and from (24.6) for $\dot{\mathbf{d}}_{n+1}$ into (24.1) leads to the relationship:

$$\mathbf{q}_{\mathrm{i},n} - \mathbf{q}_{\mathrm{e},n+1} + \mathbf{K}_{\mathrm{t},n}\Delta\mathbf{d} + \mathbf{M}\left(\frac{4}{\Delta t^2}\Delta\mathbf{d} - \frac{4}{\Delta t}\dot{\mathbf{d}}_n - \ddot{\mathbf{d}}_n\right) + \mathbf{C}\left(\frac{2}{\Delta t}\Delta\mathbf{d} - \dot{\mathbf{d}}_n\right) = \mathbf{0} \tag{24.9}$$

from which:

$$\Delta\bar{\mathbf{q}}_{\mathrm{e}} = \bar{\mathbf{K}}_{\mathrm{t},n}\Delta\mathbf{d} \tag{24.10}$$

where

$$\bar{\mathbf{K}}_{\mathrm{t},n} = \mathbf{K}_{\mathrm{t},n} + \frac{4}{\Delta t^2}\mathbf{M} + \frac{2}{\Delta t}\mathbf{C} \tag{24.11}$$

and

$$\Delta\bar{\mathbf{q}}_{\mathrm{e}} = \mathbf{q}_{\mathrm{e},n+1} - \mathbf{q}_{\mathrm{i},n} + \mathbf{M}\left(\frac{4}{\Delta t}\dot{\mathbf{d}}_n + \ddot{\mathbf{d}}_n\right) + \mathbf{C}\dot{\mathbf{d}}_n \tag{24.12}$$

or

$$\Delta\bar{\mathbf{q}}_{\mathrm{e}} = \Delta\mathbf{q}_{\mathrm{e}} + \mathbf{M}\left(\frac{4}{\Delta t}\dot{\mathbf{d}}_n + 2\ddot{\mathbf{d}}_n\right) + 2\mathbf{C}\dot{\mathbf{d}}_n \tag{24.13}$$

where in deriving (24.13), we have used (24.1) at n, thereby assuming exact satisfaction of dynamic equilibrium at the previous time step.

Equation (24.10) provides a conventional incremental 'predictor step' although it now uses an equivalent dynamic tangent stiffness matrix, $\bar{\mathbf{K}}_{\mathrm{t},n}$ which includes contributions from both the mass and damping matrices.

24.4.2 The 'corrector'

Having solved (24.10) for $\Delta\mathbf{d}$, the displacement at step $n+1$ can be obtained as $\mathbf{d}_{n+1} = \mathbf{d}_n + \Delta\mathbf{d}$ and we can use (24.6) to obtain $\dot{\mathbf{d}}_{n+1}$ and (24.5) to obtain $\ddot{\mathbf{d}}_{n+1}$. Knowing $\mathbf{d}_{n+1}$, we can also compute the stresses at $n+1$ and hence obtain the internal forces $\mathbf{q}_{\mathrm{i},n+1}$ as if we were using a static algorithm. Again, as in statics, substitution into (24.1) will, in general, lead to a residual, $\bar{\mathbf{g}}_{n+1}$ that is not zero. Consequently, we now employ a Newton–Raphson (or modified Newton–Raphson or quasi-Newton) corrector. To

this end, a truncated Taylor series is first applied to $\mathbf{g}_{n+1}$ so that:

$$\mathbf{g}_{n+1,\text{new}} = \mathbf{g}_{n+1,\text{old}} + \frac{\partial \mathbf{g}}{\partial \mathbf{d}} \delta \mathbf{d}_{n+1} = \mathbf{g}_{n+1,\text{old}} + \mathbf{K}_{t,n+1} \delta \mathbf{d}_{n+1} \tag{24.14}$$

while from (24.6):

$$\delta \dot{\mathbf{d}}_{n+1} = \frac{2}{\Delta t} \delta \mathbf{d}_{n+1} \tag{24.15}$$

and from (24.5) and (24.15):

$$\delta \ddot{\mathbf{d}}_{n+1} = \frac{4}{\Delta t^2} \delta \mathbf{d}_{n+1} \tag{24.16}$$

We can now use (24.14)–(24.16) to apply a truncated Taylor series on (24.1) so that:

$$\bar{\mathbf{g}}_{n+1,\text{new}} = \bar{\mathbf{g}}_{n+1,\text{old}} + \bar{\mathbf{K}}_{t,n+1} \delta \mathbf{d}_{n+1} \tag{24.17}$$

where $\bar{\mathbf{K}}_{t,n+1}$ is given by

$$\bar{\mathbf{K}}_{t,n+1} = \mathbf{K}_{t,n+1} + \frac{4}{\Delta t^2} \mathbf{M} + \frac{2}{\Delta t} \mathbf{C} \tag{24.18}$$

which takes the same form as that previously given in (24.11) for the predictor step. If $\bar{\mathbf{g}}_{n+1,\text{old}} \neq \mathbf{0}$, we assume that by setting $\bar{\mathbf{g}}_{n+1,\text{new}} = \mathbf{0}$ in (24.17), we will obtain an improvement $\delta \mathbf{d}_{n+1}$ to $\mathbf{d}_{n+1}$ so that:

$$\delta \mathbf{d}_{n+1} = -\bar{\mathbf{K}}^{-1}_{t,n+1} \bar{\mathbf{g}}_{n+1} \tag{24.19}$$

where we have dropped the 'old' subscript on $\bar{\mathbf{g}}_{n+1}$ but, as with the usual static Newton–Raphson iterations, it is implied.

The predictor-corrector algorithm of Sections 24.4.1 and 24.4.2 takes a very similar form to conventional non-linear static procedures. However, it is worth emphasising one very important distinction. With a static procedure, without material non-linearity, a converged solution corresponding to a particular set of external loads, should be independent of the adopted 'incremental steps'. This should strictly be true provided there is no material non-linearity and provided the converged equilibrium state is stable—i.e. we are ignoring the issue of multiple equilibrium states associated with limit points or bifurcations. However, in non-linear dynamics, even if we have converged to a configuration whereby $\bar{\mathbf{g}}_{n+1} = \mathbf{0}$, in general there will still be an error associated with the 'time integration'. This error will be related to the size of the 'time steps' and can be controlled if methods are introduced so that the 'time steps are limited' (see Section 24.13).

The implicit solution technique has so far been described in relation to the 'average acceleration method' or 'trapezoidal rule', but the methodology could equally be applied to other 'time integration techniques'.

24.5 AN EXPLICIT SOLUTION PROCEDURE

Explicit solution schemes have been described by Belytschko and Schwer [B3.17], and Belytschko [B2, B3] among others. By setting $\gamma = 1/2$ and $\beta = 0$ in (24.2) and (24.3), we

obtain:

$$\mathbf{d}_{n+1} = \mathbf{d}_n + \Delta t \dot{\mathbf{d}}_n + \frac{\Delta t^2}{2} \ddot{\mathbf{d}}_n \tag{24.20}$$

and

$$\dot{\mathbf{d}}_{n+1} = \dot{\mathbf{d}}_n + \frac{\Delta t}{2} \{ \ddot{\mathbf{d}}_n + \ddot{\mathbf{d}}_{n+1} \} \tag{24.21}$$

It will again assumed that all of the information is available at step n. Hence, from (24.20), we can obtain $\mathbf{d}_{n+1}$ and hence both the stresses at $n+1$ and the 'static internal forces' $\mathbf{q}_{i,n+1}$ at $n+1$ so that the 'static residual', $\mathbf{g}_{n+1}$ is known. Substituting from (24.21) into (24.1), we obtain:

$$\mathbf{g}_{n+1} + \mathbf{C}\left(\dot{\mathbf{d}}_n + \frac{\Delta t}{2} \ddot{\mathbf{d}}_n \right) + \left(\mathbf{M} + \frac{\Delta t}{2} \mathbf{C} \right) \ddot{\mathbf{d}}_{n+1} = \dot{\mathbf{g}}_{n+1} + \left[\mathbf{M} + \frac{\Delta t}{2} \mathbf{C} \right] \ddot{\mathbf{d}}_{n+1} = \mathbf{0} \tag{24.22}$$

which can be solved to give:

$$\ddot{\mathbf{d}}_{n+1} = - \left[\mathbf{M} + \frac{\Delta t}{2} \mathbf{C} \right]^{-1} \dot{\mathbf{g}}_{n+1} \tag{24.23}$$

In explicit dynamics it is assumed that the mass matrix $\mathbf{M}$ can be diagonalised (possibly using a technique such as that in [H5]). If diagonal matrices are assumed for both $\mathbf{M}$ and $\mathbf{C}$, the computation of $\ddot{\mathbf{d}}_{n+1}$ from (24.23) is trivial. However, in many circumstances, it is unrealistic to use a lumped damping matrix, and one is forced to make the algorithm asynchronous by introducing $\mathbf{c}\dot{\mathbf{d}}_n$ rather than $\mathbf{C}\dot{\mathbf{d}}_{n+1}$ in (24.1). In these circumstances, in place of (24.23), we obtain:

$$\ddot{\mathbf{d}}_{n+1} = - \mathbf{M}^{-1} (\mathbf{g}_{n+1} + \mathbf{C}\dot{\mathbf{d}}_n) \tag{24.24}$$

Having obtained $\ddot{\mathbf{d}}_{n+1}$ from (24.23) and (24.24), we can use (24.20) to obtain $\mathbf{d}_{n+2}$ and (24.21) to obtain $\dot{\mathbf{d}}_{n+1}$ so that all of the information is now known at step $n+1$ and we are ready to move on to the next step.

24.6 A STRAGGERED, CENTRAL DIFFERENCE, EXPLICIT SOLUTION PROCEDURE

Most 'explicit dynamics' computer programs adapt a slightly different, staggered, time-marching procedure with the nodal velocities being computed at the half time steps (i.e. $\dot{\mathbf{d}}_{n+1/2}$) and the stresses, displacements and accelerations at the whole time steps (i.e $\boldsymbol{\sigma}_{n+1}$ and $\mathbf{d}_{n+1}$ and $\ddot{\mathbf{d}}_{n+1}$). The time integration algorithms are then:

$$\ddot{\mathbf{d}}_n = \frac{1}{\Delta t} (\dot{\mathbf{d}}_{n+1/2} - \dot{\mathbf{d}}_{n-1/2}) \tag{24.25}$$

$$\dot{\mathbf{d}}_{n+1/2} = \frac{1}{\Delta t} (\mathbf{d}_{n+1} - \mathbf{d}_n) \tag{24.26}$$

which involve central difference approximations.

It will be assumed that we know the velocity at step $n-\frac{1}{2}$ and the displacements (or coordinates) at step n. Also, the stresses will be known at step n and hence the internal force vector $\mathbf{q}_{i,n}$ may be obtained. This will usually involve a Eulerian formulation (Chapter 12). (Details of the stress-updating algorithm, which uses the Jaumann rate in conjunction with this staggered updating scheme, are given in Section 19.4.)

If it is assumed that the damping matrix, $\mathbf{C}$, is non-diagonal we must again introduce an asynchronous term so that, in place of (24.24), we now obtain:

$$\ddot{\mathbf{d}}_n = -\mathbf{M}^{-1}(\mathbf{g}_n + \mathbf{C}\dot{\mathbf{d}}_{n-1/2}) \tag{24.27}$$

As a start, both the displacements $\mathbf{d}_0$ and velocities $\dot{\mathbf{d}}_0$ will be assumed known as will any initial stresses. There are a number of variants on the starting procedure. Here, it will also be assumed that $\dot{\mathbf{d}}_{-1/2}$ is equal to $\dot{\mathbf{d}}_0$. To start the algorithm, we compute $\mathbf{g}_0$ (possibly zero) and then begin with a modified form of (24.27) so that the complete algorithm takes the form:

(1) $\ddot{\mathbf{d}}_0 = -\mathbf{M}^{-1}(\mathbf{g}_0 + \mathbf{C}\dot{\mathbf{d}}_0)$.
(2) $\dot{\mathbf{d}}_{1/2} = \Delta t\ddot{\mathbf{d}}_0 + \dot{\mathbf{d}}_{-1/2} = \Delta t\ddot{\mathbf{d}}_0 + \dot{\mathbf{d}}_0$ (from (24.25).
(3) $\mathbf{d}_1 = \Delta t\dot{\mathbf{d}}_{1/2} + \mathbf{d}_0$ from (24.26).
(4) Compute $\boldsymbol{\sigma}_1$ and $\mathbf{q}_{i,1}$ using the methods of Section 19.4.
(5) $\ddot{\mathbf{d}}_1 = -\mathbf{M}^{-1}(\mathbf{g}_1 + \mathbf{C}\dot{\mathbf{d}}_{1/2})$ from (24.27).
(6) $\dot{\mathbf{d}}_{3/2} = \Delta t\ddot{\mathbf{d}}_1 + \dot{\mathbf{d}}_{1/2}$ from (24.25).
(7) $\mathbf{d}_2 = \Delta t\dot{\mathbf{d}}_{3/2} + \mathbf{d}_1$ from (24.26, et.)

Algorithm 24.1 A staggered explicit, time-marching procedure.

If variable time steps are to be introduced, we can replace Δt in (24.25) by Δt_n and Δt in (24.26) by $\Delta t_{n+1/2}$ where:

$$\Delta t_{n+1/2} = \tfrac{1}{2}(\Delta t_n + \Delta t_{n+1}) \tag{24.28}$$

In relation to the stress updating, in (19.41), (19.43) and (19.44), we would replace Δt by $\Delta t_{n+1/2}$. Generally, for explicit computer codes, the time step size is governed by issues of stability.

24.7 STABILITY

Although much work has been devoted to the stability of time-marching algorithms [H8, H3.13, Z1.14], a lot of this work strictly relates to the linear regime. For such problems, assuming $\mathbf{C} = \mathbf{0}$ and that there are no external forces (24.1) becomes:

$$\mathbf{K}\mathbf{d} + \mathbf{M}\ddot{\mathbf{d}} = \mathbf{0} \tag{24.29}$$

We will assume that the solution takes the from:

$$\mathbf{d} = \mathbf{a}e^{i\omega t} \tag{24.30}$$

so that equation (24.29) can be re-expressed as an eigenvalue problem to obtain the frequency, ω, and the equivalent eigenvectors, $\mathbf{a}$, so that:

$$[\mathbf{K} - \omega^2\mathbf{M}]\mathbf{a} = [\mathbf{K} - \lambda\mathbf{M}]\mathbf{a} = \mathbf{0} \tag{24.31}$$

In a particular mode, the period is given by $2\pi/\omega$. For linear systems, it can be shown that the 'average acceleration' or trapezoidal rule (Newmark with $\beta = 1/4$ and $\gamma = 1/2$)

is unconditionally stable (irrespective of the size of the time step) while the equivalent explicit method (Newmark with $\beta = 0$ and $\gamma = 1/2$) is conditionally stable so that the time step is limited by

$$\Delta t \leqslant \Delta t_{\text{crit}} = \frac{2}{\omega_{\max}} \tag{24.32}$$

Strictly, to obtain $\omega_{\max}$, we should solve the structural eigenvalue problem in (22.31). Fortunately, however we can bracket $\omega_{\max}$ using:

$$\omega_{\max} \leqslant \max_{\text{all } e} \omega_{\max}^{(e)} \tag{24.33}$$

where the e symbol relates to the elements. In other words, we can use the maximum of the maximum ω over all of the elements. In practice, we do not even need to conduct the eigenvalue analysis at the element level, but may instead use Gorschgerin's theorem [J2] or alternatively simple formulae that have been given for a range of elements by Belytschko [B2, B3].

It was stated earlier that the 'average acceleration' or 'trapezoidal rule' was unconditionally stable. Unfortunately this is only true for 'linear systems' and, among others Simo and co-workers [S3–S5] and the author and co-workers [C2–C4, G1] have shown that severe numerical instabilities can arise for non-linear problems.

These difficulties are illustrated in Figures 24.2–24.4 which involves the analysis of the simple pendulum of Figure 24.1 which was originally analysed and discussed by Bathe in his book [B1.10] and study guide [B1]. In both cases, the pendulum was dropped from the horizontal position while for the results shown in Figures 24.2–24.4 (details in [C2]), the mass was 'fired' with an initial horizontal velocity of 772.5 cm/sec from the vertical position. (The basic behaviour is very similar for the two cases.)

The results in Figures 24.2–24.4 that are labelled Newmark relate to the 'average acceleration method' or 'trapezoidal rule' with $\beta = 1/4$ and $\gamma = 1/2$ (Section 24.3 and 24.4). From the response in Figure 24.2, it can be seen that, using this method, a time step of the order of 0.025s is required (in comparison with the period of the order of

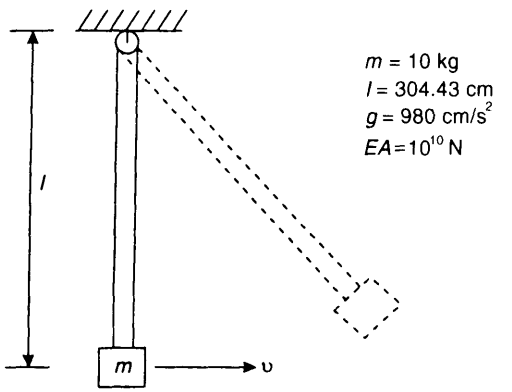

Figure 24.1 Simple pendulum.

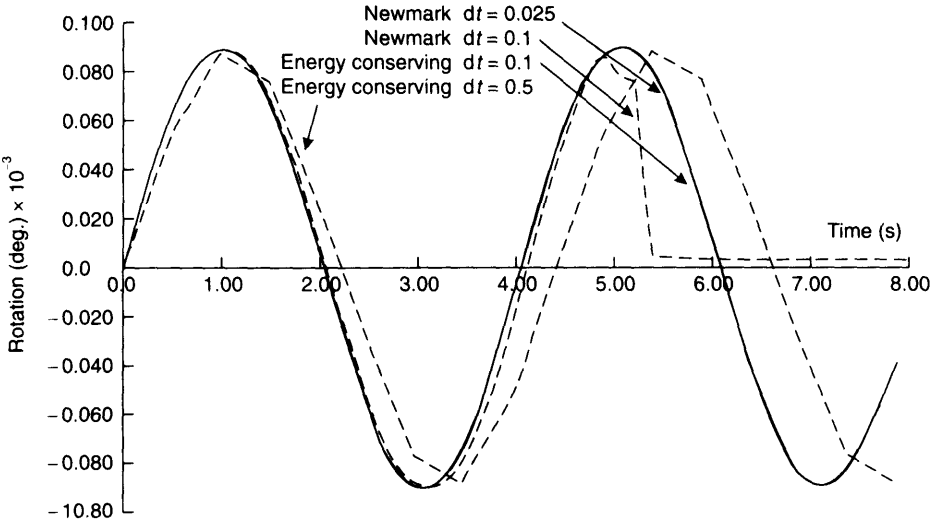

Figure 24.2 Computed responses for simple pendulum.

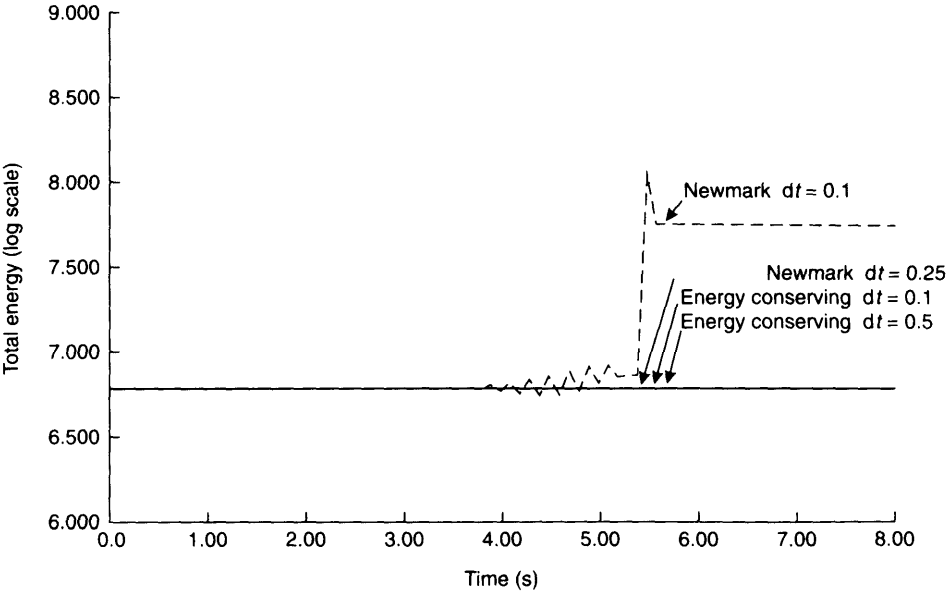

Figure 24.3 Variation of energy with time.

4.0 s) to obtain a satisfactory (but for how long?) solution. If a time step of 0.1 s is adopted, the solution 'locks' at a position close to the initial position after one and a quarter periods. Figure 24.3 shows that, prior to this 'locking', there has been a build-up of energy with an increasing percentage going into strain energy rather than kinetic energy. This increase is associated (Figure 24.4) with an oscillating axial strain

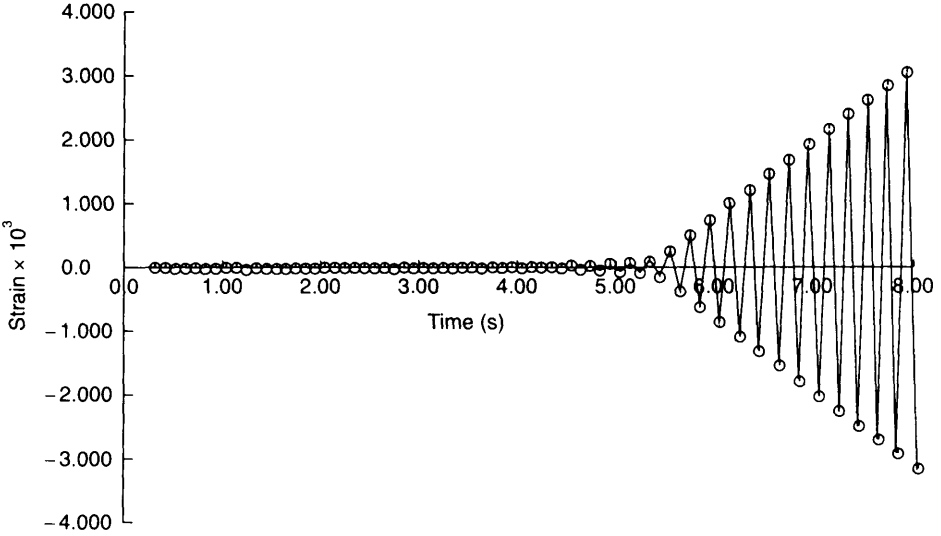

Figure 24.4 Variation of axial strain with time (with Newmark method)

(Figure 24.4). It should be emphasised that there are no numerical difficulties in obtaining the 'locked solutions' shown in Figures 24.2 and 24.3. The predictor-corrector procedure does not 'blow up', but rather converges to the 'wrong solution'. Indeed in some cases [C3], these 'wrong solutions' are not obviously wrong (see also Stewart [S8] on the general pitfalls that can result from numerical time-integration schemes).

One possible remedy is the development of 'energy-conserving algorithms' which will be discussed later in Sections 24.10–24.12 and for which the results labelled 'energy conserving' in Figures 24.2 and 24.3 were obtained. Another possibility is to use an algorithm with some built-in 'numerical dissipation'. A popular method that falls into this category is described below.

24.8 THE HILBER–HUGHES–TAYLOR α METHOD

The Hilbert–Hughes–Taylor method [H4] was originally formulated in a linear context as a variant of the Newmark algorithm. We will here directly consider its application in a non-linear context and will rewrite (24.1) as

$$\bar{\mathbf{g}}_{n+1} = \dot{\mathbf{g}}_{n+1}(\alpha) + \mathbf{M}\ddot{\mathbf{d}}_{n+1} = \mathbf{0} \tag{24.34}$$

where

$$\begin{aligned}\mathbf{g}^{*}_{n+1}(\alpha) &= (1+\alpha)\{\mathbf{q}_{\mathrm{i},n+1} - \mathbf{q}_{\mathrm{e},n+1} + \mathbf{C}\dot{\mathbf{d}}_{n+1}\} - \alpha\{\mathbf{q}_{\mathrm{i},n} - \mathbf{q}_{\mathrm{e},n} + \mathbf{C}\dot{\mathbf{d}}_{n}\} \\ &= (1+\alpha)\{\mathbf{g}_{n+1} + \mathbf{C}\dot{\mathbf{d}}_{n+1}\} - \alpha\{\mathbf{g}_{n} + \mathbf{C}\dot{\mathbf{d}}_{n}\}\end{aligned} \tag{24.35}$$

In re-expressing the dynamic equilibrium equations in this way, we have effectively

related the inertia terms $\mathbf{M}\ddot{\mathbf{d}}_{n+1}$ to the 'end point' $n+1$ (or $\alpha=0$) while the static and damping terms are related to some point α (with $\alpha<0$). In this way we include a component of the terms from the previous step. The equilibrium equations of (24.34) and (24.35) are now combined with the time integration updates of (24.2) and (24.3).

To obtain an expression for the predictor step, we substitute into (24.34) and (24.35) from the truncated Taylor expansion for $\mathbf{q}_{i,n+1}$ previously given in (24.8) and from (24.3) and (24.2) for $\dot{\mathbf{d}}_{n+1}$ and from (24.2) for $\ddot{\mathbf{d}}_{n+1}$. This process leads to the incremental relationship of (24.10) ($\Delta\bar{\mathbf{q}}_e = \bar{\mathbf{K}}_{t,n}\Delta\mathbf{d}$) with:

$$\bar{\mathbf{K}}_{t,n} = (1+\alpha)\left[\mathbf{K}_{t,n} + \frac{\gamma}{\beta\Delta t}\mathbf{C}\right] + \frac{1}{\beta\Delta t^2}\mathbf{M} \tag{24.36}$$

and

$$\Delta\bar{\mathbf{q}}_e = (1+\alpha)(\mathbf{q}_{e,n+1} - \mathbf{q}_{i,n}) - \alpha(\mathbf{q}_{e,n} - \mathbf{q}_{i,n}) + \mathbf{M}\left(\frac{1}{\beta\Delta t}\dot{\mathbf{d}}_n + \frac{(1-2\beta)}{2\beta}\ddot{\mathbf{d}}_n\right)$$
$$+\left(-1+(1+\alpha)\frac{\gamma}{\beta}\right)\mathbf{C}\dot{\mathbf{d}}_n + \left(\frac{(1+\alpha)(\gamma-2\beta)\Delta t}{2\beta}\right)\mathbf{C}\ddot{\mathbf{d}}_n \tag{24.37}$$

With a view to obtaining the 'corrector', from the variation of (24.2), we have:

$$\delta\ddot{\mathbf{d}}_{n+1} = \frac{1}{\beta\Delta t^2}\delta\mathbf{d}_{n+1} \tag{24.38}$$

and from the variation of (24.3) in conjunction with (24.38), we have:

$$\delta\dot{\mathbf{d}}_{n+1} = \frac{\gamma}{\beta\Delta t}\delta\mathbf{d}_{n+1} \tag{24.39}$$

Substitution from (24.14), (24.38) and (24.39) into a truncated Taylor series from (24.34) to (24.35) leads to (24.17) where $\bar{\mathbf{K}}_{t,n+1}$ is now given by

$$\bar{\mathbf{K}}_{t,n+1} = (1+\alpha)\left[\mathbf{K}_{t,n+1} + \frac{\gamma}{\beta\Delta t}\mathbf{C}\right] + \frac{1}{\beta\Delta t^2}\mathbf{M} \tag{24.40}$$

and the Newton–Raphson iterative change is given by the standard equation (24.19).

For a linear system, if the parameters α, β and γ are chosen so that:

$$-1/3 \leqslant \alpha \leqslant 0; \qquad \beta=(1-\alpha)^2/4; \qquad \gamma=(1-2\alpha)/2 \tag{24.41}$$

an unconditionally stable, second-order accurate scheme results [H2, H3]. In a non-linear environment (where the method can be unstable [C5]), analysts typically use the scheme with $\alpha = -0.05$ [H2, H3]. When α is set to zero, the conventional implicit Newmark method is recovered.

24.9 MORE ON THE DYNAMIC EQUILIBRIUM EQUATIONS

If (as in all of the following), we neglect any damping terms, the previous dynamic equilibrium equations (24.1), can be considered as stemming from a weak form of the differential equation of dynamic equilibrium whereby:

$$\sigma_{ij,j} + b_i = \rho\ddot{x}_i \tag{24.42}$$

with b_i as the body forces and $\ddot{x}_i$ as the components of acceleration. For the present, we will not be precise regarding the definition of the 'type of stress'.

The weak form of (24.42) can be written as

$$\int \boldsymbol{\sigma}^{\mathrm{T}} \delta \boldsymbol{\varepsilon}_{\mathrm{v}} \, \mathrm{d}V - \int \delta \mathbf{u}_{\mathrm{v}}^{\mathrm{T}} \mathbf{b} \, \mathrm{d}V + \int \rho \delta \mathbf{u}_{\mathrm{v}}^{\mathrm{T}} \ddot{\mathbf{u}} \, \mathrm{d}V = 0 \tag{24.43}$$

where the subscript v means virtual. Following from the finite element discretisations whereby:

$$\mathbf{u} = \mathbf{H}\mathbf{d}; \qquad \delta \mathbf{u} = \mathbf{H}\delta \mathbf{d}; \qquad \ddot{\mathbf{u}} = \mathbf{H}\ddot{\mathbf{d}}; \qquad \delta \boldsymbol{\varepsilon} = \mathbf{B}\delta \mathbf{d} \tag{24.44}$$

we arrive at the equations:

$$\delta \mathbf{d}_{\mathrm{v}}^{\mathrm{T}} \bar{\mathbf{g}} = 0 \tag{24.45}$$

where $\bar{\mathbf{g}}$ is the dynamic residual given by

$$\bar{\mathbf{g}} = \mathbf{q}_{\mathrm{i}} - \mathbf{q}_{\mathrm{e}} + \mathbf{M}\ddot{\mathbf{d}} = \mathbf{g} + \mathbf{M}\ddot{\mathbf{d}} \tag{24.46}$$

with

$$\mathbf{q}_{\mathrm{i}} = \int \mathbf{B}^{\mathrm{T}} \boldsymbol{\sigma} \, \mathrm{d}V \tag{24.47}$$

$$\mathbf{M} = \int \rho \mathbf{H}^{\mathrm{T}} \mathbf{H} \, \mathrm{d}V \tag{24.48}$$

It is clear that, apart from the D'Alembert inertia terms, equation (24.26) takes the same form as the static equilibrium equations. Indeed, apart from the exclusion of a damping term $\mathbf{C}\dot{\mathbf{d}}$, these equations coincide with (24.1) which formed the starting-point for all of the work in the previous sections. In the next section, we will consider a 'total Lagrangian formulation' and in this case the static internal force vector in (24.47) would involve $\mathbf{B}_{nl}$ which is a function of the current displacements while, in place of $\boldsymbol{\sigma}$, we would have the second Piola–Kirchhoff stresses, $\mathbf{S}$.

The main aim of the work in the current section is to emphasise that (24.1) or (24.46) represent dynamic equilibrium equations for a single point in time and stem from (24.42) which also represented a single point in time. However, just as we use the finite element procedure to discretise in space and hence introduce an approximation, so we are now approximating in time and there are a number of ways in which the finite element method can be used for this purpose. Many methods start with equations (24.42) or (24.46). However, the starting-point can precede equations (24.42) and can stem from Hamilton's principle which gives:

$$\delta \int_{t_1}^{t_2} (K - \phi) \mathrm{d}t = 0 \tag{24.49}$$

where K is the kinetic energy and ϕ is the total potential energy.

In the following, we will start by giving the developments for a simple system with one degree of freedom. In this case, we have:

$$\delta \int_{t_1}^{t_2} (\tfrac{1}{2} m \dot{x}^2 - \phi) \mathrm{d}t = 0 \tag{24.50}$$

from which we can obtain:

$$\int_{t_1}^{t_2}\left(m\dot{x}\delta\dot{x}-\frac{\mathrm{d}\phi}{\mathrm{d}x}\delta x\right)\mathrm{d}t=\int_{t_1}^{t_2}(m\dot{x}\delta\dot{x}-g\delta x)\mathrm{d}t=0 \tag{24.51}$$

The first term can be integrated by parts so that:

$$(m\dot{x}\delta x)_{t_1}^{t_2}-\int_{t_1}^{t_2}(m\ddot{x}\delta x+g\delta x)\mathrm{d}t=-\int_{t_1}^{t_2}(m\ddot{x}\delta x+g\delta x)\mathrm{d}t=0 \tag{24.52}$$

where the first term in (24.52) vanishes because x is specified at the end points [S1.16]. If equation (24.52) is to be valid irrespective of δx, we arrive at the differential equation:

$$m\ddot{x}+g(x)=0 \tag{24.53}$$

which is the one-dimensional equivalent of (24.42). However, we could maintain the time integral in (24.52) and indeed we could adopt a form of Petrov–Galerkin approach [Z1.13, Z1.14] so that the δx's are simply 'test functions' and are not derived from the x's.

24.10 AN ENERGY CONSERVING TOTAL LAGRANGIAN FORMULATION

In a finite element context, energy-conserving methods seem to have been first considered by Haug *et al.* [H1] and Hughes *et al.* [H6] who used Lagrangian multipliers to enforce the conservation as a constraint. Simo and co-workers [S1, S2] then explored the idea of a form of 'mid-point equilibrium' which follows on from the ideas of Hilber *et al.* [H4] and Zienkiewicz *et al.* [Z1]. It would seem that the key to the success of the method related to the precise form of the 'mid-point stresses' [S3–S5, C2–C4, G1, S8]. In particular, they should be the average of those stresses at the beginning and end of the steps and should *not* be computed from the average of the displacements at the beginning and end of the steps.

We will now explore the ideas further by extending the work of the previous section to the multi-dimensional case and by adopting a total Lagrangian approach with Green strains so that the equivalent of (24.52) can now be expressed as

$$\int_{t_1}^{t_2}\delta\bar{\mathbf{d}}^{\mathrm{T}}\mathbf{M}\ddot{\mathbf{d}}\,\mathrm{d}t+\int_{t_1}^{t_2}\int\mathbf{S}^{\mathrm{T}}\delta\bar{\mathbf{E}}\,\mathrm{d}V_{\mathrm{o}}\mathrm{d}t-\int_{t_1}^{t_2}\mathbf{q}_{\mathrm{e}}^{\mathrm{T}}\delta\bar{\mathbf{d}}\,\mathrm{d}t=\mathbf{0} \tag{24.54}$$

where $\mathbf{S}$ are the second Piola–Kirchhoff stresses and $\mathbf{E}$ are the Green strains. The bars on the $\delta\mathbf{d}$'s and $\delta\mathbf{E}$'s emphasise that (considering a Galerkin approach), they do not have to be derived from the $\mathbf{d}$'s which are required for the computation of the $\mathbf{S}$ and $\ddot{\mathbf{d}}$.

We can use various approximate procedures to integrate (24.54) in time. A particular form involves a combination of trapezoidal and mid-point approximations so as to produce:

$$\delta\bar{\mathbf{d}}_{\mathrm{m}}^{\mathrm{T}}\mathbf{M}\left(\frac{\dot{\mathbf{d}}_2-\dot{\mathbf{d}}_1}{\Delta t}\right)+\delta\bar{\mathbf{d}}_{\mathrm{m}}^{\mathrm{T}}\int\mathbf{B}_{\mathrm{m}}^{\mathrm{T}}\left(\frac{\mathbf{S}_1+\mathbf{S}_2}{2}\right)\mathrm{d}V_{\mathrm{o}}-\delta\bar{\mathbf{d}}_{\mathrm{m}}^{\mathrm{T}}\mathbf{q}_{\mathrm{em}}=0 \tag{24.55}$$

Here the subscript m means 'mid-point' and we are writing:

$$\delta\bar{\mathbf{E}}_m = \mathbf{B}(\mathbf{d}_m)\delta\bar{\mathbf{d}}_m = \mathbf{B}\left(\frac{\mathbf{d}_1+\mathbf{d}_2}{2}\right)\delta\bar{\mathbf{d}}_m = \tfrac{1}{2}(\mathbf{B}(\mathbf{d}_1)+\mathbf{B}(\mathbf{d}_2))\delta\bar{\mathbf{d}}_m \tag{24.56}$$

where the $\mathbf{B}$'s are those appropriate to a total Lagrangian formulation (Chapter 5) and were previously referred to as $\mathbf{B}_{nl}$ (see (5.19) or (12.5)). In (24.55), $\mathbf{S}_1$ are the second Piola–Kirchhoff stresses computed at time t_1 (from $\mathbf{d}_1$) and $\mathbf{S}_2$ are the second Piola–Kirchhoff stresses computed at time t_2 (from $\mathbf{d}_2$). It should be noted that the vector $\frac{1}{2}(\mathbf{S}_1+\mathbf{S}_2)$ is *not* computed from the mid-point displacements $\mathbf{d}_m = \frac{1}{2}(\mathbf{d}_1+\mathbf{d}_2)$ so that we are using a form of Petrov–Galerkin procedure.

Equation (24.55) can be re-expressed as

$$\delta\bar{\mathbf{d}}_m^{\mathrm{T}}\bar{\mathbf{g}}_m = 0 \tag{24.57}$$

where the dynamic, mid-point residual $\bar{\mathbf{g}}_m$ is given by

$$\begin{aligned}\bar{\mathbf{g}}_m &= \int \frac{(\mathbf{B}_1+\mathbf{B}_2)^{\mathrm{T}}}{2}\frac{(\mathbf{S}_1+\mathbf{S}_2)}{2}\mathrm{d}V_0 - \mathbf{q}_{em} + \mathbf{M}\left(\frac{\dot{\mathbf{d}}_2-\dot{\mathbf{d}}_1}{\Delta t}\right)\\ &= \mathbf{q}_{im} - \mathbf{q}_{em} + \mathbf{M}\left(\frac{\dot{\mathbf{d}}_2-\dot{\mathbf{d}}_1}{\Delta t}\right) = \mathbf{0}\end{aligned} \tag{24.58}$$

As the time step tends to zero, (25.58) tends to (24.46) with:

$$\mathbf{q}_i = \int \mathbf{B}(\mathbf{d})^{\mathrm{T}}\mathbf{S}(\mathbf{d})\mathrm{d}V_0 \tag{24.59}$$

The motivation for the particular form of integration in (24.55) relates to energy conservation [S3].

For the strain energy change over the step, we may write:

$$\Delta\varphi = \int \frac{(\mathbf{S}_1+\mathbf{S}_2)^{\mathrm{T}}}{2}\Delta\mathbf{E}\mathrm{d}V_0 = \int \frac{(\mathbf{S}_1+\mathbf{S}_2)^{\mathrm{T}}}{2}\left(\frac{(\mathbf{B}_1+\mathbf{B}_2)}{2}\Delta\mathbf{d}\right)\mathrm{d}V_0 = \mathbf{q}_{im}^{\mathrm{T}}\Delta\mathbf{d} \tag{24.60}$$

where $\Delta\mathbf{d}$ are the displacement changes from time step 1 to time step 2 (i.e. $\mathbf{d}_2-\mathbf{d}_1$) and the vector $\mathbf{q}_{im}$ is that given in (24.58). (More discussion on the relationships in (24.60) is given in the next section.) For the kinetic energy change over the step, with the aid of (24.6), we can write:

$$\Delta K = \tfrac{1}{2}\dot{\mathbf{d}}_2^{\mathrm{T}}\mathbf{M}\dot{\mathbf{d}}_2 - \tfrac{1}{2}\dot{\mathbf{d}}_1^{\mathrm{T}}\mathbf{M}\dot{\mathbf{d}}_1 = \tfrac{1}{2}(\dot{\mathbf{d}}_2-\dot{\mathbf{d}}_1)^{\mathrm{T}}\mathbf{M}(\dot{\mathbf{d}}_2+\dot{\mathbf{d}}_1) = \left(\frac{\dot{\mathbf{d}}_2-\dot{\mathbf{d}}_1}{\Delta t}\right)^{\mathrm{T}}\mathbf{M}\Delta\mathbf{d} \tag{24.61}$$

Hence, assuming a fixed external load vector (as with gravity loading), the total energy change is

$$\Delta K + \Delta\varphi + \Delta P = \Delta\mathbf{d}^{\mathrm{T}}\left(\mathbf{M}\left(\frac{\dot{\mathbf{d}}_2-\dot{\mathbf{d}}_1}{\Delta t}\right) + \mathbf{q}_{im} - \mathbf{q}_e\right) = \Delta\mathbf{d}^{\mathrm{T}}\bar{\mathbf{g}}_m \tag{24.62}$$

where $\bar{\mathbf{g}}_m$ was defined in (24.58). Having iterated to dynamic equilibrium, this vector will be zero and hence, from (24.62), there will be no energy change over the time increment [53]. While it is true that for most structural systems damping or dissipation will be involved, it none the less makes sense to start with an algorithm that is satisfactory

in the absence of such damping. In this context, the author believes that the main advantage of the 'energy-conserving algorithms' is not necessarily that they conserve energy, but rather that they are stable in the non-linear regime.

In describing the predictor–corrector steps for the energy-conserving algorithm, instead of using time steps 1 and 2, we will revert to using steps such as $n-1$ and n. The essential background for the method has already been described apart from the velocity update for which we use (24.6), which, for convenience is reproduced here as:

$$\dot{\mathbf{d}}_{n+1} = \frac{2}{\Delta t}\Delta\mathbf{d} - \dot{\mathbf{d}}_n = \frac{2}{\Delta t}(\mathbf{d}_{n+1} - \mathbf{d}_n) - \dot{\mathbf{d}}_n \tag{24.63}$$

24.10.1 The 'predictor step'

If we assume dynamic equilibrium at step $m- = n-1/2$, using a truncated Taylor series, we can write:

$$\begin{aligned}\mathbf{q}_{i,m+} &= \mathbf{q}_{i,n+1/2} = \mathbf{q}_{im-} + \frac{\partial \mathbf{q}_{i,m-}}{\partial \mathbf{d}_n}(\mathbf{d}_{n+1} - \mathbf{d}_n) \\ &= \mathbf{q}_{i,m-} + \mathbf{K}_{t,m-}\Delta\mathbf{d}\end{aligned} \tag{24.64}$$

where, from (24.58)

$$\mathbf{K}_{t,m-} = \int\left(\frac{\mathbf{B}_{n-1} + \mathbf{B}_n}{4}\right)^{\mathrm{T}} \mathbf{C}_{t,n}\mathbf{B}_n \mathrm{d}V_0 + \mathbf{K}_{t\sigma}\left(\frac{\mathbf{S}_{n-1} + \mathbf{S}_n}{4}\right) \tag{24.65}$$

where $\mathbf{K}_{t\sigma}$ takes the form given in (5.25) or (12.6) and is symmetric while the first term in (24.65) is non-symmetric. This non-symmetry relates to the Petrov–Galerkin nature of the earlier derivation. As the step size tends to zero, symmetry is restored. Substitution from (24.64) for $\mathbf{q}_{i,m+}$ and from (24.63) for $\dot{\mathbf{d}}_{n+1}$ into $\bar{\mathbf{g}}_{m+}$ using (24.58)leads to the relationship:

$$\Delta\bar{\mathbf{q}}_e = \bar{\mathbf{K}}_{t,m-}\Delta\mathbf{d} = \bar{\mathbf{K}}_{t,m}(\mathbf{d}_{n+1} - \mathbf{d}_n) \tag{24.66}$$

where

$$\bar{\mathbf{K}}_{t,m-} = \mathbf{K}_{t,m-} + \frac{2}{\Delta t^2}\mathbf{M} \tag{24.67}$$

with $\mathbf{K}_{t,m}$ from (24.65) and:

$$\Delta\bar{\mathbf{q}}_e = \mathbf{q}_{e,m+} - \mathbf{q}_{i,m-} + \frac{2}{\Delta t}\mathbf{M}\dot{\mathbf{d}}_n \tag{24.68}$$

24.10.2 The 'corrector'

Having solved (24.66) for $\Delta\mathbf{d}$, the displacements at step $n+1$ can be obtained as $\mathbf{d}_{n+1} = \mathbf{d}_n + \Delta\mathbf{d}$ and we can use (24.63) to obtain $\dot{\mathbf{d}}_{n+1}$. Knowing $\mathbf{d}_{n+1}$, we can also compute the stresses at $\mathbf{S}_{n+1}$ and hence obtain the internal forces $\mathbf{q}_{i,m+}$ using (24.58) (with subscript n replacing subscript 1 and subscript $n+1$ replacing subscript 2) from

which the dynamic residual, which will not generally be zero, will be given by

$$\bar{\mathbf{g}}_{m+} = \int \left(\frac{\mathbf{B}_n + \mathbf{B}_{n+1}}{2}\right)^{\mathrm{T}} \left(\frac{\mathbf{S}_n + \mathbf{S}_{n+1}}{2}\right) \mathrm{d}V_0 - \mathbf{q}_{\mathrm{e},m+} + \mathbf{M}\left(\frac{\dot{\mathbf{d}}_{n+1} - \dot{\mathbf{d}}_n}{\Delta t}\right)$$

$$= \mathbf{q}_{\mathrm{i},m+} - \mathbf{q}_{\mathrm{e},m+} + \mathbf{M}\left(\frac{\dot{\mathbf{d}}_{n+1} - \dot{\mathbf{d}}_n}{\Delta t}\right) = \mathbf{g}_{m+} + \mathbf{M}\left(\frac{\dot{\mathbf{d}}_{n+1} - \dot{\mathbf{d}}_n}{\Delta t}\right) = \mathbf{0} \quad (24.69)$$

Applying a truncated Taylor series to $\mathbf{g}_{m+}$ in (24.69), we obtain:

$$\mathbf{g}_{m+,\mathrm{new}} = \mathbf{g}_{m+,\mathrm{old}} + \frac{\partial \mathbf{g}}{\partial \mathbf{d}} \delta \mathbf{d}_{n+1} = \mathbf{g}_{m+,\mathrm{old}} + \mathbf{K}_{\mathrm{t},m+} \delta \mathbf{d}_{n+1} \quad (24.70)$$

where

$$\mathbf{K}_{\mathrm{t},m+} = \int \left(\frac{\mathbf{B}_{n+1} + \mathbf{B}_n}{4}\right) \mathbf{C}_{\mathrm{t},n+1} \mathbf{B}_{n+1}^{\mathrm{T}} \mathrm{d}V_0 + \mathbf{K}_{\mathrm{t}\sigma}\left(\frac{\mathbf{S}_{n+1} + \mathbf{S}_n}{4}\right) \quad (24.71)$$

which takes the same form as (24.65). To complete the process, from (24.63) we have:

$$\delta \dot{\mathbf{d}}_{n+1} = \frac{2}{\Delta t} \delta \mathbf{d}_{n+1} \quad (24.72)$$

We can now use (24.70) and (24.72) to apply a truncated Taylor series to (24.69) so that:

$$\bar{\mathbf{g}}_{m+,\mathrm{new}} = \bar{\mathbf{g}}_{m+,\mathrm{old}} + \bar{\mathbf{K}}_{\mathrm{t},m+} \delta \mathbf{d}_{n+1} \quad (24.73)$$

where $\bar{\mathbf{K}}_{\mathrm{t},m+}$ is given by

$$\bar{\mathbf{K}}_{\mathrm{t},m+} = \mathbf{K}_{\mathrm{t},m+} + \frac{2}{\Delta t^2} \mathbf{M} \quad (24.74)$$

which takes the same form as that previously given in (24.67) for the predictor step. We can now apply the standard method to (24.73) to obtain the Newton–Raphson iterative change, $\delta \mathbf{d}_{n+1}$ with:

$$\delta \mathbf{d}_{n+1} = -\bar{\mathbf{K}}_{\mathrm{t},m+}^{-1} \bar{\mathbf{g}}_{m+} \quad (24.75)$$

where, as usual, we are dropping the subscript 'old'.

24.11 A CO-ROTATIONAL ENERGY-CONSERVING PROCEDURE FOR TWO-DIMENSIONAL BEAMS

The concepts of Section 24.10 can be adapted to apply to two-dimensional beams [G1]. To this end, we will start with an approximate co-rotational approach which does not exactly conserve energy. The starting equation is closely related to (24.58) and involves:

$$\bar{\mathbf{g}}_{\mathrm{m}} = \left(\frac{\mathbf{T}_n + \mathbf{T}_{n+1}}{2}\right)^{\mathrm{T}} \left(\frac{\mathbf{q}_{il,n} + \mathbf{q}_{il,n+1}}{2}\right) - \mathbf{q}_{\mathrm{em}} + \mathbf{M}\left(\frac{\dot{\mathbf{p}}_{n+1} - \dot{\mathbf{p}}_n}{\Delta t}\right)$$

$$= \mathbf{q}_{\mathrm{im}} - \mathbf{q}_{\mathrm{em}} + \mathbf{M}\left(\frac{\dot{\mathbf{p}}_{n+1} - \dot{\mathbf{p}}_n}{\Delta t}\right) = \mathbf{0} \quad (24.76)$$

Here, we are following the usual co-rotational approach (see Sections 7.2, 7.3, 17.1 and Chapter 18) whereby $\mathbf{q}_{il,n+1}$ are the local internal forces at step $n+1$ and the 'transformation matrix', $\mathbf{T}_{n+1}$, is such that, at step $n+1$, the local nodal 'displacement changes' (here including rotations), $\delta\mathbf{p}_{l,n+1}$ are related to the global nodal 'displacement changes', $\delta\mathbf{p}$, via:

$$\delta\mathbf{p}_{l,n+1} = \mathbf{T}_{n+1}\delta\mathbf{p} \tag{24.77}$$

With the more usual 'end-point' equilibrium relationship, in place of (24.76), the dynamic equilibrium equations would read:

$$\begin{aligned}\tilde{\mathbf{g}}_{n+1} &= \mathbf{T}_{n+1}^{\mathrm{T}}\mathbf{q}_{il,n+1} - \mathbf{q}_{e,n+1} + \mathbf{M}\ddot{\mathbf{p}}_{n+1} \\ &= \mathbf{q}_{i,n+1} - \mathbf{q}_{e,n+1} + \mathbf{M}\ddot{\mathbf{p}}_{n+1} = \mathbf{0}\end{aligned} \tag{24.78}$$

In relation to energy conservation, we observe that:

$$\Delta\mathbf{p}_l \simeq \left(\frac{\mathbf{T}_n + \mathbf{T}_{n+1}}{2}\right)\Delta\mathbf{p} \tag{24.79}$$

Equation (24.79) can be considered as being derived from the average of:

$$\mathbf{p}_{l,n+1} \simeq \mathbf{p}_{l,n} + \left.\frac{\partial\mathbf{p}_l}{\partial\mathbf{p}}\right|_n \Delta\mathbf{p} \tag{24.80a}$$

and

$$\mathbf{p}_{l,n} \simeq \mathbf{p}_{l,n+1} - \left.\frac{\partial\mathbf{p}_l}{\partial\mathbf{p}}\right|_{n+1} \Delta\mathbf{p} \tag{24.80b}$$

The equivalent relationship to (24.79) for the total Lagrangian continuum formulation of Section 24.10 is

$$\Delta\mathbf{E} = \left(\frac{\mathbf{B}_n + \mathbf{B}_{n+1}}{2}\right)\Delta\mathbf{p} \tag{24.81}$$

where

$$\delta\mathbf{E}_{n+1} = \mathbf{B}_{n+1}\delta\mathbf{p}_{n+1} \tag{24.82}$$

Because of the quadratic nature of the Green strain, there is no approximation in (24.81).

For the co-rotational approach, although (24.79) does involve an approximation, it is a reasonably good one and so we can still use this equation as the starting-point for energy conservation. (Sophistications aimed at the removal of the approximation will be discussed later.) Having adopted (24.79), we can now write the change in strain energy over the step as

$$\begin{aligned}\Delta\varphi &= \Delta\mathbf{p}_l^{\mathrm{T}}\left(\frac{\mathbf{q}_{il,n} + \mathbf{q}_{il,n+1}}{2}\right) \\ &= \Delta\mathbf{p}^{\mathrm{T}}\left(\frac{\mathbf{T}_n + \mathbf{T}_{n+1}}{2}\right)^{\mathrm{T}}\left(\frac{\mathbf{q}_{il,n} + \mathbf{q}_{il,n+1}}{2}\right) = \Delta\mathbf{p}^{\mathrm{T}}\mathbf{q}_{\mathrm{im}}\end{aligned} \tag{24.83}$$

In addition, (24.61) still applies for the change in kinetic energy (although now with $\mathbf{p}$'s instead of $\mathbf{d}$'s because we are including rotational variables). Consequently, we can

again write an equation of the form of (24.62) whereby:

$$\Delta T + \Delta\varphi + \Delta P = \Delta\mathbf{p}^{\mathrm{T}}\left(\mathbf{M}\left(\frac{\dot{\mathbf{p}}_{n+1} - \dot{\mathbf{p}}_n}{\Delta t}\right) + \mathbf{q}_{\mathrm{im}} - \mathbf{q}_{\mathrm{e}}\right) = \Delta\mathbf{p}^{\mathrm{T}}\bar{\mathbf{g}}_{\mathrm{m}} \tag{24.84}$$

As with the total Lagrangian formulation of Section 24.10, once we have iterated to 'dynamic mid-point equilibrium' so that (24.76) is satisfied, the energy change over the step will vanish.

Before considering refinements whereby we overcome the approximation in (24.79), some discussion will be given on the mass matrix **M** that was introduced in (24.76). For this matrix, either a 'lumped' or a 'consistent' form can be used and because an 'implicit procedure' is being adopted, there will not be any advantages from adopting the former. For the latter, a 'Timoshenko beam' approach can be simply applied, with the mass matrix being derived from interpolations on the global translations and on the global rotation. Assuming a linear interpolation, this leads to the relationship:

$$\delta\mathbf{p}_{\mathrm{v}}^{\mathrm{T}}\mathbf{M}\ddot{\mathbf{p}} = \delta\mathbf{p}_{\mathrm{v}}^{\mathrm{T}}\frac{\rho l_{\mathrm{o}}}{6}\begin{bmatrix} 2\mathbf{D} & \mathbf{D} \\ \mathbf{D} & 2\mathbf{D} \end{bmatrix}\ddot{\mathbf{p}} \tag{24.85a}$$

where ρ is the density and **D** is a 3×3 diagonal matrix given by

$$\mathbf{D} = \begin{bmatrix} A & 0 & 0 \\ 0 & A & 0 \\ 0 & 0 & \mathrm{I} \end{bmatrix} \tag{24.85b}$$

where A is the area of the beam and I is the second moment of area.

Following the 'element independent' co-rotational procedure of Section 17.1 and Chapter 18, in (24.76) and in subsequent developments, the local internal force vectors, $\mathbf{q}_{\mathrm{il}}$, are unspecified and could be obtained from either a Timoshenko formulation or from a Bernoulli formulation. However, because of the movement of the local element frame, there would be considerable difficulties in deriving appropriate mass relationships for the latter (see Section 17.5.3). Consequently in [G1], the author and co-worker adopted a Timoshenko formulation for the mass terms even if a Bernoulli formulation was being used for the 'static internal forces'.

24.11.1 Sophistications

In the following, it will be assumed that the variables are ordered as $u_1, v_1, \theta_1, u_2, v_2, \theta_2$. It can then be shown [G1] that a better approximation than (24.79) is given by

$$\Delta\mathbf{p}_l = \Delta\mathbf{p}_{\mathrm{r}} + \mathbf{P}\left(\frac{\mathbf{T}_n + \mathbf{T}_{n+1}}{2}\right)\Delta\mathbf{p}_{\mathrm{t}} \tag{24.86}$$

where $\Delta\mathbf{p}_{\mathrm{r}}$ contains the incremental global rotations (in their usual positions) with all of the other variables zero, while $\Delta\mathbf{p}_{\mathrm{t}}$ contains the incremental translations (in their usual positions) with the rotations being set to zero. In (24.86), **P** is a diagonal matrix with:

$$\mathrm{Diag}(\mathbf{P}) = \left(*, *, \frac{\Delta\alpha}{\sin\Delta\alpha}, \frac{2}{1+\cos\Delta\alpha}, *, \frac{\Delta\alpha}{\sin\Delta\alpha}\right) \tag{24.87}$$

and $\Delta\alpha$ is the rigid-body rotation between steps n and $n+1$. The latter can be computed from the relationship:

$$\sin\Delta\alpha = \| \mathbf{x}_{21}, n \times \mathbf{x}_{21}, n+1 \| / l_n l_{n+1} \tag{24.88}$$

where the $\mathbf{x}_{21}$'s are the vectors lying between nodes 1 and 2 and the l's are the equivalent (straight) lengths.

Because of the adopted ordering of the nodal variables, following an equivalent two-dimensional approach to the two-dimensional approach in Section 17.1, only the third and sixth rows (relating to rotations) and the fourth row (relating to the extension) in the $\mathbf{T}$ matrices in (24.86) will be non-zero. Consequently, the asterisks in (24.87) can take any value. Equation (24.86) is effectively exact for small strains. In these circumstances, as the step size tends to zero, the approximation in (24.79) also becomes exact. It will be useful to re-express (24.86) as

$$\Delta\mathbf{p}_l = \left[\bar{\mathbf{I}} + \mathbf{P}\left(\frac{\mathbf{T}_n^{\circ} + \mathbf{T}_{n+1}^{\circ}}{2} \right) \right] \Delta\mathbf{p} \tag{24.89}$$

where $\bar{\mathbf{I}}$ is the diagonal matrix:

$$\text{Diag}(\bar{\mathbf{I}}) = (0, 0, 1, 0, 0, 1) \tag{24.90}$$

and the matrices $\mathbf{T}_n^{\circ}$ and $\mathbf{T}_{n+1}^{\circ}$ are the conventional transformation matrices after the diagonal terms corresponding to the nodal rotations have been set to zero. In place of (24.83), the change of strain energy over the step can now be expressed as

$$\Delta\varphi = \Delta\mathbf{p}_l^{\mathrm{T}} \left(\frac{\mathbf{q}_{il,n} + \mathbf{q}_{il,n+1}}{2} \right) = \Delta\mathbf{p}^{\mathrm{T}} \left[\bar{\mathbf{I}} + \mathbf{P}\left(\frac{\mathbf{T}_n^{\circ} + \mathbf{T}_{n+1}^{\circ}}{2} \right) \right]^{\mathrm{T}} \left(\frac{\mathbf{q}_{il,n} + \mathbf{q}_{il,n+1}}{2} \right) \tag{24.91}$$

Hence, in order to ensure energy conservation, we must equate (24.91) to $\Delta\mathbf{p}^{\mathrm{T}}\mathbf{q}_{\mathrm{im}}$ so that the modified mid-point internal force vector is now:

$$\mathbf{q}_{\mathrm{im}} = \left[\bar{\mathbf{I}} + \left(\frac{\mathbf{T}_n^{\circ} + \mathbf{T}_{n+1}^{\circ}}{2} \right)^{\mathrm{T}} \mathbf{P} \right] \left(\frac{\mathbf{q}_{il,n} + \mathbf{q}_{il,n+1}}{2} \right) \tag{24.92}$$

24.11.2 Numerical solution

To apply the method, we combine (24.76) with the modified (24.92) (for approximate energy conservation there is no need to include the 'sophistications') in conjunction with a trapezoidal update of the form of (24.6), i.e.

$$\mathbf{p}_{n+1} = \mathbf{p}_n + \frac{\Delta t}{2} \{ \dot{\mathbf{p}}_n + \dot{\mathbf{p}}_{n+1} \} \tag{24.93}$$

The derivation of the predictor–corrector algorithm follows very similar lines to that adopted in Section 24.10. The key issue is the variation of the mid-point dynamic

residual, $\bar{\mathbf{g}}_m$, which from (24.76) and (24.92) involves:

$$\delta\bar{\mathbf{g}}_m = \bar{\mathbf{K}}_{t,m}\delta\mathbf{p}_{n+1} = \left[\mathbf{K}_{t,m} + \frac{2}{\Delta t^2}\mathbf{M}\right]\delta\mathbf{p}_{n+1} \tag{24.94}$$

where

$$\begin{aligned}\mathbf{K}_{t,m}\delta\mathbf{p}_{n+1} &= \frac{1}{2}\left[\bar{\mathbf{I}} + \left(\frac{\mathbf{T}_n^o + \mathbf{T}_{n+1}^o}{2}\right)^T\mathbf{P}\right]\delta\mathbf{q}_{il,n+1} \\ &\quad + \left(\frac{\delta\mathbf{T}_n^o + \mathbf{T}_{n+1}^o}{2}\right)^T\mathbf{P}\left(\frac{\mathbf{q}_{il,n} + \mathbf{q}_{il,n+1}}{2}\right) + \left(\frac{\mathbf{T}_n^o + \mathbf{T}_{n+1}^o}{2}\right)^T\delta\mathbf{P}\left(\frac{\mathbf{q}_{il,n} + \mathbf{q}_{il,n+1}}{2}\right) \\ &= \left[\mathbf{K}_{t1} + \mathbf{K}_{t\sigma}\left(\mathbf{P}\left(\frac{\mathbf{q}_{il,n} + \mathbf{q}_{il,n+1}}{2}\right)\right) + \mathbf{K}_{t2} + \mathbf{K}_{t3}\right]\delta\mathbf{p}_{n+1}\end{aligned} \tag{24.95}$$

and

$$\mathbf{K}_{t1} = \frac{1}{2}\left[\bar{\mathbf{I}} + \left(\frac{\mathbf{T}_n^o + \mathbf{T}_{n+1}^o}{2}\right)^T\mathbf{P}\right]\mathbf{K}_l\mathbf{T}_{n+1} \tag{24.96}$$

The latter matrix is non-symmetric while $\mathbf{K}_{t\sigma}$ in (24.95) takes precisely the same form as the conventional static co-rotational stress matrix (although now as a function of a modified local internal force vector). The matrices $\mathbf{K}_{t2}$ and $\mathbf{K}_{t3}$ stem from the $\delta\mathbf{P}$ term in (24.95). From (24.87) we will require $\delta\alpha$, where $\Delta\alpha$ is the incremental rigid body rotation. From (7.65), this is given by

$$\delta\alpha = \frac{1}{l_{n+1}}\mathbf{e}_{2,n+1}^T(\delta\mathbf{d}_2 - \delta\mathbf{d}_1)_{n+1} \tag{24.97}$$

where $\mathbf{e}_2$ is the unit vector at right angles to the current vector lying along the beam, $\mathbf{e}_1$ (see Figure 7.7) and $\delta\mathbf{d}_1$ and $\delta\mathbf{d}_2$ are the variations in translational displacements at nodes 1 and 2 respectively. With the aid of (24.97), the matrices $\mathbf{K}_{t2}$ and $\mathbf{K}_{t3}$ can be computed as

$$\mathbf{K}_{t2} = \frac{\sin\Delta\alpha - \Delta\alpha\cos\Delta\alpha}{4l_{n+1}\sin^2\Delta\alpha}(\mathbf{q}_{il,n}(3) + \mathbf{q}_{il,n+1}(3) + \mathbf{q}_{il,n}(6) + \mathbf{q}_{il,n+1}(6))\begin{bmatrix}\mathbf{B} & -\mathbf{B}\\ -\mathbf{B} & \mathbf{B}\end{bmatrix} \tag{24.98a}$$

$$\mathbf{K}_{t3} = \frac{\sin\Delta\alpha}{2l_{n+1}(1+\cos\Delta\alpha)^2}(\mathbf{q}_{il,n}(4) + \mathbf{q}_{il,n+1}(4))\begin{bmatrix}\mathbf{C} & -\mathbf{C}\\ -\mathbf{C} & \mathbf{C}\end{bmatrix} \tag{24.98b}$$

with

$$\mathbf{B} = \begin{bmatrix}\mathbf{B}_{11} & \mathbf{0}\\ \mathbf{0}^T & 0\end{bmatrix}; \qquad \mathbf{B}_{11} = -\left(\frac{\mathbf{e}_{2,n}}{l_n} + \frac{\mathbf{e}_{2,n+1}}{l_{n+1}}\right)\mathbf{e}_{2,n+1}^T \tag{24.99a}$$

$$\mathbf{C} = \begin{bmatrix}\mathbf{C}_{11} & \mathbf{0}\\ \mathbf{0}^T & 0\end{bmatrix}; \qquad \mathbf{C}_{11} = \{\mathbf{e}_{1,n} + \mathbf{e}_{1,n+1}\}\mathbf{e}_{2,n+1}^T \tag{24.99b}$$

24.12 AN ALTERNATIVE ENERGY-CONSERVING PROCEDURE FOR TWO-DIMENSIONAL BEAMS

In Section 7.4, we described a formulation for two-dimensional beams that was based on Reissner's beam theory. This formulation can be considered as the two-dimensional equivalent of the three-dimensional formulation due to Simo and Vu-Quoc [S3.16] that was discussed in Section 17.2.1. In relation to dynamics, Stander and Stein [S7] have incorporated the static two-dimensional formulation (Section 7.2) within an energy-conserving dynamic framework. Many of the adopted concepts are very similar to those discussed in the previous section for the co-rotational formulation. In the current section, we will outline the extension of the static formulation of Section 7.4 so as to produce an energy-conserving dynamic technique. The derivations will rely heavily on those already given in Section 7.4 for the 'static case' and frequent reference will be made to equations from that section which will not be rederived here.

The starting motivation can be considered as the desire to be able to express the change of energy over the step in the form of (24.84) and, in particular, the change of strain energy in the form of (24.83) so that $\Delta\varphi = \Delta\mathbf{p}^{\mathrm{T}}\mathbf{q}_{\mathrm{im}}$. We can use this concept to define the required 'static mid-point internal force vector', $\mathbf{q}_{\mathrm{im}}$. To this end, we will start by considering the change in axial strain energy over the step which can be expressed via:

$$\Delta\varphi_{\mathrm{a}} = \tfrac{1}{2}(N_n + N_{n+1})l_{\mathrm{o}}(\varepsilon_{l,n+1} - \varepsilon_{l,n}) = N_{\mathrm{m}}l_{\mathrm{o}}(\varepsilon_{l,n+1} - \varepsilon_{l,n}) \tag{24.100}$$

In the above, the 'local strain', ε_l, is defined via (7.112) and using this equation, we can write:

$$\begin{aligned} l_{\mathrm{o}}(\varepsilon_{l,n+1} - \varepsilon_{l,n}) = &\begin{pmatrix} \cos\theta_{\mathrm{av},n+1} \\ \sin\theta_{\mathrm{an},n+1} \end{pmatrix}^{\mathrm{T}} \begin{pmatrix} x'_{21\mathrm{m}} + \Delta u_{21}/2 \\ z'_{21\mathrm{m}} + \Delta w_{21}/2 \end{pmatrix} \\ &- \begin{pmatrix} \cos\theta_{\mathrm{av},n+1} \\ \sin\theta_{\mathrm{an},n+1} \end{pmatrix}^{\mathrm{T}} \begin{pmatrix} x'_{21\mathrm{m}} - \Delta u_{21}/2 \\ z'_{21\mathrm{m}} - \Delta w_{21}/2 \end{pmatrix} \end{aligned} \tag{24.101}$$

Here, $x'_{21\mathrm{m}}$ and $z'_{21\mathrm{m}}$ are the components of the vector $\mathbf{x}'_{21\mathrm{m}}$ which is related to (7.111) although now with respect to the 'mid-point configuration' so that:

$$\mathbf{x}'_{21\mathrm{m}} = \mathbf{x}_{21} + \tfrac{1}{2}(\mathbf{d}_{21,n+1} + \mathbf{d}_{21,n}) = \tfrac{1}{2}(\mathbf{x}'_{21,n+1} + \mathbf{x}'_{21,n}) \tag{24.102}$$

In the above and in subsequent developments the subscript 'av' means the average of the variables at nodes 1 and 2 (see (7.109)), while the subscript 'm' relates to the mid-point in time. The terms $\Delta u_{21\mathrm{m}}$ and $\Delta w_{21\mathrm{m}}$ in (24.101) are the incremental differences in the u (related to x—see Figure 7.9) and w (related to z—see Figure 7.9) displacements.

Equation (24.101) can be re-expressed as

$$\begin{aligned} l_{\mathrm{o}}(\varepsilon_{l,n+1} - \varepsilon_{l,n}) = &\begin{pmatrix} \cos\theta_{\mathrm{av},n+1} - \cos\theta_{\mathrm{av},n} \\ \sin\theta_{\mathrm{an},n+1} - \sin\theta_{\mathrm{av},n} \end{pmatrix}^{\mathrm{T}} \begin{pmatrix} x'_{21\mathrm{m}} \\ z'_{21\mathrm{m}} \end{pmatrix} \\ &+ \frac{1}{2}\begin{pmatrix} \cos\theta_{\mathrm{av},n+1} + \cos\theta_{\mathrm{av},n} \\ \sin\theta_{\mathrm{av},n+1} + \sin\theta_{\mathrm{av},n} \end{pmatrix}^{\mathrm{T}} \begin{pmatrix} \Delta u_{21} \\ \Delta w_{21} \end{pmatrix} \end{aligned} \tag{24.103}$$

The key step is the subsequent expression of:

$$\theta_{\mathrm{av},n+1} = \theta_{\mathrm{av,m}} + \Delta\theta_{\mathrm{av}}/2$$
$$\theta_{\mathrm{av},n} = \theta_{\mathrm{av,m}} - \Delta\theta_{\mathrm{av}}/2 \tag{24.104}$$

followed by the expansion using expressions for terms such as $\cos(a+b)$. This process allows (24.103) to be re-expressed as

$$l_{\mathrm{o}}(\varepsilon_{l,n+1} - \varepsilon_{l,n}) = 2\sin(\Delta\theta_{\mathrm{av}}/2)\begin{pmatrix} -\sin\theta_{\mathrm{av,m}} \\ \cos\theta_{\mathrm{av,m}} \end{pmatrix}^{\mathrm{T}}\begin{pmatrix} x'_{21\mathrm{m}} \\ z'_{21\mathrm{m}} \end{pmatrix}$$
$$+ \cos(\Delta\theta_{\mathrm{av}}/2)\begin{pmatrix} \cos\theta_{\mathrm{av,m}} \\ \sin\theta_{\mathrm{av,m}} \end{pmatrix}^{\mathrm{T}}\begin{pmatrix} \Delta u_{21} \\ \Delta w_{21} \end{pmatrix} \tag{24.105}$$

and hence, introducing more of the notation of Section 7.4, we obtain:

$$l_{\mathrm{o}}(\varepsilon_{l,n+1} - \varepsilon_{l,n}) = \{\bar{\mathbf{r}}_{\mathrm{m}} + \bar{c}_2\mathbf{s}\}^{\mathrm{T}}\Delta\mathbf{p} = \{\bar{\mathbf{r}}_{\mathrm{m}} + \bar{c}_2\mathbf{s}\}^{\mathrm{T}}\{\mathbf{p}_{n+1} - \mathbf{p}_n\} \tag{24.106}$$

where $\mathbf{s}$ was defined in (7.119) and $\bar{\mathbf{r}}_{\mathrm{m}}$ is related to $\mathbf{r}$ in (7.112) which was defined in (7.62) so that we now have:

$$\bar{\mathbf{r}}_{\mathrm{m}}^{\mathrm{T}} = \cos(\Delta\theta_{\mathrm{av}}/2)\{-c, -s, 0, c, s, 0\} \tag{24.107}$$

with

$$\mathrm{c} = \cos(\theta_{\mathrm{av,m}}); \qquad s = \sin(\theta_{\mathrm{av,m}}) \tag{24.108}$$

The constant $\bar{c}_2$ in (24.106) is related to c_2 in (7.121) but now takes the form:

$$\bar{c}_2 = \frac{1}{\Delta\theta_{\mathrm{av}}}\sin(\Delta\theta_{\mathrm{av}}/2)(\bar{\mathbf{t}}_2^{\mathrm{T}}\mathbf{x}'_{21\mathrm{m}}) \tag{24.109}$$

The vector $\bar{\mathbf{t}}_2$ is related to $\mathbf{t}_2$ in (7.110) but is now given by

$$\bar{\mathbf{t}}_2^{\mathrm{T}} = \{-s, c\} \tag{24.110}$$

where s and c were defined in (24.108). The vector $\mathbf{s}$ in (24.106) was defined in (7.119).

A very similar procedure can now be applied to the change in shear strain energy over the step so that:

$$\Delta\varphi_{\mathrm{s}} = \tfrac{1}{2}(Q_n + Q_{n+1})l_{\mathrm{o}}(\gamma_{n+1} - \gamma_n) = Q_{\mathrm{m}}l_{\mathrm{o}}(\gamma_{n+1} - \gamma_n) \tag{24.111}$$

In the above, the shear strain, γ, was defined via (7.114) and using this equation, we can write:

$$l_{\mathrm{o}}(\gamma_{n+1} - \gamma_n) = \begin{pmatrix} -\sin\theta_{\mathrm{av},n+1} \\ \cos\theta_{\mathrm{av},n+1} \end{pmatrix}^{\mathrm{T}}\begin{pmatrix} x'_{21\mathrm{m}} + \Delta u_{21}/2 \\ z'_{21\mathrm{m}} + \Delta w_{21}/2 \end{pmatrix}$$
$$- \begin{pmatrix} -\sin\theta_{\mathrm{av},n} \\ \cos\theta_{\mathrm{av},n} \end{pmatrix}^{\mathrm{T}}\begin{pmatrix} x'_{21\mathrm{m}} - \Delta u_{21}/2 \\ z'_{21\mathrm{m}} - \Delta w_{21}/2 \end{pmatrix} \tag{24.112}$$

with subsequent developments eventually leading to

$$l_{\mathrm{o}}(\gamma_{n+1} - \gamma_n) = -2\sin(\Delta\theta_{\mathrm{av}}/2)\begin{pmatrix} c \\ s \end{pmatrix}^{\mathrm{T}}\begin{pmatrix} x'_{21\mathrm{m}} \\ z'_{21\mathrm{m}} \end{pmatrix}$$
$$+ \cos(\Delta\theta_{\mathrm{av}}/2)\begin{pmatrix} -s \\ c \end{pmatrix}^{\mathrm{T}}\begin{pmatrix} \Delta u_{21} \\ \Delta w_{21} \end{pmatrix} \tag{24.113}$$

Introducing more of the notation of Section 7.4, we obtain:

$$l_o(\gamma_{n+1} - \gamma_n) = \{\bar{\mathbf{z}}_m + \bar{c}_1\mathbf{s}\}^T\Delta\mathbf{p} \tag{24.114}$$

where $\bar{\mathbf{z}}_m$ is related to $\mathbf{z}$ in (7.114) so that we now have:

$$\bar{\mathbf{z}}_m^T = \cos(\Delta\theta_{av}/2)\{s, -c, 0, -s, c, 0\} \tag{24.115}$$

with c and s having been defined in (24.108). The vector $\mathbf{s}$ was defined in (7.119) while the constant $\bar{c}_1$ in (24.114) is related to c_1 in (7.120) but now takes the form:

$$\bar{c}_1 = -\frac{1}{\Delta\theta_{av}}\sin(\Delta\theta_{av}/2)(\bar{\mathbf{t}}_1^T\mathbf{x}'_{21m}) \tag{24.116}$$

The vector $\bar{\mathbf{t}}_1$ is related to $\mathbf{t}_1$ in (7.110) but is now given by

$$\bar{\mathbf{t}}_1^T = \{c, s\} \tag{24.117}$$

where c and s have been defined in (24.108).

For the bending strain energy, the change over the step is very simply expressed as

$$\begin{aligned}\Delta\varphi_b &= \tfrac{1}{2}(M_n + M_{n+1})l_o(\chi_{n+1} - \chi_n) = M_m(\theta_{21,n+1} - \theta_{21,n}) \\ &= M_m\{0, 0, -1, 0, 0, 1\}\Delta\mathbf{p} = M_m\mathbf{a}^T\Delta\mathbf{p}\end{aligned} \tag{24.118}$$

By combining the three strain energy changes, we arrive at the relationship:

$$\Delta\varphi = \Delta\mathbf{p}^T\mathbf{q}_{im} = \Delta\mathbf{p}^T\mathbf{B}^T\begin{bmatrix}N_m\\M_m\\Q_m\end{bmatrix} = \Delta\mathbf{p}^T[\bar{\mathbf{r}}_m + \bar{c}_2\mathbf{s}, \mathbf{a}, \bar{\mathbf{z}}_m + \bar{c}_1\mathbf{s}]\begin{bmatrix}N_m\\M_m\\Q_m\end{bmatrix} \tag{24.119}$$

which defines the 'static internal force vector', $\mathbf{q}_{im}$ required to ensure energy conservation. The tangent stiffness matrix follows from the variation of $\mathbf{q}_{im}$ (and the inertia terms—see Section 24.11) in the usual way. As with the co-rotational technique of the previous section, a non-symmetric tangent stiffness matrix is again produced [S7].

24.13 AUTOMATIC TIME-STEPPING

As indicated in Sections 24.6 and 24.7, for explicit methods, the time step is best related to an estimate of the maximum eigenvalue of the system (which can change with time) in order to ensure stability (see also [P1, U1]). In the current section, we will be concerned with automatic time-stepping for implicit methods.

Hibbitt and Karlsson [H2, H3] observe that having obtained solutions at steps n and $n+1$, one can interpolate the acceleration over the step via:

$$\ddot{\mathbf{d}} = (1-\tau)\ddot{\mathbf{d}}_n + \tau\ddot{\mathbf{d}}_{n+1} \tag{24.120}$$

where τ varies from 0 to 1. (We are here reverting to the use of $\mathbf{d}$ for the nodal displacement variables. Certainly, for two-dimensional beams, we could use $\mathbf{p}$ instead, implying the inclusion of 'rotational displacements'. As will be discussed in Section 24.14, the issue of interpolating three-dimensional rotational variables is more complicated). If we now use the Newmark formula (24.2) for $\ddot{\mathbf{d}}_{n+1}$, the acceleration at τ, can be

written as

$$\ddot{\mathbf{d}} = \frac{\tau}{\beta \Delta t^2} \Delta \mathbf{d} - \frac{\tau}{\beta \Delta t} \dot{\mathbf{d}}_n + \left[1 - \frac{\tau}{2\beta} \right] \ddot{\mathbf{d}}_n \tag{24.121a}$$

This equation can be integrated with respect to τ and the constants of integration inserted so that the Newmark end conditions (24.2) and (24.3) are satisfied and we obtain:

$$\dot{\mathbf{d}} = \frac{\tau^2 \gamma}{\beta \Delta t} \Delta \mathbf{d} + \left(1 - \frac{\tau^2 \gamma}{\beta} \right) \dot{\mathbf{d}}_n + \tau \Delta t \left(1 - \frac{\gamma \tau}{2\beta} \right) \ddot{\mathbf{d}}_n \tag{24.121b}$$

A further integration leads to

$$\mathbf{d} = \mathbf{d}_n + \tau^3 \Delta \mathbf{d} + \tau(1 - \tau^2) \Delta t \dot{\mathbf{d}}_n + \tau^2 (1 - \tau) \frac{\Delta t^2}{2} \ddot{\mathbf{d}}_n \tag{24.121c}$$

Hibbitt and Karlsson [H2, H3] were adopting an end-point dynamic equilibrium procedure (as modified by the α method—see Section 24.8) and noted that having obtained such an equilibrium point they could insert (24.121) into the dynamic equilibrium equations to obtain the dynamic residual at any point within the step, τ. In particular they considered $\tau = 1/2$. It was argued that, if the adopted time step was small enough for an accurate solution, this residual would be small, whereas if it were too large, the computed mid-point residual (and in particular its max-norm) would be significant in comparison with a typical real force. From numerical experiments, they considered that if the maximum mid-point residual was of the order of 1 per cent of such a real force, the solution had a high accuracy, while if the same percentage was of the order 10, moderate accuracy was being obtained and if the percentage were of the order of 100, the accuracy was considered poor. Using these observations they developed an empirical algorithm for adjusting the time steps.

In order to apply this technique, once dynamic equilibrium is obtained, the stress updating routines must be re-entered with the mid-point displacements so that the mid-point residual can be evaluated. If the solution is considered too inaccurate and a time step reduction is required, the current increment is resolved with a reduced time step.

Bergan and Mollestad [B4] have proposed an alternative procedure in which one uses the Rayleigh quotient to evaluate the 'current frequency', ω_n at time step n via:

$$\omega^2 = \frac{\Delta \mathbf{d}^{\mathrm{T}} \mathbf{K} \Delta \mathbf{d}}{\Delta \mathbf{d}^{\mathrm{T}} \mathbf{M} \Delta \mathbf{d}} \tag{24.122}$$

In detail, Bergain and Mollestad [B4] mainly discussed linear problems. For non-linear work, the author and co-worker [Z1] have computed this quantity immediately after convergence at the end of step n so that $\Delta \mathbf{d} = \mathbf{d}_{n+1} - \mathbf{d}_n$ while $\mathbf{K}$ is the tangent stiffness at the end of step n (or at the beginning of step $n+1$). The current period is then computed via:

$$T = \frac{2\pi}{|\omega^2|} \tag{24.123}$$

The absolute value is taken because ω^2 may be negative. Zhong and Crisfield [Z1] then use the period T so computed to adjust the step at the next increment $(n+1)$. Bergan and Mollestad [B4] suggest the computation of preliminary time step via:

$$\Delta t^*_{n+1} = \varphi T \tag{24.124}$$

where the input factor φ may lie between 0.001 (high accuracy) and 0.1 (low accuracy). In the author's implementation [Z1], a maximum ratio for the time step increase is set to 2.0, while no limit is set for a reduction. If the incremental displacements become very small or vanish (as when passing through points of maximum amplitude), the current frequency computation is abandoned and the present time step is used for the next time step.

The present author and a co-worker [Z1] have successfully applied this algorithm which is very easy to implement. It can be used with both the end-point equilibrium methods of Sections 24.2–24.8 and the mid-point equilibrium methods of Sections 24.9–24.12. Particularly in the former case, it is important that the analysis should commence with a small time step. If this is too small, the automatic algorithm will quickly allow it to grow. However, if the initial time step is too large, the solution may never recover [Z1].

24.14 DYNAMIC EQUILIBRIUM WITH ROTATIONS

In relation to finite elements, the issue of non-linear dynamics with rotations has been discussed in the papers by Simo and co-workers [S1–S6] and those by Cardona and Geradin [C1, C1.17, C2.17]. In the following we will start by considering a point with a position vector $\mathbf{x}$, which is assumed to rotate about the origin so that:

$$\dot{\mathbf{x}} = \dot{\boldsymbol{\theta}} \times \mathbf{x} = \boldsymbol{\omega} \times \mathbf{x} = \mathbf{S}(\boldsymbol{\omega})\mathbf{x} = -\mathbf{S}(\mathbf{x})\boldsymbol{\omega} \tag{24.125}$$

where $\boldsymbol{\omega}$ is the angular velocity and $\mathbf{S}(\boldsymbol{\omega})$ is the skew-symmetric matrix of (16.8). The rotational kinetic energy can be written as

$$K = \frac{1}{2}\int \rho \dot{\mathbf{x}}^{\mathrm{T}}\dot{\mathbf{x}}\,\mathrm{d}V = -\frac{1}{2}\boldsymbol{\omega}^{\mathrm{T}}\int \rho \mathbf{S}(\mathbf{x})\mathbf{S}(\mathbf{x})\mathrm{d}V\boldsymbol{\omega} = \tfrac{1}{2}\boldsymbol{\omega}^{\mathrm{T}}\mathbf{J}_{\mathrm{u}}\boldsymbol{\omega} \tag{24.126}$$

where:

$$\mathbf{J}_{\mathrm{u}} = -\int \rho \mathbf{S}(\mathbf{x})\mathbf{S}(\mathbf{x})\mathrm{d}V = \int (\rho(\mathbf{x}^{\mathrm{T}}\mathbf{x})\mathbf{I} - \mathbf{x}\mathbf{x}^{\mathrm{T}})\mathrm{d}V \tag{24.127}$$

and we have made use of (16.86). Equation (24.127) can be expanded to give:

$$\mathbf{J}_{\mathrm{u}} = \int \rho(x_1^2 + x_2^2 + x_3^2)\begin{bmatrix} 1 & 0 & 0 \\ 0 & 1 & 0 \\ 0 & 0 & 1 \end{bmatrix}\mathrm{d}V - \int \begin{bmatrix} x_1^2 & x_1x_2 & x_1x_3 \\ x_2x_1 & x_2^2 & x_2x_3 \\ x_3x_1 & x_3x_2 & x_3^2 \end{bmatrix}\rho\,\mathrm{d}V \tag{24.128}$$

Assuming that the axes are chosen to coincide with the principal directions of inertia,

the terms such as $\int x_1 x_2 \rho \, dV$ are zero. We can then write:

$$J_{u11} = \int (x_2^2 + x_3^2)\rho \, dV$$

$$J_{u22} = \int (x_1^2 + x_3^2)\rho \, dV \tag{24.129}$$

$$J_{u33} = \int (x_1^2 + x_2^2)\rho \, dV$$

so that:

$$\mathbf{J}_u = \begin{bmatrix} J_{u11} & 0 & 0 \\ 0 & J_{u22} & 0 \\ 0 & 0 & J_{u33} \end{bmatrix} \tag{24.130}$$

However, when the body rotates (Figure 24.5), the principal directions of inertia will change and hence the previous computations are only valid in a rotating coordinate system (although $\mathbf{J}_u$ need only be computed once—in the initial coordinate system). In

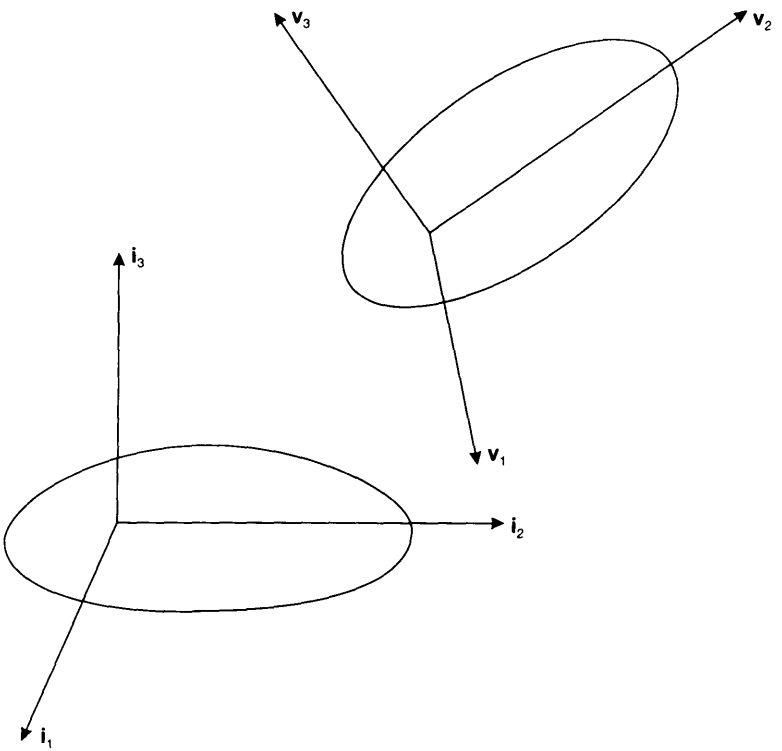

Figure 24.5 Rotating body.

the following, we will introduce a subscript u for all quantities that are related to this rotating coordinate system.

Suppose that the initial axes $[\mathbf{i}_1, \mathbf{i}_2, \mathbf{i}_3]$ rotate with time to axes $\mathbf{U} = [\mathbf{u}_1, \mathbf{u}_2, \mathbf{u}_3]$ (Figure 24.5), then the inertia matrix with respect to the fixed frame $[\mathbf{i}_1, \mathbf{i}_2, \mathbf{i}_3]$ can be expressed as

$$\mathbf{J}(t) = \mathbf{U}\mathbf{J}_u\mathbf{U}^T \tag{24.131}$$

We can check this assertion, using the procedure of Section 4.3, with a transformation matrix $\mathbf{T} = \mathbf{U}^T$ so that we obtain:

$$\mathbf{J}_u = \mathbf{T}\mathbf{J}(t)\mathbf{T}^T = \mathbf{U}^T[\mathbf{U}\mathbf{J}_u\mathbf{U}^T]\mathbf{U} = \mathbf{J}_u \tag{24.132}$$

Consequently, as intended, the inertia matrix with respect to the rotating frame remains fixed. This rotating frame is often referred to as the 'body attached frame' (or convected frame) and it will here be considered as having its origin at the centre of mass.

We will now write down the rotational equilibrium equations as

$$\frac{\mathrm{d}}{\mathrm{d}t}(\mathbf{J}(t)\boldsymbol{\omega}) = \frac{\mathrm{d}}{\mathrm{d}t}[\mathbf{U}\mathbf{J}_u\mathbf{U}^T\boldsymbol{\omega}) = \mathbf{M}_e \tag{24.133}$$

where $\mathbf{M}_e$ are the external moments and $\mathbf{J}(t)\boldsymbol{\omega}$ is the angular momentum. Evaluating the time derivative in (24.133) and noting that $\mathbf{J}_u$ is fixed, we obtain:

$$\mathbf{U}\mathbf{J}_u(\mathbf{U}^T\boldsymbol{\omega})^{\cdot} + \dot{\mathbf{U}}\mathbf{J}_u\mathbf{U}^T\boldsymbol{\omega} = \mathbf{M}_e \tag{24.134}$$

Writing:

$$\boldsymbol{\omega}_u = \mathbf{U}^T\boldsymbol{\omega} \tag{24.135}$$

as the angular velocity with respect to the rotating 'body frame', then premultiplication of (24.134) by $\mathbf{U}^T$ leads to

$$\mathbf{J}_u\dot{\boldsymbol{\omega}}_u + \mathbf{U}^T\dot{\mathbf{U}}\mathbf{J}_u\boldsymbol{\omega}_u = \mathbf{U}^T\mathbf{M}_e = \mathbf{M}_{eu} \tag{24.136}$$

From previous work (see (16.81c)), we can write:

$$\mathbf{S}(\boldsymbol{\omega}) = \dot{\mathbf{U}}\mathbf{U}^T \tag{24.137}$$

so that with respect to the rotating frame:

$$\mathbf{S}(\boldsymbol{\omega}_u) = \mathbf{U}^T[\dot{\mathbf{U}}\mathbf{U}^T]\mathbf{U} = \mathbf{U}^T\dot{\mathbf{U}} \tag{24.138}$$

and we can rewrite (24.136) as

$$\mathbf{J}_u\dot{\boldsymbol{\omega}}_u + \mathbf{S}(\boldsymbol{\omega}_u)\mathbf{J}_u\boldsymbol{\omega}_u = \mathbf{J}_u\dot{\boldsymbol{\omega}}_u + \boldsymbol{\omega}_u \times \mathbf{J}_u\boldsymbol{\omega}_u = \mathbf{M}_{eu} \tag{24.139}$$

Expanding (24.139) and assuming that $\mathbf{J}_u$ is given by (24.130), we now obtain:

$$\begin{aligned}
J_{u11}\dot{\omega}_{u1} + (J_{u33} - J_{u22})\omega_{u2}\omega_{u3} &= M_{eu1} \\
J_{u22}\dot{\omega}_{u2} + (J_{u11} - J_{u33})\omega_{u1}\omega_{u3} &= M_{eu2} \\
J_{u33}\dot{\omega}_{u3} + (J_{u22} - J_{u11})\omega_{u1}\omega_{u2} &= M_{eu3}
\end{aligned} \tag{24.140}$$

24.15 AN 'EXPLICIT CO-ROTATIONAL PROCEDURE' FOR BEAMS

The first dynamic co-rotational solutions would seem to have been described by Belytschko and Schwer [B3.17]. While in the following, we will concentrate on beams, many of the concepts are also relevant to shells.

As a first stage, we set up the initial element frames, $\mathbf{E}$ and compute the lumped inertia matrices with respect to these frames, $\mathbf{J}_E$. The contributions to a particular node (from different elements) are then transformed to the fixed global axes $[\mathbf{i}_1, \mathbf{i}_2, \mathbf{i}_3]$ and summed to give:

$$\mathbf{J} = \sum \mathbf{E}\mathbf{J}_E\mathbf{E}^T \tag{24.141}$$

Assuming that the element lies along the local 1 axis, for the element contribution to a node, Belytschko [B3] and Belytschko and Schwer [B3.17] take half the torsional inertia for the 11 term in $\mathbf{J}_E$ and a half of $A\rho l^2/12$ for the 22 and 33 contributions. Having formed $\mathbf{J}$ via (24.141), an eigenvalue analysis gives:

$$\mathbf{J} = \mathbf{U}\,\mathbf{Diag}(\mathbf{J}_u)\mathbf{U}^T \tag{24.142}$$

where $\mathbf{Diag}(\mathbf{J}_u)$ is now fixed as the rotating principal inertia matrix (previously $\mathbf{J}_u$) and $\mathbf{U}$ defines the initial orientation of the nodal triad $\mathbf{U}$.

As a starting-point let us assume that we know the current values of the element frame $\mathbf{E}$ and the nodal frames $\mathbf{U}_i$. Using the techniques of Section 17.1 or Chapter 18, we can now compute the local internal forces $\mathbf{q}_{il}$ and hence the global internal forces via:

$$\mathbf{q}_i = \mathbf{T}^T\mathbf{q}_{il} \tag{24.143}$$

where the transformation matrix, $\mathbf{T}$ has been discussed in Chapters 17.1 (where it was called $\mathbf{F}$) and in Chapter 18. At this stage, the internal forces (and residuals) are divided into translational forces, $\mathbf{q}_{it}$ and 'rotational forces', $\mathbf{q}_{ir}$. For the former, the method of Section 24.6 is directly applied so that, at a particular node:

$$\ddot{\mathbf{d}}_n = -\mathbf{M}^{-1}(\mathbf{g}_{t,n} + \mathbf{C}\dot{\mathbf{d}}_{n-1/2}) \tag{24.144}$$

where the subscript t on the vector $\mathbf{g}$ means 'translational'. The 'rotational forces' are now transformed to relate to the 'body attached' nodal frame so that a step n, at a particular node, we have:

$$\mathbf{g}_{ur,n} = \mathbf{U}_n^T\mathbf{g}_{r,n} \tag{24.145}$$

where the subscript r means 'rotational'. Neglecting any rotational damping, (24.136) can now be used to obtain:

$$\dot{\boldsymbol{\omega}}_{u,n} = -\mathbf{J}_u^{-1}\{\mathbf{g}_{ur,n} + \mathbf{S}(\boldsymbol{\omega}_{u,n-1/2})\mathbf{J}_u\omega_{u,n-1/2}\} \tag{24.146}$$

At this stage, the translational velocities are updated via:

$$\dot{\mathbf{d}}_{n+1/2} = \dot{\mathbf{d}}_{n-1/2} + \Delta t\ddot{\mathbf{d}}_n \tag{24.147}$$

while, in the body attached frame, the angular velocities, $\boldsymbol{\omega}_u$ are updated via:

$$\boldsymbol{\omega}_{u,n+1/2} = \boldsymbol{\omega}_{u,n-1/2} + \Delta t\dot{\boldsymbol{\omega}}_{u,n} \tag{24.148}$$

The translational displacements (or coordinates) can be updated via:

$$\mathbf{d}_{n+1} = \mathbf{d}_n + \Delta t \dot{\mathbf{d}}_{n+1/2} \tag{24.149}$$

and finally the nodal triad $\mathbf{U}$ can be updated via:

$$\mathbf{U}_{n+1} = \mathbf{U}_n[\mathbf{I} + \Delta t \mathbf{S}(\boldsymbol{\omega}_{u,n+1/2})] \tag{24.150}$$

The usual equation for updating a triad (see (16.47) or (17.10)) is

$$\mathbf{U}_{n+1} = \Delta \mathbf{U} \mathbf{U}_n \tag{24.151}$$

In deriving (24.150), we have used the simplest approximation to the rotation matrix $\Delta\mathbf{U}$ (see (16.5)) in the body attached frame, i.e.

$$\Delta \mathbf{U}_u = [\mathbf{I} + \Delta t \mathbf{S}(\boldsymbol{\omega}_{u,n+1/2})] \tag{24.152}$$

so that:

$$\Delta \mathbf{U} = \mathbf{U}_n \Delta \mathbf{U}_u \mathbf{U}_n^T = \mathbf{U}_n[\mathbf{I} + \Delta t \mathbf{S}(\boldsymbol{\omega}_{u,n+1/2})]\mathbf{U}_n^T \tag{24.153}$$

Substitution from (24.153) into (24.151) leads to the relationship given in (24.150).

24.16 UPDATING THE ROTATIONAL VELOCITIES AND ACCELERATIONS

In (24.148), the update for the rotational velocities was applied in the 'body attached frame'. We will now use an illustration from Simo and Wong [S1] to show that this is indeed the correct way to introduce the update.

Suppose that on top of the motion of our nodal triad $\mathbf{U}(t)$, we superimpose a constant rotation $\mathbf{Q}$ to produce a motion:

$$\mathbf{U}^+(t) = \mathbf{Q}\mathbf{U}(t) \tag{24.154}$$

Because $\mathbf{Q}$ is fixed,

$$\dot{\mathbf{U}}^+(t) = \mathbf{Q}\dot{\mathbf{U}}(t) \tag{24.155}$$

and the angular velocity for this modified motion is given by

$$\mathbf{S}(\boldsymbol{\omega}^+) = \dot{\mathbf{U}}^+(t)\mathbf{U}^+(t)^T = \mathbf{Q}[\dot{\mathbf{U}}(t)\mathbf{U}(t)^T]\mathbf{Q}^T = \mathbf{Q}\mathbf{S}(\boldsymbol{\omega})\mathbf{Q}^T \tag{24.156}$$

or

$$\boldsymbol{\omega}^+ = \mathbf{Q}\boldsymbol{\omega} \tag{24.157}$$

Suppose we now consider the angular velocity with respect to the body attached frame, $\boldsymbol{\omega}_u$, where (see (24.138)):

$$\mathbf{S}(\boldsymbol{\omega}_u) = \mathbf{U}^T[\dot{\mathbf{U}}\mathbf{U}^T]\mathbf{U} = \mathbf{U}^T\dot{\mathbf{U}} \tag{24.158}$$

or

$$\boldsymbol{\omega}_u = \mathbf{U}^T\boldsymbol{\omega} \tag{24.159}$$

If the same procedure is now applied to the modified motion (with superscript +), we

obtain:

$$\mathbf{S}(\boldsymbol{\omega}_u^+) = \mathbf{U}^{+\mathrm{T}}\dot{\mathbf{U}}^+ = \mathbf{U}^{\mathrm{T}}\mathbf{Q}^{\mathrm{T}}\mathbf{Q}\dot{\mathbf{U}} = \mathbf{U}^{\mathrm{T}}\dot{\mathbf{U}} = \mathbf{S}(\boldsymbol{\omega}_u) \tag{24.160}$$

or

$$\boldsymbol{\omega}_u^+ = \boldsymbol{\omega}_u \tag{24.161}$$

The relationships in (24.160) and (24.161) clearly provide the appropriate updating (no updating) in the current situation. In order words, in body attached coordinates, the superimposition of a constant rotation does not change the angular velocity and hence this description is appropriate for applying the updates.

We will consider the updates for the trapezoidal rule of (24.5) and (24.6). (An equivalent procedure could equally be applied to the general Newmark updates (24.2) and (24.3)). The rotational equivalent of (24.6) can be written as

$$\boldsymbol{\omega}_{u,n+1} + \boldsymbol{\omega}_{u,n} = \frac{2}{\Delta t}\Delta\boldsymbol{\theta}_u \tag{24.162}$$

where the subscript u implies that we are working in 'body attached (to **U**) coordinates'. In fixed coordinate, the $\Delta\boldsymbol{\theta}$ vector in (24.162) is related to that the obtained from the relationship:

$$\mathbf{U}_{n+1} = \Delta\mathbf{U}(\Delta\boldsymbol{\theta})\mathbf{U}_n \tag{24.163}$$

Knowing $\mathbf{U}_{n+1}$ and $\mathbf{U}_n$, $\Delta\boldsymbol{\theta}$ can be obtained from $\Delta\mathbf{U}$ using the method of Section 16.8 or that of Section 16.10. The vector $\Delta\boldsymbol{\theta}_u$ in (24.162) is the body attached equivalent of $\Delta\boldsymbol{\theta}$. Using (24.135), we might expect this to be computed either from

$$\Delta\boldsymbol{\theta}_u = \mathbf{U}_n^{\mathrm{T}}\Delta\boldsymbol{\theta} \tag{24.164a}$$

or else from

$$\Delta\boldsymbol{\theta}_u = \mathbf{U}_{n+1}^{\mathrm{T}}\Delta\boldsymbol{\theta} \tag{24.164b}$$

It can be shown that these two expressions are equivalent because:

$$\mathbf{U}_{n+1}^{\mathrm{T}}\Delta\boldsymbol{\theta} = \mathbf{U}_n^{\mathrm{T}}\Delta\mathbf{U}^{\mathrm{T}}\Delta\boldsymbol{\theta} = \mathbf{U}_n^{\mathrm{T}}\Delta\boldsymbol{\theta} \tag{24.165}$$

In the last step, we have used the fact (see (16.30)) that $\Delta\boldsymbol{\theta}$ is the eigenvalue of $\Delta\mathbf{U}$ and $\Delta\boldsymbol{\theta}/\Delta\theta$ it eigenvector so that:

$$\Delta\mathbf{U}\Delta\boldsymbol{\theta} = \Delta\boldsymbol{\theta} \tag{24.166a}$$

and multiplying (24.166a) by $\Delta\mathbf{U}^{\mathrm{T}}$:

$$\Delta\mathbf{U}^{\mathrm{T}}\Delta\boldsymbol{\theta} = \Delta\boldsymbol{\theta} \tag{24.166b}$$

For the angular accelerations, the equivalent of (24.5) now follows as

$$\dot{\boldsymbol{\omega}}_{u,n+1} + \dot{\boldsymbol{\omega}}_{u,n} = \frac{2}{\Delta t}(\boldsymbol{\omega}_{u,n+1} - \boldsymbol{\omega}_{u,n}) \tag{24.167}$$

In deriving both the predictors and correctors for the implicit solution procedures of Sections 24.3 and 24.8, we required the variations of the adopted updating algorithms (see i.e. (24.15) and (24.16)). The only difficulty relates to the variation of (24.162) when

combined with (24.164a), from which we obtain:

$$\delta\boldsymbol{\omega}_{\mathrm{u},n+1} = \frac{2}{\Delta t}\mathbf{U}_n^{\mathrm{T}}\delta\boldsymbol{\theta}_{n+1} = \frac{2}{\Delta t}\mathbf{U}_n^{\mathrm{T}}\mathbf{H}(\Delta\boldsymbol{\theta})^{-1}\delta\bar{\boldsymbol{\theta}}_{n+1} \tag{24.168}$$

where $\mathbf{H}(\Delta\boldsymbol{\theta})$ is given in (16.90) and its inverse in (16.94). The vector $\delta\bar{\boldsymbol{\theta}}_{n+1}$ contains the finite element spin variables that would be obtained from the iterative solver. Following the discussion in Section 16.11, unlike $\delta\boldsymbol{\theta}_{n+1}$ in (24.168), the bared terms are non-additive to $\Delta\boldsymbol{\theta}$. Combining (24.168) with the variation of (24.167), we can now obtain:

$$\delta\dot{\boldsymbol{\omega}}_{\mathrm{u},n+1} = \frac{2}{\Delta t}\delta\boldsymbol{\omega}_{\mathrm{u},n+1} = \frac{4}{\Delta t^2}\mathbf{U}_n^{\mathrm{T}}\mathbf{H}(\Delta\boldsymbol{\theta})^{-1}\delta\bar{\boldsymbol{\theta}}_{n+1} \tag{24.169}$$

24.17 A SIMPLE IMPLICIT CO-ROTATIONAL PROCEDURE USING ROTATIONS

An explicit procedure with rotation variables was described in Section 24.15. We will now consider an equivalent implicit procedure based on the trapezoidal rule. For the present, we will still adopt a lumped mass matrix for which the rotary inertia matrix ($\mathbf{J}_{\mathrm{u}}$) would again be computed using the method of Section 24.15 in a 'once-only', preprocessing pass.

It will be assumed that we know all of the variables at step n and have estimates for the variables at step $n+1$ (possibly via a predictor stage for which the reader could provide the relevant equations as an exercise). The techniques of Section 17.1 or Chapter 18 can then be used to provide the local static internal forces at step $n+1$ and hence the internal forces in relation to the fixed cartesian axes via (24.143). For the translational variables, we now have the equilibrium equations:

$$\bar{\mathbf{g}}_{n+1} = \mathbf{g}_{n+1} + \mathbf{M}\ddot{\mathbf{d}}_{n+1} = \mathbf{q}_{\mathrm{i},n+1} - \mathbf{q}_{\mathrm{e},n+1} + \mathbf{M}\ddot{\mathbf{d}}_{n+1} = 0 \tag{24.170}$$

while for the rotational variables at a particular node (see (24.139) premultiplied by $\mathbf{U}_{n+1}$), we have:

$$\bar{\mathbf{g}}_{n+1} = \mathbf{g}_{n+1} + \mathbf{U}_{n+1}\mathbf{J}_{\mathrm{u}}\dot{\boldsymbol{\omega}}_{\mathrm{u},n+1} + \mathbf{U}_{n+1}\mathbf{S}(\boldsymbol{\omega}_{\mathrm{u},n+1})\mathbf{J}_{\mathrm{u}}\boldsymbol{\omega}_{\mathrm{u},n+1} = 0 \tag{24.171}$$

To derive the equations for a 'corrector' iteration, we apply a truncated Taylor series to (24.171) so that:

$$\begin{aligned}\bar{\mathbf{g}}_{n+1,\mathrm{new}} = \bar{\mathbf{g}}_{n+1,\mathrm{old}} &+ \mathbf{K}_{\mathrm{t},n+1}\delta\mathbf{p} + \mathbf{U}_{n+1}\mathbf{J}_{\mathrm{u}}\delta\dot{\boldsymbol{\omega}}_{\mathrm{u},n+1} \\ &+ \mathbf{S}(\delta\bar{\boldsymbol{\theta}})\{\mathbf{U}_{n+1}\mathbf{J}_{\mathrm{u}}\dot{\boldsymbol{\omega}}_{\mathrm{u},n+1} + \mathbf{U}_{n+1}\mathbf{S}(\boldsymbol{\omega}_{\mathrm{u},n+1})\mathbf{J}_{\mathrm{u}}\boldsymbol{\omega}_{\mathrm{u},n+1}\} \\ &+ \mathbf{U}_{n+1}\mathbf{S}(\boldsymbol{\omega}_{\mathrm{u},n+1})\mathbf{J}_{\mathrm{u}}\delta\boldsymbol{\omega}_{\mathrm{u},n+1} - \mathbf{U}_{n+1}\mathbf{S}(\mathbf{J}_{\mathrm{u}}\boldsymbol{\omega}_{\mathrm{u},n+1})\delta\boldsymbol{\omega}_{\mathrm{u},n+1}\end{aligned} \tag{24.172}$$

where, because we are only dealing with the rotational variables at a node, the term $\mathbf{K}_{\mathrm{t}}$ only includes the relevant contributions. Using (24.168) and (24.169), (24.172) can be

re-expressed as

$$\bar{\mathbf{g}}_{n+1,\text{new}} = \bar{\mathbf{g}}_{n+1,\text{old}} + \mathbf{K}_{t,n+1}\delta\mathbf{p} + \frac{4}{\Delta t^2}\mathbf{U}_{n+1}\mathbf{J}_u\mathbf{U}_n^T\mathbf{H}(\Delta\boldsymbol{\theta})^{-1}\delta\bar{\boldsymbol{\theta}}$$
$$- \mathbf{S}\{\mathbf{U}_{n+1}\mathbf{J}_u\dot{\boldsymbol{\omega}}_{u,n+1} + \mathbf{U}_{n+1}\mathbf{S}(\boldsymbol{\omega}_{u,n+1})\mathbf{J}_u\boldsymbol{\omega}_{u,n+1}\}\delta\bar{\boldsymbol{\theta}}$$
$$+ \frac{2}{\Delta t}\{\mathbf{U}_{n+1}\mathbf{S}(\boldsymbol{\omega}_{u,n+1})\mathbf{J}_u - \mathbf{U}_{n+1}\mathbf{S}(\mathbf{J}_u\boldsymbol{\omega}_{u,n+1})\}\mathbf{U}_n^T\mathbf{H}(\Delta\boldsymbol{\theta})^{-1}\delta\bar{\theta} \qquad (24.173)$$

In Section 24.19, we will describe an alternative co-rotational procedure which does not involve a lumped mass formulation. However, we will first outline an isoparametric formulation.

24.18 AN ISOPARAMETRIC FORMULATION FOR THREE-DIMENSIONAL BEAMS

In this section, we will outline the extension by Simo and Vu Quoc [S6] of their original work on the static analysis of three-dimensional beams [S3.17]. The latter was described earlier in Section 17.2. We will here concentrate on the inertia terms and, in particular with those related to the rotations. Using the isoparametric approach, in place of (24.171), we can write the element contribution to the dynamic residual associated with the rotation variables at a node as

$$\bar{\mathbf{g}}_{n+1} = \mathbf{g}_{n+1} + \int h(\zeta)(\mathbf{U}_{n+1}\mathbf{J}'_u\dot{\boldsymbol{\omega}}_{u,n+1} + \mathbf{U}_{n+1}\mathbf{S}(\boldsymbol{\omega}_{u,n+1})\mathbf{J}'_u\boldsymbol{\omega}_{u,n+1})\,dS \qquad (24.174)$$

where $h(\zeta)$ is the shape function associated with the node and $\mathbf{J}'_u$ is given by

$$\mathbf{J}'_u = \int \begin{bmatrix} (x_2^2 + x_3^2) & 0 & 0 \\ 0 & x_3^2 & 0 \\ 0 & 0 & x_2^2 \end{bmatrix} \rho\, dx_2 dx_3 \qquad (24.175)$$

with the beam being assumed to lie along the x_1 axis. In contrast to the relationships in (24.171), in (24.175), $\mathbf{U}_{n+1}$, $\boldsymbol{\omega}_{n+1}$ and $\dot{\boldsymbol{\omega}}_{u,n+1}$, are now functions of ζ, the non-dimensional coordinate along the beam. In particular, the current triad $\mathbf{U}$ is the triad $\mathbf{T}$ of Section 17.2.

For the static formulation of Section 17.2, once we had obtained the nodal changes in rotation variables, the latter were interpolated to the Gauss points using (17.93) and the triad $\mathbf{T}$ (here $\mathbf{U}$) was updated in the usual way. For dynamics, we can also use the interpolated $\delta\bar{\boldsymbol{\theta}}$ at the Gauss points to obtain the change in angular velocities $\delta\boldsymbol{\omega}_{u,n+1}$ via (24.168) and hence we can update the angular velocities at the Gauss points. The angular accelerations at the Gauss points can then be updated using (24.167).

Having performed the updates, the dynamic residual can be computed using numerical integration, in conjunction with (24.175) for the rotation terms. If we write the dynamic equilibrium equation as

$$\bar{\mathbf{g}}_{n+1} = \mathbf{g}_{n+1} + \mathbf{q}_{\text{mas}} = \mathbf{0} \qquad (24.176)$$

with $\mathbf{q}_{\text{mas}}$ as the inertia (or mass) terms, for a two-noded element we can write the latter

as

$$\mathbf{q}_{\text{mas}} = \int \begin{bmatrix} h_1 A\rho \ddot{\mathbf{d}} \\ h_1 \mathbf{U}\{\mathbf{J}'_u \dot{\boldsymbol{\omega}}_u + \mathbf{S}(\boldsymbol{\omega})\mathbf{J}'_u \boldsymbol{\omega}_u\} \\ h_2 A\rho \mathrm{d} \\ h_2 \mathbf{U}\{\mathbf{J}'_u \dot{\boldsymbol{\omega}}_u + \mathbf{S}(\boldsymbol{\omega})\mathbf{J}'_u \boldsymbol{\omega}_u\} \end{bmatrix} \mathrm{d}S \tag{24.177}$$

where the subscript $n+1$ has been omitted but is implied.

For the Newton–Raphson iterations, we require the relationship:

$$\delta \mathbf{q}_{\text{mas}} = \mathbf{K}_{\text{t,mas}} \delta \mathbf{p} \tag{27.178}$$

With the aid of (24.168) and (24.169), we can obtain:

$$\mathbf{K}_{\text{t,mas}} = \begin{bmatrix} \mathbf{K}_{11} & \mathbf{0} & \mathbf{K}_{13} & \mathbf{0} \\ \mathbf{0} & \mathbf{K}_{22} & \mathbf{0} & \mathbf{K}_{24} \\ \mathbf{K}_{31} & \mathbf{0} & \mathbf{K}_{33} & \mathbf{0} \\ \mathbf{0} & \mathbf{K}_{42} & \mathbf{0} & \mathbf{K}_{44} \end{bmatrix} \tag{24.179}$$

where

$$\mathbf{K}_{11} = \frac{4}{\Delta t^2} \int A\rho h_1^2 \, \mathrm{d}S = \frac{4A\rho l}{3\Delta t^2} \mathbf{I} \tag{24.180a}$$

$$\mathbf{K}_{13} = K_{31} = \frac{4}{\Delta t^2} \int A\rho h_1 h_2 \, \mathrm{d}S = \frac{4A\rho l}{6\Delta t^2} \mathbf{I} \tag{24.180b}$$

$$\mathbf{K}_{33} = \frac{4}{\Delta t^2} \int A\rho h_2^2 \, \mathrm{d}S = \frac{4A\rho l}{3\Delta t^2} \mathbf{I} \tag{24.180c}$$

$$\begin{aligned} \mathbf{K}_{2i,2j} = & \int h_i h_j (-\mathbf{S}(\mathbf{U}_{n+1}\mathbf{S}(\boldsymbol{\omega}_{\mathrm{u},n+1})\mathbf{J}'_u \boldsymbol{\omega}_{\mathrm{u},n+1} + \mathbf{U}_{n+1}\mathbf{J}'_u \dot{\boldsymbol{\omega}}_{\mathrm{u},n+1})) \, \mathrm{d}S \\ & + \frac{2}{\Delta t} \int h_i h_j (\mathbf{U}_{n+1}\mathbf{S}(\boldsymbol{\omega}_{\mathrm{u},n+1})\mathbf{J}'_u - \mathbf{U}_{n+1}\mathbf{S}(\mathbf{J}'_u \boldsymbol{\omega}_{\mathrm{u},n+1})) \, \mathbf{U}_n^{\mathrm{T}} \mathbf{H}(\Delta\boldsymbol{\theta})^{-1} \mathrm{d}S \\ & + \frac{4}{\Delta t^2} \int h_i h_j \mathbf{U}_{n+1}\mathbf{J}'_u \mathbf{U}_n^{\mathrm{T}} \mathbf{H}(\Delta\boldsymbol{\theta})^{-1} \, \mathrm{d}S \end{aligned} \tag{24.180d}$$

In deriving the last expressions in (24.180a)–(24.180c), it has been assumed that the area of the element is constant. Equation (24.180d) applies for $i = 1, 2$ and $j = 1, 2$ and therefore defines the submatrices $\mathbf{K}_{22}$, $\mathbf{K}_{44}$, $\mathbf{K}_{24}$ and $\mathbf{K}_{42}$ in (24.179). The expressions in (24.180d) are closely related to (24.173) which was derived in more detail earlier.

It is worth noting that for the isoparametric formulation there are some difficulties associated with the numerical integration. For example, with a two-noded element, to avoid shear locking, we should use one-point integration for the static terms (see Section 7.2), while for the mass or inertia terms a two-point integration scheme is required. Also we are updating and storing triads (possibly via quaternions—see Section 16.9) at both sets of integration points with the angular velocities and accelerations also being stored at the latter.

24.19 AN ALTERNATIVE IMPLICIT CO-ROTATIONAL FORMULATION

In Section 24.17, we considered a simple co-rotational procedure which depended on a lumped formulation for the inertia terms. In the present section, we will consider an alternative procedure [J1] for which the starting-point can be considered to be a modified form of (24.177) with **U** being replaced by the fixed element frame, **E** (see Section 17.1 and Chapter 18). We can then write:

$$\mathbf{q}_{\text{mas}} = \begin{bmatrix} \mathbf{I} & & & \\ & \mathbf{E} & & \\ & & \mathbf{I} & \\ & & & \mathbf{E} \end{bmatrix} \int \begin{bmatrix} h_1 A\rho \ddot{\mathbf{d}} \\ h_1\{\mathbf{J}'_u\dot{\boldsymbol{\omega}}_u + \mathbf{S}(\boldsymbol{\omega})\mathbf{J}'_u\boldsymbol{\omega}_u\} \\ h_2 A\rho \ddot{\mathbf{d}} \\ h_2\{\mathbf{J}'_u\dot{\boldsymbol{\omega}}_u + \mathbf{S}(\boldsymbol{\omega})\mathbf{J}'_u\boldsymbol{\omega}_u\} \end{bmatrix} dS$$

$$= \bar{\mathbf{E}} \int \begin{bmatrix} h_1 A\rho \ddot{\mathbf{d}} \\ h_1\{\mathbf{J}'_u\dot{\boldsymbol{\omega}}_u + \mathbf{S}(\boldsymbol{\omega})\mathbf{J}'_u\boldsymbol{\omega}_u\} \\ h_2 A\rho \ddot{\mathbf{d}} \\ h_2\{\mathbf{J}'_u\dot{\boldsymbol{\omega}}_u + \mathbf{S}(\boldsymbol{\omega})\mathbf{J}'_u\boldsymbol{\omega}_u\} \end{bmatrix} dS \tag{24.181}$$

If the accelerations, rotational velocities, $\boldsymbol{\omega}_u$, and accelerations, $\dot{\boldsymbol{\omega}}_u$, (in the body attached frame) are now assumed to be interpolated using the conventional isoparametric shape functions, we can replace (24.181) with the relationship:

$$\mathbf{q}_{\text{mas}} = \bar{\mathbf{E}} \left[\mathbf{M}\ddot{\mathbf{p}} + \frac{l}{12} \begin{bmatrix} \mathbf{0} \\ 3\mathbf{S}(\boldsymbol{\omega}_1)\mathbf{J}'_u\boldsymbol{\omega}_1 + \mathbf{S}(\boldsymbol{\omega}_1)\mathbf{J}'_u\boldsymbol{\omega}_2 + \mathbf{S}(\boldsymbol{\omega}_2)\mathbf{J}'_u\boldsymbol{\omega}_1 + \mathbf{S}(\boldsymbol{\omega}_2)\mathbf{J}'_u\boldsymbol{\omega}_2 \\ \mathbf{0} \\ 3\mathbf{S}(\boldsymbol{\omega}_2)\mathbf{J}'_u\boldsymbol{\omega}_2 + \mathbf{S}(\boldsymbol{\omega}_2\mathbf{J}'_u)\boldsymbol{\omega}_1 + \mathbf{S}(\boldsymbol{\omega}_1)\mathbf{J}'_u\boldsymbol{\omega}_2 + \mathbf{S}(\boldsymbol{\omega}_1)\mathbf{J}'_u\boldsymbol{\omega}_1 \end{bmatrix} \right] \tag{24.182}$$

where

$$\ddot{\mathbf{p}}^{\mathrm{T}} = (\ddot{\mathbf{d}}_1^{\mathrm{T}}, \dot{\boldsymbol{\omega}}_1^{\mathrm{T}}, \ddot{\mathbf{d}}_2^{\mathrm{T}}, \dot{\boldsymbol{\omega}}_2^{\mathrm{T}}) \tag{24.183}$$

The matrix **M** in (24.182) is the conventional fixed mass matrix (see (24.85) in two-dimensional) that would relate to a linear isoparametric formulation. In (24.182) and (24.183), we have dropped the subscript u on the $\boldsymbol{\omega}$'s and $\dot{\boldsymbol{\omega}}$'s, but none the less, they are implied so that these quantities relate to a body-attached frame.

In contrast to the previous isoparametric formulation (Section 24.18), the rotational nodal velocities and accelerations (in a body attached frame) are now updated at the nodes rather than at the Gauss points. In order to apply Newton–Raphson iterations, we require the variation of (24.182) which leads to an equation of the form of (24.178) with:

$$\mathbf{K}_{\text{t,mas}} = \mathbf{K}_{\text{mas1}} + \mathbf{K}_{\text{mas2}} + \mathbf{K}_{\text{mas3}} \tag{24.184}$$

The matrix $\mathbf{K}_{\text{mas1}}$ stems from the variation of $\bar{\mathbf{E}}$ in (24.182). If we are using the co-rotational procedure of Section 17.1, the individual variations, $\delta\mathbf{e}_1$, $\delta\mathbf{e}_2$ and $\delta\mathbf{e}_3$ can be taken from (17.21) and (17.32). Alternatively, using the co-rotational procedure of

Section 18.10, we could use (18.27) so that:

$$\delta \mathbf{e}_i = -\mathbf{S}(\mathbf{e}_i)\mathbf{V}^{\mathrm{T}}\delta\mathbf{p} \tag{24.185}$$

If we adopt the former, we obtain:

$$\mathbf{K}_{\mathrm{mas}1} = \begin{bmatrix} \mathbf{0} & \mathbf{0} & \mathbf{0} & \mathbf{0} \\ \bar{q}_{\mathrm{m}}(4)[-\mathbf{A},\mathbf{0},\mathbf{A},\mathbf{0}] + \bar{q}_{\mathrm{m}}(5)\mathbf{L}(\mathbf{r}_2)^{\mathrm{T}} + \bar{q}_{\mathrm{m}}(6)\mathbf{L}(\mathbf{r}_3)^{\mathrm{T}} & & & \\ \mathbf{0} & \mathbf{0} & \mathbf{0} & \mathbf{0}\ \mathbf{0} \\ \bar{q}_{\mathrm{m}}(10)[-\mathbf{A},\mathbf{0},\mathbf{A},\mathbf{0}] + \bar{q}_{\mathrm{m}}(11)\mathbf{L}(\mathbf{r}_2)^{\mathrm{T}} + \bar{q}_{\mathrm{m}}(12)\mathbf{L}(\mathbf{r}_3)^{\mathrm{T}} & & & \end{bmatrix} \tag{24.186}$$

where

$$\bar{\mathbf{q}}_{\mathrm{m}} = \bar{\mathbf{E}}_{n+1}^{\mathrm{T}}\mathbf{q}_{\mathrm{mas}} \tag{24.187}$$

The second matrix $\mathbf{K}_{\mathrm{mas}2}$ is obtained from the variation of the acceleration terms in $\ddot{\mathbf{p}}$. For these, we require (24.16) and (24.169) and obtain:

$$\begin{aligned} \mathbf{K}_{\mathrm{mas}2} &= \frac{4}{\Delta t^2}\bar{\mathbf{E}}_{n+1}\mathbf{M}\begin{bmatrix} \mathbf{I} & & & \\ & \mathbf{U}_{n,1}^{\mathrm{T}}\mathbf{H}(\Delta\boldsymbol{\theta}_1)^{-1} & & \\ & & \mathbf{I} & \\ & & & \mathbf{U}_{n,2}^{\mathrm{T}}\mathbf{H}(\Delta\boldsymbol{\theta}_2)^{-1} \end{bmatrix} \\ &= \frac{4}{\Delta t^2}\bar{\mathbf{E}}_{n+1}\mathbf{M}\mathbf{B} \end{aligned} \tag{24.188}$$

where $\mathbf{U}_{n,1}$ is the nodal triad at node 1 at step n and $\mathbf{U}_{n,2}$ is the equivalent triad at node 2.

The final term $\mathbf{K}_{\mathrm{mas}3}$ stems from the variations of the (body attached) rotational velocity terms in (24.182) and hence we require the use of (24.168) to obtain:

$$\mathbf{K}_{\mathrm{mas}3} = \frac{l}{12}\frac{2}{\Delta t}\bar{\mathbf{E}}_{n+1}\begin{bmatrix} \mathbf{0} & \mathbf{0} & \mathbf{0} & \mathbf{0} \\ \mathbf{0} & 3\mathbf{F}_1+\mathbf{F}_2 & \mathbf{0} & \mathbf{F}_1+\mathbf{F}_2 \\ \mathbf{0} & \mathbf{0} & \mathbf{0} & \mathbf{0} \\ \mathbf{0} & \mathbf{F}_1+\mathbf{F}_2 & \mathbf{0} & \mathbf{F}_1+3\mathbf{F}_2 \end{bmatrix}\mathbf{B} \tag{24.189}$$

where

$$\mathbf{F}_i = \mathbf{S}(\boldsymbol{\omega}_i)\mathbf{J}'_{\mathrm{u}} - \mathbf{S}(\mathbf{J}'_{\mathrm{u}}\boldsymbol{\omega}_i) \tag{24.190}$$

and $\mathbf{B}$ was defined in (24.188).

24.20 (APPROXIMATELY) ENERGY-CONSERVING CO-ROTATIONAL PROCEDURES

Section 24.11 described an energy-conserving procedure for two-dimensional co-rotational beams. To this end, it first described a formulation that effectively conserved energy for moderate-sized steps and later, in Section 24.11, sophistications were added to remove the restrictions. In this section, we will apply a similar (approximate) method to modify the co-rotational procedures of Sections 24.17 and 24.19. In relation to the translational variables, the starting point is the mid-point dynamic equilibrium

relationship of (24.76). With regard to the rotational variables, a similar procedure is applied to the static internal forces, while for the dynamic rotational forces, instead of applying (24.171) whereby:

$$\mathbf{q}_{\text{mas}} = \frac{\mathrm{d}}{\mathrm{d}t}\{\mathbf{U}\mathbf{J}_{\text{u}}\mathbf{U}\boldsymbol{\omega}\}|_{n+1} = \mathbf{U}_{n+1}\mathbf{J}_{\text{u}}\dot{\boldsymbol{\omega}}_{\text{u},n+1} + \mathbf{U}_{n+1}\mathbf{S}(\boldsymbol{\omega}_{\text{u},n+1})\mathbf{J}_{\text{u}}\boldsymbol{\omega}_{\text{u},n+1} \tag{24.191}$$

(see also (24.133)), we now apply:

$$\mathbf{q}_{\text{mas}} = \frac{1}{\Delta t}(\mathbf{U}_{n+1}\mathbf{J}_{\text{u}}\boldsymbol{\omega}_{\text{u},n+1} - \mathbf{U}_{n}\mathbf{J}_{\text{u}}\boldsymbol{\omega}_{\text{u},n}) \tag{24.192}$$

For the present, we will concentrate on a 'lumped mass formulation' (see Section 24.17). In these circumstances, the change of kinetic energy can be expressed as:

$$\begin{aligned}\Delta K &= \tfrac{1}{2}((\boldsymbol{\omega}_{\text{u},n+1}^{\text{T}}\mathbf{J}_{\text{u}}\boldsymbol{\omega}_{\text{u},n+1}) - (\boldsymbol{\omega}_{\text{u},n}^{\text{T}}\mathbf{J}_{\text{u}}\boldsymbol{\omega}_{\text{u},n})) \\ &= \tfrac{1}{2}((\boldsymbol{\omega}_{\text{u},n+1} + \boldsymbol{\omega}_{\text{u},n})^{\text{T}}\mathbf{J}_{\text{u}}(\boldsymbol{\omega}_{\text{u},n+1} - \boldsymbol{\omega}_{\text{u},n}))\end{aligned} \tag{24.193}$$

Substitution from the updating formula of (24.162) into (24.193) gives:

$$\Delta K = \frac{1}{\Delta t}\Delta\boldsymbol{\theta}_{\text{u}}{}^{\text{T}}\mathbf{J}_{\text{u}}(\boldsymbol{\omega}_{\text{u},n+1} - \boldsymbol{\omega}_{\text{u},n}) \tag{24.194}$$

while premultiplication of $\mathbf{q}_{\text{mas}}$ from (24.192) by $\Delta\boldsymbol{\theta}^{\text{T}}$ gives:

$$\begin{aligned}\Delta\boldsymbol{\theta}^{\text{T}}\mathbf{q}_{\text{mas}} &= \frac{1}{\Delta t}\Delta\boldsymbol{\theta}^{\text{T}}(\mathbf{U}_{n+1}\mathbf{J}_{\text{u}}\boldsymbol{\omega}_{\text{u},n+1} - \mathbf{U}_{n}\mathbf{J}_{\text{u}}\boldsymbol{\omega}_{\text{u},n}) \\ &= \Delta\boldsymbol{\theta}_{\text{u}}^{\text{T}}\frac{1}{\Delta t}(\mathbf{J}_{\text{u}}\boldsymbol{\omega}_{\text{u},n+1} - \mathbf{J}_{\text{u}}\boldsymbol{\omega}_{\text{u},n}) = \Delta K\end{aligned} \tag{24.195}$$

where use has been made of (24.164) and (24.194). Following the approach of Section 24.11, we can also argue that:

$$\Delta\mathbf{p}^{\text{T}}\mathbf{q}_{\text{im}} \simeq \Delta\varphi \tag{24.196}$$

where $\mathbf{q}_{\text{im}}$ are the 'mid-point' static internal forces and $\Delta\varphi$ is the change in strain energy over the step. Consequently (for fixed external forces), the energy is (approximately) conserved once the combined residual $\mathbf{q}_{\text{im}} - \mathbf{q}_{\text{em}} + \mathbf{q}_{\text{mas}}$ is zero.

Rather than apply this 'lumped procedure', the present author and co-workers [C5, C6] have modified the co-rotational approach of Section 24.19 so that instead of (24.181), we start with:

$$\begin{aligned}\mathbf{q}_{\text{mas}} = \frac{1}{\Delta t}\int \begin{bmatrix} h_1 A\rho\{\dot{\mathbf{d}}_{n+1} - \dot{\mathbf{d}}_{\text{n}}\} \\ \mathbf{0} \\ h_2 A\rho\{\dot{\mathbf{d}}_{n+1} - \dot{\mathbf{d}}_{\text{n}}\} \\ \mathbf{0} \end{bmatrix} \mathrm{d}S \\ + \frac{1}{\Delta t}\bar{\mathbf{U}}_{n+1}\int \begin{bmatrix} \mathbf{0} \\ h_1\mathbf{J}'_{\text{u}}\boldsymbol{\omega}_{\text{u},n+1} \\ \mathbf{0} \\ h_2\mathbf{J}'_{\text{u}}\boldsymbol{\omega}_{\text{u},n+1} \end{bmatrix} \mathrm{d}S - \frac{1}{\Delta t}\bar{\mathbf{U}}_{n}\int \begin{bmatrix} \mathbf{0} \\ h_1\mathbf{J}'_{\text{u}}\boldsymbol{\omega}_{\text{u},n+1} \\ \mathbf{0} \\ h_2\mathbf{J}'_{\text{u}}\boldsymbol{\omega}_{\text{u},n+1} \end{bmatrix} \mathrm{d}S\end{aligned} \tag{24.197a}$$

where $\bar{\mathbf{U}}$ is defined (in similar fashion to $\bar{\mathbf{E}}$ from (24.181)) via:

$$\bar{\mathbf{U}} = \begin{bmatrix} \mathbf{I} & & & \\ & \mathbf{U}_1 & & \\ & & \mathbf{I} & \\ & & & \mathbf{U}_2 \end{bmatrix} \tag{24.197b}$$

with $\mathbf{U}_1$ as the nodal triad at node 1 and $\mathbf{U}_2$ as the equivalent triad at node 2. (It is probable that the 'nodal-point formulation' of Section 24.19 could be improved by introducing the $\bar{\mathbf{U}}$ matrix instead of the $\bar{\mathbf{E}}$ matrix.) Equation (24.197a) can be re-expressed as:

$$\mathbf{q}_{\text{mas}} = \frac{1}{\Delta t}\mathbf{M}_{\text{t}}\{\dot{\mathbf{p}}_{\text{t},n+1} - \dot{\mathbf{p}}_{\text{t},n}\} + \frac{1}{\Delta t}\bar{\mathbf{U}}_{n+1}\mathbf{M}_{\text{r}}\dot{\mathbf{p}}_{\text{r},n+1} - \frac{1}{\Delta t}\bar{\mathbf{U}}_{n}\mathbf{M}_{\text{r}}\dot{\mathbf{p}}_{\text{r},n} \tag{24.198}$$

where $\mathbf{M}_{\text{t}}$ contains the translational parts of the conventional fixed mass matrix and $\mathbf{M}_{\text{r}}$ the rotational parts. Also $\dot{\mathbf{p}}_{\text{t}}$ contains the translational nodal velocities (with the rotational terms set to zero) while $\dot{\mathbf{p}}_{\text{r}}$ contains the (body attached) rotational nodal velocities (with the translational terms set to zero).

In oder to apply Newton–Raphson iterations, we require the variation of (24.198)which leads to an equation of the form of (24.178) so that:

$$\delta\mathbf{q}_{\text{mas}} = \mathbf{K}_{\text{mas1}}\delta\mathbf{p}_{\text{r},n+1} + \mathbf{K}_{\text{mas2}}\delta\mathbf{p}_{\text{t},n+1} + \mathbf{K}_{\text{mas3}}\delta\mathbf{p}_{\text{r},n+1} \tag{24.199a}$$

The matrix $\mathbf{K}_{\text{mas1}}$ stems from the variation of $\bar{\mathbf{U}}_{n+1}$ in (24.198) and we obtain:

$$\mathbf{K}_{\text{mas1}} = \begin{bmatrix} \mathbf{0} & \mathbf{0} & \mathbf{0} & \mathbf{0} \\ \mathbf{0} & -\mathbf{S}(\bar{\mathbf{q}}_{\text{m}}(4\text{–}6)) & \mathbf{0} & \mathbf{0} \\ \mathbf{0} & \mathbf{0} & \mathbf{0} & \mathbf{0} \\ \mathbf{0} & \mathbf{0} & \mathbf{0} & -\mathbf{S}(\bar{\mathbf{q}}_{\text{m}}(10\text{–}12)) \end{bmatrix} \tag{24.199b}$$

where:

$$\bar{\mathbf{q}}_{\text{m}} = \frac{1}{\Delta t}\bar{\mathbf{U}}_{n+1}\mathbf{M}_{\text{r}}\dot{\mathbf{p}}_{\text{r},n+1} \tag{24.200}$$

The second matrix $\mathbf{K}_{\text{mas2}}$ is obtained from the variation of the translational velocity terms in (24.198) and, with the aid of (24.15), leads to

$$\mathbf{K}_{\text{mas2}} = \frac{2}{\Delta t^2}\mathbf{M}_{\text{t}} \tag{24.201}$$

The final matrix $\mathbf{K}_{\text{mas3}}$ in (24.199a) is obtained from the variation of the (body attached) rotational velocities in $\dot{\mathbf{p}}_{\text{r},n+1}$. With the aid of (24.168), we obtain:

$$\mathbf{K}_{\text{mas3}} = \frac{2}{\Delta t^2}\bar{\mathbf{U}}_{n+1}\mathbf{M}_{\text{r}}\begin{bmatrix} \mathbf{0} & & \\ & \mathbf{U}_{n,1}^{\text{T}}\mathbf{H}(\Delta\boldsymbol{\theta}_1)^{-1} & \\ & \mathbf{0} & \\ & & \mathbf{U}_{n,2}^{\text{T}}\mathbf{H}(\Delta\boldsymbol{\theta}_2)^{-1} \end{bmatrix} \tag{24.202}$$

where $\mathbf{U}_{n,1}$ is the nodal triad at node 1 at step n and $\mathbf{U}_{n,2}$ is the equivalent triad at node 2.

Sophistications can probably be made to the method in order to achieve full energy conservation. Ideas on this topic are discussed in [C5, C6] where it is shown that even the current 'approximately energy conserving' procedure leads to a dramatic improvement in the 'non-linear stability' in comparison with the conventional end-point Newmark method.

24.21 ENERGY-CONSERVING ISOPARAMETRIC FORMULATIONS

An energy-conserving formulation for beams has been described by Simo et al. in [S5] while a formulation for shells has been described by Simo and Tarnow in [S4]. In the following we will consider beams.

The developments start with the expression (17.79) derived for the static internal forces. Combining the latter with (17.74):

$$\mathbf{q}_i = \frac{1}{2}\begin{bmatrix} -2\mathbf{U} & \mathbf{0} \\ -\mathbf{S}(\mathbf{x}'_{21})\mathbf{U} & -2\mathbf{U} \\ 2\mathbf{U} & \mathbf{0} \\ -\mathbf{S}(\mathbf{x}'_{21})\mathbf{U} & 2\mathbf{U} \end{bmatrix} \begin{pmatrix} \mathbf{N} \\ \mathbf{M} \end{pmatrix} \tag{24.203}$$

These equations relate to a two-noded element, but the extension to a more general isoparametric element is straightforward (see Section 17.2.6).

In (24.203), we have adopted the current notation whereby $\mathbf{U}$ is the triad which was labelled $\mathbf{T}$ in Section 17.2. This triad would be computed at the Gauss point (here centre point) using (see 17.65). In Section 17.2, the internal force vector (here (24.203)) was related to the end point, $n+1$. A modification, aimed at energy conservation, would be to replace (24.203) with a mid-point relationship:

$$\mathbf{q}_{im} = \frac{1}{2}\begin{bmatrix} -2\mathbf{U}_m & \mathbf{0} \\ -\mathbf{S}(\mathbf{x}'_{21m})\mathbf{U}_m & -2\mathbf{U}^*_m \\ 2\mathbf{U}_m & \mathbf{0} \\ -\mathbf{S}(\mathbf{x}'_{21m})\mathbf{U}_m & 2\mathbf{U}^*_m \end{bmatrix} \begin{pmatrix} \mathbf{N}_m \\ \mathbf{M}_m \end{pmatrix} \tag{24.204}$$

where the reason for the asterisks will be given shortly. In (24.204) (see (17.66a) and (24.102)), we would use:

$$\mathbf{x}'_{21m} = \mathbf{x}_{21} + \tfrac{1}{2}(\mathbf{d}_{21,n} + \mathbf{d}_{21,n+1}) \tag{24.205}$$

while

$$\mathbf{N}_m = \tfrac{1}{2}(\mathbf{N}_n + \mathbf{N}_{n+1}); \qquad \mathbf{M}_m = \tfrac{1}{2}(\mathbf{M}_n + \mathbf{M}_{n+1}) \tag{24.206}$$

The matrix $\mathbf{U}_m$ has yet to be defined. To this end, Simo *et al.* [S5] used the non-orthogonal:

$$\mathbf{U}_m = \tfrac{1}{2}[\mathbf{U}_{n+1} + \mathbf{U}_n] \tag{24.207}$$

and:

$$\mathbf{U}^*_m = \det(\mathbf{U}_m)\mathbf{U}_m^{-T} \tag{24.208}$$

It can now be shown [S5] (see (24.60) and (24.196)) that:

$$\Delta \mathbf{p}^{\mathrm{T}} \mathbf{q}_{\mathrm{im}} = \Delta \varphi \tag{24.209}$$

where $\Delta \mathbf{p}$ are the incremental displacements over the step and $\Delta \varphi$ is the change of strain energy over the step. However, $\Delta \mathbf{p}$ in (24.209) must be defined in such a way that the incremental rotation variables involve tangent scaled pseudo-vector components (see (16.34)). Indeed the up-dating procedures must also involve the latter. In addition, in contrast to the static work of Section 17.2, we must now use the shape functions to interpolate 'incremental' rather than 'iterative' (see (17.64) and (17.93)) (tangent scaled) rotational quantities.

The procedure of Simo *et al.* [S5] fully conserves both energy and the components of angular momentum. However, because of the use of the tangent scaled pseudo-vector, it does not seem to be possible to implement this formulation as a direct extension (including the up-dating procedures) of the static formulation of Chapter 17. The present author and a co-worker have developed such an extension [J1] which uses:

$$\exp[\mathbf{S}(\boldsymbol{\theta})] = \mathbf{U}_{n+1} \mathbf{U}_n^{\mathrm{T}} \tag{24.210}$$

$$\mathbf{U}_m = \exp[\mathbf{S}(\boldsymbol{\theta}/2)]\mathbf{U}_n = \exp[\mathbf{S}(-\boldsymbol{\theta}/2)]\mathbf{U}_{n+1} \tag{24.211}$$

(As with the formulation of Simo *et al.* [S5], the shape function interpolations must again be made to 'incremental rotations'—here not tangent scaled). While an approximately energy conserving procedure can be obtained by directly using (24.204) (without the asterisks), a fully energy-conserving procedure can be obtained by modifying (24.204) so that:

$$\mathbf{q}_{\mathrm{im}} = \frac{1}{2} \begin{bmatrix} -2\mathbf{A}_1 \mathbf{U}_{\mathrm{m}} & \mathbf{0} \\ -\mathbf{A}_2 \mathbf{S}(\mathbf{x}'_{21\mathrm{m}}) \mathbf{U}_{\mathrm{m}} & -2\mathbf{A}_3 \mathbf{U}_{\mathrm{m}} \\ 2\mathbf{A}_1 \mathbf{U}_{\mathrm{m}} & \mathbf{0} \\ -\mathbf{A}_2 \mathbf{S}(\mathbf{x}'_{21\mathrm{m}}) \mathbf{U}_{\mathrm{m}} & 2\mathbf{A}_3 \mathbf{U}_{\mathrm{m}} \end{bmatrix} \begin{pmatrix} \mathbf{N}_{\mathrm{m}} \\ \mathbf{M}_{\mathrm{m}} \end{pmatrix} \tag{24.212}$$

with

$$\mathbf{A}_1 = \left[[\mathbf{I}] + \frac{1 - \cos(\theta/2)}{\theta^2} \mathbf{S}(\boldsymbol{\theta}) \mathbf{S}(\boldsymbol{\theta}) \right] \tag{24.213a}$$

$$\mathbf{A}_2 = \frac{2 \sin(\theta/2)}{\theta} [\mathbf{I}] \tag{24.213b}$$

$$\mathbf{A}_3 = \left[[\mathbf{I}] + \left(1 - \left(\frac{\sin(\theta/2)}{(\theta/2)} \right) \right) \frac{\mathbf{S}(\boldsymbol{\theta}) \mathbf{S}(\boldsymbol{\theta})}{\theta^2} \right] \tag{24.213c}$$

and $\boldsymbol{\theta}$ is the incremental pseudo-vector at the centre of the beam. In the two-dimensional case, it can be shown that this procedure coincides with the method of Stander and Stein [S7] which was discussed in Section 24.12. While the present technique leads to a fully energy-conserving procedure [J1], the algorithm does not conserve angular momentum (except in the limit at $\Delta t \to 0$). None the less, numerical experiments show that the angular momentum remains bounded and that the formulation inherits the important property of remaining stable in the non-linear regime. However, these same numerical experiments currently indicate some convergence difficulties (see also [B5]). These convergence problems do not seem to arise with the method of Simo *et al.* [S5].

For the mass terms, we modify (24.177) from Section 24.18 using the ideas from Section 24.20 so as to obtain:

$$\mathbf{q}_{\text{mas}} = \frac{1}{\Delta t}\int \begin{bmatrix} h_1 A\rho\{\dot{\mathbf{d}}_{n+1} - \dot{\mathbf{d}}_n\} \\ h_1\{\mathbf{U}_{n+1}\mathbf{J}'_u\boldsymbol{\omega}_{u.n+1} - \mathbf{U}_n\mathbf{J}'_u\boldsymbol{\omega}_{u.n}\} \\ h_2 A\rho\{\dot{\mathbf{d}}_{n+1} - \dot{\mathbf{d}}_n\} \\ h_2\{\mathbf{U}_{n+1}\mathbf{J}'_u\boldsymbol{\omega}_{u.n+1} - \mathbf{U}_u\mathbf{J}'_u\boldsymbol{\omega}_{u.n}\} \end{bmatrix} dS \tag{24.214}$$

As pointed out at the end of Section 24.18, we might require a different numerical integration procedure for the static and inertia terms. Further details on the formulations can be found in [S5] and [J1]. It is worth noting that while for continua and two-dimensional beams, the energy-conserving formulations have the disadvantage of leading to non-symmetric stiffness matrices, for three-dimensional beams there are no such disadvantages because the conventional end-point formulations also lead to non-symmetry (Sections 24.17–24.19).

24.22 SPECIAL NOTATION

A = area
$\mathbf{A}_1, \mathbf{A}_2, \mathbf{A}_3$ = see (24.213)
$\mathbf{C}$ = damping matrix
$\mathbf{C}_t$ = tangent constitutive matrix
$\mathbf{d}$ = displacement vector
$\dot{\mathbf{d}}$ = velocity vector
$\ddot{\mathbf{d}}$ = acceleration vector
$\mathbf{E}$ = element triad, composed of unit vector $\mathbf{e}_1$–$\mathbf{e}_3$
$\bar{\mathbf{E}}$ = see (24.181)
$\mathbf{E}$ = (Section 24.10)—Green strain
$\mathbf{g}$ = static residual or out-of-balance force vector
$\bar{\mathbf{g}}$ = dyanmic residual or out-of-balance force vector
h_i = shape functions
$\mathbf{H}$ = shape function matrix
$\mathbf{H}(\boldsymbol{\theta})$ = matrix connecting $\delta\bar{\boldsymbol{\theta}}$ to $\delta\theta$ (see (17.173) and (16.89) and (16.90)). Here first used in Section 24.16
$\mathbf{J}_u$ = rotary inertia matrix in body attached frame (see (24.128)–(24.130))
$\mathbf{J}'_u$ = rotary inertia matrix in body attached frame (see (24.175))
K = kinetic energy
$\mathbf{K}_t$ = static tangent stiffness matrix
$\bar{\mathbf{K}}_t$ = tangent stiffness matrix including inertia terms
$\mathbf{L}$ = matrix connecting $\delta\mathbf{e}$'s to $\delta\mathbf{p}$'s (see (17.32)). Here first used in Section 24.19
$\mathbf{M}$ = mass matrix
$\mathbf{M}$ = (Section 24.21) vector of local bending moments
$\mathbf{N}$ = axial force
$\mathbf{N}$ = vector of local axial and shear stress resultants in Section 17.3
$\mathbf{p}$ = nodal displacement vector (including rotations)
$\dot{\mathbf{p}}$ = velocity vector (including rotational velocities)

$\ddot{\mathbf{p}}$ = acceleration vector (including rotational accelerations)
$\mathbf{P}$ = see (24.87)
$\mathbf{q}_i$ = internal force vector
$\bar{\mathbf{q}}_m$ = see (24.187) and (24.200)
$\mathbf{q}_{mas}$ = internal forces due to mass or inertia terms
$\mathbf{S}$ = skew-symmetric matrix or (Section 24.10) second Piola–Kirchhoff stresses
$\mathbf{T}$ = transformation matrix relating small changes in local variables to small changes in global variables
$\mathbf{U}$ = body attached triad (possibly related to a node)
$\mathbf{x}$ = initial coordinate vector
$\mathbf{x}'$ = current coordinate vector
l_o, l_n = old and new length of beam (straight between nodes)
α = constant for 'α method'—see Section 24.8
α = rigid body rotation in Section 24.11
β, γ = Newmark constants
ω = frequency or angular velocity
$\boldsymbol{\omega}$ = vector of angular velocities
$\dot{\boldsymbol{\omega}}$ = vector of angular accelerations
φ = strain energy
ϕ = total potential energy
ρ = density
ζ = non-dimensional coordinate along beam

Subscripts

l = local
m = mid-point
mas = relates to mass or inertia
r = rotational
t = translational (or tagential)
u = related to triad $\mathbf{U}$ and hence 'body attached'

24.23 REFERENCES

[A1] Argyris, J. & Mlejnek, H.-P., *Dynamics of Structures*, North-Holland (1991).
[B1] Bathe, K.-J., *Finite Element Procedures for Solids and Structures—Nonlinear Analysis*, MIT Centre for Advanced Engineering Stufies (1986).
[B2] Belytschko, T., An overview of semidiscretisation and time integration procedures, *Computational Methods for Transient Analysis*, ed. T. Belytschko & T. J. R. Hughes, Elsevier Science, pp. 1–65 (1983).
[B3] Belytschko, T., A survey of numerical methods and computer programs for dynamic structural analysis, *Nucl. Engng. Design*, **37**, 23–34 (1976).
[B4] Bergan, P. G. & Mollestad, E., An automatic time-stepping algorithm for dynamic problems, *Comp. Meth. in Appl. Mech. & Engng.*, **49**, 299–318 (1985).

[B5] Bauchau, O. A., Damilano, G. & Theron, N. J., Numerical integration of nonlinear elastic multi-body systems, *Int. J. for Num. Meth. in Engng.*, **38**, 2727–2751 (1995).

[C1] Cardona, A. & Geradin, M., Time integration of the equations of motion in mechanism analysis, *Computers & Structs.*, **33**, 801–820 (1989).

[C2] Crisfield, M. A. & J. Shi, A co-rotational element/time integration strategy for non-linear dynamics, *Int. J. for Num. Meth. in Engng.*, **37**, 1897–1913 (1994).

[C3] Crisfield, M. A., Shri, J. & Lim, K. L., Finite elements and non-linear dynamics, *Modern Practice in Stress and Vibration Analysis*, The Stress Analysis Group of the Institute of Physics, Sheffield (1993) pp. 3–13.

[C4] Crisfield, M. A. & Shi, J., in: *Computational Analysis of Rigid and Flexible Mechanical Systems*, Vol. 2, ed. M. S. Pereira *et al.*, IDMEC, Univ. of Lisbon, Portugal, pp. 197–214 and in extended form in *Nonlinear Dynamics*, **9**, 37–52 (1996).

[C5] Crisfield, M. A., Jelenic, G., Fan, Z. & Zhong, H.-G., Static and dynamic non-linear analysis of structures, in *Computational Methods in Applied Sciences '96*, ed. J.-A. Désidéri, C. Hirsch, P. Le Tallec, E. Oñate, M. Pandolfi, J. Périaux, E. Stein, John Wiley & Sons, Chichester, pp. 9–21 (1996).

[C6] Crisfield, M. A., Jelenic, G., Mi, Y., Zhong, H.-G. & Fan, Z., Some aspects of the non-linear finite element method, to be published in *Finite Elements in Analysis and Design*.

[G1] Galvanetto, U. & Crisfield, M. A., An energy conserving co-rotational procedure for the dynamics of planar structures, *Int. J. for Num. Meth. in Engng.*, **39**, 2265–2282 (1996)

[H1] Naug, E., Nguyen, O. S. & De Rouvray, A. L., An improved energy conserving implicit time integration algorithm for nonlinear dynamic structural analysis, in *Proceedings of the Fourth Conference on Structural Mechanics in Reactor Technology*, San Francisco, Aug. (1977).

[H2] Hibbitt, H. D. & B. I. Karlsson, Analysis of pipe whip, *ASME Pressure Vessel and Piping Conf.*, San Francisco, 25–29 June, (1979).

[H3] Hibbitt, H. D. & Karlsson, B. I. *Analysis of Pipe Whip*, Report No. EPRI NP-1208, Electric Power Res. Inst., Palo Alto, Nov. (1979).

[H4] Hilber, H. M., Hughes, T. J. R. & Taylor, R. L., Improved numerical dissipation for time integration algorithms, *Earthquake Engineering and Structural Dynamics*, **5**, 283–292 (1977).

[H5] Hinton, E., Rock, A. & O. C. Zienkiewicz, A note on mass lumping and related processes in the finite element method, *Int. J. for Earthquake Eng. Struct. Dyn.*, **4**, 245–249 (1970).

[H6] Hughes, T. J. R., Liu, W. K. & Caughy, 'Transient finite element formulations that preserve energy', *Journal of Applied Mechanics*, **45**, 366–370 (1978).

[H7] Hughes, T. J. R. & Belytschko, T., A precis of developments in computational methods for transient analysis, *J. of Appl. Mech.*, **50**, 1033–1041 (1983).

[H8] Hughes, T. J. R., Analysis of transient algorithms with particular reference to stability behaviour, *Comp. Meth. in Mechanics*, ed. T. Belytschko & T. J. R. Hughes, North-Holland, Amsterdam (1983).

[J1] Jelenic, G. & Crisfield, M. A., Co-rotational and isoparametric formulations for non-linear dynamics with finite elements, paper in preparation.

[J2] Jennings, A. & McKeown, J. J., *Matrix Computation*, 2nd edn, Wiley, London (1992).

[N1] Newmark, N. M., A method of computation for structural dynamics, *J. Eng. Mech. Div., ASCE, EM3*, **85**, 67–94 (1959).

[P1] Park, K. C. & Underwood, P. G., A variable central difference method for structural dynamic analysis—Part 1, Theoretical aspects, *Comp. Meth. in Appl. Mech. & Engng.*, **22**, 241–258 (1980).

[S1] Simo, J. C. & Wong, K. K., Unconditionally stable algorithms for rigid body dynamics that exactly preserve energy and momentum, *Int. J. for Num. Meth. in Engng.*, **31**, 19–52 (1991).

[S2] Simo, J. C., Rifai, M. S. & Fox, D. D., On a stress resultant geometrically exact shell model, Part VI: Conserving algorithms for non-linear dynamics, *Int. J. for Num. Meth. in Engg.*, **34**, 1117–1164 (1992).

[S3] Simo, J. C. & Tarnow, N., The discrete energy-momentum method. Conserving algorithms for nonlinear elastodynamics, *Z. angew. Math. und Phys.*, **43**, 757–792 (1992).

[S4] Simo, J. C. & Tarnow, N., A new energy conserving algorithm for the nonlinear dynamics of shells, *Int. J. for Num. Meth. in Engng.*, **37**, 2527–2549 (1994).

[S5] Simo, J. C., Tarnow, N. & Doblare, M., Nonlinear dynamics of 3-D rods: exact energy and momentum conserving algorithms, *Int. J. for Num. Meth. in Engng.*, **38**, 1431–1474 (1995).

[S6] Simo, J. C. & Vu Quoc, L., On the dynamics in space of rods undergoing large motions—a geometrically exact approach, *Comp. Meth. in Appl. Mech. & Engng.*, **66**, 125–161 (1988).

[S7] Stander, N. & Stein, E., An energy conserving planar finite beam element for dynamic flexible mechanisms, submitted to *Engineeing Computations*.

[S8] Stewart, I., Warning—handle with care!, *Nature*, **355**, 16–17 (1992).

[U1] Underwood, P. G. & Park, K. C., A variable central difference method for structural dynamic analysis—Part 2, Implementation and performance evaluation, *Comp. Meth. in Appl. Mech. & Engng.*, **23**, 259–279 (1980).

[Z1] Zienkiewicz, O. C., Wood, W. L. & Taylor, R. L., An alternative single-step algorithm for dynamic problems, *Earthquake Engineering and Structural Dynamics*, **8**, 31–40 (1980).

[Z2] Zhong, H. G. & Crisfield, M. A., Application of an automatic time-stepping procedure in dynamic non-linear finite element computations, IC Aero Report 96-02, Dept. of Aeronautics, Imperial College, London (1996).

Index

Index compiled by Geoffrey C. Jones